



Odyssée au fil des interfaces: de la physico-chimie des macromolécules à l'enveloppe bactérienne, plate-forme interactive du micro-organisme avec son micro-environnement

Cécile Duclairoir Poc

► To cite this version:

Cécile Duclairoir Poc. Odyssée au fil des interfaces: de la physico-chimie des macromolécules à l'enveloppe bactérienne, plate-forme interactive du micro-organisme avec son micro-environnement. Bactériologie. Université de Rouen Normandie, 2018. tel-02367371

HAL Id: tel-02367371

<https://normandie-univ.hal.science/tel-02367371>

Submitted on 18 Nov 2019

HAL is a multi-disciplinary open access archive for the deposit and dissemination of scientific research documents, whether they are published or not. The documents may come from teaching and research institutions in France or abroad, or from public or private research centers.

L'archive ouverte pluridisciplinaire **HAL**, est destinée au dépôt et à la diffusion de documents scientifiques de niveau recherche, publiés ou non, émanant des établissements d'enseignement et de recherche français ou étrangers, des laboratoires publics ou privés.

HABILITATION A DIRIGER DES RECHERCHES

Mémoire présenté en vue d'obtenir
l'habilitation à diriger des recherches

Spécialité ASPECTS MOLECULAIRES ET CELLULAIRES DE LA BIOLOGIE

Préparée au sein de l'Université de Rouen Normandie

Odyssée au fil des interfaces: de la physico-chimie des macromolécules à l'enveloppe bactérienne, plate-forme interactive du micro-organisme avec son micro-environnement.

Présentée et soutenue par
Cécile DUCLAIRoir POC
le 14 novembre 2018

Thèse soutenue publiquement le 14 novembre 2018
devant le jury composé de

Dr Catherine SANTAELLA	Chargée de recherche, BIAM-LEMIRE UMR CNRS-CEA Aix Marseille Université 7265	Rapporteur
Pr Jean-Marc BERJEAUD	Professeur directeur du laboratoire Ecologie et Biologie des Interactions UMR CNRS 7267, Université de Poitiers	Rapporteur
Pr Raphaël DELEPEE	Professeur au laboratoire ABTE-ToxEMAC EA4651, Université de Caen Normandie	Rapporteur
Dr Céline PICARD	Maître de conférences laboratoire URCOM UMR CNRS 3038, Université du Havre Normandie	Examinateur
Pr Nicole ORANGE	Professeur Laboratoire de Microbiologie Signaux et Microenvironnement EA 4312, Université de Rouen Normandie	Examinateur et garant

Garant : Pr Nicole ORANGE, Laboratoire de Microbiologie Signaux et Microenvironnement, EA 4312

Table des matières

<u>AVANT-PROPOS</u>	<u>1</u>
<u>RESUME DES ACTIVITES DU DR CECILE DUCLAIROR POC EN VUE DE SOUTENIR L'HABILITATION A DIRIGER LES RECHERCHES</u>	<u>2</u>
<u>CURRICULUM VITAE DETAILLE</u>	<u>5</u>
<u>BILAN DE MES RECHERCHES</u>	<u>25</u>
I) <u>INTERFACE : QUELLE REALITE PHYSIQUE ?</u>	<u>27</u>
II) <u>CREATION D'INTERFACES A L'AIDE DE BIOMOLECULES</u>	<u>27</u>
III) <u>BIOSURFACTANTS, EXOPRODUITS BACTERIENS AMPHIPHILES</u>	<u>29</u>
A) <u>Production de cyclolipopeptides par de nombreuses souches de <i>P. fluorescens</i> de toute niche environnementale</u>	<u>31</u>
(1) <u>Origine rhizosphérique</u>	<u>31</u>
(2) <u>Origine aéroportée</u>	<u>32</u>
(3) <u>Origine clinique</u>	<u>33</u>
B) <u>Valorisation de CLPs en réponse à une pollution environnementale</u>	<u>34</u>
C) <u>Rôle des BSs : élément de la réponse adaptative de <i>Pseudomonas</i> à leur microenvironnement</u>	<u>35</u>
(1) <u>Physiologie bactérienne</u>	<u>35</u>
(a) <u>Mobilité</u>	<u>35</u>
(b) <u>Adhésion</u>	<u>37</u>
(c) <u>Biofilm</u>	<u>38</u>
(2) <u>Réponse au stress biologique provoqué par un hôte</u>	<u>42</u>
(3) <u>Communication cell-to-cell</u>	<u>43</u>
IV) <u>EVALUATION DE LA VIRULENCE BACTERIENNE : APPROCHE ORIGINALE EN QUALITE DE L'AIR</u>	<u>45</u>
V) <u>IMPACT DE STRESS SUR L'ADAPTATION ET LA VIRULENCE BACTERIENNE</u>	<u>49</u>
A) <u>Stress biologique</u>	<u>49</u>
(1) <u>Signaux eucaryotes</u>	<u>49</u>
(a) <u>Acide γ-aminobutyrique (GABA)</u>	<u>49</u>
(b) <u>Substance P</u>	<u>50</u>
(c) <u>Calcitonin Gene Related Peptide (CGRP)</u>	<u>51</u>
(2) <u>Systèmes de sécrétion</u>	<u>51</u>

B) Stress chimique : la pollution diésel promeut-elle la virulence bactérienne via sa propre réponse adaptative ?	53
(1) <u>Implémentation de l'imagerie HPTLC-MALDI TOF MS et application à l'étude du lipidome de bactéries <i>P. fluorescens</i></u>	<u>54</u>
(2) <u>Mise en place de l'exposition bactérienne</u>	<u>58</u>
(a) <u>Matériel biologique</u>	<u>58</u>
(b) <u>Choix et concentration en polluant</u>	<u>58</u>
(3) <u>Impact du NO₂ sur la physiologie et la virulence des souches <i>P. fluorescens</i> aéroportée MFAF76a et clinique MFN1032</u>	<u>60</u>
(a) <u>Approche lipidomique</u>	<u>60</u>
(b) <u>Réponse des 2 souches via leur comportement social et leur résistance aux antibiotiques aux 3 concentrations de NO₂</u>	<u>63</u>
(4) <u>Impact du NO₂ sur l'homéostasie membranaire de la souche <i>P. fluorescens</i> aéroportée MFAF76a</u>	<u>70</u>
(a) <u>Impact du NO₂ sur la réponse de <i>P. fluorescens</i> aéroportée MFAF76a à l'aide d'analyses « omics »</u>	<u>71</u>
(b) <u>Eléments de réponse à propos de l'impact du NO₂, polluant automobile sur la réponse adaptative de <i>P. fluorescens</i></u>	<u>73</u>
C) Stress physique : impact d'une matrice cosmétique complexe	74
(1) <u>Impact du microenvironnement sur <i>Cutibacterium acnes</i></u>	<u>75</u>
(2) <u>Impact d'une matrice cosmétique complexe de type lotion solaire sur la croissance de deux souches modèles cutanées : <i>Staphylococcus aureus</i> MFP 05 et <i>Pseudomonas fluorescens</i> MFP04</u>	<u>76</u>
(3) <u>Etude préliminaire de la réponse adaptative bactérienne interagissant avec des NPs</u>	<u>78</u>
(a) <u>Impact du stress de NPs hydrophiles sur la croissance les bactéries cutanées <i>Staphylococcus aureus</i> MFP05 et <i>Pseudomonas fluorescens</i> MFP04</u>	<u>78</u>
(b) <u>Impact du stress de NPs hydrophiles sur la physiologie de la <i>Pseudomonas fluorescens</i> aéroportée MFAF76a</u>	<u>79</u>
MES PERSPECTIVES DE RECHERCHE	81
I) <u>SECURITE SANITAIRE DE L'AIR : ADAPTATION BACTERIENNE AUX NOx</u>	<u>81</u>
II) <u>ADAPTATION DE BACTERIES EN CONTACT AVEC UN MILIEU DENSE</u>	<u>85</u>
A) <u><i>NanoToxBactR</i> : étude de faisabilité d'un test cytotoxicité des NPs</u>	<u>85</u>
B) <u>Evaluation de l'activité antibactérienne de nanomatériaux NMx d'argent</u>	<u>87</u>
C) <u>Evaluation de l'activité antibactérienne de NPs en matrice cosmétique</u>	<u>90</u>
(1) <u>Evaluation de l'activité antibactérienne des émulsions</u>	<u>91</u>
(2) <u>Evaluation de l'activité antibactérienne du rayonnement UV</u>	<u>91</u>
(3) <u>Evaluation de l'activité antibactérienne de NPs en matrice cosmétique</u>	<u>92</u>
III) <u>FEUILLE DE ROUTE !</u>	<u>93</u>
BIBLIOGRAPHIE	95
MES PUBLICATIONS	115

Remerciements

Remerciements

Cette tranche de vie, relatée dans ce mémoire, a été rendue possible, comme les perspectives le seront, que grâce au concours de plusieurs personnes à qui je voudrais témoigner toute ma reconnaissance.

Je voudrais tout d'abord adresser toute ma gratitude aux rapporteurs et examinateurs qui ont accepté d'évaluer mes travaux : Mesdames Catherine SANTAELLA et Céline PICARD ; Messieurs Jean-Marc BERJEAUD et Raphaël DELEPEE. Je ne t'oublie pas, Nicole ! Tu as accepté d'être mon garant. Tu as été celle qui m'a proposé d'intégrer notre laboratoire, le Laboratoire de Microbiologie du Froid, qui, depuis, est devenu le Laboratoire de Microbiologie Signaux et Microenvironnement. Tout au long de ces années, tu as tenté de m'initier à « surfer sur la vague ». J'en profite pour remercier le directoire actuel : Marc FEUILLOLEY et Sylvie CHEVALIER de leur confiance, soutien, conseils et expertises scientifiques.

Ces dernières années ont été riches scientifiquement grâce à l'ensemble des membres du LMSM : aussi bien enseignants-chercheurs, techniciens, doctorants, post-doctorants, stagiaires. Certains d'entre vous ont partagé un peu plus que de la science ! Ces échanges peuvent remplir les coffres de voiture, aussi bien de cartons pleins que de laurier. Une pensée toute particulière à Annabelle, qui a relu la quasi-totalité de ce manuscrit (Une phrase : sujet, verbe, complément. Il y a encore du boulot !), à Josette et à notre regretté JeF.

Ces travaux ne pourraient être présentés sans l'implication de l'ensemble des « stagiaires » que j'ai l'occasion d'encadrer. Merci, plus particulièrement, aux post-doctorants : Magdalena, Maryse et Juju, mais aussi aux doctorants : Sandra, Tatiana, Ségo et le nouveau venu Thibault, sans oublier les externes : Laura et Davina. Des nuages se sont parfois accumulés, mais j'ai pris plaisir à vous encadrer de mon mieux pour que nous grandissions ensemble ! Merci à Anne de nous avoir accompagné, Nicole et moi, quelques années sur la thématique de la qualité de l'air.

Je n'oublie pas nos collaborateurs ébroïciens (Florence, Nadine), normands (Jean-Paul, Frédéric, David, Frantz, Julie, Céline Nicolas, Michel), de Paris (Marie-Noëlle, Thierry, Jean-

Marie, Magalie, Pascal), du Poitou (et oui la filière n'est pas mauvaise ;- !), de l'étranger (Hermann, Angela) et j'en oublie... Merci à tous !

Je désire aussi remercier mes collègues croisés en enseignement : bien sûr ceux de Génie Biologique (Je sais je suis structurante ;- !), de Pack (J'ai du mal avec Pec !), d'IQBio, de M2 Microbio, d'ESITech (ah cette semaine bloquée !), tous les acteurs de formation que sont les personnels administratifs et techniques et formateurs d'autres cursus (ancien Ecopic, CQP, CMQ et IFSI d'Evreux).

Un grand merci à mes parents, à mes « petites » sœurs, aux Poc et valeurs ajoutées, aux très proches : Josette & Michel, Florence & Christophe !

Enfin merci pour votre amour, soutien et patience inconditionnels à vous deux, Xavier et Anne-Elisabeth.

Cette citation était en début de mon manuscrit de thèse et reste d'actualité :

« Donnez leur envie de bien faire et vous aurez tout gagné ! »

Mère Sainte Marie, Principes d'éducation
(Douvres-La Délivrande, Calvados, 1832)

Partons pour cette odyssée au travers des interfaces !



Avant-propos

Avant-Propos

Cher lecteur,

Vous voici à l'orée d'un mémoire d'habilitation à diriger les recherches, dont l'objectif est de revisiter ma vie d'enseignant-chercheur.

Mon application a été de vous rendre le moins fastidieux et le plus cohérent possible cet odyssée au travers d'une vingtaine d'années d'enseignements et de recherche qui ont été riches en interfaces et évolutions. Dans un premier temps, un résumé de mon parcours comme enseignant et comme chercheur sera complété par mes perspectives de recherche. Suivra mon *curriculum vitae* détaillant exhaustivement mon cursus, mes enseignements, mes responsabilités administratives, mes activités d'expertise et de conseil et survolant mes activités recherche, compilant mes encadrements et mes publications-communications. Par la suite, je réaliseraï un bilan plus approfondi de ma recherche. Je conclurai par les perspectives de recherche que j'aimerais poursuivre dans les années à venir.

Débutons cet odyssée !

Résumé d'activité

Résumé des activités du Dr Cécile Duclairoir Poc en vue de soutenir l'habilitation à diriger les recherches

Titulaire d'un DEUG Sciences et Structure de la Matière préparé à l'antenne universitaire naissante de Cherbourg (Université de Caen Normandie, 1993), j'ai poursuivi mon cursus universitaire, à Caen, en chimie, puis chimie des matériaux en me spécialisant en physico-chimie des interfaces. Effectivement mes recherches doctorales, sous la direction des Pr E NAKACHE et AM ORECCHIONI, ont débuté en 1997 au sein de l'équipe Polymères et Interfaces d'un laboratoire de Chimie, Laboratoire de Chimie Moléculaire Thio-organique LCMT UMR-CNRS 6507 de l'Université de Caen Normandie. Elles ont ciblé des biomolécules. J'ai étudié la physico-chimie, voire la structure de ces macromolécules naturelles afin de les valoriser sous une forme galénique toujours d'actualité : l'encapsulation. J'ai ensuite évalué la faisabilité de leur vectorisation en y incorporant des molécules actives.

Les compétences développées en galénique et en formulation cosmétique m'ont permis d'assurer des formations intra-entreprises dès 1997 et comme enseignante vacataire à l'Université de Caen Normandie (1998-1999), à l'Ecole d'ingénieurs de Cherbourg (1999-2000) et à l'Université de Rouen Normandie pour un DESTU dispensé à l'IUT d'Evreux (2001).

Suite à mon recrutement par l'Université de Rouen Normandie, comme ATER (2001), puis maître de conférences (2002), j'ai intégré l'équipe de formation du DUT Génie Biologique. Mon service statutaire concerne les domaines des industries pharmaceutiques et cosmétiques et leurs problématiques qualité. Ces enseignements sont réalisés en partie au sein de la Halle Technologique de Pharmacie Industrielle dont j'ai la responsabilité depuis 2001. Au cours des années, j'ai fait bénéficier de ce plateau technique unique à d'autres formations : le DUT Packaging naissant (2003-2015), l'IUP/ Master Ingénierie de la Santé IQBio (UFR Sciences et Techniques, Université de Rouen Normandie ; 2003-à ce jour), l'ESITech (Ecole d'ingénieurs co-habillée Université de Rouen Normandie-INSA de Rouen ; 2015-à ce jour), mais aussi à des formations préparatoires au Certificat de Qualification Professionnelle pour les salariés de l'industrie pharmaceutique (partenariat avec l'AFPI de l'Eure, labellisé par les entreprises du médicament). Depuis 2011, je dispense des enseignements davantage centrés sur ma recherche aux étudiants des 2 parcours du Master Microbiologie (co-acrédité Universités de Rouen Normandie et Caen Normandie).

Quant à mon implication administrative, elle est effective. Ma participation a pu être ponctuelle : responsabilité de parcours DUT ou de formation (2 licences professionnelles) ; représentativité dans diverses commissions (conseil de département, d'institut, jurys de VAE, de DUT, de LP). Cependant un engagement fort sur le long terme est démontré par ma coordination des stages en Génie Biologique depuis 2001 ou ma représentation de l'Université de Rouen Normandie depuis 2013 auprès de formations en soins infirmiers (IFSI d'Evreux, DRDJSCS de Normandie).

Parmi mes autres charges administratives, j'assure depuis 2013 des expertises de dossiers Crédit d'Impôt Recherche et Jeune Entreprise Innovante.

Les occupations précédentes sont importantes et nécessaires, mais moins motivantes que la recherche. Dès mon recrutement par l'Université de Rouen Normandie en 2001, je me suis intéressée aux biosurfactants bactériens au sein du Laboratoire de Microbiologie du Froid, EA 2123, dirigé alors par le Pr. N ORANGE qui a évolué en EA 4312 nommée Laboratoire de Microbiologie du Froid – Signaux et MicroEnvironnement (LMDF-SME), puis en 2011 en Laboratoire de Microbiologie-Signaux et Microenvironnement (LMSM, EA 4312) dirigé actuellement par le Pr M FEUILLOLEY. La production de ces molécules amphiphiles modifie la physico-chimie de la surface bactérienne et, par conséquent, influence son adaptation à son micro-environnement, voire sa virulence. Au long des années, ma formation en microbiologie s'étoffant, j'ai élargi mon champ de recherche débutant par l'identification et l'établissement des conditions de sécrétion des biosurfactants. J'ai ensuite évalué leur implication dans le comportement adhésif bactérien, dans la virulence bactérienne, voire leur rôle dans la communication bactérienne en participant alors à une collaboration avec le Dr M.N. Bellon-Fontaine (UBHM, UMR INRA AgroParitech, Massy). Parallèlement, j'ai étudié une possible valorisation de ces biomolécules en bioremédiation de sédiments estuariens avec le Laboratoire COBRA UMR CNRS 6014 (Université de Rouen Normandie).

Suite à ma participation à une étude sur la qualité de l'air, un questionnement est apparu : les bactéries aéroportées ne seraient-elles pas l'interface catalysée par la pollution automobile déclenchant chez l'humain de pneumopathies bactériennes exacerbées en période de forte pollution ? Après avoir étudié l'impact sur la physiologie d'une souche aéroportée de *Pseudomonas fluorescens* à des expositions au NO₂, marqueur de pollution automobile, nous avons approfondi le sujet pour évaluer l'impact de ce même stress chimique au niveau de la paroi bactérienne, interface da la bactérie avec son microenvironnement. Y a-t'il simple diffusion du NO₂ sans autre réponse bactérienne, comme le sous-entend l'approche traditionnelle de l'immuno-suppression humaine provoquée par la pollution ? Ou la bactérie met-elle en œuvre une réponse plus ou moins complexe dont l'un des sites est sa paroi, interface avec l'environnement extérieur?

Parallèlement, j'ai eu l'opportunité de collaborer sur une autre thématique de sécurité sanitaire, concernant les produits cosmétiques. L'objectif était de documenter le vieillissement de nanoparticules (NPs) de TiO₂ en lotion solaire sur deux bactéries représentatives du microbiote cutané. Suite à la formulation de deux lotions solaires modèles contenant des NPs hydrophiles ou hydrophobes, la croissance bactérienne a été étudiée lors de deux scenarii soit mimant le stockage du produit, soit lors de l'application de la formule solaire sur la peau. Désirant évaluer le cas d'une biocontamination ponctuelle d'un cosmétique lors de sa production ou lors du prélèvement consommateur avant application, une souche *P. fluorescens* d'origine aéroportée a été mise en contact avec de NPs de TiO₂ hydrophiles. La membrane bactérienne s'en trouve-t'elle impactée, voire perméabilisée ?

Ainsi les pistes de ces recherches convergent vers la réponse bactérienne au niveau de sa paroi, interface entre la bactérie et son microenvironnement. Ces travaux m'ont permis d'encadrer 11 étudiants Bac +2/3, 19 Bac+4, 6 Master 2, 3 doctorants et 3 post-doctorants.

J'aimerais poursuivre cette approche de la réponse membranaire bactérienne en approfondissant, voire en fragmentant les stress étudiés. En documentant leur conséquences physiologiques, métaboliques, génétiques, nous pourrons appréhender les mécanismes stratégiques implantés. En sécurité sanitaire de l'air, la caractérisation de l'adaptation bactérienne au NO₂ sera poursuivie au travers de la réponse membranaire. Le doctorant recruté (RIN 2018-2021) a pour objectif d'en évaluer les conséquences et d'en décoder les mécanismes sous-tendant grâce aux collaborations nationales et internationales. A la suite d'exposition de mélanges NO₂/NO, nous espérons déconvoluer les stratégies bactériennes (dont membranaires) mises en œuvre en condition de stress nitrosant en phase gaz. Ce stress est souvent intégré au stress oxydant qui est l'un des principaux acteurs des mécanismes antimicrobiens. Dans un premier temps, afin d'éviter les ROS (espèces réactives oxydantes) en solution, je débuterai par l'effet des rayonnements UV (producteurs de ROS) sur la réponse bactérienne, thématique d'un financement Cifre déposé à l'été 2018 avec BASF Beauty Care Solutions France SAS. Fin 2018, j'aimerais déposer auprès de l'ANSES une version amendée du projet NanoToxBactR. Cette étude de faisabilité concerne un test original d'évaluation de toxicité de NPs, via leur effet antibactérien en aérosol. Pour compléter mes compétences, je collaborerai avec l'équipe NanoCARE (GPM UMR CNRS 6634, Université de Rouen Normandie-INSA de Rouen) et, de nouveau, avec le CERTAM. Poursuivant ma collaboration avec le département matériaux du LIST (Luxembourg), j'explorerai les conséquences du contact nanomatériau imprégné/ bactérie sur son homéostasie membranaire et les répercussions métaboliques, voire génétiques. Cette expertise accumulée me permettra d'aborder, à plus long terme, l'interaction bactérie/matrice cosmétique solaire, préoccupant l'industrie cosmétique. Un tel modèle nécessite une fragmentation de ce système en « contacts élémentaires » de la bactérie avec les divers partenaires : globule d'émulsion, irradiation solaire, filtre physique type NP. Les stratégies bactériennes mises en place via sa membrane pourront être évaluées, en identifiant la participation relative de chaque partenaire.

Toute cette trajectoire scientifique a été possible et ne pourra se poursuivre que grâce à des encadrements de stagiaires et de doctorants et à des réponses positives aux programmes de financements que j'ai déjà pu obtenir et que je développerai activement dans les années à venir.

Mon objectif est de poursuivre ma quête sur le rôle de la membrane bactérienne, interface intelligente et sélective entre la bactérie et son microenvironnement !

Evreux, le 5 septembre 2018



Cécile DUCLAIRoir

Curriculum vitae détaillé

DUCLAIROIR POC

Cécile

Née le 16 juillet 1973
à Clermont-Fd (63)
Mariée, 1 enfant
31 rue Saint Louis
27000 EVREUX
t : +33 613 426 051
e : cecile.poc@univ-rouen.fr

Maître de conférences
Université de Rouen



**Laboratoire De Microbiologie
Signaux et Microenvironnement**
EA 4312
CSSN, Bureau I109;
55 rue Saint Germain, 27000 Evreux



**Halle Technologique de
Pharmacie Industrielle**
IUT d'Evreux
CS 40486
27004 Evreux Cedex

□ CURSUS/FORMATION

- 1997-2000 Doctorat en Sciences des Matériaux à l'Université de Caen** soutenu le 4 octobre 2000, obtenu avec mention très honorable.
- Mai 1998 Formation à la diffusion de neutrons aux petits angles**, lors des Journées de la Diffusion Neutronique 7, à Albé (Vosges)
- 1996-1997 DEA de Sciences de Matériaux à l'Université de Caen** (mention assez-bien, 1^{ère} session)
- 1996-1998 Maîtrise de Chimie option "Catalyse et Propriétés des Interfaces" à l'Université de Caen** (session de juin)
- 1993-1995 Licence de Chimie à l'Université de Caen** (session de juin)
- 1991-1993 DEUG A voie ASP (Sciences-Physiques) option Sciences pour l'Ingénieur à l'Université de Caen** (session de juin)

□ PARCOURS PROFESSIONNEL

2016-à ce jour Titulaire de la Prime d'Encadrement Doctorale et de Recherche

2002-à ce jour Maître de Conférences, Laboratoire de Microbiologie du Froid- Signaux et MicroEnvironnement, EA 4312, Université de Rouen

"Mécanismes adaptatifs bactériens, en particulier membranaires, lors de stress physique lié à une matrice complexe (émulsion, nanoparticules, nanomatériaux)"

"Impact de stress : thermique et chimique (HAP, substance P et NOx) sur la virulence bactérienne"

"Evolution de la virulence bactérienne lors d'interactions biotiques ou abiotiques"

"Production et caractérisation de biosurfactants bactériens, facteurs de virulence"

"Qualité microbiologique de l'air urbain"

"Qualité microbiologique de produits cosmétiques"

2001-2002 Agent Temporaire d'Enseignement et de Recherche, Laboratoire de Microbiologie du Froid (actuel LMSM, EA 4312), Université de Rouen Normandie

"Evaluation de propriétés de surface de souches bactériennes, en particuliers *Pseudomonas*"

2001 Vacataire en galénique pour le Diplôme d'Etudes Scientifiques et Techniques d'Université Industrie Pharmaceutique, Institut Universitaire Technologique d'Evreux, Université de Rouen Normandie.

1996-2000 Doctorante, Equipe Polymères et Interfaces, UMR CNRS 6507, ISMRA-Caen

"Elaboration de nanoparticules de biopolymères (chitosane et gliadines, protéines du blé) et encapsulation de diverses substances actives (vitamine, parfum et bactéricide tensio-actif)"

en collaboration avec le laboratoire de Pharmacie galénique et biopharmacie de Rouen, l'INRA de Nantes, le Laboratoire Léon Brillouin du CEA-Saclay dans le cadre d'échanges de chercheurs du Réseau Régional Normand Matériaux-Polymères-Plasturgie.

1996 Technicienne, Département d'Applications Techniques, Société Française HOECHST, Lillebonne (76). Etude physico-mécanique, détermination de la transition vitreuse au moyen des différentes méthodes de choc et la stabilité de coloration du polypropylène chargé en colorant

FONCTIONS EN ENSEIGNEMENT & ADMINISTRATIF PEDAGOGIQUE
➤ AU SEIN DE NORMANDIE UNIVERSITE

✓ Au sein de l’Institut Universitaire Technologique d’Evreux, Université de Rouen Normandie

2017 à ce jour Membre du Conseil d’Institut de l’Institut Universitaire Technologique d’Evreux
2017 à ce jour Membre du Section Locale Hygiène Sécurité Conditions de Travail Environnement, Institut Universitaire Technologique d’Evreux.

2015- à ce jour Membre du jury de Validation de la Licence Professionnelle Toxicologie et Gestion des risques toxiques, Institut Universitaire Technologique d’Evreux.

2001-à ce jour Responsable pédagogique de la Halle Technologique de pharmacie Industrielle
Sept-oct 2014 Formations préparatoires au Certificat de qualification professionnelle pour les salariés de l’industrie pharmaceutique (CQP Pharma) réalisées par C DUCLAIRIOIR POC, partenariat avec l’AFPI de l’Eure, formations labellisées par le LEEM

2007-2012 Vice-présidente et membre du jury de Validation des Acquis de l’Expérience, Institut Universitaire Technologique d’Evreux.

2007-2012 Membre du jury de Validation des Licences Professionnelles, Institut Universitaire Technologique d’Evreux.

2007-2010 Responsable pédagogique de la Licence Professionnelle Gestion de la Production Option : Animateur Qualité, Département de Génie Biologique, Institut Universitaire Technologique d’Evreux en partenariat avec la CCI de l’Eure au sein de l’Institut Européen de la Qualité Totale.

2003-2006 Participation aux jurys de validation des DUT, Institut Universitaire Technologique d’Evreux.

•*Département Génie Biologique*

2015- à ce jour Membre du Conseil de Perfectionnement de la Licence Professionnelle Toxicologie et Gestion des risques toxiques

2015- à ce jour Responsable des modules d’enseignement et enseignante en Licence Professionnelle Toxicologie et Gestion des risques toxiques

- M32 : Gestion des Risques en production
- M42 : Aspects Réglementaires et normatifs

2001-à ce jour Responsable des modules et enseignante en DUT Génie Biologique concernant les industries pharmaceutiques et cosmétiques et la qualité afférente

- Option Industries Agro-alimentaires et Biologique : M32I03, M41I06C, M33I01C et M42I01C
- Option Analyses Biochimiques et Biologiques : M33B01, M41B06, M42B01.

2001-à ce jour Co-responsable des stages du DUT Génie Biologique options Industries Agro-alimentaires et Biologiques et Analyses Biochimiques et Biologiques

2013-2017 Membre du Conseil de Département Génie Biologique

2006-2007 Responsable pédagogique de la Licence Professionnelle Biotechnologique Option : Modélisation et Validation, cohabilité avec l’université de Cergy-Pontoise

2003-2006 Responsable pédagogique de la 2^{ème} Année Génie Biologique Option : Industries Agro-alimentaires et Biologiques Adaptation locale : Industries Pharmaceutiques

2001 Vacataire en galénique pour le Diplôme d’Etudes Scientifiques et Techniques d’Université Industrie Pharmaceutique, Institut Universitaire Technologique d’Evreux, Université de Rouen Normandie.

•*Département Génie du Conditionnement et de l’Emballage (créé en 2003)*

2003-2015 Enseignante sur les interactions contenu-contenant en bio-industries

✓ Au sein de l'UFR Sciences et Techniques, Université de Rouen Normandie

2017- à ce jour Responsable du module Sécurité microbiologique : normes et qualité du Master 2 Biosciences Microbiologie option Microbiologie industrielle et Biotechnologie (MIB), co-habilités avec l'Université de Caen Normandie <site Mont St Aignan, 76>.

2017- à ce jour Enseignante en Interaction surfaces abiotiques du Master 1 Microbiologie <site Mont St Aignan, 76>.

2012-à ce jour Tuteur de stages d'initiation à la recherche en Master 1 Biosciences Microbiologie, Université de Rouen Normandie.

2012- à ce jour Enseignante en Microbiologie, Master 2 Biosciences Microbiologie, cohabilité avec Université de Caen Normandie, subdivisé depuis 2017 en 2 options : Microbiologie industrielle et Biotechnologie (MIB) et Mécanismes Moléculaires Microbiens (MMM) <site Mont St Aignan, 76>.

2011- à ce jour Membre des jurys de soutenance de Master 2 Microbiologie Microbiologie industrielle et Biotechnologie (MIB), cohabilité avec l'Université de Caen Normandie

2003-à ce jour Enseignante en Microbiologie pharmaceutique, en Master 1 Professionnel Biosciences, Ingénierie Qualité Bioproduits <Antenne d'Evreux, 27>;

2012-2016 Enseignante en Qualité dans les bio-industries en Licence 3 SVT Ingénierie de la Santé <Antenne d'Evreux, 27>;

2003-2015 Enseignante en Management de la Qualité en bio-industries, en Master 2 Professionnel Biosciences, Ingénierie Qualité Bioproduits <Antenne d'Evreux, 27>.

✓ Au sein de l'ESITech, Ecole d'ingénieurs co-habilléée Université de Rouen Normandie-INSA de Rouen (créeée en septembre 2014) <site St Etienne du Rouvray, 76>.

2018- à ce jour Membre du Conseil de Perfectionnement de l'ESITech

2015- à ce jour Responsable des modules d'enseignement et enseignante de 2^{ème} année Spécialité Technologie du Vivant

- TV41-Génie des procédés
- TV42-Formulation

✓ Au sein de l'UFR Sciences et Techniques, Université de Caen Normandie

1999-2000 Chargée de Travaux Pratiques de chimie, Ecole d'Ingénieurs de Cherbourg (EIC) <Site de Cherbourg>.

1998-1999 Chargée de Travaux Dirigés, Institut de Biologie et Biochimie appliquées <CampusI, Caen>.

➤ EN DEHORS DE NORMANDIE UNIVERSITE

2016- à ce jour Membre du jury régional d'attribution du Diplôme d'Etat d'Infirmier, DRDJSCS de Normandie

2013- à ce jour Membre du Conseil Pédagogique et de la Commission d'Attribution des Crédits de l'Institut de Formation paramédical de l'Eure.

2006-2010 Enseignante en Connaissance des Entreprises Industrielles de la Santé et Projet tutoré de la Licence Professionnelle Biotechnologique option Production et Diagnostic, Université de Cergy-Pontoise <site St Martin>.

1996-2006 Formatrice au cours de 6 formations permanentes *intra muros* de la Société L'Oréal d'Initiation aux Agents de Surfaces (tensio-actifs).

FONCTIONS ADMINISTRATIVES RECHERCHE

2001-2004 Qualifiée aux fonctions de maîtres de conférences des sections CNU : 31, 32 et 39 (actuellement 85).

2002-2013 Membre de la 39^{ème} section du CNU, devenue la 85^{ème}.

Septembre 2013 Intégration de la 64^{ème} section du CNU.

✓ Au sein de Normandie Université

2017 Vice-présidente du comité de sélection pour le recrutement du maître de conférences emploi n°1287 (section 64), IUT d'Evreux, Génie Biologique / LMSM, Université de Rouen Normandie.

- 2017** Membre du comité de sélection pour le recrutement du maître de conférences emploi n°325 (sections 31 et 33), UFR Sciences et Technique / Laboratoire URCOM, Université du Havre Normandie.
- 2015-2017** Référent de thèse pour l'Ecole Doctorale Normande de Chimie – ED 508, Université du Havre Normandie.
- 2015-2016** Membre des jurys de soutenance à mi-parcours des thèses de l'Ecole Doctorale Normande de Biologie Intégrative Santé Environnement ED 497 de l'Université de Rouen Normandie.
- 2015** Membre du comité de sélection pour le recrutement du maître de conférences emploi n°586 (section 65), ESITech / LMSM, Université de Rouen Normandie.
- 20 Nov 2015** Membre du jury de la soutenance du Doctorat Européen en Microbiologie de Tatiana KONDAKOVA de l'Université de Rouen, intitulé “*Pseudomonas adaptation to stress factors: role of membrane lipids and Pseudomonas fluorescens response to NO₂*”.
- 2013- à ce jour** Membre suppléant de la Commission consultative de spécialités d'établissement de la 64ème section du Conseil National des Universités (CNU), Université de Rouen Normandie.
- Normandie.
- 2004-2006** Membre de la commission de spécialistes 39^{ème} section CNU (actuelle 85^{ème}), Université de Rouen Normandie.
- ✓ Au sein du Laboratoire de Microbiologie Signaux Microenvironnement EA4312
- 2012-à ce jour** Membre du conseil du laboratoire LMSM, EA 4312, Université de Rouen

• *Recherche de financement pour mes thématiques de recherche*

- Janvier 2018** Soumission d'une demande d'allocation doctorale au concours du Réseau d'Intérêts Normand Normandie Biomédicale et Chimie axe Sécurité sanitaire, bien-être et aliments durables intitulée « NOxBBEE : NOx, polluants automobiles : détermination de Biomarqueurs Bactériens d'Exposition Environnementale par inhalation», porteur C DUCLAIROIR POC, Direction LMSM (Encadrement : Pr N ORANGE 50%- Dr C DUCLAIROIR POC 50%) concrétisée par le recrutement de T CHAUTRAND au 1^{er} septembre 2018. *Obtention.*
- Novembre 2017** Soumission d'une lettre d'intention pour une étude de faisabilité en réponse aux Appels à projets de recherche sur la santé environnement et la santé au travail intitulé « Développement d'un outil bactérien rapide et robuste d'identification des dangers liés à l'inhalation de nanomatériaux » par C DUCLAIROIR POC (budget 50k€ dont 1 an de post-doc). *Non retenu.*
- Octobre 2017** Participation à la soumission d'une ANR portée par M FEUILLOLEY intitulée «LipiDyn : Dynamique adaptative des lipides membranaires des bactéries à Gram négatif : relations environnementales et évolutives» (budget 681,42k€, durée 48 mois). *Non retenue.*
- Mars 2015** Soumission d'une demande d'allocation doctorale au concours du Groupe Régional de Recherches Haut-Normand Sécurité Sanitaire SéSa intitulée « NO₂BactAIR : Exposition au polluant automobile NO₂, adaptation d'une BACTérie Aéroportée via son homéostase membranaire et sa viRulence», porteur C DUCLAIROIR POC, Direction LMSM (Pr N ORANGE 50%- Dr C DUCLAIROIR POC 50%) concrétisé par le recrutement de S DEPAYRAS au 1^{er} octobre 2015. *Obtention.*
- Mars 2015** Soumission d'un projet au concours du Groupe Régional de Recherches Haut-Normand Sécurité Sanitaire SéSa intitulée « NitroBactAIR : Qualité de l'air : stress Nitrosant provoqué par les polluants automobiles (NOx) et adaptation d'une Bactérie Aéroportée via son homéostase membranaire et sa viRulence.», porteur C DUCLAIROIR POC (budget 31,5k€ sur 3 ans). *Obtention.*
- Janvier 2014** Soumission d'un projet en réponse aux Appels à projets de recherche sur la santé environnement et la santé au travail intitulé « Impact de NO₂ gaz sur la virulence d'une bactérie aéroportée : stratégies de dénitrification et de mobilité membranaire » par C DUCLAIROIR POC (budget 50k€ dont 1 an de post-doc). *Non retenu.*

Mars 2012 Soumission d'une **demande d'allocation doctorale au concours de Groupe Régional de Recherches Haut-Normand Sécurité Sanitaire et Environnement SSE** intitulée « Impact de marqueurs de pollution que sont NO et NO₂ sur la physiologie et la virulence de Pseudomonas », porteur C DUCLAIROIR POC, Co-direction LMSM (Pr N Orange)/ CERTAM (Dr F Dionnet), concrétisé par le recrutement de T Kondakova au 1^{er} octobre 2012. *Obtention.*

Janvier 2012 Soumission d'une **ANR Jeunes Chercheuses et Jeunes Chercheurs par C DUCLAIROIR POC** intitulée «Impact du stress nitrosant sur l'expression de la virulence d'une bactérie aérienne via la régulation lipidique et des systèmes de sécrétion» (**budget 241k€**) labellisée par le pôle de compétitivité MOV'EO. *Non retenue.*

Nov. 2011 Soumission d'une lettre d'intention pour un projet en réponse aux Appels à projets de recherche sur la santé environnement et la santé au travail intitulé « Impact des NOx sur la virulence d'aérosols bactériens» par N ORANGE, C DUCLAIROIR POC, A GROBOILLOT (budget 200k€ dont 7 mois de post-doc). *Non retenue.*

• *Participation à des axes transversaux de recherche du LMSM EA 4312*
2013-2017 **Contribution aux travaux de thèse de Laura ROWENCZYK** intitulés « Vieillissement de nanoparticules de TiO₂ en lotion solaire : évolution de leur impact sur des germes représentatifs du microbiote cutané » codirigée par l'URCOM (Pr M GRISSEL), Université du Havre Normandie et par le LMSM (Pr M FEUILLOLEY)-Université de Rouen Normandie, soutenue le 7 décembre 2016 au Havre.

Depuis 2015 **Contribution aux travaux de thèse de Davina DESPLAN** codirigée par l'UMR 8029 SATIE (Pr P GRIESMAR), Université de Cergy-Pontoise et par le LMSM (Pr N ORANGE)-Université de Rouen Normandie <soutenance prévue décembre 2017>

Mais aussi des **participations ponctuelles aux travaux des diverses thèses suivantes**

Nom	Prénom	Directeur(s) de thèse	Date de début de thèse	Date de soutenance (pour les diplômés)
HILLION	Mélanie	FEUILLOLEY M.	nov.-09	11/01/13
DAGORN	Audrey	FEUILLOLEY M.	oct.-09	01/02/13
MIJOUN	Lily	FEUILLOLEY M.	nov.-09	18/12/13
DECOPIN	Victorien	ORANGE N., MERIEAU A.	oct.-11	01/11/14
ROSAY	Thibaut	LESOUHAITIER O.	oct.-12	14/12/15
N'DIAYE	Awa	FEUILLOLEY M.	oct.-13	oct-2016
GALLIQUE	Mathias	MERIEAU A.	oct.-14	déc-2017
GANNESSEN	Andrei	PLAKUNOV V FEUILLOLEY M.	oct.-15	en cours
BORREL	Valérie	FEUILLOLEY M. KONTO Y.	janv.-16	en cours
LE TOQUIN	Esther	ORANGE N., CEA Marcoul	oct.-15	en cours
CLABAUT	Maximilien	FEUILLOLEY M. CHEVALIER S.	déc.-17	en cours

□ ENCADREMENTS

☞ Encadrement de **11 étudiants au cours d'un stage de niveau 1^{er} cycle universitaire** de l'Université de Rouen Normandie.

☞ Encadrement de **6 étudiants au cours d'un stage de Master 1** de l'Université de Rouen Normandie, de Lille

☞ Encadrement de **12 étudiants au cours d'un stage de Master 1 d'immersion en laboratoire** de l'Université de Rouen Normandie

☞ Encadrement d'**1 élève-ingénieur au cours d'un stage d'immersion de 6 mois en laboratoire** de l'ESITech, Rouen

☞ Encadrement de **6 étudiants au cours d'un stage de Master 2** de l'Université de Rouen Normandie.

☞ Co-encadrement de **3 doctorantes en Microbiologie** de l'Université de Rouen Normandie

☞ Co-encadrement de **3 chercheurs post-doctorants**.

La liste exhaustive des encadrements est dressée en annexe 1.

□ RAYONNEMENT ET VULGARISATION

La diffusion de mes travaux de recherche peut s'adresser à mes pairs, comme être vulgarisée afin d'informer, voire de faire découvrir la science.

➤ Membre de sociétés savantes

✓ American Society for Microbiology <2014-2017>

✓ Groupements De Recherche CNRS

• Combavir <2012-2013>

• Cosmactifs GDR 3711 <depuis sa création en septembre 2015>

Membre du bureau <depuis mars 2018>, participation à l'écriture du dossier renouvellement <été 2018>

✓ Réseau d'Intérêts Normand (RIN)

• RIN Normandie Biomédicale et Chimie CBS

○ **principalement axe Sécurité sanitaire, bien-être et aliments durables (SESAL) <2017-à ce jour> préalablement SéSa (Sécurité Sanitaire), puis SSE (Sécurité sanitaire et Environnement)<2010-2017>**

○ IRIB HN (Institut de Recherche et d'Innovation Biomédicale de Haute Normandie) <2014- à ce jour>

• TERA (Territoire, Environnement, Risques, Agronomie) - SCALE (Sciences appliquées à environnement) <2010-2014>

• EEM (Energie, Electronique, Matériaux) - Energie : Performances environnementales et effets sur l'environnement <2012-2015>

➤ Actrice de collaborations scientifiques

Collaborateur(s)	Institution	Pays	Date	thème de recherche
Dr H HEIPIEPER	Helmoltz Institute, DBE, Leipzig	Allemagne	2013 - à ce jour	Stress chimique (lipidomique)
Dr M NUSSER, Dr G BRENNER-WEISS	Karlsruhe Institute of Technology, IFG	Allemagne	2015	Stress chimique (biofilm)
Pr A CORCELLI	Università degli Studi di Bari, DSMBNOS	Italie	2015 - à ce jour	Stress chimique (lipidomique)
Dr T KONDAKOVA	University of Illinois, Department of Microbiology	USA	2015 - à ce jour	Stress chimique
Dr M MORENO	Luxembourg Institute of Science and Technology, Département Recherche et Technologie en matériaux	Luxembourg	2018	Stress physique (nanomatériaux)
Dr J VERDON	Université de Poitiers, LEBI UMR CNRS 7267	France	2011- à ce jour	Evaluation de la virulence
Dr A BENAMAR	Université du Havre, LOMC UMR 6294	France	2010-2014	Biosurfactants
Pr M GRISEL, Dr C PICARD, Dr N HUCHET	Université du Havre, URCOM EA 3221	France	2013- à ce jour	Stress physique (matrice cosmétique)
Dr F DIONNET, Dr D PRETERRE, Dr F GOURIOU	CERTAM	France	2009- à ce jour	Evaluation de la virulence, Stress chimique, Stress physique
Pr J-P MORIN	Université de Rouen, INSERM UMR U1096	France	2009-2015	Evaluation de la virulence, Stress
Dr F KOLTALO	Université de Rouen, COBRA UMR 6014	France	2010-2014	Biosurfactants
Dr J VIEILLARD	Université de Rouen, COBRA UMR 6014	France	2014	connexe: physico-chimie des surfaces
Dr N MACHOUR-MERLET	Université de Rouen, COBRA UMR 6014	France	2013- à ce jour	Stress chimique (lipidomique)
Dr J HARDOUIN	Université de Rouen, PBS UMR 6270	France	2014- à ce jour	Stress chimique (protéomique)

➤ **Organisation de colloques scientifiques**

- ✓ Participation à l'organisation du *3rd day of Institute for Research and Innovation in Biomedecine*, Caugé, Normandie, 20 juin 2014
- ✓ Coorganisatrice du *colloque Intelligence Economique* de la PFT Normandie Sanitaire "*Lutte contre la contrefaçon et Sécurisation des savoirs des bioindustries*", Evreux, 18 novembre 2014.
- ✓ Organisatrice du *symposium recherche "Membranes cellulaires"*, Evreux, 19 novembre 2015
 - "Multiples roles of cardiolipin in biomembranes"

Pr Angela Corcelli, *Coordinatore Centro Interdipartimentale di Ricerca sulla Pace, Dipartimento Scienze Mediche di Base Neuroscienze e Organi di Senso, Università degli Studi di Bari, Bari Italy*

- "Ice nucleation activity in fungi"

Dr Janine Frölich, *Max Planck Institute for Chemistry, research group leader in Multiphase Chemistry Department, Mainz, Germany*

- "Microbial Adaptation to Toxic Organic Solvents and other Forms of Stress - Mechanisms and Applications"

Dr Hermann Heipieper, *Head of the group Microbial Processes, Department Environmental Biotechnology*

Helmholtz Centre for Environmental Research - UFZ, Leipzig, Germany

- ✓ Coorganisatrice du *3^{ème} Colloque du GDR Cosm'actifs* (GDR 3711) "*Hot spots de la Cosmétomique*", Rennes, 27-28 novembre 2018.

□ **PRODUCTION SCIENTIFIQUE**

- ☞ **30 Publications dans des revues internationales ou nationales avec comité de lecture** répertoriées par l'AERES ou dans les bases de données internationales (ISI Web of Knowledge, Pub Med...),
 - ☞ **4 chapitres de livre,**
 - ☞ **2 articles de diffusion de connaissance,**
 - ☞ **33 communications orales avec actes dans un congrès international ou national, dont 2 plénières internationales.**
- ☞ **44 communications par affiche** avec actes dans des congrès internationaux ou nationaux.

Cette production scientifique est compilée en annexe 2.

FONCTIONS EN VALORISATION & TRANSFERT DE TECHNOLOGIE

- 2002-2010** Consultante au sein du **CRITT ADIPpharm**, Anticiper et Développer l'Innovation de votre Projet pharmaceutique, Evreux pour les projets galéniques et aspects qualité.
- 2003- 2010** Secrétaire du bureau du **CRITT ADIPpharm**, Evreux.
- 2004- à ce jour** Experte pour la Plate-Forme Technologique "Normandie Sécurité Sanitaire", pour la Plate-Forme Mutualisée d'Innovation Cosmetomics@Normandie et la Société Biogalenys (Evreux, 27)

□ **EXPERTISES**

- 2010- à ce jour** Reviewer pour des publications internationales à comité de lecture :Plant and Soil ; International Journal of Food, Research in Microbiology, FEMS Microbiology Letters ;
- 2012- à ce jour** Experte pour le **Crédit d'Impôt Recherche et Jeune Entreprise Innovante** pour le gouvernement français

□ **DIVERS**

Promotion de l'enseignement des sciences : forums régionaux, conférences en lycée

- 2017-2018** Formation CERPEP d'enseignants du secondaire sur les « Technologies émergentes sur la conservation des bioproduits : du laboratoire au monde industriel »

- 2018** Formation « Savoir manipuler les bouteilles de gaz »

2005- à ce jour Sauveteur Secouriste du travail

2005- à ce jour Habilitation à la conduite d'autoclave

Annexe 1

Encadrements réalisés par C Duclairoir Poc

Signification des abréviations:

Imm : immersion en laboratoire

L: diplôme préparé d'un niveau 1er cycle universitaire

M1: diplôme préparé Master 1

D: diplôme préparé doctorat

Ing : diplôme préparé ingénieur

M2: diplôme préparé Master 2

PD: statut post-doc

M2_1 : Sandra N'Goya, DEA Microbiologie, Rouen (Septembre 2002- Septembre 2003)

Co-encadrement par N Orange & C Poc

Pseudomonas fluorescens : Etude de leur potentialité à produire des biosurfactants et impact sur leur comportement bioadhésif

M1_1 : Mathieu SABATTIER, MasterI Ingénierie de la santé, Evreux (Avril-juin 2002)

Mise en place du SMQ de la HTPI Evreux

L1: Bruno JEHL, DUT Génie Biologique option IAB, Evreux (Avril-juin 2002)

Recherche de facteurs influençant la production de biosurfactant sur la souche hospitalière de *Pseudomonas fluorescens*

D1: Sandra N'GOYA, Thèse en Microbiologie, Université de Rouen (Septembre 2003-2007)

Co-encadrement par N Orange, MN Bellon-Fontaine, T Meylheuc & C Poc

Etude de la production de biosurfactants par les *Pseudomonas fluorescens*, de sa conséquence sur la surface bactérienne et sur son potentiel adhésif (soutenue le 24 septembre 2007)

M1_2: Marie-Hélène AUDEON, MasterI Ingénierie de la santé, Evreux (Mai-juin 2006)

Caractérisation de quelques bactéries par la mise en évidence de leur production de biosurfactant de nature ionique déterminée et par caractérisation physico-chimique de leur membrane externe

L2 : Marion COUVE, L3 Ingénierie de la Santé, Evreux (Mai-Juillet 2008)•

Co-dirigé par A Groboillot & C Poc

Influence des HAP sur la physiologie de *Pseudomonas fluorescens* DSS73 et de son mutant

M1_3 : Etienne LENOBLE, MasterI Ingénierie de la Santé, Evreux (Mai-Juin 2008)

Co-dirigé par A Groboillot & C Poc

Mise en place d'une base de données concernant les bactéries de l'air dans le cadre du projet PUC2MP

L3 : Sahed SELIM, L3 Ingénierie de la Santé, Evreux (Mai-Juillet 2009)

dirigé par F Koltalo et appui technique sur l'aspect biosurfactant C Poc

Analyse de polluants de type hydrocarbure aromatique polycyclique à l'interface eau/sédiment.
Désorption par agents tensio-actifs

L4 : Jessica BLONDEL, L3 Ingénierie de la Santé, Evreux (Mai-Juillet 2009)

Etude de la production de biosurfactants et du comportement adhésif de deux souches *Pseudomonas fluorescens* de niches écologiques différentes

L5 : Philadelphia GRESSENT, L3 Ingénierie de la Santé, Evreux (Mai-Juillet 2009)

Etude du comportement adhésif de deux souches nosocomiales de *Pseudomonas fluorescens* productrice et non-productrice de biosurfactant.

PDI : Maddalena MORETTI, Post-doc (Mars-octobre 2009)

Co-dirigé par A Groboillot & C Poc

Identification fongique des campagnes de prélèvement du projet PUC2MP

L6 : Priscilla Morice, BTS Bioanalyse et contrôles, Evreux (Novembre-décembre 2009)

Co-dirigé par M Moretti & C Poc

Identification bactérienne et fongique des campagnes de prélèvement du projet PUC2MP

M2_2 : Seyed Mohsen HOSSEINI, M2R Microbiologie, Rouen (Janvier- mars 2010)

Co-encadrement A Merieau & C Poc

Etude de la régulation et de la production de CLP «viscosinamide-like» par deux souches de *Pseudomonas fluorescens* hospitalières: MFN1032 et MFY162

L7 : Célia Augé, L3 Ingénierie de la Santé, Evreux (Mai-juillet 2010)

Co- encadrement par A Groboillot & C Poc

Influence des hydrocarbures aromatiques aromatiques polycycliques (HAP) sur la physiologie d'une souche productrice de biosurfactant dans le cadre d'un projet de restauration de sédiments pollués par des HAP.

PD2: Julien VERDON, Post-doc (Octobre 2010-Août 2011)

Co-dirigé par A Groboillot & C Poc

Financement FEDER Virulence

NOx influence on outdoor bacterial air quality

M1_4: Hervé TOUCOUROU, Master1 Ingénierie de la santé, Evreux (Mai-Juillet 2012•)

Caractérisation de biosurfactants produits par des souches de *Pseudomonas* collectées dans l'air

M1_5: Lylia DRICI, Master 1 Pro Protéomique, Lille (Mars-Juillet 2012)

Co-dirigé par J Verdon & C Poc

Mise en place de l'analyse des protéines bactériennes à l'aide d'un spectromètre de masse MALDI TOF/TOF.

L8 & L9: Rachel DUCHESNE & Mélanie LE GOFF, stages volontaires L3 Biologie, Rouen (Mai-Juin 2012)

Co-dirigées par J Verdon & C Poc

M2_3: Hervé TOUCOUROU, Master 2 Pro Ingénierie de la santé, Evreux (Février-Juillet 2012)

Impact de l'exposition de souches de *Pseudomonas* à des polluants atmosphériques: Etude physiologique et mise au point d'un test cytotoxique vis-à-vis de *Dictyostelium discoideum*

PD3: Maryse BONNIN JUSSERAND, Post-doc (Janvier-Août 2012)

Co-dirigé par A Groboillot & C Poc

Financement FEDER Virulence

NOx influence on outdoor bacterial air quality

D2: Tatiana KONDAKOVA, Thèse en Microbiologie, Université de Rouen Normandie (Octobre 2012- Septembre 2015)

Co-direction par N Orange & F Dionnet

Encadrement scientifique : C Poc

Financement GRR SSE

Impact de marqueurs de pollution que sont NO et NO₂ sur la physiologie et la virulence de *Pseudomonas*.

M1 Imm_1-> M1 Imm_4 : A HAMON, F OUSALEM, W ODJO et S COCHENNEC, Stage M1 immersion en laboratoire, Rouen (printemps 2013)

Characterization of surface properties of *Pseudomonas fluorescens* MFAF76a strain and its GFP transformed

M1_6: Ishac Si Hadj Mohand, Master 1 Microbiologie, Rouen (Mai-Juin 2013)

Caractérisation des propriétés de surface de deux souches *Pseudomonas fluorescens*: l'aéroportée MFAF76a et l'hospitalière MFN1032 et de leurs transformées chromophores.

M1 Imm_5-> M1 Imm_8 : T CLAMENS, A DUPUIS, S HAULARD et R VERGER, Stage M1 immersion en laboratoire, Rouen (printemps 2014)

Elaboration d'un protocole de séparation de protéines à pH basique

M2_4 : Andry TSIFERANA, Master 2 Master Pro Biosciences, Ingénierie Qualité Bioproduits, Rouen (Février-Juillet 2014)

Impacts de l'exposition de *Pseudomonas* aéroportées aux NOx sur leur profil protéomique et leur virulence

M2_5 : Chloé CATOVIC, Master 2 Recherche Microbiologie, Rouen (Janvier-Juin 2015)

Co-encadrement par T Kondakova & C Poc

Etude de la réponse bactérienne moléculaire et physiologique de *Pseudomonas fluorescens* suite à son exposition au NO₂, polluant atmosphérique

D_3 : Sérgolène DEPAYRAS, Thèse GRR SeSa, Université de Rouen Normandie (Octobre 2015-soutenance prévue décembre 2018)

Co-encadrement 50% CDP avec direction du Pr N Orange

NitroBactAIR : Qualité de l'air : stress Nitrosant provoqué par les polluants automobiles (NOx) et adaptation d'une Bactérie Aéroportée via son homéostase membranaire et sa virulence

M1 Imm_9-> M1 Imm_10 : P HOULEMARE et E LIEVIN, stage M1 immersion en laboratoire, Rouen (printemps 2016)

Co-encadrement: Cécile Duclairoir-Poc & Sérgolène Depayras

Evaluation par cytométrie en flux de l'influence des NOx sur *Pseudomonas fluorescens*

M2_6 : Marine RINGUEDÉ, Master 2 Microbiologie, Rouen (Janvier-Juillet 2017)

Evaluation de l'innocuité en utilisation d'une formule solaire contenant comme filtre UV des nanoparticules de TiO₂ et contaminée par une souche de *Pseudomonas fluorescens* aéroportée.

L10: Sarah MAERTEN, BTS 2A, Lycée Léopold Sedar Senghor, Evreux (Mai-Juillet 2017)

Co-encadrement: Cécile Duclairoir-Poc & Sérgolène Depayras

Etude d'un système de communication chez *P. fluorescens* : Le Quorum Sensing

Ing1_1 : Candice AUGER, stage d'immersion en laboratoire s'étalant sur 6 mois (de plus de 600h), ESITech 1^{ère} année d'ingénieurs, Rouen (Février-Juillet 2018)

Co-encadrement: Cécile Duclairoir-Poc & Sérgolène Depayras

Dans le cadre de l'étude de l'impact de marqueurs de pollution automobile (oxydes d'azote) sur la physiologie et la virulence de souches de *Pseudomonas* : Réponse membranaire de mutants d'une *Pseudomonas fluorescens* aéroportée suite à l'exposition à deux polluants automobiles NOx en synergie.

M1 Imm_11-> M1 Imm_12 : J MARTEL et F FECAMP, stage M1 immersion en laboratoire, Rouen (Printemps 2018)

Mise au point de protocole de lipidomique HPTLC MALDI sur extraits bactériens

L11 : Mathieu CLAIRET, BTS 2A, Lycée Léopold Sedar Senghor, Evreux (Mai-Juillet 2018)

Évaluation de l'activité antibactérienne de nanomatériaux à base d'argent

Annexe 2

Publications et communications de C Duclairoir Poc

➤ 30 publications dans des revues internationales ou nationales avec comité de lecture répertoriées par l'AERES ou dans les bases de données internationales (ISI Web of Knowledge, Pub Med...).

P1- Formation of Gliadin Nanoparticles: Influence of the Solubility Parameter of the Gliadin Solvent

C Duclairoir, E Nakache, H Marchais, A-M Orecchioni, Colloid and Interface Science. (1998) **276** : 321-327.

P2- Gliadin Nanoparticles : Formation ; All-trans Retinoic Acid Entrapment and Release, Size Optimization

C Duclairoir, JM Irache, E Nakache, A-M Orecchioni, C Chabenat, Y Popineau, Polymer International., (1999) **79** :327-333.

P3- Maîtrise de la taille de nanoparticules de gliadines de blé par la détermination de leur paramètre de solubilité

A-M Orecchioni, C Duclairoir, E Nakache, Annales Pharmaceutiques Françaises. (2001) **59** : 402-406.

P4- α -tocopherol encapsulation and *in vitro* release from wheat gliadin nanoparticles

C Duclairoir, A-M Orecchioni, P Depraetere, E Nakache, Journal of Microencapsulation. (2002), **19** : 53-60.

P5- Polymer Nanoparticles Characterization in Aqueous Suspension

C Duclairoir, E Nakache, International Journal of Polymer Analysis and Characterization. (2002) **7** : 284-313.

P6- Biopolymeric colloidal carriers for encapsulation or controlled release

D. Renard, P. Robert, L. Lavenant, D. Melcion, Y. Popineau, J. Guéguen, C. Duclairoir, E. Nakache, C. Sanchez and C. Schmitt, International Journal of Pharmaceutics. (2002) 242(1-2) : 163-166.

P7- Evaluation of Gliadins Nanoparticles as Drug Delivery Systems: a Study of Three Different Drugs

C Duclairoir, A-M Orecchioni, P Depraetere, F Osterstock, E Nakache, International Journal of Pharmaceutics. (2003) 253: 133-144.

P8- Gliadin characterization by SANS and gliadin nanoparticle growth modelization.

A-M Orecchioni, C Duclairoir, Denid Renard and E Nakache., Journal of nanoscience and nanotechnology. (2006) **6** :3171-3178.

P9- Phenotypic variation in the *Pseudomonas fluorescens* clinical strain MFN1032

G Rossignol, D Sperandio , J Guerillon, C Duclairoir Poc, E Soum-Soutera, N Orange, MGJ Feuilloley, A Merieau. Res Microbiol. (2009) 160(5):337-44

P10- Pollution des sédiments de dragage : Procédés de bioremédiation alliés à l'électromigration.

F Portet-Koltalo, M Ammami, A Benamar, A Groboillot, N Orange. C Duclairoir Poc Spectra Analyse. (2010) 277 : 54-58.

P11- Déséquéstration de polluants de type hydrocarbures aromatiques polycycliques à l'interface de sédiments au moyen de tensioactifs d'origine biologique. "

F Portet-Koltalo, M Ammami, A Benamar, A Groboillot, N Orange. C Duclairoir Poc Spectra Analyse. (2011) 278 : 21-27.

P12- Novel Application of Cyclolipopeptide Amphisin: Faisability Study as Additive to Remediate PAHs Contaminated Sediments.

A Groboillot, F Koltalo, F Lederf, M Feuilloley, N Orange, C Duclairoir Poc, Int. J. Mol. Sci. (2011) 12 : 1787-1806

P13- *Caenorhabditis elegans* as a model to monitor air bacterial quality"
C Duclairoir Poc, A Groboillot, O Lesouhaitier, M Feuilloley, J-P Morin, N Orange, BMC Res. Notes. (2011) 4:503.

P14- The Major Outer Membrane Protein Oprf is Required for Rhamnolipid Production in *Pseudomonas aeruginosa*

E Bouffartigues, G Gicquel, A Bazire, L Fito-Boncompte, L Taupin, O Maillot, A Groboillot, C Poc-Duclairoir, N Orange, M Feuilloley, A Dufour, S Chevalier. J. Bacteriol. Parasitol. (2011) 2 : 118; DOI : 10.4172/2155-9597.1000118

P15- Influence of growth temperature on cyclolipopeptides production and on adhesion behaviour in environmental strains of *Pseudomonas fluorescens*.

C Duclairoir Poc, T Meylheuc, S Ngoya, A Groboillot, J Bodilis, L Taupin, A Merieau, M Feuilloley, N Orange. J. Bacteriol. Parasitol. (2011) S1-002. <http://dx.doi.org/10.4172/2155-9597.S1-002>.

P16- Gamma-aminobutyric acid acts as a specific virulence regulator in *Pseudomonas aeruginosa*

A Dagorn, M Hillion, A Chapalain, O Lesouhaitier, C Duclairoir Poc, J Vieillard, S Chevalier, L Taupin, F Le Derf, MGJ Feuilloley, Microbiology. (2013) 159:339-351

P17- Investigation of the release of PAHs from artificially contaminated sediments using cyclolipopeptidic biosurfactants

F Portet-Koltalo, MT Ammami, A Benamar, H Wang, F Le Derf, C Duclairoir-Poc, Journal of Hazardous Materials. (2013) 261:593– 601.

P18- Effect of GABA, a bacterial metabolite, on *Pseudomonas fluorescens* surface properties and cytotoxicity

A Dagorn, A Chapalain, L Mijouin, M Hillion, C Duclairoir-Poc, S Chevalier, L Taupin, N Orange, MGJ Feuilloley, Int. J. Mol. Sci. (2013) 14 : 12186-12204; DOI : 10.3390/ijms140612186.

P19- Effects of a Skin Neuropeptide (Substance P) on Cutaneous Microflora

L Mijouin, M Hillion, Y Ramdani, T Jaouen, C Duclairoir-Poc, ML Gueye, E Lati, F Yvergnaux, A Driouich, L Lefevre, L Misery, MGJ Feuilloley, PLoS ONE. (2013) 8(11): e78773 ; DOI : 10.1371/journal.pone.0078773:..

P20- Airborne fluorescent pseudomonads : what potential for virulence ?

C Duclairoir Poc, J Verdon, A Groboillot, M Barreau, H Toucourou, L Mijouin, C Leclerc, C Hulen, T Kondakova JP Morin, MGJ Feuilloley, A Merieau, N Orange, International Journal of Current microbiology and applied sciences.(2014) 3(8) : 708-722.

P21- A new tool for studying bacterial lipidome: HPTLC-MALDI-TOF Imaging enlightening virulence traits of the airborne *Pseudomonas fluorescens* MFAF76a

T Kondakova, N Merlet-Machour, M Chapelle, D Preterre, F Dionet, MJ Feuilloley, N Orange, C Duclairoir Poc, Research in Microbiology. (2015) 166 : 1-8; DOI : 10.1016/j.resmic.2014.11.003

P22- Application of biosurfactants and periodic voltage gradient for enhanced electrokinetic remediation of metals and PAHs in dredged marine sediments

M T Ammami, F Portet-Koltalo, A Benamar, C Duclairoir Poc, H Wang, F Le Derf, Chemosphere. (2015) 125 : 1–8.

P23- Surface functionalization of cyclic olefin copolymer witharyldiazonium salts: A covalent grafting method

F Brisset, J Vieillard, B Berton, S Morin-Grognet,C Duclairoir-Poc, F Le Derf, Applied Surface Science. (2015) 329 : 337–346.

P24- Glycerophospholipid synthesis and functions in *Pseudomonas*: eukaryotic lipid exploitation

T Kondakova; F D'Heygère ; M J. Feuilloley; N Orange; H J Heipieper; C Duclairoir Poc, Chemistry and Physics of Lipids. (2015) 190:27-42; DOI : 10.1016/j.chemphyslip.2015.06.006.

P25- A *Pseudomonas fluorescens* type 6 secretion system is related to mucoidy, motility and bacterial competition

V Decoin, M Gallique, C Barbey, F Le Mauff, C Duclairoir Poc, MGJ Feuilloley, N Orange, A Merieau, BMC Microbiology. (2015) 15(1); DOI: 10.1186/s12866-015-0405-9.

P26- Response to Gaseous NO₂ Air Pollutant of *P. fluorescens* Airborne Strain MFAF76a and Clinical Strain MFN1032

T Kondakova, C Catovic, M Barreau, M Nusser, G Brenner-Weiss, M Feuilloley, F Dionnet, N Orange, C Duclairoir Poc, Front Microbiol. (2016) 7:379; DOI : 10.3389/fmicb.2016.00379.

P27- Development of preservative-free nanoparticles-based emulsions: Effects of NP surface properties and sterilization process.

L Rowenczyk, C Picard, C Duclairoir Poc, N Hucher, N Orange, M Feuilloley, M Grisel. Int J Pharm. (2016) 510(1) : 125-34; DOI : 10.1016/j.ijpharm.2016.06.014.

P28- Skin-bacteria communication: Involvement of the neurohormone Calcitonin Gene Related Peptide (CGRP) in the regulation of *Staphylococcus epidermidis* virulence.

A N'Diaye, C Leclerc, T Kentache, J Hardouin, C Duclairoir Poc, Y Konto-Ghiorghi, S Chevalier, O Lesouhaitier, MG Feuilloley. Sci Rep. (2016) 6: 35379; DOI : 10.1038/srep35379.

P29- Impact of coated TiO₂-nanoparticles used in sunscreens on two representative strains of the human microbiota: Effect of the particle surface nature and aging

L Rowenczyk, C Duclairoir Poc, M Barreau, C Picard, N Hucher, N Orange, M Grisel, M Feuilloley. Colloids and Surfaces B: Biointerfaces. (2017)[158](#) : 339-348; DOI : 10.1016/j.colsurfb.2017.07.013.

P30- Impact of gaseous NO₂ on *P. fluorescens* strain in the membrane adaptation and virulence.

S Depayras, T Kondakova, N Merlet-Machour, H J Heipieper, M Barreau, C Catovic, M Feuilloley, N Orange, C Duclairoir Poc, *Int. J. Environ. Impacts.* (2018), 1(3) : 1–10.

➤ *Chapitres de livre: 4*

Ch1- Creation of biopolymeric colloidal carriers dedicated to controlled release applications

D Renard, P Robert, L Lavenant, D Melcion, Y Popineau, J Gueguen, C Duclairoir, E Nakache, C Sanchez and C Schmitt

In Plant biopolymer science: food and non-food applications p.119-124, Denis Renard, Guy Della Valle, Yves Popineau, eds, Royal Society of Chemistry (Great Britain 2002)

Ch2- Plant protein-based nanoparticles

A-M Orecchioni, C Duclairoir, J Manuel Irache and E Nakache,
in "Nanotechnologies for the life sciences" vol.2, Biological and pharmaceutical nanomaterials, p.117-144, Challa S. S. R. Kumar Ed., Wiley-VCH Verlag GmbH&Co. KGaA, Weinheim (2006)

Ch3- HPTLC-MALDI TOF MS Imaging analysis of phospholipids

T Kondakova, N Merlet Machour, C Duclairoir Poc
In Neuromethods: Lipidomics, vol. 125 Chapter 12; Paul L. Wood (ed.); Series Editor: Wolfgang Walz, eds, Springer (Germany 2017), DOI 10.1007/978-1-4939-6946-3_12.

Ch4- The hidden face of Nitrogen oxides species – from toxicity effect to potential cure?

S Depayras, T Kondakova, H J. Heipieper, M Feuilloley, N Orange and C Duclairoir Poc
In Emerging Pollutants - Some Strategies for the Quality Preservation of Our Environment", p.19-44, edited by Sonia Soloneski and Marcelo L. Laramendy, Ed. IntechOpen, London (United Kingdom, 2018); <http://dx.doi.org/10.5772/intechopen.75822>

➤ *Publications de revue ou de diffusion de connaissance : 2*

Pdc1- Encapsulation et applications industrielles

C Duclairoir, L'Actualité Chimique. (2000) 6 : 24-27.

Pdc2- Particules Urbaines et Céréalières, Microorganismes Mycotoxines et Pesticides

JP Morin, D Preterre, F Gouriou, V Delmas, A François, N Orange, A Groboillot, C Duclairoir-Poc, M Moretti, O Maillot, O Lesouhaitier, Pollution atmosphérique. (2013)217; URL : <http://lodel.irevues.inist.fr/pollution-atmospherique/index.php?id=759>.

➤ **Publications de compte-rendu de congrés : 77**

✓ **Conférence plénière internationale : 2**

CInt1- "Polymer Nanoparticles Characterization in Aqueous Suspension"

C Duclairoir, E Nakache, International Symposium of Polymer Analysis and Characterization, 26-30 juin 1999, la Rochelle-France.

CInt2- Response of commensal Staphylococci to sub-lethal concentrations of skin antimicrobial peptides

Cécile Duclairoir-Poc, FEMS, Leipzig, Germany, July 21-25th 2013.

✓ **Communications orales : 31**

C1- Nanoparticules de gliadines obtenues par coacervation

C Duclairoir, E Nakache, H Marchais, A-M Orecchioni, *Journée de l'Ecole Doctorale Normande de Chimie-Biologie*, 27 mars 1997, Caen.

C2- Elaboration de nanoparticules de gliadines par coacervation

C Duclairoir, E Nakache, H Marchais, A-M Orecchioni, *Rencontre de la Société Française de Chimie (section Basse-Normandie-Sarthe)*, 30 mai 1997, Caen.

C3- Nanoparticules de polymère végétal

C Duclairoir, E Nakache, A-M Orecchioni, H Marchais, *Journées GFP Ouest-SFC*, 15-17 octobre 1997, Thiais.

C4- Préparation de nanoparticules de polymère végétal. Optimisation de leur taille

C Duclairoir, E Nakache, A-M Orecchioni, H Marchais, *Congrès Annuel du GFP*, 18-20 novembre 1997, Louvain-La-Neuve, Belgique.

C5- Encapsulation de vitamines dans des nanoparticules de protéines végétales

C Duclairoir, E Nakache, A-M Orecchioni, J Irache, Y Popineau, D Renard, *Journées GFP-Ouest*, 2-3 juin 1999, Alençon.

C6- Nanoparticules de protéines végétales : caractérisation structurale et potentialités d'encapsulation

C Duclairoir, D Renard, A-M Orecchioni, Y Popineau, E Nakache, *Journées d'Etudes des Polymères*, 5-10 septembre 1999, Trégastel.

C7- Impact de la production de biosurfactants sur la réactivité de souches de *Pseudomonas fluorescens* vis-à-vis d'un micro-environnement solide.

S Ngoya, C Duclairoir, N Orange. *9^{ème} journée de l'Ecole doctorale Normande chimie-biologie*, 17 mars 2006, Rouen.

C8- Caractérisation des biosurfactants chez plusieurs souches de *Pseudomonas fluorescens* provenant d'environnements différents,

S Ngoya, C Duclairoir, N Orange. *BIOADH' 2007*, 09 mars 2007, Strasbourg.

C9- Analyse de la biodiversité de la flore bactérienne et fongique d'environnements aériens en zones urbaines et portuaire

M Moretti, A Groboillot, C Duclairoir-Poc, O Maillet, O Lesouhaitier, J. P Morin., M. G. J.Feuilloley, N Orange. *MicrobAERO 2009*, 6-8 octobre 2009, Narbonne.

C10- *Pseudomonas fluorescens* : Interactions potentielles de la microflore bactérienne avec la neurophysiologie humaine.

L Mijouin, M Hillion, A Dagorn, A-S Blier, A Madi, T Jaouen, W Veron, N Connil, C Poc, A Groboillot, O Lesouhaitier, N Orange, S Chevalier, MGJ Feuilloley. *17^{ème} Journée Scientifique de l'IFRMP23*, Mont-Saint-Aignan, 17 juin 2011.

C11- Extracellular gamma aminobutyric acid (GABA) regulates *Pseudomonas* virulence.

A Dagorn, A Chapalain, O Lesouhaitier, C Poc, J Vieillard, S Chevalier, L Taupin, F Le Derf, N Orange, MGJ Feuilloley. *Journée de l'EdNBISE*, Rouen, 23 mars 2012.

C12- NitroBactAIR : Impact du stress nitrosant sur l'expression de la virulence d'une bactérie aéroportée

C Duclairoir Poc, *Plénière MOVE'O*, 7 novembre 2012, Rouen.

C13- Impact du stress nitrosant sur l'expression de la virulence d'une bactérie aéroportée

C Duclairoir Poc, déjeuner-débat des professionnels de l'Automobile intitulé "L'automobile et l'Environnement sous la loupe des Scientifiques" Automobile Club de France, mardi 12 février 2013; Paris.

C14- Response of commensal *Staphylococci* to sub-lethal concentrations of skin antimicrobial peptides.

M Hillion, L Mijouin , C Leneveu, E Gerault , T Jaouen , L Lefevre , N Orange, G Redziniak , C Duclairoir-Poc, MJG Feuilloley. *5th FEMS Congress of European Microbiologists*. July 21-25th 2013, Leipzig, Germany.

C15- Etude de la virulence de *Pseudomonas* aéroportées à l'aide d'un nouvel outil lipidomique

T Kondakova , N Merlet-Machour, D Preterre, F Dionnet, N Orange, C Duclairoir Poc, *Journées Interdisciplinaires Qualité Air-8^{ème} édition*, 10-11 février 2014, Villeneuve d'Ascq.

C16- Study of *Pseudomonas* airborne virulence using a new lipidomic tools

T Kondakova, N Merlet-Machour, D Preterre, F Dionnet, N Orange, C Duclairoir-Poc. *17^{ème} Journée de l'EdNBISE*, 10 avril 2014, Le Havre.

C17- Bacterial phospholipid adaptation to human temperature.

T Kondakova, N Merlet-Machour, J Bodilis, F Dionnet,M Feuilloley, O Orange, HJ Heipieper, C Duclairoir Poc. *13th Euro Fed Lipid Congress*, 27-30 September 2015, Florence, Italy.

C18- Aging of coated TiO₂ nanoparticles in oil-in-water emulsion : bactericidal toxicity

L Rowenczyk, C Picard, C Duclairoir-Poc, N Hucher, N Orange, M Feuilloley and M Grisel, *Journées Nord-Ouest Européennes des Jeunes Chercheurs*, 11-12 Mai 2015, Rouen.

C19- Evaluation du potentiel applicatif en cosmétique de biosurfactants microbiens secrétés par des souches de *Pseudomonas* fluorescent aéroportées

S Depayras, C Duclairoir-Poc, *1^{er} colloque du GDR Cosm'actifs*, Moulin d'Andé, 26-27 Septembre 2018, Andé, France.

C20- Aging of TiO₂-nanoparticle surface in cosmetic emulsions: their impact on bacteria of the cutaneous microbiota

L Rowenczyk , C Picard, C Duclairoir-Poc, N Hucher, N Orange, M Feuilloley and M Grisel, *1^{er} colloque du GDR Cosm'actifs*, Moulin d'Andé, 26-27 Septembre 2018, Andé, France.

C21- Impact of gaseous NO₂ on *P. fluorescens* strain in the membrane adaptation and virulence

S Depayras, T Kondakova, N Merlet-Machour, HJ Heipieper, M Barreau, C Catovic, M Feuilloley, N Orange, C Duclairoir-Poc, *WIT Air Pollution* , 25 -27 April 2017, Cadiz, Spain.

C22- Développement de formulations sans conservateurs pour des modèles de crèmes solaires contenant des dispersions TiO₂ nanoparticulaires. Effet des processus de stérilisation sur la stabilité.

L Rowenczyk, C Picard, C Duclairoir-Poc, N Hucher, N Orange, M Feuilloley, M Grisel. *2^{ème} colloque du GDR Cosm'actifs*, 25 & 26 Septembre 2017, Domaine de Chalès, Nouan le Fuzelier, France.

C23- Impact des nanoparticules de TiO₂ passivées formulées en lotion solaire sur des bactéries cutanées ou aéroportée biocontaminante,

L Rowenczyk, M Ringuedé, M Barreau, C Picard, N Hucher, M Grisel, M Feuilloley, N Orange et C Duclairoir-Poc. *2^{ème} colloque du GDR Cosm'actifs*, 25 & 26 Septembre 2017, Domaine de Chalès, Nouan le Fuzelier, France.

C24- Impact of gaseous NO₂ on *P. fluorescens* strain in the membrane adaptation and virulence

S Depayras, T Kondakova, N Merlet-Machour, HJ Heipieper, M Barreau, C Catovic, Feuilloley M, Orange N, C Duclairoir-Poc, *Congrès de la Société Française de Microbiologie 2017*, 09-11 Octobre 2017, Paris.

C25- Interactions [nano]particules et micro-organismes cutanés

N Hucher, C Duclairoir-Poc. *Inauguration de la plate-forme d'Innovations Cosmetomics*, 3 octobre 2017, Evreux.

C26- Production de viscosinamides par la souche clinique de *Pseudomonas fluorescens* MFN1032: Implication dans le développement du biofilm.

D Depayras, A Merieau, M Barreau, T Kondakova, C Barbey, M Feuilloley, N Orange, C Duclairoir Poc. *Colloque Bioadh'2017*, Domaine de Frémigny, 15 & 16 Novembre 2017, Bouray sur Juine, France.

C27- Nitrogen dioxide: from a simple diffusible gas to a potential antibacterial against *P. fluorescens*?

S Depayras, T Kondakova, HJ Heipieper, M Feuilloley, N Orange, C Duclairoir Poc, *21^{ème} Journée de l'EdNBISE*, 22-23 mars 2018, Rouen.

C28- Microenvironment impact on *Cutibacterium acnes*: growth, virulence and biofilm formation of acneic and non-acneic strains.

V Borrel, Y Konto-Ghiorgi, L Lefevre, C Duclairoir-Poc, MGJ Feuilloley, *21^{ème} Journée de l'EdNBISE*, 22-23 mars 2018, Rouen.

C29- NO₂: simple gaz diffusible ou agent antibactérien anti- *P. fluorescens* potentiel?

S Depayras, T Kondakova, HJ Heipieper, J Hardouin, M Feuilloley, N Orange, C Duclairoir Poc, *Mini-colloque Pseudomonas*, 17-18septembre 2018, Marseille.

C30- Régulation et Rôle de CmpX chez *Pseudomonas aeruginosa*

E Bouffartigues, D Tortuel, O Maillot, A David, J Omnes, A Tahiroui, CO Azuama, L Taupin, S Depayras, C Duclairoir Poc, HJ Heipieper, A Dufour, O Lesouhaitier, N Orange, MGJ. Feuilloley, P Cornelis, S Chevalier, *Mini-colloque Pseudomonas*, 17-18septembre 2018, Marseille.

C31- Nitrogen dioxide: from a simple diffusible gas to a potential antibacterial against *P. fluorescens*?

S Depayras, T Kondakova, HJ Heipieper, M Feuilloley, N Orange, C Duclairoir Poc, *Congrès SFM 2018*, 1-3 octobre 2018, Paris.

✓ **Affiches : 44**

A1- Elaboration de nanoparticules de gliadines par coacervation

C Duclairoir, E Nakache, H Marchais, A-M Orecchioni, Rencontre de la Société Française de Chimie (section Basse-Normandie-Sarthe), 30 mai 1997, Caen-France.

A2-Elaboration de nanoparticules de gliadines de blé

C Duclairoir, E Nakache, H Marchais, A-M Orecchioni congrès international SFC97, 7-12 septembre 1997, Bordeaux-France.

A3-Influence du paramètre de solubilité sur la taille des nanoparticules de gliadines

C Duclairoir, E Nakache, H Marchais, A-M Orecchioni, 12th Annual meeting of the GTRV, décembre 1997, Bruxelles-Belgique.

A4- Wheat Gluten Nanopaticles as Drug Carriers : Encapsulation Mechanism and Size Optimization

A-M Orecchioni, J M Irache, C Duclairoir, E Nakache, Symposium on Natural Origin Substances in Drug Formulation, 4-6 novembre 1998, Beijing-Japan.

A5- Elaboration of Nanoparticles from Vegetal Polymer : Size Optimization Study

C Duclairoir, E Nakache, A-M Orecchioni, J Irache, Y Popineau, Symposium International sur les Polymères en Milieu Dispersionné, 11-16 avril 1999, Lyon-France.

A6- Nanoparticles Preparation by Vesicle Polymerization or by Controlled Coacervation

E Nakache, N Poulain, C Duclairoir, A-M Orecchioni, Gordon Research Conferences, 27 juin- 2 juillet 1999, Cambridge-USA.

A7- Solvent Effect on the Size Optimization of Submicronic Wheat Proteins Drug Carriers

A-M Orecchioni, D Renard, C Duclairoir, Y Popineau, E Nakache, 12th International Symposium on Microencapsulation, 6-8 septembre 1999, London-United Kingdom.

A8- Development of Carbohydrate Polymer-Based Submicron Colloidal System in Reverse Micelles

A-M Orecchioni, C Duclairoir, E Nakache, Lipid and Surfactant Dispersed System, 26-28 octobre 1999, Moscow, CEI.

A9- Vitamin E Encapsulation and Release from Wheat Protein Nanoparticles

A-M Orecchioni, C Duclairoir, P Depraetere, Y Popineau, E Nakache, 3rd Word Meeting on pharmaceutics, Biopharmaceutics Pharmaceutical Technology, 3-6 avril 2000, Berlin-Deutschland.

A10- Encapsulation de l'alpha-tocophérol au sein de suspensions colloïdales nanométriques de gliadines de blé

A-M Orecchioni, C Duclairoir, E Nakache, XXIV Congresso internazionale della societa farmaceutica del mediterraneo latino, 20-23 septembre 2000, Assisi-Italia.

A11- Elaboration de nanoparticules de protéines végétales et application comme système de libération contrôlée de vitamine E

C Duclairoir, D Renard, P Depraetere, Y Popineau, A-M Orecchioni, E Nakache, 19èmes Journées du club émulsion, 6-7 novembre 2000, Bordeaux-France.

A12- Biofilm, biosurfactant, temperature : dependency for 9 wild *Pseudomonas fluorescens* environmental strains and for two of their biosurfactant non-producing mutants.

C Duclairoir-Poc, T Meylheuc, S Nogoya, A Groboillot, L Taupin, A Merieau, MGJ Feuilloley, N Orange Eurobiofilms, First European Congress on Microbial Biofilms, September 2 – 5 2009, Rome, Italy.

A13- Analyse de la biodiversité de la flore bactérienne et fongique d'environnements aériens en zones urbaines et portuaire.

M Moretti, A Groboillot., C Duclairoir-Poc, O Maillot, O Lesouhaitier, JP Morin, MGJ Feuilloley, N Orange *MicrobAERO2009*, 6 – 8 octobre 2009 Narbonne.

A14- Evaluation de la qualité microbiologique de l'air de deux zones urbaines en Haute-Normandie.

C Duclairoir-Poc, A Groboillot, O Maillot, M Moretti, O Lesouhaitier, MGJ Feuilloley, JP Morin, N Orange *1^{er} Congrès Européen sur les Pathologies Environnementales*. 9-10 octobre 2009, Rouen.

A15- Influence de la température sur le comportement adhésif et sur la production de biosurfactant chez *Pseudomonas fluorescens* d'origine environnementale.

C Duclairoir-Poc, T Meylheuc, S Nogoya, A Groboillot, L Taupin, A Merieau, MGJ Feuilloley, N Orange Bioadh 2009, 17-19 Novembre 2009, Le Mans.

A16- Déséqustration de polluants de type hydrocarbures aromatiques polycycliques à l'interface eau/sédiments à l'aide de tensioactifs d'origine synthétique ou biologique.

F Portet-Koltalo, S Sahed, A Groboillot, C Duclairoir-Poc, N Orange. SEP 2009, 30 nov-3 décembre 2009, Marseille.

A17- GABA and benzodiazepine receptors ligands: Promising molecules as bacterial virulence inhibitors.

A Dagorn, A Chapalain, S Chevalier, C Poc, N Orange, V Papadopoulos, MGJ Feuilloley *3^{ème} rencontres normandes en Chimie-Biologie-Santé: La biologie, inspiratrice de nouveaux médicaments*. 10 décembre 2009, Rouen.

A18- Evaluation de la qualité bactérienne d'écosystèmes aériens en zones urbaines et portuaires grâce à deux approches : Les antibiogrammes et les tests de virulence vis-à-vis de *Caenorhabditis elegans*.

A Groboillot, C Duclairoir-Poc, O Maillot, M Moretti, O Lesouhaitier, MGJ Feuilloley, JP Morin, N Orange. *VIII^{eme} Congrès de la SFM*, 2-4 juin 2010, Marseille.

A19- Effect of a cyclolipopeptidic biosurfactant on PAHs sorption by sediments.

F Portet-Koltalo, F.; Ammami, M.T.; Benamar, A.; Duclairoir-Poc, C.; Le Derf, F. *12th European Meeting on Environmental Chemistry (EMEC 12)*, 7-10 décembre 2011, Clermont-Ferrand.

A20- *Pseudomonas fluorescens*, a member of the gut-brain-skin axis.

M Hillion, L Mijouin, A Dagorn, T Rosay, A Madi, T Jaouen, N Connil, C Poc, A Groboillot, O Lesouhaitier, N Orange, S Chevalier, MGJ Feuilloley. *1^{ère} journée scientifique de l'Institut de Recherche et d'Innovation Biomedicale (IRIB)*, 1^{er} juin 2012, Rouen.

A21- *Pseudomonas* aéroportées : Caractérisation phénotypique et évaluation de leur potentiel virulent à l'aide de différents modèles.

C Duclairoir Poc, J Verdon, A Groboillot, O Lesouhaitier, O Maillot, M Barreau, N Orange. *Congrès de la Société Française de Microbiologie 2013*, Février 2013, Lille.

A22- L'acide gamma-aminobutyrique (GABA) module la virulence et la cytotoxicité des *Pseudomonas*

A Dagorn, M Hillion, A Chapalain, O Lesouhaitier, C Duclairoir-Poc, S Chevalier, MJG Feuilloley. *Congrès de la Société Française de Microbiologie 2013*, Février 2013, Lille.

A23- La Substance P, un médiateur entre microflore et homéostasie cutanée

L Mijouin, M Hillion, T Jaouen, C Duclairoir-Poc, MJG Feuilloley, Y Ramdani. *Congrès de la Société Française de Microbiologie 2013*, Février 2013, Lille.

A24- Another paradigm in antibacterial treatments : Why a diplomatic approach should be more efficient than weapons of mass destruction ?

M Hillion, L Mijouin, A Dagorn, C Leneveu, AS Blier, A Madi, T Jaouen, T Rosay, K Biaggini, N Connil, C Poc, A Groboillot, C Hulen, N Lomri, O Lesouhaitier, N Orange, MGJ Feuilloley. *ESF-EMBO Symposium Bacterial Networks*. 16-21 March 2013, Pultusk, Poland.

A25- Regulation of *Pseudomonas* cytotoxicity and virulence by gamma aminobutyric acid (GABA), an inter-kingdom communication signal.

A Dagorn, A Chapalain, L Mijouin, M Hillion, C Duclairoir-Poc, J Vieillard, S Chevalier, L Taupin, F Le Derf, N Orange, MGJ Feuilloley. *2nd Scientific meeting of Institute for Research and Innovation in Biomedicine (IRIB)*, June 21th 2013, Rouen.

A26- Air: a potential biohazard niche for fluorescent Pseudomonads.

C Duclairoir Poc, J Verdon, A Groboillot, M Barreau, H Toucourou, L Mijouin, O Maillet, C Hulen, O Lesouhaitier, JP Morin, MGJ Feuilloley, A Merieau, N Orange. *5th FEMS Congress of European Microbiologists*, 19-23 July 2013, Leipzig, Germany.

A27- Regulation of *Pseudomonas aeruginosa* virulence by Gamma-aminobutyric Acid

A. Dagorn, M. Hillion, A. Chapalain, O. Lesouhaitier, C. Duclairoir-Poc, N. Orange, S. Chevalier, M. Feuilloley. *5th FEMS Congress of European Microbiologists*, 19-23 July 2013, Leipzig, Germany.

A28- The virulence of cutaneous bacteria can be locally regulated by Substance P, a skin neuropeptide.

L. Mijouin, M. Hillion, Y. Ramdani, T. Jaouen, M.-L. Follet-Gueye, C. Duclairoir-Poc, M.G.J. Feuilloley. *5th FEMS Congress of European Microbiologists*, 19-23 July 2013, Leipzig, Germany.

A29- *Pseudomonas* cytotoxicity and virulence are regulated by gamma aminobutyric acid (GABA).

Dagorn A, Chapalain A, Mijouin L, Hillion M, Duclairoir-Poc C, Vieillard J, Chevalier S, Taupin L, Le Derf F, Orange N, Feuilloley MGJ. *16^{ème} journée de l'école doctorale EdNBISE*, 11-12 juillet 2013, Caen.

A30- Airborne fluorescent pseudomonads: in vitro assessment for identification of a potentiel biohazard.

C Duclairoir Poc, J Verdon, A Groboillot, M Barreau, H Toucourou, L Mijouin, O Maillet, C Hulen, O Lesouhaitier, JP Morin, MGJ Feuilloley, A Merieau, N Orange, *Pseudomonas 2013*, September 2013, Lausanne.

A31- New role for T6SS in the *Pseudomonas fluorescens* strain MFE01.

V Decoin, D Sperandio, D Bergeau, C Barbey, C Duclairoir-Poc, X Latour, N Orange, A Merieau, *Pseudomonas 2013*, September 2013, Lausanne.

A32- Gamma-aminobutyric Acid (GABA) modulates *Pseudomonas* cytotoxicity and virulence.

A. Dagorn, A Chapalain, L Mijouin, M. Hillion, C. Duclairoir-Poc, J Vieillard, S. Chevalier, L Taupin, F Le Derf, N. Orange, M. Feuilloley, *Pseudomonas 2013*, September 2013, Lausanne.

A33- Evaluation of *Pseudomonas* aerosolisation for physiological studies.

F Gouriou, P Penalva, S Berthout, C Duclairoir-Poc, A Agoulon, D Preterre, F Dionnet, MGJ Feuilloley, N Orange, A Groboillot, *Pseudomonas 2013*, September 2013, Lausanne.

A34 -La Substance P, une cible nouvelle pour un contrôle optimal des interactions peau/microbiote cutané

L Mijouin., M Hillion, Y Ramdani, T Jaouen, C Duclairoir-Poc, ML Follet-Gueye, E Lati, F Yvergniaux, A Driouch, L Lefeuvre, MGJ Feuilloley. *Cosminnov 2013*, 8-9 octobre 2013, Orléans.

A35 -Lipidome of airborne *Pseudomonas* sp. by HPTLC-MALDI-TOF MSI : remarkable presence of eucaryotic lipid – phosphatidylcholine

T Kondakova, N Merlet-Machour, D Preterre, F Dionnet, N Orange, C Duclairoir Poc, *3^{ème} day of Institute for Research and Innovation in Biomedecine*, 20 juin 2014, Caugé, Normandie.

A36 – Effet des NOx sur une souche de *Pseudomonas fluorescens* du microbiote cutané

F Ousalem, C Barbey, M Barreau, C Duclairoir-Poc, F Gouriou, A Groboillot, MJG Feuilloley, *11^{ème} congrès national de la Société Française de Microbiologie*, 24 et 25 mars 2015, Paris.

A37- Effect of temperature on *Pseudomonas* phospholipid composition.

T Kondakova, N Merlet-Machour, J Bodilis, F Dionnet, M Feuilloley, N Orange, HJ Heipieper, C Duclairoir Poc. 18^{ème} Journée de l'Ecole Doctorale EdNBISE, 26 - 27 mars 2015, Rouen.

A38 – *Pseudomonas fluorescens* lipidome screening : effect of temperature and growth phase on *Pseudomonas* phospholipids

T Kondakova, N. Merlet-Machour, J. Bodilis, F Dionnet, M Feuilloley, N Orange, HJ Heipieper, C Duclairoir Poc. 6th FEMS Congress of European Microbiologists. June 7-11th 2015, Maastricht, Netherlands.

A39- The nitrogen dioxide increases *Pseudomonas fluorescens* biofilm formation: identification of the bacterial response to air pollutant.

T Kondakova, T Kentache, A Garreau, M Barreau, A Groboillot, J Hardouin, F Dionnet, M Feuilloley, N Orange, HJ Heipieper, C Duclairoir Poc. 6th FEMS Congress of European Microbiologists. June 7-11th 2015, Maastricht, Netherlands.

A40- Bacterial phospholipid adaptation to human temperature.

T Kondakova, N Merlet-Machour, J Bodilis, F Dionnet, M Feuilloley, N Orange, HJ Heipieper, C Duclairoir Poc. Euro Fed Lipid Congress, 27-30 September 2015, Florence, Italy.

A41- Impact of nanoparticles used in cosmetics on skin microflora representative bacteria.

L Rowenczyk, C Picard, C Duclairoir Poc., N Hucher, N Orange, M Feuilloley, M Grisel. Journées Paul Marty SFC, 8-9 décembre 2015, Paris. Prix du meilleur poster.

A42- Investigation in the potential roles of viscosinamides produced by *P. fluorescens*

S Depayras, A Merieau, M Barreau, T Kondakova, C Barbey, H Toucourou, M Feuilloley, N Orange, C Duclairoir-Poc. 7th FEMS Congress of European Microbiologists. July 9-13th 2017, Valencia, Spain.

A43- Impact of gaseous NO₂ on *P. fluorescens* strain in the membrane adaptation and virulence

S Depayras, T Kondakova, N Merlet-Machour, HJ Heipieper, M Barreau, C Catovic, M Feuilloley, N Orange, C Duclairoir-Poc. 7th FEMS Congress of European Microbiologists. July 9-13th 2017, Valencia, Spain.

A44- Investigation in the potential roles of viscosinamides produced by *P. fluorescens*

S Depayras, A Merieau, M Barreau, T Kondakova, C Barbey, H Toucourou, M Feuilloley, N Orange, C Duclairoir-Poc. Congrès de la Société Française de Microbiologie 2017, 09-11 Octobre 2017, Paris.

Bilan & perspectives

en recherche

Lors de la rédaction de ce mémoire d'habilitation à diriger les recherches, mon laboratoire de rattachement a pour thématique clef le « Rôle de la communication et des facteurs environnementaux ou eucaryotes dans l'adaptation et la virulence bactérienne. ». Ces divers mots clefs semblent à première vue éloignés des centres d'intérêt de la jeune étudiante en DEUG Sciences et Structure de la Matière que j'étais au siècle dernier. Cependant ce parcours transdisciplinaire allant des sciences dites « dures » au monde du vivant m'a permis d'évoluer des interfaces et phénomènes physico-chimiques à l'enveloppe microbienne. A force de communication, mon adaptation s'est réalisée au travers de différents environnements : de la matière abiotique à biotique. Ainsi ai-je quelques traits communs avec nos chères souches modèles, les *Pseudomonas fluorescens* ! Le mot interface sous divers aspects a rythmé ma recherche comme un leitmotiv, comme vous pourrez le découvrir dans les pages qui vont suivre.

Bilan de mes recherches

Bilan de mes recherches

Mes recherches doctorales, sous la direction des Pr E NAKACHE et AM ORECCHIONI, ont débuté au sein de l'équipe Polymères et Interfaces d'un laboratoire de Chimie, Laboratoire de Chimie Moléculaire Thio-organique LCMT UMR-CNRS 6507, à l'Université de Caen et ont ciblé des biomolécules. J'ai appréhendé la physico-chimie, voire la structure de ces macromolécules naturelles, afin de les valoriser sous une forme galénique toujours d'actualité : l'encapsulation. Puis j'ai évalué la faisabilité de la vectorisation en y incorporant des molécules actives.

Suite à mon recrutement par l'Université de Rouen, comme ATER (2001), puis comme maître de conférences (2002), je me suis intéressée dans un premier temps aux biosurfactants (BSs) bactériens -autres biomolécules- au sein du Laboratoire de Microbiologie du Froid, EA 2123, devenu Laboratoire de Microbiologie du Froid – Signaux et MicroEnvironnement (LMDF-SME) EA 4312, puis en 2011 en Laboratoire de Microbiologie-Signaux et Microenvironnement (LMSM, EA 4312) dirigés par le Pr. N ORANGE, puis par le Pr M FEUILLOLEY. La production des BSs, molécules amphiphiles, modifie la physico-chimie de la surface bactérienne et, par conséquent, influence son adaptation à son micro-environnement, voire sa virulence. Au long des années, ma formation en microbiologie s'étoffant, j'ai élargi mon champ de recherche débutant par l'identification et l'établissement des conditions de sécrétion des BSs. J'ai ensuite évalué leur implication dans le comportement adhésif bactérien, dans la virulence bactérienne, voire leur rôle dans la communication bactérienne. Parallèlement, j'ai collaboré à une possible valorisation de ces biomolécules en bioremédiation des sédiments estuariens.

Suite à ma participation à une étude sur la qualité de l'air, un questionnement est apparu : les bactéries aéroportées ne seraient-elles pas l'interface catalysée par la pollution automobile déclenchant chez l'humain des pneumopathies bactériennes exacerbées en période de forte pollution. Après avoir étudié l'impact sur la physiologie d'une souche aéroportée de *Pseudomonas fluorescens* d'expositions au NO₂, marqueur de pollution automobile, nous avons approfondi cette thématique pour évaluer l'impact de ce même stress chimique au niveau de la paroi bactérienne, interface de la bactérie avec son microenvironnement. Y a-t'il simple diffusion du NO₂ sans autre réponse bactérienne, comme le sous-entend l'approche traditionnelle de l'immuno-suppression humaine provoquée par la pollution ? Ou la bactérie met-elle en œuvre une réponse plus ou moins complexe localisée dans sa paroi, interface avec l'environnement extérieur?

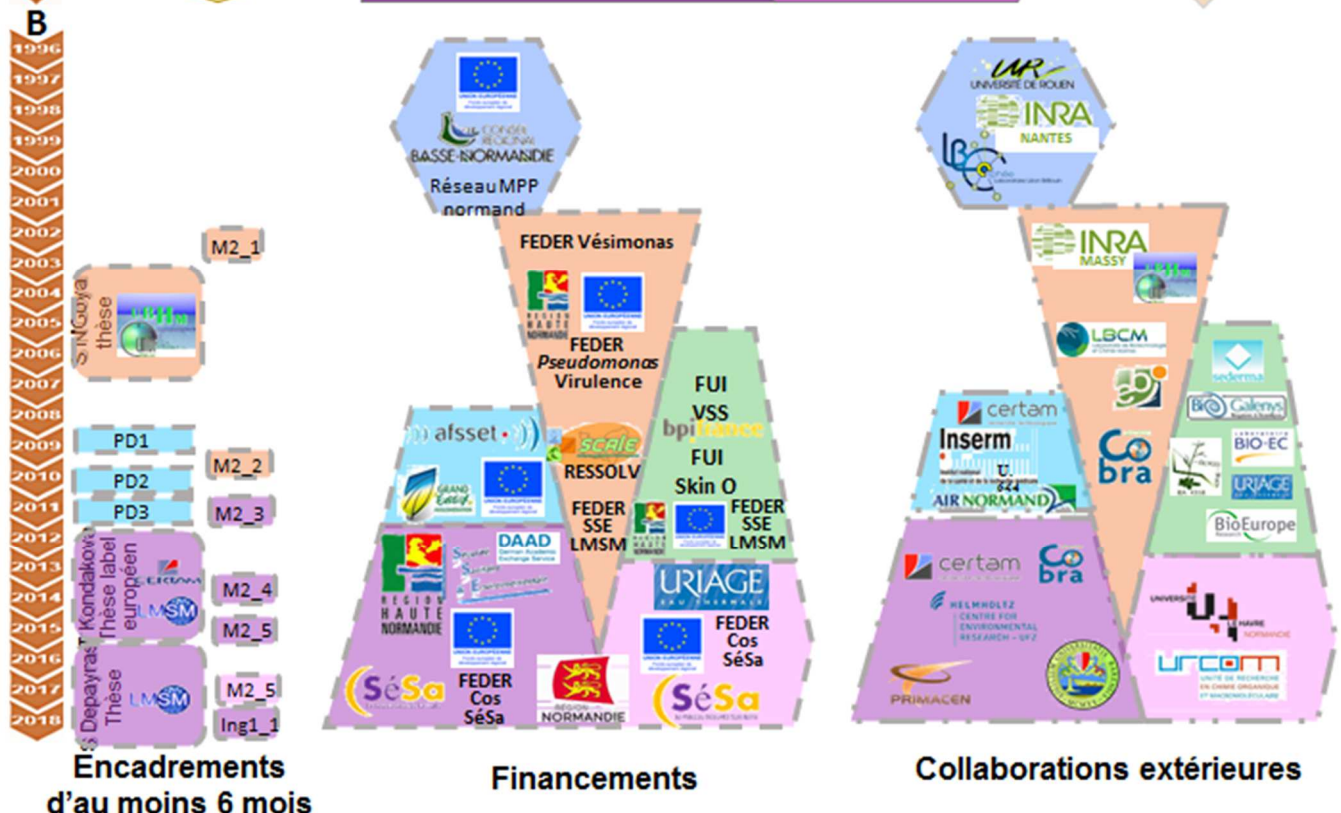
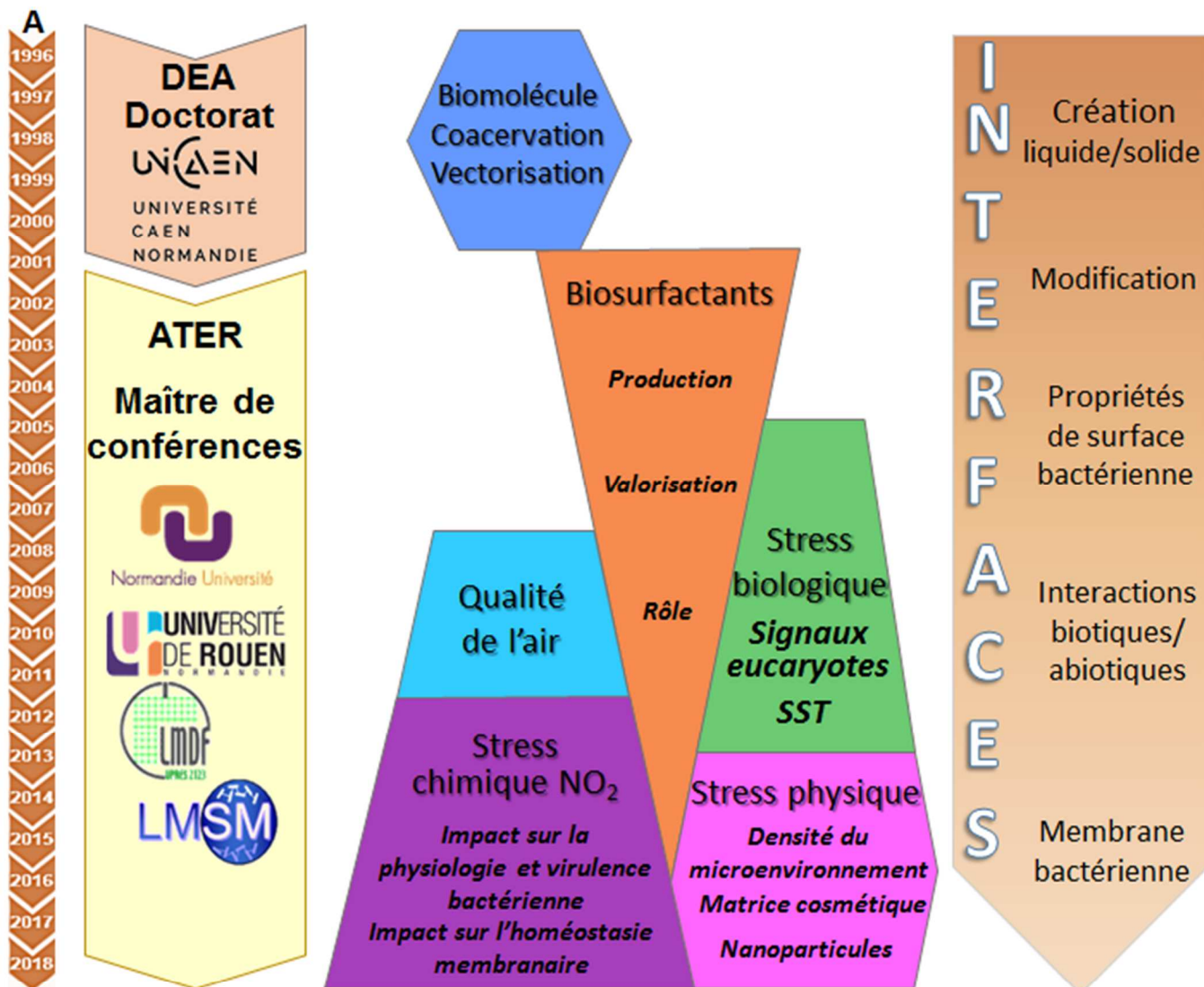


Figure 1 : Synoptiques de mes travaux en recherche. A : Synthèse thématique. B : Encadrements, financements et collaborations.

Parallèlement j'ai eu l'opportunité de collaborer sur une autre thématique de sécurité sanitaire, concernant les produits cosmétiques. L'objectif était de documenter le vieillissement de nanoparticules (NPs) de TiO₂ en lotion solaire sur deux bactéries représentatives du microbiote cutané. Suite à la formulation de deux lotions solaires modèles contenant des NPs hydrophiles ou hydrophobes, la croissance bactérienne a été étudiée lors de deux scenarii mimant soit le stockage du produit, soit l'application de la formule solaire sur la peau. Désirant évaluer le cas d'une biocontamination ponctuelle d'un cosmétique lors de sa production ou lors du prélèvement consommateur avant application, une souche *P. fluorescens* d'origine aéroportée a été mise en contact avec de NPs de TiO₂ hydrophiles. La membrane bactérienne s'en trouve-t-elle impactée, voire perméabilisée ?

Ces diverses recherches ont été mises en œuvre au travers d'encadrements, de collaborations, dont le synoptique est présenté en Figure 1.

I) Interface : quelle réalité physique ?

Dans un premier temps, quelle réalité physique désigne le terme « interface » ? Le dictionnaire Le Grand Robert (2017) indique pour cet anglicisme « Surface de séparation entre deux phases distinctes (solide-liquide, solide-gaz, liquide-gaz) ». D'après l'*Encyclopædia Universalis*, une interface peut être définie, d'une façon plus générale, comme étant la zone qui sépare deux milieux condensés qui peuvent différer par leur composition et / ou structure chimique (BOUQUET and LANGERON, n.d.).

Deux différences apparaissent. L'interface a-t'elle 2 ou 3 dimensions ? Est-elle d'épaisseur nulle ou correspond-elle à un volume « transitoire » où localement les propriétés commencent à être différentes de celles des deux phases dites en contact, tout en formant un gradient (un continuum de l'une à l'autre) ? Ici, nous plaçant à terme à l'échelle bactérienne, nous resterons sur la vision classique d'une interface d'épaisseur nulle, évitant le chausse-trappe d'interphase qui pourrait être à l'origine de quiproquo entre chimistes et biologistes !

Le second point de litige concerne la nature des phases en contact. Dans le cadre de ce mémoire, nous prendrons en compte tous les systèmes évoqués par le dictionnaire Le Grand Robert, complétés par le contact de deux liquides non miscibles, donc zone de forte hétérogénéité à courte distance. Débutons donc notre périple !

II) Crédit d'interfaces à l'aide de biomolécules

Au cours de ma recherche doctorale (DEA et thèse), je me suis intéressée au chitosane, polysaccharide extrait de crustacés ou champignons, mais aussi aux gliadines, protéines extraites du gluten de blé. Ces études ont bénéficié du soutien financier du réseau Matériaux-Polymères-Plasturgie Normand. Le cœur de ces travaux a reposé sur la solubilité de ces deux biomolécules dans différents

systèmes de solvants. Plus particulièrement pour les gliadines, grâce à une collaboration avec les Dr RENARD (Laboratoire de Physico-chimie des Macromolécules, INRA de Nantes) et. POPINEAU (Laboratoire de Biochimie et Biotechnologies des Protéines, INRA de Nantes), fournisseur de ces protéines, nous avons mené la caractérisation des protéines solubilisées par diffusion dynamique et statique de la lumière grâce à des mesures en diffusion de neutrons aux petits angles, effectuées au sein du Laboratoire Léon Brillouin du CEA-Saclay. Pour cela, j'ai suivi une formation préalable lors des Journées de la Société Neutronique Française à Albé (Vosges) en juillet 1997. Ces expériences de diffusion de neutrons aux petits angles ont permis d'apprécier, pour les différentes fractions protéiques (α , β , γ et ω -gliadine), leur conformation et leur influence sur le comportement en solution de deux extraits « bruts », mélanges de ces diverses fractions polluées faiblement par des gluténines. Cette étude en milieu deutéré a mis en lumière un comportement similaire pour les fractions α , β et γ - gliadine de masse moléculaire très proche (25-40 kDa) et constituants majoritaires des extraits bruts, alors que les ω -gliadines (65-80 kDa) se comportent davantage comme les gluténines (80-100 kDa). La solubilité des fractions les plus légères n'est pas modifiée par la présence des ω -gliadines, ni des gluténines. En bilan, meilleure est la solubilité des gliadines, plus expansive est leur conformation en solution (Orecchioni et al., 2006).

La solubilité des deux extraits en milieu hydroalcoolique deutéré par diffusion de neutrons aux petits angles a été confrontée à l'étude similaire en turbidimétrie en eau/éthanol. Ces deux approches expérimentales désignent la même composition en solvants comme optimum de solubilisation, qui s'avère dépendante de la composition relative en α , β et γ - gliadines (Orecchioni et al., 2006).

La voie de valorisation pressentie pour ces extraits bruts de gliadines était la formation par précipitation de particules, intéressant le domaine de l'encapsulation (Duclairoir, 2000; Duclairoir et al., 1999; Orecchioni et al., 2007; Denis Renard et al., 2002a, 2002b; D Renard et al., 2002; Renard and Reddy, 2007). Le procédé mis en œuvre a été la coacervation simple (Duclairoir et al., 1998; Orecchioni et al., 2006; Denis Renard et al., 2002a; D Renard et al., 2002). Ainsi la séparation de phase est induite par le phénomène physico-chimique de sursaturation menant au « compactage » du biopolymère par désolvatation rendant le milieu moins favorable à la solubilité des macromolécules. Ce procédé interfacial peut être obtenu par divers stress dont la variation de la composition du milieu en solvant qui a été mis en œuvre (Duclairoir et al., 1998, 1999; Orecchioni et al., 2001, 2006, 2007; Denis Renard et al., 2002a; Renard and Reddy, 2007).

J'ai optimisé le procédé en étudiant l'influence de divers paramètres expérimentaux sur la taille des particules, me conférant une expertise granulométrique de tout type d'objet en solution de quelques nanomètres à quelques millimètres (Duclairoir and Nakache, 2002). La taille des nanoparticules optimisées a été d'un diamètre de l'ordre de 900 nm (Duclairoir et al., 2002, 1999, 1998).

La modélisation de la formation des nanoparticules a été montrée comme une nucléation très rapide, voire instantanée lors de la première phase de la désolvatation des gliadines, puis l'intégration de nouvelles macromolécules à leur surface assurant la croissance particulaire (Orecchioni et al., 2006).

L'étude de valorisation a aboutie à la faisabilité de l'encapsulation et le relargage de 4 actifs de polarité différente : la vitamine A (Duclairoir et al., 1999), la vitamine E hydrophobe (Duclairoir et al., 2003, 2002), l'extrait de lavande peu polaire et le chlorure de benzalkonium, un amphiphile cationique (Duclairoir et al., 2003; D Renard et al., 2002). L'encapsulation est d'autant plus intéressante que le principe actif présente une polarité similaire aux protéines hydrophobes. Le relargage se réalise en deux phases. Dans un premier temps, suite au processus de désolvatation, une partie du principe actif, quelle que soit sa nature chimique, se trouve en surface des particules et donc se désorbe par un relargage rapide, qualifié d'“effet burst”. Le relargage se poursuit plus lentement, car il est tributaire de la migration du principe actif au sein de la particule assimilable à une sphère homogène jusqu'à sa surface, interface avec le milieu extérieur (Duclairoir et al., 2003; D Renard et al., 2002).

Production scientifique correspondante : P1-P8 ; Ch1-ch2 ; Pdc1 ; CInt1 ; C1-C6 ; A1-A11.

Cette caractérisation de biopolymères en solution m'a ouvert une porte sur la physico-chimie des biomolécules. Depuis mon intégration en 2001 à l'actuel LMSM, les biomolécules que sont les biosurfactants (BSs) m'ont permis de découvrir et d'apprivoiser le monde du vivant et plus particulièrement les bactéries et leurs réponses à leur microenvironnement.

III) Biosurfactants, exoproduits bactériens amphiphiles

Les BSs bactériens, comme les surfactants synthétiques, sont des molécules amphiphiles, dénommées aussi amphipathiques, ou bien, plus rarement, amphilyophiles ou amphiolaires. Elles sont constituées d'une partie présentant une affinité pour l'eau, mais aussi une seconde partie plus hydrophobe. Les anglo-saxons désignent par le substantif « amphiphiles », équivalent à « surfactants », les tensioactifs, alors qu'« amphiphilic » ou « amphipathic » sont les adjectifs correspondants.

Cette nature chimique ambivalente confère aux tensioactifs leur capacité à se localiser préférentiellement à toute interface, abiotique (solide, gaz, liquide) ou biotique (organismes producteurs ou non producteurs). Si leur concentration est telle que la saturation des interfaces disponibles est obtenue, alors l'excès de molécules amphiphiles s'organise pour former des microdomaines de polarité opposée à celle de la phase continue sous la forme de micelles. La Concentration Micellaire Critique (CMC) correspond à la concentration de tensioactifs nécessaire à la saturation des diverses interfaces (Van Hamme et al., 2006).

Les BSs intéressent grandement les industriels pour leur image de produit « naturel » liée à leur faible toxicité, leur haute biodégradabilité, leur coût modique surtout lors de valorisation de sous-produits bioindustriels (Martinotti et al., 2013). Ces biomolécules amphiphiles peuvent être des matières

premières de nombreux produits : médicaments (Satpute et al., 2016), aliments (Nitschke and Silva, 2018), cosmétiques, pesticides (Sitaraman, 2015), lubrifiants (Das et al., 2014), dépolluants environnementaux (bioremédiation de pollution aux hydrocarbures ou métaux lourds) (Mao et al., 2015; Novik and Kiseleva, 2015; Santos et al., 2017).

Par définition, les BSs sont des biomolécules amphiphiles produites à la surface ou excrétées par de nombreux êtres vivants, principalement microbiens. Cette production est dépendante de la souche et de son microenvironnement (pH, agitation, température, oxygène disponible...) (Desai and Banat, 1997). Les BSs sont habituellement classés selon leur structure chimique assurant leur amphiphilie. Ainsi la partie hydrophobe est constituée d'une chaîne lipidique (insaturée, linaire ou plus complexe), alors que la partie hydrophile peut être glucidique ou peptidique. Les BSs comprennent principalement

- des glycolipides (Rosenberg and Ron, 1999) : rhamnolipides (de Araujo et al., 2016; Kiran et al., 2016), les tréhalolipides (Soberón-Chávez et al., 2005), les sophorolipides (Hirata et al., 2009) ;
- des lipopeptides-lipoprotéines : non cycliques (Seghal Kiran et al., 2010) et cycliques -les CLPs- dont, plus particulièrement, la surfactine (Loiseau et al., 2015; Ongena and Jacques, 2008), l'amphisine, la viscosine (Nielsen et al., 2002; Nielsen and Sorensen, 2003; Raaijmakers et al., 2006)... ;
- des lipides (acides gras, lipides neutres, phospholipides) (Desai and Banat, 1997) ;
- des polymères tensioactifs : emulsan, liposan (Calvo et al., 2009) ; des particules tensioactives (toute ou partie cellulaire du microorganisme) (Desai and Banat, 1997).

Leur rôle dans la physiologie microbienne, et plus particulièrement bactérienne, a été documenté de plus en plus largement ces vingt dernières années (Ron and Rosenberg, 2001).

Les BSs s'avèrent incontournables pour toute forme de vie communautaire (biofilms, films surfaciques, agrégats...), ils interviennent dans la transition du mode planctonique au mode sessile. Effectivement les microorganismes interagissent avec leur micro-environnement en modulant les phénomènes interfaciaux existant via leur production de BSs. Ainsi, ces molécules amphiphiles agissent comme des médiateurs. Dans la nature, ils peuvent avoir un rôle physiologique en améliorant la biodisponibilité des nutriments, en favorisant leur solubilisation, voire leur assimilation. Ainsi, les bactéries dégradant des hydrocarbures produisent souvent des BSs favorisant une meilleure biodégradation de ces composés. Ils peuvent être aussi impliqués dans la mobilité bactérienne, mais aussi participer aux mécanismes cellulaires tels que la communication et la différenciation. Ils prennent part à la formation des biofilms, interagissent avec d'autres exoproduits microbiens (protéines, enzymes...) en modifiant leur conformation, leur spécificité et, par conséquent, en modulant leur activité (Singh et al., 2007). Ainsi les BSs secrétés par les microorganismes leur permettent la régulation des transferts de nutriments, de déchets, de molécules de communication, mais aussi impactent les interactions hôtes-microorganismes et donc participent à la virulence

microbienne. De plus, ils influencent la croissance microbienne en réduisant la disponibilité des substrats nutritifs, en modifiant le pH et en séquestrant des métabolites toxiques (Van Hamme et al., 2006).

Les espèces bactériennes productrices de BSs comptent parmi elles l'espèce *Pseudomonas* qui était le modèle de prédilection du laboratoire lors de mon intégration comme ATER, puis maître de conférences.

A) Production de cyclolipopeptides par de nombreuses souches de *P. fluorescens* de toute niche environnementale

Beaucoup de travaux dans la littérature traitent des rhamnolipides, BSs produits, entre autres, par *P. aeruginosa* (de Araujo et al., 2016; Kiran et al., 2016). Comme l'indique leur nom, ces BSs sont constitués d'unités osidiques comme partie hydrophile, liés à une chaîne carbonée hydrophobe. Cependant ce savoir n'est pas transposable à l'espèce *P. fluorescens* dont j'ai pu caractériser un certain nombre des souches de diverses origines. Effectivement certaines des souches *Pseudomonas* fluorescent spp. sont connues pour produire des cyclolipopeptides (CLPs) (Kruijt et al., 2009; Poc et al., 2011; Raaijmakers et al., 2010; Rokni-Zadeh et al., 2011a; Roongsawang et al., 2003) dont la surfactine (Loiseau et al., 2015; Ongena and Jacques, 2008; Rivardo et al., 2009; Vlamakis et al., 2013). Ce BS est caractérisé par sa queue lipidique formée d'un cycle de 7 acides aminés (Nielsen et al., 2002). Selon les souches *Pseudomonas* spp., d'autres familles de CLPs sont décrites avec des chaînes apolaires carbonées plus ou moins longues, reliées à des peptides cyclisés dont le nombre d'acides aminés varie selon l'organisme et les conditions de culture. Cependant, les acides aminés habituellement constitutifs de ces CLPs comptent parmi eux l'acide aspartique (Asp ou E), l'acide glutamique (Glu ou E), la glutamine (Gln ou Q), l'isoleucine (Ile ou I), la leucine (Leu ou L), la sérine (Ser ou S), la thréonine (Thr ou T) et la valine (Val ou V) (Ongena and Jacques, 2008). Parmi ces CLPs, sont déjà identifiées l'amphisine, la viscosine (Bak et al., 2015; Kruijt et al., 2009; Nielsen et al., 1999; Raaijmakers et al., 2010, 2006; Roongsawang et al., 2003) ...

Depuis mon intégration à l'Université de Rouen, j'ai eu l'opportunité de caractériser les CLPs produits par des souches de *Pseudomonas* issues de trois compartiments : la rhizosphère, l'air et les patients atteints de pneumopathies. Le Tableau 1 synthétise ces identifications.

(1) Origine rhizosphérique

Lors du travail doctoral du Dr NGOYA (2003-2007), que j'ai co-encadré avec le Pr ORANGE et l'unité de recherche en Bioadhésion et Hygiène des Matériaux, INRA de Massy (Pr BELLON-FONTAINE et Dr MEYLHEUC), nous avons évalué la production de BSs sur une trentaine de souches *Pseudomonas fluorescens* issues de la rhizosphère. Puis, ce panel a été réduit à 13 souches plus spécifiques. Leur production de BS a été observée à deux températures : 8°C (mimant les conditions de stockage en chambre froide) et 17°C (optimum de production des BSs et température

en salle d'opération hospitalière). Après une longue mise au point des conditions de production, nous avons mis en évidence, dans ces conditions, la production de 22 BSs différents identifiés et caractérisés par HPLC-MS comme des cyclolipopeptides (CLPs) apparentés à l'amphisine, à la viscosine et à la viscosinamide. 7 ont été identifiés pour la première fois. Ces familles de CLPs sont caractérisées par le nombre d'acides aminés formant la tête polaire et impliqués dans le cycle, ainsi que par le nombre de carbones de la queue hydrophobe dont la substitution peut être variable. La tête hydrophile des apparentés de l'amphisine (amphisine-like), de la viscosine et de la viscosinamide (viscosine-like) est constituée de deux résidus aminés reliés à la queue apolaire, complétés par un cycle comprenant, respectivement, 11 et 9 acides aminés. J'ai pu proposer une technique d'identification rapide entre ces 3 familles de BSs en croisant leur charge ionique et leur signature hémolytique.

La température de croissance à 17°C s'est avérée être davantage favorable à la production de CLPs en abondance et en quantité qu'à celle à 8°C.

Production scientifique correspondante : P15 ; C7-C8 ; A12 ; A15.

Encadrements : L4-L5 ; M1-2 ; M2-1 ; D1.

(2) Origine aéroportée

Avec le Dr GROBOILLOT et le Pr ORANGE, j'ai co-dirigé, depuis 2008, le volet micro-organisme du projet Particules Urbaines et Céréalières, Microorganismes Mycotoxines et Pesticides (PUC2MP) financé par l'AFSSET. Ce projet sera présenté plus largement ultérieurement. Il a été l'occasion de constituer une souchothèque de microorganismes aéroportés parmi lesquelles 15 souches de *Pseudomonas spp.* ont été étudiées pour leur potentiel de production de BSs à l'aide du tensiomètre Krüss DSA30, financé par le FEDER Virulence *Pseudomonas*. 4 souches se sont avérées productrices de BSs. Suite à la mise au point d'un protocole de purification avec l'aide du Dr KOLTALO (COBRA, Université de Rouen), les caractéristiques physico-chimiques de ces BS purifiés ont été évaluées. Ces biomolécules ont été caractérisées comme des CLPs : la souche MFAF88 produisant des amphisine-like, MFAO2 des putisolvine-like et MFAD21c et MFAH4a des CLPs non connus. Plus récemment, grâce à une collaboration avec l'EBI, université de Poitiers (Pr BERJEAUD et Dr VERDON) lors de la thèse de S DEPAYRAS (thèse 2015- soutenance prévue en 2018), les BSs ont pu être plus finement identifiés, d'autant que la famille des CLPs a été complétée par les apparentés PPZPM, constitués de 10 acides aminés dont 8 formant un cycle polaire (Weisshoff et al., 2014). Les CLPs produits par les souches MFAD21c et MFAH4a appartiennent à cette nouvelle famille.

En conclusion, la niche « air » recèle des souches *Pseudomonas* aéroportées productrices de CLPs de structures variées. La production ne semble pas spécifique à un habitat particulier.

Production scientifique correspondante : P14; P20 ; Pdc2 ; C19 ; A21 ; A26 ; A30.

Encadrements : M1_4 ; D3 ; PD2.

Niche	Souche	CLP	Molar mass (g.mol ⁻¹)	STRUCTURE												
				Fatty Acid	1	2	3	4	5	6	7	8	9	10	11	12
RHYZOSPHERE	<i>P. fluorescens</i> PfA7B	Massetolide E	1112	CH ₃ (CH ₂) ₇ CH(OH)-CO	L-Leu	D-Glu	D-allo-Thr	D-Val	L-Leu	D-Ser	L-Leu	D-Ser	L-Val			
		Viscosin	1126	CH ₃ (CH ₂) ₇ CH(OH)-CO	L-Leu	D-Glu	D-allo-Thr	D-Val	L-Leu	D-Ser	L-Leu	D-Ser	L-Ile			
	<i>P. fluorescens</i> DSS73	Amphisin	1395	CH ₃ (CH ₂) ₇ CH(OH)-CO	D-Leu	D-Asp	D-allo-Thr	D-Leu	D-Leu	D-Ser	L-Leu	D-Gln	L-Ser	L-Ile	L-Asp	
	<i>P. fluorescens</i> CTS22	Lokisin	1354	CH ₃ (CH ₂) ₇ CH(OH)-CO	D-Leu	D-Asp	D-allo-Thr	D-Leu	D-Leu	D-Ser	L-Leu	D-Ser	L-Leu			
	<i>P. fluorescens</i> CTS38	2	1112	CH ₃ (CH ₂) ₇ CH(OH)-CO	X-Leu/Ile	x-Glu	x-Thr	x-Val	X-Leu/Ile	x-Ser	X-Leu/Ile	x-Ser	x-Val			
		Massetolide F	1126	CH ₃ (CH ₂) ₇ CH(OH)-CO	L-Leu	D-Glu	D-allo-Thr	D-Val	L-Leu	D-Ser	L-Leu	D-Ser	L-Leu			
		6	1152	CH ₃ (CH ₂) ₉ CH(OH)-CO	X-cyclopr	x-Glu	x-Thr	x-Val	X-Leu/Ile	x-Ser	X-Leu/Ile	x-Ser	X-Leu/Ile			
		Massetolide B / Massetolide H	1154	(CH ₃) ₂ CH-(CH ₂) ₆ CH(OH)-CO / CH ₃ (CH ₂) ₅ CH(OH)-CO	L-Leu	D-Glu	D-allo-Thr	D-Ile/Val	L-Leu	D-Ser	L-Leu	D-Ser	L-Ile			
	<i>P. fluorescens</i> CTS50	2	1112	CH ₃ (CH ₂) ₇ CH(OH)-CO	X-Leu/Ile	x-Glu	x-Thr	x-Val	X-Leu/Ile	x-Ser	X-Leu/Ile	x-Ser	x-Val			
		Massetolide F	1126	CH ₃ (CH ₂) ₇ CH(OH)-CO	L-Leu	D-Glu	D-allo-Thr	D-Val	L-Leu	D-Ser	L-Leu	D-Ser	L-Leu			
		Massetolide A / Massetolide D /	1140	CH ₃ (CH ₂) ₇ CH(OH)-CO	L-Leu	D-Glu	D-allo-Thr	D-Ile	L-Leu	D-Ser	L-Leu	D-Ser	L-Ile/Leu			
		Pseudophomin A		(CH ₃) ₂ CH-(CH ₂) ₆ CH(OH)-CO	L-Leu	D-Glu	D-allo-Thr	D-Ile	D-Leu	D-Ser	L-Leu	D-Ser	L-Ile			
		7	1166	C _x H _y O ₂	Z	W	x-Thr	x-Val	X-Leu/Ile	x-Ser	X-Leu/Ile	x-Ser	X-Leu/Ile			
	<i>P. fluorescens</i> CTS70	Massetolide C/ Pseudophomin B	1168	CH ₃ (CH ₂) ₉ CH(OH)-CO	L-Leu	D-Glu	D-allo-Thr	D-Ile	L/D-Leu	D-Ser	L-Leu	D-Ser	L-Ile/Leu			
		Amphisin	1395	CH ₃ (CH ₂) ₇ CH(OH)-CO	D-Leu	D-Asp	D-allo-Thr	D-Leu	D-Leu	D-Ser	L-Leu	D-Gln	L-Ser	L-Ile	L-Asp	
	Tensin	1409	CH ₃ (CH ₂) ₇ CH(OH)-CO	D-Leu	D-Asp	D-allo-Thr	D-Leu	D-Leu	D-Ser	L-Leu	D-Gln	L-Leu	L-Ile	L-Glu		
	<i>P. fluorescens</i> CTS117	Massetolide E	1112	CH ₃ (CH ₂) ₇ CH(OH)-CO	L-Leu	D-Glu	D-allo-Thr	D-Val	L-Leu	D-Ser	L-Leu	D-Ser	L-Val			
		1	1126	CH ₃ (CH ₂) ₇ CH(OH)-CO	X-Leu/Ile	x-Glu	x-Thr	x-Val	X-Leu/Ile	x-Ser	X-Leu/Ile	x-Ser	X-Leu/Ile			
	<i>P. fluorescens</i> CTS193	Hodersin	1409	CH ₃ (CH ₂) ₇ C(OH) ₂ -CO	x-Leu	x-Asp	x-allo-Thr	x-Leu	x-Leu	x-Ser	x-Leu	x-Gln	x-Leu	x-Ile	x-Glu	
	<i>P. fluorescens</i> DR54	Viscosinamide B	1111	CH ₃ (CH ₂) ₇ CH(OH)-CO	L-Leu	D-Gln	D-allo-Thr	D-Val	L-Leu	D-Ser	L-Leu	D-Ser	L-Val			
		Viscosinamide C	1125	CH ₃ (CH ₂) ₇ CH(OH)-CO	L-Leu	D-Gln	D-allo-Thr	D-Val	L-Leu	D-Ser	L-Leu	D-Ser	L-Leu			
		Viscosinamide A	1125	CH ₃ (CH ₂) ₇ CH(OH)-CO	L-Leu	D-Gln	D-allo-Thr	D-Val	L-Leu	D-Ser	L-Leu	D-Ser	L-Ile			
		4	1151	CH ₃ (CH ₂) ₉ CH(OH)-CO	X-cycloproAla	x-Gln	x-Thr	x-Val	X-Leu/Ile	x-Ser	X-Leu/Ile	x-Ser	X-Leu/Ile			
		Viscosinamide D	1153	CH ₃ (CH ₂) ₉ CH(OH)-CO	L-Leu	D-Gln	D-allo-Thr	D-Val	L-Leu	D-Ser	L-Leu	D-Ser	L-Ile			
AIR	<i>P. fluorescens</i> MFAD21c	PPZPM-2	1254	CH ₃ (CH ₂) ₇ CH(OH)-CO	Leu	Glu	Thr	Ile	Leu	Ser	Leu	Leu	Ser	Ile		
		PPZPM-1	1240	CH ₃ (CH ₂) ₇ CH(OH)-CO	Leu	Glu	Thr	Val	Leu	Ser	Leu	Leu	Ser	Ile		
	<i>P. putida</i> MFAF88	Putisolvine I	1380	CH ₃ (CH ₂) ₄ CO	Leu	Glu	Leu	Ile	Gln	Ser	Val	Ile	Ser	Leu	Val	Ser
		Putisolvine II	1394	CH ₃ (CH ₂) ₄ CO	Leu	Glu	Leu	Ile	Gln	Ser	Val	Ile	Ser	Leu	Leu	Ser
	<i>P. fluorescens</i> MFAH4a	PPZPM-6	1226	CH ₃ (CH ₂) ₇ C(OH)-CO	Leu	Glu	Thr	Val	Leu	Ser	Leu	Leu	Ser	Val		
		PPZPM-2	1254	CH ₃ (CH ₂) ₇ CH(OH)-CO	Leu	Glu	Thr	Ile	Leu	Ser	Leu	Leu	Ser	Ile		
	<i>P. fluorescens</i> MFAO2	PPZPM-1	1240	CH ₃ (CH ₂) ₇ CH(OH)-CO	Leu	Glu	Thr	Val	Leu	Ser	Leu	Leu	Ser	Ile		
		Amphisine	1396	CH ₃ (CH ₂) ₇ CH(OH)-CO	Leu	Asp	Thr	Leu	Leu	Ser	Leu	Gln	Leu	Ile	Asp	
	Tensine	1410	CH ₃ (CH ₂) ₇ CH(OH)-CO	Leu	Asp	Thr	Leu	Leu	Ser	Leu	Gln	Leu	Ile	Glu		
HOPITAL	<i>P. fluorescens</i> MFN1032	Viscosinamide B	1111	CH ₃ (CH ₂) ₇ CH(OH)-CO	L-Leu	D-Gln	D-allo-Thr	D-Val	L-Leu	D-Ser	L-Leu	D-Ser	L-Val			
		Viscosinamide A	1125	CH ₃ (CH ₂) ₇ CH(OH)-CO	L-Leu	D-Gln	D-allo-Thr	D-Val	L-Leu	D-Ser	L-Leu	D-Ser	L-Ile			
		4	1151	CH ₃ (CH ₂) ₉ CH(OH)-CO	X-cycloproAla	x-Gln	x-Thr	x-Val	L-Leu/Ile	x-Ser	X-Leu/Ile	x-Ser	X-Leu/Ile			
		Viscosinamide D	1153	CH ₃ (CH ₂) ₉ CH(OH)-CO	L-Leu	D-Gln	D-allo-Thr	D-Val	L-Leu	D-Ser	L-Leu	D-Ser	L-Ile			
	<i>P. fluorescens</i> MFY162	Pseudodesmin B	1111	CH ₃ (CH ₂) ₇ CH(OH)-CO	L-Leu	D-Gln	D-allo-Thr	D-Val	D-Leu	D-Ser	L-Leu	D-Ser	L-Val			
		Pseudodesmin C	1125	CH ₃ (CH ₂) ₇ CH(OH)-CO	L-Leu	D-Gln	D-allo-Thr	D-Val	D-Leu	D-Ser	L-Leu	D-Ser	L-Leu			
		Pseudodesmin A	1125	CH ₃ (CH ₂) ₇ CH(OH)-CO	L-Leu	D-Gln	D-allo-Thr	D-Val	D-Leu	D-Ser	L-Leu	D-Ser	L-Ile			
		4"	1151	CH ₃ (CH ₂) ₉ CH(OH)-CO	X-cycloproAla	x-Gln	x-Thr	x-Val	D-Leu/Ile	x-Ser	X-Leu/Ile	x-Ser	X-Leu/Ile			
		Pseudodesmin D	1153	CH ₃ (CH ₂) ₉ CH(OH)-CO	L-Leu	D-Gln	D-allo-Thr	D-Val	D-Leu	D-Ser	L-Leu	D-Ser	L-Ile			

Tableau 1 : Les diverses souches productrices de BSs, que j'ai eu l'occasion d'étudier et de caractériser.

(3) Origine clinique

Le panel bactérien du travail doctoral du Dr NGOYA (2003-2007) contenait aussi trois souches *P. fluorescens* cliniques, à l'origine de pneumopathies. MF2256 s'est avérée non productrice de BS, alors que MFN1032 et MFY162 produisent des CLPs de la famille de la viscosinamide, peu étudiée (Geudens et al., 2014; Nielsen et al., 1999). Une approche de la régulation de la production

des CLP par modélisation informatique a été effectuée lors d'une collaboration avec des bioinformaticien l'I3S du CNRS de Sophia-Antipolis (Richard et al., 2012).

Depuis quelques années, la biosynthèse des CLPs a été décrite et repose sur les peptides synthases non ribosomiales (NRPSs). Ces systèmes multifonctionnels sont constitués de plusieurs modules dont le nombre est fonction de celui des acides aminés constitutants les CLP. Effectivement un premier module initie la n-acylation entre le premier acide aminé et la queue acide gras β -hydroxylé via un domaine NRPS de condensation (C1) qui est réputé spécifique à ces BSs. Puis la chaîne peptidique s'accroît par l'action consécutive de modules NRPS d'elongation. Après le clivage d'un domaine thioesterase, une intracyclisation se produit et permet la libération du CLP (Rokni-Zadeh et al., 2011b; Zhao et al., 2016). Suite au financement FEDER SSE LMSM d'un séquençage de la souche *P. fluorescens* MFN1032, le Dr MERIEAU a confirmé par bioinformatique la présence des gènes NRPS codant le domaine C1 de lipoinitiation des CLPs. Son étude phylogénique sur ce domaine C1 a mis en évidence une très forte homologie entre celui de la souche *P. fluorescens* MFN1032 et celui de la souche rhizosphérique *P. fluorescens* DR54, productrice de viscosinamide et apparentés (Geudens et al., 2014; Nielsen et al., 1999). S DEPAYRAS a établi la production de 4 viscosinamides-like par la souche *P. fluorescens* MFN1032 à 28°C en milieu pauvre (Davis medium), dont le CLP majoritaire est la viscosinamide A. Sa production s'est révélée effective dès la phase exponentielle de croissance par imagerie HPTLC MALDI-TOF (high-performance thin-layer chromatography couplée matrix-assisted laser desorption ionization), dont le développement a été réalisé lors de la thèse du Dr KONDAKOVA (2012-2015) au LMSM qui sera évoquée ultérieurement.

Production scientifique correspondante : P9 ; C8 ; C26 ; A42 ; A44.

Encadrements : L1 ; M1_4; M2_1 ; M2_2; D1-D3.

Prise dans son intégralité, cette étude confirme que la production des CLPs n'est pas liée à un habitat particulier. De plus, la structure chimique des CLPs est spécifique à chaque *Pseudomonas* fluorescent producteur, mais est aussi dépendante des conditions de production. Ainsi le Tableau 1 récapitule l'ensemble des CLPs identifiés ou pressentis. Une telle variété soulève une interrogation sur leur utilité pour leurs organismes producteurs, mais aussi de leur valorisation potentielle.

B) Valorisation de CLPs en réponse à une pollution environnementale

Parmi les traitements de dépollutions de sols pollués par des hydrocarbures poly-insaturés (HAP), l'utilisation de tensioactifs est reconnue comme efficace, car elle s'appuie sur des procédés de lavage des sols (Lim et al., 2016). Les rhamnolipides ainsi que la surfactine, un CLP, sont traditionnellement étudiés en bioremédiation. Dans le cadre des projets interreg RESSOLV, puis SCALE, en collaboration avec le Dr KOLTALO du LASOC (devenu équipe SIMA de l'UMR

COBRA, Université de Rouen Normandie), nous avons étudié l’alternative qu’est le cyclolipopéptide anionique : l’amphisine, ayant une activité tensio-active plus importante que les BSs précédemment cités. Mon rôle était de produire ce BS, mais aussi, en collaboration avec les Dr GROBOILLOT et Pr ORANGE, d’évaluer, sur la physiologie de la souche bactérienne productrice d’amphisine, *P. fluorescens* DSS73, l’impact de la présence de différents HAP modèles : naphtalène, phénantrène, pyrène et fluorène (Groboillot et al., 2011). D’autre part, le Dr F KOLTALO a comparé une autre famille de CLPs, la viscosine et le Massetolide E avec les surfactants synthétiques lors de la remédiation de sédiments pollués par séparation électrocinétique, afin de désorber les polluants HAP et métaux lourds (Ammami et al., 2015; Portet-Koltalo et al., 2013, 2011, 2010). Les BSs s’avèrent plus efficaces lors de la remédiation des métaux lourds que des HAP, mais moins efficaces que les surfactants synthétiques. Cependant il pourrait être intéressant de tester de plus fortes concentrations de ces BSs pour favoriser la formation de micelles évacuant les contaminants.

Production scientifique correspondante : P10-P12 ; P17 ; P22 ; A16 ; A19.

Encadrements : L2-L3 ; L7.

C) Rôle des BSs : élément de la réponse adaptative de *Pseudomonas* à leur microenvironnement

Toute production microbienne ne peut être gratuite au vu du coût énergétique correspondant (Ferenci, 2007). Aussi nous avons évalué le potentiel adaptatif bactérien lié aux BSs. Tout d’abord nous avons examiné l’impact des BSs sur la physiologie en termes de capacité à coloniser, via la mobilité bactérienne et la formation de biofilm, puis comme réponse bactérienne à des stress abiotiques et biotiques. Commençons à enquêter sur l’apport des BSs dans l’habileté de la bactérie à se mouvoir.

(1) Physiologie bactérienne

(a) Mobilité

Les BSs, comme leurs homologues synthétiques, par leur constitution sont connus pour réduire les frictions entre bactéries et n’importe quelle surface et peuvent faciliter leur déplacement. Ils s’avèrent impliqués aussi bien lors de mode de mobilité active, i.e. motilité, (swarming, gliding) ou passive (sliding) (Harshey, 2003). Le gliding n’a été décrit que pour certaines espèces microbiennes et parmi le phylum Bacteroidetes, pour l’espèce *Flavobacterium johnsoniae*, fortement éloignée des *Pseudomonas* spp. Ce mouvement fluide généralement le long du plus grand axe microbien, sur gélose de 1 à 1,5% d’agar, est obtenu grâce aux BSs excrétés et par la complexation de sulfolipides de la membrane externe (Harshey, 2003) permettant une « focal-adhesion » à la surface abiotique (Kearns, 2010). Cependant cette motilité ne semble pas concerner les micro-organismes que j’ai pu étudier. Le swarming, autre mode de motilité, est défini comme un déplacement bactérien collectif et rapide sur une surface semi-solide, résultant de la force motrice liée à la rotation flagellaire (Kearns,

2010). Elle se caractérise par une activité intercellulaire, ainsi qu'une différenciation morphologique des cellules (Tremblay and Déziel, 2008) en présence d'exoproduits, le plus fréquemment des BSs (Kearns, 2010). Il est détectable sur gélose de 0,5 à 2% d'agar (Harshey, 2003; Tremblay and Déziel, 2008) en milieu riche, mais son observation est largement dépendante de l'espèce (Kearns, 2010) et des conditions expérimentales (Tremblay and Déziel, 2008). Le déplacement passif de glisse (sliding ou spreading) a été décrit comme favorisé par les BSs, confortés par la présence de polysaccharides, en l'absence de tout appendice moteur fonctionnel tel que flagelle ou pili. Il est visuellement observable en milieu gélosé contenant 0,2 à 0,7% d'agar. Les forces d'expansion lors de la croissance bactérienne se combine avec l'abaissement de tension de surface liée aux BSs (Harshey, 2003; Kearns, 2010). Alsohim *et al.* (Alsohim et al., 2014) indiquent que les deux mobilités peuvent se cumuler, rendant les interprétations délicates, surtout que la prépondérance de l'une ou l'autre est soumise aux conditions expérimentales, pouvant de plus être impactée par la qualité de l'eau ou de l'agar utilisée lors de la préparation des milieux gélosés. Cette étude est d'autant plus intéressante qu'elle étudie la mobilité de la souche *P. fluorescens* SBW25 productrice de viscosine, CLP différent de la viscoinamide, l'acide aminé Glu se substituant à Gln. La viscosine s'avère indispensable pour le sliding, qualifié de spidery spreading, i.e. diffusion fractale. Le swarming est dépendant de flagelle(s) fonctionnel(s), mais la viscosine, optionnelle, accélère la vitesse de diffusion sur la surface semi-solide. Elle serait responsable du front humide précédent la zone du swarming, mais aussi de la morphologie plus ou moins accidentée du front de diffusion.

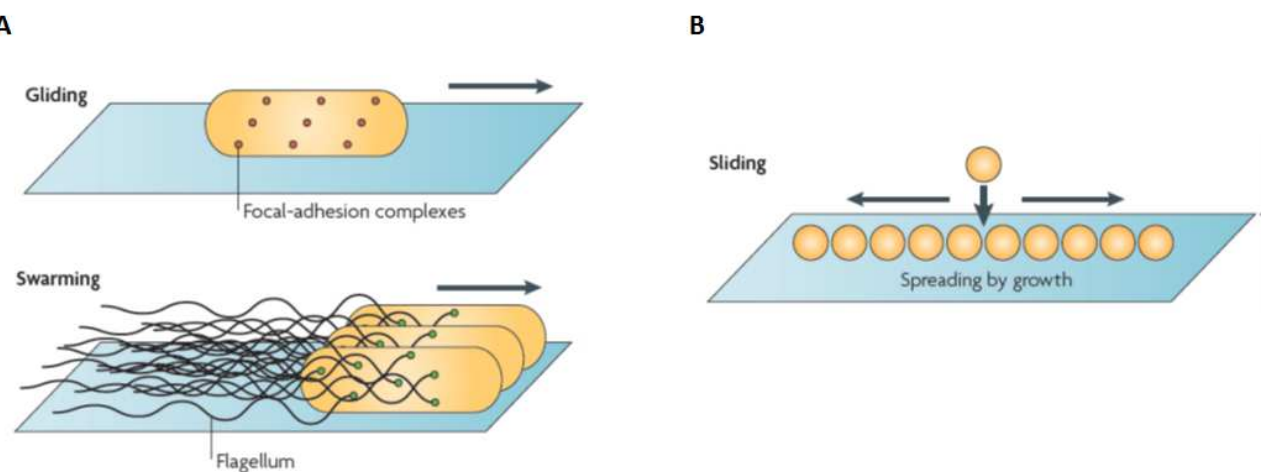


Figure 2 : Mobilités bactériennes impliquant les BSs. A : mobilité active – motilité ; B : mobilité passive adapté de Kearns (Kearns, 2010).

L'ensemble des souches de *P. fluorescens* que j'ai pu étudier présentait une mobilité de type swarm, (communication personnelle). Cependant les morphologies des zones de diffusion et de leur front pouvaient être très variables. Ainsi toutes les non productrices, comme la souche aéroportée MFAF76a (Duclairoir Poc et al., 2014), présentent un zone de diffusion circulaire, alors que des festons, voire des dendrites se forment pour les productrices de biosurfactants. Ainsi est visible le « film d'eau » contenant probablement la viscoinamide et précédant le front de diffusion lié au swarm de la souche clinique MFN1032.

L'ensemble de ces mobilités, passive ou active, ont un rôle significatif dans la colonisation des surfaces par les bactéries qui débute toujours par une étape d'adhésion.

(b) Adhésion

Pour d'étudier l'impact des BSs dans l'adhésion bactérienne, j'ai évalué l'adhésion de deux souches rhizosphériques productrices de BSs couplées à un mutant non producteur. Il s'agit des *P. fluorescens* PFA7b et DSS73 produisant des CLPs de type viscosine et amphisine respectivement, et de Pf1 Vis- et DSS73-15C2, leurs mutants relatifs. Les conditions optimales de production de BSs ont été constatées à 17°C en milieu DMB. Le temps de contact pour l'adhésion est défini comme un temps de génération.

Le phénomène d'adhésion se concrétise par des interactions à plus ou moins longue portée et des détachements du support abiotique, tous gouvernés, en partie, par les propriétés de surface des bactéries. L'hydrophilie de chaque souche sauvage et de son mutant s'avère similaire suite à des tests Microbial Adhesion To Solvents (MATS) ciblés, comme présenté Figure 3, éliminant ainsi un biais possible. De plus, la souche sauvage adhère moins à la surface de la microplaqué que son mutant quels que soient les CLPs qu'elle produit. Donc les CLPs pénaliseraient l'adhésion de leur propre producteur.

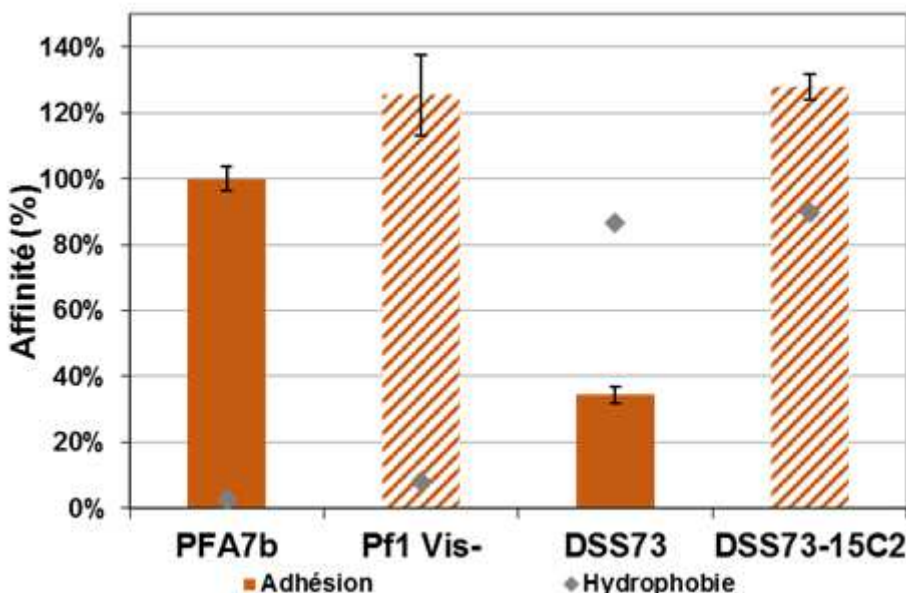


Figure 3 : Evaluation de l'adhésion bactérienne en microplaqué à 17°C en DMM, après un temps de génération pour les souches rhizosphériques PFA7b et DSS73 et leur mutant respectif non producteur de BS, ainsi que leur hydrophobie. L'adhésion est normalisée par rapport à celle de PFA7b.

Cependant, une mutation qui abolit l'expression d'un gène localisé dans une non ribosomique peptide synthétase (NRPS) ne peut pas uniquement ciblée la production de CLP, mais peut implémenter d'autres modifications pouvant impacter l'adhésion, telles que la production d'exopolysaccharides (EPS) (Alsohim et al., 2014).

La souche clinique *P. fluorescens* MFN1032 présente des variants spontanés, dont V1 et V3 sont non producteurs de viscosinamides (Rossignol et al., 2009). Mettant à profit ce panel de souches, j'ai caractérisé le rôle des viscosinamides dans l'adhésion bactérienne et la formation de biofilm. Ces études ont été menées à 2 températures : l'optimum de production de BSs (17°C) et la température optimale de croissance de ces souches (28°C). La température de croissance n'a pas d'impact sur l'hydrophilie des souches. Cependant leur hydrophilie est différente, conséquences de mutations génétiques chez les variants par rapport à la souche sauvage (Richard et al., 2012).

Quelle que soit la température d'incubation, les CLPs amoindrissent l'adhésion des deux mutants par rapport à la souche sauvage.

En résumé, l'étape d'adhésion entre bactérie et surface n'est pas favorisée par les CLPs. Ils peuvent la contrecarrer selon la température d'expérience ou la niche écologique des souches *Pseudomonas fluorescens* étudiées.

(c) Biofilm

Après l'adhésion, la colonisation bactérienne à une surface se poursuit par l'élaboration d'un biofilm qui est le lieu d'un comportement bactérien coopératif, conduisant à des phénotypes différenciés d'où son hétérogénéité de structure. Les bactéries aux divers phénotypes sont encastrées dans une matrice extracellulaire composée principalement d'exopolysaccharides (EPS) (Stoodley et al., 2002).

Les CLPs ne semblent pas impacter le développement du biofilm bactérien en microplaques à 17°C. Au contraire à 28°C, ils semblent favoriser son développement : le biofilm de MFN1032 contient plus de deux fois plus de bactéries que ceux de ses variants. L'apport exogène de CLPs n'augmente pas l'importance du biofilm des variants aux deux températures 17 et 28°C. Cependant l'efficacité de l'ajout de BSs est plus variable à 28°C. La tendance n'est pas similaire à 28°C pour ces mêmes variants. Quant à la souche sauvage, suite à cet ajout, ses biofilms sont aussi amoindris aux deux températures. (Bonnichsen et al., 2015), les viscosinamides favoriseraient la dispersion du biofilm en le dissolvant comme la viscosine produite dissout les biofilms de la souche *P. fluorescens* SBW25 (Bonnichsen et al., 2015; Raaijmakers et al., 2010). Viscosine est considérée comme un catalyseur du départ des bactéries du biofilm existant suite à des altérations de l'hydrophilie de leur surface et de la structure matricielle du biofilm. (Bonnichsen et al., 2015). Ces résultats font échos aux contradictions de la littérature sur l'implication des CLPs au cours de la colonisation bactérienne. Ainsi les sessilines de *Pseudomonas* CMR12 (D'aes et al., 2014) ou les viscosine et apparentés de *P. fluorescens* SBW25 (de Bruijn et al., 2007) favorisent la formation du biofilm en conditions d'incubation statiques. Au contraire un mutant de SBW25 déficient en viscosine montre une augmentation du biofilm (Bonnichsen et al., 2015), comme d'autres *Pseudomonas* productrices d'arthrofactine, orfamide et putisolvine (D'aes et al., 2010; Kruijt et al., 2009; Roongsawang et al.,

2003). Les viscosinamides semblent participer à l’édification du biofilm en fonction des températures d’incubation, mais ils favorisent aussi systématiquement sa dispersion.

Afin de poursuivre nos investigations, nous avons eu recours à un transformant de la souche MFN1032, portant le gène *gfp*, MFN1032*gfp* (Decoin et al., 2014). Le transformant et la souche sauvage présentent la même hydrophobie, la même charge de surface et la même acidité-basicité de Lewis, réputées gouverner l’adhésion, les interactions et le détachement bactérien avec les surfaces abiotiques (Gallardo-Moreno et al., 2011). La cinétique de croissance de MFN1032*gfp* a été réalisée pendant 48h à 28°C en DMB sur lame de verre, sa rigidité favorisant le biofilm microbien (Saha et al., 2013). Le biofilm a été observé par microscopie confocale à 2, 24 et 48h, Figure 4A.

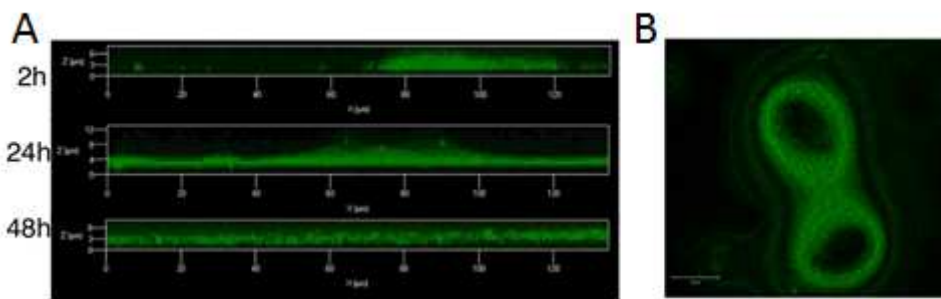


Figure 4 : Formation de biofilm de MFN1032*gfp* sur lame de verre à 28°C en DMB. A : coupe longitudinale à 2, 24 et 48h, B : coupe transversale à 24h.

Dès 2h de croissance, des structures en forme de champignon, Figure 4B, apparaissent. Elles sont liées à l’hétérogénéité des mobilités bactériennes, en particuliers le swarm nécessitant la production de BSs (Mann and Wozniak, 2012). Ces superstructures restent jusqu’à 24h alors que le biofilm s’épaissit (doublement par rapport à celui de 2h). A 48h, la hauteur de biofilm chute significativement ; cette dispersion pourrait correspondre à la perte de ces suprastructures. Un tel process a été décrit pour *P. aeruginosa*, lié aux rhamnolipides via la motilité, les interactions cellule-cellule, la différenciation et la formation de canaux hydriques (Mann and Wozniak, 2012). D’autre part la viscosine, chez *P. fluorescens* SBW25, a été suggérée comme promoteur de la dispersion du biofilm (Bonnicksen et al., 2015), comme la putisolvine, produite par une souche *P. putida* (Cárcamo-Oyarce et al., 2015). A l’instar, les viscosinamides pourraient rester à la surface de leurs bactéries productrices, favorisant l’échappement individuel de ces mêmes bactéries du biofilm. Jusqu’ici ce phénomène n’a été décrit qu’après plusieurs jours et non 2h comme pour *P. fluorescens* MFN1032 (Bonnicksen et al., 2015; Cárcamo-Oyarce et al., 2015; Mann and Wozniak, 2012). Quant aux proéminences, elles pourraient être provoquées par les conditions stressantes : limitation d’un ou plusieurs nutriments du milieu minimum (Barraud et al., 2015; Cárcamo-Oyarce et al., 2015; Davies, 2011; Petrova and Sauer, 2016). De plus, leur disparition marque l’étape finale du développement du biofilm ; les bactéries sont « relâchées » de l’intérieur du biofilm par les canaux hydriques (Davies, 2011)

Pour confirmer cette potentielle implication des BSs dans la formation de biofilm, une cinétique similaire a été réalisée sur des filtres Anapore™ transparents au microscope confocal,

augmentant la surface de contact entre filtre/biofilm mimant davantage le développement de *P. fluorescens* MFN1032 au sein des poumons, son lieu d'isolement (Chapalain et al., 2008). De plus ce type de support « souple » m'a permis d'envisager un suivi cinétique de l'hydrophobie de la face externe du biofilm à l'aide de la technique de la goutte captive via l'angle de contact θ , Figure 5A.

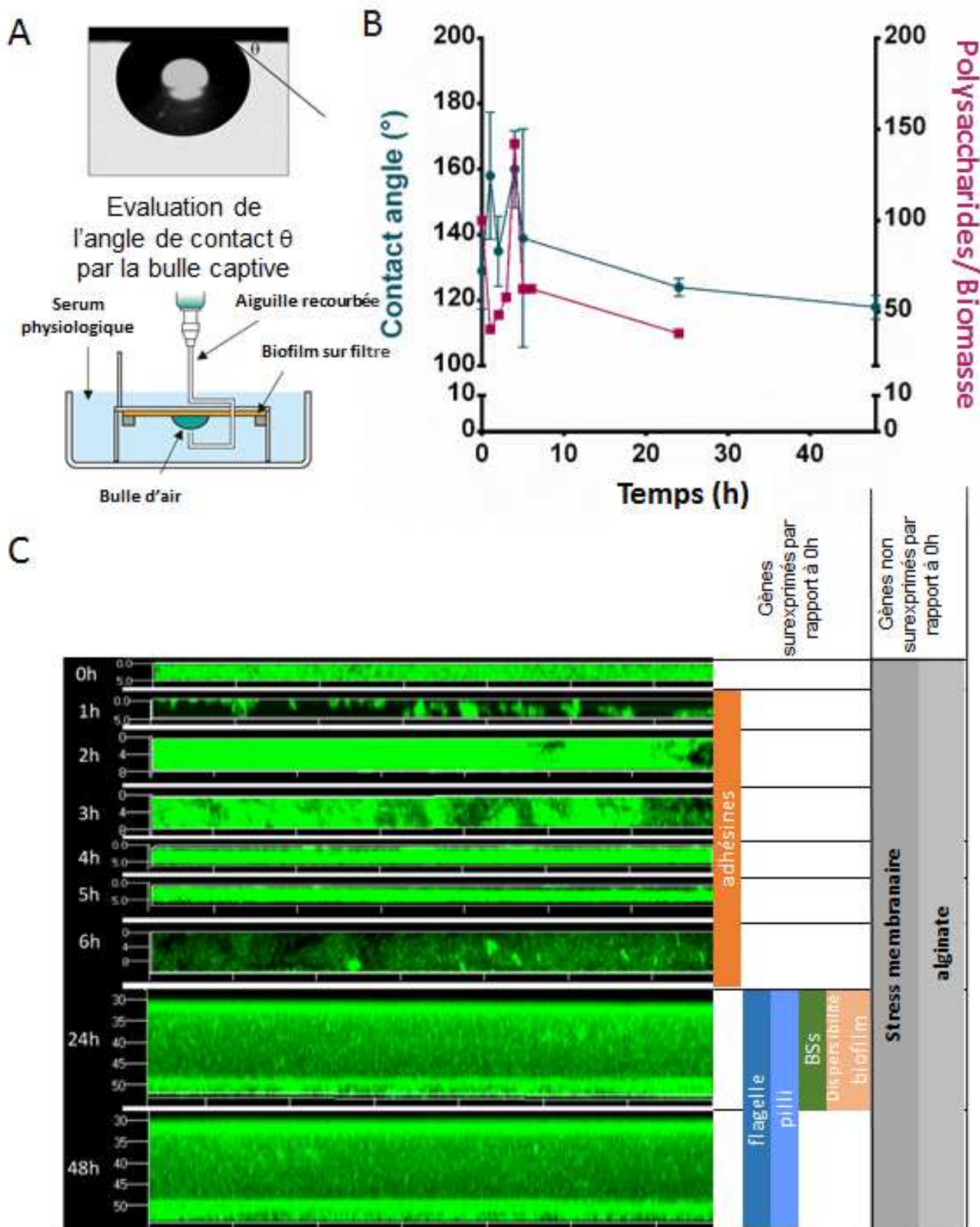


Figure 5 : Formation de biofilm de MFN1032gfp sur filtre Anapore à 28°C en DMB. A : méthode de la bulle captive ; B : cinétique de l'évolution de l'hydrophobie et du rapport biovolume polysaccharide/biomasse ; C : Suivi de la formation du biofilm en microscopie confocale et par transcriptomique ciblée.

Les BSs sont à même d'impacter l'hydrophilie de surface, comme intrinsèquement ils se localisent aux interfaces ou dès la création de nouvelles surfaces, ils s'y implantent. *In vitro* la surfactine, autre cyclolipopeptide, interagit avec l'enveloppe bactérienne en profondeur au niveau de la tête des phospholipides (Otzen, 2017), modifiant ainsi l'hydrophobie cellulaire, donc du biofilm. Cependant l'hydrophobie de biofilm peut refléter aussi l'évolution de la composition en surface du biofilm c'est-à-dire le ratio matrice polysaccharidique/ biomasse (Barraud et al., 2015; Cárcamo-Oyarce et al., 2015; Davies, 2011; Petrova and Sauer, 2016).

La littérature fait mention de quelques mesures d'hydrophobie de biofilm (Baumgarten et al., 2012b; Feng et al., 2016), mais uniquement via la méthode de la goutte posée qui implique un dessèchement du biofilm, voire sa restructuration (Gallardo-Moreno et al., 2011), donc un stress du tapis bactérien. La bulle captive évalue l'angle de contact θ que forme la bulle d'air mise en contact avec le biofilm bactérien immergé en sérum physiologique, comme présenté en Figure5A avec des biais moindres qu'avec la goutte posée (Gallardo-Moreno et al., 2011).

L'implémentation innovante de la bulle captive nous a permis d'établir l'évolution sur 48h de l'hydrophobie du biofilm se développant à 28°C en DMB, Figure 5B, parallèlement à sa caractérisation en microscopie confocale, Figure5C. Pour affiner notre compréhension, les polysaccharides ont été localisés par coloration spécifique des motifs β -glucosidiques via le calcofluor (Harris and Fincher, 2009). Leur proportion a été quantifiée relativement à la biomasse par le rapport des biovolumes respectifs du calcofluor (polysaccharides) et de la biomasse, représenté en Figure5B.

La Figure 5B&C montre l'évolution du biofilm pendant 48 h à 28°C sous différents aspects. Bien que le biofilm croît, son épaisseur n'augmente pas linéairement dans le temps (Figure 5C). Toutefois, cette cinétique de formation n'est pas en cohérence avec la croissance obtenue sur lame de verre. La rugosité du filtre étant supérieure à celle de la lame de verre, l'adhérence bactérienne est accrue sur les surfaces les plus rugueuses et leurs défauts favorisant le contact filtre/bactéries (Song et al., 2015). La première étape, transitoire, commence par une phase très précoce de l'adhérence (Figure 5C: 0 & 1h) ; un certain nombre de bactéries recouvre le filtre, mais sans s'y fixer. Aussi le rapport polysaccharide/biomasse chute. De plus l'hydrophilie augmente de 129° à 158°, car les bactéries *P. fluorescens* MFN1032, plutôt hydrophobes, s'en détachent. Globalement la surface du biofilm est hydrophile, mais des fluctuations d'hydrophobie sont observées, lors des premiers temps d'adhésion. Les colonies grossissent et s'étendent durant l'attachement irréversible comme en témoignent l'augmentation du rapport polysaccharide/biomasse, mais aussi de la surexpression des adhésines, protéines en amont de la biosynthèse de la matrice polysaccharidique (Barraud et al., 2015). L'épaisseur maximale atteinte est 8 μ m tout en laissant des zones non couvertes du filtre (Figure 5B & C: 2 & 3h). A 4h, le biofilm bactérien est à confluence, mais son épaisseur se réduit à 5 μ m. Les polysaccharides atteignent leur maximum de production, confortent la densification du biofilm (de Araujo et al., 2016) et entraînent une augmentation d'hydrophobie (Figure 5B: 4h). Comme la

surfactine (Vlamakis et al., 2013) ou la viscosine (Bonnichsen et al., 2015), les viscosinamides pourraient stimuler la production de polysaccharides (de Araujo et al., 2016). L'écart type de l'hydrophobie se trouve doublé entre 4 et 5 h ; elle atteint 24 % à 5 h attestant de l'instabilité de l'interface. Ceci pourrait être rapproché d'un réarrangement cellulaire tel que des bactéries libérées du biofilm par les canaux hydriques (Davies, 2011) Cependant cette instabilité pourrait aussi avoir pour origine la production, même débutante de BSs (Figure 5B: 5h). Le mélange de viscosinamides homologues pourrait augmenter cette instabilité par leur diversité de structure. La surexpression à 24h des gènes en liaison avec les pili, les flagelles, les BSs et la dispersion du biofilm indiquerait une synergie entre ces deux phénomènes (Figure 5C: 24h), simultanément à un rapport matrice polysaccharidique/ biomasse fléchissant. Le biofilm observé à 6 h est moins dense qu'auparavant et quelques proéminences sont apparues, mais la hauteur atteint au maximum 10 µm. Le biofilm mature est atteint après 24h, alors que sa hauteur maximale moyenne est d'environ 22 µm (Figure 5C : 24 & 48h). Aucune évolution n'est observée après 24h. Ces observations sont cohérentes avec le cycle de vie d'un biofilm (Barraud et al., 2015; Davies, 2011; Petrova and Sauer, 2016). Néanmoins, l'interruption de l'expérience après 48h pourrait biaiser l'observation de la dernière phase, c'est-à-dire l'altération du biofilm par la dissémination bactérienne.

Ainsi, ces bactéries peuvent rester en interaction avec leur microenvironnement : surface abiotique ou hôte, *i.e.* cellules ou organismes Aussi l'impact des CLPs sur les interactions avec des partenaires biotiques semble intéressant à étudier.

Production scientifique correspondante : P15 ; C26 ; A12 ; A42 ; A44.

Encadrements : L4-L5 ; M1-6 ; M2_1-M2_2 ; D1 ; D3.

(2) Réponse au stress biologique provoqué par un hôte

Au vu de l'isolement de *P. fluorescens* MFN1032 suite à une pathologie pulmonaire (Rossignol et al., 2008; Sperandio et al., 2010), une étude en cytotoxicité a été réalisée vis-à-vis de pneumocytes A549.

Ce modèle de toxicologie *in vitro* a pour objectif de se rapprocher du mode de contamination par voie pulmonaire pouvant provoquer une pneumopathie. Ainsi cette lignée cellulaire a été exposée à la souche *P. fluorescens* MFN1032, mais aussi à son surnageant de culture stérile, contenant des viscosinamides.

La croissance bactérienne a été réalisée à 28°C, température optimale de croissance de cette souche (Chapalain et al., 2008), mais aussi à 37°C, température humaine. Le contact des bactéries avec les pneumocytes entraîne une lyse cellulaire limitée (au plus 30% à 28°C, comme représenté Figure 6). Il pourrait être dû au système de sécrétion de type 3, SST3, identifié par ma collègue, le Dr A MERIEAU, chez *P. fluorescens* MFN1032 (Sperandio et al., 2012). Au contraire le contact surnageant/ A549 est bien plus dévastateur. Plus de la moitié des pneumocytes s'en trouve lysée, mais l'action du SST3 ne peut être envisagée.

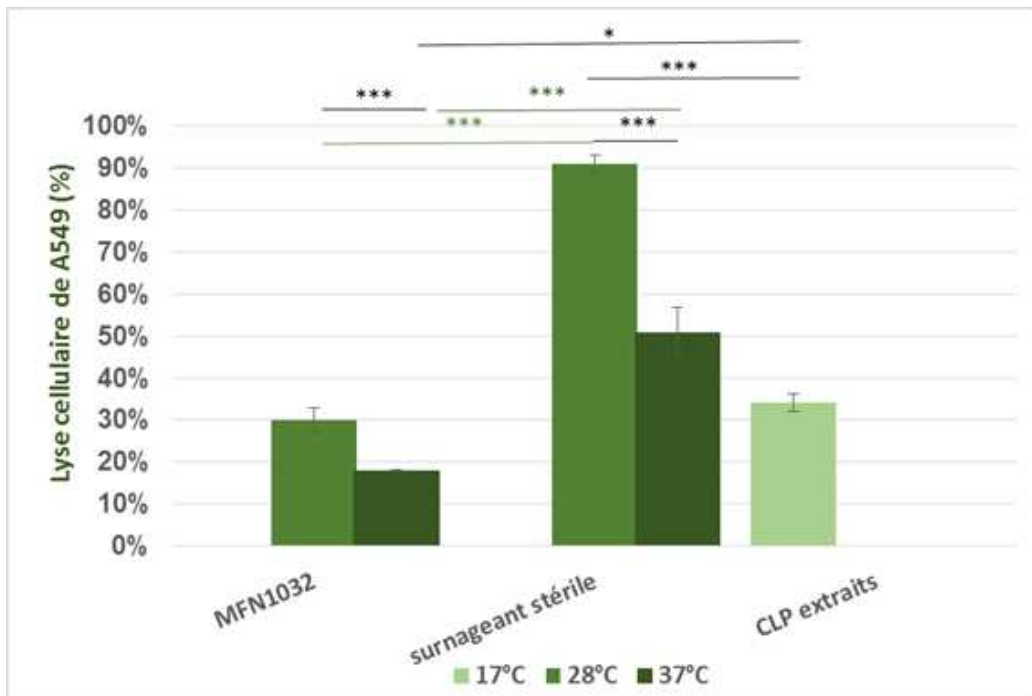


Figure 6 : Cytotoxicité envers des pneumocytes A549. A : souche MFN1032, B : son surnageant de culture en DMB, C : solution de CLPs purifiés. (* : $P=0,05$; ** : $P=0,01$; *** : $P=0,001$).

A cette température de 28°C, la sécrétion d'exoproduits tels que les CLPs est plus importante qu'à 37°C, ce qui se traduit par une réduction de la virulence de la souche clinique à 37°C. Les mécanismes d'interactions bactéries/A549 sont donc liés aux exoproduits, dont les viscosinamides, les enzymes, les LPS (Picot et al., 2004) ou les sidérophores (Rossignol et al., 2008). Pour confirmer l'action des CLPs, un extrait purifié a été mis en contact et a entraîné une lyse pneumocytaire de 34%, prouvant leur participation active dans la virulence de la souche *P. fluorescens* MFN1032. Ainsi les viscosinamides, comme CLPs, confirment leur capacité à interagir avec les membranes ou protéines d'organismes vivants (Otzen, 2017).

Production scientifique correspondante : P20 ; C26 ; A26 ; A30 ; A42 ; A44.

Encadrements : M2_3 ; D3.

(3) Communication cell-to-cell

Ces viscosinamides ne pourraient-ils pas prendre part au « bavardage bactérien », i.e. Quorum Sensing -QS- (Bjarnsholt et al., 2011) ? Les CLPs pourraient agir comme des molécules de signalisation (D'aes et al., 2014), cependant leur implication dans le QS reste mystérieuse (Cárcamo-Oyarce et al., 2015; D'aes et al., 2014; Fazli et al., 2014; Vlamakis et al., 2013b). La production de molécules de signalisation, N-AcylHomoserine Lactones (NAHLs), a été évaluée chez la souche MFN1032, mise en présence de deux souches biosenseurs: *Agrobacterium tumefaciens* NTI, révélant la production de NAHLs de C₆ à C₁₂ (McClean et al., 1997) et *Chromobacterium violaceum* CV026, indicateur pour ceux de C₄ à C₈ (Farrand et al., 1996), en collaboration avec mes collègues les Dr A MERIEAU et C BARBEY.

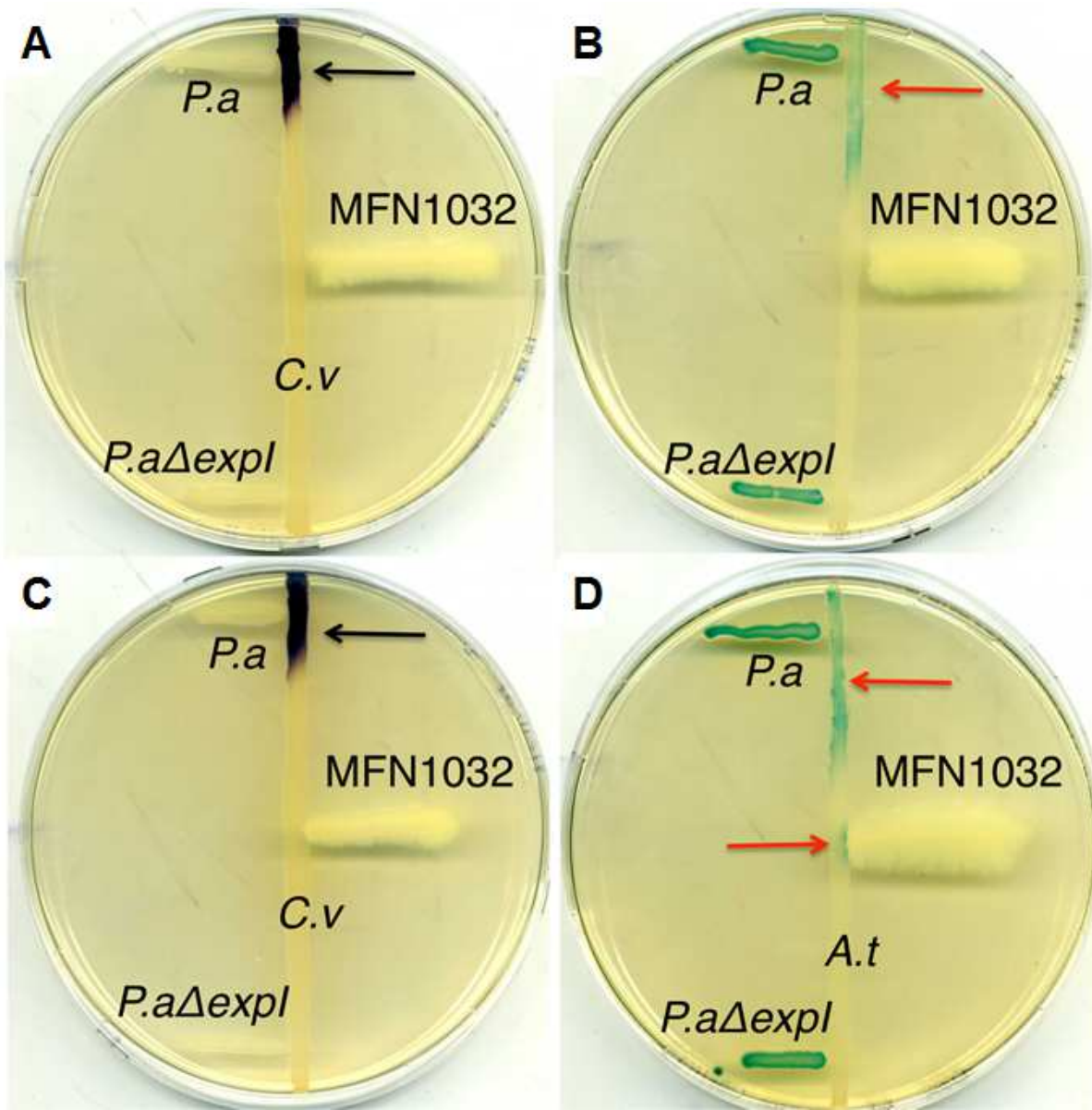


Figure 7 : Evaluation de la production de molécules de signalisation, N-AcylHomoserine Lactones (NAHLs) de la souche MFN1032 à l'aide des biosenseurs *C. violaceum* CV026 (A &C) et *A. tumefaciens* NTI (B &D). A & B : sans contact ; C&D : avec contact.

A la Figure 7, la souche clinique ne provoque pas leur coloration (pas d'activation du senseur), aussi elle ne semble produire aucun type de NAHLs, ce qui n'est pas contradictoire avec la littérature très contrastée des molécules de signalisation chez les *Pseudomonas* fluorescent. Ainsi les souches *P. fluorescens* 07A and 041 ne produisent pas de telles molécules (Martins et al., 2014). De plus, la production de CLPs est parfois indépendante de NAHLs produits (Bonnichsen et al., 2015; De Bruijn et al., 2008). Les BSs présentent une structure similaire aux NAHLs et partagent leur efficacité à faibles concentrations (Primo et al., 2015). Cependant ils s'avèrent beaucoup plus diffusibles (Williams et al., 2007).

De plus la souche *P. fluorescens* 2-79 est reportée utilisant une forme en C₆ trihydroxylée comme signal de quorum (Khan et al., 2005). Ainsi les viscosinamides étant moins diffusibles que les NAHLs, les essais ont été réitérés en mettant en contact direct la souche MFN1032 et les biosenseurs. Une réponse positive d'*A. tumefaciens* NTI suite à ce contact direct, Figure 7D, indique que

MFN1032 produits des composés similaires aux NAHLs. Ne serait-ce pas les viscosinamides qui seraient impliquées comme médiatrices d'une communication cellule-cellule ? Beaucoup de zones d'ombre persistent !

Production scientifique correspondante : A42 ; A44.

Encadrements : M2_3 ; D3.

Que les bactéries aient une croissance planctonique ou sessile, en interaction avec une interface abiotique ou biotique, les BSs, dont les CLPs, sont effectivement un des éléments de la réponse adaptative des *Pseudomonas* à leur microenvironnement. Cependant cette réponse ne s'exprime pas uniquement via ces biomolécules. Quand il s'agit de se développer, voire de survivre, la bactérie doit faire face à un microenvironnement. Même si celui-ci est des plus favorables à son développement, la bactérie doit contrecarrer l'intrusion d'autres organismes en s'en défendant. Aussi avons-nous décidé avec un certain nombre de mes collègues du LMSM d'explorer la virulence bactérienne comme une approche de leur réponse adaptative pour une niche écologie rarement étudiée : l'air extérieur.

IV) Evaluation de la virulence bactérienne : approche originale en qualité de l'air

Avec le Dr A GROBOILLOT et le Pr N ORANGE, j'ai co-ordonné, entre 2008 et 2010, le volet micro-organisme du projet Particules Urbaines et Céréalières, Microorganismes Mycotoxines et Pesticides (PUC2MP), saisine financée par l'AFSSET. Ce travail a été rendu possible grâce une collaboration entre Air Normand, agence de surveillance de la qualité de l'air en Haute-Normandie à l'époque (V DELMAS, A FRANCOIS), le CERTAM (Centre d'Etudes et de Recherche en Aérothermique Moteur, Dr F DIONNET, Dr D PRETERRE D et Dr F GOURIOU) et les laboratoires de l'Université de Rouen : unité U644 de l'INSERM (Pr J-P MORIN) et notre équipe.

Cette saisine avait pour objectif d'évaluer l'impact sanitaire de poussières de déchagements céréaliers en fonction des pressions environnementales (température, pollution...). L'identification par microbiologie pasteurienne, métabolique et par biologie moléculaire des diverses communautés bactériennes et fongiques a mobilisé, en plus des 3 enseignants-chercheurs que nous étions, 3 techniciens (permanent : O MAILLOT et contractuels : E GERAULT et S PIRES), 3 stagiaires, dont un post-doctorant (Dr M MORETTI), spécialiste fongique. Suite aux 9 prélèvements d'air «céréaliers» ou urbains, une souchothèque a été constituée contenant 280 souches fongiques et plus de 2000 bactéries aéroportées.

Afin d'appréhender l'aspect sanitaire de cette biocharge bactérienne, la virulence de souches représentatives de chaque grande famille bactérienne lors des divers prélèvements a été évaluée grâce au test alternatif toxicologique du nématode *Caenorhabditis elegans*, implanté au sein de notre laboratoire par mon collègue le Dr O LESOUHAITIER. Ce modèle cytotoxique *in vitro* de type

« Slow killing » est d'autant plus pertinent qu'il est adapté à de nombreux pathogènes humains (Darby, 2005) et, plus particulièrement, pour des pathologies pulmonaires (Rea et al., 2010). Les bactéries sont une source de nourriture pour ces nématodes. Plus la cinétique de survie des *C. elegans* est longue, moins la souche bactérienne est virulente vis-à-vis de ce modèle. Afin de comparer les cinétiques obtenues pour les différentes souches, une approche analytique a consisté à considérer la durée nécessaire pour que la moitié de la population des vers ait disparu, cette valeur est qualifiée de DL50. *Pseudomonas aeruginosa* PAO1 (par la suite PAO1) est utilisée comme témoin de virulence (DL50 de l'ordre de 6 jours) et la souche *Escherichia coli* OP50 (par la suite OP50) comme témoin non virulent avec une DL50 d'environ 16 jours. La Figure 8 présente une des comparaisons de telles cinétiques de survie.

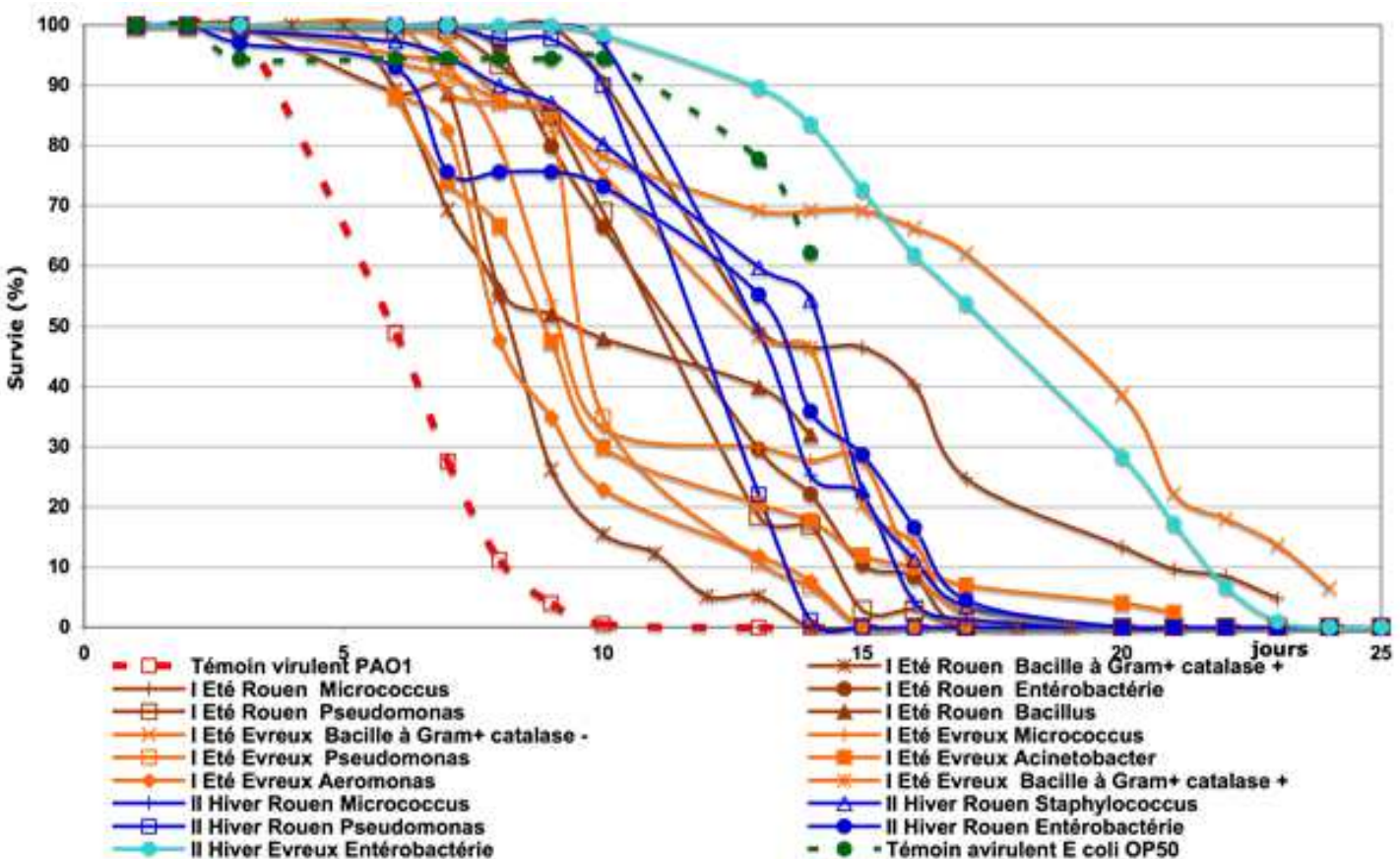


Figure 8 : Cinétiques de survie de *C. elegans* pour quelques souches bactériennes prélevées dans l'air urbain à Rouen ou à Evreux en période estivale ou hivernale.
Souche OP50 : témoin de non-virulence ; Souche PAO1 : témoin de virulence.

Traditionnellement les souches ayant une DL50 se situant entre 9 et 14 jours sont considérées de virulence intermédiaire, donc sans grand danger sanitaire pour des personnes en bonne santé, non immuno-déprimées. Suite à l'étude de virulence des souches représentatives, les populations bactériennes prélevées au niveau des silos ne présentent pas un danger plus important que celui de l'air urbain. (Morin et al., 2013).

Le test de survie de *C. elegans* a été adapté pour une culture globale de la population bactérienne récoltée lors du prélèvement, comme présenté Figure 9.

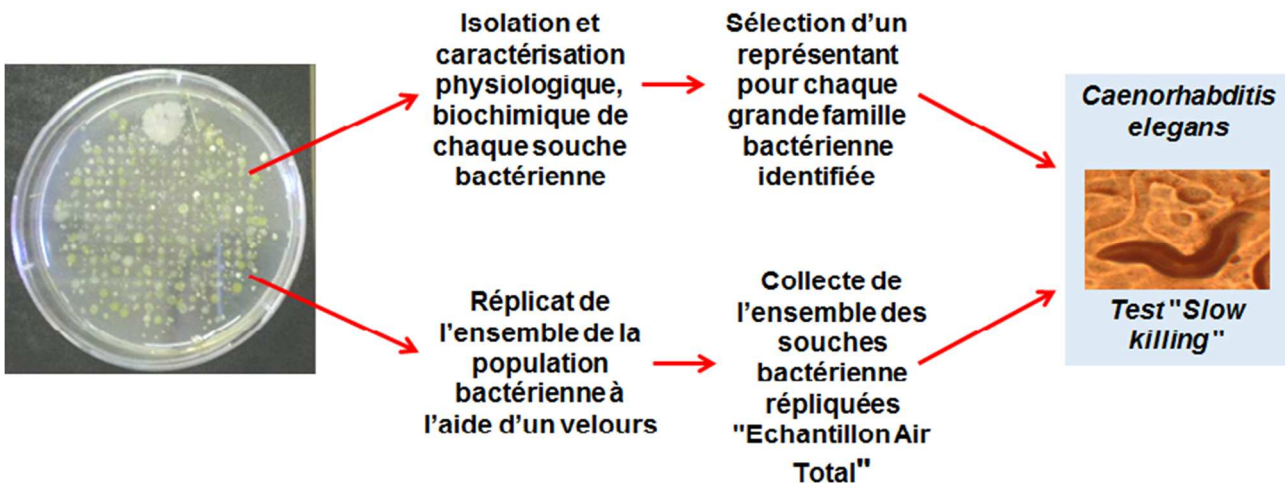


Figure 9 : Stratégie pour évaluer la virulence de bactéries aéroportées.

La cinétique de survie paraît constituer un bon indicateur de la virulence de l'ensemble des souches prélevées, comme présenté à la Figure 10.

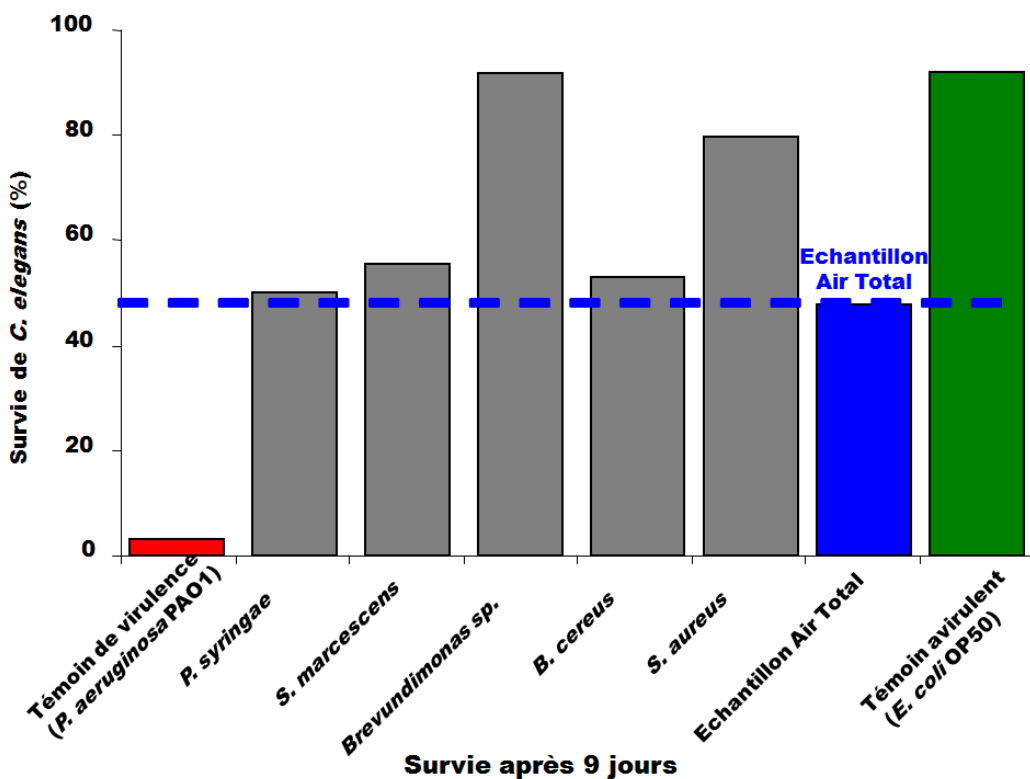


Figure 10 : Comparaison de la survie des nématodes *C. elegans* exposés aux bactéries à jour 9.

Ainsi l'établissement fastidieux de chacune des cinétiques de survie du nématode vis-à-vis de chaque isolat purifié ne s'avère pas nécessaire. Cette approche originale a permis de proposer un nouvel outil de surveillance de la qualité biologique de l'air (Duclairoir Poc et al., 2011).

Afin d'améliorer la fiabilité du traitement des données de survie du modèle nématode, avec mes collègues Dr A GROBOILLOT et O LESOUHAITIER, nous participons au projet régional PIFS (Plateforme Probabilités, Informatique Fondamentale et Statistique) dirigé par le Dr V BARBU (Laboratoire de Mathématiques Raphaël Salem, UMR 6085 CNRS de l'Université de Rouen-Normandie) qui désire travailler sur la modélisation de la survie en biologie.

D'autre part, lors des prélèvements hivernaux au cours de déchargements céréaliers sur les quais rouennais, les *P. fluorescens* et apparentées s'avèrent être présentes et prépondérantes (Duclairoir Poc et al., 2014). Malgré le caractère psychotrophe de l'espèce, quelques unes de ces souches aéroportées sont capables de se développer à 37°C, comme d'autres souches cliniques telles que *P. fluorescens*, MFN1032, rendant envisageable leur implication lors d'infections pulmonaires. Dans le cadre du FEDER « *Pseudomonas* Virulence », un post-doctorant, Dr VERDON, que je co-encadrais avec ma collègue Dr A GROBOILLOT, a caractérisé le biophysiome, à 30 et 37°C, de ces souches aéroportées (croissance, facteurs de virulence : mobilité, formation de biofilm, production d'exoproduits, systèmes de sécrétion), mais aussi leur sensibilité aux antibiotiques. Ainsi, au sein du panel bactérien, deux souches aéroportées modèles ont été sélectionnées : *P. fluorescens* MFAF76a et *P. putida* MFAF88, au vu de la similarité de leur biophysiome avec la souche *P. fluorescens* MFN1032, témoin clinique. Parallèlement avec l'aide d'une stagiaire spécialisée en protéomique (M1_5), le Dr VERDON a établi l'exoprotéome de ces souches aéroportées dans différentes conditions (culture à 28 ou à 37°C et phase de croissance fin d'exponentielle ou stationnaire avancée). Ces facteurs de virulence précédemment déterminés ont été corroborés à l'aide de trois modèles cytotoxiques : nématode *Caenorhabditis elegans*, amibe *Dictyostelium discoideum* et la lignée cellulaire pneumocytaire A549.

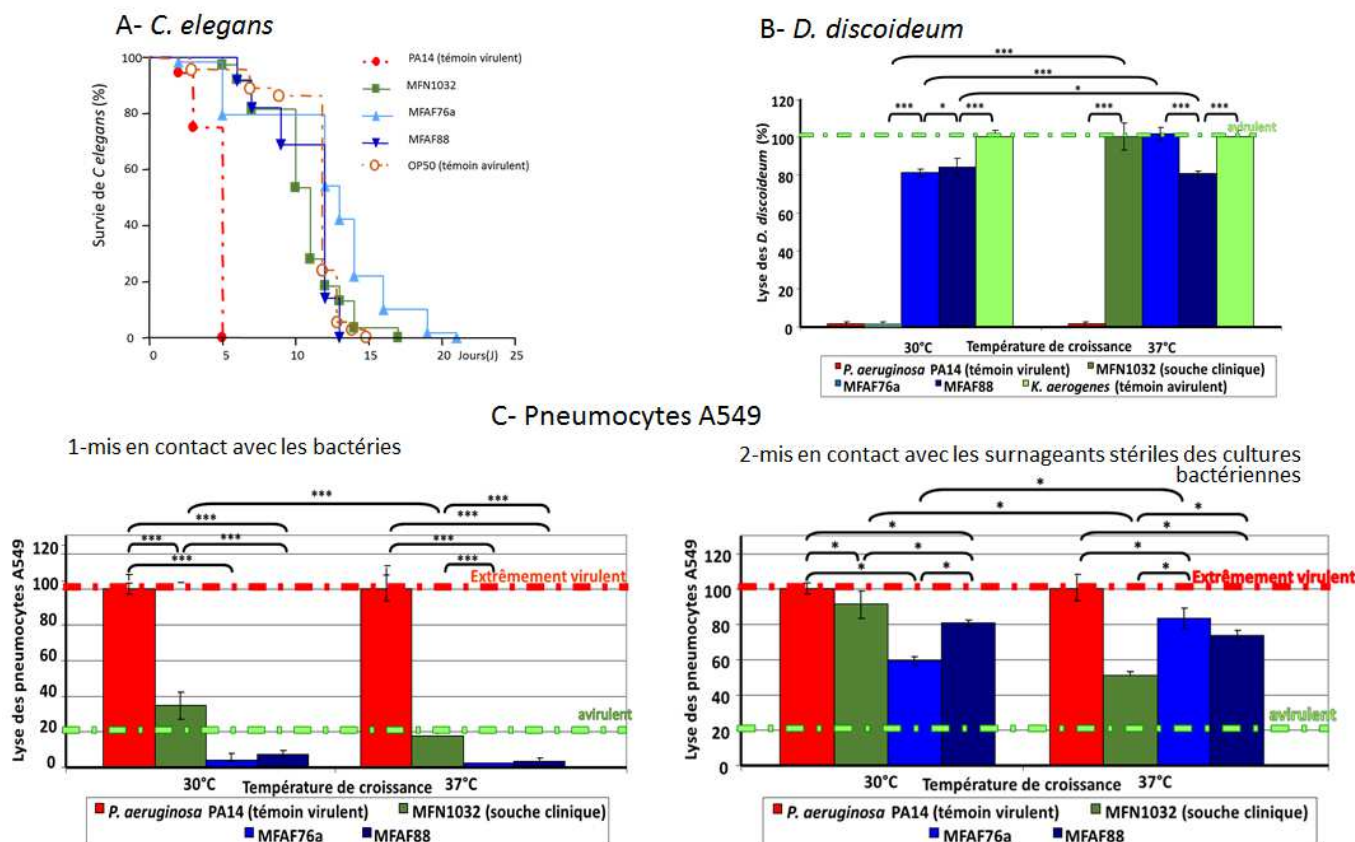


Figure 11 : Cytotoxicité des souches aéroportées MFAF76a, MFAF88 et clinique MFN1032 à l'aide de 3 types de modèle. A : *C. elegans* ; B : *D. discoideum* ; C : Pneumocytes A549. (* : P=0,05 ; ** : P=0,01 ; * : P=0,001).**

L'approche via le test *C. elegans* s'est avérée peu discriminante, Figure 11A, d'autant que la survie des nématodes est favorisée par la production de CLP bactériens (Bjørnlund et al., 2009), dont

les souches *P. fluorescens* MFN1032 et *P. putida* MFA88 sont productrices (Duclairoir Poc et al., 2014). *D. discoideum* mime l’interaction des macrophages humains avec les microorganismes en vue d’établir leur virulence (Pukatzki et al., 2006) en un test de courte durée (Carilla-Latorre et al., 2008). La souche MFN1032 présente une virulence uniquement à 30°C, Figure 11B, qui est corrélée à l’activité du système de sécrétion de type 3 (SST3) identifiée à 28°C (Sperandio et al., 2012), mais qui n’est plus fonctionnel à 37°C. L’absence de virulence observée pour les deux souches aéroportées vis-à-vis de *D. discoideum* laisse à penser que les souches MFAF76a et MFAF88 ne possèderaient pas ce type de SST3 fonctionnel à 30 et 37°C.

Mises en contact direct avec les pneumocytes A549, les trois souches ne démontrent aucune virulence significative, Figure 11C1. Cependant leurs surnageants de culture stérilisés provoquent une lyse patente des pneumocytes, mais variable selon les conditions. Grâce à leur sécrétion, Figure 11C2, les souches aéroportées MFAF76a et MFAF88 induisent une réponse inflammatoire des cellules pulmonaires, spécialement à 37°C, aussi le risque sanitaire correspondant n’est pas à négliger (Duclairoir Poc et al., 2014). De plus, dans une approche sanitaire rigoureuse, plusieurs modèles toxicologiques doivent être mis en œuvre simultanément afin de corroborer leurs résultats, pour éviter tout biais lié à des modèles peu sensibles ou trop spécifiques.

Production scientifique correspondante : P13 ; P20 ; Pdc2 ; C9 ; A13-A14 ; A18 ; A26 ; A30.

Encadrements : L6 ; M1_3 ; M2_3 ; PD1.

Cette incursion dans le domaine de l’air extérieur doublée de l’intérêt pour la sécurité sanitaire m’a naturellement menée à m’interroger à l’impact de différents stress sur la physiologie bactérienne, voire sa virulence. Aussi ma curiosité scientifique m’a entraînée à approfondir la concrétisation de la réponse bactérienne en me focalisant de plus en plus sur l’interface qu’est la membrane bactérienne lors de modifications de son microenvironnement lors de stress chimiques ou physiques.

V) Impact de stress sur l’adaptation et la virulence bactérienne

A) Stress biologique

(1) Signaux eucaryotes

(a) Acide γ -aminobutyrique (GABA)

Les BSs sont une des réponses bactériennes adaptatives à la pression environnementale, comme nous l’avons développé plus spécifiquement pour les CLPs. Pour l’espèce *Pseudomonas aeruginosa*, le rôle de ses BSs, les rhamnolipides, a été largement documenté dans l’adhésion bactérienne et la virulence (Fazli et al., 2014). Les thèses des Dr A Chapalain et A Dagorn (encadrées par les Pr S CHEVALIER et M FEUILOLEY) se sont intéressées à la communication entre bactéries de l’espèce *Pseudomonas* grâce à l’acide gamma aminobutyrique (GABA). Ce neurotransmetteur des animaux, et aussi molécule de défense chez les plantes, permet la communication inter-règnes et

présente la particularité d'être produit par certaines espèces bactériennes, dont les *Pseudomonas* (Lesouhaitier et al., 2009). Lors de notre étude, *P. fluorescens* MF37, en présence de faible de concentration de GABA, voit sa virulence modifiée comme chez *P. aeruginosa* PAO1, mais les mécanismes impliqués, modifications de surface et changement de profil de sécrétion, apparaissent différents chez ces deux espèces. Effectivement, j'ai établi que *P. fluorescens* MF37 n'est pas productrice de BS et sa virulence est reliée à la production d'exoproduits et aux variations structurales des liposaccharides. Cette altération des LPS a été pressentie au travers de la variation des propriétés de la surface bactérienne que j'ai évaluée à l'aide de tests Microbial Adhesion To Solvents (MATS) (Dagorn et al., 2013a). Un autre mécanisme de virulence a été démontré pour *P. aeruginosa* PAO1 qui produit des rhamnolipides. Cette production est modulée par le faible ajout de GABA. Suite à une fine analyse tensiométrique, j'ai pu aider à mettre en évidence l'évolution de l'activité tensioactive des rhamnolipides, dénotant une modification de leur nature liée à l'ajout de GABA (Dagorn et al., 2013b). Ainsi clairement la virulence de *P. aeruginosa* est contrôlée via la production de ses BSs par le GABA, molécule de communication inter-règnes.

(b) Substance P

La peau est un microbiome au sein duquel la flore bactérienne endogène est soumise à une multitude de signaux eucaryotes potentiellement capables d'en faire varier la virulence, avec les réactions inflammatoires cutanées bien connues des personnes à peau sensible. Le LMSM a commencé à explorer l'existence d'un lien entre signaux eucaryotes et virulence de ces bactéries cutanées dans le cadre du contrat FUI « Skin O Flor ». Dans ce contexte, l'effet de la substance P, molécule eucaryote cutanée (Lesouhaitier et al., 2009), a été évaluée sur la modulation de la virulence d'une bactérie endogène, *Bacillus cereus*.

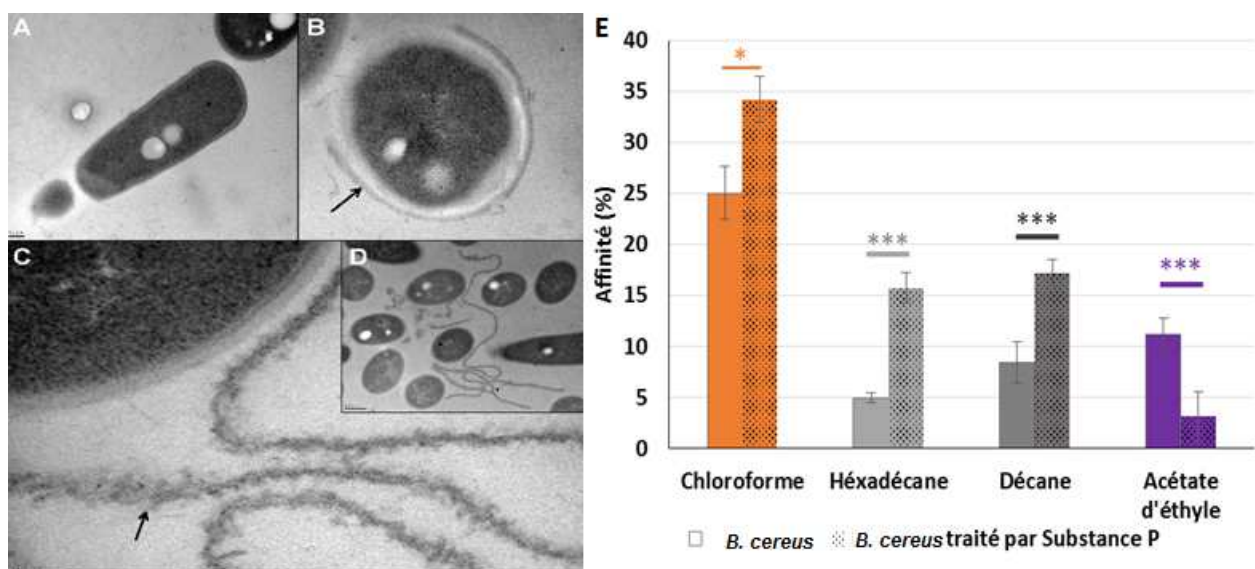


Figure 12 : Pelage de la S layer de *B. cereus* par la substance P. A: Coupe de microscopie électronique de la surface bactérienne intacte. B, C & D : Clichés de détachement de la S Layer (→) suite au traitement par la substance P. E : Affinité relative aux solvants de la souche *B. cereus* non-traitée et traitée par la substance P. (* : $P=0,05$; ** : $P=0,01$; * : $P=0,001$). Adaptée de Mijouin (Mijouin et al., 2013).**

Ma contribution a confirmé le mécanisme de relargage de facteurs de virulence : les protéines de la S layer bactérienne. Effectivement le phénomène de pelage de cette S layer, visualisée par microscopie à balayage (MEB) en Figure 12A-D, a été corrélée aux variations de polarité surfacique de *B. cereus* que j'ai quantifiées au travers de tests MATS, Figure 12E. Ce pelage de la S layer conduit à une augmentation de virulence bactérienne (Mijouin et al., 2013).

(c) Calcitonin Gene Related Peptide (CGRP)

Au LMSM, une autre molécule de signalisation eucaryote a été étudiée la Calcitonin Gene Related Peptide (CGRP). Elle est co-localisée et co-secrétée avec la Substance P dans la peau (Lesouhaitier et al., 2009). Son impact a été caractérisé sur une bactérie cutanée *Staphylococcus epidermidis*. Aucune variation parmi les facteurs de virulence secrétés n'est démontrée, alors que les propriétés de la surface bactérienne que j'ai quantifiées sont altérées. Cette augmentation d'hydrophobie bactérienne a été corrélée à une moindre adhésion de cette souche *S. epidermidis* sur kératinocytes (N'Diaye et al., 2016). Ainsi *S. epidermidis* est capable d'intégrer le signal CGRP et d'adapter en conséquence sa virulence.

Production scientifique correspondante : P16 ; P18-P19 ; P28 ; CInt2 ; C10-C11 ; C14 ; C30 ; A17 ; A20 ; A22-A25 ; A27-A29 ; A32 ; A34.

(2) Systèmes de sécrétion

En plus des stress biologiques liés aux sécrétions cellulaires eucaryotes, les bactéries doivent aussi faire face aux microorganismes sécréteurs. Comme décrit précédemment, la souche *P. fluorescens* MFN1032 présente un système de sécrétion de type SST3 fonctionnel à 28°C (Sperandio et al., 2012). Elle possède, de plus, selon des études bioinformatiques, un système de sécrétion de type 6, SST6. Les SST6 sont des nanomachines dédiés à l'injections d'effecteurs, directement de la bactérie à la cellule cible (Gallique et al., 2017). Au LMSM, j'ai collaboré à la caractérisation d'une autre souche *P. fluorescens* environnementale : MFE01. Elle présente un SST6 très actif.

Lors d'une co-culture avec la souche *P. fluorescens* MFE01, MFN1032 est confinée par MFE01 qui l'entoure Figure 15A-C. Ce phénomène n'est pas reproduit par le mutant de délétion MFE01 $\Delta hcp1$, mutant du SST6, mais conservé chez le mutant MFE01 $\Delta hcp2$ qui endigue le swarming de MFN1032, Figure 15 A&B. Les gènes *hcp1* et *hcp2* codent pour deux protéines Hcp différentes, présentes chez la souche MFE01, mais absente pour MFN1032, Figure 15D.

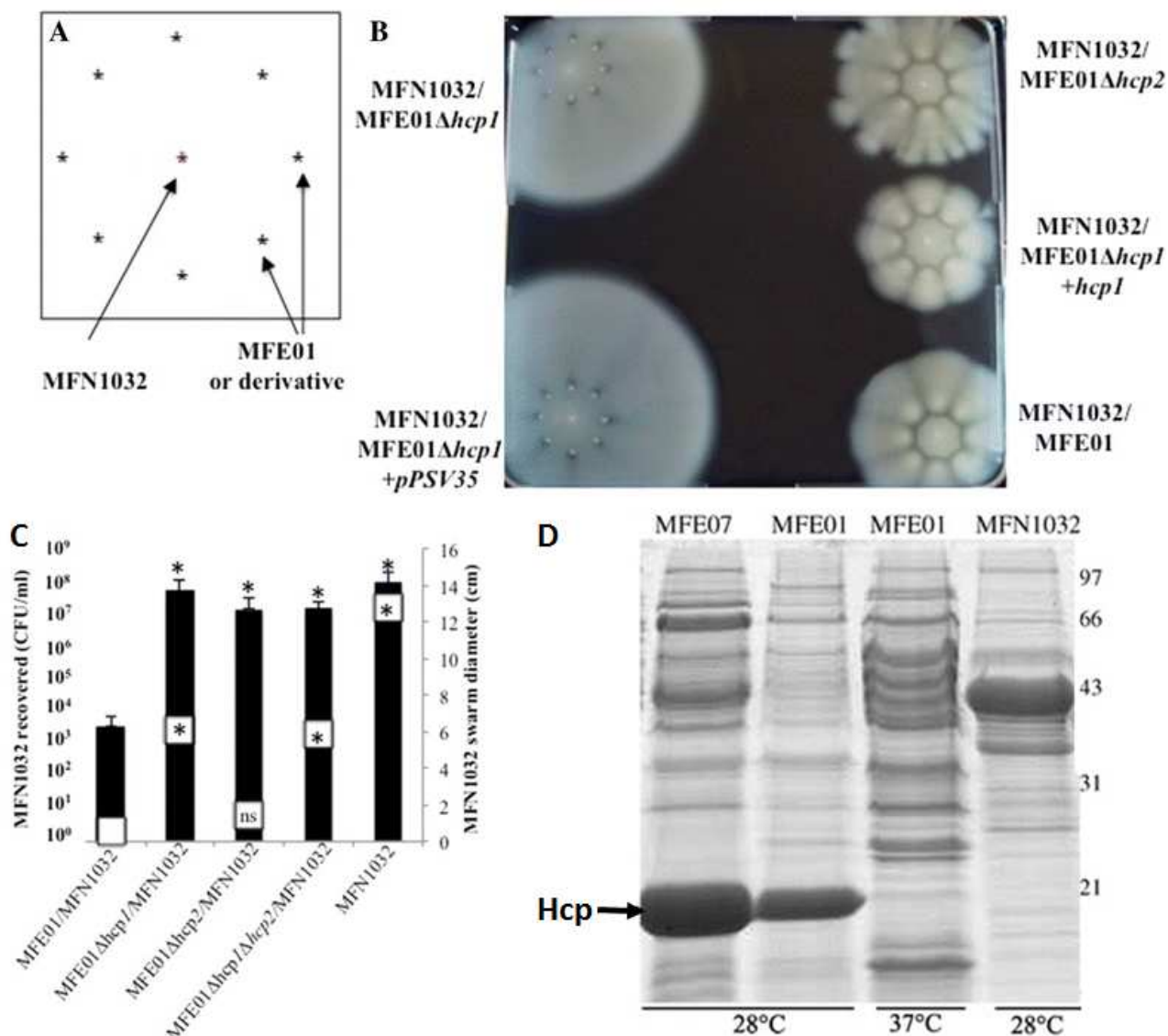


Figure 13 : Effet de *P. fluorescens* MFE01 et de ses mutants en co-culture bactérienne. A: Plan expérimental : *P. fluorescens* MFN1032 entourée concentriquement par MFE01 et ses mutants. B: Swimming de MFN1032 en co-culture avec MFE01 ou ses mutants. C: Survie de MFN1032 (histogramme) et diamètres de swarm de MFN1032 (\square). D: Elution sur SDS-PAGE des surnageants concentrés de culture en phase exponentielle de MFE07, MFE01 et MFN1032 à 28°C et MFE01 à 37°C. La protéine Hcp, majoritaire à 28°C, a été identifiée par spectrométrie de masse. (* : $P=0,05$). Adaptée de Decoin (Decoin et al., 2015).

Ces protéines sont constitutives du SST6 et en démontrent la fonctionnalité lors d'interactions avec des hôtes par contact direct. La souche MFE01 est capable en réponse à son microenvironnement d'adopter une stratégie antibactérienne. En relation avec Hcp1, elle limite la mobilité d'autres souches. Par Hcp2, elle exerce une activité bactéricide (Decoin et al., 2015).

Production scientifique correspondante : P25 ; A31.

Le SST6 est présent chez certaines de nos souches aéroportées, aussi avec ma collègue le Dr MERIEAU, nous aimerais confirmer leur activité et évaluer leur expression en situation de stress exogène chimique, par exemple.

B) Stress chimique : la pollution diésel promeut-elle la virulence bactérienne via sa propre réponse adaptative ?

Pour poursuivre la dynamique initiée par le projet qualité de l'air et intéressée par l'aspect pulmonaire suite à l'adaptation du modèle cytotoxique A549, j'ai proposé de poursuivre dans une démarche de sécurité sanitaire en étudiant, à l'aide de quelques souches de *Pseudomonas* collectées, l'influence de polluants tels que les oxydes d'azote sur leur physiologie, leur potentiel d'adaptation et leur virulence.

«La pollution est la plus grande cause environnementale de maladies et de décès dans le monde aujourd'hui, responsable d'environ 9 millions de décès prématurés» a statué dernièrement la commission du Lancet (Landrigan et al., 2018). Parmi ces contaminants, les oxydes d'azote, NOx, et plus particulièrement le dioxyde d'azote, NO₂, sont nommément identifiés comme des polluants très préoccupants pour la santé publique par l'OMS (WHO Regional Office for Europe, 2013) et marqueurs de la pollution automobile (*Air quality in Europe — 2017 report*, 2017). Ainsi dès 2012, l'ANSES a fait une de ses priorités les conséquences du NO₂ pour la qualité de l'air. Or ce dernier est réputé pour favoriser le développement d'infections pulmonaires, principalement bactériennes (Latza et al., 2009).

Traditionnellement les épidémiologistes expliquent l'augmentation de pneumopathies d'origine bactérienne par une immunodépression humaine consécutive au caractère irritant des polluants sur les tissus pulmonaires facilitant ainsi la colonisation bactérienne (Silveyra et al., 2017). Notre approche a été de documenter une argumentation alternative : la pollution pourrait augmenter (aggraver) la virulence bactérienne *per se* ce qui favoriserait l'infection plus aisée de l'hôte humain par les bactéries en contact avec la pollution. Lors d'une étude au sein de services d'urgences européens, les *Pseudomonas* spp. s'avèrent l'un des genres bactériens prépondérants (14%) de ces cas pulmonaires et qui accroissent le taux de mortalité (Vincent et al., 2006).

Nous avions envisagé différentes approches d'exposition : culture liquide bactérienne, aérosolisation ou monocouche bactérienne. Au vu de la question sanitaire à laquelle nous voulions répondre, nous avons favorisé l'approche par contact le plus direct polluant gaz/ bactérie, surtout en s'affranchissant au maximum du facteur eau qui pourrait facilement interférer et altérer la répétabilité de notre système d'étude. Ainsi le périmètre de notre approche aurait été modifié en ne nous limitant plus au stress nitrosant, mais en élargissant au stress oxydant plus globalisant. Cette réflexion s'est accompagnée d'un dépôt de lettre d'intention auprès de l'ANSES au printemps 2011, non retenue. Cependant notre projet a été financé au travers du projet Européen-Etat-Région Virulence *Pseudomonas* finançant 18 mois de stagiaire postdoctoral (les Dr J VERDON et M BONNIN-JUSSERAND) et 40k€ d'équipement. Grâce à cette dotation, le LMSM a pu acquérir un tensiomètre Krüss DSA30 qui a soutenu toute la caractérisation des BSs évoquée lors des parties précédentes, mais aussi les fournitures pour le prototype d'exposition, dont la conception et la réalisation

n'auraient pu avoir lieu sans l'appui du CERTAM et les mains expertes des Dr F GOURIOU et D PRETERRE.

Le genre bactérien *Pseudomonas* est connu pour contrecarrer le stress nitrosant provoqué par NO₂ et son congénère NO grâce à la mise en œuvre de stratégies de dénitritification impactant leur perméabilité membranaire et leur régulation protéique (Arai, 2011; Van Alst et al., 2007). Le phénomène plus global qu'est le stress oxydant, entraîne une modulation de la régulation lipidique et de la virulence. Suite à ces stress, les biomolécules (ADN, lipides, protéines) subissent des dommages délétères (Spiro, 2007). Après un travail de sélection des modèles bactériens d'intérêt et de leur caractérisation en parallèle du témoin clinique *P. fluorescens* MFN1032 mené par le Dr J VERDON, une seconde post-doctorante, le Dr M BONNIN-JUSSERAND a défriché la méthodologie d'exposition, dont la préparation du matériel biologique, et a réalisé des essais préliminaires avec un mélange (NO/NO₂/O₂/N₂). Parallèlement, pressentant que, suite aux expositions, les bactéries pourraient ne subir que des variations modérées de virulence, avec un étudiant de Master 2 (M2_3), j'ai adapté un test cytotoxique vis-à-vis des amibes *Dictyostelium discoideum* permettant d'avoir une quantification graduée de virulence bactérienne.

Concomitamment, au début 2012, j'ai déposé un dossier ANR Jeune Chercheur-Jeune Chercheuse intitulé NitroBactAIR, ayant obtenu la labellisation du pôle de compétitivité MOV'EO, mais non retenu pour financement par l'ANR. Profitant de ce dossier, j'ai postulé au printemps pour une bourse de thèse en région Haute-Normandie. Ainsi à partir d'octobre 2013, j'ai été la responsable scientifique de la thèse de T KONDAKOVA, financée par le GRR SSE et sous la co-direction du LMSM (Pr N ORANGE) et du CERTAM (Dr F DIONNET). Ce projet a visé tout d'abord à compléter les outils d'étude de la virulence et plus spécifiquement du stress nitrosant par la mise au point de la caractérisation des lipides bactériens par HPTLC couplée au MALDI-TOF/TOF (lipidome) de souches de *P. fluorescens*, puis de réaliser des expositions bactériennes.

(1) Implémentation de l'imagerie HPTLC-MALDI TOF MS et application à l'étude du lipidome de bactéries *P. fluorescens*

La technique innovante d'analyse des lipides par HPTLC couplée au MALDI-TOF/TOF a été adaptée aux lipides bactériens et décrite à la Figure 14 (Kondakova et al., 2015b, 2017). Ainsi une expertise a été acquise sur le lipidome des *Pseudomonas* spp. (Kondakova et al., 2015a). Cette concrétisation a été permise grâce à l'expertise du dépouillement spectral du Dr N MERLET-MACHOUR de l'UMR COBRA (Université de Rouen-Normandie).

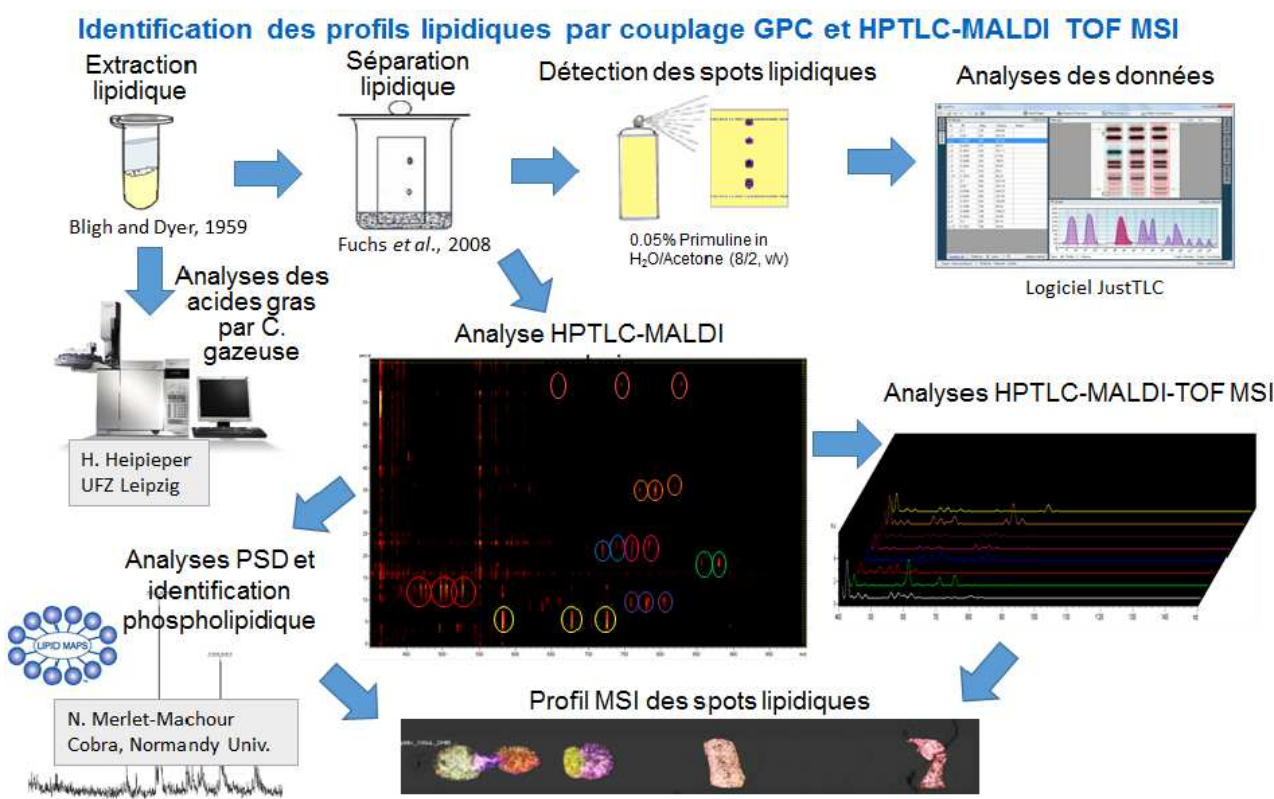


Figure 14 : Principe de la lipodomique couplant analyse des acides gras et imagerie HPTLC-MALDI TOF MS

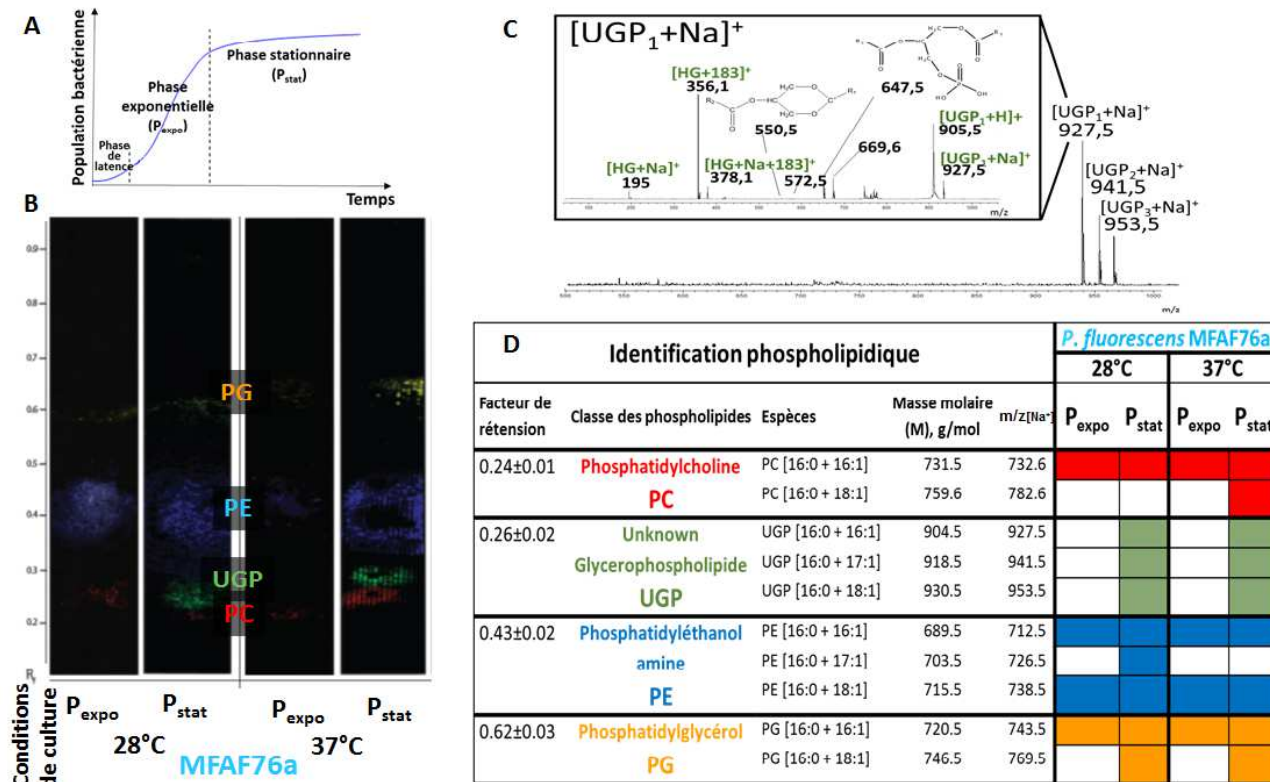


Figure 15 : Lipidome de la souche *P. fluorescens* MFAF76a selon les phase et température de croissance. A : profil d'une courbe de croissance bactérienne. B : Profils HPTLC-MSI en phase exponentielle (P_{expo}) et stationnaire (P_{stat}) à 28 et 37°C. C : spectre MSMS du phospholipide inconnu, UGP. D : Synthèse de l'analyse lipidomique selon les phases et températures de croissance.

Les lipidomes de la souche aéroportée *P. fluorescens* MFAF76a et de son témoin clinique MFN1032 ont été établis en fonction des conditions de croissance : température (28 et 37°C) et phase physiologique exponentielle (P_{expo}) et statique (P_{stat}), rappelées en Figure 15A. Les profils HPTLC MALDI TOF MSI de MFAF76a sont présentés en Figure 15B.

Trois familles lipidiques sont systématiquement identifiées : la phosphatidylcholine (PC ; R_f 0.24±0.01 – colorée en rouge), la phosphatidyléthanolamine (PE ; R_f 0.43±0.02 – en bleu) et le phosphatidylglycérol (PG ; R_f 0.62±0.03 – en jaune) (Kondakova et al., 2015b). Les PE et PG sont les lipides "communs" dans le lipidome bactérien et jouent un rôle incontournable dans la structuration de la paroi bactérienne (Kondakova et al., 2015a). Par contre, la présence de la PC est inhabituelle dans le lipidome des procaryotes (Fuchs et al., 2007) et est un composant majeur de la membrane des eucaryotes. C'est également le phospholipide principal du plasma, constituants des lipoprotéines et du cholestérol (Cole et al., 2012). Il est cependant rarement retrouvé dans le lipidome bactérien (uniquement pour environ 10% des espèces bactériennes) (Cole et al., 2012; Kondakova et al., 2015a).

Un quatrième spot est observé avec un R_f 0.26±0.02, (Figure 15B, coloré en vert). Les données accumulées par MS et MS tandem, présentées à la Figure 15C, ne nous a pas encore permis l'identification complète de ce phospholipide, codé UGP pour unknown glycerophospholipid. La fragmentation suite à la MSMS semble typique de celle décrite pour les phospholipides par Al-Saad (Al-Saad et al., 2003), avec des réarrangements spécifiques pour la tête polaire (HG). Certains des pics présents en MSMS sont similaires à ceux du PG. La similitude des acides gras a été confirmée par notre collaborateur le Dr H HEIPIEPER, Figure 15D, mais le m/z est nettement plus important que celui du PG, et pourrait laisser pressentir des Phosphatidylinositol 4,5-bisphosphates (PIP) qui possèdent eux habituellement 4 chaînes d'acides gras. Cependant la fragmentation n'est pas compatible avec de tels PLs.

D'autre part un autre PL, la cardiolipine (CL) est fréquemment constitutive des membranes bactériennes (Grimard et al., 2014) dont celles de certaines *Pseudomonas* (Fouchard et al., 2005; Kondakova et al., 2015a). Cependant sa détection peut être aléatoire selon le type de technique d'analyse mise en œuvre (Romantsov and Wood, 2017), même si l'approche couche mince assure sa révélation (Cronan, 2003). La biosynthèse de la CL est décrite chez les bactéries via la réaction de deux molécules de PG (Kondakova et al., 2015a; Ortega et al., 2017), ou, plus rarement à partir de PG et PE (Dowhan et al., 2017). L'analyse *in silico* du génome de *P. fluorescens* MFAF76a, Figure 16, réalisée dernièrement par S DEPAYRAS, a visé à mieux caractériser cette voie métabolique chez *P. fluorescens* MFAF76a et a mis en évidence l'existence de la machinerie de production de la CL, sans que sa production ne soit effectivement observée.

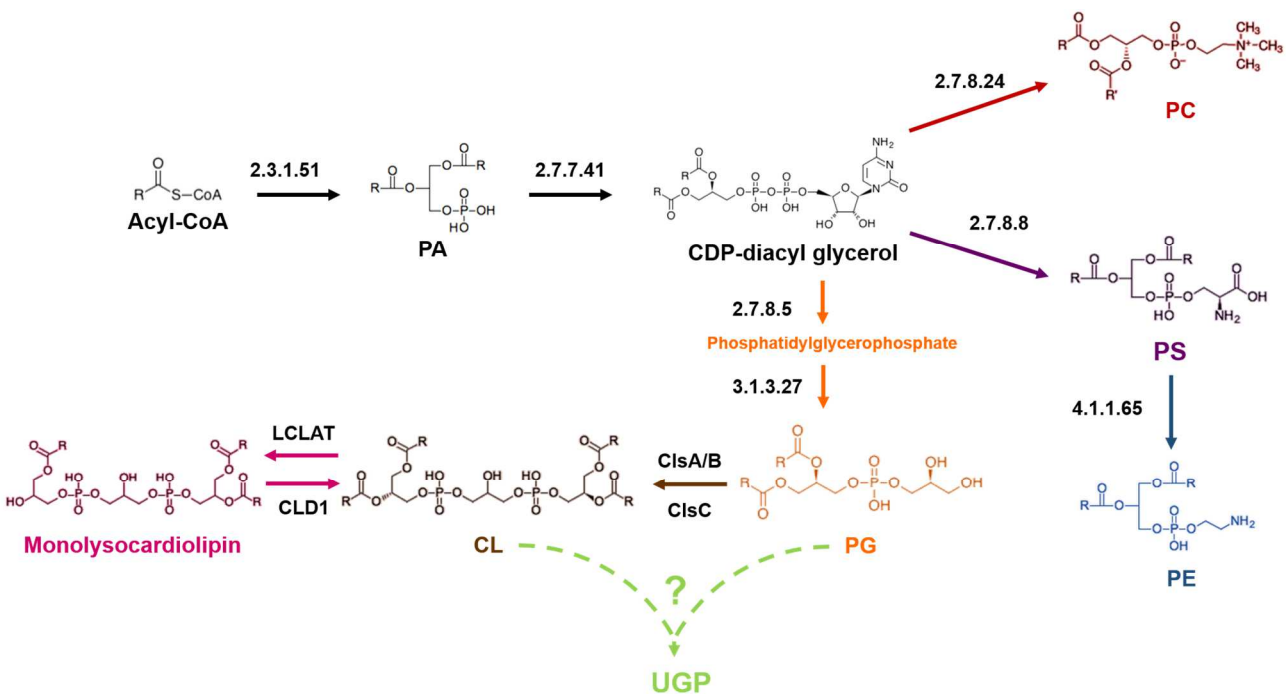


Figure 16 : Analyse *in silico* de *P. fluorescens* MFAF76a concernant le métabolisme des glycérophospholipides.

Ce faisceau de données couplé à la valeur de m/z de 905 nous interroge et nous permet d'émettre l'hypothèse que l'UGP pourrait être un « hybride » de la CL, il pourrait ne compter que 3 chaînes d'acides gras au lieu des 4 usuelles. L'UGP1 pourrait avoir la structure présentée en Figure 17, correspondant à un m/z de 905. Grâce à une collaboration avec le Pr A CORCELLI (Università degli Studi di Bari, Italie), nous espérons mener à bien cette identification.

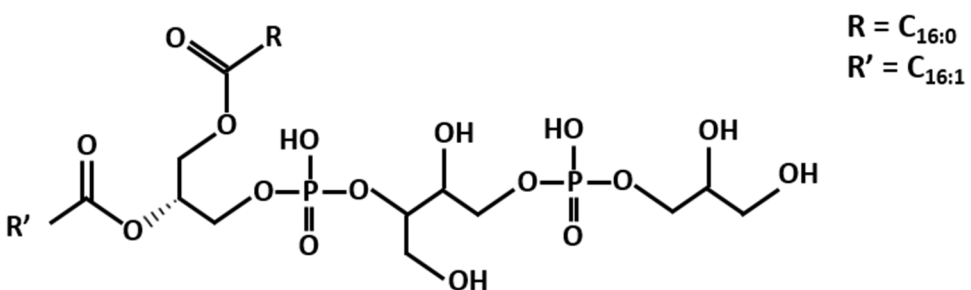


Figure 17 : Structure hypothétique de l'UGP1

D'autre part, cet UGP ne s'avère qu'être produit en phase stationnaire à 28°C et 37°C, mais sa révélation n'est pas toujours systématique. Un profil similaire est obtenu pour *P. fluorescens* MFN1032 à l'exception d'un cinquième spot supplémentaire au R_f 0,50 qui correspond à la viscosinamide A (communication personnelle).

Pour compléter ce lipidome, l'analyse des acides gras a été réalisée par T KONDAKOVA au Helmholtz Institute, chez le Dr H HEIPIEPER (Leipzig, Allemagne), ce qui lui a permis d'obtenir le label de doctorat européen. Comme le montre le lipidome de la souche aéroportée à la Figure 15D, la composition globale en PLs ne varie ni avec la température, ni avec la phase de croissance. Cependant des modifications à la marge concernent les longueurs de chaînes latérales, qui se traduisent par une augmentation du degré de saturation à 37°C par rapport à 28°C. Ce phénomène est connu chez les

Pseudomonas spp. pour préserver leur stabilité membranaire (Mansilla et al., 2004). Ainsi pour endiguer une élévation de la température, ces bactéries synthétisent davantage d'acides gras saturés pour maîtriser les propriétés de leur bicouche lipidique.

Production scientifique correspondante : P21 ; P24 ; Ch3 ; C15-C17 ; A35 ; A37 ; A38.

Encadrements : M1 Imm_11->M1 Imm_12 ; D2-D3.

(2) Mise en place de l'exposition bactérienne

(a) Matériel biologique

Lors de ses travaux doctoraux (2012-2015), le Dr T KONDAKOVA a finalisé un système original, Figure 18, mettant en contact direct les bactéries avec le gaz polluant (Kondakova et al., 2016), contrairement à d'autres installations exposant des cultures bactériennes liquides (Spiro, 2008).

Suite à une préculture en milieu pauvre (Davies Minimum Broth), les bactéries sont ensemencées sur des filtres à hauteur de 3.10^7 bactéries par filtre sous la forme d'une monocouche, qui, après avoir été déposée sur une gélose DMA, est incubée pendant 4h. Ensuite, les filtres sont transférés sur une gélose qui sera alors déposée dans une des chambres d'exposition.

Le système d'exposition permet d'exposer la même culture dans deux chambres d'exposition thermostatées et à humidité contrôlée : une première est sous flux d'air synthétique et la seconde sous atmosphère polluée, soit de l'air synthétique additionné du polluant choisi.

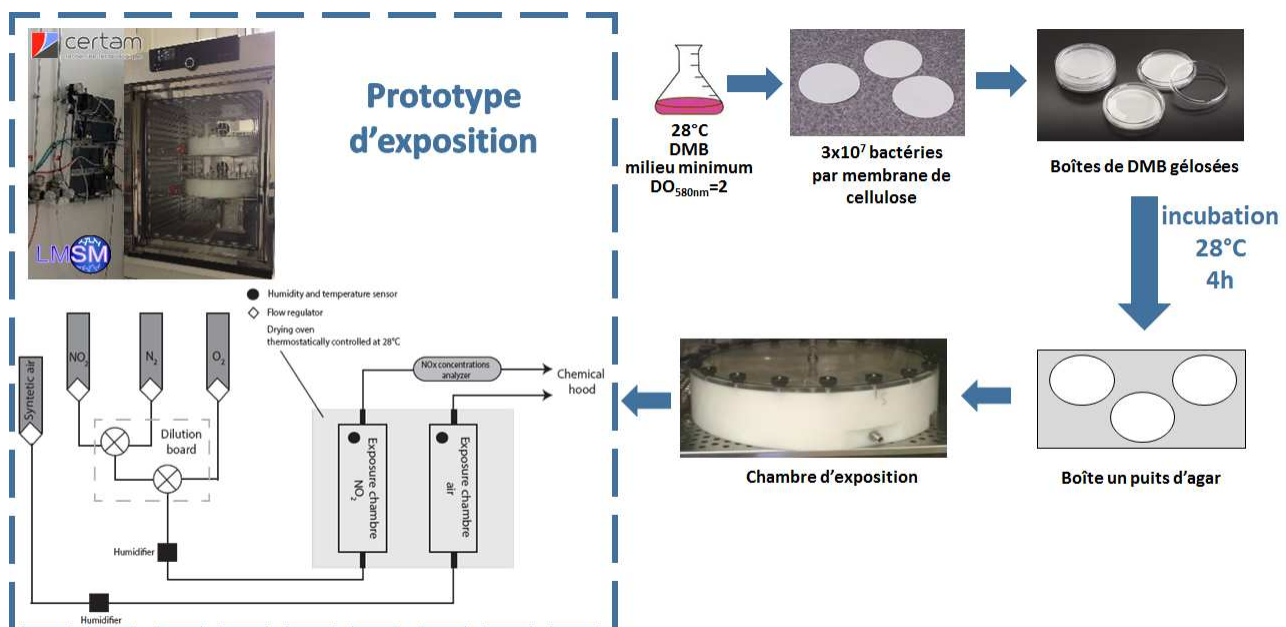


Figure 18 : Procédé d'exposition de bactéries en monocouche à un polluant gazeux.

Ainsi, ce système permet l'exposition concomitante de bactéries issues de la même culture en présence ou non de polluant(s), de façon à mimer l'exposition réelle aux polluants atmosphériques.

(b) Choix et concentration en polluant

Parmi ces contaminants, les oxydes d'azote, NOx, et plus particulièrement le dioxyde d'azote, NO₂, sont nommément identifiés comme des polluants très préoccupants pour la santé publique par l'OMS (WHO Regional Office for Europe, 2013) et marqueurs de la pollution automobile (*Air quality*

in Europe — 2017 report, 2017). D'origine principalement anthropogénique, les oxydes d'azote sont loin d'être des molécules inconnues dans le monde biologique. Effectivement les NOx interagissent avec de nombreux matériaux biologiques ; ainsi ils provoquent l'altération de membranes biologiques et de nombreuses biomolécules telles que les protéines, les lipides voire l'ADN, entraînant de nombreuses pathologies. Dans le chapitre "The hidden face of Nitrogen oxides species – from toxicity effect to potential cure?" du livre « Emerging Pollutants » (Depayras et al., 2018a), nous avons compilé les méfaits des radicaux libres NO et NO₂, liés à leur électron non-apparié (Figure 19A), mais aussi leur potentiel en thérapie humaine. Cependant, en qualité de l'air, depuis 2012, l'Agence nationale de sécurité sanitaire de l'alimentation, de l'environnement et du travail (ANSES) a fait une de ses priorités les conséquences du NO₂ sur la santé humaine. Or ce dernier est réputé pour favoriser le développement d'infections pulmonaires, principalement bactériennes (Latza et al., 2009).

L'impact d'un polluant aéroporté est fonction de sa concentration et de la durée d'exposition. Suite à des revues, les organismes sanitaires de référence ont émis des limites toxicologiques (Figure 19B &C) pour chacun de ces deux radicaux desquelles les instances gouvernementales se sont inspirées pour établir des limites environnementales (Figure 19D & E).

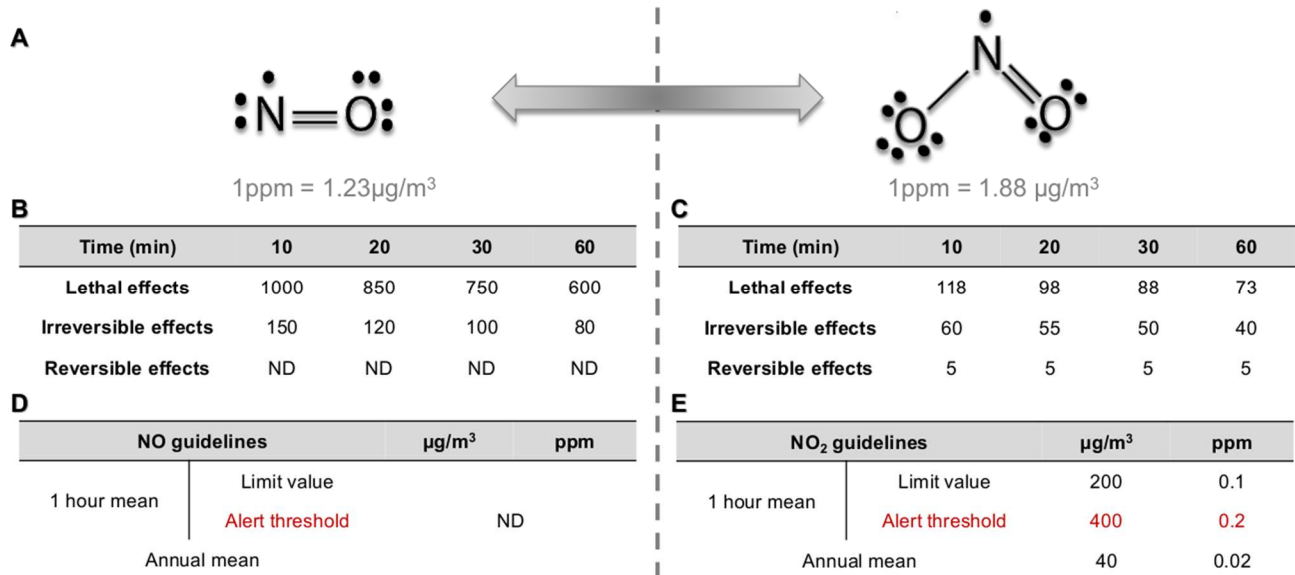


Figure 19 : Caractéristiques clefs des NOx. A: leur structure de Lewis et facteur de conversion. B: seuils du NO (ppm) (Bisson et al., 2011); C: seuils du NO₂ (ppm) (Bisson et al., 2011); D et E: Valeurs limites du NO et du NO₂ respectivement (*Air quality in Europe — 2017 report*, 2017); ppm: partie par million; ND: non déterminée.

Concernant les références toxicologiques, l'effet létal correspond aux concentrations en NO ou NO₂ en deçà desquelles aucune mortalité n'est observée chez la population exposée. Quant aux effets réversibles ou irréversibles, ils décrivent le constat de pathologies humaines réversibles ou irréversibles dans la population exposée.

Les moyennes horaires d'exposition en NO₂ pouvaient excéder 940 µg/m³ (0,5 ppm) à proximité d'un trafic chargé (Svartengren et al., 2000). Depuis une quinzaine d'année, la réglementation est devenue davantage contraignante suite aux signatures de la convention de Genève et des protocoles de Kyoto, Gothenburg et Paris (Europe and Unece, 2015). Ainsi cette moyenne horaire en habitacle automobile

a été évaluée entre 200 à 250 µg/m³ (>0,1 ppm) de NO₂ (Morin et al., 2009). Cependant la lettre Recherche N°21 de l’ADEME indique des pics de concentrations en NOx 9 fois supérieures à celles à l’extérieur de l’habitacle (Adème, 2017).

Les concentrations choisies en NO₂ lors de cette étude, dans un premier temps, ont pour objectif de décrire 3 cas très différents (Kondakova et al., 2016) :

* une situation « environnementale » où la qualité de l’air est saine: 0,1 ppm ;

* une situation critique où des effets réversibles sur la santé humaine peuvent se produire :

5 ppm,

* et enfin une situation toxique pour laquelle des effets irréversibles seraient observés en santé humaine : 45 ppm.

Dans la suite de cette étude, d’autres concentrations seront envisagées, dont la concentration de 0,2 ppm pouvant correspondre à une concentration en NOx observable ponctuellement dans un habitacle automobile dans un tunnel parisien (Morin et al., 2009) !

Production scientifique correspondante : P21 ; Ch4 ; A33 ; A35.

Encadrements : D2-D3 ; PD2-PD3.

(3) Impact du NO₂ sur la physiologie et la virulence des souches *P. fluorescens* aéroportée MFAF76a et clinique MFN1032

La seconde partie des travaux doctoraux du Dr T KONDAKOVA a été de caractériser l’impact de l’exposition au NO₂ sur le biophysiome des souches *P. fluorescens* aéroportée MFAF76a et clinique MFN1032. Afin de poursuivre ces travaux présentés lors de la soutenance du doctorat européen du Dr T KONDAKOVA (20 Novembre 2015), j’ai déposé une lettre d’intention auprès de l’ANSES dès janvier 2014 intitulée «Impact du NO₂ gaz sur la virulence d’une bactérie aéroportée : stratégies de dénitrification et de mobilité membranaire », non retenue. Suite au dépôt d’une demande régionale d’allocation doctorale, sélectionnée et financée par le GRR haut-normand SéSa (Sécurité Sanitaire), j’assure la responsabilité scientifique et le co-encadrement, avec le Pr N ORANGE, de S DEPAYRAS depuis septembre 2015 (soutenance d’ici fin 2018) sur la consolidation et l’approfondissement des résultats précédemment acquis.

(a) Approche lipidomique

Mettant à profit l’implémentation de l’imagerie HPTLC MALDI TOF MS complétée par l’analyse des acides gras lors de ses séjours en Allemagne auprès du Dr H HEIPIEPER (Helmoltz Institute, Leipzig, Allemagne), le Dr T KONDAKOVA a caractérisé les lipidomes de la souche *P. fluorescens* aéroportée MFAF76a et de son témoin clinique MFN1032 suite à leur exposition à trois concentrations : 0,1 ; 5 et 45 ppm en NO₂. La Figure 20 met en évidence que seul le lipidome résultant de l’exposition à 45 ppm est significativement altéré par rapport à celui du témoin (exposition à l’air synthétique).

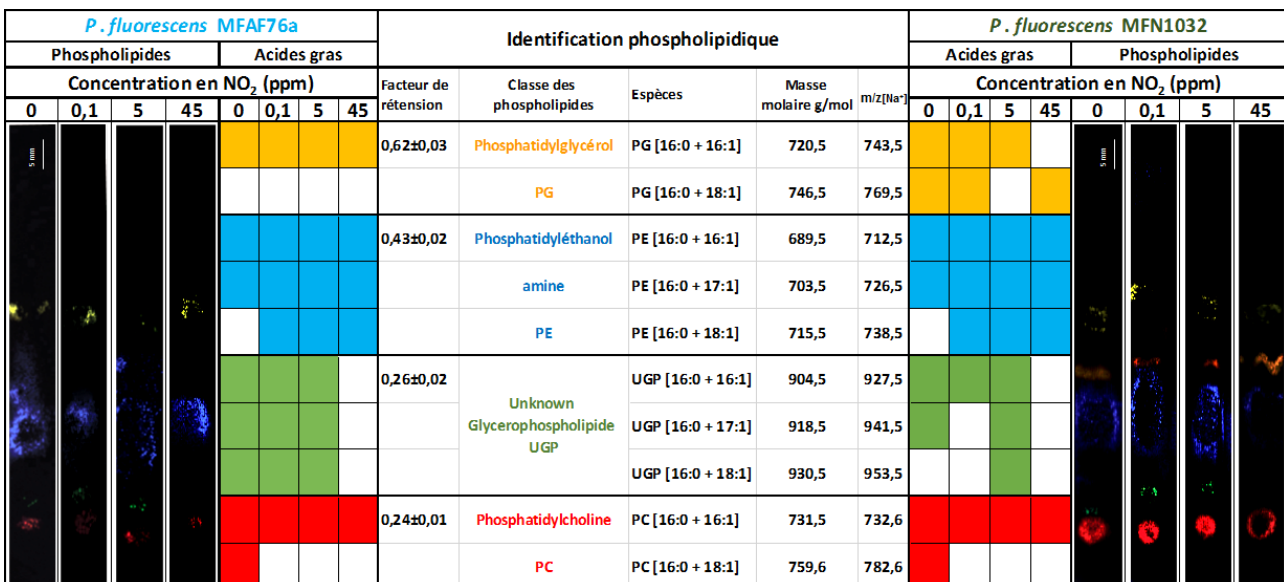


Figure 20 :Lipidome des souches *P. fluorescens* MFAF76a et MFN1032 suite à leur exposition à 0 ; 0,1 ; 5 et 45 ppm de NO₂. Synthèse de l’analyse lipidomique : profils HPTLC-MSI et analyse des acide gras.

La disparition de l'UGP est constatée pour les deux souches étudiées à 45 ppm de NO₂. Quant aux autres familles de phospholipides, PE, PC et PG restent présentes, mais leur profil en acides gras se trouve modifié selon la concentration en NO₂. La souche aéroportée laisserait entrevoir que les longueurs de chaînes seraient moindres aux fortes teneurs en NO₂ pour PC et PG au contraire de PE, la réponse de la souche clinique n'est pas aussi tranchée. Tout en étant le produit de nombreuses biomolécules essentielles (acides gras, acide phosphatidyl, diacylglycérol), PE est connu pour être le phospholipide prépondérant chez les *Pseudomonas*, structurant leur membrane bactérienne et principalement cytoplasmique (Grimard et al., 2014). Aussi pour assurer sa survie en évitant la déstabilisation de sa propre paroi, la bactérie peut être amenée à privilégier la variété de ce PL (longueur de chaînes, insaturation) par rapport à d'autres PLs minoritaires. L'existence de chaînes d'acide gras en C₁₈ est uniquement observée pour PE lors du stress drastique qu'est l'exposition à 45 ppm de NO₂. Ceci pourrait s'expliquer par le coût énergétique non négligeable que représente l'allongement des chaînes d'acide gras de 2 C (C₁₆->C₁₈) (Marella et al., 2018). Cet allongement n'est qu'uniquement observé pour le PE, PL primordial du point de vue prépondérance et structuration au niveau membranaire (Grimard et al., 2014; Kondakova et al., 2015a). Cependant l'altération des chaînes grasses reste modérée, aucune modification drastique des spectres de MS n'a démontré la réaction du NO₂ avec les lipides conduisant à l'apparition d'adduits hydroperoxydes, alcools ou aldéhydes (Möller et al., 2008). Ceci est largement décrit chez les eucaryotes, connus pour leurs teneurs membranaires importantes en acides gras polyinsaturés (Augusto et al., 2002), ce qui n'est pas la caractéristique des deux bactéries étudiées, qui ne possèdent que des monoinsaturations (Figure 20).

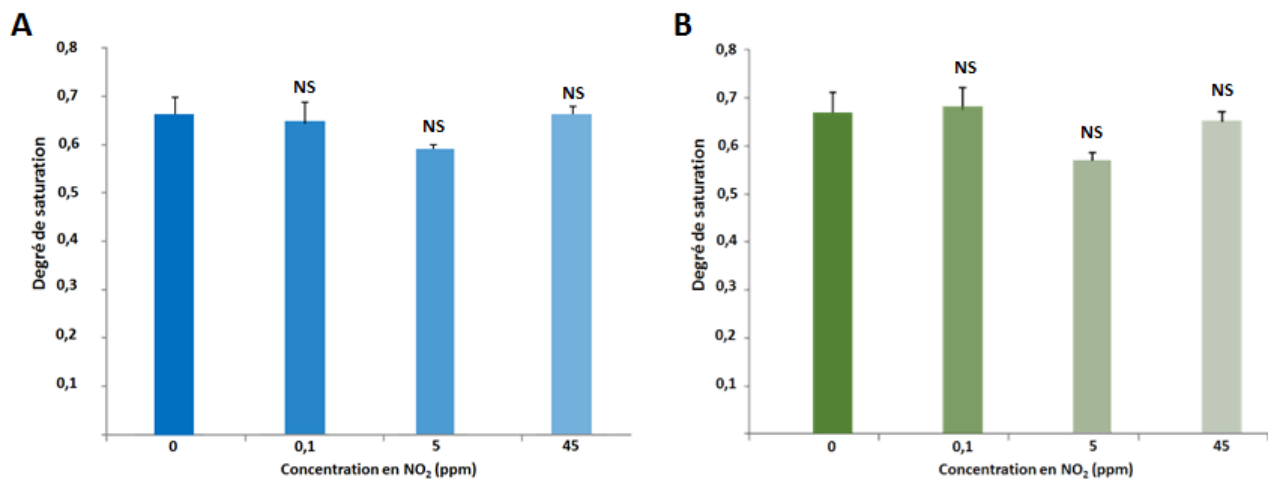


Figure 21 : Degré de saturation en acides gras des souches *P. fluorescens* MFAF76a et MFN1032 suite à leur exposition à 0 ; 0,1 ; 5 et 45 ppm de NO₂. NS : non significatif ($P>0,05$)

Le degré de saturation des acides gras, selon la souche et la concentration en NO₂, présenté en Figure 21, n'évolue pas, par conséquent la libre diffusion du NO₂ est confirmée au travers de la membrane bactérienne, confortant la simulation de Signorelli démontrant que les lipides membranaires ne font pas obstacle au transport du NO₂ (Signorelli et al., 2011).

Au vu de son caractère lipophile, le NO₂ pourrait s'accumuler dans la membrane (Fukuto et al., 2000). Bien que ne réagissant pas avec les lipides, il pourrait réagir avec d'autres constituants (protéines, liposaccharides) (Cheng et al., 2013). Aussi nous avons envisagé d'évaluer les propriétés de surface à l'aide du test Microbial Adhesion To Solvents (MATS) suite aux expositions uniquement pour la souche aéroportée MFAF76a, incapable de produire des BSs qui pourraient modifier par leur ad/(b)sorption les propriétés pariétales bactériennes.

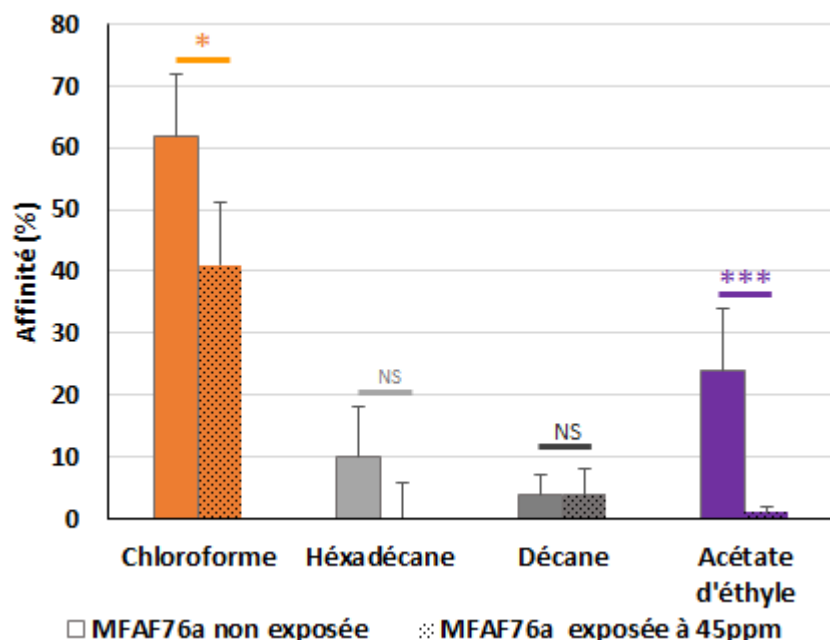


Figure 22 :Affinité relative aux solvants de la souche *P. fluorescens* MFAF76a exposée, respectivement à l'air synthétique et à 45 ppm de NO₂.

Par souci de clarté, seules les affinités aux solvants sont présentées Figure 22 lors d'exposition en absence de NO₂ et à 45 ppm. La surface de la souche MFAF76a reste hydrophile quelle que soit la concentration d'exposition au NO₂, confortant l'absence de changement drastique des charges présentes sur la paroi membranaire externe. Cette réponse au NO₂ est différente de celle provoquée à la membrane bactérienne par les solvants organiques (octanol, par exemple) qui impactent les lipopolysaccharides (LPS) et modifient la charge globale de la surface bactérienne (Baumgarten et al., 2012a). Cependant la diminution du caractère basique de Lewis (couple décane/acétate d'éthyle) indique que des accepteurs de doublets non liants sont moins nombreux en surface suite à l'exposition à 45 ppm en NO₂. Cela pourrait s'expliquer par des modifications impactant aussi bien les protéines membranaires que les lipides, d'autant que l'adaptation bactérienne en réponse aux oxydes d'azote peut s'exprimer par une surproduction de protéines membranaires telles que les pompes à efflux (Fetar et al., 2011), mais aussi par le glissement/ translocation des PLs entre cytosol et membrane externe (Sanyal and Menon, 2009). Ainsi cette diminution pourrait être en partie imputable à la substitution entre des PLs zwitterioniques (pas de changement global de charge), mais avec des caractéristiques acido-basiques différentes. PE et PC sont des PLs zwitterioniques présents chez la souche aéroportée MFAF76a, mais PC est moins électroaccepteur que PE (Romantsov and Wood, 2017), par conséquent sa présence pourrait être favorisée dans la membrane externe après exposition à 45 ppm de NO₂, sans oublier la prépondérance du PE et la diminution drastique , voire disparition de l'UGP.

Dans tous les cas, l'exposition au NO₂ chez les *P. fluorescens* étudiées provoque une réponse impactant visiblement leur homéostasie membranaire via, entre autres, leurs PLs.

(b) Réponse des 2 souches via leur comportement social et leur résistance aux antibiotiques aux 3 concentrations de NO₂

Pour poursuivre notre évaluation de l'impact du polluant automobile NO₂ sur la virulence bactérienne, notre attention s'est portée sur une analyse fine des phénotypes de comportement social (motilité, biofilm) et de résistance aux antibiotiques sur les deux souches de *Pseudomonas fluorescens* : l'environnementale MFAF76a et la témoin MFN1032, souche clinique. Les trois concentrations : 0,1 ; 5 et 45 ppm en NO₂ ont été étudiées pour évaluer des situations, respectivement, « environnementale », critique et toxique (cf choix et concentration en polluant). Seule la concentration dite « toxique » (45 ppm) a conduit à des variations phénotypiques significatives, aussi elles seront les seules présentées par la suite.

(i) Impact du NO₂ sur le comportement social bactérien

La première étape de formation des biofilms correspond à l'adhésion et nécessite des appendices tels que flagelles et pili de type IV (Caiazza et al., 2007), caractérisables via la motilité bactérienne de type swimming et swarming. Le NO₂ gazeux réduit significativement la motilité des deux souches (swim et swarm si existant), Figure 23 (Kondakova et al., 2016).

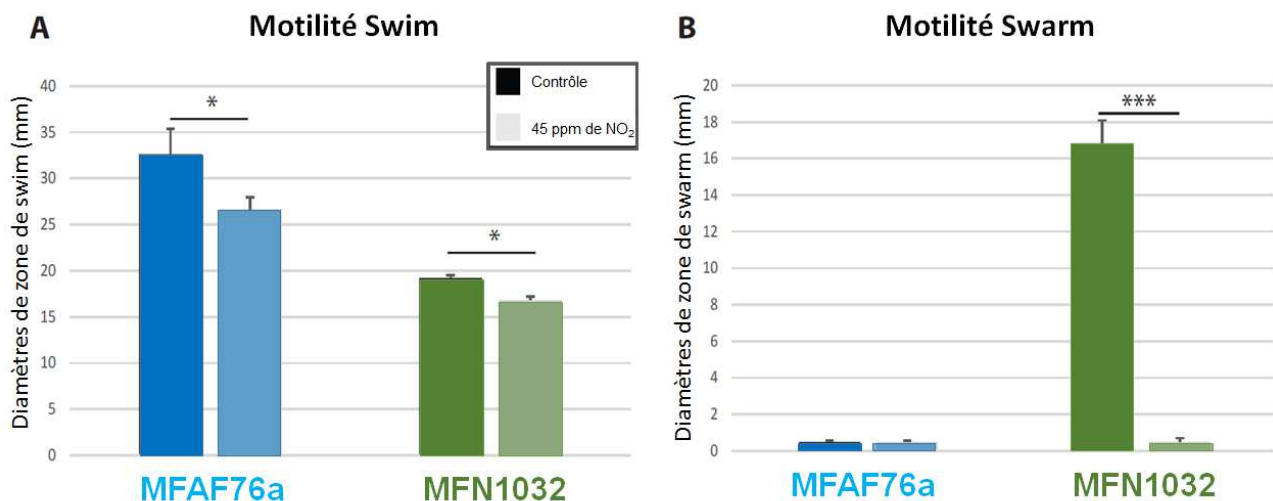


Figure 23 : Motilité swim et swarm des souches *P. fluorescens* MFAF76a et MFN1032 exposées, respectivement à l'air synthétique et à 45 ppm de NO₂. (* : P=0,05 ; ** : P=0,01 ; * : P=0,001).**

Cette sédentarisation accrue des deux souches devrait faciliter leur capacité à former des biofilms.

Suite à l'exposition à 45 ppm de NO₂, les deux souches forment des biofilms, mais une densification du biofilm est observée Figure 24 : augmentatio du biovolume pour les deux souches, alors que la souche MFAF76a triple l'épaisseur de son biofilm. Aucune modification patente de celui de MFN1032 n'est observée (Kondakova et al., 2016). Même si la réponse diffère, le NO₂ impacte le biofilm des deux souches, à l'instar du NO chez *P. aeruginosa* (Barraud et al., 2015), suggérant une similitude des mécanismes d'action des NOx vis-vis des *Pseudomonas*.

En présence de NO, la formation de biofilm est corrélée à une augmentation de la production de bis-(3', 5')-cyclic dimeric guanosine monophosphate, c-di-GMP (Ha and O'Toole, 2015). Suite à l'exposition au NO₂, aucune variation de sa concentration intracellulaire n'est notée chez les deux souches. Par conséquent, le NO₂ n'induit pas exactement la même réponse que le NO gazeux provoque chez *P. aeruginosa* (Cutruzzolà and Frankenberg-Dinkel, 2016; Li et al., 2013), via la production des enzymes DipA, MucR, NdbA and BdIA (Petrova and Sauer, 2016; Roy et al., 2012). L'analyse transcriptomique des gènes respectifs, suite à l'exposition des 2 souches d'intérêt à 45 ppm de NO₂, n'a révélé aucune altération de leur expression (Kondakova et al., 2016).

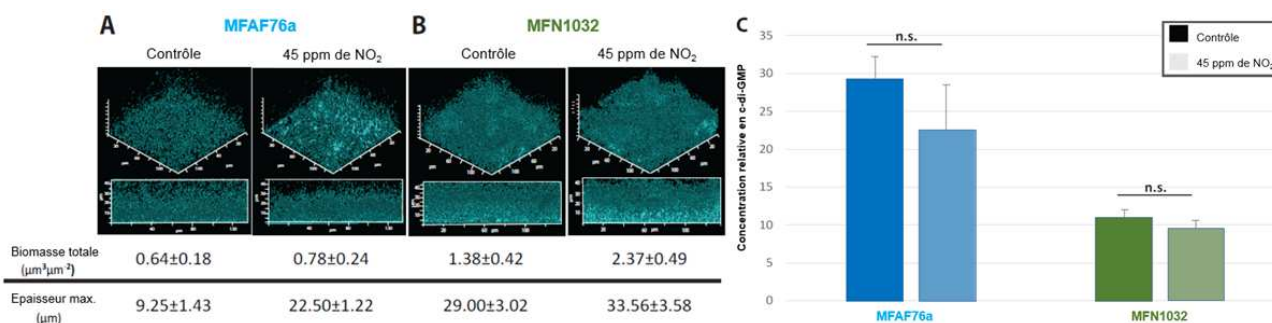


Figure 24 : Biofilm des deux souches *P. fluorescens* exposées, respectivement à l'air synthétique et à 45 ppm de NO₂. A : souche MFAF76a. B : souche MFN1032. C : Quantification du bis-(3', 5')-cyclic dimeric guanosine monophosphate (c-di-GMP). (NS : non significatif P>0,05).

D'autre part, cette exposition au NO₂ engendre davantage d'agrégats bactériens, présentés Figure 25. Présent chez les 2 souches productrice ou non de biosurfactant, ce phénomène, en plus de densifier le biofilm, pourrait être relié au stress périétal. Effectivement l'augmentation d'agrégats a été observée lors de la délétion de la porine membranaire majoritaire OprF chez *P. aeruginosa* H103 (Bouffartigues et al., 2015).

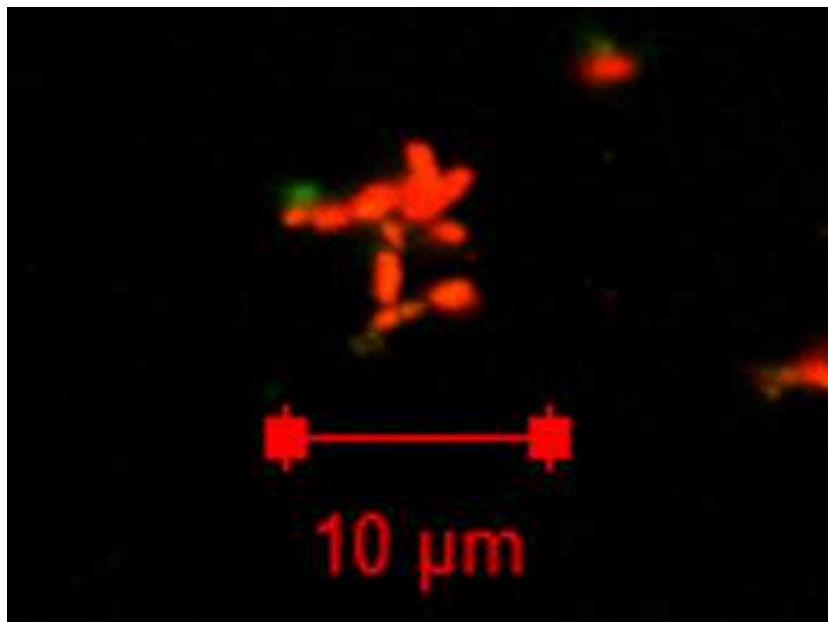


Figure 25 : Exemple d'agrégats bactériens observés chez la souche MFAF76a après exposition à 45 ppm de NO₂.

Par conséquent, le NO₂ perturbe bien l'intégrité membranaire des souches étudiées en modifiant leur capacité à former des biofilms.

(ii) Impact du NO₂ sur la résistance des souches environnementale et clinique aux antibiotiques

Si son intégrité membranaire est modifiée, le microorganisme peut voir sa résistance aux antibiotiques modulée. Or le NO induit l'expression des gènes *mexEF-oprN* (Fetar et al., 2011) et module ainsi la résistance aux antibiotiques fluoroquinolones, chloramphenicol and aminoglycosides (Gusarov et al., 2009; McCollister et al., 2011; van Sorge et al., 2013), que nous avons, par conséquent, étudiée.

Le NO₂ favorise l'expression de la pompe à efflux MexEF-OprN, de type RND - Resistance-Nodulation-Division- transporteurs intramembranaires, impliquée dans l'antibiorésistance aux fluoroquinolones (e.g. ciprofloxacin) (Köhler et al., 1997). Ainsi, suite à l'exposition à 45 ppm de NO₂, l'expression des différents gènes est accrue entre 3,5 et plus de 100 fois pour certains d'entre eux et, de plus, la pompe est fonctionnelle comme le démontre la résistance plus importante à la ciprofloxacin, Figure 26 (Kondakova et al., 2016).

A

Souche	concentration en NO ₂ (ppm)	Ciprofloxacine MIC(µg/mL)	Chloramphénicol MIC(µg/mL)
MFAF76a	0	6.25	50
	45	12.5	> 100
MFN1032	0	3.125	150
	45	6.25	200

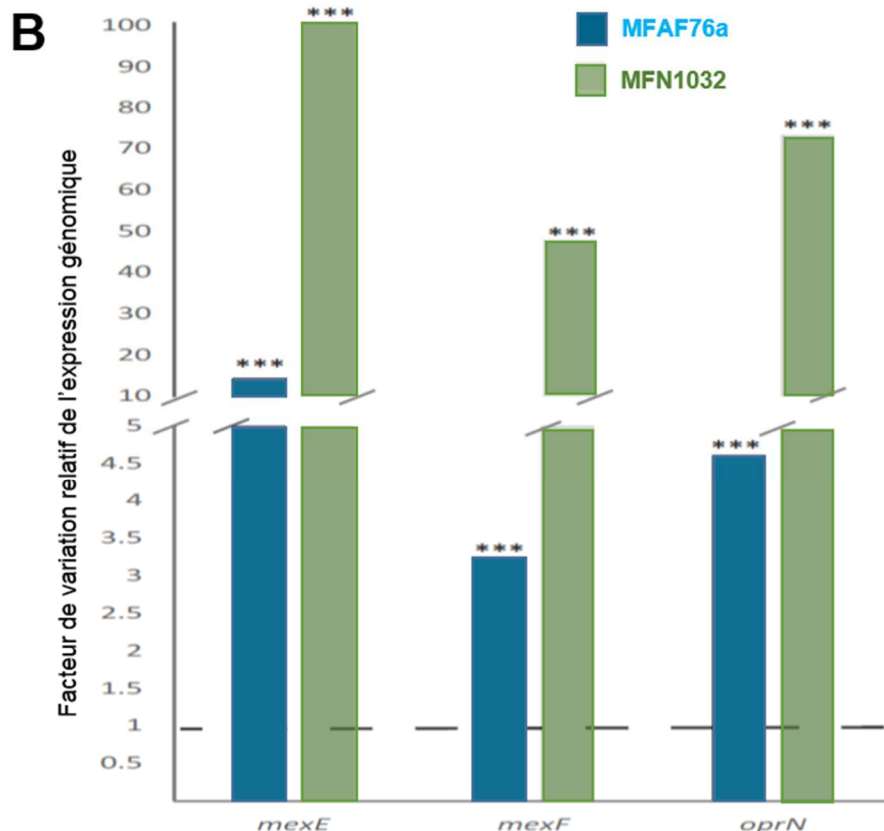


Figure 26 : Virulence des deux souches *P. fluorescens* MFAF76a et MFN1032 exposées. A : Résistance à 2 antibiotiques suite à l'exposition à l'air synthétique et à 45 ppm de NO₂. B : Quantification de leur expression génomique de *mexE*, *mexF* et *oprN* suite à l'exposition au NO₂. (* : P=0,05 ; ** : P=0,01 ; * : P=0,001).**

Un second antibiotique a été étudié le chloramphénicol antimicrobien nitroaromatique, substrat de la pompe MexEF-OprN (Köhler et al., 1997; Sobel et al., 2005). La résistance à cet antibiotique, présentée Figure 26, est doublée suite à l'exposition (Kondakova et al., 2016).

Aussi, même si le NO₂ diffuse librement au travers de la membrane bactérienne, celle-ci possède un ou plusieurs mécanismes de résistance, voire de détoxicification.

Une des voies de dénitrification du NO₂ chez les *Pseudomonas* spp. implémente la réduction du NO₂ via les enzymes nitrite réductases (NIR), impliquant le cytochrome respiratoire cd1 (Arai et al., 2005; Shiro, 2012). Il s'avère qu'*in silico* nos deux souches sont dénuées des gènes codant pour les enzymes NIR, mais, comme la majorité des *P. fluorescens*, présentent l'opéron *nirBD* codant des nitrites réductases assimilatrice (NAS) (Redondo-Nieto et al., 2013). Ainsi les souches MFAF76a et MFN1032 possèdent la machinerie pouvant réduire les nitrates en nitrites, puis en ammonium (Jeter, 1984; Moreno-Vivián et al., 1999). Cependant, la production de l'ARN messager *NirBD* n'est pas modifiée par la présence du polluant (Kondakova et al., 2016). Par conséquent les deux souches n'utilisent pas cette voie d'assimilation des oxydes azotés lors de ces expositions.

Comme le NO₂ reste chimiquement proche de NO, dont les voies de détoxication ont largement été explorées, notre intérêt s'est porté sur la voie la plus connue de détoxicification du NO, transformé en nitrates via l'action de la flavohémoglobine (FlavoHb) (Hmp chez *Escherichia coli* et Fhp chez *P. aeruginosa*) (Arai et al., 2005; Corker and Poole, n.d.). Testée chez les deux souches suite à l'exposition au NO₂, l'expression du gène homologue à *hmp* a été observée et est multipliée par 25 pour MFAF76a et 23 pour MFN1032, Figure 27 (Kondakova et al., 2016).

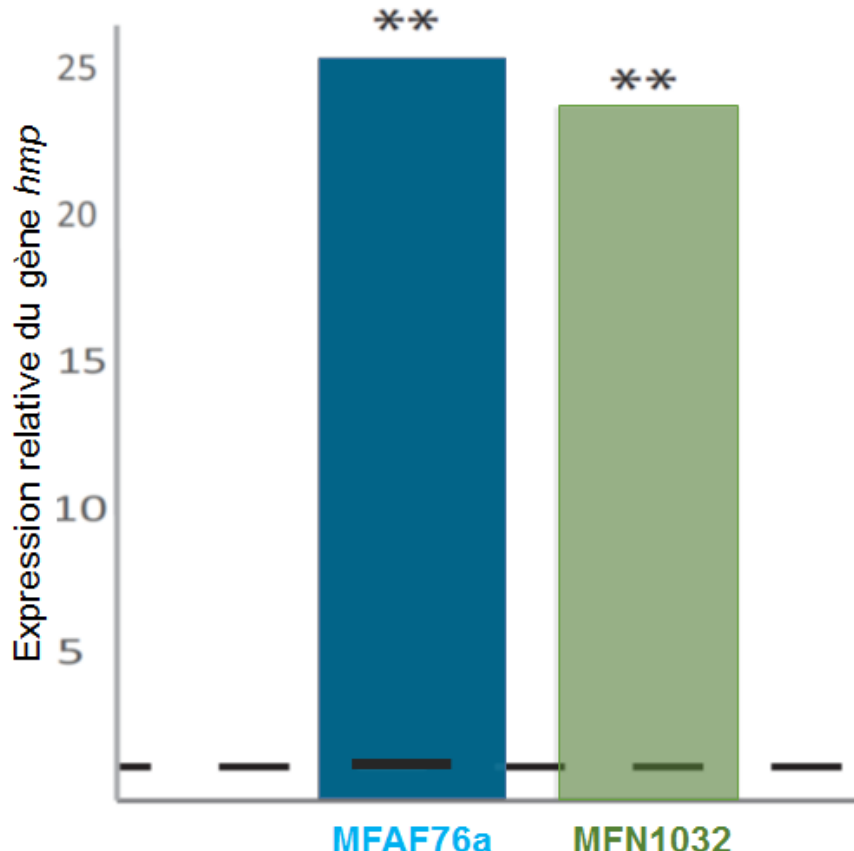


Figure 27 : Quantification de l'expression du gène *hmp*, codant pour la flavohémoglobine, par les souches *P. fluorescens* MFAF76a et MFN1032 exposées à 45ppm de NO₂. (: P=0,01).**

La flavohémoglobine est donc activée suite à une exposition à 45ppm en NO₂ de ces *P. fluorescens*. Ainsi le NO₂ pourrait activer un mécanisme mis habituellement en œuvre par le NO. Une détoxicification par le NO₂ activant Hmp a déjà été reportée, aussi le NO₂ a été tenu pour être réduit en NO (Poole et al., 1996).

A l'issue de travaux de thèse du Dr T KONDAKOVA en novembre 2015, l'hypothèse a été émise qu'après exposition à 45ppm de NO₂, le polluant, ayant diffusé dans le cytosol, pourrait être transformé en partie par Hmp en nitrates. Ces derniers, avec les autres produits de dégradation, pourraient être expulsés à l'extérieur des *P. fluorescens* à l'aide de la pompe RND MexEF-oprN (cf la surexpression de *mexE*, *mexF* et *oprN*).

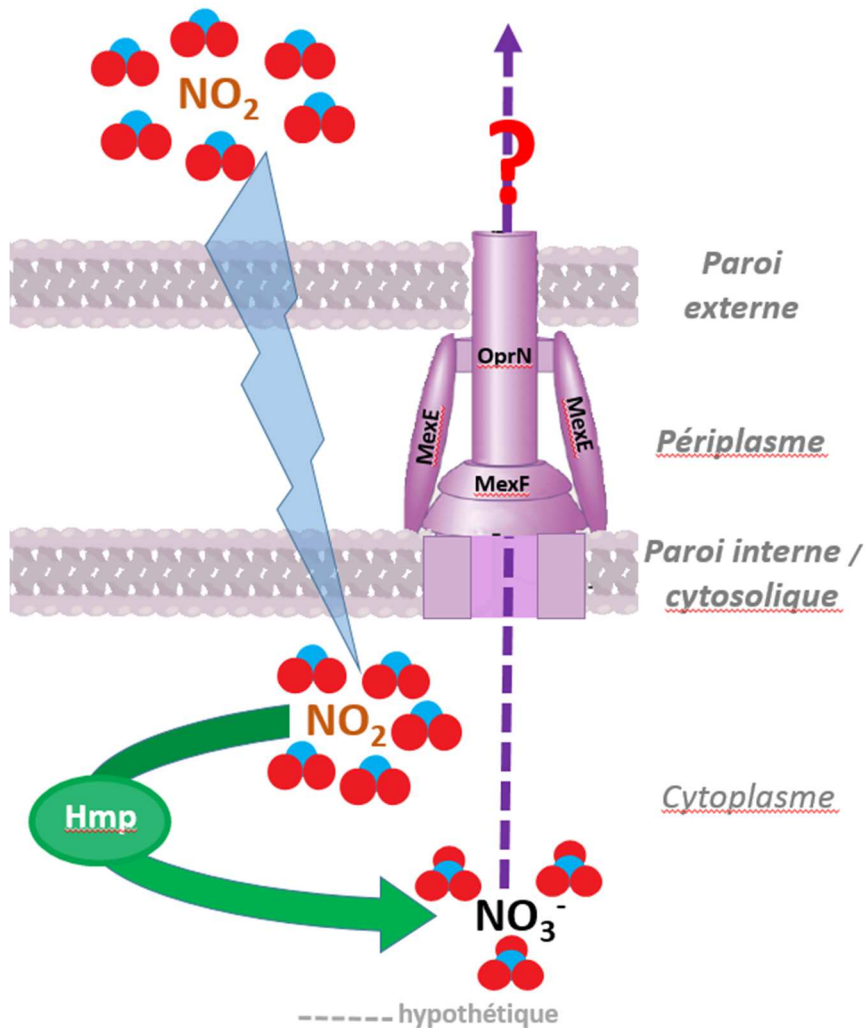


Figure 28 : Stratégie hypothétique mise en œuvre par les souches *P. fluorescens* étudiées suite à leur exposition à 45ppm de NO₂ gazeux, proposée par T Kondakova lors de sa soutenance de thèse le 20 novembre 2015.

Dans tous les cas, l'exposition à 45ppm en NO₂ provoque une réponse complexe des *P. fluorescens* MFAF76a et MFN1032 impactant sans conteste leur intégrité membranaire de diverses manières (variabilité des phospholipides, altération de la motilité bactérienne et surproduction de la pompe MexEF-OprN), complétée par un des mécanismes de détoxification. Cette réponse nécessite un coût énergétique fort important, voire fatal. Les travaux de S DEPAYRAS (thèse débutée en 2015) ont débuté par l'étude de la viabilité bactérienne suite au stress NO₂. Ses travaux se sont principalement focalisés sur la souche aéroportée et non productrice de biosurfactant MFAF76a.

(iii) Impact du NO₂ sur la viabilité de *P. fluorescens* aéroportée MFAF76a

La densité bactérienne est traditionnellement quantifiée à l'aide de la densité optique (DO) de la suspension à 580 nm suite à l'établissement de la correspondance DO et dénombrement cultural bactérien (Unité formant colonies-UFC), directement proportionnels via la loi de Beer-Lambert. La quantification de la population bactérienne grâce à la DO, réalisée en quelques minutes, est rapide et économique par rapport au dénombrement cultural bactérien nécessitant plus d'une journée. La viabilité bactérienne correspond, ici, à quantifier le nombre de bactéries ayant été exposées au NO₂ et encore vivantes. Une pigmentation jaune de la biocharge apparaît plus ou moins intense selon les

souches lors de leur exposition au NO₂ et biaise la lecture de la DO. D'autre part, selon nos études, le NO₂ entraîne des modifications au niveau de la membrane bactérienne, dont l'incursion et la composition peuvent mener à la déformation de la cellule, rendant caduque l'application de la loi de Beer-Lambert. Aussi la viabilité a été établie par dénombrement cultural. Suite à leur exposition à 45 ppm, la souche MFAF76a a sa viabilité diminuée (perte d'un log), Figure 29A (Depayras et al., 2018b).

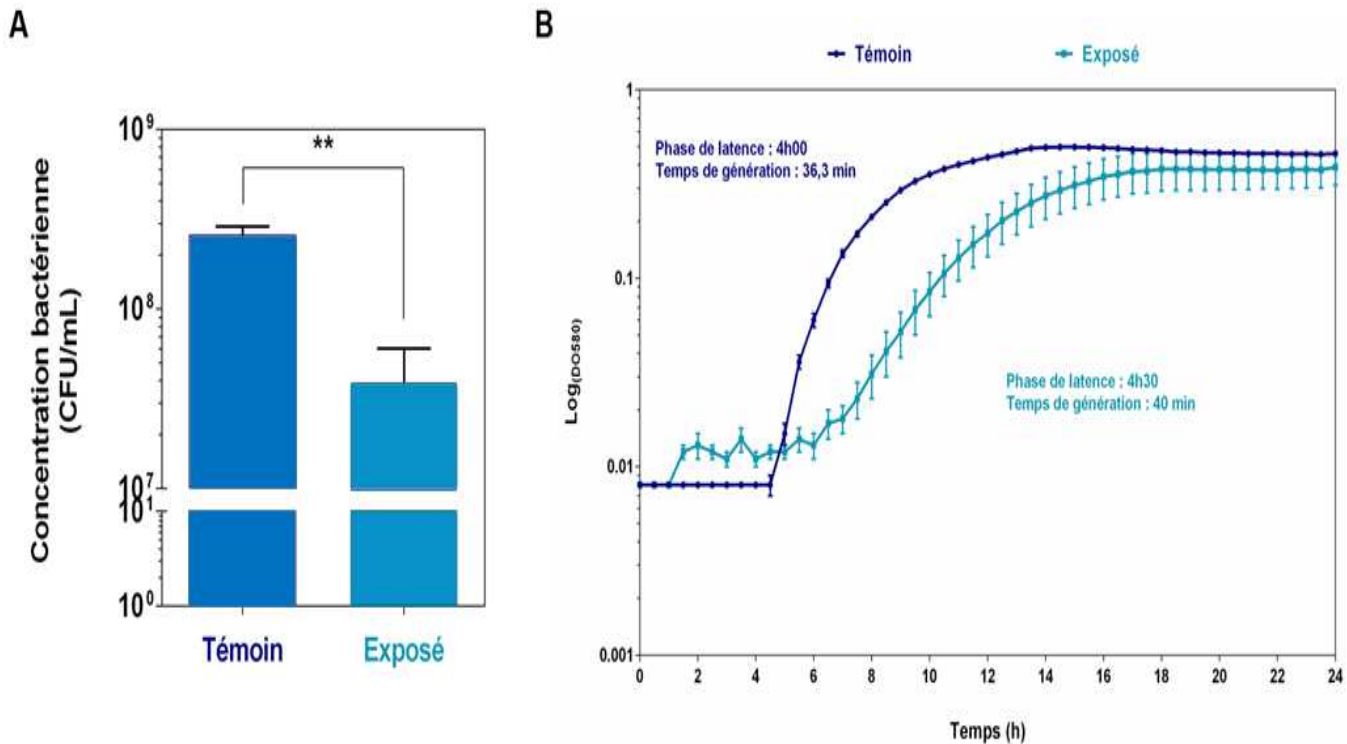


Figure 29 : Impacts physiologiques suite à l'exposition à 45ppm NO₂ de *P. fluorescens* MFAF76a. A : viabilité. B : suivi de croissance en DMB à 28°C. (: $P=0,01$).**

Quelque soient les biais expérimentaux évoqués, cette perte de viabilité signifie soit la présence de bactéries viables, mais non cultivables, soit la mort cellulaire. Quant à la croissance de MFAF76a, le temps de latence est augmenté d'une demi-heure suite à l'exposition, mais sans impact sur le temps de génération (Figure 29B). Le NO₂ ne semble pas impacter significativement le métabolisme bactérien relatif à la division cellulaire, mais d'autres voies métaboliques le sont, corroborant les diverses altérations phénotypiques que nous avons déjà établies.

Pour approfondir cette approche viabilité après exposition au NO₂, la permabilisation membranaire a été évaluée grâce au test Live Dead (Depayras et al., 2018b). Il permet de discriminer les membranes cellulaires intactes (correspondant aux bactéries vivantes, colorées en vert) de celles endommagées (*i.e.* bactéries incultivables, voire mortes, colorées en rouge), Figure 30.

Suite à l'analyse d'image des champs d'observation par microscopie confocale des bactéries colorées par le kit Live Dead, la perméabilisation membranaire de MFAF76a est augmentée d'environ 50% par la présence du polluant, diminuant par conséquent de moitié la population viable bactérienne.

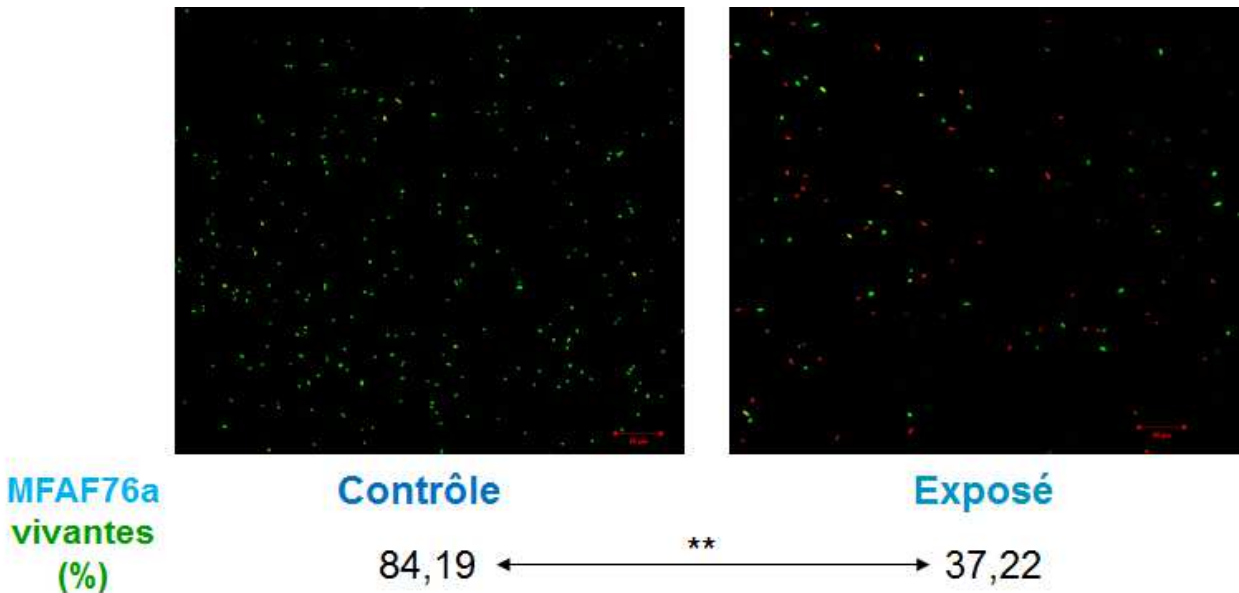


Figure 30 : Impact de 45 ppm de NO₂ sur la perméabilisation membranaire de *P. fluorescens* MFAF76a. Quantification par analyse d'image de clichés de microscopie confocale. (: P=0,01).**

Nos travaux démontrent, chez les souches *P. fluorescens* étudiées,

- que NO₂ impacte fortement la viabilité bactérienne
- que, chez les bactéries viables, même s'il diffuse librement au travers de la membrane bactérienne, le métabolisme se trouve modifié par la présence du NO₂
 - ✓ au niveau lipidique, dont les phospholipides membranaires
 - ✓ de son comportement social (appendices membranaires, protéine membranaire OprN)
 - ✓ de sa résistance aux antibiotiques (pompe membranaire MexEF-OprN)
 - ✓ et de détoxification originale par activation de la flavohémoglobine, inhabituelle chez les *P. fluorescens*.

Le plus souvent, la réponse bactérienne au NO₂ passe par l'intervention de la membrane bactérienne, voire plus précisément son homéostasie.

En parallèle des expositions à faible concentration en NO₂ (0,2 ppm) ont été effectuées sur la souche aéroportée et son témoin clinique en phase exponentielle et stationnaire de croissance. Les tests physiologiques post-exposition ont permis d'observer peu, voire pas, de toxicité du NO₂ dans de telles conditions de concentration, mais aussi peu de perméabilisation membranaire. Aussi, pour l'instant, l'exclusivité de nos efforts se maintient sur l'exposition de la souche aéroportée à 45ppm de NO₂.

Production scientifique correspondante : P26 ; P30; Ch4 ; C12-C13 ; C21 ; C24 ; C27 ; C29 ; A36 ; A39 ; A43.

Encadrements : L8-L9 ; M1_5 ; M1_Imm_1->M1_Imm_12 ; M1_6 ; M2_4->M2_5 ; D2-D3 ; PD3.

(4) Impact du NO₂ sur l'homéostasie membranaire de la souche *P. fluorescens* aéroportée MFAF76a

Afin de mieux cerner l'ampleur de cette réponse, S DEPAYRAS a systématisé les approches « omics » : génomique, transcriptomique pour expliciter les phénotypes observés précédemment.

*(a) Impact du NO₂ sur la réponse de *P. fluorescens* aéroportée MFAF76a à l'aide d'analyses « omics »*

L'analyse *in silico* du génome de *P. fluorescens* MFAF76a réalisée dernièrement par S DEPAYRAS, a permis d'identifier certains gènes par homologie à des souches *Pseudomonas* déjà séquencées et annotées, principalement *P. fluorescens* A506 et F113. Les gènes ciblés ont leur expression impliquée dans les mécanismes de détoxicification des NOx, du stress pariétal, d'antibio-résistance, mais aussi dans la formation des appendices membranaires (flagelle, pili), de la matrice extracellulaire, sans oublier des systèmes de sécrétion.

Ensuite l'expression d'une trentaine de gènes chez *P. fluorescens* MFAF76 a été quantifiée en phases exponentielle et stationnaire de croissance en absence et en présence de 45 ppm et de 0,2 ppm de NO₂, Tableau 2.

Catégorie	Sous-catégorie	Souche <i>P. fluorescens</i> MFAF76a
Motilité	Flagelle	5
	Pili type IV	4
Biosurfactant	Massetolides	1
Antibiorésistance	β-lactame	10
Dénitrification		4
Biofilm	Alginate	3
	Adhésine	1
Système de sécrétion	SST3	0
	SST6	1
QS	phénazine	0
Stress pariétal		3
Total		32

Tableau 2 : Nombre de gènes dont l'expression a été ciblée lors des expositions en absence et en présence de 45 ppm et de 0,2 ppm de NO₂ en phase exponentielle et stationnaire de croissance.

Seuls les échantillons obtenus après exposition à 45 ppm de NO₂ ont permis de montrer des modifications significatives dans l'expression de gènes. Les gènes surexprimés significativement, Figure 31, sont notamment impliqués dans la formation et le fonctionnement du flagelle (*flaA*, *flgE*, *fliA*, *fliF*), la production d'alginate (*algD*, *oprF*), la réponse au stress pariétal (*oprF*, *oprN*), l'antibio-résistance (pompe à efflux : *mexE*, *mexF*, *oprN*) et la détoxicification (*hmp*).

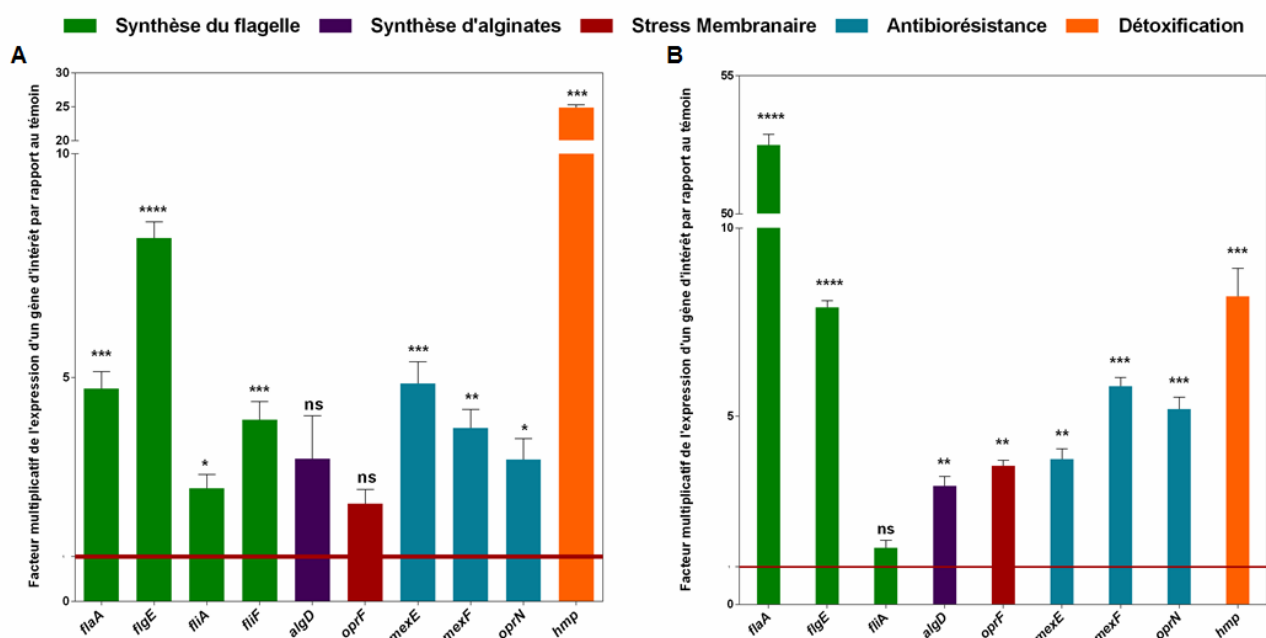


Figure 31 : Gènes de *P. fluorescens* MFAF76a dont l'expression est significativement surexprimée suite à une exposition à 45 ppm de NO₂. A : Phase exponentielle de croissance. B : Phase stationnaire de croissance. (NS : $P > 0,005$; * : $P=0,05$; ** : $P=0,01$; *** : $P=0,001$; **** : $P=0,0001$).

Une analyse en protéomique, *i.e.* la concrétisation de l'expression génomique sous la forme de la production des protéines correspondantes, a été menée en parallèle en collaboration avec le Dr J HARDOUIN, PBS UMR 6270, Université de Rouen Normandie. Elle a confirmé en partie ces données, Figure 32.

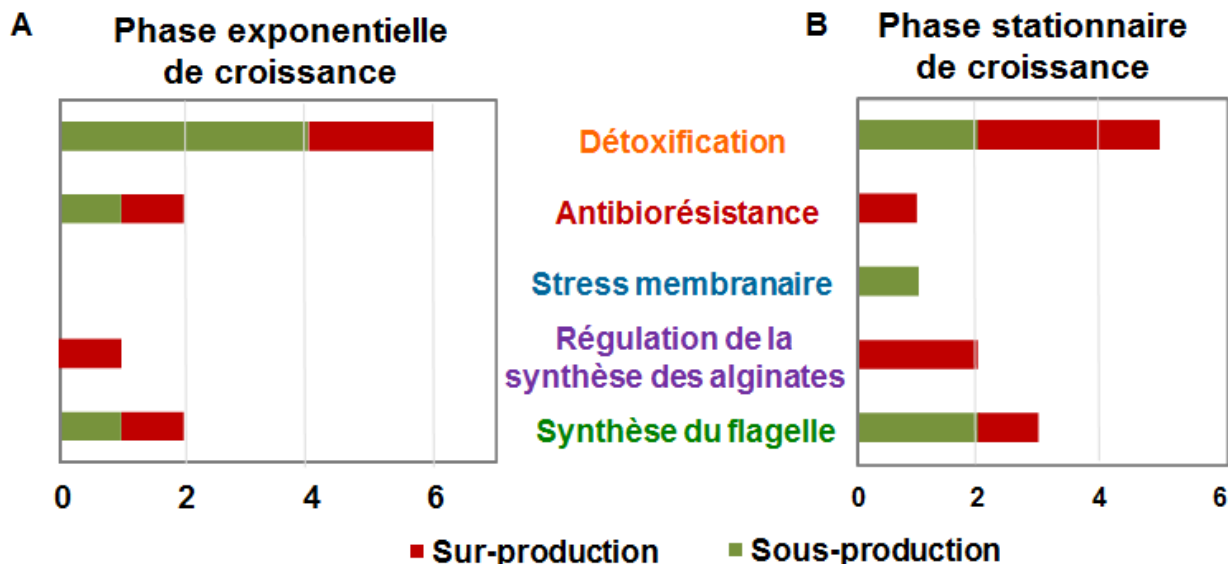


Figure 32 : Comparaison de l'expression protéique, décrite par grandes familles fonctionnelles, de *P. fluorescens* MFAF76a lors d'une exposition à 45ppm de NO₂ versus air synthétique selon la phase de croissance.

A : Phase exponentielle. B : Phase stationnaire.

Pour les deux phases de croissance, le profil protéique se voit modifié suite à l'exposition à 45 ppm de NO₂. Ces résultats très préliminaires, Figure 32, indiquent des modulations et pas uniquement des surproductions protéiques. Aussi les surexpressions génétiques ne se concrétisent pas uniquement en une production augmentée des protéines correspondantes, mais peuvent conduire aussi à des

répressions de certaines, voire des interconnexions plus complexes. Une analyse plus fouillée des résultats de protéomique est en cours, cependant, nous pouvons déjà explorer les pistes présentes dans la littérature et cohérentes avec les résultats déjà compilés.

*(b) Eléments de réponse à propos de l'impact du NO₂, polluant automobile sur la réponse adaptative de *P. fluorescens**

La compilation de l'ensemble de ces données nous mène actuellement au schéma synthétique Figure 33.



Figure 33 : Récapitulatif des données acquises et réponse bactérienne supposée suite à l'exposition à 45ppm de NO₂ d'après notre avancée actuelle.

Le degré de saturation des acides gras indique que le NO₂ diffuse librement au travers de la membrane. Une partie ou la totalité du NO₂ entré dans le cytosol pourrait être pris en charge par l'enzyme de détoxicification flavohémoglobine qui le convertit en produits de dégradation azotés (NX) moins toxiques pour la bactérie. Comme pour NO, les nitrates (NO₃⁻) pourraient compter parmi ces NX qui seront sûrement métabolisés en d'autres composés plus élémentaires. Ce mécanisme de détoxicification par la flavohémoglobine est connu pour permettre la réparation chez *E. coli* des dommages du stress nitrosant au niveau des lipides membranaires (Bonamore et al., 2003). Si ce même mécanisme est présent chez *P. fluorescens*, il pourrait masquer l'apparition d'adduits hydroperoxydes, alcools ou aldéhydes (Möller et al., 2008) qui seraient « corrigés » en se concrétisant par les modifications lipidiques que nous avons constatées et confirmées par l'altération du caractère de base de Lewis. La membrane voit aussi son homéostasie modifiée par la surexpression d'un certain nombre de porines (OprF et OprN) qui sont des protéines de la membrane externe contribuant à la stabilisation membranaire et permettant le passage de solutés (Henderson et al., 2016). Chez *P. aeruginosa*, OprF est un canal aqueux non spécifique pour les ions (Bellido et al., 1992). En condition anaérobie, elle pourrait potentiellement assurer le transport de nitrates et nitrites (Hassett et al., 2002). Dans ces mêmes conditions, la formation de biofilm est accentuée et s'effectue dans une matrice d'exoproduits polymériques, principalement des exopolysaccharides (Yoon et al., 2002). Suite à l'exposition au NO₂, les *P. fluorescens* étudiées pourraient éliminer les nitrates et d'autres produits de dégradation via la porine OprF tout en favorisant la formation de biofilms et d'agrégats que nous avons observée. De plus, OprF assure l'intégrité de la membrane bactérienne via ses interconnexions

de régulation d'expression avec d'autres porines et le peptidoglycane (Chevalier et al., 2017). La synthèse des alginates, impliqués dans le peptidoglycane et exopolysaccharides, est sous le contrôle du promoteur *algD* (Hay et al., 2014) qui se trouve être surexprimé par l'exposition au NO₂. *AlgD* impacte aussi indirectement la production des flagelles en la réprimant (Hay et al., 2014), confortant la réduction de la motilité observée. Ceci est en contradiction avec la surexpression des gènes *flgA*, *flgE*. Flag et FlgE contribuent à la présence de flagelles. Cette surexpression n'implique pas la fonctionnalité des flagelles. La transcription de *flgA* et *flgE* sont sous le contrôle de FliA, de même que la transcription d'OprD. Or il s'avère que cette même porine a son production réprimée lors d'une surproduction de la pompe à efflux MexEF-OprN (Köhler et al., 1999). Cette surproduction de ce complexe macromoléculaire encastré dans la membrane externe est un élément supplémentaire de perturbation de l'homéostasie membranaire et contrebalancerait la perte de l'UGP. Elle pourrait être à l'origine de l'efflux des NX, voire de leurs produits de dégradation plus complète dans le microenvironnement de la bactérie. De plus, ces efflux entraîneraient l'entrée de proton (H⁺) dans le cytosol, qui pourrait modifier le potentiel de membrane, entraînant des dysfonctionnements des protéines membranaires le régulant. De telles modifications ont concouru chez *P. aeruginosa* une susceptibilité accrue à des antibiotiques (Pan et al., 2017), comme nous l'avons aussi constatée. En résumé, le marqueur de pollution automobile NO₂ catalyse une augmentation de la virulence bactérienne avec un stress pariétal notable. Cependant beaucoup de zones d'ombres persistent.

Production scientifique correspondante : C 28 ; C30.

Encadrements : Ing1_1 ; D3.

C) Stress physique : impact d'une matrice cosmétique complexe

Profitant du développement d'un autre axe de sécurité sanitaire au LMSM concernant les produits cosmétiques, j'ai eu l'opportunité d'étudier les interactions des bactéries avec la matrice complexe qu'est un produit cosmétique. Tout laboratoire cosmétique se doit d'étudier et de communiquer sur l'innocuité de son produit commercialisé en Europe. Le règlement cosmétique européen 1223/2009 (*Règlement (CE) no 1223/2009 du Parlement européen et du Conseil du 30 novembre 2009 relatif aux produits cosmétiques*, 2009), appliqué depuis juillet 2013, impose aux producteurs la transparence, mais aussi un effort de recherche pour enrichir le dossier d'information produit de toute étude illustrant l'innocuité (chimique, physique, microbiologique) de leurs produits. La majorité des matrices cosmétiques peuvent être définies comme une dispersion d'un liquide en fines gouttelettes dans un milieu continu liquide (Doumeix, 2011). Deux grandes familles coexistent les émulsions dites Huile-dans-Eau (H/E) et celles Eau-dans-Huile (E/H). Ces dernières E/H sont connues pour limiter la prolifération de microorganismes (Schubert and Engel, 2004), car l'huile, phase dispersante, crée un milieu anaérobie et rend l'eau indisponible pour les germes. Mais ces formes laissent un résidu « huileux, gras » sur la peau, peu vendable auprès du consommateur. Aussi

les émulsions cosmétiques H/E sont les plus retrouvées sur le marché, mais présentent une stabilité microbiologique plus fragile.

Ce monde des émulsions pourrait paraître fort éloigné, voire incohérent avec mes préoccupations précédentes sur l'homéostasie membranaire. Revenons à la définition d'interface. Elle correspond à la séparation entre deux milieux non miscibles et différant en composition et/ou structure chimique. Ainsi les microorganismes en suspension dans une des phases de l'émulsion perçoivent l'interface formée par le milieu non miscible comme un stress physique. Le contact avec les gouttelettes peut entraîner la déstabilisation membranaire et la lyse rapide des cellules (Hamouda and Baker, 2000). De même l'interface créée par un milieu plus dense comme la surface solide de nanoparticules peut induire une réponse adaptative des bactéries et plus spécifiquement au niveau de leur paroi (Persat, 2017). D'où mon intérêt pour ces sujets en cours de développement et encore peu documentés *in situ*, i.e. en produit cosmétique.

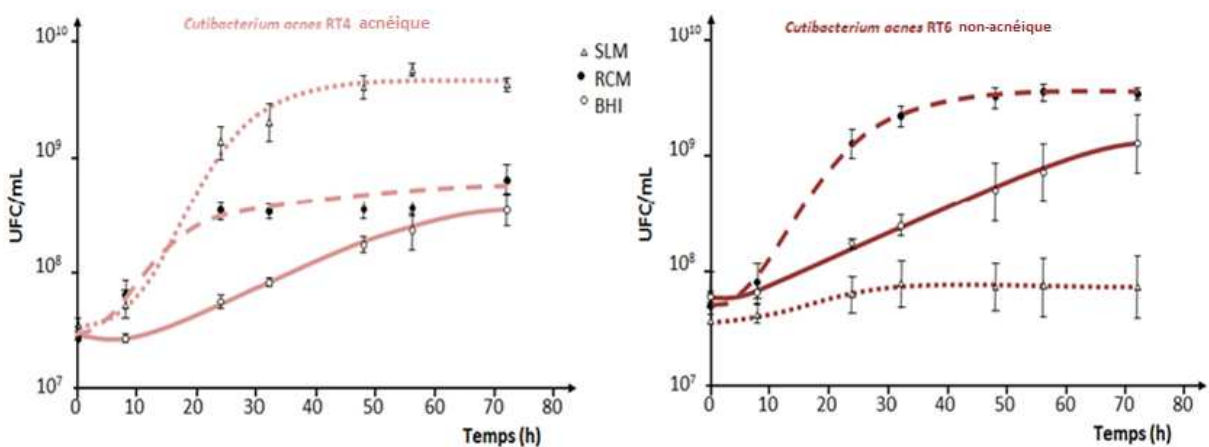
(1) Impact du microenvironnement sur *Cutibacterium acnes*

L'*Acne vulgaris* (i.e. acné) est l'une des maladies cutanées les plus répandues (White, 1998).

Le Gram positif *Propionibacterium acnes*, dénommé dorénavant *Cutibacterium acnes* - *C. acnes*, est considéré comme un des fréquents promoteurs de l'acné (Scholz and Kilian, 2016). Récemment, V BORREL, co-encadrée par le Pr FEUILLOLEY et le Dr KONTO-GHIORGHI, a développé un milieu mimant le sébum qui, lors de l'acné, est hypersécrété et s'accumule au niveau du follicule pilo-sébacé. Ce milieu, appelé SLM pour Sebum Like Medium, est à base du milieu classique Brain Heart Infusion medium (BHI) complété par du squalène, de la trioléine et de l'acide oléique. Il constitue une émulsion.

La croissance de deux souches de *C. acnes* RT4 (acnéique) et RT6 (non-acnéique) a été réalisée en SLM, BHI et RCM (Reinforced Clostridial Medium), milieu traditionnel de ces bactéries. Leur croissance diverge selon les milieux, Figure 34A. La souche acnéique RT4 se développe plus facilement en SLM et plus rapidement en SLM et RCM qu'en BHI. Au contraire la non-acnéique, RT6 croît davantage et plus rapidement en RCM qu'en BHI et ne fait que se « maintenir » en SLM. Ces résultats conformes au profil virulent (acné) des souches pourraient être liés à une hydrophilie bactérienne plus ou moins importante. Suite aux tests MATS en BHI et RCM, milieux homogènes, Figure 34B, RT4, l'acnéique est plus hydrophobe que la non acnéique RT6. Aussi sa croissance au sein d'une émulsion, comme SLM, est favorisée. La stabilité du profil d'acido-basicité de Lewis de RT6 dans les deux milieux conforte sa faible affinité pour la phase lipophile donc SLM, surtout la forme émulsion (Hamouda et al., 2001), et sa préférence pour le RCM.

A



B

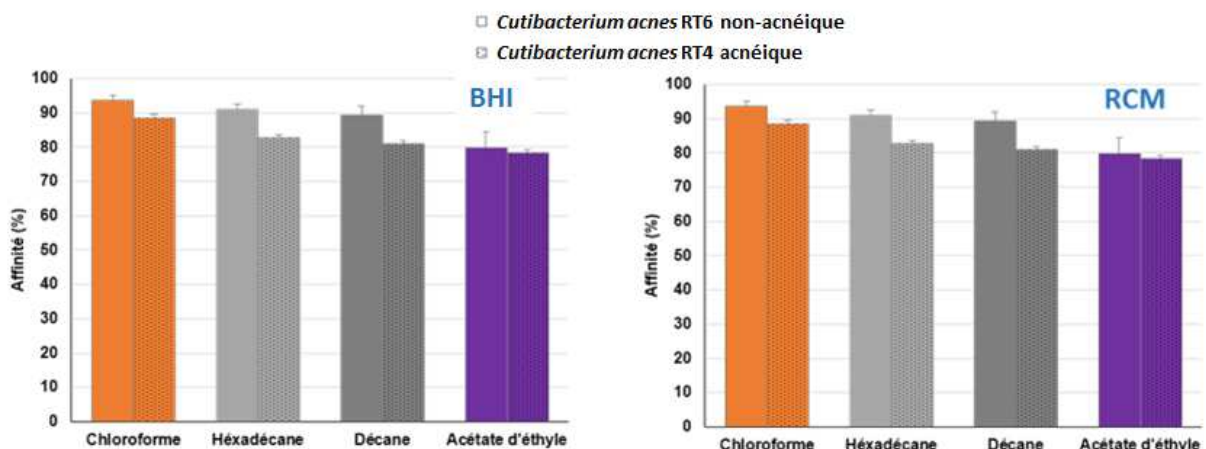


Figure 34 : Caractérisations physiologiques des souches *C. acnes* RT4 (acnéique) et RT6 (non acnéique). A : Cinétiques de croissance à 37°C selon les milieux. B : Affinités aux solvants selon le milieu.

Production scientifique correspondante : C28.

(2) Impact d'une matrice cosmétique complexe de type lotion solaire sur la croissance de deux souches modèles cutanées : *Staphylococcus aureus* MFP 05 et *Pseudomonas fluorescens* MFP04

Les cosmétiques peuvent modifier de façon radicale, voire irréversible la composition et la diversité du microbiote cutané, d'autant plus s'ils sont utilisés régulièrement. Ainsi quelques études ont été menées sur l'impact à long terme de l'utilisation quotidienne de cosmétiques sur la peau (Urban et al., 2016). Les lotions solaires ont la caractéristique de protéger la peau contre les effets néfastes d'une exposition solaire due aux rayonnements UVB (les coups de soleil), mais aussi une protection contre le vieillissement cellulaire relatif aux UVA, voire aux UV artificiels (Debacq-Chainiaux et al., 2012). Parmi les alternatives offertes aux formulateurs de l'industrie cosmétique, le seul filtre UV inorganique que l'Europe autorise sont les nanoparticules (NPs) de l'oxyde de titane (TiO_2) à condition de mentionner [nano] sur l'étiquette produit (*Règlement (CE) no 1223/2009 du Parlement européen et du Conseil du 30 novembre 2009 relatif aux produits cosmétiques*, 2009). Plus récemment, les NPs de ZnO , moins utilisées, ont été permises (Journal officiel de l'Union européenne, 2017). Leur pouvoir anti-rayonnement provient de leurs propriétés optiques, mais

demeurent aussi transparentes après application cutanée (Stark et al., 2015; Wawrzynczak et al., 2016).

La thèse régionale NanoBact du Dr L ROWENCZYK s'est déroulée de 2014 à 2017 en codirection entre l'URCOM, de l'Université du Havre (Pr M GRISEL, Dr C PICARD et Dr N HUCHET) et le LMSM (Pr M FEUILLOLEY et moi-même). Suite à la formulation de deux lotions solaires modèles contenant des NPs hydrophiles ou hydrophobes (Rowenczyk et al., 2016), la croissance de deux bactéries représentatives de la peau humaine *Staphylococcus aureus* MFP 05 et *Pseudomonas fluorescens* MFP04 (Hillion et al., 2013) a été étudiée lors de deux scenarii mimant soit le stockage du produit (formule fraîche), soit lors de l'application de la formule solaire sur la peau (formule vieillie), Figure 35A (Rowenczyk et al., 2017).

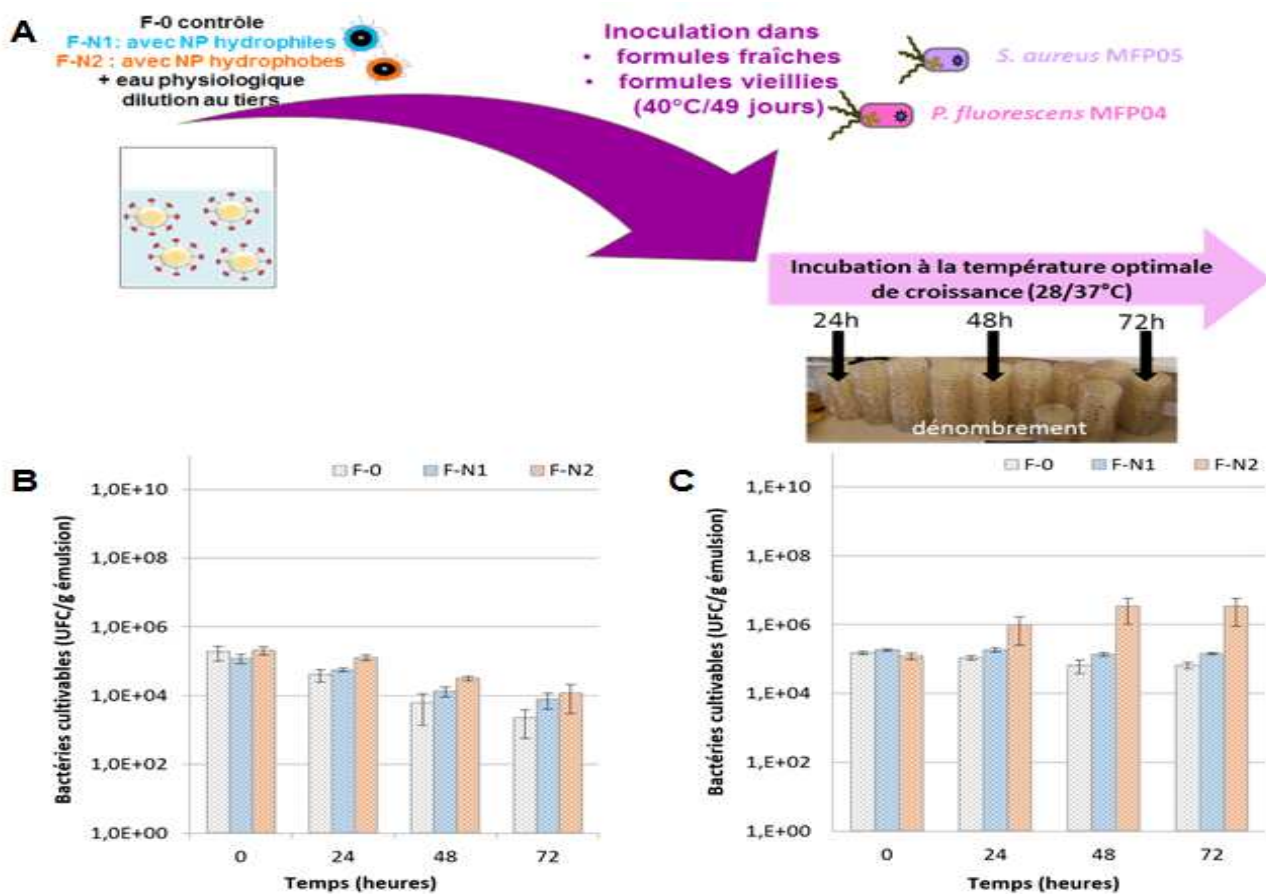


Figure 35 : Impact de la formulation cosmétique sur la croissance de bactéries cutanées. A : Protocole synthétique. B et C : Croissance de la souche *Staphylococcus aureus* MFP05 en formule fraîche et vieillie respectivement.

Pour les deux souches cutanées, la population diminue progressivement suite à leur inoculation en formule fraîche. La Figure 35B présente la croissance de *Staphylococcus aureus* MFP05. Cette diminution ne semble pas imputable à la présence des NPs, ni de leur hydrophilie, mais peut être reliée à l'effet bactéricide de l'émulsion galénique quelle que soit son type (Teixeira et al., 2007). Quant à la croissance en formule vieillie, les deux souches survivent, à l'exception de *S. aureus* MFP05 en présence des NPs hydrophobes favorisant leur développement (Rowenczyk et al., 2017).

Production scientifique correspondante : P27 ; C22 ; C25 ;

Encadrements : Contribution aux travaux de thèse de Laura ROWENCZYK, soutenue le 7 décembre 2016 au Havre.

Ma curiosité a été piquée par ce résultat et je m'interrogeais sur l'impact réel des NPs sur physiologie, voire sur l'homéostasie membranaire bactérienne.

(3) Etude préliminaire de la réponse adaptative bactérienne interagissant avec des NPs

(a) Impact du stress de NPs hydrophiles sur la croissance les bactéries cutanées

Staphylococcus aureus MFP05 et Pseudomonas fluorescens MFP04

Le Dr L ROWENCZYK a poursuivi ses travaux doctoraux en démontrant que la surface des NPs se modifiait au cours du vieillissement du cosmétique en absorbant divers constituants de l'émulsion (Rowenczyk et al., 2016). Aussi il nous est apparu intéressant d'étudier l'impact des particules hydrophiles brutes et extraites de formules fraîche et vieillie sur la croissance des deux souches *S. aureus* MFP05 et *P. fluorescens* MFP04. Les NPs hydrophobes ont été écartées au vu du biais que représente l'ajout d'un tensio-actif nécessaire à la dispersion de ces NPs, mais que les bactéries pourraient métaboliser et surtout qui biaiserait les propriétés de surface des NPs et des bactéries ! Le mode opératoire, présenté en Figure 36A, mime le devenir après bains de mer et de soleil : les NPs en contact avec les bactéries (Rowenczyk et al., 2017).

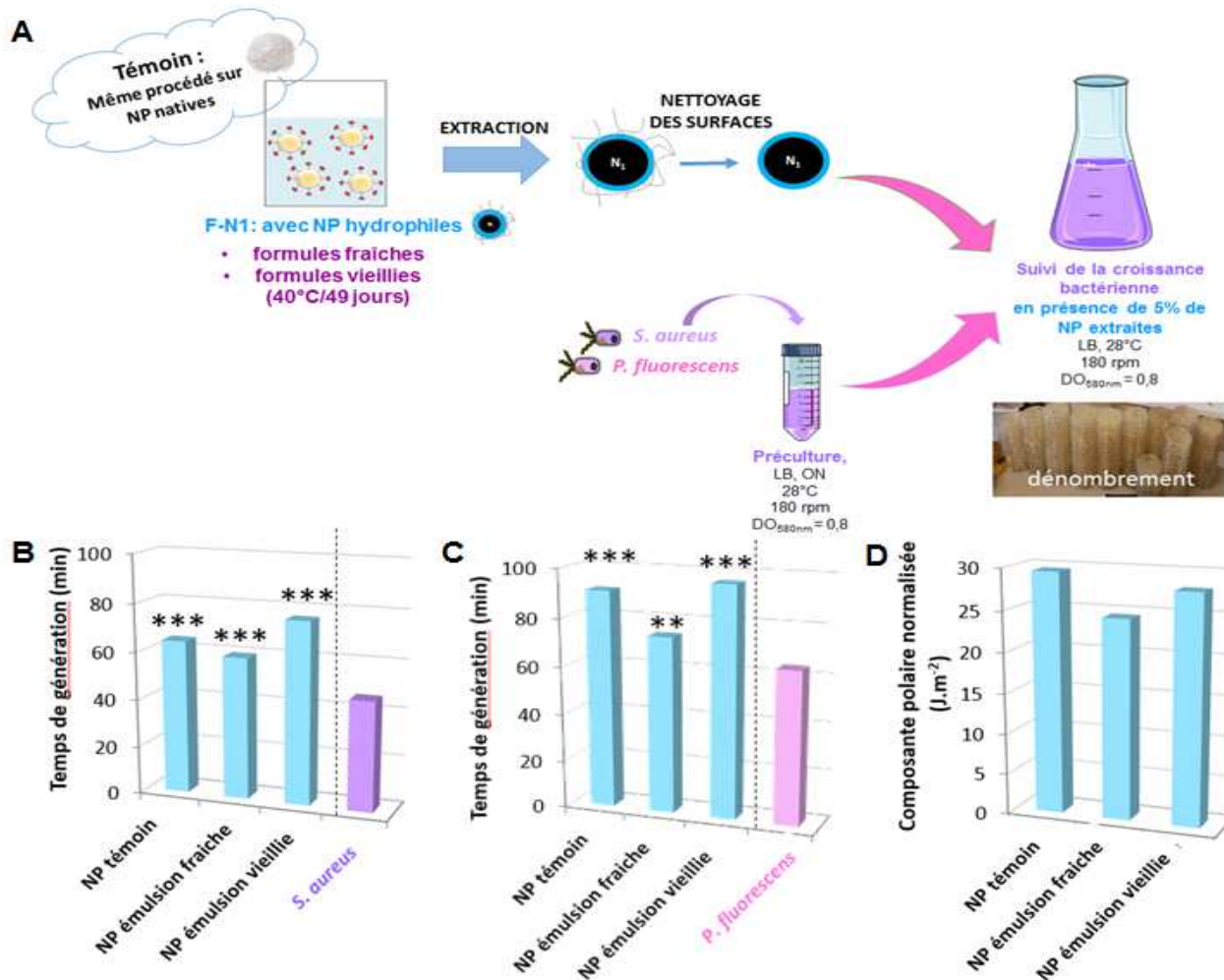


Figure 36 :Impact de NPs hydrophiles sur la croissance de bactéries cutanées. A : Protocole synthétique. B et C : Croissance des souches *Staphylococcus aureus* MFP05 et *P. fluorescens* MFP04, respectivement, en présence de NPs brutes et extraites de formules fraîche et vieillie. D : Polarité des diverses NPs.

Le temps de génération augmente, Figure 36B et C, systématiquement en présence des NPs hydrophiles, par conséquent elles ont un effet inhibiteur sur les souches cutanées (Hamouda et al., 2001; Teixeira et al., 2007). Cependant l'importance de l'inhibition de la croissance est fonction du vécu des NPs en émulsion. Les NPs issues de la formule fraîche inhibent moins la croissance bactérienne que les NPs brutes ou celles extraites de formulation vieillie. Figure 36D présente la polarité de surface des diverses NPs présentant une répartition similaire aux temps de croissance selon le type de NPs. Ainsi les nanoparticules hydrophiles de TiO₂ étalées sur la peau n'ont pas le même impact sur les bactéries cutanées selon le degré de vieillissement d'une lotion solaire (Rowenczyk et al., 2017).

La présentation de ces résultats a permis à L ROWENZYCK d'obtenir son doctorat le 7 décembre 2016, mais aussi de gagner le prix du meilleur poster de la Société Française de Cosmétologie ; elle s'est vu décerner son inscription complète au congrès international IFSCC à Orlando à l'automne 2016 (30 octobre-2 novembre 2016). D'autre part, ces travaux ont été communiqués lors des Journées du GDR Cosm'actifs 2017 (25-26 septembre 2017) lors de deux communications orales l'une réalisée par le Dr N HUCHET et l'autre par moi-même. Ils ont été aussi le support d'une conférence plénière que j'ai réalisée en tandem avec le Dr N HUCHET lors de l'inauguration de la plateforme d'innovation Cosmetomics@Evreux, le 3 octobre 2017.

Production scientifique correspondante : P29 ; C18 ; C20 ; C23 ; C25 ; A41 ;

Encadrements : Contribution aux travaux de thèse de Laura ROWENCZYK, soutenue le 7 décembre 2016 au Havre.

(b) Impact du stress de NPs hydrophiles sur la physiologie de la *Pseudomonas fluorescens* aéroportée MFAF76a

Désirant évaluer le cas d'une biocontamination ponctuelle d'un cosmétique lors de sa production ou lors du prélèvement consommateur avant application, la souche *P. fluorescens* aéroportée MFAF76a (Duclairoir Poc et al., 2014) a été mise en contact avec des formules modèles contenant ou pas de NPs de TiO₂ hydrophiles (Rowenczyk et al., 2017, 2016), Figure 37A. Leurs propriétés optiques, leur conférant leur pouvoir anti-rayonnement UV, perturbent toute mesure spectrophotométrique, aussi seules les approches par dénombrement cultural sont envisageables (Planchon et al., 2013). Ma récente participation au travail doctoral de D DESPLAN co-dirigée par les Pr GRIESMAR (SATIE, Université de Cergy-Pontoise) et Pr ORANGE (LMSM, Université de Rouen) concourra au développement d'une nouvelle technique de caractérisation *in situ* de la croissance bactérienne par le suivi des propriétés mécaniques et électriques de la biomasse. Par ailleurs, nous sommes en cours de développement d'une méthodologie par cytométrie de flux, nécessitant d'utiliser, par conséquent des souches portant un chromophore, d'où l'utilisation de la souche MFAF76abpf, *i.e.* transformant de la souche aéroportée portant la protéine fluorescente bleue, pour cette étude.

Parallèlement, par dénombrement cultural, l'effet inhibiteur des NPs de TiO₂ hydrophiles sur la croissance de la souche est constatée, Figure 37B, déjà observé pour *E. coli* (Foster et al., 2011; Planchon et al., 2013; Wang et al., 2017).

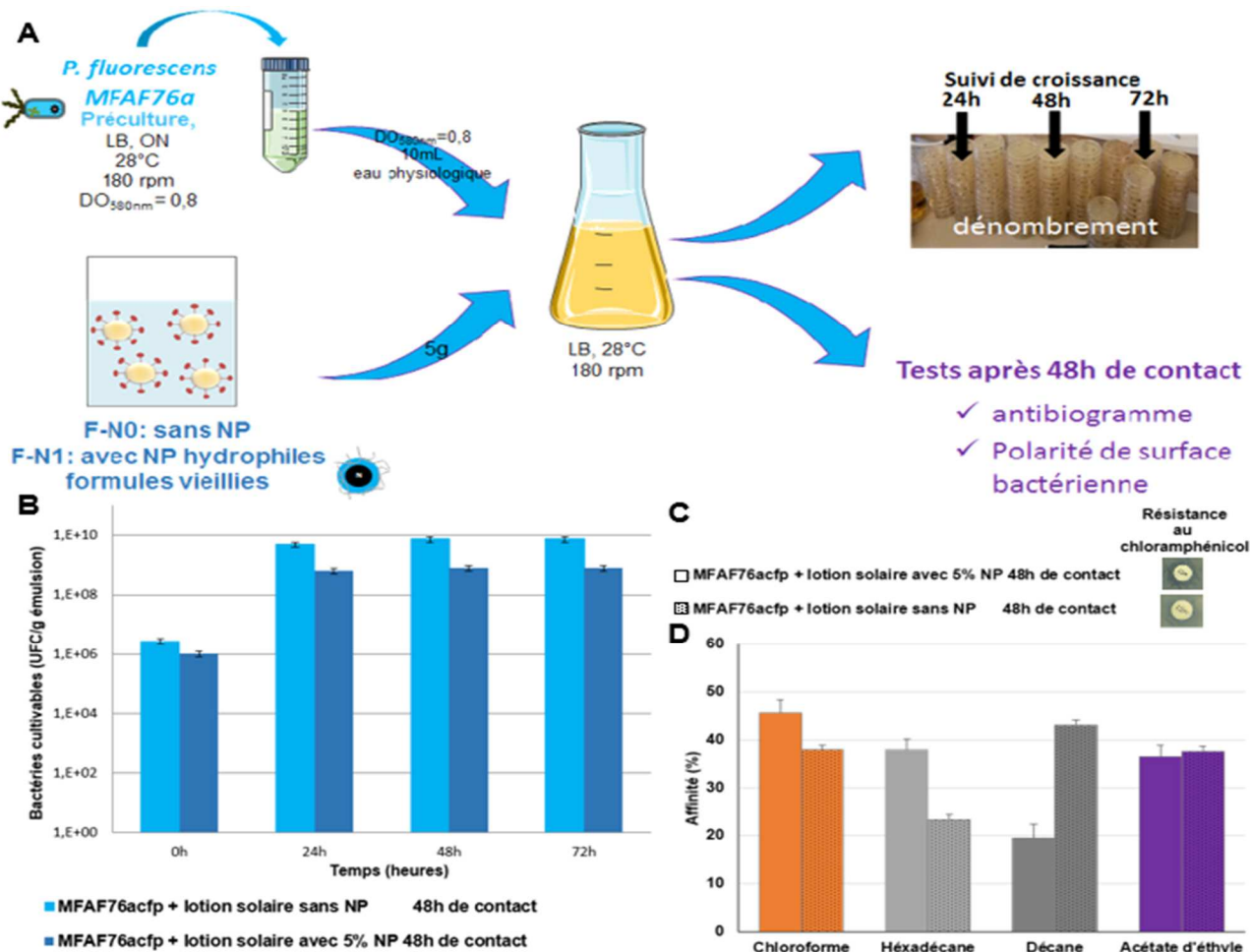


Figure 37 : Caractérisation de la physiologie et des phénotypes de *P. fluorescens* aéroportée MFAF76a en absence et présence de NPs hydrophiles brutes. A : Protocole synthétique. B : Croissance bactérienne C : Résistance au chloramphénicol D : Affinités bactériennes aux divers solvants.

D'autre part, la variation de virulence bactérienne a été évaluée en comparant l'antibiorésistance des bactéries inoculées dans des formulations avec ou sans NP vis-à-vis du chloramphénicol, qui est un antibiotique nitroaromatique et un substrat transporté par la pompe MexEF-OprN (Köhler et al., 1997; Sobel et al., 2005). À la Figure 37C, la présence des NPs hydrophiles favorise la résistance de la bactérie au chloramphénicol et par conséquent laisse à penser à la suractivité des pompes MexEF-OprN, c'est-à-dire une perméabilisation de l'enveloppe bactérienne, voire potentiellement une altération membranaire liée à la porine OprN. Les NPs impactent les propriétés surfaciques de la bactérie qui devient plus hydrophile et son acidité de Lewis se transforme en basicité, Figure 37D. De telles modifications ont déjà été rapportées et peuvent aboutir à la mort cellulaire (Foster et al., 2011). L'homéostasie membranaire se trouve altérée par les NPs hydrophile de TiO₂ étudiées et présentes dans cette matrice cosmétique complexe.

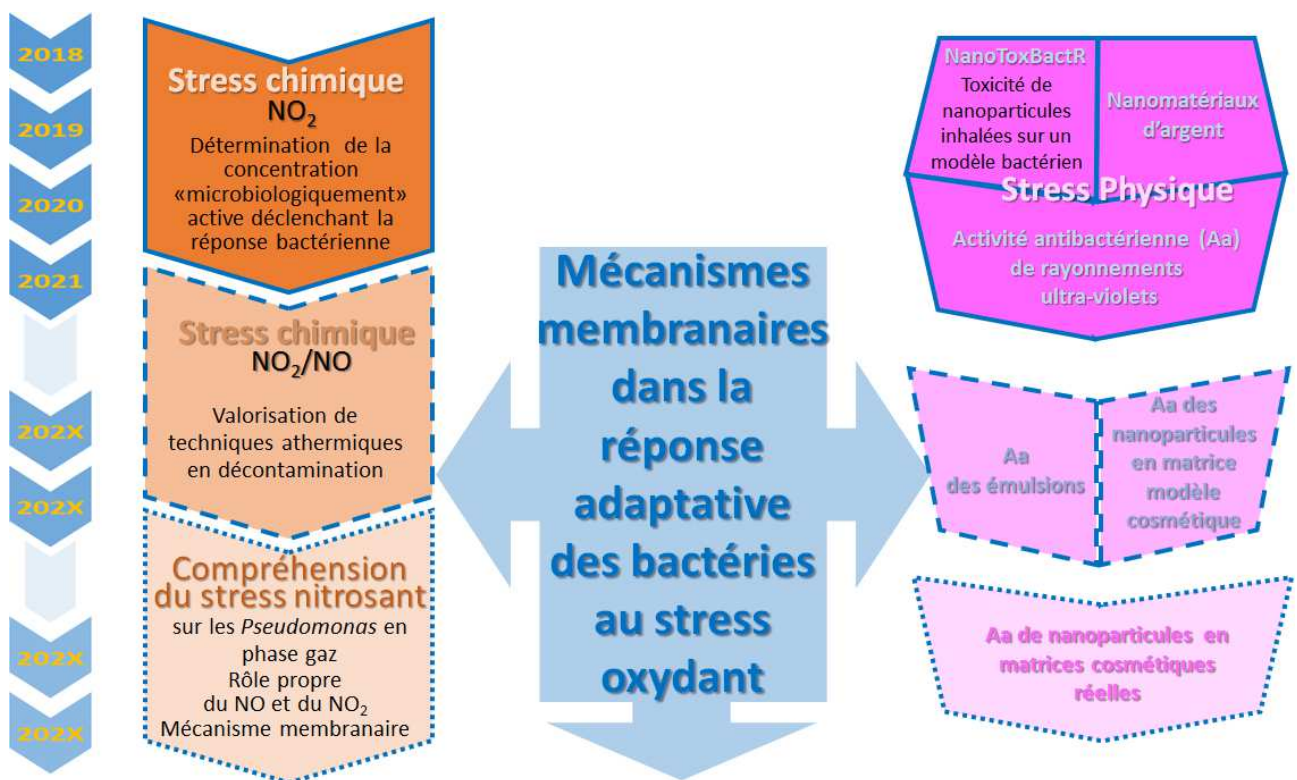
Production scientifique correspondante : C23 ; C25.

Encadrements : M2_6.

Mes perspectives de recherche

Mes perspectives de recherche

La synthèse de mes travaux ayant été réalisée, maintenant quel regard puis-je porter vers l'avenir ? Des voies se dessinent. Il s'agit de l'aspect sécurité sanitaire déclinée au moins dans deux domaines : la niche air et le produit cosmétique dans son contexte cutané. L'autre angle d'approche, dans lequel je désire poursuivre, concerne la réponse bactérienne via les mécanismes mis en œuvre par sa paroi bactérienne, interface de la bactérie avec son microenvironnement. Dans les quelques pages qui vont suivre, je vais vous développer comment je pense pouvoir développer ces différents projets, synthétisés Figure 38. Leur nombre pourrait vous faire craindre que je me puisse m'égarer dans des chemins de traverse. Actuellement je pressens une similitude sur l'ensemble de ces thèmes et c'est cette ligne de force que j'aimerais confirmer, voire documenter par la suite de mes travaux.



I) Sécurité sanitaire de l'air : adaptation bactérienne aux NOx

Comme déjà évoqué précédemment, la pollution est une préoccupation sanitaire de première importance. Le marqueur de pollution automobile NO₂ restera au moins encore quelques décennies d'actualité, bien que des « résultats encourageants de diminution des niveaux des polluants de l'air ont été notés entre 2010 et 2015 (*Air quality in Europe — 2017 report*, 2017). Certains organismes gouvernementaux ou non (e.g. WHO, EEA, et INERIS) désirent réduire drastiquement le parc des véhicules diésel suite aux protocoles de Kyoto, Gothenburg et accord de Paris, signés respectivement en 1997, 1999 et 2015. Néanmoins perdureront les autres sources de pollutions en NO₂ : production

et distribution d'énergie, industries, transport non routier, agriculture, et les secteurs du commerce, des institutions ou des ménages, ces sources représentent actuellement plus de 60% de cette pollution (*Air quality in Europe — 2017 report*, 2017; Depayras et al., 2018a).

Traditionnellement les épidémiologistes expliquent l'augmentation de pneumopathies d'origine bactérienne par une immunodépression humaine consécutive au caractère irritant des polluants sur les tissus pulmonaires facilitant ainsi la colonisation bactérienne (Silveyra et al., 2017). Notre approche a été de documenter une argumentation alternative : la pollution pourrait augmenter (aggraver) la virulence bactérienne *per se* ce qui favoriserait l'infection plus aisée de l'hôte humain par les bactéries en contact avec la pollution. En amont d'une approche intégrative de l'exposition environnementale d'un humain tout au long de sa vie de type exposome (Wild et al., 2013), le modèle bactérien reste un outil unicellulaire beaucoup plus simple de mise en œuvre, par rapport à des organismes plus complexes. De plus sa réponse à un quelconque stress reste appréhendable relativement aisément dans sa globalité par des approches phénotypiques, macroscopiques ou ciblées, aussi bien physiologiques qu'«omics» (protéomique, lipidomique, transcriptomique, génomique, voire métabolomique). Ainsi l'identification de biomarqueurs bactériens suite à l'exposition aux NOx peut venir documenter la toxicité par inhalation du NO₂, du NO et/ou leur synergie, en amont d'une évaluation du risque sanitaire aéroporté. Cette connaissance du stress nitrosant induit en phase gaz pourrait trouver un potentiel applicatif en médecine, en industrie automobile (habitacle).

Suite à l'approche physiologique, transcriptomique, protéomique et lipidomique menée par S DEPAYRAS suite à l'exposition de la souche aéroportée MFAF76a à 45 ppm de NO₂, cette doctorante a désiré clôturer ses travaux (soutenance prévue d'ici fin 2018), avec l'aide d'une étudiante Ingénieur, par la réalisation de mutants de délétion, complémentation et surexpression concernant trois gènes. Actuellement seuls deux jeux ont été concrétisés, ceux d'*oprN* et de *hmp*. L'intérêt pour *oprN* est lié à son implication dans l'homéostasie de la membrane bactérienne. Quant à *hmp*, il est lui relié à la production de protéines impliquées dans l'adaptation du métabolisme respiratoire, voire à la détoxicification. Ainsi les mutants de délétion, complémentation et surexpression ont été obtenus MFAF76aΔ*oprN*, MFAF76aΔ*oprN+oprN* et MFAF76a+*oprN* respectivement pour *oprN* et pour *hmp* MFAF76aΔ*hmp*, MFAF76aΔ*hmp+hmp* et MFAF76a+*hmp*, sans oublier les témoins avec le vecteur vide correspondant. D'ici la fin de ses travaux doctoraux, S DEPAYRAS devrait pouvoir caractériser la réponse physiologique de ces mutants à 45 ppm de NO₂ par l'évaluation de leur survie (cultivabilité, cinétique de croissance, test de perméabilité) et ainsi vérifier l'implication de ces gènes dans la réponse au stress nitrosant.

A moyen terme, je vais poursuivre ces travaux, grâce à une allocation doctorale financée au travers du Réseau d'Intérêt Normand (RIN) Sécurité Sanitaire, bien-être et ALiments durables (SéSAL) par la région Normandie. Le doctorant, recruté début septembre 2018, s'attellera, entre septembre 2018 et Août 2021, à déterminer des Biomarqueurs Bactériens d'Exposition Environnementale (BE²) par inhalation de NOx, polluants automobiles (NOxBBEE). Effectivement, au vu des résultats acquis,

des biomarqueurs bactériens tels que l'homéostasie membranaire, comportement social bactérien, voire les lipides sont clairement pertinents.

Ainsi, en complément des mutants déjà élaborés par S DEPAYRAS, j'aimerais étoffer la banque de mutants en vue de choisir les BE² au NO₂ gazeux par inhalation. Deux voies métaboliques semblent très attrayantes suite à notre précédente étude protéomique : la synthèse de glycérophospholipides (GPs) et le chimiotactisme. D'autant plus que concernant les GPs, j'aimerais concrétiser l'identification (avec le Pr A CORCELLI de l'Università degli Studi di Bari, Italie), voire comprendre la biosynthèse de l'UGP. En d'autres termes, cela me permettrait de poursuivre mon approfondissement de l'adaptation de la membrane bactérienne à l'exposition au NO₂. Quant au chimiotactisme, il est largement impliqué dans le comportement social bactérien. Son évaluation peut être obtenue, chez la souche aéroportée MFAF76a, par la caractérisation de phénotypes : biofilm, appendices cellulaires (pili, flagelles).

Il faudra peut-être prévoir des mutants à mutation multiple. Effectivement l'absence de réponse physiologique discriminante aux concentrations inférieures ou de 5 ppm en NO₂ laisse présager un mécanisme d'adaptation multi-échelle de la souche MFAF76a. Il pourrait être implanté simultanément au niveau de plusieurs gènes. Cette mutation multiple pourra être encore plus complexe à mettre en œuvre qu'une « simple » mutation.

Dans un second temps, le doctorant sera amené à évaluer la réponse des divers mutants qu'il aura pu obtenir suite à leur exposition à 45 ppm de NO₂. Une approche multi-échelle (physiologique, motilité, biofilm, antibiorésistance, protéomique, lipidomique, transcriptomique) sera adaptée selon le gène étudié. Ainsi nous poursuivrons nos collaborations : en région, avec la plateforme PRIMACEN pour la protéomique (Dr J HARDOUIN) et pour l'observation des appendices cellulaires (flagelles) via la microscopie électronique (Dr M-L GUEYE) et, à l'internationale avec le Pr H HEIPER (Helmoltz Institute, Leipzig, Allemagne) pour l'approche lipidomique via les acides gras. Suite à la compilation des divers résultats, un faisceau de régulation devrait apparaître ; ainsi des voies métaboliques préférentiellement mises en œuvre devraient être mises en évidence. Au sein de ces voies activées, nous sélectionnerons les BE². De plus, grâce à la comparaison des réponses de mutants de délétion *ad hoc*, les mécanismes de réponse au NO₂ gazeux et leur synergie pourront être finement établis.

Par la suite, l'exposition de la souche MFAF76a sera menée sur une gamme de concentration en NO₂ mimant l'environnement urbain (0,2 ppm) jusqu'à sa toxicité (45 ppm). Ainsi seront étudiées les relations entre la concentration du polluant automobile et les BE². De cette manière, la concentration en polluant activant la réponse bactérienne ou concentration minimale « effective » devrait être établie. Cette concentration biologiquement active en NO₂ sera confirmée à l'aide de l'exposition des mutants à la même gamme de concentrations et documentera la toxicité par inhalation de ce polluant préoccupant.

Par la suite, une étude similaire sera envisagée avec le NO gazeux à l'aide de la souche MFAF76a et de sa collection de mutants. L'approche multi-échelle précédemment évoquée pourrait être enrichie à l'aide d'analyses RNAseq ciblées voire métabolomiques, grâce aux équipements respectivement acquis par le RIN 2017 et demandé lors du RIN 2018. Grâce à ce dernier équipement, je collaborerai avec un nouveau partenaire normand le Pr R DELEPEE, Plateforme PRISM et laboratoire Aliments Bioprocédés Toxicologie Environnements (ABTE), équipe Toxicologie de l'Environnement Milieux Aériens et Cancers (ToxEMAC) de l'Université de Caen Normandie. Après corrélation des résultats ainsi obtenus et ceux observés avec NO₂, au maximum 2 mutants seront retenus pour envisager les expositions à des mélanges de NO/NO₂.

Parallèlement, des essais de destruction des germes exposés les plus virulents seront développés à l'aide de techniques athermiques, par exemple la photocatalyse. L'objectif serait d'explorer des potentiels applicatifs aussi bien en médecine, qu'en industrie, voire en industrie automobile.

Ainsi à plus long terme, la mise en œuvre d'exposition à des mélanges de NO/NO₂ devrait nous permettre d'affiner la connaissance du stress nitrosant et de découpler le rôle de chacun de ces composés azotés. Une étude, même restreinte, à l'aide de *P. fluorescens* MFN1032 pourrait être fort informative, quant à l'impact des NOx sur la synthèse des biosurfactants ou du rôle de ces exoproducts dans la détoxicification bactérienne.

Quant à l'impact des NOx sur des bactéries, ces travaux aideront à la définition du lien entre NOx - polluants automobiles-, l'homéostasie membranaire et la modulation de la virulence bactérienne. Ensuite l'origine chimique ou bactérienne de l'immuno-suppression humaine pourra être établie dans le cas d'infections pulmonaires bactériennes en présence d'air pollué. De plus, cette démarche, en amont d'évaluation du risque sanitaire aéroporté, permettra de documenter la toxicité par inhalation de ces polluants préoccupants. Les concentrations biologiquement actives déterminées pourraient contribuer à long terme à l'établissement des valeurs toxicologiques en qualité de l'air. Un prolongement industriel serait d'améliorer la qualité de l'atmosphère dans l'habitacle automobile, lieu d'exposition quotidien et important aux NOx. Une implémentation industrielle pourrait être relative à la lutte contre les biofilms de biocontaminants aéroportés en milieu industriel. Quant aux perspectives thérapeutiques, elles pourraient concerner la lutte d'infections opportunistes soit à l'encontre des *Pseudomonas spp.* en dégradant leur paroi, soit en utilisant leurs modes d'action contre d'autres pathogènes en tirant avantage du stress nitrosant. Une meilleure compréhension du mode d'action des RNS (reactive nitrogen species) intéresse le monde médical dans son défi contre les stratégies d'antibiorésistance développées par les microorganismes (Jamil et al., 2017; Pelgrift and Friedman, 2013).

II) Adaptation de bactéries en contact avec un milieu dense

Suite à la thèse du Dr L ROWENZYCK en codirection avec l'URCOM, Université du Havre (Pr M GRISEL, les Dr C PICARD et N HUCHER) et aux travaux ultérieurs, ma curiosité avait été attisée par l'impact des interfaces denses (globules d'émulsion ou nanoparticules) sur la physiologie bactérienne et encore plus intriguée par leurs altérations potentielles envers l'enveloppe bactérienne. D'autant que, suite à son attachement à des NPs de fer valence 0 (Fe^0), *Pseudomonas stutzeri* met en place deux mécanismes de défense prépondérants (Saccà et al., 2014). L'un est d'adapter l'homéostasie membranaire via une répression protéique permettant de maîtriser l'absorption en fer et le second est de contrecarrer les espèces oxydantes (ROS) en les piégeant dans les replis « inhabituels » de protéines surproduites telles que des chaperones, des protéines de choc chaud ou de superoxyde dismutases (SOD). De nombreuses NPs de nature différente sont reportées comme pouvant prévenir de la formation de biofilms bactériens, voire les éliminer. Le pouvoir antibactérien des NPs est fréquemment sous-tendu par 4 processus : 1) perturbation de la membrane bactérienne, 2) génération de ROS; 3) diffusion à travers la membrane bactérienne; et 4) induction d'activités antibactérienne au sein de la cellule, dont des interactions avec l'ADN et les protéines (Wang et al., 2017).

N'ayant pas encore finalisé la mise au point de la méthodologie alternative de dénombrement bactérien en matrice complexe par cytométrie de flux, je me suis réorientée vers une mise en contact des NPs sous forme aérosol avec les bactéries. Cette approche originale pouvant être intéressante en approche de sécurité sanitaire concernant les nanomatériaux (NMx) dont les NPs, qui attirent l'attention de nombreux organismes sanitaires français comme internationaux (*Etat des connaissances relatif aux nanoparticules de dioxyde de titane et d'oxyde de zinc dans les produits cosmétiques en termes de pénétration cutanée, de génotoxicité et de cancérogenèse*, 2011; European Commission and Directorate General for Health & Consumers, 2013; Sccs and Chaudhry, 2015; Scientific Committee on Consumer Safety (SCCS) and Chaudhry, 2016). De plus, la terminologie de « nano-antimicrobial » démontre l'intérêt croissant porté aux NMx, au sens large, pour contrecarrer l'antibiorésistance croissante d'un certain nombre de micro-organismes pathogènes (Jamil et al., 2017; Wang et al., 2017).

Aussi ai-je en novembre 2017 déposé une lettre d'intention intitulée NanoToxBactR auprès de l'ANSES.

A) NanoToxBactR : étude de faisabilité d'un test cytotoxicité des NPs

NanoToxBactR correspond à une étude de faisabilité d'un test cytotoxicité sous forme d'une monocouche de la bactérie aéroportée *P. fluorescens* MFAF76a pour identifier les dangers des nanoparticules (NPs) inhalées. L'objectif serait de mettre à disposition de la communauté un outil

sensible, « rapide » et « simple ». Ainsi, à l'aide de matériel biologique bactérien, une réponse à la mise en contact NPs/bactéries pourrait être obtenue en moins de 24h sans culture, par la quantification de bioindicateur(s) pertinent(s) ne nécessitant aucun post-traitement biochimique et n'entrant aucun biais quantitatif lié à la présence de NPs (Bitounis et al., 2016).

L'originalité de ce travail réside, en partie, dans le contact des NPs aérosolisées avec la monocouche bactérienne conservée sur gélose, et non en milieu liquide, pour mimer l'exposition pulmonaire où les NPs s'accumulent engendrant une réponse inflammatoire (Geiser et al., 2017; Khatri et al., 2017) et stress oxydant (Das and Patra, 2017; Khatri et al., 2017; Wang et al., 2017). Habituellement les concentrations en NPs sont limitées par leur solubilité en phase aqueuse, ici l'élément limitatif sera leur surface spécifique par rapport à celle offerte par la monocouche. Les 2 aérocontaminants choisis sont des NPs de noir de carbone (NPnC), de type céramique, et de cuivre (NPCu), de type métallique. Les NPCu, souvent utilisées comme pigment, dopant électronique ou catalyseur (Rager et al., 2016; Stark et al., 2015). Elles sont aussi connues comme antibactérien, car le cuivre endommage la membrane bactérienne et dégrade son ADN (Vincent et al., 2018). Elles sont fréquemment mises en œuvre dans des procédés industriels par des salariés certes équipés de protections individuelles, mais dont l'efficacité reste relative pour des nanoobjets de quelques dizaines de nanomètres (Honnert and Grzebyk, 2013). Quant aux NPnC, elles relèvent davantage de la qualité de l'air extérieur, car elles miment souvent les suies automobiles (Morin et al., 2009; Stark et al., 2015). De plus, elles sont largement utilisées en cosmétique comme base colorante (0,001 à 10%) pour des soins, des vernis et de nombreux cosmétiques pour les yeux (mascaras, fards...) (Scientific Committee on Consumer Safety (SCCS) and Chaudhry, 2016). L'adaptation du système d'exposition précédemment décrit pourrait être réalisée par nos collaborateurs du CERTAM (les Dr D Préterre & F Gouriou, St Etienne du Rouvray, 76) en y introduisant des aérosols de NPCu ou NPnC générés en amont du système et contrôlés par un granulomètre.

Les monocouches avant et après exposition seraient caractérisées à l'aide de microscopie et d'imagerie par microsonde ionique SIMS. La quantité de NPs déposées selon la surface de la monocouche bactérienne, non hydratée, pourrait être évaluée par microscopie confocale. La qualité du dépôt (homogénéité, répartition des NPs) sur la charge bactérienne serait observée par confocal, MEB et SIMS. Cette technique lourde et innovante sur des matrices biologiques nous serait accessible au travers d'une collaboration avec l'équipe NanoCARE du GPM UMR CNRS 6634 de l'Université de Rouen Normandie-INSA de Rouen (les Dr A Cabin Flaman & A Delaune, D Gibouin).

Dans un premier temps sera établie la concentration nécessaire pour recouvrir intégralement la couche bactérienne qui sera définie comme concentration maximale pour chacune des NPs. Puis l'exposition de la monocouche bactérienne sera réalisée à 2 autres concentrations. Parallèlement à la caractérisation des dépôts, les phénotypes bactériens de viabilité, morphologie et perméabilité seront évalués, et corroborés à l'aide d'une étude de transcriptomique ciblée.

Les travaux de Sacca (Saccà et al., 2014) sur l'exposition de suspension de *P. stutzeri* planctoniques à des NPs de Fe⁰ nous confortent dans notre approche phénotypique et transcriptomique, mais aussi sur nos choix de biomarqueurs : viabilité bactérienne et perméabilisation membranaire.

Cette étude NanoToxBactR confirmerait, en premier lieu, la pertinence du critère perméabilité membranaire des bactéries suite à leur exposition aux NPs comme indication de la toxicité particulière. Actuellement ce type d'évaluation semble biaisée par les interférences que provoquent les NPs lors des dosages biochimiques ou spectrophotométriques, compromettant leur robustesse (Bitounis et al., 2016). Ainsi cet outil robuste serait applicable à tout aérosol de NPs, indépendamment de ses caractéristiques (métallique, céramique, greffé, enrobé...). A plus long terme, il pourrait aussi selon la durée ou la fréquence d'exposition aider à statuer pour des expositions chroniques et/ou cumulées en pollution de l'air (Geiser et al., 2017).

Malheureusement, ce projet n'a pas été retenu par l'ANSES. Nous affinons notre stratégie en vue d'une nouvelle soumission fin 2018.

B) Evaluation de l'activité antibactérienne de nanomatériaux NMx d'argent

En Novembre 2017, j'ai présenté une communication intitulée « Production de viscosinamides par la souche clinique de *Pseudomonas fluorescens* MFN1032: Implication dans le développement du biofilm » à Bioadh2017, où j'ai fait la connaissance du Dr M MORENO (Luxembourg Institute of Science and Technology, Département Recherche et Technologie en matériaux). Ce chercheur fonctionnalise des surfaces de matériaux à l'aide de nanoparticules d'argent par procédé plasma qu'elle développe et se trouve vivement intéressée pour évaluer leur activité antibactérienne.

En cours de rédaction de la lettre d'intention NanoToxBactR à l'ANSES, dont je ne connaissais pas l'issue, je désirais étudier l'impact du contact de NPs / bactérie sur la physiologie et la perméabilité membranaire bactérienne. Les "silver nanomaterials" sont définis comme tout matériau contenant de l'argent dont l'activité est accrue grâce à la structure nanométrique (Marambio-Jones and Hoek, 2010). Un nanomatériau (NM) est un matériau dont au moins une de ses dimensions ou une de ses unités tridimensionnelles est nanométrique (1-100nm) (Wang et al., 2017). Par son procédé, Figure 39, le Dr M MORENO produit des surfaces présentant des clusters nanométriques d'argent métallique Ag⁰.

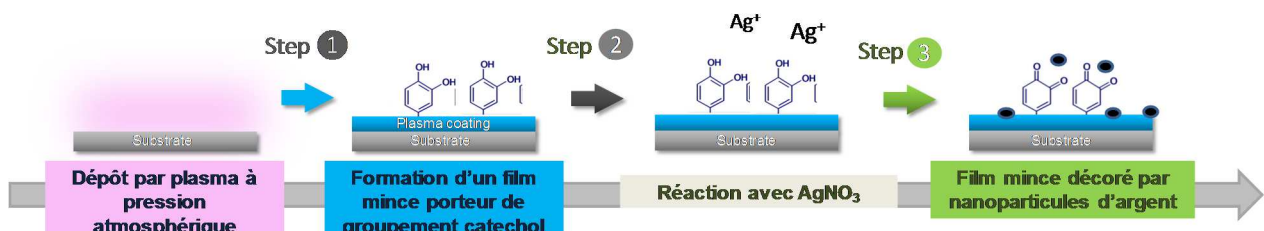


Figure 39 : Procédé d'obtention des nanomatériaux (NMx) d'argent, réalisé par le Dr M MORENO.

L'argent est utilisé depuis des siècles comme antibactérien avec une utilisation moindre depuis la découverte des antibiotiques. Cependant un regain d'intérêt existe suite aux phénomènes d'antibiorésistance développés par de nombreux pathogènes (Chen and Schluesener, 2008; Jamil et al., 2017; Wang et al., 2017) et de nombreux nano-antibiotiques sont développés (Jamil et al., 2017; Marambio-Jones and Hoek, 2010; Zheng et al., 2018), voire industrialisés largement (habillement, biens de consommation, de soin, de santé...). Cette utilisation est si présente que la dissémination des NMx, plus particulièrement des silver NMx, dans l'environnement préoccupent les instances sanitaires européennes (Hartemann et al., 2015; Kapuścińska and Nowak, 2016).

L'activité antibactérienne des silver NMx se réalise via la libération d'ions argent Ag^+ , forme oxydée d' Ag^0 facilement obtenable à pH acide. Ils interagissent directement avec la membrane. Le transport de NPAg (d'environ 80nm) a été constaté au travers de la membrane de *P. aeruginosa* et est reliée à l'expression de la pompe membranaire MexAB-OprM (Picard et al., 2018; Xu et al., 2004), dont le diamètre maximal est dix fois plus petit (Phan et al., 2010). Des zones d'ombres persistent. D'autre part, les Ag^+ réagissent aussi avec l'oxygène de l'air ou de l'eau et induisent la production extra- et intracellulaire de ROS, plus spécifiquement d'ions et de radicaux hydroxyles (Wang et al., 2017). Ils peuvent entraîner, sélectivement ou concomitamment, une augmentation de la perméabilité membranaire, une perte de force motrice protonique induisant une perte énergétique de la bactérie avec un efflux phosphate, une fuite du cytosol, des modifications protéiques, lipidiques, voire une perturbation de la réPLICATION de l'ADN (Das and Patra, 2017; Marambio-Jones and Hoek, 2010; Wang et al., 2017).

De plus la toxicité des silver matériaux est liée à leurs propres caractéristiques intrinsèques : taille, forme, cristallinité, chimie, mais aussi selon les caractéristiques propres à son microenvironnement aqueux ou non (Marambio-Jones and Hoek, 2010). Habituellement l'activité antibactérienne est quantifiée par une mise en contact des NMx en suspension dans une suspension bactérienne (Das and Patra, 2017; Marambio-Jones and Hoek, 2010), qui est biaisée par les interférences provoquées par les NPs lors des dosages (Bitounis et al., 2016). Une autre quantification est de déposer la suspension de nanomatériaux sur un tapis bactérien (Zodrow et al., 2009). Ces protocoles ne sont pas envisageables pour les échantillons matriciels et monofaces fournis par le Dr MORENO. Récemment un stagiaires de BTS a adapté le protocole présenté Figure 40 de la norme ISO 22196 :2011 intitulée Plastiques -- Mesurage de l'action antibactérienne sur les surfaces en plastique.

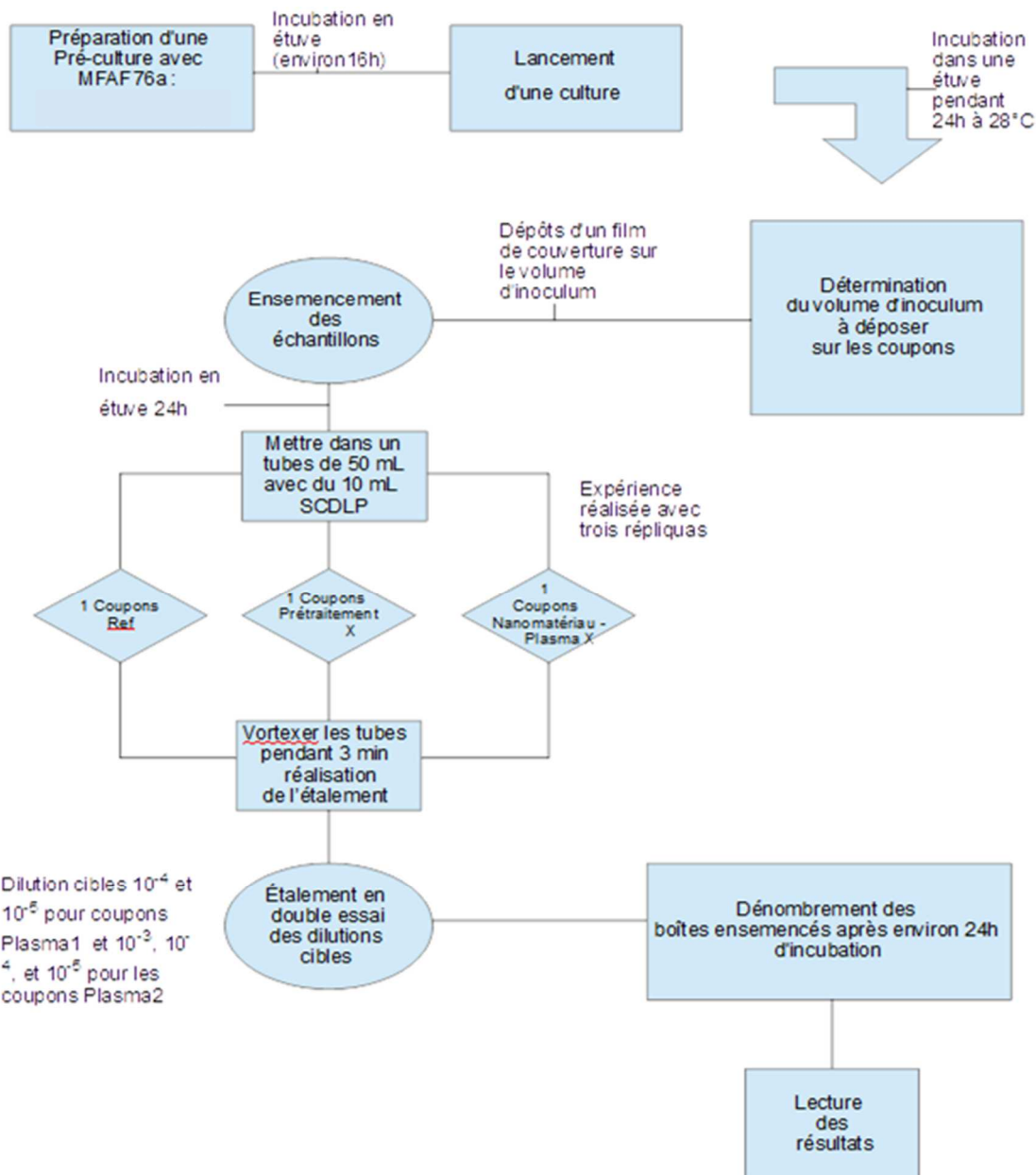


Figure 40 : Protocole d'évaluation de l'activité antibactérienne par dépôt de suspension bactérienne sur la face de NMx.

Le Dr MORENO a fourni deux lots préparés lors de conditions de plasma impactant la quantité et la qualité des dépôts de NPsAg, qui sont en cours de caractérisation. Quant à leur activité antimicrobienne, les essais préliminaires à l'aide de la souche *P. fluorescens* MFAF76a retracent aussi cette différence d'état de surface.

Dans la seconde partie du stage de BTS à l'automne 2018, des essais complémentaires vont permettre de conforter ce protocole. La mise au point de la méthodologie alternative de dénombrement bactérien par cytométrie de flux pourrait être effective alors. Aussi nous pourrions envisager de développer un protocole alternatif grâce à la souche MFAF76abfp, *i.e.* portant une protéine fluorescente bleue. Il éviterait les fastidieux dénombremens sur boîtes de Petri et serait affranchi du biais lié à la présence potentielle de NMx. Cette approche nous permettrait aussi d'évaluer grossièrement la proportion de bactéries partiellement, totalement ou non perméabilisées (Chau et al., 2008). Ainsi nous pourrions discriminer les conditions de préparation plasma représentatives d'un

panel large d'activité antimicrobienne au travers d'une sélection de traitements plasma définis et caractérisés.

Au vu des mécanismes décrits dans la littérature, nous pourrons mettre à profit l'expérience accumulée sur le stress membranaire, mais aussi le stress oxydant, qui inclut le stress nitrosant. Ainsi des approches transcriptomiques ciblées dans un premier temps seront envisagées. Elles pourront être affinées par la suite par des approches complémentaires omics, voire la mise en œuvre de mutants pour affiner la connaissance des mécanismes mis en œuvre par *P. fluorescens* MFAF76a en contact avec les silver nanomatériaux développés par le Dr M MORENO.

C) Evaluation de l'activité antibactérienne de NPs en matrice cosmétique

Les opportunités précédentes concernant les NMx ne m'ont pas détournée de l'approche en sécurité sanitaire des produits cosmétiques, d'autant que les autorités sanitaires européennes imposent depuis mai 2018 une analyse de risque lors du dépôt de nouveaux ingrédients cosmétiques de type NM (SCCS, 2017).

Le contact bactérie/matrice cosmétique que j'ai eu l'opportunité de caractériser a impacté la physiologie bactérienne au niveau viabilité et/ou homéostasie membranaire. Pour appréhender les synergies mises en œuvre lors de la réponse bactérienne, il me semble nécessaire d'étudier les différents partenaires présents dans le microenvironnement bactérien qu'est la lotion solaire. Elle consiste en la dispersion de gouttelettes (émulsion) contenant des particules solides dispersées, les NPs de TiO₂ comme filtres inorganiques. Il s'agit donc d'un système à phases multiples qui apparaît encore plus complexe qu'une simple émulsion. De plus, les NPs de TiO₂ protègent la peau lors d'exposition aux rayonnements UV (Wawrzynczak et al., 2016), mais alors produisent des ROS (Das and Patra, 2017; Wang et al., 2017; Yadav et al., 2016). Ces propriétés photocatalytiques peuvent avoir des conséquences sur la réponse bactérienne, même en absence de rayonnement (Jamil et al., 2017; Pelgrift and Friedman, 2013).

Aussi pour envisager la réponse bactérienne au sein de cette matrice complexe, une scission en plusieurs problématiques s'impose : le contact avec l'émulsion et le contact avec le système photocatalytique. Ce dernier point nécessite d'être à nouveau fragmenté en l'impact du rayonnement et celui du filtre solaire. Au cœur de la lotion solaire, ce filtre photocatalytique générera des ROS qui inévitablement vont déclencher des adaptations bactériennes : métaboliques, membranaires, voire génétiques. Ces conséquences se concrétiseront, en partie, macroscopiquement sous la forme d'activité antibactérienne. Cette activité, dans ce système complexe, reflètera aussi l'interaction avec l'émulsion. Aussi, par ces études, j'entends caractériser l'origine des diverses contributions à la réponse bactérienne *in situ*, i.e. en produit cosmétique.

(1) Evaluation de l'activité antibactérienne des émulsions

Les nano-émulsions (émulsions dont le diamètre moyen des globules est inférieur au micromètre) sont réputées d'une activité antimicrobienne plus importante que les émulsions, liée à leur granulométrie plus fine (Teixeira et al., 2007). Suite à une revue fournie, El Kadri et al. (Kadri et al., 2017) contestent que les survie et croissance bactérienne soient impactées par la granulométrie de l'émulsion, voire que la membrane soit dégradée lors de ce contact (Hamouda et al., 2001; Hamouda and Baker, 2000; Teixeira et al., 2007). L'analogie avec l'interaction bactérie/NM laisserait penser qu'en contact direct avec une interface plus dense, la bactérie pourrait voir sa perméabilité membranaire modifiée (changements structuraux phospholipidiques, protéiques, altération de l'activité respiratoire). Cette réponse membranaire pourrait impactée la communication de la bactérie, voire aboutir à la mort cellulaire (Das and Patra, 2017; Wang et al., 2017). Le débat reste ouvert !

Les travaux doctoraux de D DESPLAN (soutenance prévue fin 2018) avec nos collaborateurs du laboratoire SATIE (Université de Cergy-Pontoise) ont implémenté une nouvelle technique de caractérisation *in situ* de la croissance bactérienne par le suivi des propriétés mécaniques et électriques de l'échantillon. Ainsi les propriétés rhéologiques : G' (module élastique) et G'' (module visco-élastique) permettent de suivre la croissance bactérienne (G''), mais aussi les modifications organisationnelles à l'interface bactérie/matrice.

A moyen terme, l'impact de l'encombrement stérique que représente un globule d'émulsion à la surface bactérienne (*e.g.* *P. fluorescens* MFAF76a) pourra être caractérisé par cette approche micro-rhéologique innovante. J'espère pouvoir la compléter par des approches transcriptomiques ciblées quantifiant l'expression de gènes liés aux ROS, à la perméabilité membranaire, à l'activité respiratoire, mais aussi des gènes méchano-senseurs (Chevalier et al., 2018; Cox et al., 2018; Persat, 2017). L'expérience acquise au cours de l'approche qualité de l'air sera aisément transposable dans ce contexte. De plus l'activité antimicrobienne de l'émulsion pourrait être évaluée en fonction de la densité de la phase globulaire, *i.e.* selon le foisonnement / l'entassement moléculaire en interface de la membrane bactérienne. Ainsi des outils omics (protéomique, lipidomique, transcriptomique, voire métabolomique ciblées) seront couplés à la micro-rhéologie, qui, je l'espère, nous permettra de clarifier les mécanismes bactériens mis en œuvre selon la densité du milieu avec lequel la bactérie crée une interface.

(2) Evaluation de l'activité antibactérienne du rayonnement UV

Une lotion solaire a pour objet de protéger contre les rayonnements solaires, parmi lesquels les rayonnements UV provoquent les plus grands dommages cutanés. Ils se subdivisent en UVA (320-400 nm), UVB (290-320 nm) et UVC (100-290 nm). Même si ces derniers concernent peu ou prou le consommateur, car ils n'atteignent pas la surface terrestre (Yadav et al., 2016). Bien que ces UVC soient réputés antibactériens, l'attention est portée davantage sur les UVB plus abondants et moins pénétrants dans la peau que les UVA plus énergétiques (Gamalier et al., 2017). Les UV induisent des

modifications lipidiques, protéiques (Santos et al., 2013) modifiant la perméabilité membranaire. L'ADN est aussi impacté par oxydation des acides nucléiques. De plus, l'irradiation UV peut accélérer la sécrétion de vésicules, signe avant-coureur de la lyse cellulaire bactérienne (Gamalier et al., 2017).

Une demande de financement de bourse doctorale Cifre a été déposée en juillet 2018 auprès de l'ANRT s'intéressant aux interactions bactérie/ irradiation UV. Ce travail collaboratif avec l'entreprise BASF Beauty Care Solutions France SAS, que je co-encadrerai avec le Pr M FEUILLOLEY, pourra contribuer à une meilleure connaissance des stratégies mises en œuvre par la bactérie dans diverses conditions d'irradiation UV, aussi bien au niveau membranaire, métabolique, voire génétique. Cette approche multi-échelle sera argumentée à l'aide des données physiologiques, protéomiques, lipidomiques, transcriptomiques et métabolomiques, que le futur doctorant acquerra.

(3) Evaluation de l'activité antibactérienne de NPs en matrice cosmétique

Dans la logique de la thèse du Dr L ROWENZYCK en codirection avec l'URCOM, Université du Havre, il semblerait intéressant d'approfondir l'impact de la présence de filtre physique cosmétique. Actuellement TiO₂ et le ZnO sont autorisés (Journal officiel de l'Union européenne, 2017; Stark et al., 2015; Yadav et al., 2016). Ces dernières années une littérature abondante de leur interaction avec les bactéries est parue (Anupama et al., 2018; Das and Patra, 2017; Planchon et al., 2013; Wang et al., 2017), dont certaines en présence d'irradiation UV ou non (Mathur et al., 2017; Qiu et al., 2017). A ma connaissance, seuls les travaux de L Rowencyk ont amorcé une étude *in situ* des interactions bactéries/ NPs en matrice complexe de type produit industriel (Rowencyk et al., 2017) que j'aimerais approfondir. Des travaux récents implémentent les approches omics dans ce contexte contact bactérie/NP TiO₂ simple. Une partie des bactéries survivent à ce contact en adaptant leur métabolisme : une sous production protéique, mais une augmentation des métabolites liés au métabolisme énergétique et à la croissance bactérienne (Planchon et al., 2017). Une étude *in silico* du contact d'un biofilm de *P. aeruginosa* avec des NPs TiO₂ décrit que le gène dont l'expression serait en premier impacté serait *katA* qui interagit ensuite avec *rpoS*, *rpoA*, *dnaK* et *hfq*. *rpoS*, *rpoA* sont reliés à la biosynthèse des ARN, mais aussi l'expression de *rpoS* impacte la motilité, la virulence et la communication bactérienne. Quant à *dnaK* et *hfq*, ils sont impliqués dans la synthèse protéique et la réponse au stress. La protéine DnaK forme un complexe ternaire avec NirC et FliC (Anupama et al., 2018). FliC est une protéine structurante du flagelle, donc relative à la motilité (Acuña et al. 2015), déjà évoquée dans la réponse au NO₂. De même que pour NirC qui chez *P. aeruginosa* est une nitrite réductase (Kondakova et al., 2016).

Ces résultats prédictifs ne sont pas directement transposables au cas du contact bactéries/ NPs en matrice complexe. Cependant nos approches omics ciblant ces différents gènes nous permettront d'affirmer, voire d'amender ce réseau qui présente des similitudes avec nos projets précédents et ceux présentés dans ce projet de recherche.

III) Feuille de route !

Les divers aspects de ces perspectives scientifiques, synthétisés Figure 38, ne seront pas développés simultanément, mais de façon séquentielle au gré de l'obtention de financements, mais aussi des avancées scientifiques, les nôtres ou celles d'autres chercheurs. Nous avons déjà à disposition de nombreux moyens, d'autres seront accessibles au sein de collaborations régionales, nationales et internationales, dont un certain nombre est déjà fonctionnel et d'autres sont à mettre en œuvre ou à créer, comme indiqué en Figure 41.

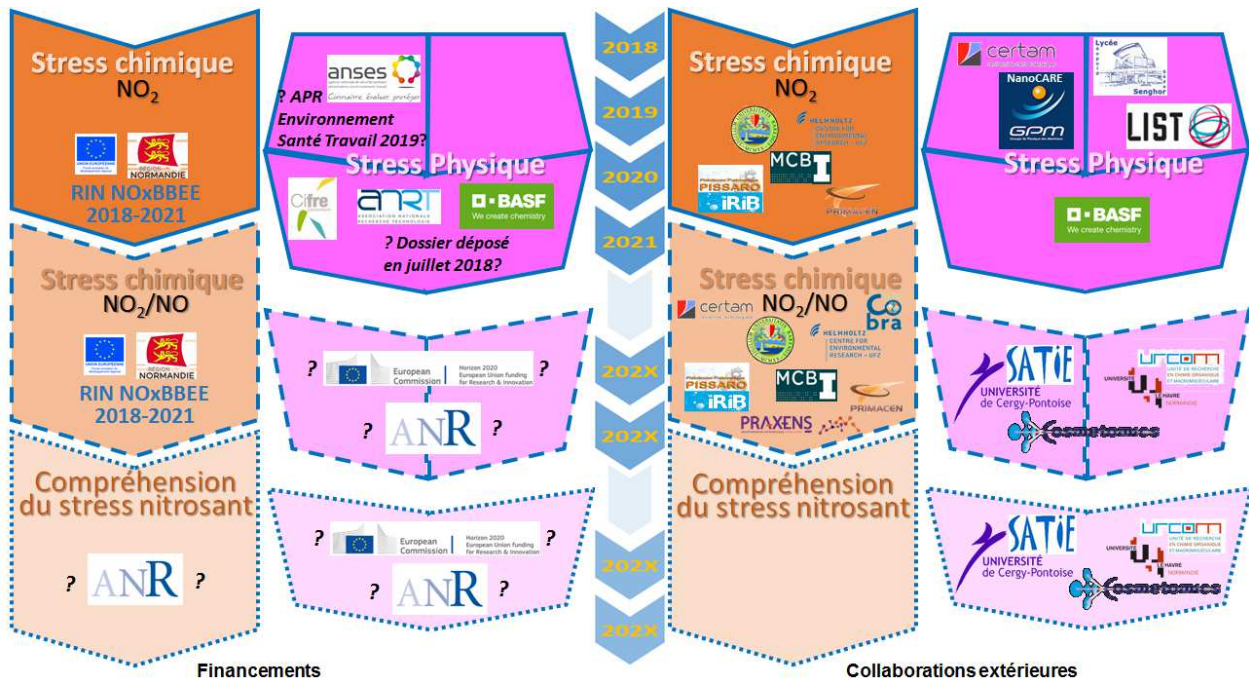


Figure 41 :Financements et collaborations acquis ou envisagés (indiqué par ? xxx ?) pour réaliser mes perspectives de recherche.

Ces thématiques de sécurité sanitaire mobilisent nos organismes gouvernementaux, qui imposent de nouvelles contraintes aux citoyens que nous sommes, mais aussi aux industriels. Aussi des demandes de financements aussi bien publics que privés semblent tout à fait motivables et concrétisables. D'ores et déjà, le retour du BTS ayant amorcé le travail sur les NMx est prévu à l'automne. Notre nouveau doctorant T CHAUTRAND, financé jusqu'en 2021 par le RIN CBS SeSAL, sur la thématique sécurité sanitaire de l'Air, sera chaperonné par l'actuelle doctorante S DEPAYRAS, bénéficiant d'un poste ATER jusqu'en août 2019. La compilation des résultats de cette thèse débutante avec les deux précédentes (T KONDAKOVA et S DEPAYRAS) permettra d'asseoir, dans les prochaines années, la construction d'un projet ANR de type ERA-NET Cofund en Résistance antimicrobienne. D'ici-là, je serai amenée à contacter de nouveaux partenaires nationaux et internationaux. Je pourrai m'appuyer sur le réseau Pseudomonas, GDR en cours de réactivation, mais aussi saisir des opportunités au cours de futurs congrès internationaux.

Suite à sa soutenance fin 2018/début 2019, S DEPAYRAS s'intéressera à la mise au point de la méthode alternative de dénombrement bactérien en matrice complexe contenant des nanoparticules. Courant de l'automne 2018, nous aurons obtenu le retour de l'ANRT concernant le

financement de la bourse doctorale CIFRE en collaboration avec BASF Beauty Care Solutions France SAS. Ainsi, d'ici fin 2018, devrait débuter l'étude de la réponse bactérienne aux rayonnements UV. Quant au contact bactérie/nanomatériaux, notre collaboration avec le Dr MORENO s'étoffera à l'automne avec de nouveaux essais réalisés lors d'un stage BTS. Pour l'aspect nanoparticules, j'envisage de soumettre une lettre d'intention amendée au sujet de NanoToxBactR au prochain appel à projets recherche de l'ANSES. Cette expertise cumulée à l'expérience acquise au travers des collaborations avec les laboratoires URCOM (Université du Havre Normandie) et SATIE (Université de Cergy-Pontoise) et la société BASF Beauty Care Solutions France SAS pourraient me permettre de participer au montage d'un projet FUI, ANR ou projet européen type H2020 permettant de documenter la sécurité sanitaire des produits cosmétiques contenant des nanoparticules par rapport au microbiote cutané, mais aussi l'impact de la pollution sur l'usage des cosmétiques.

Fondamentalement, mon intérêt pour les interfaces a été un fil rouge tout au long de ma vie de chercheur. Ayant débuté par les interfaces physico-chimiques, comprendre comment la membrane bactérienne est une plate-forme intelligente et sélective d'interactions du micro-organisme avec son microenvironnement m'enthousiasme. De plus, je cherche à appréhender les stratégies membranaires, métaboliques et génétiques en réponse à des stress exogènes.

Je poursuis ce chemin qui se trace au gré des interfaces ! En avant pour de nouvelles aventures !

Références bibliographiques

Bibliographie

Adème, 2017. Caractériser et améliorer la qualité de l'air dans les habitacles; qualitifier et limiter les particules émises hors échappement par les véhicules. Adème Vous Lett. Rech. 3–4.

Air quality in Europe — 2017 report (Publication No. 13/2017), 2017. , EEA Report. European Environment Agency, Luxembourg. <https://doi.org/10.2800/850018>

Al-Saad, K.A., Siems, W.F., Hill, H.H., Zabrouskov, V., Knowles, N.R., 2003. Structural analysis of phosphatidylcholines by post-source decay matrix-assisted laser desorption/ionization time-of-flight mass spectrometry. *J. Am. Soc. Mass Spectrom.* 14, 373–382. [https://doi.org/10.1016/S1044-0305\(03\)00068-0](https://doi.org/10.1016/S1044-0305(03)00068-0)

Alsohim, A.S., Taylor, T.B., Barrett, G.A., Gallie, J., Zhang, X.-X., Altamirano-Junqueira, A.E., Johnson, L.J., Rainey, P.B., Jackson, R.W., 2014. The biosurfactant viscosin produced by *Pseudomonas fluorescens* SBW25 aids spreading motility and plant growth promotion: Viscosin mediates sliding motility and plant protection. *Environ. Microbiol.* 16, 2267–2281. <https://doi.org/10.1111/1462-2920.12469>

Ammami, M.T., Portet-Koltalo, F., Benamar, A., Duclairoir-Poc, C., Wang, H., Le Derf, F., 2015. Application of biosurfactants and periodic voltage gradient for enhanced electrokinetic remediation of metals and PAHs in dredged marine sediments. *Chemosphere* 125, 1–8. <https://doi.org/10.1016/j.chemosphere.2014.12.087>

Anupama, R., Sajitha Lulu, S., Mukherjee, A., Babu, S., 2018. Cross-regulatory network in *Pseudomonas aeruginosa* biofilm genes and TiO₂ anatase induced molecular perturbations in key proteins unraveled by a systems biology approach. *Gene* 647, 289–296. <https://doi.org/10.1016/j.gene.2018.01.042>

Arai, H., 2011. Regulation and Function of Versatile Aerobic and Anaerobic Respiratory Metabolism in *Pseudomonas aeruginosa*. *Front. Microbiol.* 2. <https://doi.org/10.3389/fmicb.2011.00103>

Arai, H., Hayashi, M., Kuroi, A., Ishii, M., Igarashi, Y., 2005. Transcriptional Regulation of the Flavohemoglobin Gene for Aerobic Nitric Oxide Detoxification by the Second Nitric Oxide-Responsive Regulator of *Pseudomonas aeruginosa*. *J. Bacteriol.* 187, 3960–3968. <https://doi.org/10.1128/JB.187.12.3960-3968.2005>

Augusto, O., Bonini, M.G., Amanso, A.M., Linares, E., Santos, C.C., De Menezes, S.L., 2002. Nitrogen dioxide and carbonate radical anion: two emerging radicals in biology. *Free Radic. Biol. Med.* 32, 841–859.

Bak, F., Bonnichsen, L., Jørgensen, N.O., Nicolaisen, M.H., Nybroe, O., 2015. The biosurfactant viscosin transiently stimulates n-hexadecane mineralization by a bacterial consortium. *Appl. Microbiol. Biotechnol.* 99, 1475–1483.

Barraud, N., Kjelleberg, S., Rice, S.A., 2015. Dispersal from Microbial Biofilms. *Microbiol. Spectr.* 3.

- Baumgarten, T., Sperling, S., Seifert, J., von Bergen, M., Steiniger, F., Wick, L.Y., Heipieper, H.J.**, 2012a. Membrane Vesicle Formation as a Multiple-Stress Response Mechanism Enhances *Pseudomonas putida* DOT-T1E Cell Surface Hydrophobicity and Biofilm Formation. *Appl. Environ. Microbiol.* 78, 6217–6224. <https://doi.org/10.1128/aem.01525-12>
- Baumgarten, T., Vazquez, J., Bastisch, C., Veron, W., Feuilloley, M.G., Nietzsche, S., Wick, L.Y., Heipieper, H.J.**, 2012b. Alkanols and chlorophenols cause different physiological adaptive responses on the level of cell surface properties and membrane vesicle formation in *Pseudomonas putida* DOT-T1E. *Appl. Microbiol. Biotechnol.* 93, 837–845.
- Bellido, F., Martin, N.L., Siehnel, R.J., Hancock, R.E.**, 1992. Reevaluation, using intact cells, of the exclusion limit and role of porin OprF in *Pseudomonas aeruginosa* outer membrane permeability. *J. Bacteriol.* 174, 5196–5203. <https://doi.org/10.1128/jb.174.16.5196-5203.1992>
- Bisson, M., Bureau, J., Del Gratta, F., Lefevre, J., Levilain, A.**, 2011. Oxydes d'azote NOx (No. DRC-11-117259-10320A), Fiche de données toxicologiques et environnementales des substances chimiques. INERIS, France.
- Bitounis, D., Pourchez, J., Forest, V., Boudard, D., Cottier, M., Klein, J.-P.**, 2016. Detection and analysis of nanoparticles in patients: A critical review of the status quo of clinical nanotoxicology. *Biomaterials* 76, 302–312. <https://doi.org/10.1016/j.biomaterials.2015.10.061>
- Bjarnsholt, T., Tolker-Nielsen, T., Givskov, M.**, 2011. Interfering with “Bacterial Gossip,” in: *Biofilm Highlights*. Springer, pp. 163–188.
- Bjørnlund, L., Rønn, R., Péchy-Tarr, M., Maurhofer, M., Keel, C., Nybroe, O.**, 2009. Functional GacS in *Pseudomonas* DSS73 prevents digestion by *Caenorhabditis elegans* and protects the nematode from killer flagellates. *ISME J.* 3, 770–779. <https://doi.org/10.1038/ismej.2009.28>
- Bonamore, A., Gentili, P., Ilari, A., Schininà, M.E., Boffi, A.**, 2003. *Escherichia coli* Flavohemoglobin Is an Efficient Alkylhydroperoxide Reductase. *J. Biol. Chem.* 278, 22272–22277. <https://doi.org/10.1074/jbc.M301285200>
- Bonnichsen, L., Svenningsen, N.B., Rybtke, M., de Bruijn, I., Raaijmakers, J.M., Tolker-Nielsen, T., Nybroe, O.**, 2015. Lipopeptide biosurfactant viscosin enhances dispersal of *Pseudomonas fluorescens* SBW25 biofilms. *Microbiology* 161, 2289–2297.
- Bouffartigues, E., Moscoso, J.A., Duchesne, R., Rosay, T., Fito-Boncompte, L., Gicquel, G., Maillet, O., Bénard, M., Bazire, A., Brenner-Weiss, G., Lesouhaitier, O., Lerouge, P., Dufour, A., Orange, N., Feuilloley, M.G.J., Overhage, J., Filloux, A., Chevalier, S.**, 2015. The absence of the *Pseudomonas aeruginosa* OprF protein leads to increased biofilm formation through variation in c-di-GMP level. *Front. Microbiol.* 6. <https://doi.org/10.3389/fmicb.2015.00630>
- BOUQUET, S., LANGERON, J.-P.**, n.d. INTERFACES.
- Caiazza, N.C., Merritt, J.H., Brothers, K.M., O’Toole, G.A.**, 2007. Inverse Regulation of Biofilm Formation and Swarming Motility by *Pseudomonas aeruginosa* PA14. *J. Bacteriol.* 189, 3603–3612. <https://doi.org/10.1128/JB.01685-06>

- Calvo, C., Manzanera, M., Silva-Castro, G.A., Uad, I., González-López, J.**, 2009. Application of bioemulsifiers in soil oil bioremediation processes. Future prospects. *Sci. Total Environ.* 407, 3634–3640. <https://doi.org/10.1016/j.scitotenv.2008.07.008>
- Cárcamo-Oyarce, G., Lumjaktase, P., Kümmerli, R., Eberl, L.**, 2015. Quorum sensing triggers the stochastic escape of individual cells from *Pseudomonas putida* biofilms. *Nat. Commun.* 6.
- Carilla-Latorre, S., Calvo-Garrido, J., Bloomfield, G., Skelton, J., Kay, R.R., Ivens, A., Martinez, J.L., Escalante, R.**, 2008. Dictyostelium transcriptional responses to *Pseudomonas aeruginosa*: common and specific effects from PAO1 and PA14 strains. *BMC Microbiol.* 8, 109. <https://doi.org/10.1186/1471-2180-8-109>
- Chapalain, A., Rossignol, G., Lesouhaitier, O., Merieau, A., Gruffaz, C., Guerillon, J., Meyer, J.-M., Orange, N., Feuilloley, M.G.J.**, 2008. Comparative study of 7 fluorescent pseudomonad clinical isolates. *Can. J. Microbiol.* 54, 19–27. <https://doi.org/10.1139/W07-110>
- Chau, F., Lefort, A., Fantin, B.**, 2008. Intérêt et applications de la cytométrie de flux en bactériologie médicale. *Antibiotiques* 10, 226–231. <https://doi.org/10.1016/j.antib.2008.08.006>
- Chen, X., Schluesener, H.J.**, 2008. Nanosilver: A nanoproduct in medical application. *Toxicol. Lett.* 176, 1–12. <https://doi.org/10.1016/j.toxlet.2007.10.004>
- Cheng, S., Lian, B., Liang, J., Shi, T., Xie, L., Zhao, Y.-L.**, 2013. Site selectivity for protein tyrosine nitration: insights from features of structure and topological network. *Mol. Biosyst.* 9, 2860–2868.
- Chevalier, S., Bouffartigues, E., Bazire, A., Tahrioui, A., Duchesne, R., Tortuel, D., Maillot, O., Clamens, T., Orange, N., Feuilloley, M.G.J., Lesouhaitier, O., Dufour, A., Cornelis, P.**, 2018. Extracytoplasmic function sigma factors in *Pseudomonas aeruginosa*. *Biochim. Biophys. Acta BBA - Gene Regul. Mech.* <https://doi.org/10.1016/j.bbagr.2018.04.008>
- Chevalier, S., Bouffartigues, E., Bodilis, J., Maillot, O., Lesouhaitier, O., Feuilloley, M.G.J., Orange, N., Dufour, A., Cornelis, P.**, 2017. Structure, function and regulation of *Pseudomonas aeruginosa* porins. *FEMS Microbiol. Rev.* 41, 698–722. <https://doi.org/10.1093/femsre/fux020>
- Cole, L.K., Vance, J.E., Vance, D.E.**, 2012. Phosphatidylcholine biosynthesis and lipoprotein metabolism. *Biochim. Biophys. Acta BBA - Mol. Cell Biol. Lipids* 1821, 754–761. <https://doi.org/10.1016/j.bbalip.2011.09.009>
- Corker, H., Poole, R.K.**, 2003. Nitric oxide formation by *Escherichia coli*: dependence on nitrite reductase, the NO-sensing regulator Fnr and flavohemoglobin Hmp 37.
- Cox, C.D., Bavi, N., Martinac, B.**, 2018. Bacterial Mechanosensors. *Annu. Rev. Physiol.* 80, 71–93. <https://doi.org/10.1146/annurev-physiol-021317-121351>
- Cronan, J.E.**, 2003. Bacterial Membrane Lipids: Where Do We Stand? *Annu. Rev. Microbiol.* 57, 203–224. <https://doi.org/10.1146/annurev.micro.57.030502.090851>
- Cutruzzolà, F., Frankenberg-Dinkel, N.**, 2016. Origin and Impact of Nitric Oxide in *Pseudomonas aeruginosa* Biofilms. *J. Bacteriol.* 198, 55–65. <https://doi.org/10.1128/JB.00371-15>

- D'aes, J., De Maeyer, K., Pauwelyn, E., Höfte, M.**, 2010. Biosurfactants in plant-*Pseudomonas* interactions and their importance to biocontrol. Environ. Microbiol. Rep. 2, 359–372. <https://doi.org/10.1111/j.1758-2229.2009.00104.x>
- D'aes, J., Kieu, N.P., Léclère, V., Tokarski, C., Olorunleke, F.E., De Maeyer, K., Jacques, P., Höfte, M., Ongena, M.**, 2014. To settle or to move? The interplay between two classes of cyclic lipopeptides in the biocontrol strain *Pseudomonas* CMR12a. Environ. Microbiol. 16, 2282–2300.
- Dagorn, A., Chapalain, A., Mijouin, L., Hillion, M., Duclairoir-Poc, C., Chevalier, S., Taupin, L., Orange, N., Feuilloley, M., Dagorn, A., Chapalain, A., Mijouin, L., Hillion, M., Duclairoir-Poc, C., Chevalier, S., Taupin, L., Orange, N., Feuilloley, M.G.J.**, 2013a. Effect of GABA, a Bacterial Metabolite, on *Pseudomonas fluorescens* Surface Properties and Cytotoxicity. Int. J. Mol. Sci. 14, 12186–12204. <https://doi.org/10.3390/ijms140612186>
- Dagorn, A., Hillion, M., Chapalain, A., Lesouhaitier, O., Duclairoir Poc, C., Vieillard, J., Chevalier, S., Taupin, L., Le Derf, F., Feuilloley, M.G.J.**, 2013b. Gamma-aminobutyric acid acts as a specific virulence regulator in *Pseudomonas aeruginosa*. Microbiology 159, 339–351. <https://doi.org/10.1099/mic.0.061267-0>
- Darby, C.**, 2005. Interactions with microbial pathogens. WormBook.
- Das, B., Patra, S.**, 2017. Antimicrobials, in: Nanostructures for Antimicrobial Therapy. Elsevier, pp. 1–22. <https://doi.org/10.1016/B978-0-323-46152-8.00001-9>
- Das, P., Yang, X.-P., Ma, L.Z.**, 2014. Analysis of biosurfactants from industrially viable *Pseudomonas* strain isolated from crude oil suggests how rhamnolipids congeners affect emulsification property and antimicrobial activity. Front. Microbiol. 5. <https://doi.org/10.3389/fmicb.2014.00696>
- Davies, D.G.**, 2011. Biofilm Dispersion, in: Biofilm Highlights. Springer, pp. 1–28.
- de Araujo, L.V., Guimarães, C.R., da Silva Marquita, R.L., Santiago, V.M., de Souza, M.P., Nitschke, M., Freire, D.M.G.**, 2016. Rhamnolipid and surfactin: Anti-adhesion/antibiofilm and antimicrobial effects. Food Control 63, 171–178.
- de Bruijn, I., de Kock, M.J., Yang, M., de Waard, P., van Beek, T.A., Raaijmakers, J.M.**, 2007. Genome-based discovery, structure prediction and functional analysis of cyclic lipopeptide antibiotics in *Pseudomonas* species. Mol. Microbiol. 63, 417–428.
- De Bruijn, I., De Kock, M.J.D., De Waard, P., Van Beek, T.A., Raaijmakers, J.M.**, 2008. Massetolide A biosynthesis in *Pseudomonas fluorescens*. J. Bacteriol. 190, 2777–2789.
- Debacq-Chainiaux, F., Leduc, C., Verbeke, A., Toussaint, O.**, 2012. UV, stress and aging. Dermatoendocrinol. 4, 236–240. <https://doi.org/10.4161/derm.23652>
- Decoin, V., Barbey, C., Bergeau, D., Latour, X., Feuilloley, M.G., Orange, N., Merieau, A.**, 2014. A type VI secretion system is involved in *Pseudomonas fluorescens* bacterial competition. PLoS One 9, e89411.

- Decoin, V., Gallique, M., Barbey, C., Le Mauff, F., Poc, C.D., Feuilloley, M.G., Orange, N., Merieau, A.**, 2015. A *Pseudomonas fluorescens* type 6 secretion system is related to mucoidy, motility and bacterial competition. BMC Microbiol. 15, 72. <https://doi.org/10.1186/s12866-015-0405-9>
- Depayras, S., Kondakova, T., Heipieper, H.J., Feuilloley, M.G., Orange, N., Duclairoir-Poc, C.,** 2018a. The Hidden Face of Nitrogen Oxides Species: From Toxic Effects to Potential Cure?, in: Soloneski, S., Larramendy, M.L. (Eds.), Emerging Pollutants - Some Strategies for the Quality Preservation of Our Environment. InTech. <https://doi.org/10.5772/intechopen.75822>
- Depayras, S., Kondakova, T., Merlet-Machour, N., Heipieper, H.J., Barreau, M., Catovic, C., Feuilloley, M., Orange, N., Duclairoir-Poc, C.**, 2018b. Impact of gaseous NO₂ on *P. fluorescens* strain in the membrane adaptation and virulence. Int. J. Environ. Impacts Manag. Mitig. Recovery 1, 183–192. <https://doi.org/10.2495/EI-V1-N2-183-192>
- Desai, J.D., Banat, I.M.**, 1997. Microbial production of surfactants and their commercial potential. | Microbiology and Molecular Biology Reviews. Microbiol. Mol. Biol. Rev. 61, 47–64.
- Doumeix, O.**, 2011. Opérations unitaires en génie biologique: Les émulsions. SCÉRÉN-CNDP-CRDP [Aquitaine].
- Dowhan, W., Bogdanov, M., Mileykovskaya, E., Vitrac, H.,** 2017. Functional roles of individual membrane phospholipids in *Escherichia coli* and *Saccharomyces cerevisiae*. Biog. Fat. Acids Lipids Membr. 1–22.
- Duclairoir, C.**, 2000. Encapsulation et applications industrielles. Actual. Chim. 8, 24–27.
- Duclairoir, C., Irache, J.M., Nakache, E., Orecchioni, A.-M., Chabenat, C., Popineau, Y.,** 1999. Gliadin nanoparticles: formation, all- trans-retinoic acid entrapment and release, size optimization. Polym. Int. 48, 327–333. [https://doi.org/10.1002/\(SICI\)1097-0126\(199904\)48:4<327::AID-PI165>3.0.CO;2-Y](https://doi.org/10.1002/(SICI)1097-0126(199904)48:4<327::AID-PI165>3.0.CO;2-Y)
- Duclairoir, C., Nakache, E.,** 2002. Polymer Nanoparticle Characterization in Aqueous Suspensions. Int. J. Polym. Anal. Charact. 7, 284–313. <https://doi.org/10.1080/10236660213159>
- Duclairoir, C., Nakache, E., Marchais, H., Orecchioni, A.-M.,** 1998. Formation of gliadin nanoparticles: Influence of the solubility parameter of the protein solvent. Colloid Polym. Sci. 276, 321–327. <https://doi.org/10.1007/s003960050246>
- Duclairoir, C., Orecchioni, A.M., Depraetere, P., Nakache, E.,** 2002. α-Tocopherol encapsulation and in vitro release from wheat gliadin nanoparticles. J. Microencapsul. 19, 53–60. <https://doi.org/10.1080/02652040110055207>
- Duclairoir, C., Orecchioni, A.-M., Depraetere, P., Osterstock, F., Nakache, E.,** 2003. Evaluation of gliadins nanoparticles as drug delivery systems: a study of three different drugs. Int. J. Pharm. 253, 133–144. [https://doi.org/10.1016/S0378-5173\(02\)00701-9](https://doi.org/10.1016/S0378-5173(02)00701-9)

- Duclairoir Poc, C., Groboillot, A., Lesouhaitier, O., Morin, J.-P., Orange, N., Feuilloley, M.J.**, 2011. *Caenorhabditis elegans* : a model to monitor bacterial air quality. BMC Res. Notes 4, 503. <https://doi.org/10.1186/1756-0500-4-503>
- Duclairoir Poc, C., Verdon, J., Groboillot, A., Barreau, M., Mijouin, L., Leclerc, C., Maillot, O., Kondakova, T., Hulen, C., Morin, J.-P., Feuilloley, M.G., Merieau, A., Orange, N.**, 2014. Airborne fluorescent pseudomonads : What potential for virulence? Int. J. Curr. Microbiol. Appl. Sci. 3, 708–722.
- Etat des connaissances relatif aux nanoparticules de dioxyde de titane et d'oxyde de zinc dans les produits cosmétiques en termes de pénétration cutanée, de génotoxicité et de cancérogenèse** (Rapport relatif aux nanomatériaux dans les produits cosmétiques No. Saisine 2008 BCT0001), 2011. . Afssaps, Paris.
- Europe, F., Unece, F.A.O.**, 2015. State of Europe's forests 2015, in: Ministerial Conference on the Protection of Forests in Europe. p. 314.
- European Commission, Directorate General for Health & Consumers**, 2013. Opinion on Titanium Dioxide (nano form): COLIPA n° S75. European Commission, Luxembourg.
- Farrand, S.K., Hwang, I., Cook, D.M.**, 1996. The tra region of the nopaline-type Ti plasmid is a chimera with elements related to the transfer systems of RSF1010, RP4, and F. J. Bacteriol. 178, 4233–4247.
- Fazli, M., Almblad, H., Rybtke, M.L., Givskov, M., Eberl, L., Tolker-Nielsen, T.**, 2014. Regulation of biofilm formation in *Pseudomonas* and *Burkholderia* species. Environ. Microbiol. 16, 1961–1981.
- Feng, J., Lamour, G., Xue, R., Mirvakili, M.N., Hatzikiriakos, S.G., Xu, J., Li, H., Wang, S., Lu, X.**, 2016. Chemical, physical and morphological properties of bacterial biofilms affect survival of encased *Campylobacter jejuni* F38011 under aerobic stress. Int. J. Food Microbiol. 238, 172–182.
- Ferenci, T.**, 2007. Bacterial Physiology, Regulation and Mutational Adaptation in a Chemostat Environment, in: Advances in Microbial Physiology. Elsevier, pp. 169–315. [https://doi.org/10.1016/S0065-2911\(07\)53003-1](https://doi.org/10.1016/S0065-2911(07)53003-1)
- Fetar, H., Gilmour, C., Klinoski, R., Daigle, D.M., Dean, C.R., Poole, K.**, 2011. *mexEF-oprN* Multidrug Efflux Operon of *Pseudomonas aeruginosa* : Regulation by the MexT Activator in Response to Nitrosative Stress and Chloramphenicol. Antimicrob. Agents Chemother. 55, 508–514. <https://doi.org/10.1128/AAC.00830-10>
- Foster, H.A., Ditta, I.B., Varghese, S., Steele, A.**, 2011. Photocatalytic disinfection using titanium dioxide: spectrum and mechanism of antimicrobial activity. Appl. Microbiol. Biotechnol. 90, 1847–1868. <https://doi.org/10.1007/s00253-011-3213-7>
- Fouchard, S., Abdellaoui-MaÃ¢ne, Z., Boulanger, A., Llopiz, P., Neunlist, S.**, 2005. Influence of growth conditions on *Pseudomonas fluorescens* strains: A link between metabolite production and

the PLFA profile. FEMS Microbiol. Lett. 251, 211–218.

<https://doi.org/10.1016/j.femsle.2005.08.003>

Fuchs, B., Schiller, J., Süß, R., Schürenberg, M., Suckau, D., 2007. A direct and simple method of coupling matrix-assisted laser desorption and ionization time-of-flight mass spectrometry (MALDI-TOF MS) to thin-layer chromatography (TLC) for the analysis of phospholipids from egg yolk. *Anal. Bioanal. Chem.* 389, 827–834. <https://doi.org/10.1007/s00216-007-1488-4>

Fukuto, J.M., Cho, J.Y., Switzer, C.H., 2000. The chemical properties of nitric oxide and related nitrogen oxides, in: Nitric Oxide. Elsevier, pp. 23–40.

Gallardo-Moreno, A.M., Navarro-Pérez, M.L., Vadillo-Rodríguez, V., Bruque, J.M., González-Martín, M.L., 2011. Insights into bacterial contact angles: Difficulties in defining hydrophobicity and surface Gibbs energy. *Colloids Surf. B Biointerfaces* 88, 373–380.

Gallique, M., Bouteiller, M., Merieau, A., 2017. The Type VI Secretion System: A Dynamic System for Bacterial Communication? *Front. Microbiol.* 8. <https://doi.org/10.3389/fmicb.2017.01454>

Gamalier, J.P., Silva, T.P., Zarantonello, V., Dias, F.F., Melo, R.C.N., 2017. Increased production of outer membrane vesicles by cultured freshwater bacteria in response to ultraviolet radiation. *Microbiol. Res.* 194, 38–46. <https://doi.org/10.1016/j.micres.2016.08.002>

Geiser, M., Jeannet, N., Fierz, M., Burtscher, H., 2017. Evaluating Adverse Effects of Inhaled Nanoparticles by Realistic In Vitro Technology. *Nanomaterials* 7, 49. <https://doi.org/10.3390/nano7020049>

Geudens, N., De Vleeschouwer, M., Fehér, K., Rokni-Zadeh, H., Ghequire, M.G.K., Madder, A., De Mot, R., Martins, J.C., Sinnaeve, D., 2014. Impact of a Stereocentre Inversion in Cyclic Lipodepsipeptides from the Viscosin Group: A Comparative Study of the Viscosinamide and Pseudodesmin Conformation and Self-Assembly. *ChemBioChem* 15, 2736–2746. <https://doi.org/10.1002/cbic.201402389>

Grimard, V., Lensink, M., Debailleul, F., Ruysschaert, J., Govaert, C., Remaut, H., Fronzes, R., 2014. The role of lipid composition on bacterial membrane protein conformation and function, in: Bacterial Membranes: Structural and Molecular Biology. Caister Academic Press, pp. 195–224.

Groboillot, A., Portet-Koltalo, F., Le Derf, F., Feuilloley, M.J.G., Orange, N., Duclairoir Poc, C., 2011. Novel Application of Cyclolipopeptide Amphisin: Feasibility Study as Additive to Remediate Polycyclic Aromatic Hydrocarbon (PAH) Contaminated Sediments. *Int. J. Mol. Sci.* 12, 1787–1806. <https://doi.org/10.3390/ijms12031787>

Gusarov, I., Shatalin, K., Starodubtseva, M., Nudler, E., 2009. Endogenous Nitric Oxide Protects Bacteria Against a Wide Spectrum of Antibiotics. *Science* 325, 1380–1384. <https://doi.org/10.1126/science.1175439>

Ha, D.-G., O'Toole, G.A., 2015. c-di-GMP and its Effects on Biofilm Formation and Dispersion: a *Pseudomonas Aeruginosa* Review. *Microbiol. Spectr.* 3. <https://doi.org/10.1128/microbiolspec.MB-0003-2014>

- Hamouda, T., Baker, J.R.**, 2000. Antimicrobial mechanism of action of surfactant lipid preparations in enteric Gram-negative bacilli. *J. Appl. Microbiol.* 89, 397–403. <https://doi.org/10.1046/j.1365-2672.2000.01127.x>
- Hamouda, T., Myc, A., Donovan, B., Shih, A.Y., Reuter, J.D., Baker, J.R.**, 2001. A novel surfactant nanoemulsion with a unique non-irritant topical antimicrobial activity against bacteria, enveloped viruses and fungi. *Microbiol. Res.* 156, 1–7. <https://doi.org/10.1078/0944-5013-00069>
- Harris, P.J., Fincher, G.B.**, 2009. Chapter 4.6 - Distribution, Fine Structure and Function of (1,3;1,4)- β -Glucans in the Grasses and Other Taxa, in: Bacic, A., Fincher, G.B., Stone, B.A. (Eds.), *Chemistry, Biochemistry, and Biology of 1-3 Beta Glucans and Related Polysaccharides*. Academic Press, San Diego, pp. 621–654. <https://doi.org/10.1016/B978-0-12-373971-1.00021-2>
- Harshey, R.M.**, 2003. Bacterial Motility on a Surface: Many Ways to a Common Goal. *Annu. Rev. Microbiol.* 57, 249–273. <https://doi.org/10.1146/annurev.micro.57.030502.091014>
- Hartemann, P., Hoet, P., Proykova, A., Fernandes, T., Baun, A., De Jong, W., Filser, J., Hensten, A., Kneuer, C., Maillard, J.-Y., Norppa, H., Scheringer, M., Wijnhoven, S.**, 2015. Nanosilver: Safety, health and environmental effects and role in antimicrobial resistance. *Mater. Today* 18, 122–123. <https://doi.org/10.1016/j.mattod.2015.02.014>
- Hassett, D.J., Cuppoletti, J., Trapnell, B., Lymar, S.V., Rowe, J.J., Sun Yoon, S., Hilliard, G.M., Parvatiyar, K., Kamani, M.C., Wozniak, D.J., Hwang, S.-H., McDermott, T.R., Ochsner, U.A.**, 2002. Anaerobic metabolism and quorum sensing by *Pseudomonas aeruginosa* biofilms in chronically infected cystic fibrosis airways: rethinking antibiotic treatment strategies and drug targets. *Adv. Drug Deliv. Rev.* 54, 1425–1443. [https://doi.org/10.1016/S0169-409X\(02\)00152-7](https://doi.org/10.1016/S0169-409X(02)00152-7)
- Hay, I.D., Wang, Y., Moradali, M.F., Rehman, Z.U., Rehm, B.H.A.**, 2014. Genetics and regulation of bacterial alginate production: Regulation of bacterial alginate. *Environ. Microbiol.* 16, 2997–3011. <https://doi.org/10.1111/1462-2920.12389>
- Henderson, J.C., Zimmerman, S.M., Crofts, A.A., Boll, J.M., Kuhns, L.G., Herrera, C.M., Trent, M.S.**, 2016. The Power of Asymmetry: Architecture and Assembly of the Gram-Negative Outer Membrane Lipid Bilayer. *Annu. Rev. Microbiol.* 70, 255–278. <https://doi.org/10.1146/annurev-micro-102215-095308>
- Hillion, M., Mijouin, L., Jaouen, T., Barreau, M., Meunier, P., Lefevre, L., Lati, E., Chevalier, S., Feuilloley, M.G.J.**, 2013. Comparative study of normal and sensitive skin aerobic bacterial populations. *MicrobiologyOpen* 2, 953–961. <https://doi.org/10.1002/mbo3.138>
- Hirata, Y., Ryu, M., Oda, Y., Igarashi, K., Nagatsuka, A., Furuta, T., Sugiura, M.**, 2009. Novel characteristics of sophorolipids, yeast glycolipid biosurfactants, as biodegradable low-foaming surfactants. *J. Biosci. Bioeng.* 108, 142–146. <https://doi.org/10.1016/j.jbiosc.2009.03.012>
- Honnert, B., Grzebyk, M.**, 2013. Manufactured Nano-objects: An Occupational Survey in Five Industries in France. *Ann. Occup. Hyg.* <https://doi.org/10.1093/annhyg/met058>

- Jamil, B., Bokhari, H., Imran, M.**, 2017. Mechanism of Action: How Nano-Antimicrobials Act? Curr. Drug Targets 18, 363–373. <https://doi.org/10.2174/1389450116666151019101826>
- Jeter, R.M., 1984. Chromosomal Location and Function of Genes Affecting *Pseudomonas aeruginosa* Nitrate Assimilation 157, 5.
- Journal officiel de l'Union européenne**, 2017. RÈGLEMENT (UE) 2017/ 1413 DE LA COMMISSION - du 3 août 2017 - modifiant l'annexe IV du règlement (CE) no 1223/ 2009 du Parlement européen et du Conseil relatif aux produits cosmétiques.
- Kadri, H.E., Devanthi, P.V.P., Overton, T.W., Gkatzionis, K.**, 2017. Do oil-in-water (O/W) nano-emulsions have an effect on survival and growth of bacteria? Food Res. Int. 101, 114–128. <https://doi.org/10.1016/j.foodres.2017.08.064>
- Kapuścińska, A., Nowak, I.**, 2016. Silver nanoparticles as a challenge for modern cosmetology and pharmacology, in: Nanobiomaterials in Galenic Formulations and Cosmetics. Elsevier, pp. 395–417. <https://doi.org/10.1016/B978-0-323-42868-2.00015-2>
- Kearns, D.B.**, 2010. A field guide to bacterial swarming motility. Nat. Rev. Microbiol. 8, 634–644. <https://doi.org/10.1038/nrmicro2405>
- Khan, S.R., Mavrodi, D.V., Jog, G.J., Suga, H., Thomashow, L.S., Farrand, S.K.**, 2005. Activation of the phz operon of *Pseudomonas fluorescens* 2-79 requires the LuxR homolog *PhzR*, N-(3-OH-hexanoyl)-L-homoserine lactone produced by the LuxI homolog *PhzI*, and a cis-acting phz box. J. Bacteriol. 187, 6517–6527.
- Khatri, M., Bello, D., Martin, J., Bello, A., Gore, R., Demokritou, P., Gaines, P.**, 2017. Chronic upper airway inflammation and systemic oxidative stress from nanoparticles in photocopier operators: Mechanistic insights. NanoImpact 5, 133–145. <https://doi.org/10.1016/j.impact.2017.01.007>
- Kiran, G.S., Ninawe, A.S., Lipton, A.N., Pandian, V., Selvin, J.**, 2016. Rhamnolipid biosurfactants: evolutionary implications, applications and future prospects from untapped marine resource. Crit. Rev. Biotechnol. 36, 399–415.
- Köhler, T., Michea-Hamzehpour, M., Epp, S.F., Pechere, J.-C.**, 1999. Carbapenem Activities against *Pseudomonas aeruginosa*: Respective Contributions of OprD and Efflux Systems. Antimicrob. Agents Chemother. 43, 4.
- Köhler, T., Michéa-Hamzehpour, M., Henze, U., Gotoh, N., Curty, L.K., Pechère, J.C.**, 1997. Characterization of MexE-MexF-OprN, a positively regulated multidrug efflux system of *Pseudomonas aeruginosa*. Mol. Microbiol. 23, 345–354.
- Kondakova, T., Catovic, C., Barreau, M., Nusser, M., Brenner-Weiss, G., Chevalier, S., Dionnet, F., Orange, N., Poc, C.D.**, 2016. Response to Gaseous NO₂ Air Pollutant of *P. fluorescens* Airborne Strain MFAF76a and Clinical Strain MFN1032. Front. Microbiol. 7. <https://doi.org/10.3389/fmicb.2016.00379>

- Kondakova, T., D'Heygère, F., Feuilloley, M.J., Orange, N., Heipieper, H.J., Duclairoir Poc, C.**, 2015a. Glycerophospholipid synthesis and functions in *Pseudomonas*. *Chem. Phys. Lipids* 190, 27–42. <https://doi.org/10.1016/j.chemphyslip.2015.06.006>
- Kondakova, T., Machour, N.M., Poc, C.D.**, 2017. HPTLC-MALDI TOF MS Imaging Analysis of Phospholipids, in: Wood, P. (Ed.), *Lipidomics, Neuromethods*. Springer New York, New York, NY, pp. 163–173. https://doi.org/10.1007/978-1-4939-6946-3_12
- Kondakova, T., Merlet-Machour, N., Chapelle, M., Preterre, D., Dionnet, F., Feuilloley, M., Orange, N., Duclairoir Poc, C.**, 2015b. A new study of the bacterial lipidome: HPTLC-MALDI-TOF imaging enlightening the presence of phosphatidylcholine in airborne *Pseudomonas fluorescens* MFAF76a. *Res. Microbiol.* 166, 1–8. <https://doi.org/10.1016/j.resmic.2014.11.003>
- Kruijt, M., Tran, H., Raaijmakers, J.M.**, 2009. Functional, genetic and chemical characterization of biosurfactants produced by plant growth-promoting *Pseudomonas putida* 267. *J. Appl. Microbiol.* 107, 546–556.
- Landrigan, P.J., Fuller, R., Acosta, N.J.R., Adeyi, O., Arnold, R., Basu, N. (Nil), Baldé, A.B., Bertollini, R., Bose-O'Reilly, S., Boufford, J.I., Breysse, P.N., Chiles, T., Mahidol, C., Coll-Seck, A.M., Cropper, M.L., Fobil, J., Fuster, V., Greenstone, M., Haines, A., Hanrahan, D., Hunter, D., Khare, M., Krupnick, A., Lanphear, B., Lohani, B., Martin, K., Mathiasen, K.V., McTeer, M.A., Murray, C.J.L., Ndaheimanjanara, J.D., Perera, F., Potočnik, J., Preker, A.S., Ramesh, J., Rockström, J., Salinas, C., Samson, L.D., Sandilya, K., Sly, P.D., Smith, K.R., Steiner, A., Stewart, R.B., Suk, W.A., van Schayck, O.C.P., Yadama, G.N., Yumkella, K., Zhong, M.**, 2018. The Lancet Commission on pollution and health. *The Lancet* 391, 462–512. [https://doi.org/10.1016/S0140-6736\(17\)32345-0](https://doi.org/10.1016/S0140-6736(17)32345-0)
- Latza, U., Gerdes, S., Baur, X.**, 2009. Effects of nitrogen dioxide on human health: Systematic review of experimental and epidemiological studies conducted between 2002 and 2006. *Int. J. Hyg. Environ. Health* 212, 271–287. <https://doi.org/10.1016/j.ijheh.2008.06.003>
- Lesouhaitier, O., Veron, W., Chapalain, A., Madi, A., Blier, A.-S., Dagorn, A., Connil, N., Chevalier, S., Orange, N., Feuilloley, M.**, 2009. Gram-Negative Bacterial Sensors for Eukaryotic Signal Molecules. *Sensors* 9, 6967–6990. <https://doi.org/10.3390/s90906967>
- Li, Y., Heine, S., Entian, M., Sauer, K., Frankenberg-Dinkel, N.**, 2013. NO-Induced Biofilm Dispersion in *Pseudomonas aeruginosa* Is Mediated by an MHYT Domain-Coupled Phosphodiesterase. *J. Bacteriol.* 195, 3531–3542. <https://doi.org/10.1128/jb.01156-12>
- Lim, M.W., Lau, E.V., Poh, P.E.**, 2016. A comprehensive guide of remediation technologies for oil contaminated soil — Present works and future directions. *Mar. Pollut. Bull.* 109, 14–45. <https://doi.org/10.1016/j.marpolbul.2016.04.023>
- Loiseau, C., Schlusselhuber, M., Bigot, R., Bertaux, J., Berjeaud, J.-M., Verdon, J.**, 2015. Surfactin from *Bacillus subtilis* displays an unexpected anti-Legionella activity. *Appl. Microbiol. Biotechnol.* 99, 5083–5093. <https://doi.org/10.1007/s00253-014-6317-z>

- Mann, E.E., Wozniak, D.J.**, 2012. Pseudomonas biofilm matrix composition and niche biology. FEMS Microbiol. Rev. 36, 893–916.
- Mansilla, M.C., Cybulski, L.E., Albanesi, D., de Mendoza, D.**, 2004. Control of Membrane Lipid Fluidity by Molecular Thermosensors. J. Bacteriol. 186, 6681–6688. <https://doi.org/10.1128/JB.186.20.6681-6688.2004>
- Mao, X., Jiang, R., Xiao, W., Yu, J.**, 2015. Use of surfactants for the remediation of contaminated soils: A review. J. Hazard. Mater. 285, 419–435. <https://doi.org/10.1016/j.jhazmat.2014.12.009>
- Marambio-Jones, C., Hoek, E.M.V.**, 2010. A review of the antibacterial effects of silver nanomaterials and potential implications for human health and the environment. J. Nanoparticle Res. 12, 1531–1551. <https://doi.org/10.1007/s11051-010-9900-y>
- Marella, E.R., Holkenbrink, C., Siewers, V., Borodina, I.**, 2018. Engineering microbial fatty acid metabolism for biofuels and biochemicals. Curr. Opin. Biotechnol. 50, 39–46. <https://doi.org/10.1016/j.copbio.2017.10.002>
- Martinotti, M.G., Allegrone, G., Cavallo, M., Fracchia, L.**, 2013. Biosurfactants, in: Sustainable Development in Chemical Engineering Innovative Technologies. Wiley-Blackwell, pp. 199–240. <https://doi.org/10.1002/9781118629703.ch9>
- Martins, M.L., Uelinton, M.P., Riedel, K., Vanetti, M.C., Mantovani, H.C., Araújo, E.F. de,** 2014. Lack of AHL-based quorum sensing in *Pseudomonas fluorescens* isolated from milk. Braz. J. Microbiol. 45, 1039–1046.
- Mathur, A., Bhuvaneshwari, M., Babu, S., Chandrasekaran, N., Mukherjee, A.**, 2017. The effect of TiO₂ nanoparticles on sulfate-reducing bacteria and their consortium under anaerobic conditions. J. Environ. Chem. Eng. 5, 3741–3748. <https://doi.org/10.1016/j.jece.2017.07.032>
- McClean, K.H., Winson, M.K., Fish, L., Taylor, A., Chhabra, S.R., Camara, M., Daykin, M., Lamb, J.H., Swift, S., Bycroft, B.W., others**, 1997. Quorum sensing and *Chromobacterium violaceum*: exploitation of violacein production and inhibition for the detection of N-acylhomoserine lactones. Microbiology 143, 3703–3711.
- McCollister, B.D., Hoffman, M., Husain, M., Vázquez-Torres, A.**, 2011. Nitric Oxide Protects Bacteria from Aminoglycosides by Blocking the Energy-Dependent Phases of Drug Uptake. Antimicrob. Agents Chemother. 55, 2189–2196. <https://doi.org/10.1128/AAC.01203-10>
- Mijouin, L., Hillion, M., Ramdani, Y., Jaouen, T., Duclairoir-Poc, C., Follet-Gueye, M.-L., Lati, E., Yvergnaux, F., Driouch, A., Lefevre, L., Farmer, C., Misery, L., Feuilloley, M.G.J.**, 2013. Effects of a Skin Neuropeptide (Substance P) on Cutaneous Microflora. PLOS ONE 8, e78773. <https://doi.org/10.1371/journal.pone.0078773>
- Möller, M.N., Lancaster Jr, J.R., Denicola, A.**, 2008. The interaction of reactive oxygen and nitrogen species with membranes. Curr. Top. Membr. 61, 23–42.

- Moreno-Vivián, C., Cabello, P., Martínez-Luque, M., Blasco, R., Castillo, F.**, 1999. Prokaryotic Nitrate Reduction: Molecular Properties and Functional Distinction among Bacterial Nitrate Reductases. *J. Bacteriol.* 181, 6573–6584.
- Morin, J.-P., Gouriou, F., Preterre, D., Bobbia, M., Delmas, V.**, 2009. Évaluation de l'exposition aux polluants atmosphériques des conducteurs de véhicules automobiles par la mise en œuvre de mesures dynamiques dans l'habitacle du véhicule. *Arch. Mal. Prof. Environ.* 70, 184–192. <https://doi.org/10.1016/j.admp.2008.10.024>
- Morin, J.-P., Preterre, D., Gouriou, F., Delmas, V., François, A., Orange, N., Grosboillot, A., Duclairoir-Poc, C., Moretti, M., Maillet, O., Lesouhaitier, O.**, 2013. Particules urbaines et céréalières, micro-organismes, mycotoxines et pesticides [WWW Document]. Http://revuesinistfrpollution-Atmospherique. <http://dx.doi.org/10.4267/pollution-atmospherique.759>
- N'Diaye, A.R., Leclerc, C., Kentache, T., Hardouin, J., Poc, C.D., Konto-Ghiorghi, Y., Chevalier, S., Lesouhaitier, O., Feuilloley, M.G.J.**, 2016. Skin-bacteria communication: Involvement of the neurohormone Calcitonin Gene Related Peptide (CGRP) in the regulation of *Staphylococcus epidermidis* virulence. *Sci. Rep.* 6, 35379.
- Nielsen, T.H., Christensen, C., Anthoni, U., Sørensen, J.**, 1999. Viscosinamide, a new cyclic depsipeptide with surfactant and antifungal properties produced by *Pseudomonas fluorescens* DR54. *J. Appl. Microbiol.* 87, 80–90. <https://doi.org/10.1046/j.1365-2672.1999.00798.x>
- Nielsen, T.H., Sorensen, D., Tobiasen, C., Andersen, J.B., Christensen, C., Givskov, M., Sorensen, J.**, 2002. Antibiotic and Biosurfactant Properties of Cyclic Lipopeptides Produced by Fluorescent *Pseudomonas* spp. from the Sugar Beet Rhizosphere. *Appl. Environ. Microbiol.* 68, 3416–3423. <https://doi.org/10.1128/AEM.68.7.3416-3423.2002>
- Nielsen, T.H., Sorensen, J.**, 2003. Production of Cyclic Lipopeptides by *Pseudomonas fluorescens* Strains in Bulk Soil and in the Sugar Beet Rhizosphere. *Appl. Environ. Microbiol.* 69, 861–868. <https://doi.org/10.1128/AEM.69.2.861-868.2003>
- Nitschke, M., Silva, S.S. e**, 2018. Recent food applications of microbial surfactants. *Crit. Rev. Food Sci. Nutr.* 58, 631–638. <https://doi.org/10.1080/10408398.2016.1208635>
- Novik, G., Kiseleva, V.S. and E.**, 2015. An Insight Into Beneficial *Pseudomonas* bacteria. *Microbiol. Agric. Hum. Health.* <https://doi.org/10.5772/60502>
- Ongena, M., Jacques, P.**, 2008. Bacillus lipopeptides: versatile weapons for plant disease biocontrol. *Trends Microbiol.* 16, 115–125. <https://doi.org/10.1016/j.tim.2007.12.009>
- Orecchioni, A.-M., Duclairoir, C., Irache, J.M., Nakache, E.**, 2007. Plant Protein-based Nanoparticles, in: Kumar, C.S.S.R. (Ed.), *Nanotechnologies for the Life Sciences*. Wiley-VCH Verlag GmbH & Co. KGaA, Weinheim, Germany. <https://doi.org/10.1002/9783527610419.ntls0016>
- Orecchioni, A.M., Duclairoir, C., Nakache, E.**, 2001. Maîtrise de la taille de nanoparticules de gliadines de blé par la détermination de leur paramètre de solubilité. *Ann. Pharm. Fr.* 59, 402–406.

- Orecchioni, A.-M., Duclairoir, C., Renard, D., Nakache, E.**, 2006. Gliadin Characterization by Sans and Gliadin Nanoparticle Growth Modelization. *J. Nanosci. Nanotechnol.* 6, 3171–3178. <https://doi.org/10.1166/jnn.2006.455>
- Ortega, A., Segura, A., Bernal, P., Pini, C., Daniels, C., Ramos, J.-L., Krell, T., Matilla, M.A.**, 2017. Membrane Composition and Modifications in Response to Aromatic Hydrocarbons in Gram-Negative Bacteria, in: Krell, Tino (Ed.), *Cellular Ecophysiology of Microbe*, Handbook of Hydrocarbon and Lipid Microbiology. Springer International Publishing, Cham, pp. 1–12. https://doi.org/10.1007/978-3-319-20796-4_48-1
- Otzen, D.E.**, 2017. Biosurfactants and surfactants interacting with membranes and proteins: Same but different? *Biochim. Biophys. Acta - Biomembr.* 1859, 639–649. <https://doi.org/10.1016/j.bbamem.2016.09.024>
- Pan, X., Dong, Y., Fan, Z., Liu, C., Xia, B., Shi, J., Bai, F., Jin, Y., Cheng, Z., Jin, S., Wu, W.**, 2017. In vivo Host Environment Alters *Pseudomonas aeruginosa* Susceptibility to Aminoglycoside Antibiotics. *Front. Cell. Infect. Microbiol.* 7. <https://doi.org/10.3389/fcimb.2017.00083>
- Pelgrift, R.Y., Friedman, A.J.**, 2013. Nanotechnology as a therapeutic tool to combat microbial resistance. *Adv. Drug Deliv. Rev.*, Nanotechnology and drug resistance 65, 1803–1815. <https://doi.org/10.1016/j.addr.2013.07.011>
- Persat, A.**, 2017. Bacterial mechanotransduction. *Curr. Opin. Microbiol.*, Cell regulation 36, 1–6. <https://doi.org/10.1016/j.mib.2016.12.002>
- Petrova, O.E., Sauer, K.**, 2016. Escaping the biofilm in more than one way: desorption, detachment or dispersion. *Curr. Opin. Microbiol.* 30, 67–78.
- Phan, G., Benabdelhak, H., Lascombe, M.-B., Benas, P., Rety, S., Picard, M., Ducruix, A., Etchebest, C., Broutin, I.**, 2010. Structural and Dynamical Insights into the Opening Mechanism of *P. aeruginosa* OprM Channel. *Structure* 18, 507–517. <https://doi.org/10.1016/j.str.2010.01.018>
- Picard, M., Tikhonova, E.B., Broutin, I., Lu, S., Verchère, A., Zgurskaya, H.I.**, 2018. Biochemical Reconstitution and Characterization of Multicomponent Drug Efflux Transporters, in: Yamaguchi, A., Nishino, K. (Eds.), *Bacterial Multidrug Exporters: Methods and Protocols*, Methods in Molecular Biology. Springer New York, New York, NY, pp. 113–145. https://doi.org/10.1007/978-1-4939-7454-2_8
- Picot, L., Mezghani-Abdelmoula, S., Chevalier, S., Merieau, A., Lesouhaitier, O., Guerillon, J., Cazin, L., Orange, N., Feuilloley, M.G.J.**, 2004. Regulation of the cytotoxic effects of *Pseudomonas fluorescens* by growth temperature. *Res. Microbiol.* 155, 39–46. <https://doi.org/10.1016/j.resmic.2003.09.014>
- Planchon, M., Ferrari, R., Guyot, F., Gélabert, A., Menguy, N., Chanéac, C., Thill, A., Benedetti, M.F., Spalla, O.**, 2013. Interaction between *Escherichia coli* and TiO₂ nanoparticles in natural and artificial waters. *Colloids Surf. B Biointerfaces* 102, 158–164. <https://doi.org/10.1016/j.colsurfb.2012.08.034>

Planchon, M., Léger, T., Spalla, O., Huber, G., Ferrari, R., 2017. Metabolomic and proteomic investigations of impacts of titanium dioxide nanoparticles on *Escherichia coli*. PLOS ONE 12, e0178437. <https://doi.org/10.1371/journal.pone.0178437>

Poc, C.D., Meylheuc, T., Ngoya, S., Groboillot, A., Bodilis, J., Taupin, L., Mérieau, A., Feuilloley, M., Orange, N., 2011. Influence of growth temperature on cyclopeptides production and on adhesion behaviour in environmental strains of *Pseudomonas fluorescens*. J. Bacteriol. Parasitol. 1, 002.

Poole, R.K., Anjum, M.F., Membrillo-Hernández, J., Kim, S.O., Hughes, M.N., Stewart, V., 1996. Nitric oxide, nitrite, and FnR regulation of hmp (flavohemoglobin) gene expression in *Escherichia coli* K-12. J. Bacteriol. 178, 5487–5492. <https://doi.org/10.1128/jb.178.18.5487-5492.1996>

Portet-Koltalo, F., Ammami, M.T., Benamar, A., Duclairoir-Poc, C., Groboillot, A., Orange, N., 2011. Déséqustration de polluants de type hydrocarbures aromatiques polycycliques à l'interface de sédiments au moyen d'un tensioactif original d'origine biologique 8.

Portet-Koltalo, F., Ammami, M.T., Benamar, A., Poc, C.D., Groboillot, A., Orange, N., 2010. Pollution des sédiments de dragage-Procédés de bioremédiation alliés à l'électromigration. Spectra Anal. 277, 54–58.

Portet-Koltalo, F., Ammami, M.T., Benamar, A., Wang, H., Le Derf, F., Duclairoir-Poc, C., 2013. Investigation of the release of PAHs from artificially contaminated sediments using cyclolipopeptidic biosurfactants. J. Hazard. Mater. 261, 593–601. <https://doi.org/10.1016/j.jhazmat.2013.07.062>

Primo, E.D., Ruiz, F., Masciarelli, O., Giordano, W., 2015. Biofilm Formation and Biosurfactant Activity in Plant-Associated Bacteria, in: Bacterial Metabolites in Sustainable Agroecosystem. Springer, pp. 337–349.

Pukatzki, S., Ma, A.T., Sturtevant, D., Krastins, B., Sarracino, D., Nelson, W.C., Heidelberg, J.F., Mekalanos, J.J., 2006. Identification of a conserved bacterial protein secretion system in *Vibrio cholerae* using the *Dictyostelium* host model system. Proc. Natl. Acad. Sci. 103, 1528–1533. <https://doi.org/10.1073/pnas.0510322103>

Qiu, T.A., Meyer, B.M., Christenson, K.G., Klaper, R.D., Haynes, C.L., 2017. A mechanistic study of TiO₂ nanoparticle toxicity on *Shewanella oneidensis* MR-1 with UV-containing simulated solar irradiation: Bacterial growth, riboflavin secretion, and gene expression. Chemosphere 168, 1158–1168. <https://doi.org/10.1016/j.chemosphere.2016.10.085>

Raaijmakers, J.M., de Bruijn, I., de Kock, M.J.D., 2006. Cyclic Lipopeptide Production by Plant-Associated *Pseudomonas* spp.: Diversity, Activity, Biosynthesis, and Regulation. Mol. Plant. Microbe Interact. 19, 699–710. <https://doi.org/10.1094/MPMI-19-0699>

- Raaijmakers, J.M., De Bruijn, I., Nybroe, O., Onghena, M.**, 2010. Natural functions of lipopeptides from *Bacillus* and *Pseudomonas*: more than surfactants and antibiotics. FEMS Microbiol. Rev. 34, 1037–1062.
- Rager, M.S., Aytug, T., Veith, G.M., Joshi, P.**, 2016. Low-Thermal-Budget Photonic Processing of Highly Conductive Cu Interconnects Based on CuO Nanoinks: Potential for Flexible Printed Electronics. ACS Appl. Mater. Interfaces 8, 2441–2448. <https://doi.org/10.1021/acsami.5b12156>
- Rea, S.L., Graham, B.H., Nakamaru-Ogiso, E., Kar, A., Falk, M.J.**, 2010. Bacteria, yeast, worms, and flies: Exploiting simple model organisms to investigate human mitochondrial diseases. Dev. Disabil. Res. Rev. 16, 200–218. <https://doi.org/10.1002/ddrr.114>
- Redondo-Nieto, M., Barret, M., Morrissey, J., Germaine, K., Martínez-Granero, F., Barahona, E., Navazo, A., Sánchez-Contreras, M., Moynihan, J.A., Muriel, C., Dowling, D., O’Gara, F., Martín, M., Rivilla, R.**, 2013. Genome sequence reveals that *Pseudomonas fluorescens* F113 possesses a large and diverse array of systems for rhizosphere function and host interaction. BMC Genomics 14, 54. <https://doi.org/10.1186/1471-2164-14-54>
- Règlement (CE) no 1223/2009 du Parlement européen et du Conseil du 30 novembre 2009 relatif aux produits cosmétiques**, 2009. , Règlement européen.
- Renard, D., Reddy, T.**, 2007. Polymères d’origine biologique pour la microencapsulation. Lavoisier: Paris, France.
- Renard, Denis, Robert, P., Lavenant, L., Melcion, D., Popineau, Y., Guéguen, J., Duclairoir, C., Nakache, E., Sanchez, C., Schmitt, C.**, 2002a. Creation of biopolymeric colloidal carriers dedicated to controlled release applications, in: Plant Biopolymer Science. pp. 119–124.
- Renard, D., Robert, P., Lavenant, L., Melcion, D., Popineau, Y., Guéguen, J., Duclairoir, C., Nakache, E., Sanchez, C., Schmitt, C.**, 2002. Biopolymeric colloidal carriers for encapsulation or controlled release applications. Int. J. Pharm. 242, 163–166. [https://doi.org/10.1016/S0378-5173\(02\)00143-6](https://doi.org/10.1016/S0378-5173(02)00143-6)
- Renard, Denis, Valle, G.D., Popineau, Y.**, 2002b. Plant Biopolymer Science: Food and Non-food Applications. Royal Society of Chemistry.
- Richard, A., Rossignol, G., Comet, J.-P., Bernot, G., Guespin-Michel, J., Merieau, A.**, 2012. Boolean Models of Biosurfactants Production in *Pseudomonas fluorescens*. PLoS ONE 7, e24651. <https://doi.org/10.1371/journal.pone.0024651>
- Rivardo, F., Turner, R.J., Allegrone, G., Ceri, H., Martinotti, M.G.**, 2009. Anti-adhesion activity of two biosurfactants produced by *Bacillus* spp. prevents biofilm formation of human bacterial pathogens. Appl. Microbiol. Biotechnol. 83, 541–553. <https://doi.org/10.1007/s00253-009-1987-7>
- Rokni-Zadeh, H., Mangas-Losada, A., De Mot, R.**, 2011a. PCR detection of novel non-ribosomal peptide synthetase genes in lipopeptide-producing *Pseudomonas*. Microb. Ecol. 62, 941–947. <https://doi.org/10.1007/s00248-011-9885-9>

- Rokni-Zadeh, H., Mangas-Losada, A., De Mot, R.**, 2011b. PCR Detection of Novel Non-ribosomal Peptide Synthetase Genes in Lipopeptide-Producing Pseudomonas. *Microb. Ecol.* 62. <https://doi.org/10.1007/s00248-011-9885-9>
- Romantsov, T., Wood, J.M.**, 2017. Contributions of membrane lipids to bacterial cell homeostasis upon osmotic challenge. *Biog. Fat. Acids Lipids Membr.* 1–23.
- Ron, E.Z., Rosenberg, E.**, 2001. Natural roles of biosurfactants. Minireview. *Environ. Microbiol.* 3, 229–236. <https://doi.org/10.1046/j.1462-2920.2001.00190.x>
- Roongsawang, N., Hase, K., Haruki, M., Imanaka, T., Morikawa, M., Kanaya, S.**, 2003. Cloning and characterization of the gene cluster encoding arthrobactin synthetase from *Pseudomonas* sp. MIS38. *Chem. Biol.* 10, 869–880.
- Rosenberg, E., Ron, E.Z.**, 1999. High- and low-molecular-mass microbial surfactants. *Appl. Microbiol. Biotechnol.* 52, 154–162. <https://doi.org/10.1007/s002530051502>
- Rossignol, G., Merieau, A., Guerillon, J., Veron, W., Lesouhaitier, O., Feuilloley, M.G., Orange, N.**, 2008. Involvement of a phospholipase C in the hemolytic activity of a clinical strain of *Pseudomonas fluorescens*. *BMC Microbiol.* 8, 189. <https://doi.org/10.1186/1471-2180-8-189>
- Rossignol, G., Sperandio, D., Guerillon, J., Duclairoir Poc, C., Soum-Soutera, E., Orange, N., Feuilloley, M.G.J., Merieau, A.**, 2009. Phenotypic variation in the *Pseudomonas fluorescens* clinical strain MFN1032. *Res. Microbiol.* 160, 337–344. <https://doi.org/10.1016/j.resmic.2009.04.004>
- Rowenczyk, L., Duclairoir-Poc, C., Barreau, M., Picard, C., Hucher, N., Orange, N., Grisel, M., Feuilloley, M.**, 2017. Impact of coated TiO₂-nanoparticles used in sunscreens on two representative strains of the human microbiota: Effect of the particle surface nature and aging. *Colloids Surf. B Biointerfaces* 158, 339–348. <https://doi.org/10.1016/j.colsurfb.2017.07.013>
- Rowenczyk, L., Picard, C., Duclairoir-Poc, C., Hucher, N., Orange, N., Feuilloley, M., Grisel, M.**, 2016. Development of preservative-free nanoparticles-based emulsions: Effects of NP surface properties and sterilization process. *Int. J. Pharm.* 510, 125–134. <https://doi.org/10.1016/j.ijpharm.2016.06.014>
- Roy, A.B., Petrova, O.E., Sauer, K.**, 2012. The Phosphodiesterase DipA (PA5017) Is Essential for *Pseudomonas aeruginosa* Biofilm Dispersion. *J. Bacteriol.* 194, 2904–2915. <https://doi.org/10.1128/JB.05346-11>
- Saccà, M.L., Fajardo, C., Martinez-Gomariz, M., Costa, G., Nande, M., Martin, M.**, 2014. Molecular Stress Responses to Nano-Sized Zero-Valent Iron (nZVI) Particles in the Soil Bacterium *Pseudomonas stutzeri*. *PLOS ONE* 9, e89677. <https://doi.org/10.1371/journal.pone.0089677>
- Saha, N., Monge, C., Dulong, V., Picart, C., Glinel, K.**, 2013. Influence of polyelectrolyte film stiffness on bacterial growth. *Biomacromolecules* 14, 520–528.
- Santos, A.L., Moreirinha, C., Lopes, D., Esteves, A.C., Henriques, I., Almeida, A., Domingues, M.R.M., Delgadillo, I., Correia, A., Cunha, Â.**, 2013. Effects of UV Radiation on the Lipids and

Proteins of Bacteria Studied by Mid-Infrared Spectroscopy. Environ. Sci. Technol. 47, 6306–6315. <https://doi.org/10.1021/es400660g>

Santos, D.K.F., Meira, H.M., Rufino, R.D., Luna, J.M., Sarubbo, L.A., 2017. Biosurfactant production from *Candida lipolytica* in bioreactor and evaluation of its toxicity for application as a bioremediation agent. Process Biochem. 54, 20–27. <https://doi.org/10.1016/j.procbio.2016.12.020>

Sanyal, S., Menon, A.K., 2009. Flipping Lipids: Why an' What's the Reason for? ACS Chem. Biol. 4, 895–909. <https://doi.org/10.1021/cb900163d>

Satpute, S.K., Kulkarni, G.R., Banpurkar, A.G., Banat, I.M., Mone, N.S., Patil, R.H., Cameotra, S.S., 2016. Biosurfactant/s from Lactobacilli species: Properties, challenges and potential biomedical applications. J. Basic Microbiol. 56, 1140–1158. <https://doi.org/10.1002/jobm.201600143>

SCCS, 2017. Checklists for Applicants Submitting Dossiers on Cosmetic Ingredients, SCCS/1588/17. European Commission, Luxembourg.

Sccs, Chaudhry, Q., 2015. Opinion of the Scientific Committee on Consumer safety (SCCS) – Revision of the opinion on the safety of the use of titanium dioxide, nano form, in cosmetic products. Regul. Toxicol. Pharmacol. 73, 669–670. <https://doi.org/10.1016/j.yrtph.2015.09.005>

Scholz, C.F.P., Kilian, M., 2016. The natural history of cutaneous propionibacteria, and reclassification of selected species within the genus *Propionibacterium* to the proposed novel genera *Acidipropionibacterium gen. nov.*, *Cutibacterium gen. nov.* and *Pseudopropionibacterium gen. nov.* Int. J. Syst. Evol. Microbiol. 66, 4422–4432. <https://doi.org/10.1099/ijsem.0.001367>

Schubert, H., Engel, R., 2004. Product and Formulation Engineering of Emulsions. Chem. Eng. Res. Des., In Honour of Professor Alvin W. Nienow 82, 1137–1143. <https://doi.org/10.1205/cerd.82.9.1137.44154>

Scientific Committee on Consumer Safety (SCCS), Chaudhry, Q., 2016. Opinion of the Scientific Committee on Consumer safety (SCCS) – Second revision of the opinion on carbon black, nano-form, in cosmetic products. Regul. Toxicol. Pharmacol. 79, 103–104. <https://doi.org/10.1016/j.yrtph.2016.02.021>

Seghal Kiran, G., Anto Thomas, T., Selvin, J., Sabarathnam, B., Lipton, A.P., 2010. Optimization and characterization of a new lipopeptide biosurfactant produced by marine *Brevibacterium aureum* MSA13 in solid state culture. Bioresour. Technol. 101, 2389–2396. <https://doi.org/10.1016/j.biortech.2009.11.023>

Shiro, Y., 2012. Structure and function of bacterial nitric oxide reductases. Biochim. Biophys. Acta - Bioenerg. 1817, 1907–1913. <https://doi.org/10.1016/j.bbabi.2012.03.001>

Signorelli, S., Möller, M.N., Coitiño, E.L., Denicola, A., 2011. Nitrogen dioxide solubility and permeation in lipid membranes. Arch. Biochem. Biophys. 512, 190–196. <https://doi.org/10.1016/j.abb.2011.06.003>

- Silveyra, P., Fuentes, N., Rivera, L.**, 2017. Understanding the Intersection of Environmental Pollution, Pneumonia, and Inflammation: Does Gender Play a Role?, in: Chroneos, Z.C. (Ed.), Contemporary Topics of Pneumonia. InTech. <https://doi.org/10.5772/intechopen.69627>
- Singh, A., Van Hamme, J.D., Ward, O.P.**, 2007. Surfactants in microbiology and biotechnology: Part 2. Application aspects. *Biotechnol. Adv.* 25, 99–121. <https://doi.org/10.1016/j.biotechadv.2006.10.004>
- Sitaraman, R.**, 2015. *Pseudomonas* spp. as models for plant-microbe interactions. *Front. Plant Sci.* 6. <https://doi.org/10.3389/fpls.2015.00787>
- Sobel, M.L., Neshat, S., Poole, K.**, 2005. Mutations in PA2491 (*mexS*) Promote *MexT*-Dependent *mexEF-oprN* Expression and Multidrug Resistance in a Clinical Strain of *Pseudomonas aeruginosa*. *J. Bacteriol.* 187, 1246–1253. <https://doi.org/10.1128/JB.187.4.1246-1253.2005>
- Soberón-Chávez, G., Lépine, F., Déziel, E.**, 2005. Production of rhamnolipids by *Pseudomonas aeruginosa*. *Appl. Microbiol. Biotechnol.* 68, 718–725. <https://doi.org/10.1007/s00253-005-0150-3>
- Song, F., Koo, H., Ren, D.**, 2015. Effects of Material Properties on Bacterial Adhesion and Biofilm Formation. *J. Dent. Res.* 94, 1027–1034. <https://doi.org/10.1177/0022034515587690>
- Sperandio, D., Decoin, V., Latour, X., Mijouin, L., Hillion, M., Feuilloley, M.G.J., Orange, N., Merieau, A.**, 2012. Virulence of the *Pseudomonas fluorescens* clinical strain MFN1032 towards *Dictyostelium discoideum* and macrophages in relation with type III secretion system. *BMC Microbiol.* 12, 223. <https://doi.org/10.1186/1471-2180-12-223>
- Sperandio, D., Rossignol, G., Guerillon, J., Connil, N., Orange, N., Feuilloley, M.G., Merieau, A.**, 2010. Cell-associated hemolysis activity in the clinical strain of *Pseudomonas fluorescens* MFN1032. *BMC Microbiol.* 10, 124. <https://doi.org/10.1186/1471-2180-10-124>
- Spiro, S.**, 2008. Metalloregulatory proteins and nitric oxide signalling in bacteria: Table 1. *Biochem. Soc. Trans.* 36, 1160–1164. <https://doi.org/10.1042/bst0361160>
- Spiro, S.**, 2007. Regulators of bacterial responses to nitric oxide. *FEMS Microbiol. Rev.* 31, 193–211. <https://doi.org/10.1111/j.1574-6976.2006.00061.x>
- Stark, W.J., Stoessel, P.R., Wohlleben, W., Hafner, A.**, 2015. Industrial applications of nanoparticles. *Chem. Soc. Rev.* 44, 5793–5805. <https://doi.org/10.1039/c4cs00362d>
- Stoodley, P., Sauer, K., Davies, D.G., Costerton, J.W.**, 2002. Biofilms as Complex Differentiated Communities. *Annu. Rev. Microbiol.* 56, 187–209. <https://doi.org/10.1146/annurev.micro.56.012302.160705>
- Svartengren, M., Strand, V., Bylin, G., Järup, L., Pershagen, G.**, 2000. Short-term exposure to air pollution in a road tunnel enhances the asthmatic response to allergen. *Eur. Respir. J.* 15, 716–724.
- Teixeira, P.C., Leite, G.M., Domingues, R.J., Silva, J., Gibbs, P.A., Ferreira, J.P.**, 2007. Antimicrobial effects of a microemulsion and a nanoemulsion on enteric and other pathogens and biofilms. *Int. J. Food Microbiol.* 118, 15–19. <https://doi.org/10.1016/j.ijfoodmicro.2007.05.008>

- Tremblay, J., Déziel, E.**, 2008. Improving the reproducibility of *Pseudomonas aeruginosa* swarming motility assays. *J. Basic Microbiol.* 48, 509–515. <https://doi.org/10.1002/jobm.200800030>
- Urban, J., Fergus, D.J., Savage, A.M., Ehlers, M., Menninger, H.L., Dunn, R.R., Horvath, J.E.**, 2016. The effect of habitual and experimental antiperspirant and deodorant product use on the armpit microbiome. *PeerJ* 4, e1605. <https://doi.org/10.7717/peerj.1605>
- Van Alst, N.E., Picardo, K.F., Iglewski, B.H., Haidaris, C.G.**, 2007. Nitrate Sensing and Metabolism Modulate Motility, Biofilm Formation, and Virulence in *Pseudomonas aeruginosa*. *Infect. Immun.* 75, 3780–3790. <https://doi.org/10.1128/IAI.00201-07>
- Van Hamme, J.D., Singh, A., Ward, O.P.**, 2006. Physiological aspects: Part 1 in a series of papers devoted to surfactants in microbiology and biotechnology. *Biotechnol. Adv.* 24, 604–620. <https://doi.org/10.1016/j.biotechadv.2006.08.001>
- van Sorge, N.M., Beasley, F.C., Gusarov, I., Gonzalez, D.J., von Köckritz-Blickwede, M., Anik, S., Borkowski, A.W., Dorrestein, P.C., Nudler, E., Nizet, V.**, 2013. Methicillin-resistant *Staphylococcus aureus* Bacterial Nitric-oxide Synthase Affects Antibiotic Sensitivity and Skin Abscess Development. *J. Biol. Chem.* 288, 6417–6426. <https://doi.org/10.1074/jbc.M112.448738>
- Vincent, J.-L., Sakr, Y., Sprung, C.L., Ranieri, V.M., Reinhart, K., Gerlach, H., Moreno, R., Carlet, J., Le Gall, J.-R., Payen, D.**, 2006. Sepsis in European intensive care units: Results of the SOAP study*. *Crit. Care Med.* 34, 344. <https://doi.org/10.1097/01.CCM.0000194725.48928.3A>
- Vincent, M., Duval, R.E., Hartemann, P., Engels-Deutsch, M.**, 2018. Contact killing and antimicrobial properties of copper. *J. Appl. Microbiol.* 124, 1032–1046. <https://doi.org/10.1111/jam.13681>
- Vlamakis, H., Chai, Y., Beauregard, P., Losick, R., Kolter, R.**, 2013. Sticking together: building a biofilm the *Bacillus subtilis* way. *Nat. Rev. Microbiol.* 11, 157–168.
- Wang, L., Hu, C., Shao, L.**, 2017. The antimicrobial activity of nanoparticles: present situation and prospects for the future. *Int. J. Nanomedicine* 12, 1227–1249. <https://doi.org/10.2147/IJN.S121956>
- Wawrzynczak, A., Feliczak-Guzik, A., Nowak, I.**, 2016. Nanosunscreens: from nanoencapsulated to nanosized cosmetic active forms, in: *Nanobiomaterials in Galenic Formulations and Cosmetics*. Elsevier, pp. 25–46. <https://doi.org/10.1016/B978-0-323-42868-2.00002-4>
- Weisshoff, H., Hentschel, S., Zaspel, I., Jarling, R., Krause, E., Pham, T.L.**, 2014. PPZPMs--a novel group of cyclic lipopeptides produced by the *Phytophthora alni* associated strain *Pseudomonas sp.* JX090307--the missing link between the viscosin and amphisin group. *Nat. Prod. Commun.* 9, 989–996.
- White, G.M.**, 1998. Recent findings in the epidemiologic evidence, classification, and subtypes of acne vulgaris. *J. Am. Acad. Dermatol.* 39, S34–S37. [https://doi.org/10.1016/S0190-9622\(98\)70442-6](https://doi.org/10.1016/S0190-9622(98)70442-6)
- WHO Regional Office for Europe**, 2013. Review of evidence on health aspects of air pollution – REVIHAAP Project: Technical Report. WHO Regional Office for Europe, Copenhagen.

- Wild, C.P., Scalbert, A., Herceg, Z.**, 2013. Measuring the exposome: A powerful basis for evaluating environmental exposures and cancer risk. *Environ. Mol. Mutagen.* 54, 480–499. <https://doi.org/10.1002/em.21777>
- Williams, P., Winzer, K., Chan, W.C., Camara, M.**, 2007. Look who's talking: communication and quorum sensing in the bacterial world. *Philos. Trans. R. Soc. B Biol. Sci.* 362, 1119–1134. <https://doi.org/10.1098/rstb.2007.2039>
- Xu, X.-H.N., Brownlow, W.J., Kyriacou, S.V., Wan, Q., Viola, J.J.**, 2004. Real-Time Probing of Membrane Transport in Living Microbial Cells Using Single Nanoparticle Optics and Living Cell Imaging [†]. *Biochemistry* 43, 10400–10413. <https://doi.org/10.1021/bi036231a>
- Yadav, H.K.S., Kasina, S., Raizaday, A.**, 2016. Sunscreens, in: *Nanobiomaterials in Galenic Formulations and Cosmetics*. Elsevier, pp. 201–230. <https://doi.org/10.1016/B978-0-323-42868-2.00009-7>
- Yoon, S.S., Hennigan, R.F., Hilliard, G.M., Ochsner, U.A., Parvatiyar, K., Kamani, M.C., Allen, H.L., DeKievit, T.R., Gardner, P.R., Schwab, U., Rowe, J.J., Iglewski, B.H., McDermott, T.R., Mason, R.P., Wozniak, D.J., Hancock, R.E.W., Parsek, M.R., Noah, T.L., Boucher, R.C., Hassett, D.J.**, 2002. *Pseudomonas aeruginosa* Anaerobic Respiration in Biofilms. *Dev. Cell* 3, 593–603. [https://doi.org/10.1016/S1534-5807\(02\)00295-2](https://doi.org/10.1016/S1534-5807(02)00295-2)
- Zhao, A., Zhu, J., Ye, X., Ge, Y., Li, J.**, 2016. Inhibition of biofilm development and spoilage potential of *Shewanella baltica* by quorum sensing signal in cell-free supernatant from *Pseudomonas fluorescens*. *Int. J. Food Microbiol.* 230, 73–80. <https://doi.org/10.1016/j.ijfoodmicro.2016.04.015>
- Zheng, K., Setyawati, M.I., Leong, D.T., Xie, J.**, 2018. Antimicrobial silver nanomaterials. *Coord. Chem. Rev.* 357, 1–17. <https://doi.org/10.1016/j.ccr.2017.11.019>
- Zodrow, K., Brunet, L., Mahendra, S., Li, D., Zhang, A., Li, Q., Alvarez, P.J.J.**, 2009. Polysulfone ultrafiltration membranes impregnated with silver nanoparticles show improved biofouling resistance and virus removal. *Water Res.* 43, 715–723. <https://doi.org/10.1016/j.watres.2008.11.014>

- Yoon, S.S., Hennigan, R.F., Hilliard, G.M., Ochsner, U.A., Parvatiyar, K., Kamani, M.C., Allen, H.L., DeKievit, T.R., Gardner, P.R., Schwab, U., Rowe, J.J., Iglewski, B.H., McDermott, T.R., Mason, R.P., Wozniak, D.J., Hancock, R.E.W., Parsek, M.R., Noah, T.L., Boucher, R.C., Hassett, D.J., 2002. *Pseudomonas aeruginosa* Anaerobic Respiration in Biofilms. *Dev. Cell* 3, 593–603. [https://doi.org/10.1016/S1534-5807\(02\)00295-2](https://doi.org/10.1016/S1534-5807(02)00295-2)
- Zhao, A., Zhu, J., Ye, X., Ge, Y., Li, J., 2016. Inhibition of biofilm development and spoilage potential of *Shewanella baltica* by quorum sensing signal in cell-free supernatant from *Pseudomonas fluorescens*. *Int. J. Food Microbiol.* 230, 73–80. <https://doi.org/10.1016/j.ijfoodmicro.2016.04.015>
- Zheng, K., Setyawati, M.I., Leong, D.T., Xie, J., 2018. Antimicrobial silver nanomaterials. *Coord. Chem. Rev.* 357, 1–17. <https://doi.org/10.1016/j.ccr.2017.11.019>
- Zodrow, K., Brunet, L., Mahendra, S., Li, D., Zhang, A., Li, Q., Alvarez, P.J.J., 2009. Polysulfone ultrafiltration membranes impregnated with silver nanoparticles show improved biofouling resistance and virus removal. *Water Res.* 43, 715–723. <https://doi.org/10.1016/j.watres.2008.11.014>

Mes publications

Publications et communications de C Duclairoir Poc

➤ 30 publications dans des revues internationales ou nationales avec comité de lecture répertoriées par l'AERES ou dans les bases de données internationales (ISI Web of Knowledge, Pub Med...).

P1- Formation of Gliadin Nanoparticles: Influence of the Solubility Parameter of the Gliadin Solvent

C Duclairoir, E Nakache, H Marchais, A-M Orecchioni, Colloid and Interface Science. (1998) **276** : 321-327.

P2- Gliadin Nanoparticles : Formation ; All-trans Retinoic Acid Entrapment and Release, Size Optimization

C Duclairoir, JM Irache, E Nakache, A-M Orecchioni, C Chabenat, Y Popineau, Polymer International., (1999) **79** :327-333.

P3- Maîtrise de la taille de nanoparticules de gliadines de blé par la détermination de leur paramètre de solubilité

A-M Orecchioni, C Duclairoir, E Nakache, Annales Pharmaceutiques Françaises. (2001) **59** : 402-406.

P4- α -tocopherol encapsulation and *in vitro* release from wheat gliadin nanoparticles

C Duclairoir, A-M Orecchioni, P Depraetere, E Nakache, Journal of Microencapsulation. (2002), **19** : 53-60.

P5- Polymer Nanoparticles Characterization in Aqueous Suspension

C Duclairoir, E Nakache, International Journal of Polymer Analysis and Characterization. (2002) **7** : 284-313.

P6- Biopolymeric colloidal carriers for encapsulation or controlled release

D. Renard, P. Robert, L. Lavenant, D. Melcion, Y. Popineau, J. Guéguen, C. Duclairoir, E. Nakache, C. Sanchez and C. Schmitt, International Journal of Pharmaceutics. (2002) 242(1-2) : 163-166.

P7- Evaluation of Gliadins Nanoparticles as Drug Delivery Systems: a Study of Three Different Drugs

C Duclairoir, A-M Orecchioni, P Depraetere, F Osterstock, E Nakache, International Journal of Pharmaceutics. (2003) 253: 133-144.

P8- Gliadin characterization by SANS and gliadin nanoparticle growth modelization.

A-M Orecchioni, C Duclairoir, Denid Renard and E Nakache., Journal of nanoscience and nanotechnology. (2006) **6** :3171-3178.

P9- Phenotypic variation in the *Pseudomonas fluorescens* clinical strain MFN1032

G Rossignol, D Sperandio , J Guerillon, C Duclairoir Poc, E Soum-Soutera, N Orange, MGJ Feuilloley, A Merieau. Res Microbiol. (2009) 160(5):337-44

P10- Pollution des sédiments de dragage : Procédés de bioremédiation alliés à l'électromigration.

F Portet-Koltalo, M Ammami, A Benamar, A Groboillot, N Orange. C Duclairoir Poc Spectra Analyse. (2010) **277** : 54-58.

P11- Déséquéstration de polluants de type hydrocarbures aromatiques polycycliques à l'interface de sédiments au moyen de tensioactifs d'origine biologique. "

F Portet-Koltalo, M Ammami, A Benamar, A Groboillot, N Orange. C Duclairoir Poc Spectra Analyse. (2011) **278** : 21-27.

P12- Novel Application of Cyclolipopeptide Amphisin: Faisability Study as Additive to Remediate PAHs Contaminated Sediments.

A Groboillot, F Koltalo, F Lederf, M Feuilloley, N Orange, C Duclairoir Poc, Int. J. Mol. Sci. (2011) 12 : 1787-1806

P13- *Caenorhabditis elegans* as a model to monitor air bacterial quality"
C Duclairoir Poc, A Groboillot, O Lesouhaitier, M Feuilloley, J-P Morin, N Orange, BMC Res. Notes. (2011) 4:503.

P14- The Major Outer Membrane Protein Oprf is Required for Rhamnolipid Production in *Pseudomonas aeruginosa*

E Bouffartigues, G Gicquel, A Bazire, L Fito-Boncompte, L Taupin, O Maillot, A Groboillot, C Poc-Duclairoir, N Orange, M Feuilloley, A Dufour, S Chevalier. J. Bacteriol. Parasitol. (2011) 2 : 118; DOI : 10.4172/2155-9597.1000118

P15- Influence of growth temperature on cyclolipopeptides production and on adhesion behaviour in environmental strains of *Pseudomonas fluorescens*.

C Duclairoir Poc, T Meylheuc, S Ngoya, A Groboillot, J Bodilis, L Taupin, A Merieau, M Feuilloley, N Orange. J. Bacteriol. Parasitol. (2011) S1-002. <http://dx.doi.org/10.4172/2155-9597.S1-002>.

P16- Gamma-aminobutyric acid acts as a specific virulence regulator in *Pseudomonas aeruginosa*

A Dagorn, M Hillion, A Chapalain, O Lesouhaitier, C Duclairoir Poc, J Vieillard, S Chevalier, L Taupin, F Le Derf, MGJ Feuilloley, Microbiology. (2013) 159:339-351

P17- Investigation of the release of PAHs from artificially contaminated sediments using cyclolipopeptidic biosurfactants

F Portet-Koltalo, MT Ammami, A Benamar, H Wang, F Le Derf, C Duclairoir-Poc, Journal of Hazardous Materials. (2013) 261:593– 601.

P18- Effect of GABA, a bacterial metabolite, on *Pseudomonas fluorescens* surface properties and cytotoxicity

A Dagorn, A Chapalain, L Mijouin, M Hillion, C Duclairoir-Poc, S Chevalier, L Taupin, N Orange, MGJ Feuilloley, Int. J. Mol. Sci. (2013) 14 : 12186-12204; DOI : 10.3390/ijms140612186.

P19- Effects of a Skin Neuropeptide (Substance P) on Cutaneous Microflora

L Mijouin, M Hillion, Y Ramdani, T Jaouen, C Duclairoir-Poc, ML Gueye, E Lati, F Yvergnaux, A Driouch, L Lefevre, L Misery, MGJ Feuilloley, PLoS ONE. (2013) 8(11): e78773 ; DOI : 10.1371/journal.pone.0078773:.

P20- Airborne fluorescent pseudomonads : what potential for virulence ?

C Duclairoir Poc, J Verdon, A Groboillot, M Barreau, H Toucourou, L Mijouin, C Leclerc, C Hulen, T Kondakova JP Morin, MGJ Feuilloley, A Merieau, N Orange, International Journal of Current microbiology and applied sciences.(2014) 3(8) : 708-722.

P21- A new tool for studying bacterial lipidome: HPTLC-MALDI-TOF Imaging enlightening virulence traits of the airborne *Pseudomonas fluorescens* MFAF76a

T Kondakova, N Merlet-Machour, M Chapelle, D Preterre, F Dionet, MJ Feuilloley, N Orange, C Duclairoir Poc, Research in Microbiology. (2015) 166 : 1-8; DOI : 10.1016/j.resmic.2014.11.003

P22- Application of biosurfactants and periodic voltage gradient for enhanced electrokinetic remediation of metals and PAHs in dredged marine sediments

M T Ammami, F Portet-Koltalo, A Benamar, C Duclairoir Poc, H Wang, F Le Derf, Chemosphere. (2015) 125 : 1–8.

P23- Surface functionalization of cyclic olefin copolymer witharyldiazonium salts: A covalent grafting method

F Brisset, J Vieillard, B Berton, S Morin-Grognet,C Duclairoir-Poc, F Le Derf, Applied Surface Science. (2015) 329 : 337–346.

P24- Glycerophospholipid synthesis and functions in *Pseudomonas*: eukaryotic lipid exploitation

T Kondakova; F D'Heygère ; M J. Feuilloley; N Orange; H J Heipieper; C Duclairoir Poc, Chemistry and Physics of Lipids. (2015) 190:27-42; DOI : 10.1016/j.chemphyslip.2015.06.006.

P25- A *Pseudomonas fluorescens* type 6 secretion system is related to mucoidy, motility and bacterial competition

V Decoin, M Gallique, C Barbey, F Le Mauff, C Duclairoir Poc, MGJ Feuilloley, N Orange, A Merieau, BMC Microbiology. (2015) 15(1); DOI: 10.1186/s12866-015-0405-9.

P26- Response to Gaseous NO₂ Air Pollutant of *P. fluorescens* Airborne Strain MFAF76a and Clinical Strain MFN1032

T Kondakova, C Catovic, M Barreau, M Nusser, G Brenner-Weiss, M Feuilloley, F Dionnet, N Orange, C Duclairoir Poc, Front Microbiol. (2016) 7:379; DOI : 10.3389/fmicb.2016.00379.

P27- Development of preservative-free nanoparticles-based emulsions: Effects of NP surface properties and sterilization process.

L Rowenczyk, C Picard, C Duclairoir Poc, N Hucher, N Orange, M Feuilloley, M Grisel. Int J Pharm. (2016) 510(1) : 125-34; DOI : 10.1016/j.ijpharm.2016.06.014.

P28- Skin-bacteria communication: Involvement of the neurohormone Calcitonin Gene Related Peptide (CGRP) in the regulation of *Staphylococcus epidermidis* virulence.

A N'Diaye, C Leclerc, T Kentache, J Hardouin, C Duclairoir Poc, Y Konto-Ghiorghi, S Chevalier, O Lesouhaitier, MG Feuilloley. Sci Rep. (2016) 6: 35379; DOI : 10.1038/srep35379.

P29- Impact of coated TiO₂-nanoparticles used in sunscreens on two representative strains of the human microbiota: Effect of the particle surface nature and aging

L Rowenczyk, C Duclairoir Poc, M Barreau, C Picard, N Hucher, N Orange, M Grisel, M Feuilloley. Colloids and Surfaces B: Biointerfaces. (2017)[158](#) : 339-348; DOI : 10.1016/j.colsurfb.2017.07.013.

P30- Impact of gaseous NO₂ on *P. fluorescens* strain in the membrane adaptation and virulence.

S Depayras, T Kondakova, N Merlet-Machour, H J Heipieper, M Barreau, C Catovic, M Feuilloley, N Orange, C Duclairoir Poc, *Int. J. Environ. Impacts.* (2018), 1(3) : 1–10.

➤ **Chapitres de livre: 4**

Ch1- Creation of biopolymeric colloidal carriers dedicated to controlled release applications

D Renard, P Robert, L Lavenant, D Melcion, Y Popineau, J Gueguen, C Duclairoir, E Nakache, C Sanchez and C Schmitt

In Plant biopolymer science: food and non-food applications p.119-124, Denis Renard, Guy Della Valle, Yves Popineau, eds, Royal Society of Chemistry (Great Britain 2002)

Ch2- Plant protein-based nanoparticles

A-M Orecchioni, C Duclairoir, J Manuel Irache and E Nakache,
in "Nanotechnologies for the life sciences" vol.2, Biological and pharmaceutical nanomaterials, p.117-144, Challa S. S. R. Kumar Ed., Wiley-VCH Verlag GmbH&Co. KGaA, Weinheim (2006)

Ch3- HPTLC-MALDI TOF MS Imaging analysis of phospholipids

T Kondakova, N Merlet Machour, C Duclairoir Poc
In Neuromethods: Lipidomics, vol. 125 Chapter 12; Paul L. Wood (ed.); Series Editor: Wolfgang Walz, eds, Springer (Germany 2017), DOI 10.1007/978-1-4939-6946-3_12.

Ch4- The hidden face of Nitrogen oxides species – from toxicity effect to potential cure?

S Depayras, T Kondakova, H J. Heipieper, M Feuilloley, N Orange and C Duclairoir Poc
In Emerging Pollutants - Some Strategies for the Quality Preservation of Our Environment", p.19-44, edited by Sonia Soloneski and Marcelo L. Laramendy, Ed. IntechOpen, London (United Kingdom, 2018); <http://dx.doi.org/10.5772/intechopen.75822>

➤ **Publications de revue ou de diffusion de connaissance : 2**

Pdc1- Encapsulation et applications industrielles

C Duclairoir, L'Actualité Chimique. (2000) 6 : 24-27.

Pdc2- Particules Urbaines et Céréalières, Microorganismes Mycotoxines et Pesticides

JP Morin, D Preterre, F Gouriou, V Delmas, A François, N Orange, A Groboillot, C Duclairoir-Poc, M Moretti, O Maillot, O Lesouhaitier, Pollution atmosphérique. (2013)217; URL : <http://lodel.irevues.inist.fr/pollution-atmospherique/index.php?id=759>.

➤ **Publications de compte-rendu de congrés : 77**

✓ **Conférence plénière internationale : 2**

CInt1- "Polymer Nanoparticles Characterization in Aqueous Suspension"

C Duclairoir, E Nakache, International Symposium of Polymer Analysis and Characterization, 26-30 juin 1999, la Rochelle-France.

CInt2- Response of commensal Staphylococci to sub-lethal concentrations of skin antimicrobial peptides

Cécile Duclairoir-Poc, FEMS, Leipzig, Germany, July 21-25th 2013.

✓ **Communications orales : 31**

C1- Nanoparticules de gliadines obtenues par coacervation

C Duclairoir, E Nakache, H Marchais, A-M Orecchioni, *Journée de l'Ecole Doctorale Normande de Chimie-Biologie*, 27 mars 1997, Caen.

C2- Elaboration de nanoparticules de gliadines par coacervation

C Duclairoir, E Nakache, H Marchais, A-M Orecchioni, *Rencontre de la Société Française de Chimie (section Basse-Normandie-Sarthe)*, 30 mai 1997, Caen.

C3- Nanoparticules de polymère végétal

C Duclairoir, E Nakache, A-M Orecchioni, H Marchais, *Journées GFP Ouest-SFC*, 15-17 octobre 1997, Thiais.

C4- Préparation de nanoparticules de polymère végétal. Optimisation de leur taille

C Duclairoir, E Nakache, A-M Orecchioni, H Marchais, *Congrès Annuel du GFP*, 18-20 novembre 1997, Louvain-La-Neuve, Belgique.

C5- Encapsulation de vitamines dans des nanoparticules de protéines végétales

C Duclairoir, E Nakache, A-M Orecchioni, J Irache, Y Popineau, D Renard, *Journées GFP-Ouest*, 2-3 juin 1999, Alençon.

C6- Nanoparticules de protéines végétales : caractérisation structurale et potentialités d'encapsulation

C Duclairoir, D Renard, A-M Orecchioni, Y Popineau, E Nakache, *Journées d'Etudes des Polymères*, 5-10 septembre 1999, Trégastel.

C7- Impact de la production de biosurfactants sur la réactivité de souches de *Pseudomonas fluorescens* vis-à-vis d'un micro-environnement solide.

S Ngoya, C Duclairoir, N Orange. *9^{ème} journée de l'Ecole doctorale Normande chimie-biologie*, 17 mars 2006, Rouen.

C8- Caractérisation des biosurfactants chez plusieurs souches de *Pseudomonas fluorescens* provenant d'environnements différents,

S Ngoya, C Duclairoir, N Orange. *BIOADH' 2007*, 09 mars 2007, Strasbourg.

C9- Analyse de la biodiversité de la flore bactérienne et fongique d'environnements aériens en zones urbaines et portuaire

M Moretti, A Groboillot, C Duclairoir-Poc, O Maillet, O Lesouhaitier, J. P Morin., M. G. J.Feuilloley, N Orange. *MicrobAERO 2009*, 6-8 octobre 2009, Narbonne.

C10- *Pseudomonas fluorescens* : Interactions potentielles de la microflore bactérienne avec la neurophysiologie humaine.

L Mijouin, M Hillion, A Dagorn, A-S Blier, A Madi, T Jaouen, W Veron, N Connil, C Poc, A Groboillot, O Lesouhaitier, N Orange, S Chevalier, MGJ Feuilloley. *17^{ème} Journée Scientifique de l'IFRMP23*, Mont-Saint-Aignan, 17 juin 2011.

C11- Extracellular gamma aminobutyric acid (GABA) regulates *Pseudomonas* virulence.

A Dagorn, A Chapalain, O Lesouhaitier, C Poc, J Vieillard, S Chevalier, L Taupin, F Le Derf, N Orange, MGJ Feuilloley. *Journée de l'EdNBISE*, Rouen, 23 mars 2012.

C12- NitroBactAIR : Impact du stress nitrosant sur l'expression de la virulence d'une bactérie aéroportée

C Duclairoir Poc, *Plénière MOVE'O*, 7 novembre 2012, Rouen.

C13- Impact du stress nitrosant sur l'expression de la virulence d'une bactérie aéroportée

C Duclairoir Poc, déjeuner-débat des professionnels de l'Automobile intitulé "L'automobile et l'Environnement sous la loupe des Scientifiques" Automobile Club de France, mardi 12 février 2013; Paris.

C14- Response of commensal *Staphylococci* to sub-lethal concentrations of skin antimicrobial peptides.

M Hillion, L Mijouin , C Leneveu, E Gerault , T Jaouen , L Lefevre , N Orange, G Redziniak , C Duclairoir-Poc, MJG Feuilloley. *5th FEMS Congress of European Microbiologists*. July 21-25th 2013, Leipzig, Germany.

C15- Etude de la virulence de *Pseudomonas* aéroportées à l'aide d'un nouvel outil lipidomique

T Kondakova , N Merlet-Machour, D Preterre, F Dionnet, N Orange, C Duclairoir Poc, *Journées Interdisciplinaires Qualité Air-8^{ème} édition*, 10-11 février 2014, Villeneuve d'Ascq.

C16- Study of *Pseudomonas* airborne virulence using a new lipidomic tools

T Kondakova, N Merlet-Machour, D Preterre, F Dionnet, N Orange, C Duclairoir-Poc. *17^{ème} Journée de l'EdNBISE*, 10 avril 2014, Le Havre.

C17- Bacterial phospholipid adaptation to human temperature.

T Kondakova, N Merlet-Machour, J Bodilis, F Dionnet,M Feuilloley, O Orange, HJ Heipieper, C Duclairoir Poc. *13th Euro Fed Lipid Congress*, 27-30 September 2015, Florence, Italy.

C18- Aging of coated TiO₂ nanoparticles in oil-in-water emulsion : bactericidal toxicity

L Rowenczyk, C Picard, C Duclairoir-Poc, N Hucher, N Orange, M Feuilloley and M Grisel, *Journées Nord-Ouest Européennes des Jeunes Chercheurs*, 11-12 Mai 2015, Rouen.

C19- Evaluation du potentiel applicatif en cosmétique de biosurfactants microbiens secrétés par des souches de *Pseudomonas* fluorescent aéroportées

S Depayras, C Duclairoir-Poc, *1^{er} colloque du GDR Cosm'actifs*, Moulin d'Andé, 26-27 Septembre 2018, Andé, France.

C20- Aging of TiO₂-nanoparticle surface in cosmetic emulsions: their impact on bacteria of the cutaneous microbiota

L Rowenczyk , C Picard, C Duclairoir-Poc, N Hucher, N Orange, M Feuilloley and M Grisel, *1^{er} colloque du GDR Cosm'actifs*, Moulin d'Andé, 26-27 Septembre 2018, Andé, France.

C21- Impact of gaseous NO₂ on *P. fluorescens* strain in the membrane adaptation and virulence

S Depayras, T Kondakova, N Merlet-Machour, HJ Heipieper, M Barreau, C Catovic, M Feuilloley, N Orange, C Duclairoir-Poc, *WIT Air Pollution* , 25 -27 April 2017, Cadiz, Spain.

C22- Développement de formulations sans conservateurs pour des modèles de crèmes solaires contenant des dispersions TiO₂ nanoparticulaires. Effet des processus de stérilisation sur la stabilité.

L Rowenczyk, C Picard, C Duclairoir-Poc, N Hucher, N Orange, M Feuilloley, M Grisel. *2^{ème} colloque du GDR Cosm'actifs*, 25 & 26 Septembre 2017, Domaine de Chalès, Nouan le Fuzelier, France.

C23- Impact des nanoparticules de TiO₂ passivées formulées en lotion solaire sur des bactéries cutanées ou aéroportée biocontaminante,

L Rowenczyk, M Ringuedé, M Barreau, C Picard, N Hucher, M Grisel, M Feuilloley, N Orange et C Duclairoir-Poc. *2^{ème} colloque du GDR Cosm'actifs*, 25 & 26 Septembre 2017, Domaine de Chalès, Nouan le Fuzelier, France.

C24- Impact of gaseous NO₂ on *P. fluorescens* strain in the membrane adaptation and virulence

S Depayras, T Kondakova, N Merlet-Machour, HJ Heipieper, M Barreau, C Catovic, Feuilloley M, Orange N, C Duclairoir-Poc, *Congrès de la Société Française de Microbiologie 2017*, 09-11 Octobre 2017, Paris.

C25- Interactions [nano]particules et micro-organismes cutanés

N Hucher, C Duclairoir-Poc. *Inauguration de la plate-forme d'Innovations Cosmetomics*, 3 octobre 2017, Evreux.

C26- Production de viscosinamides par la souche clinique de *Pseudomonas fluorescens* MFN1032: Implication dans le développement du biofilm.

D Depayras, A Merieau, M Barreau, T Kondakova, C Barbey, M Feuilloley, N Orange, C Duclairoir Poc. *Colloque Bioadh'2017*, Domaine de Frémigny, 15 & 16 Novembre 2017, Bouray sur Juine, France.

C27- Nitrogen dioxide: from a simple diffusible gas to a potential antibacterial against *P. fluorescens*?

S Depayras, T Kondakova, HJ Heipieper, M Feuilloley, N Orange, C Duclairoir Poc, *21^{ème} Journée de l'EdNBISE*, 22-23 mars 2018, Rouen.

C28- Microenvironment impact on *Cutibacterium acnes*: growth, virulence and biofilm formation of acneic and non-acneic strains.

V Borrel, Y Konto-Ghiorgi, L Lefevre, C Duclairoir-Poc, MGJ Feuilloley, *21^{ème} Journée de l'EdNBISE*, 22-23 mars 2018, Rouen.

C29- NO₂: simple gaz diffusible ou agent antibactérien anti- *P. fluorescens* potentiel?

S Depayras, T Kondakova, HJ Heipieper, J Hardouin, M Feuilloley, N Orange, C Duclairoir Poc, *Mini-colloque Pseudomonas*, 17-18septembre 2018, Marseille.

C30- Régulation et Rôle de CmpX chez *Pseudomonas aeruginosa*

E Bouffartigues, D Tortuel, O Maillot, A David, J Omnes, A Tahiroui, CO Azuama, L Taupin, S Depayras, C Duclairoir Poc, HJ Heipieper, A Dufour, O Lesouhaitier, N Orange, MGJ. Feuilloley, P Cornelis, S Chevalier, *Mini-colloque Pseudomonas*, 17-18septembre 2018, Marseille.

C31- Nitrogen dioxide: from a simple diffusible gas to a potential antibacterial against *P. fluorescens*?

S Depayras, T Kondakova, HJ Heipieper, M Feuilloley, N Orange, C Duclairoir Poc, *Congrès SFM 2018*, 1-3 octobre 2018, Paris.

✓ **Affiches : 44**

A1- Elaboration de nanoparticules de gliadines par coacervation

C Duclairoir, E Nakache, H Marchais, A-M Orecchioni, Rencontre de la Société Française de Chimie (section Basse-Normandie-Sarthe), 30 mai 1997, Caen-France.

A2-Elaboration de nanoparticules de gliadines de blé

C Duclairoir, E Nakache, H Marchais, A-M Orecchioni congrès international SFC97, 7-12 septembre 1997, Bordeaux-France.

A3-Influence du paramètre de solubilité sur la taille des nanoparticules de gliadines

C Duclairoir, E Nakache, H Marchais, A-M Orecchioni, 12th Annual meeting of the GTRV, décembre 1997, Bruxelles-Belgique.

A4- Wheat Gluten Nanopaticles as Drug Carriers : Encapsulation Mechanism and Size Optimization

A-M Orecchioni, J M Irache, C Duclairoir, E Nakache, Symposium on Natural Origin Substances in Drug Formulation, 4-6 novembre 1998, Beijing-Japan.

A5- Elaboration of Nanoparticles from Vegetal Polymer : Size Optimization Study

C Duclairoir, E Nakache, A-M Orecchioni, J Irache, Y Popineau, Symposium International sur les Polymères en Milieu Dispersé, 11-16 avril 1999, Lyon-France.

A6- Nanoparticles Preparation by Vesicle Polymerization or by Controlled Coacervation

E Nakache, N Poulain, C Duclairoir, A-M Orecchioni, Gordon Research Conferences, 27 juin- 2 juillet 1999, Cambridge-USA.

A7- Solvent Effect on the Size Optimization of Submicronic Wheat Proteins Drug Carriers

A-M Orecchioni, D Renard, C Duclairoir, Y Popineau, E Nakache, 12th International Symposium on Microencapsulation, 6-8 septembre 1999, London-United Kingdom.

A8- Development of Carbohydrate Polymer-Based Submicron Colloidal System in Reverse Micelles

A-M Orecchioni, C Duclairoir, E Nakache, Lipid and Surfactant Dispersed System, 26-28 octobre 1999, Moscow, CEI.

A9- Vitamin E Encapsulation and Release from Wheat Protein Nanoparticles

A-M Orecchioni, C Duclairoir, P Depraetere, Y Popineau, E Nakache, 3rd Word Meeting on pharmaceutics, Biopharmaceutics Pharmaceutical Technology, 3-6 avril 2000, Berlin-Deutschland.

A10- Encapsulation de l'alpha-tocophérol au sein de suspensions colloïdales nanométriques de gliadines de blé

A-M Orecchioni, C Duclairoir, E Nakache, XXIV Congresso internazionale della societa farmaceutica del mediterraneo latino, 20-23 septembre 2000, Assisi-Italia.

A11- Elaboration de nanoparticules de protéines végétales et application comme système de libération contrôlée de vitamine E

C Duclairoir, D Renard, P Depraetere, Y Popineau, A-M Orecchioni, E Nakache, 19èmes Journées du club émulsion, 6-7 novembre 2000, Bordeaux-France.

A12- Biofilm, biosurfactant, temperature : dependency for 9 wild *Pseudomonas fluorescens* environmental strains and for two of their biosurfactant non-producing mutants.

C Duclairoir-Poc, T Meylheuc, S Nogoya, A Groboillot, L Taupin, A Merieau, MGJ Feuilloley, N Orange Eurobiofilms, First European Congress on Microbial Biofilms, September 2 – 5 2009, Rome, Italy.

A13- Analyse de la biodiversité de la flore bactérienne et fongique d'environnements aériens en zones urbaines et portuaire.

M Moretti, A Groboillot., C Duclairoir-Poc, O Maillot, O Lesouhaitier, JP Morin, MGJ Feuilloley, N Orange *MicrobAERO2009*, 6 – 8 octobre 2009 Narbonne.

A14- Evaluation de la qualité microbiologique de l'air de deux zones urbaines en Haute-Normandie.

C Duclairoir-Poc, A Groboillot, O Maillot, M Moretti, O Lesouhaitier, MGJ Feuilloley, JP Morin, N Orange *1^{er} Congrès Européen sur les Pathologies Environnementales*. 9-10 octobre 2009, Rouen.

A15- Influence de la température sur le comportement adhésif et sur la production de biosurfactant chez *Pseudomonas fluorescens* d'origine environnementale.

C Duclairoir-Poc, T Meylheuc, S Nogoya, A Groboillot, L Taupin, A Merieau, MGJ Feuilloley, N Orange Bioadh 2009, 17-19 Novembre 2009, Le Mans.

A16- Déséqustration de polluants de type hydrocarbures aromatiques polycycliques à l'interface eau/sédiments à l'aide de tensioactifs d'origine synthétique ou biologique.

F Portet-Koltalo, S Sahed, A Groboillot, C Duclairoir-Poc, N Orange. SEP 2009, 30 nov-3 décembre 2009, Marseille.

A17- GABA and benzodiazepine receptors ligands: Promising molecules as bacterial virulence inhibitors.

A Dagorn, A Chapalain, S Chevalier, C Poc, N Orange, V Papadopoulos, MGJ Feuilloley *3^{ème} rencontres normandes en Chimie-Biologie-Santé: La biologie, inspiratrice de nouveaux médicaments*. 10 décembre 2009, Rouen.

A18- Evaluation de la qualité bactérienne d'écosystèmes aériens en zones urbaines et portuaires grâce à deux approches : Les antibiogrammes et les tests de virulence vis-à-vis de *Caenorhabditis elegans*.

A Groboillot, C Duclairoir-Poc, O Maillot, M Moretti, O Lesouhaitier, MGJ Feuilloley, JP Morin, N Orange. *VIII^{ème} Congrès de la SFM*, 2-4 juin 2010, Marseille.

A19- Effect of a cyclolipopeptidic biosurfactant on PAHs sorption by sediments.

F Portet-Koltalo, F.; Ammami, M.T.; Benamar, A.; Duclairoir-Poc, C.; Le Derf, F. *12th European Meeting on Environmental Chemistry (EMEC 12)*, 7-10 décembre 2011, Clermont-Ferrand.

A20- *Pseudomonas fluorescens*, a member of the gut-brain-skin axis.

M Hillion, L Mijouin, A Dagorn, T Rosay, A Madi, T Jaouen, N Connil, C Poc, A Groboillot, O Lesouhaitier, N Orange, S Chevalier, MGJ Feuilloley. *1^{ère} journée scientifique de l'Institut de Recherche et d'Innovation Biomedicale (IRIB)*, 1^{er} juin 2012, Rouen.

A21- *Pseudomonas* aéroportées : Caractérisation phénotypique et évaluation de leur potentiel virulent à l'aide de différents modèles.

C Duclairoir Poc, J Verdon, A Groboillot, O Lesouhaitier, O Maillot, M Barreau, N Orange. *Congrès de la Société Française de Microbiologie 2013*, Février 2013, Lille.

A22- L'acide gamma-aminobutyrique (GABA) module la virulence et la cytotoxicité des *Pseudomonas*

A Dagorn, M Hillion., A Chapalain., O Lesouhaitier, C Duclairoir-Poc, S Chevalier, MJG Feuilloley. *Congrès de la Société Française de Microbiologie 2013*, Février 2013, Lille.

A23- La Substance P, un médiateur entre microflore et homéostasie cutanée

L Mijouin, M Hillion, T Jaouen, C Duclairoir-Poc, MJG Feuilloley, Y Ramdani. *Congrès de la Société Française de Microbiologie 2013*, Février 2013, Lille.

A24- Another paradigm in antibacterial treatments : Why a diplomatic approach should be more efficient than weapons of mass destruction ?

M Hillion, L Mijouin, A Dagorn, C Leneuve, AS Blier, A Madi, T Jaouen, T Rosay, K Biaggini, N Connil, C Poc, A Groboillot, C Hulen, N Lomri, O Lesouhaitier, N Orange, MGJ Feuilloley. *ESF-EMBO Symposium Bacterial Networks*. 16-21 March 2013, Pultusk, Poland.

A25- Regulation of *Pseudomonas* cytotoxicity and virulence by gamma aminobutyric acid (GABA), an inter-kingdom communication signal.

A Dagorn, A Chapalain, L Mijouin, M Hillion, C Duclairoir-Poc, J Vieillard, S Chevalier, L Taupin, F Le Derf, N Orange, MGJ Feuilloley. *2nd Scientific meeting of Institute for Research and Innovation in Biomedicine (IRIB)*, June 21th 2013, Rouen.

A26- Air: a potential biohazard niche for fluorescent Pseudomonads.

C Duclairoir Poc, J Verdon, A Groboillot, M Barreau, H Toucourou, L Mijouin, O Maillet, C Hulen, O Lesouhaitier, JP Morin, MGJ Feuilloley, A Merieau, N Orange. *5th FEMS Congress of European Microbiologists*, 19-23 July 2013, Leipzig, Germany.

A27- Regulation of *Pseudomonas aeruginosa* virulence by Gamma-aminobutyric Acid

A. Dagorn, M. Hillion, A. Chapalain, O. Lesouhaitier, C. Duclairoir-Poc, N. Orange, S. Chevalier, M. Feuilloley. *5th FEMS Congress of European Microbiologists*, 19-23 July 2013, Leipzig, Germany.

A28- The virulence of cutaneous bacteria can be locally regulated by Substance P, a skin neuropeptide.

L. Mijouin, M. Hillion, Y. Ramdani, T. Jaouen, M.-L. Follet-Gueye, C. Duclairoir-Poc, M.G.J. Feuilloley. *5th FEMS Congress of European Microbiologists*, 19-23 July 2013, Leipzig, Germany.

A29- *Pseudomonas* cytotoxicity and virulence are regulated by gamma aminobutyric acid (GABA).

Dagorn A, Chapalain A, Mijouin L, Hillion M, Duclairoir-Poc C, Vieillard J, Chevalier S, Taupin L, Le Derf F, Orange N, Feuilloley MGJ. *16^{ème} journée de l'école doctorale EdNBISE*, 11-12 juillet 2013, Caen.

A30- Airborne fluorescent pseudomonads: in vitro assessment for identification of a potentiel biohazard.

C Duclairoir Poc, J Verdon, A Groboillot, M Barreau, H Toucourou, L Mijouin, O Maillet, C Hulen, O Lesouhaitier, JP Morin, MGJ Feuilloley, A Merieau, N Orange, *Pseudomonas 2013*, September 2013, Lausanne.

A31- New role for T6SS in the *Pseudomonas fluorescens* strain MFE01.

V Decoin, D Sperandio, D Bergeau, C Barbey, C Duclairoir-Poc, X Latour, N Orange, A Merieau, *Pseudomonas 2013*, September 2013, Lausanne.

A32- Gamma-aminobutyric Acid (GABA) modulates *Pseudomonas* cytotoxicity and virulence.

A. Dagorn, A Chapalain, L Mijouin, M. Hillion, C. Duclairoir-Poc, J Vieillard, S. Chevalier, L Taupin, F Le Derf, N. Orange, M. Feuilloley, *Pseudomonas 2013*, September 2013, Lausanne.

A33- Evaluation of *Pseudomonas* aerosolisation for physiological studies.

F Gouriou, P Penalva, S Berthout, C Duclairoir-Poc, A Agoulon, D Preterre, F Dionnet, MGJ Feuilloley, N Orange, A Groboillot, *Pseudomonas 2013*, September 2013, Lausanne.

A34 -La Substance P, une cible nouvelle pour un contrôle optimal des interactions peau/microbiote cutané

L Mijouin., M Hillion, Y Ramdani, T Jaouen, C Duclairoir-Poc, ML Follet-Gueye, E Lati, F Yvergniaux, A Driouch, L Lefeuvre, MGJ Feuilloley. *Cosminnov 2013*, 8-9 octobre 2013, Orléans.

A35 -Lipidome of airborne *Pseudomonas* sp. by HPTLC-MALDI-TOF MSI : remarkable presence of eucaryotic lipid – phosphatidylcholine

T Kondakova, N Merlet-Machour, D Preterre, F Dionnet, N Orange, C Duclairoir Poc, *3^{ème} day of Institute for Research and Innovation in Biomedecine*, 20 juin 2014, Caugé, Normandie.

A36 – Effet des NOx sur une souche de *Pseudomonas fluorescens* du microbiote cutané

F Ousalem, C Barbey, M Barreau, C Duclairoir-Poc, F Gouriou, A Groboillot, MJG Feuilloley, *11^{ème} congrès national de la Société Française de Microbiologie*, 24 et 25 mars 2015, Paris.

A37- Effect of temperature on *Pseudomonas* phospholipid composition.

T Kondakova, N Merlet-Machour, J Bodilis, F Dionnet, M Feuilloley, N Orange, HJ Heipieper, C Duclairoir Poc. 18^{ème} Journée de l'Ecole Doctorale EdNBISE, 26 - 27 mars 2015, Rouen.

A38 – *Pseudomonas fluorescens* lipidome screening : effect of temperature and growth phase on *Pseudomonas* phospholipids

T Kondakova, N. Merlet-Machour, J. Bodilis, F Dionnet, M Feuilloley, N Orange, HJ Heipieper, C Duclairoir Poc. 6th FEMS Congress of European Microbiologists. June 7-11th 2015, Maastricht, Netherlands.

A39- The nitrogen dioxide increases *Pseudomonas fluorescens* biofilm formation: identification of the bacterial response to air pollutant.

T Kondakova, T Kentache, A Garreau, M Barreau, A Groboillot, J Hardouin, F Dionnet, M Feuilloley, N Orange, HJ Heipieper, C Duclairoir Poc. 6th FEMS Congress of European Microbiologists. June 7-11th 2015, Maastricht, Netherlands.

A40- Bacterial phospholipid adaptation to human temperature.

T Kondakova, N Merlet-Machour, J Bodilis, F Dionnet, M Feuilloley, N Orange, HJ Heipieper, C Duclairoir Poc. Euro Fed Lipid Congress, 27-30 September 2015, Florence, Italy.

A41- Impact of nanoparticles used in cosmetics on skin microflora representative bacteria.

L Rowenczyk, C Picard, C Duclairoir Poc., N Hucher, N Orange, M Feuilloley, M Grisel. Journées Paul Marty SFC, 8-9 décembre 2015, Paris. Prix du meilleur poster.

A42- Investigation in the potential roles of viscosinamides produced by *P. fluorescens*

S Depayras, A Merieau, M Barreau, T Kondakova, C Barbey, H Toucourou, M Feuilloley, N Orange, C Duclairoir-Poc. 7th FEMS Congress of European Microbiologists. July 9-13th 2017, Valencia, Spain.

A43- Impact of gaseous NO₂ on *P. fluorescens* strain in the membrane adaptation and virulence

S Depayras, T Kondakova, N Merlet-Machour, HJ Heipieper, M Barreau, C Catovic, M Feuilloley, N Orange, C Duclairoir-Poc. 7th FEMS Congress of European Microbiologists. July 9-13th 2017, Valencia, Spain.

A44- Investigation in the potential roles of viscosinamides produced by *P. fluorescens*

S Depayras, A Merieau, M Barreau, T Kondakova, C Barbey, H Toucourou, M Feuilloley, N Orange, C Duclairoir-Poc. Congrès de la Société Française de Microbiologie 2017, 09-11 Octobre 2017, Paris.

Publications à comité de lecture

P1

C. Duclairoir
E. Nakache
H. Marchais
A.-M. Orecchioni

Formation of gliadin nanoparticles: Influence of the solubility parameter of the protein solvent

Received: 9 September 1997
Accepted: 16 December 1997

C. Duclairoir · E. Nakache (✉)
Groupe Polymères-Interfaces
LCMT, UMR 6507, ISMRA
6 boulevard du Maréchal Juin
F-14050 Caen Cedex
France

H. Marchais · A.-M. Orecchioni
Laboratoire de Pharmacie Galénique
et Biopharmacie
Université de Rouen
76803 Saint-Etienne du Rouvray Cedex
France

Abstract Nanoparticles are produced from gliadin, a wheat gluten fraction, by precipitation in a non-solvent. In order to control their size, the solvent effect is studied by solubilizing the protein in different mixtures whose solubility parameters are close or equal to the gliadin parameter, δ_G . The determination of δ_G is performed by turbidity. The size of the nanoparticles is evaluated by QELS (quasi-elastic light scattering). The study of the size as a function of the solubility

parameter of the protein solvent allows the determination of the optimal conditions for nanoparticle formation.

Key words Nanoparticles – gliadin – solubility parameter – desolvatation method

Introduction

Nanoparticles obtained from natural or synthetic polymers are currently attracting much interest as specific carriers in pharmacy, in cosmetology, in the agro-chemical industry and in other industrial fields [1–3]. For biological applications, vegetal particles have been derived from proteins [4, 5], such as gliadin extracted from gluten of wheat and vicillin or legumin extracted from pea seeds. Their potential appears to be large, especially in the targeting of active principles.

The formation of gliadin nanoparticles by desolvatation method in a non-solvent mixture, as well as their loading and controlled release capacity of all trans-retinoic acid have recently been shown [5]. It is concluded that the coacervate formation is very sensitive to environmental parameters and to the structural characteristics of the protein.

In this paper, we propose to understand the influence of the environmental parameters by a thermodynamical approach. The solubility parameters will be used to opti-

mize the preparation of gliadin nanoparticles with the aim of estimating their size.

Theory

Mixing enthalpy $\Delta^M H$ of polymer/solvent system

Flory [6] evaluated the mixing enthalpy for a regular system, i.e., for real polymer/solvent mixtures in the case of a weak thermic effect. The total energy of the interaction ΔE_{12} is a function of the elementary interaction energies of solvent/solvent (E_{11}), of polymer segment/polymer segment (E_{22}) and of solvent/polymer segment (E_{12}):

$$\Delta E_{12} = \frac{1}{2}(E_{11} + E_{22}) - E_{12} . \quad (1)$$

If z is the coordination number of polymer network and N_1 the number of moles of the solvent and ϕ_2 the volume fraction of the polymer, the mixing enthalpy is

$$\Delta^M H = (z - 2)N_1 \phi_2 \Delta E_{12} . \quad (2)$$

Solubility parameter δ and interaction energies

Hildebrand proposed the following relation for ΔE_{12} for endothermic "simple" mixtures:

$$\Delta E_{12} = [(E_{11}^{1/2} - E_{22}^{1/2})/2]^2 \quad (3)$$

from which the definitive form of $\Delta^M H$ is

$$\Delta^M H = V \phi_1 \phi_2 (\delta_1 - \delta_2)^2 \quad (4)$$

with V the molar mixture volume, ϕ_1 and ϕ_2 are, respectively, the volume fraction of the solvent and of the polymer.

δ_i is the solubility parameter of the compound defined as

$$\delta_i = [E_{ii}(z - 2)/(2V_i)]^{1/2} \quad (5)$$

i , i.e. 1 or 2, means, respectively, the solvent or the polymer. V_i is the molar volume of the compound i . For classical solvents, the parameter can be found in the literature data [7] and is expressed in $(J\text{ cm}^{-3})^{1/2}$ or in $(\text{MPa})^{1/2}$.

Relation (4) shows that the miscibility of a polymer in a solvent is possible if

$$\delta_1 = \delta_2 . \quad (7)$$

The solubility parameter δ_M of a mixture, for instance water/ethanol, is determined with the help of the following relation:

$$\delta_M = \phi \delta + \phi' \delta' \quad (8)$$

with δ and δ' the solubility parameters of ethanol and water and ϕ and ϕ' their volume fractions, respectively.

$$(\phi + \phi' = 1).$$

In this study, we are assuming that the protein/water/ethanol mixture is a simple regular mixture. In fact the protein is very diluted (0.1%).

Material and methods

Material

Gliadin was obtained from a common wheat flour (variety Hardy) and purified by INRA de Nantes laboratories, and then dialysed. Its method of purification is as follows:

Gluten was extracted on a preparative scale from the wheat flour. It was freeze-dried, ground in a refrigerated grinder and defatted by two extractions with dichloromethane for 2 h at 20 °C (gluten/solvent ratio: 1/10 w/v). After filtering, the residue was evaporated from the gluten at 20 °C under reduced pressure. Samples of dried gluten powder (50 g) were stirred gently in an ethanol/water mixture (70/30 v/v) in a gluten/solvent ratio: 1/10 w/v for 4 h at 20 °C. The suspension was centrifuged (10 000 g for

20 min). The soluble fraction was dialysed exhaustively, first against water, and then against 0.05 M acetic acid. Finally, gliadin was freeze-dried.

Analysis of the extracted gliadin fraction was carried out by reverse phase-HPLC [9] and polyacrylamide gel electrophoresis at acid pH [10]. In this way, the amount of protein in the gliadin freeze-dried extract was calculated to be around 85% w/w and the proportions of the different gliadin groups were 55% w/w for α and β -gliadins, 15% w/w for γ -gliadin, and for ω -gliadin.

All aqueous solutions were prepared from ultra pure water (Milli Q Plus-Millipore). The physiological saline phase was prepared from NaCl provided by Merck.

Pure absolute ethanol at 99.5% was provided by Carlo Erba.

Pure propylene glycol (PG) or 1,2-propanediol greater than 98% was provided by Fluka.

Pure ethylene glycol (EG) greater than 99.8% R.P. was provided by Prolabo.

The surface-active agent which disperses the nanoparticles is Synperonic® PE/F68 provided by ICI.

Ethanol was eliminated by evaporation with Rotavapor R-114, provided by Büchi, under reduced pressure (Divac 2.4L provided by Leybold).

Nanoparticle separation by ultracentrifugation was carried out with the help of Sigma 3K30 (Bioblock Scientific). The solutions' turbidity was determinated by UV-visible Lambda 5 photometer (Perkin-Elmer). Particle diameters were estimated by quasi-elastic light scattering (QELS), with the help of a photogoniiodiffusometer and a RTG correlator (ΣEMATech) with 12 digital counters.

Preparation of different-solubility-parameter solutions

According to Hildebrand, the solubility parameter of gliadin can be determined using a panel of solvents or mixtures of them. The solvent which best solubilizes gliadin has the same solubility parameter (δ_G) as this protein.

Different mixtures were prepared with solvents such as ethylene glycol (EG) or propylene glycol (PG) and ultra pure water. Table 1 displays the solubility parameters of the solvents used [7].

0.1% gliadin solutions were prepared in solvents mixtures where δ_M was chosen between 30.2 and 36.9 MPa^{1/2}.

Preparation of gliadin nanoparticles by desolvation method

This method is based on the fact that gliadin is not soluble in a non-solvent medium such as water, in contact of which the protein precipitates.

Table 1 Solubility parameters of the solvents used

Solvents	Water	Ethylene glycol	Propylene glycol	Ethanol
δ (MPa ^{1/2})	47.8	32.9	30.2	26.5

Two solutions prepared separately were mixed. The method is as follows:

- 0.5% (w/v) Gliadin is solubilized at 25 °C in 20 ml of an ethanol/water mixture A of required δ_M , prepared and then filtered on 0.45 µm.
- Solution B is made from 40 ml of physiological saline solution (i.e. 0.9% NaCl aqueous solution), filtered on 0.45 µm, and from Syneronic® PE/F68 at 25 °C. The surface-active agent concentration is 0.5% w/w.
- The solution B is slowly poured with the help of a funnel, 4 mm in diameter, diving into the solvent phase A at 25 °C, under magnetic stirring (500 r.p.m) for about 10 min. The stirring and the temperature are maintained for 5 min after this operation. We call this coacervation step of the nanoparticles “*nano precipitation*”.
- The suspension of nanoparticles is concentrated by *evaporation* with a rotavapor in order to eliminate most of the ethanol.
- Then the nanoparticles are purified by *centrifugation* for 15 min at 20 000 r.p.m and at 4 °C. The supernatant is removed and then the pellets are resuspended in 2 ml of supernatant by three sessions of 5 min ultrasonic waves.

The different steps of the preparation are described in Fig. 1.

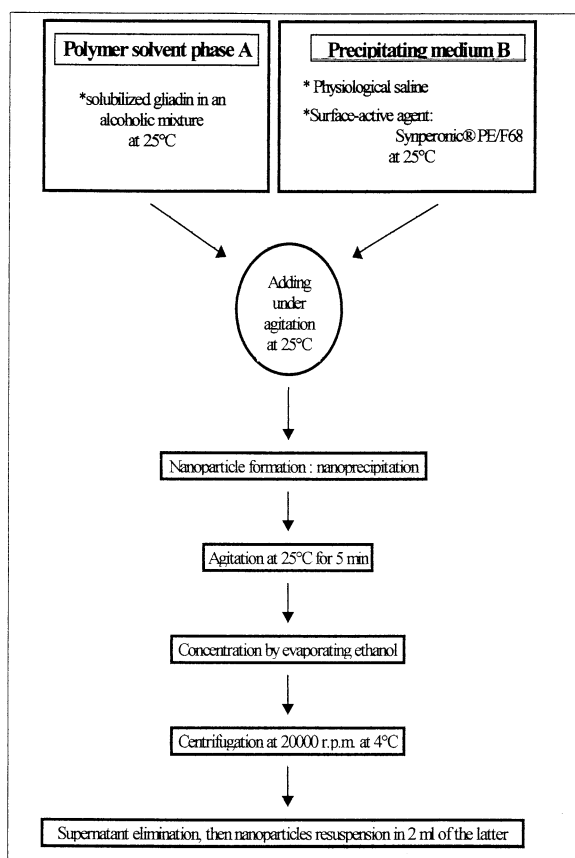
Cross-linking of gliadin nanoparticles

This stage is reached by adding glutaraldehyde to the suspension. Freshly prepared particles were cross-linked with 1.64 mg glutaraldehyde/mg nanoparticles for 2 h at room temperature. This colloidal system was then purified twice by centrifugation in physiological saline solution.

Characterization of desolvation method media and of gliadin nanoparticles

Turbidity

For the determination of its solubility parameter, the solubility of a compound dissolved in media of different δ_M is usually inspected visually for homogeneity and transparency of the mixtures. More accurate measurement can be made by turbidity experiments. The more opaque the

**Fig. 1** Preparation of gliadin nanoparticles by desolvation method

solution, the more attenuated the intensity of the incident beam. The observed absorption is related to the turbidity τ and to the thickness of the cell l .

The measurement is performed by determining the difference between a suspension and the pure solvent:

$$(Abs)_{1+2} - (Abs)_1 = l(\tau_{1+2} - \tau_1) = l\Delta\tau \quad (9)$$

with $(Abs)_i = \log(I/I_0)$; the subscripts 1 and 2 denote solvent and solute, respectively, in this case gliadin.

Quasielastic light scattering (QELS)

Particle-size measurements are carried out using quasi-elastic light scattering (QELS). By this method, mean particle diameters and sample polydispersity are determined. This technique is concerned with the time dependence of the fluctuations on the intensity of light scattered by a suspension of nanoparticles. The correlator accumulates the value of the light correlation function in 12 digital counters. Before an analysis, the sample is warmed up at 25 °C for, at least, a quarter of an hour; each change of one

degree centigrade promotes an error of 2% on the size estimation.

For a system of rigid monodisperse particles, the correlation function is

$$C(t) = A \exp(-2\Gamma t) + B \quad (10)$$

with A and B constants and t the measurement time. $C(t)$ is related to the fluctuation relaxation time τ by

$$\Gamma = Dq^2 = 1/\tau \quad (11)$$

where q is the scattering fluctuation wave vector amplitude. D is the translational diffusion coefficient which allows the determination of the size of a particle at high dilution limit through the Stokes-Einstein equation by extrapolation at zero volume fraction:

$$D = kT/3\pi\eta d \quad (12)$$

with k the Boltzmann constant, T the absolute temperature and η the viscosity of the medium in which the particles of hydrodynamic diameter d are suspended. Particle size measurements are performed with diluted solutions close to the dilution limit. And, for spherical particles, only scattering at one angle, 90° , is required. In our case, the gliadin nanoparticles had been shown spherical by SEM [5].

Experimental results

Determination of gliadin solubility parameter, δ_G (Hildebrand's method)

The visual observation of 0.1% gliadin solutions gives the results shown in Table 2. The solvents used are usually considered as references for the determination of solubility parameters.

This first approach leads to the conclusion that the solutions are clearer between 30.2 and 36.9 MPa^{1/2}. Then the gliadine solubility parameter, δ_G is located at 35 ± 1 MPa^{1/2}.

To improve and quantify this result, a turbidity study has been performed at 25 °C with similar ethanol/water mixtures of δ_M from 34.0 to 36.1 MPa^{1/2}. This couple of solvents was chosen because it will concern the preparation of gliadin nanoparticles. Figure 2 shows the obtained results.

It can be concluded more precisely that δ_G value is 34.5 ± 0.5 MPa^{1/2}.

Gliadin nanoparticle size by QELS

In a first step, the nanoparticles not reticulated were studied.

Table 2 Visual observations of 0.1% gliadin solutions

δ [MPa ^{1/2}]	Mixture [%]	T [°C]	Appearance
30.2	100 PG	14.6	Very cloudy
30.6	96 PG/4 Water	14.6	Cloudy
31.8	91 PG/9 Water	14.6	Very cloudy
32.8	85 PG/15 Water	14.6	Very cloudy
32.9	100 EG	17.2	Cloudy
33.9	79 PG/21 Water	14.6	Clear
34.2	91 EG/9 Water	17.2	Very clear
35.0	73 PG/27 Water	14.6	Very clear
35.1	85 EG/15 Water	17.2	Very clear
36.0	79 EG/21 Water	17.2	Clear
36.9	73 EG/27 Water	17.2	Cloudy

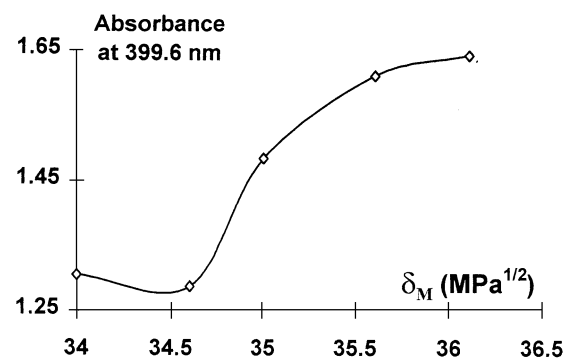


Fig. 2 Turbidity of gliadin mixtures

This study is based on three different batches of nanoparticles. Each shown diameter is an average of, at least, three measurements by QELS.

Evolution of nanoparticles with the process step

Figure 3 shows the nanoparticle diameters plotted versus the solubility parameters δ_M of the solvent mixtures used for the desolvation, 24 h after the desolvatation process.

The curves show a minimum size of the diameter when δ_M corresponds to the gliadin solubility parameter δ_G for the steps of nanoprecipitation and evaporation by rotavapor. This minimum size has been observed in three different sets of experiments. For the centrifugation step, the behavior is not the same: an inflection point can be observed at δ_G on the decreasing plot. As shown by Table 3, the size is doubled with respect to the nanoprecipitation step at δ_G .

A similar observation is noted, in Fig. 3, between 32.9 and 35.0 MPa^{1/2}. A possible explanation could be the aggregation of the particles in both by the action of the centrifugal force. But, from 36.1 to 37.9 MPa^{1/2}, diameters

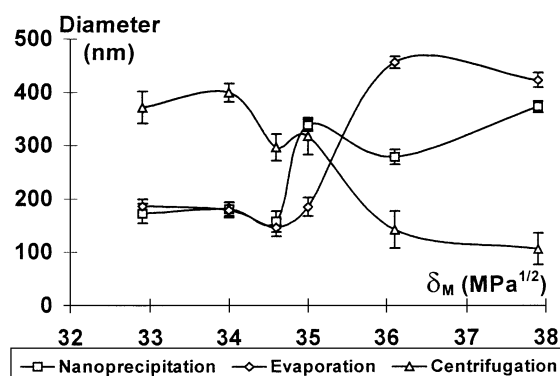


Fig. 3 Size evolution of gliadin nanoparticles as a function of the process step, 24 h after desolvation. The error bars represent the polydispersity of the size distribution

Table 3 Minimum size of gliadin particles 24 h after desolvation

Process stage	Nanoprecipitation	Rotavapor	Centrifugation
Diameter (nm)	157.4	146.2	296.4

decrease and the polydispersity values increase between 20 and 35%. This different behavior is not easy to explain. None of the parameters or experimental conditions were changed during the experiments.

Nanoparticle size as a function of δ and time

Figure 4 shows the evolution of the nanoparticle size from 24 h after their nanoprecipitation to 39 days after ($d + 39$).

During the step of nanoprecipitation, the nanoparticles were subjected neither to evaporation, nor to centrifugation. This plot and Fig. 5 show that, after 28 days ($d + 28$), the graphs are not complete. In these plots, several points are missing since $d + 28$. In fact flocculation is achieved and the colloidal concentration is too small to be measured by QELS.

Figure 5 shows the evolution of nanoparticle size from 24 h after their evaporation until 39 days after ($d + 39$). These particles were not subjected to centrifugation.

Figures 4 and 5 show a similar shape of the curves for nanoprecipitation and solvent evaporation stages with a minimum diameter obtained in the vicinity of δ_G . As for the general shape of the graphs, time does not seem to have a great influence on the minimum size. Nevertheless, for a given δ_M different from δ_G , the mean diameter of the nanoparticles changes with time.

The centrifugation (Fig. 6) has three effects: it affects the size of particles after the nanoprecipitation, and in-

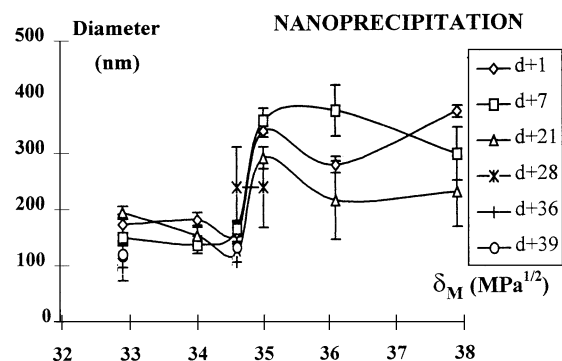


Fig. 4 Evolution of nanoparticle size after precipitation as a function of δ_M and time

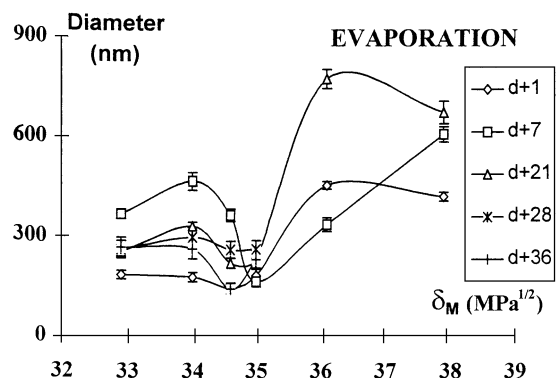


Fig. 5 Evolution of nanoparticle size after precipitation and after evaporation by rotavapor as a function of δ_M and of the time. The symbols are the same as in Fig. 4

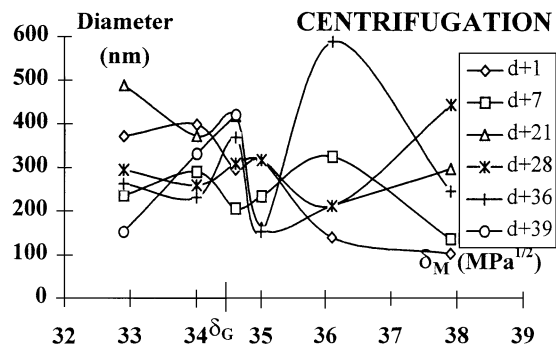


Fig. 6 Evolution of nanoparticle size after precipitation, solvent evaporation and centrifugation as a function of δ_M and time. The symbols are the same as in Fig. 4

fluences the temporal size of the suspension, and increases the polydispersity of size distributions. However, in the area of solubility parameters around δ_G , the evolution of the nanoparticle size is less important. Then a greater stability of size at δ_G can be deduced.

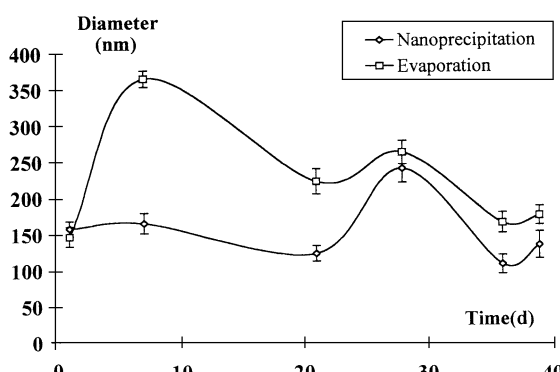


Fig. 7 Size evolution of gliadin nanoparticles (62EtOH/38H₂O) in time after nanoprecipitation and rotavapor

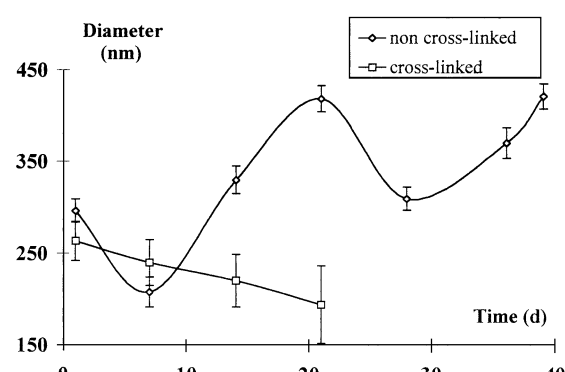


Fig. 8 Time evolution of gliadin nanoparticles cross-linked or not after centrifugation

Nanoparticle size as a function of time

The former studies show a minimum and rather "stable" size at δ_G . A comparison of the evolution of the nanoparticles diameter prepared at δ_G after nanoprecipitation and after solvent evaporation follows.

Figure 7 displays a similarity in the relationship between the size evolution and time. Nevertheless, after the rotavapor stage, which eliminates most of ethanol, the size becomes more important than after nanoprecipitation. This is probably correlated to the higher concentration of nanoparticles, which are brought closer to each other and tend to aggregate. It can be also observed that the difference between the two curves fades away in time. After 40 days, the size is approximately the same as that 24 h after the preparation of nanoparticles.

Compared evolution of the size of cross-linked and non-cross-linked particles in time

To prevent any size variations in time, a set of nanoparticles was cross-linked after the process of centrifugation and re-suspended in physiological saline.

Two interesting observations can be made from Fig. 8: the size of the non-cross-linked particles oscillates with time and their mean size increases also with time.

Contrarily to what might be expected [5], the size of the cross-linked nanoparticles reduces with time and the solution flocculates. The glutaraldehyde is known to react with the NH₂ groups of the protein. From this, it may be assumed that the charge of such groups in aqueous solution is neutralized by glutaraldehyde and, consequently, on one side, the protein is more confined, then the size decreases. On the other side, the suspension flocculates by lack of electrostatic repulsions between nanoparticles, because all NH₃⁺ groups were changed into NH₂ ones.

Conclusion

This study shows that the method of the formation of gliadin nanoparticles by the solubility parameters allows the control of their size. Indeed, when the gliadin is solubilized in its good solvent, whose solubility parameter is as that of the protein, the smallest size of the particles is obtained whatever the conditions of protein extraction and purification. This size varies with the different stages of the process, the most disturbing of which being centrifugation. Time, and chemical cross-linking affect the evolution of particle size.

Acknowledgments The authors thanks the "Réseau Matériaux Polymères, Plasturgie de Basse-Normandie" for financial support.

References

1. Fessi H, Devissaguet JP, Puisieux F (1986) French Patent Application 8618446
2. Couvreur P, Buri P, Puisieux F, Doelker E, Benoit JP (1985) In: Formes pharmaceutiques nouvelles. Eds Techniques et Documentation Lavoisier, Paris, pp 577–611
3. Stainmesse S, Orecchioni A-M, Nakache E, Puisieux F, Fessi H (1995) Colloid Polym Sci 273:505–511

4. Ezpeleta I, Irache JM, Stainmesse S, Gueguen J, Orecchioni A-M (1996) Eur J Pharm Biopharm 42:36–41
5. Ezpeleta I, Irache JM, Stainmesse S, Chabenat C, Gueguen J, Popineau Y, Orecchioni A-M (1996) Int J Pharmaceuticals 131:191–200
6. Flory JP (1953) In: Principles of Polymer Chemistry. Cornell University Press, Ithaca
7. Barton AFM (1991) In: Handbook of Solubility Parameters and Other Cohesion Parameters, 2nd Ed. CRC Press, Boca Raton
8. Small JP (1953) J Appl Chem, 371
9. Wieser H, Seilmmer W, Belitz HD (1994) J Cereal Sci 19:149–155
10. Larré C, Popineau Y, Loisel W (1991) J Cereal Chem 14:231–241

P2

Gliadin nanoparticles: formation, all-trans-retinoic acid entrapment and release, size optimization

Cécile Duclairoir,^{1,*} Juan Manuel Irache,² Evelyne Nakache,¹ Anne-Marie Orecchioni,² Christiane Chabenat³ and Yves Popineau⁴

¹ Groupe Polymères-Interfaces, LCMT, UMR 6507, ISMRA, 6 boulevard du Maréchal Juin, 14050 Caen Cedex, France

² Laboratoire de Pharmacie Galénique et Biopharmacie, Université de Rouen, 76803 Saint Etienne du Rouvray Cedex, France

³ Laboratoire de Chimie Analytique, Université de Rouen, 76803 Saint-Etienne du Rouvray Cedex, France

⁴ Laboratoire de Biochimie et Technologie des Protéines, INRA de Nantes, rue de la Géraudière, BP 71627, 44316 Nantes Cedex, France

Abstract: Gliadin nanoparticles were prepared by a desolvatation method. They showed good stability during several weeks in PBS or aqueous medium. Assayed as carriers for all-trans-retinoic acid (RA), they have a quite good entrapment efficiency: about 75% of added drug at 60 µg·(mg gliadin)⁻¹ and a payload of 76.4 µg·(mg gliadin)⁻¹ nanoparticles. A rapid release of 20% of the drug after 15 min in sink conditions and a diffusion process in a second step are observed.

According to the nature of vegetal proteins, the size control of the nanoparticles may be reached by varying the nature of the solvent, the pH and the ionic strength. Because gliadin is poorly solubilized in aqueous solutions, the first method was chosen. In order to quantify more precisely the solvent effect, the size diameter was optimized through a solubility parameter study. The smallest size was reached for protein solubility solvent equal to that of gliadin. Size differences were observed with respect to the process steps; the diameter obtained after nanoprecipitation fluctuates with time.

© 1999 Society of Chemical Industry

Keywords: gliadin nanoparticles; all-trans-retinoic acid; encapsulation; size optimization; solubility parameter

INTRODUCTION

At the beginning of the twentieth century, Ehrlich¹ first conceived 'magic bullets' to treat patients. In his opinion, drugs could be introduced into the body and released next to the site responsible for the disease. The last few decades have witnessed concerted efforts to enhance the drug effectiveness by improving their selectivity, which, with a few exceptions, is generally poor.² For instance, in cancer chemotherapy cytostatic agents also damage normal, rapidly dividing cells.

A possible approach to enhance drug effectiveness consists in the use of site-specific drug delivery, which would not only increase the amount of drug reaching the site but also simultaneously decrease the amount being distributed to other parts of the body, thus reducing unwanted side-effects.¹ Site-specific or targeted delivery, therefore, would also enable a reduction in the necessary dose to be administered. By decreasing the side-effects, it would also increase the therapeutic index of the drug.^{3,4} In this context, a large number of drug delivery systems or drug carriers have been conceived and developed. Among

these systems, colloidal drug delivery systems ie liposomes and nanoparticles, and microparticles hold great promise for reaching the goal of site-specific delivery or drug targeting.

Liposomes are vesicular colloidal drug delivery systems. They consist of one or more concentric spheres of lipid bilayer(s) surrounding aqueous compartment(s).⁵ These bilayers are usually formed by amphiphilic lipids, ie phosphatidylcholine or dipalmitoyl phosphatidylcholine, and cholesterol which is used to alter the membrane permeability.⁶

Microparticles can be defined as polymeric entities falling in the range 1–250 µm (ideally less than 125 µm in diameter). At present, there is no universally accepted size range that particles must have in order to be classified as microparticles. However, many workers classify particles smaller than 1 µm as nanoparticles and particles larger than 1000 µm as macroparticles.⁷ Similarly, nanoparticles are solid colloidal polymeric particles ranging in size from 10 to 1000 nm. Both nano- and microparticles are made of artificial or natural material.⁸ The role of these polymers in the preparation methods of carriers

* Correspondence to: Cécile Duclairoir, Groupe Polymères-Interfaces, LCMT UMR 6507, ISMRA, 6 boulevard du Maréchal Juin, 14050 Caen Cedex, France
Contract/grant sponsor: Réseau Matériaux Polymères, Plasturgie

de Basse-Normandie.

(Received 28 May 1998; revised version received 15 January 1999; accepted 18 January 1999)

exceeds that of inert excipients. The components have an influence, not only on the biodegradation kinetics but also on the drug loading, compatibility with tissues and *in vivo* drug stability.⁹

In addition to the properties of the carrier material, bioacceptability is also influenced by the particle size. A reduction of the particle size enables intravenous injection. The diameter of the smallest blood capillaries is 4 µm; consequently, solid particles have to have a smaller diameter, in order to be able to traverse all capillaries.⁴ Furthermore, small colloidal carriers have a tendency to accumulate in areas of inflammation in the body and in certain tumours.¹⁰ Moreover, it has been demonstrated that a reduction in particle size of polymeric particles minimizes possible irritant reactions at the injection site.⁴

Finally, it is also interesting to note that for topical and oral applications it can be interesting to design small colloidal carriers. In principle, a decrease of the size allows an increase of the specific surface and, therefore, an increase of the possibilities of interaction with the skin and/or the mucosa. Therefore, a longer residence time of the drug delivery system could be expected from a decrease of its size.

The aim of this work was to form particles from a vegetal protein, gliadin (a fraction of wheat gluten), by a method of desolvating macromolecules.^{11,12} This method of precipitation has several names in the literature, including nanoprecipitation,^{12–14} coacervation,¹⁵ solvent displacement¹⁶ or drowning-out.¹⁷ These submicronic carriers could entrap different drugs (hydrophilic, hydrophobic and amphiphilic). All-*trans*-retinoic acid was chosen for its application in skin treatments.¹¹ This acid, slightly ionized in water, behaves like a lipophilic drug when it is introduced in an aqueous medium. However, if the pH of the medium is increased, this acid becomes better dissociated and may behave as a slightly polar molecule.

MATERIALS AND METHODS

Materials

Pure propylene glycol or 1,2-propanediol was purchased from Fluka, Switzerland. Synperonic® PE/F68 was graciously donated by ICI, UK. This surface-active agent is a tribloc copolymer polyethylene oxide-propylene oxide-polyethylene oxide. All-*trans*-retinoic acid (RA) or tretinoin ($C_{20}H_{20}O_2$, *M* 300.4), glutaraldehyde and trypsin type I from bovine pancreas were purchased from Sigma Chemical Co, USA. The physiological saline phase was prepared with NaCl provided by Merck, Germany and ultrapure water (Milli Q Plus, Millipore), as for all aqueous preparations. Other organic solvents (acetone, ethanol, etc) and chemical products used to prepare the phosphate buffer (PBS) were purchased from Prolabo, France.

Ethanol evaporation was realized by a rotavapor

R-114, provided by Büchi, Switzerland under reduced pressure. Nanoparticle separation was carried out by centrifugation with a Sigma 3K30 (Bioblock Scientific, France). UV-visible spectroscopy was carried out with a UV-visible Lambda 5 photometer (Perkin Elmer, USA). The particle diameters were measured by Quasi-Elastic Light Scattering (QELS), also known as photon correlation spectrometry (PCS) using two pieces of apparatus: a N4MD submicron analyser (Coultronics) was used for the characterization of gliadin nanoparticles, and a photogonioidiffusometer and an RTG correlator (SEMA Tech, France) with 12 digital counters were used for size optimization. The determination of loading and releasing capacities of gliadin nanoparticles made use of an original HPLC assembly described in detail later.

Gliadin nanoparticles

Gliadin extraction and purification

Gliadin was obtained from a common wheat flour (variety Hardy), purified at the Nantes Laboratories of INRA and then dialysed. Its method of purification is the following.

Gluten was extracted on a preparative scale from wheat flour. It was freeze-dried, ground in a refrigerated grinder and defatted by two extractions with dichloromethane for 2 h at 20°C (gluten/solvent ratio 1/10 w/v). After filtering, the residue was evaporated from the gluten at 20°C under reduced pressure. Samples of dried gluten powder (50 g) were stirred gently in an ethanol/water mixture (70/30 v/v) in a gluten/solvent ratio of 1/10 w/v for 4 h at 20°C. The suspension was centrifuged (10 000 g for 20 min). The soluble fraction was dialysed exhaustively, firstly against water, and then against 0.05 M acetic acid. Finally, gliadin was freeze-dried.

Analysis of the extracted gliadin fraction was carried out by reverse phase-HPLC¹⁸ and polyacrylamide gel electrophoresis at acid pH.¹⁹ In this way, the amount of protein in the gliadin freeze-dried extract was calculated to be around 85% w/w and the proportions of the different gliadin groups were 55% w/w for α - and β -gliadins, 15% w/w for γ -gliadin, and 15% w/w for ω -gliadin.

Preparation of gliadin nanoparticles by desolvatation

This method is based on the insolubility of gliadin in a non-solvent medium such as water, in contact with which the protein precipitates. The different steps of preparation are described in Fig 1. Two solutions prepared separately were mixed: Solution A containing 0.5% w/v gliadin solubilized at 25°C in 20 ml of an ethanol/water mixture, was prepared and then filtered through a 0.45 µm membrane. Solution B was made from 40 ml of physiological saline solution (i.e. 0.9% NaCl aqueous solution), filtered through a 0.45 µm membrane, and from Synperonic® PE/F68 at 25°C. The surface-active agent concentration was 0.5% w/w.

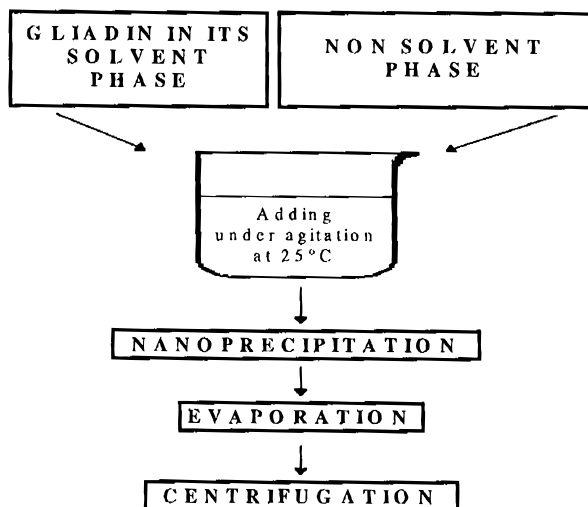


Figure 1. Formulation of gliadin nanoparticles by a macromolecule desolvatation.

The solvent phase A was then slowly poured with the help of a funnel, 4 mm in diameter, placed into the solution B at 25°C, under magnetic stirring (500 rev min⁻¹) for 2 min. Stirring and temperature were maintained for 5 min after this operation. This coacervation of the nanoparticles is named here as nanoprecipitation. The nanoparticle suspension was concentrated by evaporation with a rotavaporator in order to eliminate most of the ethanol. Then the nanoparticles were purified by centrifugation for 15 min at 20 000 rev min⁻¹ at 4°C. The supernatant was removed and the pellets resuspended in 2 ml of supernatant by ultrasonication for three sessions of 5 min.

Eventually, some batches were cross-linked with 1.64 mg glutaraldehyde per mg nanoparticles for 2 h at room temperature. This colloidal system was then purified twice by centrifugation in physiological saline solution.

Finally, RA-loaded gliadin nanoparticles were prepared by adding the drug in the organic phase before nanoprecipitation. In addition, the nanoparticle preparation procedure was performed in the dark in order to avoid RA degradation.

Evaluation of nanoparticle size by QELS

Particle-size measurements are carried out using quasi-elastic light scattering (QELS). The correlator accumulates the value of the light correlation function in 12 digital counters. Before an analysis, the sample is warmed to 25°C during at least 15 min: each change of 1°C promotes an error of 2% on the size estimation. Particle diameters are deduced from the Stokes-Einstein relation:

$$D = kT/3\pi\eta d \quad (1)$$

where k is the Boltzmann constant, T the absolute temperature and η the viscosity of the medium in which the particles of hydrodynamic diameter d are suspended. Particle size measurements are per-

formed with diluted solutions close to the dilution limit. For spherical particles, only scattering at one angle (90°) is required. In this study, the gliadin nanoparticles had been shown to be spherical by scanning electron microscopy.¹¹

Evaluation of transformed gliadin

The amount of gliadin transformed into nanoparticles was determinated as follows: 5 ml of suspension was centrifuged (20 000 rev min⁻¹ for 15 min) and the residue was dissolved with ethanol/water (7/3 v/v) mixture at room temperature for 10 min. The samples were assayed by UV-visible spectrophotometry at 280 nm. In preliminary experiments, absorbance at 280 nm had been shown to depend only on the concentration of the protein and to be linear up to 2 mg gliadin/ml.¹¹

RA entrapment

RA HPLC analysis

A liquid chromatography (Beckman Instruments) equipped with a 20 µl sample loop injector was used. RA was analysed by using a modification of an isocratic procedure previously reported.²⁰ Samples were chromatographed using a 15 cm × 4.6 mm i.d. stainless-steel column packed with octadecyl silane C18 (Ultrasphere ODS, 5 µm, Beckman) and a flow rate of 1.8 ml min⁻¹. The mobile phase, filtered through a 0.45 µm filter and degassed before use, consisted of methanol and water containing 10 mM ammonium acetate (75/25 v/v). The column effluent was monitored using a UV detector set at 350 nm. RA stock solutions in methanol were refrigerated and kept in the dark.

Calibration curves were constructed from a methanolic RA stock solution over the range 0.5–60 µg/ml. The curves were linear and passed through the origin ($r^2 = 0.998$, $n = 6$). The repeatability (variation coefficient) was determinated to be 0.45% for the RA concentration 60 µg ml⁻¹. Finally, the detection limit was calculated to be 0.2 µg ml⁻¹.

RA loading

RA-loaded gliadin nanoparticles (1–2 mg) were dissolved in 10 ml of a methanol/water mixture (7/3 v/v) at room temperature in the dark. The samples were then assayed for drug content by UV-visible spectroscopy at 350 nm. Although gliadin molecules did not interfere, empty nanoparticles were treated in the same way and used as references for these determinations. Moreover the supernatants obtained from the two washing steps were analysed by the HPLC method described above. This technique allowed the determination of the amount of non-associated RA with gliadin nanoparticles. The drug loading (payload) and the entrapment efficiency were calculated as follows:

$$\text{Payload (\%)} = \frac{100C_1}{\text{gliadin nanoparticle yield (mg)}} \quad (2)$$

Table 1 Solubility parameters of the solvents used

Solvent	δ (MPa $^{1/2}$)
Water	47.8
Ethylene glycol	32.9
Propylene glycol	30.2
Ethanol	26.5

$$\text{Entrapment efficiency (\%)} = \frac{100C_1}{(C_1 + C_2)} \quad (3)$$

where C_1 is the amount of RA loaded in the nanoparticles (determined from spectroscopy experiments), and C_2 is the amount of free RA (data from HPLC).

In vitro RA release

About 15 mg of gliadin nanoparticles (containing 0.85 mg of RA) were suspended in 100 ml of PBS at pH 7.4. To prevent drug loss due to photo-degradation during the dissolution study, the experimental assembly was protected from the light. The medium was maintained at 37°C and stirred at 200 rev min $^{-1}$. Samples of 1 ml were collected at successive time intervals, and centrifuged for 15 min at 20 000 rev min $^{-1}$. These samples were immediately analysed by HPLC using the procedure described above, for their RA content (each measurement was made in triplicate). Finally, in order to avoid possible thermal RA degradation during the experiments, the *in vitro* drug release tests were performed for only 3 h.

Solubility parameters

Theory

Hildebrand²¹ defined the solubility parameter δ , correlated to the mixing enthalpy for endothermic simple mixtures. In that case, the miscibility of a polymer in a solvent is possible if

$$\delta_1 = \delta_2 \quad (4)$$

with 1 and 2 meaning solvent and polymer. For classical solvents, the parameter can be found in the literature²² and is expressed in (J · cm $^{-3}$) $^{1/2}$ or in (MPa) $^{1/2}$.

The solubility parameter δ_M of a mixture (for instance, water/ethanol) is determined with the help of the following relation:

$$\delta_M = \phi\delta + \phi'\delta' \quad (5)$$

where δ and δ' are the solubility parameters of ethanol and water, and ϕ and ϕ' are their volume fractions ($\phi + \phi' = 1$).

This approach is better adapted to non-polar molecules because their mixing enthalpy values are

slightly endothermic. Because gliadin is one of the non polar proteins, the preceding relation can be applied conveniently.

In this study, the protein/water/ethanol mixture is assumed to be a simple regular mixture. In fact the protein is very dilute (0.1%).

Preparation of different solubility parameter solutions

According to Hildebrand,²¹ the solubility parameter of gliadin can be determined using a panel of solvents or mixtures of them. Logically, the solvent which best solubilizes gliadin has the same solubility parameter (δ_G) as this protein.

Different mixtures were prepared with solvents such as ethylene glycol (EG) or propylene glycol (PG) and ultra pure water. Table 1 displays the solubility parameters of the solvents used.²² 0.1% gliadin solutions were prepared in solvent mixtures where δ_M ranged between 30.2 and 36.9 MPa $^{1/2}$.

Turbidity

For the determination of its solubility parameter, the solubility of a compound dissolved in media of different δ_M values could be estimated visually from the homogeneity and transparency of the mixtures. More accurate estimates can be made by turbidity measurements: the more opaque the solution, the more attenuated the intensity of the incident beam. The observed absorption is related to the turbidity τ and to the thickness of the cell l . The measurement is performed by determining the difference between a suspension and the pure solvent; then

$$\begin{aligned} (\text{Abs})_{1+2} - (\text{Abs})_1 &= 1(\tau_{1+2} - \tau_1) \\ &= 1\Delta\tau \end{aligned} \quad (6)$$

where $(\text{Abs})_i = \log(I/I_0)$, and subscripts 1 and 2 denote solvent and solute, respectively, in this case gliadin.

RESULTS AND DISCUSSION

The term gliadin defines a group of proteins extracted from gluten by 70% ethanol.¹⁹ These proteins are polymorphic and can be classified on the basis of their electrophoretic mobility in the following four fractions: α -gliadin molecular mass about 25–35 kDa; β -gliadin, 30–35 kDa; γ -gliadin 35–40 kDa; ω -gliadin, 55–70 kDa.¹⁹ Other characteristics of these proteins are, (i) their low solubility in aqueous solution; (ii) the presence of interpeptide S–S bonds and hydrophobic interactions which induce protein chains to assume a folded shape;²³ (iii) a high proline content and a very low proportion of charged amino acids.¹⁹

The method used to prepare gliadin nanoparticles in this study is based on the desolvatation of macromolecules by adding a solvent phase of the protein to a non-solvent phase (Fig 1).

Gliadin was dissolved in different organic media.¹¹ The solutions were poured into a physiological saline phase, followed by the further process steps. The

nanoparticle diameters depend on the organic medium. In fact, the smallest particles were produced with the ethanolic mixture (7/3 v/v); their size was about 500 nm.¹¹ The non-solvent phase was always an aqueous solution containing NaCl 0.9% w/v (in order to increase the yield of gliadin nanoparticles) and Synperonic PE/F 68 which inhibited particle aggregation. It is interesting to note that both water and ethanol are considered to be safe for the preparation of drugs. Moreover, gliadin nanoparticles prepared in this way were stable, and further treatment by heat or chemical crosslinking was not necessary to stabilize them. However, some batches have been hardened, because it is known that the stability and drug release characteristics can be modulated by crosslinkage.¹⁴

RA-loaded gliadin nanoparticles

All-trans retinoic acid (RA) appears to be involved in the proliferation and differentiation of epithelial tissues. These properties make it an attractive agent for the treatment of skin disorders, such as acne, psoriasis, hyperkeratosis, ichthyosis and epithelial tumours.²⁴ However, several drawbacks and undesirable effects have been reported for the currently available dosage forms (eg teratogenicity).²⁴ One possibility to overcome these difficulties and attempt to increase the therapeutic efficacy, consists of the use of drug delivery systems possessing the capacity to control drug release. For this purpose micro-emulsions,²⁵ topical liposomes²⁶ and gliadin nanoparticles¹¹ have been proposed.

The drug content was measured by spectrophotometry after dissolving RA-loaded gliadin nanoparticles in an ethanol/water mixture (7 : 3). These data correspond to parameter C_1 in eqns (2) and (3). Similarly, the amount of non-entrapped RA, which corresponds to C_2 in eqn (3), was calculated after HPLC analysis of the supernatants obtained from the washing steps. From these results, the payload was calculated and plotted against the ratio between the amounts of drug and gliadin used for the preparation of RA-loaded gliadin nanoparticles (Fig 2). It is clear that the drug content associated with nanoparticles (payload) increases with the concentration of drug; however, at ratios greater than 90 µg mg⁻¹ the stability of RA delivery systems was impaired.

In contrast, the efficiency of RA entrapment (calculated from eqn 3) was greater than 85% of the added drug for ratios lower than 60 µg mg⁻¹. Above this ratio, a significant amount of drug remained free (about 25% for a ratio of 90 µg mg⁻¹) which was responsible for the partial loss of physicochemical stability.

RA release from gliadin nanoparticles

Gliadin nanoparticle formulations were tested for *in vitro* release for 3 h at 37°C in the absence of light. The *in vitro* release profiles give an indication of the capacity of the delivery system for the controlled

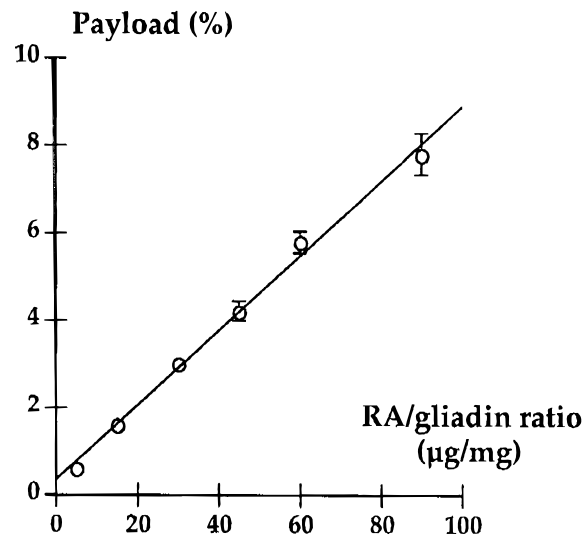


Figure 2. Influence of the RA/Initial protein ratio on the payload of RA associated with gliadin nanoparticles.

release of drugs or active molecules. Figure 3 shows the plot of the data expressed as the cumulative amounts of RA released from the gliadin nanoparticles as a function of time. RA was released into a two-step mechanism, characterized by an initial rapid release followed by a continuous diffusion process (Fig 3). The first release was found to be about 20% of the loaded drug and can be related either to the release of the drug entrapped in the peripheral domains of the nanoparticle matrix²⁷ or to a simple desorption of superficial RA, whilst the second slower period was linear with respect to time and appeared to be a diffusion phenomenon.²⁸ Furthermore, in this second step, about 20% of the drug was released by diffusion in 3 h.

Size optimization of gliadin nanoparticles: influence of the solubility parameter of the protein solvent phase

The preceding results show clearly that the gliadin nanoparticles are able to entrap and to release a lipophilic drug such as RA. The size is also a determinant parameter in the optimization of their efficacy and their bioacceptability.⁵ Indeed the smaller the nanoparticles, the better their penetration into small capillary blood vessels.

Precipitation and coacervation can be considered part of the general area of solubility parameter and phase equilibria.²⁹ A correlation between the solubility parameter and the particle diameter should lead to optimization of their size. This correlation was studied with gliadin in various solvents. In order to simplify the experiments, the nanoparticles were not crosslinked and RA and PBS were absent.

Determination of gliadin solubility parameter δ_G (Hildebrand's parameter)

The solubility parameter of gliadin δ_G , was measured at 25°C in ethanol/water mixtures of solubility

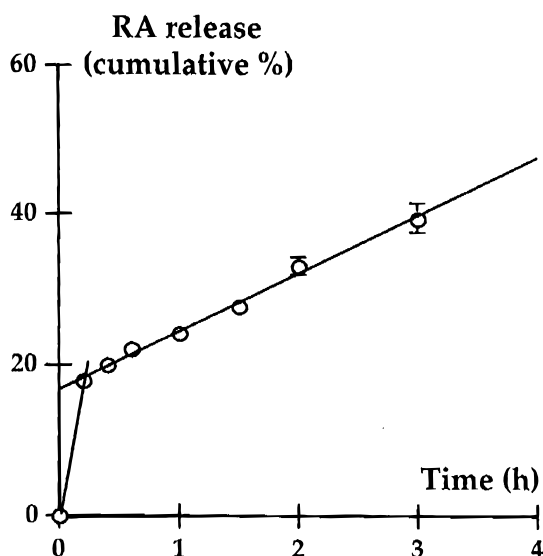


Figure 3. *In vitro* release of RA from gliadin nanoparticles (expressed as cumulative release). Gliadin nanoparticles were prepared from a drug/protein ratio of $60 \mu\text{g mg}^{-1}$.

parameter δ_M , in the range $33.9\text{--}36 \text{ MPa}^{1/2}$. In Fig 4, minimum turbidity is observed at $34.5 \pm 0.5 \text{ MPa}^{1/2}$, which corresponds to the clearest solution. It can therefore be accurately concluded that the δ_G value is $34.5 \pm 0.5 \text{ MPa}^{1/2}$.

Change of nanoparticle size with the process step

This study is based on three different batches of nanoparticles. Each diameter is a mean value of at least three measurements by QELS. At the end of the nanoprecipitation, evaporation and centrifugation steps, the solutions in which the nanoparticles are suspended, contain, respectively, 20%, nearly 0% and 0% ethanol.

Figure 5 shows the variation of nanoparticle size 24 h after desolvatation of one batch of gliadin. The nanoparticle diameters are plotted versus the solubility parameters δ_M of the initial solvent mixtures used for nanoprecipitation. The curves show a minimum diameter of 150 nm when δ_M corresponds to the gliadin solubility parameter δ_G for the steps of nanoprecipitation and evaporation by a rotavapor. This behaviour is not observed for the centrifugation

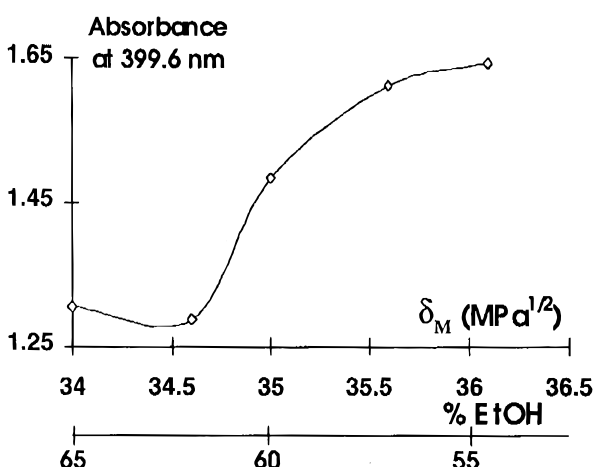


Figure 4. Turbidity of gliadin mixtures.

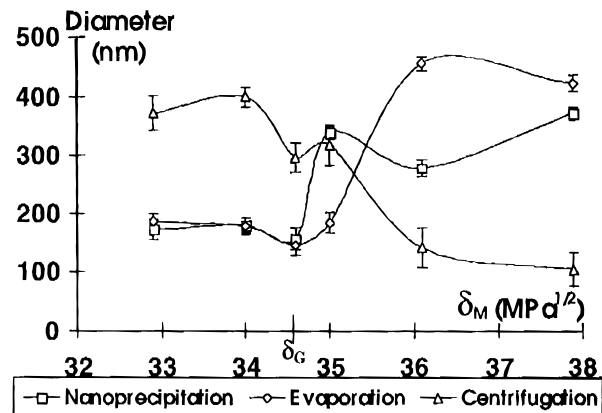


Figure 5. Size change of gliadin nanoparticles as a function of the process step 24 h after desolvatation. The polydispersity of the size distribution is represented by error bars.

step. Compared to the nanoprecipitation and evaporation steps, the nanoparticle size is doubled at δ_G . The nanoparticle size is also doubled between 32.9 and $35.0 \text{ MPa}^{1/2}$. A possible explanation could be the aggregation of the particles by pairing through the action of the centrifugal force. However, from 36.1 to $37.9 \text{ MPa}^{1/2}$, the diameters decrease and the polydispersity values increase to between 20 and 35%. This different behaviour is not easy to explain: none of the parameters or experimental conditions were changed during the experiments.

The size of the nanoparticles obtained was followed for 39 days. After 28 days for the nanoprecipitation and evaporation steps, some batches flocculated, but the nanoparticles obtained with solvent media close to δ_G remained in suspension. The minimum diameter obtained is in the vicinity of δ_G . The centrifugation study (not shown here²⁴) has two effects: it affects the size of the particles after nanoprecipitation, and influences the temporal shape of the suspension.

Nanoparticle size at δ_G as a function of time

A comparison of the change of the diameter of non-crosslinked nanoparticles prepared at δ_G after nanoprecipitation and solvent evaporation follows. Figure 6 shows a similarity in the relationship between the

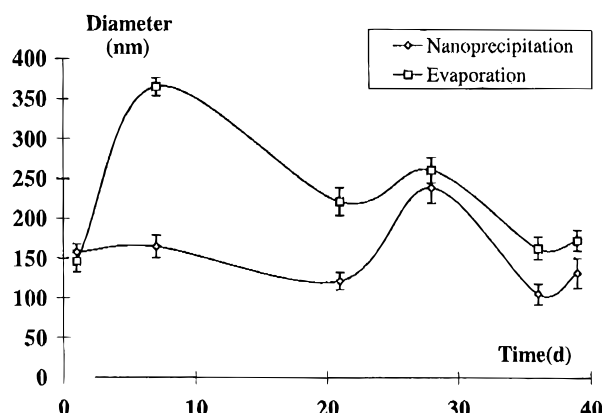


Figure 6. Size change of gliadin nanoparticles with time after nanoprecipitation and evaporation steps. The polydispersity of the size distribution is represented by error bars.

diameter size and time. Nevertheless, after the rotavapor stage, which eliminates most ethanol, size becomes more important than after nanoprecipitation. This is probably correlated to the higher concentration of nanoparticles, which are brought closer to each other and tend to aggregate. It can also be observed that the difference between the two curves decreases with time. After 40 days, the size is approximatively the same as the 24 h after the preparation of the nanoparticles. The oscillations are probably related to degradation processes of the nanoparticles, which might be worth examining in future experiments.

CONCLUSIONS

Gliadin nanoparticles can be obtained by using only environmentally acceptable solvents such as ethanol and water. Their size, which is one of the determinant characteristics for medical purposes can be optimized by investigating the solubility parameter δ of the protein solvent phase: the closer δ is to the protein solubility parameter, the smaller the size of the nanoparticles. Furthermore, these delivery systems were found to be good carriers for slightly polar molecules such as RA. In this context, the limit payload for RA was fixed at 76.4 μg drug per mg nanoparticle, which corresponds to an entrapment efficiency of about 75% of added RA. RA was released in a biphasic way, characterized by an initial rapid release period (20% of the entrapped drug) followed by a continuous and slower release characterized by a diffusion process. The nanoparticle size varies with time, but the mean diameter is almost the same 40 days after precipitation, which gives a good indication of their stability.

ACKNOWLEDGEMENTS

The authors thank the Réseau Matériaux Polymères, Plasturgie for financial support.

REFERENCES

- 1 Ehrlich P, *Collected Studies on Immunity*, Vol 2. New York, John Wiley & Sons. p 422, 1906.
- 2 Gregoriadis G, *J Antimicrob Chem* **28** (Suppl. B) 39:1991.
- 3 Douglas SJ, Davis SS, Illum E, *CRC Crit Rev Ther Drug Carrier Sys* **3**:233 (1987).
- 4 Puiseux F, Barrat G, Couarraze G, Couvreur P, Devissaguet JP, Dubernet C, Fattal E, Fessi H, Vauthier C, Benita S, in *Polymeric Biometaterials*, Ed by Dimitriu S. Marcel Dekker, New York. pp 749–794 (1994).
- 5 Fattal E, Couvreur P and Puiseux F, in *Les Liposomes, Aspects Technologiques, Biologiques et Pharmacologiques*, Ed by Delatre J, Couvreur P, Puiseux F, Philipot J and Schuber F, Les Editions INSERM Tec & Doc Lavoisier, Paris. pp 43–62, (1993).
- 6 Marsch D, *Handbook of Lipid Bilayers*, CRC Press, Boston (1990).
- 7 Benoit JP, Marchais H, Rolland H and Vaude Velde V, in *Microencapsulation Methods and Industrial Applications*, Ed by Benita S, Marcel Dekker, New York. pp 35–71 (1996).
- 8 Chasin M and Langer R, *Biodegradable Polymer as Drug Delivery Systems*, Marcel Dekker, New York. (1990).
- 9 di Silvio L, Gurav N, Kayser M, Braden M and Downes S, *Biomaterials* **15**:931 (1994).
- 10 Gipps EM, Arshady R, Kreuter J, Groscurth P and Speiser PP, *J Pharm Sci* **75**:256 (1986).
- 11 Ezpelleta I, Irache JM, Stainmesse S, Chabenat C, Gueguen J, Popineau Y and Orecchioni AM, *Int J Pharm* **131**:191 (1996).
- 12 Duclairoir C, Nakache E, Marchais H, Orecchioni AM, *Colloid Polymer Sci* **276**:321 (1998).
- 13 Kreuter J, *Int J Pharm* **58**:196 (1983).
- 14 Rubino OP, Kowalsky R and Swarbrick J, *Pharm Res* **10**:1059 (1993).
- 15 Naim JG, *Adv Pharm Sci* **7**:93 (1995).
- 16 Alonso MJ, in *Microparticulate Systems for the Delivery of Proteins and Vaccines*, Ed by Cohen S and Bernstein H, Marcel Dekker, New York. p 203 (1996).
- 17 Plasari E, Grisoni Ph and Villermaux J, *Trans Inst Chem Eng* **75**:237 (1997).
- 18 Wieser H, Seilmer W and Belitz HD, *J, Cereal Sci* **19**:149 (1994).
- 19 Larré C, Popineau Y, and Loisel W, *J Cereal Chem* **14**:231 (1991).
- 20 Furr HC, Barna AB and Olson JA, *Modern Chromatographic Analysis of Vitamins*, 2nd edn, Ed by Leenheer D, Lambert WE and Wellis HJ, Marcel Dekker, New York. pp 1–71 (1992).
- 21 Hildebrand JH, Scott RL, *The Solubility of Nonelectrolytes*, Dover Publications, New York (1964).
- 22 Barton AFM, *Handbook of Solubility Parameters and Other Cohesion Parameters*, 2nd Edn, CRC Press, Boca Raton (1991).
- 23 Bietz JA and Rothfus JA, *Cereal Chem* **47**:381 (1970).
- 24 Lewin AH, Bos ME, Zusi FC, Nair X, Whiting G, Bouquin P, Tetrault G and Carroll FI, *Pharm Res* **11**:192 (1994).
- 25 Takino T, Koishi K, Takakura Y and Hashida M, *Biol Pharm Bull* **17**:121 (1994).
- 26 Masini V, Bonte F, Meybeck A and Wepierre J, *J Pharm Sci* **82**:17 (1993).
- 27 Jeyanthi R and Rao KP, *Int J Pharm* **55**:31 (1989).
- 28 Gupta PK, Hung CT and Perrier DG, *Int J Pharm* **33**:137 (1986).
- 29 Dervichian DG, *Discuss Faraday Soc*, **18**:231 (1954).

P3

Article original

Maîtrise de la taille de nanoparticules de gliadines de blé par la détermination de leur paramètre de solubilité

A.-M. Orecchioni (1), C. Duclairoir (2), E. Nakache (2)

Résumé. Des nanoparticules de gliadines, complexes protéiques issus du gluten de blé, ont été préparées par coacervation (désolvatation). L'objectif était d'obtenir des systèmes colloïdaux dont la taille et l'indice de polydispersité soient les plus faibles possibles. Le choix du solvant est primordial d'autant que la solvatation totale permet de contrôler le processus de désolvatation et de maîtriser subséquemment la taille des particules dispersées.

Différents solvants pharmaceutiques ont été essayés. Pour sélectionner le meilleur, on s'en est remis à une approche thermodynamique qui repose sur la détermination du paramètre de solubilité δ_G du complexe gliadines. Le solvant le mieux adapté est celui dont le paramètre de solubilité (calculé ou déterminé expérimentalement) est égal à celui des protéines végétales en question.

Mots-clés : Nanoparticules, Paramètre de solubilité, Gliadines, Protéines végétales.

Summary. Gliadins nanoparticles, protein complex from wheat gluten, were prepared by coacervation (macromolecules desolvatation). The objective was to prepare nanometric colloidal systems with both smallest particle size and polydispersity index. Macromolecules solvent choice is predominant. Their total solvation enables of control the desolvatation process and thence particle sizes.

Different pharmaceutical solvents were assayed. In order to select the best of them, a thermodynamical approach was used. It rests on the determination of the solubility parameter δ_G of the gliadins complex. The best solvent is the one whose solubility parameter (calculated or experimentally determinated) is equal to the plant protein's.

Key-words: Nanoparticles, Solubility parameter, Gliadins, Vegetable proteins.

Wheat gliadins nanoparticles size control by determination of the solubility parameter of these plant proteins
A.-M. Orecchioni, C. Duclairoir, E. Nakache. Ann Pharm Fr 2001, 59 : 402-406.

Introduction

La mise au point de formes pharmaceutiques et notamment de suspensions colloïdales nanométriques à base de macromolécules naturelles ou syn-

thétiques requiert la parfaite connaissance des propriétés physicochimiques de chacun des composants de la formule. Doivent être également connues les interactions des matières premières entre elles (substances actives et excipients), et, de manière plus approfondie, les interactions avec les solvants, surtout s'il s'agit de formes liquides. Ainsi, pour ces dernières, la connaissance des forces de cohésion qui lient entre elles atomes et molécules de la substance à dissoudre (forces électrostatiques, forces de Van de Waals, liaisons hydrogène...) devrait permettre de mieux apprécier les mécanismes qui régissent leur solubilité

Présentation devant L'Académie nationale de Pharmacie, séance du 6 décembre 2000.

(1) Laboratoire de Pharmacie galénique et de Biopharmacie, Université de Rouen, 22, boulevard Gambetta, F 76183 Rouen Cedex.

(2) Groupe Polymères-Interfaces, LCMT, UMR 6507, ISMRA, 6, boulevard du Maréchal Juin, F 14050 Caen Cedex.

Tirés à part : A.M. Orecchioni, à l'adresse ci-dessus.

Nanoparticules de gliadines de blé : maîtrise de leur taille

et, en conséquence, permettre le choix du meilleur solvant [1].

Dans le présent travail, l'objectif était de mettre au point de nanoparticules de gliadines tout en maîtrisant parfaitement la taille et l'indice de polydispersité afin qu'ils soient les plus faibles possibles. La taille est en effet étroitement liée à la biodisponibilité. Ainsi, dans le cas, par exemple, de préparations destinées à une application topique, une importante surface spécifique favorise les interactions avec la peau et/ou les muqueuses garantissant un temps de résidence plus long dans les diverses assises cutanées d'où un effet thérapeutique prolongé.

Pour la formulation des suspensions colloïdales de gliadines (protéines issues du gluten de blé), une méthode classique de coacervation a été employée. Pratiquement, la technique consiste à précipiter les protéines en solution par modification des propriétés physicochimiques du solvant : ajout d'un électrolyte, d'un non solvant des macromolécules, action de l'élévation de la température, modification du pH... Dans une première étape, il a donc été nécessaire de rechercher le solvant le plus apte à permettre la solvatation totale des gliadines. La deuxième étape a consisté à maîtriser la réaction de désolvatation en vue d'obtenir une précipitation sous forme de nanoparticules et non une précipitation massive sous forme de gel. Cette démarche s'est appuyée sur une approche thermodynamique.

Rappels sur la théorie de Hildebrand

L'énergie de cohésion qui permet aux atomes et aux molécules d'une substance d'être liés entre eux peut être quantifiée de différentes manières. La plus habituelle est la détermination du paramètre de solubilité δ (Hildebrand et Scott) [2-4] de ladite substance. Le paramètre de solubilité est une valeur numérique qui permet de caractériser le pouvoir solvant de différents composés à l'équilibre. D'après la théorie de Hildebrand, quand deux substances sont mélangées, la chaleur de mélange ΔH , ou enthalpie, est donnée par la relation :

$$\Delta H = V_T (\delta_1 - \delta_2)^2 \cdot \phi_1 \cdot \phi_2 \quad (\text{relation 1})$$

où V_T = volume total des corps en présence

δ = paramètre de solubilité

ϕ = fraction volumique.

Les indices 1 et 2 correspondent respectivement au solvant et au corps à dissoudre.

Le paramètre de solubilité de chacun des composants est défini par la relation :

$$\delta = (\Delta E_v / V_m)^{0.5} \quad (\text{relation 2})$$

où ΔE_v = variation d'énergie de vaporisation
 V_m = volume molaire.

Quand les paramètres de solubilité de deux substances sont égaux, la relation 1 permet de prédire qu'elles sont solubles l'une dans l'autre. Il en résulte donc que, pour que la miscibilité ou la solubilité soient les meilleures, ΔH doit avoir une valeur voisine de zéro. Les valeurs de δ s'expriment en $(J/cm^3)^{0.5}$ ou en $(MPa)^{0.5}$.

Les paramètres de solubilité de la plupart des solvants usuels ont été déterminés, soit par calcul, soit expérimentalement, par différents auteurs [5, 6]. Ils figurent sur des tableaux auxquels il est aisément de se référer lorsqu'on souhaite dissoudre un composé quelconque. Il suffit de chercher dans une série de solvants de δ variés celui qui assure la dissolution totale du produit. Toutefois l'expérimentation a montré qu'il n'est pas toujours possible de trouver un solvant de même δ que celui de la substance à mettre en solution. Dans ce cas, il est possible de faire appel à un mélange de solvants. Le paramètre de solubilité δ_M du mélange est donné par la relation 3.

$$\delta_M = \phi_1 \cdot \delta_1 + \phi_2 \cdot \delta_2 \quad (\text{relation 3})$$

avec $\phi_1 + \phi_2 = 1$

Le δ du corps à dissoudre correspond alors au δ_M du meilleur mélange.

L'application de la théorie de Hildebrand aux gliadines devrait permettre de déterminer le paramètre de solubilité (δ_G) de ces dernières à l'aide d'une série de solvants pharmaceutiques utilisés seuls ou en mélange afin de permettre la solvatation totale de ces protéines et, par suite, la formulation de suspensions nanoparticulaires.

Matériel et méthodes

Les solutions aqueuses ont été préparées avec de l'eau ultrapure (Milli Q Plus, Millipore).

Le chlorure de sodium a été fourni par Merck.

L'éthanol absolu (EtOH) provenait de chez Carlo Erba.

Le propylène glycol (PG) de pureté supérieure à 98 % a été fourni par Fluka.

L'éthylène glycol (EG) de pureté supérieure à 99,5 % a été fourni par Prolabo.

L'agent de surface utilisé pour disperser les nanoparticules a été du Synperonic® PE/F 68 de chez ICI.

Les gliadines ont été extraites et purifiées au sein du Laboratoire de Biochimie et Technologie des protéines de l'INRA de Nantes. Issues du gluten de blé (variété « Hardi »), elles ont été obtenues par une méthode générale d'extraction des protéines qui repose sur les différences de solubilité dans des solutions alcooliques en présence de sels (NaCl le plus souvent). Dans le cas particulier de ces protéines végétales, le solvant utilisé a été un mélange éthanol/eau (70/30 v/v) pour un rapport gluten/solvant égal à 1/10 p/v. Les gliadines, fraction soluble, représentent 85 % p/p de la fraction protéique. Il s'agit en fait d'un complexe protéique qui peut être subdivisé en quatre groupes (α , β , γ et ω gliadines) selon leur mobilité électrophorétique en milieu acide, ou en trois groupes ($\alpha\beta$, γ et ω gliadines) selon la séquence des acides aminés N-terminaux [7].

Préparation d'une gamme de solvants de différents paramètres de solubilité

Parmi les solvants susceptibles d'assurer la solvation du complexe-gliadines, le choix s'est porté sur l'éthylène glycol (EG), le propylène glycol (PG), l'éthanol (EtOH) et l'eau ultra pure. Leurs paramètres de solubilité respectifs sont reportés dans le tableau I, les valeurs sont données en (Mpa)^{0,5}.

Les solvants ont été utilisés seuls ou en mélange, la gamme de δ s'étalant de 30,2 à 36,9. La concentration en gliadines dans chacune des solutions organiques a été de 0,1 % p/v.

Tableau I. — Paramètres de solubilité des solvants utilisés (Mpa^{0,5}).
Solubility parameters of the solvents used (Mpa^{0,5}).

Solvants	Eau	EG	PG	EtOH
δ	47,8	32,9	30,2	26,5

Préparation des nanoparticules de gliadines par coacervation

Cette méthode est également appelée nanoprécipitation, désolvatation des macromolécules, déplacement de solvant. Elle repose sur le fait que les gliadines sont insolubles dans l'eau au sein de laquelle elles précipitent [8-10].

Deux solutions préparées séparément à la température de 25 °C ont été filtrées sur membrane 0,45 µm puis mélangées.

Une première solution, constituée de 20 ml d'un mélange éthanol/eau de δ_M requis et contenant 0,5 % p/v de gliadines a été versée lentement (2 min) sous agitation magnétique (500 rev/min) au sein de 40 ml d'une solution aqueuse saline (NaCl 0,9 % p/v) contenant 0,5 % p/v de Synperonic®PE/F68. L'agitation a été encore maintenue pendant 5 min. La suspension de nanoparticules ainsi obtenue a été concentrée sous vide (Rotavapor R-114, Büchi). La suspension nanoparticulaire a ensuite été purifiée par ultracentrifugation (15 min à 20 000 rev/m) à la température de 4 °C. Après élimination du surnageant, le culot de centrifugation a été remis en suspension dans 2 ml de surnageant et soumis aux ultrasons afin de disperser les nanoparticules. Les différentes étapes sont reportées (fig. 1).

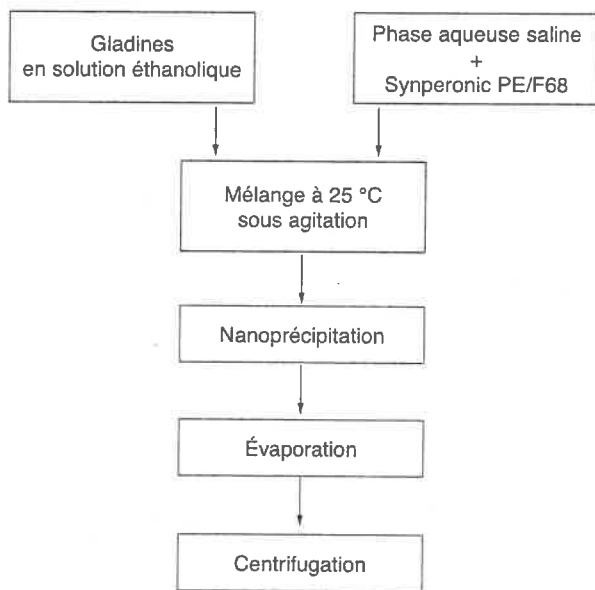


Figure 1. Préparation des nanoparticules par coacervation.
Nanoparticles preparation by coacervation.

Nanoparticules de gliadines de blé : maîtrise de leur taille

Tableau II. — Observation de solutions de gliadines à 0,1 % p/v.
Visual observations of 0.1 % w/v gliadins solutions.

δ Mpa ^{0,5}	mélange %	Temp. °C	Aspect
30,2	PG 100	14,6	très trouble
30,6	PG/Eau 96/4	14,6	trouble
31,8	PG/Eau 91/9	14,6	très trouble
32,8	PG/Eau 85/15	14,6	très trouble
32,9	EG 100	17,2	trouble
33,9	PG/Eau 79/21	14,6	clair
34,2	EG/Eau 91/9	17,2	très clair
35,0	PG/Eau 73/27	14,6	très clair
35,1	EG/Eau 85/15	17,2	très clair
36,0	EG/Eau 79/21	17,2	clair
36,9	EG/Eau 73/27	17,2	trouble

Mesure de la taille des nanoparticules par diffusion quasi élastique de la lumière (QELS)

La mesure a été effectuée sur des suspensions nanoparticulaires diluées. Des études en microscopie électronique à balayage (résultats non présentés ici) ont montré que les particules sont sphériques ; les mesures ont donc été faites à l'angle de 90°.

Résultats et discussion

Détermination du paramètre de solubilité des gliadines δ_G par la méthode de Hildebrand

Les solvants utilisés dans cette étude pour la détermination des paramètres de solubilité sont généralement considérés comme les solvants de référence.

Dans une première approche, l'observation visuelle des différentes solutions de gliadines à 0,1 % p/v au sein des solvants seuls ou associés a permis de les classer en fonction de leur aspect en solutions transparentes ou non. Les résultats sont reportés dans le tableau II.

Il est ainsi possible de constater que les solutions colloïdales les plus claires sont obtenues pour des valeurs de δ comprises entre 33,9 et

36 MPa^{0,5}. Le paramètre de solubilité δ_G des gliadines devrait donc se situer à 35 ± 1 Mpa^{0,5}.

En vue de mieux préciser ces observations préliminaires, des études turbidimétriques ont été effectuées à 25 °C avec des mélanges éthanol-eau de δ_M compris entre 34,0 et 36,1 Mpa^{0,5}. Ce couple de solvants a été choisi car il est utilisé pour la préparation des nanoparticules. Les résultats obtenus (*fig. 2*) permettent de déterminer le δ_G des gliadines avec précision. Il se situe à une valeur :

$$\delta_G = 34,5 \pm 0,5 \text{ Mpa}^{0,5}$$

valeur pour laquelle la turbidité est minimum. Le mélange solvant correspond aux proportions suivantes : EtOH/H₂O 62/38.

Mesure de la taille des nanoparticules par QELS

Les mesures ont été faites sur trois lots différents. Chaque résultat est la moyenne de trois mesures. Ces dernières ont été effectuées aux différentes étapes de la réaction de nanoprecipitation. Aussitôt après que cette dernière se soit produite, après évaporation et après centrifugation, les résultats sont reportés sur la *fig. 3*.

Les observations suivantes peuvent être faites lorsque sont reportés sur un graphe les diamètres nanoparticulaires en fonction des paramètres de solubilité des solvants du complexe gliadines :

— le diamètre des nanoparticules présente une valeur minimum de 150 nm lorsque le paramètre de solubilité δ_M du mélange correspond au paramètre de solubilité δ_G des gliadines ;

— ce minimum est observé aux deux étapes du processus de coacervation : nanoprecipitation instantanée et évaporation avec un faible indice de polydispersité ;

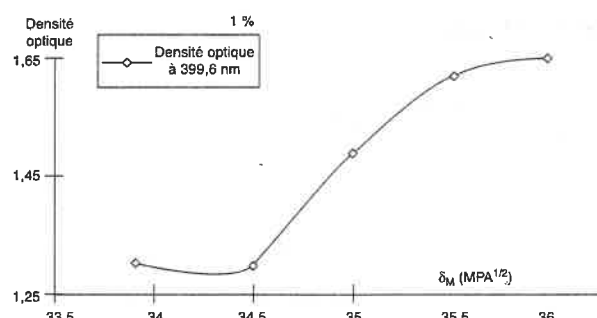


Figure 2. Turbidité des solutions de gliadines.
Turbidity of gliadins solutions.

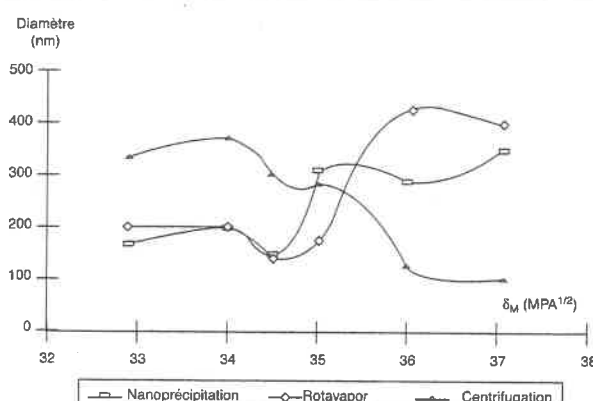


Figure 3. Évolution de la taille des nanoparticules en fonction de l'étape du processus 24 h. après nanoprecipitation.
Size evolution of gliadins nanoparticles as a function of the process step 24 h. after desolvatation.

— la courbe correspondant à l'étape de centrifugation ne présente pas le même profil que les deux précédentes. Si un minimum est observable pour la valeur $\delta_M = \delta_G$, la taille est toutefois le double de celles observées pour les autres étapes (300 nm environ). Cette taille est également le double pour des valeurs de δ_M comprises entre 32,9 et 35,0 MPa^{0,5}. Cela pourrait être dû à l'action des forces de centrifugation qui provoquerait la formation d'agrégats. Nous ne pouvons cependant pas expliquer pourquoi la taille diminue tandis que l'indice de polydispersité augmente pour des valeurs de δ_M comprises entre 36,1 et 37,9 MPa^{0,5} ;

— le suivi de l'évaluation des tailles au cours du temps (suivi sur 39 jours, non montré ici) a permis de constater que, bien que quelques lots aient fluctué, les tailles des particules restées en suspension dans un mélange solvant de $\delta_M = \delta_G$ ont conservé une valeur minimale.

Conclusion

La détermination du paramètre de solubilité des gliadines a permis de maîtriser la taille des nanoparticules obtenues par le processus de coacervation. Ainsi, lorsque le complexe protéique est solvaté dans un « bon solvant », dont le paramètre de solubilité est égal à celui des protéines, la taille des vecteurs nanoparticulaires obtenus est minimale quelles que soient les conditions d'extraction et de purification du matériau macromoléculaire. Si tou-

tefois cette taille est sous la dépendance de certaines étapes du processus de fabrication, il n'en reste pas moins qu'elle passe par un minimum, et que celui-ci se maintient au cours du stockage, ce qui est de bon augure pour ce qui est de la stabilité du système colloïdal. Celui-ci pourrait d'ailleurs être « figé » par cryodessiccation sans inconvénients majeurs puisque la suspension nanoparticulaire est obtenue en milieu aqueux. Des études sont actuellement en cours au sein du laboratoire pour l'encapsulation de diverses substances actives en vue d'applications dermatologiques des vecteurs ainsi obtenus.

Remerciements

Les auteurs remercient le « Réseau Matériaux, Polymères, Plasturgie de Haute-Normandie » pour son soutien financier.

Références

- Hancock BC, York P, Rowe RC. The use of solubility parameters in pharmaceutical dosage form design. *Int J Pharm* 1997; 148: 1-21.
- Hildebrand JH and Scott RL. The Solubility of Nonelectrolytes. 3rd Edn. New York: Reinhold; 1949.
- Hansen CM. The universality of the solubility parameter. *Ind Eng chem Prod Res Dev* 1969; 8: 2-11.
- Barton AFM. Handbook of solubility parameters and other cohesion parameters. 2nd Edn. Boca Raton: CRC Press; 1991.
- Vaughan CD. Using solubility parameters in cosmetic formulation. *J Soc Cosmetic Chem* 1985; 36: 319-33.
- Bustamente PB, Martin A and Gonzalez-Guisandez A. Partial solubility parameters and solvatochromic parameters for predicting the solubility of single and multiple drugs in individual solvents. *J Pharm Sci* 1993b; 82: 635-40.
- Larré C, Popineau Y and Loisel W. Fractionation of gliadins from common wheat by cation exchange FPLC. *J Cereal Chim* 1991; 14: 231-41.
- Ezpeleta I, Irache JM, Stainmesse S, Chabenat C, Gueguen J, Popineau Y, Orecchioni AM. Gliadins nanoparticles for the controlled release of all-trans-retinoic acid. *Int J Pharm* 1996; 131: 191-200.
- Duclairoir C, Nakache E, Marchais H, Orecchioni AM. Formation of gliadin nanoparticles: influence of the solubility parameter of the protein solvent. *Colloid Polym Sci* 1998; 276: 321-7.
- Duclairoir C, Irache JM, Nakache E, Orecchioni AM, Chabenat C and Popineau Y. Gliadin nanoparticles: formation, all trans-retinoic acid entrapment and release, size optimization. *Polym Int* 1999; 79: 327-33.

P4

α -Tocopherol encapsulation and *in vitro* release from wheat gliadin nanoparticles

C. DUCLAIRIOIR[†], A. M. ORECCHIONI^{‡*}, P. DEPRAETERE[§]
and E. NAKACHE[†]

[†] Equipe Polymères-Interfaces, ISMRA, LCMT UMR 6507, 14050 Caen Cedex, France

[‡] Université de Rouen, UFR de Médecine et Pharmacie, 76183 Rouen, France
[§] Laboratoire de Pharmacie Galénique, Bd Becquerel, Hérouville St Clair, 14032 Caen, France

(Received 3 December 2000; accepted 23 February 2001)

α -Tocopherol, or vitamin E (VE), is widely used as a strong antioxidant in many medical and cosmetic applications, but is rapidly degraded, because of its light, heat and oxygen sensitivity. Thus, all of its formulation has to avoid contact with light, heat or air. Drug loaded carriers are an attractive opportunity, especially if they are made for bioacceptable macromolecules such as vegetal proteins. For instance, gliadins, extracted from wheat gluten, generate nanoparticles by a desolvatation method and may interact with epidermal keratin for therapeutic or cosmetic formulations. Their lipophilic drug loading capacities have been investigated. The VE loaded gliadin nanoparticles have been characterized by their size, by their zeta potential, by their VE payload, and by their entrapment efficiency. When VE loaded, the gliadin particle size is ~900 nm and their charge is close to zero. They are suitable VE drug carriers with an optimum encapsulation rate ~100 VE μ g/gliadin mg with an efficiency of more than 77%. The release behaviour of VE loaded nanoparticles may be interpreted as a ‘burst effect’, followed by a diffusion process through an homogeneous sphere.

Keywords: Vitamin E, gliadins, nanoparticles, desolvation method, release.

Introduction

α -Tocopherol (vitamin E) (VE) is known to act as a strong antioxidant or nitrosamine blocker to prevent the build up of cellular peroxides (Idson 1992, Marty and Wepierre 1994). The exposure to free oxygen species induces a rise in lipid peroxidation which may cause injury at different sites of the body. For instance, the action of free radicals produced by a variety of environmental stresses (among them sun exposure) may promote cataratogenesis (Trevithick *et al.* 1992), cardiovascular disease due to the toxicity of lipid peroxides towards endothelial cells of the blood vessels (Kaneko *et al.* 1991), or skin damage such as premature skin ageing (Epstein 1983), skin fragility, and even skin cancers (melanoma or others) (Sober 1987) related to a decrease in cellular immunity of the skin. VE appears to be one of the strongest free radical scavengers by its action as a chain breaking antioxidant in membranes (Tappel 1962), preventing acute or chronic

* To whom correspondence should be addressed

damage (Kligman and Kligman 1986). When applied on the skin, this drug has been found to be active in reducing cell membrane phospholipid peroxidation (Burton and Ingold 1986). Besides these biological activities, VE also exerts cosmetic functions; notably, it helps delay the progression of ageing (Wester and Maibach 1997) and possesses a skin moisturizing power (Mayer *et al.* 1993) and emolliency (Marty 1998, Tamburic *et al.* 1999). VE is naturally present in the skin and can ensure a natural protection against UV light damage (Fuchs *et al.* 1989). Its absorbance spectrum is maximum at 295 nm and extends into the solar spectrum: VE itself may absorb solar UV light and become itself a free radical, the tocopheroxyl radical (Kagan *et al.* 1992). It is well known that reductive antioxidants such as vitamin C can promote the recycling of VE (Kagan *et al.* 1992), but this mechanism depletes other antioxidants enhancing light-induced oxidative damages (Kagan *et al.* 1992). The consequent observation is that VE may act in two opposite manners : as a peroxy radical scavenger and as an endogenous photosensitizer. Nevertheless, in spite of these unwanted drawbacks, VE had been proved effective against malignancies and is widely used as a potent free radical scavenger.

However, VE is degraded by oxygen and must be carefully protected from light, heat and prolonged contact with air for dosage forms. To overcome these inconveniences liposome dosage forms were formulated (Kagan *et al.* 1992, Koga and Terao 1996). Another interesting system for controlled drug release could be nanoparticulate carriers from bioacceptable macromolecules. It is for this reason that vegetal protein fractions have been chosen from wheat gluten, i.e. gliadins. In previous works (Ezpeleta *et al.* 1996), it has been shown the value of using such vegetal materials, particularly because they can incorporate a wide variety of lipophilic substances. Moreover, gliadins possess the ability to interact with epidermal keratin due to their richness in proline (Tegila and Secchi 1994).

Materials and methods

Materials

α -Tocopherol (VE) was obtained from Sigma Chemical Co (St Louis, Mo, USA). Synperonic[®] PEF 68 was furnished by ICI Surfactant (Cleveland, UK). All the aqueous solutions were prepared with ultrapure water (Milli Q Plus, Millipore, Molsheim, France). Solvents and other chemicals were of analytical grade and obtained from Prolabo (Paris, France).

Gliadin extraction and purification

Gliadins were extracted from a common wheat flour (Hardi variety) Larré *et al.* 1991). Briefly, gluten was freeze dried, ground in a refrigerated grinder and defatted by two extractions with dichloromethane (gluten/solvent ratio : 1/10) for 2 h at 20 °C. After filtration and residual solvent evaporation under reduced pressure, samples of dried powder were stored in an ethanol/water mixture (70/30 V/V) for 4 h at 20 °C. The soluble fractions were then dialysed against distilled water and finally freeze dried.

Preparation of VE loaded gliadin nanoparticles

The gliadin nanoparticles were prepared by a desolvation method described elsewhere (Duclairoir *et al.* 1999). The nanoparticle procedure was performed under a flow of nitrogen in the dark, in order to avoid VE degradation. Proteins were solubilized in an ethanol/water mixture (62/38 v/v) at 25 °C, and the resulting solution filtered through a 0.1 µm pore-sized membrane. Various amounts of VE in ethanolic solutions were added to the gliadin solution. Nanoparticle formation occurred when 20 mL of this solution was poured into a 0.9% w/v NaCl/water solution containing Synperonic® PE/F 68 (0.5% v/v) as a stabilizer at 25 °C with stirring (500 rpm). The organic solvent was evaporated under reduced pressure, and the resulting suspension was centrifuged (20 000 rpm, 15 min). The supernatant was removed and, after three washes in ultra pure water, the loaded pellets were freeze dried and stored at 4 °C in the dark.

Physicochemical characterization of the nanoparticles

The yield of gliadin transformed into particles was analysed by measuring the gliadin amount in the supernatant after the first centrifugation. The samples were analysed in a Perkin-Elmer Lambda 8 spectrophotometer at 25 °C at 278 nm.

The size was characterized by a Malvern Mastersizer (Malvern, Worcestershire, UK) and by scanning electron microscopy (Jeol, T330A, Japan).

The surface properties of gliadin nanoparticles, loaded and non-loaded, were analysed by determining their zeta potential in a unimillimolar KNO₃ solution at room temperature. The nanoparticles were observed in very dilute conditions by a Sephy Zetaphorimeter III (Sephy, Limours, France).

VE loading

About 1 mg of gliadin nanoparticles containing different amounts of VE mg/gliadin g was digested in 10 mL of the ethanol/water mixture (62/38 v/v) at 25 °C in the dark. The drug content C_1 was assayed by High Performance Liquid Chromatography-Reverse Phase (HPLC-RP) at room temperature using a photo-diode array detector (Waters 600, Millenium³² software, Waters, Milford, USA) at 295 nm and a 250 × 3 mm Nucleosil® 100-5, packed with C_{18} column (Macherey Nagel, Düren, Germany).

Non-encapsulated VE remaining in the supernatant after the first centrifugation C_2 was measured by HPLC. From these data, the drug loading (payload) was calculated as the ratio of amount of entrapped drug in nanoparticles (mg) C_1 /gliadin nanoparticles yield (mg), i.e.:

$$\text{Payload}(\%) = \frac{C_1(\text{mg})}{\text{gliadin nanoparticles yield}} * 100 \quad (1)$$

and the entrapment efficiency was calculated as the ratio between the VE amount in particles and the initial drug content ($C_1 + C_2$), i.e.:

$$\text{Entrapment efficiency} = \frac{C_1[\text{amount of VE in nanoparticles (mg)}]}{(C_1 + C_2) [\text{initial drug content (mg)}]} * 100 \quad (2)$$

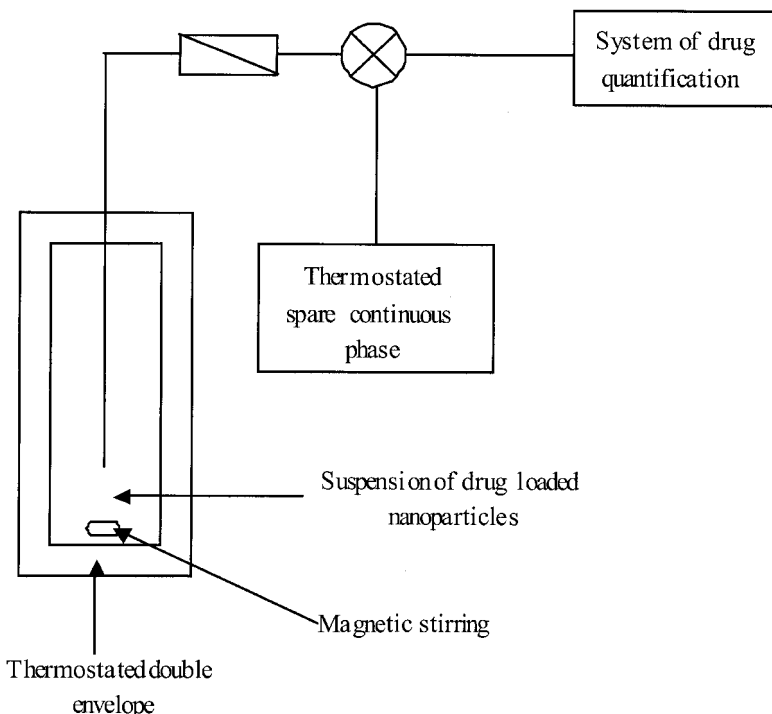


Figure 1. Homemade release cell.

In vitro drug release

About 1 mg of gliadin nanoparticles containing 102.7 VE mg/gliadin mg were suspended in 10 mL of decane under stirring, under nitrogen and in the dark, in order to prevent drug loss. The medium was then maintained at 25 °C in a homemade release cell, represented in figure 1.

This original cell is a double shell leading to efficient thermostating and an access allowing easy collecting of aliquots (100 µL) free of nanoparticles by filtration by a 0.1 µm pore sized membrane. After each sample collection at successive time intervals, an equal amount of decane was introduced into the medium. Thus, during the whole release, the nanoparticle concentration remained unchanged. The amount of released drug was evaluated by HPLC, as previously described.

Results

Gliadin nanoparticle characterization

Gliadins, wheat gluten proteins, precipitate into nanoparticles by the desolvation method known as 'nanoprecipitation' (Fessi *et al.* 1986, Stainmesse *et al.* 1995, Alonso 1996), coacervation, solvent displacement or drawing-out phenomenon (Mersmann 1994). At least 90% of gliadins were transformed into nanoparticles.

These particles, loaded or non-loaded, are spherical, as shown in figure 2 by scanning electron microscopy. The mean diameter of VE nanoparticles is 900 nm by laser granulometry. The zeta potential of loaded and non-loaded nanoparticles is essentially zero.

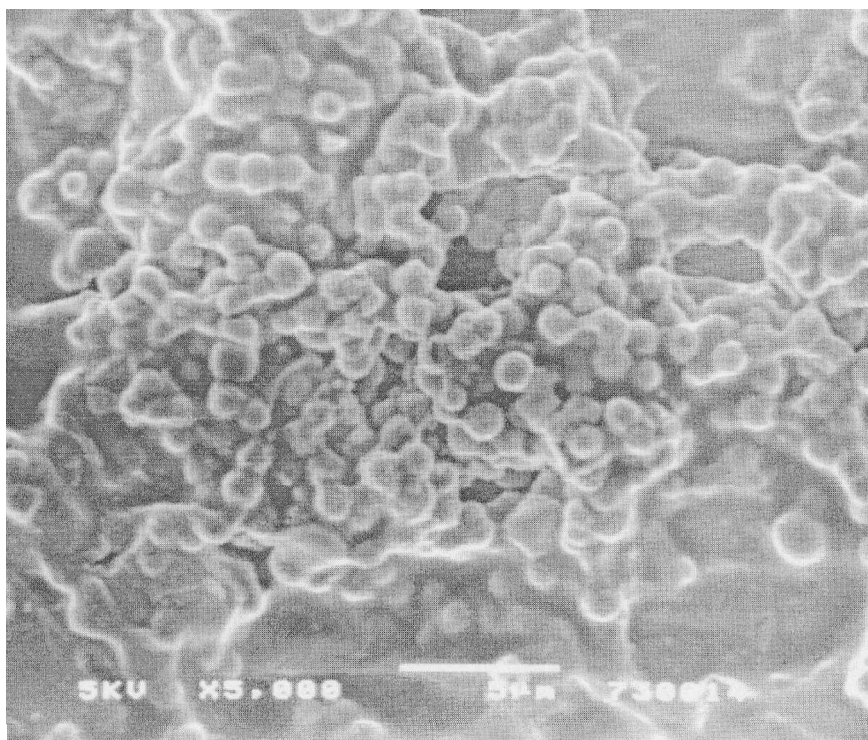


Figure 2. Freeze dried VE loaded gliadin nanoparticles by SEM.

VE encapsulation study

Payload and entrapment efficiency are dependent on the drug/initial protein ratio. The payload encapsulated (drug/initial drug amount) increases from 0 to 40% and the efficiency of encapsulation (drug/initial drug content) decreases from 65 to 100%. Figure 3 represents the payload and the efficiency versus the ratio VE/gliadins amount. The best compromise of these two parameters is obtained for 972 VE μg /gliadin mg, with an efficiency of 79.2%. (figure 3).

VE in vitro release study

Gliadin nanoparticles were tested for *in vitro* release for 100 h at 25 °C under nitrogen in the dark. During the experimental period, no VE or particle degradation was observed. Figure 4 shows the plot of the amount of VE released from the carrier as a function of time. It can be observed that VE is released in a biphasic way, characterized by an initial rapid release (under 1 h) which can be attributed to the release of the encapsulated or adsorbed drug in the superficial external zone of the spheres.

The second releasing period shows a dependency on time and is related to the drug diffusivity inside the matrix system, the surface area and, of course, the drug content.

During the first period, both VE and surfactant (Synperonic® PE/F68) are released in the medium because of their weak affinity for the gliadins. As soon as the nanoparticles are suspended in decane, both VE and Synperonic® PE/F68 are

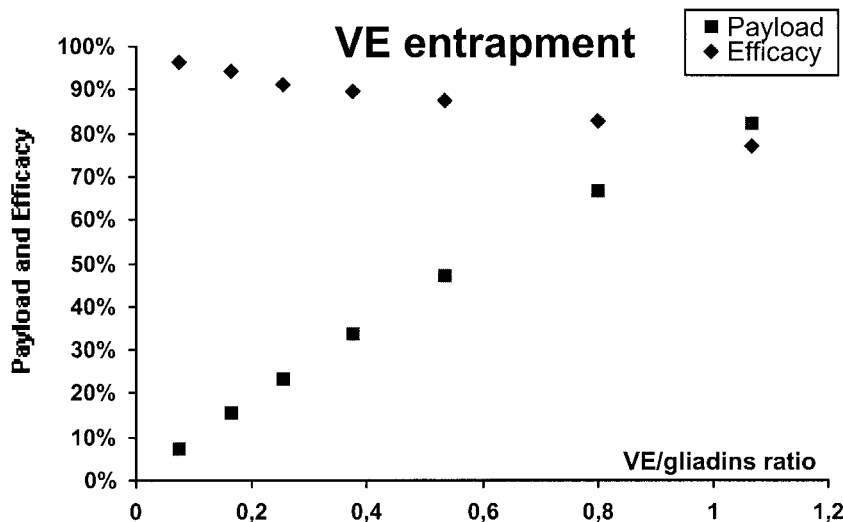


Figure 3. Payload and entrapment efficiency of VE in gliadin nanoparticles.

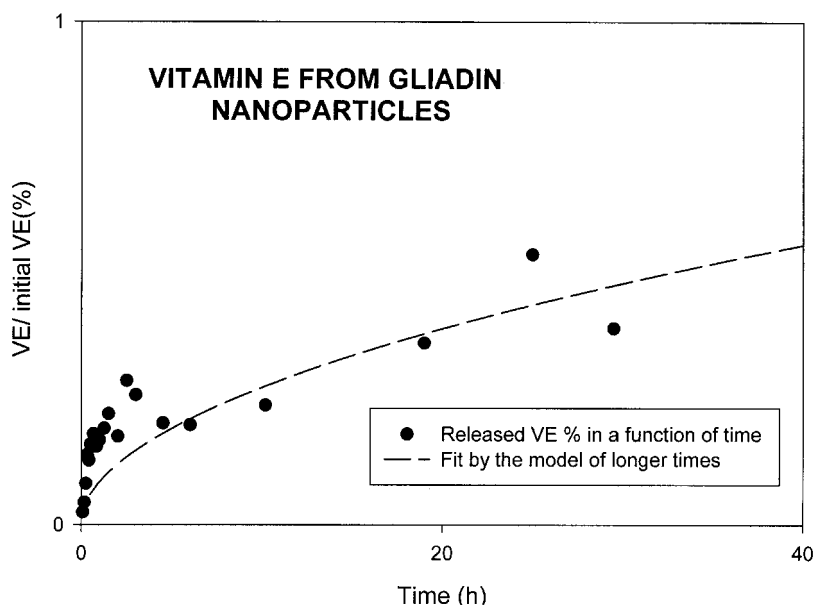


Figure 4. VE release in decane from 102.7 VE $\mu\text{g}/\text{protein mg}$ loaded nanoparticles at 25°C.

released. The surfactant concentration may be high in the vicinity of nanoparticles, and micelles may form. These micelles are able then to subsidize a part of the released VE, playing the role of drug-reservoirs. This should explain the fall in VE concentration observed.

During the second part, both VE and surfactant continue to be released into the medium.

In order to explain this release profile, some analytical models have been applied (Washington 1996). The particles are spherical and, assuming that the

drug is uniformly distributed inside the carrier and that these latter remained undegraded during the experimental period, then if M_t is the amount of released drug at t time, and $(1 - M_t/M_0)$ the released amount, the following relation can be written:

$$\frac{M_t}{M_0} = 1 - \frac{6}{\pi^2} \sum_{n=1}^{\alpha} \left[\frac{1}{n^2} \exp(-n^2 \pi^2 \tau) \right] \quad (3)$$

where τ is given by the relation:

$$\tau = \frac{Dt}{R^2} \quad (4)$$

with D the diffusion coefficient of the drug in the particle and R the particle radius.

This relation can be simplified for the first release period:

$$\frac{M_t}{M_0} = 6 \sqrt{\frac{\tau}{\pi}} \quad (5)$$

For the second period, this relation becomes, for longer release times:

$$\frac{M_t}{M_0} = 6 \sqrt{\frac{\tau}{\pi}} - 3\tau \quad (6)$$

The release has been fitted to this model for the first release period and for longer times. The values of the correlation coefficient, r^2 , are 0.73 and 0.90. Obviously, the model for the first release does not describe the experimental data. This underestimates the fast release of adsorbed drug on the particle surface and in the region close to it, usually called the ‘burst effect’.

In conclusion, by the desolvation method, gliadin nanoparticles are obtained with a mean diameter of 900 nm and essentially uncharged. These gliadin nanoparticles are suitable vitamin E drug release carriers, with an optimum payload of 972 drug $\mu\text{g}/\text{protein mg}$ with an entrapment efficiency of at least 77% of vitamin E. Their *in vitro* release consists of two periods: a ‘burst effect’ and a slower diffusion process.

Acknowledgements

The authors thank the ‘Réseau Matériaux, Polymères, Plasturgie’ of Basse Normandie (France) for financial support.

References

- ALONSO, M. J., 1996, Nanoparticle drug carrier technology. *Drug and Pharmaceutical Science*, **77**, 203–242.
- BURTON, G. W., and INGOLD, K. U., 1986, Vitamin E. Application of the principles of physical organic-chemistry to the exploration of its structure and function. *Accounts of Chemical Research*, **19**, 194–201.
- DUCLAIRIOU, C., IRACHE, J. M., NAKACHE, E., ORECCHIONI, A. M., CHABENAT, C., and POPINEAU, Y., 1999, Gliadin nanoparticles: formation, all-trans-retinoic acid entrapment and release, size optimization. *Polymer International*, **79**, 327–333.
- EPSTEIN, J. H., 1983, Photocarcinogenesis, skincancer and aging. *Journal of the American Academy of Dermatology*, **9**, 487–502.

- EZPELATA, I., IRACHE, J. M., STAINMESSE, S., CHABENAT, C., GUEGUEN, J., POPINEAU, Y., and ORECCHIONI, A. M., 1996, Gliadin nanoparticles for the controlled release of all-trans-retinoic acid. *International Journal of Pharmaceutics*, **131**, 191–200.
- FESSI, H., DEVISSAGUET, J. P., and PUISIEUX, F., 1986, Procédés de préparation de systèmes colloïdaux sous forme de nanoparticules. *Fr. Patent Application*, **8**, 618–446.
- FUCHS, J., HUFLEJT, M. E., ROTHFUSS, L. M., WILSON, D. S., GARCAMO, G., and PACKER, L., 1989, Acute effect of near ultraviolet and visible light on the cutaneous antioxidant defense system. *Photochemistry and Photobiology*, **50**, 739–744.
- IDSON, B., 1992, Dry skin moisturizing and emolliency. *Cosmetics and Toiletries*, **107**, 69–78.
- KAGAN, V., WITT, E., GOLDMAN, R., SCITA, G., and PACKER, L., 1992, Ultraviolet light induced generation of vitamin E radicals and their recycling. A possible photosensitizing effect of vitamin E in the skin. *Free Radical Research Communications*, **16**, 51–54.
- KANEKO, T., NAKANO, S., and MATSUMOTO, M., 1991, Protective effects of vitamin E on linoleic acid hydroperoxide induced injury to human endothelial cells. *Lipids*, **26**, 345–348.
- KLIGMAN, L. H., and KLIGMAN, A. M., 1986, Photoaging in dermatology. *Photodermatology*, **3**, 215–227.
- KOGA, T., and TERAO, J., 1996, Antioxidant behaviours of vitamin E analogues in unilamellar vesicles. *Bioscience Biotechnology Biochemistry*, **60**, 1043–1045.
- LARRÉ, C., POPINEAU, Y., and LOISEL, W., 1991, Fractionation of gliadins from common wheat by cation exchange FPLC. *Journal of Cereal Chemistry*, **14**, 231–241.
- MARTY, J. P., 1998, Vitamins and skin aging. In *Intensive course in Dermato-cosmetic sciences* (Brussels: Vrije Universiteit Brussel), pp. 115–140.
- MARTY, J. P., and WEPIERRE, J., 1994, Percutaneous absorption of cosmetics: implication in safety and efficacy. In *Cosmetic Dermatology*, edited by R. Baran and H. I. Maibach (London: Martin Dunitz Ltd).
- MAYER, P., PITTERMANN, W., and WALLAT, S., 1993, The effects of Vitamin E on the skin. *Cosmetics and Toiletries*, **108**, 99–109.
- MERSMANN, A., 1994, *Crystallization Technology Handbook* (New York: Marcel Dekker Inc.).
- SOBER, A. J., 1987, Solar exposure in the etiology of cutaneous melanoma. *Photodermatology*, **4**, 23–31.
- STAINMESSE, S., ORECCHIONI, A.-M., NAKACHE, E., PUISIEUX, F., and FESSI, H., 1995, Formation and stabilization of a biodegradable polymeric colloidal suspension of nanoparticles. *Colloid Polymer Science*, **273**, 505–511.
- TAMBURIC, S., ABAMA, G., and RYAN, J., 1999, Moisturizing potential of D- α -Tocopherol. *Cosmetics and Toiletries*, **114**, 73–82.
- TAPPEL, A. L., 1962, Vitamin E as the biological lipid antioxidant. *Vitamins and Hormones*, **20**, 493–510.
- TEGLIA, A., and SECCHI, G., 1994, New protein ingredients for skin detergency: relative wheat protein-surfactant complexes. *International Journal of Cosmetic Science*, **16**, 235–246.
- TREVITHICK, J. R., XIONG, H., LEE, S., SHUM, D. T., SANFORD, S. E., KARLICK, S. J., NORLEY, C., and DILWORTH, G. R., 1992, Topical tocopherol acetate reduces post UVB sunburn-associated erythema, edema and skin sensibility in hairless mice. *Archives of Biochemistry and Biophysics*, **296**, 575–582.
- WASHINGTON, C., 1996, Drug release from microparticulate systems. In *Microencapsulation: Methods and Industrial Applications*, edited by S. Benita (New York: Marcel Dekker, Inc.), pp. 155–181.
- WESTER, R. C., and MAIBACH, H. I., 1997, Absorption of tocopherol into and through human skin. *Cosmetics and Toiletries*, **112**, 53–57.

P5

This article was downloaded by: [Dicle University]

On: 16 November 2014, At: 14:38

Publisher: Taylor & Francis

Informa Ltd Registered in England and Wales Registered Number: 1072954

Registered office: Mortimer House, 37-41 Mortimer Street, London W1T 3JH,
UK



International Journal of Polymer Analysis and Characterization

Publication details, including instructions for
authors and subscription information:

<http://www.tandfonline.com/loi/gpac20>

Polymer Nanoparticle Characterization in Aqueous Suspensions

Cécile Duclairoir ^a & Evelyne Nakache ^a

^a Equipe Polyme'res-Interfaces , ISMRA , Caen Cedex,
France

Published online: 27 Oct 2010.

To cite this article: Cécile Duclairoir & Evelyne Nakache (2002) Polymer Nanoparticle Characterization in Aqueous Suspensions, International Journal of Polymer Analysis and Characterization, 7:4, 284-313, DOI: [10.1080/10236660213159](https://doi.org/10.1080/10236660213159)

To link to this article: <http://dx.doi.org/10.1080/10236660213159>

PLEASE SCROLL DOWN FOR ARTICLE

Taylor & Francis makes every effort to ensure the accuracy of all the information (the "Content") contained in the publications on our platform. However, Taylor & Francis, our agents, and our licensors make no representations or warranties whatsoever as to the accuracy, completeness, or suitability for any purpose of the Content. Any opinions and views expressed in this publication are the opinions and views of the authors, and are not the views of or endorsed by Taylor & Francis. The accuracy of the Content should not be relied upon and should be independently verified with primary sources of information. Taylor and Francis shall not be liable for any losses, actions, claims, proceedings, demands, costs, expenses, damages, and other liabilities whatsoever or howsoever caused arising directly or indirectly in connection with, in relation to or arising out of the use of the Content.

This article may be used for research, teaching, and private study purposes. Any substantial or systematic reproduction, redistribution, reselling, loan, sub-licensing, systematic supply, or distribution in any form to anyone is expressly forbidden. Terms & Conditions of access and use can be found at <http://www.tandfonline.com/page/terms-and-conditions>



Polymer Nanoparticle Characterization in Aqueous Suspensions

Cécile Duclairoir and Evelyne Nakache

Equipe Polymères-Interfaces, ISMRA, Caen Cedex,
France

This article evaluates several techniques for measuring nanoparticle size in suspension. The direct techniques measure the nanoparticle size by electron microscopy. However, with this technique, the particles must be observed dry, except in the case of environmental microscopy, and their distribution is calculated by performing image analysis. Other indirect methods, based on measurements of intensity fluctuations allow size measurement but these methods are dependent on sample preparation (concentration, polydispersity, etc.). Two types of materials are characterized and discussed herein: model polystyrene latex particles used for size standardization in several devices and polydisperse wheat protein nanoparticles prepared in our laboratory. Our results show that no size characterization method is totally universal and absolute. Coupling at least two different methods allows for more rigorous size characterization.

Keywords: Size characterization techniques; Nanoparticles; Suspension; Polydispersity; Multimodal

Received 12 July 2000; accepted 15 February 2001.

Financial support of Matériaux-Polymères-Plasturgie Network of Normandie, France, is acknowledged. The authors are gratefully indebted for fruitful discussions and technical help to Dr. D. Renard, INRA of Nantes LPCM, LS and Laser Granulometry; Dr. P. Depraetere and M. Massard ERA Zétamétrie of Caen University; M. Vizcaïno, Sté Séphy (DLS device); and Dr. F. Osterstock, LERMAT ISMRA (SEM).

Address correspondence to Dr. Cécile Duclairoir, Laboratoire de Microbiologie du Froid, IUT d'Evreux, 55 rue Saint Germain, Evreux, 27000, France. E-mail: cecile.duclairoir@univ-rouen.fr

Nowadays, polymer colloids are of great interest in many fields: drug vectorization, agrochemistry, varnishes, paints, inks, and so on. Their industrial use is related to their efficiency, which is a function of several parameters: their particle size, surface properties, loading capacity, and release capacity. In pharmaceutical applications, for instance, sub-micronic vectors such as drug loaded polymer nanoparticles have to reach the extremity of the smallest blood capillaries, whose diameter is about 4 µm. Their small sizes are therefore obviously of great importance.

Numerous techniques have been used to characterize colloids, but their applications may be limited by theoretical considerations or by experimental limitations. The purpose of this article is, first, to review some size characterization techniques used to characterize nano- or microparticles. Some techniques (light scattering, laser granulometry, electron microscopy) will be described extensively. This presentation will also discuss, in a less systematic way, the applications of the Coulter counter, ultrasonic or confocal microscopy, and sedimentation techniques. Second, we will illustrate some of these techniques by analyzing data on very dilute suspension of standard latexes and plant protein nanoparticles^[1], studied in our laboratory. Both theoretical background and practical applications will be discussed here. Usually nanoparticles are formed from synthetic polymers, but they may also be formed from animal proteins. The nanoparticles studied herein are biocompatible, biodegradable, and, contrarily to animal proteins, they are free from prions.

The sample polydispersity is also a very important parameter, but it can be hard to estimate. We will discuss here how to overcome this difficulty.

REVIEW OF NANOPARTICLES SIZE CHARACTERIZATION TECHNIQUES IN AQUEOUS SUSPENSIONS

Methods for measuring nanoparticle size may be divided into two categories: nondestructive methods and destructive methods. These methods may also be categorized according to practical advantages and disadvantages, such as limitations on size range, etc.

Nondestructive Methods

The nondestructive techniques allow the study of particles in an aqueous medium, which may or may not be diluted. For easy size characterization, the sample must be either monomodal (a unique size distribution) or multimodal (several size classes) with a limited polydispersity (narrow size distribution).

Light Scattering

Light scattering (LS) requires the use of highly diluted samples in order to avoid multiple scattering. The particles in suspension are subjected to Brownian motion and scatter^[2] the monochromatic incident light (wavelength λ) in the diffusion volume shown in Figure 1^[3]. In order to avoid particle interactions, the sample has to be highly diluted with the continuous phase of the suspension. In such an ideal case without any particle interactions, the intensity fluctuations are collected by a photo-detector. The data may be treated in two ways:

- Data averaged over a period of time: so-called dynamic light scattering (SLS)
- Time dependent acquisition: so-called dynamic light scattering (DLS) and then fitted by theoretical models

When a size determination is carried out by LS, it can be difficult to choose the best algorithm to use for the interpretation of the data. These algorithms will be discussed in the sample studies section. Nowadays, any LS apparatus gives a size evaluation, but care must be taken to assure proper data interpretation. Rayleigh^[4], considering time-averaged scattering of isolated spherical scatterers, treated the simplest case. Rayleigh scattering only applies to particles smaller than $\lambda/20$ ^[5]. When particles are larger than about $\lambda/20$, the method commonly called SLS gives the radius of gyration, the molecular weight and the second virial coefficient

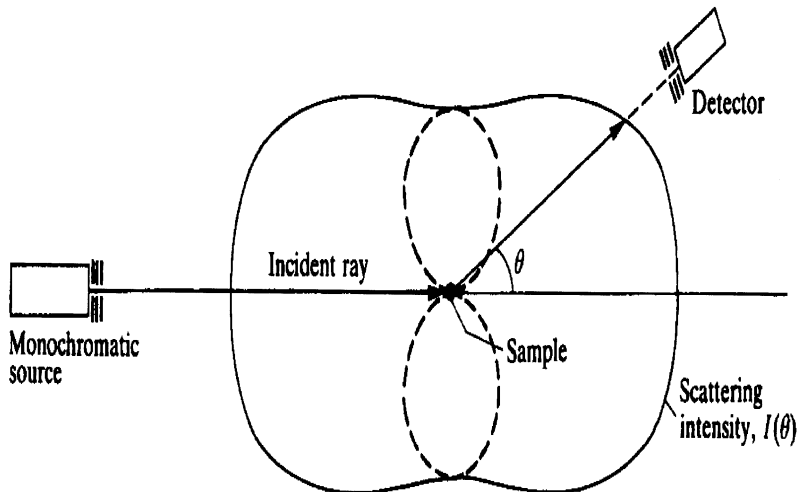


FIGURE 1 Light scattering device (courtesy of Oxford University Press^[3]).

of the polymer. By a more complex approach, Rayleigh–Gans–Debye theory^[6, 7], investigates particles in interaction in a diluted medium. Sizes up to $\lambda/2$ can be measured. The usual incident light is a red or green laser (λ is less than 640 nm), so the biggest observed size is about 300 nm^[5].

DLS is a broadly applied size characterization technique, also known as photon correlation spectroscopy (PCS) or quasi-elastic light scattering (QELS). By this technique, the intensity fluctuations are fitted, with the help of a correlator, by an autocorrelation function G_1 as a function of time (Eq. 1).

$$G_1(t) = \exp(-Dq^2t) \quad (1)$$

with D the translational diffusion coefficient, n solvent refractive index, and λ the wavelength of the incident beam. The wave vector q is given by

$$q = \frac{4\pi n}{\lambda} \sin\left(\frac{\theta}{2}\right) \quad (2)$$

with θ the observation scattering angle and n the refractive index of the medium. Different algorithms or theoretical models can be used for data treatment and by Stokes law and Einstein's equation of Brownian motion, they can yield the diffusion coefficient D and, consequently, the hydrodynamic radius R_h (radius of sphere having the same diffusion coefficient as the polymer) as given in Equation 3.

$$R_h = \frac{kT}{6\pi\eta D} \quad (3)$$

with k the Boltzman constant, T the absolute temperature, and η the sample viscosity. No calibration is needed, and the measured value is absolute. For spherical particles smaller than $\lambda/2$, a single measurement at 90° is sufficient, although for polydisperse materials angular dependence on the measured D values may be observed.

In the two LS methods, plots of the particle diameter versus the size distribution are generated as shown later in the sample studies. These two approaches do not take into account the angular dependency of the intensity fluctuations, even if they are accumulated at different angles between 30° and 150°. For larger particles, which are bigger than λ , the intensity fluctuations depend dramatically on the observation angle. The Mie theory^[8], based on refractive index fluctuations, covers up this angular dependence and gives the closest size classes to the real size distribution. The two LS approaches diverge from each other for particle size greater than 350 nm (i.e., $\lambda/2$) and the differences increase dramatically. For instance, for a same relative scattering intensity at 90°, the displacement could reach more than 100 nm for submicronic particles.

The Mie theory allows the observation of particles of, at least, a few micrometers.

The DLS drawbacks are as follows:

- Several angle acquisitions are necessary, except for spherical particles. In that case, acquisition at a single angle of 90° is enough.
- The preparative conditions must avoid any pollutant such as oil on the glassware or ambient dust during experiments and even before. The glassware has to be cleaned carefully with sulfochromide or surfactant mixtures and solvents have to be filtered.
- The sample has to be very diluted, which may provoke a dilution shock. A slightly blue coloration appears for very diluted suspensions of particles smaller than the light wavelength.
- Numerous algorithms are necessary to interpret light fluctuations and to discriminate their various meanings.
- The proportions of the different size classes are related to peak areas, and, due to theoretical assumptions, they could diverge from reality.

Laser Granulometry

Laser granulometry is based on light diffraction by a beam whose λ is smaller than the particle size. The particle refractive index must be different from that of the aqueous medium. A concentric annular detector at small angles collects the diffracted light. The difference between the refractive indexes of the particles and the medium leads to the particle size. The study of the intensity fluctuations allows measurements of the size distribution, $X(d)$, as given by Eq. (4) with the help of Mie theory^[8].

$$X(d) = N \sum_{n=1}^{\infty} [(2n+1)/(n(n+1))] \{a_n \pi_n(\cos \theta) + b_n \tau_n(\cos \theta)\} \times (-1)^{n+1} \quad (4)$$

where π_n and τ_n are related to Legendre polynomials as given in Eqs. (5a) and (5b)

$$\pi_n(\cos \theta) = P_n^{(1)}(\cos \theta)/\sin \theta \quad (5a)$$

and

$$\tau_n(\cos \theta) = \frac{d}{d\theta} (P_n^{(1)}(\cos \theta)) \quad (5b)$$

and a_n and b_n are dependent on the particle size, d , and on the relative refractive index of the particles to their medium, m , as shown in Eqs. (6a) and (6b).

$$a_n = \{\Psi_n(\alpha)\Psi_n(\beta) - m\Psi_n(\beta)\Psi_n(\alpha)\}/\{\zeta_n(\alpha)\zeta_n(\beta) - m\zeta_n(\beta)\zeta_n(\alpha)\} \quad (6a)$$

$$b_n = \{m\Psi_n(\alpha)\Psi_n(\beta) - \Psi_n(\beta)\Psi_n(\alpha)\}/\{m\zeta_n(\alpha)\zeta_n(\beta) - \zeta_n(\beta)\zeta_n(\alpha)\} \quad (6b)$$

with $\alpha = 2\pi d/\lambda$ and $\beta = m\alpha$ and Ψ Riccati-Bessel functions and ζ Hankel functions.

A lens with a focal length of 45 μm situated between the incident beam and the sample cell, as shown on Figure 2, allows the observation of particles between 0.1 and 80 μm and a lens with a focal length of 100 μm positioned after the sample cell and before the detector, as represented in Figure 3, characterizes sizes from 0.5 to 170 μm . Thus different optical systems allow the measurement of different size ranges.

Laser granulometry requires some caution during sample preparation:

- Elimination of dust (glassware cleaning, filtered solvents, etc.)
- Use of the ideal sample concentration, which is often a balance between a limited sample quantity and systematic dilution. This dilution may disturb particle stability. Usually, prior to the measure, a concentration test is done by the estimation of an obscuration factor of the suspension.
- Prevention of possible gas bubbles during the stirring or ultrasonication of the sample

Reverse Fourier Optics

Focal length = 45mm

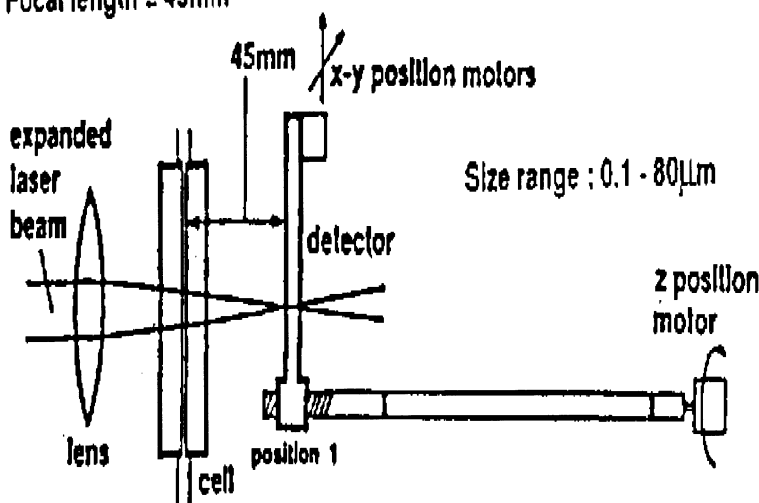


FIGURE 2 Laser granulometry device: 45 mm lens focal (courtesy of Malvern Instrument Limited).

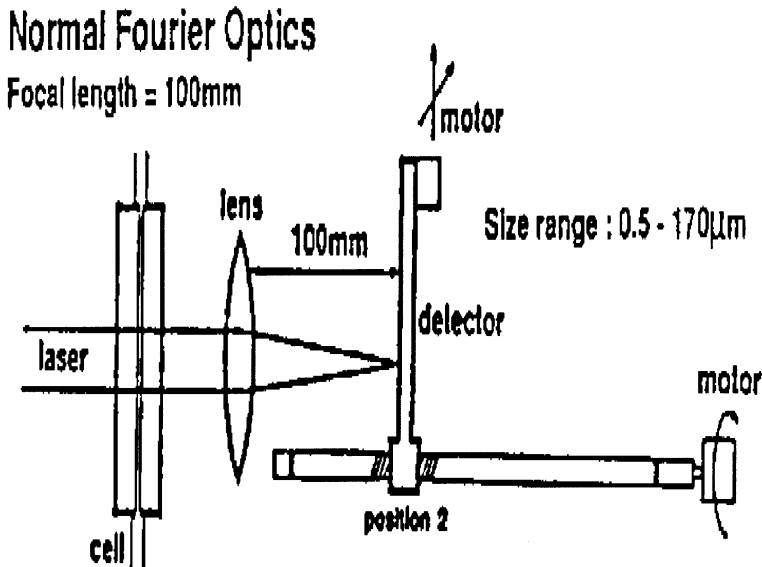


FIGURE 3 Laser granulometry device: 100 mm focal lens (courtesy of Malvern Instrument Limited).

The resulting plot is similar to the plot generated in DLS: size distribution vs. volume-average diameters.

Coulter Counter

Largely used by the paint and pharmaceutical industries, this method is an electronic size measuring technique. It is based on the Coulter principle^[9] of allowing the dispersion to flow through a narrow aperture, where particles cause a change in the conductivity of the medium (see Figure 4). This conductivity variation, R , is a function of particle diameter, d , and its volume, V , as shown in Eq. (7).

$$R = \frac{\frac{r_e V}{A^2} \left(1 - \frac{r_e}{r_p}\right)}{1 - \left(1 - \frac{r_e}{r_p}\right) \frac{d}{A}} \quad (7)$$

with A the aperture section, r_e the electrolyte resistivity, r_p particle resistivity. This method is not very sensitive to submicron sized particles. This instrument was one of the first particle size instruments on the market and it is simple and quick to use.

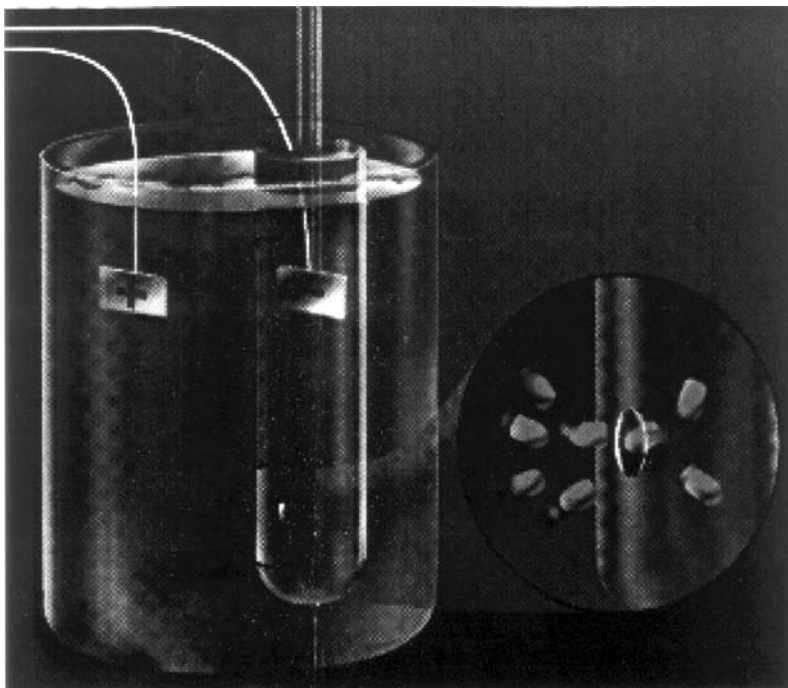


FIGURE 4 Scheme of Coulter counter apparatus (courtesy of Micromeritics).

The drawbacks are encountered in the following:

- The sample preparation must be without pollutant (i.e., oil on the glassware or ambient dust).
- The difference in the conductivity between particles and the medium has to be significant. The ideal case consists of a conducting medium with a nonconducting particle.

Ultrasonic Spectroscopy

Since the beginning of the 1990s, vesicle and polymer particle diameters have been measured by ultrasonic velocity^[10]. In the emulsion domain, this technique is very common and facilitates size investigation from 10 nm to 1,000 µm. For high frequencies (i.e., study of large particles), the ultrasound can be destructive, so this method should be used with caution. This is especially the case for fragile objects such as vesicles or emulsions.

The main advantage of this technique is its application to concentrated particle suspensions. Caution has to be observed in preparing samples without gas bubbles, which may disturb ultrasonic wave displacement.

Confocal Microscopy

Confocal fluorescent microscopy^[11] involves the study of labeled core particles. It can be easily achieved with the help of fluorescent markers for polymerized particles. In confocal microscopy, all objects out of focus are suppressed from image formation. The minimum measured size is 200 nm. Three-dimensional representations can be built up from two-dimensional image analyses.

By such microscopy, very small quantities, even of polydisperse samples, can be observed. This technique also generates very high quality reflected images in brightfield. The disadvantages are necessary fluorescent core and matching solvent in order to reduce light scattering.

Environmental Microscopy

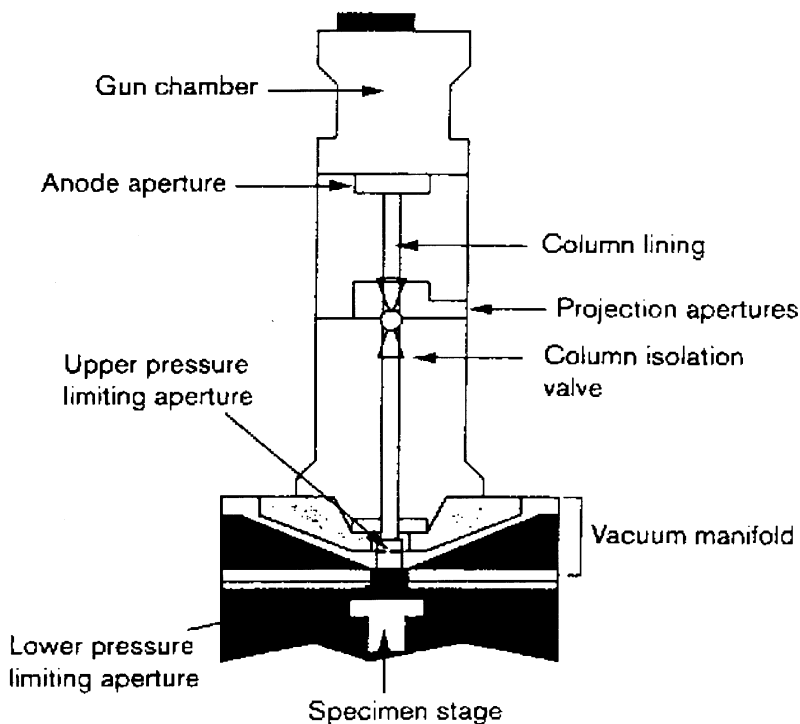
This most recent technique is based on scanning electron microscopy, but the aqueous environment of the particles is preserved (no need to dry sample). Performing measurements involves exposing a drop of the solution sample to an electron beam with a pressure gradient in the specimen chamber, as shown in Figure 5^[12]. This allows a sufficient sample hydration instead of the high vacuum required in traditional electronical microscopies. Following irradiation, the sample emits secondary electrons collected by a detector, as shown in Figure 6. Their topography is observed in the sample micrograph. Recent work has shown that by minimizing the electron beam path through the vapor and by working at the lowest acceptable pressure, remote electron scattering and artifact X-ray production can be reduced to an acceptable level^[13]. This technique is suitable for characterizing polydisperse sample.

Sedimentation

The theory and practice of free sedimentation are ruled by the well-known Stokes law. Free sedimentation means that a particle sediments in a manner independent of the neighboring particles^[5]. The heavier the particle is, the shorter the sedimentation time is.

Traditional sedimentation. Gravity-induced sedimentation is too slow with submicronic objects. In fact, Brownian motion for such particles is very important and disturbs the sedimentation kinetics. As a consequence, centrifugation and ultracentrifugation are employed.

Centrifugation and ultracentrifugation. These methods separate particles into size classes by sedimentation resulting from the earth's gravity



Pressure range		Pressure zone
10^{-7} torr	□	Gun chamber
10^{-6} torr	□	Upper column
10^{-4} torr	□	EC2
10^{-1} torr	■	EC1
10 torr	■	Specimen

FIGURE 5 Environmental scanning, electronical microscopy apparatus (courtesy of Elsevier Science Editors^[12]).

and centrifugal acceleration. An optical system is generally used to detect the displacement of the sedimentation front. The centrifugal speed is less than 10,000 rpm for centrifugation. The minimum particle size is 250 nm^[9]. With ultracentrifugation, for inorganic particles, the accessible size can be as small as a few nanometers^[14].

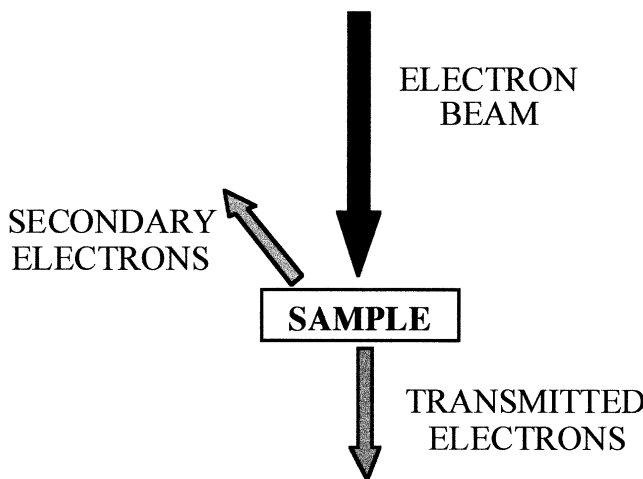


FIGURE 6 Sample submitting to an electronic beam.

The drawbacks are as follows:

- Nonspherical particles require a more complex treatment.
- Hard particles are required because of strength of the centrifugal field, which may deform soft particles.
- Finding an adequate optical system, particularly in the case of turbid suspensions.
- Several dilutions may be necessary in order to avoid particle interactions. Optimal concentration up to 1% (v/v) is usually obtained^[9].

1. Destructive Methods

With destructive methods the particles are removed from the aqueous environment.

Electron Microscopy

Electron microscopy^[15] is a common name for several techniques where the sample is submitted to an electron beam of modulated power. In the observation chamber the pressure conditions are strictly controlled, and most measurements are performed under vacuum. A scanning electron microscopy (SEM) micrograph is a topography of the intensity of the secondary electrons. For transmission electron microscopy (TEM), the intensity of the transmitted electrons is collected (see Figure 6). The size range and resolution of these techniques are

dependent on the beam power. For example, 20 kV is enough to observe submicronic particles with a resolution of 50 nm. The sample preparation is specific to each technique. By these methods, an image of the particles themselves is obtained. A mean size characterization requires an image analysis, which must be more elaborate if the sample is polydisperse. In the latter case, the mean diameter is normally calculated as a number-averaged diameter. One has to be aware that the electron beam can fuse particles, such as polymer gels.

Scanning Electron Microscopy (SEM)

The “dried” sample is submitted to an electron beam and the topography of secondary electron intensity leads to particle size evaluation. The smallest observed particles are about 200 nm. The preparation method of the “dried” sample leads to the distinction between classical and cryofracture methods.

In the classical case, the aqueous sample is placed on a sample-support and evaporated under vacuum before covering it with colloidal metal. In cryofracture SEC, the aqueous sample is frozen by immersion in liquid nitrogen prior to fracturing. It is then submitting to a gentle cleaning of the fracture plane surface. The ice quality is of great importance; it has to be amorphous to form the best replica of the surface.

Platinum, then carbon are deposited in order to obtain a rigid and SEM observable replica.

Cryofracture TEM

Several preparation methods may be employed depending on the nature of the sample.

- Small drops of the sample are projected onto a cryogenically cooled metal surface and mechanically fractured afterward. A replica is formed by metal vapor deposition and then submitted to the electron beam.
- A thin layer of the sample is frozen and then submitted to the electron beam. The transmitted electrons are collected to evaluate their intensity topography. The sample is frozen so rapidly that amorphous and transparent ice is formed.

Scanning Tunneling Microscopy (STM) and Atomic Force Microscopy (AFM)

The “hydrated” and slightly conductive sample, where the solvent is not completely evaporated, can be studied with the help of a sharp metal tip bound to a piezoelectric crystal.

For STM^[15], the sample surface has to be conducting or metallized. A voltage increase of the piezocrystal moves the tip to a distance where a tunneling current is detected. For AFM^[15], the tip scans over the surface

and its deflections are detected by a laser system on its backside. The size resolution is less than one nanometer. The main disadvantage is that the tip cannot scan convex topology. In this case, tapping (push and pull STM) may be used, which allows measurements of diameters.

Let us now give some examples of experimental measurements in order to illustrate some of these techniques and how to choose the appropriate one.

STUDY OF AN IDEAL SAMPLE: LATEXES

The first example is a standard sample of calibrated polystyrene nanoparticles, provided by Interfacial Dynamics Corp. (Portland, Oregon, USA). The number-average diameter was given as 310 (± 10) nm (based upon TEM). This ideal suspension was characterized by three techniques: DLS, laser granulometry, and SEM.

DLS Study

The complete DLS study was performed on a SEMATech photogoniometer (Nice, France) with the help of a Malvern 7032CN correlator (Malvern, Worcestershire, UK). The Malvern software PCS 1.32 was used to analyze the data. As stated earlier, the sample preparation has to be done with caution (no dust, contaminants, or multiple scattering).

For each sample, at least five acquisitions of ten sub-runs were made. The software for each subacquisition checks off the measurement quality for each mathematical treatment (monomodal-cumulants, Contin described later). The intensity ratio suspension/solvent has to be more than ten. In our case, it is fifty times larger.

The correlator gives results that are highly dependent on the chosen algorithm (i.e., a mathematical model) and the different theoretical approaches: monomodal-cumulants, Contin, non-negatively constrained least squared (NNLS), inverse Laplace transformation (ILT), and so on. Several such methods are described in the literature, especially in an exhaustive review by Stepanek^[16]. Here, monomodal-cumulants and Contin treatments are presented, since they are the most used routine algorithms.

Each algorithm induces some assumptions about the sample composition and its polydispersity. The monomodal algorithm assumes nothing about the distribution. It consists in fitting a polynomial to the log of the normalized correlation function. Contin mode, developed by the Provencher team^[17], analyses the correlation through an inverse transformation. Its consists in adding a constraint—the regulariser—to an ordinary least-squares criteria for achieving the best fit. This mode is convenient for several populations. An automatic mode exists, which is a

combination of monomodal and Contin mode with a priority to the monomodal.

In Table I various averaged diameters obtained by different analysis are compiled.

Three average diameters can be obtained:

- Intensity-average, d_I , (also called z-average diameter) calculated by

$$d_I = \frac{\sum_i n_i d_i^7}{\sum_i n_i d_i^6} \quad (8)$$

with n_i the relative particle proportion in the corresponding class size d_i

- Volume-average, d_v , (also called weight-average) is obtained by assuming that the particles are spherical and multiplying the relative contribution of each size class d_i by the volume corresponding to a sphere in that size class

$$d_v = \frac{\sum_i n_i d_i^4}{\sum_i n_i d_i^3} \quad (9)$$

- Number-average, d_n obtained with the help of

$$d_n = \frac{\sum_i n_i d_i}{\sum_i n_i} \quad (10)$$

In the case of particle diameters larger than λ , a part of the light is adsorbed and the intensity average diameter estimation is a function of the particle refractive index which has to be known precisely. Then, the other average representations are calculated by the chosen method (Eqs. 8–10). Thus, if the refractive index is not properly defined, these average-diameters can be erroneous.

The intensity value is more appropriate for reporting results from a DLS analysis based on intensity fluctuations, but the mean number

TABLE I Latex Mean Diameters by Monomodal Algorithm and Relative Proportion

Analysis	Intensity	Volume	Number
Mean (nm)	307.8	350	316.1
Width	109	146	175
%	100	100	100

diameter also has to be considered, because it can be more easily compared to microscopic results.

Monomodal-Cumulants Model

Here the chosen model is the monomodal one. In Figure 7a, the plot of the autocorrelation function G_1 versus sample time, τ , is represented. Function G_1 quantifies the similarity between two acquisitions on a same small suspension volume taken at two different moments separated by τ , the sample time.

When two acquisitions are identical, $G_1(\tau) = 1$, the most information about the suspension is obtained. In the opposite case, when $G_1(\tau)$ equals zero, i.e., when two acquisitions are totally different, no information about the system can be extracted.

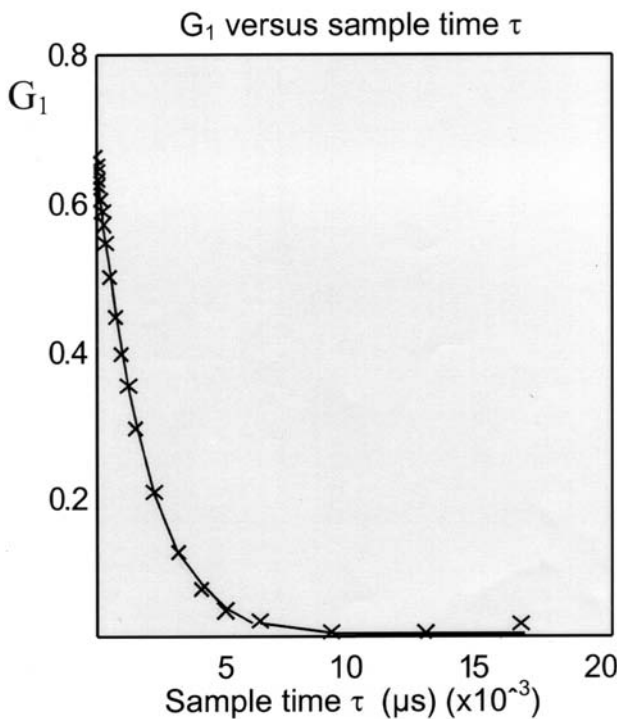


FIGURE 7a QELS G_1 autocorrelation function of latexes in a function of the sample time τ fitted by monomodal algorithm (at least five acquisitions of ten subruns, suspension/solvent intensity ratio > 50).

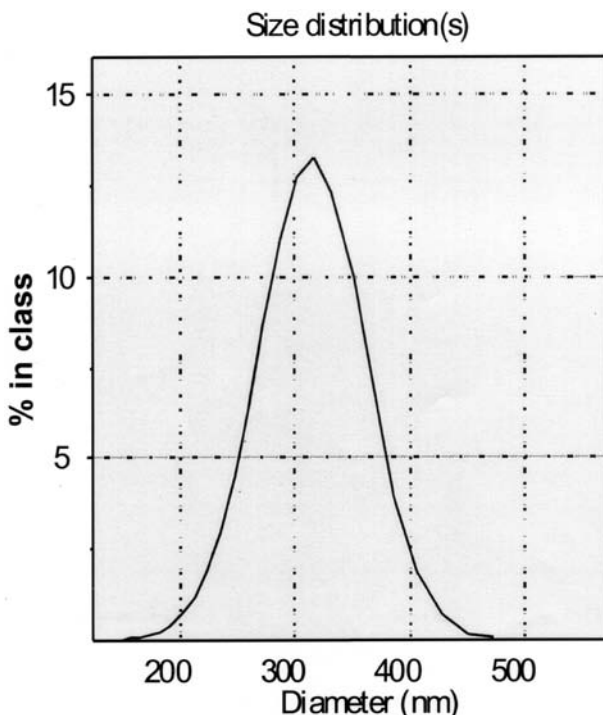


FIGURE 7b QELS intensity-average size distribution of latexes obtained by monomodal algorithm (at least five acquisitions of ten sub-runs, suspension/solvent intensity ratio > 50).

The first τ for which $G_1(\tau)$ equals zero, is called the relaxaton time, t_r . In other words, the shorter the sample time τ is, the bigger the ratio t_r/τ is, and the better the statistics (number of accumulations) are.

In Figure 7a, the experimental data are represented by crosses and fitted by the monomodal model curve. The fit is good for most of the data, and only the data corresponding to the smallest G_1 values are not correctly fitted. The relaxation time, t_r , equals 20 ms, which can be considered as a covenient value.

In Figure 7b, the size class distribution in intensity is shown versus the particle diameters analyzed. Only one peak appears centered about 310 nm. It is a Gaussian curve.

Table I shows that the mean intensity value is very close to the one measured by TEM, given by Interfacial Dynamics Corp. However, the measured polydispersity is around 15%. Polydispersity is often an

important parameter for nanoparticles. The mean volume and mean number averages are obtained by calculation. One can note that the mean number value is very close to the mean intensity one.

Contin Model

The same data may be analyzed via use of the Contin algorithm. G_1 versus sample time and size distribution versus intensity diameters are represented, respectively, in Figures 8a and 8b. Here, the relaxation time, t_r , is about 30 ms, which is longer than with monomodal cumulant model. As explained below, the shorter the sample time is, the better the statistics are. Thus, the Contin model does not seem to be the most convenient model.

The distribution peak form is not as close as the monomodal treatment to a Gaussian distribution. It proves that the Contin analysis, in this case of a nearly monodisperse sample, is not the more convenient algorithm. The intensity mean diameter, shown in Table II, is not as close to the given standard value 310 nm as the monomodal value. The other mean values are out of range, especially because of their width, which is as large as the diameter itself.

In conclusion, in the DLS study of nearly monodisperse samples, the use of the monomodal algorithm is recommended.

Laser Granulometry Study

The use of laser granulometry requires some caution during sample preparation as mentioned earlier. Similarly to DLS, laser granulometry results are represented as the size distribution versus volume-average diameters. Each sample is diluted with the help of the continuum medium in order to achieve the ideal experimental condition with an adequate obscuration coefficient (about 0.3). Then acquisitions are made until five consecutive runs give similar results, in order to achieve good repeatability.

In Figure 9, the size distribution was observed with the 45 μm focal lens and, in Figure 10, the same observation was carried out with the 100 μm focal lens. With the former, only one population appears centered on 300 nm and, for the latter, four different size classes are observed, with three of them being obviously artifacts. The optical system, in relation to the size range observed, is of great importance if meaningful results are to be obtained.

Table III gives the results of the 45 μm focal measurements. Among the various averaged diameters compiled, which are obtained by different calculations, the two most important are the volume and number representations. The number diameter will be taken into account in the following, since it can be easily compared to microscopy results.

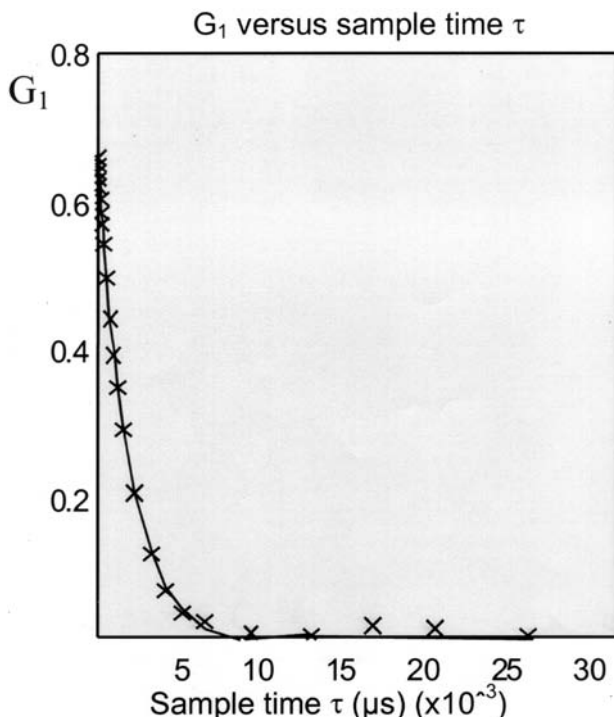


FIGURE 8a QELS G_1 autocorrelation function of latexes in a function of the sample time τ fitted by Contin algorithm (at least five acquisitions of ten sub-runs, suspension/solvent intensity ratio >50).

STUDY OF PLANT PROTEIN NANOPARTICLES

The suspension used was a plant protein nanoparticle system described earlier^[1]. It was obtained by a coacervation method. The desolvatation of macromolecules was caused by addition of a solvent phase, an ethanolic aqueous solution of the protein, to a nonsolvent phase. The chosen protein is gliadins, extracted from wheat flour. Several techniques were applied, DLS (cumulants and Contin), laser granulometry, and SEM, in order to determinate the most representative distribution for the sample.

DLS Study

The same preparation caution is taken for the DLS sample as described earlier (no pollutants and no multiple scattering). For each sample, at least five acquisitions of ten sub-runs are made. The software

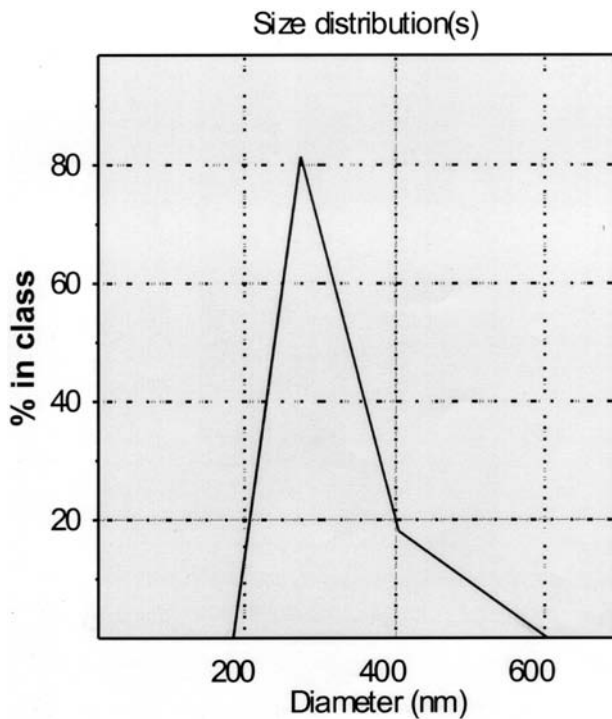


FIGURE 8b QELS intensity-average size distribution of latexes obtained by Contin algorithm (at least five acquisitions of ten sub-runs, suspension/solvent intensity ratio > 50).

for each subacquisition checks off the measurement quality for each mathematical treatment (monomodal-cumulants, Contin described later). The intensity ratio suspension/solvent is fifty.

Monomodal-Cumulants Model

The relaxation time, t_r , of the G_1 fit, Figure 11a, is large (longer than 100 ms). The application of monomodal model here seems to be poor.

TABLE II Latex Mean Diameters by Contin Algorithm

Analysis	Intensity	Volume	Number
Mean (nm)	297	391	354
Width	131.4	341.9	351.2

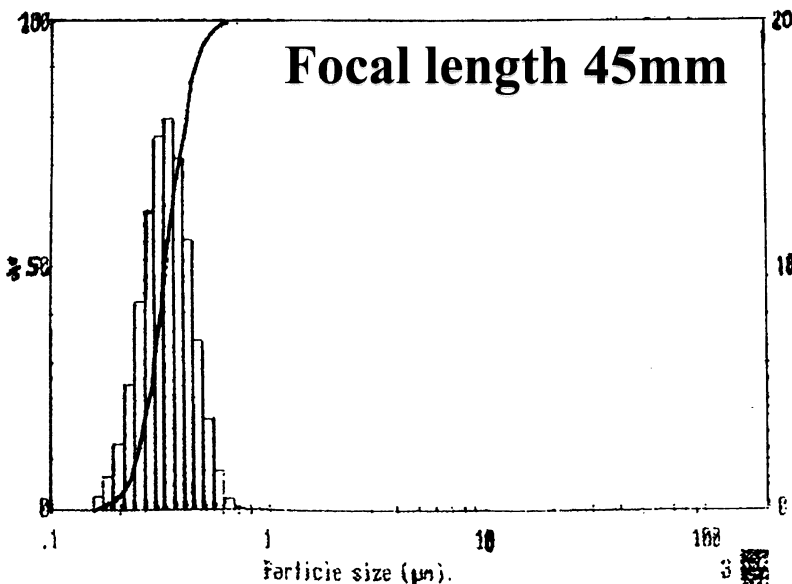


FIGURE 9 Volume-average size distribution of latexes obtained by laser granulometry with the 45 mm focal length (obscuration coefficient around 0.3, five consecutive acquisitions given similar results).

The intensity size distribution, Figure 11b, presents one peak, but the number distribution, Figure 11c, presents several. Table IV does not give narrow values of the mean diameter. This heterogeneity of results shows that the monomodel assumption is not appropriate for this particular case.

Contin Model

With the Contin analysis, Figure 12a, t_r of G_1 is less than 25 ms. The results are better than those from the monomodal-cumulant model. A single peak is seen in the size distribution curve, Figure 12b. Its form is nearly Gaussian and it is centered around 800 nm. The mean intensity value is around 800 nm, but the width is important. The two other analyses, in volume and in number, given in Table V, are out of sense and are probably due to calculation artifacts. In fact DLS analysis points out a quite polydisperse population with a mean size greater than λ (i.e., about 800 nm).

To conclude, DLS analysis shows several distributions, with one of them composed of particles larger than λ .

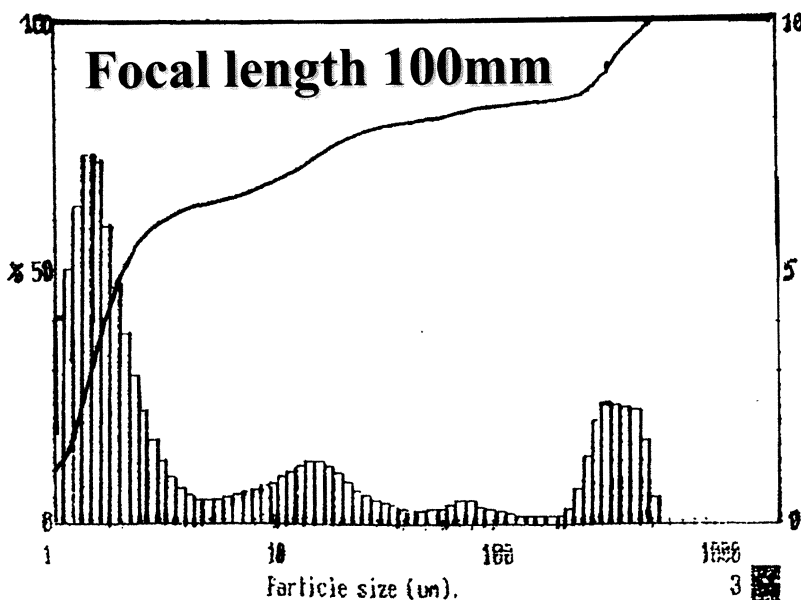


FIGURE 10 Volume-average size distribution of latexes by laser granulometry with the 100 mm focal length (obscuration coefficient around 0.3, five consecutive acquisitions given similar results).

Laser Granulometry Study

From the plant protein nanoparticles suspension, a laser granulometry sample without any pollutants or gas bubbles was prepared. The size distribution plot, Figure 13, shows two size classes: one around 500 nm and another at 6 μm. It is now clear why light scattering was not usable. The latter class represents less than 10% of the sample population. The mean volume diameter is 1 μm while 50% of the particle size are less than 550 nm. These results are coherent, but very different. Let us now consider an SEM image of the particles.

TABLE III Latex Mean Diameters by Laser Granulometry

Analysis	Intensity	Volume
Mean (nm)	340	290
Width	28	21

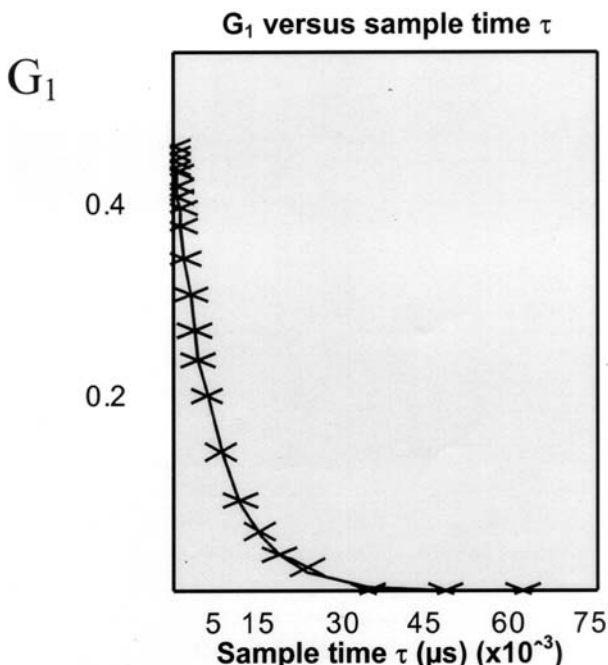


FIGURE 11a QELS G_1 autocorrelation function of plant protein nanoparticles fitted by monomodal algorithm (at least five acquisitions of ten sub-runs, suspension/solvent intensity ratio > 50).

SEM

The sample preparation was evaporated in a vacuum chamber, and then the deposition of a colloidal metal was performed. This layer conducts on the sample surface the electron beam and generates the secondary electrons forming the SEM image. Should the beam fuse the particles of gel or of soft polymers, cryo-SEM could be used.

Several micrographs (at least 10) of the same sample are taken. Figure 14 is representative of all of them and shows spherical particles. The diameter of most of them is less than 700 nm in a “dry” state. A few of them are bigger than 2 μm such as the one next to the 1 μm bar. This image confirms the previous results: the Contin DLS diameter of 800 nm, which has been found in the aqueous medium, and the laser granulometry two size classes whose diameters are upper than 1 μm . It would be interesting now to perform an image analysis in order to confirm the four peaks seen by Contin analysis.

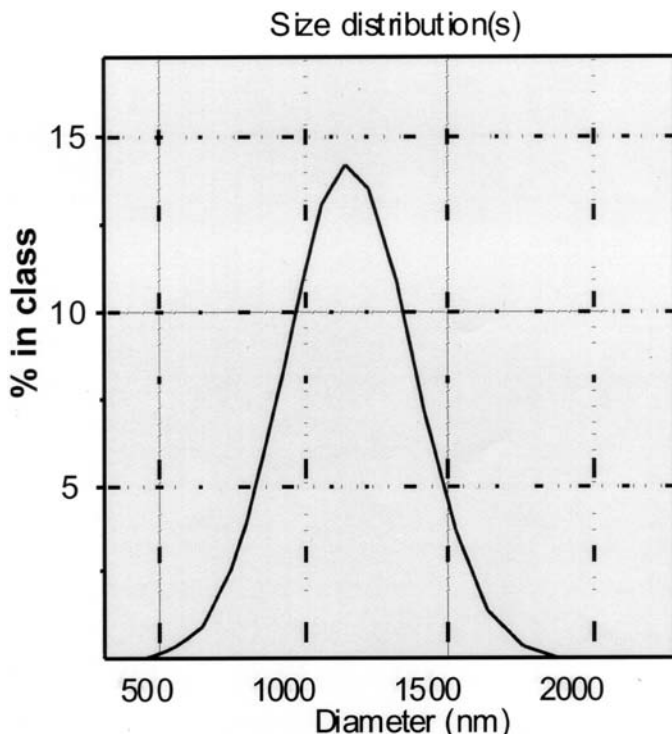


FIGURE 11b QELS intensity-average size distribution of plant protein nanoparticles obtained by monomodal algorithm (at least five acquisitions of ten subruns, suspension/solvent intensity ratio > 50).

This example shows that a characterization of nanoparticles size, for such a non-ideal sample, is not evident. The sample polydispersity leads to many difficulties. To resolve them, a solution could be to separate the different size classes, and then to characterize them. Different solutions may also be used, as reviewed in the following section.

POTENTIAL SOLUTIONS TO PROBLEMS ASSOCIATED WITH POLYDISPERSITY

Sedimentation

Generally speaking, sedimentation gives access to information over a wide size range, from a few nanometers up to several micrometers. This is

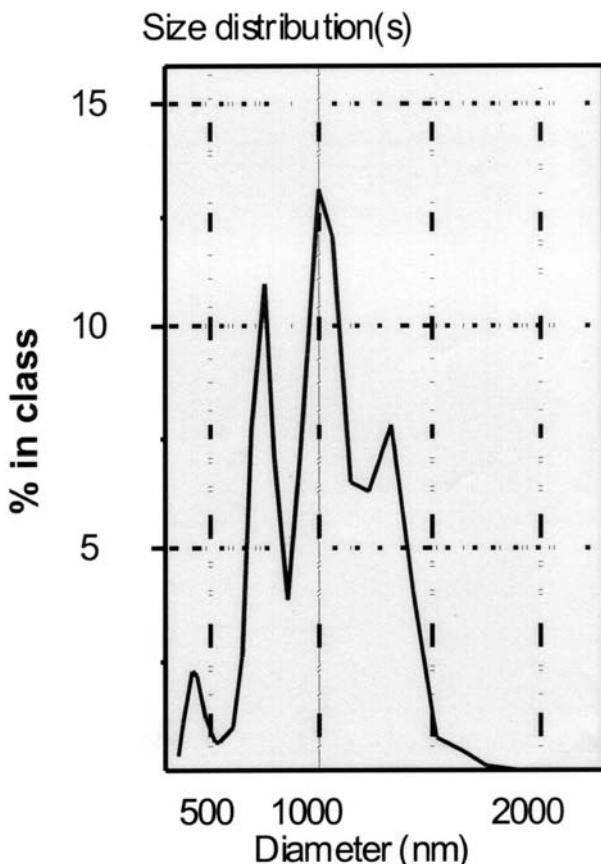


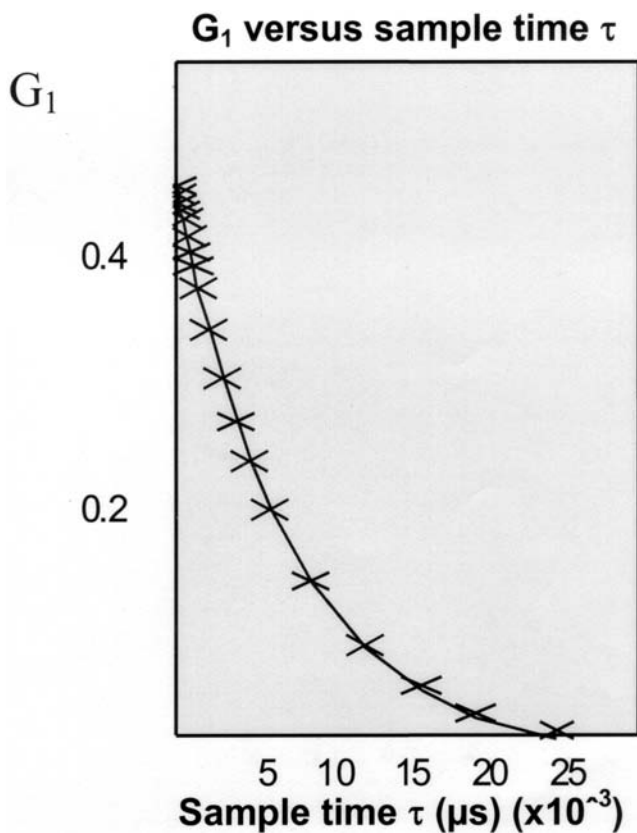
FIGURE 11c QELS number-average size distribution of plant protein nanoparticles obtained by monomodal algorithm (at least five acquisitions of ten sub-runs, suspension/solvent intensity ratio > 50).

especially true with the ultracentrifugation for nanosized objects. With an appropriated optical system, the size analysis is made easier with the help of time used as a separator. A unique size class passes in front of the optical system at any point in time. In fact, monodisperse and uncharged hard spherical particles are quickly size characterized in very diluted suspension if the sedimentation occurs rapidly enough.

These techniques are based on the free and unhindered sedimentation of particles. The potential complicating factors for such a characterization are polydispersity—i.e., size distribution mixture, attractive and charged particles, non-ideal shapes, temperature, dilution shock, vessel

TABLE IV Plant Protein Nanoparticle Mean Diameters by Monomodal Algorithm and Relative Proportion

Analysis	Intensity		Volume			Number		
	Mean (nm)	752.5	1023.7	1313.2	446.5	738.5	1035.6	1327.7
Width	523.9	120.5	134.5	205	96.8	156	234.5	102.4
%	100	12.4	39.2	47.8	7.3	30.6	44.4	17.7

**FIGURE 12a** QELS G_1 autocorrelation function of plant protein nanoparticles fitted by Contin algorithm (at least five acquisitions of ten sub-runs, suspension/solvent intensity ratio > 50).

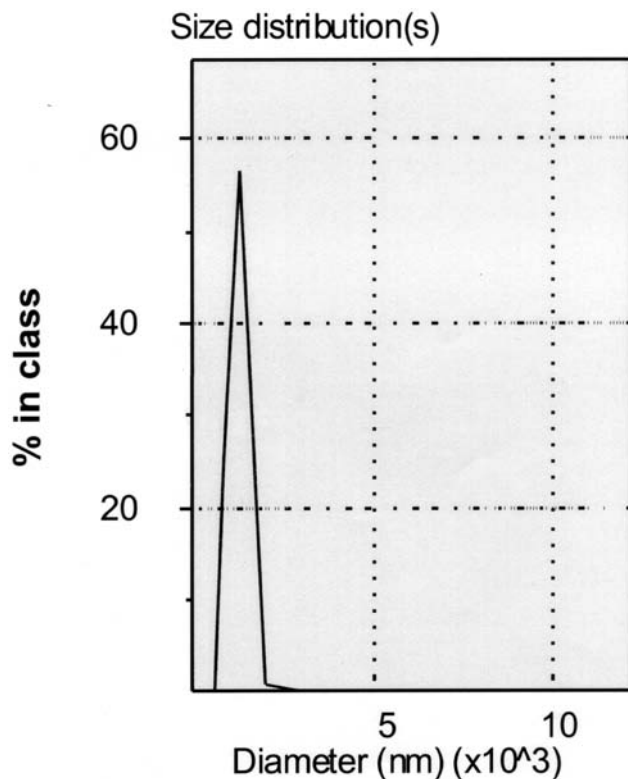


FIGURE 12b QELS intensity-average size distribution of plant protein nanoparticles obtained by Contin algorithm (at least five acquisitions of ten sub-runs, suspension/solvent intensity ratio > 50).

geometry, and softness of the particles surface. Nowadays some of these difficulties are partially covered up. Philipse^[18] has written an interesting review about this point.

TABLE V Plant Protein Nanoparticles Mean Diameters by Contin Algorithm and their Relative Proportion

Analysis	Intensity	Volume	Number
Mean (nm)	7.8	745.8	1.9
Width	16.2	1219	0.7
%	16.9	83.1	100

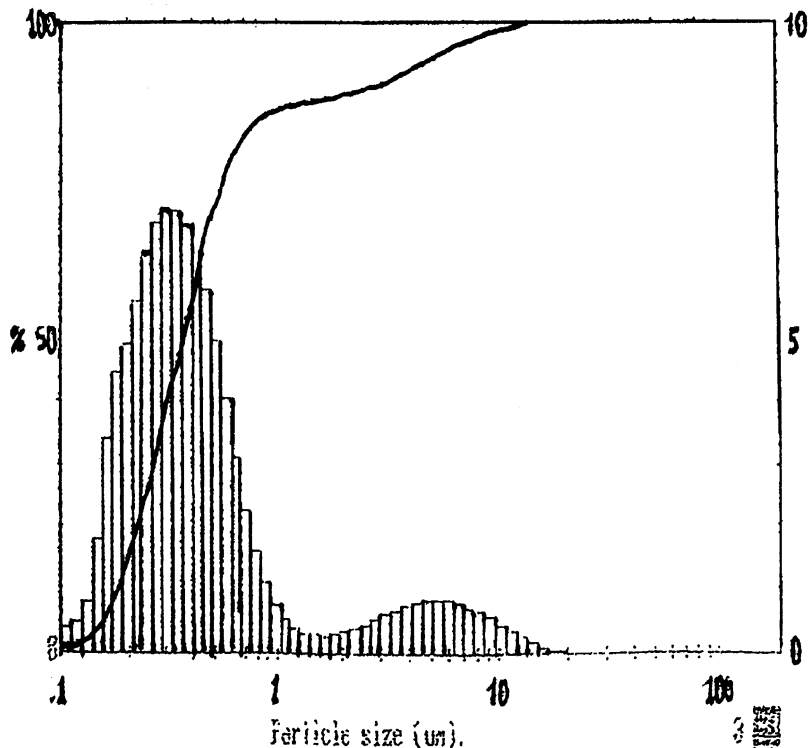


FIGURE 13 Volume-average size distribution of plant protein nanoparticles obtained by laser granulometry with the 45 mm focal length (obscuration coefficient around 0.3, five consecutive acquisitions given similar results).

Another approach, for a very diluted complex sample, is to couple DLS with SLS. This method is known as multiangle dynamic light scattering.

Multiangle Dynamic Light Scattering^[19,20]

At different angles, the fluctuation intensities data are cumulated and, then, integrated in two ways: averaged over a period of time (SLS) and time dependent (DLS). The two results are correlated: the dynamical data are evaluated by the Mie scattering function and then related to the statistical intensity values. The obtained results are more reliable than the ones generated only by DLS or SLS. Several classes are now resolved and characterized even if they are close together.

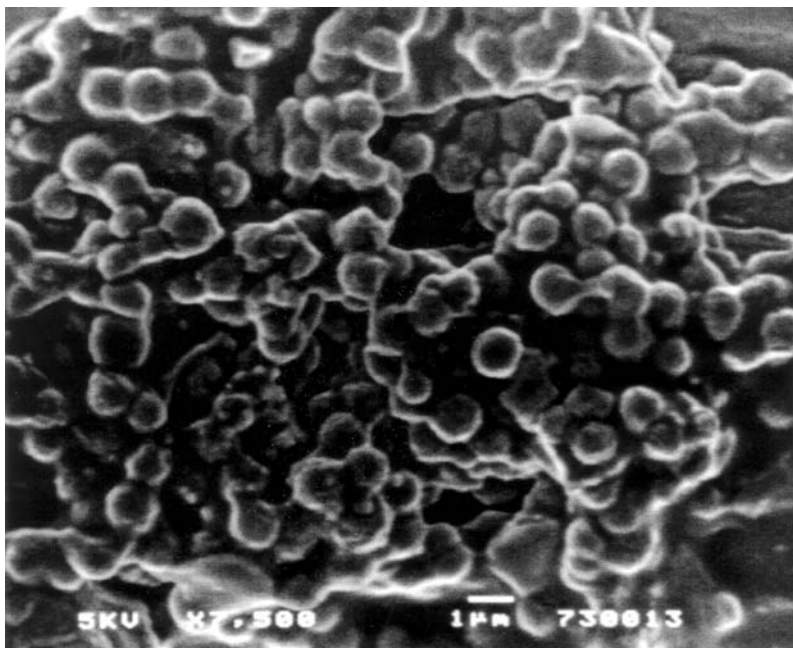


FIGURE 14 Plant protein nanoparticles SEM image.

Another point of view is, first, to separate the size distribution fractions and, then, to analyse them. The separation could occur by one of the flow field fractionation (FFF) family techniques.

Flow Field Fractionation Techniques

FFF methods^[21] are direct and non-invasive methods. The different fractions of the polydisperse sample are first separated, and then their mean diameters are evaluated. The separation occurs by differential retention related to a physicochemical parameter difference in a stream liquid flowing through a thin channel (50–300 μm). The separated components are eluted one by one into a detector, often a MALS detector (multi-angle light scattering). The size range spreads from a few nm to 100 μm with the help of the Rayleigh–Debye–Gans and Lorentz–Mie combination algorithms.

Sedimentation Flow Field Fractionation

The discriminating parameter involved in the sedimentation FFF is the specific gravity difference between the particles and the aqueous

phase. A circular channel spins around a centrifuge axis and the species are separated by the radially induced acceleration. For each peak, the retention time is related to the particle size through MALS measurements, and these results could be complemented by other microscopic characterizations.

Sedimentation FFF is not convenient for smaller sized particles (< 30 nm), whose sedimentation process is too slow. In such case, FFF is convenient. The separation in this latter technique is driven by a “cross-flow” field obtained by a second stream at a right angle to the main one.

Environmental Microscopy

Environmental microscopy, as shown earlier, avoids the inconvenience and possible artifacts of “dried” sample. The sample hydration is controlled by varying the vapor pressure in the chamber while maintaining the temperature constant^[13]. The thermal conductivity of the sample can be critical. In addition the water can condense or evaporate. Before the pump-down sequence, the chamber has to be saturated to minimize the sample water evaporation. This microscopy method needs no prior sample preparation^[18]. The image is a picture of nanoparticles; this method is less invasive than SEM and the diameters are reliable. With the use of an image analysis, the size distribution curve is easily obtained. Such a method affords direct particle observation in their own medium without any dilution.

CONCLUSION

The different examples presented show that size characterization is not such an easy analysis especially with a complex sample composed of several size populations.

Nanosized objects are observable by many techniques. Most of them are adversely affected by concentrated conditions, polydisperse distributions, and irregular particle shapes. Multiangle dynamic light scattering can be very helpful in overcoming the last two disadvantages.

The concentration dependency is avoided by eluting and by separating each size class before identifying them. For instance, multiangle dynamic light scattering is fruitfully coupled with sedimentation FFF. In this case, the particles are observed by indirect ways, for example light intensity fluctuations.

Particles are directly seen by methods such as electronic microscopy. The major disadvantage of these techniques is that the particles are not characterized in solution but in a “dried” state, environmental microscopy being an exception. This method is a less invasive technique and gives results that are most representative of the real sample size

distribution if it is coupled with an image analysis. Its development seems to be very promising in the next decades, but currently it is rarely applied.

Finally, to prevent making excessive assumptions, the preferred solution is to couple several size characterization techniques. It is preferred that at least one *in situ* technique be combined with electronic microscopy.

REFERENCES

- [1] Duclairoir, C., Irache, J. M., Nakache, E., Orecchioni, A.-M., Chabenat, C., and Popineau, Y. (1999). *Polymer International*, **79**, 327.
- [2] Pusey, P. N. (1973). In: *Industrial Polymers: Characterization by Molecular Weight*, J. H. S. Green and R. Dietz, Ed. (Transcripta Books: London).
- [3] Atkins, P. W. (1999). In: *Physical Chemistry*, 4th ed. (Oxford University Press: Oxford, UK).
- [4] Rayleigh, L. (1871). *Phil. Mag.*, **41**, 107, 274, 447.
- [5] Kralchëvsky, P. A., Danov, K. D., Denkov, N. D. (1997). In: *Handbook of Surface and Colloid Chemistry*. K. S. Birdy, Ed., 448–494 (CRC Press: Boca Raton, Florida).
- [6] Debye, P. (1915). *Ann. Phys.*, **46**, 809.
- [7] Gans, R. (1921). *Ann. Phys.*, **65**, 37; (1923). *Ann. Phys.*, **67**, 353; (1925). *Ann. Phys.*, **76**, 29.
- [8] Mie, G. (1908). *Ann. Phys.*, **25**, 377.
- [9] Carr, W. (1976) In: *Progress in Organic Coatings*, **4**, 161.
- [10] McClements, D. J., and Coupland, J. N. (1996). *Colloids and Surfaces A*, **117**, 161.
- [11] Chestnut, M. H. (1997). *Current Opinion in Colloid & Interface Science*, **2**, 158.
- [12] Donald, A. M. (1998). *Current Opinion in Colloid & Interfaces Science*, **3**, 143.
- [13] Griffith, E., and Newbury, D. E. (1996). *Scanning*, **18**, 465.
- [14] Wyatt, P. J. (1998). *Journal of Colloid & Interface Science*, **197**, 9.
- [15] Fennell, E. D., and Wennerström, H. (1994). In: *The Colloidal Domain Where Physics, Chemistry, Biology, and Technology Meet* (VCH Editions: New York).
- [16] Stepanek, P. (1993). In: *Dynamic Light Scattering*, W. Brown, Ed., pp. 177–241 (Oxford University Press: Oxford, UK).
- [17] Provencher, S. W. (1982). *Comput. Phys. Comm.*, **27**, 213–227.
- [18] Philipse, A. (1997). *Current Opinion in Colloid & Interface Science*, **2**, 200.
- [19] Bryant, G., and Thomas, J. C. (1995). *Langmuir*, **11**, 2480.
- [20] Bryant, G., Abeynayake, C., and Thomas, J. C. (1996). *Langmuir*, **12**, 6224.
- [21] Giddings, J. C. (1993). *Science*, **260**, 1456.

P6



ELSEVIER

International Journal of Pharmaceutics 242 (2002) 163–166

international
journal of
pharmaceutics

www.elsevier.com/locate/ijpharm

Note

Biopolymeric colloidal carriers for encapsulation or controlled release applications

D. Renard ^{a,*}, P. Robert ^a, L. Lavenant ^a, D. Melcion ^a, Y. Popineau ^a, J. Guéguen ^a, C. Duclairoir ^b, E. Nakache ^b, C. Sanchez ^c, C. Schmitt ^d

^a INRA Centre de Recherches de Nantes, rue de la Geraudiere, BP 71627 44316 Nantes Cedex 3, France

^b Equipe Polymères-interfaces LCMT UMR 6507 ISMRA 14050 Caen Cedex, France

^c LPCGA ENSAIA/INPL 54505 Vandoeuvre-Les-Nancy, France

^d Nestle Research Center, CH-1000 Lausanne 26, Switzerland

Received 24 December 2001; received in revised form 10 January 2002; accepted 16 January 2002

Abstract

Biopolymers represent an interesting alternative to synthetic polymers in order to be used as structured carriers for controlled release and encapsulation applications. In particular, the ability of these carriers to entrap both hydrophilic and hydrophobic drugs may be very promising for many applications. In addition, the absence of chemical compounds and organic solvents used to produce biopolymeric matrices could be very interesting for some industrial applications. Simple or complex coacervation methods involving proteins or protein and polysaccharide mixtures were used to create new matrices dedicated to controlled release applications. Controlled release experiments with model compounds were conducted in order to evaluate the performance of such matrices. An alternative and promising research field deals with particles obtained from hydrogel systems. Totally transparent solid matrices resulting from the dehydration of new protein gels were formed and swelling capacities of these matrices were studied.

© 2002 Elsevier Science B.V. All rights reserved.

Keywords: Coacervation; Encapsulation; Hydrogels; Swelling; Proteins; Arabic gum

In the last decades, micro and nanosized colloidal carriers have received a growing scientific and industrial interest (Thies, 1996). These vectors may be capsules (with liquid core surrounded by a solid shell), particles (polymeric matrices), vesicles or liposomes, multiple or single emulsions and

found a wide range of applications. They may be loaded by living cells, enzymes, flavour oils, pharmaceuticals, vitamins, adhesives, agrochemicals, catalysts and offer considerable advantages at use. Liquids can be handled as solids, odour or taste can be effectively masked in a food product, sensitive substances can be protected from deleterious effects of the surrounding environment, toxic materials can be safely handled, and drug delivery can be controlled and targeted (Robinson, 1997).

* Corresponding author. Tel.: +33-2-40-67-50-52; fax: +33-2-40-67-50-43

E-mail address: drenard@nantes.inra.fr (D. Renard).

In the aforementioned laboratories, we started with a new strategy based on phase separation in order to prepare natural particles. Simple or complex coacervation methods involving proteins or protein and polysaccharide mixtures (Schmitt et al., 1998) were used to create new matrices dedicated to controlled release applications. The colloidal carriers produced were in the micrometer or nanometer size range depending on the substrates or the methods used.

Wheat proteins, gliadins, were implicated in simple coacervation to produce nanospheres. Nanoparticles were obtained by desolvation of the protein using physiological salt solution as non-solvent. Synperonic PE F68 was used to stabilize the nanoparticles suspension (Duclairoir et al., 1998). Gliadins nanospheres typical size was around 900 nm (Duclairoir et al., 1998). Particles size and polydispersity increased with the increase of the solvent/non-solvent ratio and with the aggregated state of the proteins. Controlled release experiments with model compounds were conducted in order to evaluate the performance of such matrices. Vitamin E-loaded nanoparticles (1 mg) were digested in 10 ml of an ethanol/water mixture (62/38 v/v) at room temperature in the dark. The vitamin E concentration encapsulated in nanoparticles (C_1) and the residual concentration in the supernatant (C_2) were then assayed by HPLC at 290 nm. Empty nanoparticles were treated in the same way and used as references for these determinations. The drug loading (rate) and the entrapment efficiency were calculated according to the equations:

$$\text{Rate (\%)} = \frac{C_1}{m_{\text{gliadins}}} \quad \text{Efficiency (\%)} = \frac{C_1}{C_1 + C_2}$$

In vitro drug release kinetic was also performed in non-sink conditions using decane as solvent (to prevent drug loss from nanoparticles dissolution) and a laboratory designed release cell. About 10 mg of gliadins nanoparticles (containing 824 µg/g gliadins) were resuspended in 10 ml of decane. Aliquots were collected at successive time intervals and replaced by the same quantity of solvent in order to get a constant volume in the release cell. The samples were analysed by HPLC as described above for encapsulation experiments.

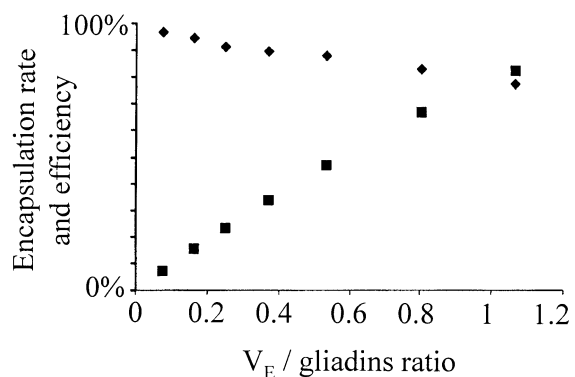


Fig. 1. Vitamin E (V_E) encapsulation rate (■) and efficiency (◆) by gliadins nanospheres as a function of V_E /gliadins ratio.

Encapsulation of vitamin E (V_E) into gliadins nanospheres revealed that the rate and efficiency decreased with the decrease of the V_E /gliadins ratio (Fig. 1). For a V_E /gliadins ratio of 1, an encapsulation rate of 824 µg/mg gliadins and an efficiency of 77% were obtained. The V_E release kinetic from loaded particles was displayed Fig. 2. The experimental points were fitted with the following equations:

$$\frac{V_E}{\text{initial } V_E} = 6 \sqrt{\frac{\tau}{\pi}} \quad (\text{short time})$$

$$\frac{V_E}{\text{initial } V_E} = 6 \sqrt{\frac{\tau}{\pi}} - 3\tau \quad (\text{intermediate time})$$

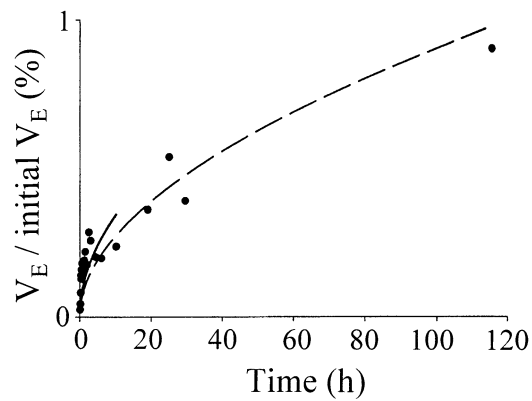


Fig. 2. Vitamin E (V_E) release kinetic by gliadins nanospheres as a function of time (h). See text for equations used in the fitting procedure: (●) released V_E (%); (—) fit (short time); (---) fit (intermediate time).

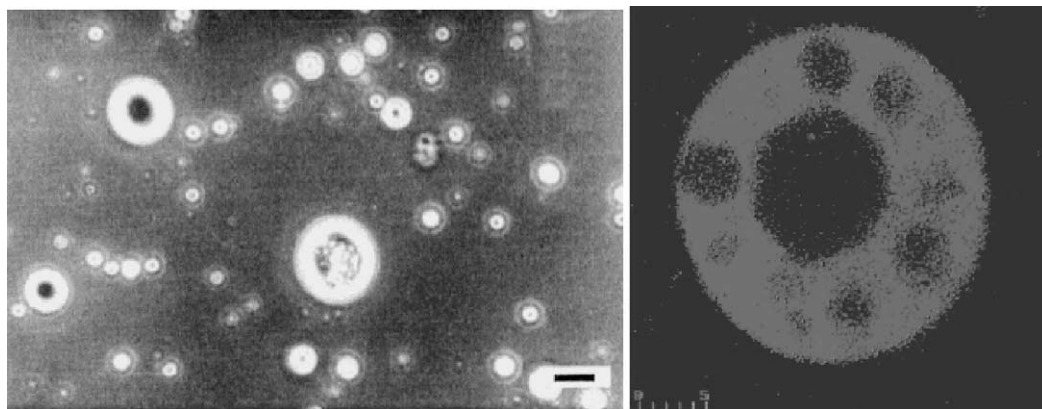


Fig. 3. (Left side) Phase contrast optical micrograph of 1 wt.% β -lactoglobulin/Arabic gum mixtures at pH 4.2 ratio 1:1. Scale bar represents 20 μm . (right side) Confocal scanning laser micrograph of a coacervate obtained with a 1 wt.% β -lactoglobulin/Arabic gum mixture at pH 4.2 ratio 1:1. Scale bar represents 5 μm .

with $\tau = Dt/r^2$, D being the diffusion coefficient of the entrapped vitamin E and r , the radius of the nanoparticles.

The kinetic profile was thus interpreted by a burst effect coupled with a drug diffusion process through the particle modelled as a homogeneous sphere. The drug diffusion coefficient was considerably reduced when entrapped in the carrier: $D_{VE} = 1.1 \cdot 10^{-20} \text{ m}^2/\text{s}$ compare to $D_{VE} = 10^{-9} \text{ m}^2/\text{s}$ in solution. The encapsulation of different drugs into nanospheres showed that carriers had more affinity for hydrophobic drugs and that the ζ -potential of the particles was directly related to the nature of the drug (Duclairoir, 2000).

In the case of complex coacervation, the β -lactoglobulin/Arabic gum couple was tested. The mechanism of formation and the structural properties of coacervates were first highlighted in order to better control the stability of these systems. Coacervation process was established at pH 4.2 in water where the two biopolymers interact electrostatically (Schmitt et al., 2000). The structure of the coacervates was explored using both phase contrast and confocal scanning laser microscopies. β -lactoglobulin/Arabic gum spherical vesicular coacervates revealed by microscopy were the hallmark of these dispersions (Fig. 3). Large 'foam-like' coacervates induced by partial coalescence of single coacervates were visible especially at the 2:1 protein to polysaccharide ratio (Schmitt

et al., 2001). Increasing dispersions stability was reached by increasing protein to polysaccharide ratio or by decreasing total biopolymer concentration. Another alternative to increase the stability is to produce composite dispersions containing both protein aggregates embedded in protein–polysaccharide coacervates and free coacervates (Schmitt et al., 2000). These systems could thus be used as multifunctional reservoirs for applications in microencapsulation.

An alternative and promising research field deals with particles obtained from hydrogel systems. The hydrogels may be sensitive to environmental stimuli such as pH, ionic strength, electric/magnetic fields, light and temperature depending on the substrate used. Totally transparent solid matrices resulting from the dehydration of new protein gels, revealed variable swelling capacities that depend on the solvent used and physical chemical conditions. The protein hydrogels were formed at pH 8 in 50% ethanol solutions (Renard et al., 2000). Swelling kinetics of cylindrical gels in both hydrated ($m_0 \sim 4.5 \text{ mg}$) and dehydrated ($m_0 \sim 1.5 \text{ mg}$) forms were followed in different solvent conditions. The swelling kinetics of β -lactoglobulin hydrogels showed that the increase of mass was the highest in water for both hydrated and dehydrated gels (Fig. 4). The capacity of swelling (or not) depended on the solvent conditions and would allow a controlled

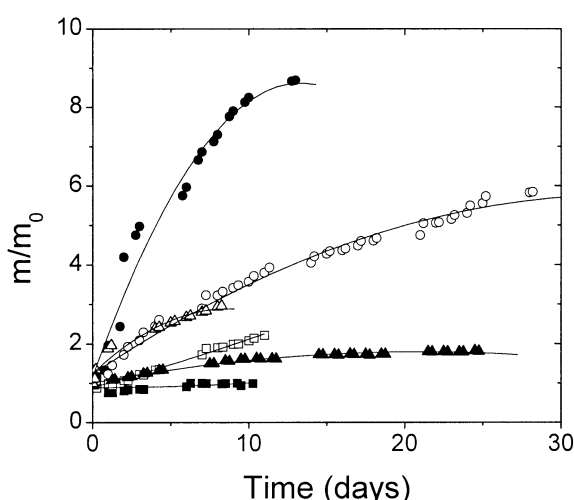


Fig. 4. Swelling kinetics of β -lactoglobulin hydrogels both in dehydrated and hydrated forms for different solvent conditions: (■) ethanol; (□) water/ethanol 50/50 (v/v); (●) water; (○) 0.1M NaCl; (▲) water/ethanol 50/50 (v/v) (hydrated gel); (Δ) water (hydrated gel).

release of both hydrophilic and hydrophobic drugs.

A new dispersion/gelation method was developed to produce micro-beads having potential applications in the encapsulation field. Basically, the dispersion of a β -lactoglobulin pre-gel in an apolar phase produced gelled droplets. These droplets were then washed and dehydrated under vacuum in order to produce particles of 500 μm mean diameter (Fig. 5). Such protein matrices were totally transparent and could be used to encapsulate large molecules or microorganisms.

References

- Thies, C., 1996. A survey of microencapsulation processes. In: Benita, S. (Ed.), Microencapsulation: Methods and Industrial Applications, vol. 73. Marcel Dekker, New York, pp. 1–19.
- Robinson, J.R., 1997. Controlled drug delivery. Past, Present, and Future. In: Park, K. (Ed.), Controlled Drug Delivery: Challenges and Strategies. American Chemical Society, Washington, pp. 1–7.
- Schmitt, C., Sanchez, C., Desobry-Banon, S., Hardy, J., 1998. Structure and technofunctional properties of protein-polysaccharide complexes: a review. *Crit. Rev. Food Sci. Nut.* 38 (8), 689–753.
- Duclairoir, C., Nakache, E., Marchais, H., Orecchioni, A.-M., 1998. Formation of gliadin nanoparticles: influence of the solubility parameter of the protein solvent. *Colloid Polym. Sci.* 276, 321–327.
- Schmitt, C., Sanchez, C., Despond, S., Renard, D., Thomas, F., Hardy, J., 2000. Effect of protein aggregates on the complex coacervation between β -lactoglobulin and acacia gum at pH 4.2. *Food Hydrocolloids* 14, 403–413.
- Renard, D., Robert, P., Garnier, C., Dufour, E., Lefebvre, J., 2000. Gelation by phase separation in a whey protein system: in-situ kinetics of aggregation. *J. Biotechnol.* 79, 231–244.
- Duclairoir, C., 2000. Préparation et caractérisation des nanoparticules de gliadiques de blé: application à l'encapsulation et au relargage de quelques substances actives. Ph.D. Thesis, Université de Caen, France.
- Schmitt, C., Sanchez, C., Lamrecht, A., Renard, D., Lehr, C.-M., de Kruif, C.G., Hardy, J., 2001. Study of β -lactoglobulin/acacia gum complex coacervation by diffusing-wave spectroscopy and confocal scanning laser microscopy. *Colloids Surf. B* 20, 267–280.

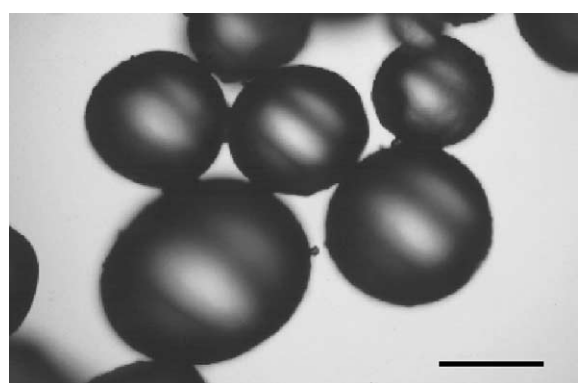


Fig. 5. Optical micrograph of β -lactoglobulin beads obtained by a gelation/emulsification method. Scale bar represents 500 μm .

P7



Available online at www.sciencedirect.com

SCIENCE @ DIRECT®

International Journal of Pharmaceutics 253 (2003) 133–144

international
journal of
pharmaceutics

www.elsevier.com/locate/ijpharm

Evaluation of gliadins nanoparticles as drug delivery systems: a study of three different drugs

C. Duclairoir^a, A.-M. Orecchioni^{b,*}, P. Depraetere^c, F. Osterstock^d, E. Nakache^a

^a *Equipe Polymères-Interfaces, ISMRA, LCMT UMR 6507, 14050 Caen Cedex, France*

^b *Université de Rouen, UFR de Médecine et Pharmacie, 76183 Rouen, France*

^c *Laboratoire de Pharmacie Galénique, Bd Becquerel, Hérouville St Clair, 14032 Caen Cedex, France*

^d *ESCTM/CRISMAT, UMR 6508, ISMRA, 14050 Caen Cedex, France*

Received 15 February 2002; received in revised form 2 December 2002; accepted 11 December 2002

Abstract

In this paper, biopolymer nanoparticles are studied, which unlike many synthetic carriers used for controlled release, are biocompatible and biodegradable systems. Gliadins nanoparticles are obtained by a desolvatation method, also known as drawing-out precipitation. These particles have been shown to be interesting as drug release systems for all-trans-retinoic acid. The aim of this paper was to study the influence of the polarity of different drugs on nanoparticle characteristics such as size and drug loading efficiency. Three drugs of three different polarities were studied: the hydrophobic Vitamin E (VE), the slightly polar mixture of linalool and of linalyl acetate (LLA) and the cationic amphiphilic benzalkonium chloride (BZC). This comparative work shows that the amount of the entrapped VE and LLA is higher than that of the cationic BZC, confirming a strong interaction between gliadins and apolar compounds, due to the apolarity of the proteins. This interaction results in a low diffusion coefficient and a partition coefficient in favour of gliadins, resulting in a low permeability coefficient. The drug release kinetics of two substances, LLA and BZC, are observed, in showing a burst effect, then a diffusion process, which can be modelled assuming that the particles are homogeneous spheres.

© 2002 Elsevier Science B.V. All rights reserved.

Keywords: Nanoparticles; Gliadins; Vitamin E; Linalool; Linalyl acetate; Benzalkonium chloride

1. Introduction

Drug delivery systems are interesting formulations to prevent numerous drawbacks related to the drug itself, for example by decreasing its degradation rate. In such a dosage form, the drug is gradually released unlike all conventional formulations. Several carriers have been studied in the last decades, among them, liposomes, vesicles, films, sponges,

simple or complex emulsions, and particles. These last named delivery systems are found as spheres or capsules for core/shell particles. Particles are classified as microparticles for micron-sized systems and as nanoparticles for sub-micronic systems (Thies, 1996). Most of them are derived from synthetic polymers and some from biopolymers (Nakache et al., 2000). Recently, gliadins, extracted from wheat gluten, have been used to elaborate nanoparticles (Ezpellesta et al., 1996; Duclairoir et al., 1999). As biopolymers, gliadins do not present the common drawbacks of synthetic materials, related to the presence of monomer or initiator residues (Chasin and Langer,

* Corresponding author. Tel.: +33-1-46612713;
fax: +33-1-46612713.

E-mail address: oreccam@wanadoo.fr (A.-M. Orecchioni).

1990). Their biocompatibility is assumed and, as plant proteins, they are recognized as prion-free unlike animal proteins. Besides gliadins are hydrophobic and slightly polar (Bigelow, 1967; Popineau and Denery-Papin, 1995). Consequently, they are able to interact with skin keratin (Teglia and Secchi, 1994). Thus, gliadin systems seem to have promise in the development of topical formulations. Moreover, previous work has shown that the preparation of gliadin particles can be easily performed by simple coacervation method (Ezpelleta et al., 1996). The obtained gliadins systems are spherical and submicron-sized, thus are nanoparticles. They proved to be interesting delivery systems for all-*trans*-retinoic acid (RA).

In this study, three drugs of different polarity have been entrapped in such gliadins nanoparticles. There are the hydrophobic Vitamin E (VE), the slightly polar linalool/linalyl acetate mixture (LLA), and the amphiphilic and cationic benzalkonium chloride (BZC), with dielectric constants (ϵ) respectively of 4, 8 and 45 (Maryott and Smith, 1951).

α -Tocopherol (Vitamin E) is known as a strong antioxidant or nitrosamine blocker to prevent built up of cellular peroxides (Idson, 1992; Marty and Wepierre, 1994). For instance, free radicals may promote skin damages such as premature skin aging (Epstein, 1983), skin fragility and even skin cancers such as melanoma (Sober, 1987) related to a decrease in cellular immunity of the skin. VE is known to delay the progression of aging (Wester and Maibach, 1997), to have skin moisturising properties (Mayer et al., 1993) and emolliency properties (Tamburic et al., 1999; Marty, 1998). However, VE is degraded by oxygen and must be carefully protected from light, heat and contact with air when it is used in formulations and dosage forms. To overcome these drawbacks, liposome dosage forms were formulated (Kagan et al., 1992; Koga and Terao, 1996). Nanoparticulate carriers from bioacceptable macromolecules, particularly gliadins, are also interesting system for controlled drug release. They are able to interact with epidermal keratin due to their being rich in proline (Teglia and Secchi, 1994).

Linalool and linalyl acetate are the major components of aromatic lavender essential oils, frequently used in aromatherapy. Moreover, linalool and linalyl acetate give antibacterial and antifungal proper-

ties (Lis-Balchin and Hart, 1999) to the formulations. In dermatologic formulations, for instance, their use may irritate the patient's skin. Gliadins encapsulation could be a fruitful method for LLA formulation. The coupling of gliadins proline, which allows a powerful attraction to the skin keratin, and of the gradual and controlled LLA release, potentially avoids all the potential drawbacks of the drug and even improves LLA disposition.

BZC is a cationic surfactant often used as antiseptic, bactericide (Patterson, 1956), spermicide (Aubeny et al., 2000) or virucide (Wainberg et al., 1990). Some original formulations of this drug, better known as Zeriphian®, are on the market. There are capsules (Wainberg et al., 1990) and vaginal Protectaid® sponges (Psychoyos et al., 1993). But the medication can promote some allergies followed by mucous lesions (Dhillon et al., 1982). Thus, a dosage form such as gliadins nanoparticles could be a good alternative and could avoid lesions promoted by the irritant BZC and, even, could improve the therapeutic dosage by delaying the delivery.

This paper reports on the characterization, entrapment and release studies on the novel drug delivery systems.

2. Materials and methods

2.1. Materials

Gliadins were extracted and purified by Y. Popineau (LBTP, INRA, Nantes, France). α -Tocopherol (VE) and benzalkonium chloride (BZC) were obtained from Sigma (St. Louis, MO, United States). The aromatic extract (LLA) was provided by Euracli (France). Synperonic® PE F68 was furnished by ICI surfactant (Cleveland, United Kingdom). All the aqueous solutions were prepared with ultrapure water (Milli Q Plus, Millipore, Molsheim, France). Ethanol and sodium chloride were of analytical grade and obtained from Prolabo (Paris, France).

For VE estimation, methanol (HPLC grade) was obtained from Carlo Erba Reagenti (Val de Reuil, France) and decane (spectroscopic grade) from Acros Organics (Geel, Belgium).

LLA quantification was performed using linalool from Touzart and Matignon (Paris, France) and

pentane (spectroscopic grade +99%) from Acros Organics (Geel, Belgium).

BZC content was estimated using chloroform (synthetic grade 99.9%) from SDS (Peypin, France), sulphuric acid (analytical grade 96%) from Carlo Erba Reagenti (Val de Reuil, France), sodium hydroxide 0.1N standard solution from Distilab (Caen, France), sodium dodecylsulfate or sodium laurylsulfate (SDS, analytical grade 99%) from Sigma (St. Louis, United States), benzethonium chloride 0.00398N standard solution from Prolabo (Paris, France), Patent blue VF or blue disulfine VN 150 from Acros Organics (Geel, Belgium), phenolphthalein from Prolabo (Paris, France), and dimidium bromide from Acros Organics (Geel, Belgium).

2.2. Gliadins extraction and purification

Gliadins were extracted from a common wheat flour (Hardi variety) (Larré et al., 1991). Briefly, gluten was freeze dried, ground in a refrigerated grinder and defatted by two extractions with dichloromethane (gluten/solvent ratio: 1/10) for 2 h at 20 °C. After filtration and residual solvent evaporation under reduced pressure, samples of dried powder were stored in an ethanol/water mixture (70/30, v/v) for 4 h at 20 °C. The soluble fractions were then dialysed against distilled water and finally freeze dried.

For this study, the gliadins extract consists of four fractions: α -, β -, γ - and ω -gliadins. The fractions are classified due to their hydrophobicity and to their mean molar mass. This extract has been characterized by high performance liquid chromatography-reverse phase (HPLC-RP). It contains 53.7% of α/β -gliadins, 39.9% of γ -gliadins and 6.4% of ω -gliadins.

2.3. Drug quantification

The choice of the three drugs (VE, LLA and BZC) was made according to their polarity difference. In consequence, their solubility behaviour differs for a given solvent.

VE could be easily characterized by its specific absorption at 295 nm by UV-spectrophotometry. VE quantification is assayed by HPLC-RP at room temperature using a photodiodes array detector (Waters 600, Millenium 32 software, Waters, Milford, United States) at 295 nm, and a 250 mm × 3 mm Nucleosil®

100-5, packed with C₁₈ column (Macherey Nagel, Düren, Germany).

The medium containing LLA is not compatible with a gas phase chromatography (GPC) analysis used to quantify the perfume. First of all, the LLA is extracted from the sample by pentane. LLA solution and pentane are mixed in equal proportion. The LLA transfer is known taking into account its partition coefficient between the two solvents. To determine this partition coefficient, a known LLA quantity is dissolved in aqueous and ethanolic media. This medium is mixed with an equivalent volume of pentane. Then the LLA concentration is quantified in pentane. After collection of the aqueous phase, it is blended with the same volume of pure pentane. The LLA quantification is assayed in pentane. It is repeated until there are no remaining LLA traces in the pentane. The LLA partition coefficient between water and pentane was calculated as a function of extraction number, the initial LLA concentration in the aqueous phase and the experimental LLA concentrations in pentane. When the extraction is completed, 5 µl of the extracted solution is analysed by GPC (Varian 3300 GC-FID, United States) equipped with a flame ionisation detector and an apolar DB 5 column (Scientific Glass Engineering, Australia). The LLA content is measured by the quantification of linalyl acetate and linalool, which are respectively 35.7 and 39.7%.

The T73-258 and T73-320 AFNOR specifications have been adapted to perform the BZC titration. In fact, this quaternary ammonium is a cationic surfactant. Its titration consists of neutralisation by an anionic surfactant, the sodium laurylsulfate (SDS) in a biphasic water/chloroform system in the presence of colour indicators mixture (ethanolic solution of dimidium bromide 0.8% w/v and Patent Blue VF 0.4% w/v). During the neutralisation, a colour indicator salt is formed and confers pink colour to the organic phase. After complete BZC neutralisation, a BZC excess transfers the indicator salt from the organic phase to the aqueous one, which becomes blue and the organic fades up.

2.4. Preparation of drug loaded gliadins nanoparticles

The gliadins nanoparticles were prepared by a desolvatation method described elsewhere (Ezpelleta

et al., 1996; Duclairoir et al., 1999). In the case of VE, to prevent its degradation, the nanoparticle procedure has to be performed in the dark, under a nitrogen flow. Proteins were dissolved in an ethanol/water mixture (62/38, v/v) at 25 °C; the resulting solution was filtered through a 0.1 µm pore sized membrane. Various amounts of drug dissolved in ethanolic solutions were then added to the previous gliadins solution. The nanoparticle formation occurred when 20 ml of this solution were poured into a 0.9% w/v NaCl/water solution containing Synperonic® PE/F 68 (0.5%, v/v) as a stabiliser, at 25 °C, under stirring (500 rpm). The organic solvent was evaporated under reduced pressure, and the resulting suspension was centrifuged (20 000 rpm or 34 900 × g, 15 min). The supernatant was removed and, after three washes in ultra pure water, the loaded pellets were freeze dried and stored at 4 °C in the dark.

2.5. Physicochemical characterization

The size of the nanoparticles was characterized by scanning electron microscopy (Jeol, T330A, Japan).

The surface properties of the nanoparticles, loaded and non-loaded, were analysed by determining their zeta potential in a unimillimolar KNO₃ solution at room temperature. The nanoparticles were observed in very diluted conditions by a Sephy Zetaphorimeter III (Sephy, Limours, France).

The thermogram of nanoparticles, loaded and non-loaded, were obtained using differential scanning calorimetry (DSC) using a Perkin-Elmer DSC7 apparatus (Überlingen, Germany) between –50 and 250 °C. The temperature gradient was 40 °C min^{−1}.

2.6. Drug loading

In order to measure the drug loading, around 1 mg of gliadins nanoparticles containing different amounts of drug was digested in 10 ml of the ethanol/water mixture (62/38, v/v) at 25 °C. The drug content C₁ was tested by the adequate analysis method according to the drug (Section 2.3). For VE, the experiments were performed in the dark under a nitrogen flow, as explained in Section 2.3.

The non-encapsulated drug remaining in the supernatant after the first centrifugation C₂ was also estimated.

With these two data, the drug loading (payload) was calculated as the entrapped drug in nanoparticles/gliadins nanoparticles yield ratio

$$\text{Payload (\%)} = \frac{C_1 \text{ (mg)}}{\text{gliadins nanoparticles yield (mg)}} \times 100 \quad (1)$$

and the entrapment efficiency was calculated as the drug amount in particles/initial drug content ratio

Entrapment efficacy (%)

$$= \frac{C_1 [\text{amount of drug in nanoparticles (mg)}]}{(C_1 + C_2) [\text{initial drug content (mg)}]} \times 100 \quad (2)$$

For comparison of the different entrapped drugs, the dimensionless entrapment efficiency is adequate. But to simplify the comparison between drugs, an optimal drug concentration has been defined as the best compromise between the payload and the entrapment efficiency. This optimal drug concentration is the drug/gliadins ratio obtained at the intersection of payload and entrapment efficiency curves versus drug/gliadins ratio.

2.7. In vitro drug release

About 1 mg of gliadins nanoparticles containing X drug mg gliadins mg^{−1} were resuspended in a release medium under stirring.

In the case of VE, the release profile was performed three times by resuspending 10.1 mg of 824.0 VE µg gliadins mg^{−1} nanoparticles in 10 ml of decane. This solvent has been chosen because of its VE affinity, like most organic solvents. The solubility parameter of gliadins and of decane are respectively 34.5 (Duclairoir et al., 1998) and 19.0 MPa^{1/2} (Barton, 1991). Considering such a difference of solubility parameters, the decane is not able to solubilize the gliadins nanoparticles and even to modify their surface. The release study was performed under nitrogen and in the dark in order to prevent VE loss.

For the BZC release, 741.5 mg of 550.3 BZC µg gliadins mg^{−1} nanoparticles were resuspended in 70 ml of ultrapure water at 25 °C. This release study has been replicated twice. The choice of water has been motivated by its inability to dissolve the gliadins nanoparticles and its ability to solubilize BZC.

For each, the medium was then maintained in a release cell at $25 \pm 0.2^\circ\text{C}$. This original cell is constituted by a double shell leading to an efficient thermostating and by an access allowing easy collecting of aliquots exempted of nanoparticles by filtration through a $0.1 \mu\text{m}$ pore sized membrane. Aliquots of 100 and $700 \mu\text{l}$ have been collected respectively for VE during 120 h and for BZC during 150 h. After each sample collection at successive time intervals, t , an equal amount of thermostated release medium was introduced into the system. Thus, during the whole release, the nanoparticles concentration remained unchanged. The released drug amount, M_t , was evaluated, for each sample, by the adequate analysis technique as regards to the drug. Then the in vitro release is found using the plot of M_t/M_0 versus the time t with M_0 the effective drug loaded amount in the nanoparticles, expressed as “X drug mg gliadins mg^{-1} ”.

3. Results and discussion

3.1. Gliadins nanoparticles characterization

Gliadins, wheat gluten proteins, precipitate into nanoparticles by the desolvatation method known as “nanoprecipitation” (Stainmesse et al., 1995; Alonso, 1996), or coacervation, solvent displacement or drawing-out phenomenon (Mersmann, 1994).

These loaded and unloaded gliadins particles are spherical, as shown by scanning electron microscopy.

3.1.1. Size characterization

The mean volume-average diameters of loaded and unloaded nanoparticles are compiled in Table 1.

To decrease the experimental error on the mean value and to approach the real mean diameter, several micrographs of different places of the sample have to be analysed. The experimental error on the mean volume-average diameter is around 10%.

Although the experimental error due to the characterization method is more important than the difference between the diameters themselves, the number-average diameters obtained by SEM seem to increase with the drug polarity (ε , their dielectric constant) (Maryott and Smith, 1951), as shown Table 1. The more polar the drug, the larger the mean diameter is of loaded particles.

3.1.2. Zeta potential study

In Table 1, are mentioned the zeta potential of loaded particles and the drug polarity represented by its dielectric constant, ε , compiled in the literature. As anticipated, the unloaded nanoparticles are almost uncharged, as are the gliadins themselves.

The VE loaded nanoparticles have a similar ζ . It is explained considering the quite low VE dielectric constant ($\varepsilon = 4$). In the case of LLA, which is slightly polar ($\varepsilon = 8$), the charge is near zero (the error with such a technique is estimated around 3 mV).

The zeta potential of BZC loaded nanoparticles differs according to the drug amount in the particles. BZC is an ionized cationic surfactant ($\varepsilon = 45$). This difference could be explained by the presence of a fraction of the drug present at the particle surface, although the zeta potential does not increase as a function of the increasing loaded BZC concentration, as shown on Fig. 1.

In fact, after zeta potential change, a step value is reached around 25 mV. Such behaviour can be related

Table 1

Size characterization, zeta potential, glass transition temperature, entrapment efficiency and optimal drug concentration obtained for drug loaded nanoparticles according to the dielectric constant of the drug

Particles	Unloaded	VE loaded	LLA loaded	BZC loaded
ε	—	4	8	45
Mean diameter $\pm 10\%$ (nm)	900	900	930	950
Zeta potential (mV)	-1	-1	-1 to -4	20–40 varying with BZC concentration
T_g	145	134	130	110
Entrapment efficiency (%)	—	79.2	82.4	52.3
Optimal drug concentration (μg gliadins mg^{-1})	—	972.0	980.0	550.3

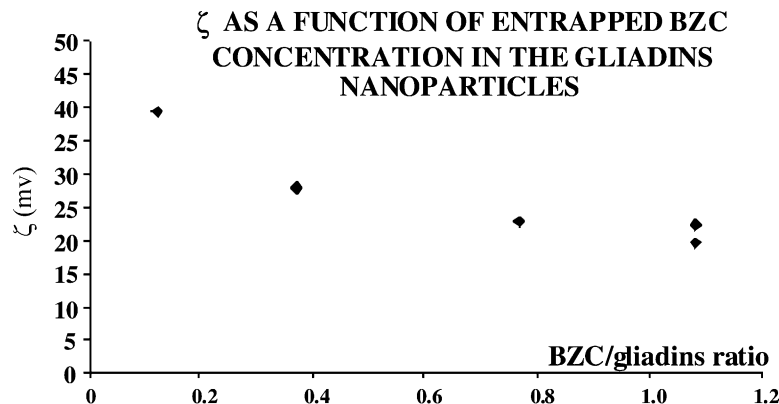


Fig. 1. Zeta potential of BZC loaded nanoparticles versus the drug entrapped concentration.

to the increased amount of charge number in the diffuse double layer inducing a shielding effect of the superficial charge decreasing the zeta potential value (Hunter, 1981).

3.1.3. DSC study

3.1.3.1. Unloaded nanoparticles. Gliadins and the surfactant (Synperonic® PE F68), as well unloaded gliadins nanoparticles were studied.

Gliadins, lead to a large glass transition temperature, T_g , around 165 °C. The surfactant thermogram shows a fusion peak at 52 °C. Then gliadins are blended with surfactant, a unique glass transition appears at 144 °C. The disappearance of the surfactant melting peak could be explained by its low amount or by perfect compatibility of the surfactant in the particle matrix. In any case, its presence is attested by decreasing glass transition temperature and can even be evaluated around 20%.

3.1.3.2. Loaded nanoparticles. Under the same conditions, thermogram of drug loaded nanoparticles show an unique transition corresponding to a glass transition. The corresponding T_g values are compiled in Table 1.

The thermogram of the drugs show no glass transition, but boiling peaks at 210 °C for VE, at 200 and 220 °C for LLA and at 36 °C for BZC. None of these peaks appear on the thermograms of drug loaded particles. For VE or LLA loaded particles, the obtained

T_g are close and their difference is less than the experimental error of 10 °C usually attributed to DSC measurements. For BZC loaded nanoparticles, the T_g seems to decrease in the presence of drug. The BZC boiling point is lower than gliadins T_g and could explain this phenomenon. These results lead to the conclusion that the drug should be, at least, dispersed quite homogeneously inside the particle.

3.2. Drug entrapment study

Payload and entrapment efficiency are dependent on the drug/initial protein ratio.

3.2.1. VE entrapment

Fig. 2 represents the payload and the efficiency versus the VE/gliadins ratio. The encapsulated/initial VE payload increases from 0 to 82% and the encapsulated/initial VE efficiency decreases from 100 to 77%.

The optimal VE concentration is obtained for 972.0 μg VE mg^{-1} gliadins, with at least, an efficiency of 79.2%.

3.2.2. LLA entrapment

The partition coefficient of LLA between gliadins solvent and pentane is 0.630 and allows us to evaluate C_1 , the effective LLA concentration contained in nanoparticles. After centrifugation, C_2 , the remaining LLA concentration in the supernatant, is evaluated with the help of the partition coefficient of LLA between the supernatant and pentane estimated to be 0.204.

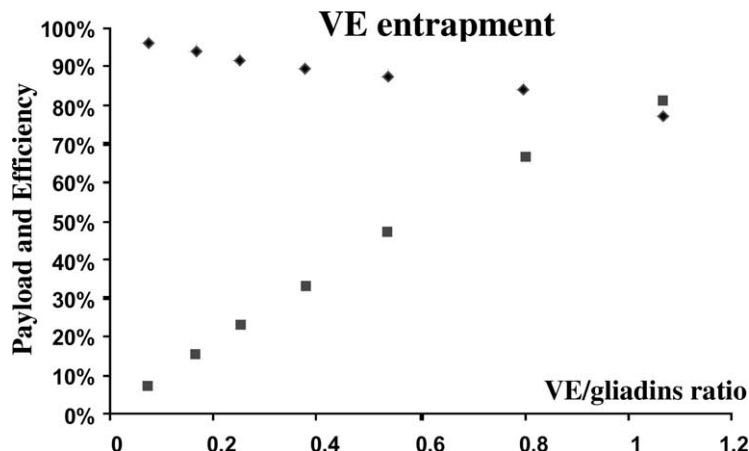


Fig. 2. Payload (■) and entrapment efficiency (◆) of VE loaded gliadins nanoparticles (experiment number $n = 3$).

On Fig. 3, the LLA payload and the LLA entrapment efficiency by gliadins nanoparticles are shown. The former increases from 0 to 94%, as the latter reduces from 100 to 76%.

The optimal LLA concentration corresponds to 980.0 LLA μg gliadins mg^{-1} with an efficiency of 82.4%.

3.2.3. BZC entrapment

BZC payload and BZC entrapment efficiency are plotted in Fig. 4. The efficiency decreases from 83 to 56% and the payload increases from 0 to 53%.

The optimal BZC concentration is achieved for 550.3 BZC μg gliadins mg^{-1} with an efficiency of 52.3%.

3.2.4. Comparison of entrapment capacity of gliadins nanoparticles

Table 1 shows the optimal drug concentration in nanoparticles and the corresponding efficiency for each drug. The close VE and LLA polarities result in similar optimum drug concentrations, including experimental error. Comparing the results of VE and BZC, molecules with a similar molar mass, indicate

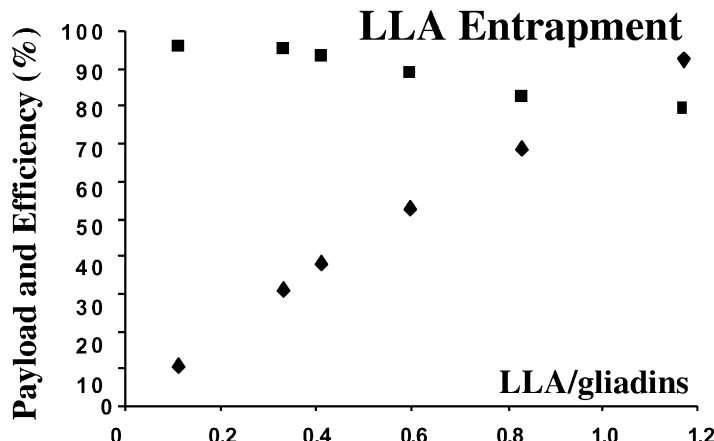


Fig. 3. Payload (■) and entrapment efficiency (◆) of LLA loaded gliadins nanoparticles ($n = 3$).

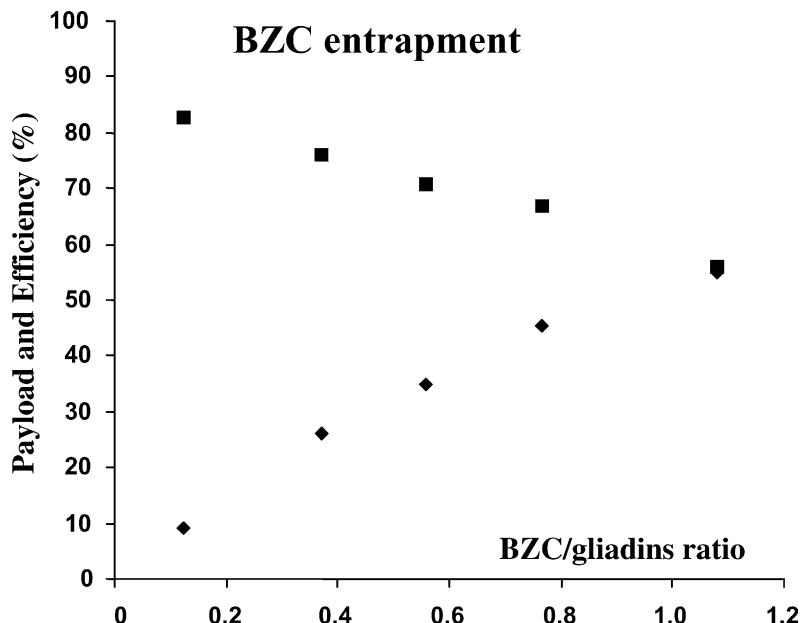


Fig. 4. Payload (■) and entrapment efficiency (◆) of BZC in gliadins nanoparticles ($n = 3$).

that the gliadins nanoparticles have more affinity for VE than for BZC, whose polarity is higher. VE is as apolar as the gliadins. Consequently, for any apolar substance, it could be assumed that gliadins nanoparticles would be able to entrap it with good results.

It can be noticed that BZC entrapment efficiency is reasonable, probably because of the hydrophobic chain of this amphiphilic molecule. These results confirm the low polarity of gliadins, whose ε is probably less than 8. Few results are described in literature concerning plant based nanoparticles and fewer about gliadins nanoparticles. The only interesting paper (Ezpelleta et al., 1996) is related to an entrapment study of all-trans-retinoic acid/gliadins. In this work, the highest ratio is just lower than 10%, the ratio used in our study is higher than 10%, but the corresponding entrapment efficiency are in concordance.

3.3. Drug in vitro release study

The release of two drugs, VE and BZC, has been studied. In fact, LLA should be studied under a controlled atmosphere and not in a liquid medium. Such differences between media used here does not allow an easy comparison to the other drugs.

3.3.1. VE in vitro release study

Gliadins nanoparticle preparations were tested for in vitro release in decane for about 120 h at 25 °C under nitrogen in the dark. During all the experimental period, no VE or no particle degradation was observed. The size and the morphology of nanoparticles have been measured before and after the release by SEM.

Fig. 5 shows that VE is released in two steps, characterized by an initial rapid release (under 1 h) which could be attributed to the adsorbed drug in the superficial zone of the spheres. This phenomenon is like a burst effect. The second releasing period shows a dependency on time and seems to be related to the drug diffusivity inside the matrix systems.

After roughly 3 h, at the break point between the two domains: burst effect and delayed release, the VE amount decreases in the release medium.

This disappearance might be explained by the following hypothesis. During the first period, both VE and surfactant (Synperonic® PE/F68) are released in the medium. This surfactant forms micelles at very low concentrations in decane (lower than 1 mg l^{-1}). Its amount in nanoparticles is evaluated around 20%. Thus, in the vicinity of the particles, its concentration could be sufficient to form micelles. These micelles

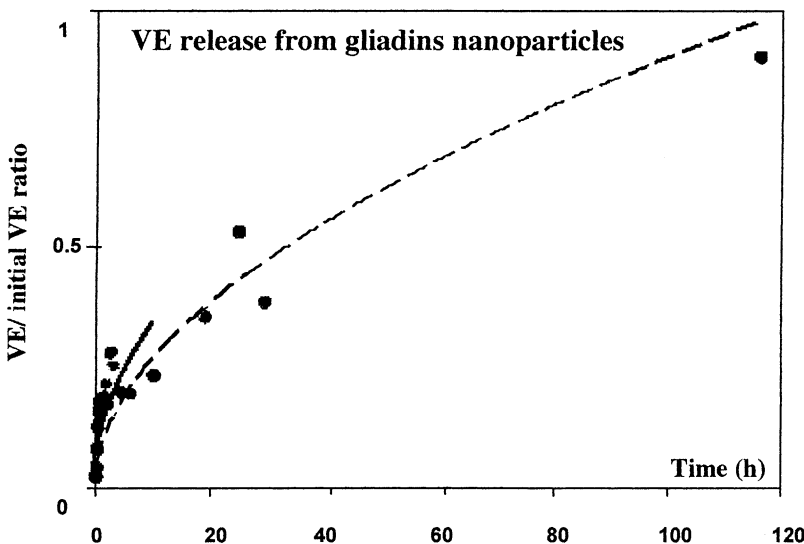


Fig. 5. VE release in decane from 824.0 VE $\mu\text{g protein mg}^{-1}$ loaded nanoparticles at 25 °C fitted by short time model (—) and by medium time model (---) ($n = 3$).

are then able to encapsulate a part of the released VE, playing the role of drug-reservoirs. As VE is entrapped in the surfactant micelles, this should explain the observed fall in VE concentration in the release medium. During the second period, both VE and surfactant continue to be released in the medium.

In order to explain this release profile, an analytical model was applied. As shown by SEM, the particles are spherical. Assuming that the drug is uniformly distributed inside the delivery system, and that these remain stable during all the experimental period, it is known that (Washington, 1996)

$$\frac{M_t}{M_0} = 1 - \frac{6}{\pi^2} \sum_{n=1}^{\infty} \left[\frac{1}{n^2} \exp(-n^2 \tau^2) \right] \quad (4)$$

where M_t is the amount of released drug at t time, and $(1 - (M_t/M_0))$ the released amount and t is given by

$$\tau = \frac{Dt}{R^2} \quad (5)$$

with D the drug diffusion coefficient through the particle and R the particle radius.

This relation is simplified for the first releasing period, i.e. the first few percent decays

$$\frac{M_t}{M_0} = 6 \sqrt{\frac{\tau}{\pi}} \quad (6)$$

For the second period, the medium release time, this relation becomes

$$\frac{M_t}{M_0} = 6 \sqrt{\frac{\tau}{\pi}} - 3\tau \quad (7)$$

For longer times, a simplification of Eq. (4) is

$$\frac{M_t}{M_0} = 1 - \frac{6}{\pi^2} \exp(-\pi^2 \tau) \quad (8)$$

Sometimes, the release can be extensively described only by the short and long time model as shown by Guy et al. (1982).

The release has been fitted by this model for the first released drug and by the one for medium times, i.e. Eqs. (6) and (7). r^2 , the correlation coefficient, is respectively 0.7321 and 0.9010. Obviously, the model of the first stage does not describe the experimental data. The difference could probably be explained by an underestimation of the burst effect by this diffusion model, and even, by experimental errors (less than 1%), but the hypothesis of drug-reservoir micelles could be an interesting complementary explanation.

For the second period, when the model for medium times is taken into account, the fit is close to the data. Then, the VE diffusion coefficient, D , through the gliadins nanoparticles can be determined; D/R^2 is $2.00 \times 10^{-4} \text{ s}^{-1}$. As the average particle radius

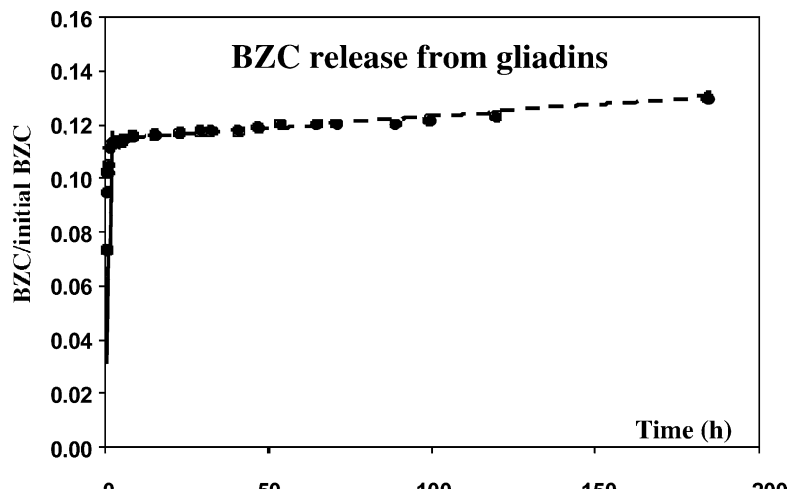


Fig. 6. BZC release in ultra pure water from $550.3 \text{ VE } \mu\text{g protein mg}^{-1}$ loaded nanoparticles at 25°C fitted by short time model (—) and by long time model (---) ($n = 3$).

is $0.45 \mu\text{m}$, the VE diffusion coefficient through the gliadins nanoparticles is estimated around $4.1 \pm 0.1 \times 10^{-5} \mu\text{m}^2 \text{ h}^{-1}$, i.e. $6.0 \pm 0.3 \times 10^{-20} \text{ m}^2 \text{ s}^{-1}$.

3.3.2. BZC *in vitro* release study

The *in vitro* release was performed at 25°C during more than 150 h in ultra pure water. The BZC release profile is represented in Fig. 6.

In less than 30 min, a rapid release occurs until 11% of the total released amount. This first period can again be attributed to the drug desorption from the particle surface. Then the drug diffuses very slowly inside the nanoparticles; in fact, in more than 150 h, only a further 2% of the drug is released after the initial rapid release.

Once again, BZC kinetics is fitted by the model of a diffusion process in a homogenous sphere. SEM confirms that nanoparticles size remains constant before and after the drug release. After fitting, the data by Eqs. (6) and (8), i.e. short and long time models, r^2 values are respectively 0.5367 and 0.9669. Again, the data are not fitted properly by the short time model. As for VE release, the diffusion process in a homogeneous sphere underestimates the “burst effect”. It can be noticed that there is no BZC decrease, as for VE. It is not surprising, because no micelle formation can occur at such concentrations of the PE F68 surfactant

in ultra pure water. Indeed in these conditions, the critical micellar concentration is 70 g l^{-1} .

The evaluation of BZC diffusion coefficient, D , is based on the long time model, for which D/R^2 equals $1.01 \times 10^{-4} \text{ s}^{-1}$. As the mean particle diameter is $0.475 \mu\text{m}$, the BZC diffusion coefficient through the gliadins nanoparticles is evaluated around $2.3 \pm 0.1 \times 10^{-5} \mu\text{m}^2 \text{ h}^{-1}$, i.e. $6.0 \pm 0.3 \times 10^{-21} \text{ m}^2 \text{ s}^{-1}$.

3.3.3. Comparison of release studies

In organic phases, diffusion coefficients are usually about $10^{-9} \text{ m}^2 \text{ s}^{-1}$. Here the coefficients are clearly much lower ($1.12 \times 10^{-20} \text{ m}^2 \text{ s}^{-1}$ for VE and $6.36 \times 10^{-21} \text{ m}^2 \text{ s}^{-1}$ for BZC). Thus, these results confirm that the drug is retained by the nanoparticle matrix Table 2.

The diffusion coefficient obtained using the homogeneous sphere model is different according to VE and BZC. This could be related to the different drug affinity for gliadins.

After 30 h, about 30% of encapsulated VE are released; on the other hand, after the same time, only 11% are released for BZC. This remark is verified more accurately after 120 h. Indeed, the release media are different for both drugs. However, the drug release process is related to the particle permeability, P , of each specific drug. In fact, this is a function of the drug

Table 2

Drug released percentage as a function of the release period and the drug diffusion coefficient through the loaded nanoparticles observed and compiled according to the drug

PA	Time (h)	Released drug (%)	Diffusion coefficient ($\text{m}^2 \text{s}^{-1}$)
VE	1	13.2	1.12×10^{-20}
	30	30.6	
	120	70.1	
BZC	1	11.1	6.36×10^{-21}
	30	11.7	
	120	12.3	

diffusion coefficient, D_{drug} , across the particle and of the drug partition coefficient, K_{drug} , between the particle and the release medium as shown in Eq. (9).

$$P = \frac{K_{\text{drug}} \times D_{\text{drug}}}{d} \quad (9)$$

with d the distance covered by the drug through the nanoparticle, i.e. in this case, the particles radius. For both drugs, the nanoparticles radii are equivalent, thus d is similar and cannot explain the factor of two between the diffusion coefficients.

The only modified parameter between the two cases is K_{drug} . The most appropriate explanation may be that K_{drug} for the (VE/gliadins nanoparticles/decane) system is lower than for the (BZC/gliadins nanoparticles/water) system.

In the literature, the all-trans-retinoic acid (RA) release has been observed from gliadins nanoparticles (Ezpellesta et al., 1996), in 100 ml of PBS at pH 7.4 with 15 mg of gliadins nanoparticles containing 60 RA μg gliadins mg^{-1} . A similar two steps profile is observed. The first 20% is released by a burst effect. After the third hour, a slower release takes place. Ezpelleta et al. (1996) had supposed that the phenomenon is ruled by a diffusion process. After 3 h, a similar amount of vitamins (RA and VE) is released by gliadins nanoparticles: around 20% for RA and 25% for VE, even if the conditions of temperature and of drug/release medium are not identical.

4. Conclusion

In conclusion, by a desolvatation method, drug loaded gliadins nanoparticles are obtained with a

mean radius about 450–475 nm. Three drugs of different polarity: hydrophobic Vitamin E, slightly polar aromatic mixture and amphiphilic cationic benzalkonium chloride were entrapped in the nanoparticles. The closer the drug and gliadins polarity, the better the drug entrapment. The release from loaded particles, of Vitamin E and of benzalkonium chloride, has been studied and interpreted as a burst effect completed by a drug diffusion process through the particle modelled as a homogenous sphere. The diffusion coefficients of the two drugs measured during the release are of several decades much smaller than in pure liquids. This confirms the strong entrapment of the drug in the nanoparticles.

These results show that the gliadins nanoparticles are suitable controlled released systems for hydrophobic and amphiphilic drugs.

Acknowledgements

Authors are indebted to the “Réseau Matériaux, Polymères, Plasturgie” (Basse Normandie—Haute Normandie, France) for financial support.

References

- Alonso, M.J., 1996. Nanoparticulate drug carrier technology. *Drug Pharm. Sci.* 77, 203–242.
- Aubeny, E., Colau, J.C., Nandeuil, A., 2000. Local spermicidal contraception: a comparative study of the acceptability and safety of a new pharmaceutical formulation of benzalkonium chloride, the vaginal capsule, with a reference formulation, the pessary. *Eur. J. Contracept. Health Care* 5, 61–67.
- Barton, A.F.M., 1991. *Handbook of Solubility Parameters and Other Cohesion Parameters*, 2nd ed. CRC Press, Boca Raton.
- Bigelow, C.C., 1967. On the average hydrophobicity of proteins and the relation between it and protein structure. *J. Theor. Biol.* 16, 187–221.
- Chasin, M., Langer, R., 1990. *Biodegradable Polymers as Drug Delivery Systems*, Marcel Dekker, New York.
- Dhillon, A.S., Winterfield, R.W., Thacker, H.L., 1982. Quaternary ammonium compound toxicity in chickens. *Avian Dis.* 26, 928–931.
- Duclairoir, C., Nakache, E., Marchais, H., Orecchioni, A.M., 1998. Formation of gliadin nanoparticles: influence of the solubility parameter of protein solvent. *Colloid Polym. Sci.* 276, 321–327.
- Duclairoir, C., Irache, J.M., Nakache, E., Orecchioni, A.M., Chabenat, C., Popineau, Y., 1999. Gliadin nanoparticles: formation, all-trans-retinoic acid entrapment and release, size optimization. *Polym. Int.* 79, 327–333.

- Epstein, J.H., 1983. Photocarcinogenesis, skincancer and aging. *J. Am. Acad. Dermatol.* 9, 487–502.
- Ezpelleta, I., Irache, J.M., Stainmesse, S., Chabenat, C., Gueguen, J., Popineau, Y., Orecchioni, A.M., 1996. Gliadin nanoparticles for the controlled release of all-trans-retinoic acid. *Int. J. Pharm.* 131, 191–200.
- Guy, R.H., Hadgraft, J., Kellaway, I.W., Taylor, M.J., 1982. Calculations of drug release rates from spherical particles. *Int. J. Pharm.* 11, 109–207.
- Hunter, R.J., 1981. Zeta Potential in Colloid Science: Principles and Applications, Academic Press, London.
- Idson, B., 1992. Dry skin moisturizing and emolliency. *Cosm. Toil.* 107, 69–78.
- Kagan, V., Witt, E., Goldman, R., Scita, G., Packer, L., 1992. Ultraviolet light induced generation of vitamin E radicals and their recycling. A possible photosensitizing effect of vitamin E in the skin. *Free Radic. Res. Comm.* 16, 51–54.
- Koga, T., Terao, J., 1996. Antioxidant behaviours of vitamin E analogues in unilamellar vesicles. *Biosci. Biotechnol. Biochem.* 60, 1043–1045.
- Larré, C., Popineau, Y., Loisel, W., 1991. Fractionation of gliadins from common wheat by cation exchange FPLC. *Cereal Chem.* 14, 231–241.
- Lis-Balchin, M., Hart, S., 1999. Studies on the mode of action of the essential oil of lavender (*Lavandula angustifolia* P. Miller). *PTR Phytother. Res.* 13, 540–542.
- Marty, J.P., 1998. Vitamins and Skin Aging. Intensive Course in Dermato-cosmetic Sciences, Vrije Universiteit Brussel, Brussels, pp. 115–140.
- Marty, J.P., Wepierre, J., 1994. Percutaneous absorption of cosmetics: implication in safety and efficacy. In: Baran, R., Maibach, H.I. (Eds.), Cosmetic Dermatology, Martin Dunitz Ltd., London, UK.
- Maryott, A.A., Smith, E.R., 1951. Table of Dielectric Constants. In Circular 514, National Bureau of Standards, New York.
- Mayer, P., Pittermann, W., Wallat, S., 1993. The effects of Vitamin E on the skin. *Cosm. Toil.* 108, 99–109.
- Mersmann, A., 1994. Crystallization Technology Handbook, Marcel Dekker, New York.
- Nakache, E., Poulain, N., Candau, F., Orecchioni, A.-M., Irache, J.M., 2000. In: Nalwa, H.S. (Ed.), Handbook of Nanostructured Materials and Nanotechnology, Academic Press, New York.
- Patterson, T.F., 1956. *Am. Rev. Tub.* 74, 284–288.
- Popineau, Y., Denery-Papin, S., 1995. Protéines de réserve du grain de blé. In: Godon, B. (Ed.), Protéines végétales, Lavoisier (collection sciences et techniques agro-alimentaires), Londres, New York, Paris, pp. 120–172.
- Psychoyos, A., Creatasas, G., Hassan, E., Georgoulas, V., Gravanis, A., 1993. Spermicidal and antiviral properties of cholic acid: contraceptive efficacy of a new marginal sponge (Protectaid) containing sodium chlorate. *Hum. Reprod.* 8, 866–869.
- Sober, A.J., 1987. Solar exposure in the etiology of cutaneous melanoma. *Photodermatology* 4, 23–31.
- Stainmesse, S., Orecchioni, A.-M., Nakache, E., Puisieux, F., Fessi, H., 1995. Formation and stabilization of a biodegradable polymeric colloidal suspension of nanoparticles. *Colloid. Polym. Sci.* 273, 505–511.
- Tamburic, S., Abamba, G., Ryan, J., 1999. Moisturizing potential of D- α -tocopherol. *Cosm. Toil.* 114, 73–82.
- Teglia, A., Secchi, G., 1994. New protein ingredients for skin detergency: relative wheat protein–surfactant complexes. *Int. J. Cosmet. Sci.* 16, 235–246.
- Thies, C., 1996. A survey of microencapsulation processes. In: Benita, S. (Ed.), Microencapsulation: Methods and Industrial Applications. Marcel Dekker, New York, pp. 1–20.
- Wainberg, M.A., Spira, B., Bleau, G., Thomas, R., 1990. Inactivation of human immunodeficiency virus type 1 in tissue culture fluid and in genital secretion by the spermicide benzalkonium chloride. *J. Clin. Microbiol.* 28, 156–158.
- Washington, C., 1996. Drug release from microparticulate systems. In: Benita, S. (Ed.), Microencapsulation: Methods and Industrial Applications. Marcel Dekker, New York, pp. 155–181.
- Wester, R.C., Maibach, H.I., 1997. Absorption of tocopherol into and through human skin. *Cosm. Toil.* 112, 53–57.

P8

Gliadin Characterization by Sans and Gliadin Nanoparticle Growth Modelization

Anne-Marie Orecchioni^{1,*}, Cécile Duclairoir², Denis Renard³, and Evelyne Nakache⁴

¹Professeur émérite, Université de Rouen, 1 allée des Tilleuls, 92330 Sceaux, France

²Laboratoire de Microbiologie du froid, UPRES 2127, IUT d'Evreux, 55 rue Saint Germain, 27000 EVREUX, France

³INRA, Centre de recherches de Nantes, rue de la Géraudière, 44316 NANTES, Cedex 3, France

⁴ENSI-CAEN-Université de Caen, UMR 6507 CNRS, Groupe "Polymères et Interfaces"

6 Avenue Maréchal Juin, 14050 CAEN, Cedex, France

Nanosized colloidal carriers can ensure a controlled and targeted therapeutic substances delivery. The original contribution of this work was to use biopolymers of vegetable source, which are an interesting alternative to synthetic polymers. The aim of this study was to prepare submicronic particles from wheat proteins: Gliadins extracted from gluten. The carrier preparation was based on the desolvatation of the macromolecules by a couple solvent/non-solvent of the proteins. In a first step, it was of interest to elucidate the gliadin macromolecular conformation in order to understand the mechanism of nanoparticle formation. The experimental work was based on SANS experiments. Because the size of the colloidal particle suspension is an important parameter to monitor, the modelization of the particle growth was thoroughly studied. Furthermore, it was observed that the determination of the solubility parameters of the proteins allowed optimization of the size of the particles. From those previous experimental results it can be concluded that there is a correlation between the protein conformation in the solvent and the size of the nanoparticles (NP).

Keywords: Nanoparticles (NP), Protein Conformation, Gliadin, Solubility Parameter, Nucleation, NP Growth, SANS Experiments.

1. INTRODUCTION

Since a few decades, nanoparticles (NP), objects of submicronic size, have focused interest in the medical or pharmaceutical field, particularly those which consist of biopolymers such as lipids, polysaccharides, or proteins. These colloidal systems are very promising for their ability to encapsulate drugs in order to protect them from degradation by environmental stress (light, oxygen, heat,...). Moreover, drug loading of such carriers may insure a controlled release of the therapeutic substance towards specific target in the organism, increase its effectiveness, decrease its losses as well as its possible harmful side effects.^{1–4} Furthermore, such nanoparticulate systems offer many potentialities in various domains other than medicine or pharmacy: food industry, cosmetology, detergency, oil industry, ...^{5,6}

NP can be formed from variety of materials including synthetic polymers⁷ and biopolymers (i.e., natural compounds) such as proteins, lipids, and carbohydrates.^{8–12} Natural macromolecules from vegetable sources appear to be a very promising alternative to synthetic polymers

owing to their safety, especially those used as a food source. The selection of a suitable structure material has a very important influence on its potential medical use. It needs to be non toxic, non antigenic, and able to be degraded *in vivo*. Comparing plant and animal proteins, it appears that vegetable proteins may be more available and cheaper than animal proteins.

In general, vegetable protein NP display a number of interesting advantages. Among them, these carriers are biocompatible, biodegradable, metabolizable, and prions free. Moreover, they can be prepared under mild conditions, without the use of toxic organic solvents or materials, and they can incorporate a wide variety of drugs in a relatively non-specific fashion.^{13–17}

Taking into account all these advantages of plant proteins, this particular contribution will focus particularly on the use of storage proteins from wheat gluten (gliadins) when used as structural material to prepare nanoparticles, and their possible applications in pharmacy and medicine.

Wheat gluten is a protein carbohydrate complex, the proteins of which are the major component. In gluten two main fractions are present: Gliadins, (a group of proteins) made of single chain polypeptides (average molecular

*Author to whom correspondence should be addressed.

weight 25–100 kDa) linked by intramolecular disulphide bonds, soluble in neutral 70% ethanol, and glutenins, alcohol-insoluble fraction, consisting of gliadin-like subunits stabilized by intermolecular disulphide bonds in large aggregates (molecular weight greater than 106 kDa).¹⁸ Gliadins are polymorphic and can be separated and classified on the basis of their electrophoretic mobility at acid pH values in four fractions: α (molecular mass 25–35 kDa), β (30–35 kDa), γ (35–40 kDa), and ω (55–70 kDa).^{19–22} All fractions have remarkably low solubility in aqueous solution, except at extreme pH. This low water solubility has been attributed to the presence of interpolyptide disulphide bonds and to the cooperative hydrophobic interactions.

In the present investigation, the preparation method of gliadin NP was studied. In a first step, the principles of gliadin extraction were reported. Then their solubilization was studied by applying the solubility parameter approach. In a third step, the gliadin macromolecular conformation was investigated by Small Angle Neutron Scattering (SANS) experiments. Finally, the NP growth was modeled. This theoretical and experimental work could allow us to determine the relation between the solubilization parameters involved in the formation of gliadin NP and the size of NP.

2. MATERIAL AND METHODS

2.1. Materials

Gliadins were extracted and purified and provided graciously by Dr. Y. Popineau of the Laboratory ... Biochimie et Technologie des protéines de l' INRA de Nantes (France)²³

2.1.1. Gliadin Extraction

For this study, 2 batches of gliadins were used: An extract from corn flour of Renan variety (gliadin G2), the other of Hardy variety (gliadin G3). Each of these batches are a mixture of the four fractions (*vide supra*). For the sake of simplicity, we will consider that each mixture is a single protein: Gliadin G2 or gliadin G3.

For gliadin G2 the flour was delipidated in order to eliminate soluble and amphiphilic proteins. This favor gliadin extraction with a very low glutenins fraction.^{24–26} Briefly gluten was obtained after extraction of 1 g of wheat flour of Renan variety in a sodium phosphate 0.05 M pH 7.8 buffer, then in a NaCl 0.1 M and triton X 114 (20 g/L) solution.^{25, 26} These different steps allow to obtain gluten without glutenins. Then gliadin G2 extraction was performed with 70/30 ethanol/water mixture (v/v). The soluble fraction is dialysed first against water, then against acetic acid 0.05 M. Finally gliadin obtained is lyophilized.

For gliadin G3, gluten was extracted on a preparative scale.²¹ It was freeze dried, ground in a refrigerated grinder and defatted by two extractions with dichloromethane for

2 h at 20 °C (gluten/solvent ratio: 1/10). After filtration, residual solvent was evaporated from the gluten at 20 °C under reduced pressure. Samples of dried gluten powder were stirred gently in an ethanol/water mixture 70/30 (v/v (gluten/solvent ratio: 1/10) for 4 hours at 20 °C. The suspension was centrifuged (10000 \times g, for 20 mn). The soluble fraction, consisting of gliadin was dialysed exhaustively first against water, and then against 0.05 M acetic acid. Finally, gliadin G3 was freeze dried.

The difference between gliadin G2 and gliadin G3 resides in the lack of glutenins in the constitution of gliadin G2.

2.1.2. Other Materials

Ultrapure water was prepared with a Milli Q Plus apparatus (Millipore, Molsheim, France). Sodium chloride NaCl was of analytical grade (Merck, Darmstadt, Germany). Pure absolute ethanol at 99.5% was provided by Carlo Erba Reagenti (Val-de-Reuil, France). Synperonic® PE F68 was furnished by ICI Surfactant (Cleveland, U.K.).

For SANS experiments: Deuterated water D₂O-99.90%D and deuterated ethanol C₂D₆O-99.00% with HDO+D₂O < 0.3% were provided by Euristop (Gif-sur-Yvette, France).

2.2. Methods

2.2.1. Gliadin G2 and G3 Solubilization

According to the nature of vegetable proteins, the size control of the NP may be reached by varying the nature of the solvent. In order to understand the solvent effect, the size diameter was examined through a solubility parameter study.^{27, 28}

Hildebrand²⁸ defined the solubility parameter δ correlated to the mixing enthalpy for endothermic simple mixtures. In the case of a polymer/solvent mixture, it was assumed that the miscibility of the polymer in the solvent is possible if $\delta_1 = \delta_2$ with 1 and 2 representing respectively the solvent and the polymer. For classical solvents, δ_1 can be found in the literature²⁹ and is expressed in (Mpa^{1/2}). The solubility parameter δ_M of a mixture (for instance water/ethanol) is determined by the relation $\delta_M = \phi\delta + \phi'\delta'$ where δ and δ' are the solubility parameters of ethanol and water and ϕ and ϕ' their volume fraction ($\phi + \phi' = 1$). Different mixtures were prepared with ultra pure water and ethanol which solubility parameters were respectively 47.8 and 26.5 (Mpa^{1/2}). 0.1% gliadin solutions were prepared in EtOH/H₂O mixtures of different δ_M ranged between 39.1 to 32.9 (Mpa^{1/2}). The determination of the solubility parameters of gliadin, was inspected for homogeneity and transparency by turbidity measurements.

2.2.2. Determination of Gliadin Structure by SANS

SANS experiments allow observation at scales smaller than light wavelength, i.e., smaller than a few ten of

nanometers. Macroscopic characteristics of a protein can be determined such as the shape and the molar mass of the molecule.

The experiments were performed in the Laboratory LLB of the Research Center of CEA (Saclay, France). The apparatus used was “G2-3 Small Angle Neutron Scattering Facility PAXY,” a SANS spectrometer for high resolution (in q space) studies. The instrument is installed at the end of the cold neutron guide G2. Incoming polychromatic neutrons are monochromatized by a mechanical velocity selector from which the spectral range extends between 3 and 20 Å with a resolution of approximatively 10%. The wave length may vary from 0.4 to 2 nm. The sample holder is equipped with a double goniometer and two independent rotating tables. The BF_3 multidetector can be positioned at any distance between 1 and 7 m from the sample in its vacuum tube. The collimation of the incident beam is carried out using diaphragms disposed at 2.5 and 5 m along the 7 m vacuum tube. The scattering angle range (2θ) extends from 0 to 60° for distance sample detector <3.5 m. The data treatments can be done by using available home programs on PC.

The neutronic diffusion corresponds to the structure observation through a disc of radius $2\pi/q$. q is the diffusion vector, it is defined by the following equation

$$Q = 4\pi \sin(2\theta)/\lambda \quad (1)$$

θ is the diffusion angle while the wave length of the incident beam is λ .

According to the diffusion vector q observed, the shape and the molar mass of the molecule can be determined.

Compared to small molecules, proteins exhibited enhanced flexibility and multiple conformations.³⁰ The gliadin conformation promoted large discussions. Some authors^{31, 32} showed that in a 70/30 v/v EtOH/H₂O mixture gliadins are prolate ellipsoids. Other authors by Small Angle X-rays Scattering (SAXS) studies³³ showed that the modelization of the gliadin conformation was represented by a cylinder. SANS experiments should allow to elucidate the proper conformation of the protein.

In the Guinier domain,³⁴ the diffusion is due to the whole structure characterized by the gyration radius R_g of the macromolecules, theoretically defined as the mean square root of the square of the distance of the chain length from the gravity center.

R_g is calculated from the slope of the curve $\ln I(q) = f(q^2)$, with $I(q)$ the diffused intensity. R_c , the radius of the section of the macromolecule, and its length L are calculated from the slope of the curve $\ln(qI) = f(q^2)$.

According to the presumed shape of the macromolecule, R_g and R_c allow to reach the characteristical parameters of the macromolecule geometry:

— for a prolate ellipsoid of major axis a and minor axis b ,

$$R_g = a^2/5 + b^2/10 \quad \text{and} \quad R_c = b\sqrt{2} \quad (2)$$

— for a cylinder of length L and radius R ,

$$R_g^2 = L^2/12 + R^2/2 \quad \text{and} \quad R_c = R\sqrt{2} \quad (3)$$

2.2.3. Preparation of Protein Nanoparticles

Several methods have been reported in the literature for the preparation of nanoparticles from protein raw materials. Coacervation or controlled desolvatation methods have been developed using solvent or electrolyte as the coacervation agent or by adjusting the pH or the ionic strength.^{14, 15, 35-37} In the coacervation methods promoted by solvents, the first step consists in dispersing the macromolecules in an adequate solvent (good solvent, GS), then adding the mixture to a second solvent which is a non solvent (NS) of the macromolecules. A required condition is that the solvent and the non solvent phases are miscible. Recent publications,^{38, 39} which were interested in the precipitation of synthetic polymers, pointed out that the “Ouzo effect,” i.e. a spontaneous emulsification process, is at the origin of the phenomenon. It enables one to create a dispersion of small droplets in a surrounding liquid phase without the use of surfactants, clouding the precipitation medium. According to this observation, the Ouzo effect could be used for preparing a variety of aqueous dispersions including NP.

The coacervation process is applied to a macromolecular solution to reduce the solubility in the system to such a degree that appropriate phase separation of the macromolecule takes place, that is the formation of a macromolecule-rich phase. The desolvatation leads to macromolecule precipitation or to coacervate formation. The phase separation is induced by a phenomenon of the polymer supersaturation (solvent evaporation, variation in temperature, pH, addition of non-solvent of the polymer, addition of ionic reactants, ...). It is assumed⁴⁰ that, before phase separation is observed, a conformational change in the macromolecule occurs. The addition of a desolvating agent (NS) shrinks the macromolecule coil which becomes smaller and smaller until the phase separation from the solvent occurs. It is possible to monitor the phenomenon by turbidity measurement. A desolvatation agent decreases the turbidity because of the decrease in macromolecular size. To prepare small particles, it is important to maintain the system just outside the coacervation region. The addition of the coacervation agent should stop as soon as the Tyndall effect bounded to the macromolecules aggregation turns the system turbid.¹³ It was interesting to point out that these observations are in contradiction with the Ouzo effect suggested by Vitale et al. and Ganachaud et al.^{38, 39} The Tyndall effect observed in the case of gliadin NP occurred at the end of the nanoprecipitation instead of promoting the precipitation.

For the preparation of gliadin nanoparticles, gliadin G3 was chosen. The desolvatation method for gliadin NP preparation was previously described by Ezpeleta et al.¹³

Briefly, 0.5% w/v of gliadin were solubilized in 20 ml of an ethanol/water phase. After filtration through a 0.45 μm membrane, the ethanolic solution was poured into a 40 ml of a constantly magnetically stirred physiological saline solution (0.9% w/v NaCl) containing 0.5% w/v Synperonic® PE/F68 as stabilizer. The ethanolic solvent was then eliminated by evaporation under reduced pressure with a Rotavapor R114 (Büchi, Switzerland). Gliadin NP thus prepared were purified by centrifugation, Sigma 3K30 centrifuge (Bioblock Scientific, Illkirch, France) equipped with a 12159 rotor. The NP were resuspended in 2 ml of supernatant by ultrasonification for 3 sessions of 5 minutes. NP were freeze dried and stored at 4 °C in the dark.

In order to determine the size of the NP, samples were taken at constant intervals of time from the mixture protein/GS/NS. The diameters were analysed by SEM using a JSM T330A (JEOL, Japan) instrument. To decrease the experimental error on the mean value and to approach the real mean diameter, at least 5 micrographs were taken from different places of each sample. Thus about 250 NP were measured, and the experimental error was about 10%.

The particle size was also determined by Quasi-elastic Light Scattering (QELS), with the help of a Malvern instrument (France) equipped with an ALV 5000 correlator having 256 digital counters.

3. THEORETICAL BACKGROUND

When the protein in its GS is introduced in the NS two kinds of precipitate can occur: Either small crystals,⁴¹ or an amorphous precipitate promoted by Van der Waals forces between macromolecules.

Works of La Mer⁴² and Mersmann⁴³ will be taken in account as models. They pointed out two consecutive and competitive steps which are nucleation and crystal growth.

3.1. Supersaturation and Precipitation Process

The energy concerned in a precipitation process (for instance by adding a non-solvent) is the chemical potential variation

$$\Delta\mu = kT \ln(C/C^*) \quad (4)$$

with C the solute concentration in the GS and C^* the saturation concentration in the NS, i.e., the maximum dissolution concentration of the macromolecule. If $C > C^*$ when the solute precipitates, the solution is called supersaturated.

If β is the ratio C/C^* , Eq. (5) becomes

$$\ln \beta = \Delta\mu/kT \quad (5)$$

Figure 1 represents the diagram of solubility of a polymer according to the concentration of the precipitating

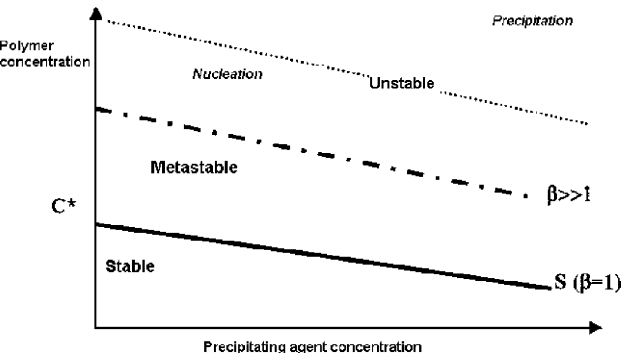


Fig. 1. Macromolecule concentration variation according to precipitating agent concentration.

solvent.⁴¹ Four zones coexist. The curve of solubility S represents the limit of solubility (or saturation) of the solute in solution, i.e. β is equal to 1. For concentrations in molecule lower than C^* , the solute is soluble in solution (stable zone). Above S , supersaturation is reached ($\beta > 1$). According to the β value, three kinds of behavior can be observed:

— $\beta \gg 1$, the solute excess precipitates instantaneously and gives an amorphous precipitate

— β is weaker but still greater than 1, the solute crystallizes in the nucleation zone. Near the precipitating zone crystallization generates very small and numerous microcrystals.

Finally for the metastable zone, β is about equal to 1, the nucleation process cannot occur. However the nuclei yet formed are growing, generating eventually new germs by shocking one to the others or against a wall (heterogeneous nucleation).

Different authors suggest that a second nucleation step occurs, called a secondary or heterogeneous nucleation.

3.2. Nucleation and Particle Growth Process

Nucleation was defined by La Mer⁴² as “the process generating from a metastable mother phase the initial fragments—nuclei or germs—of a new more stable phase which will evolve thereafter and spontaneously towards the stable entities of more important size.”

According to Galkin,⁴⁴ classical models established by La Mer and Mersmann were a good approximation of what happens in fact. Indeed several authors^{45,46} considered that classical nucleation theories account perfectly for crystallisation or precipitation of amorphous objects. They suggested that, in spite of the complexity of the structure of the proteins and their behavior in solution, there are important similarities between the mechanisms and the kinetics of precipitation of proteins and those of inorganic salts.

However, for proteins the nucleation step is very limited in time. For a high saturation, the nucleation rate is important even instantaneous.^{47–50}

3.3. Particle Growth Process

The growth process of a colloidal particle was studied by Sugimoto.⁵¹ According to this author, for a colloidal particle, the first step of growth begins by diffusion of a solute molecule towards the surface of the solution. It is followed by the integration of this molecule to the surface.

Assuming that R is the particle radius, δ the thickness layer, and x the distance from the particle center, the molecular diffusion flux J passing through the spherical surface of radius x in the diffusion layer is given by Fick's law.

If C_1 is the solute concentration at the solution/surface interface, the diffusion flux is given by relation (6)

$$J = 4\pi DR(R + \delta)(C - C_1)/\delta \quad (6)$$

D is the diffusion coefficient

J is related, on the other hand, to dR/dt

$$J = 4\pi R^2/V_m \cdot dR/dt \quad (7)$$

V_m is the macromolecule molar volume

The diffusion process is followed by the integration process of a molecule in the surface

$$J = 4\pi R^2 k(C_1 - C^*) \quad (8)$$

k is the integration constant. The integration process is assumed to be a first order process.

From the two previous equations, it can be deduced

$$(C_1 - C^*)/(C - C_1) = D(1 + R/\delta)/kR \quad (9)$$

According to the literature, two approaches seemed to be the more appropriate to explain protein precipitation.^{41,48}

3.3.1. Growth Controlled by the Diffusion Process

If growth is controlled by the diffusion process, the diffusion coefficient D could be expressed by the relation $D \ll kR$, which leads to $C_1 = C^*$. It can be shown that:

$$dR/dt = DV_m(1/R + 1/\delta)(C - C^*) \quad (10)$$

It can be noticed that dR/dt decreases when R increases, which means that the variation of R with time becomes smaller as the particle grows, if $(C - C^*)$ can be regarded as constant. The growth curve of a NP, $R = f(t)$, tends to be asymptotic.

3.3.2. Growth Controlled by the Integration Reaction

If $D \gg kR$, then $C = C_1$ and the growth is limited by the integration reaction at the surface. In this case,

$$dR/dt = kV_m(C - C^*) \quad (11)$$

This equation shows that if the concentration gradient is constant, R is a linear function of time, provided that $(C - C^*)$ can be regarded as constant.

4. RESULTS AND DISCUSSION

4.1. Gliadin G2 and G3 Solubilization

As previously described, it is assumed that the solvent which best solubilizes a gliadin has the same solubility parameter as this protein.²⁸

When varying the ratio ethanol/water (EtOH/H₂O) from 50/50 to 70/30 v/v, the solubility parameter varied from 39.1 to 32.9 (Mpa^{1/2}). We observed that the clearest solution was obtained for a solubility parameter of: 34.5 ± 0.5 (Mpa^{1/2}) for G3 corresponding to an ethanol/water ratio of 62/38 (v/v), and 38.5 ± 0.5 (Mpa^{1/2}) for G2, corresponding to an ethanol/water ratio of 52/48 (v/v).

These values signified that G2 was the most soluble in an ethanolic/water mixture 52/48 (v/v), while the best mixture was 62/38 (v/v) for G3. It can be assumed that gliadins were in an expanded conformation in these solvents. To control this hypothesis, the conformation of gliadins was investigated by SANS.

4.2. Determination of Gliadin Structure by SANS

Because of the lack of contrast between water and ethanol, the experiments were performed with deuterated solvents: D₂O and EtOD.

G2 was chosen because of its relative purity, compared to G3, particularly because it contains a very few amount of glutenins.

Different experiments involving gliadin in different mixtures EtOD/D₂O v/v were performed.

4.2.1. Modelization of the Experimental Results

Figure 2a and Figure 2b showed the variation of $\ln(I)$ versus q^2 and $\ln(qI)$ versus q^2 . The slope analysis and the value of I at q equals zero allow the determination of the characteristic parameters of prolate ellipsoid or of cylinder. With these characteristic parameters, the theoretical $I/I(0) = f(q)$ curves could be calculated and plotted. These graphs are then superposed on the experimental values $I/I(0)$, in order to determine if the protein conformation is a prolate ellipsoid or a cylinder.

When this modelization was applied to our experimental results, the mean square variation could not allow to distinguish between the two shapes.

In order to distinguish them, L_c , the contour length, independent of R_c and R_g , defined by

$$L_c = \pi \cdot I(0)/I_c(0), \quad \text{with} \quad I_c(0) = F * I(0),$$

was calculated. F was the normalization factor. Table I displayed the parameters of the two conformations. By comparing L_c with on the one hand, the cylinder length L , and on the other hand, the major ellipsoid axis $2a$ for different mixtures, one could not distinguish between the two shapes. We chose the cylinder shape because its

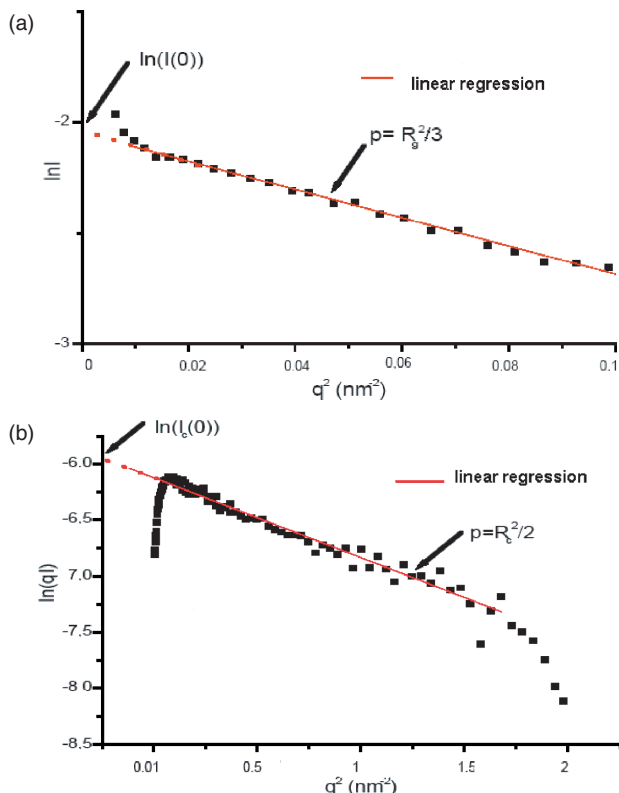


Fig. 2. (a) Guinier representation of diffused intensity $\ln I$ versus q^2 .
 (b) Representation of $\ln qI = f(q^2)$ for gliadin G2.

treatment is simpler. Table I presented in its last column the parameters obtained after modelization. They confirmed the experimental values of d and L . They are close to the experimental dimensions of the rods of γ Gliadin and ω Gliadin in solution obtained by Thompson.³¹

4.2.2. Correlation Between the Solubility Parameter of the Good Solvent and the Gliadin Conformation

The values of L and d obtained from the different experiments showed that the largest conformation was obtained for the mixture 62/38: The value of L is maximum (25 nm), as the value of d is 3.5 nm.

From other experiments we observed that, in deuterated solvents the solubility parameter of G2 was changed: The best solvent mixture was obtained for 62/38 EtOD/D₂O v/v, which corresponded to $\delta_G = 34.5 \pm 0.5$ (MPa^{1/2}).

When considering the two previous observations, we could conclude that the greatest conformation of gliadin G2 was obtained when the solubility parameter of the solvent was the same as the gliadin's one $\delta_G = 34.5 \pm 0.5$ (MPa^{1/2}).

A similar study was performed for gliadin G3, and similar results were obtained: considering the cylinder model, the greatest conformation of gliadin G3 ($L = 18$ nm, $d = 2.6$ nm) is obtained when the solubility parameter of the solvent is the same as the gliadin's one.

4.3. Experimental Nanoparticle Formation and Process of Nucleation

Figure 3a showed NP obtained by SEM and Figure 3b the distribution curve obtained by QELS. They are observed two hours after their preparation.

The initial gliadin concentration in GS (62/38 H₂O/EtOH v/v) was 4.25 g/L. The saturation concentration of gliadin in NS (H₂O + NaCl 0.9% + Synperonic®) was 0.869 g/L. This value could seem rather high because gliadin is not soluble in salted water but the little amount of surfactant PE F68 favours the dissolution of gliadin.

The value of $(C - C^*)$, which characterized the saturation, was then 3.381 g/L. As $\beta = C/C^* \gg 1$, the conditions were fulfilled an amorphous protein precipitation, as seen before.

Observing the NP with a polarizing microscope, it could be concluded that no sign of crystallization occurred because no birefringence and no color were observed, so that NP were amorphous.

Figure 4 shows the evolution of G3 gliadin NP sizes with time. As soon as the non solvent was added in the medium, particles formed, which is in favour of an instantaneous nucleation.⁴⁷

Moreover two different curves could be observed:
 — a linear curve for the minimum particles diameter, parallel to the abscissa,
 — a linear curve for the mean particles diameter.

This means that the distribution of size is bimodal:
 — small particles, about 70 nm in size, which size did not change with time. It may be assumed that these small particles could generate nucleation growth.
 — larger particles growing with time.

Table I. Gliadin G2 characterization by SANS.

EtOD/D ₂ O (v/v)	C (g · L ⁻¹)	R_g (nm) (±2%)	R_s (nm) (±3%)	d (nm) cylinder	L (nm) cylinder	2a (nm)	L_c (nm) (±5%)	Cylinder parameters after modelization (nm)
52/48	3.5	4.38	1.18	3.32	14.6	19.45	18.85	$d = 3.6$; $L = 16$
52/48	5.5	4.41	1.4	3.96	14.5	19.5	16.4	$d = 4.0$; $L = 15.5$
55/45	17.1	6.17	0.85*	2.4*	21.2	27.5	26.7	$d = 3.5$; $L = 23$
62/38	18.3	6.97	1.24	3.5	23.8	21.9	26.8	$d = 3.5$; $L = 25$
70/30	12.9	5.76	0.81*	2.29*	19.75	25.7	23.7	$d = 3.0$; $L = 21$

*Imprecision (lack of data at large q).

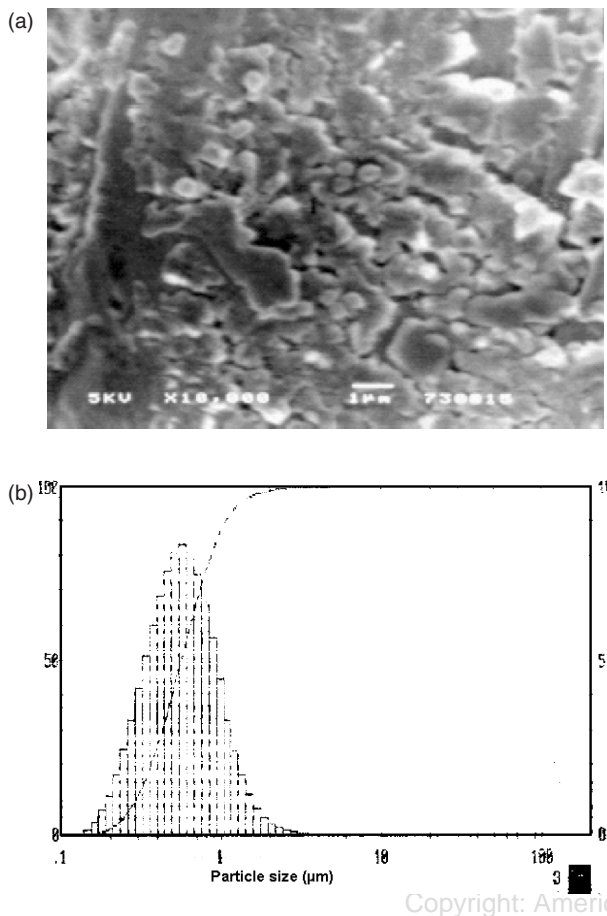


Fig. 3. (a) SEM micrograph of gliadin NP. (b) Distribution curve of gliadin NP obtained by QELS.

As the evolution of the mean diameter versus time appeared linear, a growth process by integration reaction could be assumed, (*vide supra* Eq. (11)). When applying Eq. (11), the value of constant k can be found: $4.12 \text{ m} \cdot \text{s}^{-1}$, which value is quite fast for a NP growth. As assumed before, this demonstrated that Galkin's approach seemed valuable for proteins nucleation and particularly for gliadin.

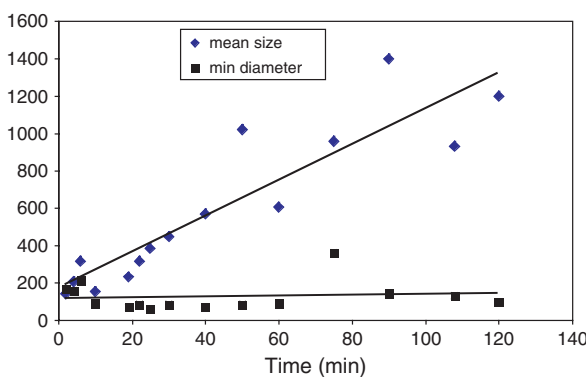


Fig. 4. Diameter kinetics during NP elaboration.

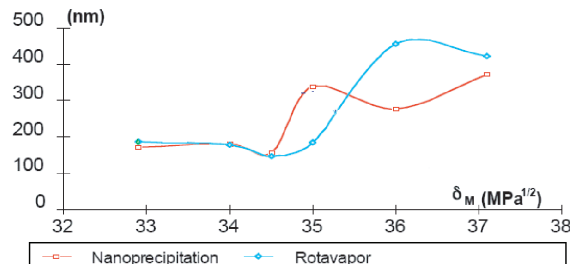


Fig. 5. Evolution of gliadin G3 NP with the solubility parameter of the solvent.

4.4. Influence of the Solubility Parameter of the Good Solvent on NP Precipitation

As the solubility parameter plays an important role in the conformation of the gliadins, it is interesting to look for the influence of this parameter on the NP size (Fig. 5).

The gliadin G3 NP were prepared and allowed to grow during 2 hours, and their size were measured by QELS.

Figure 5 showed that the size falls to a minimum (about 150 nm) when the solubility parameter of the solvent was the same as the gliadin one, i.e. $34.5 \pm 0.5 \text{ (MPa}^{1/2}\text{)}$.

4.5. Relation Between the Gliadin Macromolecular Size and the NP Size

In the conclusion of Section 4.2.2, the macromolecular size of the protein was the greatest when the solubility parameter of the GS corresponded to the solubility parameter of the protein. For this same solubility parameter, in Section 4.4, the NP size was the smallest.

Thus the proteins solubilization played a capital influence on the size of NP. Indeed, the more the solubility parameter of the good solvent was close to that of the proteins, the smaller were the particles. It could be deduced from this observation that the more expanded was the conformation of the macromolecules at the time of precipitation, the more the surface of contact between proteins and their non-solvent was important, the more the macromolecules contracted and formed small particles.

5. CONCLUSION

The study of the formation of the particles indicated that nucleation was instantaneous and that the distribution size was bimodal. In addition the growth of the particles was carried out mainly by integration: The incorporation of a macromolecule to the edifice, which was the particle, was the predominant process.

The curve of gliadin NP growth was elucidated: the evolution of their mean diameter with time was linear. This signified that one could stop the growth at a given size if it could be possible to freeze the system, at a minimal particle size or at another required size.

Moreover, the proteins solubilization plays a capital influence on the size of NP. Indeed, the more the solubility

parameter of the good solvent was close to that of the proteins, the smaller were the particles. It could be deduced from this observation that the more expanded was the conformation of the macromolecules at the time of precipitation, the more the surface of contact between proteins and their bad solvent was important, the more the macromolecules contracted forming the smaller particles. Briefly, the smallest particles were obtained from the protein solution in which the protein was the more expanded.

Acknowledgments:

The authors thank:
— The interregional “Réseau Matériaux, Polymères, Plasturgie” (Basse-Normandie, Haute-Normandie) for financial support.
— Dr. Y. Popineau, Laboratory LBTP, INRA, Nantes (France), for providing gracefully purified gliadins, and for fruitful discussions.
— Dr. A. Lapp, Laboratory LLB of CEA Saclay (France), for his help in the characterization of gliadins in solution by SANS.
— Dr. F. Osterstock, for his technical assistance in SEM experiments.

References and Notes

1. F. Puisieux, G. Barratt, G. Couarrazé, P. Couvreur, J. P. Devissaguet, C. P. Dubernet, E. Fattal, H. Fessi, C. Vauthier and S. Benita, in Polymeric Biomaterials, edited by S. Dimitriu, Marcel Dekker, New York (**1994**), p. 747.
2. M. J. Alonso, *Drug. Pharm. Sci.* **77**, 203 (**1996**).
3. J. R. Robinson, in Controlled Drug Delivery Challenges, edited by K. Park, American Chemical Society, Washington (**1997**).
4. F. De Jaeghere, E. Doelker, and R. Gurny, in Encyclopedia of Controlled Drug Delivery, edited by E. Mathiowitz, John Wiley, New York (**1999**).
5. S. Stainmesse, A. M. Orecchioni, E. Nakache, F. Puisieux, and H. Fessi, *Colloid. Polym. Sci.* **273**, 505 (**1995**).
6. C. Duclairoir, J. M. Irache, E. Nakache, A. M. Orecchioni, C. Chabenat, and Y. Popineau, *Polym. Int.* **79**, 327 (**1999**).
7. E. Nakache, N. Poulain, F. Candau, A. M. Orecchioni, and J. M. Irache, in Handbook of Nanostructured Materials and Nanotechnology, edited by H. S. Nalwa, Academic Press, New York (**2000**), Vol. 5, p. 577.
8. C. Duclairoir, A. M. Orecchioni, P. Depraetere, F. Osterstock, and E. Nakache, *Int. J. Pharm.* **353**, 133 (**2003**).
9. C. Duclairoir, Ph.D. Thesis, Université de Caen/Basse-Normandie, UFR Sciences, Caen (**2000**).
10. P. Couvreur, G. Barratt, E. Fattal, P. Legrand, and C. Vauthier, *Crit. Rev. Ther. Drug Carrier Syst.* **19**, 99 (**2002**).
11. C. Duclairoir, A. M. Orecchioni, P. Depraetere, and E. Nakache, *J. Microencapsul.* **19**, 61 (**2002**).
12. J. C. Daniel and C. Pichot, in Les Latex Synthétiques, Tec & Doc-Lavoisier, Paris (**2006**).
13. I. Ezpeleta, J. M. Irache, S. Stainmesse, C. Chabenat, J. Gueguen, Y. Popineau, and A. M. Orecchioni, *Int. J. Pharm.* **131**, 191 (**1996**).
14. J. M. Irache, L. Bergougnoux, I. Ezpeleta, J. Gueguen, and A. M. Orecchioni, *Int. J. Pharm.* **126**, 103 (**1995**).
15. T. Mirshahi, J. M. Irache, J. Gueguen, and A. M. Orecchioni, *Drug. Dev. Ind. Pharm.* **22**, 841 (**1996**).
16. T. Mirshahi, J. M. Irache, C. Nicolas, M. Mirshahi, J. P. Faure, J. Gueguen, C. Hequet, and A. M. Orecchioni, *Drug Target* **10**, 625 (**2002**).
17. A. M. Orecchioni, C. Duclairoir, J. M. Irache, and E. Nakache, Nanotechnologies for the Life Sciences, edited by Challa S. S. R. Kumar, Wiley-VCH, Weinheim, Germany (**2006**).
18. J. A. Bietz and J. A. Rothfus, *Cereal Chem.* **47**, 381 (**1970**).
19. M. Byers, J. Mifflin, and S. J. Smith, *J. Sci. Food Agric.* **34**, 447 (**1983**).
20. D. L. Du Cros and C. W. Wrigley, *J. Sci. Food Agric.* **30**, 785 (**1979**).
21. C. Larré, Y. Popineau, and W. Loisel, *J. Cereal Chem.* **14**, 231 (**1999**).
22. H. Wieser, W. Seilmmer, and H. D. Belitz, *J. Cereal Sci.* **19**, 149 (**1994**).
23. Y. Popineau and S. Denery-Papini, in Protéines végétales, Lavoisier, Paris (**1996**).
24. R. C. Bootmley, M. F. Kearns, and J. D. Shoffield, *J. Sci. Food Agric.* **33**, 481 (**1982**).
25. D. Marion, Y. Nicolas, Y. Popineau, G. Branland, and J. Landry, in Proceedings of the International Meeting Wheat Kernel Proteins, Voberto, Italy (**1994**), p. 197.
26. Y. Nicolas, J. P. Martinant, S. Denery-Papini, and Y. Popineau, *J. Sci. Food Agric.* **77**, 96 (**1998**).
27. C. Duclairoir, E. Nakache, H. Marchais, and A. M. Orecchioni, *Colloid. Polym. Sci.* **276**, 321 (**1998**).
28. J. H. Hildebrand and R. L. Scott, in Regular Solutions, Prentice-Hall, Englewood Cliffs, NJ (**1962**).
29. A. F. M. Barton, in Handbook of Solubility Parameters and other Cohesion Parameters, CRC Press, Boca Raton (**1991**).
30. R. K. Scopes, in Protein Purification, Principles and Practice, Springer Verlag, New York (**1982**).
31. N. H. Thomson, M. J. Miles, Y. Popineau, J. Harries, P. R. Shewry, and A. S. Tatham, *Biochem. Biophys. Acta, Prot. Struct. Mol. Enzymol.* **1430** (**1999**).
32. E. W. Cole, D. D. Kasarda, and D. Lafiandra, *Biochem. Biophys. Acta* **787** (**1984**).
33. K. J. I'Anson, V. J. Morris, P. R. Shewry, and A. S. Tatham, *Biochem. J.* **287**, 183 (**1992**).
34. Guinier and G. Fournet, in Small Angle Scattering of X-Rays, Wiley, New York (**1955**).
35. D. J. Burgess and O. N. Singh, *J. Pharm. Pharmacol.* **45**, 586 (**1993**).
36. Ezpeleta, J. M. Irache, S. Stainmesse, J. Gueguen, and A. M. Orecchioni, *Eur. J. Pharm. Biopharm.* **42**, 36 (**1996**).
37. S. Galindo-Rodríguez, E. Allémann, H. Fessi, and E. Doelker, *Pharm. Res.* **21**, 1428 (**2004**).
38. S. A. Vitale and J. L. Katz, *Langmuir* **19**, 4105 (**2003**).
39. F. Ganachaud and L. Katz, *Chem. Phys. Chem.* **6**, 209 (**2005**).
40. S. P. Sanghvi and J. P. Nairn, *J. Pharm. Sci.* **80**, 394 (**1991**).
41. V. Mikol and R. Giegé, in Crystallization of Nucleic Acids and Proteins: A Practical Approach, edited by A. Ducruix and R. Giegé, IRL Press at Oxford University Press, Oxford (**1992**).
42. V. K. La Mer, *Ind. Eng. Chem.* **44**, 1270 (**1952**).
43. Mersmann, in Crystallization Technology Handbook, Marcel Dekker, New York, Basel, Hong Kong (**1994**).
44. O. Galkin and P. G. Vekilov, *J. Am. Chem. Soc.* **122**, 156 (**2000**).
45. Z. Kam, H. B. Shore, and G. Feher, *J. Mol. Biol.* **123**, 539 (**1978**).
46. A. J. Malkin and A. J. Mc Pherson, *Acta Crystallogr. Sect. D* **50**, 385 (**1994**).
47. A. Teglia and G. Secchi, *Int. J. Cosm. Sci.* **16** (**1994**).
48. E. Plasari, P. Grisoni, and J. Villermaux, *Trans. Inst. Chem. Eng. Part A* **75**, 237 (**1997**).
49. J. Schlichtkrull, *Acta Chem. Scand.* **11**, 299 (**1957**).
50. M. Ataka and T. Tanaka, *Biophys. J.* **58**, 807 (**1990**).
51. T. Sugimoto, *Adv. Coll. Interface Sci.* **28**, 65 (**1987**).

Received: 15 December 2005. Revised/Accepted: 25 February 2006.

P9



Phenotypic variation in the *Pseudomonas fluorescens* clinical strain MFN1032

G. Rossignol^a, D. Sperandio^a, J. Guerillon^a, C. Duclairoir Poc^a, E. Soum-Soutera^b, N. Orange^a, M.G.J. Feuilloley^a, A. Merieau^{a,*}

^a Laboratoire de Microbiologie Du Froid-Signaux MicroEnvironnement (LMDF-SME), UPRES EA 4312, Centre Normandie Sécurité Sanitaire, Université de Rouen, 55 rue Saint Germain, 27000 Evreux, France

^b Laboratoire de Biotechnologie et Chimie Marines (LBCM), EA 3884, Université Bretagne Sud, Lorient, France

Received 17 December 2008; accepted 14 April 2009

Available online 3 May 2009

Abstract

Pseudomonas fluorescens is a highly heterogeneous species and includes both avirulent strains and clinical strains involved in nosocomial infections. We previously demonstrated that clinical strain MFN1032 has hemolytic activity involving phospholipase C (PlcC) and biosurfactants (BSs), similar to that of the opportunistic pathogen *Pseudomonas aeruginosa*. When incubated under specific conditions, MFN1032 forms translucent phenotypic variant colonies defective in hemolysis, but not necessarily in PlcC. We analyzed eight variants of the original strain MFN1032 and found that they clustered into two groups. Mutations of genes encoding the two-component regulatory system GacS/GacA are responsible for phenotypic variation in the first group of variants. These group 1 variants did not produce secondary metabolites and had impaired biofilm formation. The second group was composed of hyperflagellated cells with enhanced biofilm capacity: they did not produce BSs and were thus unable to swarm. Artificial reduction of the intracellular level of c-di-GMP restored the ability to form biofilm to levels shown by the wild type, but production of BSs was still repressed. Phenotypic variation might increase the virulence potential of this strain.

© 2009 Elsevier Masson SAS. All rights reserved.

Keywords: *Pseudomonas fluorescens*; Phenotypic variation; Biofilm; c-di-GMP; Biosurfactants

1. Introduction

Environmental adaptability of microorganisms results from genetic diversity and natural selection. Bacteria also have complex regulatory networks enabling them to colonize a variety of environments [1].

This adaptive behavior can be correlated with phenotypic variation, which is mainly, but not necessarily, influenced by the external environment. One process involved in phenotype

diversification is phase variation, which is usually a reversible, high-frequency phenotype switching corresponding to differential expression of one or several genes. Phase variation generates subpopulations within a clonal population. The switch between the various states is generally a stochastic event which can be modulated by external factors [14]. Reversion is a requirement to be considered as phase variation, but it cannot be observed under laboratory conditions [32]. Several studies have described mechanisms involved in phase variation, and although observations of phase variation are increasing, few mechanisms have been reported. These can be divided into genetic rearrangements (DNA inversion or duplication, transposition, homologous recombination, slipped-strand mispairing) or epigenetic modification/regulation [11].

In *Pseudomonas* sp., phenotypic variation has been described for rhizospheric bacteria and the opportunistic pathogen

* Corresponding author. Tel.: +33 232291562; fax: +33 232291550.

E-mail addresses: gaelle.rossignol@univ-rouen.fr (G. Rossignol), daniel.sperandio@etu.univ-rouen.fr (D. Sperandio), josette.guerillon@univ-rouen.fr (J. Guerillon), cecile.poc@univ-rouen.fr (C. Duclairoir Poc), emmanuelle.soutera@univ-ubs.fr (E. Soum-Soutera), nicole.orange@univ-rouen.fr (N. Orange), marc.feuilloley@univ-rouen.fr (M.G.J. Feuilloley), annabelle.merieau@univ-rouen.fr (A. Merieau).

Pseudomonas aeruginosa, representative of the genus. Phenotypic variation in crop-protective bacteria *Pseudomonas* was shown to affect mainly the production of exo-enzymes, secondary metabolites and colonization properties [2,26,28,31]. Most of the strains displayed increased motility, generally associated with a longer length of flagellum. These phenotypic variations are correlated with the accumulation of spontaneous mutations in the *gacS* or *gacA* genes [29]. These genes encode the GacA/GacS two-component regulatory system which regulates secondary metabolism, exo-enzyme production and biofilm formation, among other functions. Random spontaneous mutations of the *gacA* and/or *gacS* genes seem to result from a dysfunction in the MutS mismatch repair system, which is negatively regulated by the general stress-response regulator RpoS, itself under the control of the Gac system [30]. These mutations seem to be mediated by site-specific recombinases, although the molecular mechanism has not yet been established [6,19]. The site-specific recombinase is probably responsible for phase variation, and *gac* mutants could be selected *a posteriori*. Phenotypic variations, mainly biofilm-related, frequently occur in the pathogen *P. aeruginosa* as a result of environmental pressure [16]. Small colony variants (SCVs) have also been isolated from the lungs of cystic fibrosis (CF) patients and this phenotype has been associated with the ability of *P. aeruginosa* to persist in the lungs and cause chronic infection [34]. Contrary to rhizobacteria, spontaneous *gac* mutations are not assumed to be involved. By sensing environmental factors, a complex regulatory network controls phenotypic variation (and perhaps the switch between acute infections and chronic persistence) [8]. The GacS/LadS/RetS pathway may play a key role by finely controlling the level of RsmZ and subsequent free RsmA, which plays a critical role in *P. aeruginosa* virulence [21]. SCV emergence is enhanced in *gacS*[−] PA14 biofilm (which could also correspond to a low level of *rsmZ*), but functional GacS is necessary for the reversion process [4].

A biofilm-related phenotype also seems to be related to the intracellular level of the second messenger c-di-GMP [12]. Although c-di-GMP regulation of biofilm has been reported in diverse bacteria, the mechanism responsible for the switch is not yet understood.

We report the first phenotypic characterization of variants from a clinical *Pseudomonas fluorescens* strain, MFN1032, isolated from a patient suffering from pulmonary tract that we had reported previously [3]. This strain displayed phenotypic variation when incubated at 37 °C. Our objectives were to determine whether these variants enhanced the virulence of this opportunistic pathogen and to identify the mechanism(s) involved.

2. Materials and methods

2.1. Bacterial strains and culture conditions

Strain MFN1032 was isolated from a patient suffering from pulmonary tract infection and identified as *P. fluorescens* biovar I [3]. The bacteria were cultured in Luria Bertani medium (LB) or King B (KB) medium and incubated at various temperatures

between 17 and 37 °C in a gyratory shaker at 180 rpm. When necessary, 15 µg/mL gentamicin and 40 µg/mL IPTG were added.

2.2. Measurement of phase variation frequencies

Aliquots of 20 mL of KB were each inoculated with one colony from KB agar plate and the cultures grown for three days, with shaking, at 28 °C or 37 °C. The optical density of the cultures was measured and they were diluted such that when plating on KB medium, an average of 300 colonies per plate were obtained. For estimations of frequency, at least 1500 colonies were counted. The frequency of switching was obtained by dividing the number of switches by the number of generations.

2.3. Extracellular activities

Lecithinase and protease activities were recorded after 48 h incubation at 28 °C on egg-yolk and milk agar plates, respectively. Agar plates supplemented with 2% sheep red blood cells (SRBCs) were used to screen for β-hemolytic activity (β-HA) after 24–48 h growth at 28 °C. The plates were examined for enzyme activities on substrates. Opaque zones showed lecithinase activity, whilst protease and hemolytic activities produced clear zones.

2.4. Biosurfactant (BS) analysis

Reverse-phase liquid chromatography coupled with mass spectrometric detection was used to identify BSs. The method was adapted from Morin [20]. When required, a drop-collapse-test was also performed as previously described [25].

2.5. Motility assays, static biofilm assay and quantification

Motility and microarray biofilm assays were performed as described previously [25].

2.6. Electron microscopy

Visualization of flagella was performed as described previously [25].

2.7. Scanning confocal laser microscopy analyses of biofilm

Biofilms were formed on glass microscope slides immersed in 30 mL of LB medium in 9 cm diameter Petri dishes. Cells were labelled with 2.5 µM of Syto 61 Red fluorochrome (Molecular Probes) for 5 min at room temperature and cellulose polymers were stained blue using the calcofluor white fluorochrome (Sigma) (0.3 mg/mL). Slides were washed twice in phosphate-buffered saline and biofilms were observed using a Leica DM6000B confocal microscope (Leica Microsystems, Heidelberg, Germany), with the immersion 63X objective.

Confocal stacks were collected and images were processed using Leica Confocal Software.

2.8. Genetic complementation

The plasmids pMP6562 (carrying the *gacS* gene), pMP5565 (carrying the *gacA* gene), pMP6603 (carrying both *gacS* and *gacA* genes) and the parental plasmid pME6010 were generous gifts from B. Lugtemberg of Leiden University [29]. pSV35 and pSV35RetS⁺ were generous gifts from S. Lory of Boston University and pJN2133 (expressing PA2133, a PDE enzyme from *P. aeruginosa* 1) [15] from C. Harwood of the University of Washington. Each plasmid was transferred to MFN1032 and variants using the technique of Enderle et al. [7].

3. Results

3.1. Phenotypic variation occurs during growth of MFN1032 on specific rich media

MFN1032 was isolated from a patient suffering from a pulmonary tract infection. The original isolate formed thick opaque colonies (most colonies in Fig. 1A). Phenotypic variation was observed when cultures were grown on KB medium or egg yolk agar (medium used to screen for lecithinase activity) (Fig. 1A and B, respectively). After three days of growth in liquid KB medium, flat and translucent colonies were found (Fig. 1A). However, a typical *P. fluorescens* laboratory strain, MF37, originally isolated from milk, displayed no phenotypic variation, even after several days of growth in liquid King B medium.

The mean frequency of MFN1032 variation was 4×10^{-5} switches per generation at 28 °C and 4×10^{-3} at 37 °C. Phenotypes of the variants were stable and were retained in subsequent cultures. No reversion to the wild type phenotype was observed under these conditions. As the frequency of variants was higher at 37 °C, we investigated virulence by

testing for potential virulence factors and colonization capacity.

3.2. MFN1032 variants display different extracellular activities

P. fluorescens phenotypic variation mainly affects extracellular enzymes and secondary metabolites. The extracellular activities of the variants were investigated and compared with MFN1032. The wild type MFN1032 produced protease and lecithinase activities. Lecithinase activity was mainly due to the production of PlcC, an enzyme involved in secreted HA (sHA) of MFN1032 [24]. These factors are involved in MFN1032 virulence, so they were screened for in eight translucent colony variants which were isolated from KB medium and then plated on appropriate media (i.e. egg yolk agar for lecithinase activity, milk agar for protease activity and SRBC agar for HA). Four of the variants expressed none of these extracellular activities (group 1) and four were only deficient for HA (group 2) (Table 1).

3.3. Phenotypic variants differ in motility, BS release and biofilm formation

Phenotypic variation is often associated with modification of motility and adhesion properties, two factors involved in virulence and colonization. To test motility on solid substrates, swimming and swarming were determined by growth on 0.3% and 0.6% agar LB plates, respectively. Diameters of colonies of MFN1032 and variants were measured after 16 h, 24 h and 40 h incubation at 28 °C (the optimal growth temperature of MFN1032). No significant difference in swimming motility was observed between the variants and MFN1032 (Fig. 2A). Concerning swarming ability, after 16 h of growth on 0.6% agar LB plates, MFN1032 had completely invaded the dish, whereas no motility was observed for group 1 and group 2 variants (Fig. 2B). Generally, swarming motility (in *P. fluorescens* and others) is a multicellular behavior resulting from

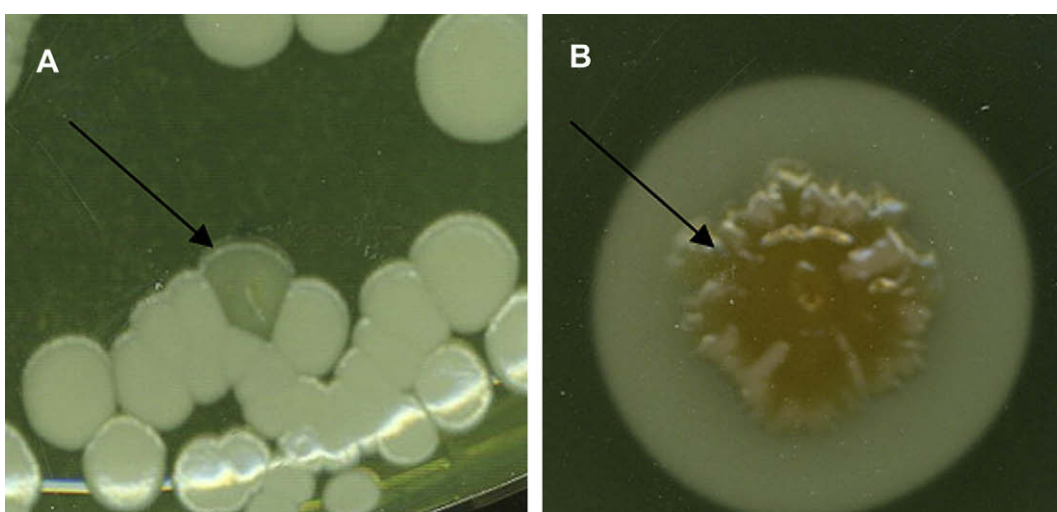


Fig. 1. Phenotypic variation in strain MFN1032 after growth on King B (A) or egg yolk agar plates (B). Colony variants are indicated by an arrow.

Table 1
Extracellular activities of strain MFN1032 and variants.

Activities	Lecithinase	Protease	Hemolysis
<i>Strains/variants</i>			
MFN1032	+	+	+
Group 1	–	–	–
Group 2	+	+	–

Lecithinase, protease and hemolytic activities were determined on egg yolk, milk or 2% SRBCs agar plates, respectively.

BS and flagellar function. The analysis of phase stationary supernatants by HPLC–MS showed that MFN1032 was able to produce at least three distinct (cyclolipopeptides) CLPs when cultured in LB medium at 28 °C. Mass spectroscopic analysis revealed the presence of two viscosinamide-like compounds (with distinct retention time in HPLC) and an unidentified CLP, presumed to be a masetolide and named “α”. No CLPs were found in group 1 or group 2 variant supernatants (Table 2).

Since the cells displayed swimming motility, loss of swarming ability could not be due to the absence of flagella. Electronic microscopy observation confirmed that MFN1032 had a single polar flagellum (Fig. 2C, photo B). Broken flagella, with a size equivalent to the MFN1032 flagellum, were observed surrounding group 1 cells (Fig. 2C, photos C and D), whereas most of group 2 displayed a hyperflagellated phenotype (most bacteria had four polar flagella) (photos E and F). We also observed that group 2 cells formed aggregates

on the drip, while most MFN1032 cells were mainly isolated (photos E and A, respectively).

These properties (autoaggregative behavior and hyperflagellated cells) are generally correlated with a biofilm-related phenotype. It has also been reported that swarming motility and biofilm are often inversely regulated [33]. We therefore used confocal laser microscopy to study biofilm formation of MFN1032 and the variants. Group 2 formed more biofilm than MFN1032 after 24 h of growth at 37 °C, whereas group 1 biofilm was sparse (Fig. 3A and C). Fluorescent coloration with the cellulose-specific dye calcofluor [27] showed that the cellulose exopolysaccharide (EPS) produced by group 2 was higher and that by group 1 was lower than that by MFN1032 (Fig. 3B and C).

3.4. Mutations in gac genes are responsible for changes in group 1 variants

Group 1 and group 2 variants were transformed by electroporation with plasmids carrying the *gacS* gene (pMP6562), the *gacA* gene (pMP5565), both (pMP6603) or neither (pME6010, as a control). The *gacS* gene restored the wild type phenotype to three group 1 variants and the *gacA* gene to the other (Fig. 4A). Most of the group 1 tested displayed a mutation in the *gacS* gene, as observed for most *Pseudomonas* rhizobacteria [29]. Gac mutants have better growth kinetics, and consequently have been described as enhancers of population fitness. We therefore determined the

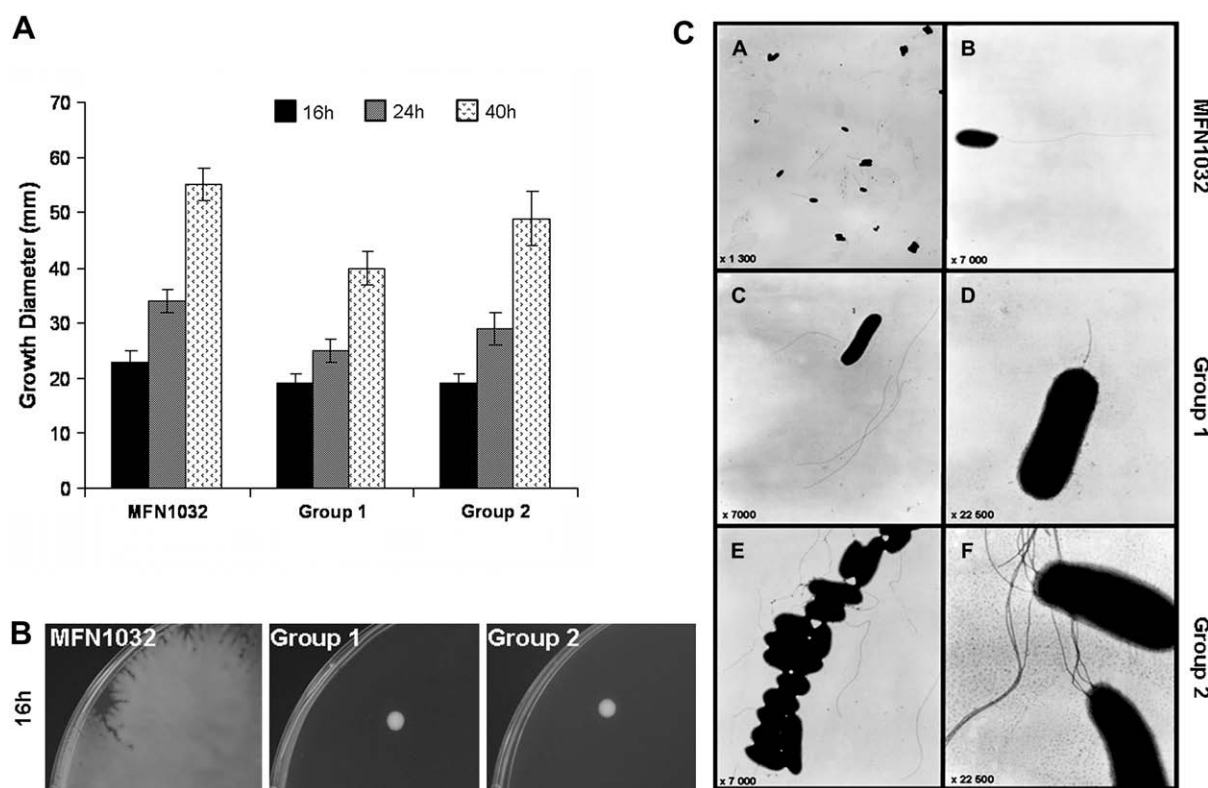


Fig. 2. Swimming (A) and swarming (B) motility of MFN1032, group 1 and group 2 variants. Swimming and swarming mobility were determined at 28 °C on LB with 0.3% or 0.6% agar. (C) TEM observations of MFN1032 and variants. Bacteria in exponential growth phase were visualized after negative staining with phosphotungstic acid (0.5%).

Table 2
Analysis of BS production by HPLC–MS.

CLPs identified	Viscosinamide-like 1	Viscosinamide-like 2	Massetolide “ α ”
Mass (in Da)	1125,8	1125,8	1111,8
<i>Strains/variants</i>			
MFN1032	+	+	+
Group 1	–	–	–
Group 2	–	–	–

generation times of group 1 variants and MFN1032 at 28 °C and 37 °C. Group 1 variants grew slightly faster at 28 °C ($G_{\text{Group}1,28^{\circ}\text{C}} = 49.5 \pm 1$ min; $G_{\text{WT},28^{\circ}\text{C}} = 54 \pm 9$ min) and much faster at 37 °C ($G_{\text{Group}1,37^{\circ}\text{C}} = 55.2 \pm 1$ min; $G_{\text{WT},37^{\circ}\text{C}} = 73.3 \pm 3$ min).

3.5. Effect of *RetS* and PDE on group 2 variants

No pMP6562, pMP5565 or pMP6603 complemented group 2 variants. The phenotype for group 2 was thus not due to defects in the *gacS* or *gacA* genes. We therefore searched for *retS*, since a mutation in the *retS* gene in *P. aeruginosa* gives a phenotype similar to that of group 2 variants [9] and *retS* orthologs are recovered from *P. fluorescens* genomes (PFL_0664 and PfI01_0661 from Pf5 and Pf01 respectively). The *retS* gene from *P. aeruginosa* (on pSV35RetS⁺) was introduced in group 2 variants (parental plasmid pSV35 was used as a control) and biofilm formation was measured in a microarray assay. The amount of biofilm was significantly greater for group 2/pSV35 than for MFN1032/pSV35, consistent with confocal microscopy findings (above). Biofilm production was lower in both group 2 and the wild type transformed by *retS* than by the control (Fig. 4B). These findings indicate that the *P. aeruginosa* *retS* gene is expressed in MFN1032 and that it negatively controls biofilm formation. Group 2/pSV35RetS⁺ did not show HA on SRBC agar and produced no BSs (Fig. 4C and D); thus, complementation by *retS* was not sufficient to fully restore the wild type phenotype.

Strong phenotypic variation was observed in both group 2- and MFN1032 *retS*-overexpressing strains, but not in MFN1032/pSV35 when incubated under the same conditions. These unexpected results were reproducible in various clones and experiments (Fig. 4C).

The effects of introducing *retS* into group 2 are probably due to a shunt of a parallel pathway, possibly that involving c-di-GMP. Indeed, biofilm phenotypes may correlate with the intracellular level of the second messenger c-di-GMP. C-di-GMP levels are finely regulated in a spatial and temporal manner by two kinds of enzymes: diguanylate cyclases (DGCs) carrying a GGDEF domain and responsible for c-di-GMP synthesis, and phosphodiesterases (PDEs) carrying an EAL domain and involved in c-di-GMP degradation. The intracellular level of this second messenger was artificially decreased in group 2 and MFN1032 by expressing a PDE enzyme from *P. aeruginosa* (PA3133 encoded by plasmid pJN2133) [15]. Biofilm formation by the transformed cells was then assayed. Both groups 2/pJN2133 and MFN1032/pJN2133 produced less biofilm than their controls (Fig. 4B). The group 2 variant transformed with the gene encoding PA3133 produced more biofilm than that transformed with the *retS* gene (35 ± 3% versus 7 ± 7% relative biofilm formation). The opposite was true for MFN1032 (0% with pJN2133 versus 12 ± 3% with pSV35RetS⁺), implicating different pathways in variants and wild type. Consistent with this possibility, group 2/pJN2133 displayed a relatively stable phenotype on SRBC agar (Fig. 4C). Nevertheless, group 2/pJN2133 variants still displayed a hemolysis- and BS-negative phenotype, suggesting that these factors are regulated independently of biofilm or that restoration of these activities requires other conditions. Expression of PDE in MFN1032 resulted in complete loss of biofilm formation capacity, BS production and hemolysis (as revealed by the drop-collapse-test from MFN1032/pJN2133 colony and culture on SRBC) (Fig. 4C and D). Expression of each PDE and *retS* in MFN1032 enhanced the phenotypic variation of the strain (Fig. 4C). These results suggest that phenotypic variation is caused by unidentified genes which

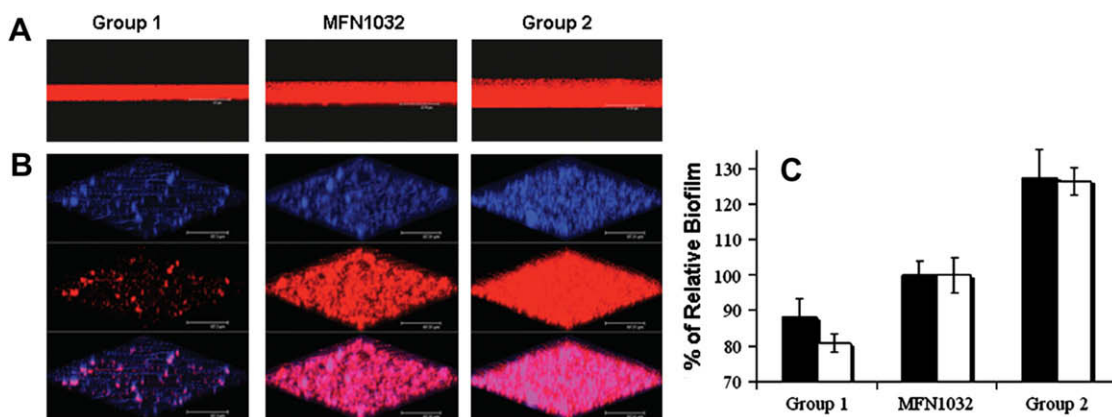


Fig. 3. Confocal laser microscopy analyses of biofilms from MFN1032 and its variants after 24 h growth in LB medium at 37 °C. Before scanning, cells were stained with Syto 61 Red. EPSs were stained blue with calcofluor white fluorochrome. Values are means of data of five images from each of two experiments. (A) Thickness of biofilm according to the (x, z) axis (the same scale is used for the 3 micrographics). (B) 3D modelling of EPS production and biofilm; middle: 3D representation of biofilm; bottom: superposition of EPS and biofilm 3D modelling. (C) Comparison of thickness of biofilm (black square) and EPS production (white square) of group 1 and group 2 variants with MFN1032 as a control.

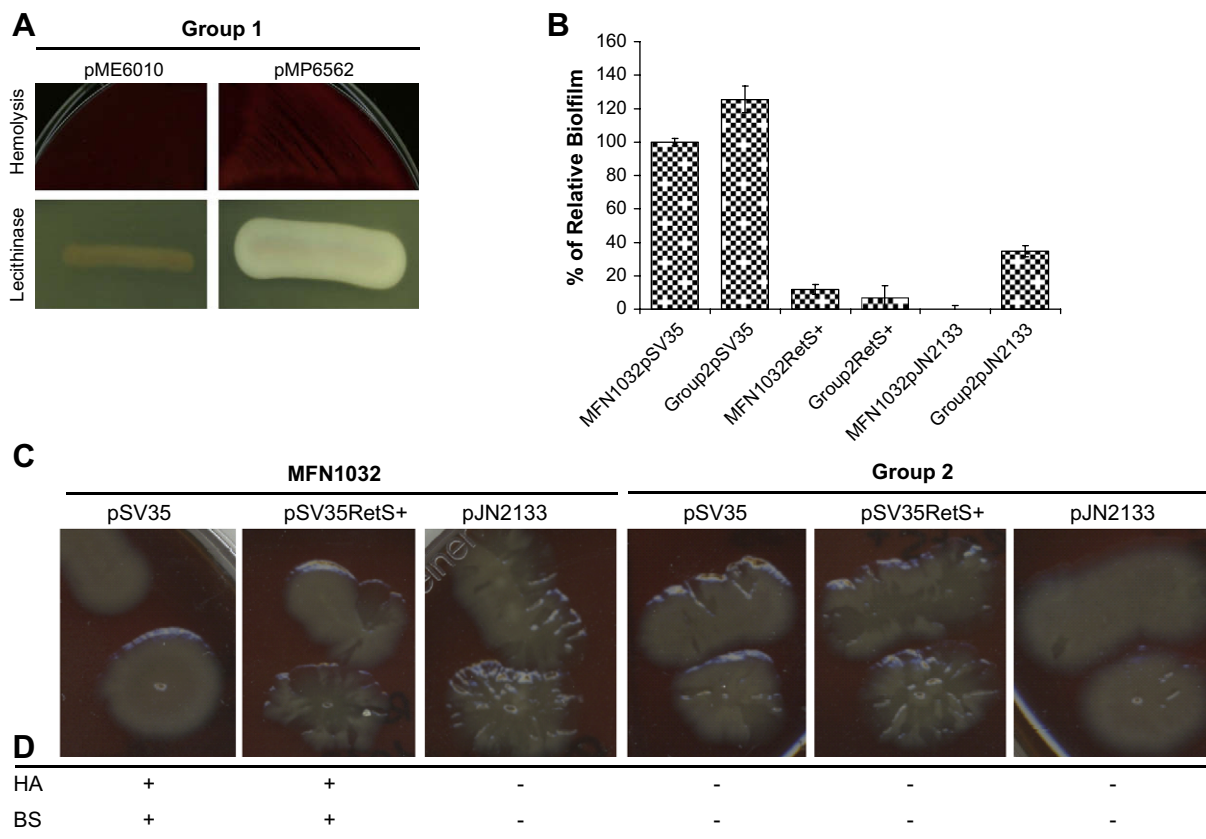


Fig. 4. (A) *gacS* complementation of a group 1 variant. Restoration of wild type phenotype in a group 1 variant (after transformation with plasmid pM6562 carrying the *gacS* gene), is tested by checking lecithinase and HA on egg yolk and SRBC agar plates, respectively. Phenotypes are compared with the same variant carrying the empty vector. (B) Effect of RetS or PA2133 (PDE) on the capacity of MFN1032 or group 2 variants to form biofilm in a static microarray assay. The quantity of biofilm was determined by measuring the OD_{595nm} after 24 h of growth at 37 °C in LB. The results are means of at least three independent experiments. (C) Phenotypic variation on SRBC agar plates. (D) HA and production of BSs from MFN1032 and group 2 variants expressing *retS* (pSV35RetS⁺) or PA2133 (pJN2133) genes. SRBC phenotypes are visualized after 48–72 h of growth at 37 °C and colonies checked for BS production by the drop-collapse-test. Plasmid pSV35 (Gm^R) was used as a control.

probably control the level of c-di-GMP in MFN1032. Thus, the nature of group 2 variants has not been fully clarified.

4. Discussion

Phenotypic variation is frequent in *Pseudomonas* and can affect competitive root colonization by rhizobacteria or persistence of the opportunistic pathogen *P. aeruginosa*. This study is the first to demonstrate that phenotypic variation can occur in a clinical strain of *P. fluorescens*. Strain MFN1032 displayed phenotypic variation under specific medium conditions (King B and egg yolk agar media) and temperature. The variation frequency was enhanced (4×10^{-3} per generation) when bacteria were incubated at 37 °C (human physiological temperature). The phenotype of all variants emerging from MFN1032 under these conditions was a translucent colony. We studied eight variants and found that four of them (group 1) were unable to produce secondary metabolites. As previously observed for rhizospheric *P. fluorescens* strains (for review, see Van den Broek et al.), a *gac* complementation in *trans* of these variants restored the original phenotype. Group 1, however, was no more motile than MFN1032, whereas

most, if not all, *gac* mutants of rhizobacteria *P. fluorescens* were more motile. A laboratory-adapted strain, MF37, was impaired in phenotypic variation, suggesting that this phenomenon is finely controlled. Specific characteristics may have evolved as a result of strain adaptation to particular niches.

Phenotypic variation in group 2 variants mainly involved their attachment properties. The greater capacity of these variants to form biofilms at solid–liquid interfaces was a consequence of cellulose exopolymer overproduction and increased flagella number. The second messenger c-di-GMP is central to regulation of surface colonization and aggregative behavior in prokaryotes [23]. In *P. fluorescens*, this molecule has been reported to regulate the wrinkly spreader phenotype of SBW25 by controlling production of acetylated cellulose exopolysaccharides at a post-transcriptional level [10]. This regulation was of the WspR regulatory protein, a GGDEF protein with DGC activity. WspR is the final gene product and primary output component of the chemotaxis-like Wsp pathway, and is activated by a currently unknown signal processed by the rest of the Wsp complex [17]. The intracellular concentration of c-di-GMP in *P. aeruginosa* is controlled by

a Wsp system (thought to function in a similar way to that in *P. fluorescens*) and the SadB/SadC/BifA pathway. In PA14, this system is believed to inversely regulate biofilm formation and swarming motility by controlling EPS production and flagellar functions [33]. We showed that PDE PA2133 overexpression restored the wild type biofilm phenotype in group 2 variants. This suggested that the biofilm was a result of an intracellular increase in the c-di-GMP level which increased cellulose EPS production. These observations agree with previously reported data [10]. In *P. aeruginosa* PAK, EPS production is also controlled by the independent parallel GacS/LadS/RetS pathway which controls the level of the non-coding small RNA RsmZ. GacS and LadS act in an opposite manner from RetS on EPS, by enhancing transcription of *rsmZ*, which in turn sequesters the post-transcriptional repressor RsmA [9]. RetS functionality has not yet been reported in *P. fluorescens*, but the GacS/Rsm pathway has been described in detail for *P. fluorescens* CHA0 [13]. The use of the *P. aeruginosa* *retS* gene in MFN1032 and its variants shows that: (1) *P. aeruginosa* *retS* is functionally similar to its ortholog in *P. fluorescens*, (2) RetS negatively controls biofilm formation and (3) overexpression of the *retS* gene is sufficient to compensate for a biofilm-related phenotype presumed to be a consequence of perturbation of intracellular c-di-GMP. This type of phenotype compensation has already been reported in *P. aeruginosa* PAK. Goodman et al. showed that PA4332 encoding a GDDEF domain protein with putative DGC activity was able to restore the wild type phenotype of the PAK *retS* mutant strain [9].

Biofilm formation and swarming motility appear to be inversely regulated in MFN1032; it is possible that loss of swarming was correlated with loss of BS production. However, swarming behavior may be related to factors other than BS (such as flagella or cell surface tension) although BS is essential to the swarming process [22]. Bruijn et al. recently demonstrated that CLP masetolide A produced by *P. fluorescens* SS01 is also essential for biofilm formation. However, they postulated that the role of CLPs in biofilm formation may be entirely different, depending on the structure and hydrophobicity of the CLP produced and the cell surface of the producing strain [5]. We demonstrated that a strain with impaired BS release (group 2 variants) did not lose its capacity to form biofilms. Thus we think that the CLPs produced by MFN1032 are not involved in biofilm formation. The regulation of CLPs in MFN1032 appeared to be very complex. As the *gac* mutants did not produce BS, the GacS/GacA system probably controls BS production, as reported in the literature. It seems, however, that this regulation is not via the RsmZ pathway, since *retS* overexpression (which also influences the RsmZ level) in MFN1032 had no effect on BS production. Gac regulation may occur at a transcriptional level, or at least by a different pathway. PDE overexpression in MFN1032 suppressed BS production; therefore, both higher (in group 2) and lower (in MFN1032/pJN2133) than wild type levels of c-di-GMP lead to a BS-negative phenotype. Compensation of this perturbation (in group 2/pJN2133 for example) was not sufficient to restore the BS wild type phenotype. In *P. aeruginosa* PA14, overexpression or mutation of the

PA4332 gene encoding a putative DGC also led to the same phenotype (enhanced cytotoxicity and biofilm formation). It has been suggested that the c-di-GMP level is finely controlled temporally and/or a spatially [24]. Note that feed forward loop regulation could explain how a single molecule can have contradictory effects in terms of concentration and kinetics [18].

In conclusion, MFN1032 phenotypic variation is mainly due to two different processes. First, spontaneous *gac* mutations lead to variants with competitive growth advantages (as observed for rhizospheric bacteria). Although these variants are completely defective in production of extracellular product, they might increase the competitiveness of the clinical strain. A second class of variants displayed a hyperbiofilm phenotype which probably facilitates persistence in the host during infection. The process responsible for the emergence of these variants has not been fully elucidated. Our findings, however, suggest a change in the intracellular level of c-di-GMP. The genes causing phenotypic variation and which are responsible for the c-di-GMP decrease have yet to be identified.

The absence of BS secretion and/or production is a common feature of all variants. Thus BS production in MFN1032 appeared to be subtly controlled. We are currently investigating a putative genetic network controlling BS production in MFN1032.

Acknowledgments

This work was supported by the Région Haute-Normandie. We are very grateful to C. Harwood, S. Lory and B. Lugtenberg for the generous gift of their plasmids.

References

- [1] Bjedov, I., Tenaillon, O., Gerard, B., Souza, V., Denamur, E., Radman, M., Taddei, F., Matic, I. (2003) Stress-induced mutagenesis in bacteria. *Science* 300, 1404–1409.
- [2] Chabeaud, P., de Groot, A., Bitter, W., Tommassen, J., Heulin, T., Achouak, W. (2001) Phase-variable expression of an operon encoding extracellular alkaline protease, a serine protease homolog, and lipase in *Pseudomonas brassicacearum*. *J. Bacteriol.* 183, 2117–2120.
- [3] Chapalain, A., Rossignol, G., Lesouhaitier, O., Merieau, A., Gruffaz, C., Guerillon, J., Meyer, J.M., Orange, N., et al. (2008) Comparative study of seven fluorescent pseudomonad clinical isolates. *Can. J. Microbiol.* 54, 19–27.
- [4] Davies, J.A., Harrison, J.J., Marques, L.L., Foglia, G.R., Stremick, C.A., Storey, D.G., Turner, R.J., Olson, M.E., et al. (2007) The GacS sensor kinase controls phenotypic reversion of small colony variants isolated from biofilms of *Pseudomonas aeruginosa* PA14. *FEMS Microbiol. Ecol.* 59, 32–46.
- [5] de Bruijn, I., de Kock, M.J., de Waard, P., van Beek, T.A., Raaijmakers, J.M. (2008) Masetolide A biosynthesis in *Pseudomonas fluorescens*. *J. Bacteriol.* 190, 2777–2789.
- [6] Dekkers, L.C., Phoelich, C.C., van der Fits, L., Lugtenberg, B.J. (1998) A site-specific recombinase is required for competitive root colonization by *Pseudomonas fluorescens* WCS365. *Proc. Natl. Acad. Sci. U.S.A.* 95, 7051–7056.
- [7] Enderle, P.J., Farwell, M.A. (1998) Electroporation of freshly plated *Escherichia coli* and *Pseudomonas aeruginosa* cells. *Biotechniques* 25, 954–956, 958.
- [8] Furukawa, S., Kuchma, S.L., O'Toole, G.A. (2006) Keeping their options open: acute versus persistent infections. *J. Bacteriol.* 188, 1211–1217.

- [9] Goodman, A.L., Kulasekara, B., Rietsch, A., Boyd, D., Smith, R.S., Lory, S. (2004) A signaling network reciprocally regulates genes associated with acute infection and chronic persistence in *Pseudomonas aeruginosa*. *Dev. Cell* 7, 745–754.
- [10] Goymer, P., Kahn, S.G., Malone, J.G., Gehrig, S.M., Spiers, A.J., Rainey, P.B. (2006) Adaptive divergence in experimental populations of *Pseudomonas fluorescens*. II. Role of the GGDEF regulator WspR in evolution and development of the wrinkly spreader phenotype. *Gene* 373, 515–526.
- [11] Hallet, B. (2001) Playing Dr. Jekyll and Mr. Hyde: combined mechanisms of phase variation in bacteria. *Curr. Opin. Microbiol.* 4, 570–581.
- [12] Haussler, S. (2004) Biofilm formation by the small colony variant phenotype of *Pseudomonas aeruginosa*. *Environ. Microbiol.* 6, 546–551.
- [13] Heeb, S., Kuehne, S.A., Bycroft, M., Crivii, S., Allen, M.D., Haas, D., Camara, M., Williams, P. (2006) Functional analysis of the post-transcriptional regulator RsmA reveals a novel RNA-binding site. *J. Mol. Biol.* 355, 1026–1036.
- [14] Henderson, I.R., Owen, P., Nataro, J.P. (1999) Molecular switches – the ON and OFF of bacterial phase variation. *Mol. Microbiol.* 33, 919–932.
- [15] Hickman, J.W., Tifrea, D.F., Harwood, C.S. (2005) A chemosensory system that regulates biofilm formation through modulation of cyclic diquanylate levels. *Proc. Natl. Acad. Sci. U.S.A.* 102, 14422–14427.
- [16] Kirisits, M.J., Prost, L., Starkey, M., Parsek, M.R. (2005) Characterization of colony morphology variants isolated from *Pseudomonas aeruginosa* biofilms. *Appl. Environ. Microbiol.* 71, 4809–4821.
- [17] Malone, J.G., Williams, R., Christen, M., Jenal, U., Spiers, A.J., Rainey, P.B. (2007) The structure–function relationship of WspR, a *Pseudomonas fluorescens* response regulator with a GGDEF output domain. *Microbiology* 153, 980–994.
- [18] Mangan, S., Zaslaver, A., Alon, U. (2003) The coherent feedforward loop serves as a sign-sensitive delay element in transcription networks. *J. Mol. Biol.* 334, 197–204.
- [19] Martinez-Granero, F., Capdevila, S., Sanchez-Contreras, M., Martin, M., Rivilla, R. (2005) Two site-specific recombinases are implicated in phenotypic variation and competitive rhizosphere colonization in *Pseudomonas fluorescens*. *Microbiology* 151, 975–983.
- [20] Morin, D., Grasland, B., Vallee-Rehel, K., Dufau, C., Haras, D. (2003) On-line high-performance liquid chromatography-mass spectrometric detection and quantification of N-acylhomoserine lactones, quorum sensing signal molecules, in the presence of biological matrices. *J. Chromatogr. A* 1002, 79–92.
- [21] Mulcahy, H., O'Callaghan, J., O'Grady, E.P., Macia, M.D., Borrell, N., Gomez, C., Casey, P.G., Hill, C., et al. (2008) *Pseudomonas aeruginosa* RsmA plays an important role during murine infection by influencing colonization, virulence, persistence, and pulmonary inflammation. *Infect. Immun.* 76, 632–638.
- [22] Raaijmakers, J.M., de Bruijn, I., de Kock, M.J. (2006) Cyclic lipopeptide production by plant-associated *Pseudomonas* spp.: diversity, activity, biosynthesis, and regulation. *Mol. Plant Microbe Interact.* 19, 699–710.
- [23] Romling, U., Amikam, D. (2006) Cyclic di-GMP as a second messenger. *Curr. Opin. Microbiol.* 9, 218–228.
- [24] Romling, U., Gomelsky, M., Galperin, M.Y. (2005) C-di-GMP: the dawning of a novel bacterial signalling system. *Mol. Microbiol.* 57, 629–639.
- [25] Rossignol, G., Merieau, A., Guerillon, J., Veron, W., Lesouhaitier, O., Feuilloley, M.G., Orange, N. (2008) Involvement of a phospholipase C in the hemolytic activity of a clinical strain of *Pseudomonas fluorescens*. *BMC Microbiol.* 8, 189.
- [26] Sanchez-Contreras, M., Martin, M., Villaceros, M., O'Gara, F., Bonilla, I., Rivilla, R. (2002) Phenotypic selection and phase variation occur during alfalfa root colonization by *Pseudomonas fluorescens* F113. *J. Bacteriol.* 184, 1587–1596.
- [27] Spiers, A.J., Bohannon, J., Gehrig, S.M., Rainey, P.B. (2003) Biofilm formation at the air–liquid interface by the *Pseudomonas fluorescens* SBW25 wrinkly spreader requires an acetylated form of cellulose. *Mol. Microbiol.* 50, 15–27.
- [28] van den Broek, D., Bloemberg, G.V., Lugtenberg, B. (2005a) The role of phenotypic variation in rhizosphere *Pseudomonas* bacteria. *Environ. Microbiol.* 7, 1686–1697.
- [29] van den Broek, D., Chin, A.W.T.F., Bloemberg, G.V., Lugtenberg, B.J. (2005c) Molecular nature of spontaneous modifications in *gacS* which cause colony phase variation in *Pseudomonas* sp. strain PCL1171. *J. Bacteriol.* 187, 593–600.
- [30] van den Broek, D., Chin, A.W.T.F., Bloemberg, G.V., Lugtenberg, B.J. (2005b) Role of RpoS and MutS in phase variation of *Pseudomonas* sp. PCL1171. *Microbiology* 151, 1403–1408.
- [31] van den Broek, D., Chin, A.W.T.F., Eijkemans, K., Mulders, I.H., Bloemberg, G.V., Lugtenberg, B.J. (2003) Biocontrol traits of *Pseudomonas* spp. are regulated by phase variation. *Mol. Plant Microbe Interact.* 16, 1003–1012.
- [32] van der Woude, M.W., Baumler, A.J. (2004) Phase and antigenic variation in bacteria. *Clin. Microbiol. Rev.* 17, 581–611.
- [33] Verstraeten, N., Braeken, K., Debkumari, B., Fauvert, M., Fransaer, J., Vermant, J., Michiels, J. (2008) Living on a surface: swarming and biofilm formation. *Trends Microbiol.* 16, 496–506.
- [34] von Gotz, F., Haussler, S., Jordan, D., Saravanamuthu, S.S., Wehmhoner, D., Strussmann, A., Lauber, J., Attree, I., et al. (2004) Expression analysis of a highly adherent and cytotoxic small colony variant of *Pseudomonas aeruginosa* isolated from a lung of a patient with cystic fibrosis. *J. Bacteriol.* 186, 3837–3847.

P10

SPECTRA ANALYSE

LA REVUE DES SCIENCES ANALYTIQUES

Comité Scientifique Programme rédactionnel Demande d'abonnement Annonceurs Newsletter Spectra Analyse Contacts Videos
Congrès JPFSA 2018

< Précédent Suivant >

La Newsletter
SPECTRA ANALYSE

 SALON ANALYSE INDUSTRIELLE Industrial Analysis Exhibition

26/27 JANVIER/JANUARY 2011 CNIT PARIS LA DÉFENSE



23 décembre 2010

– Dans le numéro 277 de Spectra Analyse –



Innovations
CONSOMMABLES Augmentation de volume pour les cryotubes

<...>



Également dans Spectra Analyse n° 277

- Technologie Appliquée LIMS QC et R&D
Renaud Acker, Mohamed Ndiaye
- Technologie Appliquée Les enjeux de la connexion instrument :
Jean-Baptiste Rio
- Technologie Appliquée Les logiciels de gestion de laboratoire (LIMS) en 2010
Jean-Baptiste Rio
- Mise à jour des connaissances Pollution des sédiments de dragage : procédés de bioremédiation alliés à l'électromigration
Florence Portet-Koltalo, Mohammed Ammami, Ahmed Benamar, Cécile Duclairoir-Poc, Anne Groboillot et Nicole Orange
- Mise à jour des connaissances Introduction à la microscopie de fluorescence en molécules uniques : principes et applications
Pascal Didier, Armelle Jouonang et Yves Mély



Florence PORTET-KOLTALO^{1*}, Mohamed Tahar AMMAMI^{1,2}, Ahmed BENAMAR², Cécile DUCLAIROR-POC³, Anne GROBOILLOT³, Nicole ORANGE³

Pollution des sédiments de dragage Procédés de bioremédiation alliés à l'électromigration

RÉSUMÉ

Afin de pouvoir valoriser les sédiments de dragage des ports (comme matériaux de remblai ou de construction), il s'avère nécessaire de les traiter afin d'atténuer leur teneur en polluants inorganiques ou organiques. Différentes méthodes de dépollution des sols peuvent être appliquées aux sédiments. Parmi elles, l'électromigration s'avère très prometteuse pour les sédiments fins de faible perméabilité. Allier cette technique à la bioremédiation s'avère encore plus encourageant : les biosurfactants, produits par des microorganismes, possèdent un potentiel intéressant pour améliorer les procédés d'électromigration.

MOTS-CLÉS

Sédiments de dragage, pollution, remédiation, électromigration, biosurfactants

Pollution of dredged sediments and remediation electrokinetic processes enhanced by biosurfactants

SUMMARY

To valorize harbour dredged sediments (as filling or building materials), it turns out necessary to treat them to limit their content in inorganic or organic pollutants. Various methods of soil remediation can be applied to sediments. Among them, electromigration is a promising technique that is proving to be suitable in cleaning fine dredged sediments. Combining a bioremediation process to electromigration seems even more promising : biosurfactants, produced by microorganisms, possess an interesting potential to improve electrokinetic processes.

KEYWORDS

polluted dredged sediments, remediation, electromigration, biosurfactants

I - Introduction

Nous évoquerons dans ce court article la problématique de la dépollution des sédiments, tout particulièrement des sédiments de dragage des ports. En effet, les anciennes pratiques de relargage des sédiments dragués pollués en milieu marin n'ont plus cours en l'état. Elles sont désormais soumises à des contraintes réglementaires. Afin de désengorger les sites de dépôt à terre, il s'avère parfois nécessaire de traiter les sédiments pollués, par des techniques proches de celles développées dans le cadre de

la dépollution des sols. Parmi ces techniques, la remédiation de la pollution de contaminants inorganiques (éléments traces métalliques) et organiques (tels les hydrocarbures aromatiques polycycliques) par un procédé d'électromigration est très prometteuse. Mais la conjonction d'une technique de remédiation physico-chimique (électromigration) avec une remédiation biologique permet d'envisager des procédés encore plus efficaces. Nous montrerons donc également les potentialités intéressantes des biosurfactants dans le cadre de la bioremédiation par électromigration.

¹ Surfaces et Interfaces Modifiées pour l'Analyse (SIMA) – Université de Rouen – UMR 6014 – 55 rue Saint Germain – 27000 Evreux – France

* auteur correspondant : Tél : +33 (0)2 32 29 15 35 – Fax : +33 (0)2 32 29 15 35 – E-mail : florence.koltalo@univ-rouen.fr

² Laboratoire Ondes et Milieux Complexes – FRE CNRS 3102 – Université du Havre – 53 rue de Prony – 76600 le Havre – France

³ Laboratoire de Microbiologie du Froid – Signaux et MicroEnvironnement – UPRES EA 4312 – Université de Rouen – 55 rue Saint Germain 27000 Evreux – France.

Pollution des sédiments de dragage procédés de bioremédiation alliés à l'électromigration

II - Pollution des sédiments de dragage

Les pratiques de dragage de sédiments accumulés dans les zones portuaires ou estuariennes constituent un enjeu pour le développement et le maintien des activités portuaires. En France, les quantités de matériaux dragués annuellement dans les ports et chenaux de navigation représentent des volumes considérables : ils sont de l'ordre de 50 millions de m³, parmi lesquels les sédiments fins, qui concentrent la majorité des polluants organiques ou inorganiques, représentent 24 millions de m³ (1). Les sédiments, une fois dragués, peuvent techniquement être immergés ou mis en dépôt à terre ou sur des îles.

La réglementation relative aux immersions de sédiments dragués a été révisée et complétée en juin 2000 et en août 2006, après les travaux du Groupe d'Etudes et d'Observations sur les Dragages et l'Environnement (GEODE). L'arrêté du 14 juin 2000 fait ainsi référence à deux niveaux, N1 et N2, entre lesquels une analyse est requise pour apprécier l'incidence de l'immersion sur les milieux concernés. Ces valeurs guides concernent essentiellement les éléments traces métalliques (ETM) et les polychlorobiphényles (PCB), mais des recommandations sont également précisées (mais encore à l'étude) pour d'autres polluants organiques tels les hydrocarbures aromatiques polycycliques (HAP). Il est désormais reconnu que les immersions sont une voie de transfert des contaminants vers le milieu marin ; Il convient donc de prendre des dispositions de nature à en limiter les impacts sur les écosystèmes. Ces dispositions tendent désormais à privilégier les dépôts terrestres (2), obligeant à terme les collectivités à prévoir un stockage des sédiments dans des sites de dépôt, voire de confinement. Contrairement à l'immersion en mer, il n'existe pas de texte réglementaire ou de guide « officiel » concernant la gestion à terre des sédiments de dragage. On prend alors généralement en compte les niveaux de référence prescrits par les textes relatifs à l'épandage des boues de station d'épuration (arrêté du 8 janvier 1998) (3).

III - Procédés de dépollution

1. Techniques conventionnelles de traitement

Divers scénarios s'offrent, depuis la décision de ne pas intervenir (mais les sites de dépôt sont d'ores et déjà saturés en Europe) jusqu'à celle d'éliminer en partie ou en totalité les contaminants présents dans les sédiments, afin de les valoriser par la suite (matériaux de remblai, de construction...). Cela amène à développer des technologies de prétraitement puis de traitement des sédiments. Les procédés de prétraitement consistent essentiellement à effectuer un tri granulométrique afin de séparer les fractions grossières (graviers,

sables), réutilisables car peu ou pas polluées, des particules fines (essentiellement des argiles), ces dernières concentrant la pollution. Les « fines » doivent également souvent être déshydratées. Après ces prétraitements, les boues fines polluées peuvent être éliminées en centre d'enfouissement, ou bien subir différentes méthodes de traitement, apparentées aux traitements de sols pollués :

- Les traitements biologiques sur les sols consistent à utiliser la capacité de certains micro-organismes à dégrader les polluants organiques (4, 5). Plusieurs techniques sont utilisées dont la biodégradation (bactérienne ou fongique) (6) activée par le compostage, la phytoremédiation, etc...
- Les traitements physico-chimiques s'appuient sur des interactions physico-chimiques ou des réactions chimiques (adsorption/désorption, oxydation/réduction, acidification...) pour laver ou immobiliser les contaminants, ou même les transformer voire les détruire. Concernant les réactions chimiques, ce sont essentiellement des réactions d'oxydation (réactions de type Fenton, ozonation...) qui conduisent à l'ultime conversion en CO₂ pour les hydrocarbures (7, 8). L'acidification, lors des procédés de lixiviation, conduit plutôt à résorber les ETM, afin de mieux les éliminer. Les traitements par lavage, moins agressifs et donc moins déstructurants pour le sol, incluent l'extraction par solvant, la flottation avec ou sans l'aide d'agents tensioactifs (9). Enfin, des procédés tels que la séparation magnétique ou l'électromigration (10, 11) permettent également d'extraire les éléments ionisés...
- Depuis quelques décennies, les traitements thermiques sont adaptés aux décontaminations de sédiments de dragage, en complément à d'autres types de traitements (biologiques, physico-chimiques). Parmi ces méthodes, on peut citer : la désorption thermique (la plus courante), la vitrification qui immobilise la pollution (12), mais également l'incinération ou la pyrolyse, d'un coût énergétique important...

2. Electromigration

Bien que ces méthodes soient éprouvées pour les sols contaminés, leur efficacité n'est pas encore avérée pour les sédiments fins de faible perméabilité. Face à ces inconvénients, l'électromigration est une méthode prometteuse, applicable *in situ*, sur des sols ou des sédiments peu perméables et vise une large variété de polluants (13-14). Elle repose sur l'induction d'un courant électrique de faible densité dans une matrice de sol contaminée afin d'y mobiliser les contaminants présents sous forme chargée ou ionisée. Le courant est appliqué par l'intermédiaire d'électrodes insérées horizontalement ou verticalement dans la matrice contaminée à traiter. Des phénomènes d'électrolyse de l'eau et d'électro-osmose apparaissent lors de l'électromigration. L'application d'un champ électrique dans le milieu, par la création d'une différence de potentiel entre des électrodes, provoque d'une part des mécanismes de transport,



MISE À JOUR DES CONNAISSANCES

appelés électrocinétiques, qui sont responsables du transport des espèces dans la phase liquide vers l'une ou l'autre électrode et d'autre part des réactions d'oxydoréduction. La mobilité ionique est principalement régie par l'intensité électrique (15) et la vitesse ionique est directement influencée par la température (16). Les réactions d'oxydoréduction permettent entre autre la fermeture du circuit, mais modifient également le pH au voisinage des électrodes (17). Ces phénomènes nécessitent une adaptation des conditions expérimentales pour favoriser la migration des polluants concernés (maintien de l'humidité et contrôle de pH). Il est également possible d'utiliser le phénomène d'électro-osmose (qui induit un mouvement de l'eau en général vers la cathode) pour éliminer certains polluants non ionisables. La performance du processus électrocinétique dépend par conséquent de l'interaction entre de nombreux paramètres interdépendants (18-20).

3. Les biosurfactants dans le cadre de la dépollution

Les biosurfactants sont un sujet d'intérêt de plus en plus grand ces dernières années. Effectivement, ces molécules d'origine microbienne présentent les mêmes caractéristiques physico-chimiques que leurs homologues synthétiques. Ainsi, grâce à leur structure amphiphile, les biosurfactants s'accumulent aux interfaces et diminuent la tension de surface. Généralement, ils ont des masses comprises entre 500 et 2 500 g.mol⁻¹ et peuvent être chargés ou non. Leur CMC (Concentration Micellaire Critique)

varie entre 1 à 200 mg.L⁻¹ (21), valeur plus faible que les tensioactifs synthétiques, ce qui confère aux biosurfactants une plus grande efficacité et les rend donc très attrayants. Leur activité tensioactive est comparable à celle de leurs homologues synthétiques, en atteignant des tensions de surface allant jusqu'à 30 mN.m⁻¹ (22). Par rapport aux tensioactifs synthétiques, les biosurfactants s'avèrent plus spécifiques, plus biodégradables et peuvent être produits de façon peu coûteuse sur des substrats renouvelables (23). Enfin le contexte réglementaire de plus en plus drastique concernant l'environnement pourrait fortement favoriser ces molécules « naturelles » par rapport à leurs homologues synthétiques (24).

Les biosurfactants sont synthétisés par certains micro-organismes, ce qui leur permet d'interagir avec leur micro-environnement en modulant les phénomènes interfaciaux. Ils jouent aussi un rôle physiologique en améliorant la biodisponibilité des nutriments hydrophobes, en favorisant leur solubilisation. Ils permettent également la régulation des transferts de déchets et des molécules signal de communication, et ont un impact sur les interactions hôtes-micro-organismes.

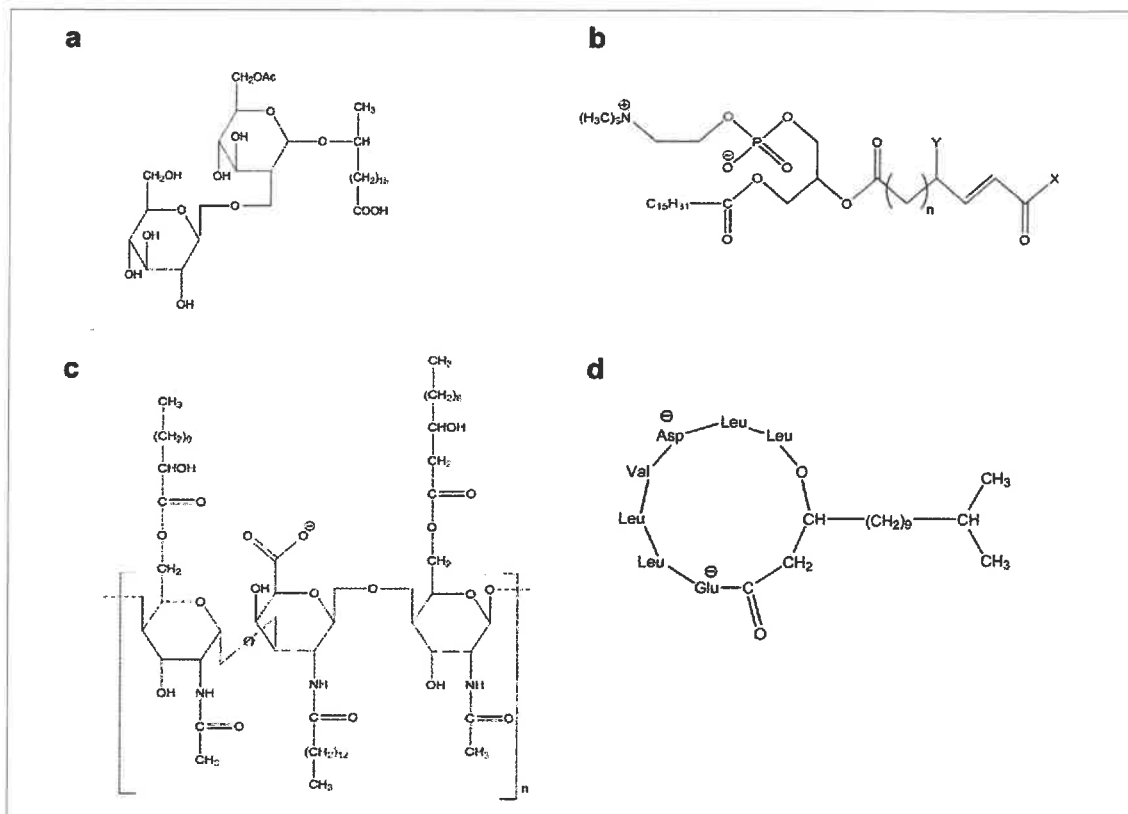
La variété structurale des biosurfactants est riche : en effet, ils sont sécrétés par un large spectre de micro-organismes (levures, moisissures et bactéries) à partir de substrats nutritifs variés et en fonction de facteurs environnementaux variables. Les biosurfactants comptent principalement (*voir figure 1*) :

- parmi les glycolipides : rhamnolipides, tréhalolipides, sophorolipides (25, 26) et les lipides (acides gras, lipides neutres, phospholipides) (27);

Figure 1

Principales familles de biosurfactants :

- (a) les rhamnolipides
- (b) les phospholipides
- (c) les biosurfactants polymères (émulsan)
- (d) les lipopeptides (surfactine)



Pollution des sédiments de dragage

procédés de bioremédiation alliés à l'électromigration

- parmi les polymères tensioactifs : emulsan, liposan (28)...

- parmi les lipopeptides-lipoprotéines : non cycliques et cycliques dont, plus particulièrement, la surfactine (29), l'amphiphine, la viscosine (30)...

Mettant en œuvre la capacité des biosurfactants à solubiliser les composés hydrophobes, un domaine d'application de choix est l'environnement (31, 32). Les rhamnolipides, produits par la souche *Pseudomonas aeruginosa*, sont intensément décrits dans la littérature et leurs applications sont nombreuses (27, 33, 34). Pour le traitement des eaux, ce sont principalement les micelles de rhamnolipides qui assurent la séquestration des métaux (35) ou des hydrocarbures (33). Afin de solubiliser les polluants hydrophobes, le sol est également traité par l'ajout de biosurfactant, qui peut être complété par un lavage à l'eau pour éliminer les hydrocarbures après désorption (36).

Une autre classe de biosurfactants peut s'avérer très intéressante : il s'agit des cyclolipopeptides (CLP), à cause de la variété des micro-organismes qui peuvent produire ce biosurfactant, principalement des *Bacillus* et des *Pseudomonas* (30, 37, 38), mais aussi grâce à la variabilité importante de leurs structures, qui les rend « modulables » en fonction des applications : la longueur de la chaîne lipophile est variable, mais également la partie peptidique, qui peut comprendre de 7 à 25 acides aminés. Les rhamnolipides, mais également la surfactine, favorisent ainsi la dépollution de terrains souillés par des HAP ou des métaux lourds (35, 39).

IV - Conclusion

Afin de dépasser les limites des différents procédés de dépollution, il peut s'avérer intéressant de combiner les avantages de plusieurs types de traitements (physico-chimiques, biologiques). Par exemple, combiner l'électromigration à la bioremédiation permet d'augmenter le transport de la bactérie et des nutriments et d'améliorer ainsi la biodégradation de polluants organiques (40) ou d'améliorer les procédés de lixiviation des métaux lourds (41). L'adjonction d'agents solubilisants, tels des agents tensioactifs synthétiques (42) mais également des biosurfactants, permet d'accroître la solubilisation de contaminants organiques peu solubles en phase aqueuse et ainsi d'améliorer le transport des polluants par électromigration (13, 43). Les biosurfactants ont également un potentiel pour remobiliser les ETM après complexation, ce qui les rend plus disponibles pour l'électro-dépollution (44). Ces techniques de dépollution innovantes, alliant les compétences de physico-chimistes et de biologistes, sont extrêmement prometteuses pour la remédiation de la pollution des sédiments fins de dragage, car les techniques employées ont-elles-mêmes un impact moindre sur l'environnement, du fait de la biodégradabilité des biosurfactants.

BIBLIOGRAPHIE

- (1) DUBOIS V, Etude du comportement physico-mécanique et caractérisation environnementale des sédiments marins. Valorisation en technique routière. Thèse de l'Université d'Artois (France), 2006.
- (2) MOO-YOUNG H. et al., Determination of the environmental impact of consolidation induced convective transport throughcappedsediment, *J. Hazard. Mater.*, 2001, 85, 53-72.
- (3) BENARD A, Impacts sur les milieux aquatiques des sédiments de dragage gérés à terre: problématique, contexte réglementaire, modélisation du transfert de contaminants organiques, Rapport d'étude de l'INERIS du 30/06/2009.
- (4) ZELLER C., CUSHING B, Panel discussion: remedy effectiveness: what works, what doesn't ?, *Integrated Environmental Assessment and Management*, 2005, 2, 75-79.
- (5) EL FRANTOUSSI SE, AGATHOS SN, Is bioaugmentation a feasible strategy for pollutant removal and site remediation?, *Curr. Opinion Microbiol.*, 2005, 8, 268-275.
- (6) REDDY MS et al., Biodegradation of phenanthrene with biosurfactant production by a new strain of *Brevibacillus* sp., *Bioresource Technol.*, 2010, 101, 7980-7983.
- (7) BOGAN BW, TRBOVIC V, PATEREK JR, Inclusion of vegetable oils in Fenton's chemistry for remediation of PAH-contaminated soils, *Chemosphere*, 2003, 50, 15-21.
- (8) ALDERMAN NS, NGUESSAN AL, NYMAN MC, Effective treatment of PAH contaminated Superfund site soil with the peroxy-acid process, *J. Hazard. Mater.*, 2007, 146, 652-660.
- (9) AHN CK, KIM YM, WOO SH, PARK JM, Soil washing using various nonionic surfactants and their recovery by selective adsorption with activated carbon, *J. Hazard. Mater.*, 2008, 154, 153-160.
- (10) KO SO, SCHLAUTMAN MA, CARRAWAY ER, Cyclodextrin enhanced elektrokinetic removal of phenanthrene from a model claysoil, *Environ. Sci. Technol.*, 2000, 34, 1535-1541.
- (11) SAWADA A., TANAKA S., FUKUSHIMA M., TATSUMI K., Electrokinetic remediation of clayey soils containing copper(II)-oximate using humic acid as a surfactant, *J. Hazard. Mater.*, 2003, 96, 145-153.
- (12) MULLIGAN CN, YONG RN, GIBBS BF, An evaluation of technologies for the heavy metal remediation of dredged sediments, *J. Hazard. Mater.*, 2001, 85, 145-163.
- (13) PAZOS M., ROSALES E., ALCANTARA T., GOMEZ J., SANROMAN MA, Decontamination of soils containing PAHs by electroremediation: a review, *J. Hazard. Mater.*, 2010, 177, 1-11.
- (14) CHEREPY NJ, WILDENSCHILD D, Electrolyte management for effective long-term electro-osmotic transport in low-permeability soils, *Environ. Sci. Technol.*, 2003, 37, 3024-3030.
- (15) BARAUD F., TELLIER S., ASTRUC M., Ion velocity in soil solution during electrokinetic remediation, *J. Hazard. Mater.*, 1997, 56, 315-332.
- (16) AL-HAMDAN AZ, REDDY KR, Electrokinetic remediation modelling incorporating geochemical effects, *J. Geot. and Geoenvir. Engr.*, ASCE, 2008, 134, 91-105.
- (17) REDDY KR, KARRI MR, Effect of voltage gradient on integrated electrochemical remediation of contaminant mixtures, *Land Cont. & Reclamation*, 2006, 14, 685-698.



MISE À JOUR DES CONNAISSANCES

- (18) YVON Y., Développement d'une méthode de décontamination active des sédiments portuaires pollués en tributylétain par électromigration, Thèse de l'Université de Pau (France), 2008.
- (19) NYSTROEM G., OTTOSEN LM, VILLUMSEN A., Electro-dialytic removal of Cu, Zn, Pb, and Cd from harbor sediment: Influence of changing experimental conditions, *Environ. Sci. Technol.*, 2005, 39, 2906-2911.
- (20) OYANADER MA, ARCE PE, Role of soil porosity and electrical and thermal resistivities on free-convective transport. Heat transfer and hydrodynamic aspects in an annular geometry, *Ind. Eng. Chem. Res.*, 2007, 46, 7627-7636.
- (21) LANG S., WAGNER F., Structure and properties of biosurfactants, *Biosurfactants and Biotechnology*, 1987, ed. Marcel Dekker, New York, 21-45.
- (22) VAN HAMME JD, SINGH A., WARD OP, Surfactants in microbiology and biotechnology: Part 1. Physiological aspects, *Biotech. Adv.*, 2006; 24, 604-620.
- (23) MUKHERJEE S., DAS P., SEN R., Towards commercial production of microbial surfactants, *Trends Biotechnol.*, 2006, 24, 509-515.
- (24) FIECHTER A., Biosurfactants - moving towards industrial application, *Trends Biotechnol.*, 1992, 10, 208-217.
- (25) SOBERÓN-CHÁVEZ G., LÉPINE F., DÉZIEL E., Production of rhamnolipids by *Pseudomonas aeruginosa*, *Appl. Microbiol. Biotechnol.*, 2005, 68, 718-725
- (26) HIRATA Y. et al., Novel characteristics of sophorolipids, yeast glycolipid biosurfactants, next term as biodegradable low-foaming surfactants, *J. Biosci. Bioeng.*, 2009, 108, 142-146.
- (27) DESAI JD, BANAT IM, Microbial production of surfactants and their commercial potential, *Microbiol. Mol. Biol. Rev.*, 1997, 61, 47-64.
- (28) CALVO C., MANZANERA M., SILVA-CASTRO GA, UAD I., GONZÁLEZ-LÓPEZ J., Application of bioemulsifiers in soil oil bioremediation processes. Future prospects, *Sci. Total Environ.*, 2009, 407, 3634-3640.
- (29) ONGENA M., JACQUES P., *Bacillus* lipopeptides: versatile weapons for plant disease biocontrol, *Trends Microbiol.*, 2008, 16, 115-125.
- (30) RAAIJMAKERS JM, DE BRUIJN I., DE KOCK MJD, Cyclic lipopeptide production by plant-associated *Pseudomonas* spp.: diversity, activity, biosynthesis, and regulation, *Mol. Plant-Microbe Interact.*, 2006, 19, 699-710.
- (31) MULLIGAN CN, Recent advances in the environmental applications of biosurfactants, *Curr. Opinion Coll. Int. Sci.*, 2009, 14, 372-378.
- (32) FRANZETTI A. et al., Potential applications of surface active compounds by *Gordonia* sp. strain BS29 in soil remediation technologies, *Chemosphere*, 2009, 75, 801-807.
- (33) BENINCASA M., MARQUES A., PINAZO A., MANRESA A., Rhamnolipidsurfactants : alternative substrates, new strategies, *Adv. Exp. Medicine Biology*, 2010, 672, 170-184.
- (34) MULLIGAN CN, Environmental applications of biosurfactants, *Environ. Pollut.*, 2005, 133, 183-198.
- (35) MULLIGAN CN, YONG RN, GIBBS BF, Metal removal from contaminated soil and sediments by the biosurfactantsurfactin, *Environ. Sci. and Technol.*, 1999, 33, 3812-3820.
- (36) OCHOA-LOZA FJ et al., Effect of clays, metal oxides, and organic matter on rhamnolipidbiosurfactant sorption by soil, *Chemosphere*, 2007, 66, 1634-1642.
- (37) ROSENBERG E., RON EZ, High and low-molecular-mass microbial surfactants, *Applied Microbiol. Biotechnol.*, 1999, 52, 154-162.
- (38) SINGH A., VAN HAMME JD, WARD OP, Surfactants in microbiology and biotechnology: part 2. Application aspects, *Biotechnol. Adv.*, 2007, 25, 99-121.
- (39) PERFUMO A., BANAT IM, MARCHANT R., VEZZULLI L., Thermally enhanced approaches for bioremediation of hydrocarbon-contaminated soils, *Chemosphere*, 2007, 66, 179-184.
- (40) KIM SH, HAN HY, LEE JL, KIM CW, YANG JW, Effect of electrokinetic remediation on indigenous microbial activity and community within diesel contaminated soil, *Sci. Total Environ.*, 2010, 408, 3162-3168.
- (41) LEE K-Y, YOON I-H, LEE B-T, KIM S-O, KIM K-W, A novel combination of anaerobic bioleaching and electrokinetics for arsenic removal from mine tailing soil, *Environ. Sci. Technol.*, 2009, 43, 9354-9360.
- (42) GAN S., LAU EV, NG HK, Remediation of soils contaminated with polycyclic aromatic hydrocarbons (PAHs), *J. Hazard. Mater.*, 2009, 172, 532-549.
- (43) JU L, ELECTOROWICZ M., In-situ phenanthrene removal provoked by electrokineticraport of on-site produced biosurfactants, Annual conference abstracts – Canadian society for Cicileengineering, 2000, 135.
- (43) JUWARKAR AA et al., Biosurfactant technology for remediation of cadmium and lead contaminated soils, *Chemosphere*, 2007, 68, 1996-2002.

PII

SPECTRA ANALYSE

LA REVUE DES SCIENCES ANALYTIQUES

Comité Scientifique Programme rédactionnel Demande d'abonnement Annonceurs Newsletter Spectra Analyse Contacts Videos

Congrès JPFSA 2018

< Précédent Suivant >

La Newsletter **SPECTRA ANALYSE**



– Dans le numéro 278 de Spectra Analyse –

04 mars 2011
PCI
PRESSE
Communication International



ANALYSE DE GAZ Sortie de la version H du MIR 9000

<...>



Également dans Spectra Analyse n° 278

- Manifestations
Au revoir Labautomation2011, bonjour SLAS2012
Patrick Marel
- Technologie Appliquée
Déséqustration de polluants de type hydrocarbures aromatiques polycycliques à l'interface de sédiments au moyen d'un tensioactif original d'origine biologique
Florence Portet-Koltalo, Mohamed Tahar Ammami, Ahmed Benamar, Anne Groboillot, Nicole Orange, Cécile Duclairroir-Poc
- Technologie Appliquée
La spectroscopie proche infrarouge : un nouvel outil pour l'optimisation des procédés de méthanisation
Mathieu Lesteur, Eric Latrille, Jean-Michel Roger, Véronique Bellon-Maurel, Catherine Gonzalez, Guillaume Junqua, Jean-Philippe Steyer
- Technologie Appliquée
L'imagerie MALDI : un nouvel outil pour les études ADME et DMPK
Raphaël Legouffe, David Bonnel, Gregory Hamm, Fabien Pamelard, Jonathan Stauber
- Mise à jour des connaissances
Microscopie STED, principe et intérêts pour l'étude du vivant
Irène Wang
- Index 2010
Les articles parus au cours de l'année 2010



Florence PORTET-KOLTALO^{1*}, Mohamed TAHAR AMMAMI^{1,2}, Ahmed BENAMAR², Anne GROBOILLOT³, Nicole ORANGE³, Cécile DUCLAIROR-POC³

Déséquestration de polluants de type hydrocarbures aromatiques polycycliques à l'interface de sédiments au moyen d'un tensioactif original d'origine biologique

RÉSUMÉ

Valoriser les sédiments de dragage des ports nécessite de les traiter afin d'atténuer leur teneur en polluants. Parmi les méthodes de remédiation de la pollution inorganique, l'électromigration s'avère prometteuse. Cependant les hydrocarbures aromatiques polycycliques (HAP), polluants particulièrement nocifs pour l'environnement, présentent un caractère lipophile qui les rend peu solubles dans l'eau et sont peu propices à une électromigration du fait de leur caractère non ionique. L'adjonction d'un agent tensioactif anionique doit permettre non seulement de les désorber du sédiment, mais également de mettre en œuvre le processus de migration électrocinétique grâce au transport des HAP dans des micelles anioniques. Un biosurfactant original (amphisine), produit par un micro-organisme (*Pseudomonas fluorescens* DSS73) a dans ce but été sélectionné. Dans un premier temps, une technique d'extraction par SPE (Solid Phase Extraction) et d'analyse par HPLC-fluorimétrie a été développée pour parvenir à doser simultanément des traces de HAP en milieu aqueux colloïdal et comprendre leur mécanisme d'adsorption à l'interface eau/sédiments. Dans un deuxième temps, l'adjonction d'amphisine a permis de montrer un processus de désorption des HAP de la surface du kaolin, matériau le plus rétensif dans le sédiment modèle. Le biosurfactant s'est même montré aussi efficace qu'un tensioactif anionique synthétique classique, le dodécyl sulfate de sodium, mais à une concentration molaire 110 fois plus faible.

MOTS-CLÉS

Hydrocarbures aromatiques polycycliques, sédiments, électromigration, remédiation, pollution, extraction liquide-solide (SPE), HPLC-fluorimétrie, biosurfactants

Desorption of strongly sorbed polycyclic aromatic hydrocarbons pollutants from sediment materials using an original biosurfactant

SUMMARY

*Electromigration is a promising technique that is proving to be suitable in cleaning fine dredged sediments of their inorganic pollutants. The electromigration process is, however, not appropriate for low water soluble, hydrophobic, non ionic hydrocarbons, such as polycyclic aromatic hydrocarbons (PAHs – a harmful pollutant to the environment). The addition of anionic surfactant should, however, allow not only PAHs desorption from the sediment by solubilising them, but will allow as well performing the electrokinetic migration process. An original biosurfactant (amphisine), produced by a microorganism (*Pseudomonas fluorescens* DSS73), has been selected for this purpose. First, a technique by extraction through SPE (solid phase extraction) and HPLC-fluorimetry has been developed to measure simultaneously traces of PAHs in the aqueous phase in order to understand their behaviour at water/sediment interfaces. Second, the addition of amphisine showed an interesting desorption process of the PAHs from the more retentive material, i.e. kaolin. The biosurfactant was even so effective as the classical anionic surfactant sodium dodecyl sulphate, but in a concentration 110 times lower.*

KEYWORDS

Polycyclic Aromatic Hydrocarbons, polluted sediments, electromigration, remediation, solid-phase extraction (SPE), HPLC-fluorimetry, biosurfactants

¹Surfaces et Interfaces Modifiées pour l'Analyse (SIMA) – UMR 6014 – Université de Rouen – 55 rue Saint Germain – 27000 Evreux, France

* auteur correspondant : Tél : +33 (0)2 32 29 15 35 – Fax : +33 (0)2 32 29 15 35 – e-mail : florence.koltalo@univ-rouen.fr

²Laboratoire Ondes et Milieux Complexes – FRE CNRS 3102 – Université du Havre – 53 rue de Prony – 76600 le Havre – France

³Laboratoire de Microbiologie du Froid – Signaux et MicroEnvironnement – EA 4312 – Université de Rouen – 55 rue Saint Germain – 27000 Evreux – France



I. Introduction

L'objectif des travaux présentés dans cet article est de montrer le potentiel de molécules possédant des propriétés tensioactives, produites par des microorganismes (biosurfactants), à re-solubiliser en phase aqueuse des micropolluants organiques très fortement adsorbés sur les particules fines des sédiments. Le but est à terme d'utiliser les propriétés de désorption et de piégeage d'un biosurfactant original, de type amphisine, afin de l'utiliser comme « transporteur » dans un réacteur fonctionnant sur le principe de l'électromigration (1, 2), afin d'atténuer la pollution dans le compartiment contenant le sédiment contaminé (procédé de bioremédiation par électromigration (3-5)).

Nous montrerons que la chromatographie en phase liquide, alliée à une détection sensible et à une technique de reconcentration de traces par SPE (solid phase extraction), est une technique de choix pour obtenir simultanément les isothermes d'adsorption d'un mélange d'hydrocarbures aromatiques polycycliques (HAP) et comprendre leurs mécanismes d'adsorption à l'interface entre le milieu aqueux et les différents constituants d'un sédiment modèle. On pourra ainsi appréhender les propriétés séquestrantes des sédiments vis-à-vis des HAP et étudier la remobilisation des HAP par l'amphisine, en vue d'une dépollution ultérieure du sédiment par électromigration.

II. Particularités des HAP

Les polluants organiques de type HAP constituent la troisième classe de polluants présents dans les sédiments après les ETM (éléments traces métalliques) et les PCB (polychlorobiphényles). Ils sont constitués d'au moins deux cycles aromatiques condensés. Leur source est désormais principalement d'origine anthropique : les HAP

sont générés par des processus de combustion incomplète de la matière organique à haute température, dans des conditions déficientes en oxygène. Ils peuvent donc provenir de la combustion de carburants automobiles – les moteurs Diesel étant les plus concernés (6) – de la combustion domestique, des productions industrielles et d'énergie...

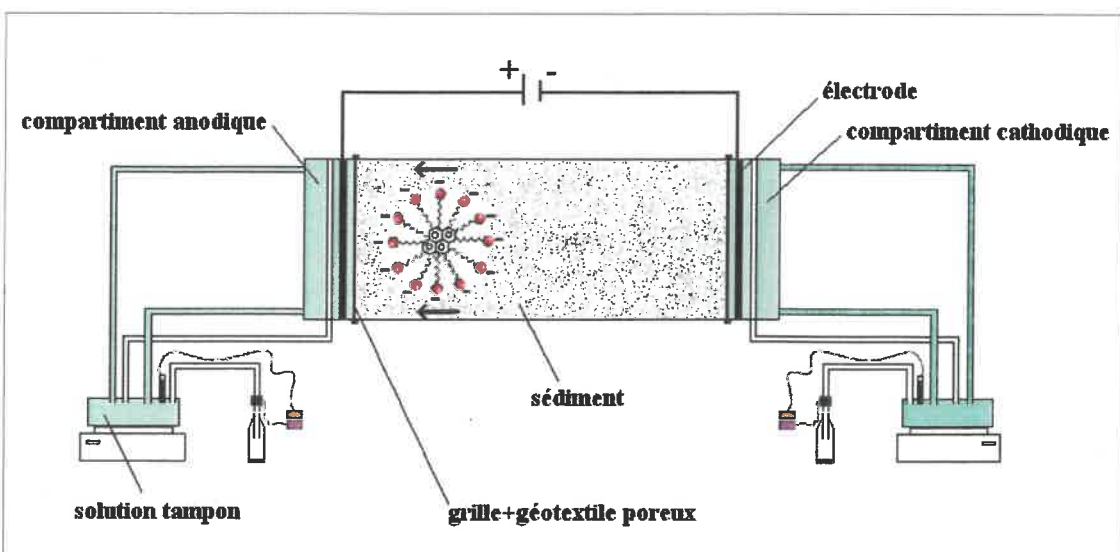
Polluants très hydrophobes et persistants, les HAP sont principalement rejetés dans l'atmosphère mais, peu ou pas solubles dans l'eau, ils finissent par s'accumuler naturellement dans les sols et sédiments. Ils présentent également un fort potentiel de bioconcentration dans les organismes (7). Or, ces polluants sont connus pour être cancérigènes, voire mutagènes et peuvent avoir par conséquent un impact non négligeable sur les organismes vivants (8).

a. Dépollution par électromigration : contraintes dues aux HAP

La technique de dépollution par électromigration consiste à atténuer la teneur en polluants ionisés en appliquant une différence de potentiel entre deux électrodes (implantées verticalement ou horizontalement dans le sédiment) qui provoque la migration des espèces chargées vers l'une au l'autre des électrodes (9). Les HAP n'étant pas ionisés, la technique d'électromigration ne semble pas particulièrement adaptée à ces micropolluants (10). L'originalité des recherches que nous allons présenter ici consiste cependant à envisager d'appliquer cette technique non seulement aux ETM, mais également aux HAP contaminant des sédiments de dragage portuaire ; les HAP doivent cependant être préalablement désorbés du sédiment et rendus solubles en milieu aqueux, grâce à l'utilisation d'agents tensioactifs anioniques, avant d'être transportés par le processus d'électromigration. En effet, les molécules amphiphiles que sont les agents tensioactifs, possédant une chaîne hydrocarbonée hydrophobe et une tête polaire anionique, ont la

Figure 1

Principe du procédé d'électromigration des HAP insérés dans des micelles anioniques.



Déséquéstration de polluants de type hydrocarbures aromatiques polycycliques à l'interface de sédiments au moyen d'un tensioactif original d'origine biologique

particularité de former des structures organisées, les micelles, au-delà d'une concentration appelée concentration micellaire critique (CMC). A l'intérieur de cette micelle anionique, une ou des molécules hydrophobes peuvent être insérées. On peut alors concevoir que cette micelle, chargée négativement, sera transportée au cours du processus d'électromigration et véhiculera ainsi les HAP, désorbés du sédiment et donc remobilisés dans le fluide interstitiel aqueux, par insertion dans le cœur hydrophobe de la micelle. La Figure 1 montre le procédé d'électromigration appliquée aux HAP, dans une cellule de conductimétrie. Le champ appliqué est d'environ 1 V.cm⁻¹.

Une quantité relativement importante d'agent tensioactif étant requise pour que ce procédé fonctionne, nous ne nous sommes pas tournés vers des tensioactifs anioniques issus de la synthèse, mais plutôt vers les biosurfactants, agents tensioactifs produits par des organismes vivants, et très facilement biodégradables, ce qui évite de rajouter une pollution supplémentaire au sédiment à traiter.

b. L'apport des biosurfactants

En ce qui concerne le biosurfactant utilisé dans le cadre de cette étude, il s'agit d'un biosurfactant anionique de type cyclolipopeptide (CLP), produit par la bactérie *Pseudomonas fluorescens* DSS73. Ce CLP (amphisine) est constitué d'une partie polaire comprenant un enchaînement de 11 acides aminés cyclisés deux acides aspartiques étant ionisés à pH > 3,9, et d'une chaîne hydrocarbonée lipophile à 10 carbones. La structure du CLP, ainsi que sa masse molaire moléculaire ($M = 1\ 394,8\ g\ mol^{-1}$), ont été déterminées par LC-MS (11) :



Figure 2

Analyse de l'amphisine produite par *Pseudomonas fluorescens* DSS73, purifiée et lyophilisée, en HPLC-UV ($\lambda = 210\ nm$).

Ce biosurfactant n'a jamais été testé dans le cadre de la dépollution des sols ou des sédiments, mais il présente l'intérêt d'abaisser fortement la tension de surface du milieu, qui passe de $69,3 \pm 0,9\ mN.m^{-1}$ avant croissance de *Pseudomonas fluorescens* DSS73 en

milieu DMB (voir matériel et méthodes) à $30,4 \pm 0,5\ mN.m^{-1}$ après croissance du micro-organisme et production de l'amphisine.

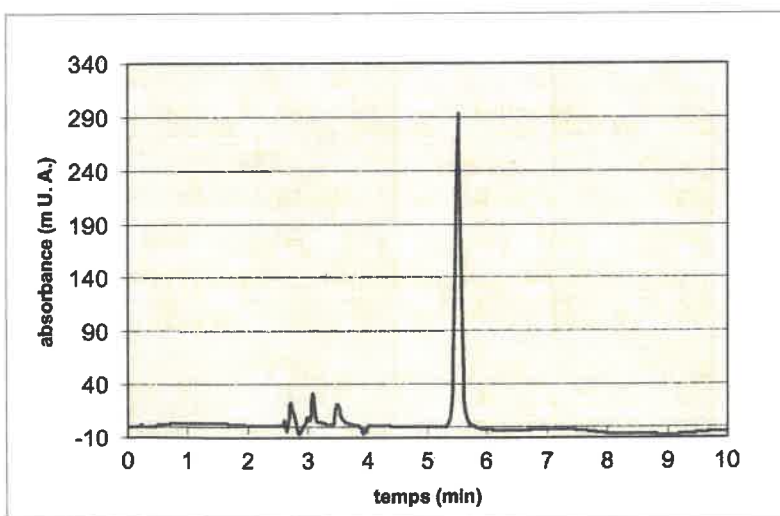
III. Adsorption des HAP à l'interface eau/sédiments et remobilisation par un biosurfactant

1. Matériel et méthodes

1.1. Production et purification du biosurfactant

La souche *Pseudomonas fluorescens* DSS73 est une souche rhizosphérique isolée d'un champ de betterave. Le milieu de culture utilisé lors de cette étude est le milieu Davis Minimal Broth ou DMB (en g.L⁻¹: K₂PO₄: 5,2; KH₂PO₄: 1,9; (NH₄)₂SO₄: 0,99; MgSO₄.7H₂O: 0,16; Glucose: 10,81; pH = 7) auquel est rajouté une solution de traces contenant des oligoéléments. Du milieu gélosé est obtenu en rajoutant de l'agar (15 g.L⁻¹). Après inoculation sur boîte de Pétri et incubation une semaine à 8°C, la totalité des tapis bactériens formés est mise en suspension dans de l'eau très peu minéralisée, par raclage en surface des géloses. La suspension obtenue est ensuite fortement agitée puis centrifugée (30 min, 18 000 g). Les mesures de tension de surface du surnageant sont effectuées par la méthode de la goutte pendante à l'aide d'un goniomètre G40 (Krüss, France).

Le surnageant contenant les biosurfactants est ensuite récupéré puis purifié par extraction liquide-solide (SPE) sur une cartouche Strata X contenant 2 g de phase polymérique (Phénomenex, Le Pecq, France) : après lavage et conditionnement, 100 mL de surnageant aqueux, auxquels ont été ajoutés 4 x 10⁻³ mol.L⁻¹ d'acide trifluoroacétique (TFA), sont percolés à travers la cartouche. L'élution se fait ensuite à l'aide de 40 mL d'acétate d'éthyle. Une seconde extraction de la phase aqueuse percolée est ensuite effectuée. Une fois les éluats réunis, la phase organique est évaporée à 40°C et 250 mBar à l'évaporateur rotatif, jusqu'à environ 10 mL. Afin de se débarrasser également de l'eau, le CLP est ensuite lyophilisé (lyophilisateur semi-pilote SMH15, Usifroid, Maurepas, France), la période de sublimation proprement dite durant au moins 48 h. On obtient alors un échantillon solide qui, après re-solubilisation dans l'acétonitrile, est analysé en HPLC-UV à 210 nm, sur une colonne C₁₈ Beckman (Fullerton, USA) (4,6 x 250 mm, particules de 5 µm) à l'aide d'une phase mobile constituée d'eau + 0,1% de TFA et d'acétonitrile (25 % de phase aqueuse, 75 % d'acétonitrile), à un débit de 1 mL.min⁻¹. La Figure 2 montre le chromatogramme obtenu : contrairement à d'autres souches bactériennes produisant des CLP, la souche *Pseudomonas fluorescens* DSS73 produit un type ultra-majoritaire de biosurfactant.





TECHNOLOGIE APPLIQUÉE

1.2. Analyse des HAP à l'interface eau/sédiments

Les études de comportement des HAP à l'interface eau/sédiments ont été réalisées dans un bain thermostaté (Fisher BioblockScientific, Illkirch, France) à une température constante de 25°C et sous agitation (300 rpm). Le dopage en HAP est réalisé en introduisant une concentration connue (C_0) à partir d'une solution mère de 16 HAP à 100 mg.L⁻¹. Lorsque l'équilibre thermodynamique est atteint, la phase aqueuse est séparée de la phase solide par centrifugation (40 minutes à 11 200 rpm). Les HAP non adsorbés restant à l'équilibre en phase aqueuse (C_{eq}) étant très peu concentrés, un protocole de purification et d'enrichissement par SPE est ensuite mis en œuvre, à l'aide de cartouches SPE Strata X (Phenomenex), contenant 60 mg de phase solide, couplées à des filtres Phenex en Téflon de 0,45 µm (Phenomenex). Afin d'obtenir des rendements d'extraction supérieurs à 80 %, il s'avère nécessaire d'homogénéiser le surnageant aqueux en rajoutant 20 % en volume d'acétone (qualité pour HPLC, Fisher Scientific), avant de procéder à sa percolation sur la cartouche SPE. Les HAP sont ensuite désorbés à l'aide de 5 mL de dichlorométhane (qualité pour HPLC, Fisher Scientific). Les analyses étant ensuite réalisées en HPLC à polarité de phases inversées, le dichlorométhane est évaporé sous flux d'azote (après adjonction de 60 µL de diméthylsulfoxyde), puis l'échantillon est re-solubilisé dans 4 mL

d'acetonitrile (qualité pour HPLC, Fisher Scientific). 10 µL d'échantillon sont ensuite injectés sur une colonne C₁₈ Envirosép PP de chez Phenomenex (150 x 4,6 mm, particules de 5 µm), avec un débit de phase mobile de 1 mL.min⁻¹, réglé par deux pompes Gold 126 Beckman Coulter. Le Tableau 1 présente les conditions du gradient d'élution mise en œuvre ainsi que la programmation des longueurs d'onde d'excitation et d'émission du détecteur fluorimétrique Prostar 363 (Varian, Palo Alto USA). La Figure 3 montre le processus analytique complet, qui permet, à l'issue du dosage par HPLC, d'obtenir la concentration de chaque HA restant à l'équilibre en phase aqueuse (C_{eq}) et par conséquent, connaissant la concentration initiale (C_0) lors du dopage du réacteur, de remonter à la concentration adsorbée sur le sédiment (C_{ads}). En faisant varier la concentration C_0 en HAP, on peut alors établir les isothermes d'adsorption à 25° pour chacun des HAP : $C_{ads} = f(C_{eq})$.

2. Résultats et discussion

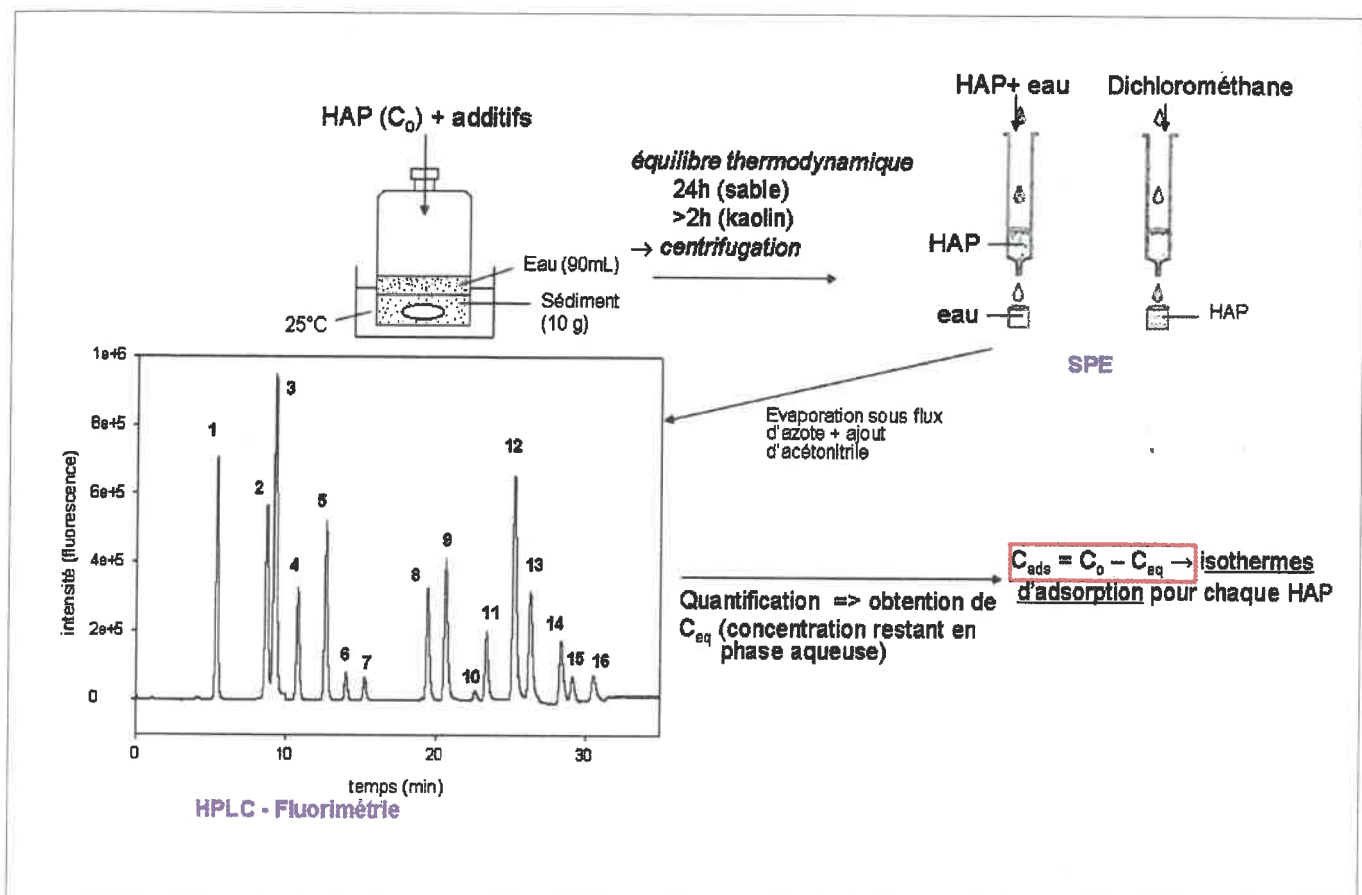
2.1. Adsorption des HAP sur le sable, le limon et le kaolin

Le sédiment est un matériau issu de l'érosion n'ayant pas encore subi de transformation diégénétique. Un sédiment se caractérise essentiellement par sa granulométrie, sa composition minérale, sa teneur en eau et en matière organique (MO). Le classement granulométrique de

Tableau I
Gradient d'élution en HPLC et
programmation des longueurs d'ondes en fluorimétrie pour
l'analyse de 16 HAP

Temps (min)	Gradient d'élution	λ_{ex} (nm)	λ_{em} (nm)	HAP détectés
0	Acetonitrile/eau 55/45% Gradient linéaire en 20 min	220	330	Naphtalène (1)
5			315	Acénaphthène (2) Fluorène (3)
7			370	Phenanthrène (4) Anthracène (5)
10			420	Fluoranthène (6) Pyrène (7)
13,4			385	Benzo[a]anthracène (8) Pyrène (9)
17		267	420	Benzo[e]pyrène (10) Benzo[b]fluoranthène (11) Benzo[k]fluoranthène (12)
21,7			420	Benzo[a]pyrène (13)
25			410	Dibenzo[a,h]anthracène (14) Benzo[g,h,i]péricrène (15)
27,4	Acetonitrile/eau 100/0%	290	500	Indéno[1,2,3-cd]pyrène (16)
29,8		245	330	
35	Acetonitrile/eau 55/45%	220		

Déséqustration de polluants de type hydrocarbures aromatiques polycycliques à l'interface de sédiments au moyen d'un tensioactif original d'origine biologique



sédiments, utilisé en géologie, différentie les plus gros blocs, galets, cailloux ou graviers, de diamètre supérieur à 2 mm, des sables (diamètre compris entre 20 µm et 2 mm), limons (2 à 20 µm) et des vases ou boues argileuses (diamètre inférieur à 2 µm). Dans notre étude, un sédiment modèle a été reconstitué, se rapprochant des sédiments présents dans une chambre de dépôt d'un grand port normand. Ce sédiment modèle contient 5 % de sable, de diamètre particulaire compris entre 125 et 315 µm (Sika, Hostun, France), 75 % de limon provenant des plateaux normands, de diamètre compris entre 4 et 100 µm (CETE, Rouen, France) et 20 % d'argile de type kaolinite, de diamètre inférieur à 80 µm, dont 54 % inférieur à 2 µm (Imerys, Poigny, France) : la proportion de particules fines, susceptibles de concentrer les pollutions, est donc particulièrement élevée. Dans un premier temps, nous nous sommes attachés à comprendre le comportement d'adsorption des HAP sur les différents constituants du sédiment. La technique d'analyse développée (SPE-HPLC-fluorimétrie) permet d'obtenir simultanément les isothermes d'adsorption des 16 HAP étudiés, mais également de comprendre leur comportement aux interfaces à des concentrations relativement faibles, comme cela peut survenir dans le cas de pollutions chroniques. La Figure 4 montre ainsi les isothermes d'adsorption de quatre des 16 HAP (pour plus de clarté) à l'interface entre l'eau et le sable, le limon ou le kaolin. On peut ainsi

dégager deux grandes tendances de l'étude de ces isothermes. En premier lieu, on voit que les HAP ne s'adsorbent pas de la même manière à la surface des différents constituants du sédiment, ceux-ci s'adsorbant beaucoup moins sur le sable (figure 4a) que sur le kaolin (figure 4c), le limon étant intermédiaire (figure 4b). Les isothermes d'adsorption atteignent en effet un plateau de saturation sur le sable à environ 0,2 mg.L⁻¹ (soit 1,8 µg de chaque HAP par gramme de sable sec), ce plateau étant plus élevé sur le limon (entre 0,4 mg.L⁻¹ et 0,9 mg.L⁻¹ selon les HAP, soit entre 3,6 et 8,1 µg.g⁻¹). Le plateau de saturation n'est du reste pas atteint sur le kaolin, dans les gammes de concentrations étudiées, ce qui montre que les particules les plus fines sont extrêmement rétensives vis-à-vis des HAP (on dépasse 9 µg de HAP adsorbé par gramme de kaolin). En deuxième lieu, on peut observer que les HAP ne s'adsorbent pas de la même manière selon qu'ils sont légers (acénaphthène, phénanthrène) ou lourds. En effet, les HAP lourds, du benz[a]anthracène à l'indéno[1,2,3-*cd*]pyrène, montrent des isothermes d'adsorption dont la pente est quasi parallèle à l'axe des y, ce qui révèle une très forte adsorption sur les particules fines du limon et surtout du kaolin, même à très faible concentration.

Des essais ont par ailleurs été effectués en fixant le pH du milieu à 4,7 (tampon acide acétique/acétate de sodium) et l'on a pu constater que seuls les HAP les plus légers étaient légèrement moins adsorbés

Figure 3
Protocole d'analyse et de dosage des HAP restant à l'équilibre dans le surmajeur aqueux. Numérotation sur le chromatogramme: voir Tableau I.



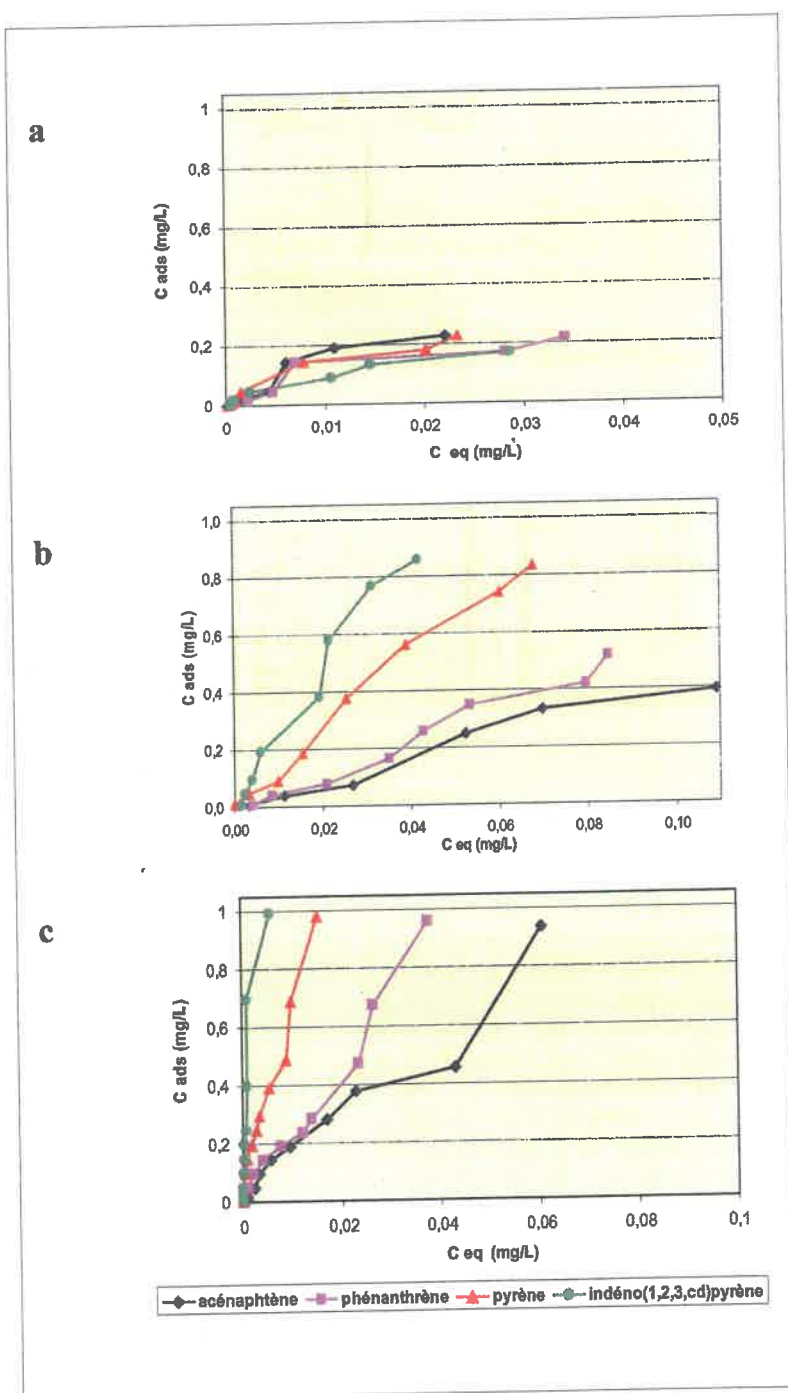
sur le kaolin dans des conditions de pH un peu plus acides. Ce pH est en fait également favorable à la migration des ETM, les métaux lourds pouvant précipiter à pH basique. Des essais ont également été réalisés en présence de chlorure de sodium (10 g.L^{-1}), puisque l'eau des bassins de stockage des sédiments, proches des zones portuaires maritimes, est saline. La présence de sel n'affecte que peu l'adsorption des HAP sur le sédiment : seuls les HAP légers sont légèrement moins adsorbés sur les particules fines, car un peu plus solubles dans la phase aqueuse, à force ionique plus élevée. Enfin, les isothermes d'adsorption des HAP ont été déterminées en présence de 1 et 5 % de matière organique (MO) dans le sédiment reconstitué, la MO étant issue de la décomposition de matière végétale (fournie par Véolia). Il s'avère que la MO adsorbe très fortement les HAP, surtout les plus lourds, et ce d'autant plus que sa teneur dans le sédiment augmente (résultats non montrés).

L'objectif est donc de parvenir à désorber, donc à remettre en solution aqueuse, une partie des HAP fortement adsorbés sur les particules du sédiment, afin qu'ils puissent migrer ultérieurement vers le compartiment anodique du pilote d'électromigration. On pourra ainsi atténuer la pollution organique séquestrée par les particules les plus fines du sédiment.

2.2. Remise en solution des HAP à l'aide de l'amphiphine

Les premiers essais ont été effectués sur du kaolin, qui, comme cela vient d'être montré, est le matériau présent dans le sédiment qui adsorbe le plus les HAP. Dans un premier temps, l'amphiphine a été introduite dans le milieu à une teneur de $0,1 \text{ g.L}^{-1}$, ce qui est probablement légèrement au-dessus de sa CMC si l'on se réfère aux CMC de cyclolipopéptides proches, tels la viscosine ($0,054 \text{ g.L}^{-1}$) (12) ou le massetolide ($0,025 \text{ mg.L}^{-1}$) (13). Malheureusement, l'amphiphine n'a pas conduit à une remobilisation nette des HAP, qu'ils soient légers ou lourds, à cette concentration. En effet, une faible proportion de biosurfactant s'adsorbe à l'interface solide/liquide et la CMC effective est, de ce fait, plus élevée que la CMC en phase aqueuse. Dans un deuxième temps, des essais ont été effectués à une teneur de 1 g.L^{-1} en CLP (soit $7,2 \cdot 10^{-4} \text{ mol.L}^{-1}$). Comme le montre la Figure 5 (deux des 16 HAP étudiés sont montrés pour plus de clarté), l'adjonction d'amphiphine au milieu a conduit à une nette diminution de la pente des isothermes d'adsorption, ce qui montre qu'une partie plus importante des HAP reste en phase aqueuse en présence de CLP. Cela est vrai pour les HAP légers, tel l'acénaphthène, comme pour les HAP les plus lourds et très fortement adsorbés, tel l'indéno[1,2,3-c,d]pyrène.

La quantité de biosurfactant nécessaire pour remobiliser efficacement les HAP des particules fines de kaolin peut sembler à première vue importante. Nous avons donc cherché à comparer son efficacité à celle d'un tensioactif synthétique classique, à savoir le dodécylsulfate de sodium (SDS). Comme pour le



CLP, l'adjonction de SDS à $10^{-2} \text{ mol.L}^{-1}$ ($2,88 \text{ g.L}^{-1}$), valeur proche de sa CMC ($8 \cdot 10^{-3} \text{ mol.L}^{-1}$), n'a pas permis de remobiliser de manière significative les HAP en phase aqueuse. En revanche, à une valeur dix fois supérieure à sa CMC ($23,07 \text{ g.L}^{-1}$), le SDS a permis de remobiliser les HAP en phase aqueuse dans des proportions à peu près équivalentes à celles de l'amphiphine (figure 5). Il est clair au vu de ces résultats que le biosurfactant anionique a un potentiel important de re-solubilisation des HAP en phase aqueuse, même pour les plus adsorbés à la surface du kaolin, et ceci à des teneurs 20 fois inférieures (en concentration massique) ou 110 fois inférieures (en concentration molaire) à un tensioactif anionique synthétique classique tel le SDS.

Figure 4

Isothermes d'adsorption à 25°C de quatre des 16 HAP testés aux interfaces : a: eau/sable; b: eau/limon; c: eau/kaolin

Déséquestration de polluants de type hydrocarbures aromatiques polycycliques à l'interface de sédiments au moyen d'un tensioactif original d'origine biologique

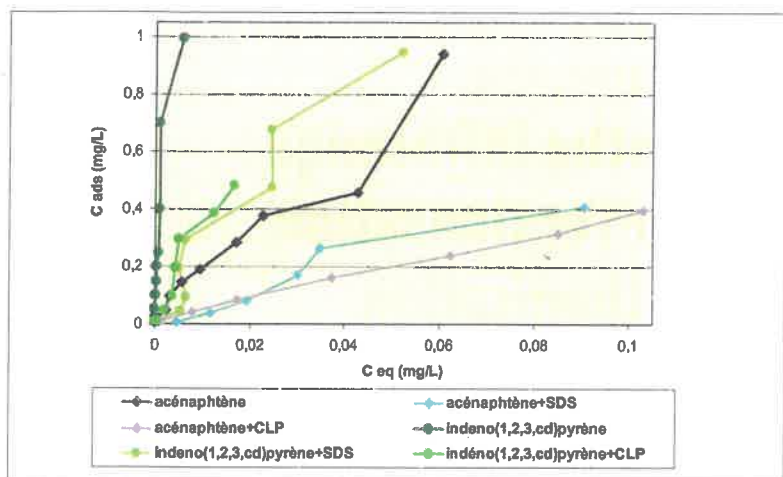


Figure 5

Isothermes d'adsorption à 25°C de deux des 16 HAP testés à l'interface eau/kaolin, en présence ou non de SDS (8.10-2 mol. L-1 ou 23,07 g.L-1) ou d'amphisine (7,2.10-4 mol.L-1 ou 1 g.L-1).

IV. Conclusion

Le développement d'une méthode d'analyse chromatographique sensible, alliée à un enrichissement de traces par SPE, a permis d'obtenir simultanément les isothermes d'adsorption d'un mélange complexe de 16 HAP et de comprendre leur mécanisme d'adsorption à l'interface eau/sédiments modèles. Le biosurfactant produit

par la souche *Pseudomonas fluorescens* DSS73, amendé au sédiment, semble très prometteur en ce qui concerne la dé-séquestration des HAP fortement adsorbés sur les particules les plus fines du sédiment, à savoir les particules de kaolin. Il est quasiment aussi efficace qu'un tensioactif synthétique classique, tel le SDS, mais à des teneurs molaires 110 fois inférieures. Il reste désormais à montrer son efficacité sur un sédiment complexe, composé du mélange sable/limon/kaolin, en présence de matière organique et en milieu salin. L'étape suivante sera bien évidemment de tester l'efficacité du biosurfactant au sein d'un pilote d'électromigration à l'échelle du laboratoire, en prenant soin de contrôler le pH et bien sûr la température du milieu, qui peuvent fortement évoluer au cours du procédé électrocinétique. À terme, il serait également très intéressant de tester la production *in situ* d'amphisine, afin d'augmenter l'efficacité du procédé de bioremédiation par électromigration en réalisant une bioaugmentation : en effet, si la souche est viable (14) et parvient à produire l'amphisine en continu dans le milieu interstitiel du sédiment, on pourra éviter de renouveler l'amendement de biosurfactant trop fréquemment, celui-ci étant facilement biodégradable.

BIBLIOGRAPHIE

- (1) ACAR YB, ALSHAWABKEH AN, Principles of electrokinetic remediation, *Environ. Sci. Technol.*, 1993, 27, 2638-47. DOI : 10.1021/es00049a002.
- (2) SUER P, GITYE K, ALLARD B, Speciation and transport of heavy metals and macroelements during electroremediation, *Environ. Sci. Technol.*, 2003, 37, 177-81. DOI : 10.1021/es010226h.
- (3) NYSTROEM GM, OTTOSEN LM, VILLUMSEN A, Electrodialytic removal of Cu, Zn, Pb and Cd from harbor sediment: influence of changing experimental conditions, *Environ. Sci. Technol.*, 2005, 39, 2906-11. DOI : 10.1021/es048930w.
- (4) WICK LY, MATTLE PA, WATTIAU P, HARMS H, Electrokinetic-transport of PAH-degrading bacteria in model aquifers and soil, *Environ. Sci. Technol.*, 2004, 38, 4596-602. DOI : 10.1021/es0354420.
- (5) PORTET-KOLTALO F, AMMAMI MT, BENAMAR A, DUCLAIR-POC C, GROBOILLOT A, ORANGE N, Pollution des sédiments de dragage : procédés de bioremédiation alliés à l'électromigration, *Spectra Analyse*, 2010, 277, 54-8.
- (6) OUKEBDANE K, PORTET-KOLTALO F, MACHOUR N, DIONNET F, DESBENE PL, Comparison of hot Soxhlet and accelerated solvent extractions with microwave and supercritical fluid extractions for the determination of polycyclic aromatic hydrocarbons and nitrated derivatives strongly adsorbed on soot collected inside a diesel particulate filter, *Talanta*, 2010, 82, 227-36. DOI : 10.1016/j.talanta.2010.04.027.
- (7) PERELO LW, In situ and bioremediation of organic pollutants in aquatic sediments, *J. Hazard. Mater.*, 2010, 177, 81-9. DOI : 10.1016/j.jhazmat.2009.12.090.
- (8) IARC (International Agency for Research on Cancer), in IARC monographs on the evaluation of the carcinogenic risk of chemicals to humans : polynuclear aromatic compounds, IARC eds., Lyon, 1983, Part I.
- (9) ALCANTARA MT, GOMEZ J, PAZOS M, SANROMAN MA, Electrokinetic remediation of PAH mixtures from kaolin, *J. Hazard. Mater.*, 2010, 179, 1156-60. DOI : 10.1016/j.jhazmat.2010.03.010.
- (10) PAZOS M, ROSALES E, ALCANTARA T, GOMEZ J, SANROMAN M, Decontamination of soils containing PAHs by electroremediation : A review, *J. Hazard. Mater.*, 2010, 177, 1-11. DOI : 10.1016/j.jhazmat.2009.11.055.
- (11) SORENSEN D, NIELSEN TH, CHRISTOPHERSEN C, SORENSEN J, GAJHEDE M, Cyclic lipopeptideamphisin from *Pseudomonas* sp. Strain DSS73, *Acta Cryst.*, 2001, C57, 1123-4.
- (12) SAINI HS, et al, Efficient purification of the biosurfactantviscosin from *Pseudomonas Libanensis* strain M9-3 and its physico-chemical and biological properties, *Journal of Natural Products*, 2008, 71, 1011-5. DOI : 10.1021/np800069u.
- (13) DE SOUZA JT, DE BOER M, DE WAARD P, VAN BEEK TA, RAAIJMAKERS JM, Biochemical, Genetic, and Zoosporicidal Properties of Cyclic Lipopeptide Surfactants Produced by *Pseudomonas fluorescens*, *Appl. Environ. Microbiol.*, 2003, 69, 7161-72. DOI : 10.1128/AEM.69.12.7161-7172.2003.
- (14) WICK LY, MATTLE PA, WATTIAU P, HARMS H, Electrokinetic Transport of PAH-Degrading Bacteria in Model Aquifers and Soil, *Environ. Sci. Technol.*, 2004, 38, 4596-602. DOI : 10.1021/es0354420.

REMERCIEMENTS
Nous tenons
à remercier la
région Haute
Normandie
pour le
financement
accordé dans le
cadre du projet
RESSOLV, inscrit
dans le réseau
de recherche
normand
SCALE.

P12

Article

Novel Application of Cyclolipopeptide Amphisin: Feasibility Study as Additive to Remediate Polycyclic Aromatic Hydrocarbon (PAH) Contaminated Sediments

Anne Groboillot ¹, Florence Portet-Koltalo ², Franck Le Derf ², Marc J. G. Feuilloley ¹, Nicole Orange ¹ and Cécile Duclairoir Poc ^{1,*}

¹ Laboratory of Cold Microbiology-Signals and Microenvironment, University of Rouen, EA 4312, 55 rue Saint Germain, 27000 Evreux, France; E-Mails: anne.groboillot@univ-rouen.fr (A.G.); marc.feuilloley@univ-rouen.fr (M.J.G.F.); nicole.orange@univ-rouen.fr (N.O.)

² UMR 6014 COBRA, University of Rouen, 55 rue Saint Germain, 27000 Evreux, France; E-Mails: florence.koltalo@univ-rouen.fr (F.P.-K.); franck.lederf@univ-rouen.fr (F.L.D.)

* Author to whom correspondence should be addressed; E-Mail: cecile.poc@univ-rouen.fr; Tel.: +33-332-291-549; Fax: +33-332-291-550.

Received: 3 November 2010; in revised form: 15 February 2011 / Accepted: 2 March 2011 /

Published: 9 March 2011

Abstract: To decontaminate dredged harbor sediments by bioremediation or electromigration processes, adding biosurfactants could enhance the bioavailability or mobility of contaminants in an aqueous phase. Pure amphisin from *Pseudomonas fluorescens* DSS73 displays increased effectiveness in releasing polycyclic aromatic hydrocarbons (PAHs) strongly adsorbed to sediments when compared to a synthetic anionic surfactant. Amphisin production by the bacteria in the natural environment was also considered. DSS73's growth is weakened by three model PAHs above saturation, but amphisin is still produced. Estuarine water feeding the dredged material disposal site of a Norman harbor (France) allows both *P. fluorescens* DSS73 growth and amphisin production.

Keywords: biosurfactant; solubility enhancement; polycyclic aromatic hydrocarbons; bioremediation; dredged sediments

1. Introduction

Recently, increasing interest has been given to biosurfactants, as these metabolites are produced by a wide variety of microorganisms [1–8]. Their amphiphilic structure leads them to accumulate at the interfaces, thus they are able to increase solubility and diffusion of insoluble compounds in water. Compared to their synthetic counterparts, biosurfactants are known for their biodegradability, their reduced toxicity, and their environmental “friendliness” [9]. Moreover, their efficiency is often higher than conventional surfactants: a similar surface tension reduction is obtained by a smaller biosurfactant quantity [3]. Their efficiency has been also proven in extreme conditions (temperature, ionic strength, pH) [10–12].

Such properties allow the biosurfactants to be potential candidates in many industrial applications, especially in the food, cosmetics, agricultural chemicals, biomedical materials or in health care and cleaning industries, *etc.* They have also been tested in environmental applications [3,7,8,13,14]. Indeed more and more environmental regulations favor these bioproducts compared to synthetic surface-active compounds [15].

Essentially, biosurfactants are classified either as low or high-molecular-mass. Whereas high-molecular-mass biosurfactants consist in particulate and polymeric amphiphiles, the low molecular-mass biosurfactants deal with three major types:

- glycolipids or lipopolysaccharides: rhamnolipids, trehalololipids [16], sophorolipids [17,18];
- lipoproteins-lipopeptides: acyclic [19] and cyclic ones (cyclolipopeptides) [20,21];
- and hydroxylated crosslinked fatty acids (mycolic acids) or phospholipids [3].

Among them, rhamnolipids, produced by *Pseudomonas aeruginosa*, are intensively described in literature and their applications also [3,14,16,22,23]. However, our interest was retained by cyclolipopeptides (thereafter mentionned as CLPs), because of the variety of microorganisms, which produce them, mainly *Bacillus* and *Pseudomonas* bacteria [4,7,21,24] and their abundant variability of structures [21,24]. They are composed of several amino-acids linked to a molecule of hydroxyalkyl acid [25]. The first discovered was surfactin [26–29]. CLPs are especially attractive for industrial applications as they present good surface tension reduction with low critical micellar concentrations (CMC, need of minimum CLPs quantity to be efficient) and versatile bioactive properties. Thus, CLPs attract attention of food and biomedical industries [30,31].

Concerning environmental remediation of any organic or inorganic contaminants [14,32], biosurfactants present a great potential in oil or metal recovery, increasing bioavailability of low solubility compounds [7,19,33,34]. Most of the more persistent organic compounds, such as polycyclic aromatic hydrocarbons (PAHs) or polychlorinated biphenyls (PCBs), are toxic and carcinogenic [35]. Among all the PAHs, 16 individual PAH compounds, consisting of two to six fused aromatic rings, have been classified as priority pollutants by the United States Environmental Protection Agency [36] due to their chronic toxic effects. Various environmental matrices, such as air, water, vegetation, soil and sediments act as environmental sinks for PAHs. Indeed, high concentrations of PAHs in benthic and aquatic organisms, but also in sediments, have already been reported [37,38].

In the case of river or harbor sediment contamination, dredging seems to be the beginning of a solution for pollution remediation [39]. In France, materials dredged annually in the harbors and the

channels represent about $50 \times 10^6 \text{ m}^3$, of that $24 \times 10^6 \text{ m}^3$ concentrate most of organic and inorganic contamination. Regulations have become more strict in Europe in the last decade. To protect the marine environment against ecological risks of dredging and capping, contaminated sludge can no longer be dumped at sea. The alternative is to store it in confinement sites, which are currently reaching capacity in Europe. Different options are now being explored in order to eliminate, or at least to weaken, the present contamination in sediments, to valorize them thereafter as filling or building materials, *etc.* The pretreatment processes primarily consist in a granulometric separation of the coarse fractions from the fine particles, where pollution is concentrated. After pretreatment, polluted fine slurries may be stored in confinement sites or submitted to processes elaborated for polluted grounds. The offered remediation strategies are mainly classified in four types: chemical, physical, or physical-chemical together, and biological [40]. Briefly, chemical treatments are largely based on oxidation with various oxidants. The physical-chemical processes are mainly extraction and washing. Washing treatments are less aggressive than physical treatments (e.g., incineration, thermal desorption, *etc.*) and thus less disturbing for the ground [41]. An alternative technique would also be an electrokinetic remediation (EK), which presents less important energy cost and is particularly adapted for fine sediments. A weak electric current, applied via electrodes inserted horizontally or vertically into the matrix to be treated, induces the mobility of the ionized species in the interstitial liquid phase towards the two electrodes permitting to reduce the contaminants level inside the sediments [42,43].

Finally, several bioremediation approaches are also proposed: first of all to diminish the risk associated to the remediation processes to human health, secondly to minimize the costs, and thirdly to be less invasive for the environment [44]. Bioremediation consists in soil detoxification by using either micro-organisms or biomass to biodegrade or absorb the pollutants. The principal processes are generally biostimulation, bioattenuation or bioaugmentation [45]. An extended definition of bioremediation would be soil or sediment amendment with additives from biological origins, (e.g., biosurfactant which contribute to the decontamination process).

To achieve better PAH removal efficiencies (extraction and/or degradation) and to pass through limitations of individual remediation techniques, physical, chemical and biological treatments can be combined [40]. For instance, the combination of an electrokinetic process and bioremediation (EK-bioremediation) enhances the transport of bacteria and nutrients for a more effective biodegradation [46,47]. Adding solubilizing agents, such as surfactants or cyclodextrines, also increases PAH removal [40,47], and in this case, even biosurfactants can be used [39,48]. Ju and Elektorowicz demonstrated that the rhamnolipids coupled with an electrokinetic process increased the solubility into the aqueous phase of phenanthrene contaminating the soil [48].

Consequently, we suggest here to work on contaminated harbor dredged sediments and to use biosurfactant-enhanced PAH solubilization with the aim of coupling it later with a physical-chemical process, such as EK. In natural conditions, *i.e.*, at the aqueous/solid interface, the biosurfactant has to be characterized by a low surface tension to improve PAHs solubility, and this is exactly the case of CLPs. Thus, in a first step, the present study focuses on the feasibility of using the anionic CLP, *i.e.*, amphisin, which is produced by *Pseudomonas fluorescens* DSS73, for a PAH solubilization purpose from polluted sediments. Hence, after a PAH's sorption study on the coarse and finest particles of a model sediment, the efficiency of amphisin will be evaluated on the desorption of a PAH mixture

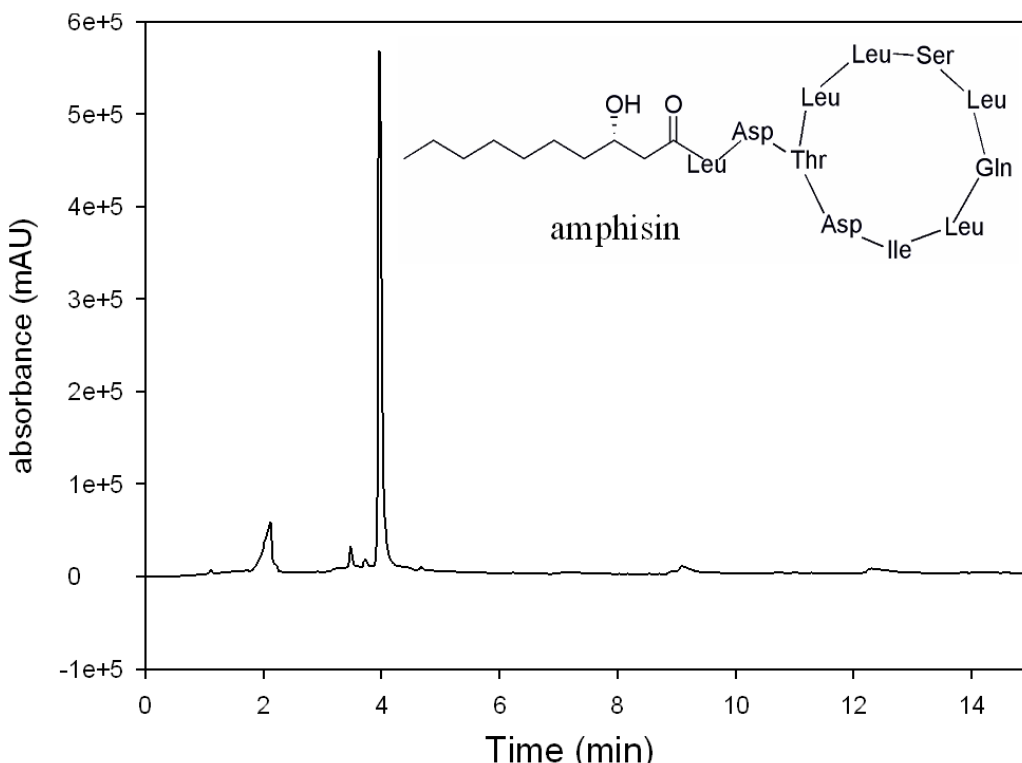
from kaolin. As regards to the *in situ* process, a convenient approach consists in direct addition of amphisin in sediments. An alternative solution would be amendment of the bacteria in the polluted sediments where they will grow and produce their biosurfactant. In that case, unlike classical bioaugmentation, bacterial addition to sediments will not lead to the pollutant biodegradation but solely to the biosurfactant production. Thus, in a second step, the feasibility of *P. fluorescens* DSS73 amendment will be evaluated. Therefore, the effect of three model PAHs, taken separately, will be studied on *P. fluorescens* DSS73 physiology, in erlenmeyer flasks and in low oxygen growth conditions. Then to mimic *in situ* conditions, the effect of estuarine water will be also investigated. Thereafter, the biosurfactant production in laboratory conditions or in real estuarine water will be verified.

2. Results and Discussion

2.1. Purity of Produced Amphisin by *Pseudomonas fluorescens* DSS73

In order to verify the production of biosurfactant by *P. fluorescens* DSS73 grown on DMA, at 8 °C, the surface tension of the rinsing solution was evaluated at $32.1 \pm 0.9 \text{ mN}\cdot\text{m}^{-1}$. Compared to the surface tension of the standard (*i.e.*, $71.7 \pm 0.3 \text{ mN}\cdot\text{m}^{-1}$), this value, which is lower than $40 \text{ mN}\cdot\text{m}^{-1}$, indicates the presence of a biosurfactant [49]. After purification and lyophilization, the purity of the biosurfactant, described earlier as amphisin [20,50] was analyzed by HPLC-UV. On the chromatogram presented in Figure 1, a single peak appeared, revealing an ultra-majority production of amphisin by *P. fluorescens* DSS73 and not a mixture of different CLPs.

Figure 1. HPLC-UV chromatogram ($\lambda = 210 \text{ nm}$) of the freeze dried biosurfactant produced by *P. fluorescens* DSS73, the amphisin and its structure.

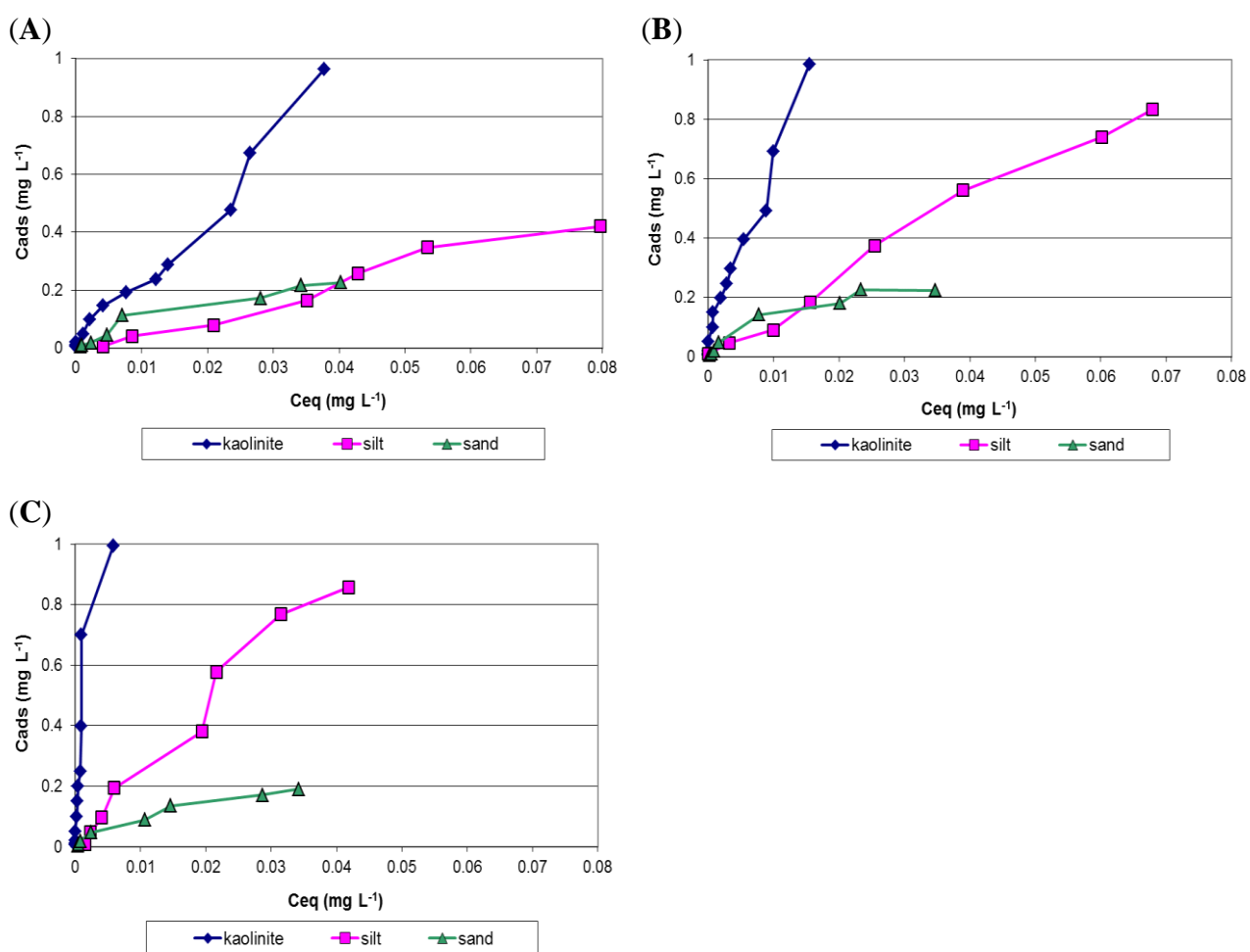


2.2. PAHs Adsorption at Water/Sediments Interface and Their Mobilization by Amphisin

2.2.1. PAHs Adsorption on Dredged Sediments Modeled by Sand, Silt and Kaolin

We worked on a model sediment which was reconstituted to mimic the existing sediments from a disposal site managed by a Norman harbor (France). Indeed such a material is able to adsorb particularly high PAHs concentrations due to its high proportion of fine particles (see Experimental section). Thus, we chose to study the behavior of 15 PAHs (among the 16 U.S. EPA priority PAHs generally found in the environment) at various water/solid interfaces, to understand which of the sediment constituents is the more retentive.

Figure 2. Adsorption isotherms of different PAHs at water/sand, water/silt and water/kaolin interfaces at 25 °C. (A) phenanthrene; (B) pyrene; (C) indeno[1,2,3,cd]pyrene.



Only the adsorption of some of the PAHs is plotted in Figure 2 (for more clarity), *i.e.*, phenanthrene, which represents a low weight PAH (Figure 2A), pyrene, which represents an intermediary PAH (Figure 2B) and indeno[1,2,3,cd]pyrene, which represents a high weight PAH (Figure 2C). The adsorption isotherms show the interfacial exchanges between water and sand, silt or kaolin, the main components of the harbor sediment. Two main trends are observed through these isotherms. Firstly, PAHs do not adsorb in the same way on the surface of the different sediment

constituents. PAH adsorption on sand is markedly weaker than on kaolin, and silt presents an intermediate. Indeed, all PAH adsorption isotherms reach a saturation level for sand at approximately $0.2 \text{ mg}\cdot\text{L}^{-1}$ ($1.8 \mu\text{g}$ of each PAH per gram of dry sand). This saturated value is higher on the silt (between $0.4 \text{ mg}\cdot\text{L}^{-1}$ and approximately $0.9 \text{ mg}\cdot\text{L}^{-1}$ according to tested PAH, *i.e.*, between 3.6 and $8.1 \mu\text{g}\cdot\text{g}^{-1}$). The saturation level is not reached on the kaolin surface in the studied concentration range. These results demonstrated that PAHs concentrate more on the finest particles, where the proportions exceed $9 \mu\text{g}\cdot\text{g}^{-1}$ of dry kaolin. Secondly, PAH adsorption is related to its structure, *i.e.*, the number of aromatic ring (three or four ring PAHs, respectively, in Figure 2 (A,B), or six ring PAHs in Figure 2C). Adsorption isotherms from fine kaolin particles are almost parallel to the y-axis for the very heavy PAHs (from benz[a]anthracene to indeno[1,2,3,cd]pyrene), meaning that they are so strongly adsorbed on the clay that we can really speak about “sequestration” of PAHs by this major constituent of the sediment.

Tests were also carried out on the presence of sodium chloride ($10 \text{ g}\cdot\text{L}^{-1}$), since the water present in the sediment pond, closed to the harbor ecosystem, is briny. The presence of salt had rather little effect on PAHs adsorption on sediments (data not shown): only light PAHs were slightly less adsorbed on fine particles, because they were a little more soluble in the aqueous phase, with a higher ionic strength.

Finally, PAHs adsorption was performed on the reconstituted sediment matrix (mixture of sand, silt and kaolin). Organic matter (OM) was introduced at 1 or 5% w/w. In such conditions, PAHs (especially the heaviest ones) were more strongly adsorbed, and this phenomenon was increased when the OM concentration rose (data not shown).

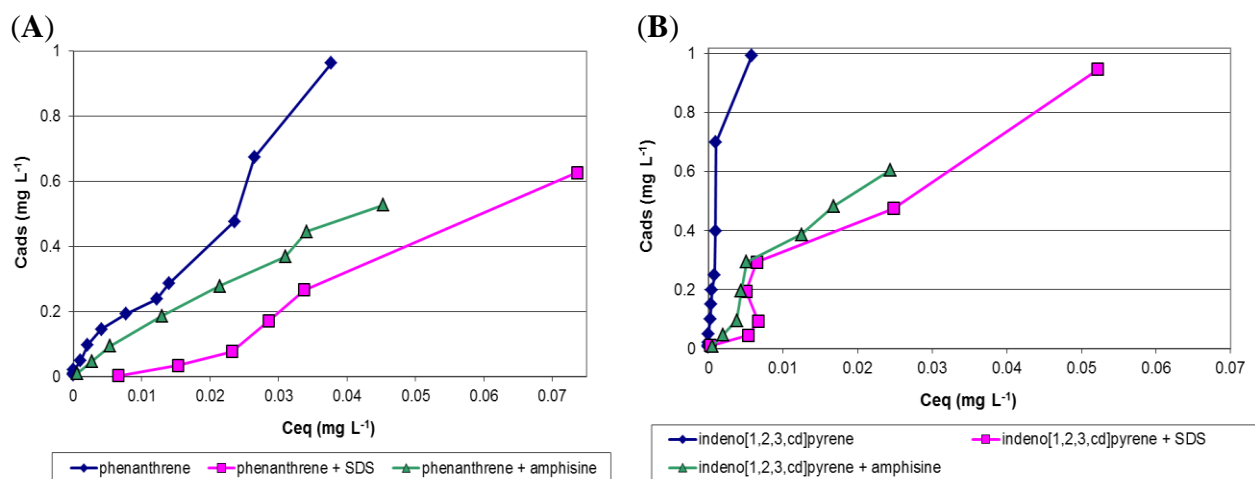
Having shown how the adsorption mechanism works, our goal was now to manage to desorb, *i.e.*, to transfer into the aqueous solution, a part of the strongly adsorbed PAHs on sediment particles, with the aim of their removal by an EK-bioremediation process. Indeed, the mobilization of sequestered PAHs by an anionic micellar system could make it possible not only to enhance the PAH solubilization in water, but also to enhance the migration towards the anodic compartment of an electromigration pilot. Our purpose was also to evaluate the desorption phenomenon in conditions close to real ones, observed in sediment disposal sites: the concentration of studied PAHs were lower than those usually found in literature [51,52], and the tested PAHs were chosen to cover different PAH characteristics (hydrophobicity, more or less complex structure).

2.2.2. PAHs Solubility Enhancement with the Help of Amphisin

Based on previous results, kaolin seems to be the most powerful PAHs adsorbent through sediment components, so amphisin efficiency was first evaluated on kaolin. The mixture of 15 PAHs was used to pollute our model sediment. In this part of the study, for more clarity, we report only phenanthrene, representing low weight PAHs (Figure 3A), and indeno[1,2,3,cd]pyrene, representing heavier PAHs (Figure 3B).

Contaminant solubilization is enhanced by any surfactant, synthetic [39] or biological [53], through micellar solubilization. Hydrophobic PAHs are entrapped inside the micelle, whose core is more hydrophobic than the matrix bulk, and PAHs solubility is greatly enhanced. As reported by Lai [54], the PAHs removal efficiency increased with a biosurfactant concentration increase, but it is not significantly related to the contact time.

Figure 3. Adsorption isotherms of different PAHs at water/kaolin interface in the presence of SDS (8×10^{-2} mol·L $^{-1}$) or amphisin (7.2×10^{-4} mol·L $^{-1}$) and in their absence at 25 °C. (A) phenanthrene; (B) indeno[1,2,3,cd]pyrene.



First, the added amphisin concentration, *i.e.*, 0.1 g·L $^{-1}$ into the system, may be slightly above its CMC, which should be closer to other CLPs, for example 0.054 g·L $^{-1}$ for viscosin [55]. Unfortunately, at this concentration, no clear PAHs mobilization was obtained for any PAHs, light or heavy. In fact, a small amphisin quantity should be adsorbed on the solid/liquid interface, increasing the effective CMC related to this model medium, which is higher than the CMC in water.

After adding more amphisin (1 g·L $^{-1}$, *i.e.*, 7.2×10^{-4} mol·L $^{-1}$), an important decrease in the slope of the adsorption isotherms was observed as shown in Figure 3. At such a concentration, amphisin kept a greater amount of PAHs in the aqueous phase. This PAH mobilization was observed for light PAHs, such as phenanthrene (Figure 3A), and for the heavier (and more adsorbed) ones, such as indeno[1,2,3,cd]pyrene (Figure 3B). At first sight, PAHs solubilizing enhancement from fine kaolin particles was managed with quite a great quantity of amphisin. To compare with a conventional synthetic surfactant, namely sodium dodecylsulfate (SDS), 10^{-2} mol·L $^{-1}$ (2.88 g·L $^{-1}$) of SDS was added to evaluate the efficiency of the solubilizing enhancement. As for amphisin, this chosen SDS quantity was close to its CMC (8×10^{-3} mol·L $^{-1}$) and did not significantly allow PAH mobilization in an aqueous phase. Yet, with a concentration “ten-fold” over its CMC (23.07 g·L $^{-1}$), SDS enhanced the PAH’s solubilization in an aqueous phase in equivalent proportions to the amphisin for heavier PAHs (Figure 3B). In summary, amphisin, an anionic CLP, presents great potential to mobilize PAHs in aqueous phase, even the most adsorbed ones on the kaolin surface, and its efficiency is noteworthy with 20-times less (in mass concentration) or 110-times less (in molar concentration) that of the anionic synthetic SDS.

Next we tested if the strain is able to grow and still to produce amphisin in the presence of pollutants and in the real interstitial aqueous medium of the dredged sediments.

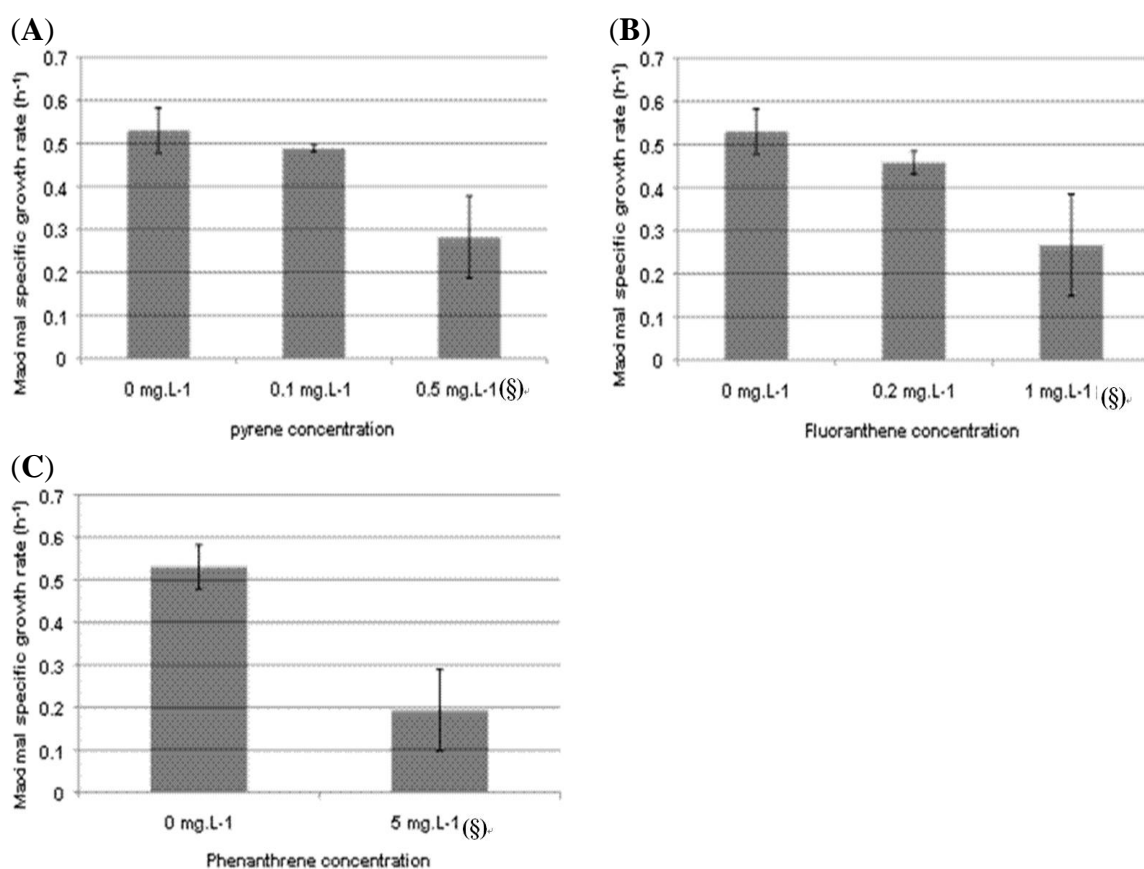
2.3. Effect of Three Model PAHs on *Pseudomonas fluorescens* DSS73 Growth Kinetics

2.3.1. Growth in Erlenmeyer Flasks

Pyrene, fluoranthene or phenanthrene was introduced, as model PAHs, before inoculation of Davis Minimal Broth (DMB) by *P. fluorescens* DSS73 to follow its growth in erlenmeyer flasks.

As PAH concentrations in the dredged sediments are generally under their solubility limit, two concentrations were tested: one just below the solubility limit and one slightly above.

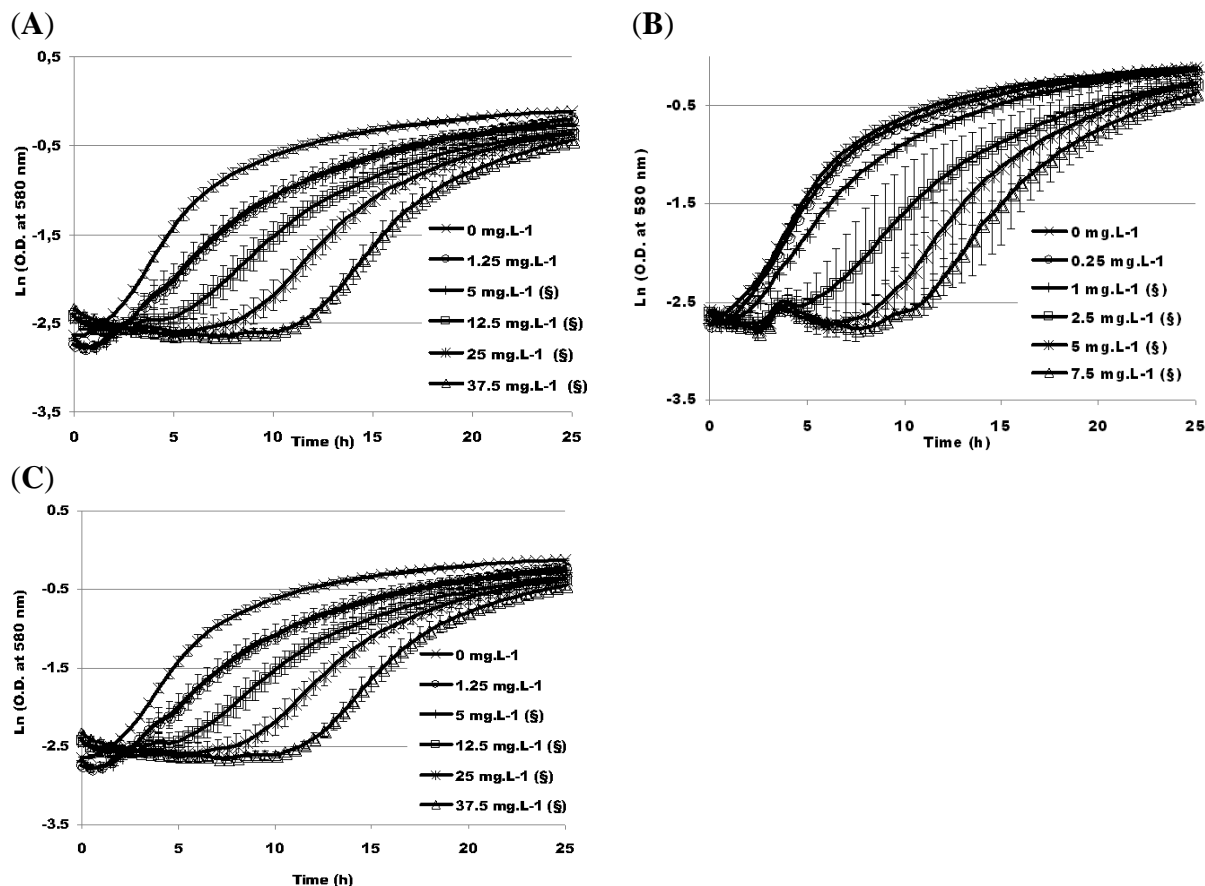
Figure 4. Effect of PAH concentration on maximal specific growth rate of *P. fluorescens* DSS73 in DMB. (§: PAH concentration higher than its solubility limit). (A) pyrene; (B) fluoranthene; (C) phenanthrene. All experiments were done in triplicate.



As shown in Figure 4, for all the tested PAHs concentrations, *P. fluorescens* DSS73 was able to grow. At concentrations lower than PAHs saturation, the maximum specific growth rates, μ_{\max} , were in the same range with or without PAH, thus the presence of pollutants did not significantly modify bacterial development. However, when the growth medium was saturated by PAHs, the bacterial growth was more disturbed: μ_{\max} decreased drastically for each of the three PAHs.

Culturing in erlenmeyer flasks favors bacterial growth in regard to those existing growth conditions in dredged sediment disposal sites, where the oxygenation of the matrix is weaker. So growth tests were also performed in oxygen-limited conditions.

Figure 5. Effect of different PAH concentrations on the growth kinetics of *P. fluorescens* DSS73 in DMB in oxygen-limited conditions. (§: PAH concentration higher than its solubility limit). (A) pyrene; (B) fluoranthene; (C) phenanthrene. All experiments were done in triplicate.



2.3.2. Growth in Oxygen-Limited Conditions

To better mimic *in situ* parameters, a similar study was made with a microplate reader. With this apparatus, same growth rates were obtained with regard to erlenmeyer cultures, when 100 μ L of culture were used in 400 μ L microplate wells (data not shown). Cultures performed with 200 μ L exhibited reduced growth that can be attributed to a lack of oxygen. Thus, the maximal growth rate was 0.53 h^{-1} for growth in erlenmeyer flasks *versus* 0.33 h^{-1} for growth in the microplate.

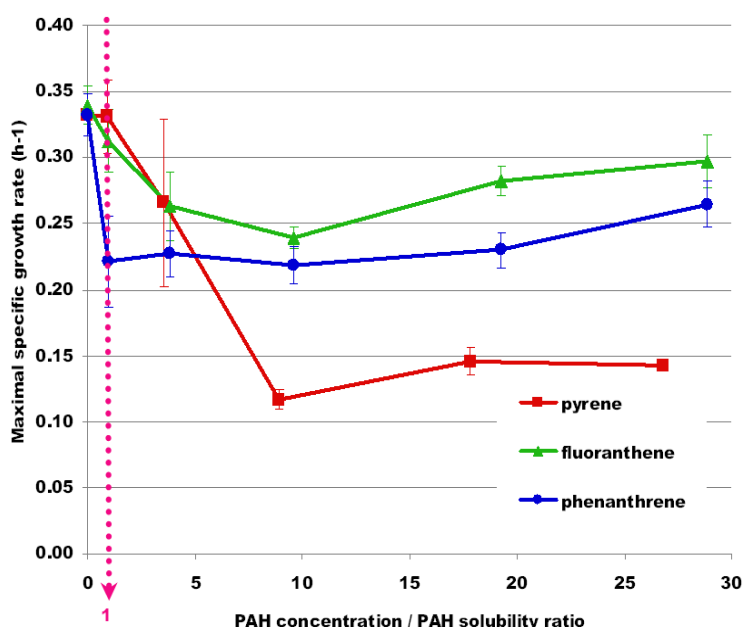
As represented in Figure 5, *P. fluorescens* DSS73 growth was stunted with increasing PAH concentration. The higher the PAH concentration was, the longer the lag phase. For some growth kinetics, an important experimental error was observed especially at high PAH concentrations. This was related to the high variability of the lag phase observed on the three replicates. In Figure 6, the previous results were summarized and normalized: μ_{\max} was reported *versus* PAH concentration normalized by PAH solubility. It appeared that when the PAH concentration was lower than its solubility (e.g., concentration over solubility ratio lower than 1), μ_{\max} was not significantly affected by PAHs ($p = 0.977$ and $p = 0.305$ for pyrene and fluoranthene, respectively, with a *t*-test) except for phenanthrene ($p = 0.007$). When the PAH concentration was higher than the solubility limit, the

maximal specific growth rate was drastically reduced with regard to a medium without contaminant. Similar trends were observed in both conditions with or without oxygen limitation.

Pyrene presented a greater inhibitory effect on *P. fluorescens* DSS73 growth than the two other PAHs. Its structure is made of four juxtaposed aromatic cycles, whereas three cycles exist for the two others. Increasing the number of aromatic cycles may lead to a greater negative impact on *P. fluorescens* DSS73 growth.

To conclude, *P. fluorescens* DSS73 is able to grow in the presence of PAHs in laboratory conditions.

Figure 6. Influence of the concentration/solubility ratio of each PAH on the maximal specific growth rate (μ_{\max}) of *P. fluorescens* DSS73 in DMB in oxygen limited conditions. All experiments were done in triplicate.



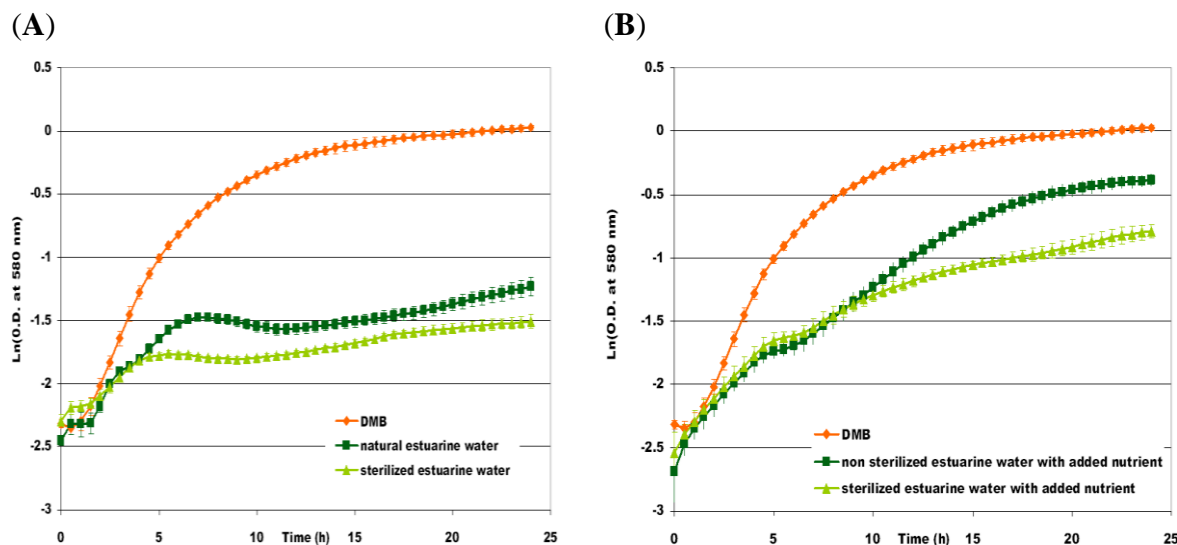
2.3.3. Growth Experiments in Estuarine Water

To approach a more *in situ* condition, the growth study in limited oxygenation was repeated, this time, with estuarine water feeding the dredged material disposal site of a Norman harbor as growth medium. Several growth experiments were performed with sterilized or crude estuarine water, with or without nutrient addition. In Figure 7, the growth kinetics were plotted in the case of estuarine water without added nutrients (Figure 7A) and supplemented with nutrients (Figure 7B). The addition of nutrients modified the profile of the growth curve. Indeed, *P. fluorescens* DSS73 growth curves, in Figure 7B, showed two phases with two different μ_{\max} (about 0.2 h^{-1} , then 0.1 h^{-1}) separated by a lag phase of 2 h. An explanation of this diauxy phenomenon may be that *P. fluorescens* DSS73 first metabolized the added nutrients, which acted as a growth stimulant, and then used the estuarine water as the second source nutrients.

With or without sterilization, growth curves showed the same trends during exponential phase, with similar growth rate values. Then, the sterilization did not improve growth, as would be expected. Indeed, it seems that the indigenous flora of estuarine water did not inhibit *P. fluorescens* DSS73 growth. Final maximum optical density (OD_{\max}) at the end of the stationary phase was higher in crude

estuarine water than in sterilized water, in the case of nutrient addition. An explanation could be that *P. fluorescens* DSS73 may inhibit other microorganisms and even metabolize their residue. Moreover, the OD_{max} values reached in crude estuarine water were equal to 0.4 without addition of nutrient and 0.7 for the supplemented growth, which leads to the conclusion that adding nutrient improves biomass production.

Figure 7. Growth kinetics of *P. fluorescens* DSS73 (A) in sterilized or natural estuarine water; (B) in sterilized or unsterilized water supplemented with nutrients, compared to DMB.



To conclude, *P. fluorescens* DSS73 is able to grow in estuarine water and addition of nutrients favors the growth.

2.4. Evaluation of Amphisin Production

2.4.1. Amphisin Production in the Presence of PAHs

Table 1. Surface tensions and associated standard deviations of *P. fluorescens* DSS73's growth in the presence of PAHs, above their solubility limit. All experiments were performed in triplicate.

Tested PAH		Surface Tension ($\text{mN} \cdot \text{m}^{-1}$)	
Name	Concentration ($\text{mg} \cdot \text{L}^{-1}$)	Before Growth	After Growth
Pyrene	0.5	52.2 ± 0.3	48.5 ± 9.1
Fluoranthene	1.0	55.0 ± 0.1	43.9 ± 7.1
Phenanthrene	5.0	55.9 ± 0.1	55.6 ± 5.2

After demonstrating the potential for *P. fluorescens* DSS73 to grow in the presence of PAHs, we could also show that the strain is still able to produce biosurfactants. Table 1 compiled the surface tension measured before inoculation and after bacterial growth in erlenmeyer flasks for each of the three PAHs, in higher concentration than their solubility limit. For pyrene and fluoranthene, the surface tension decreased slightly, but for phenanthrene no modification was noted. The difference of surface tension did not reach $20 \text{ mN} \cdot \text{m}^{-1}$ [52] after bacterial growth, which could suggest that no biosurfactant

was produced. However, it was interesting to note the enormous relative standard deviation associated to the mean values of surface tension after growth (between 9.4% and 18.8%), so interfacial exchanges were effectively modified. It may be correlated to the PAH's entrapment into amphisin micelles; amphisin mobilized at interface DMB/PAH could not help to decrease the surface tension relative to DMB/air interface. Although it was not clearly established, amphisin could be produced in PAH's presence.

2.4.2. Amphisin Production by *Pseudomonas fluorescens* DSS73 Growing in Estuarine Water

As already shown, *P. fluorescens* DSS73 growth may occur in estuarine water, and it was still able to produce amphisin (Table 2).

Table 2. Surface tension and associated standard deviations of *P. fluorescens* DSS73's growth in estuarine water with or without nutrients. All experiments were performed in triplicate.

Tested Medium	Surface Tension ($\text{mN}\cdot\text{m}^{-1}$)		Amphisin Production
	Before Growth	After Growth	
DMB	69.3 ± 0.9	30.4 ± 0.5	+
Estuarine water without nutrient	60.9 ± 0.5	32.8 ± 0.2	+
Estuarine water with nutrients		29.8 ± 0.6	+

In all cases, after bacterial growth in estuarine water, the surface tension was less than $40 \text{ mN}\cdot\text{m}^{-1}$, criterion required to detect biosurfactant production according to Carillo [49]; moreover the growth in estuarine water resulted in a decrease of surface tension of more than $30 \text{ mN}\cdot\text{m}^{-1}$. Without any doubt, amphisin is produced by DSS73 in estuarine water, with or without nutrient addition.

3. Experimental Section

3.1. Microorganism

P. fluorescens DSS73 is a strain from sugar beet rhizospheric environment and was graciously provided by Dr. O. Nybroe (Royal Veterinary & Agricultural University-Thorvaldsensvej, Denmark).

3.2. Growth Medium

The bacteria were grown in Davis Minimal Broth (DMB: $30 \text{ mmol}\cdot\text{L}^{-1} \text{ K}_2\text{HPO}_4$, $14 \text{ mmol}\cdot\text{L}^{-1} \text{ KHPO}_4$, $0.4 \text{ mmol}\cdot\text{L}^{-1} \text{ MgSO}_4$, $7.6 \text{ mmol}\cdot\text{L}^{-1} (\text{NH}_4)_2\text{SO}_4$, $120 \text{ mmol}\cdot\text{L}^{-1}$ glucose, and 1 mL of trace element solution per liter (pH 7.3). The trace element solution contained per liter of pure water 20 mg of $\text{CoCl}_2\cdot6\text{H}_2\text{O}$, 30 mg of H_3BO_3 , 10 mg of $\text{ZnSO}_4\cdot7\text{H}_2\text{O}$, 1 mg of $\text{CuCl}_2\cdot2\text{H}_2\text{O}$, 2 mg of $\text{NiCl}_2\cdot6\text{H}_2\text{O}$, 3 mg of $\text{NaMoO}_4\cdot2\text{H}_2\text{O}$, 10 mg of $\text{FeSO}_4\cdot7\text{H}_2\text{O}$, and 2.6 mg of $\text{MnSO}_4\cdot\text{H}_2\text{O}$. The glucose and trace elements were sterilized separately by filtration (Steriltop, Millipore, France) and aseptically added to the rest of the medium. Growth on solid medium was performed on DMA (Davis Minimal Agar) with the same composition as DMB supplemented with agar ($15 \text{ g}\cdot\text{L}^{-1}$).

Cultures were also carried out in estuarine water that was collected in sterile bottles, in an estuarine canal feeding the dredged material disposal site (Normandy, France). Then the estuarine water was stored at 4 °C and used for the cultures in the following 24 h. The pH of the water was adjusted to 7. Bacterial growth was tested in unsterilized or sterilized (by filtration) estuarine water. Cultures were done using unsterilized or sterilized estuarine water as aqueous base with DMB components. The addition of nutrients resulted in ion precipitation. The precipitate was eliminated by centrifugation (7000 g, 10 min).

3.3. Biosurfactant Recovery

To test for biosurfactant production, the bacterial colonies were grown on Davis minimal agar. DMA culture plates were inoculated with 40 µL of stocked suspension. After incubation for at least a week at 8 °C, bacterial colonies were scraped off, transferred to 15 mL of sterile mineral water and dispersed by agitation. This mineral spring water was used as its low level in mineral charge ensures a good repeatability and high values for tensiometry. After centrifugation (30 min, 4 °C, 18,000 g), the surface tension of the supernatant could be determined by the direct method of the pendant drop using a G40 goniometer (Krüss, France).

The biosurfactant purification was performed by liquid-liquid extraction: 100 mL of aqueous supernatant completed with 4×10^{-3} mol·L⁻¹ of trifluoroacetic acid (TFA), was mixed and agitated one hour with 150 mL of ethyl acetate, and then transferred into a separatory funnel. A second extraction of the aqueous phase was carried out each time. After collection of all organic phases, they were evaporated at 40 °C and 250 mbar with the rotary evaporator, to obtain approximately 10 mL of extract. In order to eliminate free water, this extract was then freeze-dried (semi-pilot freeze-drier SMH15, Usifroid, Maurepas, France), the sublimation took at least 2 days. The solid lyophilized sample was then solubilized in acetonitrile and was analyzed in liquid chromatography (HPLC) with UV detection (at 210 nm): The purified amphisin was separated on a hydrophobic C₁₈ bonded column (Beckman, Fullerton, USA) (4.6 mm × 250 mm, particles of 5 µm), using as a mobile phase a solvent mixture composed of: 25% water containing 0.1% TFA and 75% acetonitrile, at 1 mL·min⁻¹.

3.4. Model Sediment for PAH Adsorption

A sediment is first characterized through its granulometry, its mineral composition, its water and organic matter (OM) content. The granulometric classification, used for sediments in geology (French standard NF P18-560), differentiates largest blocks, rollers, stones or gravels, of diameters greater than 2 mm, sands (diameter ranging between 20 µm and 2 mm), silts (2 to 20 µm) and clay sludges or muds (diameters less than 2 µm). The reconstituted studied sediment contained 5% sand, with a particle diameter between 125 and 315 µm (Sika, Hostun, France), 75% silt from the Normandy shelves, with a diameter between 4 and 100 µm (CETE, Rouen, France) and 20% kaolinite clay, with a diameter being less than 80 µm, including 54% of particles less than 2 µm (Imerys, Poigny, France).

3.5. PAH Quantification at the Water/Sediment Interface

The PAH adsorption at the water/sediment interface was carried out in reactors containing 10 g of model sediment for 90 mL of aqueous phase (ratio 10/90 in weight or 111 g of dry sediment per liter), maintained at a constant temperature (25 °C) in a thermostated bath (Fisher Bioblock Scientific, Illkirch, France) and under agitation (300 rpm). In many experiments, sodium chloride could be added into water at a concentration of 10 g L⁻¹. In other experiments, organic matter could be mixed with the model sediment, in variable proportions (1 to 5% w/w). This organic matter was obtained from the decomposition of a vegetable material (VEOLIA-France): it was then dried 48 h at 50 °C, crushed and sieved to obtain particle diameters less than 355 µm. PAH introduction in reactors was done from a known concentration (C_o) of a stock solution of 16 PAHs (100 mg·L⁻¹) in water. When thermodynamic equilibrium was reached (2 h for kaolin alone, 12 h for sand alone, 4 h for the model sediment), the solid phase was eliminated by centrifugation (40 min, 11,200 rpm). Then an enrichment protocol by SPE (solid phase extraction) was done to concentrate the traces of non-adsorbed PAH still present in the aqueous phase at the end of the equilibrium step (C_{eq}). Indeed, direct PAH analysis and quantification by HPLC would have been impossible without SPE enrichment because non-adsorbed PAHs were found under the limits of detection of the fluorimetric detector. It must be added that even after centrifugation, ultra-fine clay particles remained in suspension in liquid phase; so SPE cartridges Strata X (Phenomenex), containing 60 mg of polymeric solid phase, had to be coupled with Phenex 0.45 µm filters, made of inert Teflon (Phenomenex), to eliminate colloid particles. Moreover, to improve PAH extraction yields, which had to be higher than 80%, it was necessary to homogenize the aqueous supernatant by adding 20% acetone in volume (HPLC grade, Fisher Scientific) before starting its percolation through the SPE cartridge. This step also made it possible to avoid the PAH sorption on the flask's glass walls, leading to high PAH losses, a particularly critical phenomenon when traces of PAH have to be analyzed quantitatively. SPE cartridges were first conditioned with methylene chloride, methanol and a mixture of acetone/water (20/80 v/v) (all solvents were of analytical grade, from Fisher Scientific France). Then, after percolation of the aqueous supernatant through the SPE cartridge associated to a filter, extracts were eluted with 5 mL of methylene chloride (HPLC grade, Fisher Scientific).

Methylene chloride was evaporated under nitrogen flow (after adding 60 µL of dimethylsulfoxide) for solvent change; then the sample was solubilized again in 4 mL of acetonitrile (HPLC grade, Fisher Scientific). 10 µL of this sample was injected on a PP Envirosep C₁₈ bonded column (Phenomenex; 150 mm × 4.6 mm, particles of 5 µm), with a flow rate of 1 mL·min⁻¹ controlled by two Beckman Coulter Gold 126 pumps.

Table 3 shows the solvent gradient conditions during chromatographic elution as well as the programmed excitation and emission wavelengths of the fluorimetric detector Prostar 363 (Varian, Palo Alto, USA). After HPLC analysis, each of the 16 PAHs could be individually quantified. Their aqueous concentration could be evaluated (as C_{eq} at equilibrium in water) and consequently, knowing their initial introduced concentration (C_o), C_{ads} could be calculated by a simple subtraction as the concentration adsorbed on sediment. Adsorption isotherms at 25 °C were then established in varying C_o and in plotting $C_{ads} = f(C_{eq})$.

Table 3. HPLC elution gradient for the analysis of the 15 priority PAHs (defined by U.S. EPA) plus benzo[e]pyrene, and conditions for the fluorimetric detection.

Time (min)	Elution Gradient	λ_{ex} (nm)	λ_{em} (nm)	Detected PAHs
0	Acetonitrile/water 55/45%	220	330	Naphthalene (1)
5	Acetonitrile/water 55/45%			
7	Linear gradient for 20 min	220	315	Acenaphthene (2) Fluorene (3)
10		250	370	Phenanthrene (4)
				Anthracene (5)
13.4		235	420	Fluoranthene (6) Pyrene (7)
17		267	385	Benz[a]anthracene (8) Pyrene (9)
21.7		260	420	Benzo[e]pyrene (10)
25	Acetonitrile/water 100/0%			Benzo[b]fluoranthene (11) Benzo[k]fluoranthene (12) Benzo[a]pyrene (13)
27.4		290	410	Dibenzo[a,h]anthracene (14) Benzo[g,h,i]perylene (15)
29.8		245	500	Indeno[1,2,3-cd]pyrene (16)
35	Acetonitrile/water 55/45%	220	330	

3.6. Solubility Enhancement of PAHs by Amphisin and SDS

The mixture of 16 PAHs was introduced into reactors containing kaolin, as further described. After mixing them for one hour at 25 °C, the purified and lyophilized biosurfactant was then introduced into the system at two different concentrations: 0.1 g·L⁻¹ and 1 g·L⁻¹. After three hours of equilibrium, the mixture was centrifuged and the non-adsorbed PAH were quantified as described elsewhere. Other similar experiments were done with a synthetic surfactant, the sodium dodecyl sulfate SDS (provided by Sigma-Aldrich), introduced in a similar way at 2.88 g·L⁻¹ or 23.07 g·L⁻¹ in the aqueous phase.

3.7. Bacterial Growth Conditions

3.7.1. Growth in Erlenmeyer Flasks with PAHs

Seed culture was carried out in 10 mL of DMB overnight at 28 °C on a rotary shaker (180 rpm). In a 500 mL erlenmeyer flask, 50 mL of DMB supplemented with PAH from stock solution in acetone, was inoculated with an aliquot of seed culture in order to obtain an initial OD of 0.05. The tested PAH concentrations were 0.1 and 0.5 mg·L⁻¹ for pyrene, 0.2 and 1 mg·L⁻¹ for fluoranthene and 5 mg·L⁻¹ for phenanthrene. The culture conditions were identical as for the seed culture. Bacterial density was determined by measuring optical density at 580 nm (Spectronic 601 spectrophotometer). For each PAH concentration, triplicate flasks were employed.

3.7.2. Growth in Oxygen-Limited Conditions

Cultures were made in polystyrene microtitration plates. 180 μL of DMB was deposited in each 400 μL well and inoculated by 20 μL of seed culture in DMB incubated at 28 °C. To study the effect of PAH on bacterial growth, PAH was added to the mixture in the wells, from PAH stock solutions in acetone, to obtain final concentrations of 0.125, 0.5, 1.25, 2.5, 3.75 $\text{mg}\cdot\text{L}^{-1}$ for pyrene, of 0.25, 1, 2.5, 5, 7.5 $\text{mg}\cdot\text{L}^{-1}$ for fluoranthene, and of 1.25, 5, 12.5, 25, 37.5 $\text{mg}\cdot\text{L}^{-1}$ for phenanthrene. To evaluate the influence of estuarine water on growth kinetics, DMB was replaced by estuarine water.

For each condition, *P. fluorescens* DSS73 growth was followed continuously in triplicate in a thermoregulated spectrometer (Xenius, Safas, Monaco) at 28 °C under rotary revolution (180 rpm).

3.8. Tensiometry

The surface tension was tested on culture supernatants after centrifugation (30 min, 4 °C, 18,000 g) from 50 mL of liquid cultures. The home-made surface tensiometer worked on the principle of the Wilhelmy plate method. All surface tensions were measured in triplicate. The measurement validity was standardized with mineral spring water of weak mineral charge ($71.7 \pm 0.3 \text{ mN}\cdot\text{m}^{-1}$).

4. Conclusions

Biosurfactant produced by *Pseudomonas fluorescens* DSS73 seems very promising with regard to mobilization in an aqueous phase of strongly adsorbed PAHs on the finest sediment particles. It was almost as efficient as conventional synthetic surfactants, such as SDS, for solubilizing the heaviest and most strongly adsorbed PAHs. However, mobilization by amphisin needs much lower quantities than those required with the synthetic surfactant. Future research needs to investigate if amphisin is also efficient in solubilizing PAHs even when another retentive material, *i.e.*, organic matter, enters the composition of the sediment; afterwards, we will also have to prove that the ionic amphisin, after its increased solubilizing effect, will be able to enhance PAH mobility through the sediment via an electromigration process. Indeed, EK remediation is a promising *in situ* method for grounds or sediments of low permeability, and is adapted to numerous pollutant types.

This study also proved that the strain was able to produce the cyclolipopeptide in hostile growth conditions corresponding to real environment, *i.e.*, in estuarine water feeding a dredged material disposal site. *P. fluorescens* DSS73 was also able to produce amphisin, in the presence of a relatively high PAH contamination, and even with low oxygen growth conditions. These very promising results suggest that bioaugmentation of the biosurfactant producer, *P. fluorescens* DSS73, could be conceivable *in situ*. As amphisin is biodegradable (which is an advantage for the environment), single amendment is not sufficient when long periods are necessary to perform pollution attenuation, which is certainly the case when EK remediation is performed *in situ*, on a large scale. Moreover, EK-bioremediation of PAHs via anionic micelles needs certainly a continuous addition of the biosurfactant, because aggregates migrate towards the anodic compartment and are consequently impoverished inside the sediment during the treatment. Thus, it would be a real advantage to continue the mobilization and migration process with biosurfactant production *in situ*.

Acknowledgements

This study was supported by grants from the Haute Normandy Region for RESSOLV project, through Norman SCALE research network. The authors thank Nybroe for gift of the different bacterial strains, Marion Couve, Céline Augé, Selime Sahed and Magalie Barreau for their technical support and Christine Farmer for her linguistic support.

References

1. Lang, S.; Wagner, F. Structure and properties of biosurfactants. In *Biosurfactants and Biotechnology*; Kosaric, N., Cairns, W.L., Gray, N.C.C., Eds.; Marcel Dekker: New York, NY, USA, 1987; pp. 21–45.
2. Kosaric, N. Biosurfactants in industry. *Pure Appl. Chem.* **1992**, *64*, 1731–1737.
3. Desai, J.D.; Banat, I.M. Microbial production of surfactants and their commercial potential. *Microbiol. Mol. Biol. Rev.* **1997**, *61*, 47–64.
4. Rosenberg, E.; Ron, E.Z. High- and low-molecular-mass microbial surfactants. *Appl. Microbiol. Biotechnol.* **1999**, *52*, 154–162.
5. Mukherjee, S.; Das, P.; Sen, R. Towards commercial production of microbial surfactants. *Trends Biotechnol.* **2006**, *24*, 509–515.
6. van Hamme, J.D.; Singh, A.; Ward, O.P. Surfactants in microbiology and biotechnology: Part 1. physiological aspects. *Biotechnol. Adv.* **2006**, *24*, 604–620.
7. Singh, A.; van Hamme, J.D.; Ward, O.P. Surfactants in microbiology and biotechnology: Part 2. Application aspects. *Biotechnol. Adv.* **2007**, *25*, 99–121.
8. Salihu, A.; Abdulkadir, I.; Almustapha, M.N. An investigation for potential development on Biosurfactants. *Biotechnol. Mol. Biol. Rev.* **2009**, *3*, 111–117.
9. Cooper, D.G. Biosurfactants. *Microbiol. Sci.* **1986**, *3*, 145–149.
10. Mukherjee, S.; Das, P.; Sen, R. Towards commercial production of microbial surfactants. *Trends Biotechnol.* **2006**, *24*, 509–515.
11. Ron, E.Z.; Rosenberg, E. Biosurfactants and oil bioremediation. *Curr. Opin. Biotechnol.* **2002**, *13*, 249–252.
12. Muthusamy, K.; Gopalakrishnan, S.; Ravi, T.K.; Sivachidambaram, P. Biosurfactants: Properties, commercial production and application. *Curr. Sci.* **2008**, *6*, 736–747.
13. Banat, I.M.; Makkar, R.S.; Cameotra, S.S. Potential commercial applications of microbial surfactants. *Appl. Microbiol. Biotechnol.* **2000**, *53*, 495–508.
14. Mulligan, C.N. Environmental applications of biosurfactants. *Environ. Pollut.* **2005**, *133*, 183–198.
15. Fiechter, A. Biosurfactants—moving towards industrial application. *Trends Biotechnol.* **1992**, *10*, 208–217.
16. Soberón-Chávez, G.; Lépine, F.; Déziel, E. Production of rhamnolipids by *Pseudomonas aeruginosa*. *Appl. Microbiol. Biotechnol.* **2005**, *68*, 718–725.
17. Uchida, Y.; Tsuchiya, R.; Chino, M.; Hirano, J.; Tabuchi, T. Extracellular accumulation of mono- and di-succinoyl trehalose lipids by a strain of *Rhodococcus erythropolis* grown on *n*-alkanes. *Agric. Biol. Chem.* **1989**, *53*, 757–763.

18. Hirata, Y.; Ryua, M.; Odaa, Y.; Igarashia, K.; Nagatsukaa, A.; Furutaa, T.; Sugiuraa, M. Novel characteristics of sophorolipids, yeast glycolipid biosurfactants, next term as biodegradable low-foaming surfactants. *J. Biosci. Bioeng.* **2009**, *108*, 142–146.
19. Kiran, G.S.; Thomas, T.A.; Selvin, J.; Sabarathnam, B.; Lipton, A.P. Optimization and characterization of a new lipopeptide biosurfactant produced by marine *Brevibacterium aureum* MSA13 in solid state culture. *Bioresour. Technol.* **2010**, *101*, 2389–2396.
20. Nielsen, T.H.; Sorensen, J. Production of cyclic lipopeptides by *Pseudomonas fluorescens* strains in bulk soil and in the sugar beet rhizosphere. *J. Appl. Environ. Microbiol.* **2003**, *69*, 861–868.
21. Raaijmakers, J.M.; De Bruijn, I.; De Kock, M.J.D. Cyclic lipopeptide production by plant-associated *Pseudomonas* spp.: diversity, activity, biosynthesis, and regulation. *Mol. Plant Microbe Interact.* **2006**, *19*, 699–710.
22. Maier, R.M.; Soberon-Chavez, G. *Pseudomonas aeruginosa* rhamnolipids: biosynthesis and potential applications. *Appl. Microbiol. Biotechnol.* **2000**, *54*, 625–633.
23. Benincasa, M.; Marqués, A.; Pinazo, A.; Manresa, A. Rhamnolipid surfactants: alternative substrates, new strategies. *Adv. Exp. Med. Biol.* **2010**, *672*, 170–184.
24. Satpute, S.K.; Banpurkar, A.G.; Dhakephalkar, P.K.; Banat, I.M.; Chopade, B.A. Methods for investigating biosurfactants and bioemulsifiers: a review. *Crit. Rev. Biotechnol.* **2010**, *30*, 127–144.
25. De Bruijn, I.; De Kock, M.J.; De Waard, P.; Van Beek, T.A.; Raaijmakers, J.M. Massetolide A Biosynthesis in *Pseudomonas fluorescens*. *J. Bacteriol.* **2008**, *190*, 2777–2789.
26. Hutchison, M.L.; Gross, D.C. Lipopeptide phytotoxins produced by *Pseudomonas syringae* pv. *syringae*: Comparison of the biosurfactant and ion channel-forming activities of syringopeptin and syringomycin. *Mol. Plant Microbe Interact.* **1997**, *10*, 347–354.
27. Pedras, M.S.C.; Ismail, N.; Quail, J.W.; Boyetchko, S.M. Structure, chemistry, and biological activity of pseudophomins A and B, new cyclic lipopeptides isolated from the biocontrol bacterium *Pseudomonas fluorescens*. *Phytochemistry* **2003**, *62*, 1105–1114.
28. Sinnaeve, D.; Michaux, C.; van hemel, J.; Vandenkerckhove, J.; Peys, E.; Borremans, F.A.M.; Sas, B.; Wouters, J.; Martins, J.C. Structure and X-ray conformation of pseudodesmins A and B, two new cyclic lipopeptides from *Pseudomonas* bacteria. *Tetrahedron* **2009**, *65*, 4173–4181.
29. Sen, R. Surfactin: Biosynthesis, genetics and potential applications. *Adv. Exp. Med. Biol.* **2010**, *672*, 316–323.
30. Mireles, J.P.; Toguchi, A.; Harshey, R.M. *Salmonella enterica* serovar typhimurium swarming mutants with altered biofilmforming abilities: Surfactin inhibits biofilm formation. *J. Bacteriol.* **2001**, *183*, 5848–5854.
31. Meylheuc, T.; Methivier, C.; Renault, M.; Herry, J.M.; Pradier, C.M.; Bellon-Fontaine, M.N. Adsorption on stainless steel surfaces of biosurfactants produced by gram-negative and gram-positive bacteria: Consequence on the bioadhesive behavior of *Listeria monocytogenes*. *Colloids Surf. B* **2006**, *52*, 128–137.
32. Nayak, A.S.; Vijaykumar, M.H.; Karegoudar, T.B. Characterization of biosurfactant produced by *Pseudoxanthomonas* sp. PNK-04 and its application in bioremediation. *Int. Biodeterior. Biodegrad.* **2009**, *63*, 73–79.

33. Bordoloi, N.K.; Konwar, C.K. Bacterial biosurfactant in enhancing solubility and metabolism of petroleum hydrocarbons. *J. Hazard. Mater.* **2009**, *170*, 495–505.
34. Mrozik, Z.; Piotrowska-Seget, S. Bioaugmentation as a strategy for cleaning up of soils contaminated with aromatic compounds. *Microbiol. Res.* **2010**, *165*, 363–375.
35. IARC (International Agency for Research on Cancer). *IARC Monographs on the Evaluation of the Carcinogenic Risk of Chemicals to Humans: Polynuclear Aromatic Compounds*; IARC Press: Lyon, France, 1983.
36. US EPA (United States Environmental Protection Agency). *Polycyclic Aromatic Hydrocarbons (PAHs)*, 2008. Available online: <http://www.epa.gov/osw/hazard/wastemin/priority.htm> (accessed on 21 February 2011).
37. Perelo, L.W. *In situ* and bioremediation of organic pollutants in aquatic sediments. *J. Hazard. Mater.* **2010**, *177*, 81–89.
38. Martínez-Jerónimo, F.; Cruz-Cisneros, J.L.; García-Hernández, L. A comparison of the response of *Simocephalus mixtus* (*Cladocera*) and *Daphnia magna* to contaminated freshwater sediments. *Ecotoxicol. Environ. Saf.* **2008**, *1*, 26–31.
39. Pazos, M.; Rosales, E.; Alcántara, T.; Gómez, J.; Sanromán, M.A. Decontamination of soils containing PAHs by electroremediation: A review. *J. Hazard. Mater.* **2010**, *177*, 1–11.
40. Gan, S.; Lau, E.V.; Ng, H.K. Remediation of soils contaminated with polycyclic aromatic hydrocarbons (PAHs). *J. Hazard. Mater.* **2009**, *172*, 532–549.
41. Perfumo, A.; Banat, I.M.; Marchant, R.; Vezzulli, L. Thermally enhanced approaches for bioremediation of hydrocarbon-contaminated soils. *Chemosphere* **2007**, *66*, 179–184.
42. Ko, S.O.; Schlautman, M.A.; Carraway, E.R. Cyclodextrin enhanced electrokinetic removal of phenanthrene from a model claysoil. *Environ. Sci. Technol.* **2000**, *34*, 1535–1541.
43. Sawada, A.; Tanaka, S.; Fukushima, M.; Tatsumi, K. Electrokinetic remediation of clayey soils containing copper(II)-oxinate using humic acid as a surfactant. *J. Hazard. Mater.* **2003**, *96*, 145–154.
44. Zeller, C.; Cushing, B. Panel discussion: remedy effectiveness: what works, what doesn't? *Integr. Environ. Assess. Manag.* **2005**, *2*, 75–79.
45. El Fantroussi, S.E.; Agathos, S.N. Is bioaugmentation a feasible strategy for pollutant removal and site remediation? *Curr. Opin. Microbiol.* **2005**, *8*, 268–275.
46. Kim, S.H.; Han, H.Y.; Lee, J.L.; Kim, C.W.; Yang, J.W. Effect of electrokinetic remediation on indigenous microbial activity and community within diesel contaminated soil. *Sci. Total Environ.* **2010**, *408*, 3162–3168.
47. Alcántara, M.T.; Gómez, J.; Pazos, M.; Sanromán, M.A. Electrokinetic remediation of PAH mixtures from kaolin. *J. Hazard. Mater.* **2010**, *179*, 1156–1160.
48. Ju, L.; Elektorowicz, M. *In-situ* phenanthrene removal provoked by electrokinetic transport of on-site produced biosurfactants. *Annu. Conf. Abstr. Can. Soc. Civil Eng.* **2000**, 135.
49. Carrillo, C.; Teruel, J.A.; Aranda, F.J.; Ortiz, A. Molecular mechanism of membrane permeabilization by the peptide antibiotic surfactin. *Biochim. Biophys. Acta* **2003**, *1611*, 91–97.

50. Sorensen, D.; Nielsen, T.H.; Christophersen, C.; Sorensen, J.; Gajhede, M. Cyclic lipoundecapeptide amphisin from *Pseudomonas* sp. strain DSS73. *Acta Crystallogr. Sect. C: Cryst. Struct. Commun.* **2001**, *57*, 1123–1124.
51. Das, P.; Mukherjee, S.; Sen, R. Antimicrobial potential of a lipopeptide biosurfactant derived from a marine *Bacillus circulans*. *J. Appl. Microbiol.* **2008**, *104*, 1675–1684.
52. Reddy, M.S.; Naresh, B.; Leela, T.; Prashanthi, M.; Madhusudhan, N.C.; Dhanasri, G.; Devi, P. Biodegradation of phenanthrene with biosurfactant production by a new strain of *Brevibacillus* sp. *Bioresour. Technol.* **2010**, *101*, 7980–7983.
53. Abouseoud, M.; Yataghene, A.; Amrane, A.; Maachi, R. Effect of pH and salinity on the emulsifying capacity and naphthalene solubility of a biosurfactant produced by *Pseudomonas fluorescens*. *J. Hazard. Mater.* **2010**, *180*, 131–136.
54. Lai, C.C.; Huang, Y.C.; Wei, Y.H.; Chang, J.S. Biosurfactant-enhanced removal of total petroleum hydrocarbons from contaminated soil. *J. Hazard. Mater.* **2009**, *167*, 609–614.
55. Saini, H.S.; Barragán-Huerta, B.E.; Lebrón-Paler, A.; Pemberton, J.E.; Vázquez, R.R.; Burns, A.M.; Marron, M.T.; Seliga, C.J.; Gunatilaka, A.A.; Maier, R.M. Efficient purification of the biosurfactant viscosin from *Pseudomonas libanensis* strain M9-3 and its physicochemical and biological properties. *J. Nat. Prod.* **2008**, *6*, 1011–1015.

© 2011 by the authors; licensee MDPI, Basel, Switzerland. This article is an open access article distributed under the terms and conditions of the Creative Commons Attribution license (<http://creativecommons.org/licenses/by/3.0/>).

P13

TECHNICAL NOTE

Open Access

Caenorhabditis elegans: a model to monitor bacterial air quality

Cécile Duclairoir Poc^{1*}, Anne Groboillot^{1*}, Olivier Lesouhaitier¹, Jean-Paul Morin², Nicole Orange¹ and Marc JG Feuilloley¹

Abstract

Background: Low environmental air quality is a significant cause of mortality and morbidity and this question is now emerging as a main concern of governmental authorities. Airborne pollution results from the combination of chemicals, fine particles, and micro-organisms quantitatively or qualitatively dangerous for health or for the environment. Increasing regulations and limitations for outdoor air quality have been decreed in regards to chemicals and particles contrary to micro-organisms. Indeed, pertinent and reliable tests to evaluate this biohazard are scarce. In this work, our purpose was to evaluate the *Caenorhabditis elegans* killing test, a model considered as an equivalent to the mouse acute toxicity test in pharmaceutical industry, in order to monitor air bacterial quality.

Findings: The present study investigates the bacterial population in dust clouds generated during crop ship loading in harbor installations (Rouen harbor, Normandy, France). With a biocollector, airborne bacteria were impacted onto the surface of agar medium. After incubation, a replicate of the colonies on a fresh agar medium was done using a velvet. All the replicated colonies were pooled creating the "Total Air Sample". Meanwhile, all the colonies on the original plate were isolated. Among which, five representative bacterial strains were chosen. The virulence of these representatives was compared to that of the "Total Air Sample" using the *Caenorhabditis elegans* killing test. The survival kinetic of nematodes fed with the "Total Air Sample" is consistent with the kinetics obtained using the five different representatives strains.

Conclusions: Bacterial air quality can now be monitored in a one shot test using the *Caenorhabditis elegans* killing test.

Background

The deep impact on health from chemical pollutants [1] is now a main concern of governmental policies in most countries. As well as airborne nanoparticles and chemicals [2], airborne bacterial and fungal contaminants are also of major importance in human health [3,4]. These micro-organisms may lead to typical respiratory tract infections but also to delayed sensitization (allergic) reactions somehow considered as the "*epidemy of the 21st century*" [5]. Some of these micro-organisms simply originate from the environment but human activities are also important sources of aerial biological contaminants [6]. It would be particularly interesting to develop a

microbial air quality alert system equivalent to that for chemical pollutants. Microbial air quality is commonly evaluated by measuring the global concentration in the air of bacteria and fungi by culture-dependant or bio-molecular methods [7]. High microbial concentrations in the air are generally associated to potential danger. The search for endotoxins has been developed [8]. The composition of microbial communities is often assessed by molecular methods [8,9] and pathogen species have been also detected by PCR with specific probes [10]. Studying airborne bacterial and fungal communities in land [4,9], urban [11-13], and occupational [14] environments now allows an almost complete description of environmental air micro-organisms biodiversity. However, the identification of microbial species and strain is not sufficient to extrapolate at the sanitary risk level, as many different parameters may affect virulence. Indeed, both contact mediated and toxin dependent virulence

* Correspondence: cecile.poc@univ-rouen.fr; anne.groboillot@univ-rouen.fr

¹Laboratory of Microbiology-Signals and MicroEnvironment, Normandy University, University of Rouen, EA 4312, 55 rue Saint Germain, 27000 Evreux, France

Full list of author information is available at the end of the article

are regulated by environmental conditions including temperature [15], bacteriophages [16] and of course microbial communication factors [17]. Sometimes bacterial strains are generally considered safe and devoid of pathogenic potential and, however, induce clinical infections [18,19]. Determining the real risk associated to airborne micro-organisms first requires collecting a maximum amount of micro-organisms in conditions which avoid the stress or even the destruction of the most sensitive micro-organisms which are usually the most metabolically active [20]. The identification of the composition of this population should be realized in a second step but the essential point is to evaluate the virulence of the complex community. This requires a cheaper and more rapid test than classical animal assays but also less sensitive than *in vitro* cytotoxicity tests. In the present study, the chosen model was the *Caenorhabditis elegans* worm. It is a versatile metazoan model previously used to assess of the virulence of many human pathogens [21,22], and especially to study primary respiratory chain dysfunction in humans [23]. Spontaneous predation and ingestion of bacteria provoke nematode death by contact dependent bacterial virulence and by the bacterial secretion of toxins [21,22]. Thus, in the present study, we investigated the risk linked to airborne bacteria in the dust cloud generated during crop ship loading in harbor installations located in close proximity of residential areas. After collection of the total microbial population, bacteria were identified by traditional phenotypic and molecular techniques. The virulence of some individual representatives chosen among the collected bacteria was compared using the nematode *C. elegans*. to that of the pooled replicated bacterial population defined as "Total Air Sample".

Methods

Aerial bacteria collection

Bacteria were collected in January 2009 at the dockside of Rouen harbour (Normandy, France) during loading from crop silo onto ship from stocking silo. All operations were done in the morning. Samples were obtained by aspiration of 30, 60, 90, or 190 L (under a flow rate $100 \text{ L} \cdot \text{min}^{-1}$) in the dust cloud of particles generated by crop transfer using an AirTest Omega Biocollector (LCB, France). In this device, air is drawn in through a 0.5 mm grid to remove macroscopic particles and the air flow is directed towards the impact medium where micro-organisms are trapped. In order to limit the stress on bacteria, a semi-solid impact medium, Trypticase Soy Agar (TSA), was made with Tryptic Soy Broth (TSB) diluted 1:5 containing agar ($10 \text{ g} \cdot \text{L}^{-1}$) and amphotericin B ($25 \text{ mg} \cdot \text{L}^{-1}$) as a fungicide.

After collection, impacted TSA plates, presented in Figure 1, were incubated at 30°C for 72 h to reveal the colonies of cultivable bacteria. Agar plates showing well separated and countable colonies were selected and before other manipulation, a velvet copy of these plates was done. This velvet was laid on a new TSA plate which afterwards was incubated at 30°C for 72 h. All the formed colonies were transferred to and grown in the same culture in 1:5 diluted TSB and then frozen at -80°C with a final glycerol concentration of 30%. This mixture of strains collected from the air impaction was designed as "Total Air Sample". Subsequently, from the original impacted TSA plate, individual colonies were removed and isolated as pure cultures on TSA for further analysis and storage at -80°C as previously described.

Bacterial characterization and identification

Each isolated bacterial strain was initially characterized by morphological observation (colony aspect, cell shape, motility, endospore), Gram staining and biochemical tests (oxidase, catalase and oxidative metabolism). These observations allowed different bacterial groups to be defined. In each group including potential pathogens, one representative strain was chosen and submitted to further characterization on API tests galleries. API kits were operated according to the manufacturer's instructions (BioMérieux, France). For Gram-positive bacteria, API 50CH was used for the identification of *Bacillus*, API ID STAPH 32 for identification of germs of the genus *Staphylococcus* or *Micrococcus* and API Coryne for Gram-positive catalase-positive non-sporing rods. For Gram-negative bacteria, API 20E was used for the identification of *Enterobacteriaceae* and API 20NE for non fermenting rods. Species identification of representative strains was confirmed by 16S RNA sequencing. For amplification of the complete 16S RNA gene, universal primers UNI_OL (5'-AGAGTGTA GCGGTGAA ATGCG-3') and UNI_OR (5'-ACGGCGGTGTGTA CAA-3') were used as suggested by Sauer et al. [24]. Amplicons were then purified through migration on agarose gel and sequenced directly by using the amplification primers UNI_OL and UNI_OR (Qiagen, Germany). Afterwards 16S RNA fragments (+/- 750 pb) were analyzed (Qiagen, Germany) and homologies with sequences of other eubacteria were determined by searching the NCBI (http://www.ncbi.nlm.nih.gov/sutils/genom_table.cgi) and RDP (http://rdp.cme.msu.edu/seqmatch/seqmatch_intro.jsp) data banks using BLAST software. An isolate was positively identified when the full-length 16S RNA gene yielded a >98.3% sequence similarity with the closest bacterial species registered in the data banks.

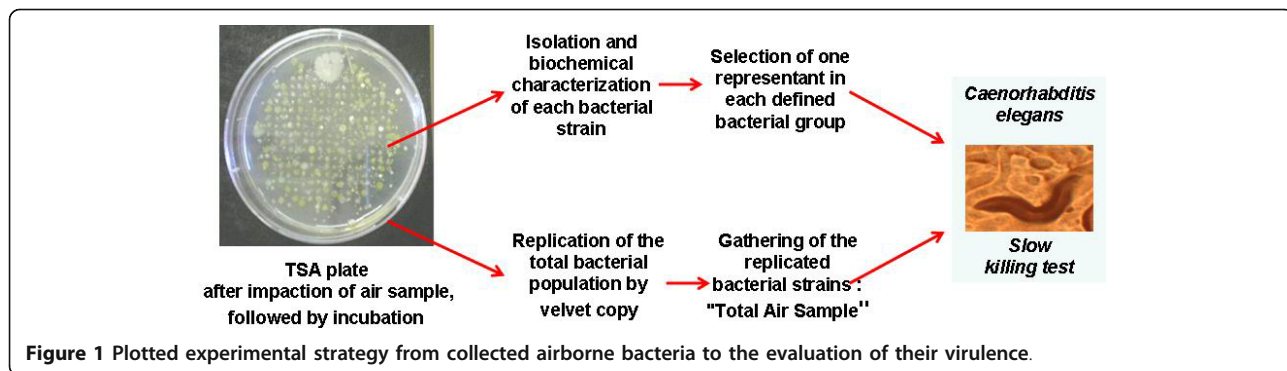


Figure 1 Plotted experimental strategy from collected airborne bacteria to the evaluation of their virulence.

Evaluation of bacterial virulence using the *Caenorhabditis elegans* killing tests

The virulence of the airborne bacterial population, i.e. the “Total Air Samples”, was compared to that of individual representatives of bacterial strains collected in the air using the slow killing tests on the nematode *Caenorhabditis elegans*, accordingly Figure 1.

Experiments were conducted using the wild-type Bristol strain N2 of *C. elegans* provided by the *Caenorhabditis* Genetics Center (Minneapolis, MN, USA). Worms were maintained under standard culturing conditions at 22°C on nematode growth medium (NGM) containing 3 g NaCl, 2.5 g peptone, 17 g agar, 5 mg cholesterol, 1 mL 1 M CaCl₂, 1 mL 1 M MgSO₄, 25 mL 1 M KH₂PO₄, H₂O for 1 L of medium. This medium was plated on Petri dishes and *Escherichia coli* OP50 as added as a normal food source [21]. For virulence tests, synchronized worms of the same development level were obtained by bleaching an adult population using sodium hypochlorite/sodium hydroxide solution [25]. The resulting eggs were incubated at 22°C on *E. coli* OP50 lawns until the worms reached the L4 life stage (48 h). The stage of development was confirmed by microscopic observation.

For bacterial virulence assays, “Total Air Samples” or individual air strain aliquots standardized by dilution (at OD₅₈₀ = 1) were prepared by spreading 100 µL on 35 mm Petri dishes containing NGM supplemented with 0.05 mg.mL⁻¹ 5-fluoro-2'-deoxyuridine (FUDR), a eukaryote DNA synthesis inhibitor preventing *C. elegans* egg offspring during the experiments. Plates were incubated overnight at 29°C and then transferred at room temperature for 4 h. In each Petri dish a mean of 20 L4 synchronized worms, harvested in M9 solution (3 g KH₂PO₄, 6 g NaHPO₄, 5 g NaCl, 1 mL 1 M MgSO₄, H₂O in 1 L) were layered. Plates were incubated at 22°C and worm survival was scored every 24 h throughout a 22 days period using an Axiovert S100 optical microscope (Zeiss, Oberkochen, Germany) equipped with a Nikon digital Camera DXM 1200F (Nikon Instruments, Melville, NY, USA). A worm was considered dead when

it remained static without grinder movements for 20 s. Results are expressed as percentage of worms surviving every day and were calculated as the mean of 3 independent assays in which each point was the average of 3 replicates. Nematode survival was calculated using the Kaplan-Meier method, and survival differences were tested for significance using the log-rank test (GraphPad Prism version 4.0; GraphPad Software, San Diego, California, USA).

Results and Discussion

Identification of airborne bacteria in the dust cloud generated by crop transfer

Plates obtained with 30 L air presented a sufficient number of colonies which remained well separated. In cultures obtained with higher air volumes, bacterial colonies were too numerous for correct isolation.

As seen Figure 1, velvet replicates of impacted TSA plates were realized to obtain the “Total Air Sample”. A total of 323 bacterial strains were isolated. The corresponding calculated bacterial concentration in the air was about 1.1×10^4 CFU.m⁻³ as shown in Table 1. This bacterial concentration in the dust cloud generated by crop loading was slightly higher than obtained in urban air, which ranged from 5.5×10^2 to 2.5×10^3 CFU.m⁻³ [7,11]. The large quantity of dusts and particles, which represents the principal support of bacteria in the air [26] can explain this result. It is also interesting to note that the values of bacterial load measured at the centre of the dust cloud are markedly lower than previously measured [27]. This difference should be attributed to the application of more recent procedures aimed at reducing particle emission during ship loading (for instance covered conveyor belts).

Morphological characters, Gram staining and biochemical tests were carried out for the 323 bacterial strains. These orientation tests allowed to distribute the bacterial population in 8 groups, i.e. Gram-negative oxidase-negative strictly aerobic rods such as *Acinetobacter*, *Pseudomonas*... (Group 1), Gram-negative oxidase-positive facultatively anaerobic rods such as *Aeromonas*...

Table 1 Airborne bacterial composition in the dust cloud resulting from crop transfer

Sample	Next to crops ship loading winter 2009	
Collected volume	30L	
Incubation conditions	30°C on 1:5 diluted TSA plate	
UFC/air m ³	10767	
Gram-negative rods	Group 1	17.6%
	Group 2	72.4%
	Group 3	39.9%
	Group 4	10.8%
Gram-positive rods	Group 5	16.4%
	Group 6	5.3%
	Group 7	11.1%
Gram-positive cocci	Group 8	6.5%
	unexploitable strains	3.7%
		2.8%
		4.6%

Eight groups were represented: Gram-negative oxidase-negative strictly aerobic rods such as *Acinetobacter*, *Pseudomonas*... (Group 1), Gram-negative oxidase-positive facultatively anaerobic rods such as *Aeromonas*... (Group 2), Gram-negative oxydase-negative facultatively anaerobic rods mainly *Enterobacteriaceae* (Group 3), Gram-negative oxidase-positive strictly aerobic rods like *Pseudomonas*... (Group 4), Gram-positive sporing rods such as *Bacillus*... (Group 5), Gram-positive catalase-positive nonsporing rods such as *Arthrobacter*... (Group 6), Gram-positive catalase-positive strictly aerobic cocci such as *Micrococcus*... (Group 7), Gram-positive catalase-positive facultatively anaerobic cocci such as *Staphylococcus*... (Group 8).

(Group 2), Gram-negative oxydase-negative facultatively anaerobic rods mainly *Enterobacteriaceae* (Group 3), Gram-negative oxidase-positive strictly aerobic rods like *Pseudomonas*... (Group 4), Gram-positive sporing rods such as *Bacillus*... (Group 5), Gram-positive catalase-positive nonsporing rods such as *Arthrobacter*... (Group 6), Gram-positive catalase-positive strictly aerobic cocci such as *Micrococcus*... (Group 7), Gram-positive catalase-positive facultatively anaerobic cocci such as *Staphylococcus*... (Group 8). No Gram-positive catalase-negative were found. Gram-negative rods accounted for the greatest part of the bacterial population (72.4%) with the following distribution: 39.9% for Group 3, 17.6% for Group 1, 10.8% for Group 4 and 4.0% for Group 2. Concerning Gram-positive bacteria, the predominant group corresponded to Group 6 (11.1%) followed by Group 5 (5.3%), Group 7 (3.7%), and Group 8 (2.8%). The bacterial composition, characterized by a predominance of Gram-negative bacilli, appeared unchanged compared to a similar study [27]. This observation is logical with regards to the nature of the material at the origin of the particles (crops). The main bacterial group, i.e. *Enterobacteriaceae*, Group 3, (39.9%), corresponds to bacterial species frequently associated with plants, and behave as epiphyte, endophyte or even pathogens [28]. These bacteria colonize crops during field growth, survive and even proliferate during storage and then are present in the dust cloud [29]. The second group of

bacteria in quantity is Group 1, represented by *P. syringae*, a germ present in the phyllosphere and generally adapted to growth at low temperature [30]. Catalase-positive non sporulated Gram-positive rods, Group 6, representing 11.1% of bacteria in the dust cloud, should correspond to bacteria of the genus *Corynebacteria*, *Rhodococcus* or *Arthrobacter* also usually present in the ground and already detected in urban air [11] and during crop manipulations [29].

The aim of this study was to monitor the bacterial air quality, and the study was focused on the groups including potential pathogens: Group 1, 3-5, and 8. From each of these groups, a representative strain was randomly chosen among the isolated strains. They were submitted to API gallery identification and 16S RNA sequencing. As shown in Table 2, all the orientation results were confirmed by those of the identification. Indeed, *P. syringae* is an oxidase-negative *Pseudomonas*, then it was pooled with *Acinetobacter*. *Brevundimonas* is related to the genus *Pseudomonas*. The correlation between the API gallery identification and 16S RNA is quite good at the genus level.

The discrepancies between identification results, especially at the species level, could be explained by the incomplete covering of clinical API galleries for the identification of environmental bacteria. This imprecision could also result from the 16S RNA strategy of identification, especially when it is applied over a large diversity of environmental bacteria whose compilation is not complete in data bases such as NCBI/PUBMED.

Comparison of population and bacterial virulence using the *Caenorhabditis elegans* killing test

This study deals with the impact of bacteria present in outdoor air on human health. A robust and practical experimental model was therefore needed in relation to respiratory diseases resulting from bacterial infection. The nematode *C. elegans* model is known to model

Table 2 Identification by API galleries and 16S RNA sequencing of the five representatives: *P. syringae*, *S. marcescens*, *Brevundimonas*, *B. cereus*, and *S. aureus*

	API Test	16S RNA identification
Group 1	<i>Pseudomonas luteola</i> (G)	<i>Pseudomonas syringae</i>
Group 3	<i>Serratia liquefaciens</i> (VG)	<i>Serratia marcescens</i>
Group 4	<i>Brevundimonas vesicularis</i>	<i>Brevundimonas</i> sp.
Group 5	<i>Bacillus cereus</i> (Exc)	<i>Bacillus thuringiensis</i> , <i>B. cereus</i> , or <i>B. anthracis</i>
Group 8	<i>Staphylococcus sciuri</i> (Exc)	<i>Staphylococcus aureus</i>

mammalian bacterial pathogenesis [21] and especially in human respiratory dysfunction [23].

The practical experimental advantages of this free-living worm are its ability to feed solely on bacteria, its short life cycle, and its easy cultivation in large number [31]. The survival kinetics of *C. elegans* in the presence of each bacterial representative (*P. syringae*, *Serratia marcescens*, *Brevundimonas*, *B. cereus*, and *S. aureus*) was studied for a maximum of 22 days (Figure 2). Even in the presence of their normal food source (*Escherichia coli* OP50) worms progressively die of age, all died after 17 days of culture. It is important to remember that the DNA synthesis inhibitor (FUDR) present in the medium prevents *C. elegans* egg offspring and population renewal. The survival of worms in the presence of these bacteria was compared to the one measured using the opportunistic pathogen *P. aeruginosa* PAO1, frequently responsible for respiratory tract infections [32]. Worms died rapidly in the presence of *P. aeruginosa* PAO1 (10 days) and none of the environmental strains collected in the air had equivalent virulence. In fact, all the survival kinetics were highly significantly different of those obtained in the presence of *P. aeruginosa* PAO1 ($P < 0.0001$ log-rank test). *P. syringae*, *S. marcescens*, and *B. cereus* presented against *C. elegans* increased or similar virulence compared to *E. coli* OP50.

Surprisingly, two strains: *Brevundimonas* sp., and *S. aureus* appeared less virulent than *E. coli* OP50 ($P < 0.0001$ log-rank test). Even if *S. aureus* is accepted as usually pathogen and *Brevundimonas* considered as an

opportunistic pathogen, we have to keep in mind that the bacterial virulence depends on the strains and is closely related to the bacterial adaptation to its microenvironment. But from the random selection of the representatives, no strain is known as strictly human pathogen. Also, according *C. elegans* test, no sanitary threat appeared because all representative strains were less virulent than the standard opportunistic pathogen *P. aeruginosa* PAO1. As isolation of all the bacterial spots on the impacted plate is rather fastidious work and complex populations should have virulence which differs from individual strains. Another approach is to test the virulence of the "global" impacted bacterial population against *C. elegans*, as shown in Figure 1. This was done with the bacterial mix, defined as "Total Air Sample". As with the representatives, virulence against nematodes was studied for the "Total Air Sample", corresponding to the bacterial population collected during crop loading on ships (plotted in Figure 2). The kinetics of the survival of worms with "Total Air Samples" was surrounded by most of the representative plots and was significantly different from that of *P. aeruginosa* PAO1 ($P < 0.0001$ log-rank test). Moreover, within the first 11 days of the study, the percentage of death of the worm population was greater using "Total Air Samples" than the avirulent standard *E. coli* OP50. This difference vanished afterwards and in both cases all worms were dead between 17 and 19 days.

The comparison of the lethal effects of the "Total Air Sample" with each environmental representative was clearly illustrated at Day 9 (Figure 3). This time corresponds to the last day of nematodes survival in the presence of *P. aeruginosa* PAO1. The survival of *C. elegans* exposed to *P. syringae* (50.00%), *Pantoae* spp (55.26%), and *B. cereus* (52.11%) was in the same range as for

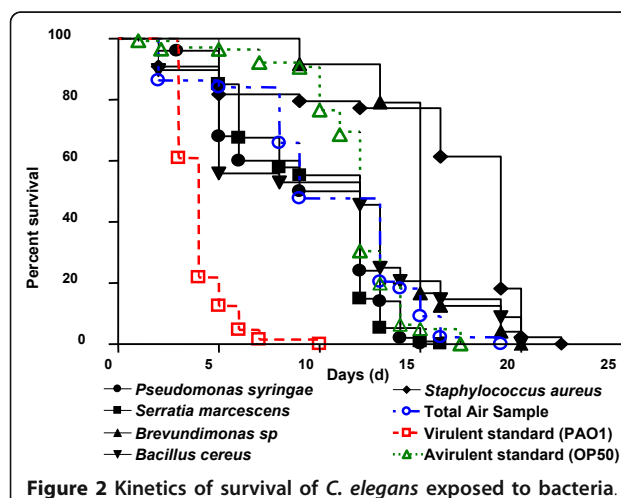


Figure 2 Kinetics of survival of *C. elegans* exposed to bacteria.

Kaplan-Meier survival plots of worms fed with the opportunistic pathogen *Pseudomonas aeruginosa* PAO1, bacterial strains isolated from air: *Pseudomonas syringae* (Group 1 : *Acinetobacter*...), *Pantoae* spp (Group 3: *Enterobacteriaceae*...), *Brevundimonas* sp (Group 4 *Pseudomonas*...), *Bacillus cereus* (Group 4: *Bacillus*...), and *Staphylococcus aureus* (Group 8: *Staphylococcus*...) and the non-virulent strain *Escherichia coli* OP50, and "Total Air Sample". Experiments were done in triplicate.

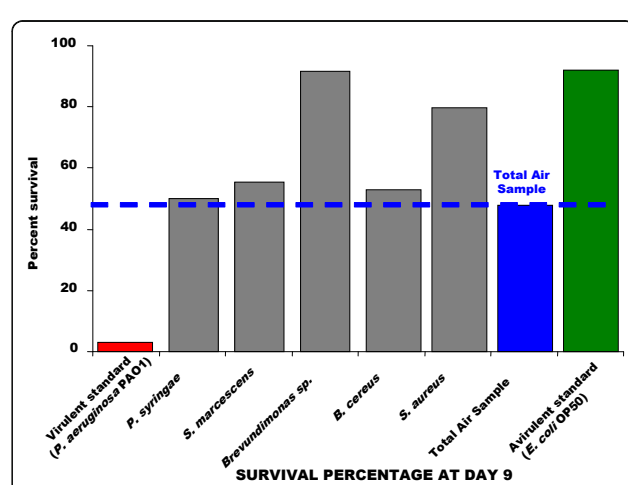


Figure 3 Comparison of the survival of worms exposed to bacteria at Day 9. Experiments were done in triplicate.

worms fed with "Total Air Sample" (47.73%). Nevertheless, as noted at Day 9, *S. aureus* and *Brevundimonas* favored the survival of nematodes with 79.55% and 91.66% of survival percentage respectively, compared to 47.73% for "Total Air Sample". Thus, nematode survival in the presence of the "Total Air Sample" seems pertinent to represent all bacteria synergies and individual virulence. The "Total Air Sample" can be considered without great sanitary risk for all healthy and non immuno-depressed people, as each representative strain.

Thence, any environmental sample with the help of a biocollector makes the assessment of the bacterial sanitary risk possible. After incubation of the softed impacted TSA plates, the total and cultivable bacterial population collected can directly feed the *C. elegans* nematode model, whose latest death shows the good quality and bacterial safety of the sample environment.

Conclusion

This study establishes that the outdoor air quality can be evaluated with the help of *C. elegans* nematodes alternative model for bacterial virulence aspects, even with high concentrations of airborne bacteria. Without the fastidious microbiological labor (isolation and bacterial identification), air quality can be monitored easily with a one-shot virulence test of the collected bacterial population obtained from a TSA plate impacted by outdoor air.

Acknowledgements

This study was supported by grants from Grand Evreux Agglomération, AFSET, and FEDER "Pseudomonas Virulence". We wish to thank Olivier Maillot and Magalie Barreau for technical assistance. We thank Dr Vlad S. Barbu (LMRS, 6085 CNRS, University of Rouen) for help with the nematode statistics and data analysis. We wish to thank Christine Farmer for linguistic insight for this manuscript.

Author details

¹Laboratory of Microbiology-Signals and MicroEnvironment, Normandy University, University of Rouen, EA 4312, 55 rue Saint Germain, 27000 Evreux, France. ²U644, Faculty of Medecine and Pharmacy, 22 boulevard Gambetta, INSERM Normandy University, University of Rouen, 76181 Rouen cedex, France.

Authors' contributions

CDP and AG conceived the study, designed and carried out some of the experiments and drafted the manuscript. OL participated in the design of the study and carried out some of the experiments. JPM encourage the use of *C. elegans* in air assessment. NO led the global project design and coordinated it. MF coordinated toxicological aspects. All authors read and approved the final manuscript.

Competing interests

The authors declare that they have no competing interests.

Received: 26 July 2011 Accepted: 18 November 2011

Published: 18 November 2011

References

- Laumbach RJ: Outdoor air pollutants and patient health. *Am Fam Physician* 2010, **81**:175-180.
- Morawska L, Wang H, Ristovski Z, Jayaratne ER, Johnson G, Cheung HC, Ling X, He C: **JEM spotlight: Environmental monitoring of airborne nanoparticles.** *Environ Monit* 2009, **11**:1758-1773.
- Douwes J, Thorne P, Pearce N, Heederik D: Bioaerosol health effects and exposure assessment: progress and prospects. *Ann Occup Hyg* 2003, **47**:187-200.
- Bugajny A, Knopkiewicz M, Piotrzeszewska-Pająk A, Sekulska-Stryjakowska M, Stach A, Filipiak M: **On the Microbiological Quality of the Outdoor Air in Poznań, Poland.** *Polish J Environ Studies* 2005, **14**:287-293.
- D'Amato G, Liccardi G, Russo M, D'Amato M: **On the interrelationship between outdoor air pollution and respiratory allergy.** *Aerobiologia* 2000, **16**:1-6.
- Lai K, Emberlin J, Colbeck I: **Outdoor environments and human pathogens in air.** *Environ Health* 2009, **8**:15.
- Fang Z, Ouyang ZY, Zheng H, Wang X, Hu L: **Culturable airborne bacteria in outdoor environments in Beijing, China.** *Microb Ecol* 2007, **54**:487-496.
- Fierer N, Liu Z, Rodríguez-Hernández M, Knight R, Henn M, Hernandez MT: **Short-term temporal variability in airborne bacterial and fungal populations.** *Appl Environ Microbiol* 2008, **74**:200-207.
- Maron PA, Lejon DPH, Carvahlo H, Bizet K, Ranjard L, Mougel C: **Assessing genetic structure and diversity of airborne bacterial communities by DNA fingerprinting and 16S rDNA clone library.** *Atmosph Environ* 2005, **39**:3687-3695.
- Létourneau V, Nehmé B, Mériaux A, Massé D, Cormier Y, Duchaine C: **Human pathogens and tetracycline-resistant bacteria in bioaerosols of swine confinement buildings and in nasal flora of hog producers.** *Int J Hyg Environ Health* 2010, **213**:444-449.
- Zhu H, Phelan PE, Duan T, Raupp GB, Fernando HJS, Che F: **Characterizations and relationships between outdoor and indoor bioaerosols in an office building.** *Aerobiologia* 2003, **19**:201-211.
- Gonçalves FL, Bauer H, Cardoso MR, Pukinskas S, Matos D, Melhem M, Puxbaum H: **Indoor and outdoor atmospheric fungal spores in the São Paulo metropolitan area (Brazil): species and numeric concentrations.** *Int J Biometeorol* 2010, **54**:347-355.
- Lee SH, Lee HJ, Kim SJ, Lee HM, Kang H, Kim YP: **Identification of airborne bacterial and fungal community structures in an urban area by T-RFLP analysis and quantitative real-time PCR.** *Sci Total Environ* 2010, **408**:1349-1357.
- Grisoli P, Rodolfi M, Villani S, Grignani E, Cottica D, Berri A, Picco AM, Dacarro C: **Assessment of airborne microorganism contamination in an industrial area characterized by an open composting facility and a wastewater treatment plant.** *Environ Res* 2009, **109**:135-142.
- Picot L, Chevalier S, Abdelmoula S, Merleau A, Guerillon J, Leroux P, Cazin L, Orange N, Feuilloley MG: **Regulation of the cytotoxic effects of Pseudomonas fluorescens by growth temperature.** *Res Microbiol* 2004, **155**:39-46.
- Casas V, Magbanua J, Sobrepeña G, Kelley ST, Maloy SR: **Reservoir of bacterial exotoxin genes in the environment.** *Int J Microbiol* 2010, **754368**.
- Antunes LC, Ferreira RB, Buckner MM, Finlay BB: **Quorum sensing in bacterial virulence.** *Microbiology* 2010, **156**:2271-2282.
- Chapalain A, Rossignol G, Lesouhaitier O, Merleau A, Gruffaz C, Guerillon J, Meyer JM, Orange N, Feuilloley MG: **Comparative study of 7 fluorescent pseudomonad clinical isolates.** *Can J Microbiol* 2008, **54**(1):19-27.
- Mondello P, Ferrari L, Carnevale G: **Nosocomial *Brevundimonas vesicularis* meningitis.** *Infez Med* 2006, **14**:235-237.
- Barer MR, Harwood CR: **Bacterial viability and culturability.** *Adv Microb Physiol* 1999, **41**:93-137.
- Darby C: **Interactions with microbial pathogens.** In *WormBook* Edited by: The *C. elegans* Research Community, WormBook 2005 [http://www.wormbook.org].
- Ruiz-Diez B, Sánchez P, Baquero F, Martínez JL, Navas A: **Differential interactions within the *Caenorhabditis elegans*-*Pseudomonas aeruginosa* pathogenesis model.** *J Theor Biol* 2003, **225**(4):469-476.
- Rea SL, Graham BH, Nakamaru-Ogiso E, Kar A, Falk MJ: **Bacteria, yeast, worms, and flies: exploiting simple model organisms to investigate human mitochondrial diseases.** *Dev Disabil Res Rev* 2010, **16**:200-218.
- Sauer P, Gallo J, Kesselova M, Kolař M, Koukalova D: **Universal primers for detection of common bacterial pathogens causing prosthetic joint infection.** *Biomed Pap Med Fac Univ Palacky Olomouc Czech Repub* 2005, **149**:285-288.

25. Stiernagle T: Maintenance of *C. elegans*. In *C elegans*. In *A practical approach*. Edited by: Hope IA. Oxford. Oxford University Press; 1999:51-67.
26. Clark RP, de Calcina-Goff ML: Some aspects of the airborne transmission of infection. *J R Soc Interface* 2009, 6:767-782.
27. Swan JR, Crook B: Airborne microorganisms associated with grain handling. *Ann Agric Environ Med* 1998, 5:7-15.
28. Holden N, Pritchard L, Toth I: Colonization outwith the colon: plants as an alternative environmental reservoir for human pathogenic enterobacteria. *FEMS Microbiol Rev* 2009, 33:689-703.
29. Gora A, Skorska C, Sitkowska J, Prazmo Z, Krysinska-Traczyk E, Urbanowicz B, Dutkiewicz J: Exposure of hop growers to bioaerosols. *Ann Agric Environ Med* 2004, 11:129-138.
30. Hirano SS, Upper CD: Bacteria in the leaf ecosystem with emphasis on *Pseudomonas syringae*-a pathogen, ice nucleus, and epiphyte. *Microbiol Mol Biol Rev* 2000, 64:624-53.
31. Ballestrieri F, Thomas T, Burke C, Egan S, Kjelleberg S: Identification of compounds with bioactivity against the nematode *Caenorhabditis elegans* by a screen based on the functional genomics of the marine bacterium *Pseudoalteromonas tunicata* D2. *Appl Environ Microbiol* 2010, 76:5710-5717.
32. Clifton IJ, Peckham DG: Defining routes of airborne transmission of *Pseudomonas aeruginosa* in people with cystic fibrosis. *Expert Rev Respir Med* 2010, 4:519-529.

doi:10.1186/1756-0500-4-503

Cite this article as: Duclairoir Poc et al: *Caenorhabditis elegans*: a model to monitor bacterial air quality. *BMC Research Notes* 2011 4:503.

**Submit your next manuscript to BioMed Central
and take full advantage of:**

- Convenient online submission
- Thorough peer review
- No space constraints or color figure charges
- Immediate publication on acceptance
- Inclusion in PubMed, CAS, Scopus and Google Scholar
- Research which is freely available for redistribution

Submit your manuscript at
www.biomedcentral.com/submit



P14

Research Article

Open Access

The Major Outer Membrane Protein Oprf is Required for Rhamnolipid Production in *Pseudomonas aeruginosa*

Emeline Bouffartigues¹, Gwendoline Gicquel¹, Alexis Bazire², Laurène Fito-Boncompte^{1,2}, Laure Taupin², Olivier Maillet¹, Anne Groboillot¹, Cécile Poc-Duclairoir¹, Nicole Orange¹, Marc Feuilloley¹, Alain Dufour² and Sylvie Chevalier^{1*}

¹Laboratoire de Microbiologie du Froid Signaux et Micro-Environnement EA 4312, Normandie Sécurité Sanitaire et Environnementale, Université de Rouen, France

²Laboratoire de Biotechnologie et Chimie Marines, EA 3884. Université de Bretagne-Sud, Université Européenne de Bretagne, France

Summary

The OprF porin is the major outer membrane protein of bacteria belonging to the *Pseudomonas* genus, and is partially exposed on the cellular surface. A study based on the comparison between *P. aeruginosa* H103 and its oprF-deficient mutant led to the finding that the absence of OprF abolished swarming but not swimming and twitching motilities. These phenotypes were explained at least in part by the inability of the oprF mutant to produce biosurfactant rhamnolipids. The levels of mRNAs encoding the rhamnolipid biosynthetic enzymes RhlA and RhlB were strongly decreased in the absence of OprF, indicating that rhamnolipid production was impaired at the transcriptional level. We suggest that the presence of OprF in the outer membrane of *P. aeruginosa* is required for environments colonization, making thus OprF a serious target for limiting *P. aeruginosa* spreading in case of cystic fibrosis.

Keywords: OprF; Porin; Rhamnolipid; Motility; *Pseudomonas*

Abbreviations: LC/MS: Liquid chromatography coupled to Mass Spectrometry

Introduction

Pseudomonas aeruginosa is an ubiquitous germ known as an important opportunistic pathogen of humans, causing a variety of infections among which chronic lung infections in cystic fibrosis patients [1-3]. *Pseudomonas* members are also described for their striking ability to adapt to various ecological niches [4]. This versatility requires a particularly well developed ability to adapt to changes of environmental conditions, to which proteins of the outer membrane may contribute, due to their partial exposition at the cell surface. Among them, OprF is one of the very few general porins [5], allowing non-specific diffusion of ionic species and of small polar nutrients [6]. OprF is also a major structural protein, anchoring the outer membrane to the peptidoglycan layer [7,8]. It is necessary for adaptation to various environments since it allows growth in low-osmolarity conditions [8], is over-produced in high salinity condition [9] and in ASM medium, which mimics the lung environment during cystic fibrosis [10]. It allows also the bacteria to respond to temperature variations by modulating the outer membrane permeability through a change in channel size [11]. OprF has been furthermore involved in adhesion to eukaryotic cells [12], and in biofilm formation under anaerobic conditions [13] enabling microcolonies formation [10]. Finally, we have recently shown that OprF is required for full virulence expression [14].

P. aeruginosa displays three types of motility: swimming in liquid or at low agar concentrations, twitching on solid surfaces, and swarming on semisolid media. Swimming and twitching result from the polar flagellum of *P. aeruginosa* and type IV pili, respectively, whereas swarming depends on both appendages and of rhamnolipids [15-17]. Rhamnolipids are biosurfactants composed of mono- or di-rhamnose linked to the lipid components 3-(3-hydroxyalkanoyloxy) alkanoic acids (HAAs) [18,19]. These glycolipids play a central role in swarming motility by acting as surface-modifying agents [20]. They can enhance cell surface hydrophobicity, by inducing LPS release from the outer membrane [21] and by adsorbing onto the cell surface [22,23], which can in turn modify the bacterium-substratum interactions. They affect

biofilm formation through microcolonies formation, motility [24], maintaining fluid channels between mushroom-like structures [25], and mediating cell detachment from biofilms [26]. Recently, rhamnolipids have been furthermore suggested to act as protective agents of *P. aeruginosa* against polymorphonuclear leukocytes, functioning as a biofilm shield *in vivo* [27,28].

Since bacterial motility plays a key role in the bacterial adaptation to environments, especially in surfaces colonization, we further investigated the function of OprF in *P. aeruginosa* motility. In this study, we show that an oprF knock out leads to impaired swarming, but not swimming or twitching motilities, at least partly through a deep alteration in rhamnolipid production.

Materials and Methods

Bacterial strains and growth conditions

The strains were *P. aeruginosa* H103 (PAO1 prototroph), its oprF mutant H636 obtained by homologous recombination with an oprF fragment containing a streptomycin cassette [29], and H636O, which corresponds to H636 complemented by plasmid pRW5 (encoding carbenicillin resistance) consisting in the functional oprF gene from *P. aeruginosa* H103 cloned into pUCP19 [14,30]. Cultures were inoculated at an initial OD₆₀₀ of 0.07, and bacteria were grown at 37°C on a rotary shaker (180 rpm) in Luria Bertani (LB) broth. In complement, 500 µg streptomycin mL⁻¹ only or with 300 µg carbenicillin mL⁻¹ were added in H636 and H636O cultures, respectively.

***Corresponding author:** Sylvie Chevalier, Laboratoire de Microbiologie du Froid, Signaux et Micro-environnement, 55 rue St Germain, 27000 Evreux, France, Tel: (+33) 2.32.29.15.60; Fax: (+33) 2.32.29.15.50; E-mail: sylvie.chevalier@univ-rouen.fr

Received May 11, 2011; **Accepted** June 15, 2011; **Published** June 25, 2011

Citation: Bouffartigues E, Gicquel G, Bazire A, Fito-Boncompte L, Taupin L, et al. (2011) The Major Outer Membrane Protein Oprf is Required for Rhamnolipid Production in *Pseudomonas aeruginosa*. J Bacteriol Parasitol 2:118. doi:[10.4172/2155-9597.1000118](http://dx.doi.org/10.4172/2155-9597.1000118)

Copyright: © 2011 Bouffartigues E, et al. This is an open-access article distributed under the terms of the Creative Commons Attribution License, which permits unrestricted use, distribution, and reproduction in any medium, provided the original author and source are credited.

Motility assays

These assays were essentially performed as described by Rashid & Kornberg [31]. Briefly, LB plates containing 0.3 % agar were point inoculated with a toothpick and incubated for 24 hours at 37°C. Swimming was quantified by measuring the circular turbid zone. The swarming assay was identical, except that LB plates contained 0.5 % agar and were incubated for 48 h. For twitching assays, cells were stab inoculated to the bottom of the Petri dish through a thin (~ 3 mm) LB agar layer (1 % agar). After incubation at 37°C for 48 h, the agar was removed, the Petri dish was washed with a stream of tap water, and the cells attached to the polystyrene surface were stained with crystal violet (1 % w/v) solution. Each assay was made at least in triplicate.

Phage PO4 sensitivity assay

10 µL of lysates that contain 102 plates forming units (PFU) of phages was mixed with 107 colonies forming units (CFU) of *P. aeruginosa* cells grown to OD600 of 0.7 and resuspended in 100µL of LB. After 10 min of incubation, 3mL of top agar was added, and the mixture was plated. Numeration of plaques was made after 16 to 24 h of incubation at 37°C.

Rhamnolipid quantification

The drop-collapse test was performed as previously described [32]. Rhamnolipids were further extracted and analyzed by liquid chromatography coupled to mass spectrometry (LC/MS) as previously described [33].

Quantitative RT-PCR

Extraction of RNAs, synthesis of cDNAs and real time PCR were achieved as previously described [9] using primers described in Table 1. PCR reactions were performed in triplicate and the standard deviations were lower than 0.15 CT. The relative quantification of the mRNAs of

Gene	sequences (5'-3')	References
<i>rhlA</i>	F: GATCGAGCTGGACGACAAGTC R: GCTGATGGTGTGGCTTTC	[33] [33]
<i>rhlB</i>	F: GAACAGGCAGACAGCAGCC R: CGCATCTTCACCCAATGGAT	[33] [33]
<i>rhlC</i>	F: ACCGGATAGACATGGCGT R: GATCGCTGTGGTGGAGTT	[33] [33]
<i>pilA</i>	F: ATTGCCATTCCCCAGTATCAGA R: CGAACGACCTTCCGAACG	This study This study
<i>fliC</i>	F: CTCGGAAACGCTACCAACG R: GCGAAGTCGGTGTCCCTTGAT	This study This study
<i>estA</i>	F: GGTTGGCCATGCCTTCT R: ACGTCATTCGTTGAACATCC	This study This study
16S	F: CAGGATTAGATAACCCTGGTAGTCCAC R: GACTTAACCCAAACATTCACGACAC	[35] [35]

Table 1: Primers used in quantitative RT-PCR experiments.

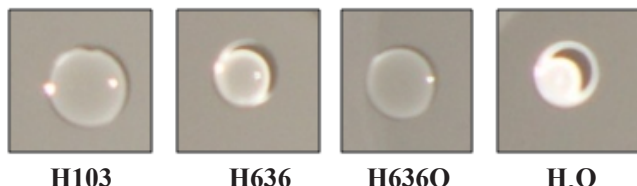


Figure 1: Drop-collapse test performed by adding 10 µL of culture supernatants of the indicated strains (48h) to water drops (20 µL) on glass slides.

interest was obtained by the comparative CT ($2^{-\Delta CT}$) method [34], using 16S rRNA as endogenous control [35]. ΔCT values were calculated by subtracting the 16S rRNA CT value from the CT value of an mRNA of interest from the same sample. ΔCT values were then obtained by calculating the difference between: i) the ΔCT value of a given mRNA resulting from *P. aeruginosa* H636 cells grown to a specific stage, and ii)

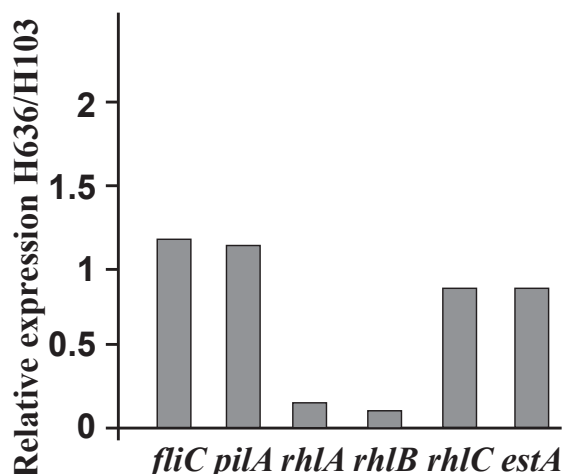


Figure 2: Expression levels of the indicated genes in the oprF mutant H636, relatively to *P. aeruginosa* H103. mRNAs were assayed by quantitative RT-PCR performed on RNA extracted from H636 and H103 strains. Values above and below 1 show a higher and a lower mRNA level in H636 than in H103, respectively. PCR reactions were performed in triplicate and the standard deviations were lower than 0.15 CT. The experiments were performed twice with independent bacterial cultures.

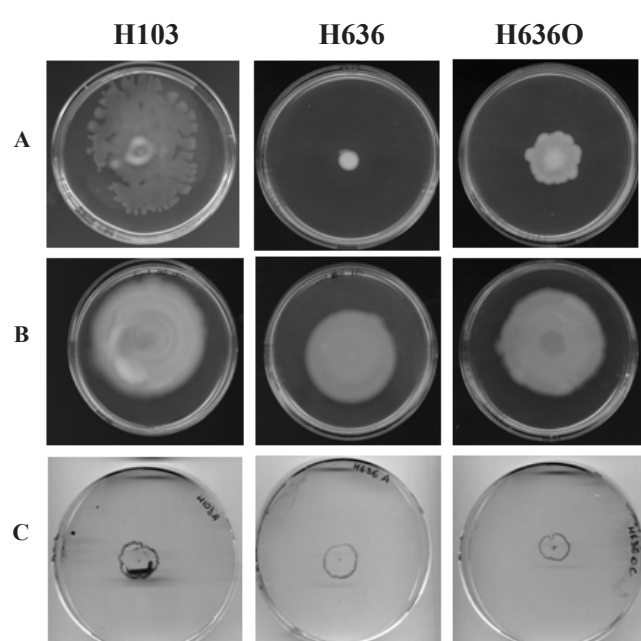


Figure 3: Swarming (A), swimming (B) and twitching (C) motilities of *P. aeruginosa* strains H103 (wild type), H636 (oprF mutant), and H636O (complemented oprF mutant).

the ΔCT value of the same mRNA from *P. aeruginosa* H103 (wild type) cells grown to the same stage. Relative mRNA level values are equal to $2^{-\Delta CT}$: values above and below 1 show a higher and a lower mRNA level in the *oprF* mutant H636 than in the wild type strain, respectively (eg a value of 0.5 indicates that the mRNA level was divided by 2 in H636).

Results

Three strains were compared in this study: the *P. aeruginosa* H103 wild type strain, its *oprF* mutant H636, and the *oprF*-complemented mutant strain H636O. The three growth curves obtained in LB medium at 37°C with shaking were similar, with a doubling time of 45 min [14].

Swarming is altered in the *oprF* mutant

The *oprF* mutant was unable to swarm, and the complementation of H636 with the *oprF* gene restores partially the swarming ability (Figure 1A). Swimming and twitching were slightly but not significantly altered (Figure 1B & Figure 1C), suggesting that both flagella and type IV pili were functional. To further dissect the swarming motility deficiency phenotype, quantitative RT-PCR experiments were performed to assay the transcription level of *fliC* and *pilA* genes, encoding the main flagellum and type IV pilus subunits, respectively. Figure 2 showed that their expression were not significantly down-regulated in the *oprF* mutant compared to H103 strain. The functionality of type IV pili was furthermore assayed by infecting the strains with the PO4 phage, which uses type IV pili as receptors [36]. The three strains were similarly sensitive to phage PO4 (the number of lysis plates being similar), indicating that type IV pili were present and functional in the H636 *oprF* mutant.

OprF is required for rhamnolipid production

Since swarming is depending on type IV pili, flagella and rhamnolipids [17], we next searched for the ability of the *oprF* mutant to produce these major biosurfactants. To achieve this rapidly, we first used the drop collapse test as previously described [32]. As shown on Figure 3, the drop spreading out in case of H103 and H636O suggested that biosurfactants were present. This was not the case for H636, suggesting a lack or a reduction in the biosurfactants amount. In supernatants of stationary phase cultures of the wild type strain, ten different ionic species, corresponding up to twelve rhamnolipids species, were identified by LC/MS (Table 2). Extra-cellular rhamnolipid production by the *oprF* mutant was nearly abolished: only three ionic species (*m/z* 675, 677, and 705) were detected in H636 supernatants, but in 25 to 50-fold lower amounts than in H103 supernatants (Table

2). Furthermore, the non detection of the ionic species *m/z* 649 in H636 supernatants indicated that Rha-Rha-C10-C10 production dropped more than 500 fold in the absence of OprF. We observed similar results when assaying rhamnolipids from supernatants of 48 and 72 h cultures (data not shown), thereby ascertaining that production of extra-cellular rhamnolipids by the *oprF* mutant is dramatically impaired, and not only delayed. The complementation of the mutation restored an efficient extra-cellular production of all rhamnolipid species, since their amounts were only 1.1 to 2.6-fold lower than in H103 supernatants (Table 2).

rhlAB expression is altered in the absence of OprF

To investigate whether the production of extra-cellular rhamnolipids by the *oprF* mutant is impaired at the biosynthesis or at the secretion level, we assayed rhamnolipids from bacterial pellets. A defect in rhamnolipid secretion was expected to lead to higher rhamnolipid accumulation in H636 OprF-negative cells than in H103 cells. This was however not the case (Table 2, intra cellular amounts), suggesting that the main defect occurred at the biosynthesis level. Mono-rhamnolipid biosynthesis specifically requires the successive actions of the enzymes RhlA and RhlB, encoded by the operon *rhlAB* [37,38]. Di-rhamnolipids are synthesized from mono-rhamnolipids by a third enzyme, the rhamnosyltransferase 2 RhlC [39]. Rhamnolipid production furthermore requires the autotransporter esterase EstA, the role of which remains unknown [40]. We therefore examined by quantitative RT-PCR whether the expression of these genes was affected in the *oprF* mutant. Whereas *rhlC* and *estA* mRNA levels were not significantly reduced in H636 mutant compared to H103 wild-type strain, the *rhlA* and *rhlB* mRNA levels were respectively 4.6 and 9-fold lower than in H103 (Figure 2). The down-regulation of the *rhlAB* operon seems strong enough to explain the rhamnolipid biosynthesis defect of the *oprF* mutant.

Discussion

OprF is the major outer membrane protein, partially exposed to the cell surface. Our study enabled us to find evidences for the involvement of OprF in swarming, but not in swimming and twitching motilities. Transcription of *fliC* and *pilA* genes are not affected, and the sensitivity to phage PO₄ indicates that the retraction function required for phage infection is maintained on the *oprF* mutant cell surface [16]. Taken together, these results suggest that flagella and type IV pili are expressed and functional in the *oprF* mutant. Since rhamnolipids are known to play a central role in swarming through their surfactant properties [20,41,42], we then focused on their production. Consistently, we found

Rhamnolipid	Ionic species* (<i>m/z</i>)	Extra cellular amount† (10^4 Area /OD ₆₀₀)			Intra cellular amount‡ (10^4 Area /OD ₆₀₀)		
		H103	H636	H636O	H103	H636	H636O
Rha-C10-C10	503	12.3 ± 1.1	ND	11.3 ± 1.9	ND	ND	ND
Rha-C10-C12:1	529	3.9 ± 0.2	ND	2.2 ± 0.3	ND	ND	ND
Rha-C12-C10 Rha-Rha-C8-C10	531	2.9 ± 0.1	ND	2 ± 0.2	ND	ND	ND
Rha-Rha-C10-C8	621	32.5 ± 7.4	ND	24.9 ± 5.2	ND	ND	ND
Rha-Rha-C8-C12:1	647	3.1 ± 0.7	ND	1.9 ± 0.1	ND	ND	ND
Rha-Rha-C10-C10	649	502.4 ± 14.5	ND	321.7 ± 55.4	13.2 ± 6.3	5.1 ± 2.2	41.5 ± 12.8
Rha-Rha-C10-C12:1	675	138.1 ± 18.1	3.3 ± 0.3	113.8 ± 13.7	5.5 ± 2.2	1.5 ± 0.7	16.1 ± 5.5
Rha-Rha-C10-C12, Rha-Rha-C12-C10	677	662.9 ± 3.6	13.2 ± 1.5	257.5 ± 16.6	15.4 ± 6.3	5.6 ± 2.8	56.9 ± 19.4
Rha-Rha-C12-C12:1	703	15.6 ± 3.3	ND	12.7 ± 1.2	0.9 ± 0.5	0.8 ± 0.1	3.7 ± 1.4
Rha-Rha-C12-C12	705	42.9 ± 25.2	1.7 ± 0.2	18.7 ± 1.5	2.9 ± 0.2	1.7 ± 0.1	5.3 ± 1.7
Total amount of rhamnolipids		1416.7 ± 74.2	18.2 ± 2	766.8 ± 1.5	37.9 ± 15.5	14.7 ± 5.9	123.5 ± 40.8

Table 2: Rhamnolipid amounts produced by *P. aeruginosa* H103, H636 and H636O grown to stationary phase in LB medium. ND: values not detected. Threshold: <0.8 x 10⁴ Area/OD₆₀₀. *Ionic species leading to LC/MS peaks. † Rhamnolipids assayed from culture supernatants. ‡ Rhamnolipids assayed from cell pellets. †,‡ The LC/MS peak surface areas were divided by the OD₆₀₀ values of the cultures. Each value is the average of three independent experiments.

that the rhamnolipid production is nearly abolished in the *oprF* mutant, which likely explains the swarming motility defect. Rhamnolipid biosynthetic genes were shown to be essential (*rhlA*) or important (*rhlB*) for *P. aeruginosa* swarming [15,20,24,37]. The roles of HAAs (3-3-hydroxyalkanoyloxy alkanoic acids), mono-rhamnolipids and di-rhamnolipids, synthesized by RhlA, RhlB and RhlC, respectively, were dissected: di-rhamnolipids and HAAs serve as attractant and repellents, respectively, while mono-rhamnolipids act as wetting agents [42]. The impairment in rhamnolipid production of the *oprF* mutant could therefore explain its inability to swarm. However, restoration of the swarming phenotype was incomplete in the complemented mutant whereas rhamnolipid production reached near wild type levels. This indicated that the lack of rhamnolipid might not be the only cause of the swarming defect in the *oprF* mutant. Alternatively, swarming might require a rhamnolipid overproduction, which might not be achieved properly in the complemented *oprF* mutant.

In the *oprF* mutant, rhamnolipids did not accumulate intracellularly at higher levels than in the wild type strain, indicating that the production is impaired at the biosynthesis level rather than at the secretion level. This impairment can be at least in part explained by lower levels of *rhlAB* mRNAs, suggesting an involvement of OprF in the *rhlAB* expression, which is already known to depend on a complex regulatory network [43]. Transcription of the *rhlAB* operon is under the direct control of the RhlR-RhlI quorum sensing (QS) system and of its cognate autoinducer molecule, N-butyryl-L-homoserine lactone (C₄-HSL) [44-47] which is itself regulated by the LasR-LasI system, encoding the *N*-(3-oxododecanoyl)-L-homoserine lactone auto inducer, (3OC₁₂-HSL) [48,49], and the MvfR-PQS (*Pseudomonas* Quinolone Signal) /HHQ (4-hydroxy-2-heptylquinoline) system [48]. We showed recently that QS molecule production was altered in the H636 *oprF* mutant since the amounts of 3OC₁₂-HSL and C₄-HSL were reduced or delayed, respectively, while that of HHQ was increased [14]. It is thus possible that these alterations in QS molecule production contribute to the observed decrease in *rhlAB* transcription.

It is unclear whether OprF plays a direct and/or indirect role in the observed phenotypes. The importance of OprF in stabilizing the outer membrane and maintaining the integrity of the cell wall of *P. aeruginosa* has been previously described [7,8,14,29]. A possibility is that the lack of OprF can change the cell surface and the composition of the outer membrane. Based on these considerations, the alteration of the QS and rhamnolipid production could be due to major modifications of the cell wall. The alternative possibility that the absence of OprF impairs the observed phenotypes by other means than outer membrane disorganization cannot be disregarded, considering the major role of OprF in binding interferon γ and activation of the QS network [50]. OprF has been indeed suggested as an environmental outer membrane sensor, perceiving variations of its micro environment, and transmitting or transducing an unknown signal leading to QS activation [14,51]. Whatever the mechanisms involved linking OprF and rhamnolipid production, it is clear that the presence of OprF in the outer membrane of *P. aeruginosa* is required for environments colonization, making thus OprF a serious target for limiting *P. aeruginosa* spreading in case of cystic fibrosis.

Acknowledgements

We are grateful to R. E. W. Hancock for kindly providing H103 and H636 strains, pRW5 plasmid and monoclonal antibodies raised against OprF. We wish to thank E. Deziel for the gift of PO₄ phage. The Laboratoire de Biotechnologie et Chimie Marines is supported by the Région Bretagne (France) and European FEDER. The LMDF-SME is supported by the Région Haute Normandie (financial

support of G. G.), the Grand Evreux Agglomération (financial support of O. M. and of L. F. B.), the Conseil Général de l'Eure (CG27), and European FEDER funds (financial support of E. B.).

References

1. Bodey GP, Bolivar R, Fainstein V, Jadeja L (1983) Infections caused by *Pseudomonas aeruginosa*. Rev Infect Dis 5: 279-313.
2. Goldberg JB (2000) *Pseudomonas*: global bacteria. Trends Microbiol 8: 55-57.
3. Ramsey DM, Wozniak DJ (2005) Understanding the control of *Pseudomonas aeruginosa* alginate synthesis and the prospect for management of chronic infections in cystic fibrosis. Mol Microbiol 56: 309-322.
4. Spiers AJ, Buckling A, Rainey PB (2000) The causes of *Pseudomonas* diversity. Microbiology 146: 2345-2350.
5. Tamber S, Hancock REW (2004) The outer membranes of *Pseudomonads*. In *Pseudomonas*, Vol. 1, pp. 575-601. Edited by J.-L. Ramos. New York, Boston, Dordrecht, Moscow: Kluwer Academic/Plenum Publishers, London.
6. Nestorovich EM, Sugawara E, Nikaido H, Bezrukov SM (2006) *Pseudomonas aeruginosa* porin OprF: properties of the channel. J Biol Chem 281: 16230-16237.
7. Woodruff WA, Hancock REW (1989) *Pseudomonas aeruginosa* outer membrane protein F: structural role and relationship to the *Escherichia coli* OmpA protein. J Bacteriol 171: 3304-3309.
8. Rawling EG, Brinkman FSL, Hancock REW (1998) Roles of the carboxy-terminal half of *Pseudomonas aeruginosa* major outer membrane protein OprF in cell shape, growth in low-osmolarity medium, and peptidoglycan association. J Bacteriol 180: 3556-3562.
9. Guyard-Nicodème M, Bazire A, Hémery G, Meyheuc T, Mollé D, et al. (2008) Outer membrane modifications of *Pseudomonas fluorescens* MF37 in response to hyperosmolarity. J Proteome Res 7: 1218-1225.
10. Sriramulu DD, Lünsdorf H, Lam JS, Römling U (2005) Microcolony formation: a novel biofilm model of *Pseudomonas aeruginosa* for the cystic fibrosis lung. J Med Microbiol 54: 667-676.
11. Jaouen T, De E, Chevalier S, Orange N (2004) Pore size dependence on growth temperature is a common characteristic of the major outer membrane protein OprF in psychrotrophic and mesophilic *Pseudomonas* species. Appl Environ Microbiol 70: 6665-6669.
12. Azghani AO, Idell S, Bains M, Hancock REW (2002) *Pseudomonas aeruginosa* outer membrane protein F is an adhesin in bacterial binding to lung epithelial cells in culture. Microb Pathog 33: 109-114.
13. Yoon SS, Hennigan RF, Hilliard GM, Ochsner UA, Parvatiyar K, et al. (2002) *Pseudomonas aeruginosa* anaerobic respiration in biofilms: relationships to cystic fibrosis pathogenesis. Dev Cell 3: 593-603.
14. Fito-Boncompte L, Chapalain A, Bouffartigues E, Chaker H, Lesouhaitier O, et al (2011) Full virulence of *Pseudomonas aeruginosa* requires OprF. Infect Immun 79: 1176-1186.
15. Köhler T, Curty LK, Barja F, van Delden C, Pechère JC (2000) Swarming of *Pseudomonas aeruginosa* is dependent on cell-to-cell signaling and requires flagella and pili. J Bacteriol 182: 5990-5996.
16. Skerker JM, Berg HC (2001) Direct observation of extension and retraction of type IV pili. Proc Natl Acad Sci USA 98: 6901-6904.
17. Overhage J, Lewenza S, Marr AK, Hancock REW (2007) Identification of genes involved in swarming motility using a *Pseudomonas aeruginosa* PAO1 mini-Tn5-lux mutant library. J Bacteriol 189: 2164-2169.
18. Soberón-Chávez G, Lépine F, Déziel E (2005) Production of rhamnolipids by *Pseudomonas aeruginosa*. Appl Microbiol Biotechnol 68: 718-725.
19. Abdel-Mawgoud AM, Lépine F, Déziel E (2010) Rhamnolipids: diversity of structures, microbial origins and roles. Appl Microbiol Biotechnol 86: 1323-1336.
20. Caiiazza NC, Shanks RM, O'Toole GA (2005) Rhamnolipids modulate swarming motility patterns of *Pseudomonas aeruginosa*. J Bacteriol 187: 7351-7361.
21. Al-Tahhan RA, Sandrin TR, Bodour AA, Maier RM (2000) Rhamnolipid-induced removal of lipopolysaccharide from *Pseudomonas aeruginosa*: effect on cell surface properties and interaction with hydrophobic substrates. Appl Environ Microbiol 66: 3262-3268.
22. Zhong H, Zeng GM, Yuan XZ, Fu HY, Huang GH et al. (2007) Adsorption

- of dirhamnolipid on four microorganisms and the effect on cell surface hydrophobicity. *Appl Microbiol Biotechnol* 77: 447-455.
23. Zhong H, Zeng GM, Liu JX, Xu XM, Yuan XZ et al. (2008) Adsorption of monorhamnolipid and dirhamnolipid on two *Pseudomonas aeruginosa* strains and the effect on cell surface hydrophobicity. *Appl Microbiol Biotechnol* 79: 671-677.
24. Pamp SJ, Tolker-Nielsen T (2007) Multiple roles of biosurfactants in structural biofilm development by *Pseudomonas aeruginosa*. *J Bacteriol* 189: 2531-2539.
25. Davey ME, Caiazza NC, O'Toole GA (2003) Rhamnolipid surfactant production affects biofilm architecture in *Pseudomonas aeruginosa* PAO1. *J Bacteriol* 185: 1027-1036.
26. Boles BR, Thoendel M, Singh PK (2005) Rhamnolipids mediate detachment of *Pseudomonas aeruginosa* from biofilms. *Mol Microbiol* 57: 1210-1223.
27. Alhede M, Bjarnsholt T, Jensen PØ, Phipps RK, Moser C, et al (2009) *Pseudomonas aeruginosa* recognizes and responds aggressively to the presence of polymorphonuclear leukocytes. *Microbiology* 155: 3500-3508.
28. Van Gennip M, Christensen LD, Alhede M, Phipps R, Jensen PØ, et al (2009) Inactivation of the *rhlA* gene in *Pseudomonas aeruginosa* prevents rhamnolipid production, disabling the protection against polymorphonuclear leukocytes. *APMIS* 117: 537-546.
29. Woodruff WA, Hancock REW (1988) Construction and characterization of *Pseudomonas aeruginosa* protein F-deficient mutants after *in vitro* and *in vivo* insertion mutagenesis of the cloned gene. *J Bacteriol* 170: 2592-2598.
30. Brinkman FSL, Schoofs G, Hancock REW, De Mot R (1999) Influence of a putative ECF Sigma factor on expression of the major outer membrane protein, OprF, in *Pseudomonas aeruginosa* and *Pseudomonas fluorescens*. *J Bacteriol* 181: 4746-4754.
31. Rashid MH, Kornberg A (2000) Inorganic polyphosphate is needed for swimming, swarming, and twitching motilities of *Pseudomonas aeruginosa*. *Proc Natl Acad Sci* 25: 4885-4890.
32. Youssef NH, Duncan KE, Nagle DP, Savage KN, Knapp RM, et al. (2004). Comparison of methods to detect biosurfactant production by diverse microorganisms. *J Microbiol Methods* 56: 339-347.
33. Bazire A, Dheilly A, Diab F, Morin D, Jebbar M, Haras D, Dufour A (2005) Osmotic stress impairs production of cell-to-cell signal molecules and rhamnolipid biosurfactant by *Pseudomonas aeruginosa*. *FEMS Microbiol Lett* 253: 125-131.
34. Livak KJ, Schmittgen TD (2001) Analysis of relative gene expression data using real-time quantitative PCR and the 2(-Delta Delta C(T)) Method. *Methods* 25: 402-408.
35. Corbella ME, Puyet A (2003) Real-time reverse transcription-PCR analysis of expression of halobenzoate and salicylate catabolism-associated operons in two strains of *Pseudomonas aeruginosa*. *Appl Environ Microbiol* 69: 2269-2275.
36. Bradley DE (1973). Basic characterization of a *Pseudomonas aeruginosa* pilus-dependent bacteriophage with a long noncontractile tail. *J Virol*. 12: 1139-1148.
37. Déziel E, Lépine F, Milot S, Villemur R (2003) *rhlA* is required for the production of a novel biosurfactant promoting swarming motility in *Pseudomonas aeruginosa*: 3-(3-hydroxyalkanoyloxy)alkanoic acids (HAAs), the precursor of rhamnolipids. *Microbiology* 149: 2005-2013.
38. Zhu K, Rock CO (2008) RhlA converts β -hydroxyacyl-acyl carrier protein intermediates in fatty acid synthesis to the β -hydroxydecanoate component of rhamnolipids in *Pseudomonas aeruginosa*. *J Bacteriol* 190: 3147-3154.
39. Rahim R, Ochsner UA, Olvera C, Graninger M, Messner P, et al. (2001) Cloning and functional characterization of the *Pseudomonas aeruginosa* *rhlC* gene that encodes rhamnosyltransferase 2, an enzyme responsible for di-rhamnolipid biosynthesis. *Mol Microbiol* 40: 708-718.
40. Wilhelm S, Gdynia A, Tielen P, Rosenau F, Jaeger KE (2007) The autotransporter esterase EstA of *Pseudomonas aeruginosa* is required for rhamnolipid production, cell motility, and biofilm formation. *J Bacteriol* 189: 6695-6703.
41. Caiazza NC, Merritt JH, Brothers KM, O'Toole GA (2007) Inverse regulation of biofilm formation and swarming motility by *Pseudomonas aeruginosa* PA14. *J Bacteriol* 189: 3603-3612.
42. Tremblay J, Richardson AP, Lépine F, Déziel E (2007) Self-produced extracellular stimuli modulate the *Pseudomonas aeruginosa* swarming motility behaviour. *Environ Microbiol* 9: 2622-2630.
43. Reis RS, Pereira AG, Neves BC, Freire DM (2011) Gene regulation of rhamnolipid production in *Pseudomonas aeruginosa*. *Bioresource Technology* 102: 6377-6384.
44. Brint JM, Ohman DE (1995) Synthesis of multiple exoproducts in *Pseudomonas aeruginosa* is under the control of RhIR-RhII, another set of regulators in strain PAO1 with homology to the autoinducer-responsive LuxR-LuxI family. *J Bacteriol* 177: 7155-7163.
45. Ochsner UA, Reiser J (1995) Autoinducer-mediated regulation of rhamnolipid biosurfactant synthesis in *Pseudomonas aeruginosa*. *Proc Natl Acad Sci USA* 92: 6424-6428.
46. Pearson JP, Pesci EC, Iglesias BH (1997) Roles of *Pseudomonas aeruginosa las* and *rhl* quorum-sensing systems in control of elastase and rhamnolipid biosynthesis genes. *J Bacteriol* 179: 5756-5767.
47. Medina G, Juárez K, Soberón-Chávez G (2003) The *Pseudomonas aeruginosa rhlAB* operon is not expressed during the logarithmic phase of growth even in the presence of its activator RhlR and the autoinducer N-butyryl-homoserine lactone. *J Bacteriol* 185: 377-380.
48. Diggle SP, Lumjaktase P, Dipilato F, Winzer K, Kunakorn M, et al. (2006) Functional genetic analysis reveals a 2-Alkyl-4-quinolone signaling system in the human pathogen *Burkholderia pseudomallei* and related bacteria. *Chem Biol* 13: 701-710.
49. Schuster M, Greenberg EP (2006) A network of networks: quorum-sensing gene regulation in *Pseudomonas aeruginosa*. *Int J Med Microbiol*. 296: 73-81.
50. Wu L, Estrada O, Zaborina O, Bains M, Shen L, et al. (2005) Recognition of host immune activation by *Pseudomonas aeruginosa*. *Science* 309: 774-777.
51. Wagner VE, Frelinger JG, Barth RK, Iglesias BH (2006) Quorum sensing: dynamic response of *Pseudomonas aeruginosa* to external signals. *Trends Microbiol* 14: 55-58.

Submit your next manuscript and get advantages of OMICS Group submissions

Unique features:

- User friendly/feasible website-translation of your paper to 50 world's leading languages
- Audio Version of published paper
- Digital articles to share and explore



Special features:

- 100 Open Access Journals
- 10,000 editorial team
- 21 days rapid review process
- Quality and quick editorial, review and publication processing
- Indexing at PubMed (partial), Scopus, DOAJ, EBSCO, Index Copernicus and Google Scholar etc
- Sharing Option Social Networking Enabled
- Authors, Reviewers and Editors rewarded with online Scientific Credits
- Better discount for your subsequent articles

Submit your manuscript at: <http://www.omicsonline.org/submission>

P15

Influence of Growth Temperature on Cyclolipopeptides Production and on Adhesion Behaviour in Environmental Strains of *Pseudomonas fluorescens*

Cécile Duclairoir-Poc^{1*}, Thierry Meylheuc², Sandra Ngoya^{1,2}, Anne Groboillot¹, Josselin Bodilis³, Laure Taupin⁴, Annabelle Merieau¹, Marc G.J. Feuilloley¹ and Nicole Orange¹

¹Laboratoire de Microbiologie-Signaux et Micro-environnement, EA4312, Normandie Université, Université de Rouen, 55 rue Saint Germain, 27000 Evreux, France

²Unité mixte de recherche en Bioadhésion et Hygiène des Matériaux, UMR 763 INRA-AgroParisTech, 25 avenue de la République, 91300 Massy, France

³Laboratoire de Morphodynamique Continentale et Côtier, UMR CNRS 6143, Normandie Université, Université de Rouen, 76821 Mont-Saint-Aignan cedex, France

⁴Laboratoire de Biotechnologie et Chimie Marines, Université de Bretagne-Sud B.P. 92116, 56321 Lorient cedex, France

Summary

The present study deals with the influence of growth temperature on biosurfactant production and the adhesion process in the psychrotrophic species *Pseudomonas fluorescens*. We studied a strain panel composed of nine wild cyclolipopeptide (CLPs) producers and by two biosurfactant mutants. Where cyclolipopeptide production was characterized at either 8°C or 17°C, cyclolipopeptide production was highlighted by hemolytic and tensiometric methods. Their ionic charge was evaluated by a double diffusion test and their identification was made as amphisin- or viscosin- or viscosinamide-like biosurfactants by Reverse Phase-High Performance Liquid Chromatography-Mass Spectroscopy. This categorization was corroborated by the 16S rRNA phylogenetic study. In *Pseudomonas fluorescens*, the number and relative quantity of cyclolipopeptide produced and bacterial adhesion differed with the growth temperature. Seven new cyclolipopeptides were characterized, of which three belong to the viscosinamide family. Biosurfactant secretion is intensive at 17°C and the highest adhesion is obtained at a lower temperature (8°C). Cyclolipopeptides appeared to antagonize the adhesion process. Strain hydrophobicity was wholly independent of growth temperature and could not be correlated with the initial attachment of bacteria, which was thermoregulated. Our study demonstrates that bacterial adhesion is controlled by the growth temperature but not by cyclolipopeptides or cell hydrophobicity.

Keywords: *Pseudomonas fluorescens*; Cyclolipopeptides; Biosurfactant; Growth temperature; Adhesion

Introduction

Surfactants are amphiphatic molecules, which are particularly well adapted to distribution at interfaces between solids, liquids or even vapour [1]. These properties were at the origin of their multiple industrial applications in petroleum production, environmental control, food transformation, agriculture, pharmaceuticals and cosmetics [2,3].

Surfactants can be obtained by chemical synthesis but a great variety of microorganisms are also able to produce such molecules designated in this case as biosurfactants. The chemical nature and surface-active properties of biosurfactants are highly variable. Although the competitive advantage of biosurfactant production for microorganisms still remains unanswered, there is now ample evidence that these molecules are essential for survival, host-interactions and growth in many bacterial species [4,5]. These molecules should increase the bioavailability of hydrophobic water-insoluble substrates and improve heavy metal binding. Through this process, biosurfactants are involved in bacterial pathogenesis and quorum sensing [6-7]. As environmental bacteria need to adapt rapidly to variations of their growth conditions [8], the production of biosurfactant is important in these species. This is particularly the case in the *Pseudomonas* genus, which is one of the most ubiquitous bacterial groups. In the present study, we focused on nine environmental *Pseudomonas* strains isolated from plants and the rhizosphere. All these bacteria have been shown to produce cyclolipopeptides (CLPs) as biosurfactants [7-15]. In literature, CLPs are described as being involved in attachment at the surfaces, inert or green, in motility, and in pathogenicity [7-8]. This last point is essential since it appears now that for clinical strain isolates virulence depends on CLP production [7,16-18]. Biosurfactant synthesis is well

documented in *Pseudomonas* [7-8], but it is remarkable that, until now, the influences of the growth temperature of *Pseudomonas fluorescens* on biosurfactant production and physico-chemical properties have not been investigated in detail. The production of exoproducts in these species is also a temperature dependent process. 17°C is known as the optimal growth temperature for many exoproducts synthesized by psychrotrophic *Pseudomonas* [19-22]. As amphiphilic exo-products, biosurfactants appear to play a role whenever a microbe encounters an interface, inert or living one. The results of these adaptation mechanisms could be adhesion, biofilm formation, quorum sensing and any response to environmental change [6]. All the knowledge on biosurfactant production in *Pseudomonas* should therefore be carefully reanalyzed taking into consideration this thermal parameter. In the present study, we investigated the influence of growth temperature on biosurfactant production at two key temperatures, 8°C and 17°C. The lower one corresponds to the temperature frequently used in cold storage conditions while the higher one represents the optimal growth temperature for many exoproducts. After sorted out genetically the studied *Pseudomonas fluorescens* strains, the decrease of surface

***Corresponding author:** Cécile Duclairoir Poc, LMDF/ LMSM, EA 4312, 55 rue Saint-Germain 27000 Evreux, France, Tel: 00 332 32 29 15 49; Fax: (00) 332 32 29 15 50; E-mail: cecile.poc@univ-rouen.fr

Received June 25, 2011; **Accepted** November 02, 2011; **Published** November 10, 2011

Citation: Duclairoir-Poc C, Meylheuc T, Ngoya S, Groboillot A, Bodilis J, Taupin L, et al. (2011) Influence of Growth Temperature on Cyclolipopeptides Production and on Adhesion Behaviour in Environmental Strains of *Pseudomonas fluorescens*. J Bacteriol Parasitol S1-002. doi:[10.4172/2155-9597.S1-002](http://dx.doi.org/10.4172/2155-9597.S1-002)

Copyright: © 2011 Duclairoir-Poc C, et al. This is an open-access article distributed under the terms of the Creative Commons Attribution License, which permits unrestricted use, distribution, and reproduction in any medium, provided the original author and source are credited.

tension is verified and reveals biosurfactant production. Their ionic characterization and the hemolytic bacterial behaviour are compared to the RP-HPLC/MS identification and then afford the proposal of a rapid CLP identification. The biosurfactant production could modify the bacterial surfacial properties and, thence, its adaptative potential in their microenvironment. Biosurfactant production are discussed in regard to the consequence of the growth temperature on the adhesive behaviour of *P. fluorescens*.

Materials and Methods

Bacterial strains

P. fluorescens PfA7B is a pathogenic strain of broccoli isolated from inflorescence. *P. fluorescens* *Pf1Vis-* is a Tn5 km^r viscosin mutant of PfA7B [13]. These two strains were provided by Dr G. Braun (Agriculture & Agri-Food, Canada). *P. fluorescens* DSS73, a strain from sugar beet rhizospheric environment, and its km^r *amsY*:tn5 amphisin mutant, *P. fluorescens* DSS73-15C2 [23], were also graciously provided by Dr O. Nybroe (Royal Veterinary & Agricultural University – Thorvaldsensvej, Denmark). Other strains of *P. fluorescens*, namely CTS22, CTS38, CTS50, CTS70, CTS117, CTS193 [11] and DR54 [10] were gifts from Dr T.H. Nielsen (Royal Veterinary & Agricultural University, Denmark). They had been isolated from Danish fallow or sugar beet fields. Both Danish fields have sandy and loamy soils.

Growth conditions and biosurfactant collection

The bacterial cultures were grown at 8°C and 17°C in Davis minimal media (DMM: 30 mmol.L⁻¹ K₂HPO₄, 14 mmol.L⁻¹ KHPO₄, 0.4 mmol.L⁻¹ MgSO₄, 7.6 mmol.L⁻¹ (NH₄)₂SO₄, 120 mmol.L⁻¹ glucose, and 1 mL of trace element solution per litre (pH 7.3). The trace element solution per litre contained 20 mg of CoCl₂.6H₂O, 30 mg of H₃BO₃, 10 mg of ZnSO₄.7H₂O, 1 mg of CuCl₂.2H₂O, 2 mg of NiCl₂.6H₂O, 3 mg of NaMoO₄.2H₂O, 10 mg of FeSO₄.7H₂O, and 2.6 mg of MnSO₄.H₂O). 15g.L⁻¹ agar was added to obtain a solid medium DMA. The glucose and trace elements were sterilized separately by filtration (Sterilipet, Millipore, France) and aseptically added to the rest of the medium. Plates were inoculated with 40µL of a stock strain suspension. To collect the potential biosurfactant production, the bacterial colonies were carefully scraped off after 4 days incubation at either 8°C or 17°C and resuspended in 15mL natural mineral water. This suspension was centrifuged 18000g at 4°C for 30 min. The rinsing solution corresponded to the obtained supernatant.

Phylogenetic study

The 16S rRNA sequences of the biosurfactant producing strains were sequenced in double stranded by Cogenics Genome Express (Meylan, France). The sequences were deposited in the Genbank database under Accession Numbers indicated in Figure 1 and Table 1.

The 16S rRNA sequences of the *Pseudomonas* type strains used for phylogenetic analyses were retrieved from the Ribosomal Database Project (<http://rdp.cme.msu.edu/index.jsp>). The 16S rRNA sequences of the *P. fluorescens* SBW25 and Pf0-1 strains were retrieved from the *Pseudomonas* Genome Database (<http://v2.Pseudomonas.com>). All the sequences were aligned using Clustal X version 1.81 with default parameters [26]. The alignment was truncated to the same size corresponding to the shortest sequence (positions 119 to 1368 in the *E. coli* numbering system). All ambiguous positions and positions with gaps were removed. A neighbour-joining tree was inferred using the Kimura-two-parameter correction with MEGA v3.0 [27]. A maximum likelihood analysis was performed using fastDNAml based on the

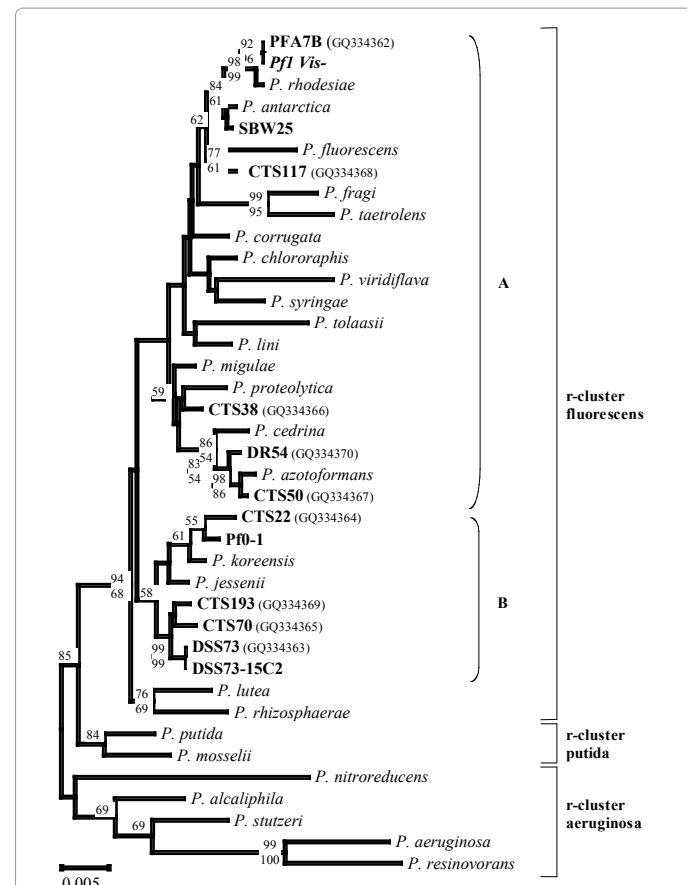


Figure 1: Phylogenetic relationships among 16S ribosomal RNA genes from the panel strain and 28 *Pseudomonas* type strains.

The nine biosurfactant-producing strains, the two biosurfactant negative mutants, SBW25 and Pf0-1 strains are in bold print. The unrooted dendrogram was carried out using the Neighbour-Joining algorithm. Numbers on tree branches report bootstrap results from Neighbour-Joining (above branch) and Maximum Likelihood (below branch) analyses for those branches having ≥50% support. A and B are two distinct phylogenetic groups in *P. fluorescens* r-cluster.

HKY model with PhyloWin v2.0 [28]. The degree of statistical support for the branches was determined with 1000 bootstrap replicates for the neighbour-joining analysis or 100 bootstrap replicates for the maximum likelihood analyses.

Hemolysis activity test

Hemolysis has been described as a potential indirect method to demonstrate surfactant production [29]. In this test, each bacterial strain was streaked onto a 2% sheep red blood cell plate and incubated for 48h at 8°C or 17°C. The plates were visually inspected for zones of clearing around the colonies, indicative of biosurfactant production.

Surface tension measurement

Surface tension measurement of a rinsing solution of bacteria cultured on solid agar medium is a direct method for determining global biosurfactant production. In this study, the rinsing solution, obtained as described in paragraph Growth conditions and biosurfactant collection, was filtered through 0.22µm filters (Sterilipet, Millipore, France) and the fluid containing the biosurfactants was collected. The surface tension of the filtered solution was determined by the direct method of the pendant drop using a G40 goniometer (Krüss, France).

Strains	Access Number	Hemolysis activities onto 2% sheep red blood cell plate and incubated for 48 h		Surface tension+/-STD mN/m		Ionic charge of the rinsing solution	
		Growth at 8°C	Growth at 17°C	Growth at 8°C	Growth at 17°C	Growth at 8°C	Growth at 17°C
PfA7B	GQ334362	β ++	β ++	27.0+/-0.0	26.7+/-0.0	anionic	anionic
Pf1 vis-		-	-	71.2+/-0.1	60.9+/-0.7	non ionic	non ionic
CTS38	GQ334368	β +	β +	63.8+/-1.2	31.1+/-0.3	anionic	anionic
CTS50	GQ334367	β ++	β +	27.5+/-0.1	27.2+/-0.1	anionic	anionic
CTS117	GQ334368	β ++	β ++	35.9+/-0.7	29.6+/-1.1	anionic	anionic
DR54	GQ334370	β +	β +	38.2+/-0.9	34.6+/-1.4	non ionic	non ionic
DSS73	GQ334363	α +	α +	32.1+/-0.9	33.2+/-0.1	anionic	anionic
DSS73-15C2		-	-	69.8+/-0.9	70.8+/-0.3	non ionic	non ionic
CTS22	GQ334364	α +	α +	57.1+/-2.3	33.2+/-0.2	anionic	anionic
CTS70	GQ334365	α +	α +	31.4+/-0.1	30.1+/-0.0	anionic	anionic
CTS193	GQ334369	α +	α +	37.6+/-1.4	35.2+/-0.1	anionic	anionic

Table 1: Registration number of sequenced 16S rRNA fragments and surfactant production evaluated by hemolytic phenotype, surface tension and ionic charge of the bacterial rinsing solution for the 11 strains.

Hemolysis on plate at 8°C and 17°C was realized as described in materials and methods. α corresponds to opaque lysis areas and β to transparent lysis areas. - : absence of clearing zone; + : lysis area≤1mm; ++: lysis area > 1mm. Surface tension of bacterial rinsing was determined as indicated in materials and methods at either 8°C or 17°C after four days (triplicate). The ionic charge determination was made with the rinsing solution of bacteria grown at either 8°C or 17°C as described in materials and methods.

Strains	Number of HPLC peaks	Molar mass (g.mol-1)	Retention time (min)		Growth at 8°C	Growth at 17°C
			Growth at 8°C	Growth at 17°C		
PfA7B	2	2	1111.7	24.0+/-0.7	24.2+/-0.0	28.7+/-0.0
Pf1 vis-			1125.7	28.5+/-0.9	ND	
DSS73	1	1	1394.8	16.0+/-0.6	16.0+/-0.6	ND
DSS73-15C2	0	0	ND	ND	ND	ND
CTS22	1	1	1353.8	16.2+/-0.6	16.0+/-0.5	ND
CTS38	2	4	1111.6	ND	22.2+/-0.5	ND
			1125.7	25.1 +/-0.6	26.2+/-0.7	ND
			1151.6	ND	34.8+/-0.4	34.8+/-0.4
			1153.7	36.9+/-0.5	38.0+/-0.0	38.0+/-0.0
CTS50	3	5	1111.6	22.1+/-0.8	22.0+/-0.5	ND
			1125.6	26.2+/-1.5	26.5+/-0.4	ND
			1139.6	31.0+/-1.0	31.0+/-1.0	ND
			1165.4	ND	38.0+/-0.9	ND
			1167.6	ND	41.1+/-1.1	ND
CTS70	2	2	1394.8	15.7 +/- 0.3	15.7+/-0.3	ND
CTS117	2	2	1408.5	16.8 +/- 0.5	16.8+/-0.5	ND
CTS193	1	1	1111.7	21.2+/-0.6	21.1+/-1.0	ND
DR54	6	6	1125.7	24.9+/-0.9	24.5+/-0.8	ND
			1408.9	13.8+/-0.8	13.8+/-0.4	ND
			1110.7	45.5 +/-0.7	45.4+/-0.6	ND
			1124.7	46.9+/-0.4	46.9+/-0.4	ND
			1110.7	47.3+/-0.5	47.3+/-0.4	ND
			1124.7	48.7+/-0.4	48.8+/-0.4	ND
			1150.5	53.7+/-0.5	53.7+/-0.3	ND
			1152.6	57.0 +/- 0.5	56.9+/-0.3	ND

Table 2: Biosurfactant characterization by HPLC for the nine wild strains grown at 8°C and 17°C

HPLC was done for biosurfactants produced by the wild strains as described in materials and methods. ND means not detected. The experiments were done in triplicate.

This method is based on the principle that the drop morphology at the apex, where it is totally independent of any contact, is correlated to the surface tension of the studied liquid. The surface tension can be calculated as the difference of pressure between the inside of the liquid and its environment divided by the sum of the inverse of the radius of the curvature of the drop.

Determining the ionic charge of biosurfactants

The ionic charge of biosurfactants was determined using the agar double diffusion technique adapted from Meylheuc [24]. Briefly, in these studies two regularly spaced rows of wells (10 mm diameter) were

made in a low hardness agar Petri dish (1% agar). Wells in the lower row were filled with the rinsing solution. Each well in the upper row was filled with a pure compound of known ionic charge. The reference anionic substance selected was sodium dodecylsulphate (SDS) 20 mmol.L⁻¹. The cationic compound was cetyltrimethylammonium bromide (CTAB) 20 mmol.L⁻¹. Appearance of a precipitation line between the wells, indicative of the ionic character of the biosurfactant, was monitored for at least one week, at room temperature.

RP-HPLC / MS analysis of biosurfactants

The biosurfactants were analyzed by reverse-phase high

Group	molar mass (g/mol)	CLP	lipidic tail	AA1	AA2	AA3	AA4	AA5	AA6	AA6	AA8	AA9	AA10	AA11
	1110.7	Pseudodesmin B	$C_{10}H_{19}O_3$	L-Leu	D-Gln	D-allo-Thr	D-Val	D-Leu	D-Ser	L-Leu	D-Ser	L-Val		
		Massetolide E	$C_{10}H_{19}O_2$	L-Leu	D-Glu	D-allo-Thr	D-Val	L-Leu	D-Ser	L-Leu	D-Ser	L-Val		
1111.7	Massetolide I	$C_{10}H_{19}O_3$	x-Leu	x-Glu	x-Thr	x-Abu	x-Leu	x-Ser	x-Leu	x-Ser	x-Ile			
		Massetolide J	$C_{10}H_{19}O_4$	x-Nva	x-Glu	x-Thr	x-Val	x-Leu	x-Ser	x-Leu	x-Ser	x-Ile		
1124.7	Pseudodesmin A	$C_{10}H_{19}O_2$	L-Leu	D-Gln	D-allo-Thr	D-Val	D-Leu	D-Ser	L-Leu	D-Ser	L-Ile			
		Viscosinamide	$C_{10}H_{19}O_2$	L-Leu	D-Gln	D-allo-Thr	D-Val	L-Leu	D-Ser	L-Leu	D-Ser	L-Ile		
		Viscosin	$C_{10}H_{19}O_2$	L-Leu	D-Glu	D-allo-Thr	D-Val	L-Leu	D-Ser	L-Leu	D-Ser	L-Ile		
1125.7	Massetolide F	$vC_{10}H_{19}O_3$	L-Leu	D-Glu	D-allo-Thr	D-Val	L-Leu	D-Ser	L-Leu	D-Ser	L-Leu			
	Massetolide L	$C_{10}H_{19}O_4$	L-Leu	D-Glu	D-allo-Thr	D-Ile	D-Leu	D-Ser	L-Leu	D-Ser	L-Val			
		Massetolide K	$C_{10}H_{19}O_5$	x-cyclopro-pAla	x-Glu	x-Thr	x-Ile	x-Leu	x-Ser	x-Leu	x-Ser	x-Val		
Viscosin-like CLP	WLIP	$C_{10}H_{19}O_6$	L-Leu	D-Glu	D-allo-Thr	D-Val	D-Leu	D-Ser	L-Leu	D-Ser	L-Leu			
		Massetolide A	$C_{10}H_{19}O_7$	L-Leu	D-Glu	D-allo-Thr	D-allo-Ile	L-Leu	D-Ser	L-Leu	D-Ser	L-Ile		
1139.7	Massetolide D	$C^{10}H_{19}O_8$	L-Leu	D-Glu	D-allo-Thr	D-allo-Ile	L-Leu	D-Ser	L-Leu	D-Ser	L-Leu			
		Massetolide G	$C_{10}H_{19}O_9$	L-Leu	D-Glu	D-allo-Thr	D-Val	L-Leu	D-Ser	L-Leu	D-Ser	L-Ile		
		Pseudophomin A	$C_{10}H_{19}O_{10}$	L-Leu	D-Glu	D-allo-Thr	D-Ile	D-Leu	D-Ser	L-Leu	D-Ser	L-Ile		
1153.8	Massetolide B	$C_{11}H_{21}O_2$	L-Leu	D-Glu	D-allo-Thr	D-allo-Ile	L-Leu	D-Ser	L-Leu	D-Ser	L-Ile			
		Massetolide H	$C_{12}H_{23}O_2$	L-Leu	D-Glu	D-allo-Thr	D-Val	L-Leu	D-Ser	L-Leu	D-Ser	L-Ile		
1167.6	Massetolide C	$C_{12}H_{23}O_2$	L-Leu	D-Glu	D-allo-Thr	D-allo-Ile	L-Leu	D-Ser	L-Leu	D-Ser	L-Ile			
		Pseudophomin B	$C_{12}H_{23}O_3$	L-Leu	D-Glu	D-allo-Thr	D-allo-Ile	D-Leu	D-Ser	L-Leu	D-Ser	L-Ile		
1353.8	Lokisin	$C_{10}H_{19}O_2$	D-Leu	D-Asp	D-allo-Thr	D-Leu	D-Leu	D-Ser	L-Leu	D-Ser	L-Leu	L-Ile	L-Asp	
Amphisin-like CLP	1394.8	Amphisin	$C_{10}H_{19}O_2$	D-Leu	D-Asp	D-allo-Thr	D-Leu	D-Leu	D-Ser	L-Leu	D-Gln	L-Leu	L-Ile	L-Asp
1408.8	Tensin	$C_{10}H_{19}O_2$	D-Leu	D-Asp	D-allo-Thr	D-Leu	D-Leu	D-Ser	L-Leu	D-Gln	L-Leu	L-Ile	L-Glu	
		Hordersin	$C_{10}H_{19}O_3$	x-Leu	x-Asp	x-Thr	x-Leu	x-Ser	x-Leu	x-Ser	x-Cln	x-Leu	x-Ile	x-Glu

Table 3: Already published CLP structures, adapted from literature [7-8,11,33-35]. AA means amino-acid number n.

performance liquid chromatography (RP-HPLC) coupled to mass spectrometry (MS) using a method adapted from Morin [25]. Before analysis the rinsing solutions were diluted at 50% in a water/acetonitrile/ammonium acetate mixture 10:90:4. An Agilent Technologies Series 1100 vacuum degasser, LC pump and autosampler (Hewlett Packard, Germany) were used. 20 μ L of the sample were injected into an analytical C18 reverse-phase column (Hypersil ODS, 2.1 x 200 mm, 5 μ m). The samples were first submitted for 4 min to an isocratic separation protocol using a water-acetonitrile-ammonium acetate mixture (65:35:4, Solution A), followed by a linear gradient from 0 to 27.3% in 5 min of Solution B consisting of a water-acetonitrile mixture (50:50, v/v). The percentage of Solution B was kept constant for 11 min to allow separation of biosurfactants in isocratic conditions. The column was then rinsed by a gradient of Solution B ranging from 27.3% to 100% for 35 min. The flow (0.4mL.min $^{-1}$) was split (1/10) using a micro-splitter valve (Upchurch Scientific, USA) turned towards the detector. The separated compounds were detected by positive-ion electrospray ionization and ion trap mass spectrometry using a Bruker Esquire-LC ESI-MS/MS (Bruker Daltonic, Germany). The relative proportions of CLPs produced at 8°C and 17°C was estimated by peak area divided by the smallest observed area. This was applied for each chromatogram from the different strains of *P. fluorescens*.

The absence of rhamnolipids was verified by parallel HPLC analysis as described by Morin [41].

Adhesion assays

Adhesion assays were adapted from the biofilm formation assay described by O'Toole [30]. The adhesion test corresponded to an incubation period not exceeding one generation time. Thus only the adhesion inherent in the bacterial contact on the inert surface was taken into account without any disruption to the growth

phenomenon. In triplicate, for each strain, three independent DMM culture were adjusted to an OD_{580nm} of 0.4. An aliquot of 100 μ L of each suspension was layered in triplicate in polystyrene micro titration plate. To determine of the adhesive ability, bacteria were incubated in static condition for 24h at 8°C and 4h at 17°C. The negative control consisted in sterile DMM. After removal of the bacterial solution and careful rinsing (x3 in 150 μ L sterile water) bacteria bound to the wells were stained by incubation for 30 min with 0.1% crystal violet. After rinsing three times with 150 μ L sterile water, remaining adherent bacteria were lysed by adding 100 μ L SDS (1% in sterile water). The adherent bacterial population was estimated by direct measurement of absorbance at 595 nm using a microtitration plate reader (Model 680XR, Biorad). To compare of the results, data were normalized as percentage of adhesion ability using as a reference the strain giving the median value in the whole study (i.e. PfA7B grown at 8°C). Results were normalized as percentage of the median value corresponding to the adhesive capability of PfA7B at 8°C. The Mann-Withney test was used to evaluate statistical significance between values.

Evaluation of bacterial surface hydrophobicity

The hydrophobicity of strains was evaluated by the microbial adhesion to solvent (MATS) test. It consisted in evaluating the affinity of the cells to apolar solvents (hexadecane). For the experiments, bacterial cells were carefully scraped off after 4 days at either 8°C or 17°C and resuspended in saline solution, then were harvested by centrifugation at 7000 g for 10 min and resuspended to Abs_{580nm}=0.4 (Abs1) in saline solution. Three rinsing, then centrifugation steps, were done to eliminate any residual CLP before evaluating the cell affinity for hexadecane. This bacterial suspension was mixed with a solvent at 1:6 (0.4 :2.4 v/v) by vigorous agitation for 1 min in order to form an emulsion. This mixture was then left for at least 15 min

until the separation of the two phases. The aqueous phase absorbance was measured ($A_{\text{abs}2}$) and the percentage of adhesion was expressed as: %affinity = $(1 - A_{\text{abs}2}/A_{\text{abs}1}) \times 100$.

Results

Phylogenetic classification of the different strains of *P. fluorescens*

The Accession Numbers of the sequenced 16S rRNA genes obtained from the 9 selected environmental strains of *P. fluorescens* and the two mutants, namely PfA7B, *PfIvis-*, DSS73, DSS73-15C2, CTS22, CTS38, CTS50, CTS70, CTS117, CTS193 and DR54, was compiled in Table 1. A phylogenetic analysis was carried out with the 16S rRNA genes of our 11 studied strains, the sequences of the *Pseudomonas (sensu stricto)* type strains close to our sequences and the sequences of the SBW25 and PfO-1 strains. According to the study of Bodilis [31], it was possible on Figure 1 to distinguish three clusters termed aeruginosa, putida and fluorescens r-clusters. The 11 strains appeared distributed in 2 distinct groups in the fluorescens r-cluster. Six strains, PfA7B, its viscosin mutant *PfIvis-*, CTS38, CTS50, CTS117 and DR54 were associated with the reference strain of *P. fluorescens* SBW25 in a first group, Group A. The second one, Group B was clearly separated from the others. It was represented by the strains DSS73, its amphisin mutant DSS73-15C2, CTS193, CTS70 and CTS22.

Hemolytic activity of the different strains of *P. fluorescens*

The 11 selected strains of *P. fluorescens* were tested for their hemolytic activity (Table 1). Blood agar lysis was observed with all strains after 4 days of incubation at either 8°C or 17°C except with the viscosin and amphisin mutants *PfIvis-* and DSS73-15C2. Two types of clearing zones, characterized by opaque or transparent lysis areas corresponding to α- and β- hemolytic activity, respectively, were observed. Hemolytic activity results to pores formation on red blood cell. α-hemolytic activity reveals incomplete lysis, β-hemolysis resulting from complete lysis [18]. It was then possible to classify the strains into three phenotypes: non-hemolytic strains (*PfIvis-* and DSS73-15C2), α-hemolytic strains (DSS73, CTS22, CTS70 and CTS193) and β-hemolytic strains (PfA7B, CTS38, CTS50, CTS117 and DR54).

Effect of the temperature on the surface tension of the rinsing solution from the culture of the different strains of *P. fluorescens*

We measured the effect of temperature on the surface tension of the rinsing solution from the culture of the different strains of *P. fluorescens*. The surface tension value of poorly mineralized water is 71.7mN.m⁻¹ and, as described by Carrillo [32], the limit tension value indicative of the presence of biosurfactant in solution is 40 mN.m⁻¹. For the 11 strains of *P. fluorescens* presently studied, the surface tension of their rinsing solution was compiled in Table 1. When bacteria were grown at 8°C, seven wild bacterial strains, i.e., PfA7B, DSS73, CTS50, CTS70, CTS117, CTS193 and DR54, should be considered as surface-active producers since the surface tension of their rinsing solution was below 40 mN.m⁻¹. As logically expected, the two mutants *PfIvis-* and DSS73-15C2 appeared negative for biosurfactant production. The two strains, CTS22 and CTS38, were also negative when grown at 8°C, but when the culture conditions were modified to a higher temperature (17°C), the production of biosurfactant was apparently stimulating. Except the mutants *PfIvis-* and DSS73-15C2 that remained negative, all the wild strains of *P. fluorescens* produced a rinsing solution which showed surface tension under 40 mN.m⁻¹.

Effect of the temperature on the ionic charge of the rinsing solution from the culture of the different strains of *P. fluorescens*

For the 11 strains of *P. fluorescens* presently studied, the ionic charge of their rinsing solution was presented in Table 1. Eight wild strains, i.e. PfA7B, DSS73, CTS22, CTS38, CTS50, CTS70, CTS117 and CTS193, produced an anionic rinsing solution, while DR54 and the two mutants had a non ionic rinsing solution at 8°C and 17°C.

Effect of the temperature on biosurfactant production by the different strains of *P. fluorescens*

Rinsing solutions from the 11 strains of *P. fluorescens* cultured at either 8°C or 17°C were analyzed by HPLC. The chromatogram analysis gave three exploitable data: number of peaks and, for each peak, its molar mass and its retention time. All data were compiled in Table 2. For all of the nine wild strains, the chromatogram revealed at least one peak for each strain, unlike non-biosurfactant producer mutants, *PfIvis-* and DSS73-15C2. These peaks could be indicative of the biosurfactant presence. After growth at 8°C, the detected compounds produced by the wild strains, with similar molar mass and retention time, were found as after incubation at 17°C, except for two wild strains, CTS38 and CTS50. They respectively produced two and three exoproducts at 8°C instead of four and five after growth at 17°C. The molar mass of these putative biosurfactants ranged from 1110.7 to 1408.5 g.mol⁻¹, as expected for cyclolipopeptides (CLPs), such as viscosin-like, and amphisin-like CLPs. To help in their identification (and according to our current knowledge), we compiled in Table 3 previously published CLPs with similar molar mass. These observed values are related to two CLP families cited above. Table 4 listed, by strain and for each related HPLC peak, its abundance in the rinsing solution obtained at either 8°C or 17°C.

In the rinsing solution obtained at either 8°C or 17°C from PfA7B, two CLPs were detected corresponding to a major peak with a molar mass of 1125.7g.mol⁻¹ and 1111.7g.mol⁻¹. The presence of Gln as amino acid in position 2, determined by mass spectroscopic (MS) –m/z: 843.2 and 714.4-, and the anionic charge of the molecule allowed us to identify the major peak as viscosin. The second peak was tentatively identified as massetolide E owing to the existence of CLP isoforms that can skew a precise identification of this molecule.

Strain DSS73 produced a more hydrophilic biosurfactant of 1394.8g.mol⁻¹ with amphisin-like characteristics. Determining the anionic charge of this compound and MS spectrum confirmed its identification as amphisin.

Strain CTS22 was also found to produce a biosurfactant that was rapidly characterized as lokisin (1394.8g.mol⁻¹) by its hydrophobicity, mass and anionic charge. In fact, the Asp and Gln residue conferred an anionic charge to amphisin.

As observed with PfA7B, strain CTS38, grown at 8°C, was found to produce two biosurfactant molecules related to the viscosin family. The same molecules are identified at 17°C, plus two new ones, whose structure appeared rather similar. MS analysis of the molecule eluting at 25.1 ± 0.6 min did not make it possible to distinguish between possible viscosin diastereoisomers or very close isomers of a same mass differing by only one amino-acid inversion between Leu or Ile. This molecule should correspond either to massetolide F or to a new molecule designated 1 with a primary structure of C10H19O2-Leu/

Ile-Glu-(Thr-Val-Leu/Ile-Ser-Leu/Ile-Ser-Leu/Ile). The second CLP generated at 8°C by CTS38 was identified as massetolide H. This molar mass corresponded to two CLPs: massetolide B or massetolide H, differing in their lipophilic tail (Table 3). The two MS peaks –m/z: 714.5 and 843.4- showed up as massetolide H. CTS38 only produced two CLPs at 8°C, yet 4 different biosurfactants were found at 17°C. In addition to the two previously identified molecules as massetolide F or 1 and massetolide H, a peak corresponding to 2 also detected at 8°C in strains CTS50 and CTS117, was identified in the rinsing solution of CTS38 grown at 17°C. Three CLPs were known with an identical molar mass and they were identified as massetolide E, I and J. Each time only one amino acid differs from viscosin's amino-acid sequence (Table 3). The MS common intense peaks: 829.5, 700.5 and 518.3 eliminated the possibility of massetolide I and J. In addition, massetolide E was already attributed to PfA7B as a co-exoproduct. The structure of 2 may be presumed similar to 1 structure, with the replacement of amino acid 9 Val to Ile/Leu. Moreover, another new CLP named 6 was

investigated. The structure study assumed the change in amino-acid 1, Leu, by its cyclic analogue, cyclopropylalanine. The MS peak, m/z 728.4, confirmed the lactone ring described for massetolide H. The putative structure of 6 could be proposed as C12H23O2-cyclopropAla-Glu-(Thr-Val-Leu/Ile-Ser-Leu/Ile-Ser-Leu/Ile).

The analysis of biosurfactants generated by strain CTS50 was more complex since it was found to produce three forms of CLPs. The first one eluted at 22.1 ± 0.8 min, for a growth temperature of 8°C, and did not correspond to previously identified CLPs. The proposed structure of this molecule designated as 2 is C₁₀H₁₉O₂-Leu/Ile-Glu-(Thr-Val-Leu/Ile-Ser-Leu/Ile-Ser-Leu/Ile-Ser-Val). Moreover, the second peak eluted at 26.2 ± 1.5 min corresponded to a CLP whose characteristics were very similar to the molecule produced by strain CTS38 and designated as 1 or massetolide F. The last compound, with a more hydrophobic character had a molar mass of 1139.6g.mol⁻¹ corresponding potentially to massetolide A, D or G or to pseudophomin A as indicated in Table

Strains	Molar mass (g.mol ⁻¹)	CLP	Putative structure	HPLC normalized peak area	
				Growth at 8°C	Growth at 17°C
PfA7B	1111.7	Massetolide E*	-	199	535
	1125.7	Viscosin	-	1100	2569
DSS73	1394.8	Amphisin	-	141	2
CTS22	1353.8	Lokisin	-	1	72
	1111.6	2 or Massetolide E	For 2 C ₁₀ H ₁₉ O ₂ -Leu/Ile-Glu-(Thr-Val-Leu/Ile-Ser-Leu/Ile-Ser-Val)	0	26
CTS38	1125.7	1 or Massetolide F	For 1 C ₁₀ H ₁₉ O ₂ -Leu/Ile-Glu-(Thr-Val-Leu/Ile-Ser-Leu/Ile-Ser-Leu/Ile)	24	303
	1151.6	6	For 6 C ₁₂ H ₂₃ O ₂ -cycloproAla-Glu-(Thr-Val-Leu/Ile-Ser-Leu/Ile-Ser-Leu/Ile)	0	33
	1153.7	Massetolide H	-	17	288
	1111.6	2 or Massetolide E	For 2 C ₁₀ H ₁₉ O ₂ -Leu/Ile-Glu-(Thr-Val-Leu/Ile-Ser-Leu/Ile-Ser-Val)	12	37
	1125.6	1 or Massetolide F	For 1 C ₁₀ H ₁₉ O ₂ -Leu/Ile-Glu-(Thr-Val-Leu/Ile-Ser-Leu/Ile-Ser-Val)	149	214
CTS50	1139.6	Massetolide A or Massetolide G or Pseudophomin A	-	750	556
	1165.4	7	at least the lactone ring (Thr-Val-Leu/Ile-Ser-Leu/Ile-Ser-Leu/Ile)	0	5
	1167.6	Massetolide C or Pseudophomin B	-	0	4
CTS70	1394.8	Amphisin	-	2	21
	1408.5	Tensin	-	43	111
CTS117	1111.7	2 or Massetolide E	For 2 C ₁₀ H ₁₉ O ₂ -Leu/Ile-Glu-(Thr-Val-Leu/Ile-Ser-Leu/Ile-Ser-Val)	18	57
	1125.7	1 or Massetolide F	For 1 C ₁₀ H ₁₉ O ₂ -Leu/Ile-Glu-(Thr-Val-Leu/Ile-Ser-Leu/Ile-Ser-Val)	21	614
CTS193	1408.9	Hodersin	-	1	2
	1110.7	3 or Pseudodesmin B	For 3 C ₁₀ H ₁₉ O ₂ -Leu/Ile-Gln-(Thr-Val-Leu/Ile-Ser-Leu/Ile-Ser-Val)	276	184
	1124.7	3 or Pseudodesmin B and Viscosinamide	-	11	49
	1110.7		-	14	41
	1124.7	Viscosinamide	-	1255	2244
DR54	1150.5	4	For 4 C ₁₂ H ₂₃ O ₂ -cycloproAla-Gln-(Thr-Val-Leu/Ile-Ser-Leu/Ile-Ser-Leu/Ile)	8	25
	1152.6	5	For 5 C ₁₂ H ₂₃ O ₂ -Leu/Ile-Gln-(Thr-Val-Leu/Ile-Ser-Leu/Ile-Ser-Leu/Ile)	14	48
		* tentatively			

Table 4: CLP identification and quantification at 8°C and 17°C

HPLC/MS was made for CLPs produced by the wild strains as described in materials and methods. CLP quantification was evaluated with the help of the chromatogram area under the peaks divided by the smallest observed area, i.e. CTS 22 and CTS193 grown at 8°C.

3. The MS spectrum of this molecule -m/z : 728.4 and 857.5- led to a 3-hydroxy decanoic acid as lipidic tail, incompatible with masetolide G. However, it was not possible to discriminate between masetolide A and D or pseudophomin A.

The number of CLPs produced by strain CTS50 went from 3 at 8°C to 5 at 17°C. The two newly detected molecules were a molecule of 1167.6 g.mol⁻¹ that should be masetolide C or pseudophomin B and a new compound called 7 characterized by a molar mass reduction of two units compared to the last product. As proposed for CTS50, it could be a change in amino acid 1 of Leu, by its cyclic analogue, cyclopropylalanine. MS data confirmed a glutamine residue bound to the lactone ring (Thr-Ile-Leu-Ser-Leu-Ser-Ile). -m/z: 714.5 and 843.4.

Two forms of amphisin-like molecules were detected in the rinsing solution of strain CTS70 grown at 8°C. Comparing them with published CLPs for this strain in different conditions, these molecules were identified as amphisin and tensin.

The analysis of biosurfactants generated by strain CTS117 revealed the presence of two CLPs previously also investigated in strain CTS50, namely the new 2 and the molecule corresponding either to masetolide F or 1.

The biosurfactant secretion profile of strain CTS193 was simpler with only one molecule of a characteristic mass of 1408.5g.mol⁻¹ identified as hodersin of the amphisin family.

Conversely, strain DR54 was at the origin of the more complex secretion pattern of biosurfactants with 6 different molecules. For growth at 17°C, the proportions and mass of the corresponding products were respectively 7.13% (1110.7g.mol⁻¹), 1.91% (1124.7g.mol⁻¹), 1.59% (1110.7g.mol⁻¹), 86.54% (1124.7g.mol⁻¹), 0.97% (1150.5g.mol⁻¹) and 1.87% (1152.6g.mol⁻¹). The major peak was clearly identified as viscosinamide [10]. The properties of other secondary compounds, i.e. hydrophobicity, non-ionic character and presence of a glutamine residue, also suggested that they were members of the viscosinamide family, subgroup of non-ionic viscosin-like CLPs. With the help of very few references on viscosinamide-like CLPs [10,35], the exoproduct of 1110.7g.mol⁻¹ could be designated like pseudodesmin B, but Sinnaeve [35] identifies this CLP at the same time as pseudodesmin A, which only differs from viscosinamide with respect to the stereochemistry of the Leu at position 5, being D rather than L. Hence an other putative biosurfactant, named 3, could be suggested as a diastereoisomer of pseudodesmin B. The two others molecules left, whose putative structure was deduced from MS analysis, were designated as 4 and 5. MS peaks revealed CLPs containing Glu in amino-acid 2 since m/z: 843.2 and 714.4 instead of 842.5 and 714.4 for Gln, as known for viscosin-like CLPs. For the two residual peaks, their elution overlapped around 47 min and was indicative of a mixture of viscosinamide and, 3 or pseudodesmin B, in minor quantity.

The biosurfactant production from bacteria grown at either 8°C or 17°C was carried out. For the majority of the strains, including PfA7B, DSS73, CTS22, CTS70, CTS117, CTS193 and DR54, growth at 17°C was not associated with changes in CLP pattern production (Table 2 & Table 4). In contrast, two strains, CTS38 and CTS50, showed their panel of CLPs markedly increased with the growth temperature.

Among the 22 different identified CLPs, seven named 1 to 7 are described for the first time, their putative structures are compiled in

Table 4. The compounds 1, 2, 6 and 7 are members of viscosin-like CLPs, as the other biosurfactants produced simultaneously by strains CTS50 and CTS117. CLPs 3, 4 and 5 own to the viscosinamid-like CLPs, as their co-produced biosurfactants by DR54. CLPs 3 and 5 present a similar hydrophilic peptidic moiety with, respectively, CLPs 2 and 1 except Glu replaced with Gln.

Effect of the growth temperature on the adhesion ability of the two wild *P. fluorescens* strains, PfA7B and DSS73

With PfA7B and DSS73 and their biosurfactant producer mutants, *Pf1vis-* and DSS73-15C2, adhesion assays were performed at either 8°C or 17°C on DMM on polystyrene microtitration plates. As represented in Figure 2, increasing the growth temperature from 8°C to 17°C was associated with a very significant decrease of the relative adhesion affinity for the both strains. At 8°C and 17°C the wild strains presented reduced adhesion compared to their surfactant mutant (ratio of 1.5 for viscosin mutant and 2 for amphisin mutant at 8°C).

Hydrophobicity

The surfacial hydrophobicity was evaluated for four strains: PfA7B, *Pf1vis-*, DSS73 and DSS73-15C2 by measuring the affinity of the cells towards the apolar solvent hexadecane. A strain with 100% affinity towards hexadecane is highly hydrophobic and a strain with 0% hexadecane affinity is highly hydrophilic. Hexadecane affinity at 8°C was illustrated in Figure 2 by white dots and affinity at 17°C by grey ones. PfA7B and *Pf1vis-* were characterized as highly hydrophilic for both growth temperature of 8°C and 17°C, as their affinity to hexadecane was evaluated less than 10% and appeared rather equal. The growth temperature for DSS73 and for its mutant only slightly modulated their hydrophobicity, at 17°C they were highly hydrophobic (hexadecane affinity greater than 85%) and at 8°C, they became only hydrophobic (hexadecane affinity about 60%).

Discussion

The 11 strains of *P. fluorescens* were selected for the present study,

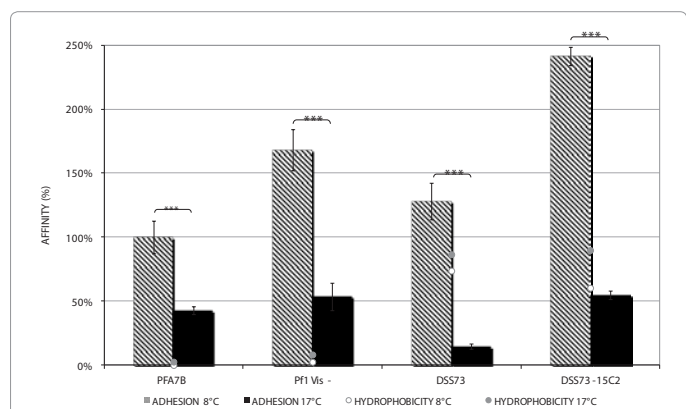


Figure 2: Influence of growth temperature on adhesion of four strains: PfA7B, *Pf1vis-*, DSS73 and DSS73-15C2 and their surface hydrophobicity after incubation at 8°C and 17°C.

Adhesion corresponds to incubation in static condition for 1 day at 8°C (cross-line pattern) and 4h at 17°C (plain black). For each strain, three independent cultures were realized in triplicate. Results were normalized as percentage of the median value corresponding to the adhesion obtained for PfA7B at 8°C. Statistical analyses were performed on these results with the help of Mann-Whitney test. NS means non significant ($p \geq 0.05$); X significant ($p \leq 0.05$); XX: highly significant ($p \leq 0.01$); XXX: extremely significant ($p \leq 0.001$).

Hydrophobicity corresponds to hexadecane affinity evaluated for bacterial cultures after 4 days of incubation at either 8°C (white dot) or 17°C (grey dot). (100%: highly hydrophobic, 0%: highly hydrophilic).

since they represent typical environmental microorganisms naturally submit to significant temperature variations. All these strains are included in the “fluorescens r-cluster” defined by Bodilis [31] in the 16S rRNA based phylogenetic tree. However the dispersion of these strains is large. In Figure 1 and as previously reported by de Bruijn [14], Group A is close to *P. fluorescens* SBW25 strain from which the genome is sequenced, whereas Group B is located at distance, i.e. near the “putida r-cluster”, and appears to be close to *P. fluorescens* Pf0-1 strain, another strain from which the genome is sequenced. This situation clearly illustrates the high heterogeneity of the species *P. fluorescens*. Recent taxonomic studies are enabled a separation into distinct species for related bacteria previously associated with *P. fluorescens*, such as *P. mosselii* [36]. Bacteria still included in the species *P. fluorescens* remain very diverse as it can be noted by analysis of siderophores expression [37]. Nevertheless, for environmental microorganisms, as for clinical strains, the very active process of gene transfer forces us to carefully consider the usually accepted taxonomical boundaries [38] and even the psychrotrophic character of *P. fluorescens* could be discussed since clinical biovar 1 of the species has been shown to grow and adapt at 37°C on rich medium [39].

The two groups presently defined in the phylogenetic study on 16S RNA are consistent with the results from the hemolytic activity study, summarized in Table 1. The strains, with β-hemolytic activity are found in Group A. Group A is distinct from Group B where strains characterized by α-hemolytic activity at either 8°C or 17°C are gathered.

Measuring surface tension from a bacterial rinsing solution was used to investigate biosurfactant production. In water, whose surface tension is about 70 mN.m⁻¹, if biosurfactants are present in solution, the surface tension falls under 40 mN.m⁻¹ [32]. Except for the two mutants *Pf1vis-* and DSS73-15C2 and strains CTS22 and CTS38 grown at 8°C, all other wild strains are positive for biosurfactant production with a surface tension of the rinsing solution between 26.7 and 35.2 mN.m⁻¹. The absence of biosurfactant in the rinsing solution of *Pf1vis-* and DSS73-15C2 grown at either 8°C or 17°C suggests that viscosin or amphisin blockage, as reported by Braun [13] and by Koch [23], is not compensated by the release of any other amphiphilic molecules. The case of the strains CTS22 and CTS38 is different since they show low but detectable α or β hemolysis activity at either 8°C and 17°C and have been previously demonstrated as amphisin- and viscosin-like producers, respectively [12]. However, surface tension measurement remains a global technique for the detection of biosurfactant production and even for very active molecules a sufficient amount is necessary to reach the limit value of 40 mN.m⁻¹ [32].

To summarize this macroscopic biosurfactant production, the 11 strains are sorted into three classes. The non-biosurfactant producers are *Pf1vis-* and DSS73-15C2 mutants. The second group consists of the α-hemolytic strains able to produce anionic biosurfactants: DSS73, CTS22, CTS70 and CTS193. The third category results from the β-hemolytic strains secreting anionic or non-ionic biosurfactants: PfA7B, CTS38, CTS50, CTS117 and DR54.

To screen rapidly a potential CLPs production by a *P. fluorescens* strain, two tests can be performed: hemolytic activity and ionic nature of the corresponding rinsing solution or culture supernatant. An α-hemolytic phenotype, with anionic rinsing solution, can be assumed to be amphisin-like CLPs producer. An anionic rinsing solution coupled with a β-hemolytic phenomenon is obtained for viscosin-like CLPs producer. Viscosinamide-like producer corresponds to a β-hemolysis with a non-ionic rinsing solution.

The CLP identification is consistent with the 16S ARN groups and the macroscopic biosurfactant evaluation. In fact Group A, in Figure 1, consists in all the viscosin- and viscosinamide-like producers. More precisely, the β-hemolytic strains secreting anionic biosurfactants are in the viscosin-like group. In addition, as a β-hemolytic strain and non-ionic biosurfactant producer, DR54 is characterized as a viscosinamide-like producer. The second category results from the α-hemolytic strains being able to produce anionic biosurfactants: DSS73, CTS22, CTS70 and CTS193. They are related in Group B, shown in Figure 1, and produce amphisin-like CLPs. The 16S rRNA phylogenetic tree corresponds with biosurfactant pattern. Structurally, the peptidic hydrophilic moiety differs among the studied CLPs. As shown by shorter retention times in RP-HPLC (Table 2), ampsin-like CLPs are more hydrophilic than viscosin and viscosinamide-like, whose ionic charge is different. Then the hemolysis mechanism could be related to CLP hydrophobicity, but not to their ionic charge. Hydrophilic amphisin-like CLPs help its producer strain to provoke pores formation and partial lysis of red blood cells, while their complete lysis is obtained with *P. fluorescens* producing hydrophobic CLPs (viscosin- or viscosinamide-like).

Over the 22 different CLPs identified in the present study (Table 4), 19 of these molecules have considerably increased production with an increase in the growth temperature of the bacteria. This increase reaches 10 and even 72 times for amphisin-like production by strains CTS70 and CTS22, but, in the vast majority, the CLP quantity detected at 17°C is twice as much as that found at 8°C. A similar temperature dependency has been reported for putisolvin, another CLP secreted by *Pseudomonas* sp. MIS38 [40] or *P. putida* PCL1445 [41] and for other different CLPs in *Bacillus subtilis* ATCC6633 [42]. But three molecules are differently regulated by temperature. In strain CTS50, production of the compound identified as massetolide A, massetolide G or pseudophomin A is reduced by 25.8 % when the bacterium was grown at 17°C. A reduction factor of the same range, -33.3%, is measured for 3 produced in strain DR54. The stronger negative effect of temperature is observed in strain DSS73 that shows its production of amphisin decrease from a mean normalized value of 141 at 8°C to only 2 at 17°C. No general trait about temperature-regulated CLPs production can be ground: the biosurfactant production seems be more strain dependant, than be ruled neither by the bacterial growth temperature neither by the produced CLPs nature. Common environmental pressures could explain such behaviour [1], yet in the present study there is no correlation between the ecology of the strains and their biosurfactant patterns.

As mentioned elsewhere, the role of biosurfactants in bacterial adhesion, and even later in biofilm production, remains to be discussed. Whereas de Bruijn [14,15] showed that in *P. fluorescens* SBW25 viscosin is essential for biofilm formation, as well massetolide A in *P. fluorescens* SS101 other CLPs, putisolvins and arthrobactins, appear to exert a negative effect on the biofilm structure in *Pseudomonas* sp. MIS38 [43] and *P. putida* PCL1445 [44].

In the present study, the adhesion of bacteria was evaluated on two wild strains: PfA7B and DSS73 and their respective CLP mutants: *Pf1vis-* and DSS73-15C2. Moreover these two wild strains produce different CLPs: PfA7B viscosine-like CLPs and DSS73 amphisin. These biosurfactants are all anionics and amphisin is largely more hydrophilic than the viscosin-like CLPs as shown by the great difference in HPLC retention time compiled in Table 2. The two wild strains are more adherent at 8°C whereas for PfA7B viscosin is more produce at 17°C as described in Figure 2. Moreover, the magnitude of adhesion is lower for the wild strains than for their CLP deficient mutants. Thus it could

be assumed that the CLP production reduces the bacterial adhesion process. As reported by Raaijmakers [7] or Palmer [48] or Simoes [49], microbial adhesion to surfaces still remains under discussion. A consensus has appeared about the initial attachment, which is the crucial step of adhesion, even if so little is still understood about it yet. Several factors seem to direct this critical step such as surface conditioning, mass transport or surface topography, but none of these factors is clearly established as dominating. The amphiphilic biosurfactant nature has led them to take part in the conditioning step of the adhesion in modulating the physico-chemical properties of the bacterial microenvironment during its deposition on an inert surface. In our study, whatever their nature, amphisin or viscosin-like, CLPs penalize the cell attachment of their own bacterial producers: the non producing mutant adheres more than the wild strain as shown in Figure 2.

Up to now, no implication of the surfacial cell itself was considered in attachment process. The hydrophobicity of the strains shown in Figure 2 corresponds to cell affinity without any adsorbed biosurfactant at their surface. Hydrophilic strain (PfA7B) and hydrophobic strain (DSS73) have similarly adhesion. Even if adherent cells number at 8°C increases with bacterial hydrophobicity, this parameter seems not dominating in adhesion process. Overall the growth temperature does not greatly modify the cell hydrophobicity.

The present results demonstrate that environmental strains of *P. fluorescens* can synthesize different forms of CLPs from the viscosin, viscosinamide and amphisin family and we propose a method for rapid CLP screening. Biosurfactant presence is determined using two analyses simultaneously: blood agar lysis and tensiometry. If both are positive, the double diffusion test is done. Afterwards the CLP class can be deduced from the hemolytic type and from the biosurfactant charge determination. Precise analysis of the data indicates that in *P. fluorescens* production of CLPs and the crucial adhesion step are both markedly affected by the growth temperature but the two events appear to be independently regulated and not correlated. Indeed, most of the presently studied environmental *P. fluorescens* CLPs producers secrete biosurfactant(s) with a great variety and in larger quantity at the optimal exoproduct secretion temperature, 17°C in our case. These CLPs disturb the bacterial adhesion process. This initial adhesion, a crucial step of biofilm formation, seems to be not controlled by strain hydrophobicity and is increased at growth temperature of 8°C. To define more precisely the origin of this behaviour difference in bacterial adhesion, some more analysis could be done on extracellular polymeric substances (EPS) or on specialized attachment structures, such as flagella or pili, also known to influence the crucial adhesion step [49]. Moreover, increase of flagella length in absence of biosurfactant has been already reported [18].

Acknowledgments

This study was supported by grants from the Communauté d'Agglomération d'Evreux, Conseil Général de l'Eure and MIATT Grand Bassin Parisien-Haute Normandie. The authors thank Drs. Braun, Nybroe and Nielsen for gift of the different bacterial strains, Magalie Barreau for her technical support and Christine Farmer for her linguistic support.

References

1. Desai JD, Banat IM (1997) Microbial production of surfactants and their commercial potential. *Microbiol Mol Biol Rev* 61: 47-64.
2. Muthusamy K, Gopalakrishnan S, Ravi TK, Sivachidambaran P (2008) Biosurfactants: Properties, commercial production and application. *Current Science* 94: 736-747.
3. Singh A, Van Hamme JD, Ward OP (2007) Surfactants in microbiology and biotechnology (Part 2): application aspects. *Biotechnol Adv* 25: 99-121.
4. Ron EZ, Rosenberg E. (2001) Natural roles of biosurfactants. *Environ Microbiol* 3: 229-236.
5. Maier RM (2003) Biosurfactants: evolution and diversity. *Adv Appl Microbiol* 52: 101-121.
6. Van Hamme J, Singh A, Ward OP (2006) Physiological aspects. Part 1 in a series of papers devoted to surfactants in microbiology and biotechnology. *Biotechnol Adv* 24: 604-620.
7. Raaijmakers JM, De Bruijn I, Nybroe O, Ongena M (2010) Natural functions of lipopeptides from *Bacillus* and *Pseudomonas*: more than surfactants and antibiotics. *FEMS Microbiol Rev* 34:1037-1062.
8. Raaijmakers JM, de Bruijn I, de Kock MJ (2006) Cyclic lipopeptide production by plant-associated *Pseudomonas* spp.: diversity, activity, biosynthesis, and regulation. *Mol Plant Microbe Interact* 19: 699-710.
9. Hildebrand PD (1989) Surfactant-like characteristics and identity of bacteria associated with broccoli head rot in Atlantic Canada. *Can J Plant Pathol* 11: 205-214.
10. Nielsen TH, Christoffersen C, Anthoni U, Sorensen J (1999) Viscosamide, a New Cyclic Depsipeptide with Surfactant and AntiFungal Properties Produced by *Pseudomonas fluorescens* DR54. *J Appl Microbiol* 87: 80-90.
11. Nielsen TH, Sorensen D, Tobiasen C, Andersen JB, Christoffersen C, et al. (2002) Antibiotic and biosurfactant properties of cyclic lipopeptides produced by Fluorescent *Pseudomonas* spp. from the sugar beet rhizosphere. *Appl Environ Microbiol* 68: 3416-3423.
12. Nielsen TH, Sorensen J (2003) Production of cyclic lipopeptides by *Pseudomonas fluorescens* strains in bulk soil and in the sugar beet rhizosphere. *Appl Environ Microbiol* 69: 861-868.
13. Braun PG, Hildebrand PD, Elis TC, Kobayashi DY (2001) Evidence and characterization of a gene cluster required for the production of viscosin, a lipopeptide biosurfactant, by a strain of *Pseudomonas fluorescens*. *Can J Microbiol* 47: 294-301.
14. de Bruijn I, de Kock MJ, Yang M, de Waard P, van Beek TA, et al. (2007) Genome-based discovery, structure prediction and functional analysis of cyclic lipopeptide antibiotics in *Pseudomonas* species. *Mol Microbiol* 63: 417-428.
15. de Bruijn I, de Kock MJ, de Waard P, van Beek TA, Raaijmakers JM (2008) Massetolide A Biosynthesis in *Pseudomonas fluorescens*. *J Bacteriol* 190: 2777-2789.
16. Bender CL, Alarcon-Chaidez F, Gross DC (1999) *Pseudomonas syringae* phytotoxins: mode of action, regulation, and biosynthesis by peptide and polyketide synthetases. *Microbiol Mol Biol Rev* 63: 266-292.
17. Rossignol G, Merieau A, Guerillon J, Veron W, Lesouhaitier O, et al. (2008) Involvement of a phospholipase C in the hemolytic activity of a clinical strain of *Pseudomonas fluorescens*. *BMC Microbiol* 8: 189.
18. Rossignol G, Sperandio D, Guerillon J, Duclairoir Poc C, Soum-Soutera E, et al. (2009) Phenotypic variation in the *Pseudomonas fluorescens* clinical strain MFN1032. *Res Microbiol* 160: 337-344.
19. Gügi B, Orange N, Hellio F, Burini J-F, Guillou C, et al. (1991) Effect of growth temperature on several exported enzyme activities in the psychrotrophic bacterium *Pseudomonas fluorescens*. *J Bacteriol* 173: 3814-3820.
20. Hellio FC, Orange N, Guespin-Michel JF (1993) Growth temperature controls the production of a single extracellular protease by *Pseudomonas fluorescens* MF0, in the presence of various inducers. *Res Microbiol* 144: 617-625.
21. Merieau A, Gügi B, Guespin-Michel JF, et al. Orange N (1993) Temperature regulation of lipase secretion by *Pseudomonas fluorescens* MF0. *Appl Microbiol Biotechnol* 39: 104-109.
22. Guillou C, Guespin-Michel JF (1996) Evidence for two domains of growth temperature for the psychrotrophic bacterium *Pseudomonas fluorescens* MF0. *Appl Environ Microbiol* 62: 3319-3324.
23. Koch B, Nielsen TH, Sorensen D, Andersen JB, Christoffersen C, et al. (2002) Lipopeptide production in *Pseudomonas* sp. strain DSS73 is regulated by components of sugar beet seed exudate via the Gac two-component regulatory system. *Appl Environ Microbiol* 68: 4509-4516.
24. Meylheuc T, Van Oss CJ, Bellon-FontaineM-N (2001) Adsorption of

- biosurfactant on solid surfaces and consequences regarding the bioadhesion of *Listeria monocytogenes* LO28. *J Appl Microbiol* 91: 822–832.
25. Morin D, Grasland B, Vallee-Rehel K, Dufau C, Haras D (2003) On-line high-performance liquid chromatography-mass spectrometric detection and quantification of N-acylhomoserine lactones, quorum sensing signal molecules, in the presence of biological matrices. *J Chromatogr A* 1002: 79–92.
26. Thompson JD, Gibson TJ, Plewniak F, Jeanmougin F, Higgins DG (1997), The CLUSTAL_X windows interface: flexible strategies for multiple sequence alignment aided by quality analysis tools. *Nucleic Acids Res* 25: 4876–4882.
27. Kumar S, Tamura K, Nei M (2004) MEGA3: Integrated software for Molecular Evolutionary Genetics Analysis and sequence alignment. *Brief Bioinform* 5: 150–163.
28. Galtier N, Gouy M (1998) Inferring pattern and process: maximum-likelihood implementation of a nonhomogeneous model of DNA sequence evolution for phylogenetic analysis. *Mol Biol Evol* 15: 871–879.
29. Youssef NH, Duncan KE, Nagle DP, Savage KN, Knapp RM, et al. (2004) Comparison of methods to detect biosurfactant production by diverse microorganisms. *J Microbiol Methods* 56: 339–47.
30. O'Toole GA, Kolter R (1998) Flagellar and twitching motility are necessary for *Pseudomonas aeruginosa* biofilm development. *Mol. Microbiol.* 30: 295–304.
31. Bodilis J, Calbrix R, Guerillon J, Merieau A, Pawlak B, et al. (2004) Phylogenetic relationships between environmental and clinical isolates of *Pseudomonas fluorescens* and related species deduced from 16S rRNA gene and OprF protein sequences. *System Appl Microbiol* 27: 93–108.
32. Carrillo PG, Mardaraz C, Pitta-Alvarez SI, Giulietti AM (1996) Isolation and selection of biosurfactant-producing bacteria. *J Microbiol Biotechnol.* 12: 82–84.
33. Gerard J, Lloyd R, Barsby T, Haden P, Kelly MT, et al. (1997) Massetolides A-H, antimycobacterial cyclic depsipeptides produced by two Pseudomonads isolated from marine habitats. *J Nat Prod* 60: 223–229.
34. Gross H, Stockwell VO, Henkels MD, Nowak-Thompson B, Loper JE et al. (2007) The genomisotopic approach: a systematic method to isolate the products of orphan biosynthetic gene clusters. *Chem Biol.* 14: 53–63.
35. Sinnaeve D, Michaux C, Van hemel J, Vandenkerckhove J, Peys E, et al. (2009) Structure and X-ray conformation of pseudodesmins A and B, two new cyclic lipopeptides from *Pseudomonas* bacteria. *Tetrahedron* 65: 4173–4181.
36. Dabboussi F, Hamze M, Singer E, Geoffroy V, Meyer JM, et al. (2002) *Pseudomonas mosselii* sp. nov., a novel species isolated from clinical specimens. *Int J Syst Evol Microbiol* 52: 363–376.
37. Meyer JM, Geoffroy VA, Baida N, Gardan L, Izard D, et al. (2002) Siderophore typing, a powerful tool for the identification of fluorescent and nonfluorescent pseudomonads. *Appl Environ Microbiol* 68: 2745–2753.
38. Baptiste E, Boucher Y (2009) Epistemological impacts of horizontal gene transfer on classification in microbiology. *Methods Mol Biol* 532: 55–72.
39. Chapalain A, Rossignol G, Lesouhaitier O, Merieau A, Gruffaz C, et al. (2008) Comparative study of 7 fluorescent pseudomonad clinical isolates. *Can J Microbiol* 54: 19–27.
40. Washio K, Lim SP, Roongsawang N, Morikawa M (2010). Identification and characterization of the genes responsible for the production of the cyclic lipopeptide arthrofactin by *Pseudomonas* sp. MIS38. *Biosci Biotechnol Biochem.* 74: 992–999.
41. Dubern JF, Lagendijk EL, Lugtenberg BJ, Bloemberg GV (2005) The heat shock genes dnaK, dnaJ, and grpE are involved in regulation of putisolvin biosynthesis in *Pseudomonas putida* PCL1445. *J Bacteriol* 187: 5967–5976.
42. Fickers P, Leclerc V, Guez JS, Béchet M, Coucheney F, et al. (2008) Temperature dependence of mycosubtilin homologue production in *Bacillus subtilis* ATCC6633. *Res Microbiol* 159: 449–457.
43. Roongsawang N, Hase K, Haruki M, Imanaka T, Morikawa M, et al. (2003) Cloning and characterization of the gene cluster encoding arthrobactin synthetase from *Pseudomonas* sp. MIS38. *Chem. Biol.* 9: 869–80
44. Kuiper I, Lagendijk EL, Pickford R, Derrick JP, Lamers GE, et al. (2004) Characterization of two *Pseudomonas putida* lipopeptide biosurfactants, putisolvin I and II, which inhibit biofilm formation and break down existing biofilms. *Mol Microbiol.* 51: 97–113
45. Palmer J, Flint S, Brooks J (2007) Bacterial cell attachment, the beginning of a biofilm. *J Ind Microbiol Biotechnol.* 34: 577–588.
46. Simões LC, Simões M, Vieira MJ (2010) Adhesion and biofilm formation on polystyrene by drinking water-isolated bacteria. *Antonie Van Leeuwenhoek.* 98: 317–329.

This article was originally published in a special issue, **Microbial Communities and Interactions** handled by Editor(s). Dr. Lesouhaitier Olivier, University of Rouen, France; Dr. Louis Lambrechts, Institut Pasteur, France; Dr. Saber Gholizadeh, Urmia University, Iran.

Submit your next manuscript and get advantages of OMICS Group submissions

Unique features:

- User friendly/feasible website-translation of your paper to 50 world's leading languages
- Audio Version of published paper
- Digital articles to share and explore

Special features:

- 200 Open Access Journals
- 15,000 editorial team
- 21 days rapid review process
- Quality and quick editorial, review and publication processing
- Indexing at PubMed (partial), Scopus, DOAJ, EBSCO, Index Copernicus and Google Scholar etc
- Sharing Option: Social Networking Enabled
- Authors, Reviewers and Editors rewarded with online Scientific Credits
- Better discount for your subsequent articles

Submit your manuscript at: <http://www.omicsonline.org/submit>

P16

Gamma-aminobutyric acid acts as a specific virulence regulator in *Pseudomonas aeruginosa*

Audrey Dagorn,¹ Mélanie Hillion,¹ Annelise Chapalain,¹ Olivier Lesouhaitier,¹ Cécile Duclairoir Poc,¹ Julien Vieillard,² Sylvie Chevalier,¹ Laure Taupin,³ Franck Le Derf² and Marc G. J. Feuilloley¹

Correspondence

Marc G. J. Feuilloley
marc.feuilloley@univ-rouen.fr

¹Laboratory of Microbiology Signals and Microenvironment (LMSM) EA 4312, University of Rouen, 27000 Evreux, France

²SIMA, UMR 6014 COBRA, University of Rouen, 27000 Evreux, France

³Laboratoire de Biotechnologie et Chimie Marines, Université de Bretagne-Sud B.P. 92116, 56321 Lorient cedex, France

Gamma-aminobutyric acid (GABA) is widespread in the environment and can be used by animal and plants as a communication molecule. *Pseudomonas* species, in particular fluorescent ones, synthesize GABA and express GABA-binding proteins. In this study, we investigated the effects of GABA on the virulence of *Pseudomonas aeruginosa*. While exposure to GABA (10 µM) did not modify either the growth kinetics or the motility of the bacterium, its cytotoxicity and virulence were strongly increased. The *Caenorhabditis elegans* 'fast killing test' model revealed that GABA acts essentially through an increase in diffusible toxin(s). GABA also modulates the biofilm formation activity and adhesion properties of PAO1. GABA has no effect on cell surface polarity, biosurfactant secretion or on the lipopolysaccharide structure. The production of several exoenzymes, pyoverdin and exotoxin A is not modified by GABA but we observed an increase in cyanogenesis which, by itself, could explain the effect of GABA on *P. aeruginosa* virulence. This mechanism appears to be regulated by quorum sensing. A proteomic analysis revealed that the effect of GABA on cyanogenesis is correlated with a reduction of oxygen accessibility and an over-expression of oxygen-scavenging proteins. GABA also promotes specific changes in the expression of thermostable and unstable elongation factors Tuf/Ts involved in the interaction of the bacterium with the host proteins. Taken together, these results suggest that GABA is a physiological regulator of *P. aeruginosa* virulence.

Received 18 June 2012

Revised 5 October 2012

Accepted 13 November 2012

INTRODUCTION

Gamma-aminobutyric acid (GABA) is a four-carbon non-protein amino acid, widespread in the environment (Bouché *et al.*, 2003). Since the 1950s, it has been known that GABA is the major inhibitory neurotransmitter in the nervous system of vertebrates and invertebrates (Owens & Kriegstein, 2002). In other living organisms, such as plants, fungi or bacteria, GABA was considered for a long time to be a stress response factor and/or a nutrient (Higuchi *et al.*, 1997; Shelp *et al.*, 1999). The hypothesis that GABA could also be a communication molecule in these organisms started with the observation that, in plants, GABA controls the guiding of the pollen tube into the female gametophyte (Palanivelu *et al.*,

2003). In plant life, GABA now appears to be a ubiquitous communication molecule produced as a defence against nematodes, insects and also bacterial phytopathogens (Shelp *et al.*, 2006). The role of GABA in communication between plants and bacteria is in line with the identification of GABA-binding proteins in different prokaryotes corresponding not only to transporters such as GabP in *Escherichia coli* or *Bacillus subtilis* (Hu & King, 1998; Brechtel & King, 1998) and Bra in *Agrobacterium tumefaciens* (Chevrot *et al.*, 2006) but also to possible specific receptors (Guthrie & Nicholson-Guthrie, 1989). In addition, many bacteria, including marine micro-organisms (Morse *et al.*, 1980), lactic bacteria (Siragusa *et al.*, 2007), *E. coli* (Richard & Foster, 2003) and *Pseudomonas* (Chou *et al.*, 2008) synthesize GABA, suggesting that, like in eukaryotes, GABA might be a conserved and ubiquitous communication molecule.

That GABA has an effect on the physiology of *Pseudomonas* is supported by several observations. A periplasmic protein

Abbreviations: 3oxoC12-HSL, 3-oxo-C12 acylhomoserine lactone; C4-HSL, C4 acylhomoserine lactone; GABA, gamma-aminobutyric acid; LDH, lactate dehydrogenase; LPS, lipopolysaccharide; POS, pseudomonas quinolone signal.

showing high affinity for GABA and biochemical characteristics similar to a subunit of the mammalian GABA_A receptor was identified in an environmental strain of *P. fluorescens* (Guthrie & Nicholson-Guthrie, 1989; Guthrie *et al.*, 2000). In *P. aeruginosa*, GABA is an intermediate metabolite of organic polycation catabolism and an inducer of the enzymic pathway controlling the intracellular polyamine levels (Chou *et al.*, 2008). The question of a possible effect of extracellular GABA on *P. aeruginosa* is of medical importance. GABA is present in significant concentrations in the brain matter but also in the cerebrospinal fluid (Tunnicliff & Malatynska, 2003) and, essentially following breaches of the meningeal barrier due to trauma, surgical acts or, more rarely, by diffusion from infected contiguous structures (paranasal sinus or inner ear), *P. aeruginosa* can invade the central nervous system causing life-threatening infections such as brain abscesses, ventriculitis or meningitis (Mesaros *et al.*, 2007). However, GABA is also present in blood (Petty *et al.*, 1999) where it has immunomodulatory functions (Jin *et al.*, 2011) and, as *P. aeruginosa* is a major cause of bloodstream infections (van Delden, 2007), the bacterium is exposed to GABA during bacteraemia or septicaemia. With the emergence of multidrug-resistant strains, it is essential to identify the hosts and communication factors capable of modulating the virulence of *P. aeruginosa*; these should represent new strategies for treatment (Fothergill *et al.*, 2012).

In the present study, we investigated the effect of GABA on *P. aeruginosa* through a multi-phenotypical study. We show that GABA stimulates *P. aeruginosa* virulence through variation of the production of a quorum-sensing-regulated factor and modulation of enzymes involved in the oxidative stress response.

METHODS

Bacterial strains and culture conditions. *P. aeruginosa* PAO1 was obtained from an international collection (University of Washington). Except for specific tests, as indicated below, bacteria were grown in Nutrient Broth (NB, Merck). The effect of GABA was studied at 0.01 mM to avoid possible direct metabolic and pH effects and since it is the mean value of the concentrations in the synaptic cleft of neurons (1.5–3 mM, Mozrzymas *et al.*, 2003), in wounded vegetal (0.1 mM, Shelp *et al.*, 1999) and in the environment (sea water concentration <0.1 µM, Johnson *et al.*, 1991). Motility assays were essentially performed as described by Rashid & Kornberg (2000). Briefly, NB plates containing 0.3% agar were point-inoculated with a toothpick previously soaked in a pellet (10 min, 10 000 g) of bacteria grown to early stationary phase that had been collected by centrifugation, and incubated for 24 h at 37 °C. The swarming assay was identical, except that NB plates contained 0.5% agar.

Bacterial virulence assays. The effect of GABA on bacterial virulence was studied by using two models, i.e. cultured rat glial cells to evaluate the cytotoxic activity of the bacteria in nerve cells (Picot *et al.*, 2001) and the nematode *Caenorhabditis elegans*, a metazoan model used to assess the general virulence of human pathogens and environmental bacteria (Duclairoir Poc *et al.*, 2011). Preliminary controls showed that exposure of *P. aeruginosa* PAO1 to GABA (0.01

mM) during the whole growth phase, or at the beginning of the stationary phase, did not modify the growth kinetics of the bacterium.

For the cytotoxic activity, *P. aeruginosa* PAO1 grown in NB was inoculated at OD₅₈₀ 0.2 in 25 ml NB containing GABA (0.01 mM) or no GABA, and cultured at 37 °C with agitation (180 r.p.m.) to early stationary phase. Bacteria were harvested by centrifugation in an Eppendorf centrifuge tube (6000 r.p.m., 4 min, 20 °C), rinsed three times with NB and resuspended at a cell density of 10⁶ c.f.u. ml⁻¹ in glial cell culture medium without antibiotics and antimycotics. The bacterial viability and density, and the absence of contamination were controlled by plating. Glial cells were incubated for 4 h with *P. aeruginosa* and glial cell death was monitored using the lactate dehydrogenase (LDH) assay release as described previously (Picot *et al.*, 2003, 2004) using the Cytotox 96 Enzymic Assay (Promega). Controls realized using bacteria alone showed that in our experimental conditions *P. aeruginosa* PAO1 does not produce molecules that interfere with this assay.

The global virulence of *P. aeruginosa* PAO1 was studied using the wild-type N2 strain of *C. elegans* kindly provided by the *Caenorhabditis* Genetics Center (Minneapolis, MN, USA). Worms were grown at 22 °C on *E. coli* OP50 cultures. Synchronous cultures of worms were obtained as described previously (Blier *et al.*, 2011). Two types of tests: ‘fast-killing’ and ‘slow-killing’ were used. In the ‘fast-killing’ test, worms are killed by bacterial diffusible toxins whose secretion is stimulated by use of a high-osmolarity medium (Aballay & Ausubel, 2002). In the ‘slow-killing’ test, worms are killed after ingestion of the bacteria (Duclairoir Poc *et al.*, 2011). Pathogen lawns used for *C. elegans* survival assays were prepared by spreading 50 µl control or GABA-treated *P. aeruginosa* PAO1 (OD₅₈₀ 1) (obtained as previously described) on 35 mm peptone-glucose-sorbitol (PGS: 1% Bacto-Peptone; 1% NaCl, 1% glucose, 0.15 M sorbitol, 1.7% Bacto-Agar) conditioned Petri dishes for ‘fast-killing’ evaluation or on 35 mm nematode growth medium (NGM: 3 g NaCl, 2.5 g peptone, 17 g agar, 5 mg cholesterol, 1 ml 1 M CaCl₂, 1 ml 1 M MgSO₄, 25 ml 1 M KH₂PO₄, H₂O to 1 l) conditioned Petri dishes supplemented with 0.05 mg 5-fluoro-2'-deoxyuridine ml⁻¹ for ‘slow-killing’ experiments. The plates were incubated overnight at 37 °C and then placed at room temperature for 4 h. Twenty L4 synchronized worms were harvested with M9 solution (3 g KH₂PO₄, 6 g NaHPO₄, 5 g NaCl, 1 ml 1 M MgSO₄, H₂O to 1 l), placed on the 35 mm assay Petri dishes and incubated at 22 °C. Worm survival was scored at 1 h, 24 h and each subsequent day, using an Axiovert S100 optical microscope (Zeiss) equipped with a Nikon digital Camera DXM 1200F (Nikon Instruments). The worms were considered dead when they remained static without grinder movements for 20 s. The results are expressed as the percentage of living worms.

Biofilm formation. The biofilm formation activity of *P. aeruginosa* PAO1 was studied using a technique adapted from O’Toole & Kolter (1998). An aliquot of 100 µl of a bacterial culture adjusted to OD₅₈₀ 0.4 was layered in a PVC microtitre plate and incubated for 24 or 48 h. In the first set of experiments, bacteria were grown in the absence of GABA but were exposed to the molecule during biofilm formation. In a second set of experiments, bacteria were grown in the presence of GABA but GABA was not added to the medium during the biofilm formation. In a third set of experiments, bacteria were grown with GABA as previously, but the medium in PVC microtitre plates was supplemented with GABA to maintain the treatment during the 24–48 h of the biofilm formation test. After removing the bacterial suspension and rinsing, bacteria and matrix bound to the wells were stained with crystal violet (0.1%, 30 min). After rinsing, the dye was recovered by adding 150 µl SDS (1% in sterile water) and the OD₅₉₅ of the solution was measured. For comparison of the results, data were normalized as a percentage of biofilm density in the absence of treatment. Results were normalized as a percentage of the median value corresponding to the mature biofilm formation activity of CTS117 at 8 °C.

Cell surface properties. The binding index of *P. aeruginosa* PAO1 on biological (cell) surfaces was determined using the gentamicin exclusion test (Mezghani-Abdelmoula *et al.*, 2004).

The binding index of bacteria on glass slides was determined by direct counting. Glass slides were cleaned with ethanol and TDF4 detergent (4% in 50 °C water) to remove any trace of lipids. A bacterial suspension [10⁸ c.f.u. ml⁻¹ in sterile water (SPW) NaCl 0.9%] was layered on each glass slide. Bacteria were allowed to adhere for 2 h at 37 °C. Non-adherent bacteria were removed by rinsing and the remaining adherent bacteria were stained with acridine orange (0.01% in sterile water). The slides were observed using an epifluorescence microscope Zeiss Axiovert 100. The binding index was determined by counting a minimum of 20 homologous fields.

The surface polarity of *P. aeruginosa* PAO1 was determined using the microbial adhesion to solvent (MATS) technique (Bellon-Fontaine *et al.*, 1996). Bacterial cultures in early stationary phase and treated or not with GABA were harvested by centrifugation at 10 000 g. Pellets were rinsed twice with 0.9% NaCl in water and diluted to OD₄₀₀ 0.8. An aliquot of bacterial suspension (2.4 ml) was mixed with 0.4 ml hexadecane. The tubes were vigorously hand-shaken and the OD₄₀₀ of the aqueous phase was measured after 15 min of decantation. The percentage of affinity for hexadecane was calculated as follows: [(OD control - OD test)/OD control] × 100.

Lipopolysaccharide (LPS) structure. LPS was purified from *P. aeruginosa* PAO1 as described by Darveau & Hancock (1983) and was analysed by MALDI-TOF MS using an Autoflex III mass spectrometer (Bruker Daltonik). For analysis, a 0.5 µl aliquot of purified LPS was spotted onto a steel target plate. An aliquot (0.5 µl) of a solution of α-cyano-4-hydroxycinnamic acid matrix (10 mg ml⁻¹ in acetonitrile/0.2% TFA, v/v) was added to each spot and these were dried at room temperature. The mass spectrometer was equipped with a pulsed YAG 200 Hz laser and was run in the positive mode. Instrument calibration was achieved by using calibration standards (Care, Bruker Daltonics) spotted on the same target plate. Each spectrum was established over 200 laser shots.

Biosurfactant production assays. The kinetics of biosurfactant production were monitored over 48 h by measuring the surface tension of the rinsing solution (SPW) of colonies of *P. aeruginosa* grown on solid NB medium, using the Wilhelmy plate technique (Hiemenz & Lagowski, 1977). Rhamnolipids were further extracted from 3 ml culture supernatant of bacteria grown for 24 h, and analysed by HPLC/MS using an Agilent Technologies 1100 system (Column YP5C18 Interchim 2 × 200 mm) coupled to a Bruker Esquire-LC ESI-MS/MS positive-ion electrospray ionization and ion trap mass spectrometer. The extraction and separation protocols were adapted from Déziel *et al.* (2000).

Secreted diffusible virulence factors assays. Secreted caseinase, esterase, lecithinase, amylase and haemolytic activities were studies by cultures on agar supplemented with milk, Tween 80, egg yolk, starch and Columbia blood, respectively. The elastase activity was measured in liquid bacterial culture medium using an elastin/Congo red assay. Filtered supernatant (50 µl) of a bacterial culture grown to early stationary phase was mixed with 1 ml Tris buffer (0.1 M, pH 7.2, 1 mM CaCl₂) containing 20 mg elastin/Congo red (Sigma). The tubes were incubated at 37 °C with agitation. After 18 h, the tubes were chilled on ice and the reaction was stopped by adding 0.1 ml 0.12 M EDTA. Non-soluble elastin/Congo red was removed by centrifugation, and the OD₄₉₀ was measured.

Pyoverdine production was monitored over 48 h. To promote pyoverdine production, bacteria were grown on King B or in Bacto Casamino Acids (CAA) medium. Pyoverdine production was

expressed as the OD₄₀₀/OD₅₈₀ ratio of the supernatant after removal of the bacteria by centrifugation (5 min, 10 000 g).

Exotoxin A was assayed in the culture supernatants of *P. aeruginosa* PAO1 grown in NB using an ELISA sandwich method on 96-well microtitre plates as described by Gaines *et al.* (2005) and Blier *et al.* (2011). Each well was coated with goat anti-exotoxin A antibody (0.25 mg ml⁻¹ in 100 mM Na₂HCO₃) and treated with BSA to block non-specific binding sites. A standard curve was made by using serial dilutions of purified exotoxin A (Sigma-Aldrich). Assays were made on 100 µl culture medium. After 1 h incubation at room temperature, the plates were washed and incubated with rabbit anti-exotoxin A. The plates were then washed and treated with goat anti-rabbit IgG conjugated to horseradish peroxidase (Sigma-Aldrich). The reaction was visualised by adding a substrate solution (Pierce Biotechnology) and was stopped after 30 min by adding H₂SO₄ (2 M). The absorbance was read at OD₄₅₀ using an ELISA plate reader (Bio-Tek Instruments). The values are expressed as the ratio of Exotoxin A (in pg ml⁻¹) versus the bacterial culture density (at 580 nm).

The HCN/CN⁻ production by *P. aeruginosa* was determined by using a polarographic method recently developed in our laboratory (Blier *et al.*, 2012). Voltametric measures were made using a Metrohm 757 VA Computrace. Analyses were carried out in a three-electrode configuration using a saturated Ag/AgCl₃ reference electrode, a platinum wire as a counter electrode and a Multi-Mode Mercury Electrode as a working electrode. All experiments were performed at room temperature. Bacterial cultures were centrifuged and filtered on a 0.22 µm filter to remove cell fragments. This medium was then diluted in 0.2 mol borate electrolyte l⁻¹ (pH 10.2). The solution was purged for 3 min with N₂ to remove dissolved oxygen and then for 20 s more between each cyanide addition. A potential scan was carried out in a negative direction from -0.1 to -0.5 V with a sweep rate of 10 mV s⁻¹. The pulse amplitude was 0.05 V with pulse duration of 0.04 s. The cyanide peak was measured at -200 mV in a differential pulse mode and the cyanide concentration was determined by adding triplicate successive (*n*=4) amounts of 10 mg potassium cyanide standard l⁻¹.

Total proteome analysis. Cultures of *P. aeruginosa* PAO1 grown to early stationary phase were centrifuged (20 min, 12 000 g). Pellets were washed three times in 50 mM Tris/HCl, pH 8. Cells were disrupted by three freeze/thaw cycles and sonication. Unbroken cells were removed by centrifugation. The supernatants were supplemented with benzonase and MgCl₂ and incubated for 30 min at 37 °C. Proteins were precipitated with cold acetone (v/v) and harvested by centrifugation at 13 000 g for 10 min at 4 °C, and resuspended in rehydration buffer containing 7 M urea, 2 M thiourea, 4% (w/v) CHAPS (Bio-Rad), 0.5% IPG buffer 3-10 (Bio-Rad), 70 mM DTT and 5 mM TCEP [Tris(2-carboxyethyl)phosphine hydrochloride] to a final volume of 300 µl. The protein concentration was controlled using the Bio-Rad protein assay (Bio-Rad) and BSA as standard.

The protein extract was then separated by 2D gel electrophoresis and in-gel trypsin digestion. For the first dimension electrophoresis, protein samples were separated by IEF using pH 4–7 IPG strips (immobilized linear pH gradients, 17 cm, Bio-Rad) as described by Barbey *et al.* (2012). After IEF, the IPG strips were reduced in an equilibration buffer [6 M urea, 50 mM Tris-maleic acid, 2% (w/v) SDS, 20% (v/v) glycerol, a few grains of bromophenol blue and 2% (w/v) DTT for reduction or 2.5% (w/v) iodoacetamide for alkylation]. The second dimension SDS-PAGE was realized on 12% polyacrylamide (37.5:1 acrylamide/bisacrylamide, Bio-Rad) gels at 50 mA for 4 h. Proteins on gels were visualized with Coomassie brilliant blue R-250 and gel images were captured using a GS-800 densitometer (Bio-Rad). Variations in spot intensity and distribution were studied using the Bio-Rad PDQuest 2D analysis software. In-gel digestion was performed as previously (Barbey *et al.*, 2012). In-gel trypsin digestion

products were then analysed using a MALDI-TOF/TOF (Autoflex III, Bruker Daltonics) in positive/reflector mode. Instrument calibration was achieved using peptide calibration standards (Care, Bruker Daltonics). Samples were spotted onto MTP 384 ground steel target, using freshly prepared matrix solution composed of 2,5-dihydroxybenzoic acid (20 mg ml^{-1}) in a solution of 0.1% TFA and 50% acetonitrile. Peptide mass fingerprints obtained from MS analysis and MS/MS spectra were used to search the NCBI no redundant database by using online MASCOT software (<http://www.matrixscience.com>). Search parameters were set as follows: taxonomy was set on bacteria; trypsin was given as the digestion enzyme and a maximum of one missed cleavage site was allowed; carbamidomethylation of cysteine and methionine oxidation were selected as fixed and variable modifications, respectively; mass values were set to monoisotopic. Searches were performed setting a peptide mass tolerance of 100 p.p.m. and a fragment ion mass tolerance of 0.5 Da. The statistical analyses of the sequences were determined by the probability-based Mowse score offered by MASCOT software. A P -value <0.05 was considered as significant.

Production of quorum-sensing factors. The kinetics of 3-oxo-C12 acylhomoserine lactone (3oxoC12-HSL) and C4 acylhomoserine lactone (C4-HSL) production by *P. aeruginosa* was measured over a 24 h period. At each time point (3, 5, 8, 12 and 24 h of incubation) an aliquot of 5 ml culture medium was collected and centrifuged for 10 min at 10 000 g. The supernatant was mixed with an equal volume of dichloromethane. This solution was shaken manually by flip-flop, and centrifuged again (10 min, 10 000 g). The aqueous phase was removed and treated for a second extraction following the same protocol. The two dichloromethane extracts were pooled and dehydrated by adding Na_2SO_4 . After removal of Na_2SO_4 crystals by centrifugation, the solvent was evaporated. The samples were then treated as described previously (Morin *et al.*, 2003) and analysed by C_{18} reversed-phase HPLC/MS analysis using an Agilent Technologies 1100 system coupled to a Bruker Esquire-LC ESI-MS/MS positive-ion electrospray ionization and ion-trap mass spectrometer.

The production of pseudomonas quinolone signal (PQS) was quantified by TLC and C_{18} reversed-phase HPLC analysis. Cultures of control or GABA-treated *P. aeruginosa* PAO1 grown for 24 h were centrifuged (5 min, 10 000 g). The supernatant was collected and acidified to pH 3 by addition of HCl. PQS was extracted three times with 10 ml acidified ethyl acetate [$1\text{ }\mu\text{l}$ acetic acid (ml ethyl acetate) $^{-1}$]. Water traces were eliminated by adding anhydrous MgSO_4 . The filtrate was evaporated under nitrogen and resuspended in 500 μl methanol. For TLC analysis, samples (10 μl) and synthetic PQS (60 nM) were spotted onto normal phase silica 60 F₂₅₄ (Merck) TLC plates, previously soaked in 5% K_2HPO_4 for 30 min and activated at 90 °C for 1 h. Extracts were separated using a dichloromethane/methanol (95:5, v/v) mobile phase, and visualized under UV light (365 nm). For HPLC analysis, samples (20 μl) were injected in a C18-Inertsil ODS3 column (5 μm , 4.6 × 250 mm) and were separated by a parabolic gradient ranging from 25 to 100% methanol in water/acetic acid (1% v/v, flow rate 0.4 ml min $^{-1}$) using a Shimadzu Prominence System equipped with a LC-20AD parallel double piston pump and a SPD-20AV UV-visible detector.

Statistical analysis. For analysis of the slow killing test results, nematode survival was calculated by using the Kaplan–Meier method, and survival differences were tested for significance by using of the log–rank test (GraphPad Prism version 4.0). For other results, each value reported for the assays is the mean of measurements from a minimum of three independent preparations. The Student *t*-test was used to compare the means within the same set of experiments.

RESULTS

Effect of GABA on *P. aeruginosa* virulence

Preliminary controls showed that exposure of *P. aeruginosa* PAO1 to GABA (0.01 mM) during the whole growth phase, or at the beginning of the stationary phase, did not modify the growth kinetics of the bacterium. When grown in the presence of GABA, *P. aeruginosa* displayed a strong increase of its cytotoxic potential on glial cells ($88.6 \pm 8.6\%$, $P < 0.001$), as revealed by the LDH release assay (Fig. 1a). Since the rat glial cells might be sensitive to GABA themselves (Angulo *et al.*, 2008), bacteria were carefully rinsed to remove any trace of free GABA prior glial cells infection. In addition, control experiments realized by direct treatment of glial cells with GABA (0.01 mM) in the absence of bacteria showed that this molecule had no direct effect on glial cell viability (data not shown).

The effect of GABA on *Pseudomonas* virulence was tested in a second model, the nematode *C. elegans*, which is

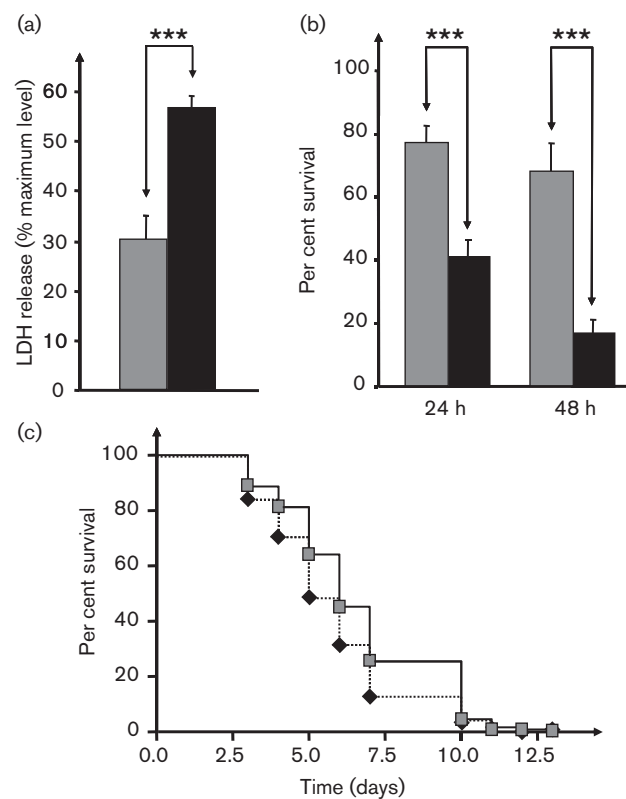


Fig. 1. Effect of GABA (0.01 mM) on the cytotoxicity and virulence of *P. aeruginosa* PAO1. The cytotoxic activity of the bacteria was evaluated on glial cells (a). The global virulence was evaluated on *C. elegans* using the ‘fast killing’ test, where the worms are killed by bacterial diffusible toxins (b) and using the ‘slow-killing’ test, in which the worms are killed through contact-mediated interactions after ingestion of the bacteria (c). *** $P < 0.001$. Grey, control PAO1; black, GABA-treated PAO1. Error bars indicate SEM.

considered to be an equivalent of the acute mouse toxicity test (Williams *et al.*, 2000) and has been adapted to compare the virulence of environmental bacteria (Duclairoir Poc *et al.*, 2011). In addition, whereas the ‘fast-killing’ test gives information on the contribution of diffusible virulence factors in the lethal activity of the bacterium, the ‘slow-killing’ test reveals global variations of virulence, including those that are due to direct contact with the bacterial surface (Aballay & Ausubel, 2002). The two tests confirmed that GABA increases the virulence of *P. aeruginosa*: the ‘fast-killing’ test clearly shows that GABA-treated bacteria provoked a sharp decrease in the number of surviving worms after 24 and 48 h (-46.3 ± 5.2 and $-75.2 \pm 4.4\%$, respectively) (Fig. 1b). While the effect of GABA was less visible in the ‘slow-killing’ test (Fig. 1c), the log-rank test analysis of the data demonstrated that GABA treated *P. aeruginosa* were also significantly more virulent ($P=0.0252$; $n=12$).

Effect of GABA on biofilm formation

As the virulence of *P. aeruginosa*, particularly in the lung, is generally associated with biofilm formation (Høiby *et al.*, 2010), the effect of GABA on the biofilm formation activity was studied *in vitro* using different protocols to take into consideration a possible metabolism of GABA during biofilm formation. Bacteria in NB medium were exposed to GABA as they were forming a biofilm or were pre-treated with GABA and were then allowed to form a biofilm in the absence or presence of GABA. When PAO1 was exposed to GABA only during the biofilm formation period, no change was observed. Conversely, when the bacteria were exposed to GABA during the growth phase, a reduction in biofilm formation was observed after 24 h (-13 ± 3 and $-15 \pm 4\%$) and 48 h (-10 ± 6 and $-18 \pm 3\%$) (Fig. 2). The reduction observed after 48 h in medium without GABA was not significant, probably because of the instability of mature biofilms.

Effect of GABA on the surface properties of *P. aeruginosa*

In order to determine more precisely the effect of GABA on the surface properties of *P. aeruginosa*, the adhesion potential and the surface polarity of the bacteria were investigated. The effect of GABA on bacterial adhesion was studied on living surfaces (glial cells) and on glass; pre-treatment of bacteria with GABA was associated with an increase in the binding index of 136 ± 21 and $138.7 \pm 8.6\%$ on glial cells and glass, respectively. However, since the global variation of adhesion is limited (it appeared only really detectable on a homogeneous surface such as glass) the increase measured on glial cells should not be significant. As bacterial adhesion depends on the surface polarity, we measured the affinity of the bacteria to hexadecane using the MATS test. Considering that the threshold for the affinity to hexadecane of polar (hydrophilic) bacteria is 20% (Bellon-Fontaine *et al.*, 1996), in our experimental conditions *P. aeruginosa* PAO1 behaved as a highly polar micro-organism ($3.5 \pm 0.2\%$ affinity to hexadecane). The surface properties of *P. aeruginosa* were not significantly modified by GABA.

Effect of GABA on contact-dependent virulence factors production

Since our results showed that GABA modulates *P. aeruginosa* virulence by acting both on surface-dependent and diffusible virulence factors, we decided to investigate the effect of GABA on the structure of the LPS, the main constituent of the outer membrane of Gram-negative bacteria. The LPS extracted from *P. aeruginosa* PAO1 was analysed by MALDI-TOF MS. Multiple peaks, essentially of *m/z* ratio <3000 , probably generated by fragments of lipid A (Veron *et al.*, 2007), were detected (Fig. 3a). Secondary peaks with a higher *m/z* ratio and considered to be compounds associated with oligosaccharide cores with different O-antigen repeating units (Veron *et al.*, 2007)

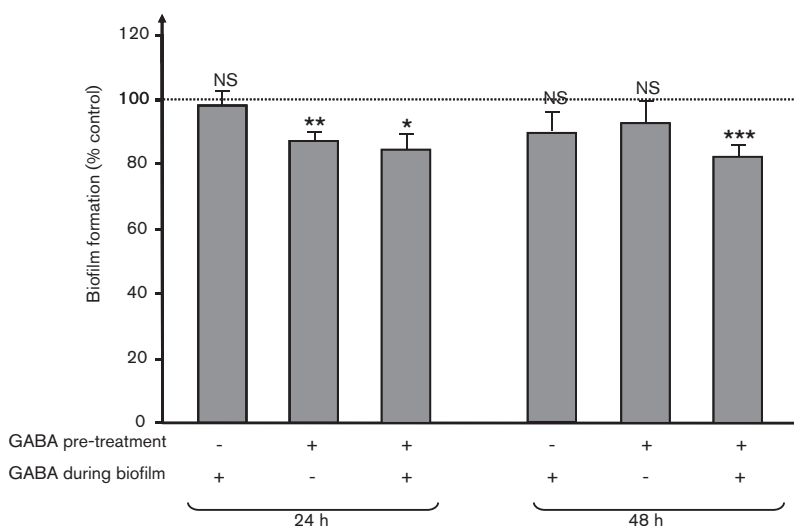


Fig. 2. Effect of GABA (0.01 mM) on the biofilm formation activity of *P. aeruginosa* PAO1, measured after 24 or 48 h of incubation. Bacteria were exposed to GABA only during the growth phase (pre-treatment), only during the biofilm formation period (during biofilm) or continuously during growth and biofilm formation (pre-treatment+during biofilm). The biofilm formation activity is expressed as a percentage of the control value. NS, non-significant; * $P<0.05$; ** $P<0.01$; *** $P<0.001$. Error bars show SEM.

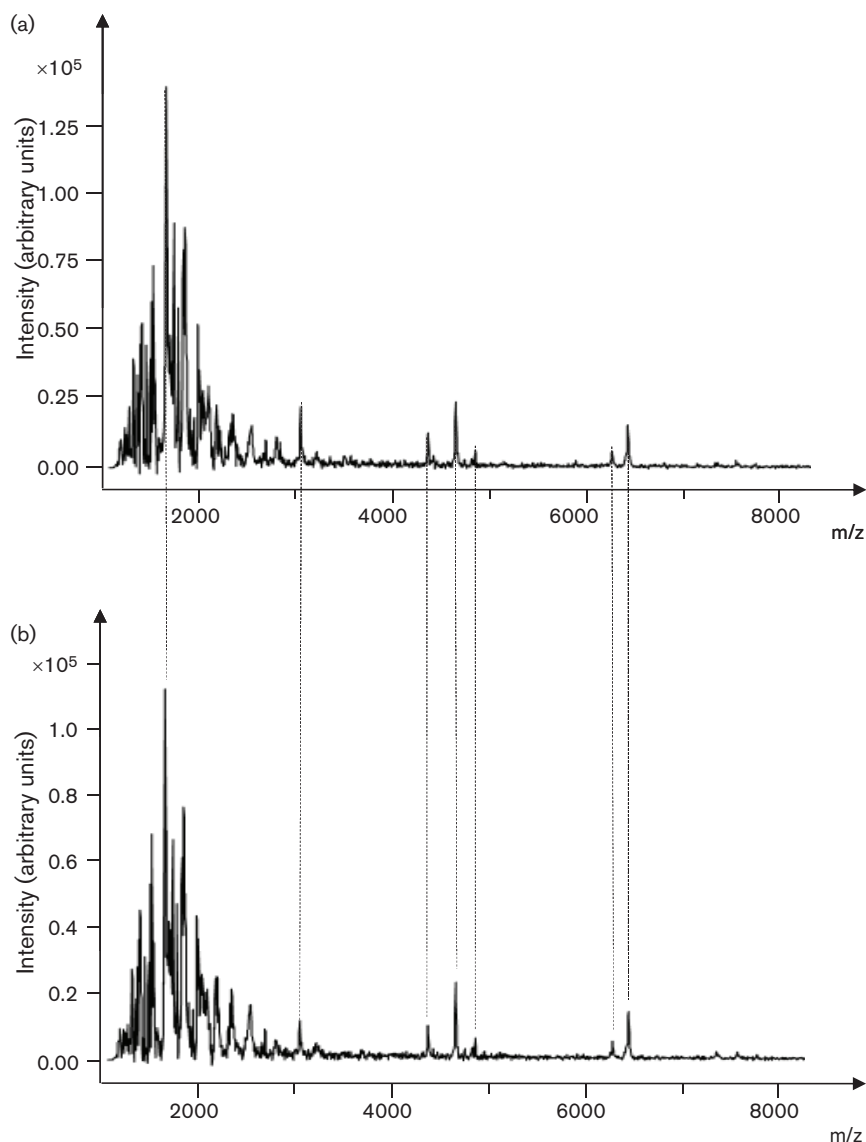


Fig. 3. MALDI-TOF analysis of LPS extracted from control (a) and GABA-treated (b) *P. aeruginosa* PAO1. Each figure is representative of three independent analyses.

were present in lower amounts. The mass spectrum of LPS extracted from GABA-treated bacteria was remarkably preserved. As noted in Fig. 3(b), the positions and relative intensities of all the peaks were the same in LPS extracted from control and GABA-treated *P. aeruginosa*, demonstrating that the LPS structure was not altered in response to GABA treatment. The surface properties of bacteria can be also influenced by the production of surfactants which modulate the surface tension between the bacterium and its immediate environment. A rapid method to check the bacterial production of surfactant involves collecting colonies on solid agar medium, cleaning them with pure water and measuring their surface tension (Carrillo *et al.*, 1996).

P. aeruginosa PAO1 colonies showed a surface tension of $39.3 \pm 1 \text{ mN m}^{-1}$, indicating the presence of surfactants in solution (the mean surface tension of poorly mineralized water is 71.7 mN m^{-1} ; Hiemenz & Lagowski, 1977). Interestingly, the surface tension of the extract of bacterial colonies grown in the presence of GABA was unchanged ($39.3 \pm 1 \text{ mN m}^{-1}$) but when this was measured on diluted extract, we observed a shift in critical micellar concentration for control and GABA-treated bacteria, suggesting a difference in the composition of the biosurfactants (data not shown). Biosurfactants from control and GABA-treated *P. aeruginosa* were then extracted and analysed by HPLC-ESI-MS/MS. A total of 10 different types of rhamnolipids were identified (Table 1). The same molecules were found in

Table 1. Rhamnolipids identified and quantified by ESI-MS analysis in cultures of *P. aeruginosa* PAO1 grown in the absence or presence of 0.01 mM GABAData are means \pm SEM.

Rhamnolipids	Intensity $\times 10^5$ (arbitrary units)	
	Control PAO1	GABA-treated PAO1
Rha-Rha-C8-C10/Rha-Rha-C10-C8	4.1 \pm 1.4	2.6 \pm 0.9
Rha-C10-C8/Rha-C8-C10	0.9 \pm 0.2	0.7 \pm 0.2
Rha-Rha-C8-C12 : 1	6.2 \pm 1.7	4.9 \pm 1.2
Rha-Rha-C10-C10	318.1 \pm 58	257.2 \pm 63.1
Rha-C10-C10	80.1 \pm 8.6	88.9 \pm 19.8
Rha-Rha-C10-C12 : 1	37.4 \pm 9.2	36.0 \pm 10.6
Rha-C10-C12 : 1	4.3 \pm 1.5	4.9 \pm 1.1
Rha-Rha-C12-C10/Rha-Rha-C10-C12	67.1 \pm 30.7	62.2 \pm 20.5
Rha-Rha-C12-C12 : 1	2.4 \pm 1.5	2.0 \pm 0.8
Rha-Rha-C12-C12	2.3 \pm 1.3	2.1 \pm 1.0

the extracts of *P. aeruginosa* exposed or not to GABA and their relatives proportions were identical, suggesting that the variations of surface tension observed in dilutions were due to other soluble factors such as proteins.

Effect of GABA on *P. aeruginosa* diffusible virulence factors

The effect of GABA on the major exoenzymic activities produced by *P. aeruginosa* PAO1, i.e. caseinase, esterase, haemolytic, amylase, lecithinase and elastase activities, was tested. None of these was altered in bacteria grown in the presence of GABA (data not shown). We investigated the effect of GABA on the principal secondary metabolites produced by *P. aeruginosa*, starting with pyoverdine, the production of which depends on iron availability in the environment and thus of the culture medium composition. We therefore studied the effect of GABA in two media known to promote pyoverdine secretion. As shown in Fig. 4(a and b), GABA has no effect on pyoverdine production in any of the tested media.

Exotoxin A is the most toxic secreted virulence factor of *P. aeruginosa* in terms of mass/activity ratio (Wolf & Elsässer-Beile, 2009). The production of exotoxin A by *P. aeruginosa* was studied in NB after 10 and 24 h of treatment with GABA. Exotoxin A was detected in the medium using a highly sensitive ELISA. As shown in Fig. 4(c), the secretion pattern of exotoxin A was unchanged in control and GABA-treated bacteria.

P. aeruginosa is also known to produce non-peptidic toxins, such as HCN. We have recently developed an original HCN polarographic assay whose sensitivity is below 1 $\mu\text{g l}^{-1}$ (Blier et al., 2012). The mean concentration of HCN in the medium of control cultures of *P. aeruginosa* after 24 h of incubation was 1.024 \pm 0.015 mg l^{-1} (Fig. 4d). The concentration of HCN in the medium of GABA-treated

bacteria was significantly increased (+35%, $P < 0.05$), reaching 1.383 \pm 0.015 mg l^{-1} .

Effect of GABA on the protein pattern expression of *P. aeruginosa*

The cell-associated proteome was investigated by analysing pellets of *P. aeruginosa* PAO1 grown in the absence or presence of GABA. The 2-D electrophoresis assays on total protein extracts showed limited differences between the proteome of control (Fig. 5a) and GABA-treated (Fig. 5b) bacteria. Two proteins (spots 1 and 2) were downregulated whereas the expression of five other proteins (spots 3–7) was clearly increased (Fig. 5c). Each spot was excised, digested in-gel with trypsin and analysed by MALDI-TOF/TOF. The seven spots corresponded to *P. aeruginosa* proteins identified in the NCBI database (Table 2). Spots 1 and 3 corresponded to the same thermo-unstable elongation factor (Tuf), as confirmed by TOF/TOF fragmentation, but the neutral form present in spot 1 was only detected in control bacteria; after treatment with GABA it was replaced as an acidic form identified as spot 3. Another protein, the thermostable elongation factor (Ts), found in spot 6, appeared to be upregulated in the presence of GABA. Spot 2, not present in bacteria exposed to GABA, was identified as an ornithine carbamoyltransferase. The other spots 4, 5 and 7 corresponded to a peroxidase, and alkyl hydroperoxide reductase and a putative USP-like protein, respectively.

Effect of GABA on *P. aeruginosa* quorum sensing factors

Since cyanogenesis is regulated by the quorum-sensing system, we investigated the effect of GABA on 3oxoC12-HSL, C4-HSL and PQS production by *P. aeruginosa*. The kinetics of 3oxoC12- and C4-HSL secretion were studied over 24 h. In the presence of GABA, the peak of

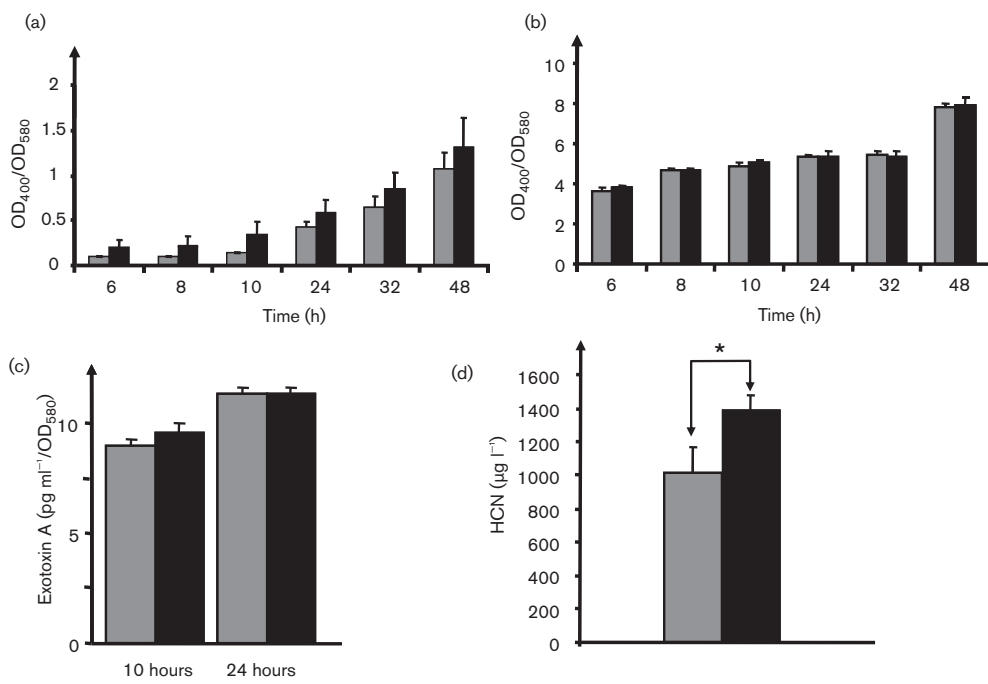


Fig. 4. Effect of GABA (0.01 mM) on pyoverdine (a, b), exotoxin A (c) and hydrogen cyanide (d) production by *P. aeruginosa* PAO1. Pyoverdine production, studied in King B (a) and CAA (b) medium, is expressed as the ratio of pyoverdine absorption (OD_{400}) versus the bacterial density (OD_{580}). Exotoxin A is expressed as the concentration measured in the medium normalized to the value of the OD_{580} of the bacterial culture. HCN concentration was determined by polarographic analysis of bacterial culture supernatant. * $P < 0.05$. Grey, control PAO1; black, GABA-treated PAO1. Error bars indicate SEM.

production of 3oxoC12-HSL was higher than in control studies (Fig. 6a). In addition, this peak was observed 8 h after the beginning of the experiment, whereas it appeared after 12 h in control bacteria. The production of C4-HSL was also stimulated in GABA-treated bacteria but the effect was of lower amplitude and statistically non-significant

(Fig. 6b). The effect of GABA on PQS production was studied by using two complementary techniques: TLC, the classical method employed to detect PQS, and HPLC, which provides a higher resolution. PQS production was measured after 24 h to allow sufficient accumulation of the molecule in the culture medium. Both techniques clearly

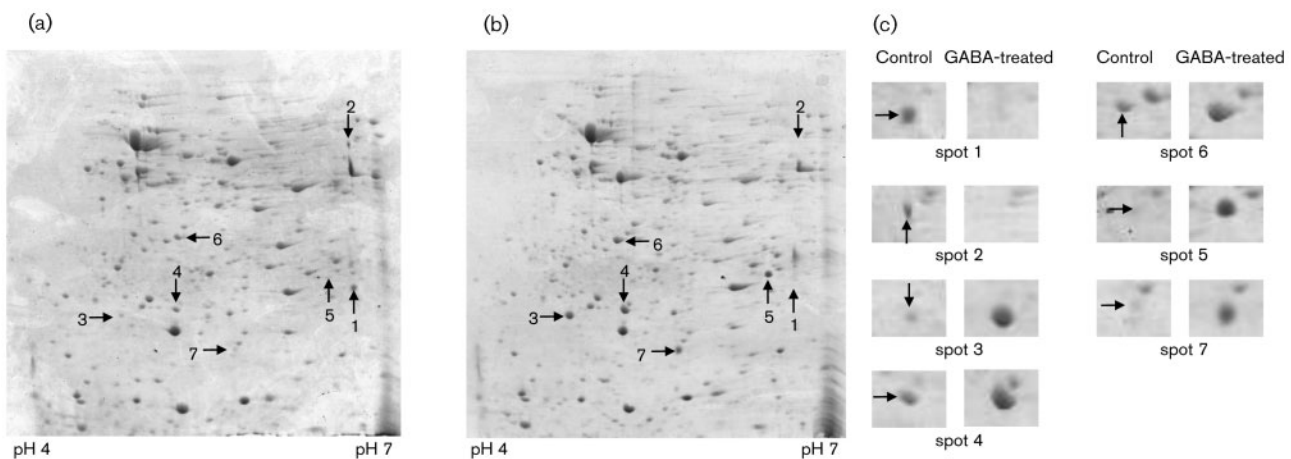


Fig. 5. 2D electrophoresis analysis of the total proteome of control (a) and GABA-treated (b) *P. aeruginosa* PAO1. Seven spots were modified after exposure of the bacteria to GABA (c). The proteins corresponding to these spots are presented in Table 2.

Table 2. MALDI-TOF/TOF identification of the proteins in Fig. 5 whose expression was modified by GABA in *P. aeruginosa* PAO1

Spot no.	NCBI accession number	Gene name	Putative function	Protein domain	Mascot score	No. matched peptides	Coverage (%)	MW (Da)/pI
1	NP_252955.1	<i>tufA</i>	Elongation factor Tu		102	14	23	43342/5.23
2	NP_253859.1	<i>arcB</i>	Ornithine carbamoyltransferase	NAD(P) ⁺ -bi-binding proteins	184	35	74	38984/6.13
3	NP_252955.1	<i>tufA</i>	Elongation factor Tuf	Peroxiredoxin (PRX) family,	89	12	28	43342/5.23
4	NP_252219.1		Putative Peroxidase	Typical 2-Cys PRX subfamily	158	13	64	21808/5.37
5	NP_248829.1	<i>ahpC</i>	Alkyl hydroperoxide reductase C	Peroxiredoxin (PRX) family,	186	15	73	20529/5.89
6	NP_252345.1	<i>tsf</i>	Elongation factor Ts	Typical 2-Cys PRX subfamily	271	23	80	30634/5.22
7	NP_251999.1		Hypothetical protein PA3309	Ubiquitin Associated domain	201	18	82	16486/5.50
				USP-Like				

showed that the production of PQS by *P. aeruginosa* PAO1 was not modified by GABA (Fig. 7).

DISCUSSION

GABA is a non-protein amino acid that is conserved in bacteria and eukaryotes (see Bouché *et al.*, 2003 for a review). In plants, GABA is secreted as a defence signal against bacterial phytopathogens (Chevrot *et al.*, 2006). In the case of *P. aeruginosa*, we observed that GABA did not affect the growth and motility of the bacterium but did increase its cytotoxicity and virulence. The *C. elegans* model gave a first indication of the mechanisms involved in the response of *P. aeruginosa* to GABA. Indeed, GABA had a strong effect on bacterial virulence in the ‘fast killing test’. In this test, the secretion of bacterial diffusible molecules is stimulated by the use of a high-osmolarity medium, suggesting that soluble toxins have a principal role in the increase in virulence. In agreement with this hypothesis, the virulence of *P. aeruginosa* in the ‘slow killing test’ appeared to be only marginally increased. However, the biofilm formation experiments revealed that the action of GABA should be more complex. When bacteria were exposed to GABA only during the biofilm formation period, GABA had no effect. Only bacteria pretreated during the growth phase showed a generally significant reduction in biofilm formation, suggesting that only the early phases of bacterial adhesion are affected by GABA.

In order to clarify the mechanism of action of GABA on *P. aeruginosa*, we focused in a first step on surface associated factors. GABA increased bacterial cell adhesion but this effect was not significant. In contrast, we observed a significant increase in the adhesion on glass of GABA-treated *Pseudomonas*. Glass is a polar surface whereas PVC, on which the biofilm formation tests were done, is hydrophobic. This is in agreement with the opposite effects of GABA on bacterial adhesion on these two surfaces. However, the MATS technique did not reveal any variation of surface polarity suggesting that GABA was acting on a specific adhesin(s). LPS, the principal component of the outer membrane of Gram-negative bacteria, was unchanged in GABA-treated bacteria. The surface tension of *P. aeruginosa* extracts was consistent with the presence of biosurfactants, and, since biosurfactants can interfere with the binding properties and biofilm formation activities of *Pseudomonas* (de Bruijn *et al.*, 2007), these molecules were analysed but, here also, the structure and concentration of rhamnolipids expressed by PAO1 were not modified in bacteria exposed to GABA.

The effect of GABA on diffusible toxins and on the proteome of *P. aeruginosa* was then investigated. The cytotoxic activity of *P. aeruginosa*, measured by LDH release from eukaryotic cells when the cytoplasmic membrane is disrupted, can be considered as an equivalent of haemolysis and it is known that this is essentially

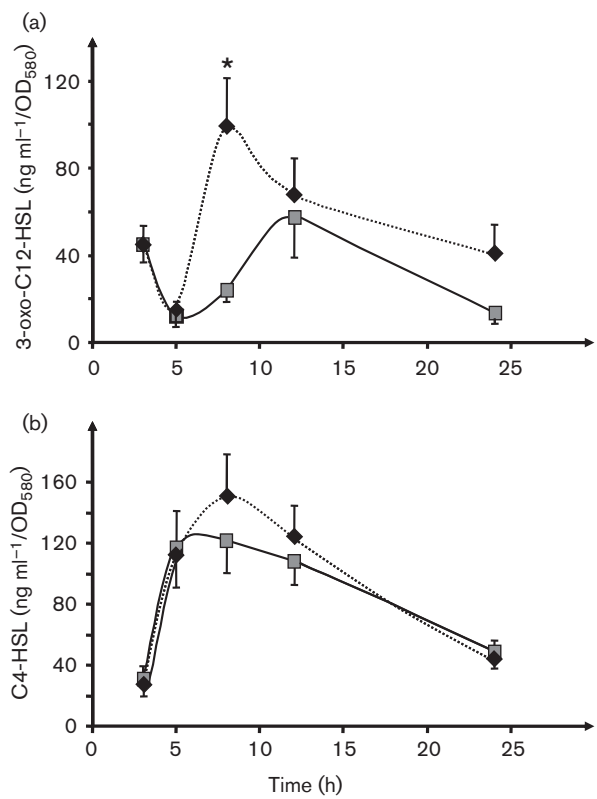


Fig. 6. Effect of GABA (0.01 mM) on the production kinetics of 3-oxo-C12-HSL and C4-HSL by *P. aeruginosa* PAO1. HSL production is expressed as the concentration measured in the medium normalized to the value of the OD₅₈₀ of the bacterial culture. *P<0.05. Grey, control PAO1; black, GABA-treated PAO1. Error bars indicate SD.

induced by a type III secretion system (Goure *et al.*, 2004) or phospholipase C (Ostroff *et al.*, 1989). The tests done on blood-supplemented agar plates showed no variation in bacterial haemolytic activity. All other exoenzymic activities studied also remained unchanged. Pyoverdine is

essential for *P. aeruginosa* virulence (Meyer *et al.*, 1996) so the production of this siderophore in GABA-treated bacteria was monitored but it appeared clearly that pyoverdine production is not modulated by GABA. Exotoxin A is the most toxic secreted virulence factor of *P. aeruginosa* in terms of mass/activity ratio (Wolf & Elsässer-Beile, 2009). Its secretion was studied in the same medium used to test the effect of GABA on *P. aeruginosa* virulence (NB). As it is a low-iron-inducible toxin, in our experimental conditions limited concentrations of exotoxin A were detected and its production was not affected by GABA. The arsenal of *P. aeruginosa* is not exclusively composed of peptidic molecules and it is interesting to note that hydrogen cyanide (HCN) is considered to be the principal diffusible lethal toxin acting on *C. elegans* (Gallagher & Manoil, 2001). In the present study, we used a polarographic assay of HCN/CN⁻ based on the redox properties of cyanide ions recently developed in our laboratory (Blier *et al.*, 2012). High quantities of HCN were measured in the growth medium of *P. aeruginosa* PAO1 and GABA induced a significant increase of HCN production. By itself, this increase of HCN (35 %) could explain the virulence of GABA-treated *P. aeruginosa* but this is not sufficient to understand the variations of surfaces properties observed in parallel. The total proteome of GABA-treated *P. aeruginosa* was then analysed and compared with that of control bacteria. The differences of expression were limited to six proteins. A first novel result was the observation of two spots (1 and 3) corresponding to the same protein but showing very different pI values. This protein, identified as the thermo-unstable elongation factor Tuf, is a GTP/GDP and ribosome binding protein, but it is also capable of binding the thermostable elongation factor Ts (Wittinghofer *et al.*, 1983), detected as spot 6 and markedly overexpressed in GABA-treated *Pseudomonas*. The existence of free or GDP+Pi tightly bound Tuf could explain the shift in pI of the molecule between control and GABA-treated bacteria. However, we cannot exclude that GABA itself could bind Tuf, and because of its acidic character decrease the pI of the

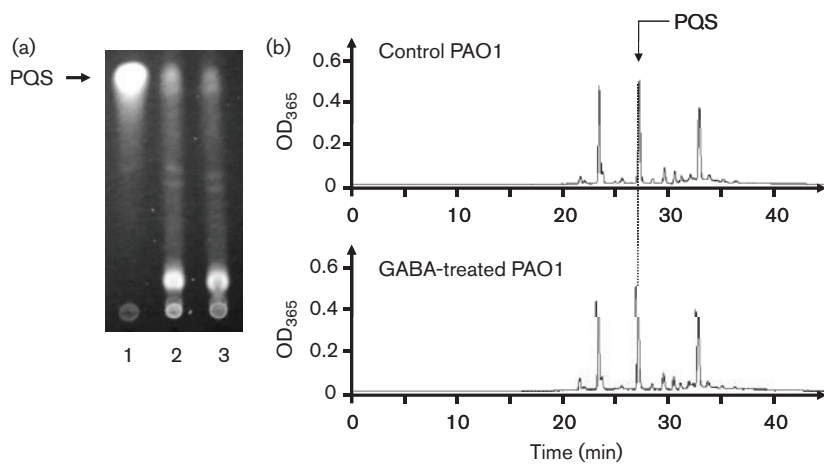


Fig. 7. Effect of GABA (0.01 mM) on the production of PQS by *P. aeruginosa* PAO1. PQS production was measured by TLC (a) (lanes: 1, synthetic PQS; 2, PQS from control PAO1; 3, PQS from GABA-treated PAO1) and RP-HPLC (b).

protein. This binding should also explain the long-term effect of GABA. In agreement with this hypothesis, which deserves further study, it has been shown that the elongation factor Tuf can be associated with the membrane of *P. aeruginosa* and it acts as a binding protein for the human plasma regulators factor H and plasminogen (Kunert *et al.*, 2007). The change of Tuf charge could also explain the specific effects of GABA on *P. aeruginosa* surface properties independently of variations in polarity, LPS or biosurfactant production. The four other proteins modulated by GABA have in common their role in oxidative metabolism. Ornithine carbamoyltransferase, identified as spot 2, is a key enzyme of the arginine deiminase pathway involved in the anaerobic metabolism of arginine (Vander Wauven *et al.*, 1984). In GABA-treated bacteria, the ornithine carbamoyltransferase was markedly repressed, whereas that of the three other proteins, a putative peroxidase, an alkyl hydroperoxide reductase and a USP-like protein, were upregulated. As for other enzymes of this family, the putative peroxidase over-expressed in the presence of GABA (spot 4) should be implicated in the removal of toxic peroxides. The alkyl hydroperoxide reductase, identified as spot 5, is essential for optimal resistance of *P. aeruginosa* to organic hydroperoxides and has an important protective role against oxidative stress (Ochsner *et al.*, 2000). The hypothetical USP-like protein PA3309 is overproduced during pyruvate fermentation and in anaerobic/aerobic stationary phases (Schreiber *et al.*, 2006). An effect of GABA on the oxidative metabolism of *P. aeruginosa* could also explain the increase in HCN observed in the present study, since cyanogenesis requires a reduced level of free oxygen (Castric *et al.*, 1981).

In *P. aeruginosa*, cyanogenesis is regulated by quorum sensing. The *hcnABC* genes encoding HCN synthases are controlled by LasR and RhlR, respectively, which are involved in the regulation of 3oxoC12-HSL and C4-HSL synthesis (Schuster & Greenberg, 2006). In agreement with this, in GABA-treated *P. aeruginosa* we observed a significant increase in 3oxoC12-HSL formation and a marginal variation in the C4-HSL kinetics. Conversely, the production of PQS, whose synthesis is also under the control of the two acylhomoserine lactones (Schuster & Greenberg, 2006), was not affected by GABA. This is also in agreement with the absence of any effect of GABA on pyoverdin production, which, through PqsE, is regulated by PQS (Diggle *et al.*, 2006). The action of GABA on *P. aeruginosa* is then fundamentally different from other Gram-negative bacteria such as *Agrobacterium tumefaciens*, where GABA provokes a decrease in acylhomoserine lactone synthesis and a reduction in virulence (Chevrot *et al.*, 2006).

To our knowledge, this is the first demonstration that GABA can regulate *P. aeruginosa* virulence. We show that a low concentration of exogenous GABA triggers an increase in virulence of *P. aeruginosa* due to a stimulation of cyanogenesis associated with a reduction in oxygen accessibility and an overexpression of oxygen-scavenging proteins. This mechanism is regulated by quorum sensing.

GABA also promotes specific changes in the expression of thermostable and unstable elongation factors involved in the interaction of the bacterium with the host proteins. As GABA is a widespread molecule, these observations should be taken into consideration in agricultural, veterinary and medical practices.

ACKNOWLEDGEMENTS

This study was supported by grants from the Conseil Général de l'Eure, the Communauté d'Agglomération d'Evreux and Europe (FEDER no. 31970). The Laboratory of Microbiology Signals and Microenvironment is a member of the PFT Normandie Sécurité Sanitaire, of the Institute for Research and Innovation in Biotechnologies (IRIB) and of the first perfumery-cosmetic worldwide network Cosmetic Valley. A.D. was a recipient of a grant from the French Ministry of Research (MRE). The authors are grateful to Christine Farmer for linguistic support. The authors thank student trainees Carole Casier (Rouen IUT) and Maxime Heude (Caen IUT) for HCN and PQS analysis.

REFERENCES

- Aballay, A. & Ausubel, F. M. (2002).** *Caenorhabditis elegans* as a host for the study of host-pathogen interactions. *Curr Opin Microbiol* **5**, 97–101.
- Angulo, M. C., Le Meur, K., Kozlov, A. S., Charpak, S. & Audinat, E. (2008).** GABA, a forgotten gliotransmitter. *Prog Neurobiol* **86**, 297–303.
- Barbey, C., Crépin, A., Cirou, A., Budin-Verneuil, A., Orange, N., Feuilloley, M., Faure, D., Dessaix, Y., Burini, J.-F. & Latour, X. (2012).** Catabolic pathway of gamma-caprolactone in the biocontrol agent *Rhodococcus erythropolis*. *J Proteome Res* **11**, 206–216.
- Bellon-Fontaine, M. N., Rault, J. & Van Oss, C. J. (1996).** Microbial adhesion to solvents: a novel method to determine the electron-donor/electron-acceptor or Lewis acid-base properties of microbial cells. *Colloids Surf B Biointerfaces* **7**, 47–53.
- Blier, A.-S., Veron, W., Bazire, A., Gérault, E., Taupin, L., Vieillard, J., Rehel, K., Dufour, A., Le Derf, F. & other authors (2011).** C-type natriuretic peptide modulates quorum sensing molecule and toxin production in *Pseudomonas aeruginosa*. *Microbiology* **157**, 1929–1944.
- Blier, A. S., Vieillard, J., Gerault, E., Dagorn, A., Varacavoudin, T., Le Derf, F., Orange, N., Feuilloley, M. & Lesouhaitier, O. (2012).** Quantification of *Pseudomonas aeruginosa* hydrogen cyanide production by a polarographic approach. *J Microbiol Methods* **90**, 20–24.
- Bouché, N., Lacombe, B. & Fromm, H. (2003).** GABA signaling: a conserved and ubiquitous mechanism. *Trends Cell Biol* **13**, 607–610.
- Brechtel, C. E. & King, S. C. (1998).** 4-Aminobutyrate (GABA) transporters from the amine-polyamine-choline superfamily: substrate specificity and ligand recognition profile of the 4-aminobutyrate permease from *Bacillus subtilis*. *Biochem J* **333**, 565–571.
- Carrillo, P. G., Mardaraz, C., Pitta-Alvarez, S. I. & Giulietti, A. M. (1996).** Isolation and selection of biosurfactant-producing bacteria. *J Microbiol Biotechnol* **12**, 82–84.
- Castric, K. F., McDevitt, D. A. & Castric, P. A. (1981).** Influence of aeration on hydrogen cyanide biosynthesis by *Pseudomonas aeruginosa*. *Curr Microbiol* **5**, 223–226.
- Chevrot, R., Rosen, R., Haudecoeur, E., Cirou, A., Shelp, B. J., Ron, E. & Faure, D. (2006).** GABA controls the level of quorum-sensing signal in *Agrobacterium tumefaciens*. *Proc Natl Acad Sci U S A* **103**, 7460–7464.

- Chou, H. T., Kwon, D. H., Hegazy, M. & Lu, C. D. (2008).** Transcriptome analysis of agmatine and putrescine catabolism in *Pseudomonas aeruginosa* PAO1. *J Bacteriol* **190**, 1966–1975.
- Darveau, R. P. & Hancock, R. E. (1983).** Procedure for isolation of bacterial lipopolysaccharides from both smooth and rough *Pseudomonas aeruginosa* and *Salmonella typhimurium* strains. *J Bacteriol* **155**, 831–838.
- de Bruijn, I., de Kock, M. J., Yang, M., de Waard, P., van Beek, T. A. & Raaijmakers, J. M. (2007).** Genome-based discovery, structure prediction and functional analysis of cyclic lipopeptide antibiotics in *Pseudomonas* species. *Mol Microbiol* **63**, 417–428.
- Déziel, E., Lépine, F., Milot, S. & Villemur, R. (2000).** Mass spectrometry monitoring of rhamnolipids from a growing culture of *Pseudomonas aeruginosa* strain 57RP. *Biochim Biophys Acta* **1485**, 145–152.
- Diggle, S. P., Cornelis, P., Williams, P. & Cámará, M. (2006).** 4-quinolone signalling in *Pseudomonas aeruginosa*: old molecules, new perspectives. *Int J Med Microbiol* **296**, 83–91.
- Duclairoir Poc, C., Groboillot, A., Lesouhaitier, O., Morin, J.-P., Orange, N. & Feuilloley, M. J. (2011).** *Caenorhabditis elegans*: a model to monitor bacterial air quality. *BMC Res Notes* **4**, 503.
- Fothergill, J. L., Winstanley, C. & James, C. E. (2012).** Novel therapeutic strategies to counter *Pseudomonas aeruginosa* infections. *Expert Rev Anti Infect Ther* **10**, 219–235.
- Gaines, J. M., Cartt, N. L., Colmer-Hamood, J. A. & Hamood, A. N. (2005).** Effect of static growth and different levels of environmental oxygen on *toxA* and *ptxR* expression in the *Pseudomonas aeruginosa* strain PAO1. *Microbiology* **151**, 2263–2275.
- Gallagher, L. A. & Manoil, C. (2001).** *Pseudomonas aeruginosa* PAO1 kills *Caenorhabditis elegans* by cyanide poisoning. *J Bacteriol* **183**, 6207–6214.
- Goure, J., Pastor, A., Faudry, E., Chabert, J., Dessen, A. & Attree, I. (2004).** The V antigen of *Pseudomonas aeruginosa* is required for assembly of the functional PopB/PopD translocation pore in host cell membranes. *Infect Immun* **72**, 4741–4750.
- Guthrie, G. D. & Nicholson-Guthrie, C. S. (1989).** gamma-Aminobutyric acid uptake by a bacterial system with neurotransmitter binding characteristics. *Proc Natl Acad Sci U S A* **86**, 7378–7381.
- Guthrie, G. D., Nicholson-Guthrie, C. S. & Leary, H. L., Jr (2000).** A bacterial high-affinity GABA binding protein: isolation and characterization. *Biochem Biophys Res Commun* **268**, 65–68.
- Hiemenz, P. C. & Lagowski, J. J. (1977).** *Principles of Colloid and Surface Chemistry*, p. 209. New York: Marcel Dekker Ed.
- Higuchi, T., Hayashi, H. & Abe, K. (1997).** Exchange of glutamate and gamma-aminobutyrate in a *Lactobacillus* strain. *J Bacteriol* **179**, 3362–3364.
- Høiby, N., Ciofu, O. & Bjarnsholt, T. (2010).** *Pseudomonas aeruginosa* biofilms in cystic fibrosis. *Future Microbiol* **5**, 1663–1674.
- Hu, L. A. & King, S. C. (1998).** Membrane topology of the *Escherichia coli* γ -aminobutyrate transporter: implications on the topography and mechanism of prokaryotic and eukaryotic transporters from the APC superfamily. *Biochem J* **336**, 69–76.
- Jin, Z., Mendu, S. K. & Birnir, B. (2011).** GABA is an effective immunomodulatory molecule. *Amino Acids*.
- Johnson, C. R., Muir, D. G. & Reysenbach, A. L. (1991).** Characteristic bacteria associated with surfaces of coralline algae: a hypothesis for bacterial induction of marine invertebrate larvae. *Mar Ecol Prog Ser* **74**, 281–294.
- Kunert, A., Losse, J., Gruszin, C., Hühn, M., Kaendler, K., Mikkat, S., Volke, D., Hoffmann, R., Jokiranta, T. S. & other authors (2007).** Immune evasion of the human pathogen *Pseudomonas aeruginosa*: elongation factor Tuf is a factor H and plasminogen binding protein. *J Immunol* **179**, 2979–2988.
- Mesaros, N., Nordmann, P., Plésiat, P., Roussel-Delvallez, M., Van Eldere, J., Glupczynski, Y., Van Laethem, Y., Jacobs, F., Lebecque, P. & other authors (2007).** *Pseudomonas aeruginosa*: resistance and therapeutic options at the turn of the new millennium. *Clin Microbiol Infect* **13**, 560–578.
- Meyer, J. M., Neely, A., Stintzi, A., Georges, C. & Holder, I. A. (1996).** Pyoverdin is essential for virulence of *Pseudomonas aeruginosa*. *Infect Immun* **64**, 518–523.
- Mezghani-Abdelmoula, S., Khémiri, A., Lesouhaitier, O., Chevalier, S., Orange, N., Cazin, L. & Feuilloley, M. G. J. (2004).** Sequential activation of constitutive and inducible nitric oxide synthase (NOS) in rat cerebellar granule neurons by *Pseudomonas fluorescens* and invasive behaviour of the bacteria. *Microbiol Res* **159**, 355–363.
- Morin, D., Grasland, B., Vallée-Réhel, K., Dufau, C. & Haras, D. (2003).** On-line high-performance liquid chromatography-mass spectrometric detection and quantification of *N*-acylhomoserine lactones, quorum sensing signal molecules, in the presence of biological matrices. *J Chromatogr A* **1002**, 79–92.
- Morse, D. E., Duncan, H., Hooker, N., Baloun, A. & Young, G. (1980).** GABA induces behavioral and developmental metamorphosis in planktonic molluscan larvae. *Fed Proc* **39**, 3237–3241.
- Mozrzymas, J. W., Zarnowska, E. D., Pytel, M. & Mercik, K. (2003).** Modulation of GABA_A receptors by hydrogen ions reveals synaptic GABA transient and a crucial role of the desensitization process. *J Neurosci* **23**, 7981–7992.
- O'Toole, G. A. & Kolter, R. (1998).** Flagellar and twitching motility are necessary for *Pseudomonas aeruginosa* biofilm development. *Mol Microbiol* **30**, 295–304.
- Ochsner, U. A., Vasil, M. L., Alsabbagh, E., Parvatiyar, K. & Hassett, D. J. (2000).** Role of the *Pseudomonas aeruginosa oxyR-recG* operon in oxidative stress defense and DNA repair: OxyR-dependent regulation of *katB-ankB*, *ahpB*, and *ahpC-ahpF*. *J Bacteriol* **182**, 4533–4544.
- Ostroff, R. M., Wretlind, B. & Vasil, M. L. (1989).** Mutations in the hemolytic-phospholipase C operon result in decreased virulence of *Pseudomonas aeruginosa* PAO1 grown under phosphate-limiting conditions. *Infect Immun* **57**, 1369–1373.
- Owens, D. F. & Kriegstein, A. R. (2002).** Is there more to GABA than synaptic inhibition? *Nat Rev Neurosci* **3**, 715–727.
- Palanivelu, R., Brass, L., Edlund, A. F. & Preuss, D. (2003).** Pollen tube growth and guidance is regulated by POP2, an *Arabidopsis* gene that controls GABA levels. *Cell* **114**, 47–59.
- Petty, F., Fulton, M., Kramer, G. L., Kram, M., Davis, L. L. & Rush, A. J. (1999).** Evidence for the segregation of a major gene for human plasma GABA levels. *Mol Psychiatry* **4**, 587–589.
- Picot, L., Abdelmoula, S. M., Merieau, A., Leroux, P., Cazin, L., Orange, N. & Feuilloley, M. G. J. (2001).** *Pseudomonas fluorescens* as a potential pathogen: adherence to nerve cells. *Microbes Infect* **3**, 985–995.
- Picot, L., Chevalier, S., Mezghani-Abdelmoula, S., Merieau, A., Lesouhaitier, O., Leroux, P., Cazin, L., Orange, N. & Feuilloley, M. G. J. (2003).** Cytotoxic effects of the lipopolysaccharide from *Pseudomonas fluorescens* on neurons and glial cells. *Microb Pathog* **35**, 95–106.
- Picot, L., Mezghani-Abdelmoula, S., Chevalier, S., Merieau, A., Lesouhaitier, O., Guerillon, J., Cazin, L., Orange, N. & Feuilloley, M. G. J. (2004).** Regulation of the cytotoxic effects of *Pseudomonas fluorescens* by growth temperature. *Res Microbiol* **155**, 39–46.
- Richard, H. T. & Foster, J. W. (2003).** Acid resistance in *Escherichia coli*. *Adv Appl Microbiol* **52**, 167–186.

- Rashid, M. H. & Kornberg, A. (2000).** Inorganic polyphosphatase is needed for swimming, swarming and twitching motilities of *Pseudomonas aeruginosa*. *Proc Natl Acad Sci U S A* **97**, 4885–4890.
- Schreiber, K., Boes, N., Eschbach, M., Jaensch, L., Wehland, J., Bjarnsholt, T., Givskov, M., Hentzer, M. & Schobert, M. (2006).** Anaerobic survival of *Pseudomonas aeruginosa* by pyruvate fermentation requires an Usp-type stress protein. *J Bacteriol* **188**, 659–668.
- Schuster, M. & Greenberg, E. P. (2006).** A network of networks: quorum-sensing gene regulation in *Pseudomonas aeruginosa*. *Int J Med Microbiol* **296**, 73–81.
- Shelp, B. J., Bown, A. W. & McLean, M. D. (1999).** Metabolism and functions of gamma-aminobutyric acid. *Trends Plant Sci* **4**, 446–452.
- Shelp, B. J., Bown, A. W. & Faure, D. (2006).** Extracellular gamma-aminobutyrate mediates communication between plants and other organisms. *Plant Physiol* **142**, 1350–1352.
- Siragusa, S., De Angelis, M., Di Cagno, R., Rizzello, C. G., Coda, R. & Gobbetti, M. (2007).** Synthesis of gamma-aminobutyric acid by lactic acid bacteria isolated from a variety of Italian cheeses. *Appl Environ Microbiol* **73**, 7283–7290.
- Tunnicliff, G. & Malatyńska, E. (2003).** Central GABAergic systems and depressive illness. *Neurochem Res* **28**, 965–976.
- van Delden, C. (2007).** *Pseudomonas aeruginosa* bloodstream infections: how should we treat them? *Int J Antimicrob Agents* **30** (Suppl. 1), S71–S75.
- Vander Wauven, C., Piérard, A., Kley-Raymann, M. & Haas, D. (1984).** *Pseudomonas aeruginosa* mutants affected in anaerobic growth on arginine: evidence for a four-gene cluster encoding the arginine deiminase pathway. *J Bacteriol* **160**, 928–934.
- Veron, W., Lesouhaitier, O., Pennanec, X., Rehel, K., Leroux, P., Orange, N. & Feuilloley, M. G. J. (2007).** Natriuretic peptides affect *Pseudomonas aeruginosa* and specifically modify lipopolysaccharide biosynthesis. *FEBS J* **274**, 5852–5864.
- Williams, P. L., Anderson, G. L., Johnstone, J. L., Nunn, A. D., Tweedle, M. F. & Wedeking, P. (2000).** *Caenorhabditis elegans* as an alternative animal species. *J Toxicol Environ Health A* **61**, 641–647.
- Wittinghofer, A., Guariguata, R. & Leberman, R. (1983).** Bacterial elongation factor Ts: isolation and reactivity with elongation factor Tu. *J Bacteriol* **153**, 1266–1271.
- Wolf, P. & Elsässer-Beile, U. (2009).** *Pseudomonas* exotoxin A: from virulence factor to anti-cancer agent. *Int J Med Microbiol* **299**, 161–176.

Edited by: W. J. Quax

P17

Accepted Manuscript

Title: Investigation of the release of PAHs from artificially contaminated sediments using cyclolipopeptidic biosurfactants

Author: F. Portet-Koltalo M.T. Ammami A. Benamar H. Wang F. Le Derf C. Duclairoir-Poc



PII: S0304-3894(13)00541-4

DOI: <http://dx.doi.org/doi:10.1016/j.jhazmat.2013.07.062>

Reference: HAZMAT 15287

To appear in: *Journal of Hazardous Materials*

Received date: 17-4-2013

Revised date: 15-7-2013

Accepted date: 26-7-2013

Please cite this article as: F. Portet-Koltalo, M.T. Ammami, A. Benamar, H. Wang, F. Le Derf, C. Duclairoir-Poc, Investigation of the release of PAHs from artificially contaminated sediments using cyclolipopeptidic biosurfactants, *Journal of Hazardous Materials* (2013), <http://dx.doi.org/10.1016/j.jhazmat.2013.07.062>

This is a PDF file of an unedited manuscript that has been accepted for publication. As a service to our customers we are providing this early version of the manuscript. The manuscript will undergo copyediting, typesetting, and review of the resulting proof before it is published in its final form. Please note that during the production process errors may be discovered which could affect the content, and all legal disclaimers that apply to the journal pertain.

1 **Investigation of the release of PAHs from artificially contaminated sediments using**
2 **cyclolipopeptidic biosurfactants**

3

4 F. Portet-Koltalo^{a,*}, M.T. Ammami^{a,b}, A. Benamar^b, H. Wang^b, F. Le Derf^a, C. Duclairoir-
5 Poc^c

6

7 a COBRA UMR CNRS 6014, Université de Rouen, 55 rue Saint Germain, 27000 Evreux,
8 France.

9 florence.koltalo@univ-rouen.fr; franck.lederf@univ-rouen.fr

10 b Laboratoire Ondes et Milieux Complexes, UMR CNRS 6294, Université du Havre, 53 rue
11 de Prony, 76600 le Havre, France.

12 ahmed.benamar@univ-lehavre.fr; mohamed-tahar.ammami@etu.univ-lehavre.fr;
13 huaqing.wang@univ-lehavre.fr

14 c Laboratoire de Microbiologie Signaux et Microenvironnement, EA 4312, Université de
15 Rouen, 55 rue Saint Germain, 27000 Evreux, France.

16 cecile.poc@univ-rouen.fr

17

18

19 * Corresponding author: F. Portet-Koltalo

20 florence.koltalo@univ-rouen.fr; Tel.: +33-232-291-535; Fax: +33-232-291-539.

21

21

22 **Abstract**

23

24 Polycyclic aromatic hydrocarbons (PAHs) can be preponderant in contaminated sediments
25 and understanding how they are sorbed in the different mineral and organic fractions of the
26 sediment is critical for effective removal strategies. For this purpose, a mixture of seven
27 PAHs was studied at the sediment/water interface and sorption isotherms were obtained. The
28 influence of various factors on the sorption behavior of PAHs was evaluated, such as the
29 nature of minerals, pH, ionic strength and amount of organic matter. Afterwards, the release
30 of PAHs from the sediment by surfactants was investigated. The effectiveness of sodium
31 dodecyl sulfate (SDS) was compared to natural biosurfactants, of cyclolipopeptidic type
32 (amphisin and viscosin-like mixture), produced by two *Pseudomonas fluorescens* strains. The
33 desorption of PAHs (from naphthalene to pyrene), from the highly retentive kaolinite fraction,
34 could be favored by adding SDS or amphisin, but viscosin-like biosurfactants were only
35 effective for 2-3 ring PAHs desorption (naphthalene to phenanthrene). Moreover, while SDS
36 favors the release of all the target PAHs from a model sediment containing organic matter, the
37 two biosurfactants tested were only effective to desorb the lowest molecular weight PAHs
38 (naphthalene to fluorene).

39

40 **Keywords**

41 Polycyclic aromatic hydrocarbons; PAHs release; Biosurfactants; Sorption isotherms;
42 Water/sediment interface

43

43 **1. Introduction**

44

45 Contaminated bottom sediments in rivers and harbors are a significant problem because of the
46 potential risks generated for aquatic organisms, wildlife, and humans. Among the
47 contaminants that can pose threats to small organisms, polycyclic aromatic hydrocarbons
48 (PAHs) are a group of organic compounds which are persistent, toxic, and are known to be
49 potential carcinogens or mutagens [1]. Sediments act as temporary or long-term sinks for this
50 class of pollutants [2, 3]. The properties of sediments differ significantly from those of soils.
51 Indeed, sediments are heterogeneous materials which are characterized by a high proportion
52 of fine particles compared to soils with also a high proportion of organic matter and water
53 content. For these reasons, decontamination methods similar to those used for soils (such as
54 soil washing) are not suitable to all types of sediments, particularly to fine-grained sediments
55 where pollutants accumulate [4]. Among different alternatives (such as bioremediation [5]),
56 electrokinetic (EK) remediation is promising for low permeability sediments. This technology
57 involves applying a low intensity electric current between two electrodes imbedded in the
58 sediment. This remediation process is limited when pollutants are nonionic and with a low
59 aqueous solubility, which is the case of PAHs [6]. Consequently, to improve decontamination
60 processes such as EK remediation, it is necessary to enhance PAH desorption from fine
61 sediment particles, and also to create a favorable environment to facilitate migration towards
62 the electrode chambers.

63 Tensioactive compounds have been shown to enhance the mobilization and solubilization of
64 PAHs from contaminated soils [7, 8]. Surfactants are amphiphilic compounds which enhance
65 the apparent solubility of the lipophilic contaminants through micellar solubilization.
66 Desirable surfactant characteristics include low surface tension, low critical micellar
67 concentration (CMC), but also low adsorption to soil or sediment. Anionic surfactants are less

likely to be adsorbed by soil particles than nonionic or cationic ones [9]. But some degradability is also required to avoid accumulation during the remediation processes. Biosurfactants, which are biologically produced from yeast or bacteria, are potentially more biodegradable and less toxic than synthetic surfactants [10]. Biosurfactants are particularly promising for enhanced remediation of soils contaminated by organic components [11, 12]. Indeed, it has been shown that biosurfactants act to enhance the process of pseudosolubilization/emulsification thereby increasing the availability of organic compounds to microbial cells in bioremediation processes [13]. Although synthetic surfactants have been more extensively studied for enhanced electrokinetic remediation of PAHs [14, 15], biosurfactants also have an interesting potential to help in EK sediment decontamination [16]. The aim of this study was to evaluate for the first time the potential of two biosurfactants of cyclolipopeptidic (CLP) type (amphisin and viscosin-like CLPs) to desorb PAHs from artificially contaminated model sediment. Indeed, a majority of studies deals with biosurfactants such as rhamnolipids [17, 18] and lipopeptides are far less studied [19, 20]. The final objective (not reported here) is to enhance the decontamination of sediments by an EK process. This paper describes first batch suspension experiments, conducted to determine the extent to which representative sediment components contribute to PAHs sorption. Sorption isotherms of a mixture of PAHs were obtained simultaneously, at trace levels, thanks to a liquid chromatographic method (HPLC) combined to a trace concentration procedure by solid phase extraction (SPE). Afterwards, three anionic surfactants were tested to enhance the aqueous solubilization of PAHs from kaolinite and from a more complex model sediment containing organic matter. A synthetic surfactant, sodium dodecyl sulfate (SDS), was compared to cyclolipopeptidic biosurfactants produced by two *Pseudomonas fluorescens* strains.

92

93 **2. Materials and methods**

94

95 **2.1. Materials and chemicals**

96

97 **2.1.1. Solvents and contaminants**

98 Acetonitrile, methylene chloride, acetone, hexane (of HPLC grade), trifluoroacetic acid
99 (TFA), dimethylsulfoxide, SDS and sodium chloride were purchased from Fisher Scientific
100 (Illkirsh, France).

101 A mixture of 15 PAHs (purchased from Sigma-Aldrich-St Quentin Fallavier, France),
102 containing 2- to 6-ring PAHs and considered as priority pollutants by the American
103 Environmental Protection Agency, was prepared in acetonitrile ($20 \mu\text{g mL}^{-1}$).

104 The model sediment was made in order to mimic the mineralogy of natural sediment collected
105 from a disposal site managed by a Norman harbor (France). It contained 5% silica sand
106 (particle diameter $\text{dp}=125\text{-}315 \mu\text{m}$) from Sika (Hostun, France), 75% quartz silt ($\text{dp}=4\text{-}100$
107 μm) collected from surface formations covering the chalk plateau in Normandy (Rouen,
108 France) and 20% kaolinite ($\text{dp}<80 \mu\text{m}$, with 54% of particles less than $2 \mu\text{m}$) from Imerys
109 (Poigny, France). Organic matter (OM) was added to this model sediment: it was kindly
110 provided by Veolia (France). OM was obtained from the decomposition of a vegetable
111 material, which was dried for 48h at 50°C , crushed and sieved to $355 \mu\text{m}$.

112

113 **2.1.2. Production and purification of biosurfactants**

114 Bacteria *P. fluorescens* DSS73 and *P. fluorescens* PfA7B were grown on Davis minimal agar
115 culture plates, as described in a previous paper [21]. After incubation for 14 days at 17°C
116 [22], colonies were scrapped off, transferred to sterile water and centrifuged 30 minutes at
117 $18000\times g$. The biosurfactant purification was slightly modified compared to a previous work

118 [21]: 100 mL of the aqueous supernatant (containing 6×10^{-3} mol.L⁻¹ TFA) was put in contact
119 and agitated one hour with 80 mL methylene chloride and then transferred into a separatory
120 funnel. Amphisin, produced by *P. fluorescens* DSS73, was extracted three times from each
121 aqueous fraction while viscosin-like mixture, produced by *P. fluorescens* PfA7B, was
122 extracted five times. After collection and evaporation of all the organic phases with a rotary
123 evaporator, concentrated extracts were freeze dried [21].

124

125 2.2. Analytical procedures

126

127 2.2.1. Biosurfactant characterization

128 Purified biosurfactants were analyzed by liquid chromatography (Beckman Coulter, Fullerton,
129 USA), on a C₁₈ bonded column from Beckman (4.6 mm i.d., d_p=5 µm and 250 mm length),
130 using a mobile phase composed of 40% water (with 0.1% TFA) and 60% acetonitrile, at 1
131 mL.min⁻¹ and with a UV detection at 206 nm. The production of *P. fluorescens* DSS73 was
132 composed of one majority CLP, named amphisin, consisting in a lyophilic chain and 11
133 amino acids (Table 1). The production of *P. fluorescens* PfA7B was composed of a mixture
134 made of two majority CLPs (viscosin-like biosurfactants), composed of a lyophilic chain and
135 polar parts containing 9 amino acids (Table 1) [22].

136 The critical micellar concentrations (CMC) of purified biosurfactants and surface tension
137 measurements were made on a tensiometer DSA30 (Krüss, Germany).

138

139 2.2.2. Sorption isotherms

140

141 2.2.2.1. Analysis of PAHs by HPLC-FLD

142 Aqueous samples containing PAHs were analyzed by HPLC using a fluorimetric (FLD)
143 detector Prostar 363 (Varian, Palo Alto, USA). 20 µL of samples were injected into a C₁₈
144 Envirosep PP column (150x4.6 mm, d_p=5 µm) purchased from Phenomenex (le Pecq,
145 France), with a flow-rate of 1 mL·min⁻¹. The mobile phase program was composed of
146 acetonitrile and water 55/45% (v/v) for 5 minutes, followed by a gradient for 20 minutes to
147 finish by 100% acetonitrile. Optimal fluorescence excitation and emission wavelengths were
148 chosen for each PAH to obtain a sensitive detection, and the limits of detection (LOD) and
149 quantification (LOQ) were evaluated (Table 2).

150

151 *2.2.2.2. Trace enrichment by SPE*

152 A trace enrichment procedure by SPE (solid phase extraction) was developed for PAHs
153 remaining in the aqueous phase after sorption experiments. 60 mg SPE cartridges (Strata X,
154 Phenomenex) were used, coupled with PTFE Phenex filters (0.45 µm) (Phenomenex). SPE
155 cartridges were conditioned with 8 mL acetone and 10 mL of a mixture acetone/water 20/80%
156 (v/v). After adding 20% acetone in volume to the aqueous medium containing PAHs, it was
157 passed through the SPE cartridge, which was finally rinsed with 10 mL of pure water. Then
158 the cartridge was dried and PAHs were eluted with 5 mL of methylene chloride. After adding
159 60 µL of dimethylsulfoxide, methylene chloride was evaporated under nitrogen flow and
160 solutes were solubilized again in acetonitrile, before injection in the HPLC system. The
161 complete procedure filtration-SPE-HPLC-FLD was evaluated on 20-100 mL aqueous samples
162 spiked with a PAH test solution at 10 µg·L⁻¹. Mean recoveries of each PAH ranged from
163 82.0±3.9% to 94.2±1.2%, which was satisfactory (Table 2).

164

165 *2.2.2.3. Batch adsorption experiments*

166 The sorption experiments were carried out using a sediment/solution ratio of 1/9 (w/w), which
167 represents a solid mass concentration $C_{\text{sed}} = 0.111 \text{ kg.L}^{-1}$. Mixtures were placed in a bath at
168 25°C (Fisher Bioblock Scientific, Illkirch, France), under agitation (250 rpm). PAH addition
169 in bottles was performed at known initial concentration ($C_o (\mu\text{g.L}^{-1})$) from a stock solution of 15
170 PAHs, mimicking the diversity of PAHs in the natural environment. After incubating the
171 samples for 24h, the bottles were centrifuged and the aqueous supernatant discarded.
172 Concentrations of PAHs remaining at equilibrium in the aqueous phase ($C_{\text{eq}} (\mu\text{g.L}^{-1})$) were
173 determined as described previously (section 2.2.2.2), with SPE concentration factors of
174 approximately 20 to 40. The concentration of sorbed PAHs ($C_{\text{ads}} (\mu\text{g.L}^{-1})$) was obtained from the
175 difference between C_o and C_{eq} . Sorption isotherms at 25°C were then established in varying
176 C_o and plotting $C_{\text{ads}} (\mu\text{g.kg}^{-1}) = f(C_{\text{eq}})$, with $C_{\text{ads}} (\mu\text{g.kg}^{-1}) = C_{\text{ads}} (\mu\text{g.L}^{-1}) / C_{\text{sed}} (\text{kg.L}^{-1})$. C_{ads} represents the
177 quantity of PAH sorbed per kg of sediment. The initial solute concentrations C_o were selected
178 to yield aqueous concentrations remaining at equilibrium distributed over a wide
179 concentration range. However, the water solubility of high molecular weight PAHs
180 ($M > 202.26 \text{ g.mol}^{-1}$) was, in many cases, lower than the desired initial concentration. So, in
181 the mass balance, precipitation of high molecular weight PAHs may contribute to the
182 immobilization of those PAHs and we cannot consider it as a sorption phenomenon.
183 Consequently, sorption isotherms and desorption by biosurfactants were studied only for the
184 seven more soluble PAHs, from naphthalene to pyrene ($M < 202.26 \text{ g.mol}^{-1}$) (Table 2).
185 The variability of the complete process (sorption-filtration-SPE enrichment-quantification by
186 HPLC-FLD) was evaluated from five experiments and Table 3 shows that sorption
187 experiments were relatively reproducible, even at very low aqueous concentrations.

188

189 *2.2.2.4. Sorption isotherms modeling*

190 The linear Henry's model for sorption isotherms was described by equation (1):

$$C_{ads} = K_d \times C_{eq} \quad (1)$$

192 Where K_d is the distribution (or partition) coefficient between the solid and the liquid phases.

193 The equation (2) of the empirical Freundlich model was expressed as:

$$C_{ads} = K_F \times C_{eq}^{1/n} \quad (2)$$

195 Where K_F is the Freundlich constant and $1/n$ is the heterogeneity factor. Finally, the
 196 monolayer Langmuir isotherm was described by the equation (3):

$$\frac{1}{C_{ads}} = \frac{1}{C_{max}} + \frac{1}{C_{max} \times K_L} \times \frac{1}{C_{eq}}$$

198 Where K_L is the Langmuir constant and C_{max} is the maximum sorption capacity of the sorbent.

200 3. Results and discussion

201

202 3.1. Sorption isotherms of PAHs on artificial sediments

203

204 Sediments are composed of particles of sand, clays, silts and of organic matter (OM).

205 According to their classification based on the grain size, stones or gravels are differentiated

from the finest particles, such as sands (diameter ranging from 50 to 2000 μm), silts (2–50

207 μm) and clays (diameter less than $2 \mu\text{m}$) (French standard NF P18-105). So, these three main

208 mineral components were tested as sorbents for PAHs. As PAHs are hydrophobic organic

209 contaminants with low aqueous solubility they were strongly sorbed onto particles. Fig. 1

210 shows the sorption isotherms of three of the seven studied PAHs (as examples). As mentioned

in section 2.2.2.3, only low molecular weight PAHs ($128.18 \text{ g mol}^{-1}$ ($M_r = 202.26 \text{ g mol}^{-1}$))

215 concentration levels were associated with the largest size fractions of harbor sediments, but
216 this result was linked to a higher association of OM with larger particles. In this reported case,
217 OM was responsible for the strongest sorption rather than the mineral particle size [23]. In our
218 study, it is clear that kaolinite is the strongest sorbent when no OM enters the composition of
219 the material. Indeed, clay has the highest specific surface area with respect to volume ratio of
220 any particle size class. In contrast, sand shows a lower capacity to adsorb all PAHs on its
221 surface.

222 Experimental data were fitted using linear regressions according to a model based on Henry's
223 isotherms, and from linear forms of Langmuir and Freundlich isotherms (section 2.2.2.4).
224 Table 4 presents the optimum isotherms and parameters for the various inorganic constituents
225 in the model sediment. From the results, sorption of the target PAHs fit better with the
226 Freundlich model than with the Langmuir one. However, it must be noted that the linear
227 model was relatively appropriate for the PAHs in the studied concentration range, except for
228 the sand material. Indeed, the saturation of sites was observed for sand and not for silt or
229 kaolinite. Since they have low porosity, silicates do not constitute high adsorption sites for
230 nonionic compounds. As highlighted, we could observe for silt and kaolinite a nearly linear
231 shape at relatively low concentrations of PAHs. At these concentration levels, Henry's model
232 is generally sufficient to describe sorption phenomena [24]. The sorption of PAHs on silt or
233 kaolinite is predominantly controlled by a partitioning process, with the specific surface area
234 being the major controlling factor. Moreover, the structure of the pollutant is also crucial.
235 Indeed, fluoranthene (three aromatic rings and a five-membered ring) is more strongly
236 adsorbed than phenanthrene (three aromatic rings), which is itself more strongly adsorbed
237 than acenaphthene (two aromatic rings and an ethylene bridge) (Fig. 1). We can observe that
238 the heavier the PAH is, the higher the sorbent-PAH partition coefficient K_d is (Table 4). Since
239 sorbents tested here did not contain OM, these results could be explained by dispersive and

240 dipole-induced dipole interactions between mineral surfaces and PAH molecules, which are
241 stronger when the number of aromatic rings is higher.

242 The model sediment was a mixture of sand, silt and clay (section 2.1.1.), which was made to
243 mimic the mineral and particle size distribution of dredged harbor sediments collected from a
244 French disposal site. The best fit for the data, for this model sediment, was also obtained with
245 the Freundlich model (Table 4), which consequently described a sorption process of
246 physisorption type through heterogeneous sites. As can be seen in Fig. 1, the sorption
247 behavior of this model sediment was intermediary between pure silt and pure kaolinite
248 sorption behavior. Table 4 indicates that in the studied concentration range, the linear model
249 fit well also.

250 As natural sediments from the French Norman disposal site come from marine channels, they
251 can contain high amounts of salts. Moreover, if we consider electrokinetic remediation as a
252 potential process to decontaminate the dredged sediments, it is important to pay particular
253 attention to the pH of the aqueous medium since this remediation process is considered to be
254 more effective at an acidic pH for co-contaminants such as metals. Consequently, we studied
255 the influence of NaCl and pH on the PAH sorption on the model sediment. Fig. 2 illustrates
256 the sorption isotherms of fluorene and pyrene with or without NaCl, at acidic or neutral pH. It
257 emerged from the results that the value of pH and NaCl concentration did not significantly
258 influence the sorption of the seven target PAHs. This can be explained by the fact that PAHs
259 are nonionic molecules that are much less strongly influenced by pH and ionic strength
260 variations than ionic compounds.

261 Many studies have demonstrated that OM plays the most important role in the sorption of
262 PAHs in marine sediments [23]. It is why amorphous OM was added, in controlled
263 proportions, to the mineral fraction of the model sediment. Fig. 3 gives the sorption isotherms
264 of three of the target PAHs with various contents of OM. It is clear that the higher the OM

265 content is, the higher the sorption is. It can be noted that even a very low content of OM (1%)
 266 leads to a strong effect. Partition coefficients could be calculated from the linear model, and
 267 the organic carbon normalized sorption coefficient K_{oc} was evaluated thanks to the equation
 268 (4), where f_{oc} is the organic carbon fraction (Table 5):

269 $K_{oc} = K_d/f_{oc}$ (4)

270 The OM percent was converted to organic carbon (OC) by the well-known relationship
 271 (equation 5) [25]:

272 $(\% \text{OM}) = 1.727 \times (\% \text{OC})$ (5)

273 Wang et al [23] found values of $\log K_{oc}$ ranging from 4.12 to 6.07 for phenanthrene, from
 274 4.62 to 6.56 for fluoranthene, and from 4.68 to 5.5 for pyrene. In our case, $\log K_{oc}$ values
 275 were 4.28 and 4.33 for phenanthrene, 4.53 and 4.66 for fluoranthene, and 4.56 and 4.70 for
 276 pyrene (Table 5). These values were similar to the lowest values reported by Wang et al.
 277 Indeed, it must be remembered that OM introduced in our studied system was amorphous and
 278 was not completely mature. But natural mature bottom sediments include also a small
 279 condensed carbon part (soot, coal...) in which interactions are stronger [26]. Even if this
 280 condensed part is not predominant in proportion in carbonaceous matter, it contributes
 281 significantly to PAH sorption and can explain the highest values of $\log K_{oc}$ in many soils or
 282 sediments.

283 PAHs are characterized by high numerical values of K_{oc} (Table 5): they strongly sorb on
 284 carbonaceous matter and the interactions that occur are not polar. So OM plays a major role in
 285 sequestering PAHs and it is well known that when K_{oc} values are high, sorbed compounds
 286 are not easy to release.

287

288 3.2. Effect of synthetic and biological surfactants on PAH desorption

289

When organic decontamination of sediments must be done using technologies such as EK remediation, the first step of the process consists of promoting an increased desorption of PAHs by reducing interfacial tension between the water and the sediment and by increasing the apparent solubility of the contaminant in the aqueous phase [6, 27]. Synthetic but also biological surfactants have been already tested to desorb PAHs from soils and sediments. Pure kaolinite is often used as a model material to test the PAH removal enhancement by surfactants, because of its particular nature [15, 28, 29]: it contains very low fractions of OM and it has a very high specific surface area. Consequently, our first experiments, which aimed at understanding the surfactant enhanced removal of PAHs from the mineral part of the sediment, were carried out with kaolinite and three anionic surfactants. Amphisin, produced by *Pseudomonas fluorescens* DSS73 and viscosin-like biosurfactants, produced by *Pseudomonas fluorescens* PfA7B, are cyclolipopeptidic (CLP) biosurfactants (Table 1). Amphisin contains two aspartic acids in its polar moiety, whose pKa are 3.9 and massetolide E and viscosin contain a glutamic acid, whose pKa is 4.1. The CMC value of the viscosin-like mixture was 0.05 g.L^{-1} , which was lower than that of amphisin (0.3 g.L^{-1}) (Fig. 4). Moreover, amphisin made it possible to lower the surface tension of pure water from $68.4 \pm 0.9 \text{ mN.m}^{-1}$ to $33.5 \pm 0.3 \text{ mN.m}^{-1}$ ($n=10$ replicates) while surface tension was lowered to $24.7 \pm 0.1 \text{ mN.m}^{-1}$ ($n=10$) when using the viscosin-like mixture.

These biosurfactants were compared to the conventional synthetic SDS. Firstly, SDS and amphisin were tested near their CMC, at 2.5 g.L^{-1} for SDS ($\text{CMC}=2.3 \text{ g.L}^{-1}$) and 0.3 g.L^{-1} for amphisin. These surfactant concentrations did not allow any significant release of the PAHs. Indeed, even if anionic surfactants are less strongly retained on kaolinite than nonionic or cationic ones, due to the repulsive negative surface charges, they are partially sorbed on the mineral surface. Such surfactant losses increase the total surfactant concentration required to form micelles in the aqueous phase. Consequently, we can speak about an effective CMC

315 (CMC_{eff}) above which PAHs can solubilize in aqueous aggregates, with $\text{CMC}_{\text{eff}} > \text{CMC}$ [30].
316 It is why the biosurfactants and SDS were tested well above their CMC, in a second step, that
317 is ten times their CMC for SDS and for the mixture of viscosin-like CLPs. Amphisin was
318 tested at 1 g.L^{-1} because it was more difficult to produce high quantities of this biosurfactant.
319 Fig. 5 shows the sorption isotherms on kaolinite of three of the seven PAHs studied, when
320 adding SDS, amphisin or viscosin-like CLPs in the aqueous phase. Adding SDS or amphisin
321 led to a significant decrease of the sorption of all the PAHs on the clayey material. In the case
322 of viscosin-like CLPs, they only contributed to a decrease of the sorption of the 2-3 ring
323 PAHs, but not of pyrene (Fig. 5c). In a majority of cases, the sorption isotherms obtained
324 when adding SDS, amphisin or viscosin-like CLPs fit slightly better with the Langmuir model
325 (and no longer with the Freundlich one). It seems that adding surfactants well above their
326 CMC tended to decrease the heterogeneity of sorption sites on kaolinite for the seven studied
327 PAHs.
328 In fact, above its CMC, it has been demonstrated that SDS can form hemimicelles at the
329 kaolinite surface, with an orientation of the hydrophobic moieties in the aqueous phase [9,
330 31]. This phenomenon has also been shown for anionic biosurfactants such as bioemulsans or
331 rhamnolipids [32, 33]. The head-on sorption of biosurfactants or SDS, even if low, can also
332 promote the incorporation of lipophilic PAHs into the hemimicelles (so-called
333 adsolubilization phenomenon). Hence, the PAH retention process can be due to two
334 mechanisms: a partition into hemimicelles formed by the sorbed surfactants and a direct
335 adsorption to the heterogeneous surface sites of kaolinite. However, a greater interaction
336 between PAHs and aqueous surfactant micelles, than between PAHs and hemimicelles, occurs
337 at high PAH concentrations, leading to a partition of PAHs in favor of the aqueous medium
338 rather than of the kaolinite surface.

339 This mechanism of partial PAH desorption thanks to their incorporation into aqueous micelles
340 cannot completely explain all the cases when the viscosin-like CLPs are used. We observe
341 that the viscosin-like mixture actually helps to enhance the release of 2-3 ring PAHs
342 (naphthalene to anthracene) from the kaolinite (Fig. 5a and 5b are given as examples). Yet, it
343 is not effective for the 4-ring more apolar PAHs, fluoranthene and pyrene (Fig. 5c). We can
344 suppose that the mixture of massetolide E and viscosin is less polar than amphisin, since they
345 possess only one ionic amino acid while amphisin possesses two ionic amino acids in its polar
346 moiety. It has been shown that relatively more hydrophilic surfactants were more effective in
347 enhancing PAH desorption from soils containing high clay contents [34].

348 Next, we tested if biosurfactants or SDS were able to enhance PAH solubilization when OM
349 was introduced into the more complex model sediment. These experiments were carried out
350 with the sediment made of sand, silt, kaolin, 2.5% OM and with 10 g.L^{-1} NaCl, to mimic the
351 natural dredged sediment collected from a Norman harbor disposal site. Fig. 6 shows the
352 sorption behavior of three of the seven studied PAHs. It appears from Fig. 6a and 6b that if
353 we consider only PAHs of low molecular weight (from naphthalene to fluorene), amphisin
354 and viscosin-like CLPs have a favorable effect on PAH release from the model sediment.
355 Indeed, based on the linear part of the isotherms, distribution coefficients Kd were calculated
356 and, for acenaphthylene (as an example), Kd decreased from 129.8 L.kg^{-1} to 103.4 L.kg^{-1} and
357 64.7 L.kg^{-1} when adding respectively amphisin or viscosin-like CLPs. But their effect on
358 desorption is weaker than that of SDS (Kd was only 11.5 L.kg^{-1} for acenaphthylene) and
359 weaker in comparison to the effect produced from a pure kaolinite surface. However, unlike
360 SDS, the two biosurfactants were unable to enhance desorption of the higher molecular
361 weight PAHs (from phenanthrene to pyrene) from the sediment particles (Fig. 6c). For
362 example, for phenanthrene, Kd values did not vary significantly, from 304.3 L.kg^{-1} to 301.7 L.kg^{-1}
363 and 291.9 L.kg^{-1} when adding respectively amphisin or viscosin-like CLPs.

364 If we compare the kaolinite/water/SDS and sediment/water/SDS systems, it appears that
365 PAHs are more sorbed on the surface of pure kaolinite than on the model sediment, in the
366 presence of SDS (see Fig. 5a/6b and Fig. 5b/6c). For example, for phenanthrene, Kd value is
367 $81.8 \text{ L}.\text{kg}^{-1}$ for the kaolinite/water/SDS system and only $12.7 \text{ L}.\text{kg}^{-1}$ for the
368 sediment/water/SDS system. On the one hand, it has been shown that SDS is less sorbed on
369 the sandy and silty parts of the sediment than on pure kaolinite [31]. Consequently, SDS
370 forms fewer hemimicelles on the model sediment than on pure kaolinite, where PAHs can be
371 adsolubilized. On the other hand, it is likely that the presence of SDS decreases the direct
372 sorption of PAHs to OM. Indeed surfactant apolar tails compete for hydrophobic sorption
373 sites on the OM surface, the ionic head being exposed to the solution in this case [31]. Thus,
374 the phenomenon of adsolubilization of PAHs, in the presence of SDS, is weaker in the case of
375 a complex sediment containing OM than in the case of pure kaolinite. It must also be
376 observed that the incorporation of PAHs into SDS hemimicelles formed at the sediment
377 surface is not really affected by PAHs structures, since Kd values are nearly the same from
378 naphthalene to pyrene (for example, $12.6 \text{ L}.\text{kg}^{-1}$ for fluorene and $13.1 \text{ L}.\text{kg}^{-1}$ for pyrene).
379 Concerning the effect of viscosin-like CLPs, it is clear that even if they were introduced at
380 levels which are ten times their CMC in the sediment/water system (like SDS), they do not
381 contribute to change the sorption of the higher weight PAHs (from phenanthrene to pyrene)
382 (Fig. 6c). And, for all the PAHs (even the lowest), the sorption is always higher on the model
383 sediment than on the pure kaolinite (Fig. 5a/6b). In the example of fluorene, Kd value is $36.4 \text{ L}.\text{kg}^{-1}$
384 at the kaolinite/water interface and $81.6 \text{ L}.\text{kg}^{-1}$ at the sediment/water interface. It
385 indicates that the favorable desorption effect noted from pure kaolinite is not as large in the
386 case of the complex sediment. All these observations are also valid for the effect of amphisin,
387 which is effective on the release of PAHs from pure kaolinite, but which helps only slightly to
388 desorb low weight PAHs (from naphthalene to fluorene) from the model sediment (Fig. 6a

389 and 6b). Indeed, in the example of fluorene, the Kd value is only 39.4 L.kg^{-1} for the
390 kaolinite/water/amphisin system but 127.1 L.kg^{-1} for the sediment/water/amphisin system.
391 In fact, the cyclolipopeptidic biosurfactants tested are less polar than SDS and consequently,
392 their sorption on OM must be greater. Clearly, SDS has one of the highest hydrophilic-
393 lipophilic balance value (HLB=40), which means that its hydrophilic part is preponderant in
394 the mass balance. Concerning amphisin and viscosin-like CLPs, their molecular structure and
395 their ability to lower the surface tension of water are near those of viscosin (27 mN.m^{-1}),
396 whose HLB is considered to be near 10. With such approximate values of HLB, it suggests
397 that the lipophilic part of our tested CLPs is more predominant than that of SDS [35]. So
398 CLPs certainly compete more with PAHs for hydrophobic sorption sites on OM. But unlike
399 SDS, their polar moiety, exposed to the aqueous phase and composed of amino acids (many
400 of them being non polar), are not repulsive for apolar PAHs, which can be likely adsolubilized
401 on the hemimicelles formed on the OM surface. Finally, the sorbed viscosin-like mixture is
402 probably slightly less attractive for PAHs than amphisin, because it contains only four or five
403 apolar amino acids in the polar heads, while amphisin contains six apolar amino acids,
404 reinforcing adsolubilization of PAHs. It is probably why amphisin contributes less in the
405 release of low weight PAHs, from the sediment to the aqueous phase, than viscosin-like CLPs
406 (Fig. 6a and 6b).

407

408 **4. Conclusions**

409

410 Batch tests made it possible to understand the sorption behavior of mixtures of PAHs at the
411 sediment surface, varying the nature of minerals, the pH, the ionic strength and the content of
412 organic matter. So it can be concluded that the fractions of kaolinite and OM in sediment play
413 the major role in PAH sorption, especially since the molecular weight of PAH increases.

414 Three anionic surfactants were tested to enhance PAHs solubilization from the particulate
415 surface to the aqueous phase. The addition of SDS causes an important reduction in the
416 sorption of all PAHs to kaolinite or to the model sediment containing OM, for two reasons.
417 The surfactant competes for sorption sites on the particle surface and adsolubilization of
418 PAHs into hemimicelles is less favorable than incorporation into micelles in the aqueous
419 phase. Two anionic cyclolipopeptidic biosurfactants, produced by *Pseudomonas fluorescens*
420 strains, were also tested. Amphisin presents an interesting potential to enhance the desorption
421 of the seven target PAHs from kaolinite to the aqueous phase. We can notice that we need 20
422 times less in mass concentration or 100 times less in molar concentration than SDS to obtain
423 good results. Viscosin-like CLPs (mixture of massetolide E and viscosin) present the same
424 interesting desorption potential from kaolinite than amphisin, but only for 2-3 aromatic ring
425 PAHs (from naphthalene to phenanthrene). Conversely, for the more lipophilic fluoranthene
426 or pyrene, adsolubilization on the kaolinite surface is unfortunately more preponderant than
427 incorporation into aqueous micelles of viscosin-like CLPs.

428 Finally, micelles of the two biosurfactants are able to release only low weight PAHs (from
429 naphthalene to fluorene) from the model sediment containing OM. Indeed, the more lipophilic
430 PAHs are not only more strongly sorbed onto the hydrophobic particles of OM, but they also
431 incorporate the surface hemimicelles formed by the biosurfactants rather than the aqueous
432 micelles. However, we can anticipate that biosurfactants, altering the distribution of low
433 weight PAHs between particulate and aqueous phases, may favor their removal from
434 sediments by remediation processes which need better solubilization of PAHs in the aqueous
435 interstitial phase (such as EK processes), or which need an increase of their bioavailability for
436 biodegradation processes.

437

438 **Acknowledgements**

439 The authors thank the “Région Haute Normandie” for financial support through Normandy
440 SCALE research network (RESSOLV program). The authors thank Dr. O. Nybroe (Royal
441 Veterinary & Agricultural University-Thorvaldsensvej, Denmark) for the gift of the
442 *Pseudomonas fluorescens* DSS73, Dr G. Braun (Agriculture & Agri-Food, Canada) for the
443 gift of *Pseudomonas fluorescens* PfA7B and C. Farmer for her linguistic support.
444

444

445 **References**

446

447 [1] M.K. Song, M. Song, H.S. Choi, Y.J. Kim, Y.K. Park, J.C. Ryu, Identification of
448 molecular signatures predicting the carcinogenicity of polycyclic aromatic hydrocarbons
449 (PAHs), Toxicology Letters 212 (2012) 18-28.

450 [2] L. Guzella, C. Roscioli, L. Vigano, M. Saha, S.K. Sarkar, B. Bhattacharya, Evaluation of
451 the concentration of HCH, DDT, HCB, PCB and PAH in the sediments along the lower
452 stretch of Hugli estuary, West Bengal, northeast India, Environment International 31 (2005)
453 523-534.

454 [3] W.X. Liu, J.L. Chen, X.M. Lin, S. Tao, Distribution and characteristics of organic
455 micropollutants in surface sediments from Bohai Sea, Environmental Pollution 140 (2006) 4-
456 8.

457 [4] C.N. Mulligan, R.N. Yong, B.F. Gibbs, An evaluation of technologies for the heavy metal
458 remediation of dredged sediments, J. Hazard. Mater. 85 (2001) 145-163.

459 [5] S. Semrany, L. Favier, H. Djelal, S. Taha, A. Amrane, Bioaugmentation: Possible solution
460 in the treatment of Bio-Refractory Organic Compounds (Bio-ROCs), Biochem. Eng. J. 69
461 (2012), 75-86.

462 [6] M. Pazos, E. Rosales, T. Alcantara, J. Gomez, M.A. Sanroman, Decontamination of soils
463 containing PAHs by electroremediation: A review, J. Hazard. Mater. 177 (2010) 1-11.

464 [7] C.N. Mulligan, R.N. Yong, B.F. Gibbs, Surfactant-enhanced remediation of contaminated
465 soil: a review, Engineering Geology 60 (2001) 371-380.

466 [8] M.T. Alcantara, J. Gomez, M. Pazos, M.A. Sanroman, PAHs soil decontamination in two
467 steps: Desorption and electrochemical treatment, J. Hazard. Mater. 166 (2009) 462-468.

- 468 [9] M.J. Sanchez-Martin, M.C. Dorado, C. del Hoyo, M.S. Rodriguez-Cruz, Influence of clay
469 mineral structure and surfactant nature on the adsorption capacity of surfactants by clays. J.
470 Hazard. Mater. 150 (2008) 115-123.
- 471 [10] S. Mukherjee, R. Das, R. Sen, Towards commercial production of microbial surfactants,
472 Trends Biotechnol. 24 (2006) 509-515.
- 473 [11] A. Franzetti, P. Carreda, C. Ruggeri, P. La Colla, E. Tamburini, M. Papacchini, G.
474 Bestetti, Potential applications of surface active compounds by Gordonia sp. strain BS29 in
475 soil remediation technologies, Chemosphere 75 (2009) 801-807.
- 476 [12] C.N. Mulligan, Recent advances in the environmental applications of biosurfactants,
477 Curr. Opin. Colloid Interface Sci. 14 (2009) 372-378.
- 478 [13] S.S. Cameotra, P. Singh, Synthesis of rhamnolipid biosurfactant and mode of hexadecane
479 uptake by Pseudomonas species, Microbial Cell Factories 8 (2009) 16-21.
- 480 [14] R.E. Saichek, K.R. Reddy, Surfactant-enhanced electrokinetic remediation of polycyclic
481 aromatic hydrocarbons in heterogeneous subsurface environments, J. Environ. Eng. Sci. 4
482 (2005) 327-339.
- 483 [15] J.W. Yang, Y.J. LeeJ, J.Y. Park, S.J. Kim, J.Y. Lee, Application of APG and Calfax 16L-
484 35 on surfactant-enhanced electrokinetic removal of phenanthrene from kaolinite,
485 Engineering Geology 77 (2005) 243-251.
- 486 [16] J.H. Chang, Z. Qiang, C.P. Huang, A.V. Ellis, Phenanthrene removal in unsaturated soils
487 treated by electrokinetics with different surfactants: Triton X-100 and rhamnolipid, Colloids
488 Surfaces A 348 (2009) 157-163.
- 489 [17] X. Pei, X. Zhan, L. Zhou, Effect of biosurfactant on the sorption of phenanthrene onto
490 original and H₂O₂-treated soils, J. Environ. Sci. 21 (2009) 1378-1385.

- 491 [18] H. Yu, G.H. Huang, C.J. An, J. Wei, Combined effects of DOM extracted from site
492 soil/compost and biosurfactant on the sorption and desorption of PAHs in a soil-water system,
493 J. Hazard. Mater. 190 (2011), 883-890.
- 494 [19] T. Lima, L. Procopio, F. Brandao, A. Carvalho, M. Totola, A. Borges, Simultaneous
495 phenanthrene and cadmium removal from contaminated soil by a ligand/biosurfactant solution
496 Biodegradation 22 (2011) 1007-1015.
- 497 [20] A.K. Singh, S.S. Cameotra, Efficiency of lipopeptide biosurfactants in removal of
498 petroleum hydrocarbons and heavy metals from contaminated soil, Environ. Sci. Pollut. Res.
499 Int. (2013) DOI 10.1007/s11356-013-1752-4.
- 500 [21] A. Groboillot, F. Portet-Koltalo, F. Le Derf, M.G.J. Feuilloley, N. Orange, C. Duclairoir-
501 Poc, Novel application of cyclolipopeptide amphisin: Feasibility study as additive to
502 remediate Polycyclic Aromatic Hydrocarbon (PAH) contaminated sediments, Int. J. Mol. Sci.
503 12 (2011) 1787-1806.
- 504 [22] C. Duclairoir-Poc, T. Meylheuc, S. Ngoya, A. Groboillot, J. Bodilis, L. Taupin, A.
505 Merieau, M.G.J. Feuilloley, N. Orange, Influence of growth temperature on cyclolipopeptides
506 production and on adhesion behaviour in environmental strains of *Pseudomonas fluorescens*,
507 J. Bacteriol. Parasitol. (2011) S1-002. doi:10.4172/2155-9597.S1-002
- 508 [23] X.C. Wang, Y.X. Zhang, R.F. Chen, Distribution and partitioning of Polycyclic Aromatic
509 Hydrocarbons (PAHs) in different size fractions in sediments from Boston Harbor, United
510 States, Marine Pollut. Bull. 42 (2001) 1139-1149.
- 511 [24] A. Mechlinska, M. Gdaniec-Pietryka, L. Wolska, J. Namiesnik, Evolution of models for
512 sorption of PAHs and PCBs on geosorbents, Trends Anal. Chem. 28 (2009) 466-482.
- 513 [25] F.J. Stevenson, Humus Chemistry. Genesis, Composition, Reactions. 2nd Ed., Wiley
514 Interscience, New York, 1994.

- 515 [26] Y. Ran, K. Sun, X. Ma, G. Wang, P. Grathwohl, E.Y. Zeng, Effect of condensed organic
516 matter on solvent extraction and aqueous leaching of polycyclic aromatic hydrocarbons in
517 soils and sediments, Environmental Pollution 148 (2007) 529-538.
- 518 [27] K.R. Reddy, P.R. Ala, S. Sharma, S.N. Kumar, Enhanced electrokinetic remediation of
519 contaminated manufactured gas plant soil, Engineering Geology 85 (2006) 132-146.
- 520 [28] R.E. Saichek, K.R. Reddy, Effect of pH control at the anode for the electrokinetic
521 removal of phenanthrene from kaolin soil, Chemosphere 51 (2003) 273-287.
- 522 [29] J. Gomez, M.T. Alcantara, M. Pazos, M.A. Sanroman, A two-stage process using
523 electrokinetic remediation and electrochemical degradation for treating benzo[a]pyrene
524 spiked kaolin, Chemosphere 74 (2009) 1516-1521.
- 525 [30] F. Bordas, P. Lafrance, R. Villemur, Conditions for effective removal of pyrene from an
526 artificially contaminated soil using *Pseudomonas aeruginosa* 57SJ rhamnolipids,
527 Environmental Pollution 138 (2005) 69-76.
- 528 [31] M.S. Rodriguez-Cruz, M.J. Sanchez-Martin, M. Sanchez-Camazano, A comparative
529 study of adsorption of an anionic and a non-ionic surfactant by soils based on
530 physicochemical and mineralogical properties of soils, Chemosphere 61 (2005) 56-64.
- 531 [32] W.H. Noordman, M.L. Brusseau, D.B. Janssen, Adsorption of a multicomponent
532 rhamnolipid surfactant to soil, Environ. Sci. Technol. 34 (2000) 832-838.
- 533 [33] M. Garcia-Junco, C. Gomez-Lahoz, J.L. Niqui-Arroyo, J.J. Ortega-Calvo, Biosurfactant-
534 and biodegradation-enhanced partitioning of Polycyclic Aromatic Hydrocarbons from
535 nonaqueous-phase liquids, Environ. Sci. Technol. 37 (2003) 2988-2996.
- 536 [34] W. Zhou, L. Zhu, Efficiency of surfactant-enhanced desorption for contaminated soils
537 depending on the component characteristics of soil-surfactant-PAHs system, Environmental
538 Pollution 147 (2007) 66-73.

539 [35] D.A. Vaza, E.J. Gudina, E.J. Alameda, J.A. Teixeira, L.R. Rodrigues, Performance of a
540 biosurfactant produced by a *Bacillus subtilis* strain isolated from crude oil samples as
541 compared to commercial chemical surfactants, *Colloids Surfaces B: Biointerfaces* 89 (2012)
542 167-174
543

543

544 **Figure captions**

545

546 Fig. 1: Sorption isotherms of PAHs on sand, silt, kaolinite and model sediment (without OM).

547 a: acenaphthene b: phenanthrene c: fluoranthene

548

549 Fig. 2: Sorption isotherms of PAHs on model sediment (without OM), with or without NaCl

550 (10 g.L^{-1}), at controlled pH or not. a: fluorene b: pyrene

551

552 Fig. 3: Sorption isotherms of PAHs on model sediment ($\text{NaCl}=10 \text{ g.L}^{-1}$, $\text{pH}=7.2$) with various

553 contents of OM. a: acenaptene b: phenanthrene c: fluoranthene

554

555 Fig. 4: Surface tension measurement of aqueous solutions containing amphisin and viscosin-

556 like biosurfactants as a function of their concentration (logarithmic scale).

557

558 Fig. 5: Sorption isotherms of PAHs on kaolinite ($\text{NaCl} = 10 \text{ g L}^{-1}$, $\text{pH} = 7.2$) with or without

559 SDS or biosurfactants (amphisin or viscosin-like mixture). a: fluorene b: phenanthrene c:

560 pyrene

561

562 Fig. 6: Sorption isotherms of PAHs ($\text{NaCl}=10 \text{ g.L}^{-1}$, $\text{pH}=7.2$, $\text{OM}=2.5\%$) on model sediment

563 with or without SDS or biosurfactants (amphisin or viscosin-like mixture). a: acenaphthene

564 b: fluorene c: phenanthrene

565

566 Table 1: Characterization of the cyclolipopeptidic biosurfactants produced by *Pseudomonas fluorescens* strains [22]

567

Strains	Molar mass (g mol ⁻¹)	CLP	Lipidic tail	Amino acids of cyclopeptidic heads										
				AA1	AA2	AA3	AA4	AA5	AA6	AA7	AA8	AA9	AA10	AA11
PfA7B	1111.7	Massetolide E	C ₁₀ H ₁₉ O ₂	L-Leu	D-Glu	D-allo-Thr	D-Val	L-Leu	D-Ser	L-Leu	D-Ser	L-Val		
	1125.7	Viscosin	C ₁₀ H ₁₉ O ₂	L-Leu	D-Glu	D-allo-Thr	D-Val	L-Leu	D-Ser	L-Leu	D-Ser	L-Ile		
DSS73	1394.8	Amphisin	C ₁₀ H ₁₉ O ₂	L-Leu	D-Asp	D-allo-Thr	D-Leu	D-Leu	D-Ser	L-Leu	D-Ser	L-Leu	L-Ile	L-Asp

568

Table 2 : Optimal fluorescence excitation and emission wavelengths, limits of detection (LOD) and quantification (LOQ) for target PAHs in HPLC-FLD, and mean recoveries and their relative standard deviation (RSD) obtained by SPE (spiked PAHs at $C_o=10 \mu\text{g.L}^{-1}$).

substance	FLD detection parameters			SPE performance	
	$\lambda_{\text{ex}}/\lambda_{\text{em}}$ (nm)	LOD ^a ($\mu\text{g L}^{-1}$)	LOQ ^b ($\mu\text{g L}^{-1}$)	Mean recovery (%)	RSD (%) (n=5)
naphthalene	220/330	0.4	1.3	82.0	3.9
acenaphthene	220/315	0.5	1.7	85.1	3.6
fluorene	220/315	0.3	1.0	85.7	3.6
phenanthrene	250/370	0.4	1.3	94.2	1.2
anthracene	250/370	0.3	1.0	82.0	2.3
fluoranthene	235/420	1.4	4.7	89.7	4.5
pyrene	235/420	1.9	6.3	90.0	1.9

a calculated as 3 times the background noise.

b calculated as 10 times the background noise.

Table 3: Reproducibility (standard deviations SD) of batch adsorption experiments for some PAHs sorbed on the model sediment, containing (or not) 2.5% of organic matter (+ or - OM) (spiked PAHs at $C_o=100 \mu\text{g.L}^{-1}$).

substance	$C_{eq} \pm SD (\mu\text{g L}^{-1})$ (n=5)	$C_{ads} \pm SD (\mu\text{g g}^{-1})$ (n=5)
naphthalene (- OM)	20.1 ± 3.3	0.727 ± 0.029
naphthalene (+ OM)	7.5 ± 1.9	0.834 ± 0.017
phenanthrene (- OM)	12.3 ± 2.7	0.791 ± 0.024
phenanthrene (+ OM)	1.3 ± 0.3	0.899 ± 0.003
fluoranthene (- OM)	3.6 ± 0.3	0.868 ± 0.004
fluoranthene (+ OM)	2.8 ± 0.5	0.898 ± 0.001

Table 4 : Best isotherms and parameters of selected PAHs for various mineral components and the model sediment (without OM).

	Acenaphthene						Phenanthrene						Fluorar		
	linear		Freundlich				linear		Freundlich				linear		
	K _d	r ²	K _F	1/n	r ²	K _d	r ²	K _F	1/n	r ²	K _d	r ²	K _F		
sand	26.4	0.569	51.2	0.861	0.920	44.8	0.843	49.2	0.922	0.926	44.2	0.777	37.1		
silt	40.7	0.962	54.6	1.183	0.986	54.0	0.978	152.9	1.376	0.964	99.7	0.988	122		
kaolinite	145.3	0.967	48.9	0.708	0.957	188.3	0.964	30.6	0.553	0.934	390.9	0.977	73.1		
model sediment	52.5	0.954	133.6	1.334	0.963	97.4	0.983	186.9	1.286	0.979	219.0	0.955	628		

Table 5: Partition coefficients K_d of PAHs (and r^2 values associated to the linear isotherm equation) for the model sediment with or without OM, and organic carbon partition coefficients K_{oc}

	Model sediment		Model sediment + 2.5% OM			Model sediment + 5% OM		
	K_d (L.kg ⁻¹)	r^2	K_d (L.kg ⁻¹)	r^2	K_{oc} (L.kg ⁻¹)	K_d (L.kg ⁻¹)	r^2	K_{oc} (L.kg ⁻¹)
naphthalene	45.2	0.943	68.1	0.911	1577	163.3	0.903	1891
acenaphthene	52.5	0.954	129.8	0.953	8967	341.9	0.958	11809
fluorene	53.8	0.993	141.6	0.940	9782	395.5	0.958	13661
phenanthrene	97.4	0.983	304.3	0.950	21021	555.0	0.935	19170
antracene	177.9	0.969	653.6	0.945	26144	809.8	0.910	27970
fluoranthene	219.0	0.955	652.2	0.943	45151	973.1	0.941	33611
pyrene	222.0	0.997	952.9	0.923	49724	1042.1	0.918	35994

- The sorption of a mixture of PAHs was studied at the sediment/water interface
- Clay and organic matter fractions were the most influent factors on PAHs sorption
- Desorption of PAHs by cyclolipopeptidic (CLP) biosurfactants was investigated
- Release of 2-4 ring PAHs from kaolinite was favored by adding SDS or amphisin
- Amphisin and viscosin-like were effective to release low weight PAHs from sediments

Adsorption isotherms of anthracene at the water/kaolinite interface (25°C)

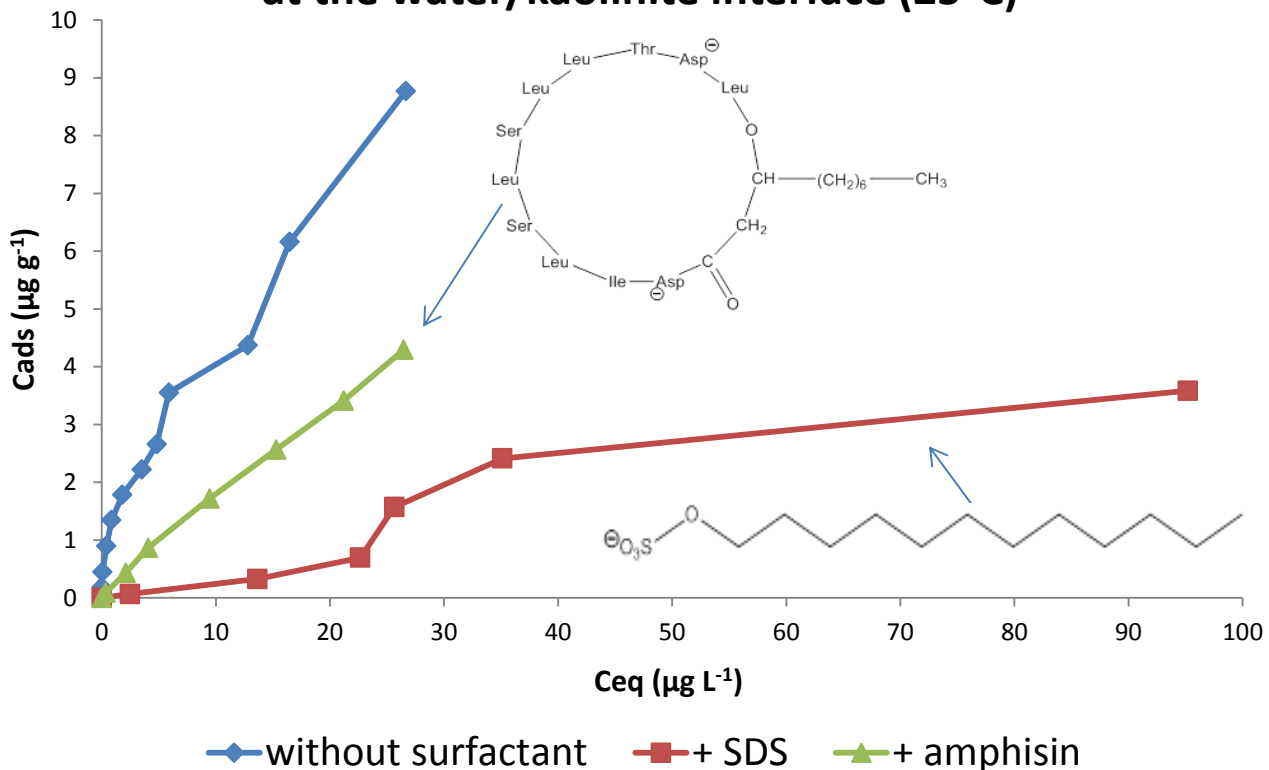


Fig. 1

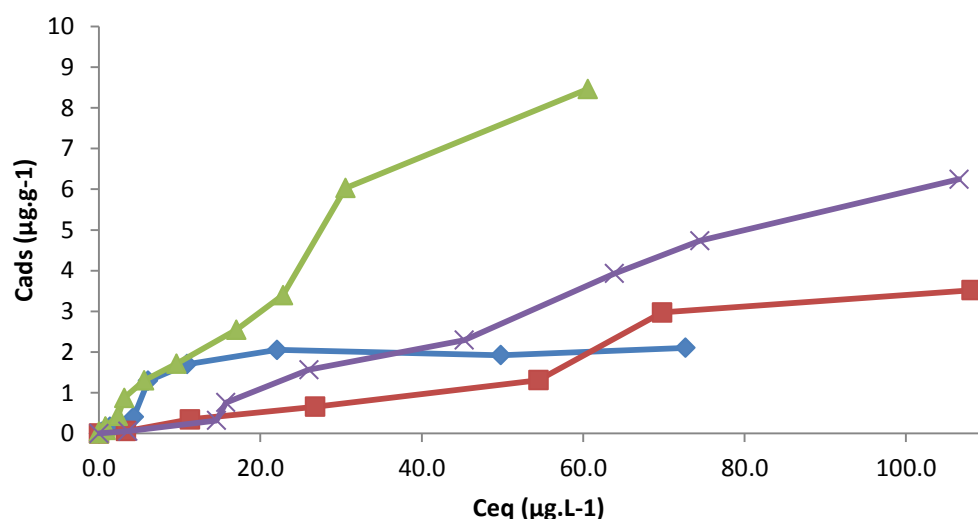
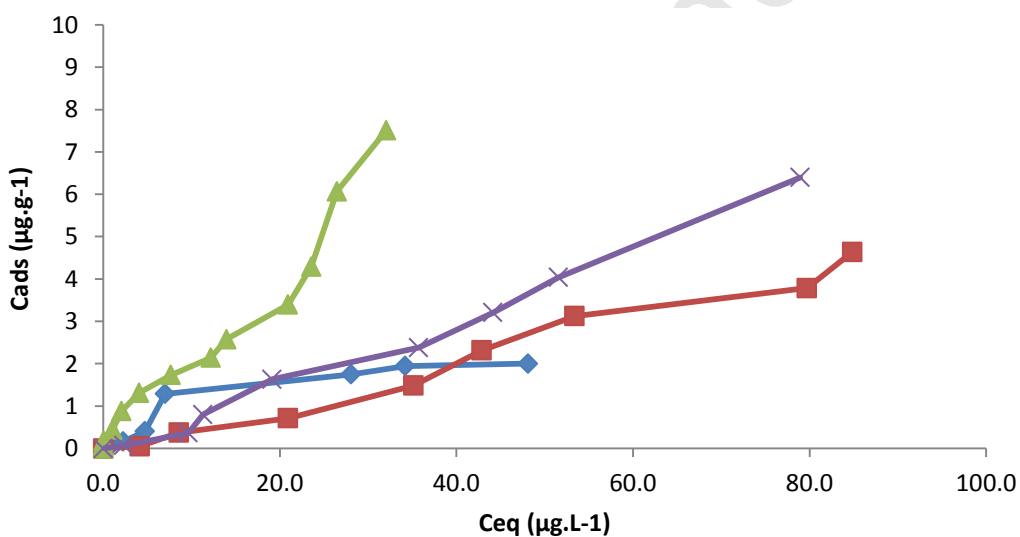
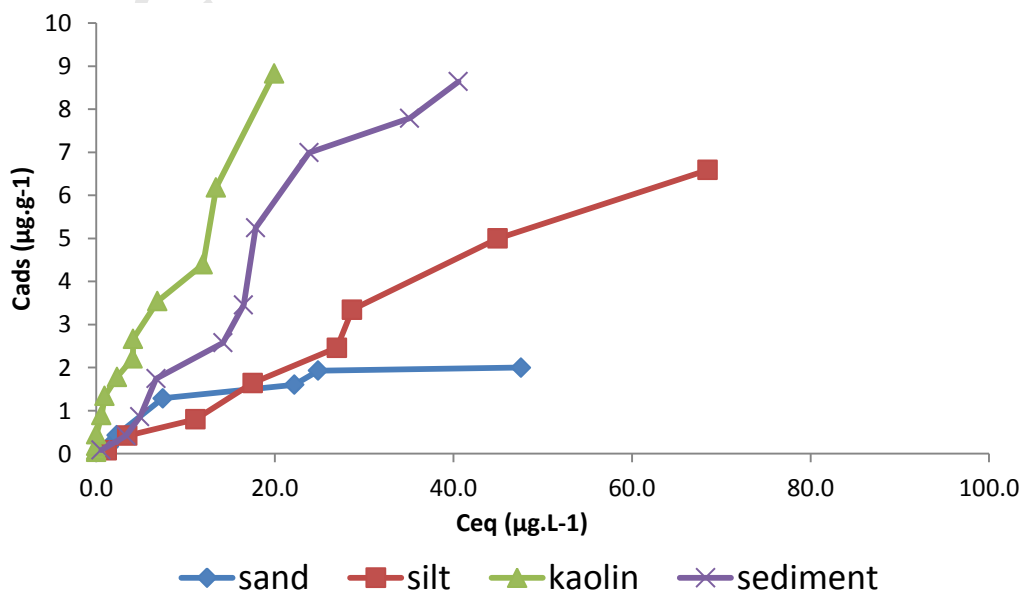
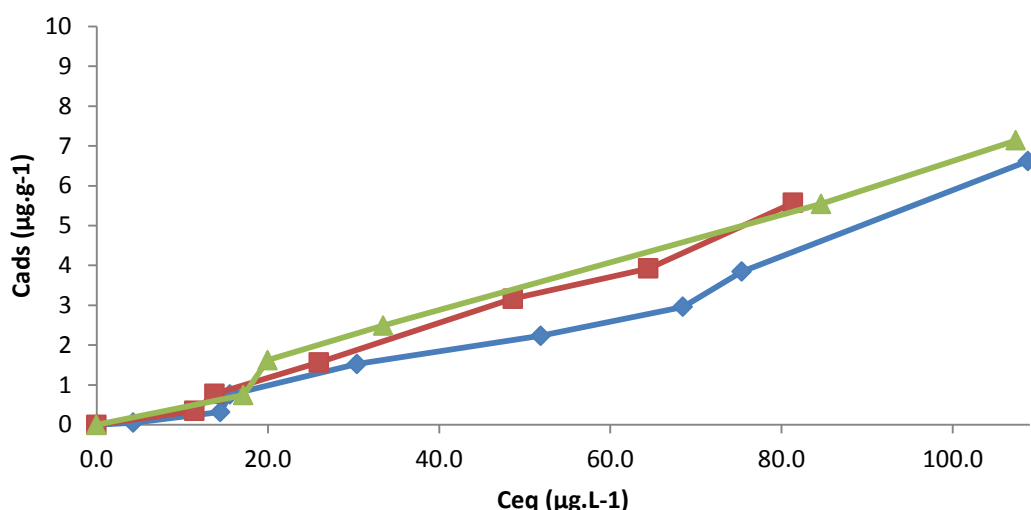
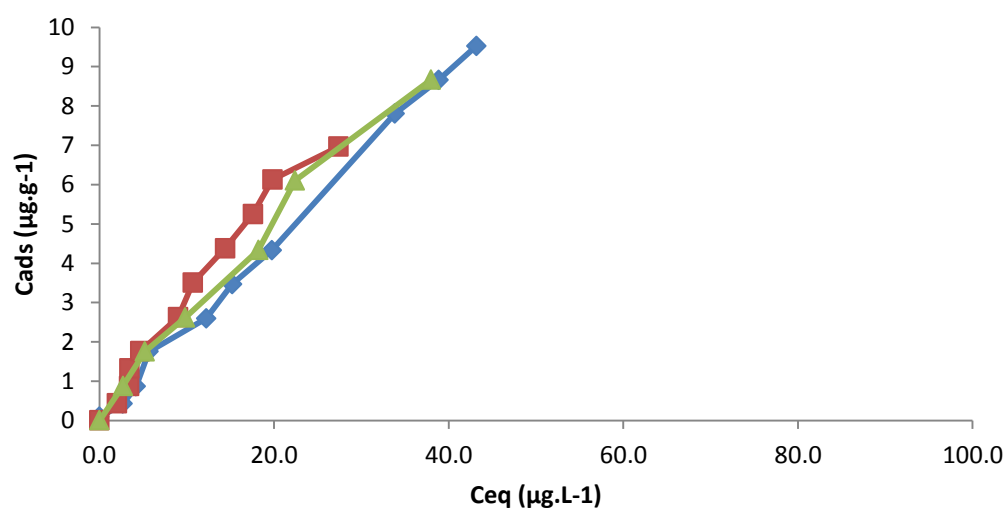
a**b****c**

Fig. 2

a**b**

—●— NaCl:0 natural pH

—▲— NaCl:10 g.L⁻¹ pH=7.2—■— NaCl:10 g.L⁻¹ pH=4.7

Fig. 3

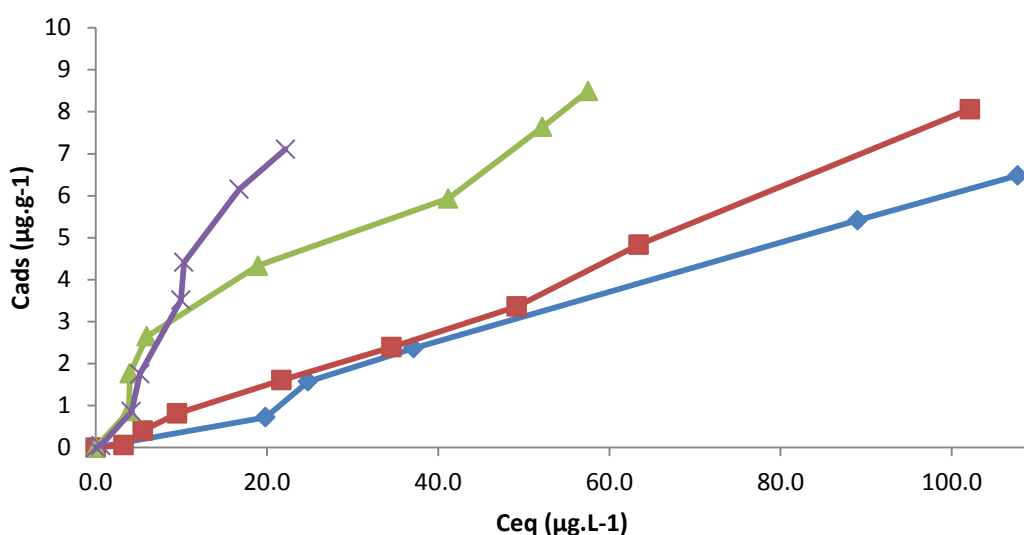
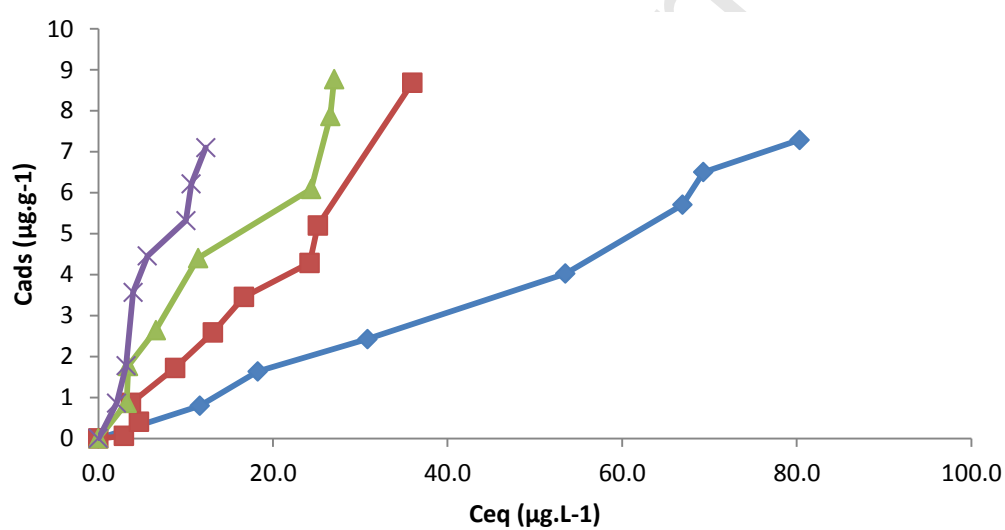
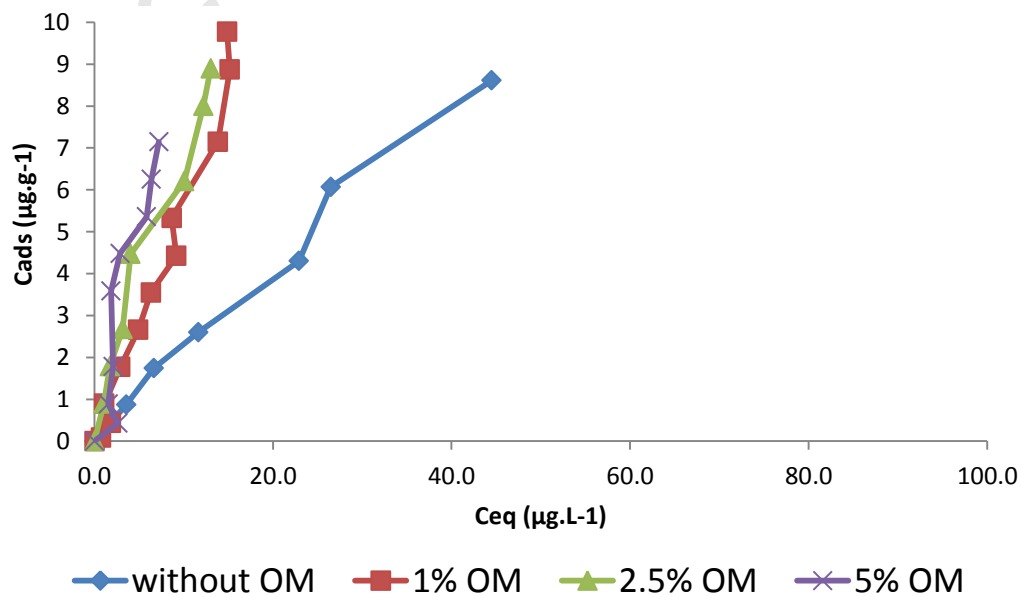
a**b****c**

Fig. 4

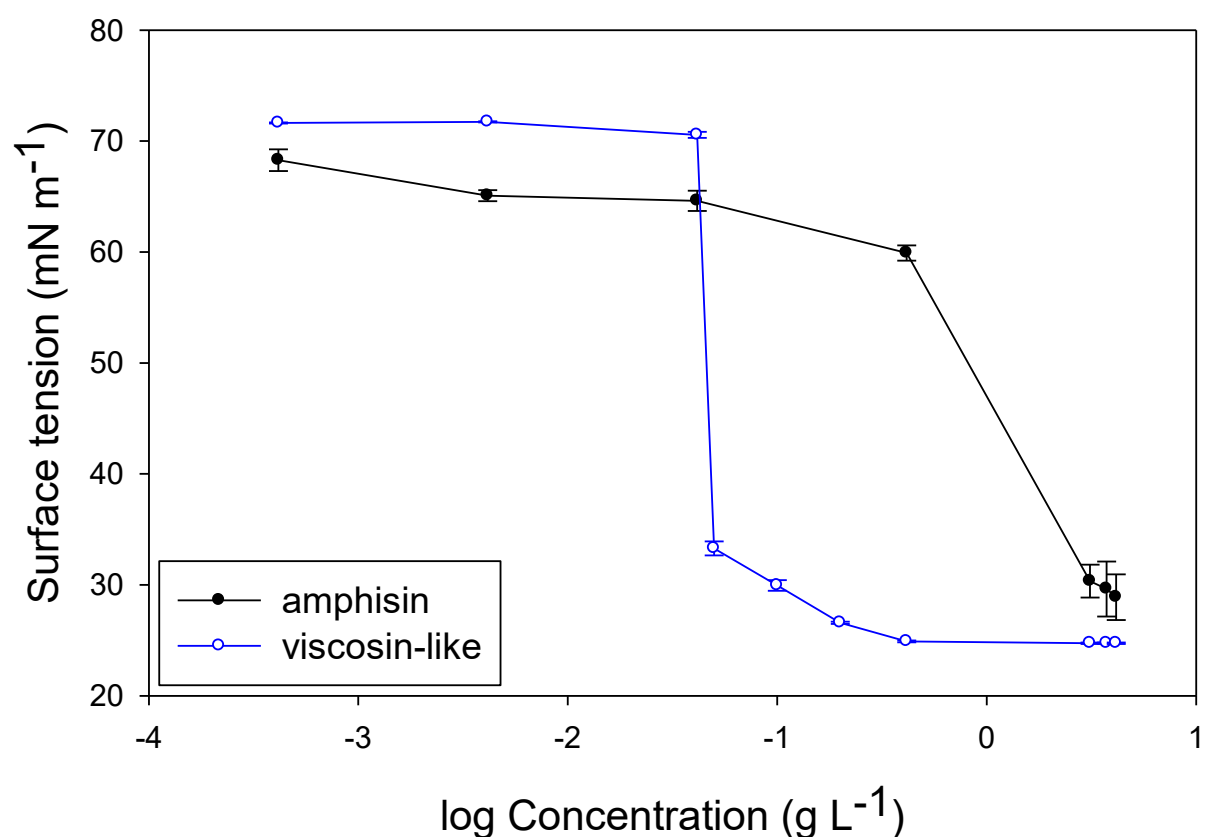


Fig. 5

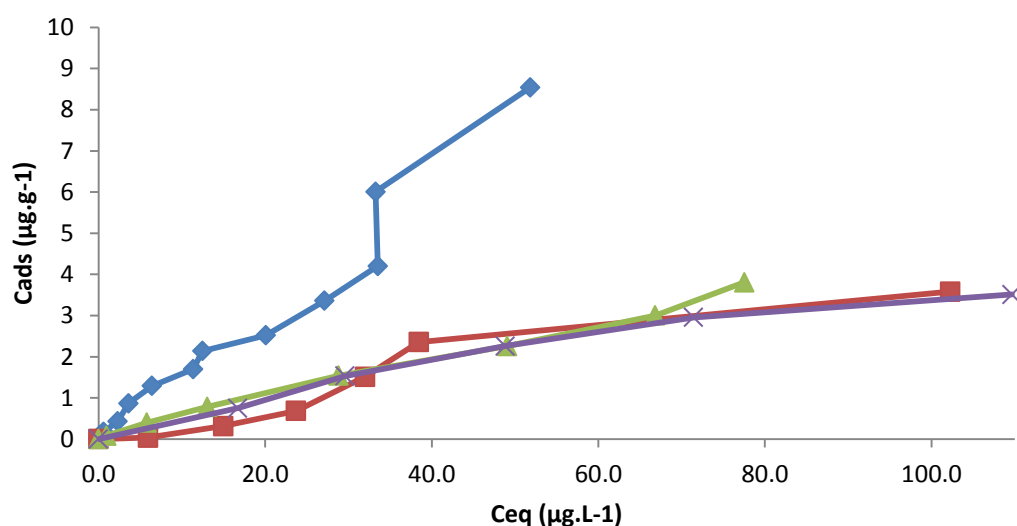
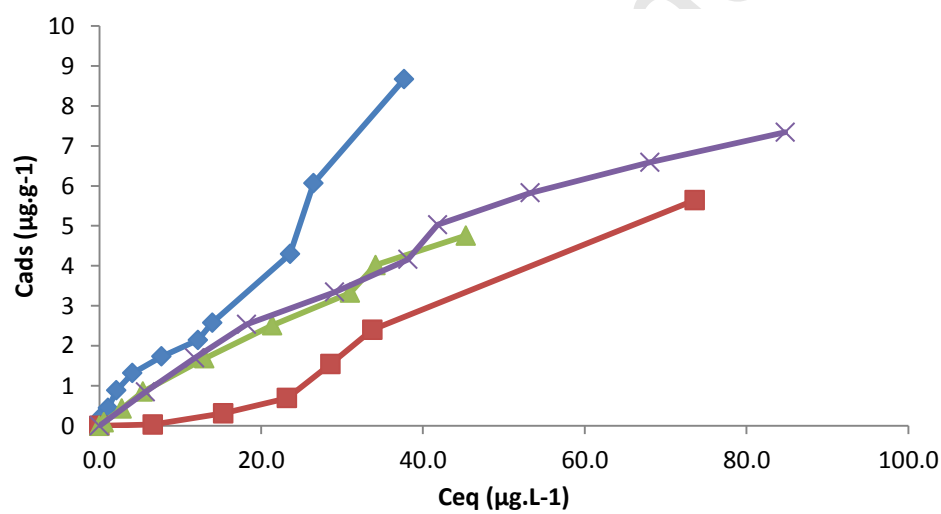
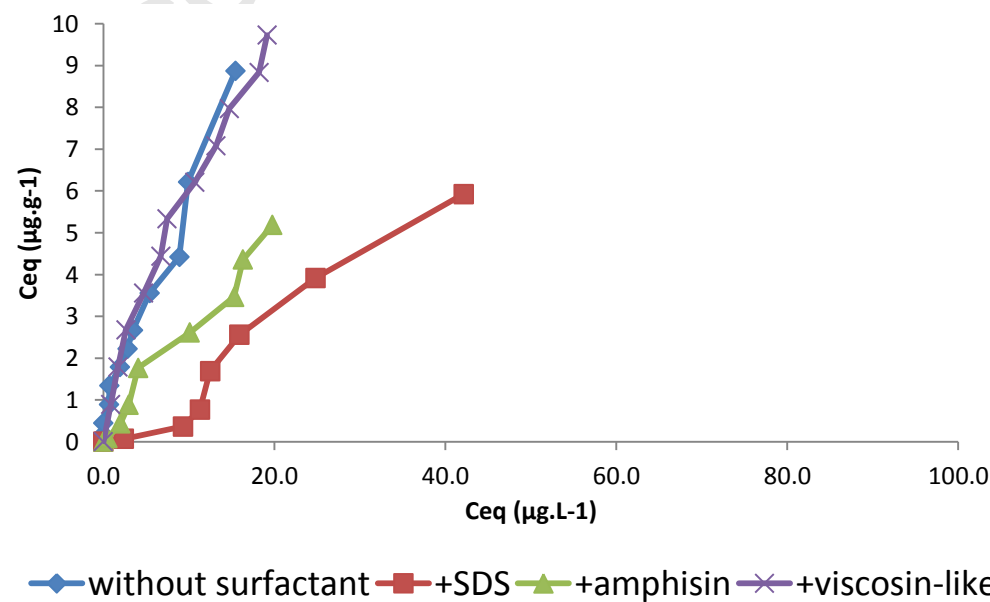
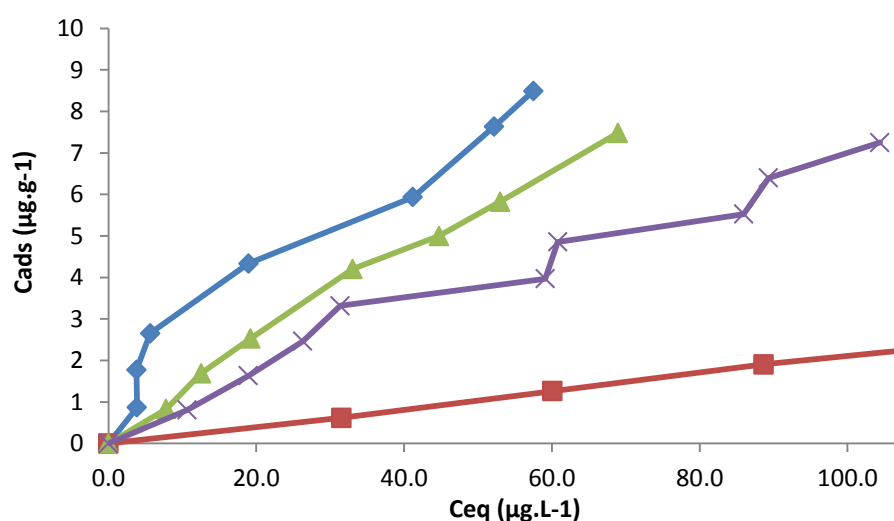
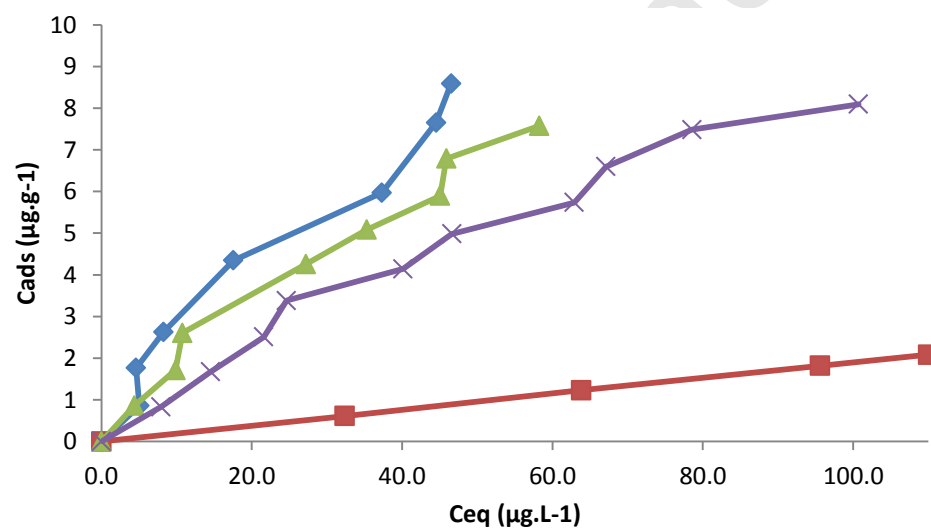
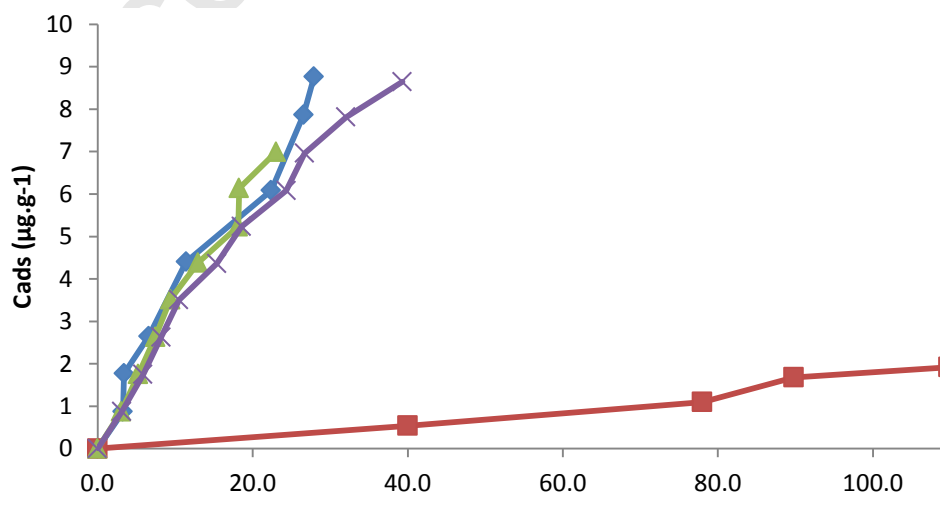
a**b****c**

Fig. 6

a**b****c**

—♦— without surfactant —■— +SDS —▲— +amphisin —×— +viscosin-like

P18

Article

Effect of GABA, a Bacterial Metabolite, on *Pseudomonas fluorescens* Surface Properties and Cytotoxicity

Audrey Dagorn ¹, Annelise Chapalain ¹, Lily Mijouin ¹, Mélanie Hillion ¹, Cécile Duclairoir-Poc ¹, Sylvie Chevalier ¹, Laure Taupin ², Nicole Orange ¹ and Marc G. J. Feuilloley ^{1,*}

¹ Laboratory of Microbiology Signal and Microenvironment LMSM, EA 4312, Normandie University, Rouen University, GRRs SSE, IRIB, VASI, Evreux F-27000, France; E-Mails: audrey.dagorn@etu.univ-rouen.fr (A.D.); Annelise.Chapalain@iaf.inrs.ca (A.C.); lily.mijouin@gmail.com (L.M.); melanie.hillion@hotmail.fr (M.H.); cecile.poc@univ-rouen.fr (C.D.-P.); sylvie.chevalier@univ-rouen.fr (S.C.); nicole.orange@univ-rouen.fr (N.O.)

² Laboratoire de Biotechnologie et Chimie Marines, Université de Bretagne-Sud B.P. 92116, Lorient cedex 56321, France; E-Mail: laure.taupin@univ-ubs.fr

* Author to whom correspondence should be addressed; E-Mail: marc.feuilloley@univ-rouen.fr; Tel.: +332-32-29-15-42; Fax: +332-32-29-15-50.

Received: 6 May 2013; in revised form: 23 May 2013 / Accepted: 27 May 2013 /

Published: 6 June 2013

Abstract: Different bacterial species and, particularly *Pseudomonas fluorescens*, can produce gamma-aminobutyric acid (GABA) and express GABA-binding proteins. In this study, we investigated the effect of GABA on the virulence and biofilm formation activity of different strains of *P. fluorescens*. Exposure of a psychotropic strain of *P. fluorescens* (MF37) to GABA (10^{-5} M) increased its necrotic-like activity on eukaryotic (glial) cells, but reduced its apoptotic effect. Conversely, muscimol and bicuculline, the selective agonist and antagonist of eukaryote GABA_A receptors, respectively, were ineffective. *P. fluorescens* MF37 did not produce biosurfactants, and its caseinase, esterase, amylase, hemolytic activity or pyoverdine productions were unchanged. In contrast, the effect of GABA was associated to rearrangements of the lipopolysaccharide (LPS) structure, particularly in the lipid A region. The surface hydrophobicity of MF37 was marginally modified, and GABA reduced its biofilm formation activity on PVC, but not on glass, although the initial adhesion was increased. Five other *P. fluorescens* strains were studied, and only one, MFP05, a strain isolated from human skin, showed structural differences of biofilm maturation after exposure to GABA. These results reveal that GABA can regulate

the LPS structure and cytotoxicity of *P. fluorescens*, but that this property is specific to some strains.

Keywords: host-microbial interactions; cytotoxicity; virulence; bacterial adhesion; lipopolysaccharide; biofilms; pyoverdine

1. Introduction

Gamma-aminobutyric acid (GABA) is a non-protein amino acid widespread in the environment [1]. Also, many bacteria, such as *Pseudomonas aeruginosa* [2,3], *Pseudomonas fluorescens* [4], marine *Pseudomonas* [5,6], lactic bacteria [7] and *Escherichia coli* [8], can synthesize GABA. Some of these bacteria release GABA, suggesting that GABA should act as a communication molecule between bacteria and their host or even between bacteria. Indeed, different GABA binding sites or sensors have been identified in bacteria. A GabP permease has been isolated in *E. coli* and *Bacillus subtilis* [9,10]. *Corynebacterium glutamicum* expresses a specific GABA transporter, also designated as GabP, but having low sequence identity with the GabP permease [11]. A selective GABA binding protein, Atu4243, was identified more recently in *Agrobacterium tumefaciens* and in several pathogenic or symbiotic Proteobacteria, including *Pseudomonas* [12]. Last year, we observed that in *P. aeruginosa*, GABA could bind the thermo-unstable ribosomal elongation factor, Tuf, a multiple function protein potentially translocated to the bacterial membrane, where it could act as a surface sensor [13]. A GABA binding protein (GBP), sharing common biochemical and pharmacological characteristics with the mammalian GABA_A receptor, was identified 20 years ago in an environmental strain of *P. fluorescens* [14], but this strain was patented and not deposited in international bacterial strains libraries. Until now, the recognition of GABA by other strains of *P. fluorescens* was not investigated, and the function of this molecule in *P. fluorescens* remains unknown.

In *Lactobacillus*, *Lactococcus lactis* and *E. coli*, GABA is involved in the resistance to acid stress [15,16], and in many species, including *Shigella flexneri* and *Listeria monocytogenes*, this system should be essential for colonization of the gastro-intestinal tract [17]. The physiological role of GABA was investigated in detail in *A. tumefaciens*, where it was shown that this molecule, which is released by plants in response to infection, induces the expression of a lactonase that cleaves *N*-3-oxo-octanoyl-L-homoserine lactone (3-oxo-C8-HSL), leading to a reduction of tumor formation [18]. GABA is also an inhibitor of virulence in the phytopathogen *Pseudomonas syringae* pv. tomato, where at high concentrations, it downregulates the expression of *hrp* genes and increases the resistance of the plant to infection [19]. Conversely, in the human opportunistic pathogen, *P. aeruginosa*, GABA reduces biofilm formation activity, but increases the production of hydrogen cyanide and its virulence [13]. It was then particularly interesting to investigate the effect of GABA on *P. fluorescens*, which is frequently found in the rhizosphere, where it can enhance the resistance of plants against bacterial pathogens, including *P. syringae* pv. tomato [20], but is also found in the clinical environment, where some strains adapted to the human physiological temperature behave clearly as opportunistic pathogens [21].

In the present study, we investigated the effect of GABA on the growth kinetic, mobility, cytotoxic activity, binding potential on biotic and abiotic surfaces, biofilm formation activity, surface polarity, biosurfactant production, lipopolysaccharide (LPS) structure, exoenzymes secretion and pyoverdine production by environmental and clinical strains of *P. fluorescens*.

2. Results

2.1. Effect of GABA on the Cytotoxic Activity, Adhesion Potential, Biofilm Formation Activity and Surface Properties of *Pseudomonas fluorescens*

Before the tests, bacteria were exposed to GABA 10^{-5} M during the whole growth phase and rinsed to remove any trace of free GABA. The concentration of 10^{-5} M was selected to avoid any possible metabolic or pH effect and because it is the mean value of the concentrations in the synaptic cleft of neurons (1.5–3 mM [22]), in wounded vegetal (10^{-4} M [23]) and in the environment (sea water concentration $<10^{-7}$ M [24]). Administration of GABA did not modify the growth kinetic or the swimming and swarming mobility of the psychrotrophic strain of *P. fluorescens* MF37 (data not shown). The cytotoxic activity of *P. fluorescens* MF37 was studied using a model of cultured rat glial cells [25], and the cell viability was determined by measurement of the release of lactate dehydrogenase (LDH) and nitrite ions in the culture medium. In comparison to the cells exposed to control bacteria, when glial cells were exposed to *P. fluorescens* MF37 treated with GABA (10^{-5} M), we observed a significant increase of LDH release ($+71.5\% \pm 5.4\%$, $p < 0.001$) (Figure 1A) and a decrease of the nitrite ion concentration ($-53.3\% \pm 2.9\%$, $p < 0.001$) (Figure 1B). Bacteria exposed to GABA 10^{-6} M also showed an increase of cytotoxicity, but this effect was not significant. Muscimol (10^{-5} M), a selective agonist of eukaryote GABA_A receptors, and bicuculline (10^{-5} M), an antagonist of these receptors, were without effect on *P. fluorescens* MF37 cytotoxicity. Because glial cells can also detect GABA [26], control studies were realized by direct treatment of glial cells with GABA (10^{-5} M), and we observed that GABA had no effect on glial cell viability. As previously demonstrated [25,27], in our experimental conditions, *P. fluorescens* MF37 did not release detectable amounts of LDH and NO.

As adhesion is a key step in the expression of bacterial virulence, we investigated the adhesion potential of GABA treated *P. fluorescens* MF37 on cultured glial cells and glass. The binding index of GABA treated bacteria on primary cultures of rat glial cells was unchanged, but we observed a significant increase of adhesion ($+55\% \pm 12\%$, $p < 0.01$) on glass surfaces (Figure 2). The effect of GABA on *P. fluorescens* MF37 biofilm formation was studied using the crystal violet technique and confocal microscopy. When *P. fluorescens* MF37 was pre-treated only during the exponential growth phase, the crystal violet technique revealed a limited, but significant reduction of biofilm formation on polyvinyl chloride (PVC) microtitration plates ($-7\% \pm 2\%$, $p < 0.05$) after 48 h incubation, whereas there was no difference after 24 h (Figure 3). Conversely, when the bacteria were pre-treated during the exponential growth phase and the biofilm formation period, we observed a significant reduction of the biofilm after 24 h ($-18\% \pm 4\%$, $p < 0.05$), but this effect was not maintained at 48 h. A unique treatment with GABA during the biofilm formation period was without effect. When the biofilm formation activity of *P. fluorescens* MF37 was studied on glass slides by confocal microscopy, we did not observe any change in the morphology or thickness of 5, 24 and 48 h-old biofilms. Other strains of

P. fluorescens originating either from agricultural soil (Pf0-1), plant leaves (SBW25), human skin (MFP05) or from the pulmonary tract and considered as an opportunistic pathogen (MFN1032) were studied in the same conditions. Only the biofilm formed by MFP05 was affected by GABA (Figure 4). There was no difference between the biofilms formed by control and GABA-treated bacteria after 5 h incubation. In contrast, the 24 h-old biofilm of GABA-treated MFP05 showed an irregular bacterial cluster and appeared more mature, its aspect being identical to a 30 h-old biofilm. This effect was transient, and after 48 h, the aspect of control and GABA-treated *P. fluorescens* MFP05 biofilms was the same.

Figure 1. Effect of GABA, the GABA_A receptor agonist muscimol and the GABA_A receptor antagonist bicuculline (10^{-5} M) on the cytotoxicity of *P. fluorescens* MF37 on eukaryotic (glial) cells. The necrotic activity of the bacterium was determined by assay of lactate dehydrogenase (LDH) in the culture medium. (A) The apoptotic activity was evaluated by the assay of nitrite; (B) in which nitrites are produced upon activation of NO-synthase in the target cell. Dotted lines indicate the production of LDH and nitrites in the medium of control eukaryotic cells not exposed to the bacterium (★★★: $p < 0.001$).

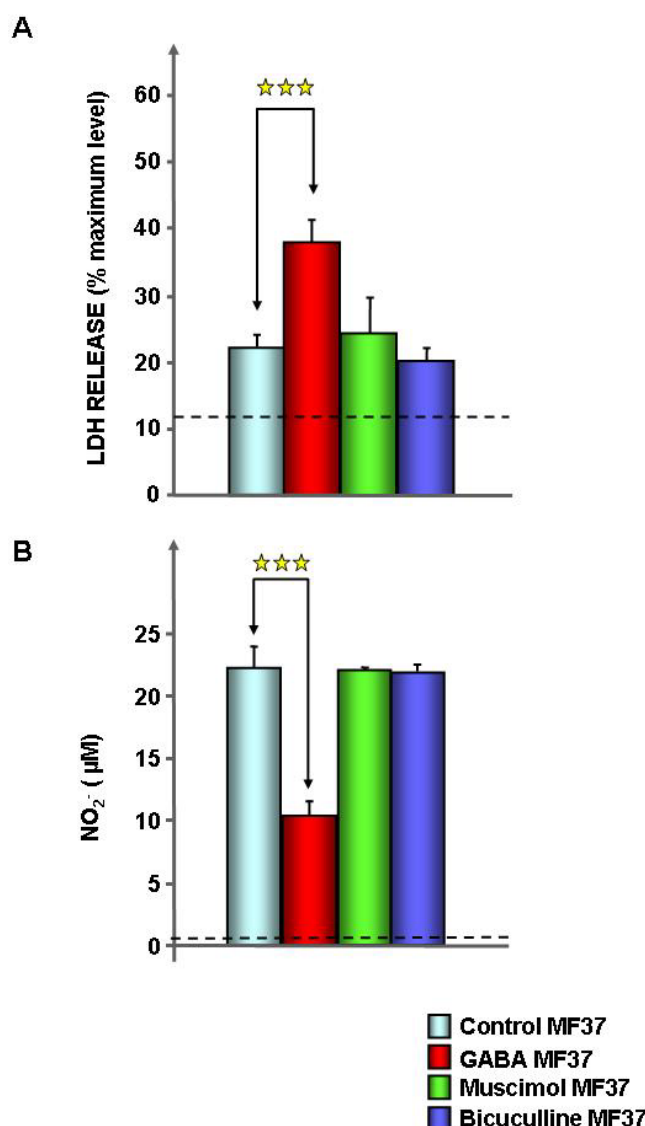


Figure 2. Effect of GABA (10^{-5} M) on the adhesion properties of *P. fluorescens* MF37 to eukaryotic cells or glass. Adhesion is expressed as the percentage of the control value (dotted line) (NS: non-significant; ★★: $p < 0.01$).

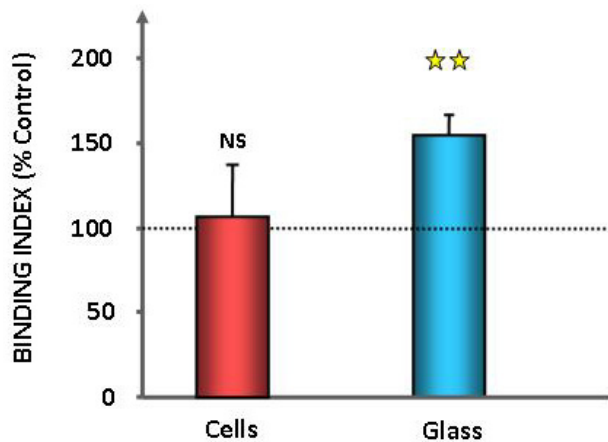


Figure 3. Effect of GABA (10^{-5} M) on the biofilm formation activity of *P. fluorescens* MF37 in 96-well PVC microtitration plates. The biofilm formation activity of bacteria was measured after 24 or 48 h of incubation. Bacteria were exposed to GABA only during the growth phase (pretreatment), only during the biofilm formation period (during biofilm) or continuously during growth and biofilm formation (pretreated + during biofilm). The biofilm formation activity is expressed as the percentage of the control value (dotted line). (NS: non-significant; ★: $p < 0.05$).

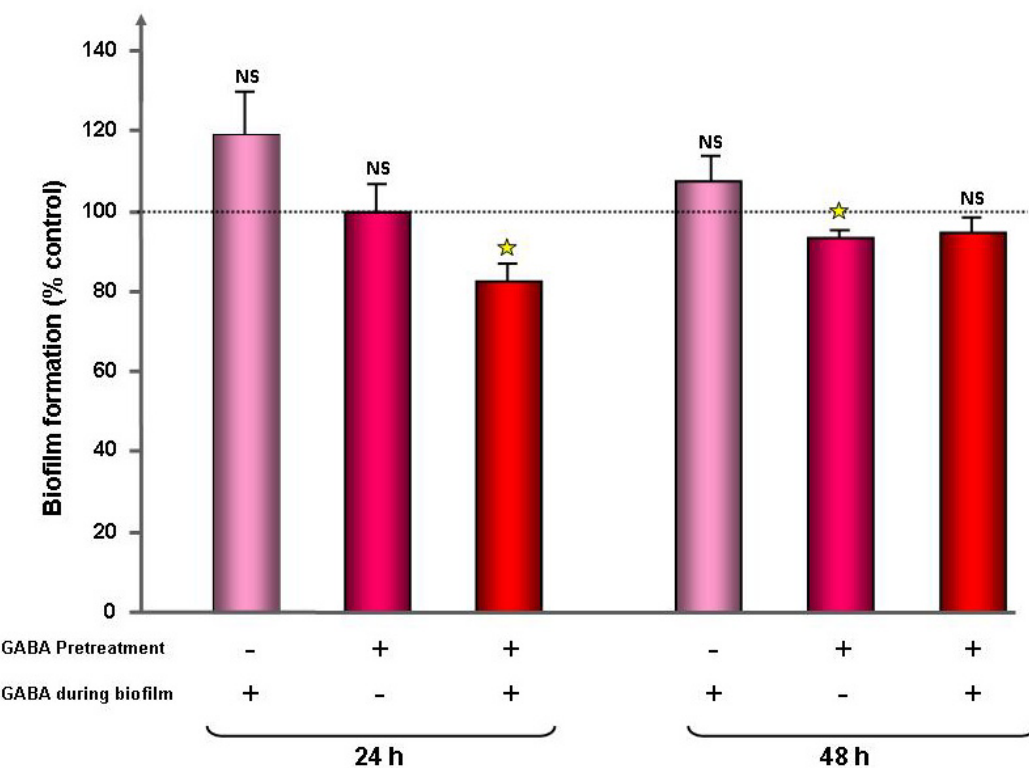
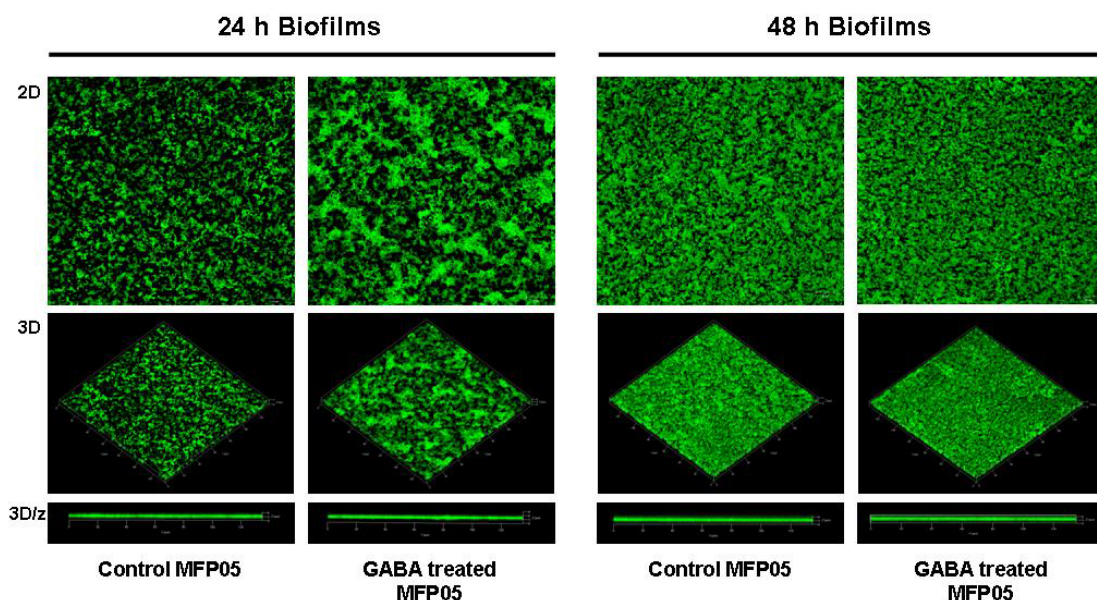


Figure 4. Effect of GABA (10^{-5} M) on the biofilm formation activity of *P. fluorescens* MFP05 on glass slides. 2D, 3D and 3D/z figures resulting from confocal laser scanning observations were realized after 24 and 48 h of biofilm formation.



As these results suggested an evolution of the surface properties of *P. fluorescens*, we investigated, by the microbial adhesion to solvent (MATS) technique, the surface hydrophilic character of the microorganism. The affinity of *P. fluorescens* MF37 to hexadecane was significantly increased after treatment by GABA ($0.6\% \pm 0.2\%$ for control, $3\% \pm 0.7\%$ for GABA-treated bacteria, $p < 0.05$) (Figure 5A), but the affinity of MF37 to hexadecane remained below 20%, which is considered the threshold value for highly hydrophilic bacteria [28]. Then, it appears that the global polarity of this strain was unchanged. Complementary studies showed that the surface tension from the rinsing medium of *P. fluorescens* MF37 colonies was also the same before or after GABA treatment ($55.7\% \pm 0.4$ and 55.8 ± 2.2 mN/m, respectively) (Figure 5B), indicating that in both conditions, *P. fluorescens* MF37 was not producing biosurfactant susceptible to modulation of bacterial adhesion.

2.2. Effect of GABA on Secreted Diffusible Factors and Lipopolysaccharide Structure

In order to identify the origin of the effect of GABA on *P. fluorescens* MF37 cytotoxicity, we investigated the effect of GABA on the caseinase, esterase, amylase, elastase and hemolytic secreted activities of the bacterium, but no difference was observed between control and GABA-treated bacteria (data not shown). Then, we investigated the effect of GABA on the production of pyoverdine, a siderophore essential for the colonizing activity of *Pseudomonas* and for virulence in plants and animals [29]. Using King B medium, a time-dependent increase of pyoverdine production was observed with both control and GABA-treated bacteria (Figure 6A). After 24, 32 and 48 h of incubation, the OD_{400}/OD_{580} ratio used to monitor pyoverdine production was higher in GABA-treated bacteria, but the difference with control bacteria was not significant. For that reason, the same experiment was repeated using Bacto Casamino Acids (CAA) medium, another pyoverdine-inducing medium. An increase of pyoverdine was observed from 6 to 48 h of incubation, but it appeared clearly that GABA was not modulating pyoverdine production (Figure 6B).

Figure 5. Effect of GABA (10^{-5} M) on the global surface polarity (A) and biosurfactant production (B) of *P. fluorescens* MF37. The surface polarity was determined by measurement of the affinity of bacteria to hexadecane. The biosurfactant production was estimated by measurement of the surface tension of rinsing solutions of bacterial colonies grown on solid agar medium. (NS: non-significant; \star : $p < 0.05$).

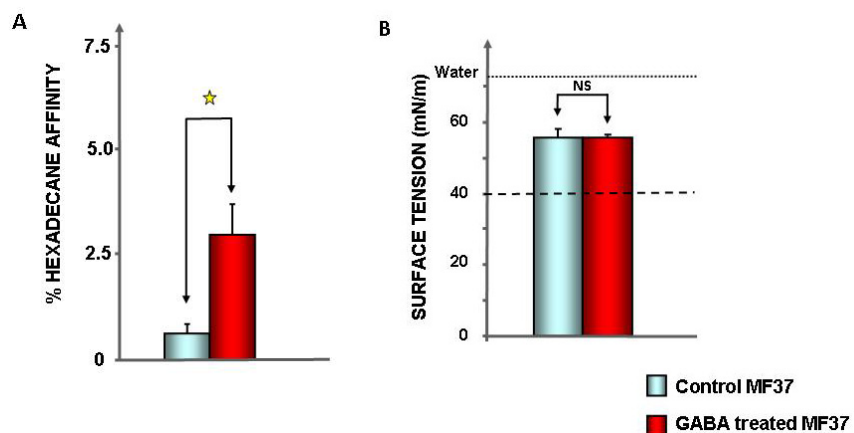
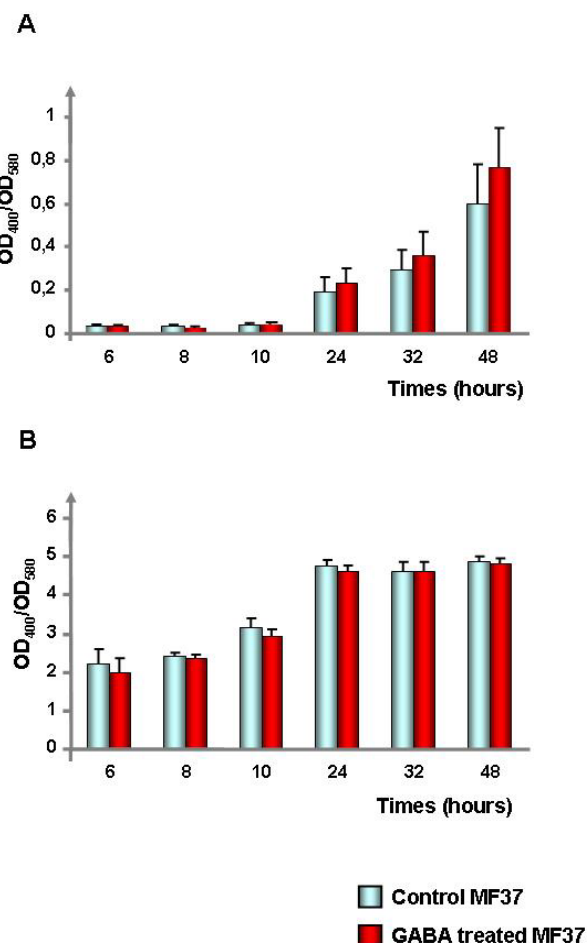
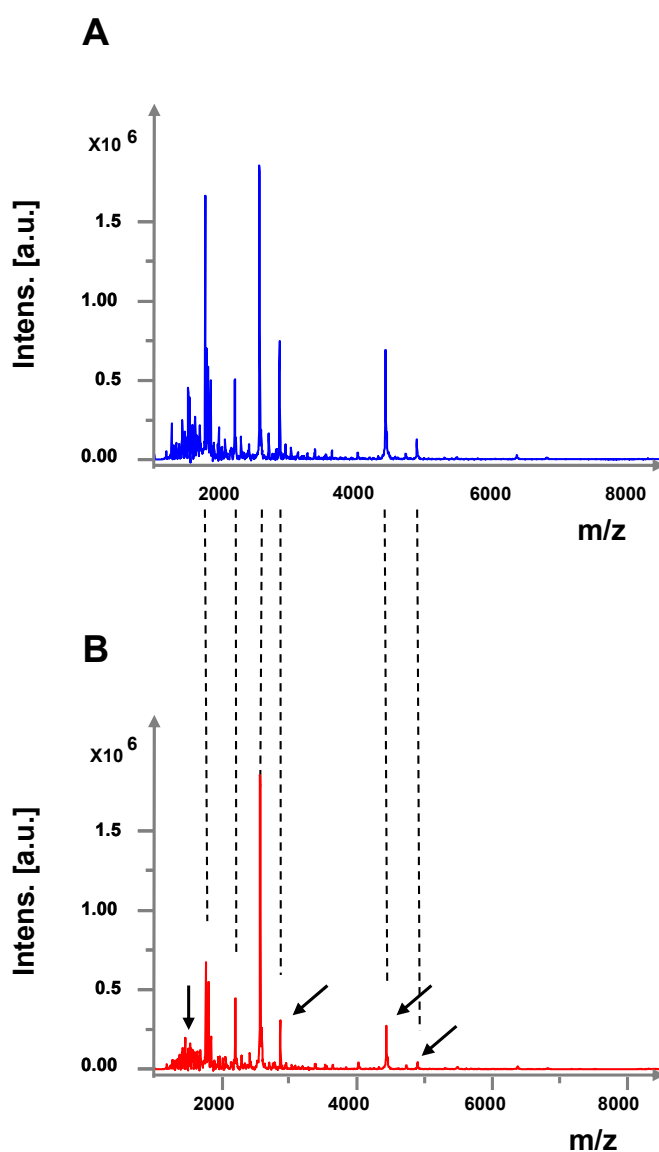


Figure 6. Effect of GABA (10^{-5} M) on pyoverdine production by *P. fluorescens* MF37. The pyoverdine production was measured in King B (A) and Bacto Casamino Acids (CAA) (B) medium. The production of pyoverdine is expressed as the ratio of pyoverdine adsorption (OD_{400}) on the OD_{580} nm of the bacterial culture.



The lipopolysaccharide (LPS) is one of the major virulence factors and the principal endotoxin of *Pseudomonas*. LPS extracted from *P. fluorescens* MF37 exposed or not to GABA was studied by MALDI-TOF mass spectrometry. We observed that the mass spectra of LPS extracted from control bacteria (Figure 7A) showed limited, but significant and repeatable, differences in comparison with the mass spectra of GABA-treated bacteria (Figure 7B). The modified peaks were found essentially in the region of low m/z fragments, considered as corresponding to lipid A fragments [30]. Three peaks of a higher m/z ratio, presumably associated with fragments of the oligosaccharide core [30], were also particularly decreased in GABA-treated bacteria, suggesting that GABA induced a large rearrangement of the LPS structure.

Figure 7. MALDI-TOF analysis of the lipopolysaccharide (LPS) extracted from control (A) and GABA-treated (B) *P. fluorescens* MF37. Each figure is a representative example of three different analysis. Arrows indicate peaks particularly modified between control and GABA-treated bacteria.



3. Discussion

GABA is present from eukaryotes to bacteria and should have a pivotal role in inter-kingdom communication [31,32]. We have recently described that GABA stimulates the virulence of the opportunistic pathogen, *P. aeruginosa* [13]. The existence of GABA binding proteins or sensors in other *Pseudomonas* and, particularly, in *P. fluorescens* has been known for a long time [14], but the physiological effect of GABA in this species was not investigated until now.

As shown with *P. aeruginosa* PAO1, GABA (10^{-5} M) had no effect on the growth kinetic and mobility of *P. fluorescens* MF37, but markedly affected the cytotoxic activity of this bacterium. LDH is a stable eukaryotic enzyme considered as a marker of necrosis or non-specific cell death, whereas nitrite ions can be employed as markers of apoptosis, since they are generated by the spontaneous conversion of nitric oxide (NO) during eukaryotic cells apoptosis [25,33]. Whereas the release of LDH from glial cells exposed to GABA-treated bacteria was increased, the concentration of NO was significantly decreased. These results are only contradictory in appearance, since the time course of necrosis is more rapid than required for induction of apoptosis [34], and a rapid induction of necrosis can prevent the activation of apoptosis [35]. It is also interesting to note that the absence of response of *P. fluorescens* MF37 to muscimol and bicuculline suggests that in this strain, the GABA sensor is not related to the muscimol-sensitive GBP protein identified by Guthrie *et al.* [36] in an environmental strain of *P. fluorescens*. The virulence of *P. fluorescens* is highly variable and appears strain- and environment-dependent. A psychrotrophic strain, such as *P. fluorescens* MF37, has a marked cytotoxic activity on animal cells [25], and some clinical strains have an infectious potential in the same range as *P. aeruginosa* [21]. Conversely, in plants, *P. fluorescens* is essentially, if not always, considered as a protecting agent [20,37]. Also, GABA appears to have opposite effects on bacterial virulence in plants and animal models. Indeed, as in *P. aeruginosa* [13], GABA acts as promoter of *P. fluorescens* cytotoxicity on rat glial cells, whereas in a phytopathogen, such as *A. tumefaciens*, GABA reduces the virulence [18]. This should be correlated to the different functions of GABA in plants, where it is a main contributor of the defense system [38], and in animals, where its protective role is apparently marginal [39]. Alternatively, these differences should reflect opposite adaptation processes between α - and γ -Proteobacteria, such as *Agrobacterium* and *Pseudomonas*.

Bacteria have two lifestyles, *i.e.*, planktonic and in biofilms. In biofilms, bacteria are protected against the action of antibiotics and host immune system molecules [40]. We tested the effect of GABA on *P. fluorescens* adhesion and biofilm formation activity on living cells, PVC (hydrophobic) and glass (hydrophilic) surfaces. GABA did not modify the initial binding index of *P. fluorescens* MF37 on living glial cells, but increased its adhesion on glass. On PVC, we observed a significant reduction of the biofilm formation activity only after 48 h, when the bacteria were pretreated with GABA during their growth phase, and after 24 h (but not after 48 h), when the bacteria were pretreated both during the growth phase and the biofilm formation period. These results suggest that only bacteria in the early growth phase are sensible to GABA either, because they express a sensor differently or, as in biofilm, GABA is unable to affect their physiology. We also tested the effect of GABA on the biofilm formation activity of bacteria on glass to observe the biofilm structure. This study was performed on *P. fluorescens* MF37, but also in other strains from environmental (Pf0-1, SBW25), clinical (MFN1032) or human skin (MFP05) origin. GABA did not affect the structure and the thickness of the

biofilms, except in the case of MFP05, where GABA induced an apparent increase of the biofilm maturation speed. GABA is synthesized and released in skin [41], and the response of MFP05 to GABA should represent an adaptation response to host signals. It is interesting to note that human skin *P. fluorescens* are special. Indeed, whereas these bacteria are found in abundance on skin regions in metagenomic studies [42], they are rarely cultivable [43], suggesting that they require specific growth conditions. In agreement with our results, this points out the high heterogeneity of *P. fluorescens* and their dependence in regards to the microenvironment.

As bacterial adhesion is governed by the surface properties, we investigated the effect of GABA on the hydrophobicity, biosurfactant production and LPS structure of *P. fluorescens* MF37. The surface hydrophobicity of the bacteria was estimated by the MATS technique. The affinity of *P. fluorescens* MF37 to hexadecane is under 20% ; then, according to Bellon-Fontaine *et al.* [28], this strain was hydrophilic in our experimental conditions. GABA significantly increased the affinity of *P. fluorescens* MF37 to hexadecane, but the general hydrophilic character of the bacterium was preserved. It is known that biosurfactants synthesized by *P. fluorescens* are implicated in surface adhesion and biofilm formation [44]. The possible effect of GABA on biosurfactants production was studied by direct measurement of the surface tension of the rinsing medium of bacterial colonies. In control medium, this value was over 40 mN/m, indicating that *P. fluorescens* MF37 was not producing biosurfactants, and this surface tension was unchanged after GABA treatment. As in parallel, GABA did not interfere with the swimming or swarming potential of *P. fluorescens* MF37; this suggests that the structure and activity of flagella and pili were not modified. This is not excluding that GABA could interfere with other adhesins, but, if any, this effect should be marginal.

P. fluorescens releases different diffusible enzymatic activities, but none was modified by GABA. Similarly, pyoverdine, which can trigger cytotoxicity [45], was also unaffected. In order to identify the factor responsible for the evolution of the cytotoxicity and surface properties of GABA-treated *P. fluorescens* MF37, we investigated the effect of GABA on the LPS structure. LPS is the major endotoxin of *Pseudomonas*, and it is known to play a key role in bacterial adhesion [46,47]. MALDI-TOF mass spectra of LPS extracted from control and GABA-treated *P. fluorescens* MF37 showed limited, but repeatable differences. These differences were essentially observed in low m/z LPS sub-fragments that should be generated by cleavage of lipid A. Interestingly, in *P. aeruginosa*, structural changes in this region have been associated with an increase in necrotic activity [30]. As observed in the case of growth temperature variations [27] or exposure to natriuretic peptides [35], the virulence of *P. fluorescens* MF37 appears modulated by a rearrangement of the LPS structure. It should be noted that NO has, by itself, a high cytotoxicity on glial cells [48], but its production by cells exposed to GABA-treated bacteria was reduced, suggesting that its contribution to glial cell death is marginal. Then, although *P. fluorescens* MF37 and *P. aeruginosa* PAO1 respond to GABA by an increase in cytotoxicity, the mechanisms appear to be very different. In *P. aeruginosa*, the effect of GABA is due to an over-production of a diffusible virulence factor (HCN) [13], whereas in *P. fluorescens*, it is essentially, if not only, dependent on the LPS structure and, then, contact-dependent.

4. Experimental Section

4.1. Bacterial Strains and Culture Conditions

P. fluorescens MF37 is a natural rifampicin-resistant mutant of the strain MF0 from raw milk [49]. This strain is a model of psychrotrophic *Pseudomonas* widely used in our laboratory. *P. fluorescens* MFN1032 is a clinical strain adapted to grow at 37 °C collected from a pulmonary tract infection [21]. It is considered to be a nosocomial bacterium. *P. fluorescens* MFP05 was collected from human skin, where this species is considered as a member of the transient bacterial microflora. *P. fluorescens* SBW25 and Pf0-1 are environmental bacteria. The SBW25 strain was isolated from plant leaves, whereas the Pf0-1 strain was isolated from agricultural soil [50]. For pre-treatment, bacteria were transferred to 25 mL of nutrient broth (NB, Merck, Darmstadt, Germany) containing or not containing GABA (10^{-5} M) and were cultured at 28 °C, until the beginning of the stationary phase. The density of the bacterial suspension was determined by absorption at 580 nm (ThermoSpectronics, Cambridge, UK).

4.2. Swimming and Swarming Mobility Tests

Cultures of *P. fluorescens* MF37 in NB in the early stationary phase were collected and centrifuged (10 min, 6000 rpm). For the swimming mobility test, plates containing 0.3% agar were inoculated on the surface using a needle previously soaked with the centrifugation pellet. The plates were incubated at 28 °C until the development of a migration halo. The diameter of the halo was measured between 4 and 48 h after inoculation. The values of mobility were determined over a minimum of 3 independent measures. For the swarming mobility test, the same protocol was used, except that NB medium was supplemented with 0.5% agar.

4.3. Cytotoxic Activity Tests

The effect of GABA, muscimol and bicuculline on the cytotoxic activity of *P. fluorescens* MF37 was investigated on primary cultures of rat glial cells using biochemical indicators of apoptosis and necrosis, as previously described [25,27]. Rat glial cells, obtained from newborn (24–48 h) rat brain, were grown in DMEM/Ham's medium (2/1) supplemented with 10% fetal calf serum, 2 mM glutamine, 0.001% insulin, 5 mM HEPES, 0.3% glucose and 1% antibiotic-antimycotic solution (Biowhittaker, Emerainville, France). The cells were layered at a concentration of 10^5 cells/well on 24 well-plates coated with poly-L-lysine ($50 \mu\text{g.mL}^{-1}$) and kept at 37 °C in a 5% CO₂ humidified atmosphere. Glial cells were allowed to grow for 12–16 days before use. For the tests, bacteria were pretreated with GABA overnight (18 h) at 28 °C. Before the tests, bacteria in the stationary phase were harvested by centrifugation (6000 rpm, 5 min) and rinsed 3 times to remove any trace of free GABA. Bacteria were then re-suspended at a density of 10^6 CFU.mL⁻¹ in glial cell culture medium without antibiotics and antimycotics and incubated with glial cells during 24 h. The concentration of LDH was determined using the Cytotox 96® Enzymatic Assay (Promega, Charbonnieres, France). Nitrite ions (NO₂⁻) resulting from the spontaneous conversion of nitric oxide (NO) in the incubation medium were measured using the Griess colorimetric reaction.

4.4. Evaluation of the Bacterial Biofilm Formation Activity by the Crystal Violet Technique

The biofilm formation activity of *P. fluorescens* MF37 was studied using the crystal violet technique adapted from O'Toole and Kolter [51]. Cultures of *P. fluorescens* MF37 grown in NB and in the early stationary phase were centrifuged for 10 min at 6000 rpm and rinsed with sterile water NaCl 0.9% (SPW). Then, an aliquot of 100 μ L of a bacterial culture adjusted to an $OD_{580} = 0.4$ was layered in a polystyrene microtitration plate (96 wells) and incubated for 24 or 48 h. In a first series of experiments, bacteria were grown in the absence of GABA, but were exposed to the molecule during the biofilm formation. In a second series of experiments, bacteria were grown in the presence of GABA, but GABA was not added to the medium during the biofilm formation step. In a third series of experiments, bacteria were grown with GABA, as previously, but the medium in PVC microtitration plates was supplemented with GABA to maintain the treatment during the 24 to 48 h of biofilm formation. At the end of the incubation time (24 h or 48 h) at 28 °C, the OD_{595} was measured. After removal of the bacterial suspension and rinsing with SPW, bacteria and matrix bound to the wells were stained with 150 μ L of crystal violet (0.1%, 30 min). After rinsing, the dye was recovered by adding 150 μ L of SDS (1% in sterile water, 15 min), and the OD_{595} nm of the solution was measured. Data were normalized as a percentage of biofilm density in the absence of treatment. The percentage of biofilm formation was evaluated by the following equation:

$$\% \text{ of biofilm formation} = (\text{OD}_{595} \text{ after crystal violet staining}/\text{OD}_{595} \text{ before crystal violet staining}) \times 100 \quad (1)$$

4.5. GFP Transformation

P. fluorescens MF37, SBW25, MFN1032, Pf0-1 and MFP05 were transformed with the pSMC2.1 plasmid [52]. The plasmid was extracted from an *E. coli* strain containing the green fluorescent protein (GFP) gene and a kanamycin resistance cassette. Briefly, 1.5 mL aliquots of bacterial cultures realized in LB medium at 28 °C and reaching an OD_{580} between 1 and 2 were centrifuged for 1 min at 13,000 rpm. The pellet was washed 3 times with 300 μ L of sucrose (300 mM) and re-suspended in 100 μ L of sucrose (300 mM). For the Pf0-1 strain, the pellet was washed and re-suspended using cold distilled water. Competent cells were mixed with 5 μ L of pSMC2.1 plasmid and electroporated at 1800 V. After electroporation, bacteria were incubated in 1 mL of LB medium for 1 h at 28 °C under 180 rpm agitation. A small volume of the culture (100 μ L) was layered on LB agar supplemented with kanamycin (200 μ g/mL). After 24 h of incubation, transformed bacteria were observed by confocal microscopy (LSM 710, Zeiss, Oberkochen, Germany) to verify the integration of the plasmid and the production of a green fluorescent signal.

4.6. Confocal Microscope Study of the Bacterial Biofilm Formation Activity on Glass Surfaces

A pre-culture and cultures of the GFP transformed strains of *P. fluorescens* were realized in NB medium, supplemented with kanamycin (200 μ g/mL) for MFN1032, MF37 and SBW25. The plasmid was stable in the strains MFP05 and Pf0-1, and the antibiotic pressure was not necessary. After 24 h of incubation with or without GABA (10^{-5} M), bacteria were centrifuged at $7000 \times g$ for 10 min at room temperature. The pellets were washed one time with SPW and adjusted at $OD_{580} = 1$ in a final volume of 25 mL. Glass slides, washed beforehand with ethanol, were placed in Petri dishes, covered with the

bacterial suspension and incubated at 28 °C in static condition. After 2 h, glass slides were washed two times with SPW. One slide was heath fixed to control the adhesion capacity of the bacteria, and the others were covered with 25 mL of NB and incubated at 28 °C. After 5, 24 and 48 h of incubation, one glass slide was washed two times with SPW, dried, fixed and observed with a confocal microscope (LSM 710, Zeiss) using an $\times 63$ immersion objective. Images were processed using Zen software (Zeiss, 2009); a median filter was applied, images were segmented and fluorescence was quantified.

4.7. Evaluation of Bacterial Surface Properties

The binding index of bacteria on biological (cell) surfaces was determined using the gentamicin exclusion test [33]. Glial cells were exposed to bacteria ($10^6 \text{ CFU} \cdot \text{mL}^{-1}$) in culture medium without antibiotics and antimycotics for 4 h. At the end of the incubation period, cultures were rinsed 3 times with fresh medium to remove unattached bacteria. A part of the wells was immediately treated with 500 μL of Triton X100 in SPW (0.1% v/v) for 15 min at 37 °C. After plating and incubation for 2 days at 28 °C, the total number of bacteria present at the surface and in the cells was determined. Other wells were exposed to gentamicin ($300 \text{ } \mu\text{g} \cdot \text{mL}^{-1}$) for 1 h at 37 °C, rinsed 3 times and then treated with Triton X100 (0.1%) for 15 min. Extracellular bacteria were killed by gentamicin, and the colonies obtained after culture correspond to bacteria exclusively present in the intracellular compartment. The number of adherent bacteria was calculated as the difference between the total number and the intracellular bacteria.

The binding index of bacteria on glass slides was determined by direct counting. Before use, glass slides were cleaned by immersion in ethanol (70% in water), rinsed in sterile water and treated with TFD4 detergent (4% in 50 °C water) for 1 h to remove any traces of lipids. Then, glass slides were rinsed in sterile water and dried under laminar air flow. A bacterial suspension ($10^8 \text{ CFU} \cdot \text{mL}^{-1}$ in SPW) was layered on each glass slide. Bacteria were allowed to adhere for 2 h at 28 °C. Non-adherent bacteria were removed by rinsing with SPW, and the remaining adherent bacteria were immediately stained with acridine orange (0.01% in SPW) for 20 min. After rinsing in SPW and drying, the slides were observed using an epifluorescence microscope Zeiss Axiovert 100 equipped with a Nikon DXM1200F color camera. The binding index was determined by counting a minimum of 20 homologous fields.

The surface polarity of bacteria was determined using the microbial adhesion to solvent (MATS) technique [28]. Bacterial cultures treated or not with GABA (10^{-5} M) were harvested by centrifugation for 10 min at $10,000 \times g$. Pellets were rinsed 2 times with SPW and diluted to $\text{OD}_{400} = 0.8$. An aliquot of bacterial suspension (2.4 mL) was mixed with 0.4 mL of hexadecane in glass tubes. The tubes were vigorously hand-shaken for 10 s, vortexed for 45 s and hand-shaken again for 10 s. After 15 min, the OD_{400} of the aqueous phase was measured. The percentage of affinity for hexadecane was calculated by the relation: $[(\text{OD control} - \text{OD test})/\text{OD control}] \times 100$.

In this relation, OD control corresponds to the OD_{400} of bacterial suspension without hexadecane, and OD test corresponds to the OD_{400} of bacterial suspension with hexadecane.

4.8. Surface Tension and Biosurfactant Production in Bacterial Culture Medium

The biosurfactant production was monitored indirectly by measuring the surface tension of the rinsing solution (SPW) of colonies of *P. fluorescens* grown during 48 h on solid NB medium, using the Wilhelmy plate technique [53].

4.9. Study of the Lipopolysaccharide Structure

The lipopolysaccharide (LPS) was purified from *P. fluorescens* MF37, as described by Darveau and Hancock [54]. Bacteria in the early stationary phase were harvested by centrifugation ($6000 \times g$, 10 min, 4 °C). Each pellet was re-suspended in 10 mM Tris-buffer 10 mM containing 2 mM MgCl₂, 200 µg mL⁻¹ pancreatic DNase and 50 µg·mL⁻¹ pancreatic RNase and was submitted to sonication (4 burst of 30 s, probe density 70). The suspension was then incubated for 2 h at 37 °C. Then, 0.5 M tetrasodium-EDTA, 100 µL of Tween 20 and 10 mM Tris-hydrochloride were added. The samples were centrifuged (10,000× g, 30 min, 20 °C) to remove the peptidoglycan. The supernatants were incubated overnight with 200 µg/mL of protease, at 37 °C, with constant shaking. Two volumes of 0.375 M MgCl₂ in 96% ethanol were added. The samples were then centrifuged (12,000× g, 15 min, 4 °C), and the pellets were sonicated in a solution of Tween 20, 0.5 M tetrasodium-EDTA and 10 mM MgCl₂. The pH of the solutions was lowered to 7 to prevent lipid saponification. The solutions were incubated for 30 min at 85 °C, to ensure that outer membrane proteins were denatured, and the pH of the solutions was increased to 9.5. Protease was then added, and the samples were incubated overnight at 37 °C. Two volumes of 0.375 M MgCl₂ in 96% ethanol were added, and the samples were centrifuged (12,000× g, 15 min, 4 °C). The pellets were re-suspended in 10 mM Tris-HCl, sonicated and centrifuged twice to remove insoluble Mg²⁺-EDTA crystals. The supernatants were then centrifuged (62,000× g, 2 h, 15 °C). The pellets containing the LPS were re-suspended in distilled water. The LPS extracts were analyzed by Matrix-Assisted Laser Desorption/Ionization Time-of-Flight mass spectrometer (MALDI-TOF) using an Autoflex III TOF/TOF 200 MALDI mass spectrometer (Bruker Daltonics Wissembourg, France). For analysis, a 1 µL aliquot of purified LPS was spotted onto a steel target plate and air dried. A volume of 1 µL of a solution of α-cyano-4-hydroxycinnamic acid matrix (14 mg/mL in acetonitrile/2.5% trifluoroacetic acid, v/v) was added on each spot and dried at room temperature. The mass spectrometer was equipped with a pulsed YAG 200 Hz laser and was run in the positive mode. Instrument calibration was achieved by using calibration standards (Care, Bruker Daltonics, Wissembourg, France) spotted on the same target plate. Each spectrum was established over 200 laser shots.

4.10. Detection of Diffusible Virulence Factors

Little is known about diffusible virulence factors produced by *P. fluorescens*. In the present study, we focused on the production of exoenzymes and pyoverdine.

Secreted caseinase, esterase, amylase and hemolytic activities were studied from cultures on milk, Tween 80, starch and Columbia blood supplemented agar medium, respectively. For these tests, the medium was inoculated on the surface using a needle previously soaked with the centrifugation pellet

and were incubated at 28 °C until the development of a halo revealing the bacterial enzymatic activity. The diameter of the halos was measured 24 h and 48 h after incubation.

The elastase activity was measured in liquid bacterial culture medium using an elastin/Congo red assay. Filtered supernatant (50 µL) was mixed with 1 mL of Tris buffer (0.1 M Tris-HCl pH 7.2, 1 mM CaCl₂) containing 20 mg of elastin/Congo red (Sigma, St Quentin Fallavier, France). The tubes were incubated at 28 °C with agitation. After 18 h, the tubes were chilled on ice, and the reaction was stopped by adding 0.1 mL EDTA 0.12 M. Non-soluble elastin/Congo red was removed by centrifugation, and the OD₄₉₀ was measured.

Pyoverdine production was monitored from 6 to 48 h of bacterial culture. To promote pyoverdine production, bacteria were grown on King B medium (for 1 L: 10 g glycerol; 20 g polypeptone; 1.5 g K₂HPO₄; 6 mM MgSO₄, 7 H₂O; pH 7) or in Bacto Casamino Acids (CAA) medium (for 1 L: 5 g of casamino acid; 0.9 g of K₂HPO₄; 2 mM MgSO₄, 7H₂O; pH 7.4). Pyoverdine production was expressed as the ratio OD₄₀₀/OD₅₈₀ of the supernatant after removal of the bacteria by centrifugation (5 min, 10,000× g).

4.11. Statistical Analysis

For all the results, each value reported for the assays is the mean of measurements from a minimum of three independent preparations. The Student *t*-test was used to compare the means within the same set of experiments.

5. Conclusions

In this present study, we demonstrate that GABA increases the cytotoxicity of *P. fluorescens* MF37 through modifications of the LPS structure. Furthermore, we observed that GABA can affect the biofilm formation activity and the surface polarity of the bacterium. These properties are not shared by all *P. fluorescens* strains, suggesting that GABA-sensitive strains adapted in response to specific environmental conditions. The mechanisms of virulence modulated by GABA in *P. fluorescens* and in *P. aeruginosa* are totally different, suggesting the existence of different detection and regulatory mechanisms.

Acknowledgements

This study was supported by grants from the Conseil Général de l'Eure, the Communauté d'Agglomération d'Evreux and Europe (FEDER n°31970). LMSM is member of the PFT Normandie Sécurité Sanitaire, of the Institute for Research and Innovation in Biotechnologies (IRIB) and of the first perfumery-cosmetic worldwide network, Cosmetic Valley. AD was a recipient from the French Ministry of Research (MRE). The authors are grateful to Christine Farmer for linguistic support.

Conflicts of Interest

The author declares no conflict of interest.

References

1. Qi, Z.; Cort, A. Free and combined amino compounds in atmospheric fine particles (PM_{2.5}) and fog waters from Northern California. *Atmos. Environ.* **2003**, *37*, 2247–2258.
2. Noe, F.F.; Nickerson, W.J. Metabolism of 2-pyrrolidone and gamma aminobutyric acid by *Pseudomonas aeruginosa*. *J. Bacteriol.* **1958**, *75*, 674–681.
3. Chou, H.T.; Kwon, D.H.; Hegazy, M.; Lu, C.D. Transcriptome analysis of agmatine and putrescine catabolism in *Pseudomonas aeruginosa* PAO1. *J. Bacteriol.* **2008**, *190*, 1966–1975.
4. Tunnicliff, G. Inhibition of 4-aminobutyrate aminotransferase from *Pseudomonas fluorescens* by ATP. *Biochem. Mol. Biol. Int.* **1993**, *31*, 41–47.
5. Kaspar, H.F.; Mountfort, D.O.; Pybus, V. Degradation of gamma-aminobutyric acid (GABA) by marine microorganisms. *FEMS Microbiol. Ecol.* **1991**, *85*, 313–318.
6. Mountfort, D.O.; Pybus, V. Regulatory influences on the production of gamma-aminobutyric acid by a marine pseudomonad. *Appl. Environ. Microbiol.* **1992**, *58*, 237–242.
7. Siragusa, S.; de Angelis, M.; di Cagno, R.; Rizzello, C.G.; Coda, R.; Gobbetti, M. Synthesis of gamma-aminobutyric acid by lactic acid bacteria isolated from a variety of Italian cheeses. *Appl. Environ. Microbiol.* **2007**, *73*, 7283–7290.
8. Richard, H.T.; Foster, J.W. Acid resistance in *Escherichia coli*. *Adv. Appl. Microbiol.* **2003**, *52*, 167–186.
9. Brechtel, C.E.; King, S.C. 4-Aminobutyrate (GABA) transporters from the amine-polyamine-choline superfamily: Substrate specificity and ligand recognition profile of the 4-aminobutyrate permease from *Bacillus subtilis*. *Biochem. J.* **1998**, *333*, 565–571.
10. Hu, L.A.; King, S.C. Membrane topology of the *Escherichia coli* γ -aminobutyrate transporter: Implications on the topography and mechanism of prokaryotic and eukaryotic transporters from the APC superfamily. *Biochem. J.* **1998**, *336*, 68–76.
11. Zhao, Z.; Ding, J.Y.; Ma, W.H.; Zhou, N.Y.; Liu, S.J. Identification and characterization of gamma-aminobutyric acid uptake system GabP_{Cg} (NCgl0464) in *Corynebacterium glutamicum*. *Appl. Environ. Microbiol.* **2012**, *78*, 2596–2601.
12. Planamente, S.; Mondy, S.; Hommais, F.; Vigouroux, A.; Moréra, S.; Faure, D. Structural basis for selective GABA binding in bacterial pathogens. *Mol. Microbiol.* **2012**, *85*, 1085–1099.
13. Dagorn, A.; Hillion, M.; Chapalain, A.; Lesouhaitier, O.; Duclairoir-Poc, C.; Vieillard, J.; Chevalier, S.; Taupin, L.; Le Derf, F.; Feuilloley, M.G.J. Gamma-aminobutyric acid acts as a specific virulence regulator in *Pseudomonas aeruginosa*. *Microbiology* **2013**, *159*, 339–351.
14. Guthrie, G.D.; Nicholson-Guthrie, C.S. Gamma-Aminobutyric acid uptake by a bacterial system with neurotransmitter binding characteristics. *Proc. Natl. Acad. Sci. USA* **1989**, *86*, 7378–7381.
15. Richard, H.; Foster, J.W. *Escherichia coli* glutamate- and arginine-dependent acid resistance systems increase internal pH and reverse transmembrane potential. *J. Bacteriol.* **2004**, *186*, 6032–6041.
16. Tramonti, A.; de Canio, M.; Delany, I.; Scarlato, V.; de Biase, D. Mechanisms of transcription activation exerted by GadX and GadW at the gadA and gadBC gene promoters of the glutamate-based acid resistance system in *Escherichia coli*. *J. Bacteriol.* **2006**, *188*, 8118–8127.

17. De Biase, D.; Pennacchietti, E. Glutamate decarboxylase-dependent acid resistance in orally acquired bacteria: Function, distribution and biomedical implications of the gadBC operon. *Mol. Microbiol.* **2012**, *86*, 770–786.
18. Chevrot, R.; Rosen, R.; Haudecoeur, E.; Cirou, A.; Shelp, B.J.; Ron, E.; Faure, D. GABA controls the level of quorum-sensing signal in *Agrobacterium tumefaciens*. *Proc. Natl. Acad. Sci. USA* **2006**, *103*, 7460–7464.
19. Park, D.H.; Mirabella, R.; Bronstein, P.A.; Preston, G.M.; Haring, M.A.; Lim, C.K.; Collmer, A.; Schuurink, R.C. Mutations in gamma-aminobutyric acid (GABA) transaminase genes in plants or *Pseudomonas syringae* reduce bacterial virulence. *Plant J.* **2010**, *64*, 318–330.
20. Van de Mortel, J.E.; de Vos, R.C.; Dekkers, E.; Pineda, A.; Guillo, L.; Bouwmeester, K.; van Loon, J.J.; Dicke, M.; Raaijmakers, J.M. Metabolic and transcriptomic changes induced in *Arabidopsis* by the rhizobacterium *Pseudomonas fluorescens* SS101. *Plant Physiol.* **2012**, *160*, 2173–2188.
21. Chapalain, A.; Rossignol, G.; Lesouhaitier, O.; Merieau, A.; Gruffaz, C.; Guerillon, J.; Meyer, J.M.; Orange, N.; Feuilloley, M.G.J. Comparative study of 7 fluorescent pseudomonad clinical isolates. *Can. J. Microbiol.* **2008**, *54*, 19–27.
22. Mozrzymas, J.W.; Zarnowska, E.; Pytel, M.; Mercik, K. Modulation of GABA_A receptors by hydrogen ions reveals synaptic GABA transient and a crucial role of the desensitization process. *J. Neurosci.* **2003**, *23*, 7981–7692.
23. Shelp, B.J.; Bown, A.W.; Faure, D. Extracellular gamma-aminobutyrate mediates communication between plants and other organisms. *Plant Physiol.* **2006**, *142*, 1350–1352.
24. Johnson, C.R.; Muir, D.G.; Reysenbach, A.L. Characteristic bacteria associated with surfaces of coralline algae: A hypothesis for bacterial induction of marine invertebrate larvae. *Mar. Ecol. Prog. Ser.* **1991**, *74*, 281–294.
25. Picot, L.; Chevalier, S.; Mezghani-Abdelmoula, S.; Merieau, A.; Lesouhaitier, O.; Leroux, P.; Cazin, L.; Orange, N.; Feuilloley, M.G.J. Cytotoxic effects of the lipopolysaccharide from *Pseudomonas fluorescens* on neurons and glial cells. *Microb. Pathog.* **2003**, *35*, 95–106.
26. Angulo, M.C.; Le Meur, K.; Kozlov, A.S.; Charpak, S.; Audinat, E. GABA, a forgotten gliotransmitter. *Prog. Neurobiol.* **2008**, *86*, 297–303.
27. Picot, L.; Mezghani-Abdelmoula, S.; Chevalier, S.; Merieau, A.; Lesouhaitier, O.; Guerillon, J.; Cazin, L.; Orange, N.; Feuilloley, M.G.J. Regulation of the cytotoxic effects of *Pseudomonas fluorescens* by growth temperature. *Res. Microbiol.* **2004**, *155*, 39–46.
28. Bellon-Fontaine, M.N.; Rault, J.; van Oss, C.J. Microbial adhesion to solvents: A novel method to determine the electron-donor/electron-acceptor or Lewis acid-base properties of microbial cells. *Colloids Surf. B Biointerfaces* **1996**, *7*, 47–53.
29. Cornelis, P. Iron uptake and metabolism in pseudomonads. *Appl. Microbiol. Biotechnol.* **2010**, *86*, 1637–1645.
30. Veron, W.; Lesouhaiter, O.; Pennanec, X.; Rehel, K.; Leroux, P.; Orange, N.; Feuilloley, M.G.J. Natriuretic peptides affect *Pseudomonas aeruginosa* and specifically modify LPS biosynthesis. *FEBS J.* **2007**, *274*, 5852–5864.
31. Owens, D.F.; Kriegstein, A.R. Is there more to GABA than synaptic inhibition? *Nat. Rev. Neurosci.* **2002**, *3*, 715–727.

32. Bouché, N.; Lacombe, B.; Fromm, H. GABA signaling: A conserved and ubiquitous mechanism. *Trends Cell. Biol.* **2003**, *13*, 607–610.
33. Mezghani-Abdelmoula, S.; Khemiri, A.; Lesouhaitier, O.; Chevalier, S.; Orange, N.; Cazin, L.; Feuilloley, M.G.J. Sequential activation of constitutive and inducible nitric oxide synthase (NOS) in rat cerebellar granule neurons by *Pseudomonas fluorescens* and invasive behaviour of the bacteria. *Microbiol. Res.* **2004**, *159*, 355–363.
34. Fink, S.L.; Cookson, B.T. Apoptosis, pyroptosis and necrosis: Mechanistic description of dead and dying eukaryotic cells. *Infect. Immun.* **2005**, *73*, 1907–1916.
35. Veron, W.; Orange, N.; Feuilloley, M.G.J.; Lesouhaitier, O. Natriuretic peptide modify *Pseudomonas fluorescens* cytotoxicity by regulating cyclic nucleotides and modifying LPS structure. *BMC Microbiol.* **2008**, *8*, 114.
36. Guthrie, G.D.; Nicholson-Guthrie, C.S.; Leary, H.L. A bacterial high-affinity GABA binding protein: Isolation and characterization. *Biochem. Biophys. Res. Commun.* **2000**, *268*, 65–68.
37. Haas, D.; Defago, G. Biological control of soil-borne pathogens by fluorescent pseudomonads. *Nat. Rev. Microbiol.* **2005**, *3*, 307–319.
38. Bown, A.W.; MacGregor, K.B.; Shelp, B.J. Gamma-aminobutyrate: Defense against invertebrate pests? *Trends Plant Sci.* **2006**, *11*, 424–427.
39. Kumar, P.; Kalonia, H.; Kumar, A. Possible GABAergic mechanism in the neuroprotective effect of gabapentin and lamotrigine against 3-nitropropionic acid induced neurotoxicity. *Eur. J. Pharmacol.* **2012**, *674*, 265–274.
40. Davey, M.E.; O'Toole, G.A. Microbial biofilms: From ecology to molecular genetics. *Microbiol. Mol. Biol. Rev.* **2000**, *64*, 847–867.
41. Ito, K.; Tanaka, K.; Nishibe, Y.; Hasegawa, J.; Ueno, H. GABA-synthesizing enzyme, GAD67, from dermal fibroblasts: Evidence for a new skin function. *Biochim. Biophys. Acta* **2007**, *1770*, 291–296.
42. Grice, E.A.; Kong, H.H.; Renaud, G.; Young, A.C.; Bouffard, G.G.; Blakesley, R.W.; Wolfsberg, T.G.; Turner, M.L.; Segre, J.A. A diversity profile of the human skin microbiota. *Genome Res.* **2008**, *18*, 1043–1050.
43. Gao, Z.; Tseng, C.; Pei, Z.; Blaser, M.J. Molecular analysis of human forearm superficial skin bacterial biota. *Proc. Natl. Acad. Sci. USA* **2007**, *104*, 2927–2932.
44. Raaijmakers, J.M.; De Bruijn, I.; Nybroe, O.; Ongena, M. Natural functions of lipopeptides from *Bacillus* and *Pseudomonas*: More than surfactants and antibiotics. *FEMS Microbiol. Rev.* **2010**, *34*, 1037–1062.
45. Becerra, C.; Albesa, I.; Eraso, A.J. Leukotoxicity of pyoverdin, production of reactive oxygen species, and effect of UV radiation. *Biochem. Biophys. Res. Commun.* **2001**, *285*, 414–418.
46. Makin, S.A.; Beveridge, T.J. The influence of A-band and B-band lipopolysaccharide on the surface characteristics and adhesion of *Pseudomonas aeruginosa* to surfaces. *Microbiology* **1996**, *142*, 299–307.
47. Yokota, S.; Fujii, N. Contributions of the lipopolysaccharide outer core oligosaccharide region on the cell surface properties of *Pseudomonas aeruginosa*. *Comp. Immunol. Microbiol. Infect. Dis.* **2007**, *30*, 97–109.

48. Mitrovic, B.; Ignarro, L.J.; Vinters, H.V.; Akers, M.-A.; Schmid, I.; Uittenbogaart, C.; Merrill, J.E. Nitric oxide induces necrotic but not apoptotic cell death in oligodendrocytes. *Neuroscience* **1995**, *65*, 531–539.
49. Burini, J.F.; Gügi, B.; Merieau, A.; Guespin-Michel, J.F. Lipase and acidic phosphatase from the psychrotrophic bacterium *Pseudomonas fluorescens*: Two enzymes whose synthesis is regulated by the growth temperature. *FEMS Microbiol. Lett.* **1994**, *122*, 13–18.
50. Silby, M.W.; Cerdeño-Tárraga, A.M.; Vernikos, G.S.; Giddens, S.R.; Jackson, R.W.; Preston, G.M.; Zhang, X.X.; Moon, C.D.; Gehrig, S.M.; Godfrey, S.A.; *et al.* Genomic and genetic analyses of diversity and plant interactions of *Pseudomonas fluorescens*. *Genome Biol.* **2009**, *10*, R51.
51. O'Toole, G.A.; Kolter, R. Flagellar and twitching motility are necessary for *Pseudomonas aeruginosa* biofilm development. *Mol. Microbiol.* **1998**, *30*, 295–304.
52. Bazire, A.; Diab, F.; Jebbar, M.; Haras, D. Influence of high salinity on biofilm formation by *Pseudomonas aeruginosa*. *J. Ind. Microbiol. Biotechnol.* **2007**, *34*, 5–8.
53. Hiemenz, P.C.; Lagowski, J.J. *Principles of Colloid and Surface Chemistry*; Lagowski, J.J., Ed.; Marcel Dekker: New York, NY, USA, 1977; p. 209.
54. Darveau, R.P.; Hancock, R.E. Procedure for isolation of bacterial lipopolysaccharides from both smooth and rough *Pseudomonas aeruginosa* and *Salmonella typhimurium* strains. *J. Bacteriol.* **1983**, *155*, 831–838.

© 2013 by the authors; licensee MDPI, Basel, Switzerland. This article is an open access article distributed under the terms and conditions of the Creative Commons Attribution license (<http://creativecommons.org/licenses/by/3.0/>).

Copyright of International Journal of Molecular Sciences is the property of MDPI Publishing and its content may not be copied or emailed to multiple sites or posted to a listserv without the copyright holder's express written permission. However, users may print, download, or email articles for individual use.

P19

Effects of a Skin Neuropeptide (Substance P) on Cutaneous Microflora

Lily Mijouin¹, Mélanie Hillion¹, Yasmina Ramdani², Thomas Jaouen¹, Cécile Duclairoir-Poc¹, Marie-Laure Follet-Gueye², Elian Lati³, Florent Yvergniaux⁴, Azzedine Driouch², Luc Lefevre⁵, Christine Farmer¹, Laurent Misery^{6,7}, Marc G. J. Feuilloley^{1*}

1 Laboratory of Microbiology Signals and Microenvironnement LMSM, EA 4312, Normandie Université, Université Rouen, Evreux, France, **2** GlycoMev EA 4358, Normandie Université, Université Rouen, Mont-Saint-Aignan, France, **3** Bio-EC Laboratory, Longjumeau, France, **4** BioEurope Research, Anet, France, **5** Dermatologic Laboratories Uriage, Courbevoie, France, **6** EA 4685 University of Western Brittany, Brest, France, **7** Department of Dermatology, University Hospital of Brest, Brest, France

Abstract

Background: Skin is the largest human neuroendocrine organ and hosts the second most numerous microbial population but the interaction of skin neuropeptides with the microflora has never been investigated. We studied the effect of Substance P (SP), a peptide released by nerve endings in the skin on bacterial virulence.

Methodology/Principal Findings: *Bacillus cereus*, a member of the skin transient microflora, was used as a model. Exposure to SP strongly stimulated the cytotoxicity of *B. cereus* ($+553 \pm 3\%$ with SP 10^{-6} M) and this effect was rapid (<5 min). Infection of keratinocytes with SP treated *B. cereus* led to a rise in caspase1 and morphological alterations of the actin cytoskeleton. Secretome analysis revealed that SP stimulated the release of collagenase and superoxide dismutase. Moreover, we also noted a shift in the surface polarity of the bacteria linked to a peel-off of the S-layer and the release of S-layer proteins. Meanwhile, the biofilm formation activity of *B. cereus* was increased. The Thermo unstable ribosomal Elongation factor (Ef-Tu) was identified as the SP binding site in *B. cereus*. Other Gram positive skin bacteria, namely *Staphylococcus aureus* and *Staphylococcus epidermidis* also reacted to SP by an increase of virulence. Thermal water from Uriage-les-Bains and an artificial polysaccharide (Teflose®) were capable to antagonize the effect of SP on bacterial virulence.

Conclusions/Significance: SP is released in sweat during stress and is known to be involved in the pathogenesis of numerous skin diseases through neurogenic inflammation. Our study suggests that a direct effect of SP on the skin microbiome should be another mechanism.

Citation: Mijouin L, Hillion M, Ramdani Y, Jaouen T, Duclairoir-Poc C, et al. (2013) Effects of a Skin Neuropeptide (Substance P) on Cutaneous Microflora. PLoS ONE 8(11): e78773. doi:10.1371/journal.pone.0078773

Editor: Roberto Amendola, ENEA, Italy

Received June 10, 2013; **Accepted** September 16, 2013; **Published** November 8, 2013

Copyright: © 2013 Mijouin et al. This is an open-access article distributed under the terms of the Creative Commons Attribution License, which permits unrestricted use, distribution, and reproduction in any medium, provided the original author and source are credited.

Funding: This work was supported by the FUI program Skin-O-Flor certified by the world's leading perfumery cosmetics network Cosmetic Valley and financed by the French Government (DGCIS), European Union (FEDER), Department of Eure et Loir and the Regions Centre and Haute-Normandie. The funders had no role in study design, data collection and analysis, decision to publish, or preparation of the manuscript.

Competing Interests: The authors have the following interests. This work was supported by public funds obtained in the framework of the FUI program Skin-O-Flor certified by the world's leading perfumery cosmetic network Cosmetic Valley. Elian Lati is employed by Bio-EC Laboratory, Florent Yvergniaux by BioEurope Research and Luc Lefevre by the Dermatologic Laboratories Uriage. Biogaleny SAS assisted with the HPLC analysis of cereulide. There are no patents, products in development of marketed products to declare. This does not alter the authors' adherence to all PLOS ONE policies on sharing data and materials, as detailed online in the guide for authors.

* E-mail: marc.feuilloley@univ-rouen.fr

Introduction

Skin is the largest neuroendocrine organ of the human body [1] and it hosts the second most numerous microbial population [2]. There is increasingly strong evidence that bacterial virulence is partly regulated by host hormones and neurotransmitters [3,4]. By sweat or direct contact with the dermis or the epidermis [5], skin micro-organisms are in contact with host communication factors. It is therefore paradoxical to note that, until now, the interaction of skin neuropeptides with the bacterial microflora was not taken into consideration.

Substance P (SP), the main neuropeptide identified in skin nerve endings, is essentially located in primary afferent C-fibers and is released in the skin [6]. This undecapeptide of the tachykinin

family has multiple bioactivities other than neurotransmission [7], such as capillary vasodilatation, fibroblast and keratinocyte proliferation or mast cell degranulation [1]. It is considered a major mediator of neurogenic inflammation [8] and itch [9]. Cutaneous neuropeptides, and particularly SP, contribute to the pathogenesis of numerous skin diseases, like psoriasis [10], atopic dermatitis [11,12], immediate and delayed hypersensitivity [13], acne [14] or rosacea [15]. These diseases have multifactorial origins and we suggest that SP could also act through interaction with the skin microflora. Indeed, SP has both direct and indirect antimicrobial activities by acting as a weak cationic antimicrobial peptide [16] and by stimulating the release of cathelicidins and defensins [17]. Different skin neuropeptides have antibacterial activities [3] but, as SP, these activities are generally observed at

high non-physiologic concentrations ($>10^{-4}$ M). At low doses, peptides, including anti-microbial ones, can affect the bacterial physiology independently of any modification in their growth rate [18]. For instance, at sub-micromolar concentrations some neuropeptides, such as dynorphin [19] or natriuretic peptides [20,21] have been shown to stimulate bacterial virulence.

In the present study, we investigated for the first time the action of SP on skin bacterial virulence using a human skin strain of *Bacillus cereus*. The mechanism of SP action on *Bacillus cereus* and its binding site were identified. We revealed that SP is acting on other Gram positive bacteria, namely *Staphylococcus aureus* and *Staphylococcus epidermidis*, suggesting that SP should act as a regulator of bacterial virulence in some of the principal skin associated bacteria. We also observed that this effect of SP on bacterial virulence can be antagonized by thermal water and an artificial polysaccharide.

Materials and Methods

Bacterial Strains, Growth Media and Culture Conditions

Bacillus cereus (MFP01), *Staphylococcus aureus* (MFP03) and *Staphylococcus epidermidis* (MFP04) originate from our library and were isolated previously from the skin of human donors in the framework of an industrial collaborative program. These bacteria, collected under control of the CRO Bio-EC (Longjumeau, France) in agreement with French and EU Ethic guidelines (ARS Biomedical Research Agreement N°2012-12-010, Bioethic Agreement DC-2008-542), have been identified using API® strips, 16S ribosomal RNA gene sequencing and whole proteome analysis by MALDI mass spectrometry and Biotype analysis (Bruker Daltonics). For confocal microscopy, these bacteria were transformed by insertion of the pTeTON-GFP plasmid [22]. Bacteria were grown at 37°C in Luria-Bertani (LB). For pre-treatment, they were diluted at a ratio of 1:40 in fresh broth and the peptides were added at the beginning of the log growth phase. Before use bacteria were rinsed to remove traces of the tested molecule. Substance P (SP) and the reversed sequence peptide (SPrev) were obtained from Polypeptide, Strasbourg, France. In all the studies, controls were carried out using SPrev.

Infection Studies

The interaction of bacteria with keratinocytes was studied using HaCaT cells (Cell Line Services, Eppelheim, Germany). Cells grown at 37°C in 5% CO₂ atmosphere in Dulbecco's modified Eagle's medium (DMEM, Lonza) were starved of antibiotics 24 h before infection assays. Cells were used between passages 41 and 65. The cytotoxic potential of bacteria was determined by measurement of lactate dehydrogenase (LDH) using the Cytotox 96 assay (Promega, Charbonnieres, France). The bacterial activation of caspase-1 was measured using a commercial kit (BioVision RP, Milpitas, California). For cytological studies *B. cereus* was treated with SPrev or SP and monolayers of HaCat cells were exposed to the bacteria at a multiplicity of infection (MOI) of 10:1. After incubation, keratinocytes were washed to remove unattached bacteria. Cells were then fixed for 10 min in 4% paraformaldehyde in water and permeabilized for 4 min in 0.2% Triton-X 100 in phosphate buffered saline (PBS). Actin was stained with anti-actin rabbit monoclonal antibody (Millipore, Molsheim, France) and revealed using goat anti-rabbit Alexa 633-labelled antibody (Molecular Probes, Saint-Aubin, France). Preparations were observed using a LSM 710 confocal laser-scanning microscope (Zeiss).

Identification of SP Stimulated *B. Cereus* Virulence Factors

For cereulide assay, *B. cereus* treated with SPrev or SP (10^{-6} M) were extracted with pentane. The solvent was evaporated and the residue was analyzed by HPLC-MS as described by Häggblom *et al.* [23]. Since cereulide is not commercially available, the calibration was made using valinomycin (Sigma, St Quentin-Fallavier, France). For the study of *B. cereus* exoproteins, supernatants from bacterial cultures were obtained by centrifugation at $7000 \times g$ for 10 min. After filtration on 0.22 µm disposable filter units, proteins were precipitated overnight on ice by addition of 10% trichloroacetic acid (TCA, v/v). Proteins were harvested at $13000 \times g$ for 20 min at 4°C, washed three times in cold acetone and dried for 1 h at room temperature. Extracted proteins were then dissolved in rehydration buffer [24] in a final volume of 350 µL. The protein concentration was determined on an aliquot by Bradford assay. Proteins were separated on 12% w/v polyacrylamide 1D gel SDS-PAGE and on 2D gels using pH 4 to 7 non-linear IEF strips and 12% w/v polyacrylamide gel [24]. The second dimension separation was run at 50 mA/gel for 4 h. Gel images were captured using a GS-800 densitometer (Bio-Rad) and analyzed using the Bio-rad PDQuest 2D analysis software. Bands or spots of interest were dissected, submitted to in-gel trypsin digestion [24], and analysed by MALDI-TOF using an AutoFlex III mass spectrometer (Bruker Daltonics) and a FlexControl software Version 3.3. The spectrometer was used in a positive/reflector mode using peptide calibration standards (Bruker Daltonics) as references. Samples were spotted onto MTP 384 ground steel targets using freshly prepared matrix solution composed of 2,5-dihydroxybenzoic acid (20 mg.mL⁻¹ in trifluoroacetic acid and acetonitrile). Each spectrum was established over an average of 500–1000 laser shots and 2,5-dihydroxybenzoic acid as matrix. The MS peak list was submitted for fingerprinting using Biotools (Version 3.2). The NCBI data base was searched using MASCOT (<http://www.matrixscience.com/cgi/nph-mascot.exe>).

Transmission Electronic Microscopy Observations

Control and SP-treated *B. cereus* were studied by Transmission Electronic Microscopy (TEM) using a Tecnai 12, FEI Company microscope. Bacteria fixed in 2% glutaraldehyde and postfixed with 1% osmium tetroxide were embedded in 2% agarose low melting point. After solidification, samples were cut into 2 mm³ slices, dehydrated, embedded in Spurr and polymerized for 24 h at 60°C. Ultrathin sections were obtained using a Leica EM UC6 ultramicrotome. The sections were contrasted with 0.5% uranyl acetate and lead citrate (10 min). The microscope was set at 60 kV. Images were processed by the PRIMACEN Platform (<http://primacen.crihan.fr>).

B. Cereus Surface Hydrophobicity and Biofilm Formation Studies

The polarity of control and SP treated *B. cereus* was studied using the MATS technique [25] and two solvent couples: chloroform/hexadecane and ethyl acetate/n-decane. The effect of SP on *B. cereus* biofilms was investigated using a LSM 710 CLSM (Zeiss). GFP-transformed bacteria grown for 13 h in the presence of SP or SPrev were poured in dishes containing sterile glass slides. After 2 h a slide was heat fixed to observe the initial adhesion. The other slides were covered by LB medium containing SP or SPrev and incubated for 5 or 24 h without agitation. In order to control their structure, the biofilms were scanned every micrometer in depth at 3 random positions. Three-dimensional (3D) images and ortho cuts (3D/z) were reconstructed using Zen® 2009 software (Zeiss). The biofilm thickness was quantified using the same software.

Identification of the *B. Cereus* SP Binding Site

For identification of the *B. cereus* SP binding site, proteins from mid-log growth phase bacteria were extracted as previously described [27]. Briefly, bacteria were harvested by centrifugation and washed with ice-cold PBS. The pellet was resuspended in non-denaturing lysis buffer (Tris 50 mM pH 8, EDTA 40 mM, NaCl 137 mM, glycerol 10%, Triton X-100 1%, Phenylmethylsulfonylfluoride 1 mM) supplemented with complete protease inhibitor cocktail (Complete Protease Inhibitor cocktail tabs, Boehringer). After sonication, cell fragments were removed by centrifugation and the supernatant was ultracentrifugated at 148,000×*g*, 50 min, 4°C. The pellet was then resuspended in a second ice cold lysis buffer (Tris 50 mM pH8, MgCl₂ 10 mM, Triton X-100 2%, Phenylmethylsulfonylfluoride 1 mM, Protease Inhibitor cocktail). The SP binding site was investigated by an immunoprecipitation technique adapted from Mijouin *et al.* [26]. SP antibody-associated beads were made by incubating G protein-coupled agarose beads (Millipore) and SP monoclonal antibody (Abcam, Paris, France) overnight. Meanwhile, 1.5 mg of *B. cereus* membrane protein extract was incubated with SP (10⁻⁶M) for 1 h at 20°C. To reduce the non-specific binding, 50 µg of rabbit polyclonal serum was added. Unlabelled agarose beads were added to fix non specific complexes. The sample was incubated 30 min at 4°C and the beads were removed by centrifugation (14000×*g*, 10 min). The supernatant, containing the SP bond ligand, was then incubated with the SP antibody-associated beads for 1 h at room temperature under slow orbital agitation. Beads were then washed by successive low speed centrifugation cycles in non-denaturing lysis buffer. The ligand was separated from the beads and denatured by adding loading buffer (Tris 200 mM pH 6.8, glycerol 45%, SDS 6%, β-mercaptoethanol 6%, bromophenol blue 0.03%) and boiling for 5 min. Before loading on 12% w/v polyacrylamide gel SDS-PAGE, the beads were eliminated by centrifugation. Proteins were visualized by colloidal coomassie brilliant blue G250 staining (Sigma). Three independent experiments were conducted. The electrophoretic band of interest was dissected, submitted to in-gel digestion and analyzed by MALDI-TOF as previously described.

Inhibition of the SP Virulence Stimulating Activity

Bacteria were diluted to a ratio of 1:40 in fresh broth and exposed at the beginning of the log growth phase to SP or SPrev (10⁻⁶M) and Uriage Thermal Water (UTW) 30% v/v or Teflose® (TF) 0.1% w/v or SRrev (10⁻⁶M). After 1 h, the micro-organisms were harvested by centrifugation, washed and the cytotoxic potential of the bacteria was determined at an MOI of 10:1 by measurement of LDH release. Controls showed that at the concentrations of TF and UTW used had no effect on the growth kinetics of the bacteria or on the survival of keratinocytes.

Statistical Analysis

Cytotoxicity (LDH), caspase 1 and MATS experiments were conducted independently at least three times at different days. The results are expressed as Means ± SEM and statistical differences were determined using the Student's *t*-test. Significant differences were noted as ★, ★★ and ★★★ for *p*-values <0.05, <0.01 and <0.001, respectively. For each biofilm, the thickness was calculated from a minimum of 20 measures in different fields using the Zen® 2009 software (Zeiss). The mean biofilm thickness was quantified over three different experiments and the Student *t*-test was used to compare the means. SDS-PAGE electrophoresis, bidimensional electrophoresis, MALDI-TOF and immunoprecip-

itation figures are representative of three independent experiments.

Results

Substance P is Stimulating the Virulence of *Bacillus Cereus*

The study was realized on *Bacillus cereus* MFP01, a strain identified on the skin of normal human volunteers. Preliminary controls showed that exposure of *B. cereus* to SP (10⁻⁶ M) during the whole growth phase or at the beginning of the stationary phase, did not modify the growth kinetics of the bacterium. SP was also without effect of the swimming and swarming activities. The peptide was not tested at higher concentrations as it is known to have possible antibacterial activities [16]. When *B. cereus* was grown in the presence of SP, the bacterium showed a strong increase in its cytotoxic potential on keratinocytes, as revealed by the LDH release assay (Fig. 1A). The threshold of SP activity was between 10⁻⁹ and 10⁻⁸ M. At a concentration of 10⁻⁶M, the cytotoxic activity of *B. cereus* reached 553±3% (*P*<0.001) of the control. Since keratinocytes might be sensitive to SP [28], bacteria were carefully rinsed to remove any trace of free SP prior cell infection. In addition, control experiments realised by direct treatment of keratinocytes with SP (10⁻⁶ M) showed that, in our experimental conditions, SP had no direct lethal effect on keratinocytes and did not modify the cytotoxic effect of SP treated bacteria. The specificity of the effect of SP on *B. cereus* was also controlled by using the SP reversed sequence peptide (SPrev). Even at the highest concentration used (10⁻⁶ M), SPrev was without any effect on *B. cereus* cytotoxicity. Then SPrev was used as a control for SP during the whole study. The response of *B. cereus* to SP was particularly rapid. A 5 min treatment of the bacterium during the mid log growth phase was sufficient to reach 90.5% of the maximal response (Fig. 1B). There was no difference of cytotoxic activity between bacteria exposed to SP for 10 min and 1 h. The cytotoxic activity of the bacteria was not modified after 1 h of treatment.

In order to characterize more precisely the effect of SP on *B. cereus* virulence we measured the production of caspase-1 by keratinocytes after infection with bacteria pretreated for 1 h with SPrev (control) or SP 10⁻⁶ M. As shown in Fig. 2A, after 30 min of infection, the production of caspase-1 by keratinocytes exposed to SP treated *Bacilli* rose significantly (+174±51%, *P*<0.05). Caspase-1 is an enzyme involved in pyroptosis and cell necrosis which is activated during the inflammasome induction [29]. An assay of other caspases and/or cytokines should be necessary to determine the precise inflammatory pathway induced by *B. cereus*. As this process is generally associated with alterations of the cellular morphology, we observed HaCaT keratinocytes exposed to SPrev and SP treated *B. cereus*. After a 30 min infection with control bacteria the histological structure of keratinocytes remained unchanged, whereas the structure of HaCaT cells exposed to SP-treated *B. cereus* was dramatically altered (Fig. 2B). In particular, we observed a complete disorganization of the actin cytoskeleton and the formation of intra-cytoplasmic vesicles. After 1 h infection with SP treated bacteria the HaCaT cell monolayer was completely disorganized. It is interesting to note that keratinocytes exposed to control bacteria for a longer period (5 h) finally presented the same aspect, suggesting that SP not only increased but also accelerated the production of virulence factors.

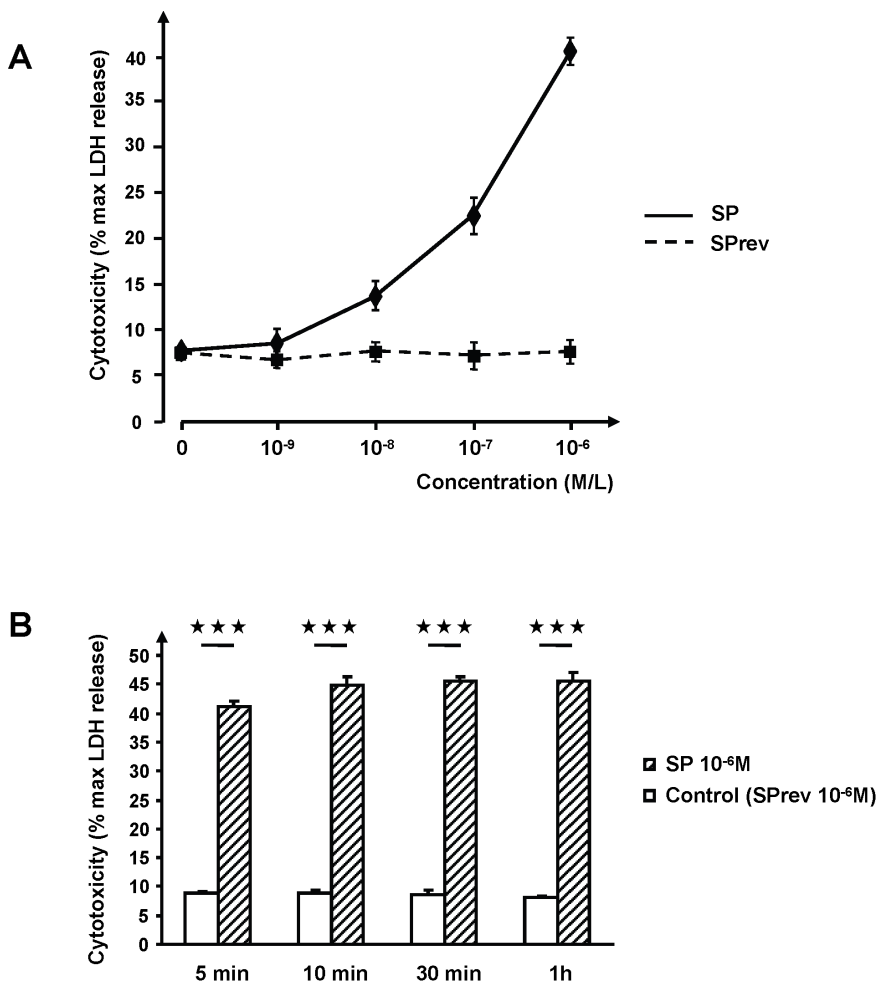


Figure 1. Effect of Substance P on the cytotoxic activity of *Bacillus cereus*. (A) Dose response curve of the effect of Substance P (SP) and of the reversed sequence peptide (SPrev). (B) Time course response of the bacteria to SP and SPrev (10^{-6} M). (★★★ = $p < 0.001$).
doi:10.1371/journal.pone.0078773.g001

Substance P Induces the Release of Superoxide Dismutase and Collagenase by *Bacillus Cereus* and a peel-off of its S-layer

The effect of SP appeared mediated through the production of diffusible virulence factors since bacterial cultures and filtered growth medium were equally cytotoxic. As the effect of SP was rapid, we first investigated a possible increase in the production of cereulide, the emetic toxin of *B. cereus* known for its very short kinetic of action [30]. HPLC-MS analysis showed that *B. cereus* MFP01 actually produced cereulide (106 ng/g wet weight of bacteria) but this production was unchanged after SP treatment. Then, exoproteins produced by *B. cereus* were studied. Image analysis of 1-D gels showed variations in 3 major bands between the control and SP treated bacteria, two in the mid-log phase culture secretome and a different one in the late stationary phase (Fig. 3). The first protein over-expressed by 1 h SP-treated *B. cereus* was identified by MALDI-TOF as a 24 kDa manganese dependent superoxide dismutase (SOD) (NCBI number ZP_00239265). The second protein was as the 66 kDa collagenase ColT (NCBI number ZP_04321651). These proteins were not over-expressed by late stationary phase bacteria but we noted an increase of a 87 kDa band corresponding to the S-layer crystal protein (NCBI number YP_002337034.1). These results were confirmed by 2-D

electrophoresis. However, *Bacillus cereus* is known to express different types of related S-layer proteins [31] and the PDQuest 2D analysis revealed that in fact two closely related 87 kDa proteins, the S-layer crystal protein (YP_002337034.1) but also the S-Layer protein Sap (HM626283.1), were over produced by *B. cereus* after a 13 h treatment with SP (Fig. 4). Conversely 10 proteins, essentially energetic and intermediate metabolism enzymes, were down regulated by SP (Table 1).

Bacteria were then examined by TEM. Control *B. cereus* showed a continuous pseudo crystalline surface (Fig. 5A). In contrast, the S-layer of bacteria treated with SP (10^{-6} M) for 13 h appeared interrupted and separated from the membrane by a gap (Fig. 5B). Long amorphous membrane-like structures were observed in the vicinity of the bacterial surface suggesting an important desquamation of the S-layer (Fig. 5C,D). These modifications were associated with a shift in the surface polarity of *B. cereus*. Considering that the threshold for the affinity to hexadecane of polar (hydrophilic) bacteria determined by the MATS technique is 20% [25], in our experimental conditions control *B. cereus* behaved as a highly polar micro-organism ($5 \pm 2\%$ and $8 \pm 2\%$ affinity to hexadecane and decane, respectively) (Fig. 6). SP treated bacteria showed a significant increase in affinity to hexadecane ($+10 \pm 2\%$) and to decane ($+9 \pm 1\%$). In agreement with these observations indicating an increase of surface hydrophobicity of SP-treated *B.*

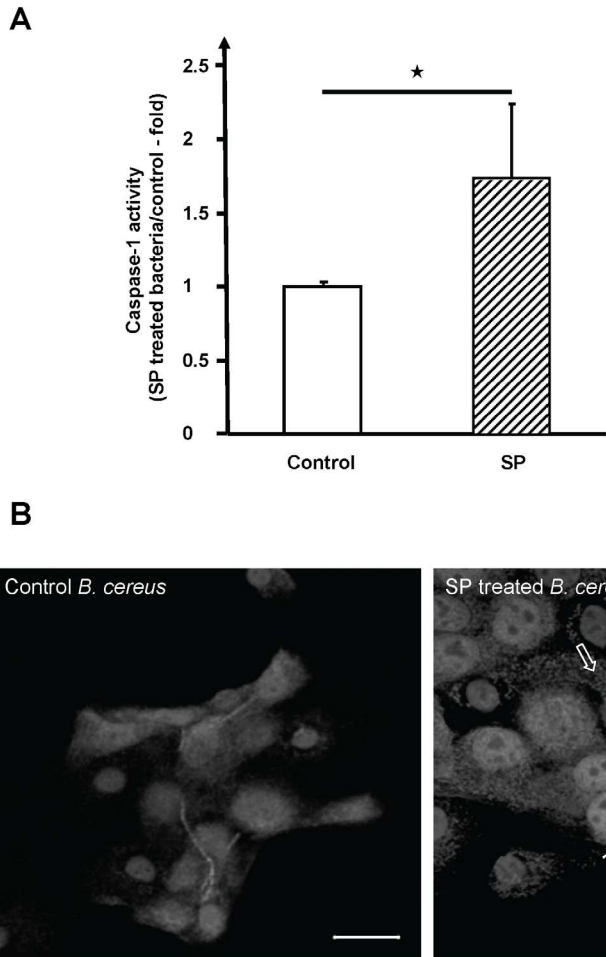


Figure 2. Effect of Substance P treated *Bacillus cereus* on caspase 1 induction and on the morphology of HaCaT cells. (A) Cells exposed to SP treated bacteria showed an increase of caspase 1 production ($\star = p < 0.05$). (B) After a 30 min infection with control bacteria the morphology of HaCaT cells remained unchanged but when the cells were exposed to SP treated *B. cereus* we observed a complete disorganization of the actin cytoskeleton (\Rightarrow) and the formation of multiple cytoplasmic vacuoles (\rightarrow). Bar = 20 μ m.

doi:10.1371/journal.pone.0078773.g002

cereus, the affinity of the bacteria to a polar solvent such as ethyl acetate was reduced. Moreover, a comparison of the affinity to the different solvent couples revealed that SP induced a shift in Lewis acid/base character of the bacterial surface. Indeed, in control bacteria the difference in the percentage of affinity between hexadecane and chloroform was about 20% while it decreased to 5% in the couple ethyl acetate/decane. In SP-treated *B. cereus*, these values were 19 and 14% respectively, showing that the bacterial surface evolved from a highly polar and strict Lewis basic character, to a mid polar and Lewis acidic-basic character.

Substance P Increases the Biofilm Formation Activity of *Bacillus Cereus*

Surface properties of *Bacillus* have a great influence on their biofilm formation activity [31]. The effect of SP on *B. cereus* biofilm formation was studied by confocal microscopy using GFP-transformed bacteria. First, we verified that the growth kinetic of GFP-pTeTON plasmid transformed bacteria was not modified in the absence or presence of SP or SPrev. After a 2 h treatment with SP (10^{-6} M), the mean surface coverage of the bacteria was unchanged except in specific points where the bacterial mat tended to form blisters (Fig. 7A). The density of the biofilm was

also unchanged after 5 h exposition to SP. Yet its thickness was increased on reconstructed 3D and transversal (3D/z) images. As calculated using Zen® software, after 5 h exposition to SP, the thickness of the biofilm rose from a mean value of 10.5 μ m to 17.1 μ m with SP treated bacteria (Fig. 7B). This effect was maintained, but to a lower degree, in 24 h old biofilms.

Substance P is Binding on the *Bacillus Cereus* Thermo Unstable Ribosomal Elongation Factor Ef-Tu

We investigated the presence of a SP binding site in the membrane of *B. cereus* considering the properties of SP (ionic charge and peptidic structure) and the very short delay required for the effect of SP on bacteria (<5 min) which suggested an interaction of SP with a surface sensor. A single band, corresponding to a 43 kDa protein, was found as the possible membrane ligand of SP in *B. cereus* (Fig. 8). No trace of non-specific or secondary binding protein was observed. We only noted a partial binding of SPrev on the same 43 kDa protein suggesting that SPrev can bind to the same site with a lower affinity. Nevertheless, SPrev is an inverted peptide and not a scramble, and some epitopes can be preserved. The SP binding site was identified by MALDI-TOF with a MASCOT score of 98 and a coverage

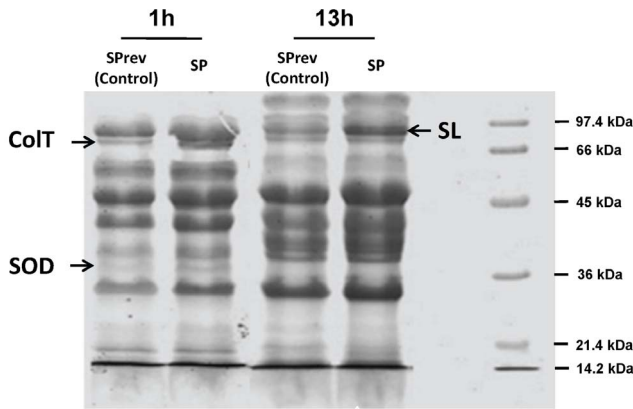


Figure 3. SDS page analysis of secreted *Bacillus cereus* proteins after 1 or 13 h treatment with Substance P (SP) or Substance P reverse (SPrev) (10^{-6} M). Bacteria exposed for 1 h to SP showed an increase in the production of the collagenase (ColT) and of superoxide dismutase (SOD). Bacteria treated for 13 h with SP presented in contrast an increase in the S-layer crystal protein (SL). Results are representative of three independent experiments.
doi:10.1371/journal.pone.0078773.g003

percentage of 59% (15 matched fragments) as the Thermo unstable ribosomal Elongation factor (Ef-Tu) (NCBI number NP_830009, 42912 Da, pI = 4.93).

Substance P also acts on *Staphylococcus Aureus* and *Staphylococcus Epidermidis* Virulence but its Effect can be Antagonized

B. cereus is responsible for severe cutaneous infections [32] but *Staphylococci* are considered as the principal Gram positive skin bacteria [2]. The effect of SP on the virulence of *B. cereus* was then compared to that of the peptide on human skin strains of *S. aureus* and *S. epidermidis*. As *B. cereus*, *S. aureus* and *S. epidermidis* responded to a 1 h exposure to SP (10^{-6} M) by a significant increase in their cytotoxicity on HaCaT cells ($+242.1 \pm 17.2\%$ and $+198.5 \pm 17\%$, respectively) (Fig. 9) suggesting that SP should have similar effects over different species of Gram positive bacteria. We also observed that a polysaccharide rich in rhamnose and obtained by fermentation, Teflose® (TF) or a thermal water from Uriage-les-Bains (UTW) were able to antagonize the effect of SP on the three Gram positive bacteria (281.6 and 181% reduction in the activity of SP on *B. cereus* for UTW and TF respectively, and total inhibition in the case of *S. aureus* and *S. epidermidis*).

Discussion

The skin microbiome is divided in two groups, the resident and the transient microflora. Bacteria of the normal resident microflora establish a quasi-symbiotic relation with the host [33]. In fact, the variations of skin bacterial population or virulence essentially concern the transient microflora that includes mostly opportunistic pathogens. *Bacillus cereus* is a member of this sub-population. In addition to food-born diseases, this bacterium is now recognized as responsible for primary cutaneous infections [32]. This species expresses a large arsenal of virulence factors, including hemolysins, phospholipases, an emetic toxin and pore forming enterotoxins [34] and was selected because of its high infectious potential that made easier the observation of cytotoxicity differences.

The stimulation of *B. cereus* cytotoxicity by SP was high (5.5 fold for SP 10^{-6} M) and rapid (5 min). The controls allowed us to exclude an artefact due to a direct action of SP on keratinocytes.

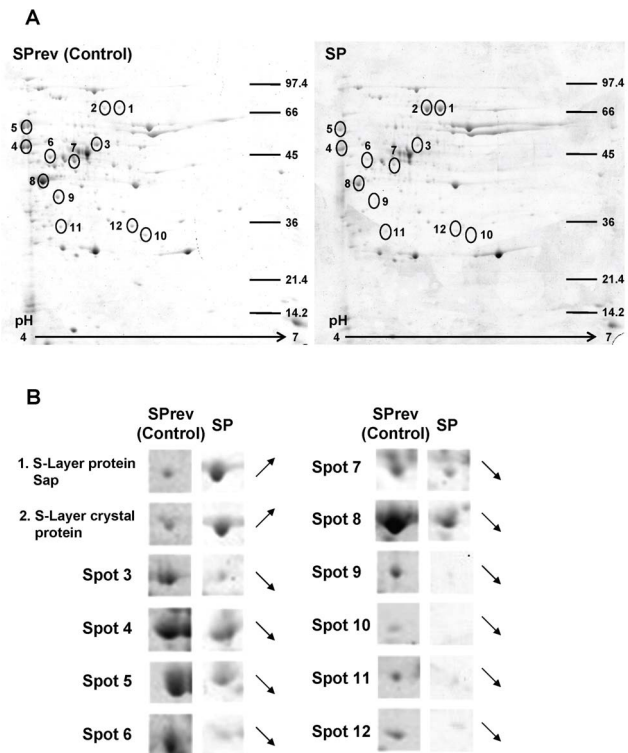


Figure 4. Bidimensional electrophoresis analysis of secreted proteins by *Bacillus cereus* after a 13 h exposure to Substance P reverse (Control) or Substance P (SP) (10^{-6} M). (A) Twelve spots were modified after exposure of the bacteria to SP. (B) Two proteins (1 and 2) were over produced whereas the expression of 10 others was down regulated. Identified proteins are presented in Table 1. Results are representative of three independent experiments.
doi:10.1371/journal.pone.0078773.g004

As the reversed sequence peptide SPrev, which has the same amino acid composition as SP was without effect, we can also exclude a metabolic action of the peptide. The assay of cereulide production showed that *B. cereus* MFP01 synthesizes this toxin and then contains the ces gene, encoded by a 270 kb plasmide, related to the PXO1 virulence plasmid of *B. anthracis* [35,36] but the expression of this plasmid is apparently not regulated by SP. *B. cereus* reacted to SP by an over production of the collagenase ColT. This should explain the disorganization of the cell monolayer and is consistent with *in-vivo* studies showing that the role of collagenase in *B. cereus* virulence is essential [37]. The increase of caspase 1 production by keratinocytes exposed to SP-treated bacteria and the morphological changes of the cells are in agreement with an induction of cell necrosis and pyroptosis [29]. However, a massive cell death, as observed with SP treated bacteria, is associated with the release of high amounts of potentially toxic oxidizing compounds. The production of SOD by SP treated *B. cereus* should be a defence reaction against this threat. This response of *B. cereus* to SP was not observed when the bacteria were exposed to SP over a long (13 h) period. In this case, we only noted an increase of the release of S-layer proteins. This result was correlated to the observation of a massive peeling-off of the S-layer of *B. cereus* and to a drop in surface polarity. These events can be interpreted as a general defence reaction of the bacterium against SP. Indeed, although SP did not affect the growth of *B. cereus*, this molecule has structural and functional homologies with antimicrobial peptides and, as recently shown, the bacterial S-layer should act as a barrier against cationic antimicrobial peptides

Table 1. MALDI-TOF/TOF identification of the proteins in Figure 4 which expression was modified by Substance P in *Bacillus cereus*.

Spot number	NCBI accession number	Gene name	Putative function	Protein domain(s)	Mascot score	Number matched peptides	Coverage (%)	Mass (Da) & pi
1	HM626283.1	<i>sap</i>	Sap (S-layer protein)	Conserved S-layer Homology Domain, bacterial Ig-like domain	352	56	62	87286/5.63
2	YP_002337034.1		Crystal protein (S-layer protein)	Conserved S-layer homology domain, bacterial Ig-like domain	246	47	59	87543/5.71
3	AE017194	<i>mmpE</i>	mmpE protein		239	35	62	43358/5.34
4	NP_981531.1	<i>eno</i>	Phosphopyruvate hydratase	Enolase	250	29	74	46371/4.68
5	ZP_03108403	<i>groL</i>	Chaperonin GroL	GroEL-like chaperonin, polypeptide binding site	237	44	72	57384/4.79
6	YP_002341293		Sulfatase	Alkaline phosphatase superfamily	185	33	47	73343/6.19
7	ZP_04302850.1		Alanine dehydrogenase	Rossmann-fold NAD(P) binding proteins	236	33	89	40084/5.22
8	ZP_00240745		Bacilloysin	Zn metalloprotease, Funga lysine, M36 Superfamily with Zn binding site	88	17	38	54586/5.30
9	ZP_04188209.1		Malate dehydrogenase		144	23	68	33535/5.05
10	YP_002532873	<i>hbd</i>	3-hydroxybutyryl-CoA dehydrogenase	Rossmann-fold NAD(P) binding proteins	126	19	59	31269/5.45
11	YP_002443562		Pyridoxal biosynthesis lyase PdxS		145	23	72	31855/5.18
12	YP_002528490.1	<i>spH</i>	Sphingomyelinase C	Metal binding site, phosphate binding site, catalytic site	201	30	69	37462/5.99

doi:10.1371/journal.pone.0078773.t001

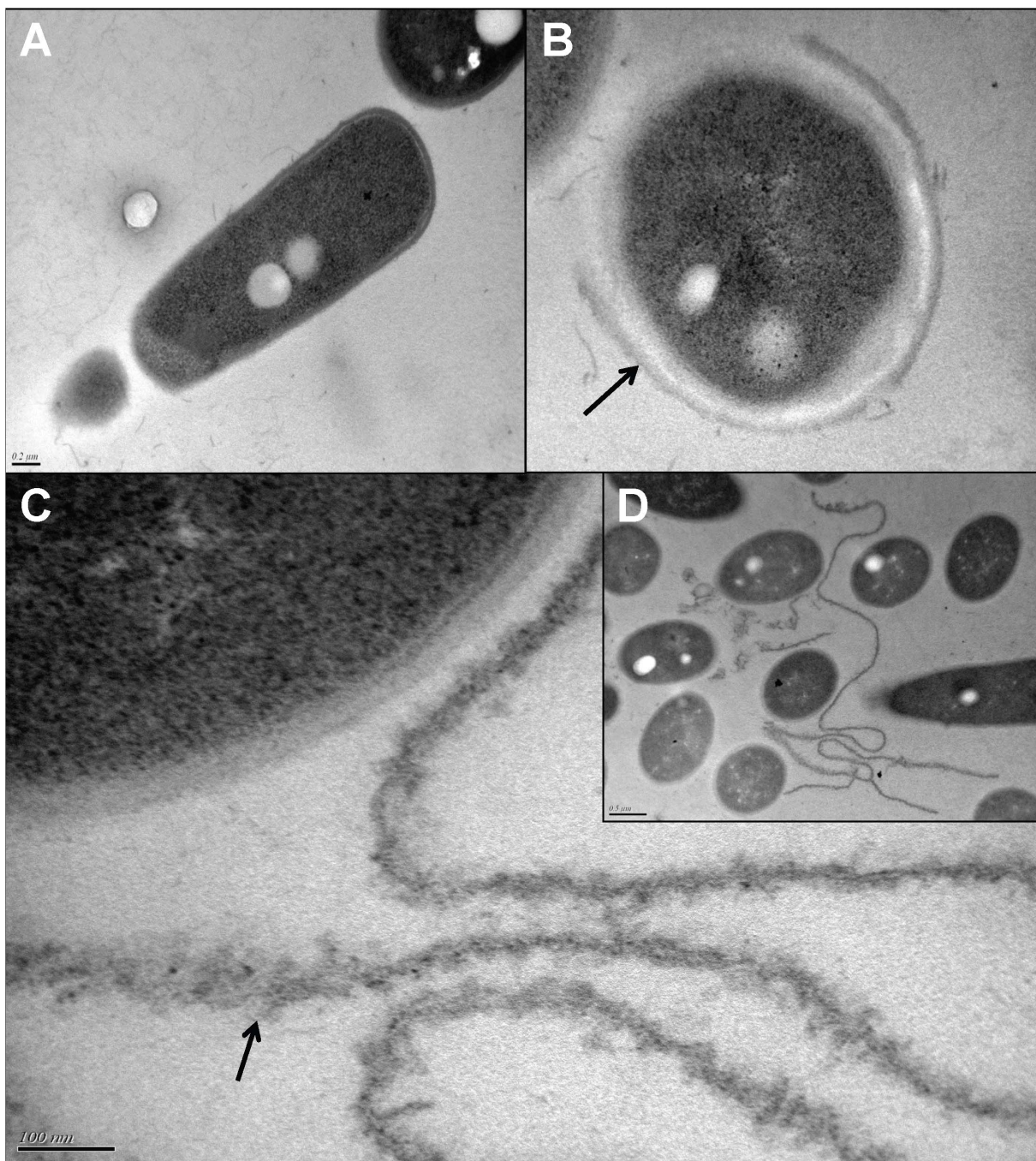


Figure 5. TEM observation of control (SPrev) and Substance P (SP) treated *Bacillus cereus*. Whereas control bacteria presented a continuous intact surface (A), bacteria exposed to SP showed a detachment of the S-layer (→) (B). Long amorphous structures were observed in the vicinity of bacterial, suggesting a desquamation of the S-layer (C, D).

doi:10.1371/journal.pone.0078773.g005

[38]. However, in the present study the concentration of SP was 3 logs below that of the more active antimicrobial peptide (LL-37) [38] and the bacterium reacted not only by releasing S-layer monomers, but by an almost complete desquamation of the S-layer. The *B. cereus* S-layer ultra structure has not been investigated in detail. Assuming that as in other species, in one *B. cereus* cell the S-layer contains an average of 40,000 monomers [39], we calculated that at a concentration of 10^{-8} M (over the threshold of SP effect) less than 1 SP molecule was available to interact with

10 S-layer proteins. Then, SP acts probably indirectly on the stabilization of the polymeric form of the S-layer. The loss of the S-layer induced by SP in *B. cereus* was associated with a decrease in the global surface polarity of the bacterium. As described in *Bacillus anthracis*, cell surface polarity plays a leading role in the adherence to mammalian cells [40] but, to the contrary of our observations, the cytotoxicity of hydrophobic strains is generally lower [41]. The correlation between surface hydrophobicity and virulence in *B. cereus* is highly strain dependant [42] but it is also

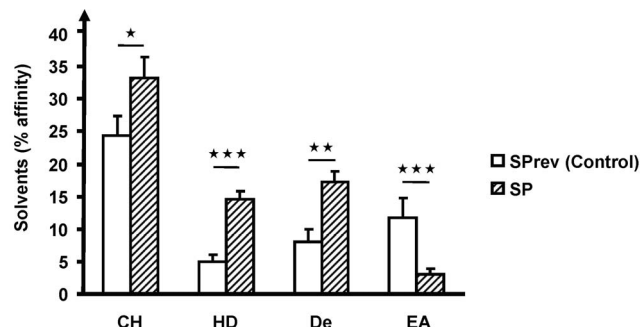


Figure 6. Effect of Substance P reverse (SPrev) and Substance P (10^{-6} M) on the affinity of *Bacillus cereus* to solvents of different polarities. chloroform (CH), hexadecane (HD), decane (De) and ethyl acetate (EA) ($\star = P < 0.05$, $\star\star = P < 0.01$, $\star\star\star = P < 0.001$). Each value represents the mean \pm SEM of three independent experiments.

doi:10.1371/journal.pone.0078773.g006

known that the surface of *B. cereus* in biofilms is more polar and hydrophilic than the surface of the planktonic bacteria [43]. However, emetic strains such as *B. cereus* MFP01 only produce a transient biofilm which tends to disorganize after 24 h. As we observed, since the bacterium remained globally hydrophilic, the surface variations are limited [31].

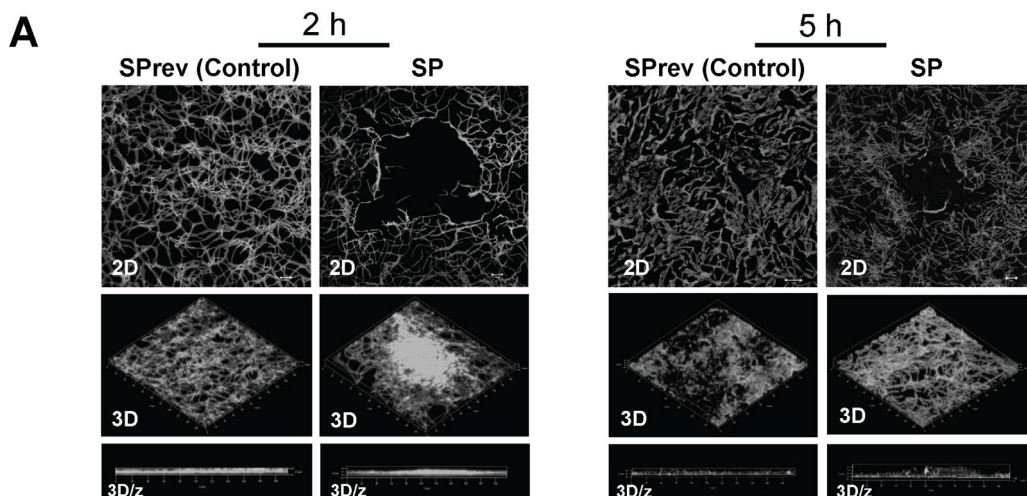


Figure 7. Effect of Substance P reverse (SPrev) and Substance P (SP) (10^{-6} M) on the biofilm formation activity of *Bacillus cereus*. The biofilm formation was observed after 2, 5 and 24 h. (A) Two dimensions (2D) and reconstructed three-dimensions (3D) and ortho cuts (3D/z) images showed that the density of the biofilm was essentially unchanged. (B) In contrast, the thickness of the biofilm was significantly increased after 5 and 24 h incubation with SP (NS = non significant; $\star\star = p < 0.01$; $\star\star\star = p < 0.001$).

doi:10.1371/journal.pone.0078773.g007

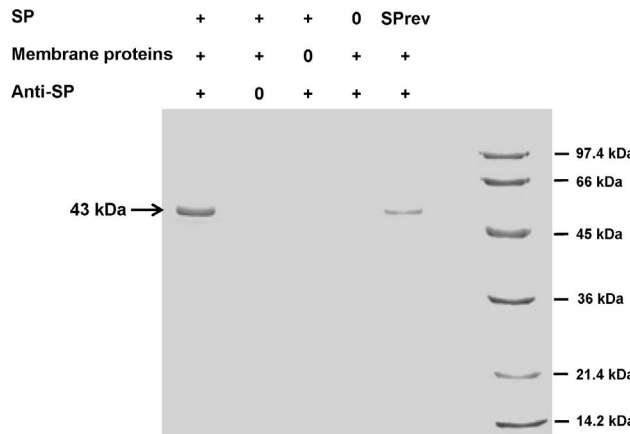


Figure 8. SDS page analysis of *Bacillus cereus* Substance P (SP) binding proteins separated by immunoprecipitation using SP antibody-associated beads. SP was found able to bind on a 43 kDa protein that was identified by MALDI-TOF/TOF as the Thermo Unstable ribosomal Elongation factor Ef-Tu (arrow: 43 kDa). SPrev was also capable of binding to this protein but with a reduced effectiveness. Results are representative of three independent experiments.

doi:10.1371/journal.pone.0078773.g008

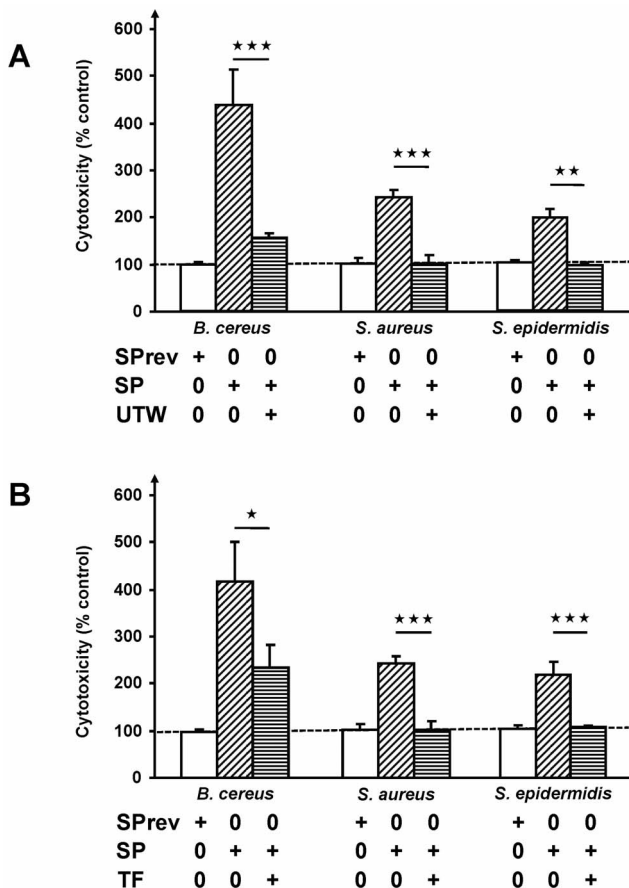


Figure 9. Inhibition of the effects of Substance P (SP) on the cytotoxic activity of *Bacillus cereus*, *Staphylococcus aureus* and *Staphylococcus epidermidis*. (A) Before infection, bacteria were exposed to SP in the presence of thermal water from Uriage-les-Bains (UTW) or (B) Teflose® (TF) ($\star = p < 0.05$, $\star\star = p < 0.01$, $\star\star\star = p < 0.001$). doi:10.1371/journal.pone.0078773.g009

The kinetic of SP on *B. cereus* requires a rapid detection of the peptide; therefore we hypothesized the presence of a surface binding site. Indeed, although untreated *B. cereus* MFP01 showed an intact S-layer protection wall, the S-layer presents multiple pores allowing the secretion of proteins [44]. Additionally, the size of these pores is sufficient to enable the passage of small exogenous peptides similar to SP [38]. We identified a 43 kDa protein, the Thermo unstable ribosomal Elongation factor Ef-Tu, as a specific SP binding site in *B. cereus*. Ef-Tu is present in large excess in bacteria [45]. In addition to its original function at the ribosomal level, it is known that in case of bacterial stress this protein is translocated to the bacterial surface [46] and in *B. anthracis* Ef-Tu was identified as a plasminogen receptor [47]. As there is no sequence homology between SP and plasminogen, Ef-Tu appears as a multifunctional sensor of host signals in *Bacilli*. Because neither SP nor plasminogen are deemed capable of crossing the membrane, Ef-Tu should be associated with a transduction system to trigger the bacterial response. In this regard, it is interesting to note that, in the membrane of *B. subtilis* Ef-Tu is colocalized and should interact with the actin-like protein MreB [48]. The bacterial cytoskeleton does not only show structural homology with its eukaryotic counterpart, but has also similar functions [49], and MreB should play a same role as actin in SP signal transduction in bacteria.

The capacity of detecting SP is shared by other Gram positive bacteria since we observed that *S. aureus* and *S. epidermidis* also reacted to SP by a marked increase in cytotoxicity. Furthermore, the specificity of SP action on *Staphylococci* was the same as in *B. cereus* with an absence of response to SPrev. *Bacilli* and *Staphylococci* are not closely related species, thus we can expect that other Gram positive bacteria should also react to SP. The bacterial diversity in neuropathic diabetic foot ulcer, which is essential in the evolution of the disease, appears dependent of host factors [50]. The decrease of SP expression observed in diabetic foot ulcer [51] should contribute to limit bacterial virulence and consequently host immune reaction, leading to the typically observed low-level chronic infection state. Alternatively, whereas the mean basal concentration of SP in sweat is picomolar [52], local concentrations at the vicinity of the producing cells or nerve terminals should be much higher. The skin concentration of SP is increased in case of atopic dermatitis [53]. Moreover, a 50 fold increase of SP is observed in sweat during depressive disorders [52] and in the case of skin breaches, as measured after surgery, the level of SP in skin exudates can be 8 to 10 nanomolar [54]. The present results should be confirmed using primary adult cells as HaCaT cells are immortalized human keratinocytes, but the threshold of SP effect on *B. cereus* is consistent with the physiological concentrations of SP suggesting that this peptide should actually act in skin as a regulator of the virulence of gram-positive bacteria.

Thermal waters have been known since antiquity to reduce or cure chronic skin inflammation. This is the case of the thermal water from Uriage-les-Bains (UTW). As it is isotonic, this water has no effect on the viability of keratinocytes but when the bacteria were exposed to SP in the presence of 30% UTW, the effect of SP on the virulence of the three bacterial species was reduced or even totally abolished. The mechanism involved was not studied but this water contains a high concentration of anions, particularly chloride (3500 mg/L) and sulfate (2862 mg/L). Then, since SP is a cationic peptide we cannot exclude that it was chelated by these ions and then unable to act on the bacteria. Another compound, Teflose® (TF), a polysaccharide containing rhamnose, glucose and glucuronic acid (BioEurope, Solabia Group) showed similar antagonist effects on SP when it was administered with the peptide. This compound claims to have an anti-adhesive effect on bacteria but because of its charge, it could also act by trapping and sequestering the peptide.

In summary, we showed that SP was able to increase the virulence of bacteria that are commonly present on the skin. The role of SP on skin infections is still controversial. Our study evidenced that the effects of this neuropeptide are not only due to SP effects on inflammation or immunity but could also relate to direct effects on bacteria, by enhancing their virulence. Moreover, the role of bacteria in the pathogenesis of psoriasis, acne or atopic dermatitis is known [33] and our results suggest that the exacerbation of these diseases by SP is not only due to a modulation of inflammation and immunity or to a direct effect of SP on keratinocytes and sebocytes: SP could also exacerbate these diseases by enhancing the virulence of some bacteria then breaking skin defences.

Acknowledgments

We thank S. Leblanc (BioGalénas SAS) for the HPLC analysis of cereulide and Dr Sastalla (NIH) for providing the pTeTON-GFP plasmid.

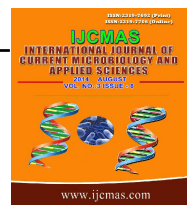
Author Contributions

Conceived and designed the experiments: L. Mijouin MGJF. Performed the experiments: L. Mijouin MH YR TJ CD-P M-LF-G. Analyzed the

References

- Roosterman D, Goerge T, Schneider SW, Bunnett NW, Steinhoff M (2006) Neuronal control of skin function: the skin as a neuroimmunoendocrine organ. *Physiol Rev* 86: 1309–1379.
- Grice EA, Segre JA (2011) The skin microbiome. *Nat Rev Microbiol* 9: 244–53.
- Lesouhaitier O, Veron W, Chapalain A, Madi A, Blier AS, et al. (2009) Gram-negative bacterial sensors for eukaryotic signal molecules. *Sensors* 9: 6967–6990.
- Hooper LV, Littman DR, Macpherson AJ (2012) Interactions between the microbiota and the immune system. *Science* 336: 1268–1273.
- Lange-Asschenfeldt B, Marenbach D, Lang C, Patzelt A, Ulrich M, et al. (2011) Distribution of bacteria in the epidermal layers and hair follicles of the human skin. *Skin Pharmacol Physiol* 24: 305–311.
- Severini C, Impronta G, Falconieri-Espamer G, Salvadori S, Espamer V (2002) The tachykinin peptide family. *Pharmacol Rev* 54: 285–322.
- Peters EM, Ericson ME, Hosoi J, Seiffert K, Hordinsky MK, et al. (2006) Neuropeptide control mechanisms in cutaneous biology: physiological and clinical significance. *J Invest Dermatol* 126: 1937–1947.
- Pereira U, Boulais N, Lebonvallet N, Lefevre L, Gougerot A, et al. (2010) Development of an *in vitro* coculture of primary sensitive pig neurons and keratinocytes for the study of cutaneous neurogenic inflammation. *Exp Dermatol* 19: 931–935.
- Raab U, Ständer S, Metz M (2011) Pathophysiology of itch and new treatments. *Curr Opin Allergy Clin Immunol* 11: 420–427.
- Ostromski SM, Belkadi A, Loyd CM, Diaconu D, Ward NL (2011) Cutaneous denervation of psoriasisform mouse skin improves acanthosis and inflammation in a sensory neuropeptide-dependant manner. *J Invest Dermatol* 131: 1530–1538.
- Hosokawa C, Takeuchi S, Furue M (2009) Severity scores, itch scores and plasma substance P levels in atop dermatitis treated with standard topical therapy with oral olopatadine hydrochloride. *J Dermatol* 36: 185–90.
- Misery L (2011) Atopic dermatitis and the nervous system. *Clin Rev Allergy Immunol* 41: 259–266.
- Wallengren J (1991) Substance P antagonist inhibits immediate and delayed type cutaneous hypersensitivity reactions. *Br J Dermatol* 124: 324–328.
- Toyoda M, Morohashi M (2001) Pathogenesis of acne. *Med Electron Microsc* 34: 29–40.
- Aubdo AA, Brain SD (2011) Neurovascular aspects of skin neurogenic inflammation. *J Investig Dermatol Symp Proc* 15: 33–39.
- Hansen CJ, Burnell KK, Brogden KA (2006) Antimicrobial activity of Substance P and Neuropeptide Y against laboratory strains of bacteria and oral microorganisms. *J Neuroimmunol* 177: 215–218.
- Brogden KA (2005) Antimicrobial peptides: pore formers or metabolic inhibitors in bacteria? *Nat Rev Microbiol* 3: 238–250.
- Hancock REW, Scott MG (2000) The role of antimicrobial peptides in animal defenses. *Proc Natl Acad Sci USA* 97: 8856–8861.
- Zaborina O, Lepine F, Xiao G, Valuckaitė V, Chen Y, et al. (2007) Dynorphin activates quorum sensing quinolone signaling in *Pseudomonas aeruginosa*. *PLoS Pathog* 3: e35.
- Veron W, Orange N, Feuilloley MGJ, Lesouhaitier O (2008) Natriuretic peptides modify *Pseudomonas fluorescens* cytotoxicity by regulating cyclic nucleotides and modifying LPS structure. *BMC Microbiol* 8: 114.
- Blier AS, Veron W, Bazire A, Gerault E, Taupin L, et al. (2011) C-type natriuretic peptide (CNP) modulates quorum sensing molecules and toxin production in *Pseudomonas aeruginosa*. *Microbiology* 157: 1929–1944.
- Sastalla I, Chim K, Cheung GY, Pomerantsev AP, Leppla SH (2009) Codon-optimized fluorescent proteins designed for expression in low-GC gram-positive bacteria. *Appl Environ Microbiol* 75: 2099–2110.
- Häggblom MM, Apetroaie C, Andersson MA, Salkinoja-Salonen MS (2002) Quantitative analysis of cereulide, the emetic toxin of *Bacillus cereus*, produced under various conditions. *Appl Environ Microbiol* 68: 2479–2483.
- Barbey C, Crépin A, Cirou A, Budin-Verneuil A, Orange N, et al. (2012) Catabolic pathway of gamma-caprolactone in the biocontrol agent *Rhodococcus erythropolis*. *J Proteome Res* 11: 206–216.
- Bellon-Fontaine MN, Rault J, Van Oss CJ (1996) Microbial adhesion to solvents: a novel method to determine the electron-donor/electron-acceptor or Lewis acid-base properties of microbial cells. *Colloids Surfaces B: Biointerfaces* 7: 47–53.
- Sinha S, Arora S, Kosala K, Namane A, Pym AS, et al. (2002) Proteome analysis of the plasma membrane of *Mycobacterium tuberculosis*. *Comp. Funct. Proteomics* 3: 470–83.
- Mijouin L, Rosselin M, Bottreau E, Pizarro-Cerdeira J, Cossart P, et al. (2012) *Salmonella enteritidis* Rck-mediated invasion requires activation of Rac1, which is dependent on the class I PI 3-kinases-Akt signaling pathway. *FASEB J* 26: 1569–1581.
- Shi X, Wang L, Li X, Sahbaie P, Kingry WS, et al. (2011) Neuropeptides contribute to peripheral nociceptive sensitization by regulating interleukin-1β production in keratinocytes. *Anesth Analg* 113: 175–183.
- Li WW, Guo TZ, Liang D, Shi X, Wei T, et al. (2009) The NALP1 inflammasome controls cytokine production and nociception in a rat fracture model of complex regional pain syndrome. *Pain* 147: 277–286.
- Jääskeläinen EL, Teplova V, Andersson MA, Andersson LC, Tammela P, et al. (2003) *In vitro* assay for human toxicity of cereulide, the emetic mitochondrial toxin produced by food poisoning *Bacillus cereus*. *Toxicol In Vitro* 17: 737–744.
- Auger S, Ramarao N, Faillie C, Fouet A, Aymerich S, et al. (2009) Biofilm formation and cell surface properties among pathogenic and nonpathogenic strains of the *Bacillus cereus* group. *Appl Environ Microbiol* 75: 6616–6618.
- Bottone EJ (2010) *Bacillus cereus*, a volatile human pathogen. *Clin Microbiol Rev* 23: 382–398.
- Gallo RL, Nakatsuji T (2011) Microbial symbiosis with the innate immune defense system of the skin. *J Invest Dermatol* 131: 1974–1980.
- Schoeni JL, Wong AC (2005) *Bacillus cereus* food poisoning and its toxins. *J Food Prot* 68: 636–648.
- Ehling-Schulz M, Fricker M, Grallert H, Rieck P, et al. (2006) Cereulide synthetase gene cluster from emetic *Bacillus cereus*: structure and location on a mega virulence plasmid related to *Bacillus anthracis* toxin plasmid pXO1. *BMC Microbiol* 6: 20.
- Rasko DA, Rosovitz MJ, Økstad OA, Fouts DE, et al. (2007) Complete sequence analysis of novel plasmids from emetic and periodontal *Bacillus cereus* isolates reveals a common evolutionary history among the *B. cereus*-group plasmids, including *Bacillus anthracis* pXO1. *J Bacteriol* 189: 52–64.
- Beecher DJ, Olsen TW, Somers EB, Wong AC (2000) Evidence for contribution of tripartite hemolysin BL, phosphatidylcholine-preferring phospholipase C, and collagenase to virulence of *Bacillus cereus* endophthalmitis. *Infect Immun* 68: 5269–5276.
- De la Fuente-Nunez C, Mertens J, Smit J, Hancock REW (2012) Bacterial surface layer protects against antimicrobial peptides. *Appl Env Microbiol* 78: 5452–5456.
- Smit J, Engelhardt H, Volker S, Smith SH, Baumeister W (1992) The S-layer of *Caulobacter crescentus*: three-dimensional image reconstruction and structure analysis by electron microscopy. *J Bacteriol* 174: 6527–6538.
- Thwaite JE, Laws TR, Atkins TP, Atkins HS (2009) Differential cell surface properties of vegetative *Bacillus*. *Lett Appl Microbiol* 48: 373–378.
- Taylor-McCabe K, Shou Y, Hong-Geller E (2012) Effects of *Bacillus anthracis* hydrophobicity and induction of host cell death on sample collection from environmental surfaces. *Gen Appl Microbiol* 58: 113–119.
- Kotiranta A, Lounatmaa K, Haapasalo M (2000) Epidemiology and pathogenesis of *Bacillus cereus* infections. *Microbes Infect* 2: 189–198.
- Karunakaran E, Biggs CA (2011) Mechanisms of *Bacillus cereus* biofilm formation: an investigation of the physicochemical characteristics of cell surfaces and extracellular proteins. *Appl Microbiol Biotechnol* 89: 1161–1175.
- Egelbrecht S, Schocher I, Sára M, Sleyter UB (1995) The S-layer from *Bacillus stearothermophilus* DSM 2358 functions as an adhesion site for a high-molecular-weight amylase. *J Bacteriol* 177: 1444–1451.
- Beck BD (1979) Polymerization of the bacterial elongation factor for protein synthesis, EF-Tu. *Eur J Biochem* 97: 495–502.
- Dallo SF, Zhang B, Denno J, Hong S, Tsai A, et al. (2012) Association of *Acinetobacter baumannii* EF-Tu with cell surface, outer membrane vesicles, and fibronectin. *ScientificWorldJournal*. 2012: 128705. doi: 10.1100/2012/128705.
- Chung MC, Tonry JH, Narayanan A, Manes NP, Mackie RS, et al. (2011) *Bacillus anthracis* interacts with plasminogen to evade C3b-dependent innate immunity. *PLoS One* 6: e18119.
- Defeu Soufo HJ, Reimold C, Linne U, Knust T, Gescher J, et al. (2010) Bacterial translation elongation factor EF-Tu interacts and colocalizes with actin-like MreB protein. *Proc Natl Acad Sci USA* 107: 3163–3168.
- Möller-Jensen J, Löwe J (2005) Increasing complexity of the bacterial cytoskeleton. *Curr Opin Cell Biol* 17: 75–81.
- Gardner SE, Hillis SL, Heilmann K, Segre JA, Grice EA (2013) The neuropathic diabetic foot ulcer microbiome is associated with clinical factors. *Diabetes* 62: 923–930.
- Galkowska H, Olszewski WL, Wojewodzka U, Rosinski G, Karnafel W (2006) Neurogenic factors in the impaired healing of diabetic foot ulcers. *J Surg Res* 134: 252–258.
- Cizza G, Marques AH, Eskandari F, Christie IC, Torvik S, et al. (2008) POWER Study Group. Elevated neuroimmune biomarkers in sweat patches and plasma of premenopausal women with major depressive disorder in remission: the POWER study. *Biol Psychiatry* 64: 907–911.
- Ostere LS, Cowen T, Rustin MH (1995) Neuropeptides in the skin of patients with atopic dermatitis. *Clin Exp Dermatol* 20: 462–467.
- Carvalho B, Clark DJ, Yeomans DC, Angst MS (2010) Continuous subcutaneous instillation of bupivacaine compared to saline reduces interleukin 10 and increases substance P in surgical wounds after cesarean delivery. *Anesth Analg* 111: 1452–1459.

P20



Original Research Article

Airborne fluorescent pseudomonads : What potential for virulence?

Cecile Duclairoir Poc^{1*}, Julien Verdon^{1,2}, Anne Groboillot¹, Magalie Barreau¹, Hervé Toucourou¹, Lily Mijouin¹, Camille Leclerc¹, Olivier Maillet¹, Tatiana Kondakova¹, Christian Hulen¹, Jean-Paul Morin³, Marc GJ Feuilloley¹, Annabelle Merieau¹ and Nicole Orange¹

¹Normandie University, France; University of Rouen, LMSM, EA 4312, 55, rue St Germain, F-27000 Evreux, France

²University of Poitiers, F-86034 Poitiers Cedex, France ; Lebi, UMR CNRS 7267, MDE, F-86022 Poitiers Cedex, France

³Normandie University, France ; University of Rouen, ABTE-ToxEMAC, EA 4651, F- 76183 Rouen Cedex, France

*Corresponding author

A B S T R A C T

Keywords

Fluorescent pseudomonads; *Pseudomonas fluorescens*; *Pseudomonas putida*; air; airborne; bio-contamination, virulence; exoproducts

The presence of human pathogens in the environment is a key concern, therefore the air needs to be evaluated as a potential source of bio-contamination. This study dealt with the characterization of fluorescent pseudomonads strains isolated from air in order to evaluate their factors of virulence. 19 strains were identified by API® strips, by MALDI-Biotyper and by 16S rDNA gene sequencing. Their growth at 30°C and 37°C, biosurfactant and biofilm production, motility and production of exoproducts were tested. A *Pseudomonas fluorescens* clinical strain was used as reference. By comparison with the virulence factors of this clinical strain, most of these strains isolated from air did not produce highly virulent factors. However a bacterial couple : *P. fluorescens* MFAF76a and *P. putida* MFAF88, was selected thanks to their observed characteristics linked to virulence quite similar with traits of the clinical reference. The cytotoxicity of their culture supernatant was investigated toward human epithelial pulmonary cells. Results revealed that these airborne fluorescent *Pseudomonas* strains secreted exoproducts, such as enzymes, surfactants and siderophores, highly virulent against the studied pneumocytes.

Introduction

For environmental policies, air quality is generally related to the presence of chemicals and particulate matter and its pollution is correlated with uncontroversial health impact. According to a survey in European intensive care units, 68% of sepsis

are lung infections and *Pseudomonadaceae* are the second most common organisms (14%), but the only ones that induce rising mortality rates (Vincent et al., 2006).

Gram-negative *Pseudomonadaceae* bacteria

present a great adaptive ability related to their large genome (Stover et al., 2000). *P. aeruginosa* is well known as prevalent pathogen in acute and chronic infections (Clifton & Peckham, 2010; Fernstrom & Goldblatt, 2013), although other fluorescent *Pseudomonas* species are ubiquitous. In fact, *Pseudomonas* are widespread Gram-negative bacteria present in various ecological niches: soil, water (Rajmohan et al., 2002), care units (Vincent et al., 2006), humans (Chapalain et al., 2008; Donnarumma et al., 2010) and air (AFSSET, 2010; Morin et al., 2013).

Moreover, some strains, isolated from a clinical environment, are able to grow at or above 37°C (Chapalain et al., 2008). *P. fluorescens* MFN1032, a clinical strain, was recently isolated from a patient with a lung infection (Chapalain et al., 2008) and induces cytotoxic responses (Rossignol et al., 2008; Madi et al., 2010; Sperandio et al., 2010; Sperandio et al., 2012). The pathogenicity of *Pseudomonas* bacteria is correlated with their enzymatic secretion (Gessner & Mortensen, 1990 ; Rossignol et al., 2008 ; Strateva & Mitov, 2011).

The purpose here was, after identification, to assess the potential for virulence of 19 airborne fluorescent pseudomonads strains, selected from Gram-negative oxidase-negative strictly aerobic rods collected during a previous study (AFSSET, 2010; Duclairoir Poc et al., 2011a ; Morin et al., 2013). For each of them, physiological characterization and determination of virulence factors were confronted. Two airborne bacteria appeared to have great similarities with the clinical standard, *P. fluorescens* MFN1032.

To compare the cytotoxicity of their secreted factors, A-549 human pulmonary type II-like epithelial cell line was implemented in

order to assess their potential virulence toward human by airways. Those cells play a critical role in coordinating both innate defence and inflammatory responses (Hawdon et al., 2010) and make it suitable to study virulence in conditions fairly close to *in vivo*.

Materials and Methods

19 airborne fluorescent *Pseudomonas* strains

In a previous study (AFSSET, 2010; Morin et al., 2013), more than 3000 bacteria were collected in air samples between June 2008 and September 2009 in 3 areas : in peri-suburban Evreux (Normandy, France), in the suburbs of Rouen (Normandy, France) and in dust clouds generated during crop ship loading in Rouen harbor installations (Normandy, France). About 3000 bacterial isolates were stored and then frozen at -80°C. Morphological characters, Gram staining and biochemical tests used to separate this bacterial population into 8 groups, which included a Gram-negative oxidase-positive strictly aerobic rods group containing *Pseudomonas* spp.

This group appeared among the most predominantly collected groups of airborne Gram-negative bacteria on harbor installations. Proportionally to their relative sample representation, 19 fluorescent *Pseudomonas* strains were randomly selected.

Clinical standard strain, MFN1032

P. fluorescens MFN1032 is a clinical strain isolated after a lung infection, related to biovar I of *P. fluorescens* species (Chapalain et al., 2008).

Identification of the 19 airborne strains API® identification

The 19 representative strains were submitted to metabolic characterization using API® 20NE strips. API® kits were operated according to the manufacturer's instructions (BioMérieux, France).

Mass spectrometric MALDI-Biotyper bacterial identification

These isolates were submitted to bacterial identification by MALDI mass spectrometry (MS) based on the total proteome screening analyzed using an algorithmic method to identify bacterium. The bacterial proteomes were obtained using an Autoflex III Matrix-Assisted Laser Desorption/Ionization-Time-Of-Flight mass spectrometer (MALDI-TOF) (Bruker, Germany) coupled to the MALDI-Biotyper 3.0 algorithmic system for microbial identification (Hillion et al., 2013). Before MS analysis, the bacterial material was spotted onto a MALDI target plate and overlaid by matrix (10g.L^{-1} α -cyano-4-hydroxycinnamic acid in 50% acetonitrile, 2.5% trifluoroacetic acid provided by Sigma-Aldrich, France).

The software generated scores evaluating the probability of correct identification of the microorganism. The species identification is considered acceptable for score values over 2.0 and, between 1.7 and 2.0, the genus identification is assumed confident. (Hillion et al., 2013)

16S rDNA gene sequencing and identification

The same isolates were identified by 16S ribosomal DNA gene sequencing. For amplification of the complete 16S RNA gene, universal primers UNI_DL (AGAGTGTGAAATGCG) and

UNI_OR (ACGGGCGGTGTACAA) were used as already described (Duclairoir Poc et al., 2011a). The nucleotide sequences were registered on GenBank, NCBI (<http://www.ncbi.nlm.nih.gov/genbank/submit/>) and were compiled in Table 1.

Partial 16S rRNA gene sequences were aligned with reference sequences using BLAST data bank (http://blast.ncbi.nlm.nih.gov/Blast.cgi?PROGRAM=blastn&PAGE_TYPE=BlastSearch&LINK_LOC=blasthome).

The minimum similarity among all members of the *Pseudomonas* genus is assumed at 77% (Balet et al., 2010). Over 95% of similarity, the species is considered surely identified.

Physiological characterization of airborne bacteria: Growth conditions

The bacteria were cultured in Luria Bertani medium (LB) (AES Chemunex, France) under shaking (180 rpm) at 30°C, close to optimum growth temperatures of *Pseudomonas fluorescens* species, i.e. 28°C (Merleau et al., 1993), and at 37°C, i.e. human body temperature. The bacterial density was determined by measuring optical density (OD) at 580 nm (Helios ε, Thermo Spectronic, USA) during at least 120h. Thanks to these growth kinetics curves, the maximum growth rate, μ_{\max} , was calculated for each strain.

Determination of virulence factors of airborne bacteria

Bacterial enzymatic characterization

Several methods were used to screen enzymatic activities. Each test was done at 30°C and 37°C.

Proteolytic activity was determined on Trypticase soy agar (TSA) (AES Chemunex, France) with skimmed milk 20%. Esterase was detected by growth on TSA (AES Chemunex, France) containing Tween 80 1% colored with Phenol red (1%).

Lecithinase and lipoproteolytic activities were analyzed by growth on TSA (AES Chemunex, France) with egg yolk 50% (VWR, Germany). Bacteria hydrolyse lecithin contrasting medium next to the inoculated streak. On the contrary a lighter colored zone shows lipoproteolytic activity. In the secreted hemolysis test, bacterial strains were streaked onto a 2% sheep red blood cell plates, whose were visually inspected the zones of clearing around the colonies. The pyoverdine production was observed by growth on King B Agar plates (AES Chemunex, France). After 48h incubation, the plates were observed with Ultra-Violet light at 365nm (VL-6LM, Vilber Lourmat, France), as the produced pyoverdine induces fluorescence.

Biosurfactant production

Surface tension measurement of a rinsing solution of bacteria cultured on solid agar medium is a direct method for determining global biosurfactant production, in ideal conditions for biosurfactant production and was done as previously described (Duclairoir Poc et al., 2011b).

Bacterial motility

Motility characters were observed through the evaluation of swim, swarm, twitch displacements after 40h at 30°C and 37°C. These motilities were obtained thanks to specific agar concentrations: 0.3% for the swim displacement, 0.5% for the swarm and 1% for the twitch. Initially, the plates were inoculated with overnight culture in LB at 30°C and 37°C (Rossignol et al., 2008).

Adhesion assays on abiotic surface

The bacterial adhesion was evaluated in triplicate in polystyrene microtitration plate at 30°C and 37°C incubated in LB during 24h and 48h. The adherent bacterial population was estimated by direct measurement (quantification) of absorbance at 595 nm after 0.1% crystal violet coloration and after cell lysis by sodium dodecylsulfate 1% (Duclairoir Poc et al., 2011b).

Evaluation of supernatant virulence using the A549 pneumocyte model

The cytotoxicity of *P. fluorescens* MFN1032, MFAF76a and MFAF88 culture supernatants, in LB at 30°C and 37°C, was evaluated toward A-549 human pulmonary type II-like epithelial cell line as described elsewhere (Pimenta et al., 2006).

The percentage (%) of total lysis was calculated as follows:

$$\%LDH = 100 \times (\text{OD}_{\text{sample}} - \text{OD}_{0\%}) / (\text{OD}_{100\%} - \text{OD}_{0\%})$$

A percentage as lower than 20% could be assumed linked to an avirulent strain. Four other classes were defined : 20-40%: weak virulence, 40-60%: virulence, 60-80%: highly virulent and greater than 80%: extremely virulent.

Results and Discussion

Identification of airborne fluorescent pseudomonads : preponderance of

Pseudomonas fluorescens cluster

The *Pseudomonas* genus is splitted into three well-supported clusters in the 16S rRNA phylogeny named aeruginosa, putida and fluorescens r-clusters (Bodilis et al., 2012). Different approaches : API/ MALDI

-Biotyper/ 16S rRNA gene sequencing, were done to identify the 19 airborne selected strains. According to the classification stated by Bodilis (Bodilis et al., 2012), a putative identification was proposed for each strain based on the more reliable identification by 16S rRNA sequencing (homology>95%) and /or by MALDI-Biotyper (score>2). The three strains : MFAE20, MFAB75 and MFAK14, were stated as *Pseudomonas* spp., their genus was surely identified, but their species could not confidently assumed. The majority of the 19 airborne strains are identified as *Pseudomonas fluorescens*.

The preponderance of *Pseudomonas fluorescens* species among the airborne Gram-negative bacteria was no surprise, due to their ubiquitous character created by their large genome (Stover et al., 2000). Moreover *P. fluorescens* is observed as the most common *Pseudomonas* species (at least 42%) in outdoor air, as already reported by Nevalainen (Nevalainen et al., 1990).

Although the pathogenicity of *P. aeruginosa* is largely described and cause several human diseases, specially in lung infections (Clifton & Peckham, 2010), the literature on other fluorescent *Pseudomonas* is poorly documented in airways transmitting route, even if such bacteria are able to induce pulmonary pathologies such as *P. fluorescens* strains (Chapalain et al., 2008).

This study aimed to contribute on a better knowledge of the impact of fluorescent pseudomonads on the safety of the air, that we breathe. To evaluate the potential of virulence on this panel of 19 airborne strains, two contamination situations were explored. Firstly, conventional airway infections at 37°C, corresponded to an internal infection such as pulmonary, and, at 30°C, temperature of an external infection

such as burned dermal injuries (Church et al., 2006) or as contamination of medical devices (Gershman et al., 2008).

Physiology of the 19 airborne bacteria : overall able to growth at 37°C

The growth rate for each of 19 airborne *Pseudomonas* strains, compiled in Table 1, was evaluated in LB medium at 30 and 37°C. Most of them were able to grow at 37°C, except MFAH4a and MFAD21c. Twelve other strains had an higher grow rate at 30°C, similar to the optimal growth temperature for *P. fluorescens* species, 28°C (Merleau et al., 1993). The first 5 strains, namely, MFAF76a, MFAF49a, MFAF88, MFAO2 and MFAF80b, presented an equivalent or increasing growth rate between 30 and 37°C. In addition to survival, they were able to multiply at human physiological temperature, which could facilitate the infectious processes.

Characterization of bacterial extracellular virulence factors : all the airborne strains produce several factors of virulence

MFN1032 was introduced in the panel to have a standard of virulence with a clinical origin that assures its pathogenic potential (Chapalain et al., 2008, Rossignol et al., 2008; Rossignol et al., 2009; Madi et al., 2010; Sperandio et al., 2010; Sperandio et al., 2012) and then makes a possible comparison of studied airborne *Pseudomonas* spp.

The 19 airborne *Pseudomonas* strains showed different patterns of secretion, as tabulated in Table 2. All strains synthesized lipoproteolytic enzymes and, except for MFAE48, induced clearing zones on sheep red blood cell plates revealing secreted hemolysis *a minima* incomplete for at least

one growth temperature. According to conventional microbiological nomenclature, the secreted hemolysis could be categorized as complete (β), incomplete (α) or no hemolysis (Luo et al., 2001). In any case, hemolytic phenomenon could result from synergy between activity of several hydrolysases, such as proteases, lecithinases, lipoproteases, and biosurfactants (Rossignol et al., 2008; Zhang et al., 2009). The hemolysis was complete for MFAF49a, MFAF80b and MFAD21c at 30°C and for MFAO2, MFAO39, MFAB75 and MFAH4a at 37°C.

Some virulence factors could be, on the one hand, strain-dependant: no protease and no lecithinase for MFAF49a, MFAF80b and for several strains less adapted at 37°C, no esterase for MFAF88 and MFAO39, no pyoverdine production for MFAF80b, MFAE88, MFAE20 and MFAH106a. On the other hand, some virulent exoproducts were strain- and temperature-dependant in the case of MFAF88 and the most of the strains were more adapted at 30°C than at 37°C.

Surprisingly, both strains, MFAH4a and MFAD21c, were not able to grow at 37°C in broth, but presented virulence factors at 37°C. To stimulate enzymatic secretion, bacterial growth was done on agar medium, promoting sessile lifestyle (i.e. in a surface adherent community). Such conditions seemed to facilitate the growth of MFAH4a and MFAD21c, contrary to more planktonic and less protective cell growth in broth. An other common character for this couple was their secretion of biosurfactant, as for MFN1032, MFAF88, MFAO2, MFAA66a, and MFAK14. This surfactive production was established through a surface tension lowered above 45mN/m (Carillo et al., 1996). Biosurfactants favor bacterial displacement, but may be affecting

adhesion, even colonisation of the host (37°C) or of a medical device or even burn injuries (30°C) (Van Hamme et al., 2006).

To conclude, only MFAF76a, MFAO2 and MFAO40 exhibit activity for all the tested enzymes like the clinical strain *P. fluorescens* MFN1032, but, among them, only MFAO2 produces biosurfactant as MFN1032.

Bacterial motility : some strains swim, all swarm and none twitch

Infection deals in part with bacterial motility to allow their colonisation in the host.

The 3 motile types : twitch, swim and swarm, were tested at 30 and 37°C.

No twitching, but swarming motility was noted for any strain at either temperature, as shown in Table 3. The swarming motility is a collective microbial motility resulting from, at least, one functional flagella, often completed by biosurfactant production (Kearns, 2010).

Although all strains were able to swim at 30°C, only 6 of them maintained the swimming mode at 37°C. This displacement allows bacteria to individually move towards the host with the help of functional flagella.

The flagella dependant motilities, i.e. swim and swarm, are involved in the development of biofilms (O'Toole & Kolter, 1998). For instance, functional flagella are needed for swarming mobility, which is related to the surface movement in the case of bacterial groups. This mobility is favored by biosurfactant production or by lipopolysaccharides, outer membrane components, for some Gram-negative bacteria (Kearns, 2010).

Bacterial adhesion on abiotic surface: different behaviours

As noted in Table 3, thicker biofilms were observed at 30°C than at 37°C. For MFAF76a, MFAF88, MFAE48 and MFAE8b, their biofilm were observed at 24h and 48h at either temperature. When the biofilm evolved between 24h and 48h, most of the time it increased, the mature structure was not yet reached, the biofilm seemed still under edification. However, for both temperatures, MFN1032 had a lowest ability to form biofilm at 48h than at 24h, this phenomenon was already reported about *P. fluorescens* biosurfactant production (Duclairoir Poc et al., 2011b). This biofilm reduction was noted at 30°C for MFAF88, MFAF80b and MFAO29 and at 37°C for MFAH4a.

Concerning contamination, the bacterial presence on biofilm is stabilized in the host or on a surface, and even protects from hostile microenvironment behind its shelf-shielding extracellular polymeric substances. Nevertheless, a biofilm could reduce over the time and persists slimmer; the lacking cells could be assumed in dispersing and colonising elsewhere in host (McDougald et al., 2012).

Selection of two airborne strains: *P.fluorescens* MFAF76A and *P. putida* MFAF88

In *P. aeruginosa* infections, tissue damage is due to the production of several extracellular and cell-associated virulence factors (Strateva & Mitov, 2011), similar exoproducts are produced by all *Pseudomonas* species and also known as factors of virulence.

Through the obtained results, two airborne strains, MFA76a and MFAF88, are of

particular interest: they are able to grow at 37°C and possibly better than at 30°C. They swim and swarm, thanks to their flagella and completed for MFAF88 by its biosurfactant production, as shown in Table 2. They present some virulent factors and form biofilm at either temperature. *P. fluorescens* MFA76a is very close to MFN1032 except for biosurfactant production and *P. putida* MFAF88 had an enzymatic pattern very different from MFN1032, but produced biosurfactant, as MFN1032.

Virulence of culture supernatant of MFN1032, MFAF76a, MFAF88 toward A-549 pneumocytes : strain-dependant virulence

Exoproducts such as lipases and proteases produced by *P. fluorescens* are known for their virulence (Rossignol et al., 2008; Zhang et al., 2009). Thus testing the growth supernatant could have a promising outcome. The need of an adequate cytotoxic model was crucial at this point and had to be ideally close to *in vivo* contamination by airway or pulmonary infection mode. The evaluation of virulence toward pneumocytes, such as cellular line A549 was assayed. The cytotoxic mechanism involved only the action of exoproducts, such as enzymes, siderophores or biosurfactants. All the supernatants, resulting from bacterial growth at 30°C and 37°C, induced lysis of the pulmonary cells by contact for 12h. Supernatant of MFAF88 induced a strong virulent response, in similar range (around 80%) at 30°C and 37°C. Furthermore, supernatants of MFN1032 and MFAF76a had significantly changed their virulence towards epithelial cells for both growth temperatures. MFN1032 was extremely virulent at 30°C and MFAF76a at 37°C and their virulence was less severe, i.e. only highly virulent, at 37°C for MFN1032, and at 30°C for MFAF76a, respectively.

Table.1 Characterization of the 19 airborne fluorescent *Pseudomonas* spp. strains

Strain	Sampling localisation & season	API® 20NE identification	MALDI Bityper: total proteomic comparison (score)	Identity percentage of 16S ribosomal RNA sequence <GenBank accession numbers>	Putative identification	μ_{max} at 30°C (h ⁻¹)	μ_{max} at 37°C (h ⁻¹)
MFAF76a	Rouen Harbor, Summer	<i>P. fluorescens</i> (excellent)	<i>P. koreensis</i> (2.122)	<i>P. koreensis</i> strain AGB-1 (96%) <KJ470785>	fluorescens r-cluster	1	1.08
MFAF49a	Rouen Harbor, Summer	<i>P. fluorescens</i> (excellent)	<i>P. abietaniphila</i> (2.094)	<i>P. lundensis</i> (85%) <KJ470784>	fluorescens r-cluster	0.79	1.05
MFAF88	Rouen Harbor, Summer	<i>Bulkholderia pseudomallei</i> (very good)	<i>Pseudomonas</i> spp. (1.982)	<i>P. putida</i> strain CG29 (99%) <KJ470787>	putida r-cluster	0.47	1.01
MFAO2	Rouen Harbor, Winter	<i>P. fluorescens</i> (excellent)	<i>P. koreensis</i> (2.001)	<i>Pseudomonas</i> sp. strain E1 (86%) <KJ470791>	fluorescens r-cluster	0.93	0.88
MFAF80b	Rouen Harbor, Summer	<i>P. fluorescens</i> (excellent)	<i>P. abietaniphila</i> (2.152)	<i>P. abietaniphila</i> strain HMGU118 (99%) <KJ470786>	fluorescens r-cluster	0.71	0.77
MFAE88	Rouen Harbor, Summer	<i>P. oryzihabitans</i> (very good)	<i>Pseudomonas</i> spp. (1.866)	<i>P. rhizosphaerae</i> strain BKB1(95%) <KJ470782>	fluorescens r-cluster	0.83	0.38
MFAO39	Rouen Harbor, Winter	<i>P. fluorescens</i> (excellent)	<i>Pseudomonas</i> spp. (1.962)	<i>P. putida</i> strain bD1 (100%) <KJ470793>	putida r-cluster	0.84	0.35
MFAA66a	Surburban Rouen, Summer	<i>P. oryzihabitans</i> (good)	<i>P. congelans</i> (2.164)	<i>P. syringae</i> pv. <i>Syringae</i> strain XJLX-2-2 (99%) <KJ470777>	fluorescens r-cluster	0.68	0.32
MFAO40	Rouen Harbor, Winter	<i>P. fluorescens</i> (excellent)	<i>P. koreensis</i> (2.149)	<i>P. fluorescens</i> strain TCA33 (99%) <KJ470794>	fluorescens r-cluster	0.85	0.3
MFAE20	Rouen Harbor, Summer	<i>P. oryzihabitans</i> (very good)	<i>Pseudomonas</i> spp. (1.917)	<i>P. graminis</i> strain 8B2 (84%) <KJ470780>	<i>Pseudomonas</i> spp.	0.64	0.26
MFAE48	Rouen Harbor, Summer	<i>P. oryzihabitans</i> (very good)	<i>P. graminis</i> (2.403)	<i>P. graminis</i> strain R5SpM3P2C1 (99%) <KJ470781>	fluorescens r-cluster	0.59	0.22
MFAB75	Surburban Rouen, Summer	<i>P. oryzihabitans</i> (very good)	<i>Pseudomonas</i> spp. (1.728)	<i>P. plecoglossicida</i> strain ETLB-3 (78%) <KJ470778>	<i>Pseudomonas</i> spp.	0.8	0.22

MFAE8b	Rouen Harbor, Summer	<i>P. fluorescens</i> (excellent)	<i>Pseudomonas</i> spp. (1.856)	<i>P. rhizosphaerae</i> strain - Y12 (79%) <KJ470783> <i>P. syringae</i> CC1557 (99%) <KJ470795>	fluorescens r-cluster	0.82	0.21
MFAO48	Rouen Harbor,Winter	<i>P. oryzihabitans</i> (very good)	<i>P. savastanoi</i> (2.098)	<i>P. putida</i> strain SCR2 (78%) <KJ470790>	fluorescens r-cluster	0.6	0.19
MFAK14	Surburban Rouen, Winter	<i>P. fluorescens</i> (good)	<i>Pseudomonas</i> spp.(1.923)	<i>P. thivervalensis</i> strain BD2-26 (99%) <KJ470792>	<i>Pseudomonas</i> spp.	0.62	0.17
MFAO29	Rouen Harbor,Winter	<i>P. fluorescens</i> (good)	<i>P. chlororaphis</i> (2.006)	<i>P. rhizosphaerae</i> strain R2-255 (99%) <KJ470788>	fluorescens r-cluster	0.6	0.15
MFAH106a	Rouen Harbor, Summer	<i>P. oryzihabitans</i> (excellent)	<i>Pseudomonas</i> spp. (1.821)	<i>P. fluorescens</i> strain RK2 (83%) <KJ470789>	fluorescens r-cluster	0.64	0.14
MFAH4a	Rouen Harbor, Summer	<i>P. fluorescens</i> (excellent)	<i>P. poae</i> (2.255)	<i>P. fluorescens</i> strain RK2 (86%) <KJ470779>	fluorescens r-cluster	0.79	No growth
MFAD21c	Residential Evreux, Summer	<i>P. fluorescens</i> (very good)	<i>P. poae</i> (2.147)		fluorescens r-cluster	0.78	No growth

Score >1.700 : probable genus

Score >2.000 : probable species,
secure genus

Air sample localisation and season; bacterial identification by API®20NE strips, by MALDI-Biotyper and by 16S rDNA gene sequencing after matching with NCBI data bank (http://blast.ncbi.nlm.nih.gov/Blast.cgi?PROGRAM=blastn&PAGE_TYPE=BlastSearch&LINK_LOC=blasthome); and maximum specific growth rate (μ_{\max}) at 30 and 37°C in LB medium, 180rpm, classified by decreasing μ_{\max} at 37°C.

Table.2 Extracellular virulence factors, at 30°C and 37°C, and biosurfactant production for MFN1032 (clinical strain) and for each airborne strain

The observed characters were proteolytic, esterase lecithinase, lipoproteinase and hemolytic activities, after 5 days, or pyoverdine production, after 2 days. The biosurfactant production was observed on Davis Minimum medium after 5 days. Experiments done in three independant assays.

Activity	Proteolytic				Esterase		Lecithinase		Lipoproteolytic		Secreted hemolytic		Pyoverdin production		Biosurfactant
	Incubation temperature (°C)		30	37	30	37	30	37	30	37	30	37	30	37	production
MFN1032	++	++	++	++	++	++	+	+	α	α	++	++	++	++	+
MFAF76a	++	++	++	++	++	++	++	++	α	α	++	++	++	++	-
MFAF49a	-	-	++	++	-	-	++	+	β	α	++	++	++	++	-
MFAF88	-	+	-	-	-	++	+	++	α	α	++	+	++	+	+
MFAO2	++	++	++	++	++	++	++	+	α	β	++	++	++	++	+
MFAF80b	-	-	++	++	-	-	++	++	β	α	-	-	-	-	-
MFAE88	-	-	-	++	-	-	++	++	α	-	-	-	-	-	-
MFAO39	-	+	-	-	++	-	+	++	β	β	++	-	-	-	-
MFAA66a	+	+	+	-	-	-	+	++	β	α	++	++	++	++	+
MFAO40	++	++	++	++	++	++	++	++	α	α	++	++	++	++	-
MFAE20	++	-	++	++	-	-	++	++	α	α	-	-	-	-	-
MFAB75	-	-	+	-	-	-	+	++	β	β	++	++	++	++	-
MFAE48	-	V	++	V	-	V	++	V	-	-	-	-	+	-	-
MFAE8b	-	-	++	++	-	-	++	+	α	α	++	-	-	-	-
MFAO48	-	-	++	++	-	V	++	V	-	α	++	-	-	-	-
MFAK14	-	+	++	-	-	-	+	++	α	α	+	-	-	-	+
MFAO29	+	V	++	V	-	V	++	V	β	α	++	-	-	-	-
MFAH106a	++	++	++	++	-	+	++	++	-	α	-	-	-	-	-
MFAH4a	++	++	++	++	-	-	+	+	β	β	++	++	++	++	+
MFAD21c	++	++	++	++	-	-	++	++	β	α	++	++	++	++	+

++: important activity

+: light activity

V: weak and variable

-: no activity

α: partial hemolysis

β: complete hemolysis

Table.3 Motility and biofilm ability, at 30°C and 37°C, for MFN1032 (clinical strain) and for each airborne strain. The observed motility characters were swim, swarm, twitch, after 40h. The biofilm formation was observed after 24h and 48h

Activity	Swim		Swarm		Twitch		Biofilm formation after 24h		Biofilm formation after 48h	
	30	37	30	37	30	37	30	37	30	37
Incubation temperature (°C)	30	37	30	37	30	37	30	37	30	37
MFN1032	++	++	+	+	-	-	++	+	+	-
MFAF76a	++	++	+	+	-	-	++	+	++	+
MFAF49a	+	-	+	+	-	-	-	-	+	+
MFAF88	++	++	+	+	-	-	++	+	+	+
MFAO2	++	+	+	+	-	-	+	-	+	-
MFAF80b	+	-	+	+	-	-	++	-	+	-
MFAE88	+	-	+	+	-	-	+	-	+	-
MFAO39	+	-	+	+	-	-	++	-	++	-
MFAA66a	+	-	+	+	-	-	-	-	-	-
MFAO40	+	-	+	+	-	-	++	-	++	-
MFAE20	+	-	+	+	-	-	+	-	+	+
MFAB75	+	-	+	+	-	-	-	-	+	-
MFAE48	+	-	+	+	-	-	+	+	+	+
MFAE8b	++	+	+	+	-	-	++	+	++	+
MFAO48	+	-	+	+	-	-	-	-	-	-
MFAK14	+	+	+	+	-	-	-	-	-	-
MFAO29	+	-	+	+	-	-	+	-	-	-
MFAH106a	+	-	+	+	-	-	+	-	+	-
MFAH4a	V	-	+	+	-	-	-	+	+	-
MFAD21c	V	-	+	+	-	-	-	-	-	-

++: displacement upper than 30mm

++: OD595 higher than 0.200

+: displacement upper than 10mm

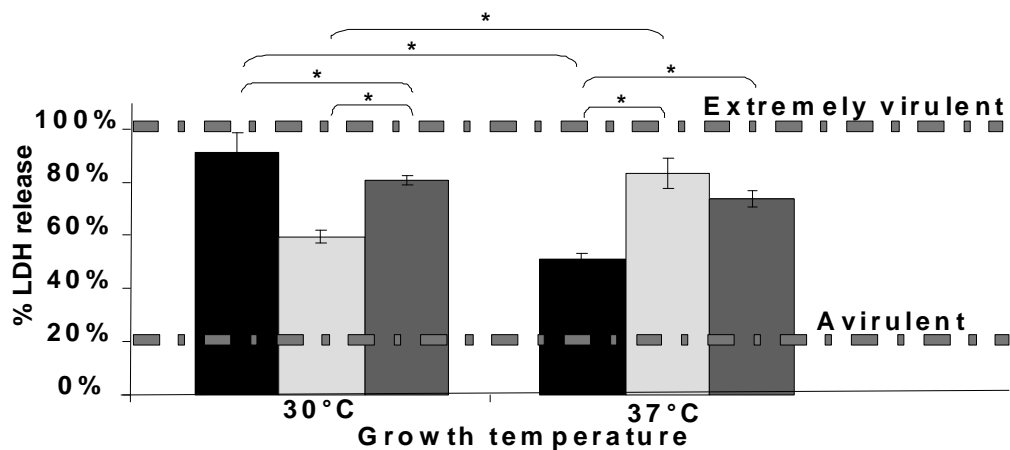
+: OD595 higher than 0.050

=: displacement lower than 10mm

-: OD595 lower than 0.050

V: weak and variable

Figure.1 Virulence towards A549 pneumocytes exposed to culture supernatants obtained at 30°C and 37°C



The virulent pattern is strain- and temperature-dependant. In fact, *P. putida* MFAF88 shows a constant virulence, its secretion varies nevertheless with temperature. Virulence could then be attributed to the common production at 30 and 37°C, i.e. lipoproteases, siderophores, and may be completed by biosurfactants, even if their quantities could be secreted quite variably at the two temperatures.

This variability in intensity of secretion could also explain the decrease in virulence for MFN1032. As shown in Table 2, all the enzymes and pyoverdine were expressed at 30°C as well as at 37°C, but no evidence was given about quantity. Rossignol and coworkers rightly note, at 37°C, a weaker production of phospholipase C, than at 28°C (Rossignol et al., 2008). This enzyme is known as a major factor of virulence.

Like MFN1032, the same families of exoproducts are secreted by *P. fluorescens* MFAF76a at both temperatures. However a slightly significative increase in virulence is noted at 37°C and again might be due in the exoproducts secretion modulation in concentration or in nature.

In any case, airborne *P. fluorescens* MFAF76a and *P. putida* MFAF88 may induce by their secretion, especially at 37°C, cytotoxic responses from A549 airway epithelial cells. Thus the biohazard, that they create as biocontamination, must be identified and not ignored. Moreover the virulence of these airborne strains and of the clinical standard, *P. fluorescens* MFN1032 operates on different ways from each other. To better understand these virulent mechanisms, an exoproteomic study would create insight.

Acknowledgements

This study was supported by grants from Grand Evreux Agglomération, AFSSET, and FEDER “*Pseudomonas* Virulence”. We wish to thank Christine Farmer for linguistic insight for this manuscript.

References

Agence française de Sécurité Sanitaire de l'environnement et du travail (became ANSES-Agence nationale de sécurité sanitaire de l'alimentation, de

- l'environnement et du travail), 2010. Project PUC2MP : Particules Urbaines et Céréalières, Microorganismes Mycotoxines et Pesticides (AFSSET-07-CRD-30) Supervisor Jean-Paul Morin, Partners: Normandie Univ, France ; Univ Rouen, INSERM U644, LMSM, CERTAM, Air Normand.
- Bodilis, J., Nsigue-Meilo, S., Besaury, L., Quillet, L. 2012. Variable Copy Number, Intra-Genomic Heterogeneities and Lateral Transfers of the 16S rRNA Gene in *Pseudomonas*. PLoS ONE. 7(4): e35647.
- Carrillo, P.G., Mardaraz, C., Pitta-Alvarez, S.I., Giulietti, A.M. 1996. Isolation and selection of biosurfactant-producing bacteria. Journal of Microbiology and Biotechnology. 12: 82-84.
- Chapalain, A., Rossignol, G., Lesouhaitier, O., Merieau, A., Gruffaz, C., Guerillon, J., Meyer, J.M., Orange, N., Feuilloley, M.G. 2008. Comparative study of 7 fluorescent pseudomonad clinical isolates. Canadian Journal of Microbiology 54(1): 19-27.
- Church, D., Elsayed, S., Reid, O., Winston, B., Lindsay, R. 2006. Burn wound infections. Clin Microbiology Reviews 19(2): 403-434.
- Clifton, I.J., Peckham, D.G. 2010. Defining routes of airborne transmission of *Pseudomonas aeruginosa* in people with cystic fibrosis. Expert Review of Respiratory Medicine. 4(4): 519-529.
- Donnarumma, G., Buommino, E., Fusco, A., Paoletti, I., Auricchio, L., Tufano, M.A. 2010. Effect of temperature on the shift of *Pseudomonas fluorescens* from an environmental microorganism to a potential human pathogen. International Journal of Immunopathology and Pharmacology. 23(1): 227-234.
- Duclairoir Poc, C., Groboillot, A., Lesouhaitier, O., Morin, J.P., Orange, N., Feuilloley, M.J.G. 2011a. *Caenorhabditis elegans*: a model to monitor bacterial air quality. BMC Research Notes 4: 503.
- Duclairoir Poc, C., Ngoya, S., Groboillot, A., Bodilis, J., Taupin, L., Merieau, A., Feuilloley, M.G., Orange, N. 2011b. Study of the influence of growth temperature on cyclolipopeptides production in environmental strains of *Pseudomonas fluorescens*. Journal of Bacteriology and Parasitology S1:002. Available <http://dx.doi.org/10.4172/2155-9597.S1-002>. Accessed 23 July 2014.
- Fernstrom, A., Goldblatt, M. 2013. Aerobiology and Its Role in the Transmission of Infectious Diseases. Journal of Pathogens, Article ID 493960, Available : <http://dx.doi.org/10.1155/2013/493960> . Accessed 23 July 2014.
- Gershman, M.D., Kennedy, D.J., Noble-Wang, J., Kim, C., Gullion, J., Kacica, M., Jensen, B., Pascoe, N., Saiman, L., McHale, J., Wilkins, M., Schoonmaker-Bopp, D., Clayton, J., Arduino, M., Srinivasan, A., *Pseudomonas fluorescens* Investigation Team. 2008. Multistate outbreak of *Pseudomonas fluorescens* bloodstream infection after exposure to contaminated heparinized saline flush prepared by a compounding pharmacy. Clinical Infectious Diseases. 47(11):1372-9.
- Gessner, A.R; and Mortensen, J.E. 1990 Pathogenic factors of *Pseudomonas cepacia* isolates from patients with cystic fibrosis. Journal of Medical Microbiology. 33 : 115-120.
- Hahn, H.P. 1997. The type-4 pilus is the major virulence-associated adhesin of *Pseudomonas aeruginosa*--a review.

- Gene 192(1): 99-108.
- Hawdon, N.A., Aval, P.S., Barnes, R.J., Gravelle, S.K., Rosengren, J., Khan, S., Ciofu, O., Johansen, H.K., Høiby, N., Ulanova, M. 2010. Cellular responses of A549 alveolar epithelial cells to serially collected *Pseudomonas aeruginosa* from cystic fibrosis patients at different stages of pulmonary infection. FEMS Immunology & Medical Microbiology. 59(2): 207-220.
- Hillion, M., Mijouin, L., Jaouen, T., Barreau, M., Meunier, P., Lefevre, L., Lati, E., Chevalier, S., Feuilloley, M.G.J. 2013. Comparative study of normal and sensitive skin aerobic bacterial populations. MicrobiologyOpen 2(6):953-961.
- Kearns, D.B. 2010. A field guide to bacterial swarming motility. Nature Reviews Microbiology. 8(9): 634-644.
- Luo, G., Samaranayake, L.P., Yau, J.Y. 2001. *Candida* species exhibit differential in vitro hemolytic activities. Journal of Clinical Microbiology. 39(8):2971-4.
- Madi, A., Lakhdari, O., Blottiére, H.M., Guyard-Nicodème, M., Le Roux, K., Groboillot, A., Svinareff, P., Doré, J., Orange, N., Feuilloley, M.G., Connal, N. 2010. The clinical *Pseudomonas fluorescens* MFN1032 strain exerts a cytotoxic effect on epithelial intestinal cells and induces Interleukin-8 via the AP-1 signaling pathway. BMC Microbiology. 10(10): 215.
- McDougald, D., Rice, S.A., Barraud, N., Steinberg, P.D., Kjelleberg, S. 2011. Should we stay or should we go: mechanisms and ecological consequences for biofilm dispersal. Nature Reviews Microbiology. 10(1): 39-50.
- Merieau, A., Gügi, B., Guespin-Michel, J.F., Orange, N. 1993. Temperature regulation of lipase B. secretion by *Pseudomonas fluorescens* strain MF0. Applied Microbiology and Biotechnology. 39: 104-109.
- Morin, J.-P., Preterre, D., Gouriou, F., Delmas, V., François, A., Orange, N., Grosboillot, A., Duclairoir-Poc, C., Moretti, M., Maillot, O., Lesouhaitier, O. 2013. Particules urbaines et céréalières, micro-organismes, mycotoxines et pesticides. Pollution atmosphérique. 217, Available: <http://lodel.irevues.inist.fr/pollution-atmospherique/index.php?id=759>.
- Mulet, M., Lalucat, J., García-Valdés, E. 2010. DNA sequence-based analysis of the *Pseudomonas* species. Environmental Microbiology. 12(6): 1513–1530.
- Nevalainen, A., Savolainen, R., Heinonen-Tanski, H. 1990. Indoor and outdoor occurrence of *Pseudomonas* bacteria. Proc. of the 5th International Conference on Indoor Air Quality and Climate, Toronto, Canada 29.07.-03.08.1990
- O'Toole, G.A., Kolter, R. 1998. Flagellar and twitching motility are necessary for *Pseudomonas aeruginosa* biofilm development. Molecular Microbiology. 30: 295-304.
- Pimenta, A.L., Di Martino, P., Blight, M.A. 2006. Positive correlation between *in vivo* and *in vitro* assays for the evaluation of *Pseudomonas* virulence. Research in Microbiology. 157(9): 885-890.
- Prüss-Ustün, A., Vickers, C., Haefliger, P., Bertollini, R. 2011. Knowns and unknowns on burden of disease due to chemicals: a systematic review. Environmental Health-Glob 10:9. Available: <http://www.ehjournal.net/content/10/1/9>. Accessed 23 July 2014..
- Rajmohan, S., Dodd, C.E., Waites, W.M.

2002. Enzymes from isolates of *Pseudomonas fluorescens* involved in food spoilage. *Journal of Applied Microbiology*. 93(2): 205-213.
- Rossignol, G., Merieau, A., Guerillon, J., Veron, W., Lesouhaitier, O., Feuilloley, M.G., Orange, N. 2008. Involvement of a phospholipase C in the hemolytic activity of a clinical strain of *Pseudomonas fluorescens*. *BMC Microbiology* 30(8): 189.
- Rossignol, G., Sperandio, D., Guerillon, J., Duclairoir Poc, C., Soum-Soutera, E., Orange, N., Feuilloley, M.G., Merieau, A. 2009. Phenotypic variation in the *Pseudomonas fluorescens* clinical strain MFN1032. *Research in Microbiology*. 160(5): 337-344.
- Semmler, A.B.T., Whitchurch, C.B., Mattick, J.S. 1999. A re-examination of twitching motility in *Pseudomonas aeruginosa*. *Microbiology+*. 145: 2863-2873.
- Sperandio, D., Rossignol, G., Guerillon, J., Connil, N., Orange, N., Feuilloley, M.G., Merieau, A. 2010. Cell-associated hemolysis activity in the clinical strain of *Pseudomonas fluorescens* MFN1032. *BMC Microbiology*. 24(10): 124.
- Sperandio, D., Decoin, V., Latour, X., Mijouin, L., Hillion, M., Feuilloley, M.G., Orange, N., Merieau, A. 2012. Virulence of the *Pseudomonas fluorescens* clinical strain MFN1032 against *Dictyostelium discoideum* and macrophages in relation with type III secretion system. *BMC Microbiology*. 12: 223.
- Stover, C.K., Pham, X.Q., Erwin, A.L., Mizoguchi, S.D., Warrener, P., Hickey, M.J., Brinkman, F.S., Hufnagle, W.O., Kowalik, D.J., Lagrou, M., Garber, R.L., Goltry, L., Tolentino, E., Westbrock-Wadman, S., Yuan, Y., Brody, L.L., Coulter, S.N., Folger, K.R., Kas, A., Larbig, K., Lim, R., Smith, K., Spencer, D., Wong, G.K., Wu, Z., Paulsen, I.T., Reizer, J., Saier, M.H., Hancock, R.E., Lory, S., Olson, M.V. 2000. Complete genome sequence of *Pseudomonas aeruginosa* PAO1, an opportunistic pathogen. *Nature*. 406(6799): 959-964.
- Strateva, T. and Mitov, I. 2011. Contribution of an arsenal of virulence factors to pathogenesis of *Pseudomonas aeruginosa* infections. *Annals of Microbiology*. 61(4): 717-732.
- Van Hamme, J.D., Singh, A., Ward, O.P. 2006. Physiological aspects. Part 1 in a series of papers devoted to surfactants in microbiology and biotechnology. *Biotechnology Advances*. 24(6): 604-620.
- Vincent, J.L., Sakr, Y., Sprung, C.L., Ranieri, V.M., Reinhart, K., Gerlach, H., Moreno, R., Carlet, J., Le Gall, J.R., Payen, D. 2006. Sepsis in European intensive care units: results of the SOAP study. *Critical Care Medicine*. 34(2): 344-353.
- Zhang, W.W., Hu, Y.H., Wang, H.L., Sun, L. 2009. Identification and characterization of a virulence-associated protease from a pathogenic *Pseudomonas fluorescens* strain. *Veterinary Microbiology*. 139(1-2): 183-188.

P21

Original article

A new study of the bacterial lipidome: HPTLC-MALDI-TOF imaging enlightening the presence of phosphatidylcholine in airborne *Pseudomonas fluorescens* MFAF76a

Tatiana Kondakova ^{a,d}, Nadine Merlet-Machour ^b, Manuel Chapelle ^c, David Preterre ^d, Frédéric Dionnet ^d, Marc Feuilloley ^a, Nicole Orange ^a, Cécile Duclairoir Poc ^{a,*}

^a Laboratory of Microbiology Signals and Microenvironment (LMSM) EA4312, Normandy Univ., Univ. Rouen, 55 rue St Germain, 27000 Evreux, France

^b Team Modified to Surface and Interface Analysis (SIMA), UMR 6014 COBRA, Normandy Univ., Univ. Rouen, 55 rue St Germain, 27000 Evreux, France

^c Bruker AXS S.A.S., 77420 Champs-sur-Marne, France

^d Aerothermic and Internal Combustion Engine Technological Research Center (CERTAM), 1 Rue Joseph Fourier, 76800 Saint Etienne du Rouvray, France

Received 6 October 2014; accepted 20 November 2014

Available online 2 December 2014

Abstract

Lipids are major functional components of bacterial cells that play fundamental roles in bacterial metabolism and the barrier function between cells and the environment. In an effort to investigate the bacterial lipidome, we adopted a protocol using MALDI-TOF MS imaging coupled to HPTLC to screen a large number of phospholipid classes in a short span of time.

With this method, phospholipids of airborne *Pseudomonas fluorescens* MFAF76a were visualized and identified in sample extracts (measurement accuracy below 0.1 Da, phospholipid identification by means of four characteristic fragment peaks). Via this technique, the *P. fluorescens* lipidome was shown to comprise three major lipid classes: phosphatidylethanolamine, phosphatidylglycerol and phosphatidylcholine.

The protocol described herein is simple, rapid and effective for screening of bacterial phospholipid classes. The remarkable presence of a eukaryotic phospholipid, phosphatidylcholine, was observed in *P. fluorescens* MFAF76a. This lipid is known to play a role in bacteria–host interactions and had not been known to be found in *P. fluorescens* cells.

© 2014 Institut Pasteur. Published by Elsevier Masson SAS. All rights reserved.

Keywords: Lipidomics; Phospholipids; Phosphatidylcholine; Mass spectrometry imaging; HPTLC MALDI TOF MSI; *Pseudomonas fluorescens*

1. Introduction

The emergence of molecular biology techniques at the end of the 20th century was at the origin of complete renewal of microbiology and, as a consequence, research focused

essentially on gene and protein expression. However, there is a growing interest in the analysis and identification of bacterial lipids [1]. Accordingly, in addition to terms such as “proteomics”, “genomics”, and “metabolomics”, the term “lipidomics” was introduced in microbiology [2].

Lipids are major compounds of bacterial cells and share a large variety of biological functions. Among these molecules, phospholipids, the major constituents of the cell membrane, play a fundamental role in metabolism, maintenance of membrane integrity, nutrient transport and signal transduction [3]. Bacterial phospholipids (PLs) are constituted by different long-chain (C₁₄–C₂₀) fatty acids linked by ester bonds to the major phosphatidyl moiety. Phosphatidic acid (PA),

* Corresponding author.

E-mail addresses: tatiana.kondakova@etu.univ-rouen.fr (T. Kondakova), nadine.merlet@univ-rouen.fr (N. Merlet-Machour), manuel.chapelle@bruker.fr (M. Chapelle), david.preterre@certam-rouen.com (D. Preterre), frederic.dionnet@certam-rouen.com (F. Dionnet), marc.feuilloley@univ-rouen.fr (M. Feuilloley), nicole.orange@univ-rouen.fr (N. Orange), cecile.poc@univ-rouen.fr (C. Duclairoir Poc).

phosphatidylcholine (PC), phosphatidylethanolamine (PE), phosphatidylglycerol (PG), phosphatidylinositol (PI), phosphatidylserine (PS) and cardiolipin (CL) represent the main classes of PLs [4].

Screening of PLs is usually performed using a variety of mass spectrometric techniques. For structural analysis fast-atom bombardment in combination with tandem mass spectrometry, electrospray ionization and matrix-assisted laser desorption ionization (MALDI) have been employed [5–7]. Electrospray ionization MS applied in negative ion mode and combined with liquid chromatography enables separating most of the different classes of phospholipids and identifying these molecules on the basis of the length of fatty acyl chains and unsaturated bond numbers or positions [8]. Although seldom used to provide detailed information for particular molecular species, MALDI is also potentially an excellent analytical method for rapid screening of lipids in biological matrices [9,10]. The use of MALDI MS for PLs analysis helps to overcome numerous problems related to the complexity and diversity of the extracts, as often encountered in bacterial material, and appears to be the most convenient method for complete screening in bacterial lipid extracts [2,11].

In the present report, we describe an analytical method coupling HPTLC to MALDI TOF for bacterial lipid analysis, fragmentation and identification. This method was used to identify PLs expressed in an airborne strain of *Pseudomonas fluorescens* MFAF76a, of particular interest. The adaptation potential of this environmental strain, elsewhere characterized [12], could reside at least by part in the composition of its outer and/or cytoplasmic membrane; thus, its lipidome was established by HPTLC-MALDI TOF imaging.

2. Materials and methods

2.1. Bacterial strain and growth conditions

P. fluorescens MFAF76a is an airborne strain isolated from a sample of air in dust clouds generated during crop ship loading in Rouen harbor installations (Normandy, France) [12]. This strain was grown at 28 °C under gentle agitation (180 rpm) in Luria-Bertani medium (AES, France). Aliquots of cells from 3 independent cultures were collected at the end of the exponential phase (OD 0.7). Cells were harvested by centrifugation at 4 °C (13,000 g) for 15 min. After removal of supernatant, cells were washed with sterile saline solution and centrifuged at 4 °C (13,000 g) for 10 min. Three successive washes were done. Aliquots of cells were resuspended in deionized water and lyophilized using a Freeze Dryer Heto PowerDry PL9000-50/HSC500 (Thermo Fisher Scientific, Saint-Herblain, France).

2.2. Reagents and chemicals

PL standards, 2,5-dihydroxybenzoic acid (DHB) and solvents (chloroform (CHCl_3), methanol (CH_3OH), ethanol ($\text{CH}_3\text{—CH}_2\text{OH}$), triethylamine ($\text{N}(\text{CH}_2\text{—CH}_3)_3$), acetone ($\text{CH}_3\text{—CO—CH}_3$) and acetonitrile ($\text{CH}_3\text{—CN}$)) were obtained

from Sigma—Aldrich (Saint-Quentin-Fallavier, France). Stock solutions of PL standards were prepared in CHCl_3 or in mixture of $\text{CHCl}_3/\text{CH}_3\text{OH}$ (2/1, v/v). All chemicals were of the highest commercially available purity and used without any further purification.

HPTLC silica gel 60 plates F₂₅₄ (75 × 50 mm, on aluminum backs) were obtained from Merck (Darmstadt, Germany). TLC chambers (80 × 120 mm) were purchased from Fisher Scientific SAS (Illkirch, France).

2.3. Bacterial lipid extraction

Lipids were extracted according to the method of Bligh and Dyer [13]. In summary, 5.5 mL of $\text{CHCl}_3/\text{CH}_3\text{OH}/\text{H}_2\text{O}$ (2/2/1.8, v/v/v) were added to about 1 g of lyophilized bacteria. Samples were mixed for 2 min and centrifuged for 10 min at 3000 g. The chloroform phase containing PLs was then collected and stored at –20 °C under N₂ atmosphere.

2.4. High performance thin-layer chromatography (HPTLC)

PLs were first separated by HPTLC using a method adapted from Fuchs et al. [10]. HPTLC plates allowing electric current conduction were washed with $\text{CHCl}_3/\text{CH}_3\text{—CH}_2\text{OH}/\text{H}_2\text{O}/\text{N}(\text{CH}_2\text{—CH}_3)_3$ (35/35/7/35, v/v/v/v) and activated at 110 °C under a vacuum for 2 h. Lipid extracts (100 μL) were deposited on HPTLC plates in triplicate and separated using $\text{CHCl}_3/\text{CH}_3\text{—CH}_2\text{OH}/\text{H}_2\text{O}/\text{N}(\text{CH}_2\text{—CH}_3)_3$ (35/35/7/35, v/v/v/v) as a running separation solution.

Individual lipid spots were visualized by UV fluorescence at 365 nm after spraying of a primulin dye solution (0.05% in $\text{CH}_3\text{—CO—CH}_3/\text{H}_2\text{O}$, 8/2, v/v). Retention factors (R_f) were calculated using the Sweday JustTLC software (v. 4.0.3, Lund, Sweden).

2.5. HPTLC-MALDI coupling

DHB was selected as the MALDI matrix, since it allows positive ion spectra of lipids and does not interfere with silica of HPTLC plates. Its peaks can be used as calibration standards.

HPTLC plates were dip-coated using a solution of DHB (200 g/L in $\text{C}_2\text{H}_3\text{N}/0.1\%$ trifluoro-acetic acid, 90/10, v/v) [7] and immediately dried under a dust-free atmosphere. This operation was repeated a second time, leading to a mean of DHB of 5 mg/cm². HPTLC plates were then fixed on a TLC MALDI target provided by Bruker Daltonics (Bremen, Germany).

2.6. MALDI TOF analysis

MALDI TOF mass spectra were acquired using an Autoflex III mass spectrometer equipped with a laser OptibeamTM Nd/YAG (355 nm) with 200-Hz tripled-frequency (Bruker Daltonics, Bremen, Germany). The excitation voltage was 19.5 kV and the reflector voltage was 21.0 kV. Laser strength

was kept about 30% above threshold for a good signal-to-noise ratio. Substantial strength is needed to desorb lipids from silica [14]. All MS spectra were obtained in reflector positive ion mode using TLC MALDI software (v. 1.1.7.0) provided by Bruker Daltonics (Bremen, Germany). 200 single laser shots were averaged for each point. The distance between two points was then determined as 1 mm. When obtained via this technique, 2D mass spectra enable rapid analysis of each lipid spot. Post-source decay (PSD) spectra were acquired on a Bruker Autoflex mass spectrometer (Bruker Daltonics), as previously described [15]. Briefly, precursor ions were isolated using a time ion selector. The fragment ions were refocused onto the detector by stepping the voltage applied to the reflectron in appropriate increments. This was done automatically using the “FAST” (“fragment analysis and structural TOF”) subroutine of FlexAnalysis software.

Calibration was performed in two steps. External calibration was performed using the DHB matrix and Peptide Calibration Standard II (ref 822570, Bruker Daltonics, Bremen, Germany) covering a mean mass range between 200 and 3500 Da. The external calibration of the apparatus was performed daily in FlexControl software. Supplementary internal calibration was made using sphingomyelin (1 µg/mL) mixed with the matrix solution before dipping. Peaks generated by these standards were used to calibrate TLC MALDI software. This double calibration method improved measurement accuracy to below 0.1 Da for lipid identification. Lipids were identified using the LIPID MAPS database.

2.7. HPTLC-MALDI TOF imaging

Mass spectrometry imaging (MSI) of each spot was performed using FlexImaging software (v. 2.1., Bruker Daltonics,

Bremen, Germany). A polygon measurement region was defined starting from the lipid migration line. The number of laser shots per pixel was set at 200 and the distance between two adjacent pixels was 200 µm, with multiple additions of single position acquisition run (every 40 shots). Following MS and MS/MS identification, the lipid line migration was reconstructed according to lipid-identified areas. Individual lipid spots were labeled by a specific color code according to *m/z*.

3. Results

3.1. HPTLC MALDI-TOF MS analysis of lipid standards

A lipid standard mixture was analyzed in order to check identification against MS and MS/MS lipid databases (www.lipidmaps.org) and to identify specific fragmentation mechanisms. The general protocol employed for standards and subsequently bacterial lipid extracts is presented in Fig. 1.

Typical HPTLC-MALDI TOF MSI of lipid standard mixture is presented in Fig. 2. The reconstructed lipid standard line migration is presented on the left side of Fig. 2. The *R_f* of lipid spots were calculated in JustTLC software using primulin-dyed HPTLC plates (data not shown). MS spectra of each lipid, identified on the basis of their *R_f* and encoded in artificial colors, are on the right side of Fig. 2. Lipid identification was completed by MS, PDS and MSI analysis directly on the HPTLC plate using TLC MALDI and FlexImaging software.

3.2. HPTLC-MALDI-TOF MSI analysis of bacterial PLs

MSI analysis of *P. fluorescens* MFAF76a lipids is presented in Fig. 3. As visible on its left side, 3 spots were separated

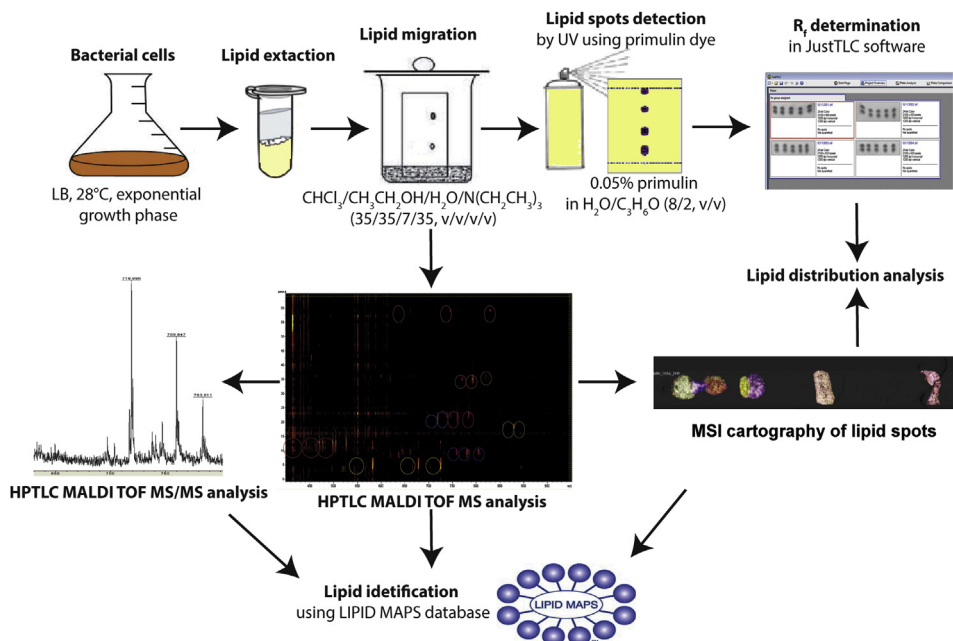


Fig. 1. Scheme illustrating the general HPTLC-MALDI TOF MSI method of PL class analysis.

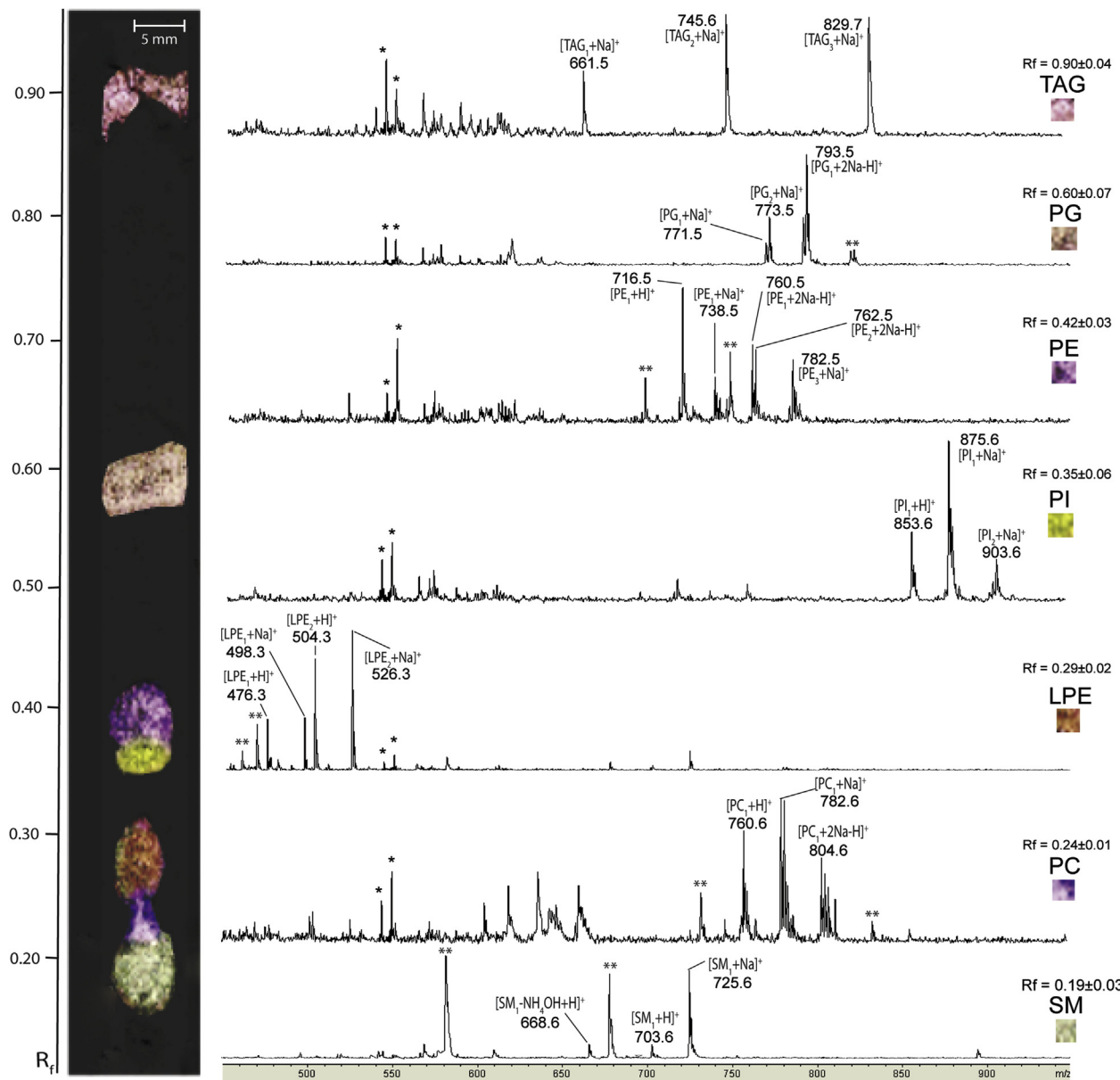


Fig. 2. HPTLC-MALDI TOF MS analysis of lipid standard mixture. Lipid mixture (100 μ L) was deposited in triplicate on the HPTLC plate and developed with $\text{CHCl}_3/\text{CH}_3\text{-CH}_2\text{OH}/\text{H}_2\text{O}/\text{N}(\text{CH}_2-\text{CH}_3)_3$ (35/35/7/35, v/v/v/v) as a solvent system. Lipid standards were purchased from Sigma-Aldrich and used in CHCl_3 or in mixture of $\text{CHCl}_3/\text{CH}_3\text{OH}$ (2/1, v/v). The DHB matrix was used as a 200 g/L solution in $\text{CH}_3\text{-CN}/0.1\%$ trifluoro-acetic acid, 90/10, v/v. After matrix application, MALDI TOF MS, PSD and MSI analyses are performed. All spectra were acquired on an Autoflex III MS equipped with a laser OptibeamTM Nd/YAG (355 nm, 200-Hz tripled-frequency) (Bruker Daltonics, Bremen, Germany). MSI analysis of lipid spots is presented on the left side of the figure. Following MS and PSD identification, the lipid line migration was reconstructed according to lipid-identified areas. Individual lipid spots were labeled with a specific color code according to m/z . Sphingomyelin (SM) — (■); PC — (■); lysophosphatidylethanolamine (LPE) — (■); PI — (■); PE — (■); PG — (■) and triglycerides (TAG) — (■); *matrix peaks; **unidentified peaks. (For interpretation of the references to color in this figure legend, the reader is referred to the web version of this article.)

with R_f 0.24 ± 0.01 ; 0.43 ± 0.02 and 0.62 ± 0.03 . On the right side of Fig. 3, the 2D representation shows the lipid line migration versus MS peak intensity (increasing m/z). The different lipid spots had specific regions of m/z localization. To eliminate most of the matrix peaks, only m/z from 500 to 2000 were studied.

Based on the response factors, the following PLs were identified: PC ($R_f = 0.24 \pm 0.01$), PE ($R_f = 0.43 \pm 0.02$) and PG ($R_f = 0.62 \pm 0.03$) (Fig. 4). Detailed MS and PDS spectra are presented on the right side of Fig. 4. PDS

spectra of selected peaks are superposed on the lipid MS spectrum.

2,5-dihydroxybenzoic acid (DHB), selected as matrix, enables cleavage of phosphate-glycerol bond and induces loss of the hydrophilic head group, i.e. $[\text{M}-\text{HG} + \text{H}]^+$, characteristic of each lipid class [1]. This loss is caused by a positive charge localized on the phosphate group [16].

The spot with $R_f = 0.62 \pm 0.03$ was identified as PG. Two most intense peaks, at m/z 743.5 and 765.5, showed one PG species singly and doubly sodiated, respectively $[\text{PG}(16:0)/$

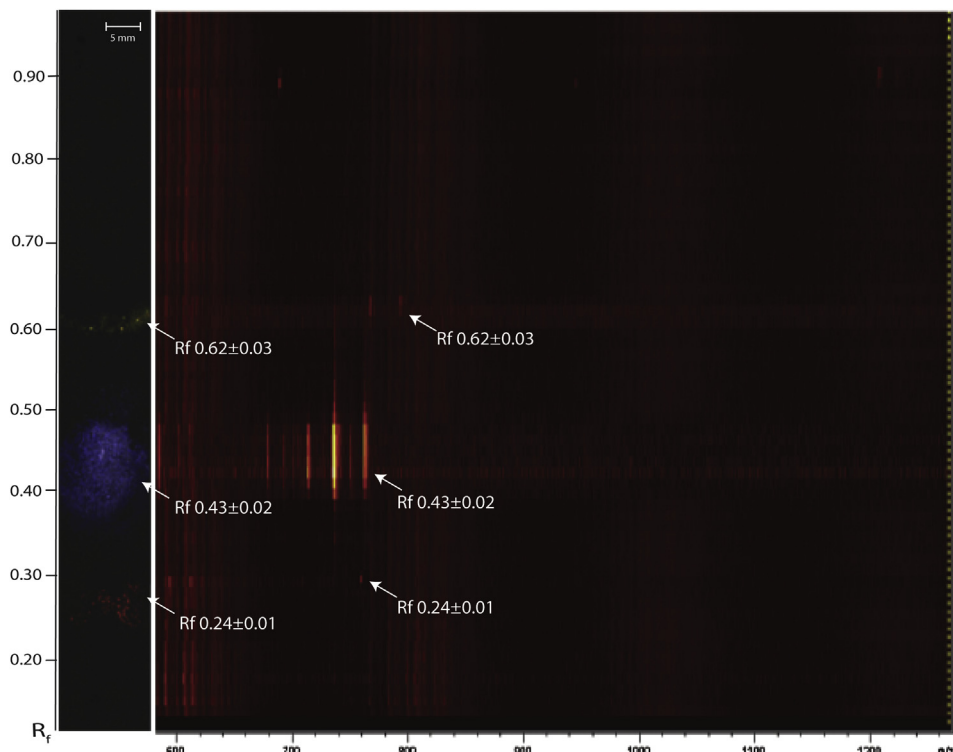


Fig. 3. HPTLC MALDI TOF MS analysis of bacterial PLs. MSI analyses were performed in triplicate using FlexImaging software (v. 2.1., Bruker Daltonics, Bremen, Germany). On the left side of the figure, MSI analysis shows *P. fluorescens* lipid distribution. On the right side, 2D MS representation obtained via TLC MALDI software is shown. The 2D MS image presents the *P. fluorescens* lipid line migration versus MS peak intensity (increasing m/z between $m/z = 500$ – 1300). PLs and retention factor (R_f): PC- 0.24 ± 0.01 (red); PE- 0.43 ± 0.02 (blue); PG- 0.62 ± 0.03 (yellow). The analyses were performed for three independent bacterial lipid extracts.

16:1)+Na] $^+$ and [PG(16:0/16:1)+2Na-H] $^+$ (Fig. 4/A). The peak at m/z 791.6 was related to another doubly sodiated PG molecule [PG(16:0/18:1)+2Na-H] $^+$. The PDS fragment at m/z 195.1 was characteristic of PG and corresponded to the sodiated head group [HG + Na] $^+$ (Fig. 4/A/1 & 2). The peaks at m/z 550.5 and 572.5, corresponding respectively to protonated and monosodiated species, illustrate loss of the head group of PG (Fig. 4/A/1). The peaks at m/z 576.5 and 598.5 indicate loss of protonated and sodiated polar head groups of PG species [PG(16:0/18:1)-HG + H] $^+$ and [PG(16:0/18:1)-HG + Na] $^+$ (Fig. 4/A/2, Table 1). The alkyl chain length was confirmed by GC MS analysis of PL fatty acids (see supplementary data Table S1).

The spot with an R_f value of 0.43 ± 0.02 led us to assume the presence of PE, a typical constituent of the *Pseudomonas* lipidome [17–19]. Two pairs of MS peaks (m/z 712.5 and 734.5; 738.5 and 760.5), separated by 22 Da, suggested the presence of two PE molecules (Fig. 4/B). This lipid class is characterized by a specific PDS fragments peak at $m/z = 123.4$ corresponding to the dehydrated PE head group [HG-H₂O] $^+$ (Fig. 4/B/3 & 4); and $m/z = 164$ to the sodiated head group: [HG + Na] $^+$ (Fig. 4/B/3 & 4). The peaks at $m/z = 669.5$ and 695.5 corresponded to loss of ethanolamine [PE(16:0/16:1)-C₂H₅N + Na] $^+$ and [PE(16:0/18:1)-C₂H₅N + Na] $^+$, respectively. For PE(16:0/16:1), two fragments at $m/z = 550.5$ and 572.5, showed loss of the protonated

and sodiated ethanolamine head groups, [PE(16:0/16:1)-HG + H] $^+$ and [PE(16:0/16:1)-HG + Na] $^+$ (Fig. 4/B/3). Peaks at $m/z = 576.5$ and 598.5 were characteristic of the loss of protonated and sodiated head groups of PE(16:0/18:1) (Fig. 4/B/4). Remarkably, the same fragments were found for PG, indicating the same length of alkyl chains in PE and PG molecules (Table 1).

The spot with $R_f = 0.24 \pm 0.01$ was unexpectedly identified as PC. Two MS peaks ($m/z = 732.6$ and 754.5) of one PC(16:0/16:0) species differentiated with 22 Da were found (Fig. 4/C). Fragments at $m/z = 184.1$ and $m/z = 147.0$ were characteristic of PC and corresponded to loss of the polar head group with specific rearrangements [HG + H] $^+$ and [HG-(CH₃)₃ + Na] $^+$ (Fig. 4/5) [20]. The peaks at $m/z = 548.5$ and 570.5, Fig. 4/5, were attributed to the loss of the sodiated and protonated polar head groups, [PC(16:0/16:0)-HG + H] $^+$ and [PC(16:0/16:0)-HG + Na] $^+$, respectively. The predominant fragment at $m/z = 697.6$ showed the loss of ammonia from the polar head group [PC(16:0/16:0)-NH₄OH + H] $^+$. The results of this study are summarized in Table 1.

4. Discussion

It is noteworthy that, up until now, the HPTLC-MALDI TOF MSI method was only used for PL analysis in eukaryotic cell lipidomes and human tissue and body fluid [21]. We

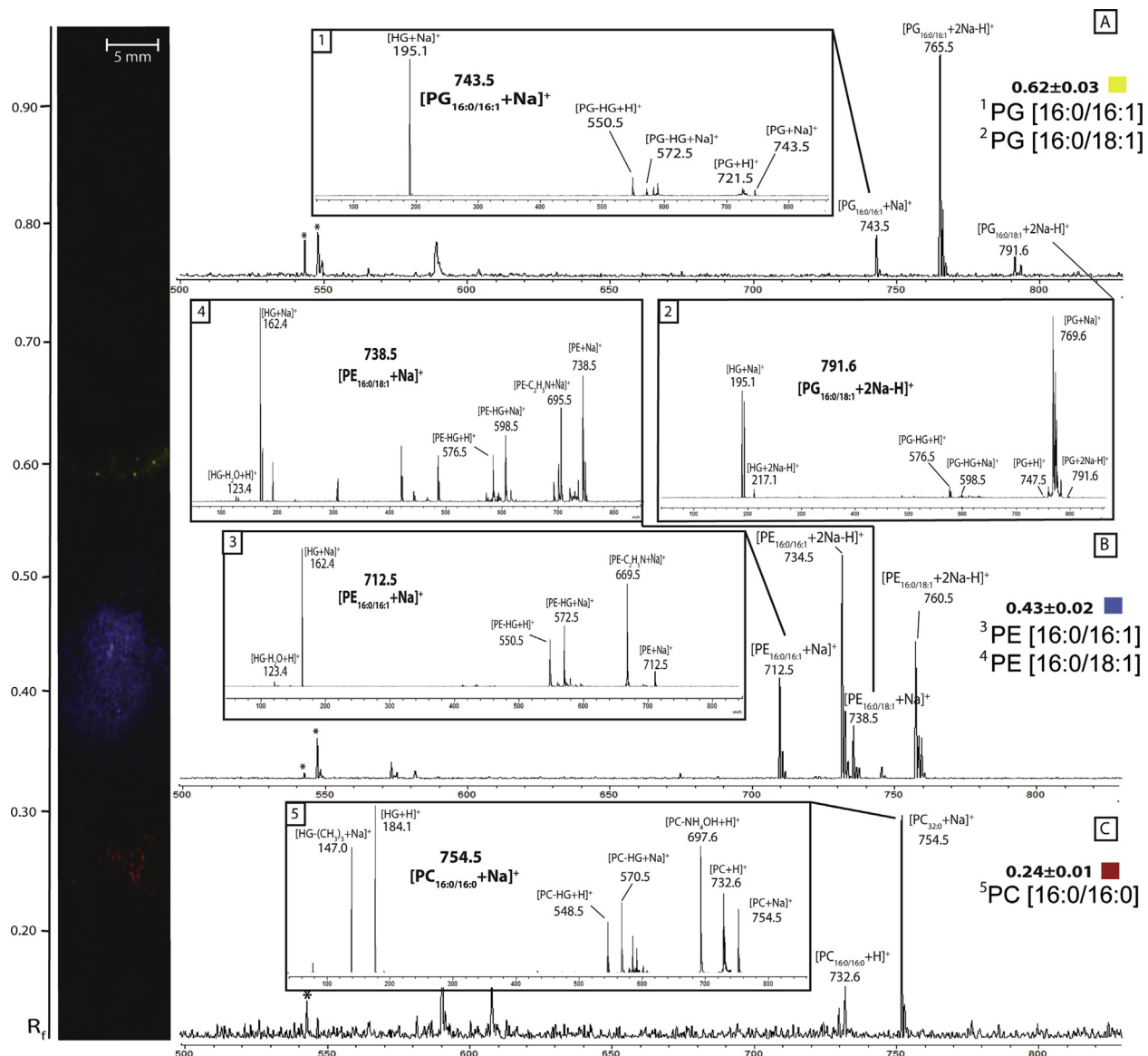


Fig. 4. HPTLC-MALDI TOF MS and PDS analysis of bacterial PLs. MS analysis of $R_f 0.24 \pm 0.01$ -PC; $R_f 0.43 \pm 0.02$ -PE and $R_f 0.62 \pm 0.03$ -PG realized in TLC MALDI software. Lipid peaks were detected in positive MALDI mode on an HPTLC plate. PSD spectra with identification of PL fragments are superimposed. Lipid identification was performed on the basis of MS, PSD and MSI analyses using the LIPID MAPS database, MS and PSD spectra of lipid standards obtained previously. The alkyl chain length was confirmed by GC MS analysis of PL fatty acids (supplementary data, Table S1). The analyses were performed for three independent bacterial lipid extracts. *DHB peaks; **unidentified peaks; HG: head group.

propose herein the first adaptation of this method to the study of the bacterial lipidome. Thus, total lipids of airborne *P. fluorescens* MFAF76a were extracted and separated on HPTLC plates to resolve individual PL spots. This HPTLC technique was coupled to MALDI TOF MS. A complete study of detected spots by MS, PDS and MSI was carried out, enabling PL identification in the lipidome of *P. fluorescens* MFAF76a. The HPTLC-MALDI TOF MSI method of PL analysis appears perfectly adapted to the analysis of bacterial lipids, as demonstrated in the present study.

This method has many key advantages: 1) due to access to a MALDI TOF spectrometer, it is inexpensive, since HPTLC plates only need to have an electric conductor metal back, but

are inserted into the spectrometer using a reusable TLC MALDI adapter; 2) HPTLC-MALDI TOF MS is a rather rapid method; TLC MALDI software enable screening of one sample in 5 min; 3) coupling between MALDI MS and HPTLC for separating individual lipids increases the sensitivity of the method compared to other existing techniques; 4) MS imaging, designed for MS analysis of tissue, is a good method for mapping individual lipid species distribution in HPTLC plates.

However, the method continues to have its drawbacks. It suffers from a lack of sensitivity; the required quantity of extracted lipid remains high. A volume of 100 μ L of bacterial lipid extract (containing a mean of 40 μ g lipids) was necessary

Table 1
PL composition of *P. fluorescens* MFAF76a.

Retention factor	Lipid class	Peak position (<i>m/z</i>) and adducts	Species	Molar mass (Da)
0.24 ± 0.01	PC	732.6 [PC + H] ⁺	PC (16:0/16:0)	731.5
		754.5 [PC + Na] ⁺		
0.43 ± 0.02	PE	712.5 [PE + Na] ⁺	PE (16:0/16:1)	689.5
		734.5 [PE+2Na-H] ⁺		
		738.5 [PE + Na] ⁺	PE (16:0/18:1)	715.5
		760.5 [PE+2Na-H] ⁺		
0.62 ± 0.03	PG	743.5 [PG + Na] ⁺	PG (16:0/16:1)	720.5
		765.5 [PG+2Na-H] ⁺		
		791.6 [PG+2Na-H] ⁺	PG (16:0/18:1)	746.5

for one migration line; this implies starting extraction from a large volume of bacterial culture (generally 100 mL).

Moreover, difficulties in PSD fragmentation and identification of PL alkyl chains remain an issue. Since analysis was performed with DHB as the MALDI matrix, the spectrometer was run in a positive mode and non-polar alkyl chain fragments have low intensity. Other experiences with other MALDI matrices, such as 9-aminoacridine or trihydroxyacetophenone in negative MALDI mode, showed weak intensity of individual lipids (data not shown). This makes PDS fragmentation of lipid peaks too insensitive and complicates lipid identification.

The HPTLC-MALDI TOF MSI method led to original results on the lipidome of *P. fluorescens*. In bacteria, most lipids are located in the cell wall. For Gram-negative bacteria like *P. fluorescens*, this cell wall consists of an association of a multiplicity of individual proteins with a somewhat limited series of major lipid species, with the main constituents of PL essentially considered to be PE, PG, CL and minor lysoPLs, like lysoPE and lysoPG [17,18,22,22–25]. The absence of CL in our results can be explained by the extraction method employed. As shown by Lopalco et al. [14], after lipidic extraction, CL is found with denatured proteins in the aqueous phase and thus not in the chloroform phase that was presently analyzed [26]. In any case, the presence of PE and PG was confirmed by our method, and these two lipid classes are considered as major components of the *Pseudomonas* lipidome [17,27]. Conversely, the detection of PC is quite unusual in a bacterial cell [9,10]. This lipid is the major constituent of the membrane bilayer in eukaryotes [28], but it is rarely found in prokaryotes, and only 10% of bacterial species are known to synthesize PC [29]. This PL is found only in the lipidome of very specific bacteria, particularly eukaryotes, symbiotic or pathogenic. Even in an opportunistic pathogen such as *P. aeruginosa*, PC is only detected in small amounts (less 4% of total lipids), but its role appears essential in virulence expression [30,31]. Thus, PC could facilitate the assembly or localization of specific proteins to *P. fluorescens*. Further proteomics studies should help to better understand the role of PC in this bacterial lipidome.

In conclusion, the HPTLC-MALDI TOF MSI technique appears to be a rapid and inexpensive method for the study of the bacterial lipidome. Mass spectrometric analysis can be realized directly after lipid separation on HPTLC plates. This method,

adapted from eukaryotic lipid analysis, should efficiently complete proteomic tools for investigating bacterial adaptation to host and stress. In the present study, HPTLC-MALDI TOF MSI enabled revealing expression of different forms of PE and PG in the lipidome of an airborne *P. fluorescens* strain. Moreover, it shows the presence of PC, suggesting potential for adaptation to interactions with eukaryotic hosts.

Conflict of interest

There is no conflict of interest.

Acknowledgments

Tatiana Kondakova is recipient of a PhD grant from the GRR SeSa (Sanitary Safety Research Network) financed by the Regional Council of Haute-Normandie (France). This study was supported by the Conseil général de l'Eure and Grand Evreux Agglomeration.

Appendix A. Supplementary data

Supplementary data related to this article can be found at <http://dx.doi.org/10.1016/j.resmic.2014.11.003>.

References

- Gidden J, Denson J, Liyanage R, Ivey DM, Lay JO. Lipid compositions in *Escherichia coli* and *Bacillus subtilis* during growth as determined by MALDI-TOF and TOF/TOF mass spectrometry. Int J Mass Spectrom 2009;283:178–84.
- Fuchs B, Süß R, Schiller J. An update of MALDI-TOF mass spectrometry in lipid research. Prog Lipid Res 2010;49:450–75.
- Zhang Y-M, Rock CO. Membrane lipid homeostasis in bacteria. Nat Rev Microbiol 2008;6:222–33.
- Wolf C, Quinn PJ. Lipidomics: practical aspects and applications. Prog Lipid Res 2008;47:15–36.
- Jensen NJ, Tomer KB, Gross ML. FAB MS/MS for phosphatidylinositol, -glycerol, -ethanolamine and other complex phospholipids. Lipids 1987;22:480–9.
- Pulfer M, Murphy RC. Electrospray mass spectrometry of phospholipids. Mass Spectrom Rev 2003;22:332–64.
- Fuchs B, Schiller J, Süß R, Zscharnack M, Bader A, Müller P, et al. Analysis of stem cell lipids by offline HPTLC-MALDI-TOF MS. Anal Bioanal Chem 2008;392:849–60.
- Milne S, Ivanova P, Forrester J, Alex Brown H. Lipidomics: an analysis of cellular lipids by ESI-MS. Methods 2006;39:92–103.
- Schiller J, Süß R, Fuchs B, Müller M, Zschornig O, Arnold K. MALDI-TOF MS in lipidomics. Front Biosci J Virtual Libr 2007;12:2568–79.
- Fuchs B, Schiller J, Süß R, Schürenberg M, Suckau D. A direct and simple method of coupling matrix-assisted laser desorption and ionization time-of-flight mass spectrometry (MALDI-TOF MS) to thin-layer chromatography (TLC) for the analysis of phospholipids from egg yolk. Anal Bioanal Chem 2007;389:827–34.
- Fuchs B, Süß R, Nimptsch A, Schiller J. MALDI-TOF-MS directly combined with TLC: a review of the current state. Chromatographia 2009;69:95–105.
- Duclairoir Poc C, Verdon J, Groboillot A, Barreau M, Toucourou H, Mijouin L, et al. Airborne fluorescent pseudomonads: what potential for virulence? Int J Curr Microbiol Appl Sci 2014;3(8):708–22.

- [13] Bligh EG, Dyer WJ. A rapid method of total lipid extraction and purification. *Biochem Cell Biol* 1959;37:911–7.
- [14] Lobasso S, Lopalco P, Angelini R, Vitale R, Huber H, Müller V, et al. Coupled TLC and MALDI-TOF/MS analyses of the lipid extract of the hyperthermophilic archaeon *Pyrococcus furiosus*. *Archaea* 2012;2012:1–10.
- [15] Fuchs B, Schober C, Richter G, Süß R, Schiller J. MALDI-TOF MS of phosphatidylethanolamines: different adducts cause different post source decay (PSD) fragment ion spectra. *J Biochem Biophys Methods* 2007;70:689–92.
- [16] Harvey DJ. Matrix-assisted laser desorption/ionization mass spectrometry of phospholipids. *J Mass Spectrom* 1995;30:1333–46.
- [17] Boeris PS, Domenech CE, Lucchesi GI. Modification of phospholipid composition in *Pseudomonas putida* A ATCC 12633 induced by contact with tetradecyltrimethylammonium. *J Appl Microbiol* 2007;103:1048–54.
- [18] Fouchard S, Abdellaoui-Mâne Z, Boulanger A, Llopiz P, Neunlist S. Influence of growth conditions on *Pseudomonas fluorescens* strains: a link between metabolite production and the PLFA profile. *FEMS Microbiol Lett* 2005;251:211–8.
- [19] Oursel D, Loutelier-Bourhis C, Orange N, Chevalier S, Norris V, Lange CM. Lipid composition of membranes of *Escherichia coli* by liquid chromatography/tandem mass spectrometry using negative electrospray ionization. *Rapid Commun Mass Spectrom* 2007;21:1721–8.
- [20] Al-Saad KA, Siems WF, Hill HH, Zabrouskov V, Knowles NR. Structural analysis of phosphatidylcholines by post-source decay matrix-assisted laser desorption/ionization time-of-flight mass spectrometry. *J Am Soc Mass Spectrom* 2003;14:373–82.
- [21] Fuchs B, Schiller J. MALDI-TOF MS analysis of lipids from cells, tissues and body fluids. *Subcell Biochem* 2008;49:541–65.
- [22] Diedrich DL, Cota-Robles EH. Heterogeneity in lipid composition of the outer membrane and cytoplasmic membrane of *Pseudomonas* BAL-31. *J Bacteriol* 1974;119:1006–18.
- [23] Gill CO. Effect of growth temperature on the lipids of *Pseudomonas fluorescens*. *J Gen Microbiol* 1975;89:293–8.
- [24] Rowe NJ, Tunstall J, Galbraith L, Wilkinson SG. Lipid composition and taxonomy of [*Pseudomonas*] *echinoides*: transfer to the genus *Sphingomonas*. *Microbiol Read Engl* 2000;146(Pt 11):3007–12.
- [25] Rühl J, Hein E-M, Hayen H, Schmid A, Blank LM. The glycerophospholipid inventory of *Pseudomonas putida* is conserved between strains and enables growth condition-related alterations. *Microb Biotechnol* 2012;5:45–58.
- [26] Lopalco P, Angelini R, Lobasso S, Köcher S, Thompson M, Müller V, et al. Adjusting membrane lipids under salt stress: the case of the moderate halophilic organism *Halobacillus halophilus*. *Environ Microbiol* 2013;15:1078–87.
- [27] Bhakoo M, Herbert RA. Fatty acid and phospholipid composition of five psychrotrophic *Pseudomonas* spp. grown at different temperatures. *Arch Microbiol* 1980;126:51–5.
- [28] Cole LK, Vance JE, Vance DE. Phosphatidylcholine biosynthesis and lipoprotein metabolism. *Biochim Biophys Acta* 2012;1821:754–61.
- [29] Conde-Alvarez R, Grilló MJ, Salcedo SP, de Miguel MJ, Fugier E, Gorvel JP, et al. Synthesis of phosphatidylcholine, a typical eukaryotic phospholipid, is necessary for full virulence of the intracellular bacterial parasite *Brucella abortus*. *Cell Microbiol* 2006;8:1322–35.
- [30] Geiger O, López-Lara IM, Sohlenkamp C. Phosphatidylcholine biosynthesis and function in bacteria. *Biochim Biophys Acta* 1831;2013:503–13.
- [31] Geiger O. Lipids and *Legionella* virulence. In: Timmis KN, editor. *Handb hydrocarb lipid microbiol*. Springer Berlin Heidelberg; 2010. p. 3195–202.

P22



Application of biosurfactants and periodic voltage gradient for enhanced electrokinetic remediation of metals and PAHs in dredged marine sediments

M.T. Ammami^a, F. Portet-Koltalo^{b,*}, A. Benamar^a, C. Duclairoir-Poc^c, H. Wang^a, F. Le Derf^b

^a Laboratoire Ondes et Milieux Complexes, UMR CNRS 6294, Université du Havre, 53 rue de Prony, 76600 le Havre, France

^b Laboratoire COBRA UMR CNRS 6014, Université de Rouen, 55 rue Saint Germain, 27000 Evreux, France

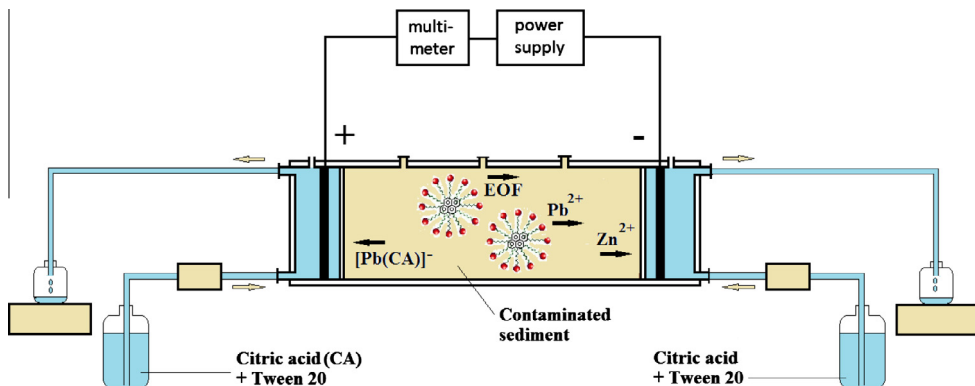
^c Laboratoire de microbiologie – signaux et micro-environnement, EA 4312, Université de Rouen, 55 rue Saint Germain, 27000 Evreux, France



HIGHLIGHTS

- Improving electrokinetic remediation of metals and PAHs in dredged harbor sediments.
- Increasing citric acid concentration, associated to Tween20 surfactant, is favorable.
- Applying a periodic voltage gradient with low concentration of additives is effective.
- Rhamnolipid and viscosin-like biosurfactants give promising results as additives.

GRAPHICAL ABSTRACT



ARTICLE INFO

Article history:

Received 28 August 2014

Received in revised form 21 November 2014

Accepted 22 December 2014

Handling Editor: E. Brillas

Keywords:

Electrokinetic remediation

Periodic voltage

Heavy metals

Polycyclic aromatic compounds

Biosurfactants

ABSTRACT

Dredged harbor sediment co-contaminated by heavy metals and polycyclic aromatic hydrocarbons (PAHs) was subjected to enhanced electrokinetic treatments, using a mixture of a chelating agent (citric acid CA) and a surfactant as additives in the processing fluids. We tested various operating conditions (at 1 V cm^{-1}): different CA concentrations, applying a periodic voltage gradient, pre-conditioning the sediment with the additives, and replacing the synthetic surfactant Tween 20 (TW20) by biosurfactants. Increasing the CA concentration was favorable for both metal and PAH removal. Applying a periodic voltage gradient associated to a low concentration of CA and TW20 provided the best results for Zn, Cd and Pb removal and also for removal of the 16 priority PAHs. Promising results were obtained with solutions containing rhamnolipids (0.028%) and a viscosin-like biosurfactant produced by *Pseudomonas fluorescens* PfA7B (0.025%), associated to a periodic voltage gradient. Although the rhamnolipid and the viscosin-like compounds involved a higher electrical current than TW20, metals were less removed from the sediment. The electroosmotic flow was lower when we used biosurfactants, hence a less effective effect on PAH removal.

© 2015 Elsevier Ltd. All rights reserved.

* Corresponding author. Tel./fax: +33 232 291 535.

E-mail addresses: mohamed-tahar.ammami@univ-lehavre.fr (M.T. Ammami), florence.koltalo@univ-rouen.fr (F. Portet-Koltalo), ahmed.benamar@univ-lehavre.fr (A. Benamar), cecile.poc@univ-rouen.fr (C. Duclairoir-Poc), huaqing.wang@univ-lehavre.fr (H. Wang), franck.lederf@univ-rouen.fr (F. Le Derf).

1. Introduction

Management of dredged sediment is of great concern for maintaining harbor activities (Benamar and Baraud, 2011). In France, chemical guidance values are provided to assess the chemical

hazard following the disposal of dredged sediment into environmental waters, as recommended by the OSPAR convention directives or French regulations such as GODE guidelines (14/06/2000). Thus the restricted disposal of dredged sediment into the marine environment has led managers to treat it ashore. However, storage on disposal sites is not a sustainable solution because of the risk of contaminants transferring to the environment. Reuse of dredged sediment in construction materials in civil engineering or habitat restoration can be proposed (Yozzo et al., 2004; Wang et al., 2012), but such sediment management requires treatments to reduce their contamination level.

In contaminated dredged sediment, inorganic metals (Peng et al., 2009) and persistent organic pollutants such as polycyclic aromatic hydrocarbons (PAHs) (Sprovieri et al., 2007) are of great concern regarding their toxicological hazard: they bioaccumulate in food chains, and induce higher mortality rates, growth reduction or disturbance of reproductive processes in marine organisms (Roberts, 2012). Powerful techniques must be developed in order to remove them from sediment, such as thermal desorption, sediment washing or flushing, solvent extraction, bioremediation (Jones et al., 2001; Libralato et al., 2008; Beolchini et al., 2009). However these technologies fail when low permeable soil or sediment is encountered.

Electrokinetic (EK) remediation is a technology that has received attention as a practical *in-situ* and *ex-situ* remediation technique for low permeable clay-rich soil or fine-grained sediment. Briefly, when a low voltage gradient is applied to the sediment *via* embedded electrodes, charged pollutants electromigrate towards the electrode of the opposite charge (Ryu et al., 2011). The electric field induces an electro-osmotic flow, and solubilized neutral pollutants can be also transported with the pore fluid (Cameselle and Reddy, 2012). Successful laboratory-scale EK tests have been reported for sediments or soils contaminated by metals or PAHs (Giannis et al., 2009; Pazos et al., 2010). Simultaneous EK removal of both metals and PAHs has been investigated lately (Maturi and Reddy, 2008; Colacicco et al., 2010; Ammami et al., 2013).

Enhanced EK technology is highly dependent on the type of processing solution used. The main reaction, inherent to the EK process, is water electrolysis. It generates H⁺ at the anode side and OH⁻ at the cathode side, and thus causes metals to precipitate near the cathode (Nogueira et al., 2007). Therefore acids are suitable candidates near the cathode as they enhance their solubilization and transport to the cathode. Adding complexing agents can also convert soil-bound metals into soluble complexes and enhance their removal (Gidarakos and Giannis, 2006). Concerning PAHs, enhancing agents that allow their better desorption from sediment particles and solubilization in the pore fluid can be used to achieve satisfactory results. Various surfactants, cyclodextrins or cosolvents have been tested (Park et al., 2007; Maturi et al., 2009; Hahladakis et al., 2013).

Mechanisms of EK PAH removal by synthetic surfactants have been investigated, but little research has been carried out using biosurfactants (Alcantara et al., 2009; Chang et al., 2009; Gonzini et al., 2010). Biosurfactants are biological surface active agents produced by certain yeasts or bacteria. They were used to clean soils polluted by organics, especially rhamnolipids produced by *Pseudomonas aeruginosa* (Bordas et al., 2005; Lai et al., 2009). Other classes of biosurfactants, such as lipopeptides or bioemulsans have also been tested for applications in soil or sediment remediation (Mulligan et al., 1999; Dahrazma and Mulligan, 2007; Juwarkar et al., 2007; Franzetti et al., 2009).

We conducted bench-scale electrokinetic tests to understand the effect of different operating parameters on the removal, in one stage, of mixed contaminants from dredged sediment, *i.e.* five metals (Cd, Cr, Cu, Pb, Zn) and the 16 priority PAHs defined by the

US-EPA. We tested the amount of chelating agent (citric acid), the nature of the surfactant (synthetic Tween 20 or biological surfactants: rhamnolipids and, for the first time, a cyclolipopeptide) and sediment pre-conditioning. Moreover, little is known about the benefits of the application of a periodic electric potential on the EK surfactant-enhanced removal of PAHs (Saichek and Reddy, 2005). So we also assessed the combination of enhancing agents, never tested together before, with the application of a periodic voltage gradient.

2. Materials and methods

2.1. Materials

2.1.1. Chemicals

Acetonitrile, methylene chloride, toluene and acetone were provided by VWR (Fontenay sous Bois, France). Nitric acid (65%), hydrochloric acid (37%), citric acid (CA) and Tween 20 (TW20) were obtained from Fisher Scientific (Illkirch, France). A standard mixture of 16 priority PAHs, perdeuterated phenanthrene, cadmium nitrate, chromium nitrate, copper sulfate, zinc nitrate and lead nitrate were provided by Sigma-Aldrich (St Quentin-Fallavier, France).

2.1.2. Sediment sampling

The dredged sediment was collected from the disposal site of a French harbor in Normandy, localized near important urban centers and industrialized areas. Its properties are presented in Table 1. pH was measured according to the NF ISO 10390 standard, electrical conductivity according to the NF ISO 11265 standard and moisture content was obtained in accordance with the French NF P 94-050 standard. Organic matter content was measured in accordance with the NF EN 12879 standard. Particle size distribution was determined using a laser particle-sizing device (Malvern Instruments, Malvern, UK).

2.1.3. Biosurfactants

The rhamnolipid biosurfactant (90% purity) was obtained from AGAE Technologies (Corvallis, USA). The other biosurfactant was our own production: *Pseudomonas fluorescens* PfA7B strain was grown on culture plates and its biosurfactant production was recovered after 14 d of incubation, as described in a previous paper (Groboillot et al., 2011). The biosurfactant, a mixture of two viscosin-like cyclolipopeptides (viscosin and masetolide E), was purified and characterized, as already described (Portet-Koltalo et al., 2013). The critical micellar concentrations (CMCs) of the biosurfactants were determined by surface tension measurements using the pendant drop method (Tensiometer DSA30, Krüss, Germany).

2.2. Electrokinetic tests

The experimental EK setup is described in a previous paper (Ammami et al., 2013). Briefly, the natural sediment was packed into a Teflon PTFE chamber. Graphite electrode plates were placed in each electrode compartment, separated from the sediment by porous glass papers. Two pumps filled the electrode reservoirs with the aqueous processing fluids (10 mL h⁻¹). A voltage gradient (1 V cm⁻¹) was applied continuously or periodically (5-d-on/2-d-off cycles) and the electrical current was periodically measured. At the end of each treatment, the sediment was extracted and cut into four slices for analysis.

Experiments 1 to 3 consisted in increasing CA concentrations while keeping the TW20 concentration constant (Table 2). Experiments 4 and 5 consisted in the same operating conditions as experiment 1, but experiment 4 was conducted under a periodic electric potential and experiment 5 with pre-conditioned sediment. In this latter case, the sediment was previously air-dried for a week and

Table 1

Properties of the dredged sediment and its metal and PAHs contaminants, compared to N1, N2 levels of GODE guidelines.

Sediment properties	Contaminants						
	Heavy metals ^{a,b} (mg kg ⁻¹)		PAHs ^{a,c} (mg kg ⁻¹)				
Particle size distribution and diameters	Clay Silt Sand	6.3% 86.2% 7.5%	$d_p < 2 \mu\text{m}$ $d_p = 2\text{--}63 \mu\text{m}$ $d_p = 63\text{--}2000 \mu\text{m}$	Cd Cr Cu Pb Zn	4.98 ± 0.12 > 2.4 (N2) 94.71 ± 3.65 > 90 (N1) 56.29 ± 1.72 > 45 (N1) 64.67 ± 1.86 < 100 (N1) 405.99 ± 12.69 > 276 (N1)	Naph Acy Ace Fluo Phen Ant Flt Pyr B(a)ant Chry B(b)flt B(k)flt B(a)pyr I(123cd)pyr Db(ah)ant B(ghi)per	0.109 ± 0.011 < 0.160 (N1) 0.055 ± 0.003 > 0.040 (N1) 0.056 ± 0.004 > 0.015 (N1) 0.062 ± 0.009 > 0.020 (N1) 0.236 ± 0.021 ~ 0.240 (N1) 0.241 ± 0.013 > 0.085 (N1) 0.470 ± 0.020 < 0.600 (N1) 0.443 ± 0.012 < 0.500 (N1) 0.296 ± 0.017 > 0.260 (N1) 0.376 ± 0.020 ~ 0.380 (N1) 0.390 ± 0.025 ~ 0.400 (N1) 0.252 ± 0.033 < 0.200 (N1) 0.313 ± 0.021 > 0.430 (N1) 0.337 ± 0.030 < 1.700 (N1) 0.065 ± 0.006 > 0.060 (N1) 0.343 ± 0.029 < 1.700 (N1)
Organic matter content	2.6%						
pH	8.4 ± 0.1						
Electrical conductivity	1.82 ± 0.2 mS cm ⁻¹						
Moisture content	93%						

^a mg kg⁻¹ dry mass, mean values obtained from 5 replicates.^b French official journal order of 6 August 2006.^c French official journal order of 8 February 2013.**Table 2**

Conditions for EK remediation experiments, mean anodic and cathodic electroosmotic flows and final energy consumption (great changes in conditions appear in bold).

Exp.	Anolytes and catholytes	Duration (d)	Voltage gradient/mode	Energy consumption (W h)	Mean anodic/cathodic EO flows (mL h ⁻¹) ^b
1	TW20 (4.94 g L ⁻¹) + CA (0.1 M)	21	1 V cm ⁻¹ /DC	18.7	-0.097/-0.075
2	TW20 (4.94 g L ⁻¹) + CA (0.5 M)	22	1 V cm ⁻¹ /DC	95.1	+0.152/+0.560
3	TW20 (4.94 g L ⁻¹) + CA (1 M)	22	1 V cm ⁻¹ /DC	109	+0.183/+1.192
4	TW20 (4.94 g L ⁻¹) + CA (0.1 M)	24	1 V cm ⁻¹ / periodic	51.1	-0.120/+0.179
5 ^a	TW20 (4.94 g L ⁻¹) + CA (0.1 M)	50	1 V cm ⁻¹ /DC	97.7	-0.296/+0.561
6	Rhamnolipid (0.275 g L ⁻¹) + CA (0.1 M)	24	1 V cm ⁻¹ / periodic	89.5	-0.004/+0.088
7	Vicosin-like (0.250 g L ⁻¹) + CA (0.1 M)	24	1 V cm ⁻¹ / periodic	108.4	-0.152/+0.267

^a Initial water content was 45% for experiment 5, unlike all the other EK tests for which water content was 93%.^b EOF is by convention positive from anode to cathode.

sieved to 2 mm, as suggested by Reddy et al. (2002). It was rehydrated with 45% moisture, using an aqueous solution containing TW20 (4×10^{-3} M) and CA (0.1 M) and the mixture was equilibrated for 24 h before starting the EK treatment. Experiments 6 and 7 were performed using CA and biosurfactants as enhancing agents, respectively rhamnolipids and a cyclolipopeptidic mixture.

Energy consumption was obtained by multiplying the mean electric current intensity (when steady state was reached), the applied voltage and the processing time (Table 2).

2.3. Analytical methods

2.3.1. Metal extraction and analysis

Three aliquots of treated sediment were collected from each sliced section and dried 48 h at 35 °C, ground, and each 0.5-g sub-sample was digested in PTFE tubes using 10 mL of nitric acid:hydrochloric acid 3:1 (v:v). The tubes were subjected to microwave irradiation at 170 °C (1200 W output) for 10 min (MarsX, CEM Corporation, Matthews, USA). The mineralized solutes were completed to 100 mL with water and filtered through PTFE filters (0.2 μm). Metal concentrations (Cd, Cr, Cu, Pb, Zn) were analyzed in triplicate using an ICP-AES (ICAP 6300, ThermoFisher Scientific, Waltham, USA). Metals in the aqueous effluents were also analyzed by ICP-AES after filtration. The linearity of the detector response was between 0.01–10 mg L⁻¹. Detection and quantification thresholds, calculated respectively as 3 and 10 times the standard deviation of the blank sample noise, were respectively 0.001/0.005 mg L⁻¹ for Cd, 0.005/0.020 mg L⁻¹ for Pb, 0.018/0.060 mg L⁻¹ for Zn, 0.003/0.010 mg L⁻¹ for Cr and 0.002/

0.080 mg L⁻¹ for Cu. Metal quantification was obtained with relative standard deviations in the 2.4–3.9% range.

2.3.2. PAH extraction and analysis

Three aliquots of sediment were taken from each sliced section and were dried one night at 35 °C, crushed, and each 5-g sub-sample was extracted by microwave-assisted extraction (MarsX) with 40 mL of toluene:acetone 1:1 (v:v) at 140 °C for 30 min (1200 W output). The extracts were filtered through PTFE filters (0.2 μm) and evaporated under vacuum to 1.5 mL. An internal standard (per-deuterated phenanthrene) was added, and then 1 μL was injected (splitless mode, 285 °C) into a gas chromatograph (6850 series, Agilent, Santa Clara, USA), equipped with a mass spectrometer detector (5975C series). Separation was performed using a 50 m × 0.25 mm i.d. DB5-MS capillary column (0.25 μm film thickness) from J&W Scientific (Folsom, CA, USA), with helium as a carrier gas (1.4 mL min⁻¹). The oven temperature was programmed at 55 °C for 1.2 min, increased to 180 °C (40 °C min⁻¹) and then to 300 °C (4.5 °C min⁻¹). The detector operated at 70 eV. Quantification was based on selected ion monitoring for better sensitivity. The linearity of the detector response was between 0.05–5 mg L⁻¹. Detection and quantification thresholds were respectively in the range 1.5–5 μg L⁻¹ and 5–16.5 μg L⁻¹. PAH quantification was obtained from relative standard deviations in the 2.7–14.1% range.

3. Results and discussion

Previous studies demonstrated that using an acidic chelatant (CA) and a nonionic surfactant (TW20) as flushing reagents was

efficient to obtain significant removal of metals (Zn, Cd, Cu, Pb) and of five PAHs from a spiked sediment mimicking the properties of our harbor sediment (Ammami et al., 2013). Consequently, we tested the CA/TW20 mixture on the natural sediment. CA and surfactants were simultaneously tested, such as in the work of Alcantara et al. (2012), and not sequentially, such as in the work of Reddy et al. (2009) or Hahladakis et al. (2014). Considering that electroosmotic flow could be reversed in some cases (Genc et al., 2009), we chose to introduce the flushing reagents at the two electrode cells.

Table 1 shows that the harbor sediment was contaminated by metals and PAHs. GEODE guidelines recommend that sediment should not be disposed of in the marine environment if contaminant concentrations exceed the N2 level: in that case the sediment is considered to have a strong impact on the environment. If contaminant concentrations are below the N1 level, dumping at sea is authorized without a toxicology impact study. If the concentration is between the N1 and N2 thresholds, the sediment is considered contaminated and its eco-toxicity impact has to be analyzed. **Table 1** shows that a major part of the pollutants was between the N1 and N2 levels and that Cd was above the N2 level: for these pollutants, assessing EK remediation conditions that could lower the contamination levels down to below the N1 level was the main objective.

As one of our upcoming objectives is to apply the EK process *in situ*, it seemed essential to use enhancing agents with low impact on the environment. Such is the case for CA; moreover, CA is selective comparatively to other chelatants (Gidarakos and Giannis,

2006). We also tested environment-friendly biosurfactants to replace TW20: commercial rhamnolipids, that have been already tested for EK remediation (Gonzini et al., 2010), and a cyclolipopeptide that has never been tested, but previous studies demonstrated that it could favor desorption of low molecular weight PAHs from sediment (Portet-Koltalo et al., 2013).

Cationic surfactants are not chosen as enhancing agents because they highly sorb onto negative sediment particles (Kaya and Yukselen, 2005). Nonionic surfactants are less sorbed and they have a low CMC; to ensure that micelles of the nonionic TW20 could form in the pore fluid, we tested it at 50 times its CMC (0.5%), which is not high compared to other studies (Colacicco et al., 2010; Alcantara et al., 2012). Concerning anionic surfactants, their strong point is that they poorly sorb onto sediment particles. So we added the anionic biosurfactants at only 5 times their CMC, evaluated at 50 mg L⁻¹ for the viscosin-like and rhamnolipid biosurfactants (**Table 2**).

3.1. Variation of the electric current and sediment parameters

Fig. 1 shows the electric current (EC) variation for the seven tests. **Fig. 1a** shows that EC initially increases to a maximum value within the first hours of treatment, and then it drops and stabilizes (Colacicco et al., 2010). The initial high values are due to the solubilization of salt precipitates which increases the EC (Mitchell, 1993). But over time, ions are depleted as they electromigrate and current intensity decreases to stabilized current values (Maturi and Reddy, 2006).

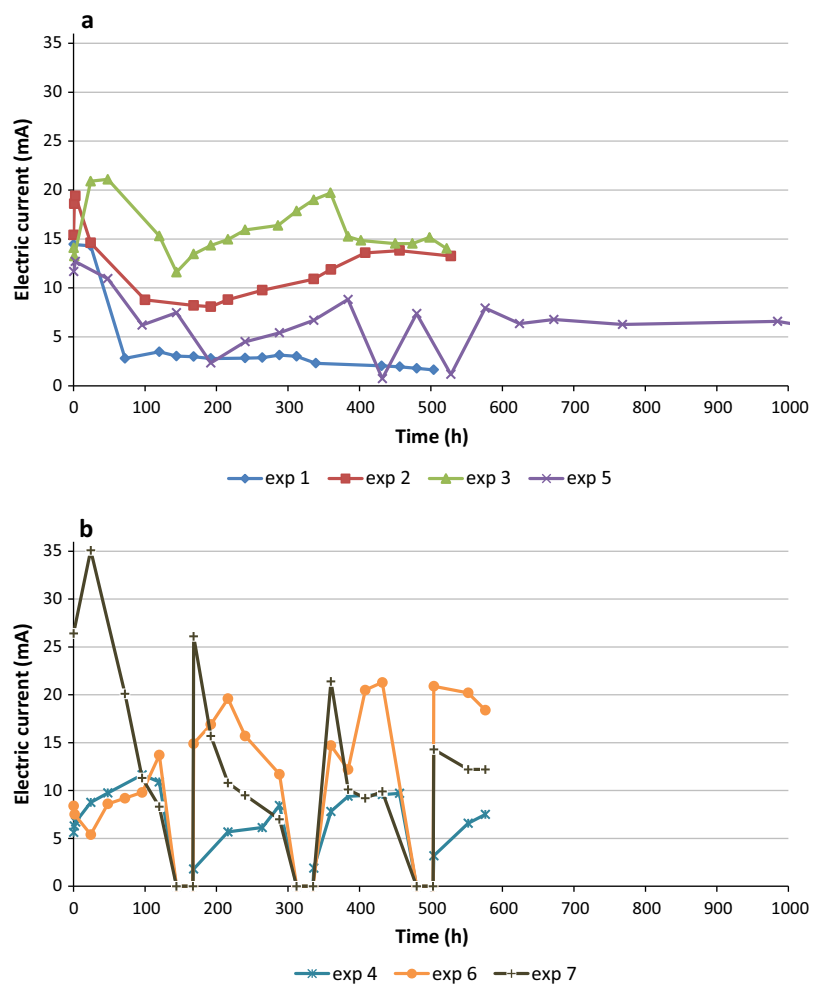


Fig. 1. Evolution of electric current with elapsed time (a) EK remediation tests 1, 2, 3 and 5 and (b) EK remediation tests 4, 6 and 7.

A higher CA concentration increased the EC because (among other things) more solubilized charged metal complexes were formed. In experiment 5, moisture content was only 45%, versus 93% for the other experiments. In the first hours of EK treatment, lowering the moisture content led to a lower EC than in experiment 1, as there were fewer available H⁺ ions from water electrolysis. It was also probably less easy for the ionic species to migrate through the less dispersed pore network (Reddy et al., 2002), which can explain the more gradual decrease of current in experiment 5 and a longer stabilization time. However, EC remained higher in experiment 5 compared to experiment 1. This behavior may be attributed to the amount of available ionic species (other than H⁺), which were better mobilized in pore fluid during the pre-conditioning step of the sediment.

Fig. 1b shows that current intensity was more fluctuating when a periodic voltage was applied. This periodicity generated an EC that followed an up-and-down pattern. When the voltage was not applied, it allowed time for the mass transfer of charged solutes from the soil to the aqueous medium, causing a higher current when the voltage was applied again (Maturi et al., 2009). Replacing TW20 by rhamnolipid or viscosin-like biosurfactants revealed that mean EC values were significantly higher (5.5 mA, 13.1 mA and 16.2 mA, respectively). The higher current obtained when we added biosurfactants may be due to their higher dielectric constant: TW20 is an uncharged surfactant, whereas rhamnolipids are in their anionic form at pH values above their pKa (4.3–5.5), and the mixture composed of masetolide E/viscosin contains glutamic acids that are in their anionic form when pH values are above their pKa (4.1).

As regards the sediment pH at the end of each test (**Fig. 2**), it underwent an overall but low acidification process compared to the initial pH value. The carbonates in the natural sediment increased its buffering capacity and impeded the progress of the acidic front from the anode towards the cathode (Ouhadi et al., 2010). **Fig. 2** shows that sediment acidification obviously increased when the CA concentration was increased. Additionally, pre-conditioning the sediment with CA and applying a longer EK treatment duration allowed for a better acidification. Lastly, applying a periodic voltage gradient seemed to hamper the acidic front migration.

We also calculated mean anodic and cathodic electroosmotic flows (EOFs), which are summarized in **Table 2** (Supplementary Fig. SM-1 shows the evolution of EOF at the cathode and the anode sides during some EK treatments). An EOF is produced when excess ions in the diffuse double-layer migrate towards the opposite

charged electrode and transfer the momentum to the surrounding pore water and to the dissolved ions or neutral species. This flow depends on the zeta-potential of the sediment particles, which is negative when the pH is above the zero point of charge of the particles: then, the positively charged diffuse double-layer migrates to the cathode (Kaya and Yukselen, 2005). At the end of our tests, the pH of the sediment did not become too acidic, even near the anode (**Fig. 2**), so overall EOFs occurred preferentially towards the cathode. Mean overall EOFs were calculated by difference between the cathodic and the anodic EOFs, which were positive by convention towards the cathode and that ranked as follows: experiment n°1 (0.023 mL h⁻¹) < n°6 (0.092 mL h⁻¹) < n°4 (0.299 mL h⁻¹) < n°2 (0.409 mL h⁻¹) < n°7 (0.419 mL h⁻¹) < n°5 (0.857 mL h⁻¹) < n°3 (1.010 mL h⁻¹).

Increasing the CA concentration in the purging fluid induced a higher overall EOF. This is a known effect of CA (Nogueira et al., 2007). So acidification of the sediment with a high CA content was favorable for sustaining a high EOF. Moreover, the use of a periodic voltage gradient (experiment 4) generated a significantly higher overall EOF compared to experiment 1; a higher EOF was also sustained in experiment 5 compared to experiment 1, although a lower moisture content is in principle detrimental to the EOF (Reddy et al., 2002). A longer contact time between sediment particles and CA (when voltage was not applied or during the preconditioning step) favors its sorption onto particles, which modifies the zeta-potential, leading to a more negative charged surface and so to a better EOF (Cameselle and Reddy, 2012).

Introducing rhamnolipid in the purging fluid was not really beneficial for the overall EOF compared to TW20, unlike viscosin-like biosurfactant. The velocity of EOF is proportional to the dielectric constant of the fluid and to the zeta potential, but inversely proportional to the viscosity of the purging solution. The higher dielectric constant of the fluid obtained when using rhamnolipids was probably counteracted by a higher viscosity.

Regarding energy consumption (**Table 2**), experiment 1 was the less expensive EK test. But experiment 4, which consisted in applying a periodic voltage gradient, should also be singled out for its low energy consumption.

3.2. Metal removal

Table 3 indicates the metal percentages removed in the seven tests. Compared to the previous results obtained on model sediment, all the metals were harder to remove from the dredged

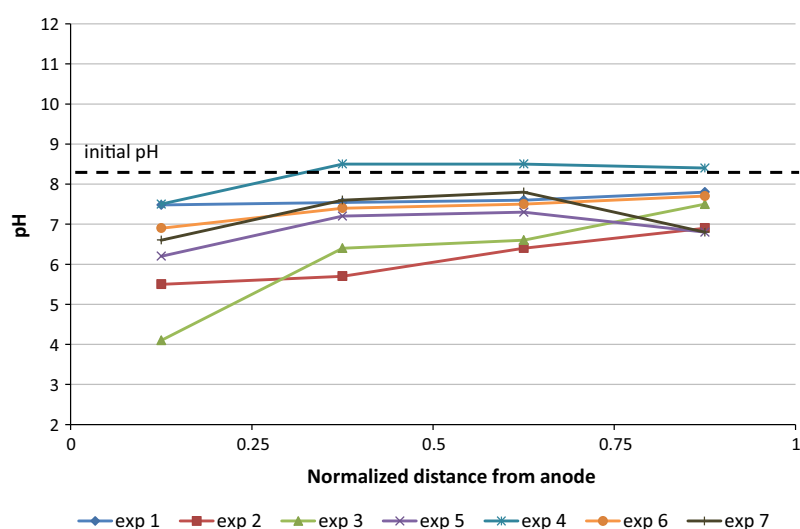


Fig. 2. Distribution of pH within sediment after EK treatments 1–7.

Table 3

Metal and PAH removals (%) after each EK treatment.

	Exp. 1	Exp. 2	Exp. 3	Exp. 4	Exp. 5	Exp. 6	Exp. 7
<i>Metals</i>							
Cd	12.8	35.6	38.6	34.9	7.4	33.5	33.0
Cr	1.3	6.1	8.5	8.5	1.6	0.1	0.1
Cu	1.6	2.8	8.7	5.6	5.0	2.0	9.2
Pb	12.9	25.5	33.4	28.8	2.2	10.6	13.1
Zn	43.0	49.4	51.6	50.2	53.0	20.2	17.2
<i>PAHs</i>							
Naph	38.4	39.0	53.3	44.5	47.2	25.6	34.8
Ace	30.4	27.9	47.8	42.2	25.3	0.0	7.7
Acy	67.5	67.3	74.3	73.1	76.0	60.5	63.9
Fluo	35.7	34.2	48.3	32.9	49.9	25.7	38.7
Phen	20.4	24.2	41.5	32.9	40.8	11.8	13.2
Ant	31.9	31.8	53.4	40.8	46.1	2.1	11.2
Flt	32.5	37.3	51.3	45.8	51.4	21.4	33.7
Pyr	30.8	35.7	50.3	44.6	52.0	19.2	29.2
B[a]ant	31.7	40.8	54.4	48.5	56.5	25.5	31.3
Chry	54.6	58.0	67.8	63.0	63.4	51.5	53.7
B[b]flt	9.1	15.5	32.9	24.3	37.7	0.0	0.6
B[k]flt	48.0	58.1	66.2	62.8	71.0	41.0	50.0
B[a]pyr	22.6	39.8	50.2	44.0	56.0	14.5	18.9
I[1.2.3-cd]pyr	43.0	59.0	61.1	57.4	71.6	34.6	41.4
D[b]ah]ant	26.0	50.5	51.9	50.1	61.3	15.8	32.3
B[ghi]per	42.8	70.9	65.0	63.3	72.2	45.7	50.1
Total PAH removal	35.3	43.1	54.4	48.1	54.9	24.7	31.9

sediment in the same operating conditions (Ammami et al., 2013). As mentioned, the buffering capacity of the natural sediment counteracts the acidification of the sediment and prevents metal solubilization and electromigration.

In most cases, at the end of the experiments, Zn and Cd were found preferentially in the cathode compartment whereas Cr, Cu and Pb were found preferentially in the anode compartment. Zn was generally the easiest to remove whereas Cr and Cu were the hardest to remove. Zn tends to precipitate as a hydroxide only at pH > 7 whereas Cr, Cu and Pb precipitate at pH values above 4–5. So Zn was easier to remove from the sediment in its cationic form at pH > 6. At this pH, Cr and Cu remained immobilized in the sediment and apparently did not form high amounts of soluble complexes with CA. Concerning Pb, which precipitates at the pH conditions of our sediment, its removal can be attributed to the formation of chelates with CA that preferentially migrate to the anode compartment. Regarding Cd, it only forms hydroxides at pH > 8. But its migration as a free cation was very low. Moreover, the stability of Cd complexes with citrate is low, so its migration to the anode was low too (Gidarakos and Giannis, 2006). In fact, Cd is most likely bound to organic matter (OM) than the other metals and is difficult to mobilize. However, increasing CA concentrations tended to enhance Cd removal, as CA contributes to dissolving large amounts of humic substances at pH > 6 and can thus favor Cd desorption (Yang et al., 2001). So increasing CA concentrations was beneficial for all metals, but the least impacted was Zn, which preferentially migrates as a free cation.

Even though metals were found preferentially in the anode or cathode compartments, the final distributions inside the sediment did not differ markedly between metals for a given test (see Supplementary Fig. SM-2). In experiments 1, 4, 5 and 6, all metal amounts tended to decrease slightly from the anode to the cathode. In experiments 2 and 3, metals tended to concentrate in the second quarter of the sediment from the anode and to be better removed near the electrodes, more particularly near the anode. Regarding experiment 7, metal amounts tended to decrease from the cathode to the anode.

In general, increasing CA concentrations helped to better remove all the metals, and the effect was improved nearby the anode. Applying a periodic voltage gradient enhanced the

decontamination of the overall sediment column: the highest pulsed current intensity was really favorable for metal removal. Reducing the moisture content and pre-conditioning the sediment was not favorable for metal removal (except for the more mobile Zn), although current intensity was higher.

Finally, swapping TW20 for biosurfactants was not beneficial for metal removal, although mean current intensity was higher. In the pH conditions of the sediment, the two biosurfactants are in their anionic form and they can theoretically help transport metals as counter-ions (Mulligan, 2009). But they electromigrate preferentially towards the anode, which counteracts EOF. Juwarkar et al. (2007) demonstrated that Cd was easy to remove by using processing solutions containing rhamnolipids, but their good removal rates were obtained with solutions containing 0.1% biosurfactant; this is much higher than the concentrations we used (0.025% and 0.028% for the viscosin-like and rhamnolipid compounds, respectively). In another case, it was necessary to use a 0.25% solution of a cyclolipopeptidic surfactant to flush Zn and Cu (Mulligan et al., 1999). So the limited effect of biosurfactants on metal removal in our tests was also probably due to their affinity for the sediment particles and to their too low concentration in the pore fluid (Ochoa-Loza et al., 2007).

3.3. PAH removal

Supplementary Fig. SM-3 shows a general decrease of all the PAHs in the sediment after EK treatments, even for the high molecular weight (HMW) PAHs, which are the most strongly sorbed to the OM and clayey fractions of the sediment (Portet-Koltalo et al., 2013). PAHs desorption and solubilization were possible owing to the presence of the surfactants in the purging solution, which can form micellar aggregates at concentrations higher than their CMC and solubilize PAHs in their hydrophobic core. But citrate ions can also play a role by increasing PAH desorption through a considerable release of OM into the solution (Yang et al., 2001).

The EOF is a major factor to consider for the transport of neutral compounds such as PAHs, alone or incorporated into nonionic surfactants. The overall EOF towards the cathode increased when TW20 was mixed with increasing concentrations of CA. Table 3 shows that total PAH removal also increased from 35.3% to

54.4%. In the same way, applying a periodic voltage gradient or equilibrating the sediment with the additives prior to EK treatment led to a better EOF, and better PAH removal along with it (Table 3). PAH desorption and solubilization are rate-limited processes; during the “down” voltage interval, re-equilibration at the solid–liquid interface occurs and more PAHs can be solubilized into micellar aggregates. For the same reasons, the equilibration time before EK experiment 5 started was beneficial for PAH removal. In this case, the benefit was more substantial for HMW PAHs (Table 3), which are more strongly bound to OM and certainly need an additional reaction time to desorb and solubilize into micelles.

PAH removal was correlated with the increase of the overall EOF towards the cathode, with a linear regression coefficient $R^2 = 0.844$ (for CA/TW20 mixtures). Supplementary Fig. SM-4a shows actually the tendency of PAHs to be depleted near the cathodic section. But when CA concentration is increased in the purging fluid, depletion in the second quarter section near the anode becomes pronounced: part of the PAHs incorporated into micelles may therefore have moved through the EOF towards the cathode, but a non-negligible part of the PAHs also electro-migrated toward the anode through their incorporation into humic substances chelated to CA (Yang et al., 2001).

Using biosurfactants instead of TW20 yielded poorer PAH removal results (Table 3). The cyclolipopeptide was mostly in its anionic form, so the migration of micelles via the EOF was probably non-significant. PAH removal near the anode compartment via electromigration of anionic micelles or via incorporation into chelated dissolved humic substances was quite efficient, but as nothing happened near the cathode, results were poorer compared to experiment 4 (Table 3).

The case of experiment 6 is different: PAHs were concentrated in the section near the anode (Supplementary Fig. SM-4b). Unlike the cyclolipopeptide, rhamnolipids allowed for PAH decontamination in the section near the cathode, but not at all near the anode. Compared to experiment 4, total removals were consequently poorer. By contrast, Chang et al. (2009) showed that EOF and phenanthrene removal were better when a nonionic surfactant was replaced by a rhamnolipid introduced at ten times its CMC. We can suppose that the more acidic pH of their treated sediment ($\text{pH} \sim 4$) was favorable to the formation of the protonated neutral form of the rhamnolipid. In that case, the rhamnolipid may be more prone to transport PAHs in the same direction as the EOF, leading to a better removal.

Table 3 shows that many structurally close PAHs with similar chemical properties have very different elimination levels. For example, acenaphthylene was consistently far less removed than acenaphthene, or benzo[k]fluoranthene was consistently much more removed than benzo[b]fluoranthene. PAHs can be more or less easily degraded by oxidation in electrochemical treatments. Moreover, the anodic oxidation of PAH mixtures occurs heterogeneously on each PAH (Alcantara et al., 2009). So part of PAH removal can be attributed not only to migration processes but also to their oxidative degradation, which is more or less effective.

4. Conclusions

The experiments involving the highest amount of CA, or performed with a lower amount of CA but applying a periodic voltage gradient, were the most powerful to remove metals, particularly Zn, Cd and Pb. Energy and additive consumption were lower with the periodic voltage gradient, and Zn, Pb and Cr were removed to levels below N1. However, Cd remained at a level above N2 and Cu at a level above N1. Our natural sediment contained high amounts of carbonates, with a high buffering capacity; therefore

in the case of Cd and Cu, associating higher amounts of CA, a periodic voltage gradient and a longer treatment seems necessary.

As regards PAHs, adding a nonionic surfactant but also CA had a positive effect on their removal, as well as applying a periodic voltage gradient. Once again, considering energy and additive consumption, experiment 4 was the most favorable. All PAH levels decreased in the sediment, and only fluorene and anthracene remained at levels above N1. Introducing TW20 at a higher concentration and extending the treatment duration can be a solution to obtain better results. For *in-situ* treatments, pre-conditioning large amounts of sediment with additives, though favorable for PAH removal, seems too expensive.

To go further, non-invasive treatments that preserve the biological characteristics of the sediment (Gonzini et al., 2010) and make it possible to reuse it after remediation can be achieved by using biosurfactants. Promising results could be obtained using not only rhamnolipids but also a cyclolipopeptidic biosurfactant, associated to the application of a periodic voltage gradient. But these biosurfactants should be tested at higher concentrations to favor the formation of micelles in the pore fluid over their sorption onto sediment particles.

Acknowledgements

This work was financially supported by the Haute-Normandie Region (France) through the research network SCALE, within the project RESSOLV.

Appendix A. Supplementary material

Supplementary data associated with this article can be found, in the online version, at <http://dx.doi.org/10.1016/j.chemosphere.2014.12.087>.

References

- Alcantara, M.T., Gomez, J., Pazos, M., Sanroman, M.A., 2009. PAHs soil decontamination in two steps: desorption and electrochemical treatment. *J. Hazard. Mater.* 166, 462–468.
- Alcantara, M., Gomez, J., Pazos, M., Sanroman, M., 2012. Electrokinetic remediation of lead and phenanthrene polluted soils. *Geoderma* 173–174, 128–133.
- Ammami, M., Benamar, A., Wang, H., Bailleul, C., Legras, M., Derf, F., Portet-Koltalo, F., 2013. Simultaneous electrokinetic removal of polycyclic aromatic hydrocarbons and metals from a sediment using mixed enhancing agents. *Int. J. Environ. Sci. Technol.* <http://dx.doi.org/10.1007/s13762-013-0395-9>.
- Benamar, A., Baraud, F., 2011. Electrokinetic remediation of dredged sediments from Le Havre harbour. *Eur. J. Environ. Civ. Eng.* 15, 215–228.
- Belochni, F., Dell'Anno, A., De Propis, L., Ubaldini, S., Cerrone, F., Danovaro, R., 2009. Auto- and heterotrophic acidophilic bacteria enhance the bioremediation efficiency of sediments contaminated by heavy metals. *Chemosphere* 74, 1321–1326.
- Bordas, F., Lafrance, P., Villemur, R., 2005. Conditions for effective removal of pyrene from an artificially contaminated soil using *Pseudomonas aeruginosa* 57S rhamnolipids. *Environ. Pollut.* 138, 69–76.
- Cameselle, C., Reddy, K.R., 2012. Development and enhancement of electro-osmotic flow for the removal of contaminants from soils. *Electrochim. Acta* 86, 10–22.
- Chang, J.H., Qiang, Z., Huang, C.P., Ellis, A.V., 2009. Phenanthrene removal in unsaturated soils treated by electrokinetics with different surfactants-Triton X-100 and rhamnolipid. *Colloids Surf. A* 348, 157–163.
- Colacicco, A., De Gioannis, G., Muntoni, A., Pettinai, E., Polettini, A., Pomi, R., 2010. Enhanced electrokinetic treatment of marine sediments contaminated by heavy metals and PAHs. *Chemosphere* 81, 46–56.
- Dahrazma, B., Mulligan, C.N., 2007. Investigation of the removal of heavy metals from sediments using rhamnolipid in a continuous flow configuration. *Chemosphere* 69, 705–711.
- Franzetti, A., Caredda, P., Ruggeri, C., Colla, P.L., Tamburini, E., Papacchini, M., Bestetti, G., 2009. Potential applications of surface active compounds by *Gordonia* sp. strain BS29 in soil remediation technologies. *Chemosphere* 75, 801–807.
- Genc, A., Chase, G., Foos, A., 2009. Electrokinetic removal of manganese from river sediment. *Water Air Soil Pollut.* 197, 131–141.
- Giannis, A., Nikolaou, A., Pentari, D., Gidarakos, E., 2009. Chelating agent-assisted electrokinetic removal of cadmium, lead and copper from contaminated soils. *Environ. Pollut.* 157, 3379–3386.

- Gidarakos, E., Giannis, A., 2006. Chelate agents enhanced electrokinetic remediation for removal cadmium and zinc by conditioning catholyte pH. *Water Air Soil Pollut.* 172, 295–312.
- Gonzini, O., Plaza, A., Di Palma, L., Lobo, M., 2010. Electrokinetic remediation of gasoil contaminated soil enhanced by rhamnolipid. *J. Appl. Electrochem.* 40, 1239–1248.
- Grobioillot, A., Portet-Koltalo, F., Le Derf, F., Feuilloley, M.G.J., Orange, N., Duclairoir Poc, C., 2011. Novel application of cyclolipopptide amphisin: feasibility study as additive to remediate polycyclic aromatic hydrocarbon (PAH) contaminated sediments. *Int. J. Mol. Sci.* 12, 1787–1806.
- Hahladakis, J.N., Calmano, W., Gidarakos, E., 2013. Use and comparison of the non-ionic surfactants Poloxamer 407 and Nonidet P40 with HP- β -CD cyclodextrin, for the enhanced electroremediation of real contaminated sediments from PAHs. *Sep. Purif. Technol.* 113, 104–113.
- Hahladakis, J.N., Lekkas, N., Smponias, A., Gidarakos, E., 2014. Sequential application of chelating agents and innovative surfactants for the enhanced electroremediation of real sediments from toxic metals and PAHs. *Chemosphere* 105, 44–52.
- Jones, K.W., Feng, H., Stern, E.A., Lodge, J., Clesceri, N.L., 2001. Dredged material decontamination demonstration for the port of New York/New Jersey. *J. Hazard. Mater.* 85, 127–143.
- Juwarkar, A.A., Nair, A., Dube, K.V., Singh, S., Devotta, S., 2007. Biosurfactant technology for remediation of cadmium and lead contaminated soils. *Chemosphere* 68, 1996–2002.
- Kaya, A., Yukselen, Y., 2005. Zeta potential of soils with surfactants and its relevance to electrokinetic remediation. *J. Hazard. Mater.* 120, 119–126.
- Lai, C.C., Huang, Y.C., Wei, Y.H., Chang, J.S., 2009. Biosurfactant-enhanced removal of total petroleum hydrocarbons from contaminated soil. *J. Hazard. Mater.* 167, 609–614.
- Libralato, G., Losso, C., Arizzi Novelli, A., Citron, M., Della Sala, S., Zanotto, E., Cepak, F., Volpi Ghirardini, A., 2008. Ecotoxicological evaluation of industrial port of Venice (Italy) sediment samples after a decontamination treatment. *Environ. Pollut.* 156, 644–650.
- Maturi, K., Reddy, K.R., 2006. Simultaneous removal of organic compounds and heavy metals from soils by electrokinetic remediation with a modified cyclodextrin. *Chemosphere* 63, 1022–1031.
- Maturi, K., Reddy, K., 2008. Cosolvent-enhanced desorption and transport of heavy metals and organic contaminants in soils during electrokinetic remediation. *Water Air Soil Pollut.* 189, 199–211.
- Maturi, K., Reddy, K., Cameselle, C., 2009. Surfactant-enhanced electrokinetic remediation of mixed contamination in low permeability soil. *Sep. Sci. Technol.* 44, 2385–2409.
- Mitchell, J.K., 1993. Fundamentals of Soil Behavior, third ed. Wiley, New York.
- Mulligan, C.N., 2009. Recent advances in the environmental applications of biosurfactants. *Curr. Opin. Colloid Interface Sci.* 14, 372–378.
- Mulligan, C.N., Yong, R.N., Gibbs, B.F., James, S., Bennett, H.P.J., 1999. Metal removal from contaminated soil and sediments by the biosurfactant surfactin. *Environ. Sci. Technol.* 33, 3812–3820.
- NF EN 12879 Standard, November 2000. Characterization of residual sludge – determination of organic matter content by loss of ignition of dry matter.
- NF ISO 10390 Standard, May 2005. Soil quality – determination of pH.
- NF ISO 11265 Standard, January 1995. Soil quality – determination of specific electrical conductivity.
- NF P 94-050 Standard, September 1995. Soils: investigation and testing – determination of moisture content by weight – oven drying method.
- Nogueira, M.G., Pazos, M., Sanroman, M., Cameselle, C., 2007. Improving on electrokinetic remediation in spiked Mn kaolinite by addition of complexing agents. *Electrochim. Acta* 52, 3349–3354.
- Ochoa-Loza, F.J., Noordman, W.H., Janssen, D.B., Brusseau, M.L., Maier, R.M., 2007. Effect of clays, metal oxides, and organic matter on rhamnolipid biosurfactant sorption by soil. *Chemosphere* 66, 1634–1642.
- Ouhadi, V., Yong, R., Shariatiadari, N., Saeidijam, S., Goodarzi, A., Safari-Zanjani, M., 2010. Impact of carbonate on the efficiency of heavy metal removal from kaolinite soil by the electrokinetic soil remediation method. *J. Hazard. Mater.* 173, 87–94.
- Park, J.Y., Lee, H.H., Kim, S.J., Lee, Y.J., Yang, J.W., 2007. Surfactant-enhanced electrokinetic removal of phenanthrene from kaolinite. *J. Hazard. Mater.* 140, 230–236.
- Pazos, M., Rosales, E., Alcantara, T., Gomez, J., Sanroman, M., 2010. Decontamination of soils containing PAHs by electroremediation: a review. *J. Hazard. Mater.* 177, 1–11.
- Peng, J.F., Song, Y.H., Yuan, P., Cui, X.Y., Qiu, G.L., 2009. The remediation of heavy metals contaminated sediment. *J. Hazard. Mater.* 161, 633–640.
- Portet-Koltalo, F., Ammami, M., Benamar, A., Wang, H., Le Derf, F., Duclairoir-Poc, C., 2013. Investigation of the release of PAHs from artificially contaminated sediments using cyclolipoppeptidic biosurfactants. *J. Hazard. Mater.* 261, 593–601.
- Reddy, K., Maturi, K., Cameselle, C., 2009. Sequential electrokinetic remediation of mixed contaminants in low permeability soils. *J. Environ. Eng.* 135, 989–998.
- Reddy, K.R., Saichek, R.E., Maturi, K., Ala, P., 2002. Effects of soil moisture and heavy metal concentrations on electrokinetic remediation. *Indian Geotech. J.* 32, 258–288.
- Roberts, D.A., 2012. Causes and ecological effects of resuspended contaminated sediments (RCS) in marine environments. *Environ. Int.* 40, 230–243.
- Ryu, B.G., Park, G.Y., Yang, J.W., Baek, K., 2011. Electrolyte conditioning for electrokinetic remediation of As, Cu, and Pb-contaminated soil. *Sep. Purif. Technol.* 79, 170–176.
- Saichek, R.E., Reddy, K.R., 2005. Surfactant-enhanced electrokinetic remediation of polycyclic aromatic hydrocarbons in heterogeneous subsurface environments. *J. Environ. Eng. Sci.* 4, 327–339.
- Sprovieri, M., Feo, M.L., Prevedello, L., Manta, D.S., Sammartino, S., Tamburino, S., Marsella, E., 2007. Heavy metals, polycyclic aromatic hydrocarbons and polychlorinated biphenyls in surface sediments of the Naples harbour (southern Italy). *Chemosphere* 67, 998–1009.
- Wang, D.X., Abriak, N.E., Zentar, R., Xu, W., 2012. Solidification/stabilization of dredged marine sediments for road construction. *Environ. Technol.* 33, 95–101.
- Yang, Y., Ratté, D., Smets, B., Pignatello, J., Grasso, D., 2001. Mobilization of soil organic matter by complexing agents and implications for polycyclic aromatic hydrocarbon desorption. *Chemosphere* 43, 1013–1021.
- Yozzo, D.J., Wilber, P., Will, R.J., 2004. Beneficial use of dredged material for habitat creation, enhancement, and restoration in New York–New Jersey Harbor. *J. Environ. Manage.* 73, 39–52.

P23



Surface functionalization of cyclic olefin copolymer with aryl diazonium salts: A covalent grafting method

Florian Brisset^a, Julien Vieillard^{a,*}, Benjamin Berton^b, Sandrine Morin-Grognet^c, Cécile Duclairoir-Poc^d, Franck Le Derf^{a,*}

^a UMR CNRS 6014 COBRA, FR 3038, Université de Rouen, 55 rue Saint Germain, 27000 Evreux, France

^b EA 3233 SMS, Université de Rouen, 1 rue du 7ème Chasseurs, BP281, 27002 Evreux Cedex, France

^c EA 3829 MERCI, Université de Rouen, 1 rue du 7ème Chasseurs, BP281, 27002 Evreux Cedex, France

^d EA 4312 LMSM, Université de Rouen, 55 rue Saint Germain, 27000 Evreux, France



ARTICLE INFO

Article history:

Received 29 October 2014

Received in revised form 8 December 2014

Accepted 8 December 2014

Available online 16 December 2014

Keywords:

Diazonium salt
Cyclic olefin copolymer
COC
Grafting
Surface treatment
Interface

ABSTRACT

Covalent immobilization of biomolecules on the surface of cyclic olefin copolymer (COC) is still a tough challenge. We developed a robust method for COC surface grafting through reaction with aryl diazonium. Chemical diazonium reduction generated an aryl radical and the formation of a grafted film layer on the organic surface. We also demonstrated that the chemical reduction of diazonium salt was not sufficient to form a film on the COC surface. UV illumination had to be combined with chemical reduction to graft an aryl layer onto the COC surface. We optimized organic film deposition by using different chemical reducers, different reaction times and reagent proportions. We characterized surface modifications by fluorescence microscopy and contact angle measurements, infrared spectroscopy, X-ray photoemission spectroscopy and Raman spectroscopy, and assessed the topography of the aryl film by atomic force microscopy. This original strategy allowed us to evidence various organic functions to graft biomolecules onto COC surfaces with a fast and efficient technique.

© 2014 Elsevier B.V. All rights reserved.

1. Introduction

Easy methods for modifying thermoplastic surfaces with specific chemicals and functionalities have been attracting scientists' attention for years. Rigid thermoplastics are increasingly used to develop biodevices (microarray chips, biosensors, cell culture devices microfluidic chips, etc.) [1,2]. Cyclic olefin copolymer (COC) has promising properties such as good transparency, high chemical resistance, low cost, high stiffness [3,4]. Despite these advantages,

COC has a chemically inert and hydrophobic surface that renders biomolecule analysis tricky. COC has been used in microfluidic channels without any modification for specific analyses [5–7]. But biomolecules (proteins, DNA, etc.) or hydrophobic impurities adsorbed onto the hydrophobic polymer usually affect the characteristics of the device (variable electroosmotic flow, unwanted fluorescence background, extra peak dispersion, etc.). Controlling surface functionalization is therefore crucial. Different approaches aimed at modifying COC surfaces have been described in the literature. A chemical method to brominate COC using a palladium catalyst has been reported [8]. This approach is interesting because the bromide group can be converted into a different group (OH, COOH, etc.) by changing the nucleophilic agent and thus yield numerous original COC polymers. However, this method modifies the whole polymer structure and thereby its physical and chemical properties, so this could result in unwanted effects. To pattern COC devices with DNA, COC surfaces were coated with silane layers to generate SiO₂-COC microarrays [3]. COC modification by dynamic or static coating has also been tried. Dynamic coating involves dissolving additives in a buffer solution to obtain a coating layer that physically adsorbs onto the surface. Thanks to this method, hydroxyethylcellulose, hydroxypropylcellulose and ethylene glycol solutions were physisorbed onto COC surfaces [4,9]. Although

Abbreviations: NBD, 4-nitrobenzenediazonium tetrafluoroborate; BBD, 4-bromobenzenediazonium tetrafluoroborate; BEBD, 4-(2-bromoethyl)benzenediazonium tetrafluoroborate; CBD, 4-(carboxymethyl)benzenediazonium tetrafluoroborate; MBD, 4-mercaptopbenzenediazonium tetrafluoroborate; COC, cyclic olefin copolymer; PMMA, polymethylmethacrylate; PET, poly(ethylene terephthalate); DI water, deionized water.

* Corresponding author at: UMR CNRS 6014 COBRA, Université de Rouen, 55, rue Saint Germain, 27000 Evreux, France. Tel.: +33 232291536.

E-mail addresses: florian.brisset@etu.univ-rouen.fr (F. Brisset), julien.vieillard@univ-rouen.fr (J. Vieillard), benjamin.berton@univ-rouen.fr (B. Berton), sandrine.morin@univ-rouen.fr (S. Morin-Grognet), cecile.duclairoir@univ-rouen.fr (C. Duclairoir-Poc), franck.lederf@univ-rouen.fr (F. Le Derf).

dynamic coating is a simple and reliable method, it requires continuous regeneration, so that its applications in the field of surface preparation are limited. COC surfaces have also been coated with different static polymer adlayers such as triblock copolymer, dimethylacrylamide copolymer and antibiofouling copolymer [10–13]. Such polymers are amphiphilic, with a hydrophobic interface in contact with COC on one side and a hydrophilic interface in contact with the aqueous solution on the other side. COCs have also been modified using covalently grafted polymers to create a robust coating with tunable chemistry. To obtain covalent coating, COCs have to be previously activated. Two main strategies have been described, based on gas plasma irradiation or on UV photoactivation. Ozone oxidation has also been successfully tested to generate polar groups such as hydroxyls, esters or carboxylic acids on COC surfaces [14,15]. In radiofrequency plasma treatment, different gasses have been tested (oxygen, nitrogen, argon, and oxygenated argon plasma), in a wide range of electrical powers (25–200 W) for various lengths of time (0–300 s). In all cases, gas radiofrequency plasmas were effective for improving COC surface wettability. However, some limitations were noted. For instance, plasma irradiation increased the surface roughness of the material, the plasma-treated sample had to be stored in air-tight conditions for its wettability to be maintained, and treatment length had to be controlled carefully to avoid “over-treatment” resulting in wettability losses [1,16,17]. So far, plasma activation of COC has been limited to surface characterization to improve the bonding process between COC and other materials [1,16,18]. Except an experiment assessing platelet adhesion onto a COC surface, plasma irradiation has not been tested for biomolecule analysis [17]. UV illumination has been tested successfully to activate COC surfaces in order to graft DNA or acrylic monomers onto them [19,20]. Another approach tested the reaction of a COC surface with UV-sensitive molecules such as an anthraquinone photolinker [21], benzophenone [22], benzoin methyl ether [23], and aryl azide [24]. Apart from these approaches, UV illumination was tested to photograft polymers onto a COC surface. That way, microfluidic channels hollowed in COC were patterned by N-vinylpyrrolidone, acrylic and methacrylate films [24–28]. As a large amount of methacrylate monomers is available, COC surfaces progressively gained new functionalities including low protein adsorption, adjustable electroosmotic flow or immobilization of reactive groups ready to use with biomolecules. Some polymeric monoliths were photo-grafted in COC microfluidic channels to develop original analytical tools [23,29]. Different ways (phenanthroline, amine, reactive silane or alkyne azide chemistry) are suitable for grafting process [30–32]. Aryldiazonium salts have been successfully grafted on many materials such as carbon, metal, semi-conductor and polymers [33,34]. The grafted aryl layers have proved efficient in sensing devices dedicated to metal ion [30,35], protein [36–38] and DNA detection [37]. Aryldiazonium salts are easy to prepare, and a wide range of reactive functional groups can be synthesized from aniline derivates or nitro precursors. Surface modification by reaction with aryldiazonium salt requires generating an aryl radical that bonds to the surface. This aryl radical is spontaneously obtained by electrochemical reduction or by chemical reduction (iron powder, hypophosphorous acid, sodium iodide, and ascorbic acid) but also by UV assistance, under ultrasonic frequency, thermolysis, solvolysis or microwave treatment [33,34,38]. Aryldiazonium salt is added as an isolated salt or generated directly *in situ* during the grafting process. Depending on the experiment, aryldiazonium is dissolved in an aprotic medium with a supporting electrolyte or in an aqueous medium [34]. Although some polymer surfaces are difficult to modify, Teflon® is modified with aryldiazonium salt to obtain a polyacrylic acid film on its surface. In this case, iron powder is added as a chemical reducer to generate the aryl radical [39]. This wet chemical treatment called Graftfast process is employed to modify

polyvinylidene fluoride membranes, poly(ethylene terephthalate), acrylonitrile–butadiene–styrene polymers and polyvinylchloride (PVC) polymers [39–42]. Chehimi et al. also observed that the aryl radical generated from aryldiazonium salt could be covalently grafted onto a polymeric surface such as poly(methyl)methacrylate [43].

The present work focuses on grafting different aryl films on COC surfaces. We tested different reducing agents prepared in aqueous media to obtain a covalent diazonium bonding on COC surfaces. We also assessed COC surface modifications by means of water angle contact, IR and Raman spectroscopy and X-ray photoelectron spectroscopy (XPS). We thus demonstrated that the properties of COC surfaces can be modulated using aryldiazonium chemistry.

2. Materials and methods

2.1. Materials and reagents

Cyclic olefin copolymer plates (MCS-TOPAS-03 and MCS-COP-04 Zeonor) were purchased from Microfluidic Chip Shop, Jena, Germany, in 1-mm thick microscopy slide format that we cut into 1 cm × 2 cm plates. The plates were rinsed with acetone in an ultrasonic bath for 20 min and dried before use. Hypophosphorous acid, sodium nitrite and all the chemicals were obtained from Sigma–Aldrich, Saint Quentin Fallavier (France).

2.2. Synthesis of diazonium salts

4-Nitrobenzenediazonium tetrafluoroborate and 4-bromobenzenediazonium tetrafluoroborate were used in their original form. $R\text{-ArN}_2^+ \text{BF}_4^-$ ($R = -\text{CH}_2\text{COOH}, -\text{CH}_2\text{CH}_2\text{Br}, -\text{OH}, -\text{SH}$) were synthesized from the corresponding anilines by diazotization as described by Khosroo and Rostami [44]. Briefly, the corresponding *para*-aniline was dissolved in HBF_4 . The mixture was cooled to 0 °C in an ice water bath. Then sodium nitrite aqueous solution was slowly added. After 20 min, the mixture was cooled to –20 °C to precipitate aryldiazonium salts. Then, the slurry was filtered by suction, washed with cold tetrafluoroboric acid and cold diethylether. Aryldiazonium tetrafluoroborate salts were kept at –20 °C. Their ^1H and ^{13}C NMR spectra (300 MHz, Bruker) are presented in Figs. A and B. In agreement with the literature, the intense band at 2290 cm^{-1} corresponding to the $-\text{N}=\text{N}$ stretch of the diazonium group was observed by IR spectroscopy [37]. For comparison purposes, aryldiazonium salts were also prepared *in situ* from the corresponding aniline prepared in aqueous HCl 0.5 M by reaction with 3 molar equivalents of sodium nitrite. Then, the COC plate was immersed and 9 molar equivalents of chemical reducer were added. The chemical reactor was incubated in a UV curing system equipped with a UV metal halide lamp (225 mW cm $^{-2}$, Dymax, Wiesbaden) for 1 h. After grafting, COC plates were sonicated with acetone for 10 min.

2.3. Characterization

2.3.1. Infrared spectroscopy (ATR-FTIR)

ATR-FTIR spectra were recorded with a Tensor 27 (Bruker) spectrometer with a ZnSe ATR crystal. For each spectrum, 20 scans were accumulated with a resolution of 4 cm^{-1} . Background spectra were recorded on air before each analysis.

2.3.2. Fluorescence microscopy

An inverted microscope (Axio Observer A1, Zeiss) equipped with a high pressure mercury lamp and a femtowatt photoreceiver (model 2151, New Focus) were used for fluorescence measurements.

2.3.3. UV-visible absorption

The optical transparency of diazonium treated COC surface was evaluated by UV-visible spectrophotometry (Shimadzu UV1650). The substrate of COC was mounted directly on the measurement setup perpendicularly to the optical pathway. Absorption spectra were monitored from 800 nm to 200 nm.

2.3.4. Raman fluorescence spectroscopy

All the Raman spectra were obtained with a Horiba Jobin Yvon LabRam HR system. A 632.8 nm HeNe laser and a confocal optical microscope were used for analysis. All the spectra were acquired with 50 \times magnification and recorded for 1 min with a spatial resolution of 2 cm $^{-1}$.

2.3.5. X-ray photoelectron spectroscopy (XPS)

X-ray photoelectron spectra were recorded on a Vacuum Generator ESCALAB 210 spectrometer using a non-monochromatic Al K α X-ray source (150 W). Pass energy was set at 160 eV for the survey and 40 eV for the core level of N_{1s}, C_{1s}, O_{1s} and Br_{3p}. The spectra were calibrated against C_{1s} set at 285 eV.

2.3.6. Contact angle analysis

COC surface wettability was determined by measuring the contact angles of deionized (DI) water using an automatic goniometer (G40, Krüss, Germany). After a 5-s equilibration, two 5 μ L water droplets were observed. The triplicate experiments were run at room temperature at 2 positions on the substrate.

2.3.7. Atomic force microscopy (AFM)

The surface 2D and 3D topography were imaged by using a PICOSPM (Molecular Imaging) in contact mode. AFM measurements were performed with silicon nitride cantilevers having a spring constant of 0.3 N/m at a fixed scan rate of 1 line/s with a resolution of 512 pixel \times 512 pixel. AFM images were analyzed with the SPIP Software (Scanning Probe Image Processor) to determine the arithmetical mean roughness (R_a) at a scale of 20 μ m \times 20 μ m areas. Samples were inspected by AFM before and after chemical modification.

3. Results and discussion

3.1. Description of surface functionalization strategy

Chehimi et al. [43] recently demonstrated that polymeric materials such as polymethylmethacrylate (PMMA) can be modified by chemical reduction of diazonium salt in the presence of a chemical reducer in acidic solution. So far this strategy has not been described in the literature to modify COC surfaces. So we tested a similar approach to modify TOPAS cyclic olefin copolymer (COC). Commercial 4-nitrobenzenediazonium (NBD) was mixed with a reducing agent in HCl for 1 h. During the reaction, the color of the solution changed, indicating sub-product (Ar–N=N–Ar) formation, and a few gas bubbles were generated, corresponding to nitrogen elimination. At the end of the reaction, a nitrobenzene film was observed on the COC surface. The ATR-FTIR spectra of our COC surfaces are presented in Fig. 1.

The IR spectrum of pristine COC displayed alkyl vibration at 3000 cm $^{-1}$ (Fig. 1, blue curve). When the COC surface was incubated with 4-nitrobenzenediazonium salt and a reducing agent, the characteristic ring vibration at 1599 cm $^{-1}$, and the NO₂ vibrations at 1522 and 1347 cm $^{-1}$ appeared (Fig. 1, pink curve). To test the strength of the molecular bonding between the first layer of the film and the COC surface, we cleaned COC samples with an organic solvent in an ultrasonic bath for 10 min. As described in Fig. 1A (green curve), the IR signatures at 1599, 1522 and 1347 cm $^{-1}$ were completely removed from the spectrum, demonstrating that, the film

was just physisorbed on the COC surface. Different approaches are presented in the literature to activate COC surfaces before molecular grafting [15,16]. Surface oxidation with ozone and UV light generated polar groups on COC surfaces [15,45]. This approach was investigated using a UV illuminator equipped with a metal halide lamp. The main part of the spectrum of this lamp was distributed in the UVA wavelength region where COC presented good transparency. The spectral distribution of the lamp is presented in Fig. C. We monitored the influence of UV illumination on COC wettability using contact angle measurements (Fig. D). Pristine COC was hydrophobic, with a 94° contact angle of water droplets. When COC was illuminated by UVA light, hydrophobicity of the material decreased with time. After 1 h of illumination, the contact angle was 77°, and it was down to 20° after 6 h of irradiation, which corresponds to hydrophilic behavior. The rate of modification of the contact angle was higher during the first hour, so we kept this reaction time to illuminate the COC surface before diazonium reaction. After illumination, the surface was incubated with aryl diazonium salt and hypophosphorous acid (H₃PO₂) for 1 h. A nitrophenyl film was observed, with nitrophenyl IR signature on the COC surface (data not shown). Nevertheless, as previously, the film was completely removed after 10 min of ultrasonic treatment.

Aryl radical may be formed by illumination of diazonium salt [46–48]. So, the grafting process of nitrobenzene diazonium salt has been tested on COC without any chemical reducer. Unfortunately, no modification of COC surface was observed by ATR-FTIR analysis (data not shown). So, light illumination was not sufficient to graft diazonium salt in our case.

Finally, we assessed another approach where the aryl diazonium salt, the COC sheet, the reducing agent and HCl are prepared in a reactor and immediately incubated under UVA light for 1 h. Thus we obtained a thick layer on the COC surface. IR signatures of nitro stretching and ring vibration before and after ultrasonic cleaning are presented in Fig. 1B (pink and green curves, respectively). Interestingly, we observed no band in the 2200–2300 cm $^{-1}$ region for the stretching of the characteristic N₂ $^{+}$ bond. COC material is chemically resistant to classical solvents (DMSO, acetonitrile, acetone, and ethanol), so we have evaluated the chemical resistance of the grafted layer using organic, basic and acidic solvents. After 5 min of rinsing with various solvent, the aryl layers are not modified. By this method, we validated that COC was covalently modified by diazonium salt reduction.

To investigate the optimal conditions for surface grafting, we tested 4-nitrobenzenediazonium surface grafting under various conditions such as different diazonium salt concentrations, reducing agent concentrations, diazonium salt/reducing agent ratios, chemical reducers, reaction times and temperatures. We first assessed the influence of the reaction time by ATR-FTIR. Fig. 2 focuses on the spectra obtained from 15 min to 180 min reaction times in the presence of a reducing agent and 4-nitrobenzenediazonium salt.

Illuminating the COC surfaces without any diazonium salt for 15 min to 3 h induced no modification (data not shown). After 15 min of reaction, we observed ring vibration at 1600 cm $^{-1}$ and NO₂ vibrations at 1525 cm $^{-1}$ and 1350 cm $^{-1}$. The intensity of these peaks increased with grafting time. These results imply that nitrophenyl films were correctly formed on COC with a multilayer pattern. The 1350 cm $^{-1}$ peak reached a highest intensity after 1 h (Fig. 2, green curve). Conversely, the ring vibration is highest after 180 min (Fig. 2, purple curve). It could be inferred that after 3 h, the NO₂ group is hidden in the multilayer. Ultrasonic waves could also generate cracks on the surface [49] that disorganize and destroy the upper layer of nitrophenyl film. We confirmed this conclusion by measuring the intensity of the 1600 cm $^{-1}$ band, which was higher before ultrasonic treatment (Fig. 1B).

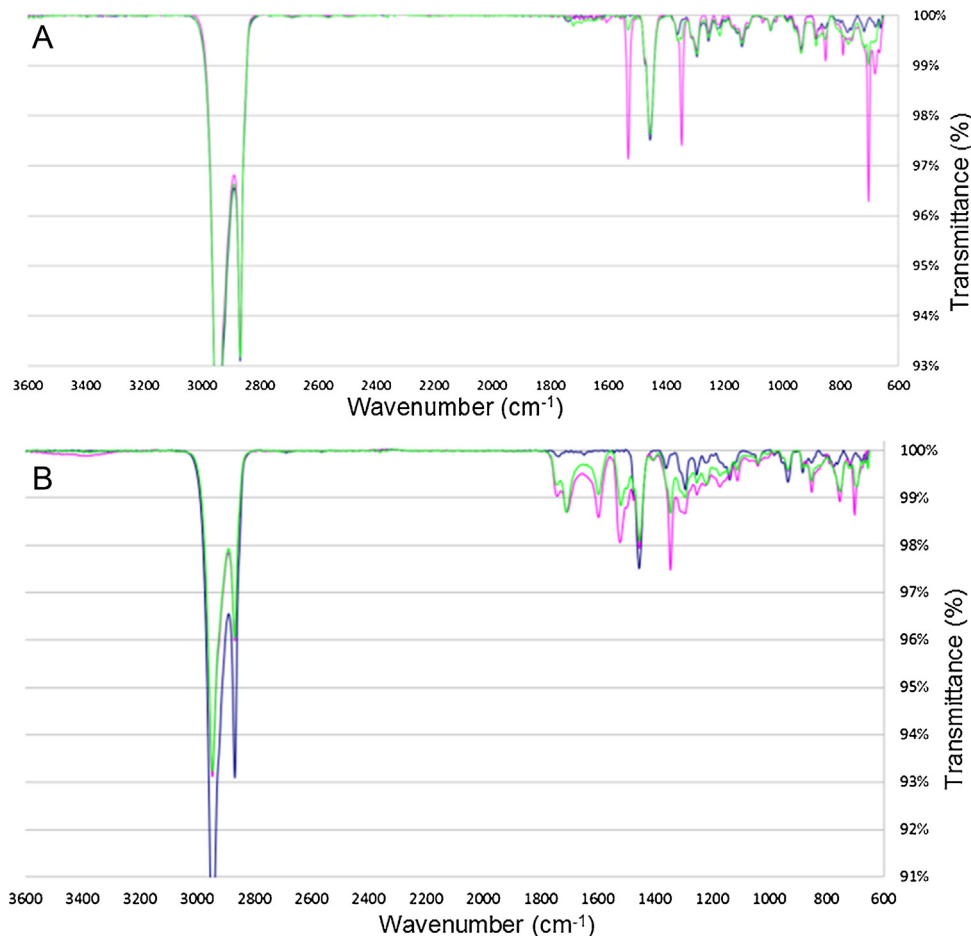


Fig. 1. IR spectra of COC surface (A) in absence or in presence (B) of UVA irradiation. Analysis of pristine COC (blue curve) of COC grafted by nitrobenzenediazonium (NBD) salt for 60 min (pink curve), and COC grafted with NBD then cleaned with ultrasonic treatment (green curve). (For interpretation of the references to color in this figure legend, the reader is referred to the web version of the article.)

Secondly, we tested different proportions of reducing agent and aryl diazonium salt with a reaction time of 1 h (Fig. 3). Hypophosphorous acid, ascorbic acid, iron filings, and sodium iodide are well known chemical reducers of diazonium salt [33]. We tested all four reducers to graft NBD salt on COC surfaces. The results are shown in Fig. 3A, H_3PO_2 was the only suitable reducer for grafting NBD on a COC surface in our conditions. A concentration of 0.1 M

aryldiazonium salt with 10 molar equivalents of reducing agent seemed to be necessary and sufficient for polyphenyl film formation (Fig. 3B). Thus, peak intensities at 1600 and 1521 cm^{-1} were similar with 10 or 50 molar equivalents of reducing agent. These results are in accordance with Chehimi et al. [43], who showed that an excess of reducing agent was required for aryl diazonium grafting.

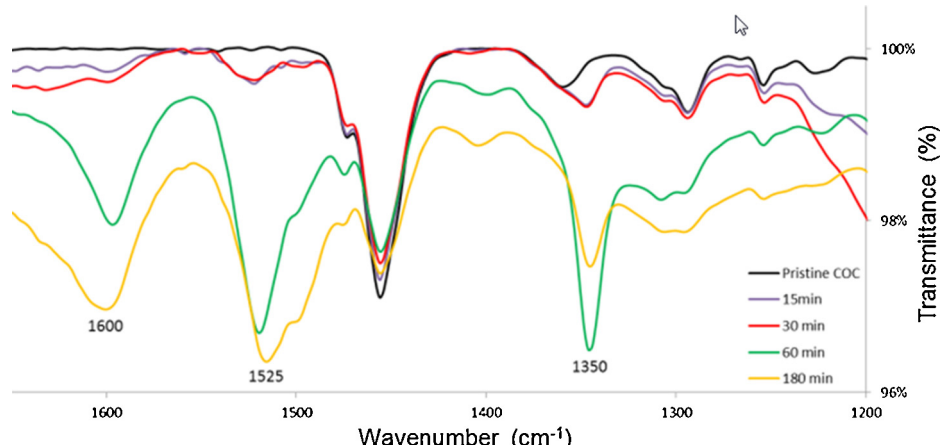


Fig. 2. Influence of reaction time on nitrophenyl film formation on COC surface. Focus between 1650 and 1200 cm^{-1} of the IR spectra of (black curve) pristine COC, and COC grafted with NBD for (purple curve) 15 min, (red curve) 30 min, (green curve) 60 min, and (yellow curve) 180 min. (For interpretation of the references to color in the text, the reader is referred to the web version of this article.)

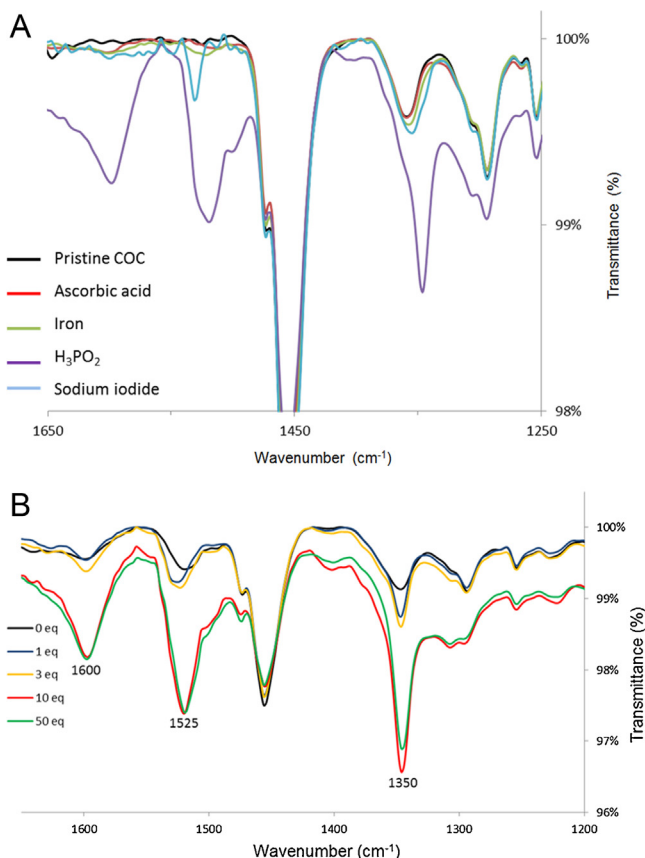


Fig. 3. Focus between 1200 and 1600 cm⁻¹ of the IR spectra of COC surface incubated with NBD for 1 h in presence of (A) various chemical reducers, and (B) various amount of molar equivalent of reducing agent.

Thirdly, we assessed the influence of the reaction temperature, as aryl radicals are temperature sensitive. During light illumination, the temperature in the illuminator increased from room temperature to 60 °C in 15 min (Fig. E). To control the temperature during diazonium reaction, the reactor was insulated with ice or liquid water (at 20 °C). The temperature of the solution increased slowly and the highest temperature measured in the chemical reactor was

no more than 47 °C after 1 h. The IR spectra obtained in the presence of a thermal insulator are presented in Fig. 4.

The characteristic band of the nitrophenyl film was higher when the temperature remained under control. These results confirm the observations of Abiman et al. [50], who tested diazonium reaction on carbon nanotubes. The topography of the film was different when the reaction started in melting ice or in liquid water at 20 °C. At 0 °C, film deposition was more heterogeneous than at room temperature. It is also important to note that the glass transition temperature (T_g) of COC is 70 °C. Thus, by controlling the reaction temperature, one can avoid it getting too close to the T_g and thus limiting possible deep modifications of the COC polymer. To sum up, we obtained the best conditions for diazonium grafting on COC when 0.1 M aryl diazonium was mixed with 10 molar equivalents of H₃PO₂ in a temperature-controlled acidic medium under UV illumination for 1 h.

In literature, COCs are presented under various names (Topas, Zeonor) corresponding to various suppliers and chemical compositions. To assess the performance of our technique, we also grafted a Zeonor device with NBD in our best conditions. As presented in Fig. 5, we grafted a nitrophenyl layer film on a Topas as well as on a Zeonor device. Interestingly, IR signals were more intensive on the Zeonor than on the Topas surface, meaning that the layers were thicker on the Zeonor sample.

There are currently just a few commercially available diazonium salts, but aryl diazonium salts could be isolated or synthesized *in situ* from aniline derivates. That way, various organic functions could be grafted onto the COC surface. To demonstrate the polyvalence of the diazonium reaction, we synthesized different aryl diazonium salts and grafted them onto COC surfaces. The IR spectra of COCs grafted with 4-(carboxymethyl)benzenediazonium (CBD), 4-bromobenzenediazonium (BBD), or 4-(2-bromoethyl)benzenediazonium (BEBD) are presented in Fig. F. We observed the poly-aryl-like layer through a Br absorption band at 735 cm⁻¹, ring vibration at 1600 cm⁻¹ (Fig. F.3) and a carbonyl (C=O) stretching band at 1715 cm⁻¹ (Fig. F.2). In the previous experiment, aryl diazonium salts had been isolated before grafting. Berthelot et al. [37], also assessed another, faster and easier method using *in situ* chemical reduction. We compared the phenyl film obtained from isolated and *in situ* reduced CBD (Fig. G). Ring vibration at 1600 cm⁻¹ and a carbonyl band at 1715 cm⁻¹ were present in the IR spectra, demonstrating the covalent bonding

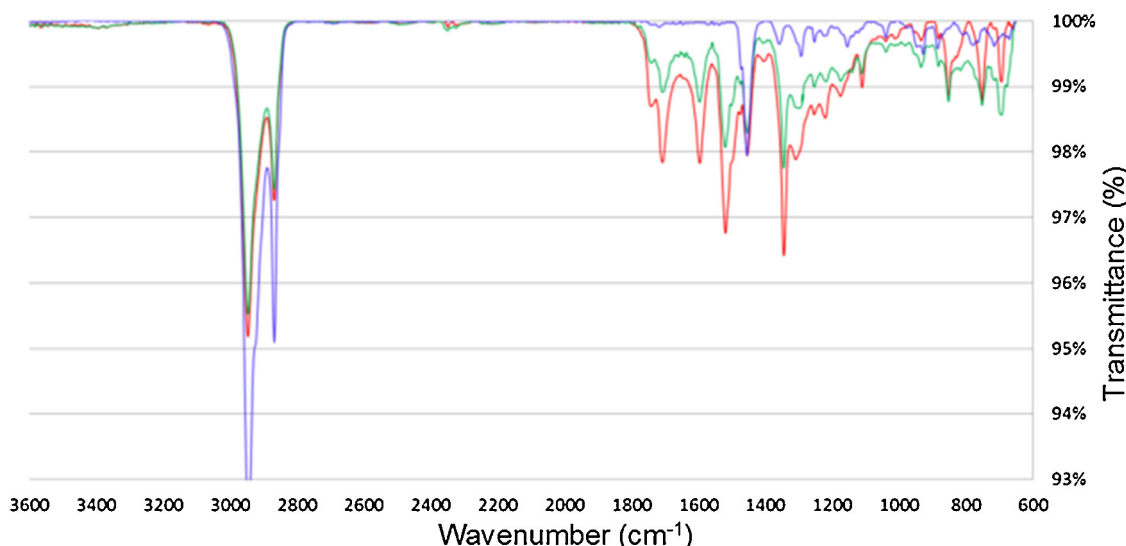


Fig. 4. IR spectra of COC surface grafted by NBD without any temperature control (blue curve), with temperature reaction initiated at 0 °C (green curve), and with temperature reaction initiated at 20 °C (red curve). (For interpretation of the references to color in this figure legend, the reader is referred to the web version of the article.)

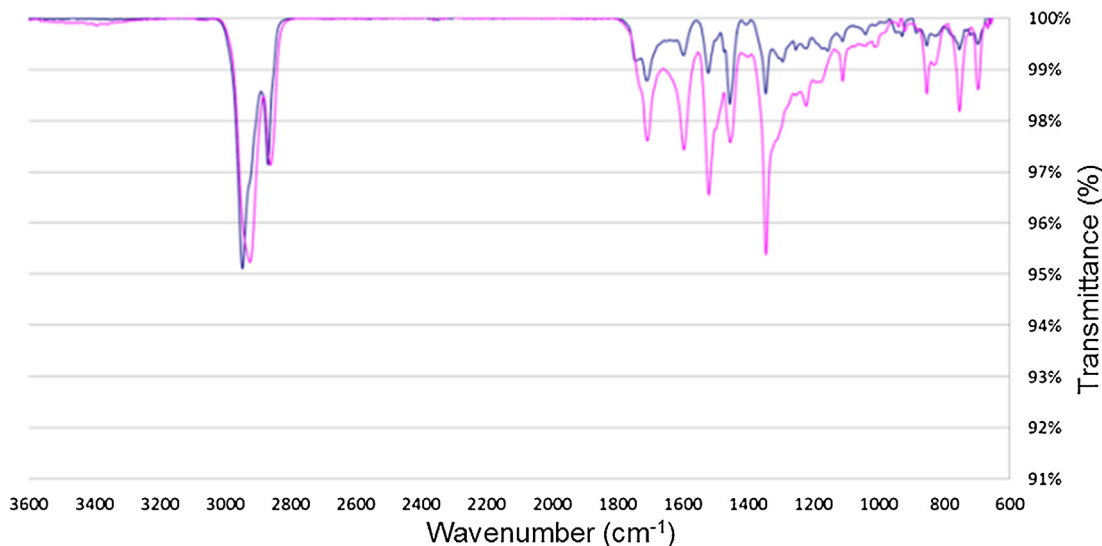


Fig. 5. IR spectra of Zeonor COC surface (pink curve) and Topas COC surface (blue curve) both chemically modified by NBD for 60 min. (For interpretation of the references to color in this figure legend, the reader is referred to the web version of the article.)

of the carboxymethylphenyl layer. Interestingly, both methods (*in situ* and from isolated diazonium salts) produced IR spectra with similar intensities for carbonyl and phenyl vibrations.

3.2. Surface chemical composition

To confirm the attachment of the diazonium film, we grafted COC surfaces with NBD and BEBD, and then examined them by XPS. We first characterized pristine COC. The XPS spectrum displayed 3 peaks at 536.2 eV, 285 eV and 286.4 eV, assignable to O_{1s}, C_{1s} and C_{2s}, respectively. The 285 eV peak was characteristic of saturated hydrocarbon. The 286.4 eV peak was assignable to a carbon atom singly bonded to an oxygen atom (*i.e.* C-OH or C-O-C) [16]. The oxygen detected at 536.2 eV probably resulted from oxygen adsorbed onto the surface or from the oxidation step during the manufacturing process of Topas COC polymer [15].

The XPS spectra recorded from the NBD-treated COC surfaces displayed 4 peaks at 533 eV, 406 eV, 400 eV and 285 eV. As previously, the 533 eV peak corresponded to O_{1s} attributed to the carbonyl group. The peaks at 400 and 406 eV corresponded to N_{1s} (Fig. 6). Mévellec et al. [39] also observed an XPS profile with two separated peaks for N_{1s} with NBD grafted onto a gold surface. The 406 eV peak corresponded to the nitro group while the 400 eV

peak was attributable to a mixture of amino groups (NH₂) and azo bridges (N=N) [39,51,52].

The Br_{3p} XPS spectra of a BEBD-coated COC displayed two large peaks at 184 eV and one small peak at 190 eV assigned to alkyl bromide [53,54]. As previously, a 285 eV peak corresponded to C_{1s} (aliphatic carbon) and 528–533 eV peaks corresponded to lattice oxygen and carbonyl groups, respectively (Fig. 6). So, the XPS results suggested that the COC surface was chemically modified after diazonium grafting.

3.3. Contact angle analysis of COC surface

The chemical composition of the COC surface changed according to the diazonium layer grafted on it, with resulting modifications of the surface properties such as wettability or light absorption. To assess the wettability of the treated material, we measured contact angles on untreated COC surfaces, light-activated surfaces and diazonium-grafted surfaces. The effects of diazonium grafting on COC surface wettability are summarized in Fig. 7.

The surface of pristine COC was expectedly hydrophobic, with a contact angle of 93.9° in DI water. NBD and BEBD grafting altered COC surface wettability, with a higher contact angle (106° and 85°, respectively) than the light-treated COC surface (77°). Conversely, CBD or MBD grafting modified COC wettability by decreasing water contact angle values (56–60°) unlike BBD grafting did not further modify wettability (73°) as shown in Fig. 7.

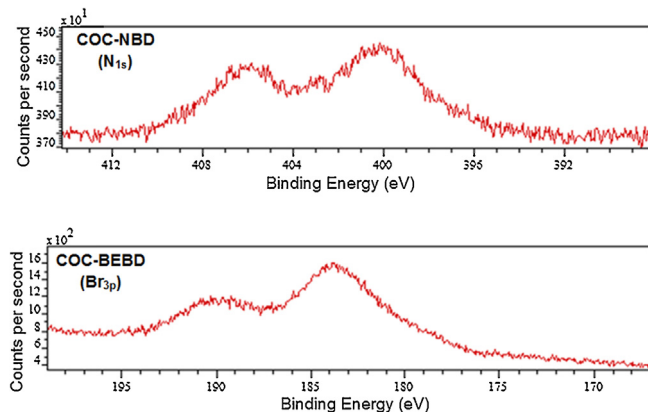


Fig. 6. N_{1s} and Br_{3p} XPS survey spectra of COC surface after chemical functionalization with NBD and BEBD respectively.

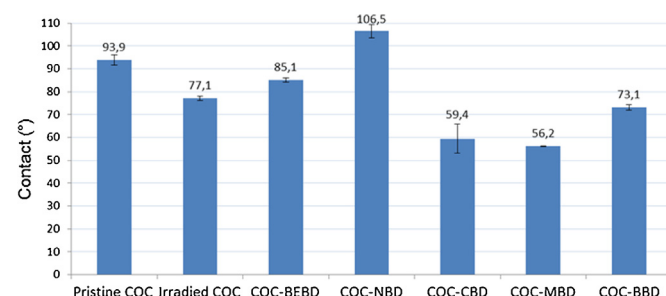


Fig. 7. Effect of various diazonium film layer on wettability of COC surface. Wettability was analyzed by water droplet contact angle measurements.

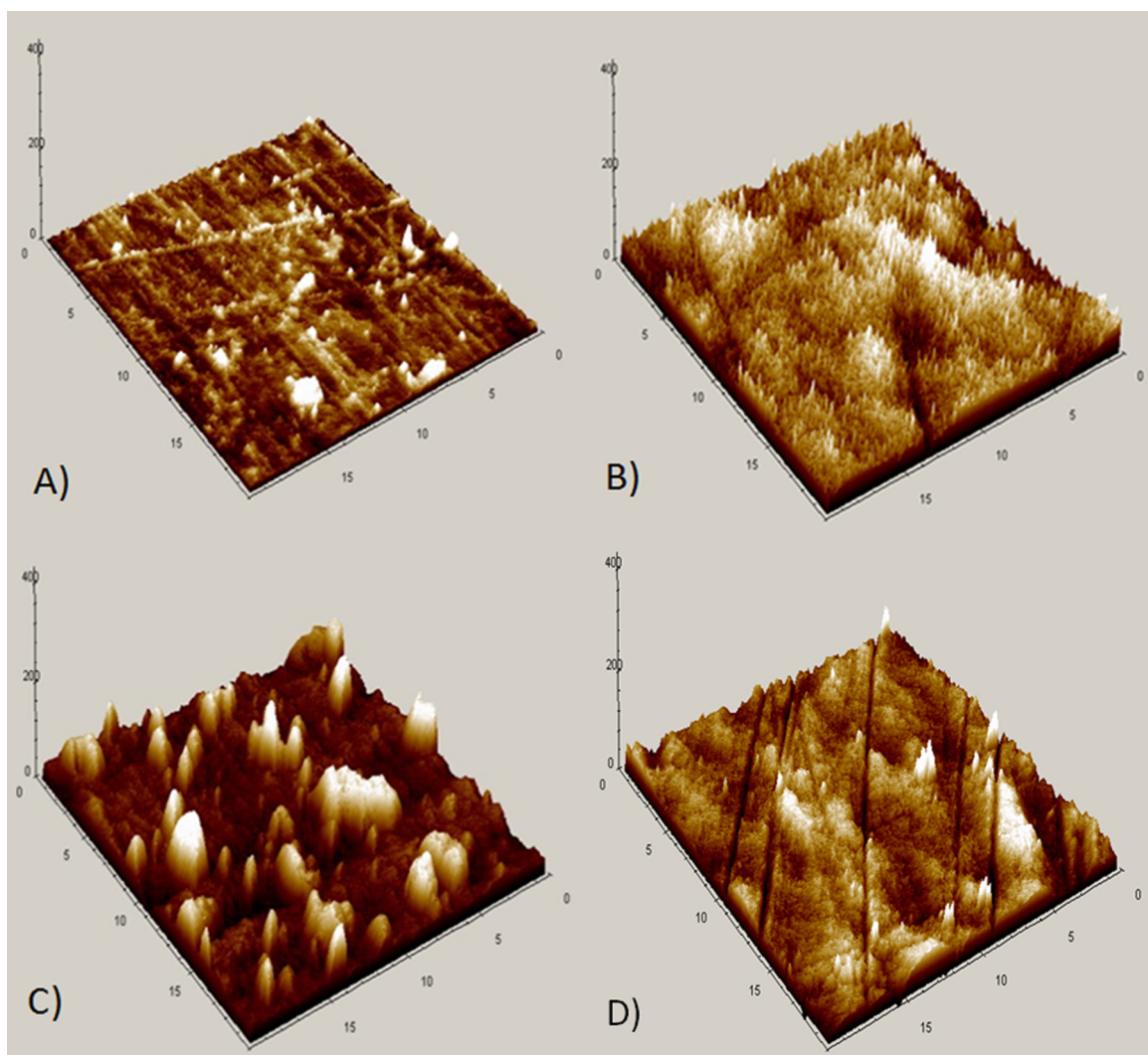


Fig. 8. 3D AFM images of COC native surface (A), NBD grafted COC (B) and CBD grafted COC (C), NBD grafted COC after 30 min of chemical reduction (D).

3.4. Surface topographies

To better understand surface wettability, we investigated surface topographies at the nanoscale. We imaged the surface morphologies of different grafted COCs by AFM (Fig. 8). Native COC had a smoother surface than grafted surfaces, and grafted layers exhibited a needle-like structure. COC slides displayed a few scratches originating from sample handling.

Using peak-to-valley analysis of the scratches, we estimated the thickness of the aryl layer. Pristine COC was 103 nm thick while NBD-, CBD- and BBD-treated COC surfaces were 350 nm, 349 nm, 630 nm thick, respectively. These results confirmed the visual aspect of the COC samples. The mean roughness value of the untreated COC surface was about 7.7 nm while mean roughness values of the NBD- and CBD- and BBD-treated samples reached 21, 22 and 25.5 nm, respectively, for 1 h reaction time. So, the nature of the aryl diazonium salt had no influence on roughness. Surface roughness increased from 7.7 nm (ground value) to 28 nm (final value) when aryl grafting time was brought to 120 min, yet, the final value was almost reached after 60 min. 30 min of reduction time is enough to graft COC surface. The aryl layer is more uniform and less thick after 30 min of reduction than after 60 min (Fig. 8D). After a reaction time of 30 min, the mean rugosity was 12 nm in comparison to 28 nm after 1 h. These results match well with the results obtained by IR spectroscopy.

3.5. Optical properties of COC surface treated by diazonium salts

Due to its optical properties (good transparency, low auto-fluorescence, and low absorption), COC is used to develop polymeric biodevices [15]. However, several authors point out that UV treatment modifies the optical properties of COC. That is why we assessed grafted COC by UV-visible spectrophotometry, epifluorescence microscopy and Raman spectroscopy. The UV-visible absorption spectra of pristine and grafted COCs are presented in Fig. H. The nitrophenyl film grafted on a COC surface generated a stronger absorption signal than pristine COC. This increase was directly related to film thickness. Thus, after a 1-h reaction time, surface absorbance at 400 nm was 0.05 A.U. for pristine COC vs. 0.32 A.U. for nitrobenzene grafted COC (Fig. H). For grafting optimization, it was interesting to work with nitrobenzene grafted COC, but for biosensor development it is important to work with transparent and low absorbance material. The absorbance of the carboxymethylbenzene grafted layer on COC is only 0.09 A.U. at 400 nm which is comparable to pristine COC (Fig. J).

Using UV light to activate COC surfaces can also generate auto-fluorescence of the material [45]. So we carried out fluorescence measurements to check if grafted diazonium COC was compatible with fluorescence detection. We made our fluorescence measurements using an inverted microscope equipped with a mercury lamp and a photodetector. We monitored fluorescence at 565 nm

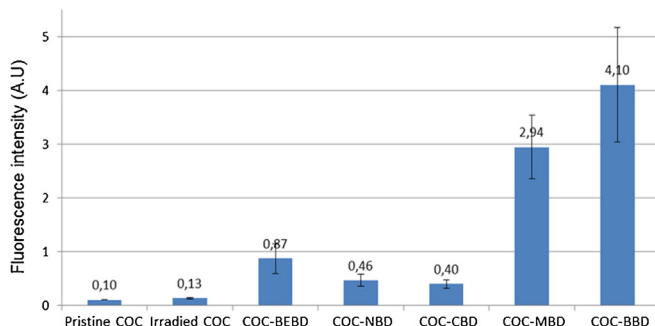


Fig. 9. Fluorescence intensity analysis of COC before and after chemical functionalization by various diazonium salts. Fluorescence measurement on oxidized COC was presented as a control.

throughout the COC polymer layer. The results are presented in Fig. 9.

Fluorescence increased with illumination time, confirming that UV light induced COC auto-fluorescence. However, in our case, the resulting auto-fluorescence was only 0.13 A.U. after 1 h of UV illumination as compared to 0.10 A.U. for pristine COC (Fig. 9). With BEBD-grafted COC surfaces, the fluorescence signal increased to 0.87 A.U. BEBD diazonium salt was not fluorescent by itself. Therefore there was a complementary effect between COC auto-fluorescence and the polyphenylene film. To improve the understanding of this phenomenon, we grafted different aryl diazonium salts onto COC surfaces for 1 h and monitored the resulting fluorescence signals (Fig. 9). MBD and BBD generated an intense fluorescence signal ranging between 2.0 and 4 A.U. Conversely, NBD and CBD generated a weak fluorescence signal ranging between 0.22 and 0.46 A.U. after 1 h of reaction time. For biosensing application, it is crucial that COC modified with carboxymethylphenyl layers keep low autofluorescence. Then, carboxylated terminated layer will be coupled with amine derivates using EDC/NHS immobilization procedure.

To establish a relationship between fluorescence measurements and chemical surface properties, we analyzed COC surfaces by Raman spectroscopy. We tested pristine COC and light irradiated-COC as controls (Fig. 1). We observed a few bands corresponding to C–H vibration ($2800\text{--}3000\text{ cm}^{-1}$), aliphatic C–C vibration ($2800\text{--}3000\text{ cm}^{-1}$) and alicyclic C–C vibration ($1300\text{--}600\text{ cm}^{-1}$) on both surfaces. No modification of the Raman spectra was induced by light oxidation. After diazonium grafting onto the COC surface, the Raman fluorescent background shifted from 200 A.U. to 6000 A.U. (Fig. 1). Except for this background modification, we observed a few characteristic bands at 1592 cm^{-1} corresponding to aromatic C=C vibration [55] and an additional single peak at 650 cm^{-1} possibly indicating vibration of the carbon–bromide bond [56].

Taking in account all our observations, we demonstrate that it is possible to covalently modify COC surfaces with diazonium salt. Different mechanisms have been suggested to describe the interaction between diazonium and COC surfaces [38]. In our case, the diazonium film was strongly bonded on the COC surface and we observed no IR band corresponding to the diazonium function, whether by IR or XPS analysis. Therefore we can infer that the diazonium film was not adsorbed onto the surface. Using radical traps, Chehimi et al. [43] demonstrated that diazonium reaction with polymers required radical formation. Diazonium reaction with COC was temperature-sensitive, probably due to the thermal sensitivity of the aryl radical. Unlike PMMA or PVC [43,46], the reactivity of the aryl radical was not sufficient for grafting onto a COC surface. Besides, there was no diazonium grafting on COC when its surface was oxidized by light irradiation before the grafting process. Thus, light illumination was required for grafting but not sufficient. Temperature was an important parameter to be controlled, but

not enough to obtain diazonium grafting because no grafting was obtained without light irradiation. Light illumination, controlled temperature and H_3PO_2 had to be combined to obtain satisfactory diazonium grafting.

In our opinion, the growth of the diazonium layer was independent of the surface properties as in the mechanism developed by Chehimi et al. on PMMA [43]. First, the aryl radical was formed, attacked the COC surface to create a bond between the aromatic ring and COC and obtain the first layer of the film. Then, diazonium multilayers were assembled. The growth of the diazonium layer was not homogenous, depending on where the first bond was created on the surface. Thus, we locally observed a few graft-free holes on the surface. It is not quite clear how the radical bonded the surface. Stachowiack et al. suggested that aryl radicals from benzophenone could bond the COC surface by hydrogen ablation when irradiated by UV wavelength [22]. Another mechanism of COC bonding could be to directly link C–H bonds on the COC surface as described for diazonium attacking carbon-based material [52]. Due to the high number of ethyl groups in COC and light requirement, COC probably needs both mechanisms to bond the first diazonium layer.

4. Conclusion

In this paper, we investigate the surface modification of cyclic olefin copolymer by aryl diazonium. Taking advantage of the reactivity of the diazonium radical, we performed a covalent grafting on COC in acidic solution in the presence of a chemical reducer. We tested the influence of temperature, reagent concentration and light irradiation time to provide optimal conditions for the covalent functionalization of the COC surface. We established the best reaction conditions as follows: One hour under UV irradiation with hypophosphorous acid and diazonium solution. Thus a thick layer of diazonium was grafted onto the surface. To show the versatility of the process, we immobilized diazoniums bearing different organic functions on the COC surface. We assessed each modified surface by IR and XPS spectroscopy, contact angle measurements, fluorescence microscopy and AFM. The aryl diazonium grafting was strong enough to withstand ultrasonic treatment, meaning that the aryl diazoniums were covalently grafted onto the COC surface. According to the diazonium we used, we modified wettability, fluorescence emission, roughness and the chemical reactivity of the COC material which is normally inert.

Compared to other treatments, the modification of the surface properties was stable for a few weeks. We observed a correlation between fluorescence intensity of the modified surface and diazonium layer thickness. This point is still under investigation. To our knowledge, this is the first time aryl diazonium has been used to functionalize a COC surface. Using aryl diazonium salt can bring benefits such as versatile chemical groups for post-functionalization, low cost and a fast process. This work give the opportunity to develop biosensor using carboxylated terminated COC surfaces to attach covalently peptide, protein or NH_2 terminated DNA. Our results are encouraging and should open onto new fields of applications for COC surfaces. For instance, aryl diazonium could be used to immobilize biomolecules randomly or with an orientated shape to develop analytical biochips.

Acknowledgments

This work was partially supported by INSA Rouen, Rouen University, CNRS, Labex SynOrg (ANR-11-LABX-0029) and the Haute-Normandie region (CRUNCH network) and Grand Evreux Agglomération.

Appendix A. Supplementary data

Supplementary data associated with this article can be found, in the online version, at <http://dx.doi.org/10.1016/j.apsusc.2014.12.060>.

References

- [1] D. Nikolova, E. Dayss, G. Leps, A. Wutzler, Surface modification of cycloolefinic copolymers for optimization of the adhesion to metals, *Surf. Interface Anal.* 36 (2004) 689–693.
- [2] P.M. Van Midwoud, A. Janse, M.T. Merema, G.M.M. Groothuis, E. Verpoorte, Comparison of biocompatibility and adsorption properties of different plastics for advanced microfluidic cell and tissue culture models, *Anal. Chem.* 84 (2012) 3938–3944.
- [3] I. Saaem, K.-S. Ma, A.N. Marchi, T.H. LaBean, J. Tian, In situ synthesis of DNA microarray on functionalized cyclic olefin copolymer substrate, *ACS Appl. Mater. Inter.* 2 (2010) 491–497.
- [4] Q. Wang, Y. Zhang, H. Ding, J. Wu, L. Wang, L. Zhou, Q. Pu, The use of ethylene glycol solution as the running buffer for highly efficient microchip-Based electrophoresis in unmodified cyclic olefin copolymer microchips, *J. Chromatogr. A* 1218 (2011) 9422–9427.
- [5] M. Castano-Alvarez, M. Fernandez-Abedul, A. Costa-Garcia, Poly(methylmethacrylate) and Topas capillary electrophoresis microchip performance with electrochemical detection, *Electrophoresis* 26 (2005) 3160–3168.
- [6] O. Gustafsson, K.B. Mogensen, J.P. Kutter, Underivatized cyclic olefin copolymer as substrate material and stationary phase for capillary and microchip electrochromatography, *Electrophoresis* 29 (2008) 3145–3152.
- [7] A. Bhattacharyya, C.M. Klapperich, Design and testing of disposable microfluidic chemiluminescent immunoassay for disease biomarkers in human serum samples, *Biomed. Microdevices* 9 (2007) 245–251.
- [8] W.-J. Huang, F.-C. Chang, P.-J. Chu, Functionalization and chemical modification of cyclic olefin copolymers (COC), *Polymer* 41 (2000) 6095–6101.
- [9] J. Zhang, C. Das, H. Fan, Dynamic coating for protein separation in cyclic olefin copolymer microfluidic devices, *Microfluid Nanofluid* 5 (2008) 327–335.
- [10] D. Sung, D.H. Shin, S. Jon, Toward immunoassay chips: facile immobilization of antibodies on cyclic olefin copolymer substrates through pre-activated polymer adlayers, *Biosens. Bioelectron.* 26 (2011) 3967–3972.
- [11] D. Sung, S. Park, S. Jon, Facile immobilization of biomolecules onto various surfaces using epoxide-containing antibiofouling polymers, *Langmuir* 28 (2012) 4507–4514.
- [12] D. Sung, S. Yang, J.W. Park, S. Jon, High-density immobilization of antibodies onto nanobead-coated cyclic olefin copolymer plastic surfaces for application as a sensitive immunoassay chip, *Biomed. Microdevices* 15 (2013) 691–698.
- [13] K.P. Perez-Toralla, J. Champ, M.R. Mohamadi, O. Braun, L. Malaquin, J.-L. Viovy, S. Descroix, New non-covalent strategies for stable surface treatment of thermoplastic chips, *Lab Chip* 13 (2013) 4409–4418.
- [14] M. Geissler, E. Roy, G.A. Diaz-Quijada, J.C. Galas, T. Veres, Microfluidic patterning of miniaturized DNA arrays on plastic substrates, *ACS Appl. Mater. Inter.* 1 (2009) 1387–1395.
- [15] G.A. Diaz-Quijada, R. Peytavi, A. Nantel, E. Roy, M.G. Bergeron, M.M. Dumoulin, T. Veres, Surface modification of thermoplastics – towards the plastic biochip high throughput screening devices, *Lab Chip* (2007) 856–862.
- [16] B. Cortese, M.C. Mowlem, H. Morgan, Characterisation of an irreversible bonding process for COC–COC and COC–PDMS–COC sandwich structures and application to microvalves, *Sens. Actuat. B* 160 (2011) 1473–1480.
- [17] S. Roy, C.Y. Yue, Y.C. Lam, Influence of plasma surface treatment on thermal bonding and flow behavior in cyclic olefin copolymer (COC) based microfluidic devices, *Vacuum* 85 (2011) 1102–1104.
- [18] S. Roy, C.Y. Yue, Surface modification of COC microfluidic devices: a comparative study of nitrogen plasma treatment and its advantages over argon and oxygen plasma treatment, *Plasma Process Polym.* 8 (2011) 432–443.
- [19] Y. Sun, I. Perch-Nielsen, M. Dufva, D. Sabourin, D. Duong Bang, J. Hogberg, A. Wolff, Direct immobilization of DNA probes on non-modified plastics by UV irradiation and integration in microfluidic devices for rapid bioassay, *Anal. Bioanal. Chem.* 402 (2012) 741–748.
- [20] G. Du, Q. Cai, L. Zhao, H. Wei, J. Wang, X. Wang, G. Guo, Q. Pu, Microfluidic patterning of miniaturized DNA arrays on plastic substrates, *Chem. Eng. J.* 195–196 (2012) 132–139.
- [21] G. Emiliyanov, P.E. Hoiby, L.H. Pederson, O. Bang, Selective serial multi-antibody biosensing with TOPAS microstructured polymer optical fibers, *Sensors* 13 (2013) 3242–3251.
- [22] T.B. Stachowiak, T. Rohr, E.F. Hilder, D.S. Peterson, M. Yi, F. Svec, J.M.J. Fréchet, Fabrication of porous monoliths covalently attached to the walls of channels in plastic microdevices, *Electrophoresis* 24 (2003) 3689–3693.
- [23] Y. Ladner, A. Bruchet, G. Crétier, V. Dugas, J. Randon, K. Faure, New “one-step” method for the simultaneous synthesis and anchoring of organic monolith inside COC microchip channels, *Lab Chip* 12 (2012) 1680–1685.
- [24] J.S. Mecomber, R.S. Murthy, S. Rajam, P.N.D. Singh, A.D. Gudmundsdottir, P.A. Limbach, Photochemical functionalization of polymer surfaces for microfabricated devices, *Langmuir* 24 (2008) 3645–3653.
- [25] S. Roy, T. Das, C.Y. Yue, High performance of cyclic olefin copolymer-based capillary electrophoretic chips, *ACS Appl. Mater. Inter.* 5 (2013) 5683–5689.
- [26] J.A. Deverell, T. Rodemann, J.A. Smith, A.J. Canty, R.M. Guijt, UV initiated formation of polymer monoliths in glass and polymer microreactors, *Sens. Actuat. B* 155 (2011) 388–396.
- [27] T. Rohr, F. Ogletree, F. Svec, J.M.J. Fréchet, Surface functionalization of thermoplastic polymers for the fabrication of microfluidic devices by photoinitiated grafting, *Adv. Funct. Mater.* 13 (2003) 264–270.
- [28] Q. Pu, O. Yesanya, B. Thompson, S. Liu, J.C. Alvarez, On-chip micropatterning of plastic (cyclic olefin copolymer, COC) microfluidic channels for the fabrication of biomolecule microarrays using photografting methods, *Langmuir* 23 (2007) 1577–1583.
- [29] Y. Ladner, G. Crétier, K. Faure, Electrochromatography on acrylate based monolith in cyclic olefin copolymer microchip: a cost-effective and easy-to-use technology, *Electrophoresis* 33 (2012) 3087–3094.
- [30] Y. Oztekin, Z. Yazicigil, A.O. Solak, Z. Ustundag, A. Okumus, Z. Kilic, A. Ramanaviciene, A. Ramanavicius, Phenanthroline derivatives electrochemically grafted to glassy carbon for Cu(II) ion detection, *Sens. Actuat. B: Chem.* 166–167 (2012) 117–127.
- [31] J. Ghilane, P. Martin, H. Randriamahazaka, J.C. Lacroix, Electrochemical oxidation of primary amine in ionic liquid media: formation of organic layer attached to electrode surface, *Electrochim. Commun.* 12 (2010) 246–249.
- [32] Andrew R. Davis, Kenneth R. Carter, Surface grafting of vinyl-functionalized poly(fluorene)s via thiolene click chemistry, *Langmuir* 30 (2014) 4427–4443.
- [33] C. Bureau, J. Pinson, Use of diazonium salt in a method for modifying insulating or semi-conductive surfaces and resulting products, *PCT Int. Appl.* (2005), WO2007 048894.
- [34] S. Gam-Derouich, S. Mahouche-Chergui, M. Turmine, J.Y. Piquemal, M. Ben-Hassen-Chehimi, M. Osmatova, M.M. Chehimi, A versatile route for surface modification of carbon, metals and semi-conductors by diazonium salt-initiated photopolymerization, *Surf. Sci.* 605 (2011) 1889–1899.
- [35] G. Liu, T. Böcking, J.J. Gooding, Diazonium salts: stable monolayers on gold electrodes for sensing applications, *J. Electroanal. Chem.* 600 (2007) 335–344.
- [36] X. Zhang, A. Tretjakov, M. Hovestaedt, G. Sun, V. Syritski, J. Reut, R. Volkmer, K. Hinrichs, J. Rappich, Electrochemical functionalization of gold and silicon surfaces by maleimide group towards biosensor for immunological application, *Acta Biomater.* 9 (2013) 5838–5844.
- [37] T. Berthelot, A. Garcia, X.T. Le, J. El Morsi, P. Jegou, S. Palacin, P. Viel, Versatile toolset for DNA or protein immobilization: toward a single-step chemistry, *Appl. Surf. Sci.* 257 (2001) 3538–3546.
- [38] S. Mahouche-Chergui, S. Gam-Derouich, C. Mangeney, M.M. Chehimi, Aryl diazonium salts: a new class of coupling agents for bonding polymers, biomacromolecules and nanoparticles to surfaces, *Chem. Soc. Rev.* 40 (2011) 4143–4166.
- [39] V. Mévellec, S. Roussel, L. Tessier, J. Chancalon, M. Maryne-L’Hermite, G. Deniau, P. Viel, S. Palacin, Grafting polymers on surfaces: a new powerful and versatile diazonium salt-based one-step process in aqueous media, *Chem. Mater.* 19 (2007) 6323–6330.
- [40] A. Garcia, N. Hanifi, B. Joussetme, P. Jégou, S. Palacin, P. Viel, T. Berthelot, Polymer grafting by inkjet printing: a direct chemical writing toolset, *Adv. Funct. Mater.* 23 (2013) 3668–3674.
- [41] A. Garcia, J. Polesel-Maris, P. Viel, S. Palacin, T. Berthelot, Localized ligand induced electroless plating (LEP) process for the fabrication of copper patterns onto flexible polymer substrates, *Adv. Funct. Mater.* 21 (2011) 2096–2102.
- [42] A. Garcia, T. Berthelot, P. Viel, A. Mesnage, P. Jégou, F. Nekelson, S. Palacin, ABS polymer electroless plating through a one-step poly(acrylic acid) covalent grafting, *ACS Appl. Mater. Inter.* 2 (2010) 1173–1183.
- [43] M. Chehimi, A. Lamouri, M. Picot, J. Pinson, Surface modification of polymers by reduction of diazonium salts: polymethylmethacrylate as an example, *J. Mater. Chem. C* 2 (2014) 356–363.
- [44] M. Khoshroo, A.A. Rostami, Characterization of the organic molecules deposited at gold surface by the electrochemical reaction of diazonium salts, *J. Electroanal. Chem.* 647 (2010) 117–122.
- [45] M. Herrmann, T. Verses, M. Tabrizian, Surface modification and characterization of a cyclic olefin copolymer for magnetic bead-based stop-flow microfluidic ELISA, in: M. Laudon (Ed.), *Technical Proceedings of the 2006 NSTI*, Vol. 2, Boston, May 7–11, Taylor and Francis, 2007.
- [46] M. Bouriga, M.M. Chehimi, C. Combellas, P. Decorse, F. Kanoufi, A. Deronzier, J. Pinson, Sensitized photografting of diazonium salts by visible light, *Chem. Mater.* 25 (2013) 90–97.
- [47] M. Busson, A. Berisha, C. Combellas, F. kanoufi, J. Pinson, Photochemical grafting of diazonium salts on metals, *Chem. Commun.* 47 (2011) 12631–12633.
- [48] S. Milanesi, M. Fagnoni, A. Albinì, The formation of radicals has been reported during the photosensitized (xanthone) cleavage of diazonium salts, *J. Org. Chem.* 70 (2005) 603–610.
- [49] V.T. Faerman, G.V. Goryachko, G.L. Slonimskii, Effect of ultrasonic vibrations of polymer films, *Polym. Sci. U.S.S.R.* 7 (1965) 1347–1353.
- [50] P. Abiman, G.G. Wildgoose, R.G. Compton, Investigating the mechanism for the covalent chemical modification of multiwalled carbon nanotubes using aryl diazonium salts, *Int. J. Electrochim. Sci.* 3 (2008) 104–117.
- [51] A. Laforgue, T. Addou, D. Bélanger, Characterization of the deposition of organic molecules at the surface of gold by the electrochemical reduction of aryl diazonium cations, *Langmuir* 21 (2005) 6855–6865.
- [52] P. Doppelt, G. Hallais, J. Pinson, F. Podvorica, D. Verneyre, Surface modification of conducting substrates. Existence of azo bonds in the structure of organic layers obtained from diazonium salts, *Chem. Mater.* 19 (2007) 4570–4575.

- [53] N. Wade, T. Pradeep, J. Shen, R.G. Cooks, Covalent chemical modification of self-assembled fluorocarbon monolayers by low-energy CH_2Br_2^+ ions: a combined ion/surface scattering and X-ray photoelectron spectroscopic investigation, *Rapid Commun. Mass Spectrom.* 13 (1999) 986–993.
- [54] S.-E. Yoo, Y.-D. Gong, J.-S. Seo, M.M. Sung, S. Lee, Y. Kim, X-ray photoelectron spectroscopy analysis of solid-phase reactions using 3-brominated Wang resin, *J. Comb. Chem.* 1 (1999) 177–180.
- [55] P. Actis, G. Cailliez, G. Shul, M. Opallo, M. Mermoux, B. Marcus, R. Boukherroub, S. Szunerits, Functionalization of glassy carbon with diazonium salts in ionic liquids, *Langmuir* 24 (2008) 6327–6333.
- [56] D. Lin-Vien, N.B. Cothup, W.G. Fateley, J.G. Grasselli, *The Handbook of Infrared and RAMAN Characteristic Frequencies of Organic Molecules*, London, Academic Press, 1991, pp. 1–501.

P24



Glycerophospholipid synthesis and functions in *Pseudomonas*

Tatiana Kondakova^a, François D'Heygère^b, Marc J. Feuilloley^a, Nicole Orange^a, Hermann J. Heipieper^c, Cécile Duclairoir Poc^{a,*}

^a Normandie University of Rouen, Laboratory of Microbiology Signals and Microenvironment (LMSM), EA 4312, 55 rue St. Germain, 27000 Evreux, France

^b Centre de Biophysique Moléculaire, CNRS, UPR4301, rue Charles Sadron, 45071 Orléans, France

^c Department of Environmental Biotechnology, UFZ Helmholtz Centre for Environmental Research, Permoserstr. 15, 04318 Leipzig, Germany

ARTICLE INFO

Article history:

Received 27 March 2015

Received in revised form 29 June 2015

Accepted 30 June 2015

Available online 3 July 2015

Keywords:

Biosynthesis

Lipidomics

Membranes

Phospholipids

Phosphatidylcholine

Lineage

Host

Interactions

ABSTRACT

The genus *Pseudomonas* is one of the most heterogeneous groups of eubacteria, presents in all major natural environments and in wide range of associations with plants and animals. The wide distribution of these bacteria is due to the use of specific mechanisms to adapt to environmental modifications. Generally, bacterial adaptation is only considered under the aspect of genes and protein expression, but lipids also play a pivotal role in bacterial functioning and homeostasis. This review resumes the mechanisms and regulations of pseudomonal glycerophospholipid synthesis, and the roles of glycerophospholipids in bacterial metabolism and homeostasis. Recently discovered specific pathways of *P. aeruginosa* lipid synthesis indicate the lineage dependent mechanisms of fatty acids homeostasis. *Pseudomonas* glycerophospholipids ensure structure functions and play important roles in bacterial adaptation to environmental modifications. The lipidome of *Pseudomonas* contains a typical eukaryotic glycerophospholipid – phosphatidylcholine –, which is involved in bacteria–host interactions. The ability of *Pseudomonas* to exploit eukaryotic lipids shows specific and original strategies developed by these microorganisms to succeed in their infectious process. All compiled data provide the demonstration of the importance of studying the *Pseudomonas* lipidome to inhibit the infectious potential of these highly versatile germs.

© 2015 Elsevier Ireland Ltd. All rights reserved.

Contents

1. Introduction	28
2. Pseudomonas lipid synthesis and functions	29
2.1. Fatty acid biosynthesis	29
2.1.1. Acyl carrier protein	29
2.1.2. Initiation of fatty acid biosynthesis	30
2.1.3. Elongation module	31
2.1.4. Introduction of the double bond	33
2.2. Transfer to the membrane	33
3. Glycerophospholipid biosynthesis and functions in <i>Pseudomonas</i>	34
3.1. Glycerophospholipid head group diversity	34
3.2. Phosphatidylethanolamine production and functions	36
3.3. Phosphatidylglycerol synthesis and functions	36
3.4. Cardiolipin biosynthesis and functions	36

Abbreviations: ACP, acyl carrier protein; AHL, N-acyl homoserine lactone; CDP, cytidine diphosphate; CL, cardiolipin; FAS, fatty acid synthesis; GP, glycerophospholipid; HG, head group; HPTLC, high performance thin-layer chromatography; IM, inner membrane; LPA, lysophosphatidic acid; LPS, lipopolysaccharide; MSI, mass spectrometry imaging; OM, outer membrane; PA, phosphatidic acid; PC, phosphatidylcholine; PE, phosphatidylethanolamine; PG, phosphatidylglycerol; PGP, phosphatidylglycerol phosphate; PI, phosphoinositide; PIP, phosphatidylinositol phosphate; PI(4,5)P2, phosphatidylinositol 4,5-bisphosphate; PI(3,4,5)P3, phosphatidylinositol 3,4,5-trisphosphate; PLD, phospholipase D; PS, phosphatidylserine; T3SS, type 3 secretion system; T6SS, type 6 secretion system.

* Corresponding author at: Laboratory of Microbiology Signals and Microenvironment (LMSM) EA 4312, Normandie Université, University of Rouen, 55 rue Saint Germain, 27000 Evreux, France. Fax: +33 232291550.

E-mail address: cecile.poc@univ-rouen.fr (C. Duclairoir Poc).

3.5. Phosphatidylcholine synthesis in <i>Pseudomonas</i>	36
4. Exploitation of host glycerophospholipids by <i>Pseudomonas</i>	37
4.1. Phosphoinositide signaling and <i>Pseudomonas</i>	37
4.2. Eukaryotic phosphatidylcholine exploitation	37
4.3. <i>Pseudomonas</i> lipids as a target for a new antibiotic development	38
5. Conclusions and perspectives	38
Acknowledgements	38
References	38

1. Introduction

The genus *Pseudomonas* is one of the most heterogeneous groups of eubacteria. These bacteria are found in all natural environments (Ringen and Drake, 1952), like water (Mena and Gerba, 2009), soil (Couillerot et al., 2009; Kiely et al., 2006) and air (Duclairoir Poc et al., 2014; Morris et al., 2007) and also in association with plants and animals. Some *Pseudomonas* species are of medical importance and count among the principal human opportunistic pathogens (Driscoll et al., 2007). The concept of *Pseudomonas* diversity originates from the biochemical studies of Stanier et al. 1966, who performed a comparative study on the growth characteristics of 267 strains on 146 different organic compounds and a wide range of physiological tests. Since their initial designation at the end of the nineteenth century and their taxonomic redefinition by Palleroni, many species have been classified in other genus (Palleroni, 2010) and, nowadays, the genus *Pseudomonas* is divided in two major lineages represented by typical species, namely *Pseudomonas aeruginosa* and *Pseudomonas fluorescens* (Mulet et al., 2010; Palleroni, 2010). The *P. aeruginosa* lineage is the most homogeneous and consists predominantly of the *P. aeruginosa* species. The *P. fluorescens* lineage is much more diverse and is by itself separated in 3 major groups: *P. fluorescens*, *Pseudomonas putida* and *Pseudomonas syringae* (Mulet et al., 2010).

The members of *P. aeruginosa* lineage are generally found in riparian soil associated with decaying plants (Jones et al., 2013; Ringen and Drake, 1952; Vasil and Ochsner, 1999). However, *P. aeruginosa* group includes important opportunistic pathogens, particularly involved in nosocomial infections in immunocompromised hosts and in cystic fibrosis (Driscoll et al., 2007). *P. aeruginosa* infections are always difficult to treat due to the natural resistance of this bacterium (Obritsch et al., 2005). Consequently, a therapy with two or three antimicrobial agents is typically used (Lodise et al., 2007; Szaff et al., 1983; Valerius et al., 1991). Thus, the utilization of antibiotics uncommonly used in clinical practice, such as polymyxins like colistin, is recommended (Gunderson et al., 2003; Sabuda et al., 2008). Bacteria of the *P. fluorescens* lineage are found preferentially in soil and in association with plants (Bodilis et al., 2006; Loper et al., 2012). Members of the *P. putida* group show an adaptation to various ecological niches and are characterized by their adaptation to grow in soils and sediments contaminated with high concentrations of heavy metals and organic contaminants (Hachicho et al., 2014; Heipieper et al., 1996; Ramos et al., 1997; Wu et al., 2011). Members of the *P. syringae* group are plant pathogens. *P. syringae* is well known for its capacity to grow epiphytically on diverse plants and for its ice-nucleation activity (Joardar et al., 2005; Kozloff et al., 1984; McCann et al., 2013). Recently, strains of *P. syringae*, virulent on diverse species of crop plants, were isolated from epilithic biofilms of rivers (Morris et al., 2007) and clouds at several kilometers altitude (Amato et al., 2007) outside the zones of agricultural production (Morris et al., 2008). Bacteria of the *P. fluorescens* group commonly found in soil (Bodilis et al., 2006) and water (Janek et al., 2010) are also able to develop in air (Duclairoir Poc et al., 2014; Kondakova et al., 2014). Some of *P. fluorescens*

group members, adapted to the human temperature are members of the skin microbiota or behave as opportunistic pathogens (Chapalain et al., 2008).

The wide distribution of *Pseudomonas* suggests a remarkable degree of physiological and genetic adaptability. Physiologically, bacterial adaptability to ecological niches and environmental modifications depends essentially on the structure and organization of their envelope. Most protective membrane functions, as osmotic or heat shock response, are traditionally attributed to proteins that are immersed in the lipid bilayer (Allan et al., 1988; Gotoh et al., 1989), but the lipids are not only a matrix to accommodate proteins but play a major role in bacterial functioning (Boughton and Pollock, 1953; Lindgren et al., 1977). As in the case of proteins, bacteria have the capacity to adjust their membrane lipid composition in response to environmental modifications (Cullen et al., 1971; Fang et al., 2000; Parsons and Rock, 2013; Pepi et al., 2008; Ramos et al., 1997). This is especially true in Gram-negative bacteria, like *Pseudomonas*, because of their double envelope with outer and inner membranes. Although a considerable diversity of lipid structures exists in the bacterial world, most predominant lipids in *Pseudomonas* membranes are glycerophospholipids (GPs). GPs are defined as acylated derivatives of *sn*-glycerol-3-phosphate composed of two fatty acid chains, a glycerol unit and a phosphate group linked to a polar head group (Zhang and Rock, 2008). The variety of chemical structures and functions of GPs is due to the polar head group (HG) and fatty acid (FA) composition. GP polar HGs determine the membrane properties and associated functions, such as the barrier function to prevent the entry of noxious compounds and the passive and active influx of nutrient molecules (Sutterlin et al., 2014; Heath et al., 2002a,b). They influence membrane-related processes such as protein export and DNA replication (Nikaido, 2003). Adjustments in FA composition are related to the formation of *trans*-unsaturated or cyclopropylated FAs. Formation of unsaturated or cyclopropylated FAs by *Pseudomonas* occurs in response to osmotic stress, solvent exposition and temperature adaptation, and are interpreted as a mechanism that modifies the permeability of the GP bilayer to minimize energy expenditure and optimize growth (Heipieper et al., 1996; Pepi et al., 2008). The recent identification of lipid signaling molecules and the involvement of GPs in bacteria/eukaryotes interactions (Sato and Frank, 2014; Vromman and Subtil, 2014) demonstrate the key role of lipids apart from cell wall. GP synthesis, composition and functions in bacterial cells were determined early in bacterial lipid metabolism and homeostasis studies realized particularly on the *Escherichia coli* lipidome (Guchhait et al., 1974; Heath and Rock, 1995; Larson et al., 1984; Parsons and Rock, 2013; Wang and Cronan, 2004). However, the high ability of *Pseudomonas* to adapt to various ecological conditions could suppose the involvement of other specific mechanisms of GP homeostasis. This review is aimed at organizing the wealth of information on GP metabolism and homeostasis in *Pseudomonas*. These data provide important insights into the mechanism and the regulation of bacterial GP synthesis, role of GPs in bacterial metabolism and homeostasis as well as in host-bacteria interactions.

2. Pseudomonas lipid synthesis and functions

2.1. Fatty acid biosynthesis

Fatty acid synthesis (FAS) in *Pseudomonas* spp. is conducted by the type II FA synthetic pathway. FAS II is found in bacteria, plants and eukaryotic parasites. This mechanism is divided in individual steps wherein each component is encoded by a separate gene that produces a unique protein, catalyzing a single step in the pathway (Heath et al., 2002a,b). Proteins in this pathway are located in the cytosol, and each has been purified and biochemically characterized (White et al., 2005). In FAS II enzymes, the active sites are usually not located on the protein surface but within a deep cavity. These active sites are connected to the protein surface through narrow tunnel. The enzymatic activity and substrate specificity are dependent on the size and the shape of the tunnels and active site chemistry (Biedermannova et al., 2012; White et al., 2005).

2.1.1. Acyl carrier protein

The major player of FA biosynthesis in bacterial cells is the acyl carrier protein (ACP). It is a small protein (about 9 kDa) containing the prosthetic group 4'-phosphopantetheine (White et al., 2005; Zhang and Rock, 2008). The ACP is produced by *acpP* gene as the apoprotein. ACP is one of the most abundant proteins in the cell and is converted to its active form by ACP-synthase (AcpS). AcpS transfers the 4'-phosphopantetheine prosthetic group from CoA to apo-ACP (White et al., 2005). The 4'-phosphopantetheine prosthetic group of ACP injects the substrate into tunnels for catalysis. ACP interacts specifically and transiently with all of the enzymes of FAS. The negative residues of ACP (its prosthetic group sulphydryl) interact with a patch of positive superficial residues of the FAS enzymes (Heath et al., 2002a,b). The ACP of *P. aeruginosa* was successively purified and characterized by Kutchma and coworkers (Kutchma et al., 1999). In addition to GP synthesis, ACP plays an essential role in synthesis of rhamnolipids, and in a broad range of other biosynthetic reactions of acyl transfer (nonribosomal peptide and depsipeptide biosynthesis). ACP is a precursor of oligosaccharides and proteins transacylation (Kutchma et al., 1999; White

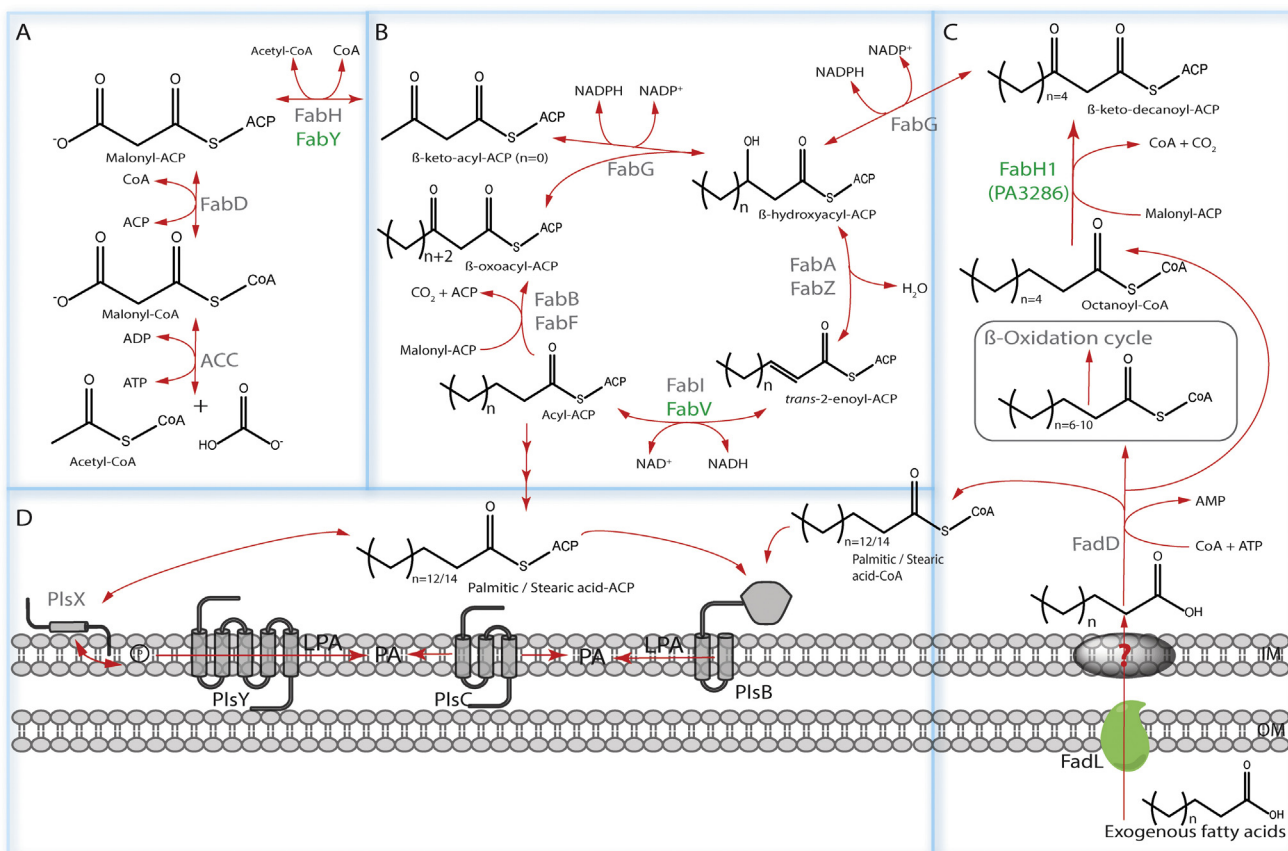


Fig. 1. Proposed pathway of fatty acid synthesis in *Pseudomonas* spp.

(A) Initiation module: the acetyl-CoA carboxylase (ACC) generates malonyl-CoA via the carboxylation of acetyl-CoA. The malonyl group is transferred to the acyl carrier protein (ACP) by malonyl-CoA:ACP acyltransferase (FabD). The initiation of the new acyl chain formation is performed by condensation of malonyl-ACP with acetyl-CoA by β-ketoacyl-ACP synthase III (FabY, PA 5174 for *P. aeruginosa* – green color – and potential FabH enzymes for *Pseudomonas* strains).

(B) Elongation module: the NADPH-dependent β-ketoacyl-ACP reductase (FabG) reduces obtained previously ketoester, and a water molecule is removed by β-hydroxyacyl-ACP dehydrases (FabA and FabZ). Then, enoyl-ACP reductases (FabI for all *Pseudomonas* spp. and FabV for *P. aeruginosa*) complete the cycle. The new cycle of elongation is initiated by β-ketoacyl-ACP synthase I and II (FabB and FabF).

(C) Incorporation of exogenous fatty acids: after diffusion across the outer membrane through FadL protein, FA is retained by FadD enzymes catalyzed esterification of FA with CoA. Further metabolism depends on acyl-CoA ester chain length. Long chains C₁₆/C₁₈-CoA esters can be incorporated directly into de novo GPs by the glycerol-phosphate and acylglycerol-phosphate acyltransferases PlsB/PlsC. Medium C₁₀ to C₁₄ acyl-CoA esters are degraded in the β-oxidation cycle. C₈-CoA esters are intercepted by FabH1 (PA3286) enzyme and condensed with malonyl-ACP to form the β-keto-decanoyl-ACP.

(D) Transfer to the membrane: C₁₆/C₁₈ fatty acids chains are transferred to the membrane by acyltransferases. The PlsB enzyme catalyzes the acylation of the sn-1-position of glycerol-3-phosphate to form lysophosphatidic acid (LPA). Alternatively, PlsX transfers the acyl group to inorganic phosphate to form reactive acylphosphate intermediate, which is acylated in sn-1-position by the integral plasma-membrane protein PlsY to form LPA. Next, PlsC transfers a FA to the sn-2-position of LPA to form phosphatidic acid (PA). OM: outer membrane; IM: inner membrane.

et al., 2005). Acyl-ACP is an acyl donor for synthesis of *N*-acyl homoserine lactones (AHLs) of the quorum sensing mechanism (Gould et al., 2004).

2.1.2. Initiation of fatty acid biosynthesis

2.1.2.1. Acetyl-CoA carboxylase and FabD acyltransferase. The acetyl-CoA-carboxylase (ACC) performs the first step of FAS in *Pseudomonas*. The malonyl-coenzyme A (malonyl-CoA) is generated through the carboxylation of acetyl-CoA (Fig. 1A) (Parsons and Rock, 2013). The ACC is a four-subunit complex consisting in a biotin carboxylase (AccC), a biotin carboxyl carrier protein (AccB), and two carboxyltransferases (AccAD) (Table 1) (Guchhait et al., 1974). This enzyme complex governs the quantity of produced FA to maintain a normal lipid/protein ratio. The organization of genes encoding the component enzyme activities of ACC varies in different organisms. In *E. coli*, the accAD and the

accBC genes are cotranscribed (Kondo et al., 1991; Li and Cronan, 1992). In *P. aeruginosa*, accBC genes are organized in one operon, and accA and accD are found in different regions of chromosome (Best and Knauf, 1993). Upon synthesis, the malonyl-CoA is transferred to ACP by a malonyl-CoA:ACP transacylase (FabD) (Fig. 1A, Table 1). The gene coordinating the production of FabD protein belongs to the fab gene cluster of *P. aeruginosa* (Kutchma et al., 1999).

2.1.2.2. Role of FabH and FabY in determining fatty acids structure in *Pseudomonas*. The following step of FAS is the initiation of new acyl chain formation by condensation of malonyl-ACP with a short-chain acyl-CoA (Fig. 1A). Usually, in γ -proteobacteria, this reaction is catalyzed by FabH enzyme. The known sequences of FabH vary according to the bacterial species, but are characterized by a conserved Cys-His-Asn catalytic triad and utilization of a ping-pong mechanism (Davies et al., 2000; Qiu et al., 1999; White et al.,

Table 1

Genes, enzymes and functions in fatty acid and glycerophospholipid synthesis.

Gene	Enzyme activity	Functions	References
acpP	Acyl carrier protein (ACP)	Production of ACP	(White et al., 2005; Kutchma et al., 1999;
accC	Acetyl-CoA carboxylase biotin carboxylase subunit (AccC)	ATP-dependent transfer of CO ₂ from bicarbonate to biotin attached to AccB	Best and Knauf, 1993)
accB	Acetyl-CoA carboxylase biotin carboxyl carrier protein subunit (AccB)	Transfer of the carboxy-biotin intermediate to the transcarboxylase enzyme composed of AccA and AccD subunits	
accA	Acetyl-CoA carboxylase carboxyl transferase (α -subunit) (AccA)	Transfer of the CO ₂ from carboxybiotin to acetyl-CoA	
accD	Acetyl-CoA carboxylase, carboxyl transferase (β -subunit) (AccD)	Transfer of the CO ₂ from carboxybiotin to acetyl-CoA	
fabD	Malonyl-CoA:ACP transacylase (FabD)	Transfer of malonyl-CoA to the ACP	(White et al., 2005; Kutchma et al., 1999)
PA3333 (fabH2)	β -Ketoacyl ACP synthase III (FabH2)	Unknown functions	(Davies et al., 2000; Yuan et al., 2012a; Yuan et al., 2012b; Six et al., 2014; Zhang and Rock, 2012)
PA3286	β -Ketoacyl ACP synthase III (FabH1)	Channelling of 8-carbon acyl-CoA intermediates	
PA5174	β -Ketoacyl ACP synthase (FabY)	Condensation of malonyl-ACP with a short-chain acyl-CoA	
fabB	β -Ketoacyl-ACP synthase I (FabB)	Complementation of acyl-ACP by two-carbon unit from malonyl-ACP	(Garwin et al., 1980; Hoang and Schweizer, 1997)
		Essential enzyme for unsaturated FAS, elongating <i>cis</i> -3-decenoyl-ACP	
fabF	β -Ketoacyl-ACP synthase II (FabF)	Complementation of acyl-ACP by two-carbon unit from malonyl-ACP Temperature-dependent production of <i>cis</i> -unsaturated FA	
fabG	3-Ketoacyl-ACP- reductase (FabG)	Reduction of ketoester to obtain the hydroxyacyl-ACP	(Fisher et al., 2000; Price et al., 2001; Ren et al., 2000)
fabA	β -Hydroxydecanoyl-ACP dehydrase (FabA)	Dehydration of hydroxyacyl-ACP to <i>trans</i> -2-ACP	(Hoang and Schweizer, 1997; Mohan et al., 1994)
fabZ	(3R)-Hydroxymyristoyl-ACP dehydratase (FabZ)	Isomerization of <i>trans</i> -2 to <i>cis</i> -3-decenoyl ACP	
fabI	NADH-dependent enoyl-ACP reductase (FabI)	Dehydration of hydroxyacyl-ACP to <i>trans</i> -2-ACP	
fabV	NADH-dependent enoyl-ACP reductase (FabV)	Formation of saturated fatty acid chains	(Zhu et al., 2010; Massengo-Tiassé and Cronan, 2008)
desA	Δ -9 fatty acid desaturase (DesA)	Introduction of double bond into acyl chains previously attached to phospholipids	(Zhu et al., 2006; Subramanian et al., 2010)
desB	Acyl-CoA Δ -9-desaturase (DesB)	Introduction of a double bond into saturated acyl-CoA specifically at the 9-position	
plsB	Glycerol-3-phosphate acyltransferase (PlsB)	Acylation of the 1-position of glycerol-3-phosphate, formation of LPA	(Röttig and Steinbüchel, 2013; Lu et al., 2007; Cronan and Bell, 1974; Yoshimura et al., 2007)
plsC	1-Acyl-sn-glycerol-3-phosphate acyltransferase (PlsC)	Formation of PA	
plsY	Glycerol-3-phosphate acyltransferase (PlsY)	Acylation of the 1-position of glyceril-3-phosphate, formation of LPA	
plsX	Glycerol-3-phosphate acyltransferase (PlsX)	Transfer of acyl group to inorganic phosphate to form reactive acylphosphate intermediate	
pssA	Phosphatidylserine synthase (PssA)	Condensation of CDP-diacylglycerol with serine, formation of PS	(Shi et al., 1993; Mileykovskaya and Dowhan, 1997)
psd	Phosphatidylserine decarboxylase (Psd)	Decarboxylation of PS, formation of PE	
pgsA	CDP-diacylglycerol-glycerol-3-phosphate 3-phosphatidyltransferase (PgsA)	Condensation of CDP-diacetylgluceral with glycerol phosphate, formation of PGP	(Heath et al., 2002a,b; Kikuchi et al., 2000; Suzuki et al., 2002)
pgpA	Phosphatidylglycerophosphatase A (PgpA)	Dephosphorylation of PGP, formation of PG	
cls	Cardiolipin synthetase (Cls)	Condensation of two PG molecules, formation of CL	(Heath et al., 2002a,b; Bernal et al., 2007)
pcs	Phosphatidylcholine synthase (Pcs)	Condensation of choline with CDP-diacylglycerol, formation of PC	(Geiger et al., 2013; Wilderman et al., 2002)

2005). FabH selectively utilizes acetyl-CoA derived from intermediary metabolism (Parsons and Rock, 2013). Only thioesters with less than four carbons are able to pass FabH active site tunnel in *E. coli* (White et al., 2005). The FabH enzyme has many similarities with FabB and FabF condensation enzymes of elongation module, which add a two-carbon unit from malonyl-ACP to growing acyl-ACP (see part Elongation module) (Parsons and Rock, 2013). The most important difference between these three enzymes is the configuration of the active site: Cys-His-His triade for FabB/FabF, and Cys-His-Asn for FabH (Davies et al., 2000). *fabH* is an essential gene for bacterial FA synthesis, thus it is a target for antibacterial development (Castillo and Pérez, 2008; Davies et al., 2000; Lai and Cronan, 2003; Zhang and Cronan, 1998). Most bacteria have a single FabH enzyme. However, in *P. aeruginosa* the FAS initiation is carried out by another enzyme PA5174, named FabY. This condensing enzyme performs a task usually attributed to FabH but uses a Cys-His-His active site of FabB/FabF enzymes (Yuan et al., 2012b). The *fabY* mutant is still viable indicating a possible alternative secondary mechanism of FAS in *P. aeruginosa* (Yuan et al., 2012a). It exhibits a growth defect and a decreased production of quorum sensing signaling molecules, rhamnolipids and siderophores (Yuan et al., 2012b). The *fabY* mutant is susceptible to a number of antibiotics, including certain β -lactams (Six et al., 2014). The study of one of *E. coli* FabH ortholog in *P. aeruginosa* (FabH1-PA3286) showed that this enzyme plays a unique role in channeling of C₈ acyl-CoA intermediates arising from FA β -oxidation (Fig. 1C green color, Table 1). Yuan and colleagues proposed that *P. aeruginosa* can incorporate exogenous FAs with C₈ via PA3286 catalysis. In this pathway exogenous FAs, intercepted by Fad enzymes, are condensed with malonyl-ACP using PA3286 to make the FAS intermediate β -keto-decanoyl-ACP (Figure 1/C) (Yuan et al., 2012a). This case of direct utilization of long-chain acyl-CoA has been demonstrated also for *E. coli* (Black et al., 2000), *Mycobacterium tuberculosis* during the synthesis of mycolic acids (Choi et al., 2000) or *Rhodococcus opacus* (Holder et al., 2011). Structural characterization of PA3286 is needed to shed more light upon how this enzyme catalyzes the reactions with long acyl chains.

The initiation of FAS in *P. fluorescens* lineage is poorly documented. We have found the open reading frames (ORF) coding FAS enzymes in genomes of five *Pseudomonas* type strains

(*P. aeruginosa* PAO1, *P. fluorescens* Pf0-1, *P. putida* KT2440, *P. fulva* 12-X, and *P. syringae* pv. *theiae*). Fig. 2 shows a phylogenetic distribution of protein translated from these ORFs. We observed that FabB and FabF have two FAS domain protein clusters well conserved among *P. aeruginosa* and *P. fluorescens* lineages. These enzymes are representatives from all five analyzed *Pseudomonas* strains, consistent with their role in FAS elongation. The FabY enzyme is not conserved suggesting strain specific role(s) outside primary FAS metabolism. The distribution of FabY in *Pseudomonas* is confined to *P. aeruginosa* PAO1 and *Pseudomonas fulva* 12-X (member of the *P. putida* group). Conversely, no *fabY* ortholog was detected in *P. putida*, *P. fluorescens*, and *P. syringae*. This indicates that this alternative metabolism observed for *P. aeruginosa* should be also active in specific members of the *P. putida* group such as *P. fulva*. However, supplementary studies are necessary to support this thesis. It is likely that FAS domain proteins should be also involved (Yuan et al., 2012b). Indeed, we found annotated sequences to *fabH* in all studied *Pseudomonas* strains. FabH proteins present two major and divergent clusters. The FabH1 enzyme was studied in *P. aeruginosa* (FabH1-PA3286) and was discussed above (Fig. 1). *fabH1* orthologous gene sequences were found in all studied *Pseudomonas* strains. This could indicate the ability of these *Pseudomonas* strains to intercept long C₈ acyl-CoA chains. Surprisingly, three strains (*P. putida* KT2440, *P. fluorescens* Pf0-1, *P. aeruginosa* PAO1) have more than one *fabH* annotated sequence (FabH2, Fig. 2). The role of FabH2 is unknown in the absence of biochemical studies of this enzyme (Zhang and Rock, 2012). Therefore, we can suppose this enzyme is involved in alternative metabolic pathway(s).

2.1.3. Elongation module

The iterative cycle of acyl chain elongation is divided in four steps catalyzed by six enzymes. In the first step, β -ketoacyl-ACP synthase I and II (FabB and FabF) complement the growing of acyl-ACP by two-carbon unit to form malonyl-ACP (Fig. 1B). The resulting ketoester is reduced by a NADPH-dependent β -ketoacyl-ACP reductase (FabG), and a water molecule is then removed by a β -hydroxyacyl-ACP dehydrases (FabA and FabZ) (Fig. 1B). The last step is catalyzed by enoyl-ACP reductases (FabI/FabV) to form a saturated acyl-ACP, which in turn serves as a substrate for another

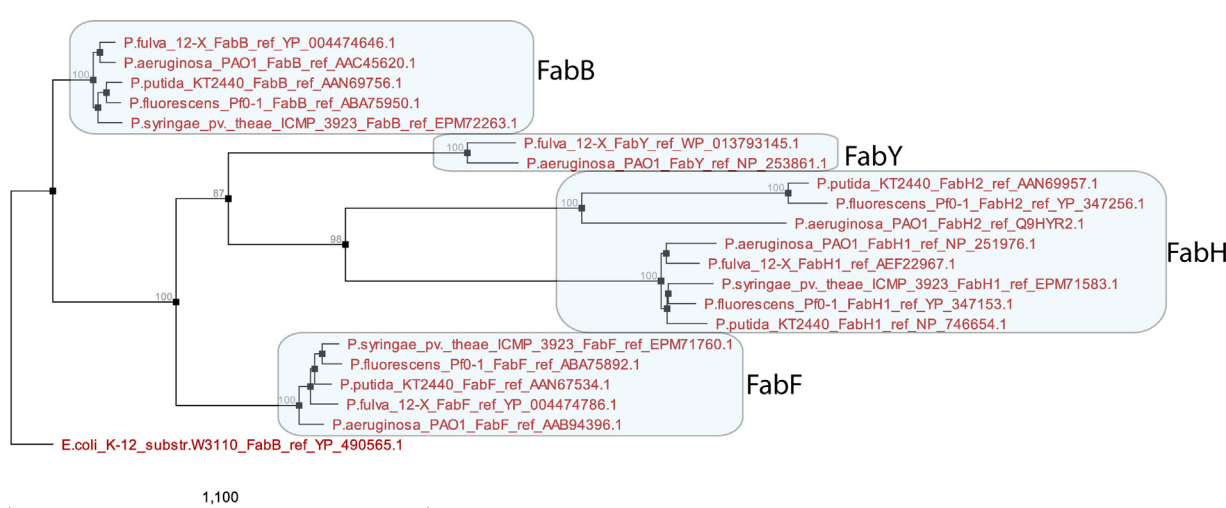


Fig. 2. Phylogenetic analysis of FabB/FabF, FabH and FabY proteins among *Pseudomonas* type strains.

A phylogenetic tree, based on protein sequences translated from open reading frames found in selected *Pseudomonas* genomes was established. Sequences coding FAS domain clusters were found in databases and analyzed using the neighbor-joining method. Analyses were conducted by using CLC Sequence Viewer 7 (CLC bio, a QIAGEN Company, Denmark). The branches of the tree are labeled by the strain name and reference in NCBI database. The percent value of the bootstrap support is present in all nodes of tree. To scale the tree, branch lengths are calculated corresponding to the number of amino acid substitutions per site. The four main clusters (FabB, FabF, FabH and FabY) are indicated in blue squares. The FabB of *E. coli* K-12 substr. W3110 is used for rooting the tree.

condensation reaction continuing the cycle of FA chain elongation (Fig. 1B) (Heath et al., 2002a,b).

Chemical structures of FabB and FabF enzymes are very similar (Huang et al., 1998; Olsen et al., 1999). However, FabF is responsible for temperature-dependent production of *cis*-unsaturated FA (Table 1) (Garwin et al., 1980). At low temperatures, FabF promotes the production of Δ11-18:1, whereas at higher temperatures, FabF is inactivated and the formation of Δ11-18:1 is reduced (Garwin et al., 1980; Zhang and Rock, 2008). FabB is an essential enzyme for unsaturated FAS (Hoang and Schweizer, 1997; Wang and Cronan, 2004) (see part Introduction of the double bond), which has the

catalytic property of elongating *cis*-3-decenoyl-ACP, whereas FabF does not (Table 1) (Hoang and Schweizer, 1997).

The next reduction of ketoester is catalyzed by a short-chain dehydrogenase/reductase family member FabG (Fig. 1B, Table 1). It is an essential protein for bacteria and plants (Fisher et al., 2000; Price et al., 2001; Ren et al., 2000).

The third step of dehydration is catalyzed by the FabA or FabZ β-hydroxyacyl-ACP dehydratases (Fig. 1B). Although FabA and FabZ are two isoforms, FabZ catalyzes the dehydration of hydroxyacyl-ACP to *trans*-2-ACP (Table 1). In addition to dehydration, FabA also carries out the isomerization of *trans*-2 to *cis*-3-decenoyl-ACP

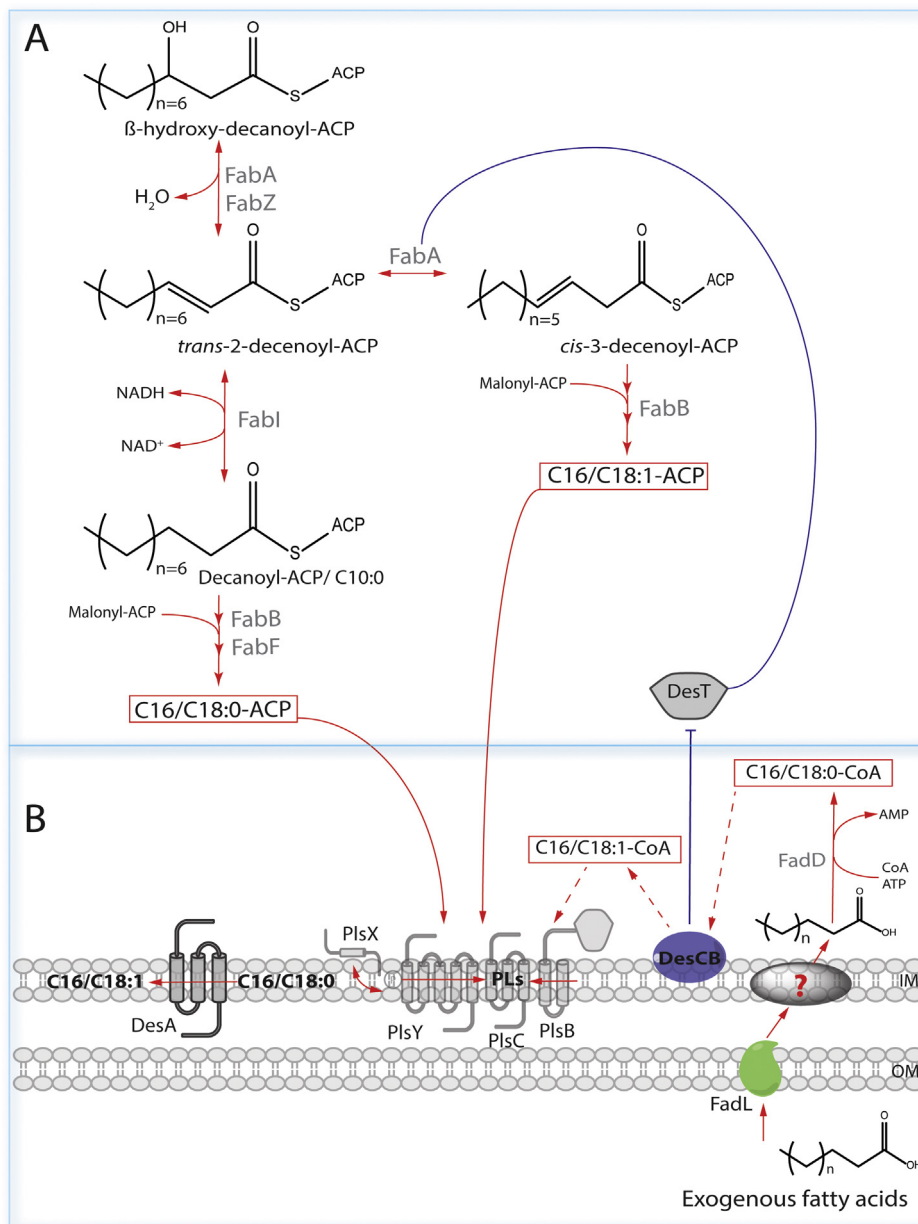


Fig. 3. Proposed mechanism of formation of unsaturated fatty acids in *Pseudomonas* strains.

(A) **FabAB pathway of double bond introduction in *Pseudomonas*:** At the 10-carbon stage of elongation module, the bifunctional FabA enzyme performs both the dehydration of β -hydroxyacyl-ACP to *trans*-2-enoyl-ACP and the isomerization of *trans*-2-enoyl-ACP to *cis*-3-enoyl-ACP. Then the enoyl-ACP reductase (FabI) reduces the *trans*-isomer to form a saturated FA chain (C16/C18:0-ACP). The *cis*-3-enoyl-ACP is elongated by the FabB enzyme to form an unsaturated FA chain (C16/C18:1-ACP), which is incorporated into GPs thought the action of acyltransferases (PlsX, PlsY, PlsB and PlsC). Production of the FabA protein is under the control of the DesT transcriptional repressor.

(B) **DesCB/DesA pathways of double bond introduction:** Exogenous FAs enter the cell and are converted to their acyl-CoA derivatives by the long-chain-fatty-acid-CoA ligase (FadD). DesA is a GP acyl-desaturase that introduces a double bond in the Δ9-position into formed GPs. The GP substrates for DesA are produced from both *de novo* FA synthesis and exogenous saturated FAs. DesB is an acyl-CoA desaturase that introduces a double bond in the Δ9-position. DesC is a predicted oxidoreductase which is probably involved in electron transport supporting FA desaturation reactions. Regulation of the DesBC system is insured by DesT. OM: outer membrane; IM: inner membrane, regulation pathways.

(Fig. 3A, Table 1) (Kimber et al., 2004). *P. aeruginosa* FabA and FabZ have very similar sequence characteristics, but they differ in active site residues, an Asp in FabA and a Glu in FabZ (Kimber et al., 2004; Mohan et al., 1994). The coupled transcription of the two genes coordinates the production of the two proteins (FabA and FabB) that are essential for unsaturated fatty acid biosynthesis (Hoang and Schweizer, 1997).

Usually, the fourth and final step in FAS is catalyzed by a NADH-dependent enoyl-ACP reductase FabI (Fig. 1B, Table 1). The active site of this enzyme has a Tyr-Lys catalytic diad (Roujeinikova et al., 1999; White et al., 2005). The FabI mechanism involves the transfer of a hydride to the C₃ of the C₂=C₃ bond and the development of an enolate anion on the C₁ carbonyl oxygen, which accepts a proton from a Tyr hydroxyl moiety. The obtained enol then undergoes tautomerization to yield the thioester (Rafferty et al., 1995). FabI is exclusively bacterial enzyme. The reduction of enoyl-ACP derivatives is thought to coordinate FA and GP biosynthesis and to regulate the degree of FA unsaturation (Hoang and Schweizer, 1999). The regulation of the ratio of unsaturated/saturated FAs is an essential mechanism of *Pseudomonas* adaptation to environmental modifications (Heath and Rock, 1995; Heipieper and Fischer, 2010; Ramos et al., 1997). FabI is the target of a group of antibacterial compounds, and is a typical triclosan-sensitive enoyl-ACP reductase (Chuanchuen et al., 2003; Heath and Rock, 1995). Triclosan is a very widely used biocide, which specifically inhibits enoyl-ACP-reductase activity. FabI is present in all *Pseudomonas* species (Zhu et al., 2010). Remarkably, *P. aeruginosa* possesses an another enoyl-ACP reductase isozyme FabV (Figure 1/B, green color, Table 1) (Zhu et al., 2010). It is considerably larger than typical short-chain dehydrogenase/reductase family members. The Tyr and the Lys active site residues of FabV are separated by eight amino acids instead of six in FabI (Massengo-Tiassé and Cronan, 2008).

In *P. aeruginosa* the genes encoding several enzymes of elongation cycle (*fabF-acpP-fabG-fabD*) are clustered (called the *fab* cluster) (Hoang and Schweizer, 1999; Kutchma et al., 1999). The genes coordinating the production of the FabH, FabY and FabZ proteins, are absent in this cluster.

2.1.4. Introduction of the double bond

Bacterial membranes should conserve the appropriate fluidity to maintain normal membrane structure and functions under various environmental changes (Heipieper and Fischer, 2010; Keweloh and Heipieper, 1996; Rühl et al., 2012). To increase membrane rigidity, *Pseudomonas* produce more saturated FAs whereas when higher fluidity is needed, unsaturated FAs are synthetized (Mansilla et al., 2004; Pepi et al., 2008; Zhu et al., 2006). A considerable diversity of mechanisms is used by *Pseudomonas* to generate unsaturated FAs. Bacteria of this genus use the bifunctional FabA enzyme which performs both the dehydration of β-hydroxyacyl-ACP to *trans*-2-enoyl-ACP and the isomerization of *trans*-2-enoyl-ACP to *cis*-3-enoyl-ACP at 10-carbon stage of elongation module (Fig. 3A, Table 1) (Parsons and Rock, 2013). Resulting *cis*-3-enoyl-ACP is then elongated by FabB enzyme. In *E. coli* the expression of *fabA* and *fabB* genes are transcriptionally regulated by the FadR activator and the FabR repressor (Feng and Cronan, 2012). In *Pseudomonas* the FabAB pathway is positively and negatively regulated by the DesT protein (PA4890) (Subramanian et al., 2010). DesT binds to a DNA palindromic site in the gene promoter. This binding is positively and negatively regulated by acyl-CoA. The DesT binds to saturated-and unsaturated-CoA with the same affinity, but the binding to DNA is enhanced when DesT is bound to an unsaturated acyl-CoA and released when DesT is bound to a saturated acyl-CoA (Miller et al., 2010; Zhang et al., 2007).

In addition to the FabAB dependent mechanism, *P. aeruginosa* generates unsaturated FAs by two other pathways (Fig. 3B). The DesA enzyme, a membrane-associated Δ9-desaturase, introduces a double bond in Δ9-position of fatty acyl chains attached to the *sn*-2 position of existing GPs (Fig. 3B, Table 1) (Parsons and Rock, 2013). We have found *P. aeruginosa* desA orthologs in a majority of *Pseudomonas* spp. (www.pseudomonas.com, data not shown). This suggests the presence of DesA dependent mechanism in most of *Pseudomonas* strains. However, the mechanism of DesA regulation is unknown and necessitates biochemical studies. Zhu et al. suppose that *desA* expression is regulated by membrane biophysical properties (Zhu et al., 2006). DesCB proteins, encoded by the *desCB* 2-genes' operon, are responsible for the introduction of a double bond specifically at the Δ9-position of acyl-CoA produced from exogenous saturated FAs (Fig. 3B, Table 1) (Subramanian et al., 2010). DesB is an acyl-CoA Δ9-desaturase, and the DesC is a predicted oxydoreductase which is probably involved in the electron transport that supports FA desaturation reactions catalyzed by DesB (Zhu et al., 2006). The *desB* mutants are known to be deficient in the synthesis of proteolytic enzymes, pyocyanin and rhamnolipids. They show impaired swarming and twitching motilities and reduced virulence in the *Caenorhabditis elegans* infection model. These data demonstrate that DesB is not only a FA desaturase but also a factor required for full virulence in *P. aeruginosa* (Schweizer and Choi, 2011). The DesBC pathway is like FabAB, regulated by a DesT dependent mechanism. However, the role of DesT in controlling *fabAB* expression likely accounts for the fact that DesT is conserved in both protein sequence and chromosomal location in all *Pseudomonas* species examined, yet only *P. aeruginosa* has a *desCB* operon (Subramanian et al., 2010). The reasons why *Pseudomonas* strains have three independent mechanisms of unsaturated FA formation need to be determined.

2.2. Transfer to the membrane

The FAS in *Pseudomonas* generally ends when the acyl chain has 16 or 18 carbons in length. The FA chain is then transferred into membrane to form GPs thanks to acyltransferases. Thus, the FA is transferred from acyl-ACP or acyl-CoA to the *sn*-1-position of glycerol-3-phosphate to form the 1-acyl-glycerol-3-phosphate, also known as lysophosphatidic acid (LPA). Next, the LPA is acylated in the *sn*-2-position to form phosphatidic acid (PA) (Fig. 1D) (Cullinane et al., 2005; Rock et al., 1981; Zhang and Rock, 2008).

The PlsB, an inner-membrane protein, catalyzes the acylation of the *sn*-1-position of glycerol-3-phosphate (Fig. 1D, Table 1). This enzyme can use both acyl donors: acyl-ACP and acyl-CoA (Lu et al., 2006) and has an eukaryotic ortholog. The second step of PA formation is always catalyzed by PlsC enzyme (Fig. 1D, Table 1), ubiquitously distributed in all bacteria (Röttig and Steinbüchel, 2013).

Alternatively, *Pseudomonas* spp. has a second acylation system PlsX/PlsY. The PlsX, a peripheral membrane protein, transfers the acyl group to inorganic phosphate to form a reactive acylphosphate intermediate (Fig. 1D, Table 1) (Zhang and Rock, 2008). Next, the PlsY an integral plasma-membrane protein acylates the *sn*-1-position of glycerol-3-phosphate and allows the PlsC enzyme to form the PA (Fig. 1D, Table 1) (Cullinane et al., 2005). Why *Pseudomonas* possesses two acylation systems is still an enigma.

PlsY is characterized as a remarkably small (23 kDa) membrane-bound enzyme in comparison to PlsB (93 kDa). It possesses five membrane-spanning segments and three cytoplasmic domains. This enzyme has no eukaryotic homologs (Röttig and Steinbüchel, 2013). Unlike PlsB, the PlsY unable to directly use acyl-ACP or acyl-CoA (Lu et al., 2007, 2006). An *E. coli*, *plsB* mutant was produced by Robert Bell's research group (Cronan and Bell,

1974). Those mutants are *sn*-glycerol 3-phosphate auxotrophs which owe their requirement to a K_m defect in *sn*-glycerol 3-phosphate acyltransferase (Cronan and Bell, 1974; Larson et al., 1984). Therefore, the *plsB* mutation was overcome by addition of exogenous glycerol-3-phosphate in the medium (Larson et al., 1984). Yoshimura et al. generated targeted *plsX*, *plsY* and *plsB* gene deletions (Yoshimura et al., 2007). *plsB* is an essential gene in *E. coli*, whereas single deletion mutants of *plsX* or *plsY* have no effect on bacterial growth. The double *plsX/plsY* mutant cannot be produced, indicating the essential role of the PlsX/PlsY complex in GP biosynthesis. Despite great therapeutic value, the transfer of FA modules to the membrane GPs remains a puzzle that will require more research to unravel.

3. Glycerophospholipid biosynthesis and functions in *Pseudomonas*

3.1. Glycerophospholipid head group diversity

An assortment of different polar HGs can be attached to the PA basic structure in bacteria, creating the optimum surface charge for membrane (Boeris et al., 2007; Parsons and Rock, 2013). The membrane charge depends on the ratio between zwitterionic GPs, e.g. phosphatidylethanolamine (PE), and GPs with acidic HGs, e.g. phosphatidylglycerol (PG). The balance in electrostatic charge is required for many integral membrane proteins to adopt the correct steric conformation in the cell membrane (Parsons and Rock, 2013). Bacteria can modify membrane charge to adapt to stress factors, like high temperature or solvent stresses (De Carvalho et al., 2008; De Carvalho, 2012).

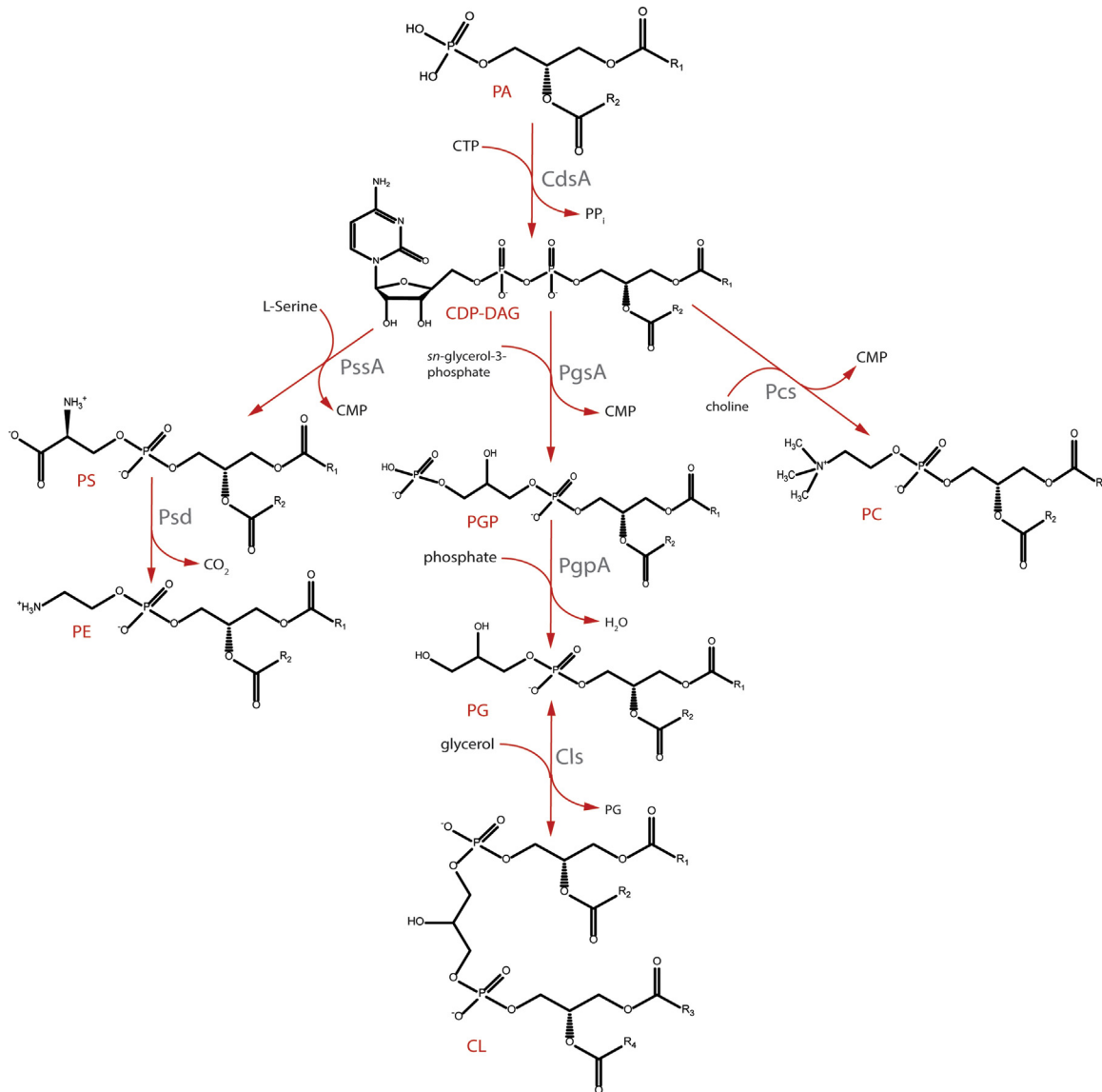


Fig. 4. Glycerophospholipid head group diversity.

Phosphatidic acid (PA) is the precursor for GPs synthesis in *Pseudomonas*. The cytidine diphosphate-diacylglycerol (CDP-DAG) is a key intermediate in the synthesis of all GPs in *Pseudomonas*. It is formed from PA and cytosine triphosphate (CTP) via CdsA catalysis. Phosphatidylethanolamine (PE), a major GP of *Pseudomonas*, is synthesized by phosphatidylserine (PS) decarboxylation. CDP-DAG is condensed with serine via the PS synthase PssA catalyze to form PS. Then, PS is decarboxylated thanks to the PS decarboxylase Psd to yield PE. For phosphatidylglycerol (PG) formation, CDP-DAG is condensed with glycerol phosphate by PgsA, to form phosphatidylglycerol phosphate (PGP). Then, PGP is dephosphorylated by a PGP phosphatase (PgpA). Cardiolipin (CL) is synthesized through condensation of two PG molecules by a CL synthase (Cls). Phosphatidylcholine (PC) is formed through the PC synthase (Pcs) pathway when choline is condensed with CDP-DAG to form the PC.

Table 2

Glycerophospholipids and their functions.

Glycerophospholipid	Chemical formula	Functions in bacterial cells	References
Phosphatidic acid (PA)		1. Basis in the synthesis of all membrane phospholipids 2. Negative membrane charge	(Parsons and Rock, 2013; Zhang and Rock, 2008) (Sutterlin et al., 2014)
Phosphatidylethanolamine (PE)		1. Most predominant phospholipid of <i>Pseudomonas</i> 2. Membrane architecture (lateral pressure and curvature stress in membranes) 3. Adaptation to organic solvents contamination and temperature stress 4. Motility and chemotaxis 5. Precursor for lipopolysaccharides synthesis	(Boeris et al., 2007; Gill, 1975; Bhakoo and Herbert, 1980) (Heath et al., 2002a,b) (Nikaido, 2003; Rühl et al., 2012; Gill, 1975; Bhakoo and Herbert, 1980) (Shi et al., 1993) (Raetz et al., 2007)
Phosphatidylserine (PS)		1. Precursor for PE synthesis	(Parsons and Rock, 2013)
Phosphatidylglycerol (PG)		1. Major anionic phospholipid of <i>Pseudomonas</i> 2. Membrane architecture 3. Adaptation to organic solvents and temperature stress	(Rühl et al., 2012; Suzuki et al., 2002) (Zhao et al., 2008) (Nikaido, 2003; Rühl et al., 2012; Gill, 1975; Bhakoo and Herbert, 1980)
Cardiolipin (CL)		1. Formation of dynamic protein-lipid membrane domains 2. Cell division 3. Resistance to organic compounds and antibiotics	(Camberg et al., 2007; Mileykovskaya and Dowhan, 2009; Romantsov et al., 2007) (Mileykovskaya and Dowhan, 2005; Dowhan et al., 2004; Mileykovskaya and Dowhan, 2009) (Ramos et al., 1997) (Bernal et al., 2007)
Phosphatidylcholine (PC)		1. Interactions symbiotic/pathogenic bacteria-eukaryotic hosts 2. Membrane structure formation 3. Resistance to heavy metals 4. Metabolic cycle, biomolecules formation	(Minder et al., 2001; Sohlenkamp et al., 2003; Martínez-Morales et al., 2003) (Geiger et al., 2013) (Boeris and Lucchesi, 2012) (Geiger et al., 2013)

Lipids composition of *Pseudomonas* spp. does not vary significantly depending on the bacterial strains (Bhakoo and Herbert, 1980; Bobo and Eagon, 1968; Boeris et al., 2007; Boeris and Lucchesi, 2012; Cullen et al., 1971; Tashiro et al., 2011). *Pseudomonas* spp. possesses four major GP species. PE and PG present the two major *Pseudomonas* spp. GPs, which together account for about 95%. Integral cellular analysis gives the composition of about 75% PE and 20% PG. Remainders are represented by cardiolipin (CL) (Diedrich and Cota-Robles, 1974) and phosphatidylcholine (PC), recently found in *Pseudomonas* strains (Boeris and Lucchesi, 2012; Geiger et al., 2013; Kondakova et al., 2014). CL is accumulated in *Pseudomonas* spp. when the cells enter the stationary growth phase. This lipid can be up to 10% of total GPs, and is required for prolonged survival of bacteria (Gill, 1975; Heath et al., 2002a,b). PC is the major component of eukaryotic cells, but it was also detected in the lipidome of *P. aeruginosa*, *P. fluorescens* and *P. putida* in small quantity (less than 4%) (Wilderman et al., 2002). The schema of *Pseudomonas* GPs synthesis is shown in Fig. 4.

3.2. Phosphatidylethanolamine production and functions

PE is a major component of the *Pseudomonas* lipidome (Table 2) (Boeris et al., 2007; Fuchs and Schiller, 2008). The bacterial PE is synthesized exclusively via phosphatidylserine (PS) decarboxylation (Dowhan, 1997; Gibellini and Smith, 2010). The first step catalyzed by PS synthase (PssA) is the condensation of cytidine diphosphate-diacylglycerol (CDP-DAG) with serine to form PS. Then PS yields PE by PS decarboxylase (Psd) (Fig. 4). PS is a minor GP of *Pseudomonas* (Bhakoo and Herbert, 1980), since it is quickly converted to PE (Table 2). It has been demonstrated that the lack of PE is lethal for bacteria, but this lethality is suppressed by media supplementation with high concentration of divalent metal cations. A pss null mutant contains no PS and PE in its lipidome and has a defect in motility (Shi et al., 1993), in Cpx dependent signal transduction pathway (Mileykovskaya and Dowhan, 1997) and in division site selection. This last was attributed to a concomitant increase in CL content (Mileykovskaya and Dowhan, 2005; Ramos et al., 1997) (see part Cardiolipin synthesis and functions). A defect in the native folding of lactose permease LacY, which causes the loss of active membrane transport, is also observed (Dowhan et al., 2004). Complete inactivation of psd indicates that this gene is required for motility and chemotaxis (Ramos and Filloux, 2007; Shi et al., 1993). PE is mostly located in the inner membrane, and may be transferred from the inner to the outer membrane by lipid flippases (Sanyal and Menon, 2009). The PE plays a major role in membrane structure, because it is able to form reversed non lamellar structures like the hexagonal phase. In membrane, PE increases lateral pressure and introduces curvature stress (Birner et al., 2001). Moreover PE is the precursor of many essential biological molecules including DAG, FAs, PA (Gibellini and Smith, 2010) and lipopolysaccharides (LPS), major *Pseudomonas* virulence factor (Ham et al., 2011; Raetz et al., 2007).

3.3. Phosphatidylglycerol synthesis and functions

The second predominant *Pseudomonas* GP is phosphatidylglycerol (PG) (Table 2) (Diedrich and Cota-Robles, 1974). Unlike PE, PG is an anionic lipid at pH 7. The hydroxyl group of PG has the potential to form intermolecular hydrogen bonds (Zhao et al., 2008). The PG synthesis is organized in two steps and starts with CDP-DAG (Fig. 4). First, the CDP-DAG is condensed with glycerol phosphate by PgsA protein, to form phosphatidylglycerol phosphate (PGP). The second step is the PGP dephosphorylation by PGP phosphatase (PgpA) (Table 1) (Rühl et al., 2012; Heath et al., 2002a, b). It has long been thought that PG is an essential bacterial GP, but

Kikuchi et al. (2000) showed that in *E. coli*, a null pgsA mutant is viable if the major outer membrane lipoprotein (Lpp) is deficient. In the null pgsA mutant, the PG production is not detected (less than 0.01% of total GPs, below the detection limit), although the PA, an acidic biosynthetic precursor, was accumulated (4%). Nonetheless, the null pgsA mutant does not grow at high temperature, in low-osmolality or minimal media, but it grows almost normally in rich media (Suzuki et al., 2002). PG is therefore nonessential for *Pseudomonas* viability or basic life GP functions, but it plays an important role in bacterial machinery. Studies of the toxic effects of organic solvents on bacteria revealed that an adaptive bacterial mechanism to solvent stress modifies the amount of PG relative to PE in the cell membrane (Fang et al., 2000; Murzyn et al., 2005). This alteration in the HG composition is the way of preserving stability and low membrane permeability (Murzyn et al., 2005).

3.4. Cardiolipin biosynthesis and functions

CL is also called diphosphatidylglycerol because of its unique dimeric molecular structure in which two phosphatidyl moieties are linked by a glycerol. This GP is one of the major participants in the formation of membrane domains in *Pseudomonas* spp. (Table 2) (Gill, 1975; Heath et al., 2002a,b). Although CL has two phosphate groups, it is not fully ionized at pH 7 due to intramolecular hydrogen bonding between the free hydroxyl residue of the central glycerol and a protonated phosphate (Kates et al., 1993). CL is produced in *Pseudomonas* species by condensation of two PG molecules (Figure 4) thanks to the CL synthase (Cls) (Table 1) (Heath et al., 2002a,b). Due to its propensity to form non-bilayer structures dependent on pH or divalent counter cations, CL is able to participate in the formation of dynamic protein–lipid membrane domains of higher curvature, for example in bacterial division sites (Table 1) (Mileykovskaya and Dowhan, 2005). This explains the co-localization of CL with some proteins, like osmosensory transporter ProP, or Eps system, found in the polar regions in bacterial cells (Camberg et al., 2007; Mileykovskaya and Dowhan, 2009; Romantsov et al., 2007). The long-term solvent response involves the increasing of CL production in *P. putida* (Bernal et al., 2007; Ramos et al., 1997). The cls null mutant has a more rigid membrane, is more sensitive to toluene stress and to several antibiotics than the parental strain, suggesting that RND efflux pumps involved in the extrusion of these drugs are not working efficiently without CL production (Bernal et al., 2007).

3.5. Phosphatidylcholine synthesis in *Pseudomonas*

PC is the major membrane-forming GP in eukaryotic cells (Cole et al., 2012). However, at least 15% of bacteria have the ability to synthesize PC (Geiger et al., 2013). For example, PC synthesis is described in *Agrobacterium tumefaciens* (Kaneshiro and Law, 1964), *Rhodobacter sphaeroides* (Arondel et al., 1993), *Sinorhizobium meliloti* (De Rudder et al., 2000), *Zymomonas mobilis* (Tahara et al., 1994), *Bradyrhizobium japonicum* (Minder et al., 2001) and many other eubacteria. PC is detected in small quantity (less than 4%) in the lipidome of *Pseudomonas* spp. (Geiger, 2010). PC and PE have a very similar chemical structure. Both have a zwitterionic state at pH 7 and possess a dipole moment across their respective head groups (Sohlenkamp et al., 2003). However, there are significant and important differences in chemistry and properties between the two GP. PC has a head group and hydrophobic domains of similar diameter and forms lipid bilayers. PE has a small head group relative to a large hydrophobic domain and favors the hexagonal II phase formation (Dowhan and Bogdanov, 2002). Two pathways for PC biosynthesis exist in bacteria: the glycerophospholipid N-methylation (Pmt) pathway and the phosphatidylcholine synthase (Pcs) pathway. In the Pmt pathway, PE is three times methylated to

yield PC involving one or more glycerophospholipid *N*-methyltransferases (Wilderman et al., 2002) whereas in the Pcs pathway, choline condenses directly with CDP-DAG to form PC (Geiger et al., 2013; Gibellini and Smith, 2010). In *P. aeruginosa* PAO1, orthologs of rhodobacterial *pmtA* (PA0798) and *pcs* (PA3857) are found (Table 1) (Wilderman et al., 2002). The *pmtA*-deficient mutant still synthesizes PC at wild type level whereas a *pcs* null mutant forms no detectable amounts of PC (Wilderman et al., 2002). These data suggest that the Pcs pathway is predominant in *P. aeruginosa* PC synthesis (Fig. 4) (Geiger et al., 2013). The both (*pcs* and *pmt* null mutants) affects the viability of PAO1, demonstrating the important role of both genes in *P. aeruginosa* (Wilderman et al., 2002). It has been shown, that *P. putida* is able to synthesize PC via the Pcs pathway (Boeris and Lucchesi, 2012). Recently, we identified the PC production in *P. fluorescens* strains (Kondakova et al., 2014). We found orthologs to *P. aeruginosa* PAO1 *pmt* and *pcs* in *P. fluorescens* PfO-1. Tblastx analyses show *pmt*: Pfl01_0427 and *pcs*: Pfl01_2093 with 28 and 66% of amino acid identity respectively (www.pseudomonas.com, BLAST analysis, data not shown). PC plays a role in membrane formation in *P. aeruginosa* and is involved in *P. putida* resistance to heavy metals (Boeris and Lucchesi, 2012) (Table 2). In addition, pseudomonal PC can function as an intermediate during the biosynthesis of other biomolecules or form part of metabolic cycle (Geiger et al., 2013, p. 201).

4. Exploitation of host glycerophospholipids by *Pseudomonas*

Lipids have been loosely defined as biological substances that are generally hydrophobic in nature and in many cases soluble in organic solvents presenting important structural materials in living organisms (Fahy et al., 2005). The role of lipid is wider than structural material formation (Ganapathy et al., 2013), and several studies help us to understand the mysterious reason why nature synthesizes thousands of different lipids (Kanfer and Kennedy, 1964, 1963). In 1989, for the first time Irvine and Berridge showed that the phosphoinositides are involved in bacterial signaling system quorum sensing (Berridge and Irvine, 1989). Then, Haucke and Di Paolo showed the lipid implication in membrane traffic (Haucke and Di Paolo, 2007).

One example of host lipid exploitation by *Pseudomonas* is illustrated in the type 3 secretion system (T3SS). This mechanism, identified in human and plant pathogens *P. aeruginosa* and *P. fluorescens* and delivering virulence effector proteins into eukaryotic cells, appears functionally dependent on lipids (Cornelis, 2002; Mavrodi et al., 2011). At the tip of the T3SS needle, bacterial proteins are inserted into the host cell membrane to form a translocon that perturbs the membrane bilayer. *P. aeruginosa* has two translocon components, PopB and PopD, capable to bind directly to two eukaryotic lipids: cholesterol and phosphatidylserine, causing a cholesterol-dependent lyse of membrane (Schoehn et al., 2003). Approximately, 28% of strains of *P. aeruginosa* encode a potent cytotoxin, ExoU (Feltman et al., 2001), which is a marker of highly virulent *P. aeruginosa* strains isolated from patients with ventilator-associated pneumonia (Diaz and Hauser, 2010; Schulert et al., 2003). The ExoU is a cytotoxic phospholipase A2 effector protein secreted by the T3SS directly into host cells (Tyson and Hauser, 2013). Among membrane GPs, ExoU possesses high affinity for phosphatidylinositol 4,5-bisphosphate or PI(4,5)P₂, and it is capable to use this phospholipid as a substrate (Kierbel et al., 2005; Sato and Frank, 2014). Lysing cell membranes, ExoU contributes to the ability of *P. aeruginosa* to disseminate rapidly from lung tissue into the bloodstream (Van der Meer-Janssen et al., 2010). Then, *Pseudomonas* strains have a large capacity to exploit eukaryotic lipids in order to improve their host interactions. Within the last few years, bacteria–host lipid interactions became a very promising research area. For earlier

studies, we highly recommend very comprehensive reviews (Ham et al., 2011; Van der Meer-Janssen et al., 2010; Vromman and Subtil, 2014).

4.1. Phosphoinositide signaling and *Pseudomonas*

Many internal organs such as epithelial sheets are composed by separate apical and basolateral surfaces that are defined by distinct lipid and protein compositions and are separated by tight junctions (Gibson and Perrimon, 2003). The apical surface plays a role of barrier to the environment. The basolateral surface is adapted for interaction with other cells and for exchange with the bloodstream.

Phosphoinositides (PIs) are small lipids derived from phosphatidylinositol. As key components of eukaryotic cell membranes, PIs have essential roles in a wide range of cellular processes, such as membrane dynamics, actin cytoskeleton arrangements and vesicle trafficking (Michell, 2007). This differential distribution of PIs in cell is regulated by PI kinases and phosphatases, which interconvert diverse PI species (Ham et al., 2011). Phosphatidylinositol 3,4,5-trisphosphate (PI(3,4,5)P₃) is described as stably localized at the basolateral membrane and is excluded from the apical plasma membrane (Vanhaesebroeck and Alessi, 2000). This GP is a key determinant of *P. aeruginosa* interaction with host cells (Botelho et al., 2000; Kierbel et al., 2005). Insertion of exogenous PI(3,4,5)P₃ into the apical surface results in the rapid transformation of regions of the apical membrane to one with basolateral constituents. *P. aeruginosa* could create a local microenvironment that facilitates colonization and entry into the cell (Kierbel et al., 2007). For this, polarized monolayers *P. aeruginosa* binds near cell-cell junctions and coopts PI₃ kinase generating PI(3,4,5)P₃ at the surface. Membrane protrusions enriched by PI(3,4,5)P₃ and actin accumulate at the apical surface in the site of bacterial binding. This causes the decreasing susceptibility of the intact epithelium to *P. aeruginosa*-mediated invasion or damage (Kierbel et al., 2007). The PI(3,4,5)P₃ pathway of cell invasion by *P. aeruginosa* depends on the phospholipase D (PLD) enzymes activity (Jiang et al., 2014). The PLD enzymes catalyze the hydrolysis of GP phosphodiester bonds to product PA, and have been identified as type 6 secretion system (T6SS) effectors (Russell et al., 2013). Two such effectors in *P. aeruginosa* are PldA (PA3487) (Russell et al., 2013) and PldB (PA5089) (Jiang et al., 2014) targeting bacterial and eukaryotic cells (Spencer and Brown, 2015). Both proteins have significant homology to eukaryotic PLDs, but not to any prokaryotic PLDs, suggesting they were acquired horizontally, perhaps from a eukaryotic organism (Wilderman et al., 2001). PLD proteins of *P. aeruginosa* imposed cell death occurs through PA accumulation, via degradation of the major membrane components: PC for eukaryotes (Jiang et al., 2014) or bacterial PE (Russell et al., 2013).

4.2. Eukaryotic phosphatidylcholine exploitation

As the major eukaryotic phospholipid, PC is supposed to play an important role in the interactions between symbiotic and pathogenic bacteria and their eukaryotic hosts (Martínez-Morales et al., 2003). But recent findings showing the PC presence in about 15 % of all bacteria put into question this hypothesis. However, plant-colonizing *P. syringae* species detects and exploits choline in hosts for osmoprotection and nutrition (Chen et al., 2013). *P. aeruginosa* in turn produces a number of virulence factors that facilitate the establishment of lung infections. Mammalian lungs are naturally coated by indispensable lung surfactant, which is composed of approximately 80% of PC (Bernhard et al., 2001). This lipid serves as an important nutrient for *P. aeruginosa* during cystic fibrosis lung infection (Sun et al., 2014). *P. aeruginosa* hemolytic phospholipase C (PlcH) is a secreted hydrolase that degrades host-

associated PC (Jackson et al., 2013; Sage and Vasil, 1997; Wargo et al., 2011). In the PC-rich environment of the lungs, the PlcH degradation products of PC, DAG, and phosphorylcholine play different roles in the disease process. DAG may induce the abnormal release of inflammatory mediators and increase the host inflammatory response, thereby promoting tissue damage (Johansen et al., 1994; Sage and Vasil, 1997). Phosphorylcholine can be converted to choline or glycine betaine. These compounds serve as osmoprotectant agents which shield bacteria against the effects of hyperosmolar environments (such as the lungs tissues) (Jackson et al., 2013; Sage and Vasil, 1997). Since *P. aeruginosa* is able to utilize choline and glycine betaine as sole sources of carbon, nitrogen and energy (Lisa et al., 1983; Sun et al., 2014). A null *P. aeruginosa* plcH mutant was less able to colonize epithelial cell monolayers and defective in biofilm formation when grown in lung (Jackson et al., 2013). In a mouse thermal injury model, plcH mutant had a 10-fold increase in its LD50, compared to that of its wild type parent (Ostroff et al., 1989). Using the transparent zebrafish model, it has been demonstrated, that the PlcH is selective for endothelial cells, and also could contribute to apoptosis in lung endothelial cells and further exacerbates chronic inflammation seen in cystic fibrosis patients (Vasil et al., 2009). However, the role of PC in *Pseudomonas* spp.–host/symbiont interactions is still a promised area of future lipidomic researches.

4.3. *Pseudomonas* lipids as a target for a new antibiotic development

The bacterial FAS II differs significantly from the mammalian and fungal system (FAS I), which uses a large complex multifunctional enzymes (White et al., 2005; Zhu et al., 2010). The differences between the FAS I and FAS II systems make the FAS II one of the most attractive biochemical pathways to be used as targets for new antibacterial agents (Heath et al., 2002a,b, 2001; Payne et al., 2001; Zhang et al., 2006). Triclosan 1 (5-chloro-2-(2,4-dichlorophenoxy)phenol), a broad spectrum antimicrobial agent, can specifically inhibit enoyl-acyl carrier protein reductase, FabI, to block lipid biosynthesis (Castillo and Pérez, 2008; McMurry et al., 1998). Through subsequent kinetic and structural studies, triclosan was shown to be a potent inhibitor of FabIs from many organisms, such as *Staphylococcus aureus* (Suller and Russell, 2000), and *Haemophilus influenzae* (Marcinkeviciene et al., 2001). However, *P. aeruginosa* is resistant to triclosan, because this species encodes triclosan-resistant enoyl-ACP reductase isoforms. As discussed above, *P. aeruginosa* contains two enoyl-ACP reductases, FabI and the triclosan resistant FabV. Upon deletion of the fabV gene, the mutant strain became extremely sensitive to triclosan (>2,000-fold more sensitive than the wild-type strain), whereas the mutant strain lacking FabI remained completely resistant to the biocide (Zhu et al., 2010).

Over the last few years, *P. aeruginosa* lipidome became a target for new antibiotic development. The family of peptidomimetic antibiotics, based on membranolytic host-defense peptide protegrin I perturbs the LPS assembly in the outer membrane (Srinivas et al., 2010). A new aminoglycoside derivative 3',4',6-tri-2-naphylmethylene (3',4',6-tri-2NM neamine) also targets *P. aeruginosa* LPS (Ouberai et al., 2011). It bound to LPS inducing membrane permeabilization. The accumulation of this drug within *P. aeruginosa* phospholipids causes the membrane destabilization. Electrostatic phospholipids/antibiotic interactions are probably critical in the 3',4',6-tri-2NM neamine efficiency. Thus the positive charge of this compound targets negatively charged phospholipids, like CL and PG (Ouberai et al., 2011). In any cases, these studies support the concept of lipid as attractive targets for drug development.

5. Conclusions and perspectives

The *Pseudomonas* genus includes ubiquitous bacteria, taming all ecological niches, which are able to adapt to highly diverse environmental modifications. In this review, we explored specific *Pseudomonas* mechanisms for FA and GP synthesis, composition and homeostasis. *Pseudomonas* spp. possesses three independent pathways to add double bonds in FA chains. These mechanisms, non-existent in many other bacteria, are known to protect *Pseudomonas* strains from stress factors. The FabV enzyme allows *P. aeruginosa* to resist to the antimicrobial agent triclosan. *P. aeruginosa* FabH enzyme was recently described as a component of the system of incorporation of long chain FAs. The *Pseudomonas* GP composition is more complex, than that one of *E. coli*. *Pseudomonas* spp. is able to synthetize the PC. This cell compound could be used by bacteria in the network of host-pathogen interactions. Improving our knowledge of GP biosynthesis in *Pseudomonas* should be helpful in understanding the physiology of these highly versatile microorganisms.

The ability of *Pseudomonas* spp. to exploit eukaryotic lipid is an emerging area of studies that will take advantage with the rapid development of high-throughput mass spectrometric, microscopic and genomic techniques. The establishment of bacterial lipid profiles should lead to the identification of the specific role of individual lipid species. Moreover the functions of minor bacterial lipids and the mechanism of lipid production in molecular level could be enlightened by the coupling of mass spectrometry with omics tools. The interactions between pseudomonad human or plant pathogens and their host, the role of individual GPs in these interactions should be investigated more finely. Hence, novel intracellular signaling or trafficking mechanisms could be revealed. This will certainly support the development of more specific drugs against *Pseudomonas* pathogens.

Acknowledgements

We wish to thank Awa N'Diaye-Renoult for linguistic insight for this manuscript. Tatiana Kondakova is recipient of a PhD grant from the GRR SeSa (Sanitary Safety Research Network) financed by the Regional Council of Haute-Normandie (France). This study was supported the Regional Council of Haute-Normandie (France) and Europe Council through the FEDER "SéSa" sponsoring.

References

- Allan, B., Linseman, M., MacDonald, L.A., Lam, J.S., Kropinski, A.M., 1988. Heat shock response of *Pseudomonas aeruginosa*. *J. Bacteriol.* 170, 3668–3674.
- Amato, P., Parazols, M., Sancelme, M., Laj, P., Mailhot, G., Delort, A.-M., 2007. Microorganisms isolated from the water phase of tropospheric clouds at the Puy de Dôme: major groups and growth abilities at low temperatures. *FEMS Microbiol. Ecol.* 59, 242–254. doi:<http://dx.doi.org/10.1111/j.1574-6941.2006.00199.x>.
- Arondel, V., Benning, C., Somerville, C.R., 1993. Isolation and functional expression in *E. coli* of a gene encoding phosphatidylethanolamine methyltransferase (EC 2.1.1.17) from *Rhodobacter sphaeroides*. *J. Biol. Chem.* 268, 16002–16008.
- Bernal, P., Muñoz-Rojas, J., Hurtado, A., Ramos, J.L., Segura, A., 2007. A *Pseudomonas putida* cardiolipin synthesis mutant exhibits increased sensitivity to drugs related to transport functionality. *Environ. Microbiol.* 9, 1135–1145. doi:<http://dx.doi.org/10.1111/j.1462-2920.2006.01236.x>.
- Bernhard, W., Hoffmann, S., Dombrowsky, H., Rau, G.A., Kamlage, A., Kappler, M., Haitsma, J.J., Freihorst, J., von der Hardt, H., Poets, C.F., 2001. Phosphatidylcholine molecular species in lung surfactant. *Am. J. Respir. Cell Mol. Biol.* 25, 725–731. doi:<http://dx.doi.org/10.1165/ajrcmb.25.6.4616>.
- Berridge, M.J., Irvine, R.F., 1989. Inositol phosphates and cell signaling. *Nature* 341, 197–205. doi:<http://dx.doi.org/10.1038/341197a0>.
- Best, E.A., Knauf, V.C., 1993. Organization and nucleotide sequences of the genes encoding the biotin carboxyl carrier protein and biotin carboxylase protein of *Pseudomonas aeruginosa* acetyl coenzyme A carboxylase. *J. Bacteriol.* 175, 6881–6889.
- Bhakoo, M., Herbert, R.A., 1980. Fatty acid and phospholipid composition of five psychrotrophic *Pseudomonas* spp. grown at different temperatures. *Arch. Microbiol.* 126, 51–55. doi:<http://dx.doi.org/10.1007/BF00421890>.

- Biedermannova, L., Prokop, Z., Gora, A., Chovancova, E., Kovacs, M., Damborsky, J., Wade, R.C., 2012. A single mutation in a tunnel to the active site changes the mechanism and kinetics of product release in haloalkane dehalogenase LinB. *J. Biol. Chem.* doi:<http://dx.doi.org/10.1074/jbc.M112.377853> jbc.M112.377853.
- Birner, R., Bürgermeister, M., Schneiter, R., Daum, G., 2001. Roles of phosphatidylethanolamine and of its several biosynthetic pathways in *Saccharomyces cerevisiae*. *Mol. Biol. Cell* 12, 997–1007.
- Black, P.N., Färgeman, N.J., DiRussso, C.C., 2000. Long-chain acyl-CoA-dependent regulation of gene expression in bacteria, yeast and mammals. *J. Nutr.* 130, 305.
- Bobo, R.A., Eagon, R.G., 1968. Lipids of cell walls of *Pseudomonas aeruginosa* and *Brucella abortus*. *Can. J. Microbiol.* 14, 503–513. doi:<http://dx.doi.org/10.1139/m68-086>.
- Bodilis, J., Heddle, M., Orange, N., Baray, S., 2006. OprF polymorphism as a marker of ecological niche in *Pseudomonas*. *Environ. Microbiol.* 8, 1544–1551. doi:<http://dx.doi.org/10.1111/j.1462-2920.2006.01045.x>.
- Boeris, P.S., Domenech, C.E., Lucchesi, G.I., 2007. Modification of phospholipid composition in *Pseudomonas putida* ATCC 12633 induced by contact with tetradecltrimethylammonium. *J. Appl. Microbiol.* 103, 1048–1054. doi:<http://dx.doi.org/10.1111/j.1365-2672.2007.03346.x>.
- Boeris, P.S., Lucchesi, G.I., 2012. The phosphatidylcholine synthase of *Pseudomonas putida* ATCC 12633 is responsible for the synthesis of phosphatidylcholine, which acts as a temporary reservoir for Al3+. *Microbiology* 158, 1249–1257. doi:<http://dx.doi.org/10.1099/mic.0.054072-0>.
- Botelho, R.J., Teruel, M., Dierckman, R., Anderson, R., Wells, A., York, J.D., Meyer, T., Grinstein, S., 2000. Localized biphasic changes in phosphatidylinositol-4,5-bisphosphate at sites of phagocytosis. *J. Cell Biol.* 151, 1353–1368.
- Boughton, B.W., Pollock, M.R., 1953. Long-chain unsaturated fatty acids as essential bacterial growth factors: further studies with *Corynebacterium 'Q'*. *Biochem. J.* 53, 261–265.
- Camberg, J.L., Johnson, T.L., Patrick, M., Abendroth, J., Hol, W.G.J., Sandkvist, M., 2007. Synergistic stimulation of EpsE ATP hydrolysis by EpsL and acidic phospholipids. *EMBO J.* 26, 19–27. doi:<http://dx.doi.org/10.1038/sj.emboj.7601481>.
- De Carvalho, C.C., Wick, L.Y., Heipieper, H.J., 2008. Cell wall adaptations of planktonic and biofilm *Rhodococcus erythropolis* cells to growth on C5 to C16 n-alkane hydrocarbons. *Appl. Microbiol. Biotechnol.* 82, 311–320. doi:<http://dx.doi.org/10.1007/s00253-008-1809-3>.
- Castillo, Y.P., Pérez, M.A., 2008. Bacterial beta-ketoacyl-acyl carrier protein synthase III (FabH): an attractive target for the design of new broad-spectrum antimicrobial agents. *Mini Rev. Med. Chem.* 8, 36–45.
- Chapalain, A., Rossignol, G., Lesouhaitier, O., Merieau, A., Gruffaz, C., Guerillon, J., Meyer, J.-M., Orange, N., Feuilloley, M.G.J., 2008. Comparative study of 7 fluorescent pseudomonad clinical isolates. *Can. J. Microbiol.* 54, 19–27. doi:<http://dx.doi.org/10.1139/w07-110>.
- Chen, C., Li, S., McKeever, D.R., Beattie, G.A., 2013. The widespread plant-colonizing bacterial species *Pseudomonas syringae* detects and exploits an extracellular pool of choline in hosts. *Plant J.* 75, 891–902. doi:<http://dx.doi.org/10.1111/tpj.12262>.
- Choi, K.-H., Kremer, L., Besra, G.S., Rock, C.O., 2000. Identification and substrate specificity of β-ketoacyl (acyl carrier protein) synthase III (mtFabH) from *Mycobacterium tuberculosis*. *J. Biol. Chem.* 275, 28201–28207.
- Chuanchuen, R., Karkhoff-Schweizer, R.R., Schweizer, H.P., 2003. High-level triclosan resistance in *Pseudomonas aeruginosa* is solely a result of efflux. *Am. J. Infect. Control* 31, 124–127. doi:<http://dx.doi.org/10.1067/mic.2003.11>.
- Cole, L.K., Vance, J.E., Vance, D.E., 2012. Phosphatidylcholine biosynthesis and lipoprotein metabolism. *Biochim. Biophys. Acta* 1821, 754–761. doi:<http://dx.doi.org/10.1016/j.bbapap.2011.09.009>.
- Cornelis, G.R., 2002. The *Yersinia* Ysc-Yop Type III weaponry. *Nat. Rev. Mol. Cell Biol.* 3, 742–754. doi:<http://dx.doi.org/10.1038/nrm932>.
- Couilleret, O., Prigent-Combaret, C., Caballero-Mellado, J., Moënne-Loccoz, Y., 2009. *Pseudomonas fluorescens* and closely-related fluorescent pseudomonads as biocontrol agents of soil-borne phytopathogens. *Lett. Appl. Microbiol.* 02566. doi:<http://dx.doi.org/10.1111/j.1472-765X>.
- Cronan, J.E., Bell, R.M., 1974. Mutants of *Escherichia coli* defective in membrane phospholipid synthesis: mapping of sn-glycerol 3-phosphate acyltransferase Km mutants. *J. Bacteriol.* 120, 227–233.
- Cullen, J., Phillips, M.C., Shipley, G.G., 1971. The effects of temperature on the composition and physical properties of the lipids of *Pseudomonas fluorescens*. *Biochem. J.* 125, 733–742.
- Cullinane, M., Baysse, C., Morrissey, J.P., O'Gara, F., 2005. Identification of two lysophosphatidic acid acyltransferase genes with overlapping function in *Pseudomonas fluorescens*. *Microbiology* 151, 3071–3080. doi:<http://dx.doi.org/10.1099/mic.0.27958-0>.
- Davies, C., Heath, R.J., White, S.W., Rock, C.O., 2000. The 1.8 Å crystal structure and active-site architecture of β-ketoacyl-acyl carrier protein synthase III (FabH) from *Escherichia coli*. *Structure* 8, 185–195. doi:[http://dx.doi.org/10.1016/S0969-2126\(00\)994-0](http://dx.doi.org/10.1016/S0969-2126(00)994-0).
- De Carvalho, C.C., 2012. Adaptation of *Rhodococcus erythropolis* cells for growth and bioremediation under extreme conditions. *Res. Microbiol.* 163, 125–136. doi:<http://dx.doi.org/10.1016/j.resmic.2011.11.003>.
- De Rudder, K.E., López-Lara, I.M., Geiger, O., 2000. Inactivation of the gene for phospholipid N-methyltransferase in *Sinorhizobium meliloti*: phosphatidylcholine is required for normal growth. *Mol. Microbiol.* 37, 763–772. doi:<http://dx.doi.org/10.1046/j.1365-2958.2000.02032.x>.
- Diaz, M.H., Hauser, A.R., 2010. *Pseudomonas aeruginosa* cytotoxin ExoU is injected into phagocytic cells during acute pneumonia. *Infect. Immun.* 78, 1447–1456. doi:<http://dx.doi.org/10.1128/IAI.01134-09>.
- Diedrich, D.L., Cota-Robles, E.H., 1974. Heterogeneity in lipid composition of the outer membrane and cytoplasmic membrane of *Pseudomonas* BAL-31. *J. Bacteriol.* 119, 1006–1018.
- Dowhan, W., 1997. Molecular basis for membrane phospholipid diversity: why are there so many lipids? *Annu. Rev. Biochem.* 66, 199–232. doi:<http://dx.doi.org/10.1146/annurev.biomed.66.1.199>.
- Dowhan, W., Bogdanov, M., 2002. Functional roles of lipids in membranes, In: Vance, D.E., Vance, J.E. (Eds.), *Biochemistry of Lipids, Lipoproteins and Membranes*. fourth ed. Elsevier Science, B.V.
- Dowhan, W., Mileykovskaya, E., Bogdanov, M., 2004. Diversity and versatility of lipid–protein interactions revealed by molecular genetic approaches. *Biochim. Biophys. Acta* 1666, 19–39. doi:<http://dx.doi.org/10.1016/j.bbamem.2004.04.010>.
- Driscoll, J.A., Brody, S.L., Kollef, M.H., 2007. The epidemiology, pathogenesis and treatment of *Pseudomonas aeruginosa* infections. *Drugs* 67, 351–368.
- Duclairoir Poc, C., Verdon, J., Groboillot, A., Barreau, M., Toucourou, H., Mijouin, L., Leclerc, C., Hulen, C., Kondakova, T., Morin, J., Feuilloley, M., Merieau, A., Orange, N., 2014. Airborne fluorescent pseudomonads: what potential for virulence? *Int. J. Curr. Microbiol. Appl. Sci.* 3, 708–722.
- Fahy, E., Subramaniam, S., Brown, H.A., Glass, C.K., Merrill, A.H., Murphy, R.C., Raetz, C.R., Russell, D.W., Seyama, Y., Shaw, W., Shimizu, T., Spener, F., van Meer, G., VanNieuwenhze, M.S., White, S.H., Witztum, J.L., Dennis, E.A., 2005. A comprehensive classification system for lipids. *J. Lipid Res.* 46, 839–862. doi:<http://dx.doi.org/10.1194/jlr.E400004-JLR200>.
- Fang, J., Barcelona, M.J., Alvarez, P.J., 2000. Phospholipid compositional changes of five pseudomonad archetypes grown with and without toluene. *Appl. Microbiol. Biotechnol.* 54, 382–389.
- Feltman, H., Schulert, G., Khan, S., Jain, M., Peterson, L., Hauser, A.R., 2001. Prevalence of type III secretion genes in clinical and environmental isolates of *Pseudomonas aeruginosa*. *Microbiology* 147, 2659–2669.
- Feng, Y., Cronan, J.E., 2012. Crosstalk of *Escherichia coli* FabR with global regulators in expression of fatty acid transport genes. *PLoS ONE* 7, e46275. doi:<http://dx.doi.org/10.1371/journal.pone.0046275>.
- Fisher, M., Kroon, J.T., Martindale, W., Stuitje, A.R., Slabas, A.R., Rafferty, J.B., 2000. The X-ray structure of *Brassica napus* beta-keto acyl carrier protein reductase and its implications for substrate binding and catalysis. *Structure* 8, 339–347 (Lond. Engl. 1993).
- Fuchs, B., Schiller, J., 2008. MALDI-TOF MS analysis of lipids from cells, tissues and body fluids. *Subcell. Biochem.* 49, 541–565. doi:http://dx.doi.org/10.1007/978-1-4020-8831-5_21.
- Ganapathy, V., Thangaraju, M., Prasad, P.D., Martin, P.M., Singh, N., 2013. Transporters and receptors for short-chain fatty acids as the molecular link between colonic bacteria and the host. *Curr. Opin. Pharmacol.* 13, 869–874. doi:<http://dx.doi.org/10.1016/j.coph.2013.08.006>.
- Garwin, J.L., Klages, A.L., Cronan, J.E., 1980. Beta-ketoacyl-acyl carrier protein synthase II of *Escherichia coli*. Evidence for function in the thermal regulation of fatty acid synthesis. *J. Biol. Chem.* 255, 3263–3265.
- Geiger, O., 2010. Lipids and *Legionella* virulence. In: Timmis, K.N. (Ed.), *Handbook of Hydrocarbon and Lipid Microbiology*. Springer, Berlin, Heidelberg, pp. 3195–3202.
- Geiger, O., López-Lara, I.M., Sohlenkamp, C., 2013. Phosphatidylcholine biosynthesis and function in bacteria. *Biochim. Biophys. Acta* 1831, 503–513. doi:<http://dx.doi.org/10.1016/j.bbapap.2012.08.009>.
- Gibellini, F., Smith, T.K., 2010. The Kennedy pathway—de novo synthesis of phosphatidylethanolamine and phosphatidylcholine. *IUBMB Life* 62, 414–428. doi:<http://dx.doi.org/10.1002/iub.337>.
- Gibson, M.C., Perrimon, N., 2003. Apical basal polarization: epithelial form and function. *Curr. Opin. Cell Biol.* 15, 747–752.
- Gill, C.O., 1975. Effect of growth temperature on the lipids of *Pseudomonas fluorescens*. *J. Gen. Microbiol.* 89, 293–298. doi:<http://dx.doi.org/10.1099/00221287-89-2-293>.
- Gotoh, N., Wakebe, H., Nishino, T., 1989. Ultrastructural aspects of fragility of *Pseudomonas aeruginosa* outer membrane devoid of protein F. *FEMS Microbiol. Lett.* 50, 51–53.
- Gould, T.A., Schweizer, H.P., Churchill, M.E.A., 2004. Structure of the *Pseudomonas aeruginosa* acyl-homoserine lactone synthase LasI. *Mol. Microbiol.* 53, 1135–1146. doi:<http://dx.doi.org/10.1111/j.1365-2958.2004.04211.x>.
- Guchhait, R.B., Polakis, S.E., Dimroth, P., Stoll, E., Moss, J., Lane, M.D., 1974. Acetyl Coenzyme A carboxylase system of *Escherichia coli*. Purification and properties of the biotin carboxylase, carboxyltransferase, and carboxyl carrier protein components. *J. Biol. Chem.* 249, 6633–6645.
- Gunderson, B.W., Ibrahim, K.H., Hovde, L.B., Fromm, T.L., Reed, M.D., Rotschafer, J.C., 2003. Synergistic activity of colistin and ceftazidime against multiantibiotic-resistant *Pseudomonas aeruginosa* in an in vitro pharmacodynamic model. *Antimicrob. Agents Chemother.* 47, 905–909. doi:<http://dx.doi.org/10.1128/AAC.47.3.905-909.2003>.
- Hachicho, N., Hoffmann, P., Ahlert, K., Heipieper, H.J., 2014. Effect of silver nanoparticles and silver ions on growth and adaptive response mechanisms of *Pseudomonas putida* mt-2. *FEMS Microbiol. Lett.* 355, 71–77. doi:<http://dx.doi.org/10.1111/1574-6968.12460>.
- Ham, H., Sreelatha, A., Orth, K., 2011. Manipulation of host membranes by bacterial effectors. *Nat. Rev. Microbiol.* 9 doi:<http://dx.doi.org/10.1038/nrmicro2602>.

- Haucke, V., Di Paolo, G., 2007. Lipids and lipid modifications in the regulation of membrane traffic. *Curr. Opin. Cell Biol.* 19, 426–435. doi:<http://dx.doi.org/10.1016/j.ceb.2007.06.003>.
- Heath, R.J., Rock, C.O., 1995. Enoyl-acyl carrier protein reductase (*fabI*) plays a determinant role in completing cycles of fatty acid elongation in *Escherichia coli*. *J. Biol. Chem.* 270, 26538–26542. doi:<http://dx.doi.org/10.1074/jbc.270.44.26538>.
- Heath, R.J., White, S.W., Rock, C.O., 2001. Lipid biosynthesis as a target for antibacterial agents. *Prog. Lipid Res.* 40, 467–497.
- Heath, R.J., Jackowski, S., Rock, C.O., 2002a. Fatty acid and phospholipid metabolism in prokaryotes. In: Vance, D.E., Vance, J.E. (Eds.), *Biochemistry of Lipids, Lipoproteins and Membranes*. fourth ed. Elsevier Science, B.V.
- Heath, R.J., White, S.W., Rock, C.O., 2002b. Inhibitors of fatty acid synthesis as antimicrobial chemotherapeutics. *Appl. Microbiol. Biotechnol.* 58, 695–703. doi:<http://dx.doi.org/10.1007/s00253-001-0918-z>.
- Heipieper, H.J., Fischer, J., 2010. Bacterial solvent responses and tolerance: *cis-trans* isomerization. In: Timmis, K.N. (Ed.), *Handbook of Hydrocarbon and Lipid Microbiology*. Springer, Berlin/Heidelberg, pp. 4203–4211.
- Heipieper, H.J., Meulenbeld, G., van Oirschot, Q., de Bont, J., 1996. Effect of environmental factors on the *trans/cis* ratio of unsaturated fatty acids in *Pseudomonas putida* S12. *Appl. Environ. Microbiol.* 62, 2773–2777.
- Hoang, T.T., Schweizer, H.P., 1999. Characterization of *Pseudomonas aeruginosa* enoyl-acyl carrier protein reductase (*FabI*): a target for the antimicrobial triclosan and its role in acylated homoserine lactone synthesis. *J. Bacteriol.* 181, 5489–5497.
- Hoang, T.T., Schweizer, H.P., 1997. Fatty acid biosynthesis in *Pseudomonas aeruginosa*: cloning and characterization of the *fabAB* operon encoding beta-hydroxyacyl-acyl carrier protein dehydratase (*FabA*) and beta-ketoacyl-acyl carrier protein synthase I (*FabB*). *J. Bacteriol.* 179, 5326–5332.
- Holder, J.W., Ulrich, J.C., DeBono, A.C., Godfrey, P.A., Desjardins, C.A., Zucker, J., Zeng, Q., Leach, A.L.B., Ghiviriga, I., Dancel, C., Abeel, T., Gevers, D., Kodira, C.D., Desany, B., Affourtit, J.P., Birren, B.W., Sinskey, A.J., 2011. Comparative and functional genomics of *Rhodococcus opacus* PD630 for biofuels development. *PLoS Genet.* 7, e1002219. doi:<http://dx.doi.org/10.1371/journal.pgen.1002219>.
- Huang, W., Jia, J., Edwards, P., Dehesh, K., Schneider, G., Lindqvist, Y., 1998. Crystal structure of beta-ketoacyl-acyl carrier protein synthase II from *E. coli* reveals the molecular architecture of condensing enzymes. *EMBO J.* 17, 1183–1191. doi:<http://dx.doi.org/10.1093/emboj/17.5.1183>.
- Jackson, A.A., Gross, M.J., Daniels, E.F., Hampton, T.H., Hammond, J.H., Vallet-Gely, I., Dove, S.L., Stanton, B.A., Hogan, D.A., 2013. Anr and its activation by PlcH activity in *Pseudomonas aeruginosa* host colonization and virulence. *J. Bacteriol.* 195, 3093–3104. doi:<http://dx.doi.org/10.1128/JB.2169-12>.
- Janek, T., Łukaszewicz, M., Rezanka, T., Krasowska, A., 2010. Isolation and characterization of two new lipopeptide biosurfactants produced by *Pseudomonas fluorescens* BD5 isolated from water from the Arctic Archipelago of Svalbard. *Bioresour. Technol.* 101, 6118–6123. doi:<http://dx.doi.org/10.1016/j.biortech.2010.02.109>.
- Jiang, F., Waterfield, N.R., Yang, J., Yang, G., Jin, Q., 2014. A *Pseudomonas aeruginosa* type VI secretion phospholipase D effector targets both prokaryotic and eukaryotic cells. *Cell Host Microbe* 15, 600–610. doi:<http://dx.doi.org/10.1016/j.chom.2014.04.010>.
- Joardar, V., Lindeberg, M., Jackson, R.W., Selengut, J., Dodson, R., Brinkac, L.M., Daugherty, S.C., DeBoy, R., Durkin, A.S., Giglio, M.G., Madupu, R., Nelson, W.C., Rosovitz, M.J., Sullivan, S., Crabtree, J., Creasy, T., Davidsen, T., Haft, D.H., Zafar, N., Zhou, L., Halpin, R., Holley, T., Khouri, H., Feldblyum, T., White, O., Fraser, C.M., Chatterjee, A.K., Cartinhour, S., Schneider, D.J., Mansfield, J., Collmer, A., Buell, C.R., 2005. Whole-genome sequence analysis of *Pseudomonas syringae* pv. *phaseolicola* 1448A reveals divergence among pathovars in genes involved in virulence and transposition. *J. Bacteriol.* 187, 6488–6498. doi:<http://dx.doi.org/10.1128/JB.187.18>.
- Johansen, T., Bjørkøy, G., Overvatn, A., Diaz-Meco, M.T., Traavik, T., Moscat, J., 1994. NIH 3T3 cells stably transfected with the gene encoding phosphatidylcholine-hydrolyzing phospholipase C from *Bacillus cereus* acquire a transformed phenotype. *Mol. Cell. Biol.* 14, 646–654.
- Jones, C., Allsopp, L., Horlick, J., Kulasekara, H., Filloux, A., 2013. Subinhibitory concentration of kanamycin induces the *Pseudomonas aeruginosa* type VI secretion system. *PLoS ONE* 8 doi:<http://dx.doi.org/10.1371/journal.pone.0081132>.
- Kaneshiro, T., Law, J.H., 1964. Phosphatidylcholine synthesis in *Agrobacterium tumefaciens*. Purification and properties of a phosphatidylethanolamine *N*-methyltransferase. *J. Biol. Chem.* 239, 1705–1713.
- Kanfer, J., Kennedy, E.P., 1964. Metabolism and function of bacterial lipids. II. Biosynthesis of phospholipids in *Escherichia coli*. *J. Biol. Chem.* 239, 1720–1726.
- Kanfer, J., Kennedy, E.P., 1963. Metabolism and function of bacterial lipids. I. Biosynthesis of phospholipids in *Escherichia coli*. *J. Biol. Chem.* 238, 2919–2922.
- Kates, M., Syz, J.Y., Gosser, D., Haines, T.H., 1993. pH-Dissociation characteristics of cardiolipin and its 2'-deoxy analogue. *Lipids* 28, 877–882.
- Keweloh, H., Heipieper, H.J., 1996. Trans unsaturated fatty acids in bacteria. *Lipids* 31, 129–137.
- Kiely, P.D., Haynes, J.M., Higgins, C.H., Franks, A., Mark, G.L., Morrissey, J.P., O'Gara, F., 2006. Exploiting new systems-based strategies to elucidate plant-bacterial interactions in the rhizosphere. *Microb. Ecol.* 51, 257–266. doi:<http://dx.doi.org/10.1007/s00248-006-9019-y>.
- Kierbel, A., Gassama-Diagne, A., Mostov, K., Engel, J.N., 2005. The phosphoinositol-3-kinase-protein kinase B/Akt pathway is critical for *Pseudomonas aeruginosa* strain PAK internalization. *Mol. Biol. Cell* 16, 2577–2585. doi:<http://dx.doi.org/10.1091/mbc.E04-08-0717>.
- Kierbel, A., Gassama-Diagne, A., Rocha, C., Radoshevich, L., Olson, J., Mostov, K., Engel, J., 2007. *Pseudomonas aeruginosa* exploits a PIP3-dependent pathway to transform apical into basolateral membrane. *J. Cell Biol.* 177, 21–27. doi:<http://dx.doi.org/10.1083/jcb.200605142>.
- Kikuchi, S., Shibuya, I., Matsumoto, K., 2000. Viability of an *Escherichia coli* *pgsA* null mutant lacking detectable phosphatidylglycerol and cardiolipin. *J. Bacteriol.* 182, 371–376.
- Kimber, M.S., Martin, F., Lu, Y., Houston, S., Vedadi, M., Dharamsi, A., Fiebig, K.M., Schmid, M., Rock, C.O., 2004. The structure of (3R)-hydroxyacyl-acyl carrier protein dehydratase (*FabZ*) from *Pseudomonas aeruginosa*. *J. Biol. Chem.* 279, 52593–52602. doi:<http://dx.doi.org/10.1074/jbc.M408105200>.
- Kondakova, T., Merlet-Machour, N., Chapelle, M., Preterre, D., Dionnet, F., Feuilloley, M., Orange, N., Duclairoir Poc, C., 2014. A new study of the bacterial lipidome: HPTLC-MALDI-TOF imaging enlightening the presence of phosphatidylcholine in airborne *Pseudomonas fluorescens* MFAF76a. *Res. Microbiol.* doi:<http://dx.doi.org/10.1016/j.resmic.2014.11.003>.
- Kondo, H., Shiratsuchi, K., Yoshimoto, T., Masuda, T., Kitazono, A., Tsuru, D., Anai, M., Sekiguchi, M., Tanabe, T., 1991. Acetyl-CoA carboxylase from *Escherichia coli*: gene organization and nucleotide sequence of the biotin carboxylase subunit. *Proc. Natl. Acad. Sci. U. S. A.* 88, 9730–9733.
- Kozloff, L.M., Lute, M., Westaway, D., 1984. Phosphatidylinositol as a component of the ice nucleating site of *Pseudomonas syringae* and *Erwinia herbicola*. *Science* 226, 845–846. doi:<http://dx.doi.org/10.1126/science.226.4676.845>.
- Kutchma, A.J., Hoang, T.T., Schweizer, H.P., 1999. Characterization of a *Pseudomonas aeruginosa* fatty acid biosynthetic gene cluster: purification of acyl carrier protein (ACP) and malonyl-coenzyme A:ACP transacylase (*FabD*). *J. Bacteriol.* 181, 5498–5504.
- Lai, C.-Y., Cronan, J.E., 2003. β -Ketoacyl-acyl carrier protein synthase III (*FabH*) is essential for bacterial fatty acid synthesis. *J. Biol. Chem.* 278, 51494–51503. doi:<http://dx.doi.org/10.1074/jbc.M308638200>.
- Larson, T.J., Ludtke, D.N., Bell, R.M., 1984. *sn*-Glycerol-3-phosphate auxotrophy of *plsB* strains of *Escherichia coli*: evidence that a second mutation, *plsX*, is required. *J. Bacteriol.* 160, 711–717.
- Lindgren, V., Holmgren, E., Rutberg, L., 1977. *Bacillus subtilis* mutant with temperature-sensitive net synthesis of phosphatidylethanolamine. *J. Bacteriol.* 132, 473–484.
- Lisa, T.A., Garrido, M.N., Domenech, C.E., 1983. Induction of acid phosphatase and cholinesterase activities in *Ps. aeruginosa* and their *in-vitro* control by choline, acetylcholine and betaine. *Mol. Cell. Biochem.* 50, 149–155.
- Li, S.J., Cronan, J.E., 1992. The gene encoding the biotin carboxylase subunit of *Escherichia coli* acetyl-CoA carboxylase. *J. Biol. Chem.* 267, 855–863.
- Lodise, T.P., Lomaestro, B., Drusano, G.L., 2007. Piperacillin-tazobactam for *Pseudomonas aeruginosa* infection: clinical implications of an extended-infusion dosing strategy. *Clin. Infect. Dis.* 44, 357–363. doi:<http://dx.doi.org/10.1086/510590>.
- Loper, J.E., Hassan, K.A., Mavrodi, D.V., Davis II, E.W., Lim, C.K., Shaffer, B.T., Elbourne, L.D.H., Stockwell, V.O., Hartney, S.L., Breakwell, K., Henkels, M.D., Tetu, S.G., Rangel, L.I., Kidarsa, T.A., Wilson, N.L., van de Mortel, J.E., Song, C., Blumhagen, R., Radune, D., Hostettler, J.B., Brinkac, L.M., Durkin, A.S., Kluepfel, D.A., Wechter, W.P., Anderson, A.J., Kim, Y.C., III, Lindow, S.E., Kobayashi, D.Y., Raaijmakers, J.M., Weller, D.M., Thomashow, L.S., Allen, A.E., Paulsen, I.T., 2012. Comparative genomics of plant-associated *Pseudomonas* spp.: insights into diversity and inheritance of traits involved in multitrophic interactions. *PLoS Genet.* 8, e1002784. doi:<http://dx.doi.org/10.1371/journal.pgen.1002784>.
- Lu, Y.-J., Zhang, F., Grimes, K.D., Lee, R.E., Rock, C.O., 2007. Topology and active site of *PlsY*: the bacterial acylphosphate: glycerol-3-phosphate acyltransferase. *J. Biol. Chem.* 282, 11339–11346. doi:<http://dx.doi.org/10.1074/jbc.M700374200>.
- Lu, Y.-J., Zhang, Y.-M., Grimes, K.D., Qi, J., Lee, R.E., Rock, C.O., 2006. Acyl-phosphates initiate membrane phospholipid synthesis in Gram-positive pathogens. *Mol. Cell* 23, 765–772. doi:<http://dx.doi.org/10.1016/j.molcel.2006.06.030>.
- Mansilla, M.C., Cybulski, L.E., Albanesi, D., de Mendoza, D., 2004. Control of membrane lipid fluidity by molecular thermosensors. *J. Bacteriol.* 186, 6681–6688. doi:<http://dx.doi.org/10.1128/JB.186.20.6681-6688>.
- Marcinkeviciene, J., Jiang, W., Kopcho, L.M., Locke, G., Luo, Y., Copeland, R.A., 2001. Enoyl-ACP reductase (*FabI*) of *Haemophilus influenzae*: steady-state kinetic mechanism and inhibition by triclosan and hexachlorophene. *Arch. Biochem. Biophys.* 390, 101–108. doi:<http://dx.doi.org/10.1006/abbi.2001.2349>.
- Martinez-Morales, F., Schobert, M., López-Lara, I.M., Geiger, O., 2003. Pathways for phosphatidylcholine biosynthesis in bacteria. *Microbiology* 149, 3461–3471. doi:<http://dx.doi.org/10.1099/mic.026522-0>.
- Massengo-Tiassé, R.P., Cronan, J.E., 2008. *Vibrio cholerae* *FabV* defines a new class of enoyl-acyl carrier protein reductase. *J. Biol. Chem.* 283, 1308–1316. doi:<http://dx.doi.org/10.1074/jbc.M708171200>.
- Mavrodi, D.V., Joe, A., Mavrodi, O.V., Hassan, K.A., Weller, D.M., Paulsen, I.T., Loper, J.E., Alfano, J.R., Thomashow, L.S., 2011. Structural and functional analysis of the type III secretion system from *Pseudomonas fluorescens* Q8r1-96. *J. Bacteriol.* 193, 177–189. doi:<http://dx.doi.org/10.1128/JB.895-10>.
- McCann, H.C., Rikkerink, E.H.A., Bertels, F., Fiers, M., Lu, A., Rees-George, J., Andersen, M.T., Gleave, A.P., Haubold, B., Wohlers, M.W., Guttman, D.S., Wang, P.W., Straub, C., Vanneste, J., Rainey, P.B., Templeton, M.D., 2013. Genomic analysis of the kiwifruit pathogen *Pseudomonas syringae* pv. *actinidiae* provides insight into the origins of an emergent plant disease. *PLoS Pathog.* 9, e1003503. doi:<http://dx.doi.org/10.1371/journal.ppat.1003503>.

- McMurry, L.M., Oethinger, M., Levy, S.B., 1998. Tricosan targets lipid synthesis. *Nature* 394, 531–532. doi:<http://dx.doi.org/10.1038/28970>.
- Mena, K.D., Gerba, C.P., 2009. Risk assessment of *Pseudomonas aeruginosa* in water. *Rev. Environ. Contam. Toxicol.* 201, 71–115. doi:http://dx.doi.org/10.1007/978-1-4419-0032-6_3.
- Michell, R.H., 2007. Evolution of the diverse biological roles of inositol. *Biochem. Soc. Symp.* 223–246. doi:<http://dx.doi.org/10.1042/BSS0740223>.
- Mileykovskaya, E., Dowhan, W., 2009. Cardiolipin membrane domains in prokaryotes and eukaryotes. *Biochim. Biophys. Acta* 1788, 2084–2091. doi:<http://dx.doi.org/10.1016/j.bbamem.2009.04.003> Biomembr., Includes Special Section: Cardiolipin.
- Mileykovskaya, E., Dowhan, W., 2005. Role of membrane lipids in bacterial division-site selection. *Curr. Opin. Microbiol.* 8, 135–142. doi:<http://dx.doi.org/10.1016/j.mib.2005.02.012>.
- Mileykovskaya, E., Dowhan, W., 1997. The Cpx two-component signal transduction pathway is activated in *Escherichia coli* mutant strains lacking phosphatidylethanolamine. *J. Bacteriol.* 179, 1029–1034.
- Miller, D.J., Zhang, Y.-M., Subramanian, C., Rock, C.O., White, S.W., 2010. Structural basis for the transcriptional regulation of membrane lipid homeostasis. *Nat. Struct. Mol. Biol.* 17, 971–975. doi:<http://dx.doi.org/10.1038/nsmb.1847>.
- Minder, A.C., De Rueter, K.E.E., Narberhaus, F., Fischer, H.-M., Hennecke, H., Geiger, O., 2001. Phosphatidylcholine levels in Bradyrhizobium japonicum membranes are critical for an efficient symbiosis with the soybean host plant. *Mol. Microbiol.* 39, 1186–1198. doi:<http://dx.doi.org/10.1111/j.1365-2958.2001.02325.x>.
- Mohan, S., Kelly, T.M., Eveland, S.S., Raetz, C.R., Anderson, M.S., 1994. An *Escherichia coli* gene (FabZ) encoding (3R)-hydroxymyristoyl acyl carrier protein dehydrase. Relation to fabA and suppression of mutations in lipid A biosynthesis. *J. Biol. Chem.* 269 (32), 896–32903.
- Morris, C.E., Kinkel, L.L., Xiao, K., Prior, P., Sands, D.C., 2007. Surprising niche for the plant pathogen *Pseudomonas syringae*. *Infect. Genet. Evol.* 7, 84–92. doi:<http://dx.doi.org/10.1016/j.meegid.2006.05.002>.
- Morris, C.E., Sands, D.C., Vinatzer, B.A., Glaux, C., Guillaud, C., Buffière, A., Yan, S., Dominguez, H., Thompson, B.M., 2008. The life history of the plant pathogen *Pseudomonas syringae* is linked to the water cycle. *ISME J.* 2, 321–334. doi:<http://dx.doi.org/10.1038/ismej.2007.113>.
- Mulet, M., Lalucat, J., García-Valdés, E., 2010. DNA sequence-based analysis of the *Pseudomonas* species. *Environ. Microbiol.* 12, 1513–1530. doi:<http://dx.doi.org/10.1111/j.1462-2920.2010.02181.x>.
- Murzyn, K., Rog, T., Pasenkiewicz-Gierula, M., 2005. Phosphatidylethanolamine-phosphatidylglycerol bilayer as a model of the inner bacterial membrane. *Biophys. J.* 88, 1091–1103. doi:<http://dx.doi.org/10.1529/biophysj.104.048835>.
- Nikaido, H., 2003. Molecular basis of bacterial outer membrane permeability revisited. *Microbiol. Mol. Biol. Rev.* 67, 593–656. doi:<http://dx.doi.org/10.1128/MMBR.67.4.593-656.2003>.
- Obritsch, M.D., Fish, D.N., MacLaren, R., Jung, R., 2005. Nosocomial infections due to multidrug-resistant *Pseudomonas aeruginosa*: epidemiology and treatment options. *Pharmacotherapy* 25, 1353–1364. doi:<http://dx.doi.org/10.1592/phco.2005.25.10.1353>.
- Olsen, J.G., Kadziola, A., von Wettstein-Knowles, P., Søgaard-Andersen, M., Lindquist, Y., Larsen, S., 1999. The X-ray crystal structure of beta-ketoacyl [acyl carrier protein] synthase I. *FEBS Lett.* 460, 46–52.
- Ostroff, R.M., Wretlind, B., Vasil, M.L., 1989. Mutations in the hemolytic-phospholipase C operon result in decreased virulence of *Pseudomonas aeruginosa* PAO1 grown under phosphate-limiting conditions. *Infect. Immun.* 57, 1369–1373.
- Uberai, M., El Garch, F., Bussiere, A., Riou, M., Alsteens, D., Lins, L., Baussanne, I., Dufrêne, Y.F., Brasseur, R., Decout, J.-L., Mingeot-Leclercq, M.-P., 2011. The *Pseudomonas aeruginosa* membranes: a target for a new amphiphilic aminoglycoside derivative. *Biochim. Biophys. Acta* 1808, 1716–1727. doi:<http://dx.doi.org/10.1016/j.bbamem.2011.01.014>.
- Palleroni, N.J., 2010. The *Pseudomonas* story. *Environ. Microbiol.* 12, 1377–1383. doi:<http://dx.doi.org/10.1111/j.1462-2920.2009.02041.x>.
- Parsons, J.B., Rock, C.O., 2013. Bacterial lipids: metabolism and membrane homeostasis. *Prog. Lipid Res.* 52, 249–276. doi:<http://dx.doi.org/10.1016/j.plipres.2013.02.002>.
- Payne, D.J., Warren, P.V., Holmes, D.J., Ji, Y., Lonsdale, J.T., 2001. Bacterial fatty-acid biosynthesis: a genomics-driven target for antibacterial drug discovery. *Drug Discov. Today* 6, 537–544.
- Pepi, M., Heipieper, H.J., Fischer, J., Ruta, M., Volterrani, M., Focardi, S.E., 2008. Membrane fatty acids adaptive profile in the simultaneous presence of arsenic and toluene in *Bacillus* sp. ORAs2 and *Pseudomonas* sp. ORAs5 strains. *Extremophiles* 12, 343–349. doi:<http://dx.doi.org/10.1007/s00792-008-0147-9>.
- Price, A.C., Zhang, Y.M., Rock, C.O., White, S.W., 2001. Structure of beta-ketoacyl-[acyl carrier protein] reductase from *Escherichia coli*: negative cooperativity and its structural basis. *Biochemistry* 40, 12772–12781 (Mosc.).
- Qiu, X., Janson, C.A., Konstantinidis, A.K., Nwagwu, S., Silverman, C., Smith, W.W., Khandekar, S., Lonsdale, J., Abdel-Meguid, S.S., 1999. Crystal structure of β-ketoacyl-acyl carrier protein synthase III: a key condensing enzyme in bacterial fatty acid biosynthesis. *J. Biol. Chem.* 274, 36465–36471. doi:<http://dx.doi.org/10.1074/jbc.274.51.36465>.
- Raetz, C.R., Reynolds, C.M., Trent, M.S., Bishop, R.E., 2007. Lipid A modification systems in gram-negative bacteria. *Annu. Rev. Biochem.* 76, 295–329. doi:<http://dx.doi.org/10.1146/annurev.biochem.76.010307.145803>.
- Rafferty, J.B., Simon, J.W., Baldock, C., Artymuik, P.J., Baker, P.J., Stuitje, A.R., Slabas, A.R., Rice, D.W., 1995. Common themes in redox chemistry emerge from the X-ray of oilseed rape (*Brassica napus*) enoyl acyl carrier protein reductase. *Structure* 3, 927–938 (Lond. Engl.).
- Ramos, J.L., Duque, E., Rodríguez-Hervá, J.-J., Godoy, P., Haïdour, A., Reyes, F., Fernández-Barbero, A., 1997. Mechanisms for solvent tolerance in bacteria. *J. Biol. Chem.* 272, 3887–3890. doi:<http://dx.doi.org/10.1074/jbc.272.7.3887>.
- Ramos, J.-L., Filloux, A., 2007. *Pseudomonas*: A Model System in Biology, vol. 5. Springer.
- Ren, Q., Sierra, N., Witholt, B., Kessler, B., 2000. FabG, an NADPH-dependent 3-ketoacyl reductase of *Pseudomonas aeruginosa*, provides precursors for medium-chain-length poly-3-hydroxyalkanoate biosynthesis in *Escherichia coli*. *J. Bacteriol.* 2000, 2978–2981. doi:<http://dx.doi.org/10.1128/JB.182.102978-2981.2000>.
- Ringen, L.M., Drake, C.H., 1952. A study of the incidence of *Pseudomonas aeruginosa* from various natural sources. *J. Bacteriol.* 64, 841–845.
- Rock, C.O., Goelz, S.E., Cronan, J.E., 1981. Phospholipid synthesis in *Escherichia coli*. Characteristics of fatty acid transfer from acyl-acyl carrier protein to sn-glycerol 3-phosphate. *J. Biol. Chem.* 256, 736–742.
- Romantsov, T., Helbig, S., Culham, D.E., Gill, C., Stalker, L., Wood, J.M., 2007. Cardiolipin promotes polar localization of osmosensory transporter Prop in *Escherichia coli*. *Mol. Microbiol.* 64, 1455–1465. doi:<http://dx.doi.org/10.1111/j.1365-2958.2007.05727.x>.
- Röttig, A., Steinbüchel, A., 2013. Acyltransferases in bacteria. *Microbiol. Mol. Biol. Rev.* 77, 277–321. doi:<http://dx.doi.org/10.1128/MMBR.10-13>.
- Roujeinikova, A., Sedelnikova, S., de Boer, G.-J., Stuitje, A.R., Slabas, A.R., Rafferty, J.B., Rice, D.W., 1999. Inhibitor binding studies on enoyl reductase reveal conformational changes related to substrate recognition. *J. Biol. Chem.* 274, 30811–30817. doi:<http://dx.doi.org/10.1074/jbc.274.43.30811>.
- Rühl, J., Hein, E.-M., Hayen, H., Schmid, A., Blank, L.M., 2012. The glycerophospholipid inventory of *Pseudomonas putida* is conserved between strains and enables growth condition-related alterations. *Microb. Biotechnol.* 5, 45–58. doi:<http://dx.doi.org/10.1111/j.1751-7915.2011.00286.x>.
- Russell, A.B., LeRoux, M., Hathazi, K., Agnello, D.M., Ishikawa, T., Wiggins, P.A., Wai, S.N., Mougous, J.D., 2013. Diverse type VI secretion phospholipases are functionally plastic antibacterial effectors. *Nature* 496, 508–512. doi:<http://dx.doi.org/10.1038/nature12074>.
- Sabuda, D.M., Laupland, K., Pitout, J., Dalton, B., Rabin, H., Louie, T., Conly, J., 2008. Utilization of colistin for treatment of multidrug-resistant *Pseudomonas aeruginosa*. *Can. J. Infect. Dis. Med. Microbiol.* 19, 413–418.
- Sage, A.E., Vasil, M.L., 1997. Osmoprotectant-dependent expression of plcH, encoding the hemolytic phospholipase C, is subject to novel catabolite repression control in *Pseudomonas aeruginosa* PAO1. *J. Bacteriol.* 179, 4874–4881.
- Sanyal, S., Menon, A.K., 2009. Flipping lipids: why an' what's the reason for? *ACS Chem. Biol.* 4, 895–909. doi:<http://dx.doi.org/10.1021/cb900163d>.
- Sato, H., Frank, D.W., 2014. Intoxication of host cells by the T3SS phospholipase ExoU: PI(4,5)P₂-associated, cytoskeletal collapse and late phase membrane blebbing. *PLoS One* 9 doi:<http://dx.doi.org/10.1371/journal.pone.0103127>.
- Schoehn, G., Di Guilmi, A.M., Lemaire, D., Attree, I., Weissenhorn, W., Dessen, A., 2003. Oligomerization of type III secretion proteins PopB and PopD precedes pore formation in *Pseudomonas*. *EMBO J.* 22, 4957–4967. doi:<http://dx.doi.org/10.1093/emboj/cdg499>.
- Schulert, G.S., Feltman, H., Rabin, S.D.P., Martin, C.G., Battle, S.E., Rello, J., Hauser, A.R., 2003. Secretion of the toxin ExoU is a marker for highly virulent *Pseudomonas aeruginosa* isolates obtained from patients with hospital-acquired pneumonia. *J. Infect. Dis.* 188, 1695–1706. doi:<http://dx.doi.org/10.1086/379372>.
- Schweizer, H.P., Choi, K.-H., 2011. *Pseudomonas aeruginosa* aerobic fatty acid desaturase DesB is important for virulence factor production. *Arch. Microbiol.* 193, 227–234. doi:<http://dx.doi.org/10.1007/s00203-010-0665-6>.
- Shi, W., Bogdanov, M., Dowhan, W., Zusman, D.R., 1993. The pss and psd genes are required for motility and chemotaxis in *Escherichia coli*. *J. Bacteriol.* 175, 7711–7714.
- Six, D.A., Yuan, Y., Leeds, J.A., Meredith, T.C., 2014. Deletion of the β-acetoacetyl synthase FabY in *Pseudomonas aeruginosa* induces hypoacetylation of lipopolysaccharide and increases antimicrobial susceptibility. *Antimicrob. Agents Chemother.* 58, 153–161. doi:<http://dx.doi.org/10.1128/AAC.1804-13>.
- Sohlenkamp, C., López-Lara, I.M., Geiger, O., 2003. Biosynthesis of phosphatidylcholine in bacteria. *Prog. Lipid Res.* 42, 115–162. doi:[http://dx.doi.org/10.1016/S0163-7827\(02\)50-4](http://dx.doi.org/10.1016/S0163-7827(02)50-4).
- Spencer, C.T., Brown, H.A., 2015. Biochemical characterization of a *Pseudomonas aeruginosa* phospholipase D. *Biochemistry* doi:<http://dx.doi.org/10.1021/bi501291t> (Mosc.).
- Srinivas, N., Jetter, P., Ueberbacher, B.J., Werneburg, M., Zerbe, K., Steinmann, J., Van der Meijden, B., Bernardini, F., Lederer, A., Dias, R.L.A., Missen, P.E., Henze, H., Zumbrunn, J., Gombert, F.O., Obrecht, D., Hunziker, P., Schauer, S., Ziegler, U., Käch, A., Eberl, L., Riedel, K., DeMarco, S.J., Robinson, J.A., 2010. Peptidomimetic antibiotics target outer-membrane biogenesis in *Pseudomonas aeruginosa*. *Science* 327, 1010–1013. doi:<http://dx.doi.org/10.1126/science.1182749>.
- Stanier, R.Y., Palleroni, N.J., Doudoroff, M., 1966. The aerobic pseudomonads a axonomic study. *J. Gen. Microbiol.* 43, 159–271. doi:<http://dx.doi.org/10.1099/00221287-43-2-159>.
- Subramanian, C., Rock, C.O., Zhang, Y.-M., 2010. DesT coordinates the expression of anaerobic and aerobic pathways for unsaturated fatty acid biosynthesis in *Pseudomonas aeruginosa*. *J. Bacteriol.* 192, 280–285. doi:<http://dx.doi.org/10.1128/JB.404-09>.

- Suller, M.T.E., Russell, A.D., 2000. Triclosan and antibiotic resistance in *Staphylococcus aureus*. *J. Antimicrob. Chemother.* 46, 11–18. doi:<http://dx.doi.org/10.1093/jac/46.1.11>.
- Sun, Z., Kang, Y., Norris, M.H., Troyer, R.M., Son, M.S., Schweizer, H.P., Dow, S.W., Hoang, T.T., 2014. Blocking phosphatidylcholine utilization in *Pseudomonas aeruginosa*, via mutagenesis of fatty acid, glycerol and choline degradation pathways, confirms the importance of this nutrient source *in vivo*. *PLoS One* 9 doi:<http://dx.doi.org/10.1371/journal.pone.0103778>.
- Sutterlin, H.A., Zhang, S., Silhavy, T.J., 2014. Accumulation of phosphatidic acid increases vancomycin resistance in *Escherichia coli*. *J. Bacteriol.* 196, 3214–3220. doi:<http://dx.doi.org/10.1128/JB.01876-14>.
- Suzuki, M., Hara, H., Matsumoto, K., 2002. Envelope disorder of *Escherichia coli* cells lacking phosphatidylglycerol. *J. Bacteriol.* 184, 5418–5425. doi:<http://dx.doi.org/10.1128/JB.184.19> 2002.
- Szaaff, M., Høiby, N., Flensburg, E.W., 1983. Frequent antibiotic therapy improves survival of cystic fibrosis patients with chronic *Pseudomonas aeruginosa* infection. *Acta Paediatr. Scand.* 72, 651–657. doi:<http://dx.doi.org/10.1111/j.1651-2227.1983.tb09789.x>.
- Tahara, Y., Yamashita, T., Sogabe, A., Ogawa, Y., 1994. Isolation and characterization of *Zymomonas mobilis* mutant defective in phosphatidylethanolamine *N*-methyltransferase. *J. Gen. Appl. Microbiol.* 40, 389–396.
- Tashiro, Y., Inagaki, A., Shimizu, M., Ichikawa, S., Takaya, N., Nakajima-Kambe, T., Uchiyama, H., Nomura, N., 2011. Characterization of phospholipids in membrane vesicles derived from *Pseudomonas aeruginosa*. *Biosci. Biotechnol. Biochem.* 75, 605–607.
- Tyson, G.H., Hauser, A.R., 2013. Phosphatidylinositol 4,5-bisphosphate is a novel coactivator of the *Pseudomonas aeruginosa* cytotoxin ExoU. *Infect. Immun.* 81, 2873–2881. doi:<http://dx.doi.org/10.1128/IAI.414-13>.
- Valerius, N.H., Koch, C., Høiby, N., 1991. Prevention of chronic *Pseudomonas aeruginosa* colonisation in cystic fibrosis by early treatment. *The Lancet* 338 (8769), 725–726. doi:[http://dx.doi.org/10.1016/0140-6736\(91\)91446-2](http://dx.doi.org/10.1016/0140-6736(91)91446-2).
- Van der Meer-Janssen, Y.P.M., van Galen, J., Batenburg, J.J., Helms, J.B., 2010. Lipids in host-pathogen interactions: pathogens exploit the complexity of the host cell lipidome. *Prog. Lipid Res.* 49, 1–26. doi:<http://dx.doi.org/10.1016/j.plipres.2009.07.003>.
- Vanhaesebroeck, B., Alessi, D.R., 2000. The PI3K-PDK1 connection: more than just a road to PKB. *Biochem. J.* 346 (Pt 3), 561–576.
- Vasil, M.L., Ochsner, U.A., 1999. The response of *Pseudomonas aeruginosa* to iron: genetics, biochemistry and virulence. *Mol. Microbiol.* 34, 399–413. doi:<http://dx.doi.org/10.1046/j.1365-2958.1999.01586.x>.
- Vasil, M.L., Stonehouse, M.J., Vasil, A.I., Wadsworth, S.J., Goldfine, H., Bolcome, R.E., Chan, J., 2009. A complex extracellular sphingomyelinase of *Pseudomonas aeruginosa* inhibits angiogenesis by selective cytotoxicity to endothelial cells. *PLoS Pathog.* 5 doi:<http://dx.doi.org/10.1371/journal.ppat.1000420>.
- Vromman, F., Subtil, A., 2014. Exploitation of host lipids by bacteria. *Curr. Opin. Microbiol.* 17, 38–45. doi:<http://dx.doi.org/10.1016/j.mib.2013.11.003> Host-microbe interactions: bacteria.
- Wang, H., Cronan, J.E., 2004. Functional replacement of the FabA and FabB proteins of *Escherichia coli* fatty acid synthesis by *Enterococcus faecalis* FabZ and FabF homologues. *J. Biol. Chem.* 279, 34489–34495. doi:<http://dx.doi.org/10.1074/jbc.M403874200>.
- Wargo, M.J., Gross, M.J., Rajamani, S., Allard, J.L., Lundblad, L.K.A., Allen, G.B., Vasil, M.L., Leclair, L.W., Hogan, D.A., 2011. Hemolytic phospholipase C inhibition protects lung function during *Pseudomonas aeruginosa* infection. *Am. J. Respir. Crit. Care Med.* 184, 345–354. doi:<http://dx.doi.org/10.1164/rccm.201103-0374OC>.
- White, S.W., Zheng, J., Zhang, Y.-M., Rock, C.O., 2005. The structural biology of type II fatty acid biosynthesis. *Annu. Rev. Biochem.* 74, 791–831. doi:<http://dx.doi.org/10.1146/annurev.biochem.74.082803.133524>.
- Wilderman, P.J., Vasil, A.I., Johnson, Z., Vasil, M.L., 2001. Genetic and biochemical analyses of a eukaryotic-like phospholipase D of *Pseudomonas aeruginosa* suggest horizontal acquisition and a role for persistence in a chronic pulmonary infection model. *Mol. Microbiol.* 39, 291–304. doi:<http://dx.doi.org/10.1046/j.1365-2958.2001.02282.x>.
- Wilderman, P.J., Vasil, A.I., Martin, W.E., Murphy, R.C., Vasil, M.L., 2002. *Pseudomonas aeruginosa* synthesizes phosphatidylcholine by use of the phosphatidylcholine synthase pathway. *J. Bacteriol.* 184, 4792–4799. doi:<http://dx.doi.org/10.1128/JB.184.17.4792-4799.2002>.
- Wu, X., Monchy, S., Taghavi, S., Zhu, W., Ramos, J., van der Lelie, D., 2011. Comparative genomics and functional analysis of niche-specific adaptation in *Pseudomonas putida*. *FEMS Microbiol. Rev.* 35, 299–323. doi:<http://dx.doi.org/10.1111/j.1574-6976.2010.00249.x>.
- Yoshimura, M., Oshima, T., Ogasawara, N., 2007. Involvement of the YneS/YgiH and PlsX proteins in phospholipid biosynthesis in both *Bacillus subtilis* and *Escherichia coli*. *BMC Microbiol.* 7, 69. doi:<http://dx.doi.org/10.1186/1471-2180-7-69>.
- Yuan, Y., Leeds, J.A., Meredith, T.C., 2012a. *Pseudomonas aeruginosa* directly shunts β-oxidation degradation intermediates into de novo fatty acid biosynthesis. *J. Bacteriol.* 194, 5185–5196. doi:<http://dx.doi.org/10.1128/JB.0860-12>.
- Yuan, Y., Sachdeva, M., Leeds, J.A., Meredith, T.C., 2012b. Fatty acid biosynthesis in *Pseudomonas aeruginosa* is initiated by the FabY class of β-ketoacyl acyl carrier protein synthases. *J. Bacteriol.* 194, 5171–5184. doi:<http://dx.doi.org/10.1128/JB.792-12>.
- Zhang, Y., Cronan, J.E., 1998. Transcriptional analysis of essential genes of the *Escherichia coli* fatty acid biosynthesis gene cluster by functional replacement with the analogous *Salmonella typhimurium* gene cluster. *J. Bacteriol.* 180, 3295–3303.
- Zhang, Y.-M., Rock, C.O., 2012. Will the initiator of fatty acid synthesis in *Pseudomonas aeruginosa* please stand up? *J. Bacteriol.* 194, 5159–5161. doi:<http://dx.doi.org/10.1128/JB.01198-12>.
- Zhang, Y.-M., Rock, C.O., 2008. Membrane lipid homeostasis in bacteria. *Nat. Rev. Microbiol.* 6, 222–233. doi:<http://dx.doi.org/10.1038/nrmicro1839>.
- Zhang, Y.-M., White, S.W., Rock, C.O., 2006. Inhibiting bacterial fatty acid synthesis. *J. Biol. Chem.* 281, 17541–17544. doi:<http://dx.doi.org/10.1074/jbc.R600004200>.
- Zhang, Y.-M., Zhu, K., Frank, M.W., Rock, C.O., 2007. A *Pseudomonas aeruginosa* transcription factor that senses fatty acid structure. *Mol. Microbiol.* 66, 622–632. doi:<http://dx.doi.org/10.1111/j.1365-2958.2007.05934.x>.
- Zhao, W., Rög, T., Gurtovenko, A.A., Vattulainen, I., Karttunen, M., 2008. Role of phosphatidylglycerols in the stability of bacterial membranes. *Biochimie* 90, 930–938. doi:<http://dx.doi.org/10.1016/j.biochi.2008.02.025>.
- Zhu, K., Choi, K.-H., Schweizer, H.P., Rock, C.O., Zhang, Y.-M., 2006. Two aerobic pathways for the formation of unsaturated fatty acids in *Pseudomonas aeruginosa*. *Mol. Microbiol.* 60, 260–273. doi:<http://dx.doi.org/10.1111/j.1365-2958.2006.05088.x>.
- Zhu, L., Lin, J., Ma, J., Cronan, J.E., Wang, H., 2010. Triclosan resistance of *Pseudomonas aeruginosa* PAO1 is due to FabV, a triclosan-resistant enoyl-acyl carrier protein reductase. *Antimicrob. Agents Chemother.* 54, 689–698. doi:<http://dx.doi.org/10.1128/AAC.01152-09>.

P25

RESEARCH ARTICLE

Open Access

A *Pseudomonas fluorescens* type 6 secretion system is related to mucoidy, motility and bacterial competition

Victorien Decoin¹, Mathias Gallique¹, Corinne Barbey¹, Francois Le Mauff², Cecile Duclairoir Poc¹, Marc GJ Feuilloley¹, Nicole Orange¹ and Annabelle Merieau^{1*}

Abstract

Background: *Pseudomonas fluorescens* strain MFE01 secretes in abundance two Hcp proteins (haemolysin co-regulated proteins) Hcp1 and Hcp2, characteristic of a functional type 6 secretion system. Phenotypic studies have shown that MFE01 has antibacterial activity against a wide range of competitor bacteria, including rhizobacteria and clinically relevant bacteria. Mutagenesis of the *hcp2* gene abolishes or reduces, depending on the target strain, MFE01 antibacterial activity. Hcp1, encoded by *hcp1*, may also be involved in bacterial competition. We therefore assessed the contribution of Hcp1 to competition of *P. fluorescens* MFE01 with other bacteria, by studying MFE01 mutants in various competitive conditions.

Results: Mutation of *hcp1* had pleiotropic effects on the MFE01 phenotype. It affected mucoidy of the strain and its motility and was associated with the loss of flagella, which were restored by introduction of plasmid expressing *hcp1*. The *hcp1* mutation had no effect on bacterial competition during incubation in solid medium. MFE01 was able to sequester another *P. fluorescens* strain, MFN1032, under swimming conditions. The *hcp2* mutant but not the *hcp1* mutant conserved this ability. In competition assays on swarming medium, MFE01 impaired MFN1032 swarming and displayed killing activity. The *hcp2* mutant, but not the *hcp1* mutant, was able to reduce MFN1032 swarming. The *hcp1* and *hcp2* mutations each abolished killing activity in these conditions.

Conclusion: Our findings implicate type 6 secretion of Hcp1 in mucoidy and motility of MFE01. Our study is the first to establish a link between a type 6 secretion system and flagellin and mucoidy. Hcp1 also appears to contribute to limiting the motility of prey cells to facilitate killing mediated by Hcp2. Inhibition of motility associated with an Hcp protein has never been described. With this work, we illustrate the importance and versatility of type 6 secretion systems in bacterial adaptation and fitness.

Keywords: *Pseudomonas fluorescens*, Type 6 secretion system, Hcp protein, Competitive inhibition, Motility, Mucoidy, Exopolysaccharides

Background

Environmental bacteria are in perpetual war against several competitors, and thus require weapons to conquer new territory. The type 6 secretion system (T6SS) of Gram-negative bacteria is an effector translocation apparatus resembling an inverted bacteriophage puncturing device [1-3]. It is involved in a broad variety of functions,

including antibacterial activity [4,5] and bacterial communication [6]. For example, *Proteus mirabilis* uses the killing activity of T6SS for self-recognition: this T6SS seems to be activated when opposing *P. mirabilis* swarms meet. The result of its action is a visible boundary called the Dienes line [7,8].

The T6SS machinery comprises at least 13 proteins, the core components, and sometimes, additional proteins [9,10]. Some of the core component proteins can affect systems other than T6SS. Hcp proteins, extracellular components of this secretion machinery, are released

* Correspondence: annabelle.merieau@univ-rouen.fr

¹LMSM, Laboratoire de Microbiologie Signaux et Microenvironnement, Normandie Université, EA 4312, IRIB, Université de Rouen, IUT d'Evreux, 55 rue Saint Germain, 27000 Evreux, France

Full list of author information is available at the end of the article

into the medium, and therefore may serve as markers of a functional T6SS apparatus [11]. Silverman and colleagues demonstrated that *P. aeruginosa* Hcp are not only structural proteins but also play a crucial role as chaperone and receptor for T6SS effectors. Various Hcp proteins transport their own effectors and this effector selection by Hcp seems to be specific [12].

The diversity of T6SS regulation reflects the vast array of its functions. The *P. aeruginosa* H1-T6SS gene cluster exhibits posttranscriptional regulation involving two sensor kinases, RetS and LadS [13–15]. High concentrations of synthetic c-di-GMP have negative effects on sensor kinase RetS, leading to *P. aeruginosa* H1-T6SS being turned on [16]. It is likely that a similar regulatory pathway controls the expression of *P. protegens* Pf-5 and *P. syringae* pv. *syringae* T6SS gene clusters [17,18]. However, T6SS regulation involves systems that regulate other genes suggesting regulatory cross-talk between T6SS and other virulence factors.

Environmental bacteria are often surrounded by an extracellular matrix, forming a protective capsule called the glycocalyx [19]. This extracellular matrix is generally composed of bacterial exopolysaccharides (EPS). EPS are involved in a variety of functions, including microcolony formation, protection against bacteriophages and mucoid phenotypes. The mucoid phenotype of *Pseudomonas* sp. is believed to be a global adaptive stress response to adverse environmental conditions [20,21]. It is characterized by overproduction of EPS alginate leading to shiny, raised and opaque colonies. The mucoid phenotype is a major factor contributing to *P. aeruginosa* infection in cystic fibrosis (CF) patients [22,23] but is unstable *in vitro* [24]. Some *P. aeruginosa* CF isolates acquire a mucoid phenotype through mutation of the anti-sigma factor MucA, a negative regulatory factor that sequesters AlgU, a positive regulator of alginate production [22,25]. A proteomic study by Rao and coworkers found that mucoid *P. aeruginosa* strains do not express T6SS genes [26]. Unlike *P. aeruginosa*, some *Vibrio cholerae* strains are mucoid and have an active T6SS [27]. Some environmental *P. fluorescens* strains produce alginate or neutral and amino sugars which give a mucoid phenotype [28,29]. The *P. fluorescens* mucoid phenotype, like that in *P. aeruginosa*, was reported to be unstable [29]. The mucoid phenotype can occur following mutation of the negative regulator of the alginate biosynthetic operon, muc [30]. We previously characterized the strain MFE01, a mucoid environmental *P. fluorescens* isolate. It constitutively secretes two characteristic T6SS proteins at 28°C: Hcp1 and Hcp2. It also exerts antibacterial activity during contact on a solid surface with competitive bacteria; this activity is associated with Hcp2 [31]. The aim of this work was to study the role of Hcp1 and the link between T6SS and the mucoid phenotype of MFE01.

Results and discussion

Some mucoid *P. fluorescens* strains secrete Hcp abundantly

The phenotypes of four *P. fluorescens* strains were observed after growth on LB agar plates at 28°C. Environmental strains MFE01 [31] and MFE07 (this study) had a stable shiny aspect, characteristic of mucoid phenotypes at 28°C. Skin strain MFP05 [32] and clinical strain MFN1032 [33] did not have a mucoid phenotype at this temperature (Figure 1A and B).

MucA is a negative regulator of the mucoid phenotype [22] in *Pseudomonas* species. We introduced the *mucA* gene of the *Pseudomonas protegens* strain Pf-5 (previously described as a *P. fluorescens* strain) [34] into MFE01. The expression of *mucA* did not switch-off mucoidy at 28°C, suggesting that the mucoid phenotype of MFE01 is not due to a mutation of the *mucA* gene or is MucA independent (Figure 1A). Scanlan and Buckling showed that the environmental *P. fluorescens* strain SBW25 has an

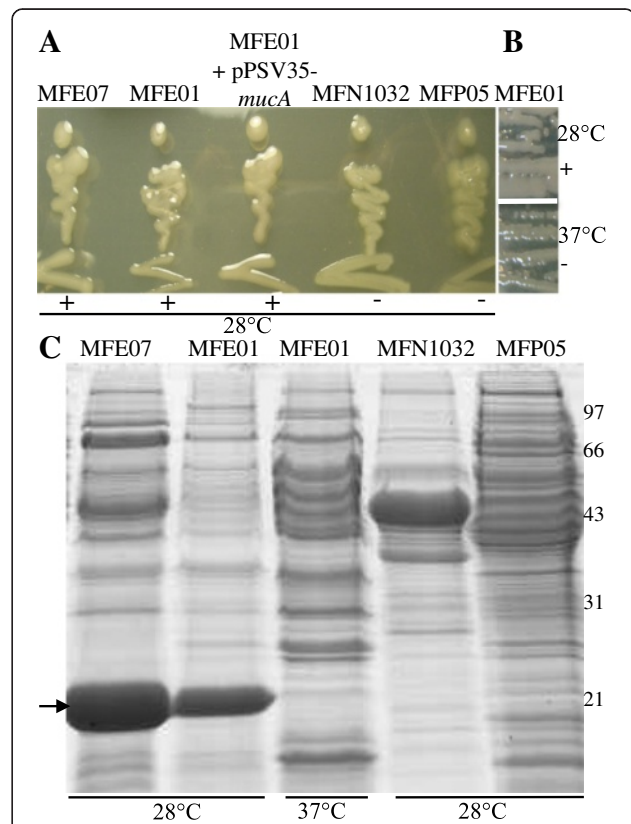


Figure 1 Hcp secretion and mucoid phenotype in *P. fluorescens* strains. **A:** Mucoidy was assessed on LB agar at 28°C. +: mucoid, -: non mucoid. **B:** Mucoidy at 28°C or 37°C of MFE01. +: mucoid, -: non mucoid. The images shown are representative of three assays. **C:** Concentrated supernatants of cultures in late exponential growth phase, grown at 28°C or 37°C, were analysed by SDS-PAGE (15% separation gel) and Coomassie staining. Bands (indicated by arrows) with an approximate molecular mass of 21 kDa were observed in MFE01 and MFE07 supernatants at 28°C. Mass spectrometry identified these major supernatant proteins as Hcp proteins.

unstable mucoid phenotype; although the genetic mechanisms of this phenotype remain unknown, they do not include mutations at many of the loci commonly reported to be involved in mucoid conversion, including *mucA* and *algU*. They also demonstrated that lytic phage exerts a selection pressure by selecting the mucoid phenotype [29].

We prepared supernatants of cultures of mucoid *P. fluorescens* strains MFE01 and MFE07 and found that these strains secreted large amounts of proteins identified as Hcp by Mass Spectroscopy (MS) (Figure 1C). The spot for the protein secreted by MFE01 matched significantly with gi: 398989489 (T6SS effector, Hcp1 family from *Pseudomonas* sp GM24) with a score of 120 for a score threshold of 84. The spot for the protein secreted by MFE07 spot matched significantly with gi:77458272 (hypothetical protein Pf01_2045 from *Pseudomonas fluorescens* Pf0-1, Hcp1 family) with a score of 65 for a score threshold of 54. The non-mucoid *P. fluorescens* strains MFP05 and MFN1032 did not secrete detectable amounts of Hcp proteins into the extracellular medium.

The optimal growth temperature of MFE01 is 28°C but it can grow at 37°C. Clearly visible at 28°C, the mucoid phenotype and Hcp secretion were both switched off at 37°C, suggesting a common regulation of these two phenotypes (Figure 1B,C).

Unterweger and colleagues observed a correlation between the mucoid phenotype and Hcp secretion in *V. cholerae* smooth strains [27]. Sigma-54 controls T6SS genes transcription, so they introduced *vasH*, encoding a sigma-54 activator protein, into rough (non mucoid) *V. cholera* strains impaired in Hcp secretion: the expression of *vasH* restored the mucoid phenotype, but not the Hcp secretion. However, *vasH* can activate transcription of genes other than T6SS genes via sigma-54 [35,36] suggesting that the correlation between mucoidy and T6SS in *V. cholerae* may be due to a common regulation system.

Hcp1 of *P. fluorescens* MFE01 is involved in mucoid phenotype

We constructed *hcp* mutants, and found that the *hcp1* mutation (MFE01Δ*hcp1* strain) lead to the loss of mucoidy at 28°C whereas the *hcp2* mutation (MFE01Δ*hcp2* strain) did not affect the mucoid phenotype (Figure 2). The introduction of a plasmid carrying the *hcp1* gene into MFE01Δ*hcp1* (MFE01Δ*hcp1*+*hcp1* strain) restored the wild-type phenotype, suggesting a direct link between *hcp1* expression and mucoidy. We analysed and compared the extracellular matrices (ECM) of MFE01 and MFE01Δ*hcp1*. The mucoid phenotype is a consequence of exopolysaccharide (EPS) accumulation [37], so we determined ECM sugar composition by Gas–liquid Chromatography (GLC). No significant difference between MFE01 and MFE01Δ*hcp1* was observed concerning the

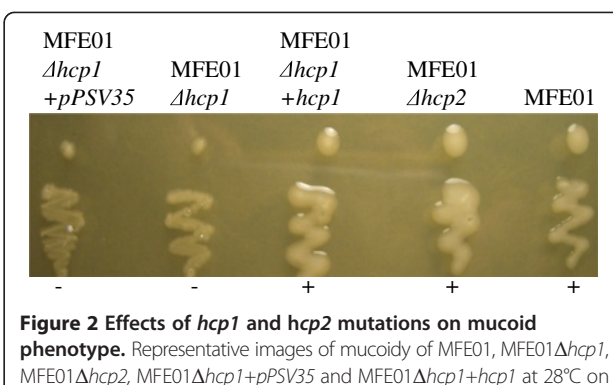


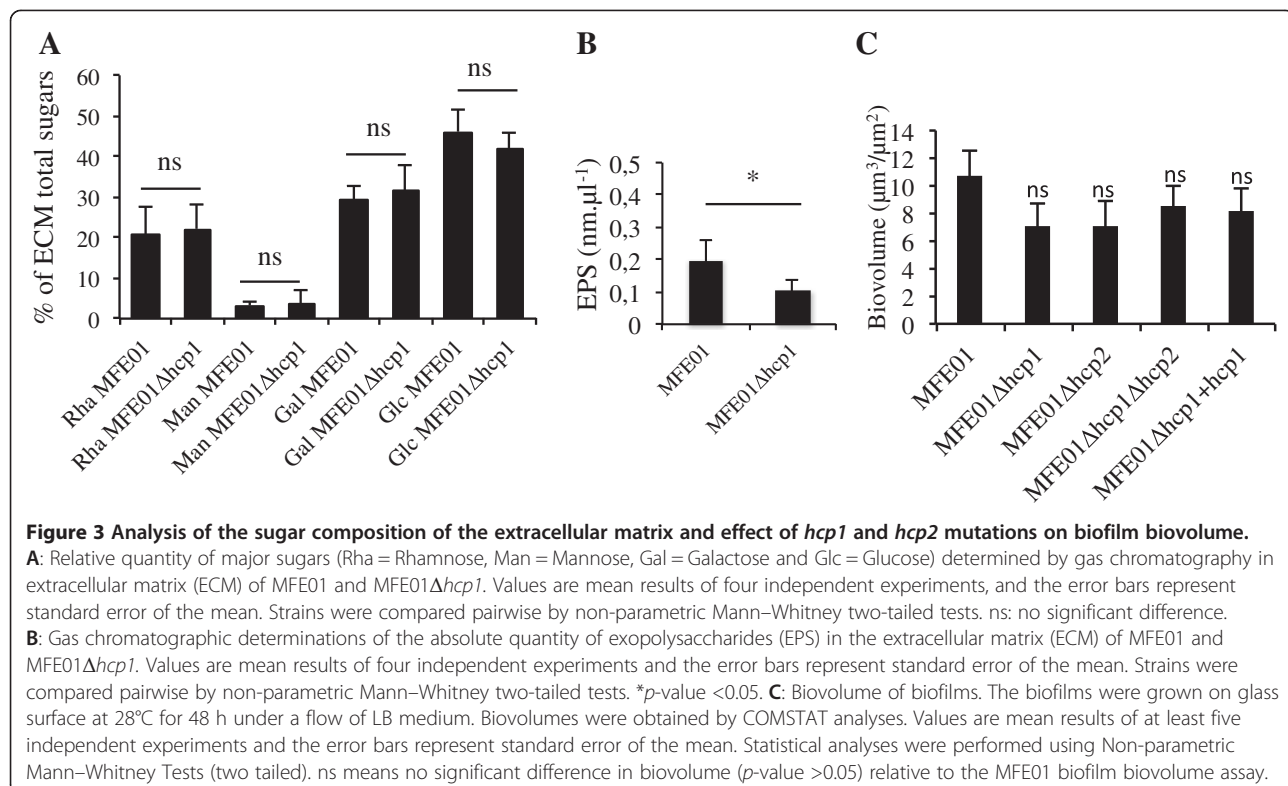
Figure 2 Effects of *hcp1* and *hcp2* mutations on mucoid phenotype. Representative images of mucoidy of MFE01, MFE01Δ*hcp1*, MFE01Δ*hcp2*, MFE01Δ*hcp1*+*pPSV35* and MFE01Δ*hcp1*+*hcp1* at 28°C on LB agar (n = 3). +: mucoid, -: non mucoid.

proportion of characteristic sugars of the *Pseudomonas* EPS (rhamnose, mannose, galactose and glucose; Figure 3A). Thus, MFE01Δ*hcp1* is able to secrete an EPS similar to that produced by MFE01. Nevertheless, the MFE01 ECM contained twice as much EPS as the MFE01Δ*hcp1* ECM suggesting that the loss of the mucoid phenotype was a consequence of less EPS accumulation (Figure 3B). In *Pseudomonas aeruginosa*, biofilm formation and T6SS expression are negatively regulated by the sensor *RetS* and *retS* mutants produce a hyperbiofilm phenotype [16]. Biofilm formation by MFE01 and mutants was then assayed. The moderate biofilm biovolume was not significantly different between MFE01 and MFE01Δ*hcp1* or MFE01Δ*hcp2* mutants (Figure 3C). These findings indicate that mucoid phenotype and biofilm formation are not co-regulated by T6SS in MFE01.

ECM protein fractions from supernatants of MFE01, MFE01Δ*hcp1* and MFE01Δ*hcp1*+*hcp1* were studied by SDS-PAGE (Figure 4A). Proteins of approximate molecular mass of 38 kDa were present in ECM extracts from MFE01 and MFE01Δ*hcp1*+*hcp1* but not in MFE01Δ*hcp1*. MS identified these 38 kDa proteins as flagellin proteins: they matched significantly with flagellin from *Pseudomonas moraviensis* (gi: 515142380) with a score of 94 for a score threshold of 86. Thus, the mucoid phenotype appears to involve the accumulation of both EPS and flagellin in ECM, which are perturbed by *hcp1* deletion. This was unexpected because the literature generally reports an inverse cross-talk between the mucoid phenotype and flagellar assembly. For example, the alternative sigma factor, σ22 (synonym *AlgT* or *AlgU*), is a positive regulator of alginate biosynthesis and a negative regulator of flagellum biosynthesis [38].

***P. fluorescens* MFE01 Hcp1 is involved in motility**

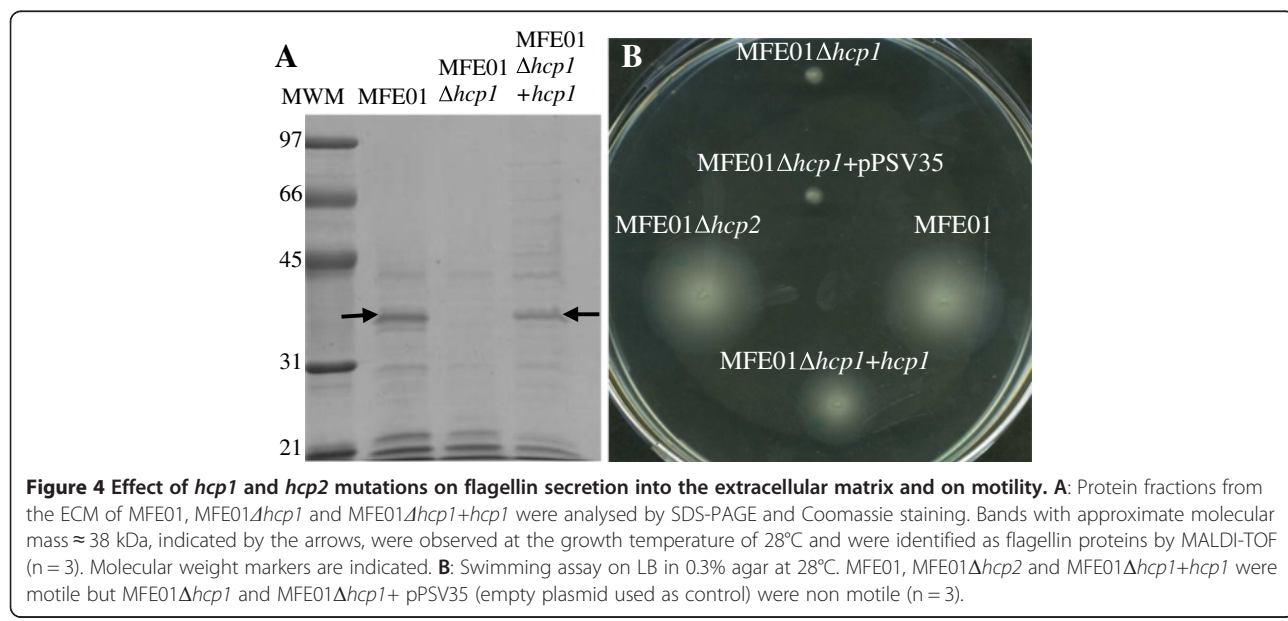
We examined motility of our various strains to elucidate the relation between flagellin accumulation in the ECM and flagellum functionality. MFE01, MFE01Δ*hcp1*, MFE01Δ*hcp2*, MFE01Δ*hcp1*+*pPSV35* (empty vector control) and MFE01Δ*hcp1*+*hcp1* were assayed for swimming;



this confirmed that MFE01 Δ hcp1 had lost motility that was restored by hcp1 introduction *in trans*. The restoration of wild-type phenotype in MFE01 Δ hcp1+hcp1 is inconsistent with a possible polar effect of the hcp1 deletion (Figure 4B).

The type 3 secretion system is related to the flagellum [39], but little is known about the relation between T6SS and the flagellar regulon. The IcmF of *Vibrio cholerae*, a

T6SS protein, is involved in motility [40]. IcmF is an inner-membrane protein of the T6SS found in numerous pathogens, and has been implicated in intracellular multiplication inside host cells [41,42]. In an avian pathogenic *E. coli*, icmF mutation impaired motility [43]; the authors indicate that this contrasts with other mutants in T6SS genes, notably clpV and hcp, which had no motility defects. Their findings suggest that the motility



defect of the *icmF* mutant was not due to a general defect of motility because of a non-functional T6SS. IcmF was somehow involved in flagellar regulation. The restoration of the motility of MFE01 Δ *hcp1* by *hcp1* introduction *in trans* implies that the function of T6SS associated to *hcp1* expression is directly involved in motility in this strain.

The *hcp1* mutant of *P. fluorescens* MFE01 retains virulence toward competitor bacteria

The Hcp concentration was slightly lower in the supernatant of MFE01 Δ *hcp1* than that of the wild-type MFE01 at 28°C (Figure 5A). This is consistent with our previous observations [31]: most of the Hcp secreted by MFE01 is produced from the expression of the *hcp2* gene. We have also demonstrated that MFE01 has a killing activity against various Gram-negative bacteria on solid medium. MFE01 Δ *hcp2* reduced prey cell populations, but significantly less than MFE01 indicating that Hcp2 contributes to the killing activity, and that another factor is also involved. To determine whether Hcp1 could be this other factor, we co-cultured mutant MFE01 Δ *hcp1* and the prey MFN1032 on a filter on solid media for 4 h at 28°C. There was no significant difference of the MFN1032 population between the co-culture with wild-type MFE01 and the co-culture with MFE01 Δ *hcp1* (Figure 5B). Thus, Hcp1 was not the key factor in this antibacterial activity even if it contributed to killing.

Whereas, the MFE01 Δ *hcp2* mutant had significantly less antibacterial activity than MFE01 and MFE01 Δ *hcp1*. The double mutant, MFE01 Δ *hcp1* Δ *hcp2*, was even less bactericidal than MFE01 Δ *hcp2* but nevertheless reduced the MFN1032 population. Another system independent of Hcp1 and Hcp2 seems to be involved in killing activity.

P. fluorescens MFE01 inhibits the motility of *P. fluorescens* strain MFN1032

The killing activity mediated by T6SS during swarming in *P. mirabilis* involves self-recognition (the Dienes effect), and we therefore studied the behaviour of MFE01 in conditions permitting its motility [7,8]. In swimming conditions (in 0.3% agar), *P. fluorescens* MFN1032 was spotted into the centre of a ring formed by MFE01 or its mutants (Figure 6A). MFE01, MFE01 Δ *hcp1*+*hcp1* and MFE01 Δ *hcp2* inhibited MFN1032 motility, but swimming MFN1032 spread through the MFE01 Δ *hcp1* and, MFE01 Δ *hcp1*+*pPSV35* mutants (Figure 6B). The *hcp1* mutation thus abolished MFE01 confining MFN1032. Introduction of the native *hcp1* gene in *trans* restored the inhibitory activity on MFN1032 swimming. Thus, in these swimming conditions, *hcp1* expression seems required for *P. fluorescens* MFE01 to control the swimming of *P. fluorescens* MFN1032. In these conditions, MFE01 Δ *hcp1* lacked motility whereas MFE01 was motile (Figure 4B). The confinement of MFN1032 could be simply due to the formation of a physical barrier by the

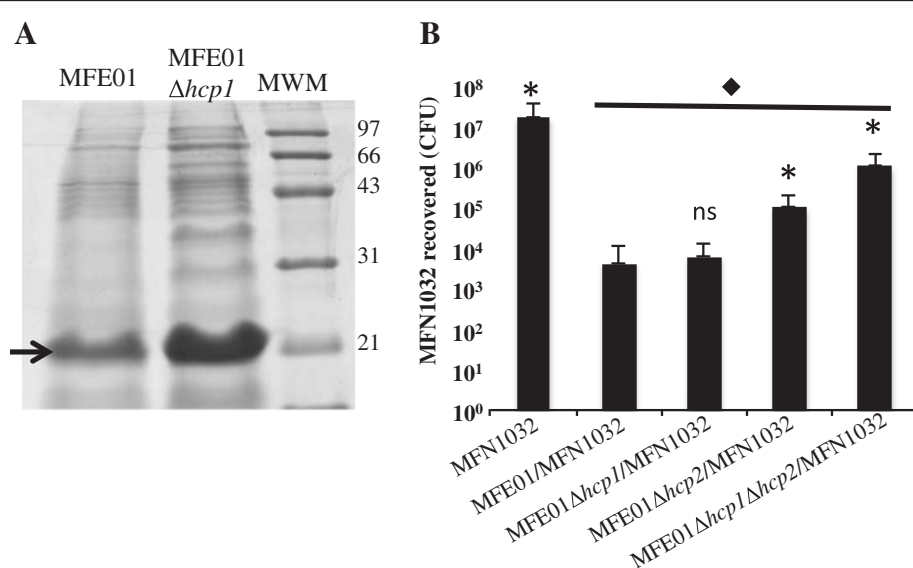


Figure 5 Hcp secretion and killing activity of *P. fluorescens* MFE01 and derivatives strains. **A:** Concentrated supernatants of MFE01 and MFE01 Δ *hcp1* cultures were analysed by SDS-PAGE and Coomassie staining. Bands with a molecular mass similar to that of an Hcp protein (\approx 20 kDa), indicated by the arrow, were observed at a growth temperature of 28°C. MWM: molecular weight markers are indicated. **B:** Quantitative co-culture assays were performed. Prey cells (MFN1032 carrying pSMC21-gfp) were or were not mixed at ratio of 1:5 with *P. fluorescens* MFE01, MFE01 Δ *hcp1*, MFE01 Δ *hcp1* Δ *hcp2* and MFE01 Δ *hcp2*; after 4 h at 28°C, MFN1032 cfu were counted ($n = 4$, the error bars represent standard error of the mean).

* Indicates a significant difference in MFN1032 cfu (p -value <0.05) relative to the MFN1032/MFE01 assay; ns means no significant difference. ♦ indicates a significant difference in MFN1032 cfu (p -value <0.05) relative to the MFN1032 alone control assay.

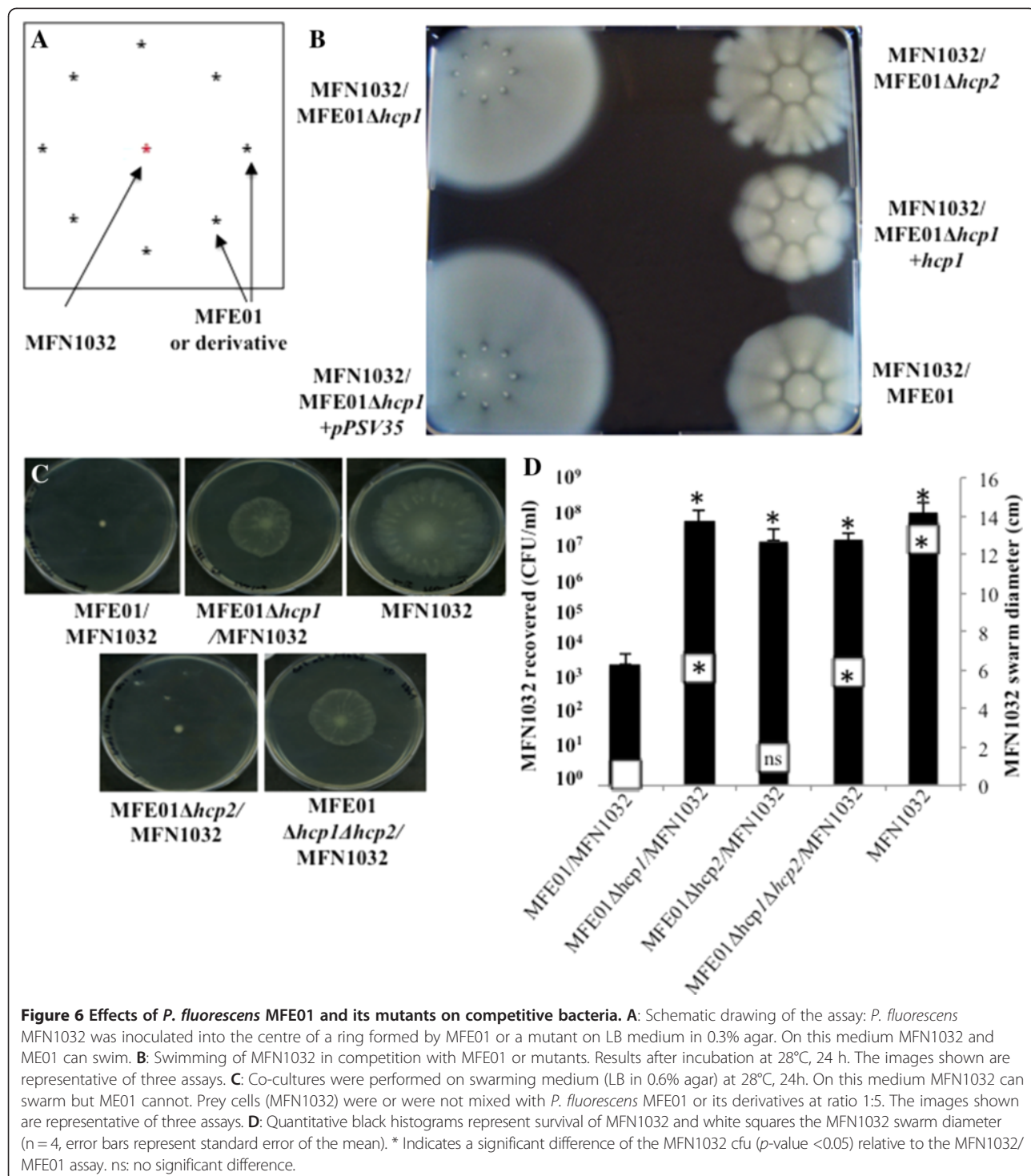


Figure 6 Effects of *P. fluorescens* MFE01 and its mutants on competitive bacteria. **A:** Schematic drawing of the assay: *P. fluorescens* MFN1032 was inoculated into the centre of a ring formed by MFE01 or a mutant on LB medium in 0.3% agar. On this medium MFN1032 and MFE01 can swim. **B:** Swimming of MFN1032 in competition with MFE01 or mutants. Results after incubation at 28°C, 24 h. The images shown are representative of three assays. **C:** Co-cultures were performed on swarming medium (LB in 0.6% agar) at 28°C, 24 h. On this medium MFN1032 can swarm but MFE01 cannot. Prey cells (MFN1032) were or were not mixed with *P. fluorescens* MFE01 or its derivatives at ratio 1:5. The images shown are representative of three assays. **D:** Quantitative black histograms represent survival of MFN1032 and white squares the MFN1032 swarm diameter (n = 4, error bars represent standard error of the mean). * Indicates a significant difference of the MFN1032 cfu (p-value <0.05) relative to the MFN1032/MFE01 assay. ns: no significant difference.

motile MFE01 whereas non-motile MFE01 Δ hcp1 could not form this barrier.

So we therefore conducted co-cultures overnight on 0.6% LB agar, conditions allowing the swarming of MFN1032. On these plates, MFE01 and mutants were unable to swarm because MFE01 lacks surfactants

essential for *P. fluorescens* swarming [44]. MFE01 and MFE01 Δ hcp2 clearly inhibited MFN1032 swarming, whereas MFE01 Δ hcp1 and MFE01 Δ hcp1 Δ hcp2 had much less effect on MFN1032 swarming (Figure 6C,D). This indicates that the inhibition of motility observed was not due to MFE01 or its derivatives forming a physical

barrier. Also, diameter of the MFN1032 swarming was reduced, albeit to a lesser extent, by the double mutant MFE01 Δ hcp1 Δ hcp2 providing further evidence for another unidentified inhibitory factor. These experiments are uninformative about whether the decrease in swarming diameter is due to a killing activity or an immobilization activity.

We consequently assayed the bactericidal activity of MFE01 and its mutants by counting MFN1032 cells in each swarming condition (Figure 6D). The MFN1032 population underwent 5-logs drops after co-culture with wild-type MFE01. Co-culture with MFE01 Δ hcp1 and MFE01 Δ hcp2 did not significantly decrease the MFN1032 population. We assumed that when co-cultured with MFE01 Δ hcp1, MFN1032 cells could swarm and thereby escape from the killing activity mediated by Hcp2, which requires close contact. When in co-culture with MFE01 Δ hcp2, MFN1032 could not be able to escape but the killing activity is abolished by hcp2 mutation. In antibacterial activity assays on solid media (Figure 5B), the MFN1032 cells were immobilized on a filter, and therefore unable to escape the killing activity of the hcp1 mutant.

These results suggest that MFE01 needs Hcp1 and Hcp2 to kill MFN1032 in conditions of motility: Hcp1 could reduce the motility of prey cells and thereby facilitate killing by Hcp2.

Phenotypes assigned to Hcp1 and Hcp2 are associated to a T6SS

Analysis of MFE01 draft genome is under way. Preliminary results indicated that this genome contains only one T6SS cluster exhibiting all core component genes but hcp genes. The two hcp genes, hcp1 and hcp2, are separately located outside this cluster and are associated with vgrG genes. Into this unique T6SS we identified a gene coding for a putative protein corresponding to a protein member of EvpB/VC_A108 family (TIGR03355). This putative protein matched with the WP_016772499.1 sequence (MULTISPECIES: type VI secretion protein [*Pseudomonas*], with 99% identity and coverage of 100%). These proteins are described as T6SS needle sheath proteins TssC and are essential components of this system. MFE01 Δ tssC, a mutant disrupted in this T6SS core component gene, was non motile in swimming conditions and non-mucoid at 28°C as well as MFE01 Δ hcp1 (Figure 7A and B) whereas MFE01 Δ hcp2 conserved the wild type phenotype (mucoid and motile). During co-culture on LBG containing X-gal at 28°C with *E.coli* containing pUC19 (*E.colipUC19*), MFE01 Δ hcp2 and MFE01 Δ tssC allowed *E.colipUC19* growth (blue spots) whereas MFE01 Δ hcp1 and MFE01 inhibited *E.colipUC19* growth (white spots) (Figure 7C). MFE01 Δ tssC phenotype seems similar to a patchwork of MFE01 Δ hcp1 and MFE01 Δ hcp2 phenotypes. These results provide a

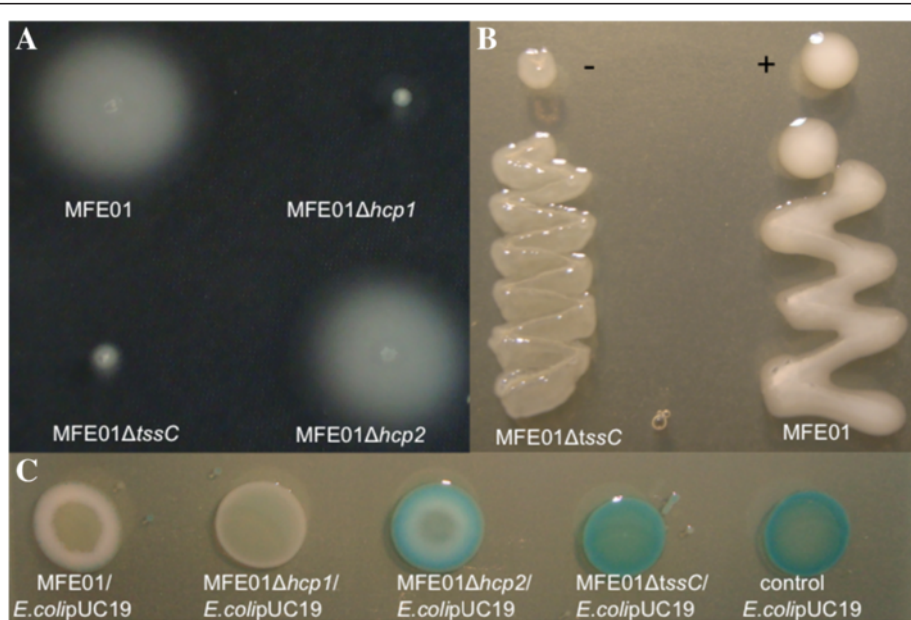


Figure 7 Phenotypes of the MFE01 Δ tssC mutant. **A:** Swimming assay on LB in 0.3% agar at 28°C during 24 h. MFE01 and MFE01 Δ hcp2 were motile contrary to MFE01 Δ hcp1 and MFE01 Δ tssC strains (n = 3). **B:** Representative images of mucoidy of MFE01 and MFE01 Δ tssC on LB agar at 28°C, 24 h (n = 3). +: mucoid, -: non mucoid. **C:** Effects of *P. fluorescens* MFE01 and its mutants on competitive *E. coli* on solid medium. Co-cultures were performed on LB medium supplemented with X-Gal (40 µg/ml) at 28°C during 24 h. Prey cells (*E. coli* DH5α^r containing pUC19) were or were not mixed with *P. fluorescens* MFE01 or its derivatives at ratio 1:1. Blue is due to X-Gal degradation by *E. colipUC19*. The images shown are representative of three assays.

strong confirmation of Hcp1 and Hcp2 involvement in a T6SS.

Conclusion

In this work, we further illustrate the importance and versatility of the T6SS in bacterial adaptation and fitness. We demonstrated cooperation between two different Hcp proteins in bacterial competition. The observations indicate that T6SS associated with Hcp1 secretion has pleiotropic effects on *P. fluorescens* MFE01: it affects mucoidy, motility and competitor inhibition in motility conditions. The relationships between T6SS and flagellin and between T6SS and mucoidy have not yet been fully elucidated. Nevertheless, we describe some of the mechanisms associated with MFE01 motility and inhibition of prey cell motility. This suggests that some effectors, that are used to inhibit competitor motility, could be accumulated in MFE01Δ, in absence of Hcp1, and consequently might inhibit the mutant's own motility. Analysis of MFE01 draft genome is under way. Numerous mutants should be constructed to analyse function of unknown putative genes surrounding these *hcp* genes to ensure an informative genomic annotation and to explain how this T6SS could impact mucoidy and motility.

Methods

Bacterial strains, plasmids and culture conditions

All strains and plasmids used are listed in Table 1. All bacterial strains were grown in LB medium with shaking (180 rpm). *Pseudomonas fluorescens* strains were grown at 28°C or 37°C and *Escherichia coli* at 37°C. Media were supplemented with antibiotics as appropriate: kanamycin (Km) 50 µg/ml (*E. coli*) or 200 µg/ml (*P. fluorescens*); tetracycline (Tc) 15 µg/ml; gentamicin (Gt) 15 µg/ml (*E. coli*), or 50 µg/ml or 100 µg/ml (*P. fluorescens* in liquid and solid media, respectively).

Hcp secretion analysis

Hcp secretion was studied by harvesting the supernatants by centrifuging the cultures at 5000 × g for 10 minutes at 20°C and passing them through a Millipore membrane with 0.22 µm pores. TCA (trichloroacetic acid, Sigma-Aldrich) was added to the supernatant to a final concentration of 10% and the mixture was incubated overnight at 4°C. The supernatant was removed by centrifugation at 13000 × g, for 30 minutes at 4°C. The protein pellet was washed twice with 5 ml of 20 mM Tris base (VWR) in cold acetone (Merck) and centrifuged at 13000 × g, for 30 minutes at 4°C. The dry pellet was then resuspended in distilled water. Proteins were separated by sodium dodecyl sulphate polyacrylamide gel electrophoresis (SDS-PAGE). Briefly, samples were mixed with an equal volume of 2 × Laemmli sample buffer

Table 1 Plasmids and strains used in the study

Strains or plasmids	Relevant characteristics	Reference/source
<i>P. fluorescens</i>		
MFE01	Air isolate, Rif ^R	[31]
MFE01Δ <hcp2></hcp2>	MFE01 with early stop codon in <i>hcp2</i>	[31]
MFE01Δ <hcp1></hcp1>	MFE01 with <i>hcp1</i> disruption	This study
MFE01Δ <hcp1></hcp1> + <i>hcp1</i>	MFE01Δ <hcp1></hcp1> with pPSV35 carrying the wild-type <i>hcp1</i> gene	This study
MFE01Δ <hcp1></hcp1> Δ <hcp2></hcp2>	MFE01 with <i>hcp1</i> and <i>hcp2</i> mutations	This study
MFE01ΔtssC	MFE01 with <i>tssC</i> disruption	This study
MFN1032	Clinical strain	[33]
MFP05	Skin isolate	[32]
Pf-5	Plant isolate	[34]
MFE07	Air isolate	This study
<i>Escherichia coli</i>		
DH5αmcr	General cloning strain	LMSM collection
S17.1	RP4-2-Tc:Mu, <i>aph</i> ::Tn7, <i>recA</i> , SmR, donor strain for conjugation	[48]
Vectors		
pPSV35	<i>P. aeruginosa</i> oriV, <i>lacq</i> mob+, <i>PlacUV5</i> , pUC18 MCS, expression vector, Gm ^R	[49]
pSMC21-gfp	Replicative plasmid, Km ^R , <i>gfp</i>	[46]
pME3087	Suicide plasmid, Tc ^R	[47]
pUC19	Replicative plasmid, <i>lacZ</i> , Ap ^R	Invitrogen®

(with β-mercaptoethanol), boiled for 5 min at 100°C and then cooled to room temperature before loading.

Mucoid phenotype and swimming assays

Strains were plated on LB agar with 0.1 mM IPTG and incubated for 24 h at 28°C; the colonies were then examined for the mucoid phenotype. Swimming assays were performed as previously described [45].

Swarming killing assay

The protocol described by Alteri and colleagues [8] was used with minor modifications. Aliquots of 5 µl of a mixture of strains at a ratio of 5:1, MFE01 or mutants: MFN1032 containing plasmid pSMC21-gfp [46] were spotted onto LB 0.6% agar with 0.1 mM IPTG. The plates were incubated overnight at 28°C, and the entire swarm was collected, and serially diluted. Aliquots of 10 µl of each dilution were plated on LB agar supplemented with 200 µg kanamycin and colony forming units counted.

Motility inhibition

Overnight cultures were centrifuged at $3000 \times g$, for 5 minutes at room temperature. The cell pellets were collected on toothpicks which was used to stab 0.3% agar LB plates, with 0.1 mM IPTG; the plates were then incubated at 28°C overnight.

Antibacterial competition assay

Antibacterial competition assays in solid media were performed as described by Decoin and coworkers [31]. To ensure pSMC21-*gfp* stability (presence or absence) in our conditions, MFN1032 containing pSMC21-*gfp* was cultivated in LB medium containing kanamycin until OD_{580 nm} of 1. Serial dilutions were then plated on LB plates without Kanamycin during 24 h at 28°C. Colonies were scrapped and suspended in NaCl 9 g/L and adjusted to OD_{580 nm} of 1. Serial dilutions were plated on selective (with kanamycin) and non-selective (without kanamycin) plates and counting. Statistics were done by pairwise strain comparisons (non-parametric Mann-Whitney-two tailed Test): no significant difference was observed between the two conditions (p-value >0.05, n = 6).

For *E.coli* growth inhibition, *Pseudomonas fluorescens* MFE01 and mutants were cultivated at 28°C in LB medium with shaking at 180 rpm overnight. *Escherichia coli* DH5αmcr transformed with pUC19 (*E.coli*pUC19), allowing blue detection on medium containing X-Gal, was cultivated at 37°C in LB with ampicillin (50 µg/ml) with shaking at 180 rpm overnight. The OD_{580 nm} was adjusted to 0.5 and the strains were mixed at a 1:1 ratio. A volume of 20 µl was spotted in LB agar plates supplemented with X-Gal (40 µg/ml) and incubated overnight at 28°C.

Disruption of the *hcp1* gene in *P. fluorescens* MFE01

MFE01Δ*hcp1* was generated by deletions in the 5' (44 bp) and 3' extremities (18 bp) of *hcp1*. 5' and 3' truncated *hcp1* was generated by PCR with the Hcp3F and Hcp4R primers (see Table 2). The resulting truncated *hcp1* construct was introduced between the *Eco*RI and *Hind*III sites (blunt-ended) of the transferable suicide plasmid pME3087 (6.9 Kb) [47]. The resulting plasmid, pME3087Δ*hcp1*, was verified by sequencing and was then transferred into MFE01 by biparental mating: *E. coli* S17-1 [48] containing pME3087Δ*hcp1* and recipient MFE01 cells were mixed and spotted onto LB agar plates and incubated overnight at 37°C. The mating mixture was then suspended in 1 ml of sterile NaCl 9 g/L and 0.1 ml aliquots were spread on LB agar plates supplemented with tetracycline (12 µg/ml), to select for the presence of the integrated plasmid, and rifampicin (25 µg/ml), to kill the *E. coli* S17-1 donor bacteria and to ensure the

Table 2 Oligonucleotides used for this study

Primer name	Primer sequence (5'-3')
PFL_1449mucAF	ATAATAAGAGCTCATGAGTCGTGAAGCCCTGC
PFL_1449mucAR	ATAATAATCTAGATTAGCGGTTTCAGGCTTG
Hcp1F	ATGGCAACACCAGCGTACATG
Hcp2R	TTAAACGACTGGAGCACGCCA
Hcp3F	CCTGATCACTGCCGGCGCTT
Hcp4R	ACGCCAGTCATCGGAACCCG
muta1tssC	CTGAGACTCCAGTAGCCAAG
muta2tssC	AAGCTTCCAGACCGAAGAAACTCGTGGGT
muta3tssC	CCAGGTGAT
muta4tssC	ATCACCTGGACCCACGAAGTATGAAGGCTCAT
	CTCCCTGAC
	ATGTCATTGAGATCGGGCAA

selection of MFE01. The resulting *hcp1* mutant (containing two truncated *hcp1* genes) was named MFE01Δ*hcp1*.

Disruption of the *hcp2* gene in *P. fluorescens* MFE01Δ*hcp1* and disruption of the *tssC* gene in *P. fluorescens* MFE01

A markerless *hcp2* mutation was introduced into MFE01Δ*hcp1* strain by the protocol described by Decoin and co-workers [31]. The resulting strain was named MFE01Δ*hcp1*Δ*hcp2*. The same protocol with PCR modifications was used to introduce a markerless *tssC* mutation into MFE01 strain. This *tssC* deletion was achieved by PCR with the muta1tssC and muta2tssC primers (<650 bp product) or the muta3tssC and muta4tssC primers (<650 bp product) (Table 2). The PCR products obtained corresponded to the upstream and downstream parts, respectively, of the *tssC* gene of MFE01, each carrying an overlapping sequence at the end. PCR parameters were as follows: annealing temperature, 62°C, extension time, 45 s; 35 cycles. A third PCR was then carried out in which the overlapping sequences of the two first products were hybridized together allowing the *tssC* deletion after PCR with the muta1tssC and muta4tssC primers. The PCR parameters were as follows: annealing temperature, 62°C; extension time, 1 m 45 s and 35 cycles. The mutant containing the *tssC* deletion was verified by DNA sequencing and named MFE01Δ*tssC*.

Heterologous expression of *mucA* in MFE01

The *mucA* (PFL_1449) sequence was amplified with the PFL_1449mucAF and PFL_1449mucAR primers (Table 2) by standard PCR from genomic DNA from *P. protegens* Pf-5. The PCR conditions were as follows: an annealing temperature of 64°C, an extension time of 30 s and 25 cycles. The polymerase used was Phusion® High-Fidelity DNA polymerase (NEB). The PCR product was digested with *Sac*I (NEB) and *Xba*I (NEB) and ligated into pPSV35 [49] digested with the same enzymes. *E. coli* was

transformed with the ligation product and the resulting plasmid was checked by PCR. Fresh MFE01 colonies were washed twice in cold sterile distilled water and transformed with 5 µl of plasmid DNA by electroporation in 1 mm cuvette at 1.8 kV (Savant electroporator). LB was then added and the mix incubated for 1 h at 28°C with shaking (180 rpm). The samples were then plated on LB agar supplemented with gentamicin and with 0.1 mM IPTG.

Insertion of the *hcp1* gene into pPSV35 and construction of strain MFE01Δ*hcp1*+*hcp1*

The *hcp1* gene was amplified from the *P. fluorescens* MFE01 genome with the Hcp1F and Hcp2R primers (Table 2). The PCR conditions were as follows: an annealing temperature of 59°C, an extension time of 30 s and 25 cycles. The polymerase used was the Phusion® High-Fidelity DNA polymerase (NEB). The amplified fragments were inserted into the pPSV35 shuttle vector at *Sma*I site by blunt-end ligation, and the resulting pPSV35-*hcp1* was used to transform *E. coli* DH5αmcr cells by electroporation. Plasmid DNA was isolated using the QIAprep Spin Miniprep Kit (Qiagen) and checked by PCR and asymmetric digestion with *Bam*H1 (NEB) to verify the orientation of the insert. MFE01Δ*hcp1* was transformed with pPSV35-*hcp1* by electroporation as described in the section “Heterologous expression of *mucA* in MFE01”. The resulting strain was called MFE01Δ*hcp1*+*hcp1*.

Preparation and purification of extracellular matrix (ECM) containing exopolysaccharides (EPS)

Strains were tested for EPS production on LB agar at 28°C. ECM was extracted as described by Dignac and colleagues with modifications [50]. Biomass was harvested and suspended in NaCl 9 g/L then sonicated at 37 Watts for 30 sec on ice and centrifuged (20,000 × g for 30 min). Clear supernatants were collected and three volumes of ice-cold ethanol were added; the samples were incubated for 24 h at 4°C, and EPS were collected by centrifugation (7000 × g, 30 min). The EPS-containing pellets were resuspended in water and lyophilised.

Analysis of the monosaccharide composition of EPS by gas chromatography – flame ionization

Lyophilised EPS were hydrolysed by treatment with 2M trifluoroacetic acid for 2 hours at 110°C. Monosaccharides were then derivatised: methanol-1M HCl (Supelco) was added and the samples incubated at 80°C overnight; then a mix of hexamethyldisiloxan:trimethylsiloxan:pyridine (3:1:9, Supelco) was added and the samples incubated at 110°C for 20 minutes. The resulting derivatives were dried then dissolved in 1 ml of cyclohexane and injected into the 3800 GC system equipped with a

CP-Sil5-CB column (Agilent Technologies). Elution was performed with the following gradient of temperature: 120°C to 160°C at a rate of 10°C per minute, 160°C to 220°C at a rate of 1.5°C per minute, 220°C to 280°C at a rate of 20°C per minute. Quantification was based on the internal standard and response factor determined previously for each monosaccharide.

Biofilm formation

Pure culture biofilms were grown in continuous-culture three-channel flow cells (channel dimensions, 1 by 4 by 40 mm). The system was assembled and prepared as follows: system sterilization during 4 h with bleach at 1.2% and rinsing with sterile NaCl 9 g/L. Before flow chamber inoculation, LB medium was injected into the system at 28°C. Overnight cultures were centrifuged at 8 000 × g during 5 min at room temperature. Pellets were recovered and washed twice with 2 mL of sterilized physiological water. Channels were inoculated with 1 mL of pure bacterial suspension at DO_{580nm} = 0.1. Bacteria were allowed to attach to the glass surface (microscope coverslip, VWR International, Fontenay sous Bois, France) during 2 h at 28°C under static conditions. Biofilm growth was then performed under a constant flow of LB medium with antibiotics at appropriate concentration if necessary (Wakson Marlow 205S, 2.5 mL/h) for 48 h at 28°C.

Confocal laser scanning microscopy (CLSM) and image analyses

Microscopic observations were performed with a LSM 710 system, Zeiss, Germany by using a 63x oil immersion objective. Biofilms were observed after a 15 min incubation with 5 µM Syto 9® green fluorescent nucleic acid stain (Life technologies) (excitation and emission λ, 488 nm and 510 nm, respectively). Biofilm stacks were analysed with COMSTAT software. The calculated parameter was the biovolume, which is the volume of bacteria (in µm³) per µm² of glass surface. The results were the mean of at least five independent experiments.

Mass spectrometry analysis

Mass spectroscopy (MS) analyses were performed with a MALDI-TOF AutoFlexIII (Bruker) in positive ion mode as described by Barbey et al. [51]. Statistical analyses of the sequences involved determining the probability based on Mowse score with MASCOT software (peptide tolerance = 100 ppm and mass values = MH⁺). A p-value of less than 0.05 was considered significant. The criteria used to accept a protein identification based on peptide mass fingerprinting (PMF) data included a score probability greater than a score threshold defined by MASCOT software.

Statistical analysis

Non-parametric Mann–Whitney Tests (two tailed) with GraphPad Prism version 6.0 (La Jolla, CA) were used for statistical analyses. A *p*-value <0.05 was considered to be statistically significant.

Competing interests

All authors declare that they have no competing interest.

Authors' contributions

VD carried out the assays with the help of MG and CB and participated in the design of the experiments and writing of the manuscript. AM designed the study, wrote the manuscript and analysed most of the data. CDP and FL were involved in ECM analysis. NO and MF were involved in scientific discussions during the design of the study. All authors read and approved the final manuscript.

Acknowledgements

This study was supported by a GRR CBS Sesa grant from the Région Haute-Normandie and FEDER funds. We are grateful to Josette Guérillon and Gaëlle Rossignol, who initiated T6SS research in the LMSM lab. We also thank Alex Edelman and Awa N'Diaye Renoult for linguistic support.

Author details

¹LMSM, Laboratoire de Microbiologie Signaux et Microenvironnement, Normandie Université, EA 4312, IRIB, Université de Rouen, IUT d'Evreux, 55 rue Saint Germain, 27000 Evreux, France. ²GlycoMEV, Laboratoire de Glycobiologie et Matrice Extracellulaire Végétale, Normandie Université, EA 4358, Université de Rouen, Faculté des sciences, Bâtiment 20 Gadeau de Kerville, IRIB 76820 Mont Saint-Aignan, France.

Received: 3 July 2014 Accepted: 11 March 2015

Published online: 26 March 2015

References

1. Jani AJ, Cotter PA. Type VI secretion: not just for pathogenesis anymore. *Cell Host Microbe*. 2010;8(1):2–6.
2. Records AR. The type VI secretion system: a multipurpose delivery system with a phage-like machinery. *Mol Plant Microbe Interact*. 2011;24(7):751–7.
3. Basler M, Mekalanos JJ. Type 6 secretion dynamics within and between bacterial cells. *Science*. 2012;337(6096):815.
4. Hood RD, Singh P, Hsu F, Guvener T, Carl MA, Trinidad RR, et al. A type VI secretion system of *Pseudomonas aeruginosa* targets a toxin to bacteria. *Cell Host Microbe*. 2010;7(1):25–37.
5. Murdoch SL, Trunk K, English G, Fritsch MJ, Pourkarimi E, Coulthurst SJ. The opportunistic pathogen *Serratia marcescens* utilizes type VI secretion to target bacterial competitors. *J Bacteriol*. 2011;193(21):6057–69.
6. Brunet YR, Espinosa L, Harchouni S, Mignot T, Cascales E. Imaging type VI secretion-mediated bacterial killing. *Cell Rep*. 2013;3(1):36–41.
7. Gibbs KA, Urbanowski ML, Greenberg EP. Genetic determinants of self identity and social recognition in bacteria. *Science*. 2008;321(5886):256–9.
8. Alteri CJ, Himpel SD, Pickens SR, Lindner JR, Zora JS, Miller JE, et al. Multicellular bacteria deploy the type VI secretion system to preemptively strike neighboring cells. *PLoS Pathog*. 2013;9(9):e1003608.
9. Aschtgen MS, Gavioli M, Dessen A, Lloubes R, Cascales E. The SciZ protein anchors the enteroaggregative *Escherichia coli* Type VI secretion system to the cell wall. *Mol Microbiol*. 2010;75(4):886–99.
10. Aschtgen MS, Thomas MS, Cascales E. Anchoring the type VI secretion system to the peptidoglycan: TssL, TagL, TagP... what else? *Virulence*. 2010;1(6):535–40.
11. Pukatzki S, McAuley SB, Miyata ST. The type VI secretion system: translocation of effectors and effector-domains. *Curr Opin Microbiol*. 2009;12(1):11–7.
12. Silverman JM, Agnello DM, Zheng H, Andrews BT, Li M, Catalano CE, et al. Haemolysin coregulated protein is an exported receptor and chaperone of type VI secretion substrates. *Mol Cell*. 2013;51(5):584–93.
13. Goodman AL, Kulasekara B, Rietsch A, Boyd D, Smith RS, Lory S. A signaling network reciprocally regulates genes associated with acute infection and chronic persistence in *Pseudomonas aeruginosa*. *Dev Cell*. 2004;7(5):745–54.
14. Mougous JD, Cuff ME, Raunser S, Shen A, Zhou M, Gifford CA, et al. A virulence locus of *Pseudomonas aeruginosa* encodes a protein secretion apparatus. *Science*. 2006;312(5779):1526–30.
15. Ventre I, Goodman AL, Vallet-Gely I, Vasseur P, Soscia C, Molin S, et al. Multiple sensors control reciprocal expression of *Pseudomonas aeruginosa* regulatory RNA and virulence genes. *Proc Natl Acad Sci U S A*. 2006;103(1):171–6.
16. Moscoso JA, Mikkelsen H, Heeb S, Williams P, Filloux A. The *Pseudomonas aeruginosa* sensor RetS switches type III and type VI secretion via c-di-GMP signalling. *Environ Microbiol*. 2011;13(12):3128–38.
17. Hassan KA, Johnson A, Shaffer BT, Ren Q, Kidarsa TA, Elbourne LD, et al. Inactivation of the GacA response regulator in *Pseudomonas fluorescens* Pf-5 has far-reaching transcriptomic consequences. *Environ Microbiol*. 2010;12(4):899–915.
18. Records AR, Gross DC. Sensor kinases RetS and LadS regulate *Pseudomonas syringae* type VI secretion and virulence factors. *J Bacteriol*. 2010;192(14):3584–96.
19. Jacques M, Marrie TJ, Costerton JW. Review: Microbial colonization of prosthetic devices. *Microb Ecol*. 1987;13(3):173–91.
20. Terry JM, Pina SE, Mattingly SJ. Role of energy metabolism in conversion of nonmucoid *Pseudomonas aeruginosa* to the mucoid phenotype. *Infect Immun*. 1992;60(4):1329–35.
21. Wood LF, Leech AJ, Ohman DE. Cell wall-inhibitory antibiotics activate the alginate biosynthesis operon in *Pseudomonas aeruginosa*: Roles of sigma (AlgT) and the AlgW and Prc proteases. *Mol Microbiol*. 2006;62(2):412–26.
22. Ramsey DM, Baynham PJ, Wozniak DJ. Binding of *Pseudomonas aeruginosa* AlgZ to sites upstream of the algZ promoter leads to repression of transcription. *J Bacteriol*. 2005;187(13):4430–43.
23. Hoiby N, Ciofu O, Bjarnsholt T. *Pseudomonas aeruginosa* biofilms in cystic fibrosis. *Future Microbiol*. 2010;5(11):1663–74.
24. Pugashetti BK, Metzger JR HM, Vadas L, Feingold DS. Phenotypic differences among clinically isolated mucoid *Pseudomonas aeruginosa* strains. *J Clin Microbiol*. 1982;16(4):686–91.
25. Wiens JR, Vasil AI, Schurr MJ, Vasil ML. Iron-regulated expression of alginate production, mucoid phenotype, and biofilm formation by *Pseudomonas aeruginosa*. *MBio*. 2014;5(1):e01010–3.
26. Rao J, Damron FH, Basler M, Digianomenico A, Sherman NE, Fox JW, et al. Comparisons of two proteomic analyses of non-mucoid and mucoid *Pseudomonas aeruginosa* clinical isolates from a cystic fibrosis patient. *Front Microbiol*. 2011;2:162.
27. Unterweger D, Kitaoka M, Miyata ST, Bachmann V, Brooks TM, Moloney J, et al. Constitutive type VI secretion system expression gives *Vibrio cholerae* intra- and interspecific competitive advantages. *PLoS One*. 2012;7(10):e48320.
28. Fett WF, Wells JM, Cescutti P, Wijey C. Identification of exopolysaccharides produced by fluorescent pseudomonads associated with commercial mushroom (*Agaricus bisporus*) production. *Appl Environ Microbiol*. 1995;61(2):513–7.
29. Scanlan PD, Buckling A. Co-evolution with lytic phage selects for the mucoid phenotype of *Pseudomonas fluorescens* SBW25. *Isme J*. 2012;6(6):1148–58.
30. Muhammadi AN. Genetics of bacterial alginate: alginate genes distribution, organization and biosynthesis in bacteria. *Curr Genomics*. 2007;8(3):191–202.
31. Decoin V, Barbey C, Bergeau D, Latour X, Feuilloley MG, Orange N, et al. A type VI secretion system is involved in *Pseudomonas fluorescens* bacterial competition. *PLoS One*. 2014;9(2):e89411.
32. Dagorn A, Chapalain A, Mijouin L, Hillion M, Duclairoir-Poc C, Chevalier S, et al. Effect of GABA, a bacterial metabolite, on *Pseudomonas fluorescens* surface properties and cytotoxicity. *Int J Mol Sci*. 2013;14(6):12186–204.
33. Chapalain A, Rossignol G, Lesouhaitier O, Merleau A, Gruffaz C, Guerillon J, et al. Comparative study of 7 fluorescent pseudomonad clinical isolates. *Can J Microbiol*. 2008;54(1):19–27.
34. Paulsen IT, Press CM, Ravel J, Kobayashi DY, Myers GS, Mavrodi DV, et al. Complete genome sequence of the plant commensal *Pseudomonas fluorescens* Pf-5. *Nat Biotechnol*. 2005;23(7):873–8.
35. Kitaoka M, Miyata ST, Brooks TM, Unterweger D, Pukatzki S. Vash is a transcriptional regulator of the type VI secretion system functional in endemic and pandemic *Vibrio cholerae*. *J Bacteriol*. 2011;193(23):6471–82.
36. Miyata ST, Kitaoka M, Brooks TM, McAuley SB, Pukatzki S. *Vibrio cholerae* requires the type VI secretion system virulence factor VasX to kill *Dictyostelium discoideum*. *Infect Immun*. 2011;79(7):2941–9.

37. Pulcrano G, Iula DV, Raia V, Rossano F, Catania MR. Different mutations in *mucA* gene of *Pseudomonas aeruginosa* mucoid strains in cystic fibrosis patients and their effect on *algU* gene expression. New Microbiol. 2012;35(3):295–305.
38. Tart AH, Wolfgang MC, Wozniak DJ. The alternative sigma factor AlgT represses *Pseudomonas aeruginosa* flagellum biosynthesis by inhibiting expression of *fleQ*. J Bacteriol. 2005;187(23):7955–62.
39. Cornelis GR. The type III secretion injectisome. Nat Rev Microbiol. 2006;4(1):811–25.
40. Das S, Chakrabortty A, Banerjee R, Chaudhuri K. Involvement of in vivo induced *icmF* gene of *Vibrio cholerae* in motility, adherence to epithelial cells, and conjugation frequency. Biochem Biophys Res Commun. 2002;295(4):922–8.
41. Hilbi H, Segal G, Shuman HA. Lcm/Dot-dependent upregulation of phagocytosis by *Legionella pneumophila*. Mol Microbiol. 2001;42(3):603–17.
42. Watarai M, Derre I, Kirby J, Grawney JD, Dietrich WF, Isberg RR. *Legionella pneumophila* is internalized by a macropinocytotic uptake pathway controlled by the Dot/lcm system and the mouse Lgn1 locus. J Exp Med. 2001;194(8):1081–96.
43. de Pace F, Boldrin De Paiva J, Nakazato G, Lancellotti M, Sircili MP, Guedes Stehling E, et al. Characterization of lcfM of the type VI secretion system in an avian pathogenic *Escherichia coli* (APEC) strain. Microbiology. 2011;157(10):2954–62.
44. Rossignol G, Sperandio D, Guerillon J, Duclairoir Poc C, Soum-Soutera E, Orange N, et al. Phenotypic variation in the *Pseudomonas fluorescens* clinical strain MFN1032. Res Microbiol. 2009;160(5):337–44.
45. Rossignol G, Merieau A, Guerillon J, Veron W, Lesouhaitier O, Feuilloley MG, et al. Involvement of a phospholipase C in the hemolytic activity of a clinical strain of *Pseudomonas fluorescens*. BMC Microbiol. 2008;8:189.
46. Davey ME, Caiazza NC, O'Toole GA. Rhamnolipid surfactant production affects biofilm architecture in *Pseudomonas aeruginosa* PAO1. J Bacteriol. 2003;185(3):1027–36.
47. Schnider U, Keel C, Voisard C, Defago G, Haas D. Tn5-directed cloning of *pqq* genes from *Pseudomonas fluorescens* CHA0: mutational inactivation of the genes results in overproduction of the antibiotic pyoluteorin. Appl Environ Microbiol. 1995;61(11):3856–64.
48. Simon R, Pehle A. A broad host range mobilization system for in vitro genetic engineering: transposon mutagenesis in Gram-negative bacteria. Biotechnology. 1983;1:784–90.
49. Rietsch A, Vallet-Gely I, Dove SL, Mekalanos JJ. ExsE, a secreted regulator of type III secretion genes in *Pseudomonas aeruginosa*. Proc Natl Acad Sci U S A. 2005;102(22):8006–11.
50. Dignac MF, Urbain V, Rybacki D, Bruchet A, Snidaro D, Scribe P. Chemical description of extracellular polymers: implication on activates sludge floc structure. Wat sci tech. 1998;8:945–53.
51. Barbe C, Crepin A, Cirou A, Budin-Verneuil A, Orange N, Feuilloley M, et al. Catabolic pathway of gamma-caprolactone in the biocontrol agent *Rhodococcus erythropolis*. J Proteome Res. 2012;11(1):206–16.

**Submit your next manuscript to BioMed Central
and take full advantage of:**

- Convenient online submission
- Thorough peer review
- No space constraints or color figure charges
- Immediate publication on acceptance
- Inclusion in PubMed, CAS, Scopus and Google Scholar
- Research which is freely available for redistribution

Submit your manuscript at
www.biomedcentral.com/submit



P26



Response to Gaseous NO₂ Air Pollutant of *P. fluorescens* Airborne Strain MFAF76a and Clinical Strain MFN1032

Tatiana Kondakova^{1,2}, Chloé Catovic¹, Magalie Barreau¹, Michael Nusser³, Gerald Brenner-Weiss³, Sylvie Chevalier¹, Frédéric Dionnet², Nicole Orange¹ and Cécile Duclairoir Poc^{1*}

¹ Laboratory of Microbiology Signals and Microenvironment EA 4312, Normandy University, University of Rouen, SéSa, IRIB, Evreux, France, ² Aerothermic and Internal Combustion Engine Technological Research Centre, Saint Etienne du Rouvray, France, ³ Institute of Functional Interfaces, Karlsruhe Institute of Technology, Karlsruhe, Germany

OPEN ACCESS

Edited by:

Steve Brian Pointing,
Auckland University of Technology,
New Zealand

Reviewed by:

Paolina Garbeva,
Netherlands Institute of Ecology,
Netherlands
Donnabella Castillo Lacap-Bugler,
Auckland University of Technology,
New Zealand

*Correspondence:

Cécile Duclairoir Poc
cecile.poc@univ-rouen.fr

Specialty section:

This article was submitted to
Terrestrial Microbiology,
a section of the journal
Frontiers in Microbiology

Received: 08 November 2015

Accepted: 09 March 2016

Published: 31 March 2016

Citation:

Kondakova T, Catovic C, Barreau M,
Nusser M, Brenner-Weiss G,
Chevalier S, Dionnet F, Orange N and
Duclairoir Poc C (2016) Response to
Gaseous NO₂ Air Pollutant of *P.
fluorescens* Airborne Strain MFAF76a
and Clinical Strain MFN1032.
Front. Microbiol. 7:379.
doi: 10.3389/fmicb.2016.00379

Human exposure to nitrogen dioxide (NO₂), an air pollutant of increasing interest in biology, results in several toxic effects to human health and also to the air microbiota. The aim of this study was to investigate the bacterial response to gaseous NO₂. Two *Pseudomonas fluorescens* strains, namely the airborne strain MFAF76a and the clinical strain MFN1032 were exposed to 0.1, 5, or 45 ppm concentrations of NO₂, and their effects on bacteria were evaluated in terms of motility, biofilm formation, antibiotic resistance, as well as expression of several chosen target genes. While 0.1 and 5 ppm of NO₂ did not lead to any detectable modification in the studied phenotypes of the two bacteria, several alterations were observed when the bacteria were exposed to 45 ppm of gaseous NO₂. We thus chose to focus on this high concentration. NO₂-exposed *P. fluorescens* strains showed reduced swimming motility, and decreased swarming in case of the strain MFN1032. Biofilm formed by NO₂-treated airborne strain MFAF76a showed increased maximum thickness compared to non-treated cells, while NO₂ had no apparent effect on the clinical MFN1032 biofilm structure. It is well known that biofilm and motility are inversely regulated by intracellular c-di-GMP level. The c-di-GMP level was however not affected in response to NO₂ treatment. Finally, NO₂-exposed *P. fluorescens* strains were found to be more resistant to ciprofloxacin and chloramphenicol. Accordingly, the resistance nodulation cell division (RND) MexEF-OprN efflux pump encoding genes were highly upregulated in the two *P. fluorescens* strains. Noticeably, similar phenotypes had been previously observed following a NO treatment. Interestingly, an *hmp*-homolog gene in *P. fluorescens* strains MFAF76a and MFN1032 encodes a NO dioxygenase that is involved in NO detoxification into nitrites. Its expression was upregulated in response to NO₂, suggesting a possible common pathway between NO and NO₂ detoxification. Taken together, our study provides evidences for the bacterial response to NO₂ toxicity.

Keywords: airborne, *Pseudomonas fluorescens*, nitrogen dioxide, biofilm, antibiotic sensitivity, motility, air pollution

INTRODUCTION

Most world-wide cities have serious air-quality problems, which have attracted attention in the past decade. One of the most common source of air pollution is engine emissions, which include, among other toxic molecules, the nitrogen oxides (NO_x; reviewed in Sher, 1998; Skalska et al., 2010). The general term NO_x includes nitric oxide (NO) and nitrogen dioxide (NO₂). NO in turn is able to damage bacterial cells interacting with bacterial proteins (McLean et al., 2010; Laver et al., 2013) and DNA (Tamir et al., 1996; Burney et al., 1999) either directly, or via formation of reactive nitrogen species (RNS), causing alterations in bacterial metabolism, among which respiration, and homeostasis. As a result, bacteria have developed specific NO detoxification pathways and defense mechanisms (Cruz-Ramos et al., 2002; Flatley et al., 2005; Spiro, 2007). In order to counteract the NO-mediated respiratory arrest (Husain et al., 2008), the detoxification processes are completed in several bacteria by metabolism reprogramming (Auger et al., 2011; Auger and Appanna, 2015). NO was furthermore identified as a signaling molecule, which promotes the biofilm dispersion in various bacterial strains, including *Pseudomonas aeruginosa* (Barraud et al., 2009; Cutruzzola and Frankenberg-Dinkel, 2015) and *P. putida* (Liu et al., 2012). This molecule is also known to modulate bacterial antibiotic sensitivity, protecting bacteria from a wide range of antibacterial agents (Gusarov et al., 2009; McCollister et al., 2011; van Sorge et al., 2013), such as vancomycin and daptomycin (van Sorge et al., 2013). Contrary to NO, NO₂ has a low solubility in water (Augusto et al., 2002). Thence NO₂ in aqueous media concerned a few reports in the microbiological context. However, in natural environments NO is unstable and quickly oxidized to form NO₂ (Skalska et al., 2010), considered as a major air pollutant. Its atmospheric level is ruled by European environmental commission and World Health Organization (INERIS, 2011; Reduction of pollutant emissions from light vehicles, 2015; WHO |Ambient (outdoor) air quality health, 2015). NO₂ toxicity to human health is well documented and is known to increase cardiovascular diseases (Chaloulakou et al., 2008), or to aggravate respiratory symptoms especially in children (Pershagen et al., 1995; Chauhan et al., 1998). On the opposite, the stress promoted by NO₂ was poorly evaluated on bacteria.

It is increasingly evident that the air is a biotic environment, containing bacteria as one of the major compounds of primary atmosphere aerosol particles (Burrows et al., 2009b; Després et al., 2012). Mean airborne bacterial concentrations can indeed be greater than $1 \cdot 10^4$ cells m⁻³ (Bauer et al., 2002; Burrows et al., 2009a). Although unstable, the air microbiota is frequently constituted with members of *Pseudomonas* genus (Fang et al., 2007; Pearce et al., 2010; Després et al., 2012; Dybwad et al., 2012; Šantl-Temkiv et al., 2015). Among these highly versatile elements, the *P. fluorescens* strains are widely adaptable and distributed (Bodilis et al., 2004) in all major natural environments, including water (Bodilis et al., 2004), soil (Varivarn et al., 2013) and clouds (Ahern et al., 2007). Several *P. fluorescens* strains were also found to promote humans acute infections and were reported in clinical samples

of immuno-compromised patients (Chapalain et al., 2008; Scales et al., 2014). All these properties make *P. fluorescens* a good model for further investigations of airborne bacteria.

We have investigated in previous studies the microbiota (bacteria, yeasts and fungi) of Rouen harbor terminal (France) (Morin et al., 2013). Thus, several *P. fluorescens* strains were isolated. Among them, the airborne *P. fluorescens* strain MFAF76a was characterized as a virulent strain, particularly its exoproducts against human epithelial pulmonary cells (Duclairoir Poc et al., 2014). The aim of this study is to investigate the physiological response of airborne *P. fluorescens* MFAF76a to NO₂ as a marker of air pollution in terms of motility, biofilm formation and antibiotic resistance. This response was compared to that of the clinical strain *P. fluorescens* MFN1032 isolated from the sputum of a pneumonia-suffering patient (Chapalain et al., 2008). The parameters of bacterial NO₂ exposure were adapted to mimic real-life air conditions. Thus, the two strains were exposed to gaseous NO₂ at three concentrations: 0.1 ppm as an annual guideline value (WHO |Air quality guidelines - global update, 2005) 5 ppm as the threshold causing reversible effects on human health, and 45 ppm as a high NO₂ concentration provoking irreversible effects (INERIS, 2011).

MATERIAL AND METHODS

Strains and Growth Conditions

Cyan Fluorescent Protein (CFP)-labeled *P. fluorescens* MFN1032 and MFAF76a were used in this study. The strains and plasmids are listed in Table S1. The 729-bp *cfpopt* gene, encoding the CFP, was extracted from pTetONCFPopt plasmid (Sastalla et al., 2009) using PstI and XmaI enzymes (NEB, Ipswich, USA). Then CFP cassette was separated by 1% agarose gel electrophoresis and purified with QIAquick Gel Extraction Kit (Qiagen, Hilden, Allemagne). The pPSV35 vector (Rietsch et al., 2005) was digested using PstI and XmaI and purified using QIAquick PCR Purification Kit (Qiagen, Hilden, Allemagne). The CFP cassette was then cloned into the PstI and XmaI sites of the pPSV35 vector. The resulting pCFP vector was introduced into One Shot® TOP10 Chemically Competent *E. coli* (LMSM collection) by heat shock. After antibiotic selection of the clones (gentamycin 15 µg/mL), the transformation was confirmed by confocal laser scanning microscope (CLSM 710, ZEISS). The obtained plasmid was then extracted from *E. coli* using QIAprep Spin Miniprep Kit (Qiagen, Hilden, Allemagne) and introduced into *P. fluorescens* strains by electroporation. The transformants were selected in LB containing 15 µg/mL of gentamycin and fluorescence was assayed using CLSM.

Bacteria were grown at 28°C under limited agitation (180 rpm) in DMB (Davis Medium Broth) minimal medium with 2.16 g/L glucose as carbon source (Duclairoir-Poc et al., 2011). Overnight cultures were diluted ($A_{580} = 0.08$) in fresh DMB and grown to the end of exponential phase ($A_{580} = 2$, 13×10^8 CFU/mL). Bacterial cultures at the end of exponential growth phase (about 3×10^7 bacteria per filter) were transferred on cellulose nitrate membrane filter (0.45 µm, pore size 0.2 µm, diameter 47 mm, Sartorius Biolab Products,

Gottingen, Germany) and grown on DMB agar plates at 28°C for 4 h to obtain a single layer's bacterial population. After 4 h of incubation, the cellulose membranes containing bacteria were placed on agar one-well dishes (size 127.8 × 85.5 mm, Thermo Scientific Nunc, Roshester, USA), which were directly transferred into the gas delivery device (**Figure 1**).

Exposition to Nitrogen Dioxide

In order to mimic the atmospheric conditions, bacterial NO₂ exposure was achieved in gas phase for 2 h, according to Ghaffari et al. (2005). The gas delivery device consisted of two sterile cylindrical Plexiglas exposure chambers (one for the NO₂ exposure, the second one for the control—exposure to synthetic air). The exposure chambers were deposited in a drying oven at 28°C (**Figure 1**). The NO₂, N₂, and O₂ obtained from Air Liquide GMP Europe (Mitry-Mory, France) were mixed together using digital mass flow regulators (Alicat Scientific, Inc., Tucson, USA) in order to get pre-calculated concentrations of NO₂ and maintain the O₂/N₂ ratio at 2/8 (v/v). The resulting gas mixture and the synthetic air were routed independently to each of the exposure chamber at a constant flow rate of 2 L/min, allowing parallel treatment of bacteria originating from the same bacterial culture. After passing through the exposure chamber, the NO₂ concentrations were monitored by AC32M nitrogen oxides analyzer (Environnement S.A, Poissy, France) and safely vented to a chemical hood. Temperature and relative humidity data were monitored to control reliable steady-state environmental conditions inside the exposure chambers. Three concentrations of NO₂ (0.1 ppm; 5 ppm and 45 ppm) were used in this study. After exposure, bacteria were diluted to A₅₈₀ = 2 in sterile saline solution and used for the subsequent experiments.

Antibiotic Sensitivity Assays

After NO₂ exposure, bacterial sensitivity to ciprofloxacin, chloramphenicol, tobramycin and kanamycin (Sigma-Aldrich, St. Quentin Fallavier, France) was assayed. The minimum inhibitory concentration (MIC) was determined by the broth microdilution method achieved in DMB. Briefly, NO₂-exposed bacteria were diluted to A₅₈₀ = 0.08 and added to a 96-well test plate (Nunc™, Roskilde, Denmark) containing different concentrations of antibiotics in triplicate. The test plates were incubated at 28°C for 24 h. Synthetic air-exposed bacteria were used as control. MIC was defined as the lowest antibiotic concentration that inhibited bacteria growth as determined by turbidimetry at A₅₈₀.

Growth inhibition assays were achieved as previously described (van Sorge et al., 2013). Exposed bacteria were diluted in DMB supplemented by the indicated antibiotics in subinhibitory concentrations (the last antibiotic concentrations allowing bacterial growth). Bacteria were added to Bioscreen Honeycomb plates (Oy Growth Curves Ab Ltd., Helsinki, Finland) in a total volume of 200 μL of DMB (A₅₈₀ = 0.08). Growth was measured every 15 min (A₅₈₀) for 24 h. The NO₂ effect on the bacterial antibiotic sensitivity was calculated as the percentage of bacterial growth with antibiotics after NO₂ exposure on the bacterial growth with antibiotics after exposure

to synthetic air, using the following formula: 100 × A₅₈₀ NO₂ exposed bacteria/A₅₈₀ synthetic air exposed bacteria (%).

Motility Assays

Swimming and swarming motility assays were performed on agar plates using DMB containing 0.2% (wt/vol) and 0.5% (wt/vol) agar, respectively, as previously described (Déziel et al., 2001). Briefly, 5 μL of NO₂ or synthetic air-exposed bacteria were spotted on the surface of agar plates. The resultant diameters of swim and swarm zones were measured after 24 h of incubation at 28°C. Motilities were assayed in three independent experiments with three replicates for each experimental condition.

Biofilm Monitoring By Confocal Laser Scanning Microscopy

NO₂ or synthetic air-exposed bacteria were diluted in sterile saline solution to A₅₈₀ = 1 to avoid bacterial multiplication, and added to glass-bottom dishes (SensoPlate™, VWR, Fontenay-sous-Bois, France). After 2 h of incubation at 28°C, planktonic bacteria were removed and bacterial adhesion on glass-bottom dishes was observed using a confocal laser scanning microscope (CLSM 710, ZEISS) with an immersion objective 63×. After addition of DMB, the samples were incubated at 28°C for 24 h. Biofilms were rinsed with saline solution and observed using CLSM. All biofilm assays were performed in three independent experiments with two replicates for each experimental condition. The biofilm thickness and related biomass (bacterial volume, μm³/μm²) were estimated from 6 fields on 3 independent experiments using COMSTAT software (Heydorn et al., 2000).

Gene Sequences Identification

The non-annotated genome drafts of MFN1032 and MFAF76a were used to identify the corresponding nucleotide sequences (data not shown). Homologous sequences search in *P. fluorescens* annotated genomes was performed using pseudomonas genome database (<http://pseudomonas.com/>). The conserved nucleotide sequences were identified in *P. fluorescens* MFN1032 and MFAF76a using Blast+ (Stand-alone) software (v. 2.2.30, NCBI) according to Altschul et al. (1997), and are listed in Table S2.

Extraction and Quantification of Bis-(3', 5')-Cyclic Dimeric Guanosine Monophosphate (c-di-GMP)

Extraction and quantification of intracellular c-di-GMP level were performed in NO₂ or synthetic air-exposed bacteria as previously described (Spangler et al., 2010; Strehmel et al., 2015). Identification and quantification of c-di-GMP was performed using three specific mass transitions from molecule ion m/z 691 to the product ions: m/z 152, m/z 135, and m/z 540. The external calibration was carried out at c-di-GMP concentrations ranging from 10 ng to 200 ng in 500 μL H₂O using the internal standard cXMP (50 ng). The resulting concentrations of c-di-GMP were normalized against total protein contents of respective cultures, which was determined by the bicinchoninic acid assay (Smith et al., 1985). All experiments were performed in three replicates for each experimental condition.

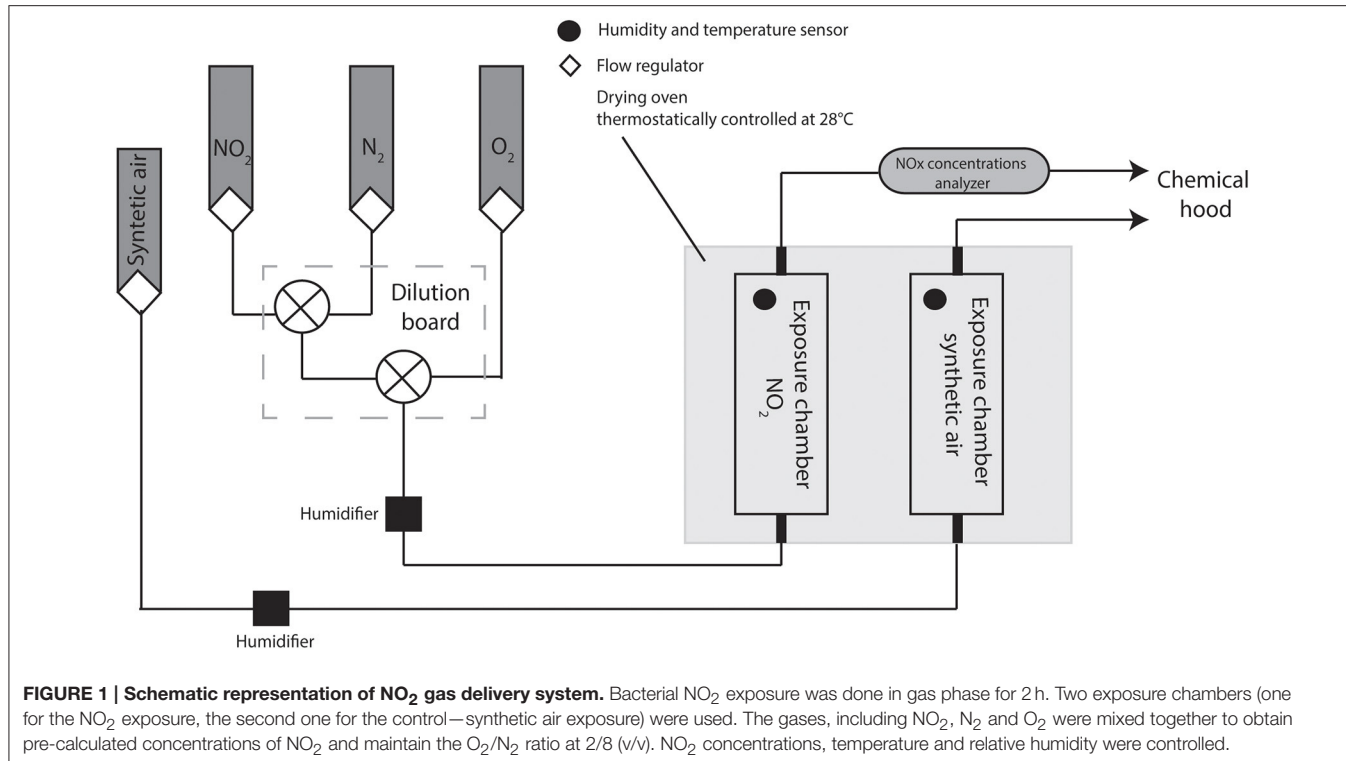


FIGURE 1 | Schematic representation of NO₂ gas delivery system. Bacterial NO₂ exposure was done in gas phase for 2 h. Two exposure chambers (one for the NO₂ exposure, the second one for the control—synthetic air exposure) were used. The gases, including NO₂, N₂ and O₂ were mixed together to obtain pre-calculated concentrations of NO₂ and maintain the O₂/N₂ ratio at 2/8 (v/v). NO₂ concentrations, temperature and relative humidity were controlled.

Quantitative RT-PCR

Total RNA was prepared by the hot acid-phenol method (Bouffartigues et al., 2012) from NO₂-exposed and not bacteria. Residual DNAs were eliminated by acid phenol treatment. The absence of DNA was confirmed by showing that PCR reactions failed without prior cDNA synthesis. RNAs were nonspecifically converted to single stranded cDNAs using the High Capacity cDNA Archive Kit (Applied Biosystems). Synthesis of cDNAs and real time PCR, allowing the quantification of mRNAs of interest were performed as previously described (Gicquel et al., 2013) using primers listed in Table S3.

Statistical Analysis

All experiments were carried out several times. To assess the significance of differences between the obtained data, Mann-Whitney test or pairwise strain comparisons (*t*-test) were applied and quantified the significance as (*) for $p < 0.05$, (**) for $p < 0.01$ and (***) for $p < 0.001$.

RESULTS AND DISCUSSION

NO₂ is one of the most common air pollutants, but its effects on the air microbiota is poorly studied. In order to assess the bacterial response to NO₂, airborne *P. fluorescens* MFAF76a and clinical control MFN1032 strains were exposed to gaseous NO₂ (as shown Figure 1) at 0.1, 5, or 45 ppm concentrations, and their effects on bacteria were evaluated in terms of motility, biofilm formation, antibiotic resistance, as well as expression of several chosen target genes. While 0.1 and 5 ppm of NO₂ did not lead to any significant modification of the studied

parameters in both the bacteria (data not shown), several alterations were observed when the bacteria were exposed to 45 ppm of gaseous NO₂. We thus chose to focus on this concentration.

NO₂-Mediated Modifications of Bacterial Biofilm

In order to test the NO₂ effect on *P. fluorescens* biofilm, both airborne MFAF76a and clinical MFN1032 were exposed to gaseous NO₂ and synthetic air and grown for 4 h in static conditions. In the control condition, the airborne strain MFAF76a produced only a poorly structured biofilm with low biomass and thickness (Figure 2A). To the best of the authors' knowledge this is the first time that the biofilm of airborne *P. fluorescens* strain was investigated. On the opposite, the clinical strain MFN1032 was able to form a structured mushroom-like biofilm, with about 2 and 3 fold more biomass and thickness than the airborne strain MFAF76a, respectively (Figure 2B, control). These data are consistent with previous studies showing that clinical strains can strongly adhere and form structured biofilms (Rossignol et al., 2008; Ma et al., 2009). After NO₂ exposition, the airborne strain MFAF76a produced biofilms with about 3 fold increase of the maximal thickness, while the biomass was similar (Figure 2A), when compared to synthetic air treatment. These data suggest that NO₂ led to induce biofilm formation in this strain. Accordingly, similar NO concentrations were previously found to promote an increase of biofilm formation in *P. aeruginosa* (Barraud et al., 2006), suggesting a common effect between NO and NO₂ treatment. On the other hand, NO₂

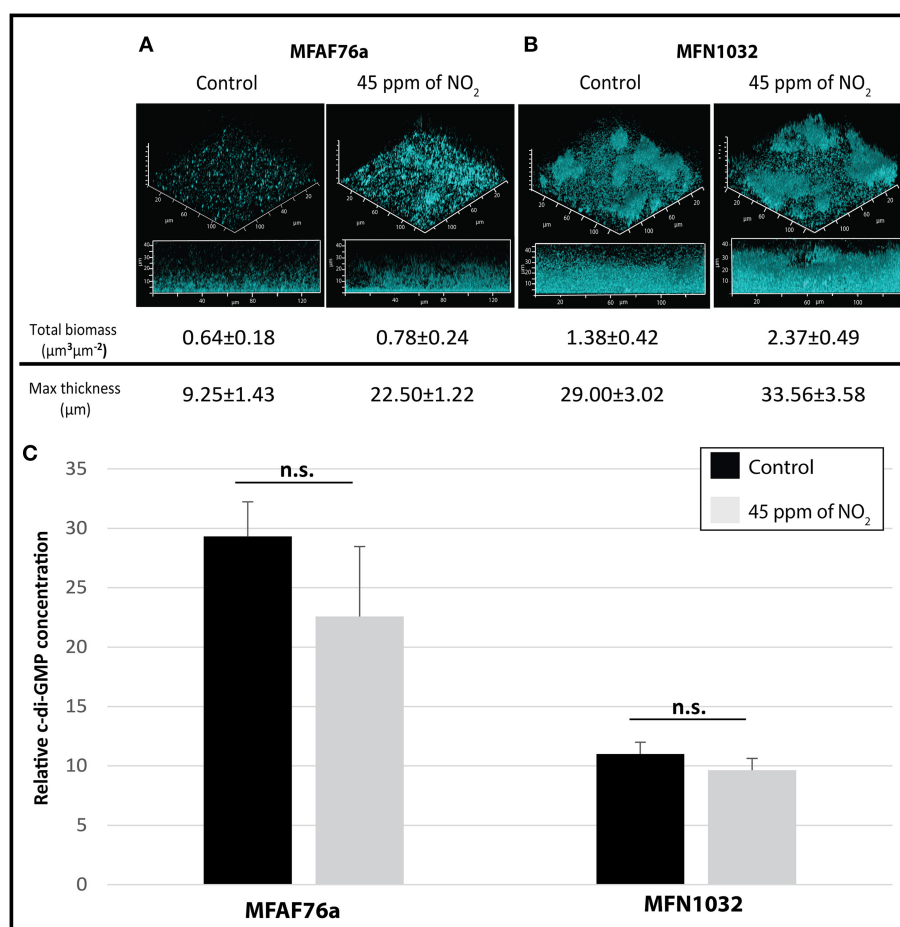


FIGURE 2 | NO₂ effect on *P. fluorescens* biofilm and intracellular c-di-GMP level. (A) Airborne MFAF76a and **(B)** clinical MFN1032 *P. fluorescens* strains were exposed in triplicate to 45 ppm of NO₂. Biofilm formation was analyzed in static conditions after 24 h development using confocal laser scanning microscope. The biofilm biomass and the maximum thickness were estimated from 6 fields on 3 independent experiments using COMSTAT software. Intracellular c-di-GMP concentrations **(C)** were measured in triplicate by LC-MS/MS for control (■) and 45 ppm of NO₂ treated (□) MFAF76a and MFN1032. Obtained results are presented as average values \pm SEM. Statistical significance was calculated by the non-parametric Mann-Whitney-Test. n.s., non-significant.

exposure of the clinical strain MFN1032 led to a 1.7 fold increase in biofilm production in terms of biomass, while the maximal thickness was unchanged (**Figure 2B**). Taken together these data suggest that the NO₂-mediated biofilm modifications are strain-dependent. Since we have shown previously that airborne MFAF76a expresses a virulence activity toward A549 epithelial pulmonary cells (Duclairoir Poc et al., 2014), these data suggest that elevated concentrations of NO₂ increases biofilm formation in potentially virulent airborne strain and may represent a sanitary risk.

Since biofilm formation is related to increased c-di-GMP production (Ha and O'Toole, 2015), we next quantified the c-di-GMP levels after NO₂ or synthetic air exposure. As shown in **Figure 2C**, both NO₂-exposed *P. fluorescens* strains did not exhibit statistically significant variations of intracellular c-di-GMP concentrations. This was quite surprising since observed in our study NO₂ mediated biofilm induction. NO-mediated reduction of the intracellular c-di-GMP level leading to dispersion of *P. aeruginosa* biofilms has been related to increase

phosphodiesterases (PDEs) activity, and as a consequence to promote the switch between the biofilm and the planktonic ways of life (Petrova and Sauer, 2012; Roy et al., 2012; Li et al., 2013; Petrova et al., 2014). In this bacterium, the following PDEs, including DipA, MucR, NdbA and BdlA, are enzymes that are involved in c-di-GMP catabolism (Petrova and Sauer, 2012; Roy et al., 2012). The mRNA levels of *dipA*, *mucR*, *ndbA* and *bdlA* genes (KT186437, KT186445, KT186444 and KT186436 respectively, Table S2) were quantified by qRT-PCR experiments, in the two strains, that were both previously exposed to NO₂ or synthetic air. For the two strains, NO₂ exposure did not lead to any modification in gene expression (data not shown). Altogether, these data suggest that (i) NO₂ may have an effect on the structure or on the biomass of the biofilm, in case of the studied airborne or clinical strains, respectively, (ii) these phenotypes would not be related to variations of the intracellular c-di-GMP levels, and (iii) NO and gaseous NO₂ may have a common and concentration-dependent effect on biofilm formation.

NO₂ Reduced Bacterial Motility

Since biofilm structure and production were not implemented by c-di-GMP level in our conditions, we next assayed the effects of NO₂ on bacterial motility, since appendices like flagella and type IV pili are also involved in the first step of biofilm formation, i.e., adhesion (Caiazza et al., 2007; Guttenplan and Kearns, 2013).

Swimming concerns motility in a liquid medium, mediated by production and activity of flagella. As shown on **Figure 3A**, gaseous NO₂ exposition significantly decreased the swimming motility of both strains, suggesting an impairment of the flagellum production and/or activity.

Swarming is a complex motility that has been related to functional flagella, type IV pili and production of biosurfactants like cyclolipopeptides (Duclairoir-Poc et al., 2011) for some *P. fluorescens* strains, or rhamnolipids for *P. aeruginosa* strains (Caiazza et al., 2005). The airborne strain MFAF76a was unable to swarm in tested experimental conditions. On the opposite, MFN1032 is a swarmer clinical strain (Rossignol et al., 2008). As shown in **Figure 3B**, exposition to NO₂ but not to synthetic air led to fully inhibit the swarming motility of this strain.

Taken together, our data show that gaseous NO₂ treatment results in a decreased motility in both of the studied strains. This decrease in motility could be a consequence of a lower production of the required appendices. Alternatively it could also be due to lower appendices activity, suggesting that they could increase the attachment of the bacterium on the glass slide. This phenotype would then be consistent with the increase in biofilm maximal thickness in case of the airborne strain, and biomass in case of the clinical strain. However, to date, the switch between motility and biofilm had frequently been associated to variations in the c-di-GMP level (Ha and O'Toole, 2015), but, herein, the gaseous NO₂-mediated differences in terms of biofilm structure could not be related to any c-di-GMP level variations.

Effect of NO₂ on MexEF-OprN Efflux Pump Expression and Antibiotic Resistance

To further characterize the effects of gaseous NO₂ on bacterial physiology, we next assayed antibiotic resistance. Since NO, a member of RNS, was found to induce the expression of *mexEF-oprN* genes (Fetar et al., 2011) and modulate bacterial resistance to fluoroquinolones, chloramphenicol and aminoglycosides (Gusarov et al., 2009; McCollister et al., 2011; van Sorge et al., 2013), we investigated the effect of gaseous NO₂ on these phenotypes.

In order to study the effect of NO₂ on MexEF-OprN efflux pump, the transcription levels of *mexE*, *mexF* and *oprN* genes (KT070324, KT070321 and KT070325 for MFAF76a; KT070323, KT070322 and KT186432 for MFN1032, respectively) were compared using qRT-PCR in two *P. fluorescens* strains exposed or not to 45 ppm of NO₂. In airborne and clinical strains, the *mexE* mRNA level was increased by almost 14- and 100-fold respectively; that of *mexF* almost 3.5- and 47-fold respectively and that of *oprN* almost 4.6- and 73-fold respectively (**Figure 4**). These data show that NO₂ promoted

TABLE 1 | NO₂ exposure increases *Pseudomonas fluorescens* antibiotic resistance.

Strain	NO ₂ concentration (ppm)	Ciprofloxacin MIC (μg/mL)	Chloramphenicol MIC (μg/mL)
MFAF76a	0	6.25	50
	45	12.5	>100
MFN1032	0	3.125	150
	45	6.25	200

mexEF-oprN expression, potentially causing modifications in *P. fluorescens* antibiotic resistance. We next tested the functionality of this pump. Since the MexEF-OprN RND efflux pump is involved in fluoroquinolone resistance, we next assayed bacterial sensitivity against ciprofloxacin by evaluating their MICs. As shown in **Table 1**, both the *P. fluorescens* strains were more resistant to this antibiotic after exposure to NO₂ than to synthetic air. Chloramphenicol is a nitroaromatic antimicrobial that is a substrate for MexEF-OprN (Köhler et al., 1997; Sobel et al., 2005). Accordingly, NO₂-exposed *P. fluorescens* strains MFAF76a and MFN1032 were about 2 fold more resistant to this antibiotic than synthetic air-treated bacteria (**Table 1**). Taken together, these data suggest a possible higher activity of this efflux pump in response to NO₂ exposure. We next followed the growth of the NO₂-exposed *P. fluorescens* strains in DMB medium containing ciprofloxacin or chloramphenicol at the higher antibiotic concentration leading to bacterial growth (**Figure 5**). Data were standardized with the control, the synthetic air treated cells growth. While ciprofloxacin had no effect on NO₂-exposed bacteria, chloramphenicol at a concentration of 25 and 100 μg/mL for strain MFAF76a and MFN1032, respectively, led to an increase in growth for the two NO₂-exposed *P. fluorescens* strains (**Figure 5**). Remarkably, the statistically significant increase of bacterial growth was maintained from 2 to 10 h, suggesting a possible NO₂ protective effect that would be conserved for 8 h after exposure. Taken together, our data show that NO₂ induced *mexEF-oprN* gene expression, and consequently increased the resistance to ciprofloxacin and chloramphenicol.

MexEF-OprN-overproducing mutants with enhanced fluoroquinolone resistance often increase bacterial susceptibility to aminoglycosides apparently owing to impairment of the MexXY system (Sobel et al., 2005; Morita et al., 2015). The effect of NO₂ on tobramycin and kanamycin sensitivity was then assayed by performing MICs. As shown in **Table 2**, NO₂ treatment led to reduce the MICs of the two tested antibiotics, suggesting that NO₂ increases *P. fluorescens* sensitivity to aminoglycosides. Tobramycin and kanamycin, at subinhibitory concentration of 1.55 and 3.1 μg/mL respectively, were found to decrease the growth of NO₂-exposed bacteria (**Figure 6**). This effect was observed only from 6 to 10 h of growth for MFN1032 and from 6 to 18 h of growth for MFAF76a, highlighting the time-limited NO₂ effect on bacterial antibiotic sensitivity. Altogether, our data show that NO₂ increases *P. fluorescens* sensitivity to tobramycin and kanamycin, accordingly its homolog NO is also found to increase *P. aeruginosa* sensitivity to tobramycin

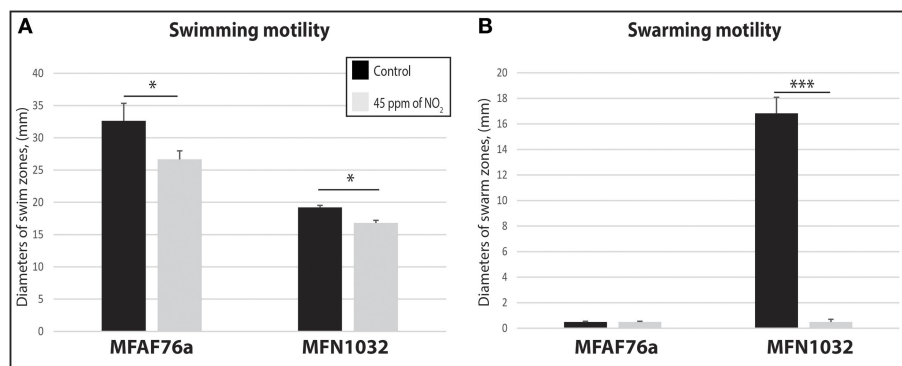


FIGURE 3 | NO₂ decreases *P. fluorescens* motility. Airborne MFAF76a and clinical MFN1032 *P. fluorescens* strains were exposed in triplicate to 45 ppm of NO₂ (■). Swimming (A) and swarming (B) motilities were assayed on DMB-swim/swarm plates after 24 h incubation. The motile bacterial movement was evaluated in three independent experiments with three replicates. The data were compared with control exposed to synthetic air (■). Obtained results are presented as average values \pm SEM. Statistical significance was calculated by the non-parametric Mann-Whitney-Test $p < 0.05$ (*) and < 0.001 (**).

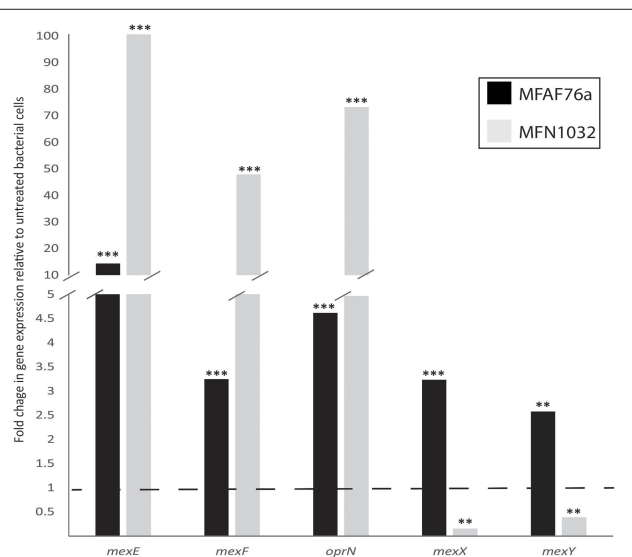


FIGURE 4 | NO₂ effect on MexEF-OprN and MexXY efflux pump gene transcription. The nucleotide sequences of the *mexEF*, *oprN*- and *mexXY*-homolog genes were obtained using the non-annotated genome drafts of airborne MFAF76a (■) and clinical MFN1032 (□) *P. fluorescens*. The GenBank accession numbers of nucleotide sequences are listed in Table S2. Quantification of mRNA level was assayed using qRT-PCR on RNAs extracted from NO₂- and synthetic air-exposed *P. fluorescens*. The PCR reactions were performed in triplicate and the standard deviations were lower than 0.15 Ct. Statistical analysis used pairwise strain comparisons (*t*-test) $p < 0.01$ (**) and < 0.001 (**). Dotted line shows the gene expression in synthetic air-exposed control.

(Barraud et al., 2006). Noticeably, this phenotype is consistent with previously published data supporting decreasing resistance to aminoglycosides of MexEF-OprN-overproducing mutant (Sobel et al., 2005; Morita et al., 2015). Since this phenotype is often associated with the impairment of the MexXY-OprM efflux pump, we next assayed the effect of NO₂ on the expression of the *mexXY* genes. As shown in Figure 4, NO₂ treatment

had an opposite effect on *mexXY* gene expression. While NO₂ increased the expression of *mexXY* in the airborne strain MFAF76a, it drastically reduced production of *mexXY* mRNA in the clinical strain MFN1032. While this latter phenotype is often described in the literature (Sobel et al., 2003) as leading to increased aminoglycoside susceptibility, the overproduction of the two RND efflux pumps MexEF-OprN and MexXY-OprM is remarkable and found in very few strains, among which the multiresistant strain PA7 (Morita et al., 2015). Nevertheless, the increased expression of *mexXY* in the airborne strain cannot be related to the increased susceptibility to aminoglycosides, which we observed. Taken together, our data indicate that the NO₂ effect on bacterial aminoglycoside resistance is complex and strain-dependent, and the up- or down- production of *mexXY* cannot account solely to explain the increased susceptibility to aminoglycosides of the two studied strains. Another hypothesis may arise related to the effects of NO₂ on membrane properties. Indeed, the NO₂ effect on *P. fluorescens* membrane was recently investigated, demonstrating the NO₂-mediated modifications in both the membrane glycerophospholipids composition (i.e., ratio zwitterionic/anionic glycerophospholipids) and in the membrane electron-accepting properties (Kondakova, personal communication). It is thus conceivable that these membrane modifications would alter bacterial membrane permeability, facilitating the aminoglycoside entry into the bacterial cell.

NO₂-Mediated Gene Expression in *P. fluorescens*

Remarkably, we have shown herein a link between gaseous NO₂ and soluble NO treatment. Indeed, NO is found to induce the expression of *mexEF oprN* genes (Fetar et al., 2011) and modulates bacterial resistance to several antibiotics (Gusarov et al., 2009; McCollister et al., 2011; van Sorge et al., 2013). Since NO₂ and NO are related chemical toxic compounds, and since NO detoxification pathways have been deeply investigated, the NO₂ effects on several chosen target genes were tested.

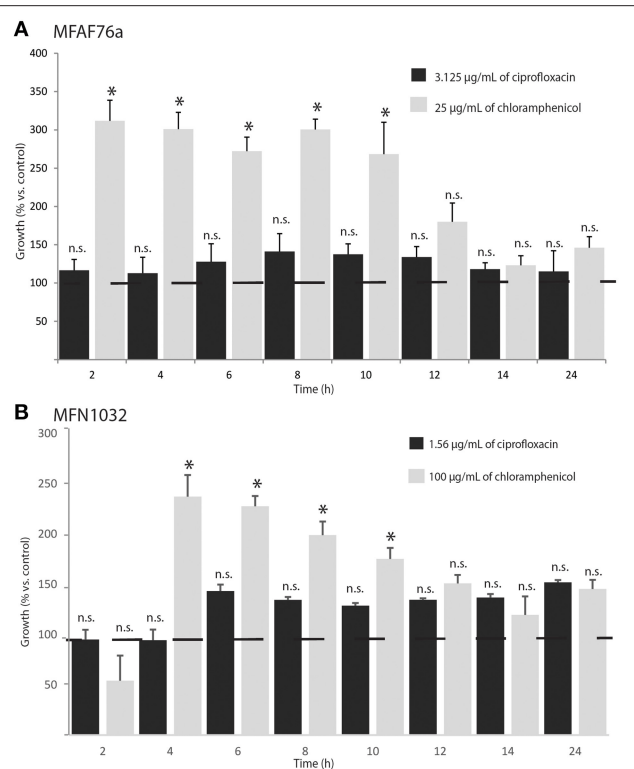


FIGURE 5 | NO₂ protects *Pseudomonas fluorescens* from chloramphenicol toxicity. After 2 h exposure to 45 ppm of NO₂, growth of airborne MFAF76a (A) and clinical MFN1032 (B) *P. fluorescens* with ciprofloxacin (■) and chloramphenicol (□) was assayed. Growth curves were performed with ciprofloxacin (3.125 µg/mL for MFAF76a and 1.56 µg/mL for MFN1032) and chloramphenicol (25 and 100 µg/mL respectively), and A₅₈₀ was recorded at the indicated time points. The control sample was bacteria exposed to synthetic air, and grown in presence of antibiotics in indicated concentrations. The data are shown as percentages of growth relative to synthetic air-exposed control. Pooled data from three independent experiments in duplicate ± SEM are reported. Statistical significance was calculated by the non-parametric Mann-Whitney-Test *p* < 0.05 (*); n.s., non-significant. Dotted line shows the control (100%).

The most well-studied pathway for NO detoxification is based on flavohemoglobin (FlavoHb) (Hmp for *E. coli* and Fhp for *P. aeruginosa*), which acts as an NO dioxygenase to transform NO to NO₃⁻ (Figure 7A) (Corker and Poole, 2003; Arai et al., 2005). After exposure to 45 ppm of NO₂, the *hmp* mRNA levels were increased almost 25- and 23-fold in MFAF76a and in MFN1032 (respectively KR818822 and KR818823 in Table S2 and Figure 8), indicating that NO₂ induces *hmp* expression in both *P. fluorescens* and suggesting a possible involvement of Hmp in NO₂ detoxification. The NO₂ effect on the Hmp synthesis was observed in other studies, where, to activate the Hmp-dependent detoxification pathway, NO₂ was proposed to be reduced to NO (Poole et al., 1996). In *Pseudomonas* spp., NO₂ reduction can be performed by nitrite reductase (NIR) enzymes (Figures 7B,C), including the well-studied respiratory cytochrome *cd1* nitrite reductase (Figure 7B) of the denitrification pathway (Arai et al., 2005; Shiro, 2012). According to the genome draft analysis

TABLE 2 | NO₂ decreases *Pseudomonas fluorescens* resistance to aminoglycosides.

Strain	NO ₂ concentration (ppm)	Kanamycin MIC (µg/mL)	Tobramycin MIC (µg/mL)
MFAF76a	0	8.3	6.2
	45	6.2	3.1
MFN1032	0	20.0	12.5
	45	16.7	8.3

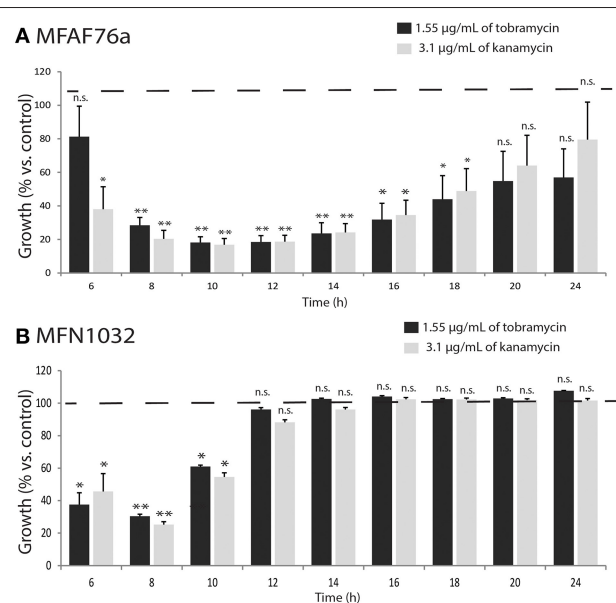


FIGURE 6 | NO₂ exposure affects *Pseudomonas fluorescens* growth with aminoglycosides. After 2 h exposure to 45 ppm of NO₂, growth of airborne MFAF76a (A) and clinical MFN1032 (B) in presence of tobramycin (1.55 µg/mL; ■) and kanamycin (3.1 µg/mL; □) was tested. A₅₈₀ was recorded at indicated time points. The control sample was bacteria exposed to synthetic air, and grown in presence of antibiotics in indicated concentrations. The data are presented as percentages of growth relative to air-exposed control. Pooled data from three independent experiments in duplicate ± SEM are reported. Statistical significance was calculated by the non-parametric Mann-Whitney-Test *p* < 0.05 (*), < 0.01 (**); n.s. non-significant. Dotted line shows the control (100%).

(data not shown), both MFAF76a and MFN1032, like the majority of *P. fluorescens* strains (Redondo-Nieto et al., 2013), do not possess denitrifying genes, but harbor the genes encoding for the assimilatory nitrite reductase NirBD (Figure 7C). The latter is part of the Nas assimilatory pathway (from nitrate assimilation), where nitrate is reduced to nitrite, which is then reduced to ammonia (Jeter et al., 1984; Moreno-Vivián et al., 1999). In order to test the NO₂ effect on the expression of *nirBD* operon, the *nirB* mRNA level (*Pfl76a_nirB* -KT186428 - and *Pfl1032_nirB* - KT070320 -, Table S2) was compared in the NO₂-exposed or non-exposed *P. fluorescens* strains. In both strains, the mRNA level of *nirB* was not modified compared to the control condition (data not shown), indicating the absence of NO₂ effect on the expression of genes coding for assimilatory NIR. To the best of

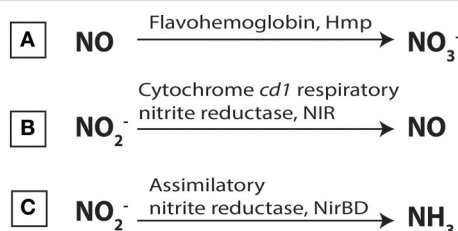


FIGURE 7 | Scheme of Hmp-mediated NO detoxification and NO₂ reduction pathways in *Pseudomonas* spp. (A) Flavohemoglobin (Hmp) is involved in NO detoxification acting as an NO dioxygenase to transform NO to NO₃⁻. The NO₂ reduction is performed by nitrite reductase enzymes, including the respiratory cytochrome *cd1* nitrite reductase, NIR (B) and the assimilatory nitrite reductase NirBD (C). The respiratory NIR is involved in NO₂⁻ reduction to NO in anaerobic conditions. NirBD takes a part of the nitrate assimilatory pathway, and reduces nitrite to ammonia.

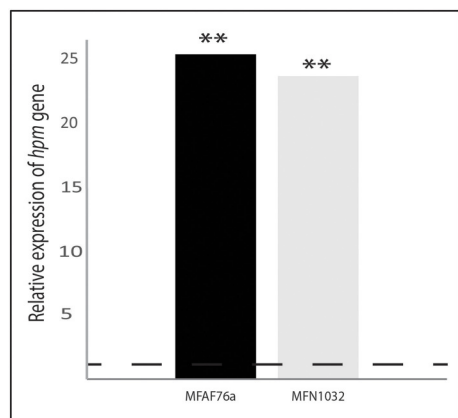


FIGURE 8 | Transcription of *hpm* is increased in response to NO₂ exposure. The nucleotide sequences of the *hpm*-homolog gene in *P. fluorescens* strains were obtained using the non-annotated genome drafts of airborne *P. fluorescens* MFAF76a (■) and clinical MFN1032 (□). The GenBank accession numbers of *hpm* nucleotide sequences are listed in Table S2. Quantification of mRNA level was assayed using qRT-PCR on RNAs extracted from NO₂⁻ and synthetic air-exposed *P. fluorescens*. The PCR reactions were performed in triplicate and the standard deviations were lower than 0.15 Ct. Statistical analysis used pairwise strain comparisons (*t*-test) $p < 0.01$ (**). Dotted line shows the gene expression in air-exposed control.

our knowledge, the involvement of Nas pathway in NO/NO₂ detoxification was not demonstrated. Given the presence of ammonium in DMB medium (Duclairoir-Poc et al., 2011), we think that the production of supplementary ammonium through the nitrite reduction is not appropriate. However, in order to better understand the mechanism of the NO₂ detoxification, the Hmp-, Nir- and Nas-mediated mechanisms should be investigated in more details.

In this study, the response of airborne *P. fluorescens* MFAF76a to gaseous NO₂, as a marker of air pollution, was for the first time investigated and compared to the response of the clinical *P. fluorescens* MFN1032 strain. We show that NO₂ leads to increased biofilm formation through a c-di-GMP independent

mechanism, reduced motility, as well as increasing ciprofloxacin, chloramphenicol resistance and aminoglycosides susceptibility. The question is now to understand how the NO₂ leads to the observed phenotypes. NO₂ has some similarities with its relative NO. NO₂, like NO, induced the expression of *mexEF-oprN* genes, encoding the RND efflux pump MexEF-OprN. Its overexpression could, among others, be involved in the observed increase of *P. fluorescens* resistance to ciprofloxacin and chloramphenicol. NO₂ induces also bacterial biofilm formation by strain-dependent mode, without c-di-GMP production variation. Thus, the high *P. fluorescens* adaptability to many environments, and a possible NO₂ propensity to increase some bacterial antibiotic resistance and biofilm formation may diminish the effectiveness of antibiotic therapies in highly polluted areas. In addition, we show the NO₂-mediated upregulation of the *hmp*-homolog gene in *P. fluorescens*, suggesting a possible common pathway between NO and NO₂ detoxification. Taken together, our data show that gaseous NO₂ can be perceived by airborne bacteria, leading to physiological modifications that may be relevant for human health (biofilm formation, antibiotic resistance). In the context of the worrying increase of atmospheric NO₂ concentrations (Bernagaud et al., 2014), these findings are of ecological relevance, especially because of the high NO₂ concentrations, found in the close vicinity of any vehicle.

AUTHOR CONTRIBUTIONS

TK contributed to the design of project, experiments, acquisition, analysis, interpretation of data, and wrote the manuscript. CC contributed in genes identification and qRT-PCR analysis. MB contributed to the transformation of *P. fluorescens* strains. MN and GB participated in c-di-GMP quantification. FD encouraged the study on the airborne bacteria. SC and NO participated in the design and drafted the manuscript. CDP led and coordinated the global project by conceiving the study, and participated in manuscript writing. All authors have read and approved the final manuscript.

ACKNOWLEDGMENTS

We thank Marc Feuilloley for his constructive comments and Yoan Konto-Ghiorghi for his advices in English editing and academic writing. We are grateful to Anne Groboillot for help with development of gas delivery system. We thank Audrey Garreau and Olivier Maillot for technical assistance. This study was supported by a PhD grant from the GRR SESA (Research Network of Sanitary Safety) and was financially supported by Europe, French Government (FEDER), Regional Council of Haute-Normandie, the Conseil Général de l'Eure and the Grand Evreux Agglomeration (France).

SUPPLEMENTARY MATERIAL

The Supplementary Material for this article can be found online at: <http://journal.frontiersin.org/article/10.3389/fmicb.2016.00379>

REFERENCES

- Ahern, H. E., Walsh, K. A., Hill, T. C. J., and Moffett, B. F. (2007). Fluorescent pseudomonads isolated from Hebridean cloud and rain water produce biosurfactants but do not cause ice nucleation. *Biogeosciences* 4, 115–124. doi: 10.5194/bg-4-115-2007
- Altschul, S. F., Madden, T. L., Schäffer, A. A., Zhang, J., Zhang, Z., Miller, W., et al. (1997). Gapped BLAST and PSI-BLAST: a new generation of protein database search programs. *Nucleic Acids Res.* 25, 3389–3402. doi: 10.1093/nar/25.17.3389
- Arai, H., Hayashi, M., Kuroi, A., Ishii, M., and Igarashi, Y. (2005). Transcriptional regulation of the flavohemoglobin gene for aerobic nitric oxide detoxification by the second nitric oxide-responsive regulator of *Pseudomonas aeruginosa*. *J. Bacteriol.* 187, 3960–3968. doi: 10.1128/JB.187.12.3960-3968.2005
- Auger, C., and Appanna, V. D. (2015). A novel ATP-generating machinery to counter nitrosative stress is mediated by substrate-level phosphorylation. *Biochim. Biophys. Acta* 1850, 43–50. doi: 10.1016/j.bbagen.2014.09.028
- Auger, C., Lemire, J., Cecchini, D., Bignucolo, A., and Appanna, V. D. (2011). The metabolic reprogramming evoked by nitrosative stress triggers the anaerobic utilization of citrate in *Pseudomonas fluorescens*. *PLoS ONE* 6:e28469. doi: 10.1371/journal.pone.0028469
- Augusto, O., Bonini, M. G., Amanso, A. M., Linares, E., Santos, C. C. X., and De Menezes, S. L. (2002). Nitrogen dioxide and carbonate radical anion: two emerging radicals in biology. *Free Radic. Biol. Med.* 32, 841–859. doi: 10.1016/S0891-5849(02)00786-4
- Barraud, N., Hassett, D. J., Hwang, S.-H., Rice, S. A., Kjelleberg, S., and Webb, J. S. (2006). Involvement of nitric oxide in biofilm dispersal of *Pseudomonas aeruginosa*. *J. Bacteriol.* 188, 7344–7353. doi: 10.1128/JB.00779-06
- Barraud, N., Storey, M. V., Moore, Z. P., Webb, J. S., Rice, S. A., and Kjelleberg, S. (2009). Nitric oxide-mediated dispersal in single- and multi-species biofilms of clinically and industrially relevant microorganisms. *Microb. Biotechnol.* 2, 370–378. doi: 10.1111/j.1751-7915.2009.00098.x
- Bauer, H., Kasper-Giebl, A., Löflund, M., Giebl, H., Hitzenberger, R., Zibuschka, F., et al. (2002). The contribution of bacteria and fungal spores to the organic carbon content of cloud water, precipitation and aerosols. *Atmospheric Res.* 64, 109–119. doi: 10.1016/S0169-8095(02)00084-4
- Bernagaud, C., Burkhardt, J.-F., Vidal, B., Lepriol, T., Petit, J.-F., Brunel, T., et al. (2014). *Observations du ratio [NO₂]/[NO_x] en tunnel routier. Pollution-Atmosphérique*. Available online at: <http://lodel.irevues.inist.fr/pollution-atmospherique/index.php?id=2659> (Accessed August 18, 2015).
- Bodilis, J., Calbrix, R., Guérillon, J., Mérieau, A., Pawlak, B., Orange, N., et al. (2004). Phylogenetic relationships between environmental and clinical isolates of *Pseudomonas fluorescens* and related species deduced from 16S rRNA gene and OprF protein sequences. *Syst. Appl. Microbiol.* 27, 93–108. doi: 10.1017/S0723-2020-00253
- Bouffartigues, E., Gicquel, G., Bazire, A., Bains, M., Maillot, M., Vieillard, J., et al. (2012). Transcription of the oprF gene of *Pseudomonas aeruginosa* is dependent mainly on the SigX sigma factor and is sucrose induced. *J. Bacteriol.* 194, 4301–4311. doi: 10.1128/JB.00509-12
- Burney, S., Caulfield, J. L., Niles, J. C., Wishnok, J. S., and Tannenbaum, S. R. (1999). The chemistry of DNA damage from nitric oxide and peroxynitrite. *Mutat. Res. Mol. Mech. Mutagen.* 424, 37–49. doi: 10.1016/S0027-5107(99)00006-8
- Burrows, S. M., Butler, T., Jöckel, P., Tost, H., Kerkweg, A., Pöschl, U., et al. (2009a). Bacteria in the global atmosphere – Part 2: modeling of emissions and transport between different ecosystems. *Atmos. Chem. Phys.* 9, 9281–9297. doi: 10.5194/acp-9-9281-2009
- Burrows, S. M., Elbert, W., Lawrence, M. G., and Pöschl, U. (2009b). Bacteria in the global atmosphere – Part 1: review and synthesis of literature data for different ecosystems. *Atmos. Chem. Phys.* 9, 9263–9280. doi: 10.5194/acp-9-9263-2009
- Caiizza, N. C., Merritt, J. H., Brothers, K. M., and O'Toole, G. A. (2007). Inverse regulation of biofilm formation and swarming motility by *Pseudomonas aeruginosa* PA14. *J. Bacteriol.* 189, 3603–3612. doi: 10.1128/JB.01685-06
- Caiizza, N. C., Shanks, R. M. Q., and O'Toole, G. A. (2005). Rhamnolipids modulate swarming motility patterns of *Pseudomonas aeruginosa*. *J. Bacteriol.* 187, 7351–7361. doi: 10.1128/JB.187.21.7351-7361.2005
- Chaloulakou, A., Mavroidis, I., and Gavriil, I. (2008). Compliance with the annual NO₂ air quality standard in Athens. Required NO_x levels and expected health implications. *Atmos. Environ.* 42, 454–465. doi: 10.1016/j.atmosenv.2007.09.067
- Chaplain, A., Rossignol, G., Lesouhaitier, O., Mérieau, A., Gruffaz, C., Guerillon, J., et al. (2008). Comparative study of 7 fluorescent pseudomonad clinical isolates. *Can. J. Microbiol.* 54, 19–27. doi: 10.1139/W07-110
- Chauhan, A. J., Krishna, M. T., Frew, A. J., and Holgate, S. T. (1998). Exposure to nitrogen dioxide (NO₂) and respiratory disease risk. *Rev. Environ. Health* 13, 73–90.
- Corker, H., and Poole, R. K. (2003). Nitric oxide formation by *Escherichia coli* dependence on nitrite reductase, the NO-sensing regulator FnR, and flavohemoglobin Hmp. *J. Biol. Chem.* 278, 31584–31592. doi: 10.1074/jbc.M303282200
- Cruz-Ramos, H., Crack, J., Wu, G., Hughes, M. N., Scott, C., Thomson, A. J., et al. (2002). NO sensing by FnR: regulation of the *Escherichia coli* NO-detoxifying flavohaemoglobin, Hmp. *EMBO J.* 21, 3235–3244. doi: 10.1093/emboj/cdf339
- Cutruzzola, F., and Frankenberg-Dinkel, N. (2015). Origin and impact of nitric oxide in *Pseudomonas aeruginosa* biofilms. *J. Bacteriol.* 198, 55–65. doi: 10.1128/JB.00371-15
- Després, V. R., Alex Huffman, J., Burrows, S. M., Hoose, C., Safatov, A. S., Buryak, G., et al. (2012). Primary biological aerosol particles in the atmosphere: a review. *Tellus B* 64. doi: 10.3402/tellusb.v64i0.15598
- Déziel, E., Comeau, Y., and Villemur, R. (2001). Initiation of biofilm formation by *Pseudomonas aeruginosa* 57R correlates with emergence of hyperpiliated and highly adherent phenotypic variants deficient in swimming, swarming, and twitching motilities. *J. Bacteriol.* 183, 1195–1204. doi: 10.1128/JB.183.4.1195-1204.2001
- Duclairoir-Poc, C., Meyheuc, T., Ngoya, S., Groboillot, A., Bodilis, J., Taupin, L., et al. (2011). Influence of growth temperature on cyclolipeptides production and on adhesion behaviour in environmental strains of *Pseudomonas fluorescens*. *J. Bacteriol. Parasitol.* S1-002. doi: 10.4172/2155-9597.S1-002
- Duclairoir Poc, C., Verdon, J., Groboillot, A., Barreau, M., Toucourou, H., Mijouin, L., et al. (2014). Airborne fluorescent pseudomonads: what potential for virulence? *Int. J. Curr. Microbiol. Appl. Sci.* 3, 708–722.
- Dybwid, M., Granum, P. E., Bruheim, P., and Blatny, J. M. (2012). Characterization of airborne bacteria at an underground subway station. *Appl. Environ. Microbiol.* 78, 1917–1929. doi: 10.1128/AEM.07212-11
- Fang, Z., Ouyang, Z., Zheng, H., Wang, X., and Hu, L. (2007). Culturable airborne bacteria in outdoor environments in Beijing, China. *Microb. Ecol.* 54, 487–496. doi: 10.1007/s00248-007-9216-3
- Fetar, H., Gilmour, C., Klinoski, R., Daigle, D. M., Dean, C. R., and Poole, K. (2011). *mexEF-oprN* Multidrug efflux operon of *Pseudomonas aeruginosa*: regulation by the MexT activator in response to nitrosative stress and chloramphenicol. *Antimicrob. Agents Chemother.* 55, 508–514. doi: 10.1128/AAC.00830-10
- Flatley, J., Barrett, J., Pullan, S. T., Hughes, M. N., Green, J., and Poole, R. K. (2005). Transcriptional responses of *Escherichia coli* to S-nitrosoglutathione under defined chemostat conditions reveal major changes in methionine biosynthesis. *J. Biol. Chem.* 280, 10065–10072. doi: 10.1074/jbc.M410393200
- Ghaffari, A., Neil, D. H., Ardakani, A., Road, J., Ghahary, A., and Miller, C. C. (2005). A direct nitric oxide gas delivery system for bacterial and mammalian cell cultures. *Nitric Oxide* 12, 129–140. doi: 10.1016/j.niox.2005.01.006
- Gicquel, G., Bouffartigues, E., Bains, M., Oxaran, V., Rosay, T., Lesouhaitier, O., et al. (2013). The extra-cytoplasmic function sigma factor SigX modulates biofilm and virulence-related properties in *Pseudomonas aeruginosa*. *PLoS ONE* 8:e80407. doi: 10.1371/journal.pone.0080407
- Gusarov, I., Shatalin, K., Starodubtseva, M., and Nudler, E. (2009). Endogenous nitric oxide protects bacteria against a wide spectrum of antibiotics. *Science* 325, 1380–1384. doi: 10.1126/science.1175439
- Guttenplan, S. B., and Kearns, D. B. (2013). Regulation of flagellar motility during biofilm formation. *FEMS Microbiol. Rev.* 37, 849–871. doi: 10.1111/1574-6976.12018

- Ha, D.-G., and O'Toole, G. A. (2015). c-di-GMP and its effects on biofilm formation and dispersion: a *Pseudomonas aeruginosa* review. *Microbiol. Spectr.* 3:MB-0003-2014. doi: 10.1128/microbiolspec.MB-0003-2014
- Heydorn, A., Nielsen, A. T., Hentzer, M., Sternberg, C., Givskov, M., Ersbøll, B. K., et al. (2000). Quantification of biofilm structures by the novel computer program comstat. *Microbiology* 146, 2395–2407. doi: 10.1099/00221287-146-10-2395
- Husain, M., Bourret, T. J., McCollister, B. D., Jones-Carson, J., Laughlin, J., and Vázquez-Torres, A. (2008). Nitric oxide evokes an adaptive response to oxidative stress by arresting respiration. *J. Biol. Chem.* 283, 7682–7689. doi: 10.1074/jbc.M708845200
- INERIS (2011). *Dioxyde d'azote: Données toxicologiques et environnementales. Portail Subst. Chim.* Available online at: <http://www.ineris.fr/substances/fr/substance/cas/10102-44-0/2> (Accessed September 17, 2015).
- Jeter, R. M., Sias, S. R., and Ingraham, J. L. (1984). Chromosomal location and function of genes affecting *Pseudomonas aeruginosa* nitrate assimilation. *J. Bacteriol.* 157, 673–677.
- Köhler, T., Michéa-Hamzehpour, M., Henze, U., Gotoh, N., Curty, L. K., and Pechère, J. C. (1997). Characterization of MexE-MexF-OprN, a positively regulated multidrug efflux system of *Pseudomonas aeruginosa*. *Mol. Microbiol.* 23, 345–354. doi: 10.1046/j.1365-2958.1997.2281594.x
- Laver, J. R., McLean, S., Bowman, L. A. H., Harrison, L. J., Read, R. C., and Poole, R. K. (2013). Nitrosothiols in bacterial pathogens and pathogenesis. *Antioxid. Redox Signal.* 18, 309–322. doi: 10.1089/ars.2012.4767
- Li, Y., Heine, S., Entian, M., Sauer, K., and Frankenberger-Dinkel, N. (2013). NO-induced biofilm dispersion in *Pseudomonas aeruginosa* is mediated by an MHYT domain-coupled phosphodiesterase. *J. Bacteriol.* 195, 3531–3542. doi: 10.1128/JB.01156-12
- Liu, P., Huang, Q., and Chen, W. (2012). Heterologous expression of bacterial nitric oxide synthase gene: a potential biological method to control biofilm development in the environment. *Can. J. Microbiol.* 58, 336–344. doi: 10.1139/w11-141
- Ma, L., Conover, M., Lu, H., Parsek, M. R., Bayles, K., and Wozniak, D. J. (2009). Assembly and development of the *Pseudomonas aeruginosa* biofilm matrix. *PLoS Pathog.* 5:e1000354. doi: 10.1371/journal.ppat.1000354
- McCollister, B. D., Hoffman, M., Husain, M., and Vazquez-Torres, A. (2011). Nitric oxide protects bacteria from aminoglycosides by blocking the energy-dependent phases of drug uptake?. *Antimicrob. Agents Chemother.* 55, 2189–2196. doi: 10.1128/AAC.01203-10
- McLean, S., Bowman, L. A. H., Sanguineti, G., Read, R. C., and Poole, R. K. (2010). Peroxynitrite toxicity in *Escherichia coli* K12 elicits expression of oxidative stress responses and protein nitration and nitrosylation. *J. Biol. Chem.* 285, 20724–20731. doi: 10.1074/jbc.M109.085506
- Moreno-Vivián, C., Cabello, P., Martínez-Luque, M., Blasco, R., and Castillo, F. (1999). Prokaryotic nitrate reduction: molecular properties and functional distinction among bacterial nitrate reductases. *J. Bacteriol.* 181, 6573–6584.
- Morin, J.-P., Preterre, D., Gouriou, F., Delmas, V., François, A., Orange, N., et al. (2013). *Particules urbaines et céréalières, micro-organismes, mycotoxines et pesticides. Pollut. Atmos.* Available online at: <http://lodel.irevues.inist.fr/pollution-atmospherique/index.php?id=759> (Accessed January 14, 2014).
- Morita, Y., Tomida, J., and Kawamura, Y. (2015). Efflux-mediated fluoroquinolone resistance in the multidrug-resistant *Pseudomonas aeruginosa* clinical isolate PA7: identification of a novel MexS variant involved in upregulation of the *mexEF oprN* multidrug efflux operon. *Antimicrob. Resist. Chemother.* 6, 8. doi: 10.3389/fmicb.2015.00008
- Pearce, D. A., Hughes, K. A., Lachlan-Cope, T., Harangozo, S. A., and Jones, A. E. (2010). Biodiversity of air-borne microorganisms at Halley Station, Antarctica. *Extrem. Life Extreme Cond.* 14, 145–159. doi: 10.1007/s00792-009-0293-8
- Pershagen, G., Rylander, E., Norberg, S., Eriksson, M., and Nordvall, S. L. (1995). Air pollution involving nitrogen dioxide exposure and wheezing bronchitis in children. *Int. J. Epidemiol.* 24, 1147–1153. doi: 10.1093/ije/24.6.1147
- Petrova, O. E., Cherny, K. E., and Sauer, K. (2014). The *Pseudomonas aeruginosa* diguanylate cyclase GcbA, a homolog of *P. fluorescens* GcbA, promotes initial attachment to surfaces, but not biofilm formation, via regulation of motility. *J. Bacteriol.* 196, 2827–2841. doi: 10.1128/JB.01628-14
- Petrova, O. E., and Sauer, K. (2012). PAS Domain residues and prosthetic group involved in BdlA-dependent dispersion response by *Pseudomonas aeruginosa* Biofilms. *J. Bacteriol.* 194, 5817–5828. doi: 10.1128/JB.00780-12
- Poole, R. K., Anjum, M. F., Membrillo-Hernández, J., Kim, S. O., Hughes, M. N., and Stewart, V. (1996). Nitric oxide, nitrite, and FnR regulation of *hmp* (flavohemoglobin) gene expression in *Escherichia coli* K-12. *J. Bacteriol.* 178, 5487–5492.
- Redondo-Nieto, M., Barret, M., Morrissey, J., Germaine, K., Martínez-Granero, F., Barahona, E., et al. (2013). Genome sequence reveals that *Pseudomonas fluorescens* F113 possesses a large and diverse array of systems for rhizosphere function and host interaction. *BMC Genomics* 14:54. doi: 10.1186/1471-2144-14-54
- Reduction of pollutant emissions from light vehicles (2015). *Access Eur. Union Law*. Available online at: <http://eur-lex.europa.eu/legal-content/EN/TXT/?uri=uriserv:l28186> (Accessed September 17, 2015).
- Rietsch, A., Vallet-Gely, I., Dove, S. L., and Mekalanos, J. J. (2005). ExsE, a secreted regulator of type III secretion genes in *Pseudomonas aeruginosa*. *Proc. Natl. Acad. Sci. U.S.A.* 102, 8006–8011. doi: 10.1073/pnas.0503005102
- Rossignol, G., Merieau, A., Guerillon, J., Veron, W., Lesouhaitier, O., Feuilloley, M. G., et al. (2008). Involvement of a phospholipase C in the hemolytic activity of a clinical strain of *Pseudomonas fluorescens*. *BMC Microbiol.* 8:189. doi: 10.1186/1471-2180-8-189
- Roy, A. B., Petrova, O. E., and Sauer, K. (2012). The phosphodiesterase DipA (PA5017) is essential for *Pseudomonas aeruginosa* biofilm dispersion. *J. Bacteriol.* 194, 2904–2915. doi: 10.1128/JB.05346-11
- Sastalla, I., Chim, K., Cheung, G. Y. C., Pomerantsev, A. P., and Leppla, S. H. (2009). Codon-optimized fluorescent proteins designed for expression in low-GC Gram-positive bacteria. *Appl. Environ. Microbiol.* 75, 2099–2110. doi: 10.1128/AEM.02066-08
- Scales, B. S., Dickson, R. P., LiPuma, J. J., and Huffnagle, G. B. (2014). Microbiology, genomics, and clinical significance of the *Pseudomonas fluorescens* species complex, an unappreciated colonizer of humans. *Clin. Microbiol. Rev.* 27, 927–948. doi: 10.1128/CMR.00044-14
- Sher, E. (1998). *Handbook of Air Pollution from Internal Combustion Engines: Pollutant Formation and Control*. San Diego, MA; Chestnut Hill, MA: Academic Press.
- Shiro, Y. (2012). Structure and function of bacterial nitric oxide reductases: nitric oxide reductase, anaerobic enzymes. *Biochim. Biophys. Acta* 1817, 1907–1913. doi: 10.1016/j.bbabi.2012.03.001
- Skalska, K., Miller, J. S., and Ledakowicz, S. (2010). Trends in NO_x abatement: a review. *Sci. Total Environ.* 408, 3976–3989. doi: 10.1016/j.scitotenv.2010.06.001
- Smith, P. K., Krohn, R. I., Hermanson, G. T., Mallia, A. K., Gartner, F. H., Provenzano, M. D., et al. (1985). Measurement of protein using bicinchoninic acid. *Anal. Biochem.* 150, 76–85. doi: 10.1016/0003-2697(85)90442-7
- Sobel, M. L., McKay, G. A., and Poole, K. (2003). Contribution of the MexXY multidrug transporter to aminoglycoside resistance in *Pseudomonas aeruginosa* clinical isolates. *Antimicrob. Agents Chemother.* 47, 3202–3207. doi: 10.1128/AAC.47.10.3202-3207.2003
- Sobel, M. L., Neshat, S., and Poole, K. (2005). Mutations in PA2491 (mexS) Promote MexT-dependent *mexEF oprN* expression and multidrug resistance in a clinical strain of *Pseudomonas aeruginosa*. *J. Bacteriol.* 187, 1246–1253. doi: 10.1128/JB.187.4.1246-1253.2005
- Spangler, C., Böhm, A., Jenal, U., Seifert, R., and Kaever, V. (2010). A liquid chromatography-coupled tandem mass spectrometry method for quantitation of cyclic di-guanosine monophosphate. *J. Microbiol. Methods* 81, 226–231. doi: 10.1016/j.mimet.2010.03.020
- Spiro, S. (2007). Regulators of bacterial responses to nitric oxide. *FEMS Microbiol. Rev.* 31, 193–211. doi: 10.1111/j.1574-6976.2006.00061.x
- Strehmel, J., Neidig, A., Nusser, M., Geffers, R., Brenner-Weiss, G., and Overhage, J. (2015). Sensor kinase PA4398 modulates swarming motility and biofilm formation in *Pseudomonas aeruginosa* PA14. *Appl. Environ. Microbiol.* 81, 1274–1285. doi: 10.1128/AEM.02832-14
- Tamir, S., Burney, S., and Tannenbaum, S. R. (1996). DNA damage by nitric oxide. *Chem. Res. Toxicol.* 9, 821–827. doi: 10.1021/tx9600311

- Šantl-Temkiv, T., Sahyoun, M., Finster, K., Hartmann, S., Augustin-Bauditz, S., Stratmann, F., et al. (2015). Characterization of airborne ice-nucleation-active bacteria and bacterial fragments. *Atmos. Environ.* 109, 105–117. doi: 10.1016/j.atmosenv.2015.02.060
- van Sorge, N. M., Beasley, F. C., Gusarov, I., Gonzalez, D. J., Köckritz-Blickwede, M., von, Anik, S., et al. (2013). Methicillin-resistant *Staphylococcus aureus* bacterial nitric oxide synthase affects antibiotic sensitivity and skin abscess development. *J. Biol. Chem.* 288, 6417–6426. doi: 10.1074/jbc.M112.448738
- Varivarn, K., Champa, L. A., Silby, M. W., and Robleto, E. A. (2013). Colonization strategies of *Pseudomonas fluorescens* Pf0-1: activation of soil-specific genes important for diverse and specific environments. *BMC Microbiol.* 13:92. doi: 10.1186/1471-2180-13-92
- WHO | Air quality guidelines - global update (2005). WHO. Available online at: http://www.who.int/phe/health_topics/outdoorair/outdoorair_aqg/en/ (Accessed September 17, 2015).

WHO | Ambient (outdoor) air quality and health (2015). WHO. Available online at: <http://www.who.int/mediacentre/factsheets/fs313/en/> (Accessed September 17, 2015).

Conflict of Interest Statement: The authors declare that the research was conducted in the absence of any commercial or financial relationships that could be construed as a potential conflict of interest.

Copyright © 2016 Kondakova, Catovic, Barreau, Nusser, Brenner-Weiss, Chevalier, Dionnet, Orange and Duclairoir Poc. This is an open-access article distributed under the terms of the Creative Commons Attribution License (CC BY). The use, distribution or reproduction in other forums is permitted, provided the original author(s) or licensor are credited and that the original publication in this journal is cited, in accordance with accepted academic practice. No use, distribution or reproduction is permitted which does not comply with these terms.

P27



Development of preservative-free nanoparticles-based emulsions: Effects of NP surface properties and sterilization process



Laura Rowenczyk^{a,b}, Céline Picard^{a,*}, Cécile Duclairoir-Poc^b, Nicolas Hucher^a, Nicole Orange^b, Marc Feuilloley^b, Michel Grisel^a

^a Normandie Univ, ULH, CNRS, URCOM, 76600 Le Havre, France

^b Laboratoire de Microbiologie Signaux et Microenvironnement EA 4312, Université de Rouen, 55 rue saint Germain 27000 Evreux, France

ARTICLE INFO

Article history:

Received 18 March 2016

Received in revised form 30 May 2016

Accepted 6 June 2016

Available online 7 June 2016

Keywords:

Emulsion formulation

Sterilization

TiO₂ NP

Particle size measurement

Rheology

Texturometry

Microbiological assays

ABSTRACT

Model emulsions were developed with or without commercial titanium dioxide nanoparticles (NP) carrying various surface treatments in order to get close physicochemical properties whatever the NP surface polarity (hydrophilic and hydrophobic). Rheology and texturometry highlighted that the macroscopic properties of the three formulated emulsions were similar. However, characterizations by optical microscopy, static light scattering and zetametry showed that their microstructures reflected the diversity of the incorporated NP surface properties. In order to use these model emulsions as tools for biological evaluations of the NP in use, they had to show the lowest initial microbiological charge and, specifically for the NP-free emulsion, the lowest bactericidal effect. Hence, formulae were developed preservative-free and a thermal sterilization step was conducted. Efficiency of the sterilization and its impact on the emulsion integrity were monitored. Results highlighted the effect of the NP surface properties: only the control emulsion and the emulsion containing hydrophilic NP fulfilled both requirements. To ensure the usability of these model emulsions as tools to evaluate the 'NP effect' on representative bacteria of the skin microflora (*S. aureus* and *P. fluorescens*), impact on the bacterial growth was measured on voluntary inoculated formulae.

© 2016 Elsevier B.V. All rights reserved.

1. Introduction

Titanium dioxide (TiO₂) NP are commonly used in Cosmetics, especially as UV filters in sunscreen emulsions. Their tiny size, enabling transparency in the visible range, makes it possible to obtain end products without any residual traces on skin in addition to a good UV-protection (Serpone et al., 2007). However, if compared to micrometric oxides, nanometric ones are more reactive and in particular photo-reactive. Therefore, such nano-objects receive a first coating with *silica* or *alumina* as it allows quenching photo-produced radicals (Serpone et al., 2006); in addition, a second coating is sometimes added in order to improve their dispersibility in formula. Whereas European Regulation (European Parliament, Council of the European Union, 2014) clearly mentions the obligation to demonstrate the safety of even coated NP, very few studies took interest on their behavior in use. Santaella et al. (Santaella et al., 2014) compared the eco-toxicity of

NP with degraded coating in aqueous environment (Auffan et al., 2010) to that of pure TiO₂. Other studies dealt with the impact of zinc oxide NP on bacteria according to their size (Pasquet et al., 2014). However, aggregation state and physicochemical behavior of NP in formula have to be taken into account and their safety in emulsions when they are layered on skin remained a critical question. Moreover, these questions are closely related to the large variety of surface treatments commercially available (polar, non-polar, hydrophilic, hydrophobic . . .).

To evaluate the only effect of NP in formula, emulsions need to be developed in order to respect three main criteria:

- Being stable and exhibiting similar microstructure and macroscopic properties whatever the coating of the incorporated NP;
- Exhibiting the lowest initial microbiological charge;
- Giving the control emulsion (without NP) the lowest bactericidal effect.

Therefore emulsions need to be developed without preservative. Hence, in order to fulfill the second criterion, alternative process, like sterilization procedures, consisting in the elimination

* Corresponding author at: University of Le Havre, 25 rue Philippe Lebon, B.P. 540 76058 Le Havre cedex, France.

E-mail address: celine.picard@univ-lehavre.fr (C. Picard).

of germs and spores in a product, has to be used. However, cosmetic form does not allow the use of technics such as filtration of emulsion systems because it could lead to a demixing phenomenon (Kocherginsky et al., 2003) or UV or gamma radiations because of presence of UV filters in this study. Sterilization by high temperature seemed the best solution especially as this kind of methods begins to be used on cosmetic emulsions (Delaunay and Legendre, 2013) associated to an adapted packaging (Devlieghere et al., 2015). Nevertheless, high temperatures could accelerate aging (Waterman and Adami, 2005) and, recently Rossano et al. (2014) demonstrated that aging of emulsions containing hydrophobic NP induced particles aggregation, adsorption of formula's compounds and coatings deterioration. Thus, as it is still relatively unexplored, it is essential to bring data concerning the effect of coatings and sterilization temperature on the emulsion properties. Our study focuses on the characterization of model emulsions in order to ensure the similarity in terms of microstructure and physicochemical properties of a control emulsion without nanoparticle and formulae containing either hydrophilic/hydrophobic NP.

Finally, microbiological evaluations were conducted on two skin bacteria strains to check the low initial microbiological charge of the model emulsions and the low bactericidal impact of the control one.

2. Experimental

2.1. Chemical and reference materials

Water with a resistivity of 18 mΩ cm used during the emulsion preparation and zetametry was purified, filtrated on 0.2 μm and treated by UV in order to eliminate germs, after described as ultrapure. Otherwise distilled water with a resistivity of 18 mΩ cm was used for other emulsion characterizations. Two different grades of TiO₂—NP were kindly given by Kobo and Merck; one hydrophilic, with a simple *silica* coating named N1 (EUSOLEX® TAVO, Merck Chimie SAS, France) and a second, hydrophobic, composed of *alumina* (*and*) *triethoxycaprylylsilane* named N2 (A10-TiO₂-11S7, Kobo Products, France). Other cosmetic grade ingredients, introduced in Table 1 were chosen to obtain simplified sunscreen, oil-in-water emulsions type, and to improve NP dispersions. Ingredients were used as received. To achieve emulsions with the lowest bactericide impact, no preservative was added.

2.2. Emulsion preparation

During preservative-free emulsion preparation, precautions were taken in order to minimize the risks of microorganisms contamination: all stainless steel materials were steamed for 45 min at 190 °C and glass bottles were rinsed with ethanol prior to drying (INRS, 2014). For technical reasons it was impossible to

make all operation under laminar flow hood in sterile conditions. But controls revealed that aerial contaminants in final formulations remained under the detection limit.

2.2.1. Emulsion without nanoparticle

Emulsion without NP was adapted from the protocol described by Rossano et al. (2014). It was developed to obtain similar emulsions, with or without NP, and to improve the NP dispersion. The gelling agent was sprinkled in water and hydrated 20 min without stirring. This mix corresponding to the phase B and the phase A were separately homogenized at 80 °C under mechanical stirring for 10 min. After water loss compensation, phase A was added to phase B off the heat and under vigorous stirring (11000 rpm for 1.5 min), by using a rotor-stator type homogenizer (Ultra-Turrax, stator diameter 25 mm, rotor diameter 18 mm, IKA). Then, the mixture was put under stirring (Turbotest, radial flow turbine of 55 mm diameter, VMI Raynerie) at 750 rpm and triethanolamin (TEA) was immediately added. After 5 min, the stirring rate was raised to 1000 rpm. A cold water bath was used once cooled below 38 °C. When the temperature of emulsion was close to 25 °C, pH was adjusted at 6.6–6.8 using HCl 0.4 M. The mixture was kept under stirring for 5 additional minutes. It was then put under vacuum to remove air bubbles incorporated during the previous process.

2.2.2. Nanoparticle dispersions

Because rotor-stator type homogenization was not sufficient to obtain an acceptable dispersion in emulsion, NP powders were first pre-dispersed in one of the emulsion phases, leading to a NP paste. Hydrophilic NP and water with a ratio of 1/2 (w/w) were sonicated 10 min (Ultrasonic cleaner, VWR, 45 kHz, 120 W). Hydrophobic NP and cetearyl ethylhexanoate with a ratio of 2/3 (w/w) were mixed. Then, this pre-dispersion was grounded on a three-cylinder mill for three times to reduce the size of agglomerates.

2.2.3. Emulsions with nanoparticles

The protocol remained the same as without NP except that just after the addition of TEA, NP paste was added under a stirring of 1000 rpm to reach the optimal dispersion in emulsion. The end of the preparation was the same than without NP.

2.2.4. Sterilization

Each emulsion was poured into several 50 mL glass autoclave-resistance bottles (VWR). After maturation at 20 ± 2 °C for 24 h, a half of them was sterilized during 20 min at 120 °C and 1 bar relative pressure in an autoclave (Laboster, Subtil-Crepieux, Chassieu, France). The second part was let at the same temperature. After heating and when the temperature cooled below 90 °C, the autoclave was opened and the bottles were let at ambient air in order to accelerate the cooling. Thus, for instance, ST-F-0 was the autoclaved version of F-0.

Table 1

Content, function and supplier of ingredients used in emulsions.

Phase	Content (%w/w)	Product INCI Name	Function	Supplier
Phase A	2.75	Steareth 2	Surfactant	Croda (UK)
	1.75	Steareth 21	Surfactant	Croda (UK)
	2.00	Paraffin	Emollient	Baëlocher (France)
	0.20	Beeswax	Emollient	Baëlocher (France)
	20.00	Cetearyl ethylhexanoate	Emollient	Stéarinerie Dubois
Phase B	0.10	Acrylates/C10-30 alkyl acrylate crosspolymer	Polymer gelling agent	Lubrizol (Belgium)
	Qs	Deionised water		
	0.13	Triethanolamin	Additive	BASF (Germany)
	5.00	TiO ₂ NP	Inorganic UV filter	–

Efficiency of the heat treatment can be evaluated by calculation of the sterility value (SV): $SV = \int 10^{(T(t)-T_{ref})/Z} dt$

- $T(t)$ is the core temperature in the time interval,
- T_{ref} is the reference temperature,
- Z is the difference of temperature required to accelerate tenfold the germs destruction reaction.

In the case of a sterilization step, T_{ref} and Z are respectively equal to 121.1 °C and 10 °C (Bimbenet et al., 2007). A temperature probe (DataTrace, CMI) was introduced into a product bottle in order to obtain the core temperature essential for the SV calculation.

2.3. Emulsions characterization

Once prepared, emulsions were characterized after a period of maturation for two days or if so, sterilization.

2.3.1. Microstructural characterization

2.3.1.1. Optical microscopy. Qualitative observations were performed using an optical microscope (DMLP/DC 300, Leica Microsystems, Wetzlar, Germany) equipped with a camera and the IM1000 software (version 1.20 Release 19). In order to visualize emulsion microstructures, droplets sizes and quality of NP dispersion, a tip of emulsion plus a water drop were placed between slide and coverslip. Pictures were obtained at a magnification of $\times 200$.

2.3.1.2. Particle size measurement. Particles sizes measurements were performed by using a laser diffractometer SALD 7500 Nano (405 nm, Shimadzu, Marne-la-Vallée, France) combined with the measure cell SALD BC 75 consisting in a 7 mL batch and a stirrer and equipped with the WingSALD II-7500 software (version 3.1). In order to reach an absorption value of the samples between 1.2 and 1.5 and the best quality of the obtained signal, particle dispersions had to be diluted and homogenized according to the following procedures. Approximately 0.1 g of NP pastes was pre-dispersed in a test tube with 5 mL of distilled water for coating 1 or of cetearyl ethylhexanoate for coating 2. This pre-dispersion was then sonicated 5 min (120 W). In the case of emulsion particle sizing measurement, approximately 0.1 g of emulsion were pre-diluted in a test tube with 5 mL of distilled water. The mix was vortexed 10 s at 1000 rpm. Finally, pre-dispersed samples were added by drop until reaching the expected absorption. All measurements were performed at least in triplicate on two different batches. D10, D50 and D90 were thereafter expressed in particle volume. By this way, for instance, D10 represented the threshold value in micrometer for which 10% of particles had a smaller size.

2.3.1.3. Zetametry. Mean zeta potentials of emulsions were performed using a Zeta Sizer Nano-Z and folded capillary cells (Malvern instruments, Malvern, UK). Emulsions were diluted at 0.5% w/w in ultrapure water containing NaCl at 10^{-4} M (conductivity of 1.70 μ S/cm). Six samples of each emulsion were adjusted at pH 2, 4, 6, 8, 10 and 12, respectively, with using NaOH or HCl (0.4 or 0.04 M).

Measurements were performed at least three times.

2.3.2. Macroscopic properties

2.3.2.1. Rheology. Rheological properties were achieved with a controlled-stress rheometer (Discovery HR1, TA instrument, Guyancourt, France) using an aluminum cone-plate geometry

(40 mm diameter, cone angle of 1.994° and truncation of 47 μ m). Data analyses were conducted with the software TRIOS® 3.0. Stress sweep was carried out at 25 °C, temperature controlled by Peltier effect, with an imposed stress gradient from 0.01 to 150 Pa and a fixed frequency of 1 Hz. This analysis highlighted the linear viscoelastic region and permitted to obtain the viscoelastic parameters, independent of the applied stress as listed below:

- $\tan(\delta)$, where δ is the phase shift between strain and stress and is equal to G''/G' ,
- G' , the elastic modulus (Pa),
- G'' , the viscous modulus (Pa),
- γ_c , the critical strain, corresponds to the percentage strain at 90% of the plateau G' value.

All measurements were performed at least twice on two different batches.

2.3.2.2. Texture analyses. Texture analyses were performed by using a TA.XT Plus (Stable Micro Systems, Cardiff, UK) and the software Texture Exponent 32 (version 5.0,6,0, 2010). It allows the characterization of mechanical properties of emulsions. The protocol was adapted from Gilbert et al. (2013). Effect of the compression was studied with the P/35 probe (35 mm diameter, aluminum). 750 μ L of emulsion were deposited on the analyzer base by using a Microman® M250 (Gilson) and compressed by the probe until a gap of 0.5 mm with a rate of 1 mm/s. Three parameters were recovered:

- the positive area, corresponding to the work required during the product compression (kg s),
- the maximum force reached (kg),
- the negative area, corresponding to the work required during the probe removal (kg s).

Ability to spreading was lead with the friction modulus A/FR. A polypropylene (PP) sheet was fixed on the analyzer base and the probe was covered with a Helioplate™ HD 2 (Helioscreen, Creil, France) consisting of a PMMA plate. Four lines of each 50 μ L of emulsion were deposited using a Microman® M250 (Gilson, Villiers-le-Bel, France) in the displacement direction. The probe was pulled on a distance of 120 mm with a speed of 3 mm/s. Pictures were taken from spreading traces on the PP sheet. In order to evaluate the corresponding traces thickness, the lightness evolution (L^* factor in the CIE $L^*a^*b^*$ color model) was measured every 2 cm, starting to the beginning of the trace (Spectrophotometer CM-5, Konica Minolta, Nieuwegein, Netherlands).

All measurements were performed at least twice on two different batches.

2.4. Microbiological assays

2.4.1. Bacteria strain and culture conditions

Pseudomonas fluorescens MFP05 and *Staphylococcus aureus* MFP 03 are normal human skin bacteria strains collected by swabbing and characterized by metabolic, proteomic and genomic analysis (Hillion et al., 2013). These strains are stored on cryobeads at -140 °C. Before use, they were sub-cultured over-night in 50 mL of Luria Bertani (LB) broth at 28 ± 2 °C for MFP05 or 37 ± 2 °C for MFP03. The cultures were then diluted again in LB broth to reach the appropriate initial bacterial density corresponding to an $OD_{580\text{nm}} = 0.08$. OD values were measured using a spectrophotometer (Helios Epsilon, ThermoSpectronics, Cambridge, UK). Bacteria were used when the cultures reached the end of the exponential growth phase.

2.4.2. Counting and detection of mesophilic aerobic bacteria

Mesophilic aerobic bacteria in emulsions were counted and detected by using the norm NF EN ISO 21149:2006 (AFNOR, 2009). It includes three culture tests. To base the study on solid grounds, we chose to correlate two of them. The first one, without enrichment, consists in diluting approximately 1 g of emulsion in ten times this exact mass in peptone water and then vortexing at 1000 rpm for 20 s. 100 µL of this mix was spread on a TSA Petri dish and incubated at 30 ± 2 °C for four days. The second test, with enrichment, was the dilution of approximately 1 g (exactly weighed) of emulsion in ten times the mass in EUGON LT 100 broth. The liquid mix was incubated at least 20 h at 30 ± 2 °C under orbital stirring at 180 rpm. Then the mix was vortexed at 1000 rpm and 100 µL were spread on a EUGON LT 100 agar Petri plate. They were then incubated at 30 ± 2 °C for four days. Three Petri dishes were prepared for each condition and emulsion. The number of mesophilic aerobic bacteria (N) was determined by the equation:

- N = m/(V × d) where,
- m is the mean number of colonies on Petri dishes,
- V is the inoculated volume on a Petri dish (mL),
- D is the dilution of the emulsion (1/10 in this case).

2.4.3. Evolution of willingly inoculated bacteria in model emulsions

Approximately 5 g of each emulsion were diluted to the third in physiologic water (NaCl 0.9%) or LB broth. Obtained solutions were inoculated with MFP03 or MFP05 at an initial concentration between 10⁵ and 10⁶ UFC/mL. The exact bacterial concentration was controlled by plating 100 µL of solutions and serial dilutions on TSA Petri Dishes immediately after bacterial inoculation. Inoculated solutions were incubated at 28 ± 2 °C in the case of MFP05 or 37 ± 2 °C for MFP03 under orbital agitation at 180 rpm. After different period of time (24 h, 48 h and 72 h, respectively), 100 µL of solutions were spread on TSA Petri dishes in order to monitor bacteria growth evolution. All Petri dishes were incubated 24 h at 28 ± 2 °C for MFP05 or 37 ± 2 °C for MFP03 before counting.

2.5. Data analyses

Results were expressed as mean ± standard deviation (SD). Statistical analyses of collected data were performed on XLSTAT software (version 2012.1.01, Addinsoft, France). Single-way analyses of variance (ANOVA) were applied to data series in order to test significance of parameters. When a significant difference was revealed between emulsions ($p < 0.05$), groups of emulsions were formed using Tukey multiple comparison test.

3. Results and discussion

3.1. Comparative study of emulsions with or without nanoparticles

Three emulsions were obtained by the lab-scale process depicted in the Material and Methods section: a control emulsion without NP (F-0), an emulsion (F-N1) with hydrophilic NP (N1) and an emulsion (F-N2) with hydrophobic NP (N2).

3.1.1. Microstructural characterization

3.1.1.1. Characterization of nanoparticles dispersions. When working with NP, emulsions and their mixtures, an important issue is to characterize size distributions, making sure that the techniques used, the operating conditions and analyses parameters fitted well.

Both NP primary sizes given by suppliers were around 10 nm diameters which correspond to the dimension of the particles

measured just after manufacturing. However, at the nanometric scale, attractive forces are intense and NP in powder are known to form aggregates-like structures of much larger dimensions (larger than 1 µm) (Aldous and Kent 2013). Thus, in the present study, several processes were tested to improve the particles dispersions in emulsions. The best one was obtained when pre-dispersion was prepared separately and added after the emulsification step. Size distributions of NP in pre-dispersion were monitored by laser granulometry as described in Materiel & Methods. Because of the thinness of the dispersions, determination of the refractive indexes (RIs) of the particles was required to use the Mie theory. Different parameters could have an impact on this RI and should be investigated. At the studied wavelength, calculation models showed that the crystallinity, the shape and the size did not impact the RI of TiO₂-particles (Auvinen et al., 2013). The coating could also have an effect on the particles refraction. Thus, calculations based on the RI of the TiO₂ or of the coating were made and gave the same results in term of size distribution.

Added to ester phase, N2 NP formed larger aggregates, with a D90 equal to 30 µm. Thanks to its high viscosity, the paste was refined using a three-cylinder mill. This method decreased the D90 under 4 µm. N1 NP in water were already well-dispersed and had a D90 already around 11 µm. Due to the low viscosity of the hydrophilic dispersion, an ultra-sonication treatment was used and reduced even more the D90 until 1.7 µm. Given in number of particles, the D50 of N2 was equal to 180 nm and the D50 of N1 to 60 nm. Consequently, N1 met the official definition of NP (Official Journal of the European Union, 2011) while N2 was really close. However, in this study, size distribution was expressed in volume as it magnifies the impact of the biggest aggregates and allows a better evidencing of the dispersion heterogeneity.

3.1.1.2. Characterization of emulsions. For the same reasons as above, emulsions size distributions were also given in volume of colloids. All colloids present in emulsions, TiO₂-particles as well as oil droplets, were detected during measurements. Since these colloids had various sizes and optical properties, the use of a RI was not applicable. For this reason, the Fraunhofer's approximation was chosen in term of calculation model. This model is generally applicable for colloids owning size larger than few micrometers; however Jones (1977) and Seville et al. (1984) demonstrated that the error made on the measured size is acceptable, when considering smaller and non-absorbing colloids like in our situation.

For F-0, even if this monomodal distribution was polydisperse (Fig. 1), the D90 value, around 7 µm and the D50 value at 2.331 µm both proved that the blank emulsion was mostly composed of small droplets. F-N1 size distribution was very similar to the blank one: only the D10 was significantly lower. NP in the emulsion

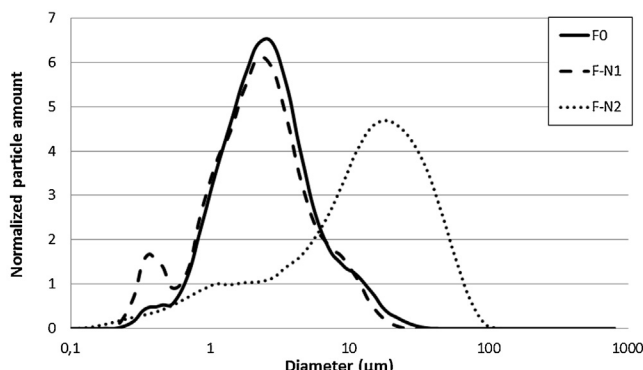


Fig. 1. Particle size distributions given in volume particle of fresh emulsions.

corresponded to a new population of colloids with a dimension around $0.6\text{ }\mu\text{m}$. Size distribution obtained for F-N2 highlighted a large distance between the D10 and the D90 values and depicted a high polydispersity. Moreover, the D50 was five time higher than the mean size value for F-0: F-N2 distribution was thus essentially formed of a new larger population around $10\text{ }\mu\text{m}$.

As sampling required for the size distribution measurement induced a dilution of emulsions and, as a consequence potential physical modifications compared to the initial droplets sizes in bulk, the microstructure of emulsions was also controlled by optical microscopy. Indeed, the lowest dilution necessary to this method allowed observations closer to the reality even if limited by the resolution around $1\text{ }\mu\text{m}$. Microscopic observations of F-0 (Fig. 2A) confirmed the thinness and the homogeneity of the emulsion and allowed to identify droplets network, appearing as a sort of spider web visible on the picture by alternation of dark areas, build of droplets, and white areas consisting of blank. This phenomenon depicted a highly flocculated system. It justified the sample preparation for the granulometry measurement that reduce the aggregation phenomena and allowed the measurement of primary sizes. Optical microscopy also confirmed that only few aggregates were formed in F-N1 and that the majority of the NP was well-dispersed once in emulsion (Fig. 2B). The important droplets network described for F-0 was no longer observed for F-N1. In this work, the high amount of tiny particles located in the continuous phase led to the formation of a new network, consisting of particles and droplets. Moreover TiO₂-particles coated with *silica* had negative surface charges (Junior and Baldo 2014) that might lead to a repulsion between droplets and prevented flocculation. The optical micrograph of F-N2 (Fig. 2C) showed large dark objects, around $10\text{--}20\text{ }\mu\text{m}$, masking droplets and corresponding to the aggregates characterized by the D90 value. Added to an oil-in-water emulsion, hydrophobic particles could not be as well dispersed as N1 and formed large vesicles of cetearyl ethylhexanoate and NP. Here again, F-N2 was less flocculated than F-0 surely because the initial emulsion was less concentrated in oil droplets: vesicles contained almost 40% of the total oil of the emulsion. To conclude, the blank emulsion and the

emulsion with hydrophilic NP were very similar in term of size distributions, while F-N2 containing hydrophobic NP was rougher. In both case, the presence of NP seemed to avoid the flocculation phenomenon.

3.1.2. Macroscopic properties

Emulsions are viscoelastic materials that have both solid and viscous liquid properties. In this study, dynamic oscillatory tests did through a stress sweep (Table 2) bring out these behaviors. On the linear viscoelastic region, the G' of F-0 was much higher than the G'' demonstrating the elastic behavior of the emulsions. This led to a tan δ equal to 0.2; this low value corresponds to a strong viscoelastic system. Approaching γ_c , emulsion structure kept up until a strong decrease of both moduli. The observed G'' overshoot is characteristic of a weak gel (not shown) usually obtained when any gelling agent is added in emulsion continuous phase.

With a similar G' value, F-N1 and F-N2 showed the same predominant elastic behavior as F-0. Even if it was demonstrated that a less flocculated networks or a higher mean size could lead to a lower elastic modulus (Tadros 2004; Pal 1996), in this study, the presence of a solid dispersion offset this fall because it strengthened the network. However, for both emulsions containing NP, tan δ was significantly higher and the G'' overshoot was no more observed. The presence of NP in emulsion gave a system considered as a weaker gel compared to F-0, sign of a reduction of the network strength. Critical strains, γ_c , were reduced showing a more polydispersed system: finally, F-N2 appeared less homogeneous than F-N1 which was less than F-0.

Texture analyses were performed on emulsions and brought out the same behaviors for F-0, F-N1 and F-N2 during compression test (Table 2). Those results highlighted that the consistency of the three emulsions was the same. Spreading tests performed in order to mimic the application of sunscreen on skin, also highlighted the same behaviors of emulsions. The presence of UV filters only raised the lightness profile of traces (Fig. 3) but did not modify the spreading quality. Finally, the slight differences observed during the microstructural characterizations did not impact the macroscopic properties of these emulsions.

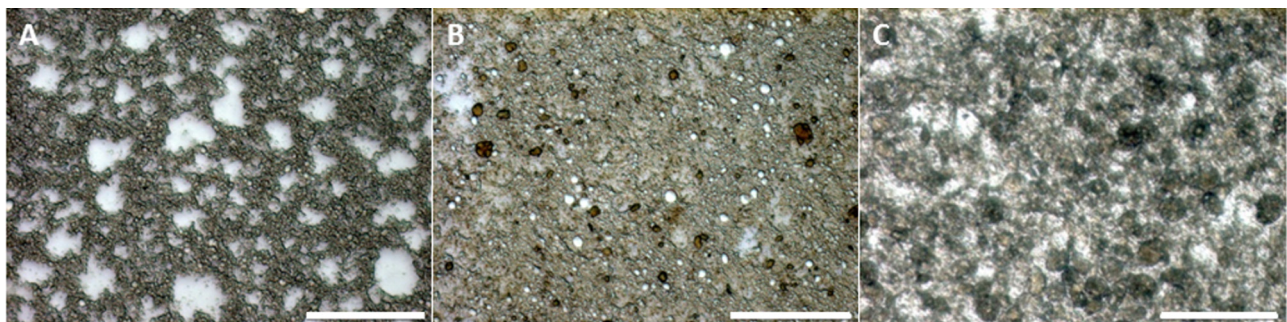


Fig. 2. Optical micrograph of; A: F-0, B: F-N1 et C: F-N2. (The scale bar corresponds to $100\text{ }\mu\text{m}$).

Table 2
Characteristic parameters of emulsions.

	Viscoelastic parameters				Compression parameters		
	G' \pm SD (Pa)	G'' \pm SD (Pa)	tan delta \pm SD	$\gamma_c \pm$ SD (%)	Positive Area \pm SD (kg s)	Maximum force (kg)	Negative Area \pm SD (kg s)
F-0	622 ^A \pm 80	122 ^{CD} \pm 13	0.20 ^C \pm 0.01	2.21 ^{AB} \pm 0.77	0.170 ^A \pm 0.023	0.363 ^{BC} \pm 0.034	-0.154 ^A \pm 0.022
ST-F-0	384 ^B \pm 28	106 ^D \pm 13	0.28 ^A \pm 0.02	2.80 ^A \pm 0.28	0.166 ^A \pm 0.012	0.337 ^C \pm 0.026	-0.157 ^A \pm 0.012
F-N1	648 ^A \pm 60	143 ^{BC} \pm 11	0.22 ^B \pm 0.01	1.88 ^{BC} \pm 0.20	0.194 ^A \pm 0.030	0.427 ^B \pm 0.051	-0.160 ^A \pm 0.032
ST-F-N1	675 ^A \pm 138	195 ^A \pm 27	0.29 ^A \pm 0.02	1.55 ^C \pm 0.57	0.285 ^B \pm 0.061	0.518 ^A \pm 0.072	-0.247 ^B \pm 0.038
F-N2	670 ^A \pm 55	159 ^B \pm 11	0.24 ^B \pm 0.00	1.18 ^C \pm 0.09	0.188 ^A \pm 0.029	0.408 ^B \pm 0.071	-0.163 ^A \pm 0.026

Different letters in the same row means significant difference between emulsions for this parameter ($p < 0.05$).

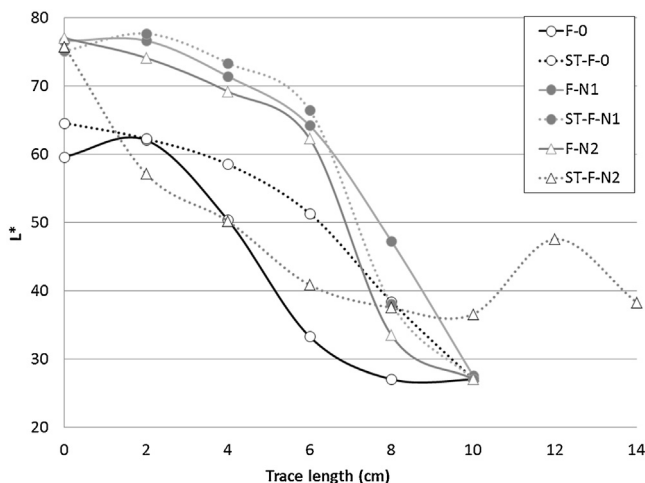


Fig. 3. Evolution percentage of lightness (L^*) along spreading traces.

3.2. Sterilization by high temperature of emulsions

In this study, a classical sterilization batch method, imitating Appertisation, was chosen and consisted in high temperature sterilization by autoclaving emulsions directly in its storage packaging (glass bottles). The calculated SV was superior to 22 min whereas the minimum value recommended by the European Pharmacopoeia (Delaunay and Legendre, 2013) is only 15 min, meaning that the treatment was efficient. By this way, three new emulsions were obtained ST-F-0, ST-F-N1 and ST-F-N2. During sterilization, high temperatures decreased the viscosity procured by the gelling agent. After cooling, ST-F-0 and ST-F-N1 restructured spontaneously and recovered a normal emulsion aspect without demixing. Sterilized formula containing N2 was no longer homogenous: a compact block stood in the middle of the glass bottle and was surrounded by a clearer liquid. After few hours

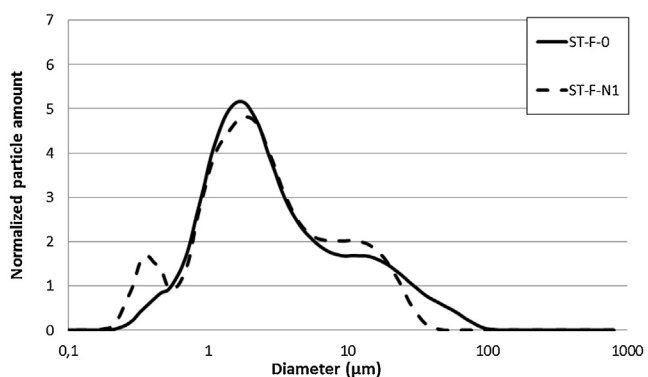


Fig. 5. Particle size distributions given in volume particle of sterilized emulsions.

cooling down, the viscosities of both phases equilibrated and the batch looked more homogenous even if lumps were still observable.

3.2.1. Microscopic characterization

The blank emulsion, ST-F-0, and the emulsion with hydrophilic NP, ST-F-N1, had droplet size distributions similar to their non-sterilized versions: only the D90 significantly increased after thermal treatment. Some larger droplets could be observed on the micrograph of ST-F-0 (arrows on Fig. 4A) confirming the presence of a new larger droplets population around 10–100 μm (Fig. 5). Large objects around 10 μm were present in F-N1 after sterilization (Figs. 4B and 5) and consisted in both droplets and particles aggregates.

Observations of ST-F-N2 phases (Figs. 4C and D) showed that the block part was constituted of around 500 μm long dark objects probably corresponding to large NP aggregates. The liquid part contained mostly fine droplets and air bubbles which appeared in the formula during the sterilization step as a consequence of the gas dilatation. The sterilized emulsion looked like after an

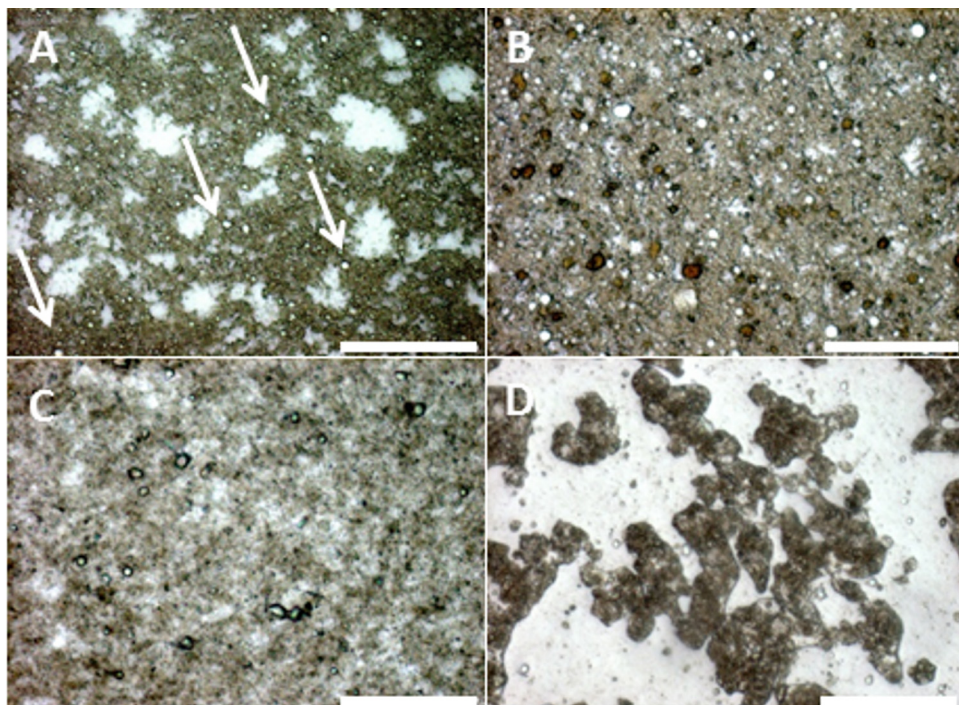


Fig. 4. Optical micrograph of; A: ST-F-0, B: ST-F-N1, C: liquid part of ST-F-N2 and D: solid part of ST-F-N2. (The scale bar corresponds to 100 μm).

accelerated aging already described by Rossano et al. (2014). These observations highlighted the high heterogeneity of ST-F-N2 that constituted a real barrier to the physicochemical characterizations of the emulsion and particle size measurements were not conducted.

Zeta potential (ZP) measurement gave a mean value that took into account surfaces of both droplets and particles (curves not shown). At pH 7, corresponding to the pH in emulsions after maturation, ZP measured for F-0 was around -30 mV . Presence of NP in F-N1 and F-N2 slightly decreased the ZP intensity at respectively -23 mV and -17 mV . After heat treatment, the measured mean zeta potential in emulsions significantly amplified for F-0 (-43 mV) and F-N1 (-33 mV) indicating that surface rearrangements occurred and increased electrostatic repulsion forces, favorable to the emulsion stability. To sum up, the thermal treatment did not impact the integrity of microstructures of the blank emulsion and of the emulsion containing hydrophilic NP while emulsion with hydrophobic NP was no longer homogeneous.

3.2.2. Macroscopic properties

As illustrated on Table 2, the G' value measured for ST-F-0 was significantly lower than the previous value obtained for F-0, while the G'' value remained the same; thus, the solid behavior of the emulsion dramatically decreased. Moreover, the $\tan \delta$ increased indicating that the gel behavior was considerably reduced. Complementary manipulations on polymer solutions showed that the G' value was divided by two whereas the G'' remained similar after the sterilization step. The viscoelastic evolutions of the emulsion during heat treatment may result from a decrease of the flocculated network but also from polymer degradation. Compression tests did not allow differentiating F-0 and ST-F-0 (Table 2); therefore, apparent texture, like firmness of the emulsion, was not impacted by the heat treatment. For ST-F-N1, the G' value was the same as its non-sterilized version whereas the G'' value was increased (Table 2). The rise of the $\tan \delta$ reflected a reduction of the viscoelastic behavior of the emulsion. Moreover, γ_c decreased indicating a loss of homogeneity, in relation with the rise of the D90 value.

The maximum force reached during the ST-F-N1 compression test (Table 2) was significantly higher when compared to other emulsions. This result revealed an high firmness for the sterilized emulsion containing hydrophilic NP (Friedman et al., 1963), in line with the high value of the viscous modulus. As this phenomenon should be explained by water losses during sterilization inducing a concentration effect of both droplets and particles, the water content of emulsions was evaluated by desiccation before and after the sterilization step but no difference was observed. Then, the increase in consistency and changes in viscoelastic behaviors of ST-F-N1 should not be explained only by the slight changes in size distributions but also by the structural rearrangements as suggested by surface modifications evidence by zetametry.

However, the γ_c remained identical in control and sterilized emulsions highlighted that their homogeneity was not impacted by the heat treatment (Table 2). Moreover, spreading tests highlighted that the important consistency of the ST-F-N1 did not affect the spreading quality as seen by comparing F-N1 and ST-F-N1 traces (Fig. 2). Nevertheless, the lightness measurement was higher along the ST-F-0 trace than along the F-0 trace. Chantrapornchai et al. already measured the bulk lightness of low concentrated emulsions with monitored flocculation. They demonstrated that in these conditions flocculated droplets decreased the L-value (Chantrapornchai et al., 2001). In this present work, as ST-F-0 and F-0 had the same granulometry profiles, ST-F-0 seemed less flocculated than the F-0 formula.

Although ST-F-N2 was not homogeneous, its spreading quality was tested in order to evaluate the impact of lumps in use.

Experiments confirmed the heterogeneity of this emulsion: at the beginning of the trace, lightness was similar to that of F-N2 but L^* quickly decreased. Previous studies have shown that the lightness of an emulsion decreases with the size of droplets (Chantrapornchai et al., 1998). Then, the presence of larger droplets in ST-F-N2 than in the other emulsions could explain the low value of measured lightness. It is also interesting to note that the trace did not end before the maximum mobile displacement and was not well-spread (Fig. 6). In fact, the emulsion seemed not to adhere on the hydrophobic surface of PP sheet but remained on the hydrophilic PMMA plate. This phenomenon should be regarded as a first sign of phase separation.

In conclusion, ST-F-0 and ST-F-N1 showed macroscopic properties slightly different than their non-sterilized versions. Mainly, the gel behavior was considerably reduced for both emulsions. However, these emulsions remained homogeneous and their qualities in term of consistency and spreading ability were acceptable. In addition to the presence of lumps in ST-F-N2, the emulsion was less covering compared to other studied emulsions and did not match the properties of sun protection cream.

3.3. Assessment of the microbiological properties of model emulsions

3.3.1. Initial microbiological charge: evaluation of aerobic mesophilic bacteria content

The efficiency of the sterilization process was evaluated following NF EN ISO 21149:2006 (AFNOR, 2009). Culture without enrichment gave the real number of mesophilic aerobic bacteria in emulsions. It was around 100 and 170 UFC/g of product and appears acceptable in regard of the acceptance limit recommended by the European Pharmacopoeia for the non-sterile cutaneous products fixed at 200 UFC/g of product (European Pharmacopoeia 8.0, 2014). Petri dishes spread with enriched non-sterilized emulsions were covered with bacteria colonies after incubation. On the contrary, in the case of sterilized emulsions, Petri dishes were devoid of any bacteria development thus proving the efficiency of the heat treatment. Hence, these results demonstrated that the initial emulsion microbiological charge of emulsions was acceptable and could not be an obstacle to future microbiological assays. For this purpose, only the non-sterilized versions were thereafter tested on bacteria strains.

3.3.2. Bactericidal effect of model emulsions

Two normal human skin bacteria strains were used: *Pseudomonas fluorescens* MFP 05, a gram negative ubiquitous bacterium representing more than 90% of the microbial flora in humid skin areas (Grice et al., 2008), *Staphylococcus aureus* MFP03, a gram positive bacterium, usually considered as a member of transient human skin flora carried by 35–60% of the human population (Percival et al., 2012).

When the control emulsion was diluted in LB broth (Fig. 7A) nutrient contribution let *P. fluorescens* and *S. aureus* to quickly develop. The growth of MFP03 (slope of the linear part of the curve) appeared more rapid than for MFP05 but this difference should only reflect their optimal growth temperature (37°C and 28°C respectively) and metabolism. In this culture condition, no bactericidal effect of the control emulsion was observed.

Thus, it appears interesting to evaluate the bactericidal effect of the presence of NP. The results highlighted that the NP did not significantly affect the growth of both bacteria. Finally, both strains grew as well in all emulsions, with or without NP. One hypothesis could be that the high nutrient contribution of LB broth hid the effect of the nanoparticle presence as well as their coatings. Therefore, dilution in physiological water was conducted as it only brings nutrients already present in the emulsion. In this second

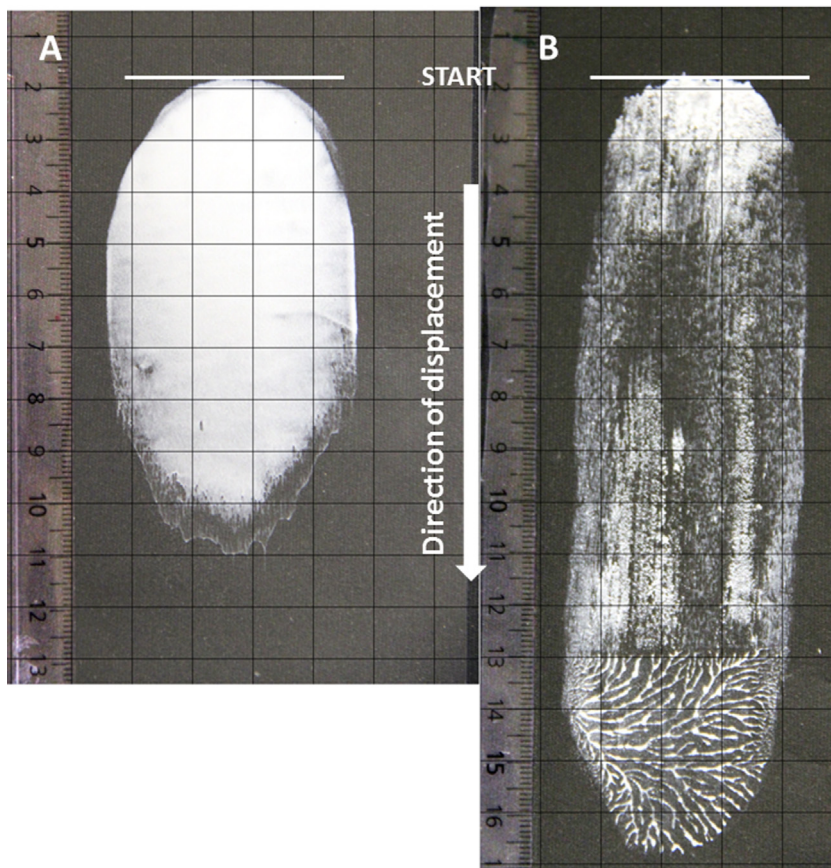


Fig. 6. Example of spreading traces, A: for F-N2, B: for ST-F-N2.

condition, the evolutions of bacteria in the diluted control emulsion were also similar and there was no NP effect (Fig. 7B). The growth kinetic of *P. fluorescens* MFP05 was reduced with a plateau, corresponding to the total biomass formed which was decreased of ten times. *P. fluorescens* MFP05 is resistant and highly adaptable to environment variations (Chapalain et al., 2008) as previously shown, emulsions are not appearing as a favorable

media for bacteria development (Teixeira et al., 2007). This was confirmed by the behavior of *S. aureus* MFP03 that was unable to grow in emulsion diluted in physiological water. This bacterium could not adapt and metabolize emulsion components. Its population was undergoing a progressive decay due to the lack of adapted resources.

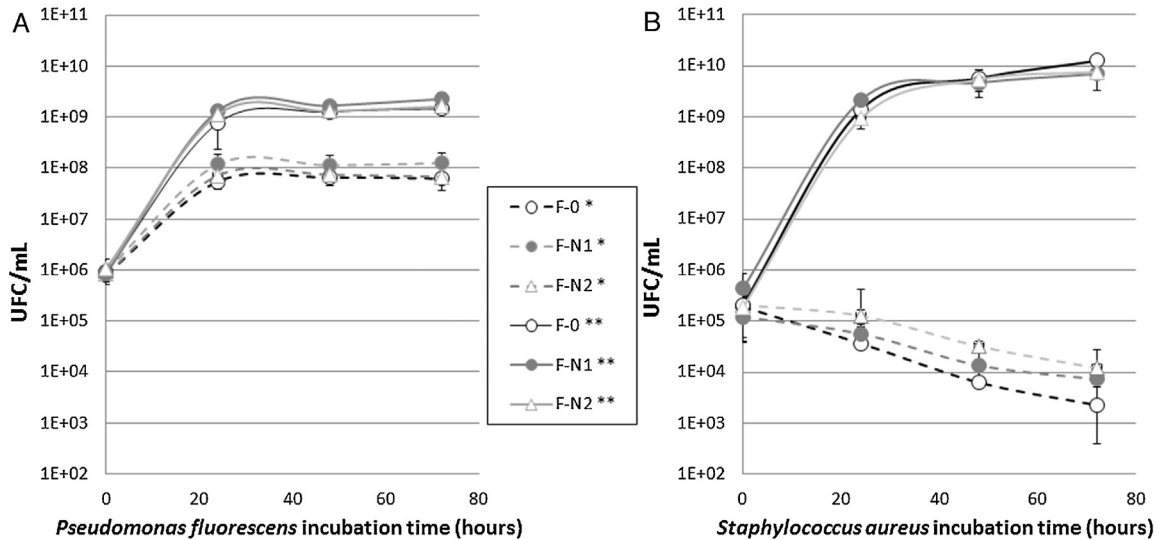


Fig. 7. Bacteria growth in different diluted emulsions ($n=3$); *emulsions diluted in physiologic water, **emulsions diluted in LB.

To conclude, the control emulsion fulfilled the defined criteria in the introduction and this test following the bacteria growth in emulsions highlighted the absence of NP effect.

4. Conclusion

In this study, formulation development was conducted to provide lab-scale preservative-free sunscreen emulsions that should contain the same major ingredients and differed only by the presence and nature of TiO_2 —NP, an inorganic UV-filter. This development phase showed that TiO_2 —NP could be difficult to implement, depending on their coating. While hydrophilic NP, coated with *silica*, was easily integrated into the continuous phase of the emulsion and did not change markedly the physicochemical characteristics of the emulsion, hydrophobic NP, coated with *alumina* (*and*) *triethoxycaprylylsilane* induced formation of large aggregates with the other ingredients during the emulsion preparation. Process had therefore to be carefully optimized and controlled in order to succeed in obtaining well dispersed and smooth emulsion. Emulsions containing NP as well as the control one had been characterized by microscopic analyses (laser diffraction granulometry and optical microscopy) and macroscopic analyses (rheology and texturometry) in order to ensure that they shared the same physicochemical properties. Even if these techniques highlighted slight differences in terms of microscopic structures between emulsions, other macroscopic analyses such as rheology and texturometry did not show bulk major differences. This should allow assessing the role of NP in use, regardless the global physicochemical properties of formulae.

We were able to show that the three emulsions fulfilled the main criteria for the evaluation of the effect of NP in formula on the microbiota. One interesting point is that non-sterile formula, developed with specific cautions taken with the formulation material and procedure, showed an initial bacterial charge well below the acceptable limit as defined by the European Pharmacopoeia 8.0.

Applicability of high temperature sterilization to cosmetic emulsions and sunscreen emulsions containing inorganic UV-filters was as well evaluated. Although this treatment should be estimated sufficient to induce emulsion demixing, the control emulsion and the emulsion containing hydrophilic NP passed through it. For both emulsions, the change in gel behaviors could not be only explained by the presence of new larger but minor populations; polymer deterioration and structural rearrangements may also explain these phenomena. Unfortunately, for emulsions containing hydrophobic NP, sterilization induced the formation of two phases; one formed by aggregated NP and larger droplets, and the other by a liquid phase containing small droplets. Even starting from an emulsion with an optimized dispersion of hydrophobic NP, heat treatment induced dramatic changes for both the microstructure as well as the macroscopic properties of this emulsion. The polymeric coating of hydrophobic NP probably makes this kind of treatment more difficult to adapt and formulation development remains to be done. As an example, additional emulsifiers may be used to stabilize NP during the sterilization step. Nevertheless the high temperature sterilization appears applicable to cosmetic emulsions and sunscreen emulsions containing, or not, inorganic hydrophilic UV-filters.

Finally, in order to verify the usability of these model emulsions, an evaluation of the microbiological effect of NP was performed on non-sterile formula. It revealed that, when bacteria were voluntary inoculated in formulae, all emulsions had the same impact on the growth of two human skin bacteria representative strains, *S. aureus* and *P. fluorescens*.

The model emulsions developed in this article are well suited for the evaluation of the 'NP effect' in formula on microbiota,

because they hide their other physicochemical aspects whatever the polarity of the coating.

Acknowledgements

The authors would like to thank A. Garreau for her contribution in the microbiological part. This project is supported by the *Région Haute-Normandie* (GRR SéSa), the *Conseil Général de l'Eure* and EU (FEDER). LR is recipient of a Doctoral fellowship from the *Région Haute-Normandie* (GRR SéSa). This research program is realized in the framework of the *PFMI Cosmétomique Haute-Normandie: Sureté, Innocuité des Produits Cosmétiques (PFMI cosmétomique SIP)* supported by the network Cosmetic Valley and of the *GDR CNRS Cosmactif*.

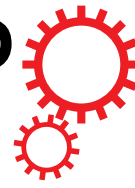
References

- AFNOR, 2009. NF EN ISO 21149:2006 – Cosmétiques – Microbiologie – Dénombrement et détection des bactéries aérobes mésophiles.
- Aldous, G., Kent, P., 2013. Conference: Titanium dioxide and zinc oxide nanoparticles in sunscreen formulations: A study of the post production particle size distribution of particles in a range of commercial emulsion variants. Available at: http://blog.ecohip.co.uk/downloads/Hamilton_Sunscreen_Nanoparticles_Paper.pdf [Consulté le aoÙt 7, 2015].
- Auffan, M., et al., 2010. Structural degradation at the surface of a TiO_2 -based nanomaterial used in cosmetics. *Environ. Sci. Technol.* 44 (7), 2689–2694.
- Auvinen, S., et al., 2013. Refractive index functions of TiO_2 nanoparticles. *J. Phys. Chem. C* 117 (7), 3503–3512.
- Bimbenet, J.-J., Duquenoy, A., Trystram, G., 2007. *Génie Des Procédés Alimentaires*, 2ème édition DUNOD/RIA, Paris.
- Chantrapornchai, W., Clydesdale, F., McClements, D.J., 1998. Influence of droplet size and concentration on the color of oil-in-water emulsions. *J. Agric. Food Chem.* 46 (8), 2914–2920.
- Chantrapornchai, W., Clydesdale, F.M., McClements, D.J., 2001. Influence of flocculation on optical properties of emulsions. *J. Food Sci.* 66 (3), 464–469.
- Chapalaïn, A., 2008. Comparative study of 7 fluorescent pseudomonad clinical isolates 54 (1), 19–27.
- Delaunay, J.-C., Legendre, F., 2013. Patent: (WO2013007755) Device and Method for Sterilizing an Emulsion at an Ultrahigh Temperature, Particularly a Cosmetic Emulsion for the Skin, Which Is Unstable at the Sterilization Temperature. Available at: <http://patentscope.wipo.int/search/en/detail.jsf;jsessionid=FCC18A3D7C5F3B1E2E316A434332886B.wapp22?docId=WO2013007755&recNum=1&maxRec=&offsite=&prevFilter=&sortOption=&queryString=&tab=PCTDescription> [Consulté le janvier 7, 2014].
- Devlieghere, F., et al., 2015. A new protocol for evaluating the efficacy of some dispensing systems of a packaging in the microbial protection of water-based preservative-free cosmetic products. *Int. J. Cosmet. Sci.* 37, 627–635.
- European Parliament, Council of the European Union, 2014. COSMETICS: Regulation (EC) No 1223/2009. Available at: <http://content.grin.com/document/v274383.pdf> [Consulté le septembre 24, 2015].
- European Pharmacopoeia 8.0, 2014. Microbiological quality of non-sterile pharmaceutical preparations and substances for pharmaceutical use, Available at: http://www.medicinalgenomics.com/wp-content/uploads/2013/04/CFU_Tolerance_European.pdf [Consulté le septembre 28, 2015].
- Friedman, H., Whitney, J., Szczesniak, A., 1963. The Texturometer—A new instrument for objective texture measurement. *J. Food Sci.* 28 (4), 390–396.
- Gilbert, L., et al., 2013. Predicting sensory texture properties of cosmetic emulsions by physical measurements. *Chemom. Intell. Lab. Syst.* 124, 21–31.
- Grice, E.A., et al., 2008. A diversity profile of the human skin microbiota. *Genome Res.* 18 (7), 1043–1050.
- Hillion, M., et al., 2013. Comparative study of normal and sensitive skin aerobic bacterial populations. *Microbiol. Open* 2 (6), 953–961.
- INRS, 2014. La désinfection des surfaces en laboratoire de biologie. Available at: <http://www.inrs.fr/dms/inrs/CataloguePapier/ED/TI-ED-6188/ed6188.pdf> [Consulté le septembre 24, 2015].
- Jones, A.R., 1977. Error contour charts relevant to particle sizing by forward-scattered lobe methods. *J. Phys. D Appl. Phys.* 10 (13), p163.
- Junior, J.A.A., Baldo, J.B., 2014. The behavior of zeta potential of silica suspensions. *New J. Glass Ceram.* 4, 29–37.
- Kocherginsky, N.M., Tan, C.L., Lu, W.F., 2003. Demulsification of water-in-oil emulsions via filtration through a hydrophilic polymer membrane. *J. Membr. Sci.* 220 (1-2), 117–128.
- Official Journal of the European Union, 2011. Commission Recommendation of 18 October 2011 on the "Definition of Nanomaterials", Available at: <http://eur-lex.europa.eu/LexUriServ/LexUriServ.do?uri=OJ:L:2011:275:0038:0040:EN:PDF> [Consulté le mars 21, 2014].
- Pal, R., 1996. Effect of droplet size on the rheology of emulsions. *AIChE J.* 42 (11), 3181–3190.
- Pasquet, J., et al., 2014. Antimicrobial activity of zinc oxide particles on five microorganisms of the Challenge Tests related to their physicochemical properties. *Int. J. Pharm.* 460 (1-2), 92–100.

- Percival, S.L., et al., 2012. Microbiology of the skin and the role of biofilms in infection. *Int. Wound J.* 9 (1), 14–32.
- Rossano, M., et al., 2014. Effects of aging on structure and stability of TiO₂ nanoparticle-containing oil-in-water emulsions. *Int. J. Pharm.* 461 (1–2), 89–96.
- Santaella, C., et al., 2014. Aged TiO₂-based nanocomposite used in sunscreens produces singlet oxygen under long-wave UV and sensitizes *Escherichia coli* to cadmium. *Environ. Sci. Technol.* 48 (9), 5245–5253.
- Serpone, N., et al., 2006. Beneficial effects of photo-inactive titanium dioxide specimens on plasmid DNA, human cells and yeast cells exposed to UVA/UVB simulated sunlight. *J. Photochem. Photobiol. A Chem.* 179 (1–2), 200–212.
- Serpone, N., Dondi, D., Albini, A., 2007. Inorganic and organic UV filters: their role and efficacy in sunscreens and sun-care products. *Inorg. Chim. Acta* 360 (3), 794–802.
- Seville, J.P., et al., 1984. Comparison of techniques for measuring the size of fine non-spherical particles. *Part. Part. Syst. Charact.* 1 (1–4), 45–52.
- Tadros, T., 2004. Application of rheology for assessment and prediction of the long-term physical stability of emulsions. *Adv. Colloid Interface Sci.* 108–109, 227–258.
- Teixeira, P.C., et al., 2007. Antimicrobial effects of a microemulsion and a nanoemulsion on enteric and other pathogens and biofilms. *Int. J. Food Microbiol.* 118 (1), 15–19.
- Waterman, K.C., Adami, R.C., 2005. Accelerated aging: prediction of chemical stability of pharmaceuticals. *Int. J. Pharm.* 293 (1–2), 101–125.

P28

SCIENTIFIC REPORTS



OPEN

Skin-bacteria communication: Involvement of the neuropeptide Calcitonin Gene Related Peptide (CGRP) in the regulation of *Staphylococcus epidermidis* virulence

Received: 06 June 2016

Accepted: 23 September 2016

Published: 14 October 2016

Awa R. N'Diaye¹, Camille Leclerc¹, Takfarinas Kentache², Julie Hardouin², Cecile Duclairoir Poc¹, Yoan Konto-Ghiorghi¹, Sylvie Chevalier¹, Olivier Lesouhaitier¹ & Marc G. J. Feuilloley¹

Staphylococci can sense Substance P (SP) in skin, but this molecule is generally released by nerve terminals along with another neuropeptide, Calcitonin Gene Related Peptide (CGRP). In this study, we investigated the effects of α CGRP on *Staphylococci*. CGRP induced a strong stimulation of *Staphylococcus epidermidis* virulence with a low threshold ($<10^{-12}$ M) whereas *Staphylococcus aureus* was insensitive to CGRP. We observed that CGRP-treated *S. epidermidis* induced interleukin 8 release by keratinocytes. This effect was associated with an increase in cathelicidin LL37 secretion. *S. epidermidis* displayed no change in virulence factors secretion but showed marked differences in surface properties. After exposure to CGRP, the adherence of *S. epidermidis* to keratinocytes increased, whereas its internalization and biofilm formation activity were reduced. These effects were correlated with an increase in surface hydrophobicity. The DnaK chaperone was identified as the *S. epidermidis* CGRP-binding protein. We further showed that the effects of CGRP were blocked by gadolinium chloride (GdCl₃), an inhibitor of MscL mechanosensitive channels. In addition, GdCl₃ inhibited the membrane translocation of EfTu, the Substance P sensor. This work reveals that through interaction with specific sensors *S. epidermidis* integrates different skin signals and consequently adapts its virulence.

Skin is the major neuroendocrine organ of the human body¹ and harbors a large and highly diverse microbiota². Skin bacteria are continuously exposed to host molecules that diffuse through the upper layers of the epidermis and are present in sweat³. Many of these molecules are released by afferent nerve terminals and show important local variations in their concentration in response to stress, inflammation or even pain^{1,4}. We have previously shown that skin bacteria of different phyla, including gram-positive species such as *Bacillus cereus*⁵, *Staphylococcus aureus*^{5,6} and *Staphylococcus epidermidis*^{5,6}, and gram-negative bacteria such as *Pseudomonas fluorescens*⁷ can detect Substance P (SP), the principle skin neuropeptide. This molecule between nano- and micro-molar concentrations acts on bacteria and leads to a general increase in virulence. There is now ample evidence that bacteria can detect a large range of neuropeptides⁸. In skin nerve terminals, SP is frequently co-localized and co-secreted with Calcitonin Gene Related Peptide (CGRP)⁹ another neuropeptide abundantly expressed in the skin¹⁰.

CGRP is a 37 amino acids peptide that belongs to the calcitonin superfamily of hormones including calcitonin, amylin, and adrenomedullin. Two isoforms of this peptide— α -CGRP (or CGRP I) and β -CGRP (or

¹Laboratory of Microbiology Signals and Microenvironnement, LMSM, EA 4312, Normandie Université, Evreux, France. ²Laboratory of Polymers, Biopolymers and Surfaces, CNRS UMR 6270, Normandie Université, Mont-Saint-Aignan, France. Correspondence and requests for materials should be addressed to M.G.J.F. (email: marc.feuilloley@univ-rouen.fr)

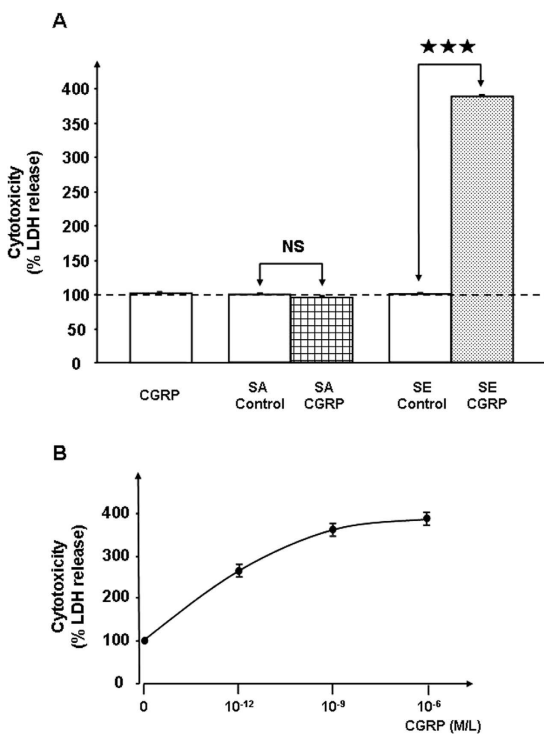


Figure 1. Effect of CGRP on the cytotoxic activities of *S. aureus* and *S. epidermidis*. (A) Comparative effect of CGRP 10^{-6} M on the cytotoxicity of *S. aureus* MFP03 (SA) and *S. epidermidis* MFP04 (SE) toward HaCaT keratinocytes. The dotted line indicates the basal cytotoxicity level (100%) in control HaCaT cell cultures. (B) Dose response curve of the effect of CGRP on *S. epidermidis* MFP04 cytotoxicity (NS = not significantly different; *** $p < 0.001$). The results are representative of three independent experiments.

CGRP II)—are produced from the same gene by alternative splicing, but α -CGRP is the major form expressed in sensory skin fibers¹. CGRP is one of the most potent vasodilatory neuromodulators and it potentiates the effects of Substance P on vascular permeability and edema formation in skin¹. In addition, CGRP exerts trophic effects on endothelial cells and melanocytes. Regarding the effects of this family of peptides on bacteria, a direct antimicrobial effect of CGRP has been described toward *Escherichia coli* and *Pseudomonas aeruginosa*¹¹ and is explained by the structural similarities between CGRP and antimicrobial peptides. However the antimicrobial spectrum of CGRP is limited and it has been shown to have no effect on *Staphylococcus aureus* viability¹¹. The ability of bacteria to detect and respond to neuropeptides through specific sensors and mechanisms was recognized only at the end of the 20th century and has diffused slowly in the scientific community under the name “Microbial Endocrinology”¹². Many peptides initially identified for entirely unrelated functions that have secondary antimicrobial activity at non-physiological concentrations, such as natriuretic peptides, have been found to be able to modulate bacterial adhesion, biofilm formation activity and virulence through specific interaction with sensor proteins¹³. However, to date the physiological effects of CGRP on bacteria and its potential detection by bacterial sensory proteins have not been investigated.

In the present report, we studied the effect of α -CGRP on *S. aureus* and *S. epidermidis*, two of the major bacterial species constituting the skin microbiota. Strains isolated from normal human skin were used to avoid the bias that are potentially encountered when library reference strains are used. The effect of α -CGRP on *S. aureus* and *S. epidermidis* virulence was investigated in cultured keratinocytes and reconstructed human epidermis to more closely simulate normal skin conditions. Although they are of the same genus, these bacteria had completely different sensitivities to CGRP. The CGRP sensor was identified in *S. epidermidis*, and the mechanism of action of the peptide was partly elucidated. A schema was then proposed to explain how *S. epidermidis* can sense and integrate different host signals and adapt its virulence in response to a cutaneous environment.

Results

CGRP stimulates the cytotoxicity of *Staphylococcus epidermidis* on cultured keratinocytes and reconstructed human epidermis. Preliminary experiments showed that exposure of *S. aureus* (MFP03) or *S. epidermidis* (MFP04) to CGRP (10^{-6} M) over the entire growth phase did not modify the growth kinetics of these bacteria. The effect of CGRP on bacterial cytotoxicity was evaluated on HaCaT keratinocytes by measurement of lactate dehydrogenase (LDH), a stable cytosolic enzyme released during cell lysis¹⁴. CGRP (10^{-6} M) did not affect the cytotoxicity of *S. aureus* toward HaCaT cells (Fig. 1A). In contrast, when *S. epidermidis* was previously treated with CGRP (10^{-6} M), the bacterium showed a strong increase in cytotoxicity ($+388 \pm 8\%$, $p < 0.001$). As a control, CGRP (10^{-6} M) was administered alone and had no effect on HaCaT keratinocytes viability. Because the bacteria were rinsed to remove any traces of free peptide before being layered on keratinocytes,

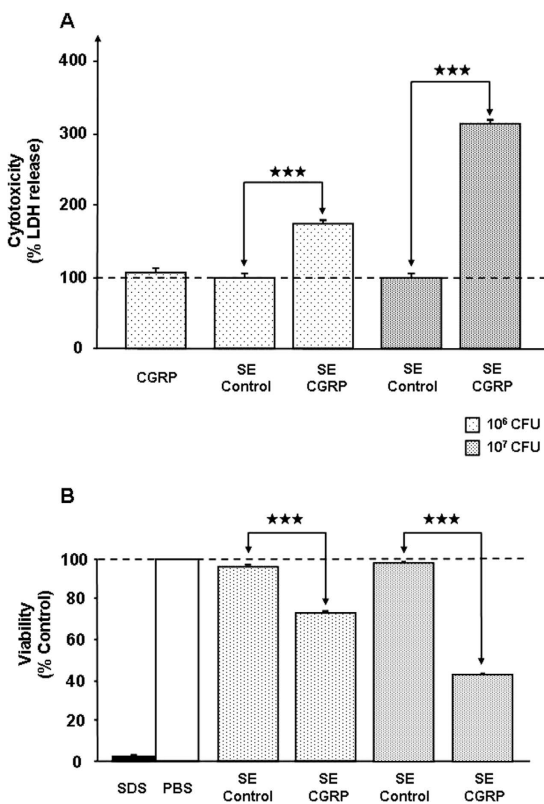


Figure 2. Effects of CGRP (10^{-6} M) on the virulence of *S. epidermidis* toward RHE. The effect of CGRP on the virulence of *S. epidermidis* MFP04 (SE) was studied on RHE (SkinEthic™) by using bacterial cultures at 10^6 and 10^7 CFU/mL and two different techniques: assay of lactate dehydrogenase (LDH) release by dying cells (A) and measure of mitochondrial respiratory activity (viability) by MTT assays (B). The dotted lines indicate the basal cytotoxicity levels (100%) measured in RHE cultures using the two techniques. (*** $p < 0.001$). The results are representative of three independent experiments.

this result can be explained only by a direct action of CGRP on *S. epidermidis*. Lower concentrations of CGRP were tested on *S. epidermidis* to investigate the dose-response relationship. This study showed that the threshold of the CGRP effect on *S. epidermidis* was remarkably low ($< 10^{-12}$ M) (Fig. 1B). These results were confirmed by using reconstructed human epidermidis (RHE) exposed to control or CGRP-treated *S. epidermidis* (10^6 and 10^7 CFU) and two different techniques to exclude any artefacts. In the first case, the cytotoxicity of bacteria was measured through assays of LDH release, as previously described. As observed with HaCaT cells, CGRP (10^{-6} M) alone had no effect on RHE viability. When RHE was exposed to 10^6 CFU *S. epidermidis*, the cytotoxicity of CGRP-treated bacteria increased ($+173 \pm 3\%$, $p < 0.001$), whereas that of the control did not (Fig. 2A). Using a ten-fold higher inoculate (10^7 CFU) did not change the cytotoxicity of the control bacteria but induced a higher increase in the cytotoxicity of CGRP-treated *S. epidermidis* ($+315 \pm 7\%$, $p < 0.001$). In a second series of experiments, the virulence of *S. epidermidis* on RHE was measured by using MTT assays, which reflect mitochondrial respiratory activity and therefore cell viability¹⁵. A significant decrease in RHE viability was observed in the presence of 10^6 and 10^7 CFU *S. epidermidis* previously exposed to CGRP ($-23 \pm 2\%$ and $-56 \pm 4\%$, $p < 0.001$, respectively) (Fig. 2B). Because CGRP stimulates the virulence of *S. epidermidis*, as previously observed using Substance P⁶ and because the two peptides are generally released by the same nerve fibers⁹, *S. epidermidis* was exposed simultaneously to Substance P and CGRP. Used alone and at the same concentration, the effect of CGRP on *S. epidermidis* cytotoxicity was stronger than that of Substance P (Fig. 3). However, when bacteria were pre-treated with both peptides simultaneously (10^{-6} M each), the cytotoxicity of *S. epidermidis* was reduced relative to that of CGRP-treated bacteria ($-50 \pm 8\%$, $p < 0.001$) and Substance P-treated bacteria ($-32 \pm 12\%$, $p < 0.001$) (Fig. 3).

CGRP-treated *Staphylococcus epidermidis* stimulates Interleukin 8 and cathelicidin secretion by keratinocytes. Because keratinocytes develop an efficient innate immune response to bacteria through activation of pro-inflammatory and antimicrobial peptides¹⁶, the production of interleukin 8 (IL8), cathelicidin (LL37) and β -defensin 2 (HBD2) by HaCaT cells and RHE was measured after exposure to control or CGRP-treated *S. epidermidis*. The basal level of IL8 secretion by HaCaT keratinocytes was not changed when the cells were exposed to CGRP (10^{-6} M) alone or to control bacteria (Fig. 4A). In contrast, CGRP-treated *S. epidermidis* triggered a significant increase in IL8 secretion ($+24 \pm 3\%$, $p < 0.001$). Similar results were obtained using RHE, although the range of the response was amplified (Fig. 4B). By itself, the cutaneous strain of *S. epidermidis* MFP04 induced a significant increase in IL8 production by RHE ($+28 \pm 5\%$, $p < 0.5$), but when the bacteria were previously exposed to CGRP, a much more substantial stimulation of IL8 secretion was observed ($+138 \pm 8\%$,

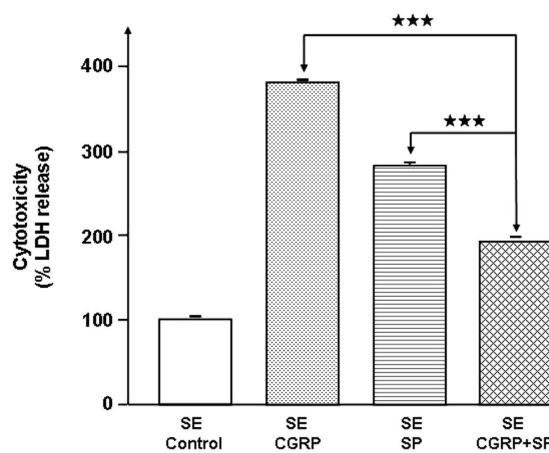


Figure 3. Combined effects of CGRP and Substance P on the cytotoxic activity of *S. epidermidis*. The comparative effects of CGRP and Substance P (SP) alone or in association (10^{-6} M each) on the cytotoxic activity of *S. epidermidis* (SE) were studied in HaCaT cells. ($***p < 0.001$). The results are representative of three independent experiments.

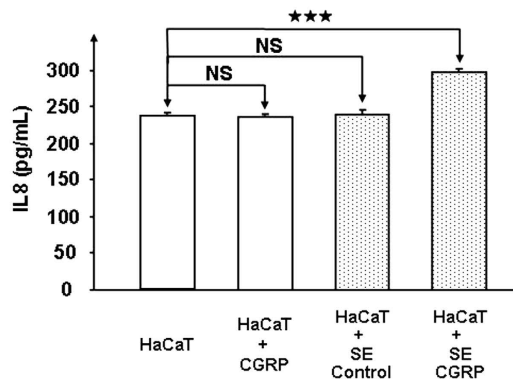
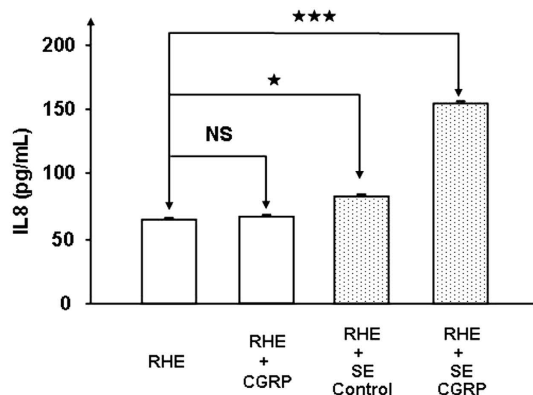
A**B**

Figure 4. Effects of CGRP (10^{-6} M) on *S. epidermidis*-induced expression of IL8 in cultured HaCaT keratinocytes (A) and RHE (B). IL8 was assayed in the culture medium of HaCaT cells and RHE (SkinEthicTM) exposed to control or CGRP-treated bacteria. (NS = not significantly different; * $p < 0.05$; *** $p < 0.001$). The results are representative of three independent experiments.

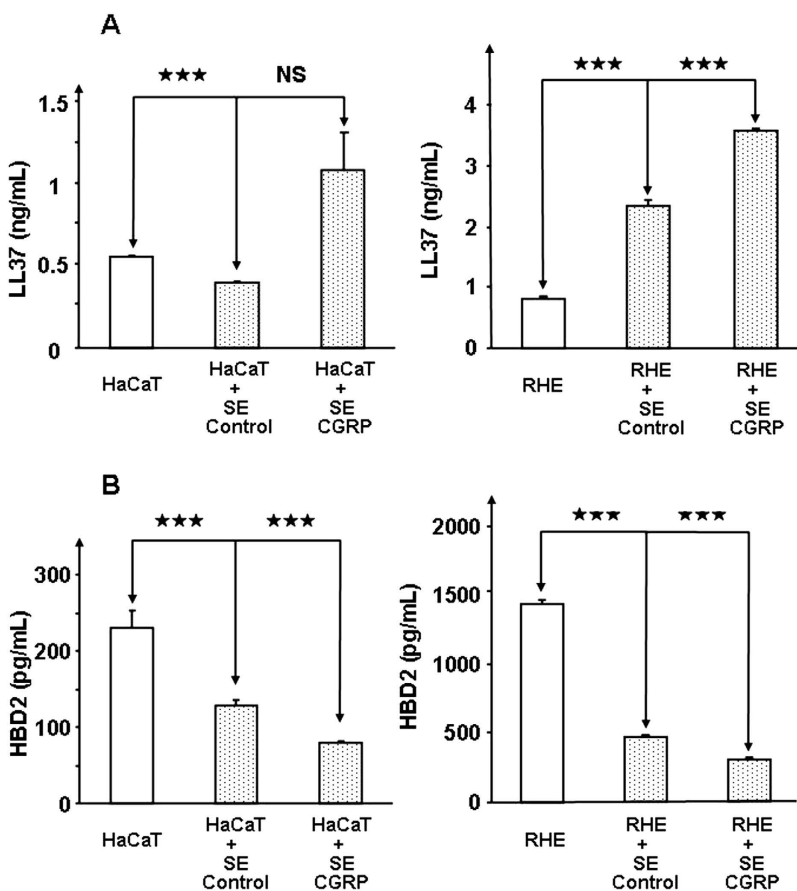


Figure 5. Effects of CGRP (10^{-6} M) on *S. epidermidis*-induced expression of antimicrobial peptides in cultured HaCaT keratinocytes (A) and RHE (B). Cathelicidin LL37 and β -defensin 2 (HBD2) were assayed in the medium of HaCaT cells and RHE (SkinEthicTM) exposed to control or CGRP-treated bacteria. (NS = not significantly different; *** $p < 0.001$). The results are representative of three independent experiments.

$p < 0.001$). HaCaT cells exposed to untreated bacteria showed a decrease in LL37 secretion ($-28 \pm 4\%$, $p < 0.001$) whereas an insignificant increase in LL37 was observed when they were exposed to CGRP-treated *S. epidermidis* (Fig. 5A). The response of RHE was more acute because control and CGRP-treated *S. epidermidis* induced a stimulation of LL37 ($+208 \pm 12\%$ $p < 0.001$ and $+343 \pm 8\%$ $p < 0.001$, respectively) (Fig. 5A). However, LL37 production was significantly higher when the cells were exposed to CGRP-treated bacteria relative to the control bacteria ($p < 0.001$). In parallel, the secretion of HBD2 by both cultured keratinocytes and RHE was significantly reduced when they were exposed to control *S. epidermidis* ($-44 \pm 12\%$ and $-67 \pm 2\%$, $p < 0.001$, respectively). The decrease in HBD2 production was more important than when keratinocytes and RHE were exposed to CGRP-treated bacteria ($-67 \pm 11\%$ and $-79 \pm 2\%$ (Fig. 5B)).

The effects of CGRP on *Staphylococcus epidermidis* cannot be explained by over-expression of virulence proteins. To investigate the origin of the increase in *S. epidermidis* virulence induced by CGRP, proteins were extracted from the secretomes of control and CGRP-treated bacteria, analyzed by 2D-gel electrophoresis and identified by Matrix-Assisted Laser Desorption Ionization Time-of-Flight mass spectrometry (MALDI-TOF/TOF). Image analysis of 3 replicates of 2D gels allowed the detection of nine major proteins over-expressed in the CGRP treated *S. epidermidis* condition compared with the control condition (Fig. 6). Interestingly, among these proteins, superoxidase dismutase (Spot 3), alkaline shock protein 23 (Spot 5), DnaK protein (Spot 7) and peroxiredoxin (Spot 9) are required for bacterial adaptation to stress (Table 1). Other identified proteins, including dihydrolipoyl dehydrogenase (Spot 1), inosine-monophosphate dehydrogenase (Spot 2) and citrate synthase (Spot 6), are involved in intermediate metabolism. Only one of the proteins over-expressed in CGRP-treated *S. epidermidis*, immunodominant surface antigen B (IsaB) (Spot 3) and its precursor (Spot 8), is considered to be a virulence factor because of its antigenic activity¹⁷. In addition, tandem mass spectrometry analysis identified a core of 170 proteins reproducibly found in the secretome of control and CGRP-treated *S. epidermidis* MFP04 and confirmed the absence of significant variations in the expression of potential cytotoxic proteins (Table S1).

CGRP affects the surface properties of *S. epidermidis*. Adhesion and internalization of *S. epidermidis* were studied using HaCaT cells and a gentamicin protection assay, as previously described¹⁸. When bacteria were pre-treated with CGRP (10^{-6} M) a significant increase in *S. epidermidis* adhesion to the surfaces of keratinocytes was

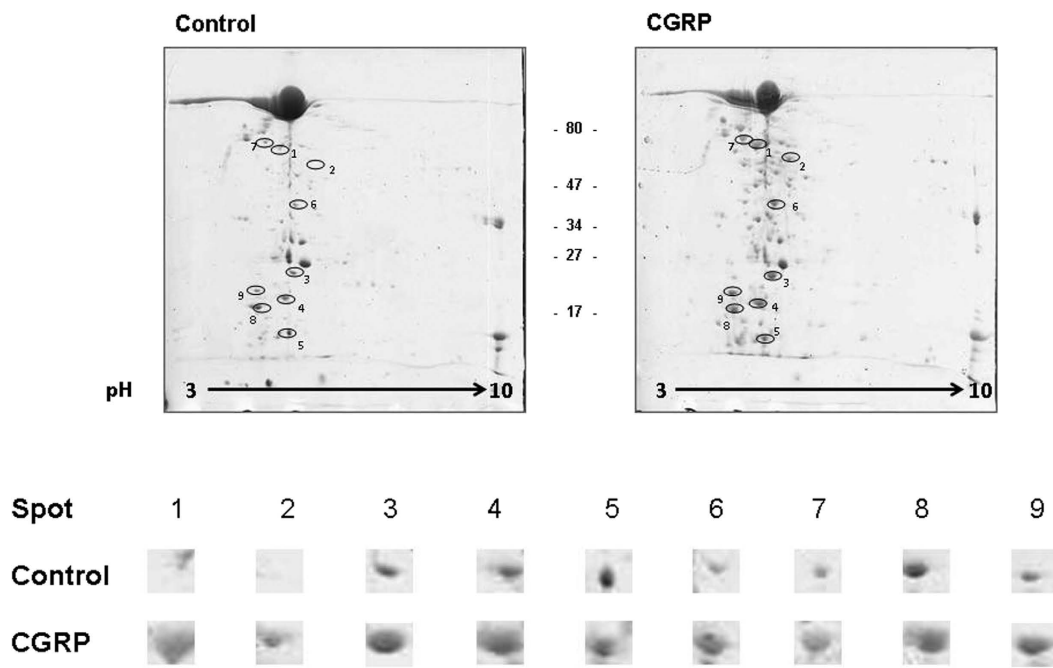


Figure 6. Bidimensional electrophoresis analysis of secreted *S. epidermidis* proteins in control conditions and after a 2 h treatment with CGRP (10^{-6} M). Nine spots were identified, corresponding to proteins significantly up-regulated after exposure of the bacteria to CGRP. Proteins corresponding to these spots are presented in Table 1. The results are representative of three independent experiments.

observed ($+29 \pm 3\%$, $p < 0.001$) (Fig. 7A). This effect was associated with a marked decrease in *S. epidermidis* internalization in HaCaT cells ($-65 \pm 4\%$, $p < 0.001$) (Fig. 7B). The effect of CGRP on biofilm formation by *S. epidermidis* was investigated by confocal laser-scanning microscopy in a flow cell system. When bacteria were pretreated with CGRP and introduced into the flow cell system, a marked decrease in biofilm formation was observed (Fig. 8). After 24 h, the mean thickness of the biofilm of control bacteria reached $23 \pm 1 \mu\text{m}$, whereas it was only of $6 \pm 1 \mu\text{m}$ with CGRP-treated *S. epidermidis*. The calculated biomass showed a similar significant decrease (-68 ± 16 , $p < 0.01$). These effects were correlated with a clear evolution of the surface polarity of CGRP-treated bacteria, as measured by the MATS technique (Microbial Adhesion To Solvents¹⁹). The higher affinity for apolar solvents (decane and hexadecane - Fig. 9) indicated that after exposure to CGRP, the surface of the bacterium evolved from having a mid-hydrophilic to a low-hydrophobic characteristic. In parallel, the affinity of the bacterium for hexadecane and chloroform, related to the Lewis acid characteristic, was marginally increased ($+6 \pm 1$ and $+15 \pm 4\%$, $p < 0.001$, respectively) whereas the affinity for decane and ethyl acetate, showing Lewis acid characteristics, was markedly enhanced ($+113 \pm 4$ and $+115 \pm 7\%$, $p < 0.001$, respectively). Thus the Lewis acid characteristic of the bacterial surface was reinforced.

The DnaK protein acts as a sensor of CGRP in *S. epidermidis*. Assuming that CGRP is unable to cross the bacterial membrane because of its charge and hook shape²⁰ and the binding of CGRP to its sensor protein is sufficiently stable, we investigated the CGRP-binding protein in *S. epidermidis* membrane extracts via an immunoprecipitation technique using CGRP antibody-coated beads as previously described⁵. A unique CGRP binding protein of an apparent mass of 70 kDa was identified in the proteome of *S. epidermidis* MFP04 (Fig. 10). In agreement with the absence of an effect of CGRP on *S. aureus*, this protein was absent in the membrane proteome in *S. aureus* MFP03 (Fig. 10). A band corresponding to this protein was subsequently dissected and analyzed by tandem mass spectrometry. This protein was identified by mass spectrometry analysis with a score of 140.29 and coverage of 64 as the 66.1 kDa chaperone protein of *S. epidermidis* DnaK.

Export of DnaK through the large conductance mechanosensitive channel MscL is required for the effects of CGRP on *S. epidermidis*. Electrophysiological approaches have demonstrated that in the membrane of *E. coli*, DnaK is exported through the large conductance mechanosensitive channel MscL²¹. MscL also triggers the export of EfTu²¹, the Substance P sensor protein in *S. epidermidis*⁶. MscL is a ubiquitous protein and is also expressed by *S. epidermidis*²². As shown herein, CGRP increases the export of DnaK by *S. epidermidis* (Spot 7 in Fig. 6 and Table 1). The effect of CGRP on *S. epidermidis* cytotoxicity was then studied in the presence of GdCl₃ (10^{-3} M) a specific inhibitor of the MscL channel²³. Exposure of bacteria to GdCl₃ resulted in a significant reduction of the cytotoxic activity of CGRP-treated bacteria ($-78 \pm 15\%$, $p < 0.001$) (Fig. 11A). In contrast, the effect of the control bacteria remained unchanged, suggesting that in the absence of CGRP, DnaK is unable to modulate bacterial cytotoxicity. In parallel, we observed through western blotting that CGRP induces a concomitant export of EfTu (Fig. 11B). Moreover, EfTu translocation through the bacterial membrane was

Spot	NCBI accession Number	Gene Name	Putative function	Mascot score	Number of matched peptides	Coverage (%)	Mass (Da) & pI
1	WP_002435425.1	Dihydrolipoyl dehydrogenase	Pyridine nucleotide-disulphide oxidoreductase fold NAD(P)(+)-binding proteins	107	16	41	49733/4.72
2	WP_002434485.1	Inosine-monophosphate dehydrogenase	The catalytic domain of the inosine-monophosphate dehydrogenase (IMPDH). IMPDH catalyzes the NAD-dependent oxidation of inosine 5'-monophosphate (IMP) to xanthosine 5' monophosphate (XMP)	100	21	43	52493/5.35
3	WP_002453341.1	Superoxidase dismutase	Inorganic ion transport and metabolism	108	15	71	22697/5.04
4	WP_002435927.1	Immunodominant surface antigen B (isaB)	Immune response during septicemia: generally classified as a virulence factor (increased expression <i>in vivo</i> during human sepsis)	98	10	62	20088/4.84
5	WP_002432778.1	Alkaline shock protein 23	Alkaline pH tolerance	120	18	72	19187/4.91
6	WP_002434679.1	Citrate synthase	CoA binding site: oxalate citrate binding site catalytic triad	144	24	55	42519/5.26
7	WP_049427550.1	DnaK	Chaperone: functions in stress-induced protein refolding and degradation	242	43	72	66071/4.54
8	WP_002436880.1	Immunodominant antigen B (isaB) precursor	IsaB pro-protein	101	8	41	18400/5.54
9	WP_030061284.1	Peroxidoxin	Controls cytokine-induced peroxide levels: confers protection to cells	141	13	91	21268/4.5

Table 1. Proteins over-expressed in the secretome of CGRP-treated *S. epidermidis* identified by MALDI-TOF/TOF.

completely inhibited by exposure to GdCl₃ (10⁻³ M) (Fig. 11B). This inhibition was observed in either the absence or presence of CGRP.

Discussion

Skin is a complex neuroendocrine organ whose physiology results from equilibrium among many local factors. In addition to the well-documented release of Substance P, skin sensory nerve terminals generally release CGRP¹. This neuropeptide is also expressed locally by monocytes and macrophages²⁴, Langerhans cells²⁵ and keratinocytes²⁶. CGRP is produced in significant amounts in skin and is now recognized as a pleiotropic signaling molecule in mammals²⁷. The present work extends this notion, showing that CGRP can also act as a regulator of bacterial physiology, modulating the virulence and surface properties of one of the principle skin associated bacteria, *S. epidermidis*.

The stimulatory effect of CGRP on *S. epidermidis* cytotoxicity is stronger than that observed under identical doses of Substance P⁵. Similarly, the threshold of CGRP activity on *S. epidermidis* is extremely low, below the picomolar level, and well below the mean concentrations of CGRP in blood ($\pm 84 \times 10^{-12}$ M)²⁸ and skin (between 5.4 and 0.3×10^{-12} M/g tissue)¹⁰. The effect of CGRP on *S. epidermidis* virulence was confirmed using RHE. RHE shows a fully differentiated stratum corneum²⁹, thus indicating that this observation is physiologically relevant. The low concentration of CGRP required to induce a bacterial response allows metabolic action of the peptide to be excluded. Moreover, the absence of the effect of CGRP on *S. aureus* indicates that it is highly specific, because this species is closely related to *S. epidermidis*. In contrast, the antagonistic effect of CGRP and Substance P towards *S. epidermidis* suggests the existence of a common step in the response of the bacterium to both peptides. This hypothesis was confirmed later in this study.

In agreement with these first results, we observed that CGRP-treated bacteria induce an up-regulation of interleukin 8 (IL8) secretion by cultured keratinocytes and RHE. In skin, as in many tissues, this result indicates the activation of an inflammatory process³⁰. Because the pro-inflammatory response of keratinocytes is generally associated with induction of antimicrobial peptide secretion¹⁶, the production of LL37 and HBD2 by HaCaT cells and RHE was measured after exposure to CGRP-treated bacteria. An increase in LL37 secretion was observed in both models when these cells were exposed to CGRP pre-treated *S. epidermidis*. *S. epidermidis* is one of the major commensal bacteria of the human skin and is normally well tolerated³¹. However, the present results demonstrate that when the bacterium is exposed to CGRP, the skin tolerance towards it is reduced, and an innate immune response is activated. Nevertheless, this response should be incomplete because a parallel decrease in HBD2 production was observed.

Analysis of the secretome of CGRP-treated bacteria by two techniques, 2D electrophoresis coupled with MALDI-TOF/TOF and tandem mass spectrometry, did not reveal significant variations in the production of diffusible proteins/enzymes with similarity to known virulence factors. The IsaB protein and its precursor were increased, but IsaB is involved in the escape mechanism from the host defense system³² and is not directly responsible for bacterial cytotoxicity. Of course, we cannot exclude the association of several individual proteins among the 170 regularly identified in the secretome of *S. epidermidis* MFP04 (this study); however, even in this list, the number of proteins or enzymes potentially capable of acting as virulence factors is very limited. In contrast, an increase in several chaperone proteins involved in bacterial adaptation was observed, suggesting that CGRP is detected by *S. epidermidis* as a stress signal. In fact, CGRP appears to modulate the surface properties of *S.*

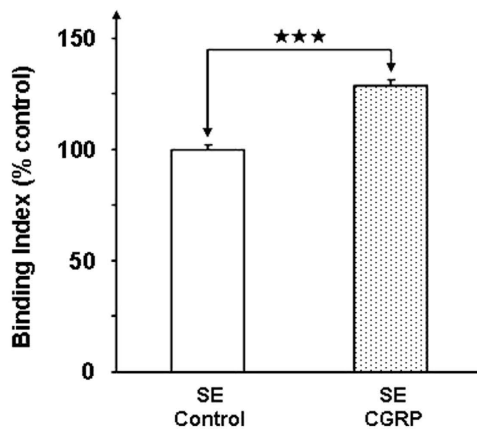
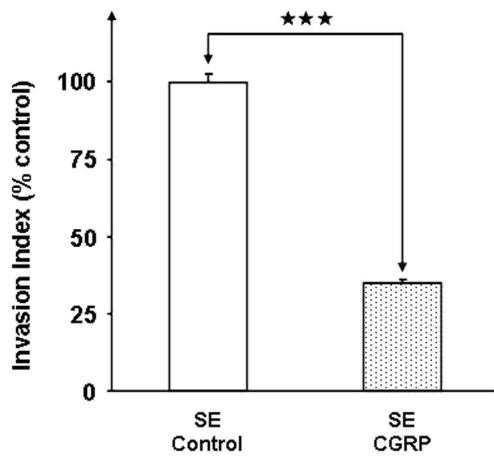
A**B**

Figure 7. Effects of CGRP (10^{-6} M) on the binding (A) and invasion activities (B) of *S. epidermidis* (SE) toward HaCaT cells. After 1 h incubation at a MOI of 10:1, the total number of cell-associated bacteria was determined by direct counting after plating. Invasive bacteria were also quantified by direct counting after elimination of extracellular bacteria by gentamicin. (**** $p < 0.001$). The results are representative of three independent experiments.

epidermidis. The bacterium showed increased adherence to keratinocytes. In contrast, its internalization process was reduced, thus suggesting that the surface properties of the bacterium hindered its penetration into the cytoplasmic compartment of the target cell. *S. epidermidis* internalization is mediated by the major autolysin/adhesin AtlE, and the eukaryotic protein Hsp70 was identified as its putative host cell receptor³³. However, in the present study we observed that CGRP induced an increase in the export of DnaK, a member of the heat shock protein 70 (Hsp70) family³⁴. Thus, we can not exclude the possibility that DnaK might interfere with AtlE on the *S. epidermidis* surface, inducing an inhibition of its adhesion potential toward target cells. In *Staphylococci*, DnaK is also involved in biofilm formation³⁵ and thus is a potential target for new antibiofilm molecules³⁶. In agreement with the hypothesis of a key role of DnaK in the response of *S. epidermidis* to CGRP, we observed that the biofilm formation activity of the bacterium was reduced after exposure to the peptide. In the present study, the biofilm formation was monitored on a glass surface and under dynamic conditions. Glass is a polar surface³⁷, and bacteria must develop sufficient adhesion forces to resist the flow. Thus, our observations suggest that CGRP-treated bacteria present a decrease in adherence to polar materials such as glass and thus present a more hydrophobic surface. This hypothesis was confirmed through use of the MATS technique, which revealed that after exposure to CGRP, the surfaces of the bacteria evolved from having a mid-hydrophilic to a low-hydrophobic characteristic. These results are also coherent with the higher adhesion on the surface of HaCaT cells, thus suggesting that CGRP-treated bacteria develop a higher affinity toward membrane phospholipids than do untreated bacteria. Although no direct relationship was found among surface polarity, biofilm formation and virulence in clinical species of *S. epidermidis*³⁸, CGRP appears to have has a coherent effect on these parameters, thus leading to increased virulence.

A central role of DnaK in the response of *S. epidermidis* to CGRP was confirmed when this protein was identified by immunoprecipitation and tandem mass spectrometry as the CGRP binding protein. In *Staphylococci*, DnaK is known for its multiple roles in environment and stress adaption³⁵ but the binding of CGRP to DnaK

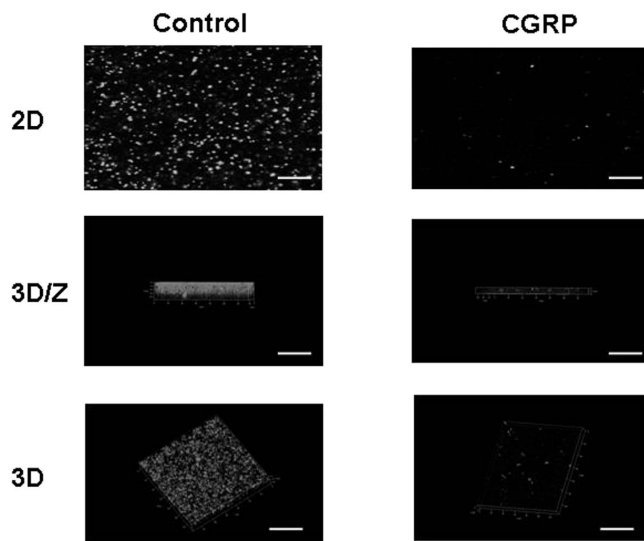


Figure 8. Effect of CGRP (10^{-6} M) on *S. epidermidis* biofilm formation under dynamic conditions. Biofilm formation by *S. epidermidis* in the absence or presence of CGRP was studied by confocal laser scanning microscopy using a flow-cell system. Two dimensional (2D) images collected at $1\text{ }\mu\text{m}$ intervals were used to reconstruct ortho cuts (3D/z) and three-dimensional (3D) images. Pictures are representative of three independent experiments. Scale bars = $20\text{ }\mu\text{m}$.

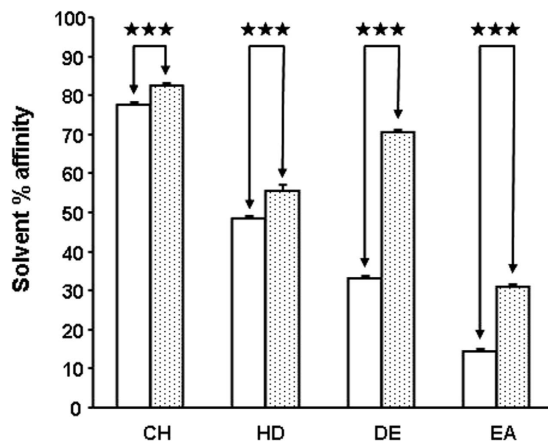


Figure 9. Effects of CGRP (10^{-6} M) on the relative affinity of *S. epidermidis* to solvents. Partition between water and solvents of different polarities and Lewis acid-base values of control (empty bars) and CGRP-treated (dotted bars) *S. epidermidis* was studied with the MATS technique using chloroform (CH), hexadecane (HD), decane (DE) and ethyl acetate (EA). ($^{***}p < 0.001$). The results are representative of three independent experiments.

was initially unexpected. However, alignment of the *S. epidermidis* DnaK amino acid sequence with eukaryotic sequences shows matches at the first rank with protein Q8T885 [www.uniprot.org] which is also designated as a CGRP receptor component protein (CGRP-RCP), a subunit of the CGRP receptor of eukaryotes necessary for signal transduction³⁹. Moreover, studies in yeast suggest that CGRP-RCP is a multifunctional protein involved in transcription⁴⁰, and in a recent study in *S. epidermidis* DnaK has been suggested to be exposed at the surface of the bacterium and to act as a receptor for endothelial cells³³. A STRING10 network analysis [http://string-db.org/] indicated that *S. epidermidis* DnaK interacts not only with other chaperone proteins but also with Eftu, the moonlighting protein previously identified as the sensor for Substance P in *Staphylococci*⁶ (Figure S1). In *E. coli*, DnaK and Eftu are released upon osmotic shock by a translocation mechanism involving the mechanosensitive channel MscL²¹. MscL can be blocked by gadolinium chloride (GdCl_3)²³, and we observed that pre-exposure of *S. epidermidis* to GdCl_3 inhibited the stimulatory effect of CGRP on *S. epidermidis* cytotoxicity. In addition, CGRP increases the release of Eftu, and this effect is antagonized by GdCl_3 , thus suggesting that the peptide induces the opening of MscL and, as shown in *E. coli*, a simultaneous translocation of DnaK and Eftu²¹. Of course the increase of DnaK in the secretome of CGRP-treated bacteria could potentially result from many other events, including increased membrane permeability, cell lysis or reduced extracellular degradation. However, in

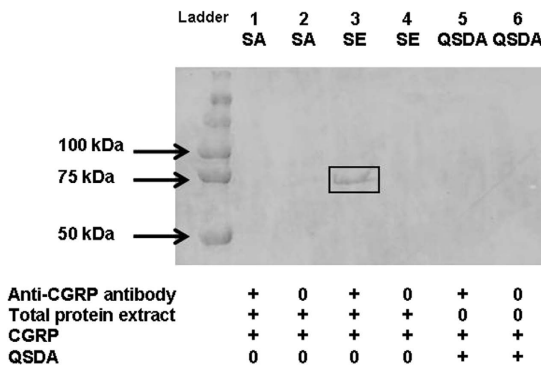


Figure 10. SDS page analysis of CGRP-binding proteins in *S. aureus* and *S. epidermidis* membrane extracts. The CGRP sensor was identified in *S. aureus* (SA) and *S. epidermidis* (SE) membrane extracts by immunoprecipitation using CGRP antibody-associated beads. CGRP was associated with a 70 kDa apparent mass protein that was identified by tandem mass spectrometry as the chaperone protein DnaK. The lactonase QSDA was used as a control. The results are representative of three independent experiments.

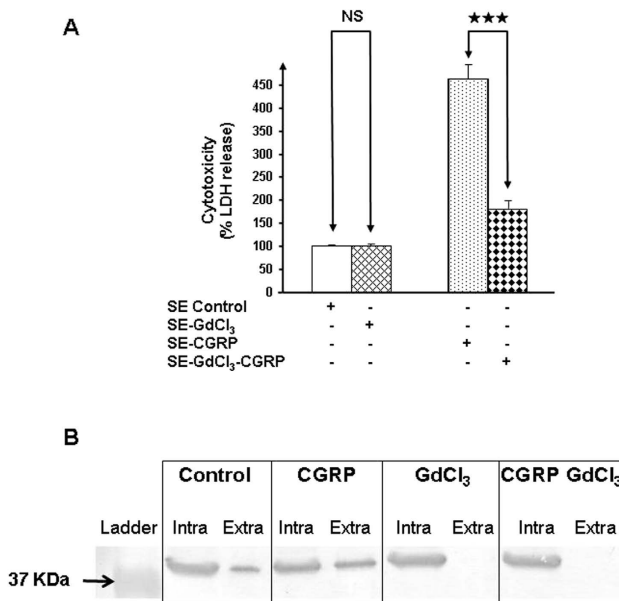


Figure 11. Effect of pre-treatment by GdCl₃ on the cytotoxicity of control and CGRP-treated *S. epidermidis* (A) and on the relative intra- and extra-cellular concentrations of EfTu produced by *S. epidermidis* in control conditions and after exposure to CGRP, GdCl₃ or CGRP and GdCl₃ (B). Bacteria (SE) exposed or not to GdCl₃ (1 mM) were subsequently grown in the absence or presence CGRP (10⁻⁶ M). Their cytotoxic potential was measured on HaCaT cells (A). EfTu was analyzed by western blotting in the stroma (intra) and growth medium (extra) of *S. epidermidis* grown in the absence (control) or presence of CGRP (10⁻⁶ M), GdCl₃ (1 mM) or both substances (CGRP and GdCl₃) (B). (NS: non significant; ***p < 0.001). The results are representative of three independent experiments.

MscL-deficient strains of *E. coli*, DnaK is not released, even after osmotic shock²¹, suggesting that DnaK export is almost exclusively controlled by MscL. Because we observed that CGRP did not affect the growth and viability of *S. epidermidis* and that as a chaperone, DnaK is a stable molecule, the effect of CGRP on DnaK export through MscL channels is the main hypothesis explaining the present results. Moreover, this hypothesis provides a potential explanation for the antagonistic effects of CGRP and Substance P. Indeed, if DnaK and EfTu are exported through the same channel, they would compete for translocation when the bacterium is simultaneously exposed to CGRP and Substance P. This hypothesis is summarized in Fig. 12. This mechanism may also explain the absence of sensitivity of *S. aureus* to CGRP. Indeed, DnaK is also expressed in *S. aureus*, but the oligomeric structure of MscL is still a matter of debate, and the diameter of this channel differs among bacterial species⁴¹. EfTu is a 43 kDa protein but DnaK is much larger (66.1 kDa) and it is possible that DnaK is unable to translocate through the *S. aureus* membrane, thus making this species insensitive to CGRP.

Reasons for the preservation or emergence of a CGRP-sensing system in *S. epidermidis* remain hypothetical. However, interestingly *S. epidermidis* not only is a commensal bacterium but also is associated with severe

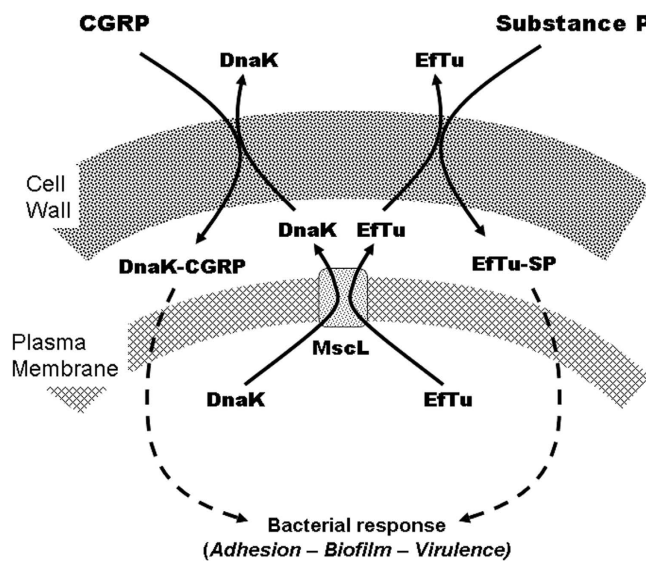


Figure 12. Schematic model representing the potential translocation of DnaK and EfTu through the membrane of *S. epidermidis*, thus leading to recognition of CGRP and Substance P. DnaK and CGRP are probably translocated in the periplasmic compartment through the MscL channel. CGRP and Substance P are binding to DnaK and EfTu, either in the periplasm or after diffusion through the cell wall, thus leading to formation of complexes able to promote the bacterial response through a yet-unknown mechanism. Competition of DnaK and EfTu for the same transporter may explain the antagonistic effects of CGRP and Substance P.

forms of atopic dermatitis⁴² and is currently regarded as the most frequent cause of nosocomial and medical device-associated infections⁴³. CGRP expression is increased during stress and in psoriatic skin and this peptide is one of the most potent vasodilatory mediators¹. Because, in parallel CGRP reduces neutrophilic accumulation¹, as has been described in the lung, where *Pseudomonas aeruginosa* uses interferon as an infection inducer⁴⁴, *S. epidermidis* should detect CGRP as a signal of favorable conditions for tissue invasion and shift from commensal to pathogenic behavior.

In conclusion, this study reveals a totally new function of CGRP in the skin as a regulator of *S. epidermidis* virulence. Our results also illustrate a new role of DnaK as a moonlighting protein⁴⁵ acting as a sensor for CGRP in *S. epidermidis*. The translocation mechanism of DnaK through MscL provides an explanation for the antagonistic effects of CGRP and Substance P on *S. epidermidis* and for the absence of the effect of CGRP on *S. aureus*. These results demonstrate that skin bacteria can integrate different signals from cutaneous origin and consequently adapt their virulence to the microenvironment.

Methods

Bacterial strains and culture conditions. *S. aureus* (MFP03) and *S. epidermidis* (MFP04) were collected from the skin of healthy volunteers⁴⁶. These bacteria were characterized by phenotypic, metabolic, MALDI-Biotyper proteomic analysis and 16S ribosomal RNA gene sequencing. All bacteria were grown at 37 °C in Luria-Bertani (LB) medium under gentle agitation (180 rpm). Bacteria were stored on cryobeads at -140 °C and subjected to two pre-culture phases. For the studies, bacteria collected at the end of the exponential growth phase were diluted in fresh broth. The peptides, diluted in sterile physiological water (NaCl 0.9%), or an equivalent volume of physiological water in control studies, were added at the beginning of the log growth phase. Before the tests, the bacteria were harvested by centrifugation (7,000 × g) and washed with sterile physiological water to remove any trace of free peptide. The bacterial density and the absence of contamination were controlled by plating. The viability of the bacteria in eukaryotic cell culture medium and under different culture conditions was controlled in preliminary studies (*data not shown*). CGRP and Substance P were obtained from Polypeptides (Strasbourg, France). Gaddolinium chloride (GdCl₃) was obtained from Sigma-Aldrich (Saint-Quentin Fallavier, France).

Cytotoxicity studies. The cytotoxicity of bacteria was studied in the human keratinocyte cell line HaCaT and in RHE. HaCaT Cells, provided by Cell Line Services (Eppelheim, Germany), were grown at 37 °C under a 5% CO₂ atmosphere, in Dulbecco's modified Eagle's medium (DMEM, Lonza, Levallois-Perret, France) supplemented with 10% fetal calf serum and 1% antibiotic cocktail (HyClone Thermo Scientific, Illkirch, France). Cells were used between passages 41 and 65. One day before use, the HaCaT cells were starved of antibiotic and fetal calf serum. The cells were incubated with control or treated bacteria at a multiplicity of infection (MOI) of 10:1.

RHE, obtained from Episkin (Lyon, France) was grown according to the specifications of the provider. Briefly, after delivery RHE was immediately incubated at 37 °C, under a 5% CO₂ atmosphere, in provider medium and

allowed to stabilize for 48h. One day before use, RHE was transferred to antibiotics-free medium. For infection tests, RHE was exposed to control or treated bacteria at a final concentration of 10^6 or 10^7 CFU.

The lethal effect of bacteria was determined by assaying LDH which is released by keratinocytes, by using a Cytotox 96 assay (Promega, Charbonnières, France) and by measurement of keratinocytes survival with MTT assays, thus allowing cellular NAD(P)H-dependent metabolic activity to be determined through evaluation of the conversion of a tetrazolium dye (MTT: 3-(4,5-dimethylthiazol-2-yl)-2,5-diphenyltetrazolium bromide) into insoluble purple formazan crystals according to the OECD Draft Revised Guideline TG431¹⁵.

Antimicrobial peptides and interleukin 8 assays. The potential effect of CGRP on *S. epidermidis*-induced expression of antimicrobial peptides and chemokines was investigated by measurement of IL8, cathelicidin (LL37) and β -defensin 2 (HBD2) production by HaCaT cells and RHE after exposure to control or CGRP-treated bacteria. IL8, LL37 and HBD2 were assayed in the culture medium of HaCaT cells and RHE by using human CXCL8/IL-8 cat. D8000C (R&D system, Lille, France), human cathelicidin cat. CSB-EL004476HU and β -defensin 2 cat. CSB-E13201h (Cusabio, Aachen, Germany) ELISA kits according to the manufacturers' protocols.

Secretome analysis. Supernatants of control or CGRP-treated *S. epidermidis* were obtained by centrifugation and filtration. Proteins were precipitated by the addition of trichloroacetic acid on ice. These proteins were harvested by centrifugation, washed in cold acetone, dried at room temperature and re-dissolved in a rehydration buffer⁴⁷. The protein concentration was determined by Bradford assays. Equal amounts of proteins (300 μ g) were loaded on each gel (12% w/v polyacrylamide) and separated. For 2D-gel electrophoresis, protein samples were first separated by isoelectric focusing (IEF) using pH 3 to 10 nonlinear IEF strips (GE Healthcare, Vélizy-Villacoublay, France) as previously described⁴⁷. The strips were then transferred horizontally onto 12% polyacrylamide gels and covered with 0.5% agarose and the second dimension separation was run. Proteins were visualized by colloidal Coomassie brilliant blue G250 staining. Gel images were captured using a GS-800 densitometer (Bio-Rad, Schiltigheim, France). Variations in spot intensity and distribution were studied using Bio-Rad PDQuest 2D® analysis software. Culture medium proteins were excluded and electrophoretic spots of interest were dissected and subjected to in-gel trypsin digestion and analyzed by MALDI-TOF/TOF using an AutoFlex III mass spectrometer (Bruker Daltonics, Wissembourg, France). The spectrometer was used in a positive/reflector mode. Samples were spotted to MTP 384 ground steel targets (Bruker Daltonics, Wissembourg, France) using a freshly prepared matrix solution composed of 2,5-dihydroxybenzoic acid in a solution of trifluoroacetic acid and acetonitrile. Each spectrum was established over an average of 500–1000 laser shots. FlexAnalysis software generated an MS peak list, which was subjected to peptide mass fingerprinting using the integrated software Biotools (Version 3.2). The NCBI database was searched using the online MASCOT software and statistical sequence analyses were performed using the probability-based Mowse score.

For tandem mass spectrometry analysis, all experiments were performed using a LTQ-Orbitrap Elite coupled with an Easy nLC II system (Thermo Scientific, Villebon-sur-Yvette, France). The samples were injected onto an enrichment column (C18 PepMap100, Thermo Scientific, Villebon-sur-Yvette, France). Separation was achieved with an analytical column needle (NTCC-360/100-5-153, NikkyoTechnos, Tokyo, Japan). The mobile phase consisted of H₂O/0.1% FA (buffer A) and ACN/FA 0.1% (buffer B). Tryptic peptides were eluted at a flowrate of 300 nL/min using a three-step linear gradient: from 2 to 40% B over 25 min. The mass spectrometer was operated in positive ion mode with a capillary voltage and a source temperature set at 1.5 kV and 275 °C, respectively. The samples were analyzed using the CID (collision induced dissociation) method. The first scan (MS spectra) was recorded in the Orbitrap analyzer ($R=60,000$) in the mass range m/z 400–1800. The 20 most intense ions were then selected for MS2 experiments. Singly charged species were excluded for MS2 analysis. Dynamic exclusion of already fragmented precursor ions was applied for 30 s, with a repeat count of 1, a repeat duration of 30 s and an exclusion mass width of ± 10 ppm. Fragmentation occurred in the linear ion trap analyzer with collision energy of 35. All measurements in the Orbitrap analyzer were performed with on-the-fly internal recalibration (lock mass) at m/z 445.12002 (polydimethylcyclosiloxane). Raw data files were processed using Proteome Discoverer 1.3 software (Thermo Scientific, Villebon-sur-Yvette, France). Peak lists were searched using the MASCOT search engine (Matrix Science, Boston, USA) against the database Swiss Prot database searches were performed with the following parameters: 1 missed trypsin cleavage site allowed; variable modifications: carbamidomethylation of cystein, and oxidation of methionine; mass tolerance on parent and daughter ions: 10 ppm and 0.5 Da respectively. Only proteins represented by more than 1 peptide sequence, by 2 folds and with power >0.8 were retained. Each protein identification was validated by an ANOVA test.

Binding and invasion studies. Binding and invasion studies were performed with HaCaT cells. Cultured keratinocytes were infected for 1 h with *S. epidermidis* (MFP04) at an MOI of 10:1. In the first series of experiments, at the end of the incubation period HaCaT cells were washed six times with DMEM to remove non-adherent bacteria and then disrupted with 1 mL of 0.9% Triton X100. The total number of cell-associated bacteria (intra- and extra-cellular) was then counted by plating serial dilutions on Tryptone Soya Agar medium (TSA). Invasive bacteria were quantified by gentamicin protection assays as described by Mezghani-Abdelmoula *et al.*¹⁸. In these experiments, at the end of the incubation period HaCaT cells were treated with 100 μ g/mL gentamicin to kill extracellular bacteria. The cells were then washed and lysed as previously described and the number of invading bacteria released from the cells was counted. Cells surface adherent bacteria were calculated by subtracting of the number of invasive bacteria from the total number of cell-associated bacteria. For each assay, serial dilutions of the whole bacterial inoculum were plated. The effect of HaCaT cell lysis buffer on the viability of *S. epidermidis* (MFP04) was controlled in preliminary tests.

Biofilm formation studies under dynamic conditions. After an overnight pre-culture in LB at 37 °C, *S. epidermidis* MFP04 was inoculated at an OD₅₈₀ of 0.08 in LB medium and sub-cultured for 2 h. CGRP (10⁻⁶ M final concentration) was added, and bacteria were grown for an additional 1 h. Bacteria were then washed and adjusted to an OD₅₈₀ of 0.1 in 0.9% NaCl supplemented with CGRP (10⁻⁶ M). The bacterial suspensions were then used to study biofilm formation under dynamic conditions at 37 °C in a three-channel flow cell as described by Bazire *et al.*⁴⁸. Briefly, each bacterial suspension was injected into a flow cell channel, and bacteria were allowed to adhere to the glass coverslip for 2 h. A flow (2.5 mL/h) of LB medium was then applied for 24 h. At the end of the experiments, the biofilms were stained with 5 × 10⁻⁶ M Syto 61 red dye or 5 × 10⁻⁶ M SytoX (Molecular Probes, Thermo Fisher Scientific, Villebon-sur-Yvette, France). Observations were made using a confocal laser scanning microscope (LSM 710 confocal laser-scanning microscope; Zeiss, Marly le Roi, France). The biofilm thicknesses and corresponding biovolumes were estimated by measuring field samples from at least 3 independent experiments using COMSTAT software (Matworks, Natick, USA)⁴⁹.

Characterization of bacterial surface polarity. Stationary phase bacteria were harvested (7,000 × g; 10 minutes) and washed twice in 0.9% NaCl. The polarity of control and CGRP-treated *S. epidermidis* MFP04 was studied using the Microbial Adhesion To Solvent (MATS) technique¹⁹ and two solvent couples: chloroform/hexadecane and ethyl acetate/n-decane. In total, 2.6 mL of bacterial suspension at OD₄₀₀ 0.8 was mixed for 60 s with 0.4 mL of each solvent indicated above. The OD of the aqueous phase was measured at 400 nm. The percentage of cells in each solvent was calculated using the following equation: (1 - A/A₀) × 100. Each experiment was repeated in triplicate using three independent cultures.

CGRP binding site identification. Mid-log growth phase bacterial cultures were centrifuged at 7,000 × g for 10 min. The pellets were resuspended in 5 mL of lysostaphin diluted in phosphate buffered saline (PBS) (10⁻⁵ g/mL). This mix was incubated for 1 h at 37 °C with shaking at 180 rpm. Then, the samples were then centrifuged for 20 min at 7,000 × g and 4 °C. Each pellet was solubilized in 6 mL of non-denaturing lysis buffer (Tris 50 × 10⁻³ M pH 8, EDTA 4 × 10⁻³ M, NaCl 137 × 10⁻³ M, glycerol 10%, Triton X100 1%, phenylmethylsulfonyl-fluoride 10⁻³ M and supplemented with protease inhibitors (Boehringer, Paris, France). Four freeze/thaw cycles were applied to the suspension at -80 °C for 20 min/37 °C for 10 min. The bacteria were lysed by sonication using a number of short pulses (1 min) with pauses (2 min) on ice to maintain a low temperature. The cell lysates were once again centrifuged at 13,000 × g for 10 min at 4 °C to remove unbroken cells. For total protein extracts, the supernatant was incubated with benzonase (0.125 × 10⁻⁶ L/mL) and MgCl₂ (1.625 × 10⁻⁶ L/mL) for 1 h at room temperature to degrade nucleic acids. The proteins were precipitated with 20% trichloroacetic acid, vortexed for 15 seconds and incubated overnight at 4 °C. Samples were then centrifuged at 13,000 × g for 20 min at 4 °C and solubilized in a rehydratation buffer (urea 7 M, 15.2% thio-urea, 4% CHAPS, 25 × 10⁻⁶ L/mL IPG buffer, 10.79 × 10⁻³ g/mL DTT and 1.43 10⁻³ g/mL TCEP in water). To extract membrane proteins, the supernatant containing the total proteins was ultracentrifuged at 35,000 rpm for 50 min at 4 °C. The pellet containing membrane proteins was solubilized in a solution containing 5 × 10⁻⁵ M Tris pH 8, 10⁻⁵ M MgCl₂, 2% Triton X100 and 10⁻⁹ M phenylmethylsulfonyl-fluoride and supplemented with protease inhibitors.

The CGRP binding site was extracted by using an immunoprecipitation technique adapted from Mijouin *et al.*⁵. Briefly, 6 × 10⁻⁶ L of G protein-coupled agarose beads (Millipore) and 1.5 10⁻⁶ g of CGRP monoclonal antibodies (Abcam, Paris, France) were allowed to associate overnight at 4 °C. Meanwhile, 1.5 × 10⁻³ g of membrane protein extracts was incubated with CGRP (10⁻⁶ M) for 1 h at room temperature under slow orbital agitation. To reduce the non-specific binding, 5 × 10⁻⁵ L of rabbit polyclonal serum was added. Unlabelled G protein-coupled agarose beads were added to remove non-specific complexes. The samples were incubated for 30 min at 4 °C under slow orbital agitation. The unlabelled beads were removed by centrifugation (10,000 × g, 4 °C, 10 min). The supernatant containing the CGRP bound ligand was then mixed with the CGRP antibody-associated beads and incubated for 1 h at room temperature under slow orbital agitation. For each sample, the beads were washed two times with 250 × 10⁻⁶ L of non-denaturing lysis buffer by low-speed centrifugation cycles. Each sample was boiled for 5 min with 5 × 10⁻⁵ L of Laemmli 2x buffer (Tris 0.2 M pH 6.8, glycerol 45%, sodium dodecyl sulfate (SDS) 6%, β-mercaptoethanol 6% and bromophenol blue 0.03%) to separate the ligand from the beads. Before loading on a 12% SDS polyacrylamide gel electrophoresis (PAGE) gel, the beads were removed by centrifugation (14,000 × g, 4 °C, 5 min). Proteins were visualized by colloidal Coomassie blue G250 staining (Sigma-Aldrich, Saint Quentin Fallavier, France). Three independent experiments were conducted.

After dissection of the band of interest and protein solubilization, the CGRP-binding proteins were identified by tandem mass spectrometry as previously described, using an LTQ-Orbitrap Elite coupled with an Easy nLC II system (Thermo Scientific, Villebon-sur-Yvette, France).

Western blot analysis of EfTu in intra- and extra-bacterial compartments. Proteins extracted from the bacterial stroma and growth medium after fractionation as previously described were separated on a 12% w/v polyacrylamide SDS-PAGE gel. After separation, proteins were transferred onto nitrocellulose membranes at 50 mA for 1 h in Tris base (0.192 M) transfer buffer containing glycine (14.5% g/L w/v) and methanol (20% v/v) using a Bio-Rad Mini TransBlot Electrophoretic Transfer Cell system. Membranes were then air-dried and immersed for 2 h in blocking buffer (Tris buffer saline (TBS): 5 × 10⁻⁵ M, 0.15 M NaCl, 5% whole milk). Membranes were incubated with primary antibody raised against bacterial EfTu⁶ (1:100 in blocking buffer) at room temperature for 2 h while shaking. After incubation, the blot was washed three times in 1x TBS supplemented with 0.05% (w/v) Tween 20 for 30 min and incubated for 1.5 h with shaking with secondary antibody diluted 1/5000 (goat anti-rabbit IgG alkaline phosphatase conjugate, Bio-Rad, Schiltigheim, France). Electrophoretic bands were detected using an alkaline phosphatase conjugate substrate kit (Bio-Rad, Schiltigheim, France).

Statistical analysis. All results are expressed as means \pm standard error (SEM) calculated over a minimum of three independent experiments. Significant differences were estimated using Student's *t* tests and are noted as ★, ★★ and ★★★ for *p*-values < 0.05 , < 0.01 and < 0.001 , respectively. For confocal microscopy studies, the biofilm thickness and biomass were calculated from a minimum of 20 measures in different fields.

References

- Roosterman, D., Goerge, T., Schneider, S. W., Bunnett, N. W. & Steinhoff, M. Neuronal control of skin function: the skin as a neuroimmunoendocrine organ. *Physiol. Rev.* **86**, 1309–1379 (2006).
- Schommer, N. N. & Gallo, R. L. Structure and function of the human skin microbiome. *Trends Microbiol.* **21**, 660–668 (2013).
- Cizza, G. *et al.* Elevated neuroimmune biomarkers in sweat patches and plasma of premenopausal women with major depressive disorder in remission: the POWER study. *Biol. Psychiatry* **64**, 907–911 (2008).
- Harrison, S. & Geppetti, P. Substance P. *Int. J. Biochem. Cell. Biol.* **33**, 555–576 (2001).
- Mijouin, L. *et al.* Effects of a skin neuropeptide (Substance P) on cutaneous microflora. *PLoS One* **8**, e78773 (2013).
- N'Diaye, A. *et al.* Effect of Substance P in *Staphylococcus aureus* and *Staphylococcus epidermidis* virulence: Implication for skin homeostasis. *Frontiers Microbiol.* **7**, 1–15, Art 506 (2016).
- Hillion, M. *et al.* *Pseudomonas fluorescens*, a forgotten member of the human cutaneous microflora sensible to skin communication and defense peptides. *Int. J. Curr. Microbiol. Appl. Sci.* **3**, 910–925 (2014).
- Lesouhaitier, O. *et al.* Gram-negative bacterial sensors for eukaryotic signal molecules. *Sensors* **9**, 6967–6990 (2009).
- Gibbins, I. L., Wattchow, D. & Coventry, B. Two immunohistochemically identified populations of calcitonin gene-related peptide (CGRP)-immunoreactive axons in human skin. *Brain Res.* **414**, 143–148 (1987).
- Eedy, D. J., Shaw, C., Johnston, C. F. & Buchanan, K. D. The regional distribution of neuropeptides in human skin as assessed by radioimmunoassay and high-performance liquid chromatography. *Clin. Exp. Dermatol.* **19**, 463–472 (1994).
- El Karim, I. A., Linden, G. J., Orr, D. F. & Lundy, F. T. Antimicrobial activity of neuropeptides against a range of micro-organisms from skin, oral, respiratory and gastrointestinal tract sites. *J. Neuroimmunol.* **200**, 11–16 (2008).
- Lyte, M. Microbial endocrinology and infectious disease in the 21st century. *Trends Microbiol.* **12**, 14–20 (2004).
- Rosay, T. *et al.* *Pseudomonas aeruginosa* expresses a functional human natriuretic peptide receptor ortholog: involvement in biofilm formation. *mBio* **6**, e01033–15 (2015).
- Picot, L. *et al.* Cytotoxic effects of the *Pseudomonas fluorescens* lipopolysaccharide in neurons and glial cells. *Microbial Pathogen.* **35**, 95–106 (2003).
- OECD Guidelines for the Testing of Chemicals. Draft Revised Guideline 431: *In vitro* skin corrosion: reconstructed human epidermis (RHE) test method (2014).
- Angrisano, T. *et al.* Epigenetic regulation of IL-8 and β -defensin genes in human keratinocytes in response to *Malassezia furfur*. *J. Invest. Dermatol.* **133**, 2101–2104 (2013).
- Mackey-Lawrence, N. M. & Jefferson, K. K. Regulation of *Staphylococcus aureus* immunodominant antigen B (IsaB). *Microbiol. Res.* **168**, 113–118 (2013).
- Mezghani-Abdelmoula, S. *et al.* Sequential activation of constitutive and inducible nitric oxide synthase (NOS) in rat cerebellar granule neurons by *Pseudomonas fluorescens* and invasive behaviour of the bacteria. *Microbiol. Res.* **159**, 355–363 (2004).
- Bellon-Fontaine, M.-N., Rault, J. & Van Oss, C. J. Microbial adhesion to solvents: a novel method to determine the electron-donor/electron-acceptor or Lewis acid-base properties of microbial cells. *Colloids Surfaces B: Biointerfaces* **7**, 47–53 (1996).
- Watkins, H. A., Rathbone, D. L., Barwell, J., Hay, D. L. & Poyner, D. R. Structure-activity relationships for α -calcitonin gene-related peptide. *Br. J. Pharmacol.* **170**, 1308–1322 (2013).
- Berrier, C., Garrigues, A., Richarme, G. & Ghazi, A. Elongation Factor Tu and DnaK are transferred from the cytoplasm to the periplasm of *Escherichia coli* during osmotic downshock presumably via the mechanosensitive channel MscL. *J. Bacteriol.* **182**, 248–251 (2000).
- Davenport, K. W. *et al.* Complete Genome Assembly of *Staphylococcus epidermidis* AmMS 205. *Genome Announc.* **2**, e01059–14 (2014).
- Berrier, C., Coulombe, A., Szabo, I., Zoratti, M. & Ghazi, A. Gadolinium ion inhibits loss of metabolites induced by osmotic shock and large stretch-activated channels in bacteria. *Eur. J. Biochem.* **206**, 559–565 (1992).
- Linscheid, P. *et al.* Expression and secretion of procalcitonin and calcitonin gene-related peptide by adherent monocytes and by macrophage-activated adipocytes. *Crit. Care Med.* **32**, 1715–1721 (2004).
- He, Y., Ding, G., Wang, X., Zhu, T. & Fan, S. Calcitonin gene-related peptide in Langerhans cells in psoriatic plaque lesions. *Chin. Med. J.* **113**, 747–751 (2000).
- Hou, Q. *et al.* Keratinocyte expression of calcitonin gene-related peptide β : implications for neuropathic and inflammatory pain mechanisms. *Pain* **152**, 2036–2051 (2011).
- Granstein, R. D., Wagner, J. A., Stohl, L. L. & Ding, W. Calcitonin gene-related peptide: key regulator of cutaneous immunity. *Acta Physiol.* **213**, 586–594 (2015).
- Birklein, F., Schmelz, M., Schifter, S. & Weber, M. The important role of neuropeptides in complex regional pain syndrome. *Neurology* **57**, 2179–2184 (2001).
- Pendaries, V. *et al.* In a three-dimensional reconstructed human epidermis filaggrin-2 is essential for proper cornification. *Cell Death Dis.* **6**, e1656 (2015).
- Nedoszytko, B. *et al.* Chemokines and cytokines network in the pathogenesis of the inflammatory skin diseases: atopic dermatitis, psoriasis and skin mastocytosis. *Postepy. Dermatol. Allergol.* **31**, 84–91 (2014).
- Scharschmidt, T. C. *et al.* A wave of regulatory T cells into neonatal skin mediates tolerance to commensal microbes. *Immunity* **43**, 1011–1021 (2015).
- Liu, P. F. *et al.* IsaB inhibits autophagic flux to promote host transmission of methicillin-resistant *Staphylococcus aureus*. *J. Invest. Dermatol.* **135**, 2714–2722 (2015).
- Hirschhausen, N. *et al.* A novel staphylococcal internalization mechanism involves the major autolysin Atl and heat shock cognate protein Hsc70 as host cell receptor. *Cell. Microbiol.* **12**, 1746–1764 (2010).
- Kampinga, H. H. & Craig, E. A. The Hsp70 chaperone machinery: J proteins as drivers of functional specificity. *Mol. Cell. Biol.* **11**, 579–592 (2010).
- Singh, V. K. *et al.* An insight into the significance of the DnaK heat shock system in *Staphylococcus aureus*. *Int. J. Med. Microbiol.* **302**, 242–252 (2012).
- Arita-Morioka, K., Yamanaka, K., Mizunoe, Y., Ogura, T. & Sugimoto, S. Novel strategy for biofilm inhibition by using small molecules targeting molecular chaperone DnaK. *Antimicrob. Agents Chemother.* **59**, 633–641 (2015).
- Gu, Y. P. Glass surfaces: Electrokinetics and wetting properties. In “Encyclopedia of Surface and Colloid Science” Vol. 4 P. Somasundaran Ed., Taylor & Francis CRC Press, Boca raton USA pp. 2711–2722 (2006).
- Cerca, N., Pier, G. B., Vilanova, M., Oliveira, R. & Azeredo, J. Quantitative analysis of adhesion and biofilm formation on hydrophilic and hydrophobic surfaces of clinical isolates of *Staphylococcus epidermidis*. *Res. Microbiol.* **156**, 506–514 (2005).
- Evans, B. N., Rosenblatt, M. I., Mnayer, L. O., Oliver, K. R. & Dickerson, I. M. CGRP-RCP, a novel protein required for signal transduction at calcitonin gene-related peptide and adrenomedullin receptors. *J. Biol. Chem.* **275**, 31438–31443 (2000).

40. Siaut, M. *et al.* An Rpb4/Rpb7-like complex in yeast RNA polymerase III contains the ortholog of mammalian CGRP-RCP. *Mol. Cell. Biol.* **23**, 195–205 (2003).
41. Dorwart, M. R., Wray, R., Brautigam, C. A., Jiang, Y. & Blount, P. S. *S. aureus* MscL is a pentamer *in vivo* but of variable stoichiometries *in vitro*: implications for detergent-solubilized membrane proteins. *PLoS Biol.* **8**, e1000555 (2010).
42. Hon, K. L., Tsang, Y. C., Pong, N. H., Leung, T. F. & Ip, M. Exploring *Staphylococcus epidermidis* in atopic eczema: friend or foe? *Clin. Exp. Dermatol.* **41**, 659–663 (2016).
43. Gomes, F., Teixeira, P. & Oliveira, R. Mini-review: *Staphylococcus epidermidis* as the most frequent cause of nosocomial infections: old and new fighting strategies. *Biofouling* **30**, 131–141 (2014).
44. Wu, L. *et al.* Recognition of host immune activation by *Pseudomonas aeruginosa*. *Science* **309**, 774–777 (2005).
45. Amblee, V. & Jeffery, C. J. Physical features of intracellular proteins that moonlight on the cell surface. *PLoS One* **10**, e0130575 (2015).
46. Hillion, M. *et al.* Comparative study of normal and sensitive skin aerobic bacterial populations. *MicrobiologyOpen* **2**, 953–961 (2013).
47. Barbey, C. *et al.* Catabolic pathway of gamma-caprolactone in the biocontrol agent *Rhodococcus erythropolis*. *J. Proteome Res.* **11**, 206–216 (2012).
48. Bazire, A. *et al.* The sigma factor AlgU plays a key role in formation of robust biofilms by nonmucoid *Pseudomonas aeruginosa*. *J. Bacteriol.* **192**, 3001–3010 (2010).
49. Heydorn, A. *et al.* Quantification of biofilm structures by the novel computer program COMSTAT. *Microbiology* **146**, 2395–2407 (2000).

Acknowledgements

We wish to thank Magalie Barreau and Olivier Maillet for technical assistance. A.R.N'Diaye is a recipient of a doctoral fellowship from the French Ministry of Research (MRE). This work was supported by grants from the Communauté d'Agglomération d'Evreux, the Conseil Général de l'Eure, the European regional development fund (ERDF) and the Normandie Regional Council.

Author Contributions

A.R.N'D. performed most of the experiments, analyzed the data and contributed to the manuscript. C.L. assisted with cytotoxicity studies. T.K. and J.H. performed tandem mass spectrometry analysis. C.D.P. analyzed MATS experiments. Y.K.-G., S.C. and O.L. assisted with experiments analysis and manuscript writing. M.G.J.F. designed the study and wrote the manuscript. All authors read and approved the final manuscript.

Additional Information

Supplementary information accompanies this paper at <http://www.nature.com/srep>

Competing financial interests: The authors declare no competing financial interests.

How to cite this article: N'Diaye, A. R. *et al.* Skin-bacteria communication: Involvement of the neurohormone Calcitonin Gene Related Peptide (CGRP) in the regulation of *Staphylococcus epidermidis* virulence. *Sci. Rep.* **6**, 35379; doi: 10.1038/srep35379 (2016).



This work is licensed under a Creative Commons Attribution 4.0 International License. The images or other third party material in this article are included in the article's Creative Commons license, unless indicated otherwise in the credit line; if the material is not included under the Creative Commons license, users will need to obtain permission from the license holder to reproduce the material. To view a copy of this license, visit <http://creativecommons.org/licenses/by/4.0/>

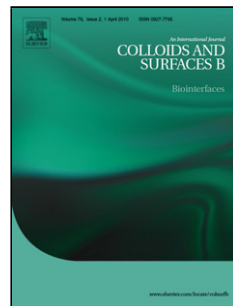
© The Author(s) 2016

P29

Accepted Manuscript

Title: Impact of coated TiO₂-nanoparticles used in sunscreens on two representative strains of the human microbiota: Effect of the particle surface nature and aging

Authors: Laura Rowenczyk, Cécile Duclairoir-Poc, Magalie Barreau, Céline Picard, Nicolas Hucher, Nicole Orange, Michel Grisel, Marc Feuilloye



PII: S0927-7765(17)30425-3

DOI: <http://dx.doi.org/doi:10.1016/j.colsurfb.2017.07.013>

Reference: COLSUB 8676

To appear in: *Colloids and Surfaces B: Biointerfaces*

Received date: 14-2-2017

Revised date: 1-6-2017

Accepted date: 5-7-2017

Please cite this article as: Laura Rowenczyk, Cécile Duclairoir-Poc, Magalie Barreau, Céline Picard, Nicolas Hucher, Nicole Orange, Michel Grisel, Marc Feuilloye, Impact of coated TiO₂-nanoparticles used in sunscreens on two representative strains of the human microbiota: Effect of the particle surface nature and aging, *Colloids and Surfaces B: Biointerfaces* <http://dx.doi.org/10.1016/j.colsurfb.2017.07.013>

This is a PDF file of an unedited manuscript that has been accepted for publication. As a service to our customers we are providing this early version of the manuscript. The manuscript will undergo copyediting, typesetting, and review of the resulting proof before it is published in its final form. Please note that during the production process errors may be discovered which could affect the content, and all legal disclaimers that apply to the journal pertain.

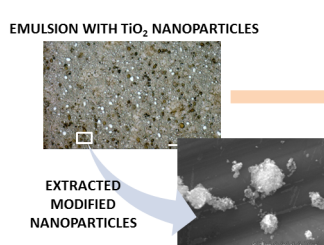
1 **Impact of coated TiO₂-nanoparticles used in sunscreens on**
 2 **two representative strains of the human microbiota:**
 3 **Effect of the particle surface nature and aging**

4
 5 *Laura Rowenczyk^{*1,2}, Cécile Duclairoir-Poc¹, Magalie Barreau¹, Céline Picard², Nicolas Hucher*
 6 *², Nicole Orange¹, Michel Grisel² and Marc Feuilloley¹*

7
 8 ¹ Laboratoire de Microbiologie Signaux et Microenvironnement EA 4312, Université de Rouen, 55 rue saint
 9 Germain 27000 Evreux, France.

10 ² Normandie Univ, UNILEHAVRE, FR3038 CNRS, URCOM, 76600 Le Havre, France.

11
 12 * Corresponding author: University of Le Havre, 25 rue Philippe Lebon, B.P. 540 76058 Le Havre cedex; Tel.: +33
 13 2327443915; E-mail address: laura.rowenczyk@univ-lehavre.fr (L. Rowenczyk)



- 16 • Surface properties of coated TiO₂-nanoparticles evolved during aging in model emulsions
 17 • Impact on skin bacteria evaluated through two exposure scenarios mimicking use conditions
 18 • Hydrophobic nanoparticles modified the physicochemical characteristics of model emulsions
 19 • Hydrophobic nanoparticles favored the development of potential pathogenic bacteria
 20 • Importance of the polarity of nanoparticles was highlighted regarding their impact on bacteria

21
 22
 23 **Keywords:** TiO₂-nanoparticles, cutaneous bacteria, bacteria growth, surface treatment,
 24 polarity, surface charge.

25 **Abstract**

26 The impact of two differently coated TiO₂-nanoparticles (NPs) was evaluated on two
 27 representative bacteria from the cutaneous microbiota (*Staphylococcus aureus* and *Pseudomonas*
 28 *fluorescens*) in conditions of use. **Particles were coated in order to exhibit either hydrophilic or**
 29 **hydrophobic behavior.** A first exposure scenario within some fresh/aged model emulsions was
 30 developed in order to measure both the impact of the NPs presence and their surface nature during
 31 the emulsions conservation. Thanks to this protocol, it was demonstrated that, during aging, the
 32 hydrophobic NPs modified the physicochemical characteristics of the emulsions, such as the pH or the
 33 colloids sizes, and favored the development of potential pathogenic bacteria. A second scenario was
 34 then envisaged, aiming to mimic the exposition of the skin, especially of the cutaneous bacteria, to
 35 NPs. Tested NPs were extracted from emulsions with different aging, and results highlighted the
 36 importance of both the NP coating nature and their history in emulsion. The different NPs impacts on
 37 the bacteria growth were discussed and linked to their surface properties modifications during aging,
 38 as polarity and charges. Finally, through two exposition scenarios, this work highlights the major
 39 impact of the NPs surface properties on bacteria.

40 **1. Introduction**

41 The TiO₂-nanoparticles (NPs) are commonly used in cosmetics due to their attractive optical
 42 properties: they protect the skin against the ultraviolet radiations, and as fine particles, they are not
 43 whitening once layered on skin. On the other hand, the TiO₂-NPs have a stronger reactivity, and
 44 especially photoreactivity, enhancing the production of reactive oxygen species (ROS) that can induce
 45 cellular damages (Dunford et al., 1997; Kamat et al., 2000; Kawaguchi et al., 1997). For this reason, NP
 46 cosmetic grades are often surface-modified by applying a passivation coating (*silica* or *alumina*), in
 47 order to quench the photo-production of radicals (Cao and Zhang, 2011; Serpone et al., 2006). In
 48 addition, in order to raise their affinity with the emulsion, a second coating is sometimes added.

49 Authors already highlighted coating deteriorations when the NPs are released after using in
 50 aqueous environment (Auffan et al., 2010; Labille et al., 2010). However, during their formulation and
 51 storage, NPs are already exposed to a variety of aggressions in emulsion which can accelerate their
 52 aging and induce particles aggregation or adsorption of sunscreen compounds (Rossano, 2014). These
 53 modifications could affect the surface properties of the NPs and thus, change their impact on human
 54 skin. Whereas the impact of these kinds of NPs on eukaryotes cells was previously documented
 55 (Rossano, 2014), there is no information concerning their impact on the skin bacteria. However these
 56 microorganisms could be in contact with these NPs through two scenarios.

- 57 - First, it has been demonstrated that for a cosmetic product, the main contamination comes
 58 from the skin microflora of the consumer (Brannan and Dille, 1990). Hence, it appeared
 59 interesting to test the impact of the emulsion containing, or not NPs, on germs of the human
 60 skin microflora. Thus, we could wonder about the effect of the NPs on the microbiological
 61 conservation of the cosmetic emulsions.
- 62 - Then, since the cutaneous bacteria represent the first skin barrier, a major consideration
 63 remains the safety of such NPs when layered on this shield. Indeed, some cosmetic ingredients
 64 have already been proved to impact the development of the cutaneous bacteria (Mijouin et
 65 al., 2013; Taylor et al., 2003) and could be involved in skin disorders (Christensen and
 66 Brüggemann, 2014).

67 For this purpose, three model emulsions containing NPs, or NPs-free (reference), were previously
 68 developed with the same major ingredients to ensure qualities, making possible to conduct
 69 microbiological testing (Rowenczyk et al., 2016). These only differed by the presence and nature of
 70 TiO₂-NPs:

- 71 · one containing hydrophilic NPs, only passivated by *silica*,
 72 · a second one containing hydrophobic NPs, coated with *alumina* and
 73 *triethoxycaprylylsilane*,
 74 · a last one NPs-free.

75 The impact of these NPs were studied though two protocols of exposure and related to their surface
 76 nature (surface charge and polarity) and modifications during aging.

77 2. Material and Methods

78 2.1. *Chemical and reference materials*

79 Ultrapure water with a resistivity of 18 MΩ.cm used during the emulsion preparation and
 80 zetametry was purified, filtrated on 0.2 µm and treated by UV in order to eliminate germs. Otherwise
 81 distilled water with a resistivity of 18 MΩ.cm was used for other emulsion characterizations.

82 Two different grades of TiO₂-nanoparticles were kindly given by Kobo and Merck; one hydrophilic,
 83 with a simple *silica* coating named N1 (EUSOLEX® TAVO, Merck Chimie SAS, France) and a second,
 84 hydrophobic, composed of *alumina* (*and*) *triethoxycaprylylsilane* named N2 (A10-TiO2-11S7, Kobo
 85 Products, France). The other cosmetic grade ingredients were chosen to obtain oil-in-water sunscreen
 86 emulsions with optimal NP dispersions. To achieve emulsions with the lowest bactericide impact, no
 87 preservative was added.

88 Solvents were used as received: diiodomethane (DIM), 99 % purity, from Avocado (La tour du pin,
89 France), decane, hexadecane, chloroform and ethyl acetate were obtained from Alfa Aesar (Karlsruhe,
90 Germany). Potassium bromide (KBr), 99 % purity, (Fisher scientific, Illkirch, France) was dried for 24 h
91 at 100°C before use.

92 **2.2. Emulsion preparation.**

93 The preparation protocol was previously described in Rowencyk *et al.* (Rowencyk et al., 2016).
94 For the preparation of the preservative-free emulsion, precautions were taken in order to minimize
95 the risk of contamination by environmental microorganisms. Stainless steel material was steamed for
96 45 min at 190°C and glass bottles were rinsed with ethanol prior to drying (INRS, 2014). For technical
97 reasons it was impossible to make all operation in sterile conditions under laminar flow hood but
98 controls revealed that, in our experimental conditions, airborne contaminants in final formulations
99 remained under the detection limit.

100 **2.3. Emulsion aging**

101 Once prepared, the emulsions were matured for 24h at ambient temperature and then
102 characterized a first time as fresh emulsions. Then, they were aged through accelerated conditions
103 which allowed quickly observing physicochemical modifications. Whereas some studies conducted on
104 aging at 50°C (André *et al.*, 2003), this temperature is high enough to reach the melting points of
105 ingredients and to change the emulsion physical state. For these reasons, the aging temperature was
106 fixed in this work at 40°C and the emulsions were characterized every week, after being slowly cooled
107 down to room temperature. At least, three batches of each emulsion were prepared and characterized.

108 **2.4. NP extraction.**

109 The NPs were extracted from the fresh and aged emulsions by a protocol adapted from Nischwitz
110 *et al.* (2012). Between 1 and 2 g of emulsions were weighed in a polypropylene tube and diluted with
111 around 8 mL of a mix of methanol/pentane (3/1) destined to break the emulsion structure. The mixture
112 was homogenized by vortexing for 2 min and ultra-sonicating for 5 min (120 W). It was then centrifuged
113 for 10 min at 8000 g to recover NPs at the bottom of the tube. The supernatant was removed. These
114 steps were repeated twice to extract the NPs from the emulsion. Then, three simple washings with
115 methanol followed in order to remove pentane traces. Remaining methanol was evaporated under
116 vacuum for 1 h and the traces of water were removed by a two-hour long freeze drying step. Extraction
117 was performed on at least three different batches of each emulsion. By this protocol, different
118 powders were obtained:

119 For N1 hydrophilic NPs:

- 120 · N1S: N1 native NP powder which underwent the protocol of extraction,
 121 · N1F: N1 NP extracted from F-N1 fresh emulsion,
 122 · N1A: N1 NP extracted from F-N1 aged emulsion.
 123 For N2 hydrophobic NPs, N2S, N2F and N2A were obtained by the same way.

124 ***2.5. Physicochemical characterizations.***

125 **2.5.1. Particle size measurement.**

126 The particle size measurements were performed by using a laser diffractometer SALD 7500
 127 Nano (405 nm, Shimadzu, Kyoto, Japan) combined with the measurement cell SALD BC 75 consisting
 128 in a 7 mL batch and a stirrer: the WingSALD II-7500 software (version 3.1, Kyoto, Japan) was used to
 129 extract the data. Emulsions were diluted and homogenized according to the following procedures until
 130 reaching absorption between 1.2 and 1.5, corresponding to a good signal. Approximately 0.1 g of
 131 emulsion was pre-diluted in a test tube with 5 mL of distilled water and then vortexed for 10 sec at
 132 1000 rpm. Finally, the pre-dispersed samples were added dropwise until reaching the expected
 133 absorption. All measurements were performed at least in triplicate on two different batches. D10, D50
 134 and D90 diameters were thereafter expressed in particle volume, with, for instance, DX representing
 135 the threshold value in micrometer for which X % of the particles had a smaller size.

136 **2.5.2. Zetametry.**

137 The zeta potentials of the NPs, bacteria and emulsion were measured using a Zeta Sizer Nano-Z and
 138 folded capillary cells (Malvern instruments, Malvern, UK). Measurements were performed at least
 139 three times and analyzed with the software Zetasizer (version 7.11, Malvern, UK).

- 140 · The hydrophilic NPs and the bacteria in exponential growth phase were dispersed at 0.5 %
 141 w/w in ultrapure water containing NaCl 3×10^{-2} M and with a conductivity of 3 mS/cm. Six
 142 samples of each culture were adjusted at pH 2, 4, 6, 8, 10 and 12, respectively, using NaOH
 143 or HCl (0.4 or 0.04M). Before measurement, the dispersions of NPs were ultra-sonicated for
 144 5 min and the suspensions of bacteria were vortexed for 20 sec at 1000 rpm.
- 145 · The measurements on hydrophobic NPs followed the same protocol as above excepted that
 146 dispersion was obtained with adding a surfactant (Tween 80 at 4 g/L).
- 147 · Prior to measurements, emulsions were diluted at 0.5% w/w in ultrapure water containing
 148 NaCl 10^{-4} M and with a conductivity of 1.70 μ S/cm. Then, six samples of each emulsion were
 149 adjusted at pH 2, 4, 6, 8, 10 and 12, respectively, using NaOH or HCl (0.4 or 0.04 M), and
 150 then vortexed for 20 sec at 1000 rpm just before ZP measurement.

151 The curve giving the ZP as a function of pH was obtained by a polynomial fit with the minimal R².
 152 Then, extrapolations allowed recovering ZP values at the other pH.

153 **2.5.3. Sessile drop method.**

154 Complementary to zetametry, we decided to use sessile drop method to characterize the NP surface.
 155 For that purpose, NPs (10 % w/w) from three different batches were first dispersed in potassium
 156 bromide (KBr). This solid dispersion was then compacted under 6 tons using a high pressure press in
 157 order to obtain homogeneous pellets. Three pellets per emulsion batch were prepared. The sessile-
 158 drop method was conducted on these pellets with a Digidrop goniometer (GBX, Dublin, Ireland) and
 159 the software Windrop ++ (1.18.04, GBX, Dublin, Ireland). Static contact angles of ultrapure water (polar
 160 component: 51.0 mN/m and dispersive component: 21.6 mN/m) and diiodomethane (DIM, polar
 161 component: 0 mN/m and dispersive component: 50.8 mN/m) were measured. The polar and dispersive
 162 components of the surface were calculated using the Owens-Wendt theory (Owens and Wendt, 1969)
 163 from the contact angle obtained with both fluids.

164 **2.5.4. Microbial adhesion to solvents test (MATS).**

165 Complementary to zetametry, we decided to use MATS to characterize the bacteria surface. The
 166 adhesion tests were performed by measuring the bacterial repartition between a bacterial suspension
 167 (DO = 0.4) in saline water (NaCl 0.15 M) and a series of solvents with different polarity: chloroform,
 168 hexadecane, decane and ethyl acetate. 1.2 mL of bacterial suspension and 0.2 mL of the solvent were
 169 poured together into a tube and vortexed for 1 min. The mixture was left at rest for 15 min to allow
 170 the phase separation. Then, the optical density (DO) was measured at 400 nm in the aqueous phase.
 171 The percentage of adhesion was calculated using the following equation (Bellon-Fontaine et al., 1996):

$$\% \text{ adhesion} = \left(1 - \frac{A}{A_0} \right) \times 100 \quad (1)$$

172 A₀, is the initial DO in the aqueous phase and A, is the DO in the aqueous phase after mixing.

$$\Delta 1 = \% \text{ adhesion hexadecane} - \% \text{ adhesion chloroform} \quad (2)$$

$$\Delta 2 = \% \text{ adhesion decane} - \% \text{ adhesion ethyl acetate} \quad (3)$$

173 If Δ1 > 10, the surface of the bacteria is a Lewis base and if Δ2 > 20, it is a Lewis acid.

174 **2.6. Microbiological tests**

175 **2.6.1. Bacteria strains and culture conditions**

176 *Pseudomonas fluorescens* MFP05 and *Staphylococcus aureus* MFP03 were collected by swabbing
 177 on normal human skin and were characterized by metabolic, proteomic and genomic analysis (Hillion
 178 et al., 2013); they were stored on cryobeads at -140°C. Before use, they were sub-cultured over-night
 179 in 10 mL of Luria Bertani (LB) broth at 28 ± 2°C for MFP05 or 37 ± 2°C for MFP03, and then diluted again
 180 in LB broth to reach the appropriate initial bacterial density corresponding to an optical density,
 181 OD_{580nm} = 0.08. OD values were measured using a spectrophotometer (Helios Epsilon,
 182 ThermoSpectronics, Cambridge, UK). Bacteria were used when the cultures reached the exponential
 183 growth phase.

184 **2.6.2. Willingly inoculated bacteria in model emulsions.**

185 Approximately 5 g of each emulsion were diluted to the third in saline water (NaCl 9 g/L) or LB
 186 broth, and then inoculated with MFP03 or MFP05 at an initial concentration between 10⁵ and 10⁶
 187 UFC/mL. The exact bacterial concentration was controlled by plating 100 µL of solutions and serial
 188 dilutions on TSA Petri Dishes immediately after bacterial inoculation. Inoculated solutions were
 189 incubated at 28 ± 2°C in the case of MFP05 or 37 ± 2°C for MFP03 under orbital agitation at 180 rpm.
 190 After 24h, 48h and 72h, 100 µL of solutions were spread on TSA plates in order to monitor bacterial
 191 growth. All Petri dishes were incubated for 24h at 28 ± 2°C for MFP05 or 37 ± 2°C for MFP03 before
 192 counting.

193 **2.6.3. Willingly inoculated bacteria in NP dispersions.**

194 The NPs were dispersed at 5 % w/w in LB broth containing 4 g/L of Tween 80. The obtained
 195 solutions were inoculated with the previous cultures of MFP03 or MFP05 in order to reach an initial
 196 DO of 0.08. The exact bacterial concentration was controlled by plating 100 µL of solutions and serial
 197 dilutions on TSA Petri Dishes immediately after bacterial inoculation. The inoculated solutions were
 198 incubated at 28 ± 2°C in the case of MFP05 or 37 ± 2°C for MFP03 under orbital agitation at 180 rpm.
 199 Every hour until 8 h, 100 µL of solutions were spread on TSA plates in order to monitor bacteria growth
 200 evolution. All Petri dishes were incubated for 24h at 28 ± 2°C for MFP05 or 37 ± 2°C for MFP03 before
 201 counting.

202 **2.7. Data analysis.**

203 Results were expressed as mean ± standard deviation (SD). Statistical analyses of collected data were
 204 performed on XLSTAT software (version 2012.1.01, Addinsoft, France). Single-way analysis of variance
 205 (ANOVA) was applied to data series in order to test significance of parameters. When a significant
 206 difference was revealed between emulsions or NPs according to the Tukey discriminant test, groups
 207 of emulsions/NPs were formed and noted with * for p<0.05, ** for p<0.01 or *** for p<0.001. In the

208 results tables, different letters in the same row mean significant difference between emulsions or
 209 nanoparticles for this parameter.

210 **3. Results and discussion**

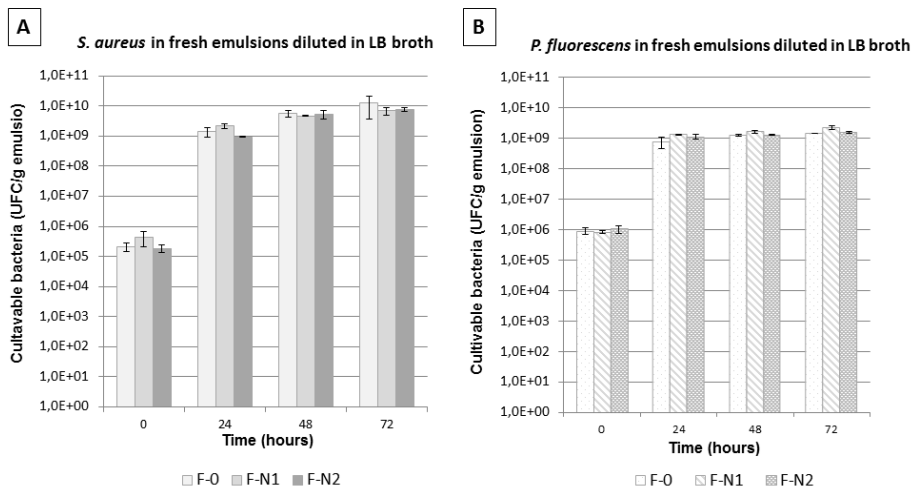
211 ***3.1. Effect of emulsion media, with or without NPs, on bacteria contamination: emulsion***
 212 ***conservation***

213 **3.1.1. Bacteria growth within fresh model emulsions**

214 This study aims to evaluate the impact of the two NPs surface nature used in sunscreen emulsions,
 215 on two bacteria commonly found on the human skin and thus, potentially introduced in use in the
 216 cosmetic product (Brannan and Dille, 1990). Two major germs of the human microbiota were selected:
 217 *Staphylococcus aureus* and *Pseudomonas fluorescens*. *S. aureus* is a Gram positive bacterium, usually
 218 considered as a member of the transient human skin flora but it is demonstrated to be carried by 35
 219 to 60 % of the human population and to behave as a commensal (Percival et al., 2012). *P. fluorescens*
 220 is a Gram negative ubiquitous bacterium representing more than 90 % of the microbial flora in humid
 221 skin areas such as the inner elbow (Grice et al., 2008). The latter is also present in abundance in the
 222 environment.

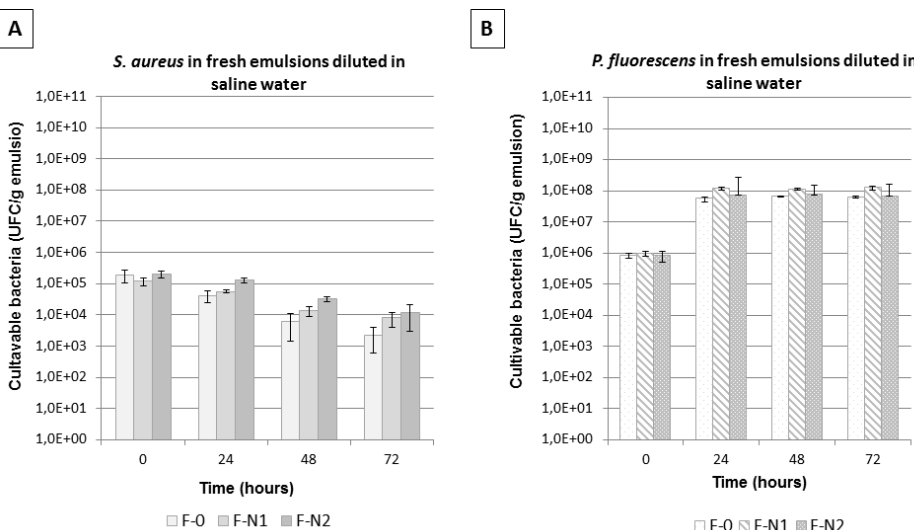
223 The control emulsion was previously developed without NPs in order to have a very low bactericidal
 224 impact and to only measure the “NP effect” on the bacterial strains (Rowenczyk et al., 2016). The three
 225 model emulsions were formulated to exhibit the lowest initial microbiological charge and the same
 226 physicochemical characteristics (pH, particle size, texture, opacity). Moreover, they are ensured to
 227 have any effect on the results of further microbiological tests. (Hamouda et al., 2001)

228 The potential of the selected germs to grow in these emulsions was evaluated. Since they were
 229 semi-solid products, a dilution by three was imposed in Luria Bertani broth (LB) before bacteria
 230 inoculation at a concentration of 10^6 UFC/g emulsion. In these conditions, both germs quickly
 231 developed since the medium brought an important nutrient contribution (Figure 1, A and B). If the
 232 maximal biomass reached by MFP03 appeared to be higher than for MFP05, this difference should only
 233 reflect the difference of optimal growth temperature (37°C and 28°C respectively) as well as
 234 metabolisms of both germs. However, both strains demonstrated a good growth rate within all
 235 emulsions, *i.e.*in the absence or presence of NPs. Thus, in these culture conditions, no detectable “NP
 236 effect” was observed on the bacterial growth regardless of their surface properties.



237
238 **Figure 1: Growths of *S. aureus* (MFP03) (A) and *P. fluorescens* (MFP05) (B) in the fresh emulsions diluted in LB broth**
239 ($n=3$).

240 It is hypothesized that the important nutrient contribution brought by the LB broth could hide the
241 potential impact of the NPs on the bacteria. Hence, in a second series of experiments the LB broth was
242 replaced by saline water (SW) and the three model emulsions were diluted the third in SW before
243 inoculation by bacteria (Figure 2, A and B). In this situation, no growth of *S. aureus* MFP03 was
244 observed (Figure 2, A). Moreover, the population of *S. aureus* showed a progressive decrease indicating
245 that the bacterium was unable to metabolize emulsion components. In contrast, the growth potential
246 of *P. fluorescens* MFP05 was preserved when the emulsions were diluted in SW although the final
247 biomass formed after 72 h was reduced by ten compared to the dilution in LB broth (Figure 2, B). These
248 result are in agreement with previous works showing that emulsions are not favorable media for
249 bacterial development (Teixeira et al., 2007), even in the case of a bacterium such as *P. fluorescens*
250 which is known for its high adaptation potential (Chapalain et al., 2008).



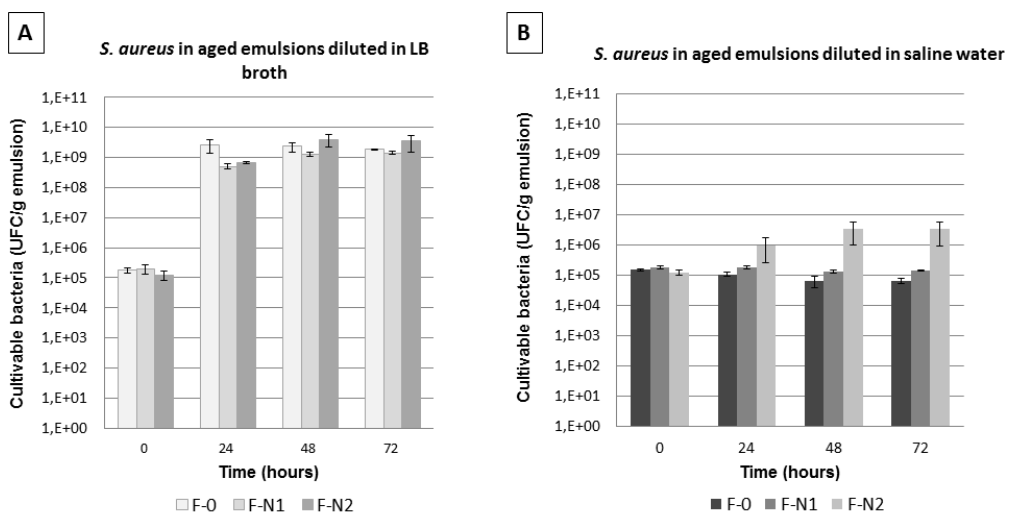
251
252 **Figure 2: Growths of *S. aureus* (MFP03) (A) and *P. fluorescens* (MFP05) (B) in the fresh emulsions diluted in saline water**
253 ($n=3$).

254 However, as for LB broth dilution, and whatever the species, the behaviors of the bacteria were
 255 the same in the three fresh model emulsions. Finally, no impact of the presence or nature of the NPs
 256 was highlighted in the fresh emulsions.

257 **3.1.2. Bacteria growth within aged model emulsions**

258 The three previous models emulsions were submitted to an accelerated aging step (40°C during
 259 49 days) to mimic the real conditions during sunscreen lotion conservation and use. Indeed, several
 260 studies have already proved that the surface of the NPs can be modified when they are rejected in
 261 aqueous environment (Auffan et al., 2010; Labille et al., 2010). On the basis of these works, it appeared
 262 interesting to study the surface modifications induced in aged emulsions. Thus, the three emulsions
 263 were tested following the same procedure than for the fresh ones, *i.e.* in absence or presence of
 264 different coated NPs.

265 In the case of *S. aureus* MFP03, no difference of growth kinetic was observed between the three
 266 aged emulsions diluted in rich medium (LB broth) (Figure 3, A). In contrast, the growth of *S. aureus* in
 267 aged emulsion diluted in poor medium (SW) was totally different when compared to the growth in
 268 fresh ones (Figure 3, B). The number of viable bacteria did not decrease, as observed for the fresh
 269 emulsions, but remained stable for the control emulsion (F0) and for the emulsion containing
 270 hydrophilic NPs (F-N1). A moderate, but significant, increase of the *S. aureus* population was even
 271 observed for the emulsion containing hydrophobic NPs (F-N2).



272
 273 **Figure 3: *S. aureus* growth in the aged emulsions; A: diluted in LB broth; B: diluted in saline water (SW) (n=3).**

274 Conversely, as previously observed, no difference of growth kinetic was observed using *P.*
 275 *fluorescens* MFP05 whatever the dilution medium used (LB broth or SW) and independently from the
 276 presence of NPs and from their surface properties (*Data not shown*).

277 **3.1.3. Evolution of the physicochemical characteristics of the emulsions during aging**

278 The evolution of the physicochemical characteristics of the three emulsions was monitored over
 279 time during aging. Each emulsion remained macroscopically stable, i.e. no demixing phenomenon was
 280 observed. However some of their microscopic parameters might evolve during aging.

281 The pH is a key parameter to consider since it was already taken into account during bacterial
 282 growth predictions due to its important impact on charges and ionic interactions (Sutherland et al.,
 283 1994). Hence, pH variations during the emulsion aging could explain the differences observed on
 284 bacterial growths. On the one hand, because of the presence of hydrophobic NPs in F-N2, the pH
 285 increased from 6.8 to 7.4 during aging (Table 1). Conversely, the pH of both F0 and F-N1 remained
 286 similar and stable (around 6.9). However, if *S. aureus* is able to grow over a large range of pH (4.5 -
 287 9.3), it is admitted that its optimal growth is between 7.0 and 7.5. Since the usual bacterial growth is
 288 strongly dependent on the pH of the media, respectively the lower or upper values leading to
 289 important reductions of its development (Bergdoll, 1989). Thus, the pH data are in accordance with
 290 the microbiological results observed for aged emulsion containing hydrophobic NPs.

291 **Table 1: pH, zeta potential (ZP) and mean diameters of emulsions (n=3). ZP values are obtained by extrapolation of the**
 292 **experimental points.**

	pH ± SD	ZP (mV)	Volumic mean diameter ± SD (μm)
Fresh F0	6.8 ± 0.1	-23	2.33 ± 0.09
Aged F0	7.0 ± 0.1	-26	2.81 ± 0.25
Fresh F-N1	6.8 ± 0.1	-30	2.11 ± 0.13
Aged F-N1	7.0 ± 0.2	-32	1.63 ± 0.28
Fresh F-N2	6.8 ± 0.1	-16	10.11 ± 0.41
Aged F-N2	7.4 ± 0.1	-14	13.16 ± 6.44

293
 294 Previous studies also pointed out the surface charges as an important parameter. Indeed, the
 295 electrostatic repulsions could prevent or enhance the bacteria/emulsion interactions (Ly et al., 2006).
 296 The fresh emulsion containing hydrophilic NPs had a more negative ZP (around -30 mV) than the
 297 control one (around -20 mV). On the contrary, the emulsion containing hydrophobic NPs had a less
 298 intense ZP value, about -15 mV. These results highlighted that F-N1 is more efficiently stabilized by
 299 electrostatic repulsions. Hence, although the presence of hydrophobic NPs (N2) clearly changed the ZP

300 of the emulsion, no difference between the bacterial growths in the three fresh emulsions was
 301 observed (3.1.1).

302 We have shown in Table 1 that the pH of the three emulsions evolved slightly differently during
 303 aging. This variation has to be taken into account for the determination of the surface charges after
 304 aging. As depicted in Table 1, the ZP measurements did not highlight major differences in terms of
 305 mean surface charges between colloids, whether in the fresh or aged emulsions.

306

307 Table 1 also reports the mean diameter of the colloids present in the emulsion, including the oil
 308 droplets and the NPs. Whereas the mean diameters for F0 and F-N1 remained similar after aging, the
 309 one for the aged F-N2 significantly increased, with large variations between tested samples, showing
 310 a more heterogeneous state for this emulsion due to aging. This result could partly explain the absence
 311 of inhibitory effects of this emulsion on the survival of *S. aureus* and the growth of the bacterium. This
 312 is consistent with previous results showing that in fine emulsions, the droplets could prevent the
 313 bacterial division by steric hindrance (Hamouda and Baker, 2000). **Moreover, the lower steric
 314 hindrance in the aged emulsion enhanced the diffusion of the ingredients in the emulsion continuous
 315 phase. Hence, bacteria could more easily access to nutriments essential for their metabolism.**

316 Hence, these results prove that the presence of hydrophobic NPs could significantly degrade the
 317 physicochemical characteristics of the emulsion F-N2 and as a consequence, reduce the
 318 microbiological conservation of this cosmetic emulsion.

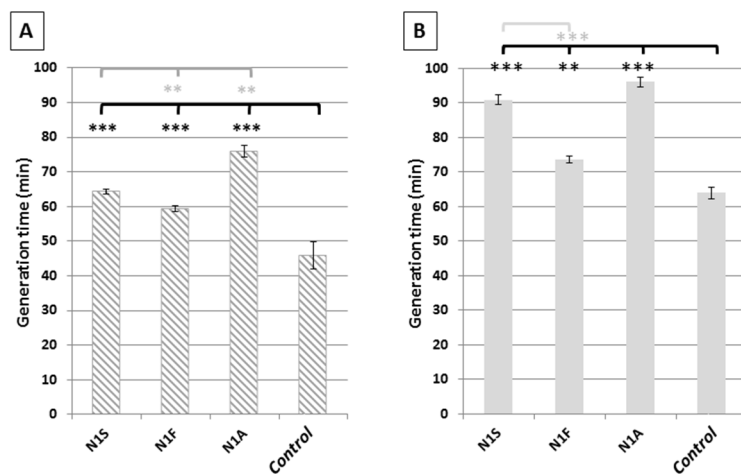
319 **3.2. Direct impact of the NPs extracted from the emulsions on two cutaneous bacteria: skin
 320 exposure**

321 **3.2.1. Bacterial growth in LB broth containing nanoparticles**

322 The second main goal of this work was to study the impact of the NPs when they are layered on
 323 the human skin. Once applied onto the skin, the aqueous and oily phases of the sunscreen emulsions
 324 are generally quickly removed (Rhodes and Diffey, 1997) and the NPs are the last component
 325 remaining at the skin surface. For that reason, the NPs were extracted and recovered from the fresh
 326 (N1F and N2F) or aged emulsions (N1A and N2A) after numerous solvent washings. This protocol was
 327 developed to mimic the skin evaporation and the leaching by sweat and sea. Then, the impact of the
 328 extracted NPs was compared to the one of control NPs corresponding to the commercial powder that
 329 underwent the same solvent washing protocol (N1S or N2S).

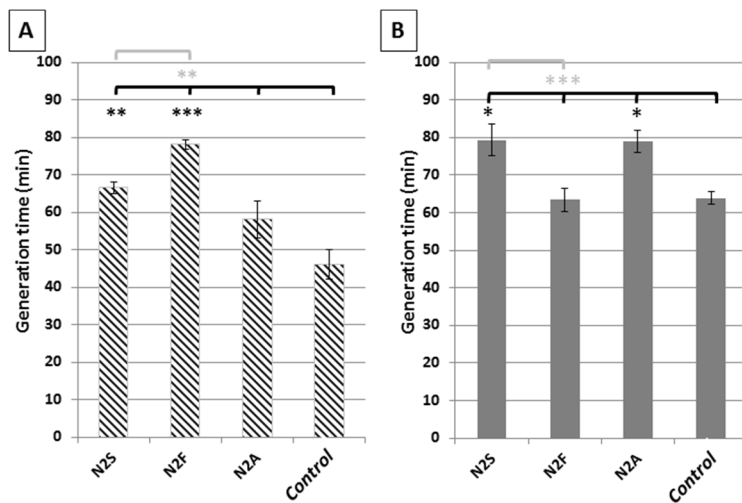
330 The growth kinetics of both bacteria were monitored in LB broth containing 5 % w/w of NPs,
 331 corresponding to the concentration added in the initial emulsions, plus a surfactant required to
 332 disperse the hydrophobic NPs. Preliminary tests allowed choosing Tween 80 (4 g/L) as a non-
 333 bactericidal surfactant efficient at a relatively low concentration (*Data not shown*).

334 The presence of the hydrophilic or hydrophobic NPs did not impact the total biomass formed by
 335 bacteria (*Data not shown*) but affected their generation times. Whereas in model emulsions the
 336 hydrophilic NPs did not affect the growth kinetics of both bacteria, in the present experimental
 337 conditions (i.e. NPs used alone after recovery from emulsions), hydrophilic NPs increased the
 338 generation time of both germs (Figures 4). It is worth mentioning that NPs extracted from aged
 339 emulsions tended to have a greater impact on the bacterial growth kinetic. This result suggests that
 340 this effect does not only result from steric hindrance but also from NP surface modifications occurring
 341 during aging.



342
 343
 344 **Figure 4: Impact of the hydrophilic N1 NPs on the generation times of;**
A: *S. aureus* (MFP03) and B: *P. fluorescens* (MFP05) (n=3).

345 The control NPs (N1S and N2S) increased only slightly the generation time of both bacteria (Figure
 346 5, A and B), thus highlighting the low impact of these NPs. Moreover, the hydrophobic NPs extracted
 347 from the fresh emulsion induced opposite effects on the two strains. Whereas they were without
 348 significant effect on the growth of *P. fluorescens* MFP05, they significantly increased the generation
 349 time of *S. aureus* MFP03. In addition, NP extracted from the aged emulsion and the control NPs had a
 350 similar effect on both bacteria.



351
352 **Figure 5: Impact of the hydrophobic N2 NPs on the generation times of;**
353 **A: *S. aureus* (MFP03) and B: *P. fluorescens* (MFP05) (n=3).**

354 All together, these results show that the hydrophilic NPs induce an intrinsic similar inhibitory
355 effect on the growth of *S. aureus* and *P. fluorescens*. This effect is minimal for NPs extracted from fresh
356 emulsion while it is slightly increases for NPs extracted from aged emulsions. Concerning the
357 hydrophobic NPs, their effect depends on the bacterial strain. Whereas it is generally limited or non-
358 significant on *P. fluorescens* MFP05, it appears more intense on *S. aureus* MFP03. Moreover, when the
359 hydrophobic NPs were extracted from fresh emulsions (N2F), they had a strong impact on *S. aureus*
360 which was not observed on *P. fluorescens*. As for a hypothesis, the impact of NPs on bacteria could
361 depend on their surface nature and their aging in emulsion.

362 **3.2.2. Influence of physicochemical properties of NP surface on their bacterial impact**

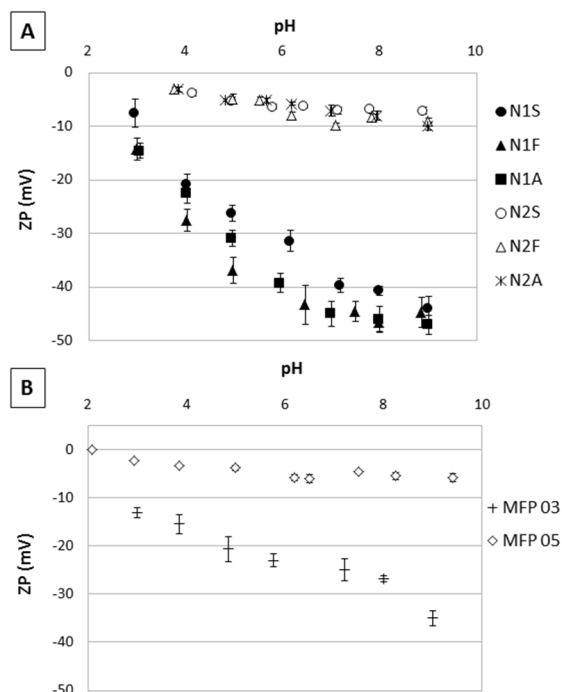
363 Results above described an “NP effect” on the bacteria growth and more precisely, a “surface
364 nature and history NP effect”. At this stage, two main hypotheses can be proposed:

- 365 · First, the outer coating of the NPs may be degraded. However, in this hypothesis, since the
366 impact of the aged NPs on the bacteria appeared fairly lowered, it seems that such a
367 degradation of the passivation coating remains limited.
- 368 · Secondly, different ingredients of the emulsion could strongly interact with and adsorb onto
369 the surface of the NPs. Part of these ingredients may remain adsorbed at the NPs surface in
370 spite of the extraction protocol. This second hypothesis is consistent with previous work.
371 (Rossano, 2014)

372 Hence, the surface properties of the extracted NPs were thereafter studied and compared.

373 • **Surface charges of NPs and bacteria**

374 The surface charges of both the bacteria and the NPs have to be considered since intense surface
 375 charges may create electrostatic repulsions and thus, prevent interactions between particles (Duffy et
 376 al., 2011). Then, the zeta potential values of NPs (Figure 6, A) and bacteria (Figure 6, B) were measured
 377 in water containing 1.8 g/L NaCl. Moreover, for the hydrophobic NPs, measurements were performed
 378 by adding 4 g/L Tween 80. This non-ionic surfactant was chosen as it does not induce any surface
 379 charge modifications.



380
 381 **Figure 6: A: Zeta potentials of NPs in water (1.8 g/L NaCl) and B: bacteria.**

382 The results given in the Figure 6 (A) show that the surface charges of the hydrophobic NPs were
 383 slightly negative (around -5 to -10 mV at pH 7). This may be explained by the outer coating made of
 384 silane, partially masking the alumina surface. Zeta Potential (ZP) of alumina is typically negative.
 385 However, since this coating is well-known to be porous (Egerton and Tooley, 2002), the positive
 386 charges of the titanium dioxide could be revealed. Hence, the apparent charge takes into account both
 387 the negative and positive charges and is, consequently, close to the isoelectric value.

388 In contrast, the hydrophilic NP appeared to be highly negatively charged with a mean value of -45
 389 mV at pH = 7, pH of LB medium (Figure 6, A). This value is consistent with the negative charges of the
 390 silica coating. It is worth mentioning that for both hydrophobic and hydrophilic NPs, native NPs and
 391 NPs from fresh or aged emulsions had almost the same zeta potential.

392 The surface of *P. fluorescens* MFP05 was close to the isoelectric value (around 0 mV) whereas the
 393 *S. aureus* MFP03 one was strongly negative. Moreover, this latter value increased with the pH (Figure

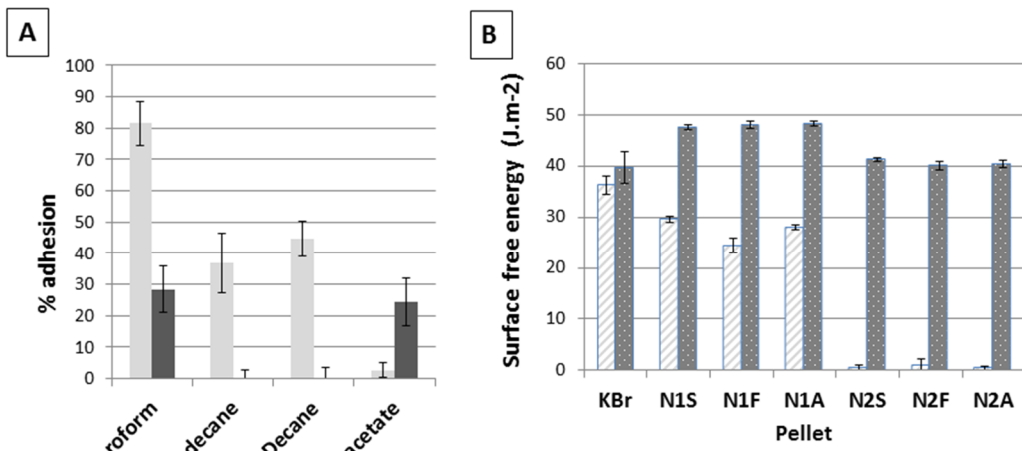
394 6, B). These differences actually reflect the surface nature of these bacteria. The surface of Gram
 395 negative bacteria, such as *P. fluorescens*, consists in a dynamic membrane allowing a rapid adaptation
 396 to the environment, including pH variations (Baysse and O'Gara, 2007). On the contrary, the surface
 397 of Gram positive bacteria, such as *S. aureus*, is made of a thick wall of peptidoglycan which does not
 398 belong the same dynamism and thus, is more directly impacted by medium charges and pH.

399 The hydrophilic NPs and *S. aureus* presented highly negatively surfaces at pH=7 (Figure 6, A and
 400 B). Then, as suggested by Duffy et al. (2011), if the surface charge was the major parameter,
 401 electrostatic repulsions should prevent interactions between hydrophilic NPs and *S. aureus*. However,
 402 in this work, the inhibitory effect on *S. aureus* MFP 03 is increased in the presence of the hydrophilic
 403 NPs, the most negatively charged particles. In contrast, the surface of *P. fluorescens* was poorly
 404 charged and could more easily interact with the hydrophilic NPs surface and even more with the
 405 hydrophobic NPs one.

406 • Surface free energies of NPs and bacteria

407 As revealed by the MATS technique, both *S. aureus* MFP03 and *P. fluorescens* MFP05 presented
 408 hydrophilic surfaces since their adhesion percentages to alkanes were low (Figure 7, A). Then, we can
 409 hypothesize that both strains, and especially *P. fluorescens* MFP05, should preferentially interact with
 410 the hydrophilic NPs (N1). Indeed, these germs are more likely able to meet and interact with the
 411 hydrophilic NPs that belong to the same emulsion phase. This explains why they were more impacted
 412 by these NPs as already shown in the present work.

413 Moreover, both strains exhibited a marked Lewis acid-base character, shown by the great
 414 difference between the affinities of each solvents couple. However, *S. aureus* MFP03 appeared to be
 415 less hydrophilic than *P. fluorescens* MFP05 strain since its adhesion percentages to alkanes was higher.
 416 These results were in accordance with the higher effect of hydrophilic NPs on *P. fluorescens* MFP05 as
 417 discussed earlier in this paper.



418
419
420
Figure 7: A: MATS results for *S. aureus* (light grey) and *P. fluorescens* (dark grey);
B: Polar (in light grey) and dispersive (in dark grey) components of the NP pellets

421 This study was completed by the measurement of the polar and dispersive components of the
422 NPs in order to qualitatively evaluate the different surface free energies between them (Figure 7, B).
423 The dispersive component of the hydrophilic NPs was significantly higher when compared to the
424 hydrophobic NPs one. Moreover, the NPs extracted from fresh emulsions (N1F) appeared to be
425 significantly less polar than the native ones (N1S) or the NPs extracted from aged emulsions (N1A).
426 Hence, this proved that the polarity of the hydrophilic NPs really depends on their history in emulsion.
427 However, the hydrophilic NPs extracted from fresh emulsions (N1F) were the one that less impacted
428 both bacteria. Then, these results confirm that the polarity of the NPs is a key parameter influencing
429 their impact on bacteria.

430 **4. General discussion**

431 A first scenario was elaborated to mimic a microbial contamination of sunscreen emulsions
432 containing NPs or NPs-free. In the absence of usable exogenous metabolites, the three fresh emulsions
433 appeared as a poorly favorable media, inducing a progressive reduction of *S. aureus* and partly
434 inhibiting the growth of a highly adaptable bacterium such as *P. fluorescens*. Moreover, it was
435 demonstrated that fresh emulsions containing NPs or NPs-free have the same impact on both Gram
436 positive and Gram negative bacteria. However, these emulsions could not prevent any potential
437 contamination if some nutriments are present, as for a rich culture medium. These results highlighted
438 that the microbial reductions observed in poor media is not due to a strong toxicity of the emulsions
439 but comes from their structures and properties. According to previous works, the emulsion
440 granulometry and pH were demonstrated as the major parameters influencing the germs growth
(Bergdoll, 1989; Hamouda and Baker, 2000; Ly et al., 2006).

442 After aging, the impact of the three model emulsions on bacteria was different and a "NP effect"
443 did appear. Even in the absence of exogenous nutrient, the aged emulsion containing hydrophobic
444 NPs showed a slower but still significant growth of *S. aureus*. In addition, this effect was observed after
445 only 24 to 72 h whereas cosmetic compounds need to undergo much longer storage time. It appeared
446 that emulsions, initially formulated in order to have similar microstructures and macroscopic
447 properties, evolved differently during aging depending on the presence and nature of NPs. After aging,
448 whereas both the control emulsion and the one formulated with hydrophilic NPs remained stable and
449 similar, the pH and the colloids size of the emulsion containing hydrophobic NPs significantly increased.
450 These results are consistent with a previous study showing that, under high temperature, NPs can
451 either stabilize or destabilize the emulsion, depending on their coating nature (Rowenczyk et al., 2016).
452 Hence, the nature of TiO₂-NPs employed in the formulation is a key parameter to be considered since
453 the presence of specific NPs in the emulsion made the cosmetic highly vulnerable to some bacteria
454 contaminations. Hence, this study revealed that long storage conditions should be a major concern in
455 regard of the microbiological safety and physicochemical modifications of those products.

456 In a second scenario mimicking the layered NPs on skin, we investigated the impact of NPs,
457 extracted from the fresh/aged emulsions, when put directly in contact with cutaneous bacteria. First,
458 it was demonstrated that the impact of the NPs on the bacteria could be related to their surface nature.
459 Hence, it seemed that this impact is the results of NPs/bacteria interaction phenomena. Whereas the
460 surface charge of the particles did not appear as a determinant parameter, the polarity of the NPs
461 should be in accordance with their impacts on bacteria. Previous works showed that the surface free
462 energy of the bacterial envelope is an important parameter in bacterial adhesion (An and Friedman,
463 1998; Sivakumar et al., 2010). More specifically, in this study, *S. aureus* and *P. fluorescens* which are
464 both hydrophilic bacteria were more impacted by the hydrophilic NPs; moreover, the most hydrophilic
465 one, *P. fluorescens*, appeared to be also the most impacted by the hydrophilic NPs. This study also
466 highlighted that the surface properties of the NPs, such as their polarity, evolved during their aging in
467 emulsion. For instance, the hydrophilic NPs extracted from a fresh emulsion were significantly less
468 polar than other hydrophilic NPs and showed the lowest impact on the growth of both bacterial
469 species.

470 There is a relation between the polarity of NPs, their interaction and their impact on some
471 cutaneous bacteria. It appeared that both the nature of the TiO₂-NPs coating and their aging have to
472 be considered regarding the NP toxicity on cutaneous bacteria. Of course, other phenomena still have
473 to be explored. For instance, it is well-known that even within a same species the results are
474 heterogeneous between strains. A given bacterial strain can modulate its surface charges and polarity
475 within a few minutes under the effect of environmental factors (Baumgarten et al., 2012). Moreover,

476 it is known that bacterial interactions are also driven by a multitude of adhesins (An and Friedman,
 477 1998).

478 **5. Conclusion**

479 In this study, we evaluated the impact of coated TiO₂-NPs on two cutaneous bacteria strains: *S. aureus* and *P. fluorescens*. To our knowledge, it is the first work dealing with the impact on bacteria of
 480 cosmetic grades of TiO₂-NPs with different surface natures and where, aging phenomena occurring
 481 during the cosmetic use were taken into consideration. For these purposes, the impact of TiO₂-NPs on
 482 bacteria was tested in multiple conditions, *i.e.* in fresh or aged formula and using native NPs or NPs
 483 extracted from these emulsions. In addition, two innovative exposure protocols were developed
 484 herein, close to the conditions encountered in emulsion or after spreading onto the skin surface. They
 485 allowed studying the impact of the NPs on the microbiological conservation of sunscreens as well as
 486 the safety of the NPs on two representative germs of the skin microbiota.

488 During the cosmetic storage, the presence of some NPs may significantly modify the emulsions
 489 properties, such as granulometry and pH. These phenomena could alter the microbiological
 490 conservation of the cosmetic towards potential pathogens. Then, once layered on skin, it was
 491 highlighted that the NP impact on bacteria highly depends on their surface characteristics, principally
 492 their polarity. Moreover, this work put emphasis on the role of the NP surface modifications during
 493 aging and highlighted that the latter had to be taken into account during the microbiological
 494 evaluations. The present surface characterizations are a first step but are not enough to fully
 495 understand the different phenomena involved and thus, in order to conclude on the nature of these
 496 modifications. In further works, their chemical nature needs to be elucidated to explain the evolution
 497 of NP properties during aging in emulsion.

498

499 **Acknowledgements**

500 This project is supported by the *Région Haute-Normandie* (*GRR SéSa*), the *Conseil Général de l'Eure*
 501 and *EU (FEDER)*. LR was recipient of a Doctoral fellowship from the *Région Haute-Normandie* (*GRR*
 502 *SéSa*). This research program is realized in the framework of the *PFMI Cosmétomique Haute-*
 503 *Normandie: Sureté, Innocuité des Produits Cosmétiques* (*PFMI cosmétomique SIP*) supported by the
 504 network *Cosmetic Valley* and of the *GDR CNRS Cosmactif*.

505

506

References

- 507 An, Y.H., Friedman, R.J., 1998. Concise review of mechanisms of bacterial adhesion to biomaterial
508 surfaces. *J. Biomed. Mater. Res.* 43, 338–348. doi:10.1002/(SICI)1097-
509 4636(199823)43:3<338::AID-JBM16>3.0.CO;2-B
- 510 André, V., Willenbacher, N., Debus, H., Börger, L., Fernandez, P., Frechen, T., Rieger, J., 2003.
511 Prediction of emulsion stability: facts and myth, *Cosmetics and Toiletries Manufacture*
512 Worldwide. ed. Aston Publishing Group.
- 513 Auffan, M., Pedeutour, M., Rose, J., Masion, A., Ziarelli, F., Borschneck, D., Chaneac, C., Botta, C.,
514 Chaurand, P., Labille, J., 2010. Structural degradation at the surface of a TiO₂-based
515 nanomaterial used in cosmetics. *Environ. Sci. Technol.* 44, 2689–2694.
516 doi:10.1021/es903767q
- 517 Baumgarten, T., Vazquez, J., Bastisch, C., Veron, W., Feuilloye, M.G.J., Nietzsche, S., Wick, L.Y.,
518 Heipeper, H.J., 2012. Alkanols and chlorophenols cause different physiological adaptive
519 responses on the level of cell surface properties and membrane vesicle formation in
520 *Pseudomonas putida* DOT-T1E. *Appl. Microbiol. Biotechnol.* 93, 837–845.
521 doi:10.1007/s00253-011-3442-9
- 522 Baysse, C., O'Gara, F., 2007. Role of Membrane Structure During Stress Signalling and Adaptation in
523 *Pseudomonas*, in: Ramos, J.-L., Filloux, A. (Eds.), *Pseudomonas: A Model System in Biology*.
524 Springer Netherlands, Dordrecht, pp. 193–224. doi:10.1007/978-1-4020-6097-7_7
- 525 Bellon-Fontaine, M.-N., Rault, J., van Oss, C.J., 1996. Microbial adhesion to solvents: a novel method
526 to determine the electron-donor/electron-acceptor or Lewis acid-base properties of
527 microbial cells. *Colloids Surf. B Biointerfaces* 7, 47–53. doi:10.1016/0927-7765(96)01272-6
- 528 Bergdoll, M.S., 1989. *Staphylococcus aureus*, in: *Foodborne Bacterial Pathogens*, Marcel Dekker Inc.
529 M.P. Doyle, pp. 463–523.
- 530 Brannan, D.K., Dille, J.C., 1990. Type of closure prevents microbial contamination of cosmetics during
531 consumer use. *Appl. Environ. Microbiol.* 56, 1476–1479.
- 532 Cao, Z., Zhang, Z., 2011. Deactivation of photocatalytically active ZnO nanoparticle and enhancement
533 of its compatibility with organic compounds by surface-capping with organically modified
534 silica. *Appl. Surf. Sci.* 257, 4151–4158. doi:10.1016/j.apsusc.2010.11.188
- 535 Chapalain, A., Rossignol, G., Lesouhaitier, O., Merieau, A., Gruffaz, C., Guerillon, J., Meyer, J.-M.,
536 Orange, N., Feuilloye, M., 2008. Comparative study of 7 fluorescent pseudomonad clinical
537 isolates (doi:) 54, 19–27. doi:10.1139/W07-110
- 538 Christensen, G.J.M., Brüggemann, H., 2014. Bacterial skin commensals and their role as host
539 guardians. *Benef. Microbes* 5, 201–215. doi:10.3920/BM2012.0062
- 540 Dunford, R., Salinaro, A., Cai, L., Serpone, N., Horikoshi, S., Hidaka, H., Knowland, J., 1997. Chemical
541 oxidation and DNA damage catalysed by inorganic sunscreen ingredients. *FEBS Lett.* 418, 87–
542 90. doi:10.1016/S0014-5793(97)01356-2
- 543 Egerton, T.A., Tooley, I.R., 2002. The surface characterisation of coated titanium dioxide by FTIR
544 spectroscopy of adsorbed nitrogen. *J. Mater. Chem.* 12, 1111–1117. doi:10.1039/b105903n
- 545 Grice, E.A., Kong, H.H., Renaud, G., Young, A.C., NISC Comparative Sequencing Program, Bouffard,
546 G.G., Blakesley, R.W., Wolfsberg, T.G., Turner, M.L., Segre, J.A., 2008. A diversity profile of
547 the human skin microbiota. *Genome Res.* 18, 1043–1050. doi:10.1101/gr.075549.107
- 548 Hamouda, T., Baker, J.R., 2000. Antimicrobial mechanism of action of surfactant lipid preparations in
549 enteric Gram-negative bacilli. *J. Appl. Microbiol.* 89, 397–403.
- 550 Hamouda, T., Mye, A., Donovan, B., Shih, A.Y., Reuter, J.D., Baker, J.R., 2001. A novel surfactant
551 nanoemulsion with a unique non-irritant topical antimicrobial activity against bacteria,
552 enveloped viruses and fungi. *Microbiol. Res.* 156, 1–7. doi:10.1078/0944-5013-00069
- 553 Hillion, M., Mijouin, L., Jouen, T., Barreau, M., Meunier, P., Lefevre, L., Lati, E., Chevalier, S.,
554 Feuilloye, M.G.J., 2013. Comparative study of normal and sensitive skin aerobic bacterial
555 populations. *MicrobiologyOpen* 2, 953–961. doi:10.1002/mbo3.138

- 556 INRS, 2014. La désinfection des surfaces en laboratoire de biologie [WWW Document]. URL
 557 <http://www.inrs.fr/dms/inrs/CataloguePapier/ED/TI-ED-6188/ed6188.pdf> (accessed
 558 9.24.15).
- 559 Kamat, J.P., Devasagayam, T.P.A., Priyadarsini, K.I., Mohan, H., 2000. Reactive oxygen species
 560 mediated membrane damage induced by fullerene derivatives and its possible biological
 561 implications. *Toxicology* 155, 55–61.
- 562 Kawaguchi, Y., Tanaka, H., Okada, T., Konishi, H., Takahashi, M., Ito, M., Asai, J., 1997. Effect of
 563 reactive oxygen species on the elastin mRNA expression in cultured human dermal
 564 fibroblasts. *Free Radic. Biol. Med.* 23, 162–165.
- 565 Labille, J., Feng, J., Botta, C., Borschneck, D., Sammut, M., Cabie, M., Auffan, M., Rose, J., Bottero, J.-
 566 Y., 2010. Aging of TiO₂ nanocomposites used in sunscreen. Dispersion and fate of the
 567 degradation products in aqueous environment. *Environ. Pollut.* 158, 3482–3489.
 568 doi:10.1016/j.envpol.2010.02.012
- 569 Ly, M.H., Nataili-Bouchez, M., Meylheuc, T., Bellon-Fontaine, M.-N., Le, T.M., Belin, J.-M., Waché, Y.,
 570 2006. Importance of bacterial surface properties to control the stability of emulsions. *Int. J.*
 571 *Microbiol.* 112, 26–34. doi:10.1016/j.ijfoodmicro.2006.05.022
- 572 Mijouin, L., Hillion, M., Ramdani, Y., Jaouen, T., Duclairoir-Poc, C., Follet-Gueye, M.-L., Lati, E.,
 573 Yvergniaux, F., Driouch, A., Lefevre, L., Farmer, C., Misery, L., Feuilloley, M.G.J., 2013. Effects
 574 of a skin neuropeptide (substance P) on cutaneous microflora. *PLoS ONE* 8, e78773.
 575 doi:10.1371/journal.pone.0078773
- 576 Nischwitz, V., Goenaga-Infante, H., 2012. Improved sample preparation and quality control for the
 577 characterisation of titanium dioxide nanoparticles in sunscreens using flow field flow
 578 fractionation on-line with inductively coupled plasma mass spectrometry. *J. Anal. At.*
 579 *Spectrom.* 27, 1084–1092. doi:10.1039/c2ja10387g
- 580 Owens, D.K., Wendt, R.C., 1969. Estimation of the surface free energy of polymers. *J. Appl. Polym.*
 581 *Sci.* 13, 1741–1747.
- 582 Percival, S.L., Emanuel, C., Cutting, K.F., Williams, D.W., 2012. Microbiology of the skin and the role of
 583 biofilms in infection. *Int. Wound J.* 9, 14–32.
- 584 Rhodes, L.E., Diffey, B.L., 1997. Fluorescence spectroscopy: a rapid, noninvasive method for
 585 measurement of skin surface thickness of topical agents. *Br. J. Dermatol.* 136, 12–17.
- 586 Rossano, M., 2014. Ph.D thesis: Utilisation des nanoparticules de dioxyde de titane dans les
 587 émulsions cosmétiques : impact sur la santé humaine et l'environnement. Université du
 588 Havre, Le Havre.
- 589 Rowenczyk, L., Picard, C., Duclairoir-Poc, C., Hucher, N., Orange, N., Feuilloley, M., Grisel, M., 2016.
 590 Development of preservative-free nanoparticles-based emulsions: Effects of NP surface
 591 properties and sterilization process. *Int. J. Pharm.* 510, 125–134.
 592 doi:10.1016/j.ijpharm.2016.06.014
- 593 Serpone, N., Salinaro, A., Hirikoshi, S., Hidaka, H., 2006. Beneficial effects of photo-inactive titanium
 594 dioxide specimens on plasmid DNA, human cells and yeast cells exposed to UVA/UVB
 595 simulated sunlight. *J. Photochem. Photobiol. Chem.* 179, 200–212.
 596 doi:10.1016/j.jphotochem.2005.08.017
- 597 Sivakumar, P.M., Iyer, G., Natesan, L., Doble, M., 2010. 3'-Hydroxy-4-methoxychalcone as a potential
 598 antibacterial coating on polymeric biomaterials. *Appl. Surf. Sci.* 256, 6018–6024.
 599 doi:10.1016/j.apsusc.2010.03.112
- 600 Sutherland, J.P., Bayliss, A.J., Roberts, T.A., 1994. Predictive modelling of growth of *Staphylococcus*
 601 *aureus*: the effects of temperature, pH and sodium chloride. *Int. J. Food Microbiol.* 21, 217–
 602 236.
- 603 Taylor, D., Daulby, A., Grimshaw, S., James, G., Mercer, J., Vaziri, S., 2003. Characterization of the
 604 microflora of the human axilla. *Int. J. Cosmet. Sci.* 25, 137–145.
- 605 Teixeira, P.C., Leite, G.M., Domingues, R.J., Silva, J., Gibbs, P.A., Ferreira, J.P., 2007. Antimicrobial
 606 effects of a microemulsion and a nanoemulsion on enteric and other pathogens and
 607 biofilms. *Int. J. Food Microbiol.* 118, 15–19. doi:10.1016/j.ijfoodmicro.2007.05.008

P30

IMPACT OF GASEOUS NO₂ ON *P. FLUORESCENS* STRAIN IN THE MEMBRANE ADAPTATION AND VIRULENCE

SÉGOLÈNE DEPAYRAS¹, TATIANA KONDAKOVA², NADINE MERLET-MACHOUR³, HERMANN J. HEIPPEL⁴, MAGALIE BARREAU¹, CHLOÉ CATOVIC¹, MARC FEUILLOLEY¹, NICOLE ORANGE¹ & CÉCILE DUCLAIR-POC¹

¹Laboratory of Microbiology Signals and Microenvironment, LMSM EA 4312, University of Rouen, France

²Cronan Lab, Department of Microbiology, University of Illinois, Urbana

³Laboratory of Organic and analytical chemistry, COBRA UMR 6014, Team 1, University of Rouen, France

⁴Microbial Processes Group, Department Environmental Biotechnology, UFZ Helmholtz Centre for Environmental Research, Germany

ABSTRACT

Nowadays air pollution is increasing due to anthropogenic activity. Among all air pollutants, nitrogen oxides (NOx) such as NO₂ are predominant. It is well known that those compounds exhibit direct toxic effects on human health. However, microorganisms are also exposed to them, but the effect of NOx on the virulence of air microbiota is still poorly understood. In this study, we evaluated the impact of NO₂ on the adaptability and virulence of an airborne strain of *P. fluorescens*, MFA76a, by exposition of this strain to 45 ppm of NO₂. The growth kinetics and cultivability were analysed. A decrease of cultivability coupled with an increase of the lag phase was observed suggesting a potential toxicity of NO₂. Since NOx particularly target lipids, the membrane permeability was assessed thanks to Live Dead tests and confocal microscopy. A significant alteration of membrane permeability was observed. Furthermore, more abundant bacterial aggregates were detected compared to the control. Thus, a lipidomic study was performed using MALDI-TOF MS Imaging coupled to HPTLC. Interestingly, bacteria exposed to NO₂ were lacking one putative glycerophospholipid molecule. In agreement with a previous study from Kondakova et al., these data demonstrate the adaptation potential of *P. fluorescens* MFA76a to an air pollutant such as NO₂.

Keywords: air pollution, antibiotic resistance, membrane, adaptation, *P. fluorescens*, toxicity.

1 INTRODUCTION

Air is a complex environment contaminated by particle matter, nitrogen oxides, ozone and hydrocarbons. It is also a biotic environment since microorganisms, mostly bacteria, are found [1]. Even if this environment is unstable, several studies highlight the presence of members of *Pseudomonas* strain in air microbiota [2, 3]. During the past decades, due to the increase of anthropogenic activities, the level of atmospheric pollutants is rising and the control of air quality remains a topic of major interest [4, 5]. Among all air pollutants, nitrogen oxides species, including nitrogen oxide (NO) and nitrogen dioxide (NO₂), are predominant [4]. It is well known that these compounds are toxic to human health, leading to cardiovascular and respiratory pathologies (allergy, asthma, bronchitis) [4, 5]. Thus, threshold values were set up by World Health Organization (WHO) to prevent the potential risks on human health. Regarding the increase of respiratory pathologies, a potential impact of NO₂ could be presumed on air microbiota. NO₂ induces cells damages, directly by interacting with proteins, DNA and lipids or either via formation of reactive nitrogen species interfering with metabolism, respiration functions and thus homeostasis [6–8]. Bacterial stress is generally leading to the expression of virulence factors; thus, NO₂ may have an impact on bacterial virulence, which could consequently alter human health. Infection by opportunistic pathogens represents a big threat for immune-compromised or cystic fibrosis patients as they are more sensitive. Indeed, this pathogens could alter the healthy microbiota and its homeostasis [9–11].

This dysbiosis and the pathogen itself could lead to an acute infection with potential lethal outcome [10]. Breathing NO₂-polluted air could potentiate this mechanism. Since *P. fluorescens* are widespread in the environment [12], including in the air [13], and had already been isolated from sputum of patients suffering from pneumonia, it seems particularly interesting to focus on this species [14]. An airborne strain *P. fluorescens* MFAF76a was previously isolated and characterized with virulent traits [13, 14]. Thus, MFAF76a seems to be the perfect candidate to test the bacterial response to NO₂ stress. Its membrane adaptability and virulence response to NO₂ contamination remain to be resolved. Therefore, several approaches were implemented in this study such as physiological tests and lipidomic analysis.

2 MATERIAL AND METHOD

2.1 Bacterial strain and growth condition

In this study, the wild-type *P. fluorescens* MFAF76a strain was used [13]. Overnight cultures in Luria Bertani medium (LB, AES) were grown at 28°C under limited agitation (180 rpm). Then cultures were diluted ($A_{580} = 0.08$) in Davis Medium Broth (DMB), a minimal medium with 2.16 g/L glucose as carbon source. The incubation was done at 28°C under agitation for 16 h to reach the stationary phase. Bacterial cultures were transferred on cellulose nitrate membrane filters (0.45 µm, pore size 0.2 µm, diameter 47 mm, Sartorius Biolab Products) and incubated on DMB agar plates at 28°C for 4 h to obtain a monolayer of bacteria. Then the membranes covered by bacteria were laid on agar one-well dishes (size 127.8 × 85.5 mm, Thermo Scientific Nunc), which were directly transferred into the gas delivery device [15].

2.2 Exposition to nitrogen dioxide

As previously described by Kondakova et al., an exposure system was developed in order to mimic the environmental exposition [15]. Briefly bacterial bed was exposed during 2 h at 28°C with a constant gas stream of 2 L/min, in two separate exposure chambers. A control was obtained using synthetic air. The NO₂-exposed bacteria were laid in contact with a mixture of N₂/O₂ 8/2 (v/v) complemented with 45 ppm of NO₂ (Air Liquide GMP Europe). After exposure, bacteria were resuspended in sterile saline solution.

2.3 Cultivability and growth kinetics

Cultivability tests were performed by serial dilution in saline solution from the bacterial suspension to reach dilution of 10⁻⁷. 100 µL of dilution range 10⁻⁴ to 10⁻⁷ were spotted onto LB agar plates in triplicate for both conditions. After incubation at 28°C for 24 h, viable colony forming unit were numerated.

After adjustment of the bacterial concentration to $A_{580} = 0.08$ in DMB, growth kinetics were done for both conditions in triplicate in a 96-well test plate (NuncTM). The bacterial population was evaluated every 15 min by turbidimetry at A_{580} during 24 h.

2.4 Lipid identification

2.4.1 Phospholipids

As previously described by Kondakova et al. [16], the lipids were extracted from lyophilized bacteria according to the method of Bligh and Dyer [17]. Then phospholipids (PLs) were first separated by HPTLC [18]. Retention factors (R_f) were calculated using the Sweday JustTLC

software (v. 4.0.3) after visualizing spots at 365 nm thanks to staining with primuline dye spray. A DHB matrix, allowing the positive ion spectra of lipids, was selected [16]. MALDI TOF mass spectra were acquired using an Autoflex III (Bruker Daltonics) and all MS spectra were obtained in reflector positive ion mode using TLC MALDI software (v. 1.1.7.0). Post-Source Decay spectra were acquired as previously described using FlexControl software (Bruker Daltonics) for each spot related to one specific lipid [16]. Lipids were identified using the LIPID MAPS database. Thanks to previous results, the MS Imaging of lipid spots was obtained using the FlexImaging software (v. 2.1.; Bruker Daltonics). According to the m/z, individual lipidic spots were labelled by a specific colour code.

2.4.2 Fatty acids

The fatty acids (FAs) methyl esters (FAME) were obtained by incubation for 15 min at 95°C in a boron trifluoride (BF_3 , 140 g/L) in methanol and extracted by hexane [19]. They were separated and analysed by gas chromatography (GC) coupled to flame ionization detection using an Agilent Technology, 6890 Network GC System. The apparatus was equipped with a CP-Sil 88 capillary column (Chrompack; length, 50 m; inner diameter, 0.25 mm; 0.25 mm film). All experiments were performed in triplicate. The degree of FAs saturation was determined as the ratio between the saturated FAs and the unsaturated FAs [20].

2.5 Microbial adhesion to solvent

The hydrophobicity of *P. fluorescens* MFAF76a strain was evaluated by the microbial adhesion to solvent (MATS) test [21]. It consisted of assessing the affinity of the cells to two solvent duos composed of a monopolar solvent and an apolar solvent. In each set, both solvents have similar surface tension, but the monopolar one was acidic (electron accepting, e.g. chloroform) or basic (electron donor, e.g. ethyl acetate). The apolar solvents were hexadecane and decane, respectively. For the experiments, bacterial cells were resuspended in saline solution to $A_{400} = 0.8$ (Abs_1). This bacterial suspension was mixed with each solvent at 1/6 (v/v) by vigorous agitation for 1 min to form an emulsion. After at least 15 min of delay, the separation of the two phases of the mixture occurred. The aqueous phase absorbance (Abs_2) was measured and the percentage of adhesion was expressed as in eqn (1):

$$\% \text{ affinity} = 1 - \frac{\text{Abs}_1}{\text{Abs}_2} \times 100 \quad (1)$$

2.6 Membrane permeability assays

After exposure, 1 mL of bacterial suspension was stained for 15 min with SYTO9 (5.01 nM) and propidium iodide (PI, 30 nM) from the Live/Dead BacLight kit (L-7012, Thermo Fisher). Prolong diamond (P36965, Thermo Fisher) was added as anti-fading agent before observation using a confocal laser scanning microscope (CLSM 710, ZEISS). Thence, with an immersion objective $\times 63$, damaged and total bacteria were respectively observed as PI and SYTO9 positive.

2.7 Statistical analysis

All experiments were carried out at least three times. Significances of differences between mean values were assessed using the Mann-Whitney test with significance set at $p < 0.05$ (*), < 0.01 (**), and < 0.001 (***)�.

3 RESULTS AND DISCUSSION

To investigate the response of air microbiota on the NO_2 air pollutant, the bacterial strain *P. fluorescens* MFAF76a was exposed to 45 ppm of NO_2 for 2 h. After exposure, several physiological tests including cultivability and growth kinetics, as well as membrane permeability and lipidomic studies were done. The results were compared with those of a control samples, coming from the same bacterial culture exposed similarly to synthetic air. In NO_2 -treated bacteria, a decrease of one log in cultivability of *P. fluorescens* MFAF76a strain was observed (Fig. 1a). Moreover, the exposure promoted an increase of half an hour of the lag phase compared with the control and no significant variation of generation time (Fig. 1b). Altogether these results suggested a diminution of the culturable bacterial density after exposure. The A_{580} do not reflect the culturable bacterial concentration. Two hypotheses could be proposed to explain such a phenomenon. The exposure to NO_2 seems to enhance the apparition of viable but non-culturable bacteria and/or the bacterial death. Moreover the treatment to NO_2 could also impact the bacterial physiology since they need to detoxify this compound first. Thence all those factors could promote the delay previously discussed. However, the generation time was not significantly impacted. This data suggest no great alteration in metabolic pathway implicated in cell division. An exposure at 45 ppm of NO_2 clearly impacts the physiological behaviour of *P. fluorescens* MFAF76a strain.

Since the membrane is the first barrier protecting bacteria from their environment, a macroscopic study by MATS technique was realized to assess the surface polarity and thence potential membrane alteration of exposed bacteria. The bacterial affinity to chloroform and hexadecane indicated no significant change in Lewis base character after exposure to NO_2 (Fig. 2). This parameter is related to the presence of lone pair usually found in unsaturations or around heteroatoms such as constituting proteins or polar head of glycerophospholipids. As no drastic modification in hydrophobicity was observed, the proteins should not be implicated. However, a decrease in acidity of Lewis (affinity relative to decane and ethyl acetate) from bacteria exposed to NO_2 was noticed and could suggest fewer electron pair acceptors

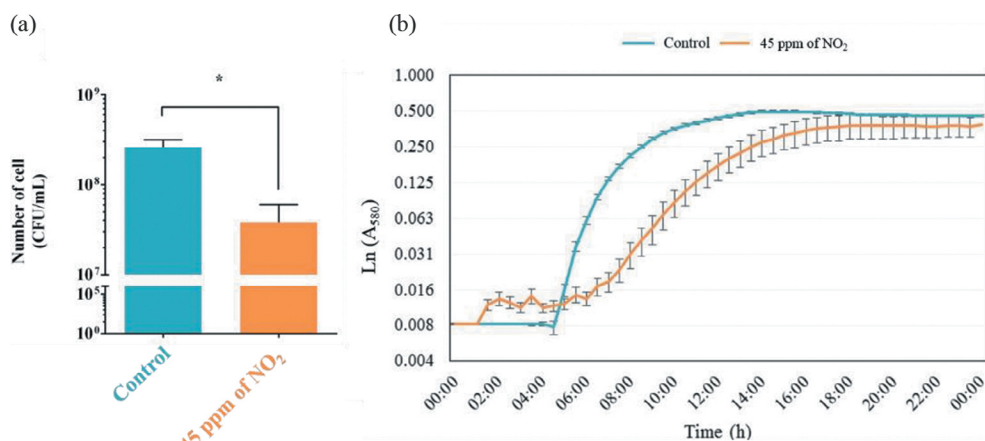


Figure 1: Physiological response of *P. fluorescens* MFAF76a strain after two hours' exposure at 45 ppm of NO_2 . (a) Bacterial cultivability. (b) Bacterial growth kinetics in DMB, a minimal medium. For each exposure condition, three independent experiments were done in three replicates.

NO ₂ concentration (ppm)	MATS : solvent affinity (%)			
	Chloroform	Hexadecane	Decane	Ethyl acetate
0	62 ± 10	10 ± 8	4 ± 3	24 ± 10
45	41 ± 10	0 ± 6	4 ± 4	1 ± 1

Figure 2: Microbial adhesion to solvent tests of *P. fluorescens* MFAF76a strain after exposed or not to NO₂. For each exposure condition, three independent experiments were done in three replicates.

outwards the membrane. These alterations reveal slight changes within the bacterial membrane, which could be limited in composition, but more surely in structure. A combination of both may also be possible. For instance, alkyl chains may swivel outwards burying electron pair acceptors inside membrane.

To better understand the nature of that membrane alteration, lipids extraction and identification using HPTLC-MALDI TOF MS were performed after exposure (Fig. 3). Indeed phosphatidylglycerol (PG), phosphatidylethanolamin (PE) and phosphatidylcholin (PC) were found in both extracts (Figs 3a and 3b). Those results are coherent with previous data [16]. Interestingly, a putative glycerophospholipid named ‘unknown glycerophospholipid’ (UGP) was identified in this study. This putative PL was only observed in control bacteria exposed to synthetic air and was absent in NO₂-treated cells, indicating its probable sensitivity to NO₂ and/or membrane

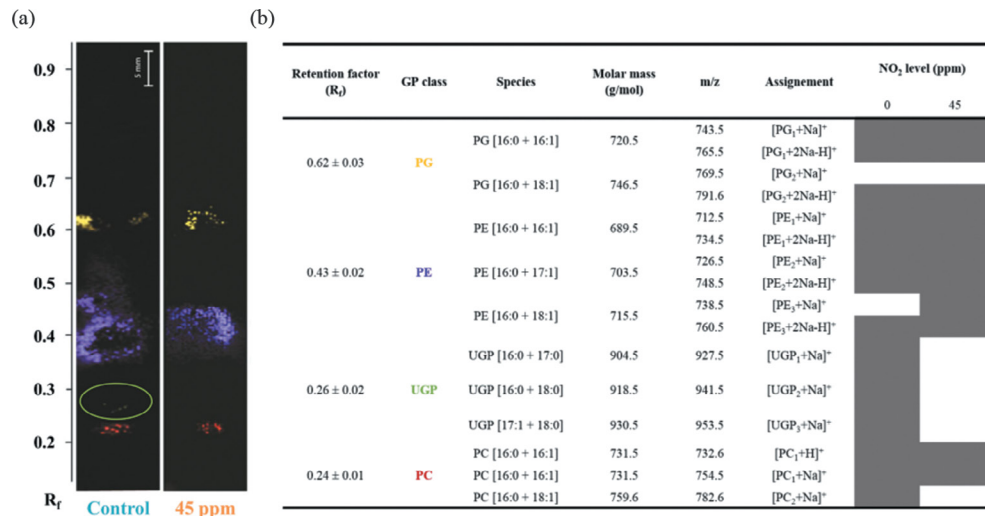


Figure 3: Lipidome of *P. fluorescens* MFAF76a strain after exposure or not to NO₂. (a) HPTLC MALDI-TOF MS Image of their glycerophospholipids. (b) List of glycerophospholipids identified. PG: Phosphatidylglycerol (yellow spot); PE: Phosphatidylethanolamin (purple spot), UGP: Unknown glycerophospholipid (green spot, circle in green), PC: Phosphatidylcholin (red spot), R_f: Retention factor. For each exposure condition, three independent experiments were done in three replicates.

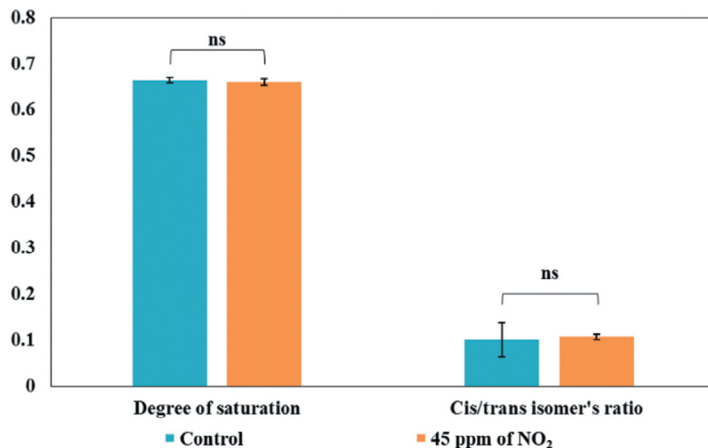


Figure 4: Fatty acid methyl esterification of *P. fluorescens* MFAF76a strain after exposition to NO₂ or synthetic air (control). For each exposure condition, three independent experiments were done in three replicates; ns: not significant.

adaptation of MFAF76A to this stress, by exclusion of this PL from the cell wall. We noted that the long FA chains of this UGP (C₁₆, C₁₇ and C₁₈) were mostly saturated. Such saturated lipids favour the membrane fluidity. Thence the absence of UGP in exposed bacteria is suggesting a decrease of membrane fluidity. However, after FAME analysis, no significant alteration in the degree of FA saturation and cis/trans isomers ratio was detected (Fig. 4). We hypothesized that bacteria, in response to the lack of UGP after exposure to NO₂, reorganizes the membrane to compensate this loss, suggesting a potential membrane adaptation to NO₂ stress.

In order to investigate potential changes of membrane permeability, Live Dead tests using SYTO9 (green) and IP (red) labels were performed and analysed using CLSM. Interestingly, the red labelling was predominant after exposure to NO₂ unlike the control (Fig. 5). IP dye entered largely in bacterial cells revealing membrane permeabilization. NO₂ alters polyunsaturated lipids through production of nitro alkyl radicals in eukaryotic cells but no literature deals on NO₂ effect on bacterial lipids [8].

An increase of cell aggregation was also observed and it is interesting to note that deletion of the main outer membrane porin OprF, which induces a parietal stress, is known to promote a similar effect in *P. aeruginosa* H103 [21]. Then the bacterial ‘community behaviour’ was investigated through biofilm formation using CLSM and a CFP-labelled *P. fluorescens* MFAF76a strain. Exposed bacteria form a thicker biofilm with some heterogeneities certainly due to the presence of bacterial amasses unlike the control [15]. This phenomenon was also observed with the oprF mutant in *P. aeruginosa* H103 [22]. Thus, the exposure to NO₂ may lead to membrane modification causing a parietal stress to *P. fluorescens* MFAF76a. Subsequently, the aggregation of the bacterial cells could promote the biofilm formation and so the bacterial survival.

Biofilms represent a threat in clinic, as their elimination is more and more challenging. Interestingly, a previous study evaluated the impact of NO₂ on antibiotic resistance using ciprofloxacin and chloramphenicol [15]. Such antibiotics are usually prescribed respectively for treatment of first and last stage of cystic fibrosis to eradicate *Pseudomonas* infection [23]. For the NO₂-treated bacteria a two-fold increase in MICs of both antibiotics was noted, indicating that in response to NO₂, *P. fluorescens* exhibits an increase in resistance against

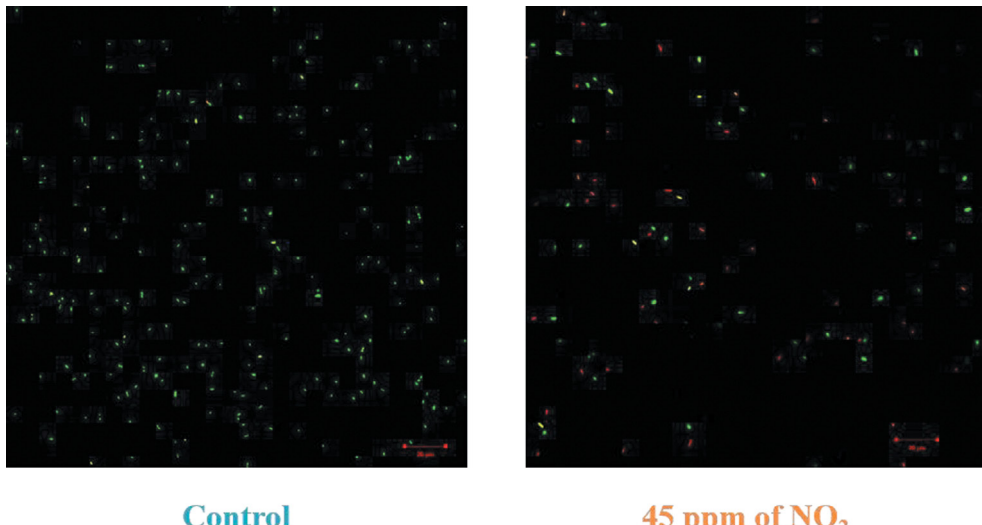


Figure 5: Membrane permeability using Live Dead test and CLSM. Green and red labels signify penetration in bacteria of SYTO9 and Propidium Iodide, respectively. For each exposure condition, three independent experiments were done in three replicates.

chloramphenicol and ciprofloxacin [15]. Surprisingly, a sub-inhibitory concentration of chloramphenicol (25 µg/mL) significantly increased the bacterial growth between 2 and 10 h of culture compared to the control. Thence a protective effect of NO₂ is conserved for 10 h after exposure. On the contrary, the growth kinetics of the exposed strain was unchanged in presence of a sub-inhibitory concentration of ciprofloxacin (3.125 µg/mL) [15]. Various stresses can lead to the modulation of bacterial resistance to antibiotics [24, 25]. Astonishingly, new therapeutic strategies are focusing nowadays on the use of gaseous nitrogen oxide as a pre-treatment to decrease the antibiotic resistance encountered in cystic fibrosis patients [26].

In correlation with previous data, a transcriptomic study on genes encoding efflux pump *mexEF-oprN* revealed a significant increase in the expression for those genes [15]. Indeed, in comparison to the controls, the expression of *mexE*, *mexF* and *oprN* genes reached almost 14-, 3.5- and 4.6-fold, respectively. These results are consistent with the antibiotic tests realized previously since the MexEF-OprN efflux pump is involved in the resistance against fluoroquinolones (such as ciprofloxacin). Moreover chloramphenicol, a nitroaromatic antimicrobial, is also a substrate for MexEF-OprN [27, 28].

As this efflux pump is a macromolecular complex enmeshed into the plasma membrane, MexEF-OprN could replace UGP to preserve the membrane integrity. Moreover, this efflux pump implements the entry of proton (H⁺), which may alter the membrane potential. Indeed H⁺ could be accumulated and, consequently, increase the positive charges within cells. Thence the alteration of the potential equilibrium may favour the increase of membrane potential. Thus, the bacterial physiology may be disturbed causing dysfunction of membrane proteins operating through this membrane potential. Indeed a decrease in membrane potential was linked with the susceptibility of *P. aeruginosa* to aminoglycosides antibiotics such as tobramycin [29]. Moreover, this H⁺ gradient could lead to a reorganization of PLs, such as a swivelling of alkyl chains outwards, which could justify the Lewis base alteration.

4 CONCLUSION

The present study provides further information concerning the adaptation of an airborne strain of *P. fluorescens* strain, with opportunistic pathogen potential behaviour, to an air pollutant such as NO₂. The bacterial stress caused by this preoccupant air pollutant induces modifications in membrane permeability certainly because of chemical and/or structural variations of cell wall constituents. Thus physiological parameters such as cultivability and growth are negatively impacted. However, the ability of the bacterium to form biofilm increases, certainly favoured by the observed bacterial amasses promoted by the parietal stress. Unfortunately, resistance to fluoroquinolone and phenicol antibiotics increases after exposure to NO₂. Those latter parameters are quiet worrying since they are implicated in bacterial virulence. However, 45 ppm of NO₂ is considered as a high concentration leading to irreversible effects on human health and does not totally reflect usual environmental concentrations measured in chronic pollution rates [29]. The next step of this project will be to focus on a lower concentration of NO₂ close to the threshold alert value [30]. Nevertheless, NO₂ has clearly a drastic impact on the physiology of *P. fluorescens* MFAF76a and these results support the hypothesis that air pollutants could promote the pathogenicity of airborne bacteria.

ACKNOWLEDGMENTS

This study was supported by a PhD grant from the GRR SESA (Région Normandie) and was financially supported by the European Union (FEDER), Région Normandie and Évreux Porte de Normandie (France).

REFERENCES

- [1] DeLeon-Rodriguez, N., Lathem, T.L., Rodriguez-R. L.M., Barazesh, J.M., Anderson, B.E. et al., Microbiome of the upper troposphere: species composition and prevalence, effects of tropical storms, and atmospheric implications. *Proceedings of the National Academy of Sciences of the United States of America*, **110**(7), pp. 2575–2580, 2013. DOI: [10.1038/ismej.2011.11](https://doi.org/10.1038/ismej.2011.11).
- [2] Dybwad, M., Granum, P. E., Bruheim, P. & Blatny, J. M., Characterization of airborne bacteria at an underground subway station. *Applied and Environmental Microbiology*, **78**(6), pp. 1917–1929, 2012. DOI: [10.1128/AEM.07212-11](https://doi.org/10.1128/AEM.07212-11).
- [3] Šantl-Temkiv, T., Sahyoun, M., Finster, K., Hartmann, S., Augustin-Bauditz, S. et al., Characterization of airborne ice-nucleation-active bacteria and bacterial fragments. *Atmospheric Environment*, **109**, 105–117, 2015. DOI: [10.1016/j.atmosenv.2015.02.060](https://doi.org/10.1016/j.atmosenv.2015.02.060).
- [4] World Health Organization, World Health Organization (WHO) guidelines for indoor air quality: selected pollutants (2010), Europe, http://www.euro.who.int/__data/assets/pdf_file/0009/128169/e94535.pdf (accessed 10 April 2017).
- [5] European Environment Agency, Air quality in Europe – 2015 report, <http://www.eea.europa.eu/publications/air-quality-in-europe-2015#tab-data-references> (accessed 30 November 2015).
- [6] Burney, S., Caulfield, J.L., Niles, J.C., Wishnok, J.S., Tannenbaum, S.R., The chemistry of DNA damage from nitric oxide and peroxy nitrite. *Mutation Research*, **424**(1–2), pp. 37–49, 1999. DOI: [10.1016/S0027-5107\(99\)00006-8](https://doi.org/10.1016/S0027-5107(99)00006-8).
- [7] Radi, R., Nitric oxide, oxidants, and protein tyrosine nitration. *Proceedings of the National Academy of Sciences of the United States of America (PNAS)*, **101**(12), pp. 4003–4008, 2004. DOI: [10.1038/84859](https://doi.org/10.1038/84859).
- [8] Augusto, O., Bonini, M.G., Amanso, A.M., Linares, E., Santosn, C.C.X. et al., Nitrogen dioxide and carbonate radical anion: Two emerging radicals in biology. *Free Radical Biology & Medicine*, **32**(9), pp. 841–859, 2002. DOI: [10.1016/S0891-5849\(02\)00786-4](https://doi.org/10.1016/S0891-5849(02)00786-4).

- [9] Harrison, F., Microbial ecology of the cystic fibrosis lung. *Microbiology*, **153(Pt 4)**, pp. 917–923, 2007. DOI: [10.1099/mic.0.2006/004077-0](https://doi.org/10.1099/mic.0.2006/004077-0).
- [10] Cullen, L. & McClean, S., Bacterial adaptation during chronic respiratory infections. *Pathogens*, **4**(1), pp. 66–89, 2015. DOI: [10.1074/jbc.R110.199703](https://doi.org/10.1074/jbc.R110.199703).
- [11] Cribbs, S.K. & Beck, J.M., Microbiome in the pathogenesis of cystic fibrosis and lung transplant-related disease. *Translational Research*, **179**, pp. 84–96, 2017. DOI: [10.1016/j.trsl.2016.07.022](https://doi.org/10.1016/j.trsl.2016.07.022).
- [12] Bodilis, J., Calbrix, R., Guérillon, J., Mérieau, A., Pawlak, B. et al., Phylogenetic relationships between environmental and clinical isolates of *Pseudomonas fluorescens* and related species deduced from 16S rRNA gene and OprF protein sequences. *Systematic and Applied Microbiology*, **27**(1), pp. 93–108, 2004. DOI: [10.1078/0723-2020-00253](https://doi.org/10.1078/0723-2020-00253).
- [13] Duclairoir Poc, C., Verdon, J., Groboillot, A., Barreau, M., Toucourou, H. et al., Air-borne fluorescent pseudomonads : What potential for virulence? *International Journal of Current Microbiology and Applied Sciences*, **3**(8), pp. 708–722, 2014. ISSN: 2319-7706.
- [14] Rossignol, G., Mérieau, A., Guerillon, J., Veron, W., Lesouhaitier, O. et al., Involvement of a phospholipase C in the hemolytic activity of a clinical strain of *Pseudomonas fluorescens*. *BMC Microbiology*, **8**, pp. 189, 2008. DOI: [10.1186/1471-2180-8-189](https://doi.org/10.1186/1471-2180-8-189).
- [15] Kondakova, T., Catovic, C., Barreau, M., Nusser, M., Brenner-Weiss, G. et al., Response to gaseous NO₂ air pollutant of *P. fluorescens* airborne strain MFAF76a and clinical strain MFN1032. *Frontiers in Microbiology*, **7**, pp. 379, 2016. DOI: [10.1186/1471-2180-13-92](https://doi.org/10.1186/1471-2180-13-92).
- [16] Kondakova, T., Merlet-Machour, N., Chapelle, M., Preterre, D., Dionnet, F. et al., A new study of the bacterial lipidome: HPTLC-MALDI-TOF imaging enlightening the presence of phosphatidylcholine in airborne *Pseudomonas fluorescens* MFAF76a. *Research in Microbiology*, **166**(1), pp. 1–8, 2015. DOI: [10.1016/j.resmic.2014.11.003](https://doi.org/10.1016/j.resmic.2014.11.003).
- [17] Bligh, E.G. & Dyer, W.J., A rapid method of total lipid extraction and purification. *Canadian Journal of Biochemistry and Physiology*, **37**(8), pp. 911–917, 1959. DOI: [10.1139/o59-099](https://doi.org/10.1139/o59-099).
- [18] Fuchs, B., Schiller, J., Süß, R., Schürenberg, M., Suckau, D., A direct and simple method of coupling matrix-assisted laser desorption and ionization time-of-flight mass spectrometry (MALDI-TOF MS) to thin-layer chromatography (TLC) for the analysis of phospholipids from egg yolk. *Analytical and Bioanalytical Chemistry*, **389**(3), pp. 827–834, 2007. DOI: [10.1007/s00216-007-1488-4](https://doi.org/10.1007/s00216-007-1488-4).
- [19] Morrison, W. & Smith, L., Preparation of fatty acid methyl esters and dimethylacetals from lipids with boron fluoride-methanol. *Journal of Lipid Research*, **5**, pp. 600–608, 1954.
- [20] Heipieper, H.J., Meulenbeld, G., van Oirschot, Q. & de Bont, J., Effect of environmental factors on the trans/cis ratio of unsaturated fatty acids in *Pseudomonas putida* S12. *Applied and Environmental Microbiology*, **62**(8), pp. 2773–2777, 1996.
- [21] Bellon-Fontaine, M.-N., Rault, J., van Oss, C.J., Microbial adhesion to solvents: a novel method to determine the electron-donor/electron-acceptor or Lewis acid-base properties of microbial cells. *Colloids Surfaces B: Biointerfaces*, **7**(1–2), pp. 47–53, 1996. DOI: [10.1016/0927-7765\(96\)01272-6](https://doi.org/10.1016/0927-7765(96)01272-6).
- [22] Bouffartigues, E., Moscoso, J.A., Duchesne, R., Rosay, T., Fito-Boncompte, L. et al., The absence of the *Pseudomonas aeruginosa* OprF protein leads to increased biofilm formation through variation in c-di-GMP level. *Frontiers in Microbiology*, **6**, pp. 630, 2015. DOI: [10.3389/fmicb.2015.00630](https://doi.org/10.3389/fmicb.2015.00630).

- [23] Banerjee, D. & Stableforth, D., The treatment of respiratory *pseudomonas* infection in cystic fibrosis: what drug and which way? *Drugs*, **60**(5), pp. 1053–1064, 2000. DOI: [10.2165/00003495-200060050-00006](https://doi.org/10.2165/00003495-200060050-00006).
- [24] Poole, K., Stress responses as determinants of antimicrobial resistance in Gram-negative bacteria. *Trends in Microbiology*, **20**(5), pp. 227–234, 2012. DOI: [10.1016/j.tim.2012.02.004](https://doi.org/10.1016/j.tim.2012.02.004).
- [25] Poole, K., Stress responses as determinants of antimicrobial resistance in *Pseudomonas aeruginosa*: multidrug efflux and more. *Canadian Journal of Microbiology*, **60**(12), pp. 783–791, 2014. DOI: [10.1139/cjm-2014-0666](https://doi.org/10.1139/cjm-2014-0666).
- [26] Deppisch, C., Herrmann, G., Graepler-Mainka, U., Wirtz, H., Heyder, S. et al., Gaseous nitric oxide to treat antibiotic resistant bacterial and fungal lung infections in patients with cystic fibrosis: a phase I clinical study. *Infection*, **44**(4), pp. 513–520, 2016. DOI: [10.1371/journal.pone.0011044](https://doi.org/10.1371/journal.pone.0011044).
- [27] Köhler, T., Michéa-Hamzehpour, M., Henze, U., Gotoh, N., Curty, L.K. et al., Characterization of MexE-MexF-OprN, a positively regulated multidrug efflux system of *Pseudomonas aeruginosa*. *Molecular Microbiology*, **23**(2), pp. 345–354, 1997. DOI: [10.1046/j.1365-2958.1997.2281594.x](https://doi.org/10.1046/j.1365-2958.1997.2281594.x).
- [28] Sobel, M.L., Neshat, S., Poole, K., Mutations in PA2491 (mexS) promote MexT-dependent mexEF-oprN expression and multidrug resistance in a clinical strain of *Pseudomonas aeruginosa*. *Journal of Bacteriol*, **187**(4), pp. 1246–1253, 2005. DOI: [10.1128/JB.187.4.1246-1253.2005](https://doi.org/10.1128/JB.187.4.1246-1253.2005).
- [29] Pan, X., Dong, Y., Fan, Z., Liu, C., Xia, B. et al., In vivo host environment alters *Pseudomonas aeruginosa* susceptibility to aminoglycoside antibiotics. *Frontiers in Cellular and Infection Microbiology*, **7**, pp. 83, 2017. DOI: [10.1128/AAC.46.6.2035-2037.2002](https://doi.org/10.1128/AAC.46.6.2035-2037.2002).
- [30] Dioxyde d'azote: Données toxicologiques et environnementales, INERIS, 2011, <http://www.ineris.fr/substances/fr/substance/cas/10102-44-0/2> (accessed 2 March 2010).

Chapitres de livre

Ch1

Creation of Biopolymeric Colloidal Carriers Dedicated to Controlled Release Applications

Denis Renard,¹ Paul Robert,¹ Laurence Lavenant,¹ Dominique Melcion,¹ Yves Popineau,¹ Jacques Guéguen,¹ Cécile Duclairoir,² Evelyne Nakache,² Christian Sanchez³ and Christophe Schmitt⁴

¹INRA CENTRE DE RECHERCHES DE NANTES, RUE DE LA GERAUDIERE, BP 71627 44316 NANTES CEDEX 3, FRANCE

²EQUIPE POLYMERES INTERFACES LCMT, UMR 6507 ISMRA, 14050 CAEN CEDEX, FRANCE

³LPCGA ENSAIA/INPL, 54505 VANDOEUVRE-LES-NANCY, FRANCE

⁴NESTLE RESEARCH CENTER, CH-1000 LAUSANNE 26,
SWITZERLAND

1 Introduction

In the last decade, micro and nanosized colloidal carriers have received a growing scientific and industrial interest.¹ These vectors may be capsules (with liquid core surrounded by a solid shell), particles (polymeric matrices), vesicles or liposomes, or multiple or single emulsions, and have found a wide range of applications. They may be loaded by living cells, enzymes, flavour oils, pharmaceuticals, vitamins, adhesives, agrochemicals or catalysts and offer considerable advantages in use. Liquids can be handled as solids, odour or taste can be effectively masked in a food product, sensitive substances can be protected from deleterious effects of the surrounding environment, toxic materials can be safely handled, and drug delivery can be controlled and targeted.²

In the forementioned laboratories, we started with a new strategy based on phase separation in order to prepare natural particles. Simple or complex coacervation methods involving proteins or protein and polysaccharide mixtures³ were used to create new matrices dedicated to controlled release applications. The colloidal carriers produced were in the micrometre or nanometre size range depending on the substrates or the methods used. Wheat proteins, gliadins, were implicated in simple coacervation to produce nanospheres. Controlled release experiments with model compounds were conducted in order to evaluate

the performance of such matrices. In the case of complex coacervation, the β -lactoglobulin/Arabic gum couple was tested. The mechanism of formation and the structural properties of coacervates were first highlighted in order to better control the stability of these systems.

An alternative and promising research field deals with particles obtained from hydrogel systems. The hydrogels may be sensitive to environmental stimuli such as pH, ionic strength, electric/magnetic fields, light and temperature depending on the substrate used. Totally transparent solid matrices resulting from the dehydration of new protein gels, revealed variable swelling capacities that depend on the solvent used and physical chemical conditions. A dispersion/gelation method was developed to produce micro-beads having potential applications in the encapsulation field.

2 Materials and Methods

2.1 Gliadins Nanoparticles

Nanoparticles were obtained by desolvation of the protein using physiological salt solution as non solvent. Synperonic PE F68 was used to stabilize the nanoparticle suspension.⁴ Vitamin E-loaded nanoparticles (1 mg) were digested in 10 ml of an ethanol/water mixture (62/38 v/v) at room temperature in the dark. The vitamin E concentration encapsulated in nanoparticles (C_1) and the residual concentration in the supernatant (C_2) were then assayed by HPLC at 290 nm. Empty nanoparticles were treated in the same way and used as references for these determinations. The drug loading (rate) and the entrapment efficiency were calculated according to the equations:

$$\text{Rate (\%)} = \frac{C_1}{m_{\text{gliadins}}} \quad \text{Efficiency (\%)} = \frac{C_1}{C_1 + C_2}$$

In vitro drug release kinetic was also performed in non-sink conditions using decane as solvent (to prevent drug loss from nanoparticles dissolution) and a laboratory designed release cell. About 10 mg of gliadins nanoparticles (containing 824 $\mu\text{g/g}$ gliadins) were resuspended in 10 ml of decane. Aliquots were collected at successive time intervals and replaced by the same quantity of solvent in order to get a constant volume in the release cell. The samples were analysed by HPLC as described above for encapsulation experiments.

2.2 β -Lactoglobulin/Arabic Gum Coacervates

Coacervation process was established at pH 4.2 in water where the two biopolymers interact electrostatically.⁵ The structure of the coacervates was explored using both phase contrast and confocal scanning laser microscopies.

2.3 β -Lactoglobulin Hydrogels

The protein hydrogels were formed at pH 8 in 50% ethanol solutions.⁶ Swelling

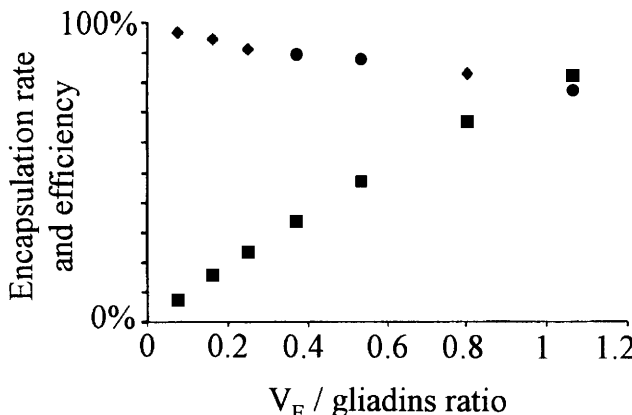


Figure 1 Vitamin E (V_E) encapsulation rate (■) and efficiency (◆) by gliadin nanospheres as a function of $V_E/\text{gliadins ratio}$

kinetics of cylindrical gels in both hydrated ($m_0 \sim 4.5 \text{ mg}$) and dehydrated ($m_0 \sim 1.5 \text{ mg}$) forms were followed in different solvent conditions.

A new method was also developed based on the dispersion of a β -lactoglobulin pre-gel in an apolar phase in order to produce gelled droplets. These droplets were then washed and dehydrated under vacuum in order to produce particles of $500 \mu\text{m}$ mean diameter.

3 Results and Discussion

Gliadin nanospheres typical size was around 900 nm .⁴ Particles size and polydispersity increased with the increase of the solvent/non solvent ratio and with the aggregated state of the proteins. Encapsulation of vitamin E (V_E) into gliadin nanospheres revealed that the rate and efficiency decreased with the decrease of the $V_E/\text{gliadins}$ ratio (Figure 1). For a $V_E/\text{gliadins}$ ratio of one, an encapsulation rate of $824 \mu\text{g}/\text{mg}$ gliadins and an efficiency of 77% were obtained. The V_E release kinetic from loaded particles is displayed in Figure 2. The experimental points were fitted with the following equations:

$$\frac{V_E}{\text{initial } V_E} = 6 \sqrt{\frac{\tau}{\pi}} (\text{short time}) \quad \frac{V_E}{\text{initial } V_E} = 6 \sqrt{\frac{\tau}{\pi}} - 3\tau (\text{intermediate time})$$

with $\tau = \frac{Dt}{r^2}$, D being the diffusion coefficient of the entrapped vitamin E and r, the radius of the nanoparticles.

The kinetic profile was thus interpreted by a burst effect coupled with a drug diffusion process through the particle modelled as a homogeneous sphere. The drug diffusion coefficient was considerably reduced when entrapped in the carrier: $D_{VE} = 1.1 \cdot 10^{-20} \text{ cm}^2 \text{ s}^{-1}$ compare to $D_{VE} = 10^{-9} \text{ m}^2 \text{ s}^{-1}$ in solution. The encapsulation of different drugs into nanospheres showed that carriers had

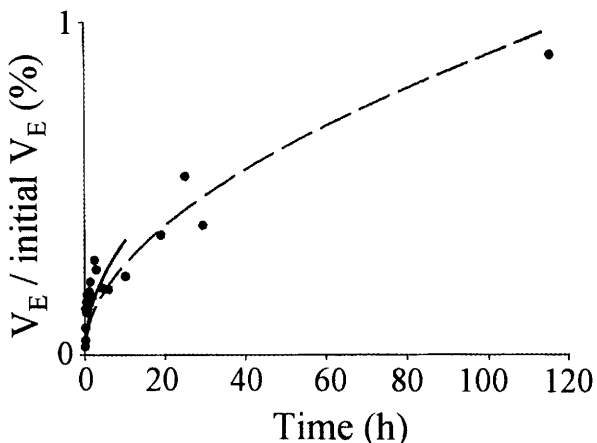


Figure 2 Vitamin E (V_E) release kinetic by gliadin nanospheres as a function of time (h). See text for equations used in the fitting procedure: (●) released V_E (%); (—) fit (short time); (---) fit (intermediate time)

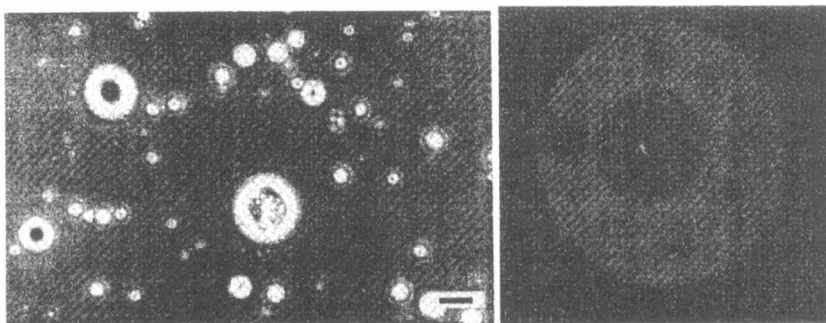


Figure 3 (Left) Phase contrast optical micrograph of 1wt% β -lactoglobulin/Arabic gum mixtures at pH 4.2 ratio 1:1. Scale bar represents 20 μm . (Right) Confocal scanning laser micrograph of a coacervate obtained with a 1wt% β -lactoglobulin/Arabic gum mixture at pH 4.2 ratio 1:1. Scale bar represents 5 μm

more affinity for hydrophobic drugs and that the ζ -potential of the particles was directly related to the nature of the drug.⁷

β -lactoglobulin/Arabic gum spherical vesicular coacervates revealed by microscopy were the hallmark of these dispersions (Figure 3). Large 'foam-like' coacervates induced by partial coalescence of single coacervates were visible especially at the 2:1 protein to polysaccharide ratio.⁸ Increasing dispersions stability was reached by increasing protein to polysaccharide ratio or by decreasing total biopolymer concentration. Another alternative to increase the stability is to produce composite dispersions containing both protein aggregates embedded in protein–polysaccharide coacervates and free coacervates.⁵ These systems could thus be used as multifunctional reservoirs for applications in microencapsulation.

The swelling kinetics of β -lactoglobulin hydrogels showed that the increase of

mass was the highest in water for both hydrated and dehydrated gels (Figure 4). The capacity of swelling (or not) depended on the solvent conditions and would allow a controlled release of both hydrophilic and hydrophobic drugs. A new method was developed based on the dispersion of a β -lactoglobulin pre-gel in an apolar phase in order to produce gelled droplets. These droplets were then washed and dehydrated under vacuum in order to produce particles of 500 μm mean diameter (Figure 5). Such protein matrices were totally transparent and could be used to encapsulate large molecules or microorganisms.

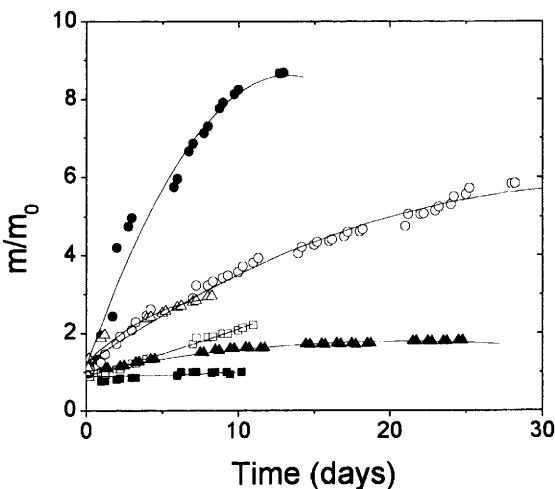


Figure 4 Swelling kinetics of β -lactoglobulin hydrogels both in dehydrated and hydrated forms for different solvent conditions: (■) ethanol; (□) water/ethanol 50/50 (v/v); (●) water; (○) 0.1M NaCl; (▲) water/ethanol 50/50 (v/v) (hydrated gel); (\triangle) water (hydrated gel)

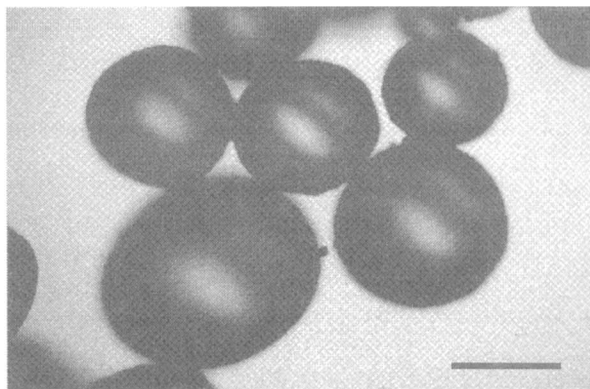


Figure 5 Optical micrograph of β -lactoglobulin beads obtained by a gelation/emulsification method. Scale bar represents 500 μm

4 Conclusion

Biopolymers represent an interesting alternative to synthetic polymers in order to be used in the route of structured carriers for controlled release and encapsulation applications. In particular, the ability of these carriers to entrap both hydrophilic and hydrophobic drugs may be very promising for many applications. In addition, the absence of chemical compounds and organic solvents used to produce biopolymeric matrices could be very interesting for some industrial applications.

References

1. C. Thies, *Microencapsulation: Methods and Industrial Applications*, S. Benita (ed.), Marcel Dekker, New York, 1996, Vol. 73, Chapter 1, p.1.
2. J. R. Robinson, *Controlled Drug Delivery: Challenges and Strategies*, K. Park (ed.), American Chemical Society, Washington, 1997, Chapter 1, p. 1.
3. C. Schmitt, C. Sanchez, S. Desobry-Banon and J. Hardy, *Crit. Rev. Food Sci. Nut.*, 1998, **38**(8), 689.
4. C. Duclairoir, E. Nakache, H. Marchais and A.-M. Orecchioni, *Colloid Polym. Sci.*, 1998, **276**, 321.
5. C. Schmitt, C. Sanchez, S. Despond, D. Renard, F. Thomas and J. Hardy, *Food Hydrocolloids*, 2000, **14**, 403.
6. D. Renard, P. Robert, C. Garnier, E. Dufour and J. Lefebvre, *J. Biotechnol.*, 2000, **79**, 231.
7. C. Duclairoir, PhD Thesis, Université de Caen, 2000.
8. C. Schmitt, C. Sanchez, A. Lamprecht, D. Renard, C.-M. Lehr, C.G. de Kruif and J. Hardy, *Colloids Surf. B*, 2001, **20**, 267.

Ch2

II

Protein & Peptide-based Nanomaterials

Nanotechnologies for the Life Sciences Vol. 2
Biological and Pharmaceutical Nanomaterials. Edited by Challa S. S. R. Kumar
Copyright © 2006 WILEY-VCH Verlag GmbH & Co. KGaA, Weinheim
ISBN: 3-527-31382-6

5**Plant Protein-based Nanoparticles**

*Anne-Marie Orecchioni, Cécile Duclairoir, Juan Manuel Irache and
Evelyne Nakache*

5.1
Introduction

Biopolymers, such as proteins, lipids or polysaccharides, are commonly used to encapsulate drugs in order to protect them from rapid degradation by environmental stress (e.g. light, heat, oxygen or pH sensitivity). Drug loading of carriers seems to be an attractive opportunity, especially if they are made from bioacceptable macromolecules, e.g. plant proteins. Colloidal carriers, in the form of nanoparticles with a diameter of 50–500 nm and up to a few micrometers, have the potential to deliver drugs to specific target sites and to achieve sustained drug release. Moreover encapsulation can modify the drug biodistribution and increase its bioavailability [1–4]. Nanoparticles can be formed from a variety of materials including synthetic polymers and biopolymers (i.e. natural compounds), such as proteins, lipids and carbohydrates [5]. Natural macromolecules from vegetable sources appear to be a very promising alternative to synthetic polymers due to their proven safety, especially those that are used as food sources. The selection of a suitable structural material has an important influence on its potential medical use. Comparing plant and animal proteins, it appears that vegetal proteins may be more disposable and cheaper than animal proteins. Moreover, for plant proteins, the purification process might be also simplified.

In general, protein nanoparticles display a number of interesting advantages. Among them, these carriers are biodegradable and metabolizable. Moreover, they can be prepared under “soft” conditions, without the use of toxic organic solvents or materials, and they can incorporate a wide variety of drugs in a relatively non-specific fashion [6]. Moreover, due to their defined primary structure, protein-based nanoparticles may offer various possibilities for surface modification and covalent attachment of drugs and ligands [7, 8].

Taking into account all of these advantages of plant proteins, this chapter will focus solely on the use of storage proteins from pea (legumin and vicilin) and wheat (gliadins) when used as a structural material to prepare nanoparticles, and their possible applications in pharmacy and medicine. These proteins are not the

only ones able to produce nano/microparticles for use as drug carriers – studies have also been performed on other plant proteins like soy glycinin from soybean seeds [9] and zein from corn [10]. However, the numbers of studies with these two proteins are very low. This chapter also includes an overview of the fabrication and applications of both conventional and “decorated” (i.e. conjugated) storage protein nanoparticles.

5.2

Description of Plant Proteins

Plant proteins are characterized by their three-dimensional organization. Two classes can be distinguished:

- Fibrous proteins composed of polypeptide chains joined together along a linear axis. They are involved in the structural material of living organisms.
- Globular proteins composed of one or, more frequently, several polypeptide chains rolled up to give a three-dimensional structure. Most of them are storage proteins.

Most vegetal proteins play an active role in biological processes, e.g. enzymes, and they can be classified by their physicochemical and extraction properties [11]. Four classes are listed:

- Vegetable albumins are hydrosoluble and rich in ionic residues (arginine, glutamic acid, lysine, tryptophan, etc.).
- Globulins are complex molecules and their amino acids composition is similar to that of albumins. However, their solubility needs an electrolyte medium.
- Prolamins are soluble in hydroalcoholic mixtures due to their high content of amino acids with hydrophilic residues.
- Glutelins cannot be dissolved in any of the aforementioned solvents, due to their high molecular mass and the presence of disulfide bonds; they are rich in lipophilic amino acids.

Storage proteins comprise proteins generated mainly during seed production and stored in the seed that serve as nitrogen sources for the developing embryo during germination [12, 13]. It is obviously more effective for the plant to use proteins instead of secondary plant products for this purpose. The average protein content of cereal grains is 10–15% of their dry weight [14], whereas for leguminous seeds it is about 20–25% [15, 16]. In addition to seeds, storage proteins can also be found in root and shoot tubers, e.g. potatoes.

No clear definition exists of what a storage protein is. The term is operational and was coined for all those proteins whose ratio in the total protein amount of the cell is greater than 5%. All of these proteins are characterized by the absence of enzymatic activity, act as a nitrogen source during seed germination and, usually, occur in an aggregated state confined in a membrane [17, 18].

Storage proteins are important for human nutrition (plant proteins), and numerous studies concerning their structure and biosynthesis have been published. For leguminosae, a simplifying rule says that they contain two types of storage proteins – legumin and vicilin. The legumins (as well as the vicilins) are very similar in different leguminose species. However, Gramineae contain a third type of storage proteins – prolamin – and, depending on the origin, it is distinguished between zein (from *Zea mays*) [19], hordein (from *Hordeum vulgare*) [20] and gliadin (from *Triticum aestivum* L.). In contrast to legumins and vicilins that are mainly located in the cotyledons of seeds, prolamines are found in the endosperm [21].

5.2.1

Pea Seed Proteins

Globulins are the main storage proteins in pea seeds [22]. These globulins were characterized by Osborne [23] according to their insolubility in distilled water and, on the contrary, by their solubility in buffered aqueous neutral salt solutions. When they are fractionated by centrifugation techniques, three different fractions have been described (with sedimentation coefficients of 2, 7 and 11S). The so-called 7 and 11S globulins represent the major pea seeds storage proteins – vicilin and legumin, respectively. These proteins display a number of similarities, including the adopted shape when solved in an aqueous solution and the similar size of the domains of the subunits forming these proteins [24, 25]. However, they can be differentiated by their molecular weight [22, 26] and different behavior at high temperature. In fact, vicilin has a size of about 200 kDa, whereas legumin is about 360 kDa [22, 26]. Furthermore, legumin does not coagulate at high temperature [27].

- Vicilin belongs to the group of so-called 7S globulins. It has a complex globular structure composed of two different types of subunits with molecular weights of about 50 and 60–70 kDa. These subunits form trimeric holoproteins in different combinations [22, 28]. Vicilin is rich in acidic amino acids (aspartic and glutamic acids), leucine and lysine [29, 30].
- Legumin belongs to the group of so-called 11S globulins [26]. This protein has a complex globular structure made of six pairs of subunits. Each of the subunits is composed of disulfide-linked acidic α -chains (molecular weight 40 kDa) and basic β -chains (molecular weight 20 kDa) [31]. Although the three-dimensional structure of legumin has not been yet determined, the sequence alignment of this protein appears to show some similarities with that of vicilin [24, 32].

5.2.2

Wheat Proteins

Storage proteins from the wheat seed are able to form a unique viscoelastic network called gluten. The properties of gluten make it useful in the production of food products such as bread, pasta and semolina, and more recently in biopackag-

ing materials [33]. The rheological properties of gluten are dependent on the protein interactions that are formed in the network, and these properties were found to be mainly influenced by physical parameters such as temperature and pressure [34–36].

Two main fractions are present in gluten – gliadin, which is soluble in 70% ethanol, made of single-chain polypeptides with an average molecular weight of 25–100 kDa linked by intramolecular disulfide bonds, and glutenin, an alcohol-insoluble fraction consisting of gliadin-like subunits stabilized by intermolecular disulfide bonds in large aggregates with a molecular weight greater than 106 kDa [37]. Because they account for about half of the total wheat gluten proteins, gliadin constitutes an important class of proteins that are involved in the various properties of the gluten [38, 39]. These proteins are polymorphic, and can be separated and classified on the basis of their electrophoretic mobility at acid pH values [40] in the following four fractions: α (molecular mass about 25–35 kDa), β (30–35 kDa), γ (35–40 kDa) and ω (55–70 kDa) groups [41–44]. All fractions have remarkably low solubility in aqueous solution except at extreme pH. This low water solubility has been attributed to the presence of interpolypeptide disulfide bonds and to the cooperative hydrophobic interactions which cause the protein chains to assume a folded shape. The amino acid composition shows that gliadin has equal amounts of apolar and neutral amino acids, mainly glutamine (about 40%). Furthermore, gliadin also has a high proline content (14%) and a very low proportion of charged amino acids [41, 45].

ω -Gliadin presents an isoelectric point (pI) ranging from 5.5 to 7 and has a few charged molecules with six to 11 basic amino acids per molecule. In contrast, α -, β - and γ -gliadins, with a pI range of 6.5–8, are still less charged than ω -gliadin [46].

5.3

Preparation of Protein Nanoparticles

Several methods have been reported in the literature for the preparation of nanoparticles from protein raw materials. Coacervation or controlled desolvation methods have been developed using solvent or electrolyte as the coacervation agent [47, 48] or by adjusting the pH or ionic strength [49, 50]. In the coacervation methods promoted by solvents, the first step consists of dispersing the macromolecules in an adequate solvent, then adding the mixture to a second solvent which is a nonsolvent of the macromolecules. A required condition is that the solvent and the nonsolvent phases are miscible.

The coacervation process is applied to a macromolecular solution to reduce the solubility in the system to such a degree that appropriate phase separation of the macromolecule takes place, i.e. the formation of a macromolecule-rich phase. The desolvation leads to macromolecule precipitation or to coacervate formation. It is assumed that, before phase separation is observed, a conformational change in the macromolecule occurs. The addition of a desolvating agent shrinks the macromolecule coil which becomes smaller and smaller until the phase separation from

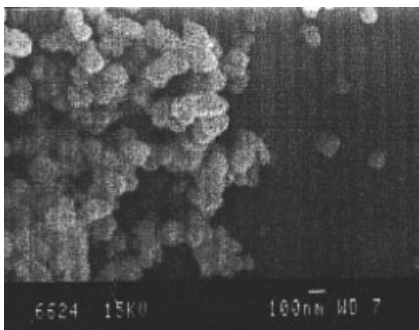


Fig. 5.1. Scanning electron micrograph of legumin nanoparticles. (From Ref. [52], permission pending).

the solvent occurs. It is possible to monitor the phenomenon by turbidity measurement. A desolvatation agent decreases the turbidity because of the decrease in macromolecular size. To prepare small particles, it is important to maintain the system just outside the coacervation region. The addition of the coacervation agent should stop as soon as the Tyndall effect bounded to aggregation of macromolecules turns the system turbid [7]

5.3.1

Preparation of Legumin and Vicilin Nanoparticles

Legumin and vicilin have an aqueous solubility that is strongly pH and ionic strength dependent [30]. Nanoparticles from these pea proteins (Figs. 5.1 and 5.2) can be obtained by a simple coacervation or controlled desolvatation method [50–52]. It was observed that extreme pH values enable their solubilization in aqueous medium. The coacervating or desolvating agent induces a progressive modification of the tertiary structure of the proteins, giving an increasing hydrophobic material which leads to submicronic aggregates or coacervates [53]. These coacervates are generally unstable and must be hardened for stabilization by physical or chemical

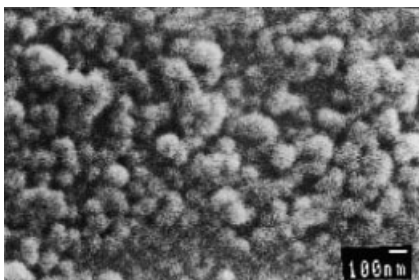


Fig. 5.2. Scanning electron micrograph of vicilin nanoparticles. (From Ref. [50]).

crosslinkage. In the case of these pea proteins, a three-step procedure can be employed to obtain nanoparticles.

In a first step, an unstable coacervate is obtained by mixing a solution of the chosen protein (pH 9) with a phosphate buffer solution. In a second step, the coacervates have to be hardened with a crosslinking agent in order to stabilize the just-forming coacervates. The most popular crosslinking agent is glutaraldehyde. This reagent reacts with the amino groups of the proteins, predominantly with the amino group of lysines, to form a Schiff base [54]. Finally, after the crosslinking, for pharmaceutical purposes, the obtained nanoparticles have to be purified. For this purpose, unreacted aldehyde can be neutralized with a sulfite and nanoparticles centrifuged in order to eliminate the nontransformed protein fraction onto particles.

Some comprehensive explanations of nanoparticles formation can be given. It is observed that, at a pH value close to 7, the coacervates show a submicronic size, but the percentages of coacervates yields are under 40% of the added protein. Similarly, the ionic strength of the buffer greatly influences the coacervate size and yield. The best experimental conditions to obtain small-sized particles (average diameter 500 nm) were found to be pH 6.8 and ionic strength 0.15 M for legumin, and pH 6.4 and ionic strength 0.10 M for vicilin [50, 52].

The isoelectric points of the two proteins are about 4.5. Thus, the balance between negative carboxyl groups (from glutamic and aspartic acids) and positive groups (from lysine and arginine) changes when the pH of the protein solution is less or greater than 4.5. Consequently, under environmental conditions close to the isoelectric point, these globulins would present a reduced interfacial charge which may enhance coacervate precipitation and phase separation. In other respects, for neutral pH values, legumin and vicilin would have a charge which may probably act against coacervate formation.

Concerning vicilin, in particular, a hypothesis for protein coacervate formation has been proposed. Under defined conditions, solubilized vicilin (7S form) may associate to yield an 11S insoluble form. This 11S form (probably a dimer of vicilin) may be responsible for the initial precipitation of vicilin which aggregates up to a critical size depending on environmental conditions (pH and ionic strength). The coacervate must be quickly hardened by crosslinkage in order to prevent the aggregates coalescing to a separate phase.

5.3.2

Preparation of Gliadin Nanoparticles

Gliadin nanoparticles (Fig. 5.3) can be prepared by a desolvation method in which a dissolution of gliadin in an organic solvent/water mixture is desolvated by the addition of a nonsolvent aqueous phase [50, 55]. Note that gliadin nanoparticles prepared in this way are stable and further treatment by heat or chemical crosslinking is not necessary to stabilize them. This fact can be explained by the extremely low solubility of gliadin in an aqueous medium and represents an advantage when compared with other protein nanoparticles (i.e. albumin, gelatin).

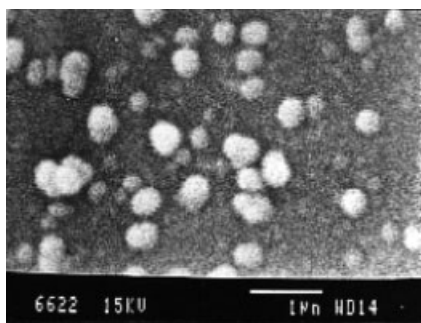


Fig. 5.3. Scanning electron micrograph of a gliadin nanoparticle. (From Ref. [8]).

In any case, gliadin nanoparticles can be hardened by chemical stabilization in order to modulate the drug release characteristics of nanoparticles or their *in vivo* distribution and interaction with the body.

Once produced (and eventually hardened by chemical crosslinkage), they have to be purified. The organic solvents are eliminated by evaporation under reduced pressure, whereas the amounts of protein not transformed onto nanoparticles and other impurities (i.e. the chemical crosslinker) are eliminated by dialysis, gel-permeation chromatography or, more frequently, subsequent centrifugations. Finally, nanoparticles can be also lyophilized to preserve their physicochemical properties for a long period of time. For lyophilization of gliadin nanoparticles, a solution of glucose 5% w/v has been proposed as a cryoprotector [56, 57].

In summary, this simple method allows the preparation of reproducible particle sizes with a narrow distribution. The main advantages are the production of nanoparticles in the absence of toxic organic solvents and the possibility of avoiding the chemical stabilization step to obtain stable nanoparticles. The selection of the solvent phase of gliadin has a significant influence on the size of the resulting nanoparticles. In this context, mixtures between either ethanol and water or acetone and water enable production of both smaller particle sizes and reproducible results. Another key factor concerns the nonsolvent of gliadin. In this case, an aqueous solution of NaCl (0.9% w/v) has been proposed [50]. When a mixture of ethanol and water is used, the size of the resulting nanoparticles is close to 450 nm and the yield of the process, determined by gravimetry and reverse-phase high-performance liquid chromatography (RP-HPLC), is about 90% [50, 56].

More recently, in order to understand the influence of environmental parameters governing gliadin nanoparticles size, a thermodynamic approach was investigated, i.e. the determination of the solubility parameter of the protein [58]. According to Hildebrand theory [59], the solubility parameter of gliadin was determined using a panel of solvents or mixtures of them. It is assumed that the solvent which best solubilizes gliadin has the same solubility parameter as the protein [60]. Different mixtures were prepared with bioacceptable solvents such as ethanol, ethylene glycol, propylene glycol and ultra-pure water. These solvents are usually considered

as references for the determination of the solubility parameters of biological compounds.

When a mixture of ethanol and water is used, the size of the resulting nanoparticles is close to 450 nm and the yield of the process, determined by gravimetry and RP-HPLC, is about 90% [50, 56]. However, a mixture of propylene glycol and water (73/27%) appears to be the best selection to obtain small gliadin nanoparticles of about 150 nm [58].

5.4

Drug Encapsulation in Plant Protein Nanoparticles

In order to evaluate the encapsulation ability of gliadin nanoparticles, different drugs were tested, chosen for their medical and/or pharmaceutical interest. The objective of this research was to determine the feasibility of nanoparticles loaded with hydrophilic or lipophilic drugs and furthermore in order to obtain as small-sized particles as possible. Attention was focused on the drug release mechanism. Four drugs were chosen – two lipophilic vitamins, i.e. all-trans retinoic acid [vitamin A (RA)] and α -tocopherol [vitamin E (VE)], and two hydrophilic drugs, i.e. a slightly polar mixture of linalool–linalyl acetate (LLA), components of the essential lavender oil, and the cationic amphiphilic benzalkonium chloride (BZC). For all these particulate systems, nanoparticles sizes were determined by scanning electron microscopy or photon correlation spectroscopy.

5.4.1

RA Encapsulation in Gliadin Nanoparticles

RA is involved in the proliferation and differentiation of epithelial tissues. This vitamin in acidic form reduces the size of sebaceous glands and sebum secretion, making it an attractive agent for the treatment of skin disorders such as acne, psoriasis, hyperkeratosis, ichthyosis and epithelial tumors [61, 62]. In the treatment of acne, it was demonstrated that RA prevents inflammatory lesions by loosening follicular impactions (microcomedones) and clearing the follicular canal of retained keratin [63]. Furthermore, RA has been proven effective against a range of malignancies in human clinical trials, although many patients relapsed after a remission [64]. *In vivo* studies have shown that RA is active against acute promyelocytic leukemia [65, 66]. Unfortunately, the limited duration of RA activity in this leukemia is a pharmacological adaptation resulting in reduced serum concentration after prolonged treatment [67]. Nevertheless, in spite of a real therapeutic interest, several drawbacks (e.g. teratogenicity) have been reported for the currently available dosage forms [62]. To overcome these inconveniences, and in an attempt to increase the therapeutic efficacy of RA, alternative dosage forms have been suggested – microemulsions [68] and liposomes for intravenous [69] and topical administration [70]. Another system suitable for controlled drug release could be nanoparticles from biopolymers. For this purpose, we have chosen nanoparticles from glia-

din. They were prepared by the aforementioned desolvatation method [50, 58]. These particles can be obtained by using only bioacceptable solvents such as ethanol and water. Their size, which is one of the determinant characteristics for medical purposes, can be optimized. These nanoparticles, showing good stability in phosphate-buffered saline (PBS), were assayed as carriers for RA. They have shown a quite good entrapment efficiency – about 75% of added drug at 60 µg (mg gliadin)⁻¹ and a payload of 74 µg (mg gliadin)⁻¹ nanoparticles [58]. In order to quantify more precisely the solvent effect, the size diameter was optimized through a solubility parameter study. The smallest size was reached for protein solubility solvent equal to that of gliadin. The average diameter of the particles was about 150 nm [58]. RA was released from these nanoparticles, in a two-step mechanism, characterized by an initial rapid release followed by a continuous diffusion process. The first release was found to be about 20% of the loaded drug and can be related either to the release of the drug entrapped in the peripheral domains of the nanoparticle matrix or to a simple desorption of superficial RA, whilst the second slower period was linear with respect to time and appeared to be a diffusion phenomenon. Furthermore, in this second step, about 20% of the drug was released by diffusion in 3 h.

These observations offer interesting prospects for the preparation of drug-loaded carriers for medical applications.

5.4.2

VE Encapsulation in Gliadin Nanoparticles

Drug carriers are interesting systems to prevent drawbacks related to the drug itself by decreasing its degradation rate. In order to test the protective power of nanoparticles against environmental stresses, a second lipophilic vitamin, VE, was encapsulated into gliadin nanoparticles. VE is known to act as a strong antioxidant or nitrosamine blocker to prevent the build-up of cellular peroxide [71]. The exposure to free oxygen species induces a rise in lipid peroxidation, which may cause injury at different sites of the body. For instance, the action of free radicals produced by a variety of environmental stresses (among them sun exposure) may promote skin damage, such as premature skin ageing [72], skin fragility and even skin cancers (melanoma or others) [73] related to a decrease in cellular immunity of the skin. VE appears to be one of the strongest free radical scavengers through its action as a chain-breaking antioxidant in membranes [74], preventing acute or chronic damage [75]. In addition to these biological activities, VE also exerts cosmetic functions; notably, it helps delay the progression of aging [76] and possesses a skin moisturizing power [77]. However, VE is degraded by oxygen, and dosage forms must be protected from light, heat and prolonged contact with air. Previous work has shown that the preparation of gliadin nanoparticles could be easily performed by a simple coacervation method. It is for this reason that gliadin has been chosen. Moreover, gliadin possesses the ability to interact with epidermal keratin due to its richness in proline [78]. VE-loaded gliadin nanoparticles have been characterized by their size, ζ potential, VE payload and entrapment efficiency.

When loaded, the gliadin particle size is about 900 nm and their charge is close to zero. They are suitable drug carriers with an optimum encapsulation rate of about 100 VE μg (mg gliadin) $^{-1}$ with an efficiency of more than 77%. The release behavior of VE-loaded nanoparticles may be interpreted as a “burst” effect, followed by a diffusion process through a homogeneous sphere [3].

5.4.3

Lipophilic, Hydrophilic or Amphiphilic Drug Encapsulation

In order to study the influence of drug polarity on nanoparticle characteristics such as particles size, drug loading and drug release, three different drugs with different polarities were chosen [79]. VE, studied in a previous paper [3], was employed as a model of a lipophilic drug, and the slightly polar LLA and the amphiphilic cationic benzalkonium chloride (BZC) as hydrophilic models. Their dielectric constants are, respectively, 4, 8 and 45 [80]. The choice of these drugs was governed by their utilization in pharmaceutical dosage forms:

- VE, widely used as strong antioxidant in many medical and cosmetic applications, is rapidly degraded because of its light, heat and oxygen sensitivity [3].
- Linalool and linalyl acetate are the major components of essential lavender oil used in aromatherapy. They possess antibacterial and antifungal properties [81]. They are used in topical formulations. They may cause skin irritation by reason of a potential caustic power. Gliadin encapsulation could be a fruitful method for LLA formulations. Furthermore, the interaction of gliadin proline with skin keratin associated with the controlled release of LLA may avoid some drawbacks of this drug.
- BZC is a quaternary ammonium used as an antiseptic and bactericide, spermicide [82], and virucide [83]. However, BZC can promote some allergies followed by mucous lesions. It is assumed that encapsulation into gliadin nanoparticles could minimize or avoid lesions promoted by this irritant quaternary ammonium and could improve the dosage form by delaying drug release.

Drug entrapment and efficiency were tested after encapsulation. The results showed that the amount of entrapped VE and LLA is higher than that of the cationic BZC, confirming a strong interaction between gliadins and apolar compounds, due to the apolarity of the proteins. When comparing drug entrapment, results show that the optimal VE concentration is obtained for 972.0 VE μg (mg gliadin) $^{-1}$, with an efficiency of 79.2%, the optimal LLA concentration corresponds to 980.0 LLA μg (mg gliadin) $^{-1}$, with an efficiency of 82.4%, and the optimal BZC concentration corresponds to 550.3 BZC μg (mg gliadin) $^{-1}$, with an efficiency of 52.3% (Table 5.1).

For drug release quantification, only VE and BZC were studied. The reason being that LLA should be studied under a controlled atmosphere and not in a liquid medium. Such differences between media used did not allow an easy comparison to other drugs. For VE and BZC, drug releases were, respectively, 13 and 11% after

Tab. 5.1. Drug encapsulation characteristics in gliadin nanoparticles.

Drug	Polarity (dielectric constant)	Payload (%)	Encapsulation efficacy (%)
VE	Apolar (4)	97.2	79.2
LLA	slightly polar (8)	82.4	98.0
BZC	polar (amphiphilic cationic) (45)	66.0	52.3

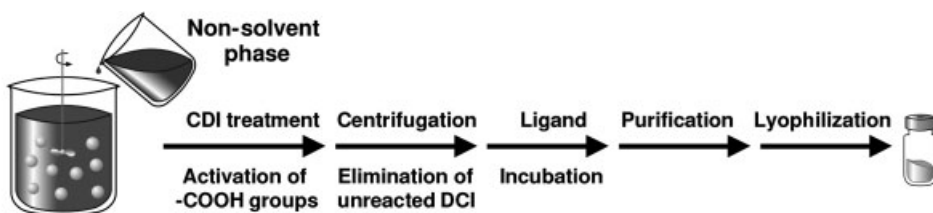
1 h, and 30.6 and 11.7% after 30 h. The phenomenon observed can be interpreted as a burst effect completed by a drug diffusion process through a homogeneous sphere. Both release diffusion parts of the profiles have been modeled with a diffusion process in a homogenous sphere. However, the diffusion coefficients are different according to VE or BZC, i.e. 1.12×10^{-20} and $6.36 \times 10^{-21} \text{ m}^2 \text{ s}^{-1}$, respectively. This could be related to the different affinity of the gliadin for the two drugs. In organic phases, diffusion coefficients are usually about $10^{-9} \text{ m}^2 \text{ s}^{-1}$. Here, the coefficients are clearly much lower, which confirm that the drug is retained by the nanoparticle matrix.

In conclusion, it can be observed that whatever the polar drug character, this gliadin nanoparticulate system is able to entrap the drug with an acceptable payload and encapsulation efficiency [79].

5.5 Preparation of Ligand–Gliadin Nanoparticle Conjugates

In general, proteins produce biodegradable particles whose physicochemical properties can be modulated by the crosslinking process employed for their stabilization. Furthermore, due to the presence of numerous functional groups (i.e. amino and carboxylic residues), proteins are excellent candidates for the preparation of conjugates, formed by the attachment of molecules capable of providing specificity to the surface of nanoparticles. In this context, different ligands have been proposed, including antibodies [84, 85], lectins [86, 87], carbohydrates [88] and other biological ligands, in order to recognize or bind particular molecules [89, 90].

However, the association of ligands with nanoparticles can be achieved by different procedures, including covalent linkage and adsorption processes [91]. Ideally, the ligand should be conjugated to particles through a covalent linkage, which is more stable than adsorption procedures, without affecting its specificity. Noncovalent attachment relies on a fortuitous process. Further, it is difficult to control the amount of ligand which is associated and this process is useful only for those proteins that will associate nonspecifically [92]. Different techniques for covalent attachment may be envisaged, depending on the principal functional groups located on the carrier surface. The most widely used methods of ligand coupling are the use of cyanogen bromide [84, 93] and periodate [94, 95] for hydroxyl



Protein solvent phase

Fig. 5.4. Route for the preparation of ligand–gliadin nanoparticle conjugates by desolvation of gliadin followed by CDI activation and further incubation with the ligand.

groups, glutaraldehyde [96, 97] and ethylene glycol diglycidyl ether [98] for amino groups, and carbodiimide (CDI) for carboxylic groups [99, 100].

This last technique is the one preferred in order to obtain conjugates between a ligand and protein nanoparticles [87, 101–103]. CDI involves the activation of carboxylic acid groups to give NH-activated carboxylic acid groups which can react with free amino groups of the ligand polypeptide chains [104]. In proteins, these carboxylic groups can be found on aspartic and glutamic acid residues. For vicilin, these amino acids represent about 19 groups per 1000 amino acid residues [101]. For gliadin, these amino acids only represent 21 and 71 groups per 1000 amino acid residues, respectively [45, 105]. In spite of gliadin having a very low proportion of these two amino acids, it appears that the coupling reaction is efficient enough to provide acceptable lectin binding.

Figure 5.4 summarizes the preparation of lectin–nanoparticle conjugates. In brief, the first step of the manufacturing protocol involves the activation of the carboxylic groups on the gliadin nanoparticles by addition of a CDI derivative [i.e. 1-(3-dimethylaminopropyl)-3-ethyl-carbodiimide hydrochloride]. After incubation, the suspension of “activated” nanoparticles has to be centrifuged in order to remove the unreacted reagent. Then, the nanoparticles are dispersed in an aqueous medium and incubated with the desired ligand for the coupling reaction by overnight incubation at room temperature [101, 102]. Finally, the resulting conjugates are purified and lyophilized using glucose as a cryoprotector [103].

Different parameters can influence the yield of the process. In spite of the fact that the CDI reaction can effectively occur up to at least pH 7.5 without any significant loss of yield, it has been reported that the optimal pH ranges between 4.7 and 6 [106]. This fact was also observed by Arangoa et al. who showed evidence of superior binding of a *Dolichus biflorus* lectin (DBA) to the surface of gliadin nanoparticles with 2-(*N*-morpholino)ethanesulfonic acid (MES) buffer (1 mM, pH 5.5) rather than with PBS (1 mM, pH 7.4) [103]. This may be explained as being due to the proton of the carboxylic group facilitating the rupture of one double link of the CDI molecule [107], forming the *O*-acylisourea intermediate. This active residue is then able to react directly with primary amines forming amide bonds and

releasing the CDI derivative. Moreover, at neutral pH, the overall charge of both the nanoparticles and the ligand would be negative. Therefore, ligand approaches to a nanoparticle surface and subsequent binding would not be favored by the phenomenon of charge repulsion [108].

Another critical factor affecting ligand binding to the surface of protein nanoparticles is the reaction time between the CDI and the gliadin. Therefore, an increase in the reaction time induced a dramatic decrease in the amount of the ligand binding to the nanoparticle surface. This could be due to the degradation of the reactive O-acylisourea complex. In fact, this complex is rapidly hydrolyzed in aqueous solution, having a constant rate measured in seconds [109]. If the target amine does not interact with the O-acylisourea intermediate before its hydrolysis, the desired binding cannot occur. This is especially problematic when the target molecule is in low concentration [106], as usually occurs in the binding of active ligands to the surface of nanoparticles. Another possible explanation for the DBA binding decrease could be the formation of the stable N-acylurea derivative [110].

However, the amount of CDI used to activate functional groups on the surface of nanoparticles is also important. A low amount of CDI may require longer reaction periods. However, the use of high amounts of CDI may induce irreversible aggregation of nanoparticles. This may be explained by the presence of both carboxylic and amine groups on the surface of the nanoparticles. Therefore, at high CDI concentrations, self-polymerization may take place [106]. In any case, in order to obtain a good binding efficiency, it is necessary to find a balance between the reaction time and the amount of CDI used to activate the nanoparticles.

Finally, another important factor concerns the amount of ligand used in the incubation with the activated nanoparticles. For gliadin nanoparticles, a maximum of ligand binding occurs when the amount of ligand incubated with activated nanoparticles is about $50 \mu\text{g} (\text{mg gliadin})^{-1}$ nanoparticles [103].

5.6

Bioadhesive Properties of Gliadin Nanoparticles

Bioadhesion is classically defined as the ability of a material to adhere to a biological substrate with the objective of improving the therapeutic efficiency of drugs by increasing the residence time at the site of activity or absorption [111, 112]. It is interesting to note that a number of drugs remain poorly available when administered by the oral route. Among other reasons, this fact can be related either to a low mucosal permeability for the drug or to its low solubility in the mucosal fluids. In both cases, an important fraction of the given dose is eliminated from the alimentary canal prior to being absorbed. The use of bioadhesive nanoparticles can be an adequate strategy to improve drug bioavailability. In fact, these carriers may enhance the drug absorption rate by reducing the diffusion barrier between the dosage form and the site of action or absorption. Similarly, they may prolong the residence time of the drug in the gut and, therefore, increase the time during which absorption can occur.

For bioadhesion studies, gliadin nanoparticles were labeled with carbazole, which is a hydrophobic fluorescent molecule.

5.6.1

Ex Vivo Studies with Gastrointestinal Mucosal Segments

In order to evaluate the bioadhesive capacity of these carriers, nanoparticles were incubated with fresh portions of rat gastrointestinal mucosa using a plate of aluminum with a slit in the center [113]. The mucosa in the slit of the plate was covered with 1 mL of suspensions (containing 4 mg mL^{-1} nanoparticles) and the incubation time was fixed for 30 min. After incubation, the suspensions were sucked off and the samples were rinsed with 5 mL 0.9% NaCl solution to eliminate the non-attached particles. Then, the mucus layer including the adsorbed particles was drawn from the membrane and digested with NaOH for 24 h. After total dissolution of mucus, carbazole extraction was performed with 1.5 mL methanol, vortexed for 1 min and centrifuged at 20 000 g for 10 min. Finally, the amounts of adhered nanoparticles or conjugates were estimated by fluorometry [103].

Gliadin nanoparticles were able to develop rapid interaction with the gut mucosa. In fact, the adsorption equilibrium for nanoparticles and conjugates was reached in less than 30 min [103]. Similarly, under the experimental conditions used [$4 \text{ mg (particles or conjugates) mL}^{-1}$], no saturation was observed on the apparent surface of mucosa delimited by the device.

Figure 5.5 shows the interactions of gliadin nanoparticles with intestinal mucosa samples. Comparing the different anatomical regions, gliadin nanoparticles

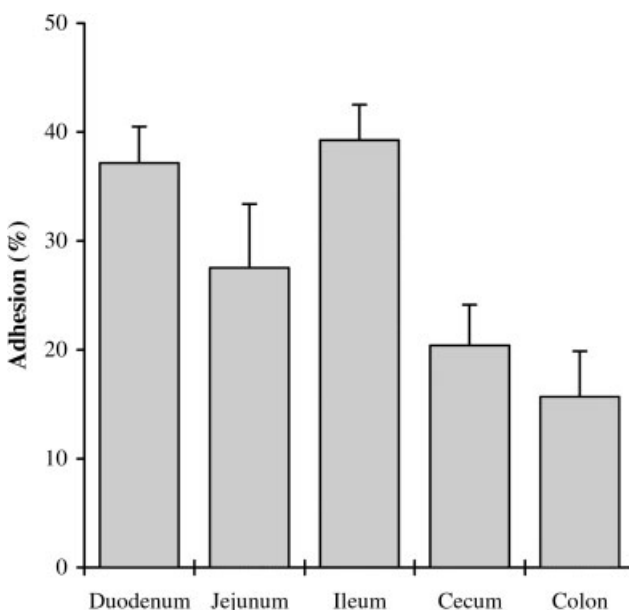


Fig. 5.5. Adhesive interactions of gliadin nanoparticles in isolated intestinal segments ($n = 4$).

showed a high affinity for the small intestine segments. However, no significant differences in the extent of interaction were found between the duodenum, jejunum and ileum ($P < 0.05$). Therefore, for ileum or duodenum portions, the amount of nanoparticles interacting with the mucosa was calculated to be close to 8 g m^{-2} , which represents about 40% of the nanoparticles placed in contact with the gastrointestinal tract. In this context, the interaction of poly(styrene) nanoparticles with intestinal segments (under similar experimental conditions) was size dependent and the largest amount of latex able to interact with the mucosa was about 1 g m^{-2} [113, 114]. Similarly, gliadin nanoparticles interacted about 8-fold more with the intestinal mucosa than poly(isobutyl cyanoacrylate) nanoparticles [115]. For large intestine portions, the interaction of gliadin nanoparticles strongly decreased. This may be explained by a reduction of both the mucosa surface and the mucin concentration along the gastrointestinal tract. According to these results, it appears that gliadin nanoparticles would be useful for improving the bioavailability of drugs. These powerfully adhesive carriers may prolong the residence time and enhance drug absorption, thus reducing the diffusion pathway.

However, DBA-gliadin nanoparticle conjugates displayed a different ability to develop adhesive interactions with the gut mucosa. In the small intestine, these conjugates showed an adhesive interaction similar to the controls ($P < 0.05$) and, for all segments, this interaction was close to 10% of the initial concentration placed in contact with the mucosa. However, in the large intestine a significant increase of about 100% was found for DBA conjugates. This fact can be explained by the reported capability of DBA to strongly react with the colonic epithelial surface [116, 117] due to the presence of *N*-acetyl- α -galactosamine (specific sugar for DBA) residues, which provide the substrate for their site-specific interaction.

Finally, concerning the interaction of gliadin nanoparticles with Peyer's patches, it was found that gliadin nanoparticles showed 3.5 times more capacity of interaction with these lymphoid tissues than DBA conjugates [103].

All of these results confirmed that gliadin nanoparticles displayed a high interactive potential with biological surfaces. However, the possible interaction between the biological substrate and these nanoparticles is of a nonspecific nature. This fact means that these colloidal systems interact in the same way with a number of components of the biological substrate, without showing target properties for a particular region or cell structure [118].

5.6.2

***In Vivo* Studies with Laboratory Animals**

In order to evaluate the *in vivo* bioadhesive capacity of gliadin nanoparticles and their influence on the pharmacokinetics of the loaded drug, animals were gavaged with a single dose of nanoparticle formulations dispersed in 0.5 mL water. For the bioadhesion study, the gastrointestinal tract of animals was cut in different portions, rinsed with saline and digested with sodium hydroxide. The fluorescent marker was extracted with methanol and determined by spectrofluorimetry. The amount of carbazole, determined in the mucosa segments, was used for the

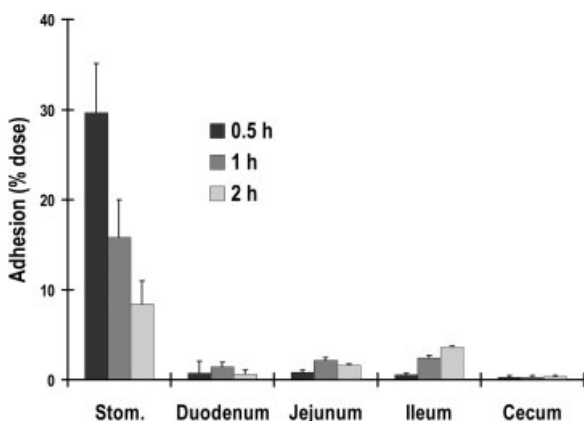


Fig. 5.6. Gastrointestinal transit profile of gliadin nanoparticles. Single administration of a single oral dose of 30 mg. Data expressed as the mean \pm SD ($n = 4$). (Adapted from Ref. [102]).

estimation of the interacted nanoparticulate fractions. For the pharmacokinetics studies, blood samples were taken from the ophthalmic venous plexus, centrifuged and assayed for carbazole content by an HPLC method with fluorescent detection [57]. *In vivo* studies demonstrated that gliadin nanoparticles displayed a high adhesive potential with a clear tropism for the stomach mucosa (Fig. 5.6). Thus, thirty minutes post-administration, about 30% of the initial dose remained adhered within the gut. However, around 90% of the adhered nanoparticles were localized in the stomach. Similarly, 1 h after administration, only 18% of the initial dose could be found in the stomach and their presence in other intestinal regions was also negligible. Finally, at 2 h post-administration, only about 8% of the given dose was found adhered to the mucosa [119]. This profile of bioadhesion (tropism for the stomach mucosa and rapid decline of the adhered fraction over the time) was not significantly affected when nanoparticles were coated with DBA [103].

Nevertheless, in order to study the influence of the degree of crosslinking on the bioadhesive profile of nanoparticles and carbazole absorption, two different formulations were prepared. The first one resulted from the crosslinking of gliadin nanoparticles with glutaraldehyde with 2 h prior purification (CL-NP). The second one (DCL-NP) was obtained after treatment of gliadin nanoparticles with a CDI derivative for 1 h and subsequent treatment with glutaraldehyde for 2 h [57] (Tab. 5.2).

Within the stomach, the bioadhesive profile of gliadin nanoparticles was found to be influenced by the crosslinkage. Thus, noncrosslinked nanoparticles displayed a higher initial ability to develop adhesive interactions than crosslinked nanoparticles. However, the elimination rate of the adhered fraction was higher for non-crosslinked than for stabilized nanoparticles [57, 119]. On the contrary, the crosslinking process allowed a similar amount of carriers adhered to the mucosa to be

Tab. 5.2. Physicochemical characteristics of the different formulations based on gliadin nanoparticles ($n = 6$).

	Size (nm)	ζ potential (mV)	Fixed ligand ($\mu\text{g mg}^{-1}$)	Loaded carbazol ($\mu\text{g mg}^{-1}$)
NP	460 ± 19	27.5 ± 0.8	—	12.6 ± 1.2
CL-NP	453 ± 24	24.5 ± 0.5	—	12.2 ± 0.8
DCL-NP	478 ± 31	21.2 ± 1.3	—	12.1 ± 1.6
BSA-NP	514 ± 18	34.7 ± 1.7	20.8 ± 1.7	12.5 ± 0.6
DBA-NP	521 ± 13	32.4 ± 0.9	23.5 ± 2.6	12.6 ± 0.9

CL-NP: nanoparticles crosslinked with glutaraldehyde; DCL-NP: nanoparticles crosslinked with CDI and glutaraldehyde; BSA-NP: bovine serum albumin–gliadin nanoparticle conjugates (control); DBA-NP: *D. biflorus* lectin–gliadin nanoparticle conjugates.

maintained for at least 1 h, which was calculated to be around 15% of the given dose (Fig. 5.7).

Another interesting point is that, within the stomach, the adhered nanoparticles appear to accumulate in the nonglandular region [119]. In this last region, cross-linked nanoparticles have a 1.5 times higher adhesive intensity than nonhardened nanoparticles. Similarly, the mean residence time of the adhered fraction to the stomach mucosa was about 95 min higher for crosslinked than for conventional gliadin nanoparticles [119].

This high adhesive capacity of gliadin nanoparticles may be explained by the protein composition with a high content of neutral and lipophilic residues. Neutral amino acids may promote hydrogen-bonding interactions with the mucosa, while

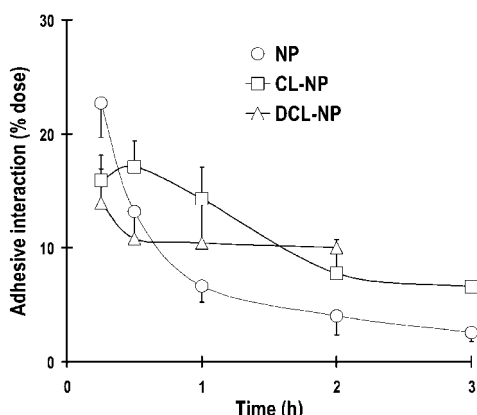


Fig. 5.7. Evolution of nonhardened gliadin nanoparticles (NP), nanoparticles crosslinked with glutaraldehyde (CL-NP), and nanoparticles crosslinked with CDI and glutaraldehyde (DCL-NP) in the stomach mucosa, as a function of time, after single oral administration 20 mg particles ($1.14 \text{ mg carbazole kg}^{-1}$). The results are expressed as the percentage of the given dose ($n = 6$).

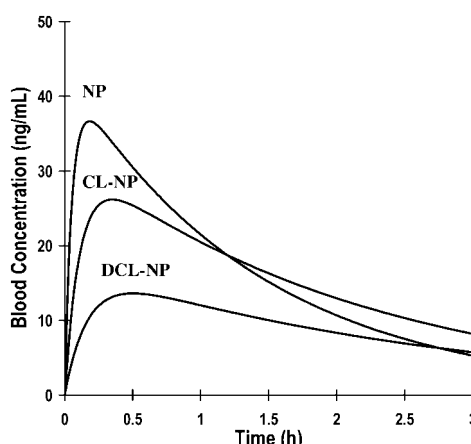


Fig. 5.8. Carbazole plasma levels after the oral administration of a single dose of $1.14 \text{ mg carbazole kg}^{-1}$ loaded in NP, CL-NP or DCL-NP ($n = 12$).

the lipophilic components may develop hydrophobic interactions with the biological support [115, 118, 120]. On the other hand, a more energetic crosslinking process reduces the ability of nanoparticles to develop adhesive interactions within the mucosa; however, this process would decrease the degradation rate of gliadin nanoparticle and, thus, provide a prolonged residence in the mucosa. For crosslinkage with glutaraldehyde, the adhered fraction of nanoparticles is constant for at least 1 h, whereas for nanoparticles crosslinked with CDI and glutaraldehyde, the adhered fraction (around 10% given dose) remained constant for at least 2 h.

Concerning the pharmacokinetic study, Fig. 5.8 shows the carbazole plasma concentration provided by nonhardened and crosslinked nanoparticles when administered by the oral route. It is interesting to note that when carbazole was formulated as an aqueous suspension it was not possible to determine the T_{\max} , C_{\max} and the elimination rate. Similarly, the area under of curve (AUC) was around zero since their absorption was negligible. This fact is typical for hydrophobic drugs with very poor aqueous solubility [121–124].

However, when formulated in nonhardened nanoparticles, the bioavailability of carbazole was calculated to be about 40% of the dose. For crosslinked nanoparticles, the bioavailability was close to the 50%. Moreover, the crosslinkage enables us to increase the T_{\max} , and to decrease the C_{\max} and the elimination rate. Similarly, the mean residence time was significantly increased in comparison with nonhardened nanoparticles and an aqueous solution of carbazole [57].

These pharmacokinetic results can be explained by the ability of gliadin nanoparticles to develop bioadhesive interactions within the stomach mucosa. Once gliadin nanoparticles are adhered to the mucosa, they would release the loaded molecules to the absorbing cell layer, minimizing losses to the luminal environment and increasing the local drug concentration. In this context, the active molecule (carbazole in this study) would be able to show a first-order absorption process. However,

the digestion of nanoparticles either in luminal fluids or adhered in the mucus may provide an instantaneous release component which may be related to a first-order absorption. In fact, the interactions developed by gliadin nanoparticles within the stomach mucosa are the key phenomena influencing carbazole absorption. This hypothesis was confirmed by a deconvolution model [57].

5.7 Future Perspectives

For pharmaceutical dosage forms it is well known that, whatever the administration mode, the principal objectives to be reached are the enhancement of the efficiency associated with a reduced toxicity and controlled drug release. Furthermore, if administered by a parenteral route, it is hoped that a major amount of the drug reaches the target site avoiding undesirable side-effects, i.e. a modification of drug distribution is required [125, 126].

Colloidal carriers in the form of nanoparticles have this potential to deliver drugs to specific target sites and to achieve sustained drug release. The bioacceptability of such nanoparticulate systems is strongly size dependent and, for intravessel administration, the diameter must be smaller than that of the smallest blood capillary. Consequently, size optimization is a very important parameter.

Furthermore, for medical applications, it is of interest to test their potential for parenteral administration, and particularly the humoral and cellular responses of protein particles after injection in animals. The first reports have been published describing these responses for native legumin and legumin nanoparticles after intradermal injection in rats [127].

5.7.1 Size Optimization

Bearing in mind this important condition, all the parameters involved in the preparation of gliadin nanoparticles have been optimized (some results are have been published [55]; other are in progress). The studied parameters were:

- Choice of the protein solvent
- Protein concentration
- Temperature during the experimental procedure
- Solvent/nonsolvent ratio
- Shear rate imposed during mixing
- Nanoparticle size evolution with time

Concerning the choice of the protein solvent, it was demonstrated that the closer the solubility parameter of the protein is to that of the solvent, the smaller the particle size (and correspondingly higher the amount of protein solubilized), under the experimental conditions chosen.

Other important experimental conditions were the solvent/nonsolvent ratio, the

temperature and the shear rate during the procedure. The data available showed that the best ratio must be less than unity and that an elevated temperature (compatible with protein thermolability, about 35 °C) decreases the particle size. Moreover, an optimum shear rate was observed for each protein concentration in the medium.

Concerning the size evolution of the nanoparticles with time, the first results showed that this parameter is a determinant for high protein concentrations. For instance, for a supersaturated solution of protein, the size increases 10 times in 100 min, ranging from 70 nm after 1 min to about 700 nm after 100 min. This is in favor of a spontaneous nucleation which occurs as soon as the non-solvent is added to the medium. In order to obtain a large range of nanoparticle sizes, it now remains to resolve the stabilization of the particles whatever their size.

In all of these abovementioned works the particle sizes of nanoparticles were greater than 100 nm. There are currently limitations on achieving nanoparticles with a size less than 100 nm and new developments are anticipated in the future.

5.7.2

Immunization in Animals

Preliminary experiments were performed on legumine nanoparticles in order to evaluate the capacities of biodegradable plant protein nanoparticles as drug delivery systems. More particularly, as it is possible to think that these nanoparticulate carriers could be considered as safe for oral or topical administrations, it was of interest to test their potential after injection [127]. In this context, humoral and cell-mediated responses were analyzed in rats. They were immunized with an intradermal injection of legumin or legumin nanoparticles of about 250 nm. Legumin and legumin nanoparticles were suspended in a sterile saline solution mixed with complete Freund's adjuvant (CFA). A control group of rats was inoculated only with saline solution and CFA.

Humoral responses. These responses against legumin and legumin nanoparticles were examined by usually appropriate techniques, i.e. Western blot and ELISA [127]. Both techniques showed that sera from rats immunized with legumin strongly expressed antibodies against this protein. On the contrary, serum samples from rats inoculated with legumin nanoparticles did not contain detectable amount of antibodies. Hence, legumin appears to be a potent inductor of the humoral immune response, while the use of legumin nanoparticles seems able to avoid the production of antibodies against them. However, the mechanism implicated in the absence of any humoral response to the legumin nanoparticles is far from clear. Mirshahi et al. [127] suggested some explanations: the chemical cross-linkage with glutaraldehyde [52] may produce some irreversible conformational changes in the protein tertiary structure making it less antigenic than the native protein [128], glutaraldehyde release could modify the surrounding cells and thus the lymphocyte response to antigens [129] or legumin nanoparticles were not sufficiently degraded to allow antigen formation during the period over which

experiment was carried out (1 month). Work is in progress to better understand this behavior.

Cell-mediated response. This was evaluated by *in vitro* lymphocyte proliferation assay 10 and 30 days after intradermal injection. Neither legumin nor legumin nanoparticles stimulated an immunogenic response [127]. This absence of response may be explained by a cytostatic effect of legumin. In a previous work (unpublished observations) it was noticed that legumin and legumin nanoparticles have a suppressive effect on *in vitro* fibroblast proliferation. These observations have to be confirmed.

Taking into consideration this cytostatic effect of legumin nanoparticles, it should be interesting to use them as pharmaceutical devices for the delivery of antitumor drugs in local cancer treatment.

Similar experimental work has to be carried out with the other plant proteins, gliadin and vicilin, in order to explore their medical and pharmaceutical potential as drug delivery systems.

From these *in vivo* and *in vitro* results, it can be assumed that plant proteins possess a role exceeding that of inert excipients. They have an influence on the entrapment efficiency of the drug and compatibility with tissues (essentially gliadin). In the future, it will be of interest to test these natural materials as encapsulating agents for the protection of sensitive drug from degradation (peptides, insulin, genes, etc.) and their ability to control drug release.

5.8 Conclusion

The method used to prepare all plant proteins nanoparticles was a controlled desolvatation method using only bioacceptable solvents. This procedure, avoiding toxic solvents, allowed the preparation of submicronic nanoparticulate systems with a narrow size distribution, and quite good yields and entrapment efficiency, making them susceptible to scale-up and industrial use. For gliadin, either hydrophilic or lipophilic drugs could be entrapped satisfactorily. Furthermore, gliadin nanoparticles possess a high interactive potential with biological surfaces, as demonstrated by *ex vivo* and *in vivo* animal experimentations. It appears that gliadin nanoparticles are interesting oral carriers to improve bioavailability of drugs. Nevertheless, in the future, efforts should be made to obtain a complete understanding of all the mechanisms implicated in the metabolism of these colloidal systems at the biomolecular level, in order to use them for medical applications.

References

- | | |
|--|---|
| <p>1 F. PUISIEUX, G. BARRATT, G. COUARRAZE, P. COUVREUR, J. P. DEVISSAGUET, C. P. DUBERNET, E.</p> | <p>FATTAL, H. FESSI, C. VAUTHIER, S. BENITA, Polymeric micro and nanoparticles as drug carriers. In</p> |
|--|---|

- Polymeric Biomaterials*, S. DIMITRIU (Ed.), Marcel Dekker, New York, 1994, pp. 747–795.
- 2 M. J. ALONSO, Nanoparticulate drug carrier technology. *Drug Pharm. Sci.* 1996, 77, 203–242.
 - 3 C. DUCLAIRROIR, A. M. ORECCHIONI, P. DEPRAETERE, E. NAKACHE, Alpha-tocopherol encapsulation and *in-vitro* release from wheat gliadin nanoparticles. *J. Microencapsul.* 2002, 19, 53–60.
 - 4 S. GOIN, Microencapsulation: industrial appraisal of industrial technologies and trends. *Trends Food Sci. Technol.* 2004, 15, 330–347.
 - 5 E. NAKACHE, N. POULAIN, F. CANDAU, A. M. ORECCHIONI, J. M. IRACHE, Biopolymer and polymer nanoparticles and their biomedical applications. In *Handbook of Nanostructured Materials and Nanotechnology*, H. S. NALWA (Ed.), Vol. 5: *Organics, Polymers and Biological Materials*, Academic Press, New York, 2000, pp. 577–638.
 - 6 P. A. KRAMER, Albumin microspheres as vehicles for achieving specificity in drug delivery. *J. Pharm. Sci.* 1974, 63, 1646–1647.
 - 7 W. LIN, A. G. A. COOMBES, M. C. DAVIES, S. S. DAVIS, L. ILLUM, Preparation of sub 100 nm human serum albumin nanospheres using a pH-coacervation method. *J. Drug Target.* 1993, 1, 237–243.
 - 8 I. EZPELETA, J. M. IRACHE, S. STAINMESSE, C. CHABENAT, J. GUEGUEN, Y. POPINEAU, A. M. ORECCHIONI, Gliadin nanoparticles for the controlled release of all *trans*- retinoic acid. *Int. J. Pharm.* 1996, 131, 191–200.
 - 9 J. LAZKO, Y. POPINEAU, J. LEGRAND, Soy glycinin microcapsules by simple coacervation method. *Colloids Surfaces B.* 2004, 37, 1–8.
 - 10 X. LIU, Q. SUN, H. WANG, L. ZHANG, J. Y. WANG, Microspheres of corn protein, Zein, for an ivermectin drug delivery. *Biomaterials* 2005, 26, 109–115.
 - 11 M. N. MIÈGE, Protein tips and distribution. In *Encyclopedia of Plant Physiology*, D. BOULTER and B. PARTHIER (Eds.), Springer, Berlin, 1982, pp. 291–345.
 - 12 C. DOMONEY, R. CASEY, Measurement of gene number for seed storage proteins in *Pisum*. *Nucleic Acids Res.* 1985, 13, 687–699.
 - 13 M. A. CHOWDHURY, A. E. SLINKARD, Genetic diversity in grass pea (*Lathyrus sativus* L.). *Genet. Resources Crop Evol.* 2000, 47, 163–169.
 - 14 K. S. G. WONG, J. WANG, L. TAO, J. TAN, J. G. ZHANG, D. A. PASSEY, J. YU, compositional gradients in Gramineae genes. *Genome Res.* 2002, 12, 851–856.
 - 15 G. H. MCINTOSH, D. L. TOPPING, Food legumes in human nutrition. In *Proceedings of the Third International Food Legumes Research Conference*, Adelaide, Australia, R. KNIGHT (Ed.), 2000, pp. 655–660.
 - 16 D. W. GRIFFITHS, D. A. LAWES, Variation in the crude protein content of field beans (*Vicia faba* L.) in relation to the possible improvement of the protein content of the crop. *Euphytica* 1978, 27, 487–495.
 - 17 H. LEVANONY, R. RUBIN, Y. ALTSCHULER, G. GALILI, Evidence for a novel route of wheat storage proteins to vacuoles. *J. Cell Biol.* 1992, 119, 1117–1128.
 - 18 I. HOHL, D. G. ROBINSON, M. J. CRISPPEELS, G. HINZ, Transport of storage proteins to the vacuole is mediated by vesicles without a clathrin coat. *J. Cell Sci.* 1996, 109, 2539–2550.
 - 19 M. I. GELI, M. TORRENT, D. LUDEVÍD, Two structural domains mediate two sequential events in γ -zein targeting: protein endoplasmic reticulum retention and protein body formation. *Plant Cell* 1994, 6, 1911–1922.
 - 20 B. G. FORDE, A. HEYWORTH, J. PYWELL, M. KREIS, Nucleotide sequence of a B1 hordein gene and the identification of possible upstream regulatory elements in endosperm storage protein genes from barley, wheat and maize. *Nucleic Acids Res.* 1985, 13, 7327–7339.
 - 21 N. ROSENBERG, Y. SHIMONI, Y. ALTSCHULER, H. LEVANONY, M. VOLOKITA, and G. GALILI, Wheat (*Triticum aestivum* L.) γ -gliadin

- accumulates in dense protein bodies within the endoplasmic reticulum of yeast. *Plant Physiol.* **1993**, *102*, 61–69.
- 22** K. MÜNTZ, Globulins from legume seeds: structure and function during storage and reactivation. In *Plant Proteins from European Crops*, J. GUEGUEN, Y. POPINEAU (Eds.), Springer, Berlin, **1998**, pp. 3–12.
- 23** T. B. OSBORNE, *The Vegetable Proteins*, 2nd edn., Longmans Green, New York, **1924**.
- 24** P. ARGOS, S. V. L. NARAYANA, N. C. NIELSEN, Structural similarity between legumin and vicilin storage proteins from legumes. *EMBO J.* **1985**, *4*, 1111–1118.
- 25** P. E. M. GIBBS, K. B. STRONGIN, A. MCPHERSON, Evolution of legume seed storage protein: a domain common to legumins and vicilins is duplicated in vicilins. *Mol. Biol. Evol.* **1989**, *6*, 614–623.
- 26** I. A. POPELO, V. V. SUCHKOV, V. Y. GRINBERG, V. B. TOLTOGUZOVA, Liquid/liquid phase equilibrium in globulin/salt/water systems: legumin. *J. Sci. Food Agric.* **1990**, *51*, 345–353.
- 27** K. D. SCHWENKE, D. ZIRWER, K. GAST, E. GÖRNITZ, K. J. LINOW, J. GUEGUEN, Changes of the oligomeric structure of legumin from pea (*Pisum sativum* L.) after succinylation. *Eur. J. Biochem.* **1990**, *194*, 621–627.
- 28** J. A. GATEHOUSE, G. W. LYCETT, A. J. DELAUNY, R. R. R. CROY, D. BOULTER, Sequence specificity of the post-translational proteolytic cleavage of vicilin, a seed storage protein of pea (*Pisum sativum* L.). *Biochem. J.* **1983**, *212*, 427–432.
- 29** E. DERBYSHIRE, D. J. WRIGHT, D. BOULTER, Legumin and vicilin, storage proteins of legume seeds. *Phytochemistry* **1976**, *13*, 3–24.
- 30** J. GUEGUEN, A. T. VU, F. SCHAEFFER, Large scale purification and characterization of pea globulins. *J. Sci. Food Agric.* **1984**, *35*, 1024–1033.
- 31** D. CAER, B. COLAS, Protease susceptibility and amino group accessibility to trinitrobenzenesulfonic acid of legumin during its glycosylation. *J. Agric. Food Chem.* **1993**, *41*, 544–546.
- 32** M. C. LAWRENCE, T. IZARD, M. BEUCHAT, R. J. BLAGROVE, P. M. COLEMAN, Structure of phaseolin at 2.2 Å resolution. Implications for a common vicilin/legumin structure and the genetic engineering of seed storage proteins. *J. Mol. Evol.* **1994**, *23*, 748–776.
- 33** S. GUILBERT, N. GONTARD, Edible and biodegradable food packaging, in *Foods and Packaging Materials – Chemical Interactions*, P. ACKERMANN, M. JÄGERSTAD, T. OHLSSON (Eds.), Royal Society of Chemistry, Cambridge, **1995**, pp. 159–168.
- 34** J. HARGREAVES, Y. POPINEAU, M. LE MESTE, M. HEMMINGGA, Molecular flexibility in wheat gluten proteins submitted to heating. *FEBS Lett.* **1995**, *373*, 103–107.
- 35** A. APICHARTSRANGKOON, A. E. BELL, D. A. LEDWARD, J. D. SCOFIELD, Dynamic viscoelastic behavior of high-pressure-treated wheat gluten. *Cereal Chem.* **1999**, *76*, 777–782.
- 36** J. LEFEBVRE, Y. POPINEAU, G. DESHAYES, L. LAVENANT, Temperature-induced changes in the dynamic rheological behavior and size distribution of polymeric proteins for glutens from wheat near-isogenic lines differing in HMW-glutenin subunit composition. *Cereal Chem.* **2000**, *77*, 193–201.
- 37** J. A. BIETZ, J. A. ROTHFUS, Comparison of peptides from wheat gliadin and glutenin. *Cereal Chem.* **1970**, *47*, 381–392.
- 38** P. R. SHEWRY, Cereal seed storage proteins. In *Seed Development and Germination*, J. KIGEL, G. GALILI (Eds.), NY Bale, Hong Kong, **1995**, pp. 45–72.
- 39** D. D. KASARDA, Structure and properties of α -gliadins. *Ann. Technol. Agric.* **1980**, *29*, 151–173.
- 40** J. H. WOYCHIK, R. A. BOUNDY, R. A. DIMLER, Starch gel electrophoresis of wheat gluten proteins with concentrated urea. *Arch. Biochem. Biophys.* **1961**, *84*, 477–482.
- 41** M. BYERS, J. MIFFLIN, S. J. SMITH, A quantitative comparison of the extraction of protein fractions from

- wheat grain by different solvents, and of the polypeptide and amino acid composition of the alcohol-soluble proteins. *J. Sci. Food Agric.* **1983**, *34*, 447–462.
- 42** D. L. DU CROS, C. W. WRIGLEY, Improved electrophoretic methods for identifying cereal varieties. *J. Sci. Food Agric.* **1979**, *30*, 785–794.
- 43** C. LARRÉ, Y. POPINEAU, W. LOISEL, Fractionation of gliadins from common wheat by cation exchange FPLC. *J. Cereal Chem.* **1991**, *14*, 231–241.
- 44** H. WIESER, W. SEILMER, H. D. BELITZ, Quantitative determination of gliadin subgroups from different wheat cultivars. *J. Cereal Sci.* **1994**, *19*, 149–155.
- 45** H. HE, R. R. ROACH, R. C. HOSENEY, Effect of nonchaotropic salts on flour bread-making properties. *Cereal Chem.* **1992**, *69*, 366–371.
- 46** Y. POPINEAU, S. DENERY-PAPINI, *Protéines Végétales*, Lavoisier, Paris, 1996.
- 47** R. BODMEIER, H. CHEN, E. PAERA-TAKUL, A novel approach to the oral delivery of micro- or nanoparticles. *Pharm. Res.* **1989**, *6*, 413–417.
- 48** M. S. EL-SAMALIGY, P. ROHDEWALD, Reconstituted collagen nanoparticles, a novel drug carrier delivery system. *J. Pharm. Pharmacol.* **1983**, *35*, 537–539.
- 49** D. J. BURGESS, O. N. SINGH, Spontaneous formation of small sized albumin/acacia coacervate particles. *J. Pharm. Pharmacol.* **1993**, *45*, 586–591.
- 50** I. EZPELETA, J. M. IRACHE, S. STAINMESSE, J. GUEGUEN, A. M. ORECCHIONI, Preparation of small-sized particles from vicilin (vegetal protein from *Pisum sativum* L.) by coacervation. *Eur. J. Pharm. Biopharm.* **1996**, *42*, 36–41.
- 51** J. M. IRACHE, L. BERGOUGNOUX, I. EZPELETA, J. GUEGUEN, A. M. ORECCHIONI, Optimization and *in vitro* stability of legumin nanoparticles obtained by a coacervation method. *Int. J. Pharm.* **1995**, *126*, 103–109.
- 52** T. MIRSHAH, J. M. IRACHE, J. GUEGUEN, A. M. ORECCHIONI, Development of drug delivery systems from vegetal proteins: legumin nanoparticles. *Drug Dev. Ind. Pharm.* **1996**, *22*, 841–846.
- 53** J. J. MARTY, R. C. OPPENHEIM, P. SPEISER, Nanoparticles: a new colloidal drug delivery system. *Pharm. Acta Helv.* **1978**, *53*, 17–23.
- 54** I. EZPELETA, J. M. IRACHE, J. GUEGUEN, A. M. ORECCHIONI, Properties of glutaraldehyde cross-linked vicilin nano- and micro-particles. *J. Microencapsul.* **1997**, *14*, 557–565.
- 55** C. DUCLAIR, E. NAKACHE, H. MARCAIS, A. M. ORECCHIONI, Formation of gliadin nanoparticles: influence of the solubility parameter of the protein solvent. *Colloid Polym. Sci.* **1998**, *276*, 321–327.
- 56** M. A. ARANGOA, M. A. CAMPANERO, Y. POPINEAU, J. M. IRACHE, Evaluation and characterization of gliadin nanoparticles and isolates by reversed-phase HPLC. *J. Cereal Sci.* **2000**, *31*, 223–228.
- 57** M. A. ARANGOA, M. A. CAMPANERO, M. J. RENEDO, G. PONCHEL, J. M. IRACHE, Gliadin nanoparticles as carriers for the oral administration of lipophilic drugs. Relationship between bioadhesion and pharmacokinetics. *Pharm. Res.* **2001**, *18*, 1521–1527.
- 58** C. DUCLAIR, J. M. IRACHE, E. NAKACHE, A. M. ORECCHIONI, C. CHABENAT, Y. POPINEAU, Gliadin nanoparticles: formation, all-*trans*-retinoic acid entrapment and release, size optimization. *Polym. Int.* **1999**, *79*, 327–333.
- 59** J. HILDEBRAND, R. SCOTT, *Regular Solutions*, Prentice-Hall, Englewood Cliffs, NJ, 1962.
- 60** A. F. M. BARTON, *Handbook of Solubility Parameters and Other Cohesion Parameters*, 2nd edn., CRC Press, Boca Raton, FL, 1991.
- 61** J. T. ELDER, A. ASTROM, U. PETTERSON, A. TAVAKKOL, C. E. GRIFFITHS, A. KRUST, P. KASTNER, P. CHAMSON, J. J. VOORHES, Differential regulation of retinoic acid receptors and binding proteins in human skin. *J. Invest. Dermatol.* **1992**, *98*, 673–679.
- 62** A. H. LEWIN, M. E. BOS, F. C. ZUSI, X.

- NAIR, G. WHITING, P. BOURQUIN, G. TETRAULT, F. I. CAROL, Evaluation of retinoids as therapeutic agents in dermatology. *Pharm. Res.* **1994**, *11*, 192–200.
- 63** R. M. LAVKER, J. J. LEYDEN, E. G. THORNE, An ultrastructural study of the effects of topical tretinoin on microcomedones. *Clin. Ther.* **1992**, *14*, 773–780.
- 64** J. DRACH, G. LOPEZ-BERESTEIN, T. MCQUEEN, M. ANDREEFF, K. METHA, Induction of differentiation in myeloid leukemia cells lines and acute promyelocytic leukemia cells by liposomal all-*trans* retinoic acid. *Cancer Res.* **1993**, *53*, 2100–2104.
- 65** S. CASTAIGNE, C. CHOMIENNE, M. T. DANIEL, P. FENAUX, R. BERGER, L. DEGOS, All-*trans* retinoic acid as a differentiation therapy in acute promyelocytic leukemias. I. Clinical results. *Blood*, **1990**, *76*, 1704–1710.
- 66** K. SEITER, W. H. MILLER, E. J. FELDMAN, T. AHMED, Z. ARLIN, Pilot study of all-*trans* retinoic acid as post-remission therapy in patients with acute promyelocytic leukemia. *Leukemia*, **1995**, *9*, 15–18.
- 67** L. DELVA, M. CORNIC, N. BALITRAND, C. CHOMIENNE, Application thérapeutique de l'acide rétinoïque dans la leucémie aiguë promyélocyttaire. *Immunoanal. Biol. Spec.* **1991**, *25*, 17–21.
- 68** T. TAKINO, K. KOISHI, Y. TAKAKURA, M. HASHIDA, Long circulating emulsion carrier systems for highly lipophilic drugs. *Biol. Pharm. Bull.* **1994**, *17*, 121–125.
- 69** K. METHA, T. SADEGHI, T. MCQUEEN, G. LOPEZ-BERESTEIN, Liposome encapsulation circumvents the hepatic clearance mechanisms of all-*trans* retinoic acid. *Leuk. Res.* **1994**, *18*, 587–596.
- 70** V. MASINI, F. BONTE, A. MEYBECK, J. WEPIERRE, Cutaneous bioavailability in hairless rats of tretinoin in liposomes or gel. *J. Pharm. Sci.* **1993**, *82*, 17–21.
- 71** B. IDSON, Dry skin moisturizing and emolliency. *Cosm. Toil.* **1992**, *107*, 69–78.
- 72** J. H. EPSTEIN, Photocarcinogenesis, skin cancer and aging. *J. Am. Acad Dermatol.* **1983**, *9*, 487–502.
- 73** A. J. SOBER, Solar exposure in the etiology of cutaneous melanoma. *Photodermatol.* **1987**, *4*, 23–31.
- 74** A. L. TAPPEL, Vitamin E as the biological lipid antioxidant. *Vitamins Hormones* **1962**, *20*, 493–510.
- 75** L. H. KLIGMAN, A. M. KLIGMAN, Photoaging in dermatology. *Photo-dermatology* **1986**, *3*, 215–227.
- 76** R. C. WESTER, H. I. MAIBACH, Absorption of tocopherol into and through human skin. *Cosm. Toil.* **1997**, *112*, 53–57.
- 77** P. M. MAYER, W. PITTERMANN, S. WALLAT, The effects of Vitamin E on the skin. *Cosm. Toil.* **1993**, *108*, 99–109.
- 78** A. TEGLIA, G. SECCHI, New protein ingredients for skin detergency: relative wheat protein–surfactant complexes. *Int. J. Cosm. Sci.* **1994**, *16*, 235–246.
- 79** C. DUCLAIRIOIR, A. M. ORECCHIONI, P. DEPRAETERE, F. OSTERSTOCK, E. NAKACHE, Evaluation of gliadins nanoparticles as drug delivery systems: a study of three different drugs. *Int. J. Pharm.* **2003**, *353*, 133–144.
- 80** A. A. MARYOTT, E. R. SMITH, Table of dielectric constants of pure liquids. In *Circular 514*, National Bureau of Standards, New York, **1951**.
- 81** M. LIS-BALCHIN, S. HART, Studies on the mode of action of the essential oil of lavender (*Lavandula angustifolia* P. MILLER). *Phytother. Res.* **1999**, *13*, 540–542.
- 82** E. AUBENY, J. C. COLAU, A. NANDEUIL, Local spermicidal contraception: a comparative study of the acceptability and safety of a new pharmaceutical formulation of benzalkonium chloride, the vaginal capsule, with a reference formulation, the pessary. *Eur. J. Contracept. Health Care* **2000**, *5*, 61–67.
- 83** M. A. WAINBERG, B. SPIRA, G. BLEAU, R. THOMAS, Inactivation of human immunodeficiency virus type 1 in tissue culture fluid and in genital secretion by the spermicide

- benzalkonium chloride. *J. Clin. Microbiol.* **1990**, *28*, 156–158.
- 84** I. H. AL-ABDULLA, G. W. MELLOR, M. S. CHILDERSTONE, A. M. SIDKI, D. S. SMITH, Comparison of three different activation methods for coupling antibodies to magnetisable cellulose particles. *J. Immunol. Methods* **1989**, *122*, 253–258.
- 85** C. WEBER, S. REISS, K. LANGER, Preparation of surface modified protein nanoparticles by introduction of sulfhydryl groups. *Int. J. Pharm.* **2000**, *211*, 67–78.
- 86** C. M. LEHR, J. A. BOUWSTRA, W. KOK, A. B. J. NAACH, A. G. DE BOER, H. E. JUNGINGER, Bioadhesion by means of specific binding of tomato lectin. *Pharm. Res.* **1992**, *9*, 547–553.
- 87** J. M. IRACHE, C. DURRER, D. DUCHÈNE, G. PONCHEL, Preparation and characterization of lectin-latex conjugates for specific bioadhesion. *Biomaterials* **1994**, *15*, 899–904.
- 88** A. MARUYAMA, T. ISHIHARA, N. ADACHI, T. AKAIKE, Preparation of nanoparticles bearing high density carbohydrate chains using carbohydrate-carrying polymers as emulsifier. *Biomaterials* **1994**, *15*, 1035–1042.
- 89** M. ROSER, D. FISCHER, T. KISSEL, Surface-modified biodegradable albumin nano- and microspheres. II: effect of surface charges on *in vitro* phagocytosis and biodistribution in rats. *Eur. J. Pharm. Biopharm.* **1998**, *46*, 255–263.
- 90** K. LANGER, C. COESTER, C. WEBER, H. VON BRIESEN, J. KREUTER, Preparation of avidin-labeled protein nanoparticles as carriers for biotinylated peptide nucleic acid. *Eur. J. Pharm. Biopharm.* **2000**, *49*, 303–307.
- 91** W. LIN, M. C. GARNETT, M. C. DAVIES, F. BIGNOTTI, P. FERRUTI, S. S. DAVIS, L. ILLUM, Preparation of surface-modified albumin nanospheres. *Biomaterials* **1997**, *18*, 559–565.
- 92** G. V. BETAGERI, C. D. V. BLACK, J. SZEBENI, L. M. WAHL, J. N. WEINSTEIN, Fc-receptor-mediated targeting of antibody-bearing liposomes containing dideoxycytidine triphosphate to human monocyte/macrophages. *J. Pharm. Pharmacol.* **1993**, *45*, 48–53.
- 93** N. G. DOLINNAYA, N. I. SOKOLOVA, D. T. ASHIRBEKOVA, Z. A. SHABAROVA, The use of BrCN for assembling modified DNA duplexes and DNA–RNA hybrids; comparison with water soluble carbodiimide. *Nucleic Acids Res.* **1991**, *19*, 3067–3072.
- 94** D. M. BOORSMA, J. G. STREEFKERK, Periodate or glutaraldehyde for preparing peroxidase conjugates? *J. Immunol. Methods* **1979**, *30*, 245–255.
- 95** P. TIJSSEN, E. KURSTACK, Highly efficient and simple methods for the preparation of peroxidase and active peroxidase–antibody conjugates for enzyme immunoassays. *Anal. Biochem.* **1984**, *136*, 451–457.
- 96** S. AVRAMEAS, B. GUILBERT, Enzyme-immunoassay for measurement of antigens using peroxidase conjugates. *Biochimie* **1972**, *54*, 837–842.
- 97** H. OTTO, H. TAKAMIYA, A. VOGL, A two-stage method for cross-linking antibody globulin to ferritin by glutaraldehyde. Comparison between the one-stage and the two-stage method. *J. Immunol. Methods* **1973**, *3*, 137–146.
- 98** S. SANO, K. KATO, Y. IKADA, Introduction of functional groups onto the surface of polyethylene for protein immobilization. *Biomaterials* **1993**, *14*, 817–822.
- 99** R. S. MOLDAY, W. J. DREYER, A. REMBAUM, S. P. S. YEN, New immunolatex spheres: visual markers of antigens on lymphocytes for scanning electron microscopy. *J. Cell Biol.* **1975**, *64*, 75–88.
- 100** N. R. SHENOY, J. M. BAILEY, J. E. SHIVELY, Carboxylic acid-modified polyethylene: a novel support for the covalent immobilization of polypeptides for C-terminal sequencing. *Protein Sci.* **1992**, *1*, 58–67.
- 101** I. EZPELETA, J. M. IRACHE, S. STAINMESSE, C. CHABENAT, J. GUEGUEN, A. M. ORECCHIONI, Preparation of lectin–vicilin nanoparticle conjugates using the

- carbodiimide coupling technique. *Int. J. Pharm.* **1996**, *142*, 227–233.
- 102** I. EZPELETA, M. A. ARANGOA, J. M. IRACHE, S. STAINMESSE, C. CHABENAT, Y. POPINEAU, A. M. ORECCHIONI, Preparation of *Ulex europaeus* lectin–gliadin nanoparticle conjugates and their interaction with gastrointestinal mucus. *Int. J. Pharm.* **1999**, *191*, 25–32.
- 103** M. A. ARANGOA, G. PONCHEL, A. M. ORECCHIONI, M. J. RENEDO, D. DUCHENE, J. M. IRACHE, Bioadhesive potential of gliadin nanoparticulate systems. *Eur. J. Pharm. Sci.* **2000**, *11*, 333–341.
- 104** L. H. OLDE DAMINK, P. J. DIJKSTRA, M. J. VAN LUYN, P. B. VAN WACHEM, P. NIEUWENHUIS, J. FEIJEN, *In vitro* degradation of dermal sheep collagen cross-linked using a water-soluble carbodiimide. *Biomaterials* **1996**, *17*, 679–684.
- 105** J. A. EWART, Slow triplet β -gliadin from Capelle-Desprez. *J. Sci. Food Agric.* **1983**, *34*, 653–656.
- 106** G. T. HERMANSON (Ed.), *Zero-length Cross-linkers. Bioconjugate Techniques*, Academic Press, Orlando, FL, **1996**.
- 107** D. BASTOS, J. L. ORTEGA, F. J. DE LAS NIEVES, R. HIDALGO, Carboxylated latexes for covalent coupling antibodies I. *J. Colloid Interface Sci.* **1995**, *176*, 232–239.
- 108** J. L. ORTEGA, D. BASTOS, R. HIDALGO, Comparative studies on physically adsorbed and chemically IgG to carboxylated latexes II. *J. Colloid Interface Sci.* **1995**, *176*, 240–247.
- 109** D. HOARE, D. KOSHLAND, A method for the quantitative modifications and estimation of carboxylic acid groups in proteins. *J. Biol. Chem.* **1967**, *242*, 2447–2453.
- 110** J. V. STAROS, R. W. WRIGHT, D. M. SWINGLE, Enhancement by *N*-hydroxysulfosuccinimide of water soluble carbodiimide-mediated coupling reactions. *Anal. Biochem.* **1986**, *156*, 220–222.
- 111** J. K. VASIR, K. TAMBWEKAR, S. GARG, Bioadhesive microspheres as a controlled drug delivery system. *Int. J. Pharm.* **2003**, *255*, 13–32.
- 112** R. GURNY, J. M. MEYER, N. A. PEPPAS, Bioadhesive intraoral release systems: design, testing and analysis. *Biomaterials* **1984**, *5*, 336–340.
- 113** C. DURRER, J. M. IRACHE, F. PUISIEUX, D. DUCHENE, G. PONCHEL, Mucoadhesion of latexes I. Analytical methods and kinetics studies. *Pharm. Res.* **1994**, *11*, 674–679.
- 114** J. M. IRACHE, C. DURRER, D. DUCHÈNE, G. PONCHEL, Bioadhesion of lectin–latex conjugates to rat intestinal mucosa. *Pharm. Res.* **1996**, *13*, 1714–1717.
- 115** G. PONCHEL, M. J. MONTISCI, A. DEMBRI, C. DURRER, D. DUCHENE, Mucoadhesion of colloidal particulate systems in the gastrointestinal tract. *Eur. J. Pharm. Biopharm.* **1997**, *44*, 25–31.
- 116** P. LANCE, R. LEV, Colonic oligosaccharide structures deduced from lectin-binding studies before and after desialylation. *Hum. Pathol.* **1991**, *22*, 307–312.
- 117** R. SHARMA, U. SCHUMACHER, The influence of diets and gut microflora on lectin binding patterns of intestinal mucin in rats. *Lab. Invest.* **1995**, *73*, 558–564.
- 118** G. PONCHEL, J. M. IRACHE, Specific and non-specific bioadhesive particulate systems for oral delivery to the gastrointestinal tract, *Adv. Drug Del. Rev.* **1998**, *34*, 191.
- 119** M. A. ARANGOA, M. A. CAMPANERO, J. M. IRACHE, Potencial bioadhesivo de las nanopartículas de gliadina en el estómago. *Rev. Colomb. Cien. Quím. Farm.* **2004**, *33*, 38–47.
- 120** J. M. GU, J. R. ROBINSON, H. S. LEUNG, Binding of acrylic polymers to mucin-epithelial surfaces. Structure/property relationship. *Crit. Rev. Ther. Drug Carrier Syst.* **1998**, *5*, 21.
- 121** N. SUBRAMANIAN, S. RAY, S. K. GHOSAL, R. BHADRA, S. P. MOULIK, Formulation design of self-micro-emulsifying drug delivery systems for improved oral bioavailability of celecoxib. *Biol. Pharm. Bull.* **2004**, *27*, 1993–1999.
- 122** A. T. M. SERAJUDDIN, P. C. SHEE, D.

- MUFSON, D. F. BERNSTEIN, M. A. AUGUSTINE, Effect of vehicle amphiphilicity on the dissolution and bioavailability of a poorly water-soluble drug from solid dispersion. *J. Pharm. Sci.* **1988**, *77*, 414–417.
- 123** B. J. AUNGST, N. NGUYEN, N. J. ROGERS, S. ROWE, M. HUSSAIN, L. SHUM, S. WHITE, Improved oral bioavailability of an HIV protease inhibitor using Gelucire 44/14 and Labrasol vehicles. *Bull Tech. Gattefosse* **1994**, *87*, 49–54.
- 124** R. N. GURSOY, S. BENITA, Self-emulsifying drug delivery systems (SEDDS) for improved oral delivery of lipophilic drugs. *Biomed. Pharmacother.* **2004**, *58*, 173–182.
- 125** S. J. DOUGLAS, S. S. DAVIS, L. ILLUM, Nanoparticles in drug delivery. *Crit. Rev. Ther. Drug Carrier System*, **1987**, *3*, 233–261.
- 126** P. ERLICH, *Collected Studies on Immunity*, Wiley, New York, **1906**.
- 127** T. MIRSHAH, J. M. IRACHE, C. NICOLAS, M. MIRSHAH, J. P. FAURE, J. GUEGUEN, C. HEQUET, A. M. ORECCHIONI, Adaptive immune responses of legumin nanoparticles. *J. Drug Target.* **2002**, *10*, 625–631.
- 128** O. SCHUSSLER, M. SHEN, L. SHEN, S. M. CARPENTIER, S. KAVERI, A. CARPENTIER, Effect of human immunoglobulins on the immunogenicity of porcine bioprostheses. *Ann. Thorac. Surg.* **2001**, *71*, S396–S400.
- 129** D. WIEBE, J. MEGERMAN, G. J. L'ITALIEN, W. M. ABBOT, Glutaraldehyde release from vascular prosthesis of biologic origin. *Surgery* **1988**, *104*, 26–33.

Ch3

Chapter 12

HPTLC-MALDI TOF MS Imaging Analysis of Phospholipids

Tatiana Kondakova, Nadine Merlet Machour, and Cécile Duclairoir Poc

Abstract

Phospholipids are major and essential functional components of all living cells playing fundamental roles in cellular metabolism and homeostasis. At molecular level, these cell compounds function as a barrier between the cell and its modifying environment and play an essential role in cell adaptation to environmental stressors. In the human body, phospholipids play a role of key metabolites in many pathways, either in health or in disease. However, because of the development of genomics and proteomics tools at the end of the twentieth century, these essential for all living cells molecules remain to be investigated in more detail. In this effort, we adopted a protocol, using MALDI-TOF MS Imaging coupled to HPTLC, to screen a large number of phospholipid classes in a short span of time. This method set the stage for future studies aimed at better defining the diversity and roles of phospholipids in all living cells.

Key words Lipidomics, Phospholipids, Mass spectrometry imaging, HPTLC MALDI TOF MSI

1 Introduction

Despite an excessive development of proteomics and genomics tools caused by the emergence of molecular biology techniques at the end of the twentieth century, there is also a growing interest in the analysis and identification of lipids [1]. All living cells, prokaryotic, as well as eukaryotic contain a myriad of lipids, whose roles are still poorly studied. Although a considerable diversity of lipid structures exists, most predominant are phospholipids (PLs) [2]. PLs are described as acylated derivatives of *sn*-glycerol-3-phosphate typically composed of two fatty acid chains, a glycerol unit, and a phosphate group linked to a polar head group [3].

PLs are the major components of all the biological membranes contributing to their biochemical and biophysical properties [2, 4, 5]. In mammalian cells, PLs play several roles, being often key metabolites in many pathways, either in health or in disease. The changes in membrane PLs' structure and composition are correlated to several diseases such as diabetes [6, 7], and Alzheimer's disease [8, 9]. The roles of PLs are especially remarkable in domains of neurology, neuro-oncology, and psychiatry. Recently, the PLs'

contribution in depression and anxiety disorders [5], as well as in synaptic communication [10], was proposed. In this way, the roles of PLs in bacteria–host interactions should also be taken into account because of the possible correlation of the human microbiota effect on the brain function [11], and multiple strategies used by bacteria to exploit eukaryotic PLs [2, 12, 13].

Altogether, these investigations encouraged development of lipidomics and metabolomics (i.e., analysis of endogenous biomolecules, generally <2000 Da, in complex biological matrices) [14]. Mass spectrometric tools, including Matrix-Assisted Laser Desorption Ionization Time-Of-Flight Mass Spectrometry (MALDI TOF MS), are some of the most robust analytical methods that provide structural data for complex biological matrices [15, 16]. The use of MALDI TOF MS for the PLs analysis helps to overcome many problems related to the complexity and diversity of the biological extracts, and appears as one of the most convenient methods to realize a complete PL screening [17, 18].

Here, we describe an analytical method for the PLs' study based on the direct coupling High Performance Thin Layer Chromatography (HPTLC) to MALDI TOF MS Imaging. This technique, adapted for the analysis of bacterial lipids, appears as a universal [15, 19], rapid, and globally cheap method for the PLs screening in all living cells. Together with another lipidomic techniques, which can be found in this volume of the Series, these protocols should be useful to explore the PL composition, localization, and role(s) in both eukaryotic and prokaryotic cells and, thus, better assess the PLs functions either in health or in disease, elucidating, among others, the role(s) of PLs in host–parasite and/or host–symbiont interactions.

2 Materials

2.1 Phospholipid Extraction

1. Extraction solution A: $\text{CHCl}_3/\text{CH}_3\text{OH}$ (1/2, v/v). Mix solution for ~1 min using vortexer to obtain the homogenous mixture (*see Note 1*).
2. Chloroform (*see Note 1*).
3. Water (*see Note 2*).
4. Centrifuge.

2.2 High-Performance Thin-Layer Chromatography (HPTLC)

1. Elution system: $\text{CHCl}_3/\text{CH}_3\text{-CH}_2\text{OH}/\text{H}_2\text{O}/\text{N}(\text{CH}_2\text{-CH}_3)_3$ (35/35/7/35, v/v/v/v) (*see Notes 1 and 3*).
2. HPTLC silica gel 60 plates F_{254} (75 × 50 mm, on aluminum backs) obtained from Merck (Darmstadt, Germany).

3. TLC chambers (e.g., TLC TANK 80 × 120 mm from Fisher Scientific SAS).
4. Primuline dye: 0.05% solution in CH₃-CO-CH₃/H₂O, (8/2, v/v) (*see Note 1*).

2.3 HPTLC-MALDI TOF Analysis

1. DHB matrix solution: 200 g/L 2,5-dihydroxybenzoic acid (DHB) in C₂H₃N/0.1% trifluoroacetic acid (TFA), (90/10, v/v) [19] (*see Notes 1 and 4*). 10 mL volume is recommended for coating of one HPTLC plate.
2. TLC MALDI target from Bruker Daltonics (Bremen, Germany).
3. Time-of-flight mass spectrometer (e.g., Autoflex III from Bruker Daltonics, Bremen, Germany).
4. TLC MALDI software (e.g., v. 1.1.7.0 from Bruker Daltonics, Bremen, Germany).
5. Peptide Calibration Standard II from Bruker Daltonics (Bremen, Germany).
6. MALDI Imaging software (e.g., FlexImaging software v. 2.1., Bruker Daltonics, Bremen, Germany).

3 Methods

3.1 Phospholipid Extraction

The quickest and simplest method to extract PLs from living cells has been described by Bligh and Dyer [20] (Fig. 1). This procedure could be applied to all biological materials (i.e., fish muscle [20], mitochondria [21], protozoa [22], and bacteria [23, 24]) and can be carried out in approximately 10 min. Briefly, a purified PL extract is obtained by homogenization of samples with a mixture of chloroform and methanol (CHCl₃/CH₃OH) in such proportions that a miscible system is formed with the water in sample. Additional dilution with chloroform and water separates the homogenate into two layers, among which the lower chloroform layer contains PLs.

1. To a 1 g sample (*see Notes 5 and 6*) add 3 mL of the extraction solution A and vortex during 3 min.
2. Add 1 mL of chloroform and vortex during 1 min.
3. Add 1 mL of water (*see Note 2*) and vortex during 3–5 min.
4. Centrifuge the mixture 10 min at 3000 × *g* to allow the formation of the two phases (i.e., upper aqueous phase and lower chloroform phase).
5. Record the lower chloroform layer in another glass tube (*see Note 7*) using a Pasteur pipette.

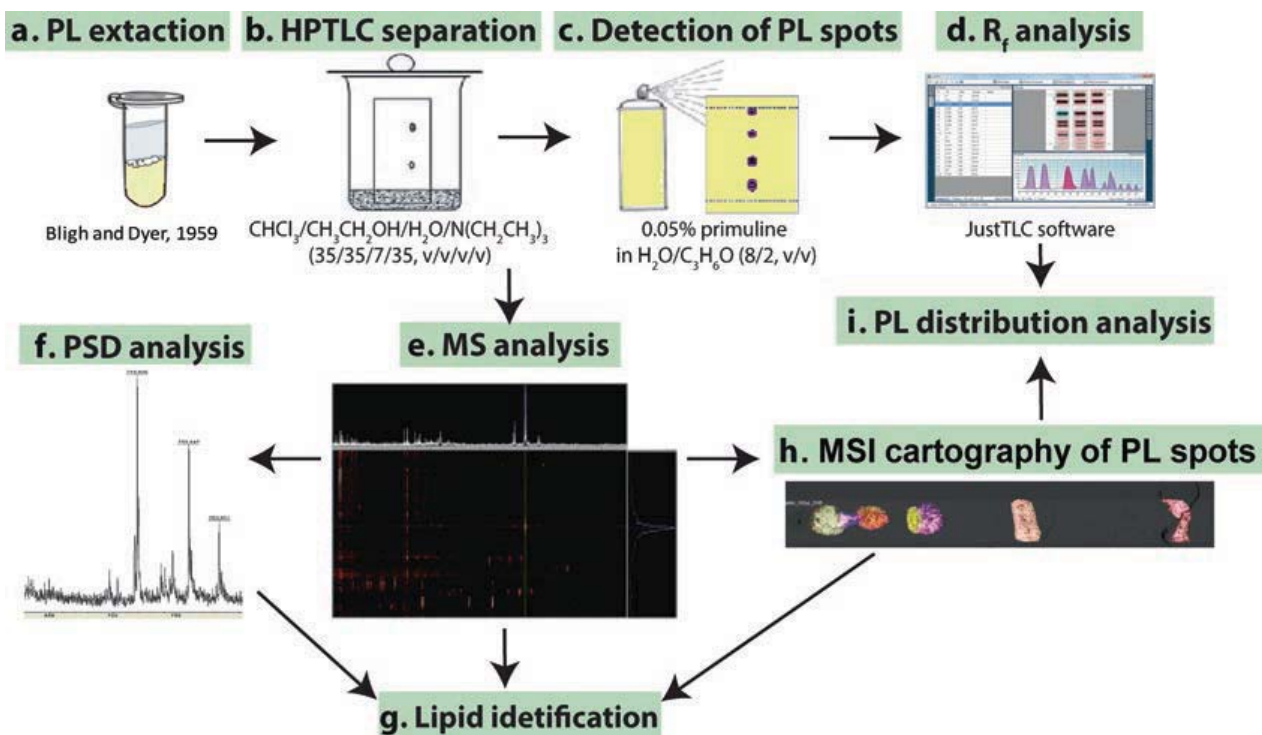


Fig. 1 Scheme illustrating the general HPTLC-MALDI TOF MSI method of phospholipid analysis. After extraction (a), phospholipids (PL) are separated on HPTLC plate (b) and detected using primuline spray (c), conducting to calculation of PL spots' retention factors (R_f) (d). MS analysis (e) of PL spots is directly performed on HPTLC plate in TLC MALDI software allowing the direct PDS analyses of each PL m/z (f) and PL identification (g). MALDI MS Imaging cartography of PL spots (h) is performed to study the PL distribution on HPTLC plate (i) according to their m/z, confirming PL identification

6. Evaporate chloroform under N₂ stream (see Note 8).
7. Measure the total lipid weight.
8. Store the extracted lipids at -20°C under N₂ atmosphere (see Note 9).

3.2 High-Performance Thin-Layer Chromatography (HPTLC)

High-Performance Thin-Layer Chromatography (HPTLC) is the simplest and well-known technique used in our work to separate individual PL species before MS and Post Source Decay (PSD) analyses (Fig. 1). We routinely use HPTLC silica gel 60 plates F₂₅₄, which allow PLs' separation according to their polar head groups (HGs) and are adapted to the future MALDI analyses. Our standard procedure is described below:

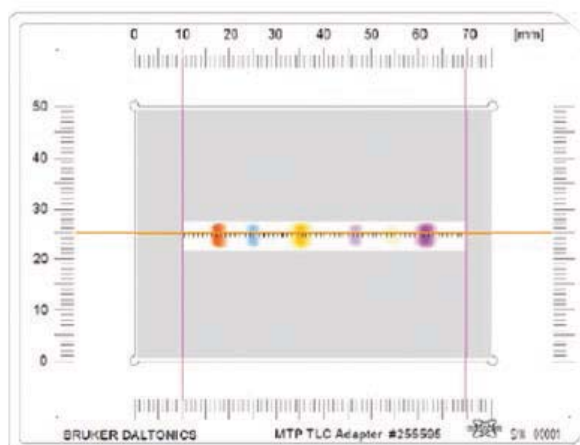
1. Wash HPTLC plate using elution system. For this, put the plate in a TLC chamber containing by a few mL of elution system and do the solvent system migration up to the top of the HPTLC plate (see Note 1).
2. Activate the HPTLC plate at 110 °C during 2 h (see Note 10).
3. To previously extracted PLs add chloroform in such a quantity to obtain the total PLs concentration ~1.5 mg/mL.

4. Spot 100 μL of lipid extract on the HPTLC plate by spotting of 2 μL 50 times (*see Note 11*).
5. Separate PL spots using $\text{CHCl}_3/\text{CH}_3\text{-CH}_2\text{OH}/\text{H}_2\text{O}/\text{N}(\text{CH}_2\text{-CH}_3)_3$ (35/35/7/35, v/v/v/v) as running separation solution (*see Note 1*) (Fig. 1b).
6. Remove HPTLC plate from the TLC chamber and dry the plate for 15 min using the chemical hood.
7. Spray primuline dye on HPTLC plate and dry for 15 min under chemical hood (Fig. 1c).
8. Visualize PL spots by UV fluorescence at 365 nm (*see Note 12*) (Figs. 3a and 4a).
9. Calculate the retention factors (R_f) of PL spots. For R_f calculation we usually use the Sweday JustTLC software (v. 4.0.3, Lund, Sweden) (Fig. 1d).

3.3 HPTLC-MALDI TOF Analysis

After separation on HPTLC plate, PLs are directly analyzed by MALDI TOF MS using TLC MALDI target (Fig. 2a). The hyphenated HPTLC-MALDI approach requires the uniform coverage of the TLC lanes with MALDI matrix and allows direct MS and PSD analyses of PLs previously separated on HPTLC plate (Fig. 1e and f). The mass spectrometric information is subsequently read out automatically using TLC software, allowing the screening of one sample in about 5 min. MALDI plate movement along the chromatographic lanes is driven by the standard movement mechanics of the MALDI ion source without additional robotic requirements. The quick analysis of PLs' MS spectra is also possible thanks to an interactive MALDI Chromatogram. MALDI MS

A TLC MALDI target



B TLC MALDI software

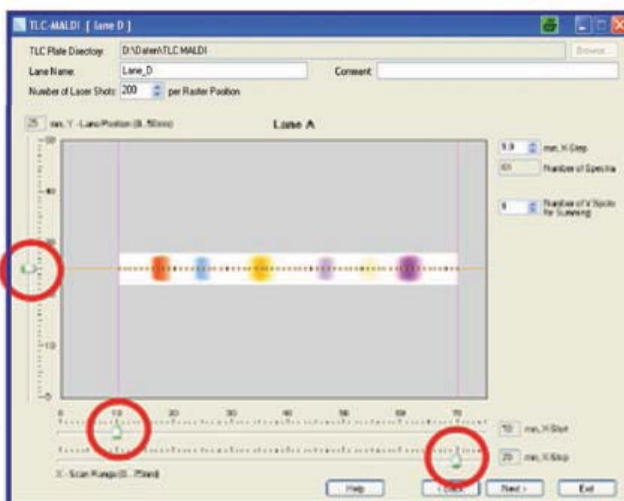


Fig. 2 HPTLC-MALDI coupling. (a) Scheme of TLC-MALDI adapter target. Orange and purple lines indicate the position of chromatographic line. (b) TLC-MALDI setup dialog

Imaging (Fig. 1h), designed for MS analysis of tissue, is also a good method for mapping individual PL species distribution in HPTLC plates, completing analysis.

3.3.1 HPTLC-MALDI TOF Coupling

1. Fill glass Petri dish with DHB matrix (200 mg/mL in C₂H₃N/0.1% TFA (90/10, v/v)) (*see Note 4*).
2. Submerge the plate in the reservoir and remove it immediately (typical immersion time: 1 s).
3. Lay the plate on a clean surface and dry it in two steps.
First step: Dry the plate with a very gentle airstream (e.g., use airstream close to a fume hood window) around 2 min until the surface becomes matt.
Second step: Dry the HPTLC plate with a hair-dryer in a stream of cold air vertically from above for about 90 s.
4. Repeat matrix application and drying procedure. This time hold the plate on the opposite edge and blow in the second step for 4 min (*see Notes 13 and 14*).
5. Insert the HPTLC plate into the dedicated adapter target (e.g., TLC MALDI target from Bruker Daltonics, Bremen, Germany) (Fig. 2a).
6. Put the HPTLC plate with the target in the desiccator for a few minutes (*see Note 15*).

3.3.2 Calibration

Automatic MALDI TOF calibration is performed in two steps.

1. External calibration of the apparatus is performed daily in FlexControl software using the DHB matrix peaks and the Peptide Calibration Standard II (ref 822570, Bruker Daltonics, Bremen, Germany) covering a mean mass range between 200 and 3500 Da (*see Note 16*).
2. Internal calibration was performed to calibrate the acquired spectra in TLC MALDI software and made using two DHB matrix peaks at 171.2 m/z and 273.0 m/z.

3.3.3 MALDI TOF Analysis

1. Using TLC MALDI software, delimit the position of PL spots and define the number of laser shoots per point (we routinely use 200 laser shoots per point). Specify the distance between points (1 mm) (Fig. 2b).
2. Adjust the voltage characteristics and laser power in FlexControl software (*see Note 17*). The extraction voltages are 19.50 and 17.30 kV. The reflector voltages are 21 and 9.40 kV. All spectra are acquired in positive reflector mode using delayed extraction.
3. Adjust the laser power about 30% above threshold to have a good signal-to-noise ratio. A major strength is needed to desorb lipids from silica [25].

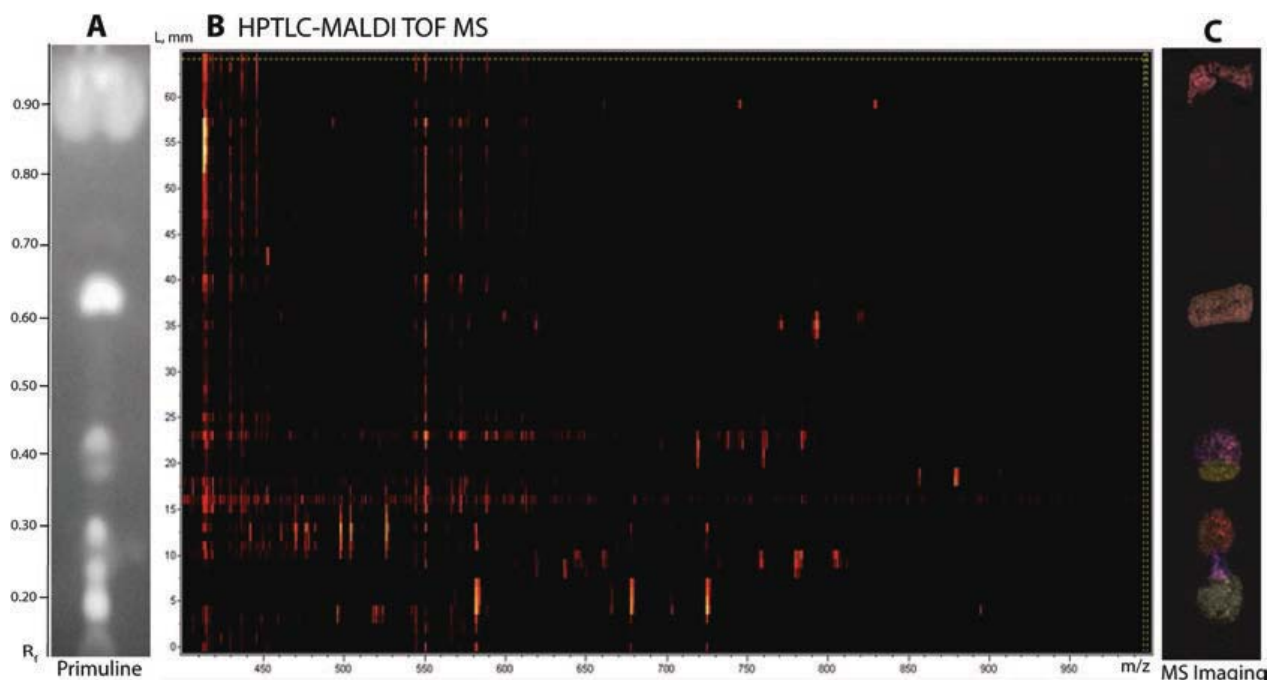


Fig. 3 HPTLC-MALDI MSI analysis. **(a)** Primuline staining of separated lipids on a HPTLC plate. **(b)** HPTLC MS readout. X- and y-axis correspond to the m/z values and the lipid spots respectively. The MS peaks' intensity is presented by red-to-yellow scale. **(c)** HPTLC-MALDI MSI analysis of identical HPTLC plate. According MS and PSD analyses, PL spots are reconstructed by color-labeling according to their m/z

4. Start an automatic spectra acquisition using TLC MALDI software. Obtained by this technique MALDI chromatogram enables the rapid (about 5 min) MS analysis of each sample (Fig. 3c). Y-axis corresponds to the chromatographic line (PL spots) (Fig. 4d) and X-axis presents MS peak intensity (increasing m/z) (Fig. 4c). To eliminate most of the DHB matrix peaks, only m/z from 500 to 2000 were studied.
5. Select and analyze the m/z of PL spots according to the peaks' intensity showing on the right of TLC MALDI software and the MS spectra of each PL spot showing at the top of the window (Fig. 4c and d).
6. In order to identify the PLs, PSD spectra are acquired as previously described [26]. The precursor ions are isolated using a time ion selector. The fragment ions are refocused onto the detector by stepping the voltage applied to the reflectron in appropriate increments. It is done automatically by using the “FAST” (“fragment analysis and structural TOF”) subroutine of the FlexAnalysis software (*see Note 17*). The obtained MS and PSD spectra are then identified using the LIPID MAPS database.

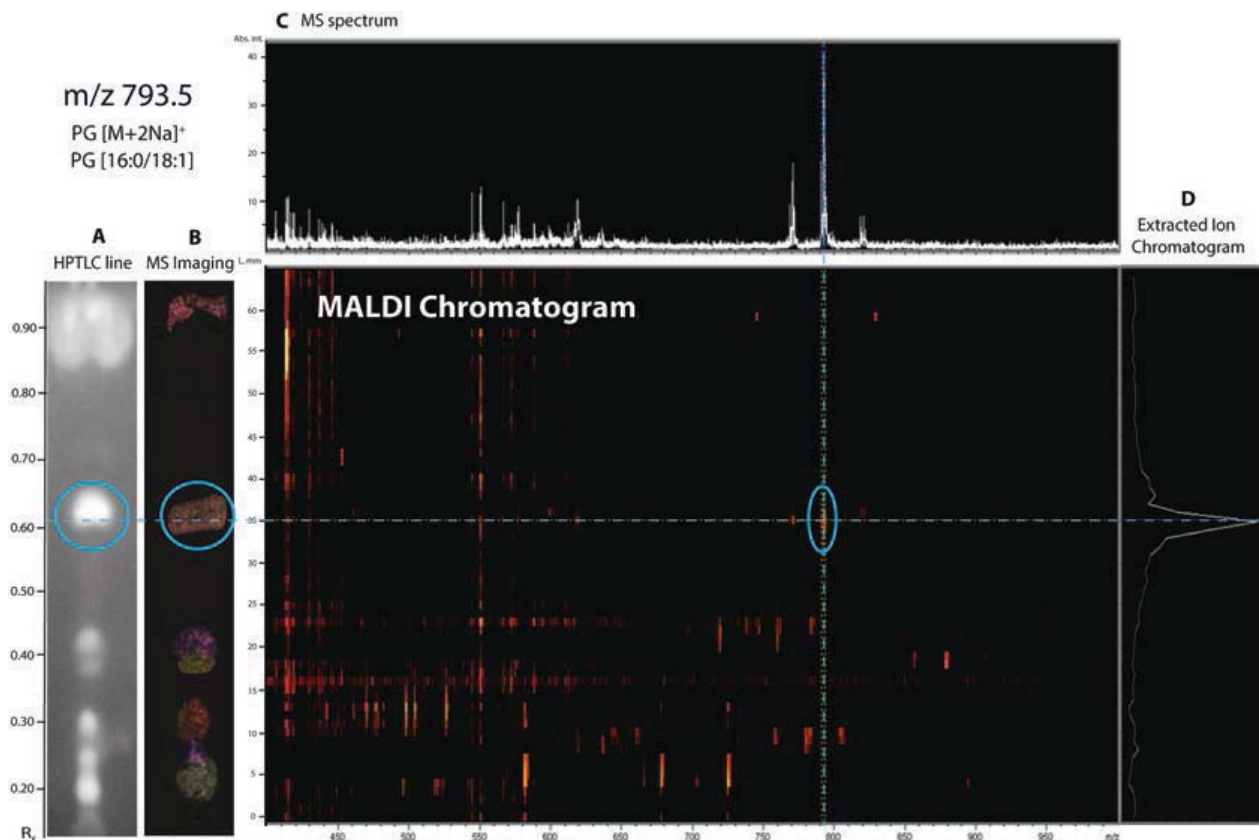


Fig. 4 HPTLC-MALDI TOF MS analysis of phosphatidylglycerol (PG). PG [16:0/18:1] with observed m/z 793.5, corresponding to PG $[M + 2Na]^+$, is shown as an example. (a) Primuline staining of separated lipids on a HPTLC plate. R_f of PG spot = 0.62 ± 0.03 (blue circle). (b) HPTLC-MALDI MSI analysis of identical HPTLC plate, showing the PG spot (m/z 793.5, rose spot in blue circle). (c) MS spectrum of $R_f = 0.62$ allows identification of PG at m/z 793.5 (blue dashed line). (d) Extracted ion chromatogram showing the intensity of PG peak at m/z 793.5. The (c) and (d) data are combined in the MALDI Chromatogram

3.3.4 HPTLC-MALDI TOF Imaging

1. Using FlexImaging software define a polygon measurement region as the HPTLC line of each sample from the PL extract depot to the solvent front.
2. Acquisition method settings: we recommend averaging 500 single laser shots for each mass spectrum (raster width 200 μm). Multiple additions of single position acquisition run (every 40 shots) are employed to obtain a minimal spectrum intensity scale of 10^4 ion counts. The obtained spectra are automatically smoothed and baselined to limit the background noise. The voltage characteristics and laser power are stetted as previously described (see Sect. 3.3.3).
3. Start spectra acquisition.
4. After the end of spectra acquisition, edit the mass filters for PLs according to their m/z identified previously (see Sect. 3.3.3) (Figs. 3b and 4b).

4 Notes

1. All chemicals are of the highest commercially available purity and used without any further purification. Solutions are best prepared in advance and conserved at room temperature.
2. We recommend using ultrapure HPLC grade water.
3. Elution system should be colorless and transparent.
4. DHB is selected as a MALDI matrix because of high signal strength and the absence of matrix adduct peaks. PSD analysis with DHB matrix allows the cleavage of phosphate-glycerol bond and induces the loss of the hydrophilic head group, i.e., $[M-HG + H]^+$, characteristic of each lipid class. This loss is caused by a positive charge localized on the phosphate group [27].
5. For phospholipid extraction, we routinely use lyophilized samples. However, Blight and Dyer's method is also adapted for samples, containing $80 \pm 1\%$ water and 1% lipids [20].
6. For tissues' study, we highly recommend homogenizing the sample before lipid extraction.
7. A small volume of the chloroform layer must be let with aqueous phase. We usually prefer to lose a few microliters of chloroform phase rather than risking contaminating PL stocks.
8. Chloroform evaporation is necessary to unsure (1) the same volume in each lipid sample and (2) the correct condition for PLs' storage. Diluted in chloroform PLs are easier oxidized during storage than dried ones.
9. The usual PLs' storage time is about 6 months.
10. "Activation" is evaporating the water in the silica. The silica gel is hygroscopic, so it adsorbs water vapor from the air and becomes hydrated. This hydration in turn, can alter chromatography and interaction of solvent system with sample.
11. All analyses are done in triplicate. We routinely spot three PL extracts on the same HPTLC plate analyzing three replicates at the same time.
12. Primuline binds noncovalently to the apolar fatty acyl residues of lipids and does not affect a subsequent MS analysis [28].
13. With two dips you get a mass occupancy of about 5 mg/cm^2 . To date, good results have been achieved by dip-coating twice. Every additional coating requires longer drying time and more repetitions can cause bleeding between the separated bands.
14. After the matrix coating the HPTLC plate should look smooth and flat. If the surface looks rough and blistered either the

organic solvent concentration in the matrix solution was too low or the drying process was not quick enough.

15. Desiccation of the HPTLC plate is likely to quickly create a vacuum in mass spectrometer.
16. We usually do the external calibration just before starting HPTLC-MALDI analysis. Thus, 1 µL of the Peptide Calibration Standard II is directly spotted on the TLC MALDI target and coated by the 1 µL DHB matrix.
17. The system utilizes an Autoflex III mass spectrometer equipped with a laser OptibeamTM Nd/YAG (355 nm) with 200-Hz tripled-frequency (Bruker Daltonics, Bremen, Germany).

Acknowledgments

TK is a recipient of a PhD grant from the GRR SeSa (Sanitary Safety Research Network) financed by the Regional Council of Haute-Normandie (France). This study was supported by the Conseil Général de l'Eure and Grand Evreux Agglomeration.

References

1. Gidden J, Denson J, Liyanage R, Ivey DM, Lay JO (2009) Lipid compositions in *Escherichia coli* and *Bacillus subtilis* during growth as determined by MALDI-TOF and TOF/TOF mass spectrometry. *Int J Mass Spectrom* 283:178–184. doi:[10.1016/j.ijms.2009.03.005](https://doi.org/10.1016/j.ijms.2009.03.005)
2. Kondakova T, D'Heygère F, Feuilloley MJ, Orange N, Heipieper HJ, Duclairoir Poc C (2015) Glycerophospholipid synthesis and functions in *Pseudomonas*. *Chem Phys Lipids* 190:27–42. doi:[10.1016/j.chemphyslip.2015.06.006](https://doi.org/10.1016/j.chemphyslip.2015.06.006)
3. Zhang Y-M, Rock CO (2008) Membrane lipid homeostasis in bacteria. *Nat Rev Microbiol* 6:222–233. doi:[10.1038/nrmicro1839](https://doi.org/10.1038/nrmicro1839)
4. O'Brien JS, Sampson EL (1965) Lipid composition of the normal human brain: gray matter, white matter, and myelin. *J Lipid Res* 6:537–544
5. Müller CP, Reichel M, Mühlé C, Rhein C, Gulbins E, Kornhuber J (2015) Brain membrane lipids in major depression and anxiety disorders. *Biochim Biophys Acta* 1851:1052–1065. doi:[10.1016/j.bbalip.2014.12.014](https://doi.org/10.1016/j.bbalip.2014.12.014)
6. Naudí A, Jové M, Ayala V, Cabré R, Portero-Otín M, Pamplona R (2013) Non-enzymatic modification of aminophospholipids by carbonyl-amine reactions. *Int J Mol Sci* 14:3285–3313. doi:[10.3390/ijms14023285](https://doi.org/10.3390/ijms14023285)
7. Solis-Calero C, Ortega-Castro J, Frau J, Munoz F (2015) Nonenzymatic reactions above phospholipid surfaces of biological membranes: reactivity of phospholipids and their oxidation derivatives. *Oxid Med Cell Longev* 2015(2015):e319505. doi:[10.1155/2015/319505](https://doi.org/10.1155/2015/319505), [10.1155/2015/319505](https://doi.org/10.1155/2015/319505)
8. Astarita G, Jung K-M, Berchtold NC, Nguyen VQ, Gillen DL, Head E et al (2010) Deficient liver biosynthesis of docosahexaenoic acid correlates with cognitive impairment in Alzheimer's disease. *PLoS One* 5(9):e12538. doi:[10.1371/journal.pone.0012538](https://doi.org/10.1371/journal.pone.0012538)
9. Wood PL (2012) Lipidomics of Alzheimer's disease: current status. *Alzheimer's Res Ther* 4:5. doi:[10.1186/alzrt103](https://doi.org/10.1186/alzrt103)
10. García-Morales V, Montero F, González-Forero D, Rodríguez-Bey G, Gómez-Pérez L, Medialdea-Wandossell MJ et al (2015) Membrane-derived phospholipids control synaptic neurotransmission and plasticity. *PLoS Biol* 13:e1002153. doi:[10.1371/journal.pbio.1002153](https://doi.org/10.1371/journal.pbio.1002153)
11. Foster JA, Lyte M, Meyer E, Cryan JF (2016) Gut microbiota and brain function: an evolving field in neuroscience. *Int J Neuropsychopharmacol* 19(5). doi:[10.1093/ijnp/pv114](https://doi.org/10.1093/ijnp/pv114)
12. van der Meer-Janssen YPM, van Galen J, Batenburg JJ, Helms JB (2010) Lipids in host-

- pathogen interactions: pathogens exploit the complexity of the host cell lipidome. *Prog Lipid Res* 49:1–26. doi:[10.1016/j.plipres.2009.07.003](https://doi.org/10.1016/j.plipres.2009.07.003)
13. Vromman F, Subtil A (2014) Exploitation of host lipids by bacteria. *Curr Opin Microbiol* 17:38–45. doi:[10.1016/j.mib.2013.11.003](https://doi.org/10.1016/j.mib.2013.11.003)
 14. Wood PL (2014) Mass spectrometry strategies for clinical metabolomics and lipidomics in psychiatry, neurology, and neuro-oncology. *Neuropsychopharmacology* 39:24–33. doi:[10.1038/npp.2013.167](https://doi.org/10.1038/npp.2013.167)
 15. Schiller J, Süß R, Fuchs B, Müller M, Zschornig O, Arnold K (2007) MALDI-TOF MS in lipidomics. *Front Biosci* 12:2568–2579
 16. Fuchs B, Schiller J, Süß R, Schürenberg M, Suckau D (2007) A direct and simple method of coupling matrix-assisted laser desorption and ionization time-of-flight mass spectrometry (MALDI-TOF MS) to thin-layer chromatography (TLC) for the analysis of phospholipids from egg yolk. *Anal Bioanal Chem* 389:827–834. doi:[10.1007/s00216-007-1488-4](https://doi.org/10.1007/s00216-007-1488-4)
 17. Fuchs B, Süß R, Nimptsch A, Schiller J (2009) MALDI-TOF-MS directly combined with TLC: a review of the current state. *Chromatographia* 69:95–105. doi:[10.1365/s10337-008-0661-z](https://doi.org/10.1365/s10337-008-0661-z)
 18. Fuchs B, Süß R, Schiller J (2010) An update of MALDI-TOF mass spectrometry in lipid research. *Prog Lipid Res* 49:450–475. doi:[10.1016/j.plipres.2010.07.001](https://doi.org/10.1016/j.plipres.2010.07.001)
 19. Fuchs B, Schiller J, Süß R, Zscharnack M, Bader A, Müller P et al (2008) Analysis of stem cell lipids by offline HPTLC-MALDI-TOF MS. *Anal Bioanal Chem* 392:849–860. doi:[10.1007/s00216-008-2301-8](https://doi.org/10.1007/s00216-008-2301-8)
 20. Bligh EG, Dyer WJ (1959) A rapid method of total lipid extraction and purification. *Biochem Cell Biol* 37:911–917. doi:[10.1139/o59-099](https://doi.org/10.1139/o59-099)
 21. Angelini R, Vitale R, Patil VA, Cocco T, Ludwig B, Greenberg ML et al (2012) Lipidomics of intact mitochondria by MALDI-TOF/MS. *J Lipid Res*. doi:[10.1194/jlr.D026203](https://doi.org/10.1194/jlr.D026203)
 22. Palusinska-Szysz M, Kania M, Turska-Szewczuk A, Danikiewicz W, Russa R, Fuchs B (2014) identification of unusual phospholipid fatty Acyl compositions of *Acanthamoeba castellanii*. *PLoS One* 9:e101243. doi:[10.1371/journal.pone.0101243](https://doi.org/10.1371/journal.pone.0101243)
 23. Lopalco P, Angelini R, Lobasso S, Köcher S, Thompson M, Müller V et al (2013) Adjusting membrane lipids under salt stress: the case of the moderate halophilic organism *Halobacillus halophilus*. *Environ Microbiol* 15:1078–1087. doi:[10.1111/j.1462-2920.2012.02870.x](https://doi.org/10.1111/j.1462-2920.2012.02870.x)
 24. Kondakova T, Merlet-Machour N, Chapelle M, Preterre D, Dionnet F, Feuilloley M et al (2014) A new study of the bacterial lipidome: HPTLC-MALDI-TOF imaging enlightening the presence of phosphatidylcholine in airborne *Pseudomonas fluorescens* MFAF76a. *Res Microbiol*. doi:[10.1016/j.resmic.2014.11.003](https://doi.org/10.1016/j.resmic.2014.11.003)
 25. Lobasso S, Lopalco P, Angelini R, Vitale R, Huber H, Müller V et al (2012) Coupled TLC and MALDI-TOF/MS analyses of the lipid extract of the hyperthermophilic archaeon *Pyrococcus furiosus*. *Archaea* 2012:1–10. doi:[10.1155/2012/957852](https://doi.org/10.1155/2012/957852)
 26. Fuchs B, Schober C, Richter G, Süß R, Schiller J (2007) MALDI-TOF MS of phosphatidylethanolamines: different adducts cause different post source decay (PSD) fragment ion spectra. *J Biochem Biophys Methods* 70:689–692. doi:[10.1016/j.jbbm.2007.03.001](https://doi.org/10.1016/j.jbbm.2007.03.001)
 27. Harvey DJ (1995) Matrix-assisted laser desorption/ionization mass spectrometry of phospholipids. *J Mass Spectrom* 30:1333–1346. doi:[10.1002/jms.1190300918](https://doi.org/10.1002/jms.1190300918)
 28. Richter G, Schober C, Süß R, Fuchs B, Müller M, Schiller J (2008) The reaction between phosphatidylethanolamines and HOCl investigated by TLC: Fading of the dye primuline is induced by dichloramines. *J Chromatogr B* 867:233–237. doi:[10.1016/j.jchromb.2008.04.010](https://doi.org/10.1016/j.jchromb.2008.04.010)

Ch4

The Hidden Face of Nitrogen Oxides Species: From Toxic Effects to Potential Cure?

Ségolène Depayras, Tatiana Kondakova,
Hermann Josef Heipieper, Marc GJ Feuilloley,
Nicole Orange and Cécile Duclairoir-Poc

Additional information is available at the end of the chapter

<http://dx.doi.org/10.5772/intechopen.75822>

Abstract

Nitrogen oxide (NOx) species represent ones of the most threatening air pollutants due to their prevalence and harmful impact on the environment and human health. The term NOx gathers mainly nitric oxide (NO) and nitrogen dioxide (NO_2), mostly produced by anthropogenic activities such as transport and industries. Several cellular constituents were already described as NOx targets. These include membranes, proteins, respiratory chain enzymes, lipids, and DNA. Such damages lead to pathologies of lungs, cardiovascular system, and skin because these organs represent the first barrier toward the environment. On the other hand, NOx is also naturally synthetized by several organisms, playing a mediator role in essential cellular functions. However, few data are yet available on NOx activity toward microorganisms. Here, we review data concerning the double face of NOx, including their use in the medical field against pathogens' infections that highlight the versatility of these compounds.

Keywords: NOx, pollutants, signalization, physiopathology, treatment

1. NOx species: the genesis of a major air pollutant

"Yet, pollution is the largest environmental cause of disease and death in the world today, responsible for an estimated 9 million premature deaths" stated The Lancet Commission in 2017. This phenomenon represents an alarming threat for human health, as a major cause of respiratory and cardiovascular pathologies as well as infertility. Moreover, those atmospheric pollutants have severe impacts on the environment and participate in climatic change,

acidification, eutrophication, and ecosystem disturbances. Several international and national organizations (e.g. WHO, EEA, and INERIS) aim at reducing the global emission of pollutants, thanks to environmental policies as Kyoto and Gothenburg protocols signed in 1997 and 1999, respectively. After that, an encouraging decrease in air pollutants' levels was measured between 2000 and 2015 [1].

Atmospheric pollutants can be classified into four families: classical, indoor, and organic or inorganic air pollutants. Among the classical ones, which are the principle in amount, sulfur dioxide (SO_2), particle matter, ozone (O_3), and nitrogen oxide (NOx) species are found [2]. The term NOx refers to a wide range of nitrogen-derived compounds, where nitric oxide (NO) and nitrogen dioxide (NO_2) are predominant [3]. Those compounds can be naturally produced at low level by lightnings [4] and volcanic eruptions [5]. However, NOx is mainly generated by anthropogenic activity (e.g., road transport, energy production, industry, and agriculture) (Figure 1) [6].

Even if NO and NO_2 represent the main species of NOx , nitrogen exists in several oxidation states in the environment, from N (-III) to N (+V). NO takes a central place in the series of reactive nitrogen species (RNS) [7]. Oxidation and reduction of NO result in the formation of several RNS, including nitrate or ammonium. NO_2 is formed by the reaction of NO with O_2 and can be dimerized to give N_2O_4 . The formed reactive species can, in turn, be involved in a wide range of reactions (Figure 2).

Nitrogen is an essential constituent of vital macromolecules (nucleic acids and proteins). This atom also constitutes the dinitrogen (N_2) gas, usually abbreviated nitrogen. This gas represents 78% of atmospheric air and is continuously recycled in our environment. First, the atmospheric nitrogen is fixed in the soil by prokaryotes to form ammonia (NH_3), which could be taken up by plants. NH_3 is then converted into ammonium (NH_4^+). Ammonium could be also

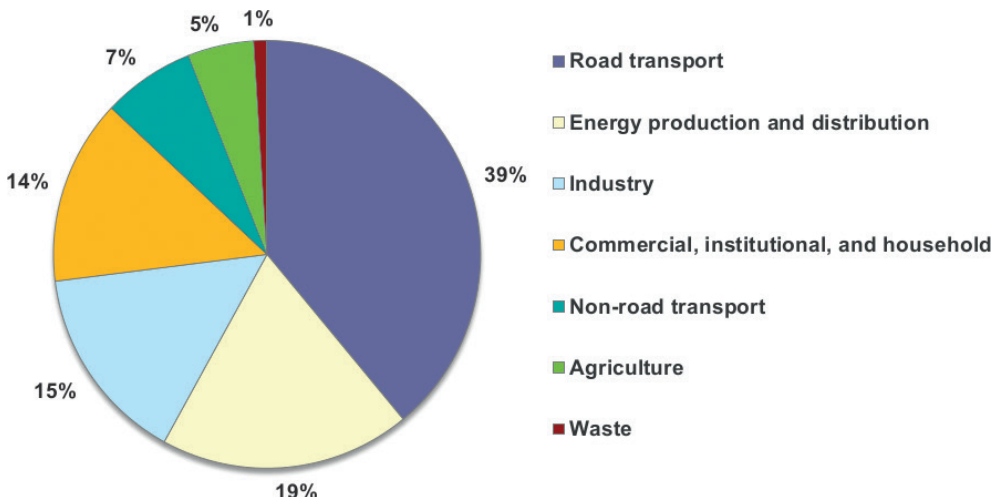


Figure 1. NOx sources linked to anthropogenic activities (according to [1]).

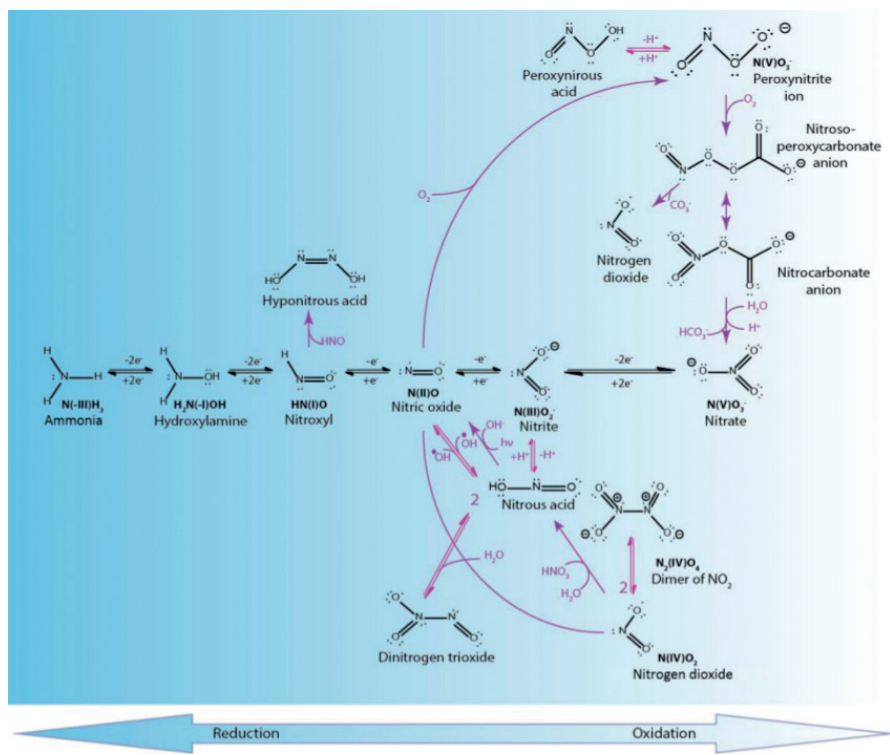


Figure 2. Redox relationships of NOx with other RNS. Black arrow: oxidation and reduction of NO; purple arrow: a wide range of reactions; roman numbers: oxidation state of the nitrogen atom; color gradient: reduction/oxidation state from (-III) to (V).

formed by mineralization of organic matter by decomposers (fungi, worms, and prokaryotes). The second part of the nitrogen cycle is the nitrification of ammonium by prokaryotes leading to nitrite (NO₂⁻) formation, which is then further oxidized into nitrate (NO₃⁻). Finally, nitrate could be assimilated by plants for their growth or converted into N₂ by denitrifying bacteria (Figure 3).

Moreover, nitrogen is also the precursor of NOx. Indeed, NOx formation can be separated into four steps. First, NO is formed in the atmosphere in combination with nitrogen, resulting from the global biogeochemical nitrogen cycle, and oxygen, following combustion (natural or anthropic). Then, this highly reactive compound can be oxidized by oxygen (O₂) to form NO₂. Alternatively, nitrogen dioxide can also be directly formed through catalytic ammonia combustion or nitrosyl chloride oxidation. Then, a temperature-dependent equilibrium is establishing between NO₂ and its dimeric form, nitrogen tetroxide (N₂O₄⁻). Finally, a photochemical reaction between NO₂ and hydroxyl radicals leads to the generation of ozone (O₃) (Figure 4).

Even if NO and NO₂ are classified as RNS, their characteristics are very different suggesting their diverse behavior and reactivity. For example, the solubility of NO is very low

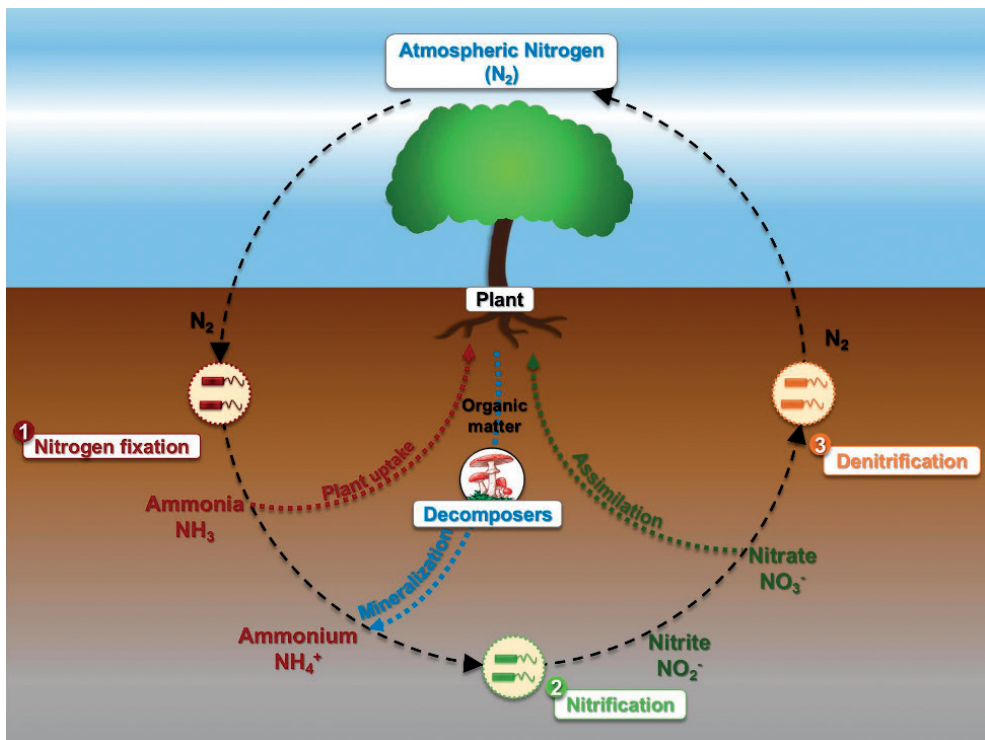


Figure 3. Nitrogen cycle at the interfaces among air, soil, and ecosystem. (1) Fixation of gaseous nitrogen by prokaryotes leading to ammonia (NH_3) and ammonium (NH_4^+); (2) nitrification of NH_4^+ by prokaryotes resulting in nitrite formation (NO_2^-) subsequently oxidized into nitrate (NO_3^-); (3) denitrifying prokaryotes catalyzing the conversion of nitrate into gaseous N_2 .

(5.7×10^2 g/L), and NO_2 is highly reactive in water resulting in the formation of HNO_2 and HNO_3 [8]. Moreover, the half-life time of those compounds highly differs because NO_2 half-life is around 35 h, whereas that of NO is almost impossible to determine because of its high reactivity [9]. The permeability of both compounds is also totally unrelated: NO has a lipophilic behavior with consequently a high-membrane permeability. This can be illustrated by the high-diffusion ability of NO toward the membrane. Conversely, the permeability coefficient of NO_2 is estimated about 5 cm s^{-1} suggesting a lower diffusion power toward biological membranes [10]. In spite of these differences, the penetration of NO and NO_2 inside cells and their high reactivity are at the origin of their pathogenic potential on human health, particularly when physiological elimination thresholds are exceeded. Since skin, respiratory tract, and lungs are the first barrier toward those gases, these organs are evidently the principle targets of these compounds and their derived species [11–13]. However, their diffusion deeper in the organism can lead afterward to other severe effects, for instance, on the cardiovascular and immune systems [12, 14]. Human health effects range from reversible (nausea, breathing difficulties, and asthma symptoms) to irreversible (cardiovascular defects, emphysema, and immunopathologies), including cancer induction in the worst cases (Figure 5) [15].

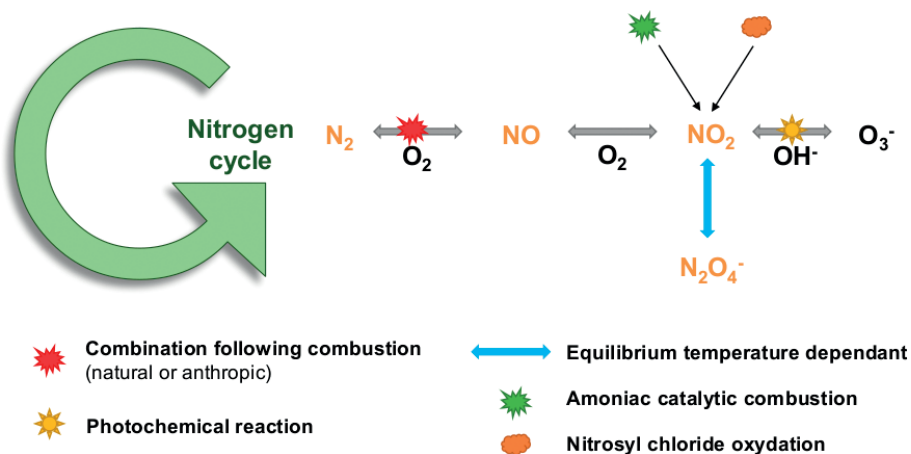


Figure 4. Atmospheric genesis of NOx (adapted from [3]).

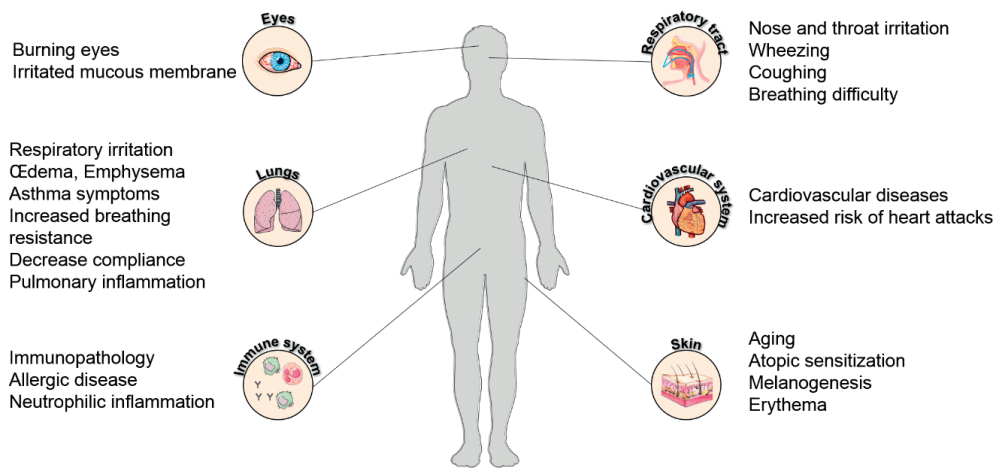


Figure 5. Representation of NOx targets and associated pathologies [11–15].

Thanks to epidemiological and clinical studies, thresholds of NO and NO₂, whose chemical structure and conversion factors are represented **Figure 6A**, have been determined for different human health effects (**Figure 6B** and **C**, respectively). However, no guideline values are available for NO (**Figure 6D**) due to its complete and rapid reaction [16]. Thus, in order to limit health issues, international organizations, such as WHO, set up guidelines for atmospheric NO₂ limit value (**Figure 6E**).

NOx is then highly toxic compounds and has a myriad of deleterious impacts on the human physiology when the bearable thresholds are exceeded. However, NOx is also naturally produced by cellular processes in a wide range of living organisms. In this case, NOx can have totally different effects as discussed later.

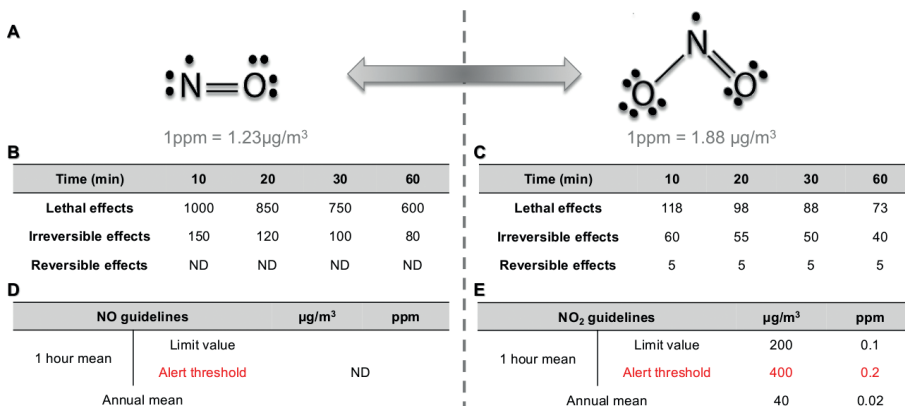


Figure 6. Key features concerning NOx. (A) Lewis structure of NOx and conversion factors; (B) NO threshold (ppm) according to [9]; (C) NO₂ threshold (ppm) according to [9]; (D) and (E) NO and NO₂ guideline values, respectively, according to [1]. ppm, parts per million; ND, not determined.

2. The double face of NOx in the eukaryotic world

To better understand why NOx impact on so many organs, it is essential to focus on the units forming each part of our body: the eukaryotic cells themselves.

2.1. Exogenous NOx: a hostile intruder inside the eukaryotic cells

Much work was already performed on NOx targets at the cell scale. NO and NO₂, thanks to their chemistry properties mentioned earlier, are highly diffusible through living membranes and exhibit a strong reactivity. It is easy to imagine the potential of such compounds. Since NO is highly reactive in lipophilic media, it can react inside the lipid bilayer, first protection of cells against the environment. Indeed, polyunsaturated fatty acids (PUFAs) are susceptible to NO in the presence of O₂ and ONOO⁻ [17]. The interaction of these toxic compounds with PUFA double bounds leads to the formation of nitrated FA. This process is considered as a protective strategy because it redirects O₂⁻ and ONOO⁻-mediated cytotoxic reactions to other oxidative pathways. Post-translational modification of several proteins is also observed in the presence of NOx and RNS. For example, tyrosine nitration on phenol residue mediated by peroxynitrite derived from OH and NO₂ leads to 3-nitrotyrosine formation [18]. This molecule represents a useful biomarker of nitrosative stress in various pathologies such as atherosclerosis [19]. Protein thiol residues are highly susceptible to NO and ONOO⁻ leading to the formation of nitrosothiol (RS-NO) and nitrothiol (RS-ONO), respectively [20]. This reversible modification modulates the activity of several proteins similar to phosphorylation. For example, S-nitrosylated cysteine thiol residue can be denitrosylated by S-nitrosoglutathione reductase or thioredoxin systems [21]. NO and other RNS can also nitrosylate [Fe—S] cluster of transition metal centers, which are essential for protein function. This modification can activate a wide range of enzymes such as the soluble guanylate cyclase (sGC) mentioned below

[22]. On the contrary, this reaction can also alter the protein function, for example, in the case of hemoglobin [23]. NO and other higher RNS products (ONOO^- or NO_2) are able to generate nitration, nitrosation, or deamination reactions on DNA bases leading to mutagenesis [24]. This phenomenon is enhanced by the inhibition of DNA repair triggered by NO [25]. More recently, a role of NO in epigenetic modification was suggested. To be more precise, this simple molecule seems to modulate histone acetylation and methylation through direct and indirect modulations of histone acetyltransferases and deacetylases, lysine demethylases, histone methyltransferases activity, thus modifying the expression of several genes [26]. These pleiotropic activities of NO and derived compounds highlight here the necessity of fine regulation pathways to prevent the development of several diseases.

2.2. Endogenous NO: an essential mediator of cellular signalization

Interestingly, NO can also be produced by several living organisms: plants, animals, and bacteria, thanks to a specific enzyme called nitric oxide synthase (NOS) [27, 28]. The large distribution of this enzyme through the different reigns emphasizes the importance of NO synthesis. Evolutionary studies highlight the necessity for the first living organisms during primitive era to eradicate toxic O_3 present in the paleoatmosphere as a survival strategy. Indeed, the liberation of gaseous NO in extracellular environment could have subsequently neutralized O_3 , thus limiting harmful oxidative reactions [29]. In eukaryotic cells, three isoforms of NOS have been described [30]. The neuronal nNOS (NOS-1) and the endothelial eNOS (NOS-3) are constitutively expressed but are only activated through calcium-dependent mechanisms. The third one is the inducible iNOS (NOS-2) expressed in macrophages following infection by pathogens, virus, or tumors. Contrary to NOS-1 and 3, NOS-2 is constitutively functional. Interestingly, these NOSs have high structural similarities with an oxygenase and a reductase domain (Figure 7) [27].

To be fully functional, NOS requires to associate with homodimers, and this form of NOS is crucial for the generation of NO [32]. When conditions are favorable (high level of L-arginine

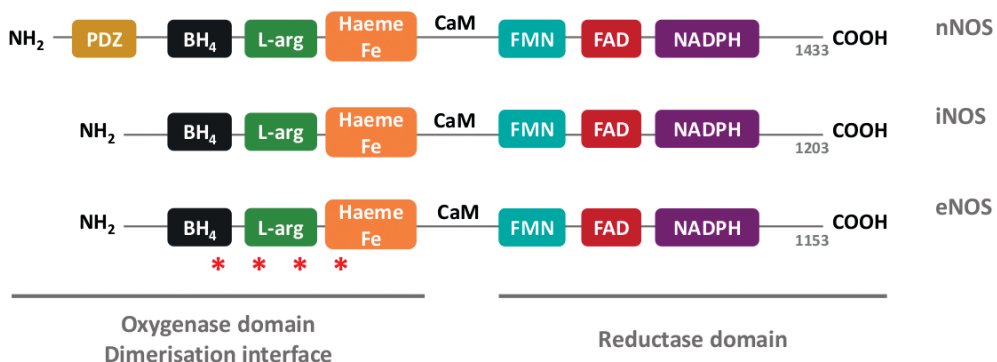


Figure 7. The structural similarities of NOS (adapted from [31]). BH₄, tetrahydrobiopterin; L-arg, L-arginine-binding site; Heme Fe, iron protoporphyrin IX; CaM, calmodulin-binding site; FMN, flavin mononucleotide-binding site; FAD, flavin adenine dinucleotide-binding site; NADPH, nicotinamide adenine dinucleotide phosphate-binding site; *, palmitoylation and myristylation of eNOS oxygenase domain.

and cofactors like BH_4), this enzyme catalyzes the conversion of L-arginine into L-citrulline using O_2 and leading to NO formation with a ratio of 1:1 [33]. However, if these parameters are not available or if NOS remains monomeric, the enzyme only produces superoxide (O_2^-) [32]. Even if NOS isoforms catalyze the same reaction, their distribution is largely related to their respective functions.

2.2.1. The endothelial eNOS and vasodilatation

Endothelial nitric oxide synthase (eNOS) can be activated through calcium-dependent and independent pathways. On the one hand, through activation of specific receptors, such as acetylcholine muscarinic receptors, bradykinin receptors, and H1 histamine receptors, distributed in the endothelial cell membrane, agonists can trigger an increase in intracellular concentration of calcium (Ca^{2+}) through the well-known polyphosphoinositides pathway. Indeed, activation of those receptors stimulates membrane-associated PLC γ and PI3K activation. This results into inositol trisphosphate (IP3) formation, which induces the release of intracellular calcium stock from endoplasmic reticulum [34]. Then, Ca^{2+} binds to calmodulin (CaM), which could later fix on the calmodulin-binding domain of eNOS controlling its enzymatic activity. On the other hand, in response to hormones or growth factors acting on their corresponding receptors, phosphate kinase A (PKA) or B (AKT) pathway can be induced mediating a phosphorylation cascade. The post-translational phosphorylation of eNOS on three specific sites (Ser617 and Ser1179 for AKt, Ser635 and Ser1177 for PKA) enhances the activity of the enzyme [35]. Moreover, the lipidation of eNOS (palmitoylation and myristoylation) could also enhance its activity [36]. This other post-translational modification promotes eNOS association with cell membrane and is stabilized by interaction with membrane chaperone proteins (caveolin-1 and HSP70/90). Both mechanisms are essential for linking upstream signal transduction pathway to eNOS activity in cells [37]. eNOS could then produce a large amount of NO, which latter diffuses freely inside smooth muscles. Herein, NO activates soluble guanylate cyclase (sGC) by reaction with the heme of the enzyme leading to the increase of cyclic guanosine monophosphate level (cGMP). cGMP subsequently activates phosphate kinase G (PKG) favoring a cytosolic Ca^{2+} reuptake into sarcoplasmic reticulum [38]. The decrease of intracellular level of Ca^{2+} leads to the relaxation of smooth muscle. Moreover, NO can inhibit caspases 3 and 8 and thus apoptosis through protein nitrosylation. NO released by endothelium is also reducing platelet aggregation and platelet or leukocyte adhesion (**Figure 8**) [39, 40].

Another source of NO inside endothelial cells was also described. Indeed, nitrite and nitrate reservoirs could be converted into NO by several enzymes such as cytochrome P450, hemoglobin, myoglobin, and others, under specific conditions [42]. However, several pathways could abolish NO production. Indeed, NO can be eliminated in combination with reactive oxygen species (ROS). eNOS could be inactivated by several phosphatases. The removal of eNOS membrane sequestration by interaction between NOS-interacting protein (NOSIP) and NOS-traffic inducer (NOSTRIN) complex favors eNOS recycling [36]. Since NO plays a central role in this phenomenon, any abnormality altering its production leads to pathogenesis and vascular disorders such as atherosclerosis and hypertension [43].

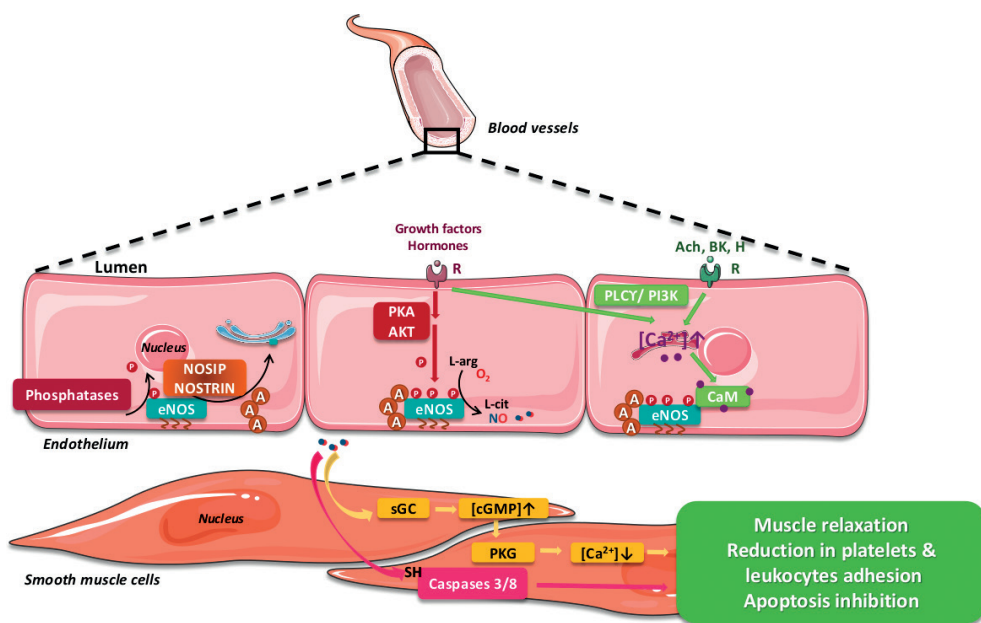


Figure 8. Physiology of vasodilatation: implication of eNOS and NO (adapted from [41]). eNOS, endothelial nitric oxide synthase; ach, acetylcholine; BK, bradykinin; H, histamine; R, receptor; CaM, calmodulin; PLC γ , phospholipase C γ ; PI3K, phosphoinositide 3-kinase; PKA, phosphate kinase A; AKT, phosphate kinase B (PKB); sGC, soluble guanylyl cyclase; cGMP, cyclic guanosine monophosphate; PKG, phosphate kinase G; A, protein complex of HSP70, HSP90, and caveolin-1; NOSIP, NOS-interacting protein; NOSTRIN, NOS traffic inducer.

2.2.2. The neuronal nNOS: a crucial element in neurotransmission

nNOS, also called NOS-1, was the first isoform discovered in the neuronal tissue. It should be distinguished between two subfamilies: nNOS α and nNOS μ , thanks to their locations and functions. Indeed, nNOS α is found in central nervous system and plays a major role in the neurotransmission at neuronal synapses, whereas nNOS μ is found in skeletal and cardiac muscle where NO controls muscle contractility and local blood flow.

2.2.2.1. nNOS α in the central nervous system

Glutamate is the major excitatory neurotransmitter in the brain. When delivered into the synapse, this molecule is activating a specific receptor (NMDAR) located inside the postsynaptic membrane. Activated NMDAR thus allows the entry of calcium. Ca^{2+} are able to activate calmodulin by physical interaction [44]. Afterward calmodulin binds to nNOS α , which, in turn, is activated. Interestingly, nNOS α can indirectly interact with the NMDAR through its fixation on an adapter protein PSD95 by their PDZ interaction domain [45]. This allows the high speed of NO synthesis in response to NMDAR activation. Thereafter, NO can diffuse back to the presynaptic area leading to an increase glutamate release in the synaptic cleft and thus neurotransmission. CAPON, a chaperon protein of DexRas, was found altering the level

of nNOS α present at the membrane [46]. Indeed, CAPON competes with the PDZ domain of nNOS α and thus promotes its detachment from the NMDAR-PSD95 complex. nNOS α interaction with CAPON-DexRas complex allows the activation of DexRas, a small protein G, through s-nitrosylation on its thiol residue [47]. Then, DexRas activates the MAPK cascade and the transcription of several genes [47]. Several shutdown systems are available to limit this process, which could dramatically affect the brain physiology by synapses hyperactivation. Indeed, kinases, such as PKC or PKII, can phosphorylate nNOS α leading to its loss of activity [48]. nNOS α can also be sequestered by two membrane proteins (caveolins 1 and 3) preventing its interaction with calmodulin (**Figure 9**).

As mentioned above, any disorder affecting NO synthesis can lead to dramatic consequences in the brain. Indeed, a lack of NO could impair the neurotransmission and hence the neuronal plasticity, such as long-term potentiation (LTP) in the hippocampus or long-term depression (LTD) in the cerebellum [50]. NO ensures also the correct irrigation of brain by its vasodilator effect on peripheral blood vessel. The synthesis of NO can be altered by a deficiency or a loss of activity of nNOS. Other regulatory elements, such as the decrease of L-arginine precursor availability or cofactors crucial for the catalytic activity of NOS, contribute also to nNOS inactivation. Conversely, in some several brain pathologies (ischemia, strokes, neurodegenerative disorders including Parkinson's and Huntington's diseases, and amyotrophic lateral sclerosis), a large amount of NO is produced [51]. It is hypothesized that NO or derived nitrogen species interact with various proteins inducing several toxic effects. Thus, pharmacological regulation of NO synthesis offers important strategies for the treatment of neurodegenerative and muscle diseases.

2.2.2.2. nNOS μ in peripheral neurotransmission

On the other hand, nNOS μ is located in skeletal and cardiac muscle where NO controls muscle contractility and local blood flow essential to support muscular effort. When the excitatory neurotransmitter acetylcholine (Ach) is released at the neuromuscular junction, it is activating specific acetylcholine nicotinic receptors present on muscle cells [52]. Activation of these receptors allows the release in the cell sarcoplasm of calcium from exogenous and/or endogenous

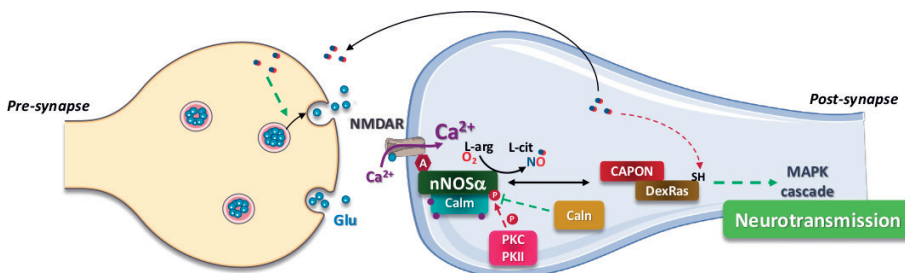


Figure 9. The neurotransmission mediated by NOS α in central nervous system (CNS) (adapted from [49]). Glu, glutamate neurotransmitter; NMDAR, N-methyl D-aspartate type-glutamate receptor; A, PSD95 protein adapter between nNOS α and NMDAR; CaM, calmodulin; PKC, phosphate kinase C; PKII, Ca^{2+}/CaM -dependent protein kinase II; CaN, calcineurin; CAPON, C-terminal PDZ domain ligand of neuronal nitric oxide synthase; MAPK, mitogen-activated protein kinase.

sources. This process is also enhanced by the activation of a voltage-dependent Ca^{2+} channel (CaCn) [53]. The increase of Ca^{2+} from exogenous origin activates ryanodine receptor present on the sarcoplasmic reticulum, which, in turn, delivers a large amount of Ca^{2+} . When the Ca^{2+} threshold is reached, it is binding on the calmodulin protein. Calmodulin can then interact with the $\text{nNOS}\mu$ to activate the generation of NO. Interestingly, $\text{nNOS}\mu$ interacts through its PDZ domain with adapter proteins (syntrophins) linked to a membrane protein complex called dystrophin [54]. Produced NO could then diffuse back to the motor neuron to enhance the liberation of neurotransmitters or the vasodilatation of blood vessels, thus increasing the local blood flow to support muscle needs during contraction efforts (Figure 10) [55].

NO synthesis is also well regulated by calpain (Calp). Indeed, this protein interacts with the PDZ domain $\text{nNOS}\mu$ provoking its detachment from the dystrophin/syntrophin membrane complex [56]. Interestingly, in muscular Duchenne dystrophy, the damages caused by dystrophin absence are enhanced in case of simultaneous lack of $\text{nNOS}\mu$ [57]. Thus, NO donors may offer a potential avenue for therapy.

2.2.3. The inducible *iNOS* and the innate immunity

NO also takes an important part in innate immunity. Indeed, NO and derived compounds are cytotoxic weapon against tumor cells, microorganisms, and viruses [58]. NO is generated by inducible nitric oxide synthases (*iNOS* and *NOS2*) within macrophages. However, more recently, studies have shown that this enzyme is also expressed in other cell line (vascular endothelial cells, hepatocytes, pulmonary, and colonic epithelial cells) [59]. Unlike nNOS or eNOS , its expression is stimulated by several pathways after activation of specific receptors by endotoxins (LPS) or cytokines (TNF α , IFN γ , and IL1 β). Briefly, the LPS endotoxins are carried by an LPS-binding (LPB) protein to its specific Toll-like receptor 4 (TLR4). Then, the transduction

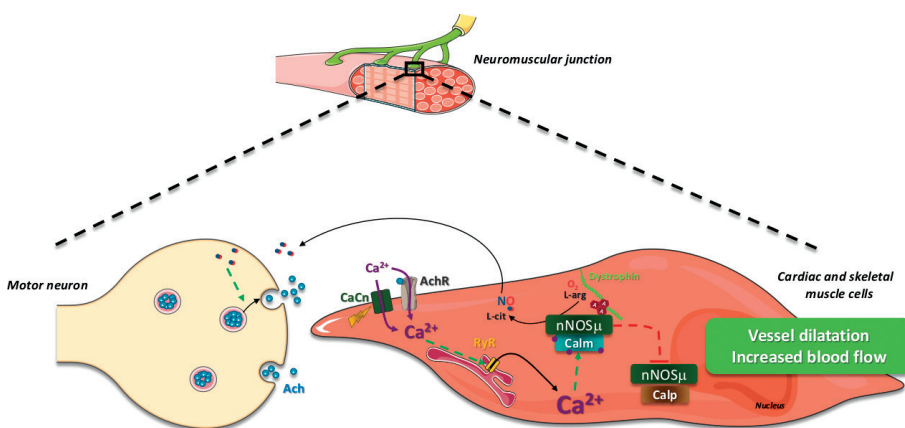


Figure 10. $\text{nNOS}\mu$ activity at the neuromuscular junction (adapted from [49]). Ach, acetylcholine; CaCn , voltage-dependent Ca^{2+} channel; AchR, acetylcholine receptor; yellow lightning symbols, membrane depolarization; Ca^{2+} , calcium; RyR, ryanodine receptor; L-cit, L-citrulline; L-arg, L-arginine; Calm, calmodulin; A, syntrophin $\alpha 1$, $\beta 1$ and $\beta 2$ adapter between dystrophin and $\text{nNOS}\mu$; Calp, calpain.

of the signal leads to the transcription of NF- κ B [60]. This transcription factor is essential for the expression of iNOS gene. On the other hand, cytokines produced by infected cells activate pathways responsible for the expression of several transcription factors (NF- κ B, AP1, and IRF1) also involved in the transcription of iNOS [61]. Both pathways are necessary to fully upregulate iNOS expression. Moreover, iNOS is constitutively active and exhibits a high affinity for calcium explaining its Ca²⁺-independent activity. iNOS produces a large amount of NO until substrate depletion [62]. Then, NO acts directly or through derived compounds (mostly ONOO⁻ and NO₂) generated through the reaction of NO with ROS formed by NADPH oxidase. These molecules can be generated inside (phagosome) or outside the cells. Altogether, NO and derivatives could act in synergy on several components within the targeted hostile elements such as proteins (thiols, metal centers, and tyrosine residues), nucleic acids, and lipids [63, 64]. Altogether, these modifications lead to irreversible damages impairing cellular metabolism and ultimately inhibit growth and replication mechanisms and even cell death (**Figure 11**).

After infection, NO generation is abolished by neutralization of iNOS activity. Indeed, iNOS undergoes a posttranslational modification called polyubiquitination leading to its proteasomal degradation. Physiological aggresome, an alternative pathway for protein degradation, is also involved in iNOS inactivation [66]. The degradation of NO can also be modulated by its own interaction with ROS. The depletion of L-arginine precursor also shuts down iNOS activity.

Overexpression of iNOS is observed during chronic infection leading to an excessive level of NO and RNS. This phenomenon can impair the host physiology because these high reactive compounds represent mutagenic sources. Thus, the NO balance is a crucial point to

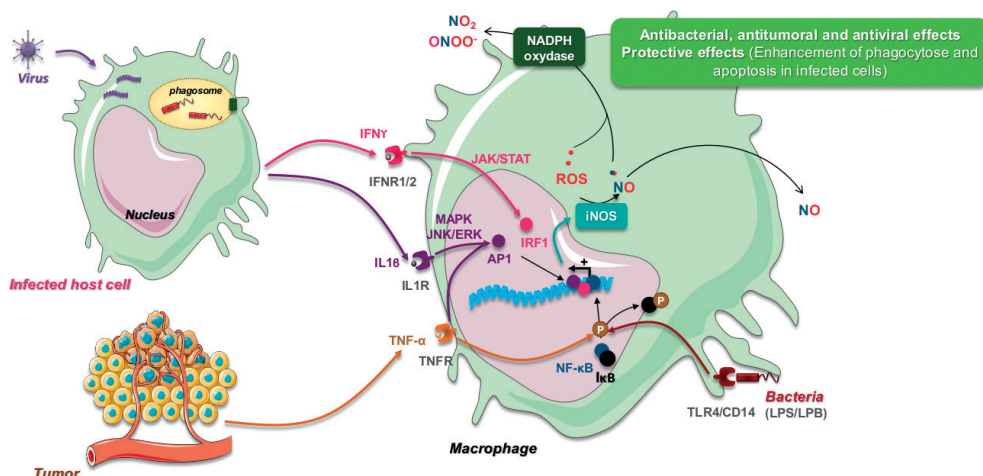


Figure 11. Implication of iNOS in the innate immunity (adapted from [65]). IFN γ , interferon γ ; IFNR1/2, IFN γ receptors 1 and 2; JAK, Janus kinase; STAT, signal transducer and activator of transcription; IRF1, interferon response factor 1; IL1 β , interleukin 1 β ; IL1R, IL1 β receptor; MAPK, mitogen-activated protein kinase; JNK, C-Jun N-terminal kinase; ERK, extracellular signal-regulated kinase; AP1, activator protein 1; TNF- α , tumor necrosis factor α ; TNFR, tumor necrosis factor receptor; NF- κ B, nuclear factor κ B; TLR4, Toll-like receptor 4; CD14, cluster of differentiation 14; LPS, lipopolysaccharide; LPB, LPS-binding protein; ROS, reactive oxygen species.

control in order to limit its tumorigenic potential. The development of iNOS inhibitors and NO-releasing agents offers interesting therapeutic strategies to struggle against cancer and microbial infections.

3. NOx versus prokaryote: “Catch me if you can”

3.1. NOx at the center of prokaryotic life, virulence, and death

Several environmental, commensal, and pathogenic prokaryotes possess an arsenal of proteins dedicated to the nitrogen metabolism under anaerobic conditions [67]. Indeed, an enzymatic chain is involved in the denitrification pathway responsible for the production of NO through nitrite reductase (NIR) as an intermediate. The outcome of this mechanism is the formation of dinitrogen (N_2). This process is crucial for the growth of bacteria in the absence of oxygen because it is coupled with ATP generation (Figure 12).

Interestingly, a shortened NOS-like protein called bNOS was discovered in Gram-positive bacteria [28]. This enzyme is deprived of the classical reductase domain already described in other NOS isoforms. However, bNOS is able to recruit other proteins exhibiting a reductase catalytic activity [69]. Similar to mammalian isoforms, bNOS catalyzes the production of NO using L-arginine precursor. However, NOx is key elements in the innate immunity to avoid infection. Indeed, similar to eukaryotic cells, prokaryotes are also sensitive to NOx activity. Thence, such compounds could alter DNA, proteins, and metal centers leading to severe alterations of bacterial growth and replication.

As previously described, NO could be endogenously produced by bacteria but is also a powerful exogenous antimicrobial agent. This highlights the requirement of systems to manage a bearable threshold of NOx within the cell. First, bacteria have developed NO sensing system

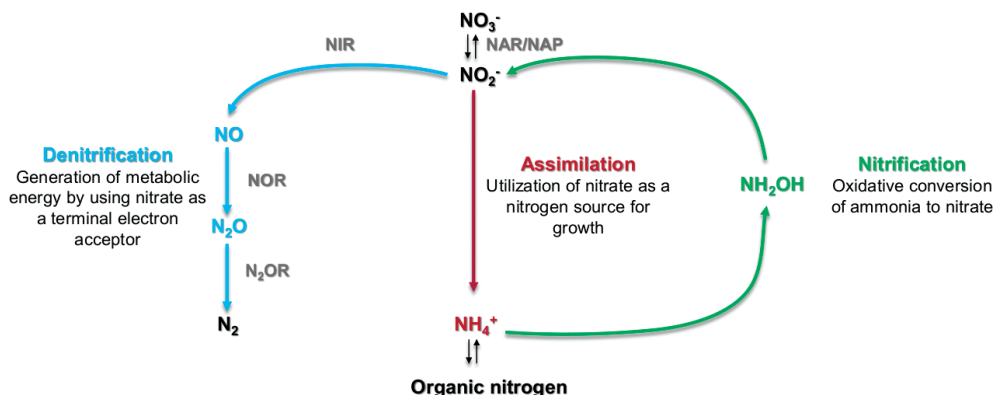


Figure 12. Bacterial nitrogen cycle (adapted from [68]). NO_3^- , nitrate; NO_2^- , nitrite; NO , nitric oxide; N_2O , nitrous oxide; N_2 , dinitrogen; NH_2OH , hydroxylamine; NH_4^+ , ammonia; NAR/NAP, nitrate reductase; NIR, nitrite reductase; NOR, nitric oxide reductase; N_2OR , nitrous oxide reductase.

through non-heme iron cluster conjugated with a wide range of detoxification mechanisms. Several pathways involving reaction of NO with non-heme iron cluster were described, mainly in *Escherichia coli* [70]. Indeed, NO can lead to a raise of the repression of sulfur assimilation operon (*suf*) exerted by ferric uptake regulator protein (Fur). This reaction is mediated by Fur nitrosylation through NO-derived S-nitrosoglutathione (GSNO). *Suf* products are required for the biogenesis of the [Fe—S] cluster, which, in turn, gives a lure to get rid of NOx collateral damages. The flavohemoglobin (*hmpA*) is another response against the nitrosative stress. This enzyme catalyzes the conversion of NO into nitrous oxide (N_2O) under anaerobic conditions. Interestingly, in the presence of NO, the S-nitrosylation of cysteine residues on MetR and FNR inactivates both the proteins. Thus, the repression exerted by MetR and the fumarate and nitrate reductase regulatory protein (FNR) is raised by *hmpA* allowing its transcription. Furthermore, NO-responsive transcriptional factor (NorR) is directly activated by NO and enhances the expression of NorVW protein catalyzing the reduction of NO into N_2O . Redox-sensitive cysteines also take part in the NO-sensing systems. Indeed, NO-activated superoxide regulon (SoxR) protein leads to the transcription increase of superoxide dismutase (*sodA*) removing O_2^- that may react with NO to form NO_2 and $ONOO^-$ [71]. Similar to SoxR, peroxide regulon (OxyR) protein is activated by S-nitrosylation. This protein induces gene expression for protective products against nitrosative stress at least by limiting the S-nitrosylation [72]. For example, the expression of catalase KatA, which could buffer free NO, is activated by OxyR [73]. Altogether, these sensing systems lead to the efficient detoxification by generation of less toxic compounds or scavenger molecules.

Moreover, bacteria also develop repairing system of DNA and [Fe—S] cluster damages related to nitrosative stress. Similar to eukaryotic cells, five DNA repair pathways are available in prokaryotes. Among them, the base excision repair (BER), to repair deaminated base, and the nucleotide excision repair (NER), to remove cross-linking in DNA, are predominant [74]. Concerning the [Fe—S] cluster repair, the iron sulfur cluster S protein (IscS), a cysteine desulfurase, can denitrosylate these protein clusters in the presence of L-cysteine [75]. Moreover, Isc regulator (IscR) protein is able to sense nitrosylated [Fe—S] cluster and thus enhances the formation and/or repair of [Fe—S] cluster [76, 77].

NO could also alter tricarboxylic acid (TCA) metabolic pathway and bacterial respiration through reaction with aconitase and cytochromes of the electron transfer chain, respectively [78]. However, these mechanisms are crucial for the generation of ATP and hence the energetic needs of bacteria [79]. To counteract the inefficiency of this enzyme, some bacteria are able to reprogram their metabolism. For example, *Pseudomonas* spp. uses the citrate lyase, phosphoenolpyruvate carboxylase, and pyruvate phosphate dikinase to convert citrate into pyruvate and ATP [80].

In nonlethal concentrations, NO interplays a signaling role in bacteria through several proteins possessing heme-nitric oxide/oxygen-binding domain and is referred under the name H-NOX proteins. H-NOX exhibits a highly conserved domain among bacteria and also shared in mammals (sGC) [81]. All H-NOX are histidine-ligated protoporphyrin IX hemoprotein able to fix NO on its ferrous iron. The H-NOX-encoding genes are found in operons with diverse bacterial signaling genes [82], whose majority is now divided in two classes: containing (i) histidine

kinase (HK) or (ii) diguanylate cyclase (DGCs) and phosphodiesterase (PDE). H-NOX could modify the function of proteins implicated in virulence such as biofilm formation and motility or even *quorum sensing* [83]. For example, H-NOX alters the function of diguanylate cyclase and enhances the phosphodiesterase activity. Altogether, this leads to the biofilm dispersion through the decrease of c-di-GMP, an essential mediator in this process. On the contrary, a more sophisticated system relative to histidine kinase (HnOK) activity leads to the accumulation of c-di-GMP in response to NO favoring the biofilm adhesion and formation. Another important virulence trait could be also modulated by H-NOX as in *Vibrio* species a cross-talk with QS seems to exist. However, a few studies are yet available.

More recently, an antibiotic resistance modulation was promoted by a bacterial NO₂ gaseous exposure. Indeed, an upregulation in expression of MexEF-OprN efflux pump was observed coupled with an increase in related antibiotic resistance [84]. The link between NO₂ and this efflux pump is yet not established, but the authors suggest here a potential role of this protein in the releasing of NOx outside the cells. Previous studies also highlight a correlation between NO endogenously generated by bNOS and increase aminoglycoside resistance [85]. NO and NO₂ could directly interact with antibiotic leading to a less toxic compound and exerted a repression of bacterial respiration preventing drug uptake.

To resume, bacteria are able to produce NO and RNS. Following endogenous burst or exogenous aggression (pollution, inflammation reactions), a physiological threshold is exceeded. However, bacteria developed an ingenious system to counteract the potential effects of NO and derived products. Various interconnected signaling pathways are implicated in this phenomenon: (i) NO detection, (ii) detoxification, (iii) repairing mechanisms, and (iv) metabolic reprogramming. Finally, these fundamental modifications modulate bacterial community behavior (QS) and virulence traits, such as biofilm and antibiotic resistance. This last point is particularly attractive in medicine. Indeed, the emergence of several antibiotic multiresistant pathogens represents a big threat for human that brings us to the last question of this review: "Does NOx therapy represent the new trends in human health care?"

3.2. The novel therapeutic strategies mediated by NOx

A lot of therapeutic strategies exploiting NOx-mediated pathways has recently emerged, particularly to treat cancer. Here we propose to classify them in three families: (i) NO-donor compounds, materials, or nanoparticles; (ii) modulators of NOS activity; and (iii) last but not least, generators of gaseous NO.

The first family NO donors consist of NO-chelating compounds that can release NO under specific conditions within the organism after administration. As shown below, several NO donors have been developed during the last decade. Their global—direct or not—anticancer effects have been exploited in the case of various carcinoma (**Table 1**).

For further information, we strongly recommend to read the review of Huang et al. [86]. Another extension of the use of NO-donor compounds is their graft on material and nanoparticles. Indeed, prosthetic biomaterials used in medical devices were modified through covalent or noncovalent binding of two NO donors (diazeniumdiolates and S-nitrosothiols).

NO-donor classes	Representative molecule	NO-release pathway	Physiological impact
Organic nitrates	Glyceril trinitrate (GTN)	Enzymatic biotransformation needed	Anticancer activity
Diazeniumdiolates	NONOates	Spontaneous and selective	Antiproliferative activity
Metal nitrosyl complexes	Sodium nitroprusside (SNP)	Spontaneous	Invasion suppression Radiosensitization
1,2,5-oxadiazole N-oxides	Furoxans	Thiol-dependant	Neuroprotective
S-nitrosothiols	S-nitroso-N-acetylpenicillamine (SNAP)	Metal ions- or superoxide-dependant	Therapeutic potential in cancers
Sydonimine	3 morpholinosydonimine (SIN1)	pH-dependant	Therapeutic potential in cancers

Table 1. The different classes of NO donor (adapted from [86]).

Several clinical trials have shown their usefulness in the context of preventing thrombus formation [87]. NO-donating nanoparticle systems represent a new promising tumoricidal agents, thanks to their unique properties: (i) strengthening NO-donor stability, (ii) loading a large amount of NO, and (iii) possibility to trigger NO releasing [88].

The modulation of NOS activity is another interesting strategy. In some pathologies inducing exacerbating inflammation (sepsis), a localized “nitrosative burst” occurs, and inhibition of NOS function is a crucial element. Thus, several L-arginine precursor analogs (N^{ω} -substituted L-arginine) were developed and tested. However, since L-arginine is the common point between all NOS isoforms, these analogs represent nonselective drugs. Moreover, such therapy did not reach clinical studies on human stage despite its effects on canine vascular tone [89]. Thus, investigation on a more selective inhibition of iNOS, crucial for inflammation, was conducted through transgenic animals. Unfortunately, iNOS knockout mice exhibit an increase in mortality following polymicrobial sepsis [90]. More recently, researcher focused on increasing NO delivery within cancers. Thus, thanks to technical progress and scientific knowledge updating, iNOS-based suicide gene therapy was investigated through viral vector use. This treatment exhibits promising tumoricidal effects and appears interesting for its specific and localized iNOS expression on animal models [91].

The third strategy is the direct gaseous delivery of NO in the treatment of various infection diseases related to antibiotic resistant bacteria. Ghaffari et al. provided a considerable work on this topic. First, they developed an ingenious delivery system usefulness for the monitoring of gNO effects on microorganisms (bacteria and fungi) and eukaryotic cells [92]. Then, they reported an effective concentration of gNO up to 200 ppm in continuous 4 h delivery exhibiting bacteriostatic effects on a representative group of microorganisms (*Staphylococcus aureus*, *Pseudomonas aeruginosa*, *E. coli*, *Candida albicans*, and *Group B Streptococcus*). Moreover, no toxic effects were observed on representative mammalian cell lines (dermal fibroblasts) of wound-healing pathology such as leg ulcer or burn injuries [93]. Thus, these promising results placed gNO as a potential topical antibiotic agent [94]. Later, they also investigated the potential use of inhaled gNO in the treatment of pathogenic infection in the case of cystic fibrosis. Indeed, this pathology is a threatening pulmonary disease where microbial infection could be lethal. However, a continuous exposure of gNO at such concentration can lead to severe

impact on the human health, particularly through methemoglobinemia. This phenomenon occurs when hemoglobin losses its vital function of oxygen carrier following the saturation of its iron heme with NO. Thus, an intermittent high-dose short-duration exposure was tested to determine the dose/duration most effective treatment. An adapted lung mammalian model was also used (macrophages and monocytes and pulmonary epithelial cells) to appreciate the potential effects of this cure on human health [95]. This study reached phase I clinical studies using a promising NO treatment at 160 ppm for 30 min three times daily for two periods of 5 days [96]. However, as reviewed by Petit et al., it is important to keep in mind that “administration of inhaled NO is associated with and unavoidable codelivery of NO₂,” thanks to the spontaneous high reactivity of NO with O₂ [97]. They also reported that the higher NO doses are used, the faster is the formation rate of NO₂. In contrast, a direct gaseous NO₂ exposure could also be benefit in the struggle against undesirable microorganism because it seems to impact their metabolism, social behavior, and growth [84]. Moreover, a continuous high-dose NO₂ exposure seems to lead in membrane alteration through an increased permeability [98].

4. Conclusion

In summary, this review of the literature shows that NOx is ubiquitous and essential in our lives. We are exposed to these compounds through environmental contaminations, but they also result from physiological processes, infections, diseases, or even drugs. NO and derivatives are implicated in a large diversity of vital functions including brain functions; motricity; cardiac, vascular, and pulmonary functions; and immunity. For these reasons, NOx is key molecules of major biochemical interest. As all active substances, NOx can exert both beneficial and adverse effects with regard to the exposition dose. The physiological adaptation to NOx results from a fine-tuned equilibrium where detoxification plays crucial roles. Myriad of finely regulated processes has emerged in response to nitrosative stress. Our knowledge still remains incomplete, and future studies are necessary to finely precise the synergy of each NOx implemented in nitrosative stress, especially when they are presented in gaseous phase that remains less explored. However, in spite of all previously described mechanisms to counteract the nitrosative stress, abnormal NOx thresholds could trigger a wide range of pathologies and even death. These antagonists, positive and negative effects, of NOx are actually intriguing. So, many researches are now focusing on NOx producing pathways to find the most effective treatments and drugs. More investigations are still needed to better understand the real potential of NOx as antitumor, antibacterial agents, and their safe clinical use.

Acknowledgements

We thank Dr. Annabelle Merieau, Djouhar Souak, and Kévin Guérin for their constructive comments. LMSM is supported by grants from Evreux Portes de Normandie, Région Normandie, French research ministry, and European Union (FEDER). S. Depayras is a recipient of a PhD grant from Région Normandie.

Conflict of interest

We have no conflict of interest to declare.

Author details

Sérgolène Depayras¹, Tatiana Kondakova², Hermann Josef Heipieper³, Marc GJ Feuilloy¹, Nicole Orange¹ and Cécile Duclairoir-Poc^{1*}

*Address all correspondence to: cecile.poc@univ-rouen.fr

1 Laboratory of Microbiology Signals and Microenvironment, LMSM EA 4312, University of Rouen, Normandy, France

2 Department of Microbiology, University of Illinois at Urbana-Champaign, Urbana, IL, United States

3 Department Environmental Biotechnology, Helmholtz Centre for Environmental Research— UFZ, Leipzig, Germany

References

- [1] Guerreiro C, González Ortiz A, Frank de Leeuw. Air Quality in Europe—2017 Report. 2017. 80 p. <https://www.eea.europa.eu/publications/air-quality-in-europe-2017>
- [2] WHO (Europe)—Guidelines for indoor air quality. 2010
- [3] Skalska K, Miller JS, Ledakowicz S. Trends in NO_x abatement: A review. Science of the Total Environment. 2010;408(19):3976-3989. DOI: 10.1016/j.scitotenv.2010.06.001
- [4] Schumann U, Huntrieser H. The global lightning-induced nitrogen oxides source. Atmospheric Chemistry and Physics Discussions. 2007;7(1):2623-2818. www.atmos-chem-phys.net/7/3823/2007/
- [5] Huebert B, Vitousek P, Sutton J, Elias T, Heath J, Coeppicus S, et al. Volcano fixes nitrogen into plant-available forms. Biogeochemistry. 1999;47(1):111-118. <https://link.springer.com/content/pdf/10.1023%2FA%3A1006276011055.pdf>
- [6] Harrison RM. Sources of air pollution. In: Air Quality Guideliees. Air Quality Guidelines. 2006. pp. 9-31. https://books.google.fr/books?id=7VbxUdlJE8wC&pg=PA29&lpg=PA29&dq=who+2006+harrison+air+quality+guideline&source=bl&ots=w225wRR7wa&sig=rgtdu2IV-o_03wIRUiVWcS-FJmY&hl=fr&sa=X&ved=0ahUKEwjk6Nr48tLYAhUGPBQKHSoyBI8Q6AEIXDAG#v=onepage&q=who2006harrisonairq
- [7] Patel RP, Mcandrew J, Sellak H, White CR, Jo H, Freeman BA, et al. Biological aspects of reactive nitrogen species; <https://ac.els-cdn.com/S0005272899000286/1-s2.0-S00052728>

- 99000286-main.pdf?_tid=80db350e-f838-11e7-9c4d-00000aacb360&acdnat=1515830910_5c2ec2c8feb9dd194a83bb07a938dfe9
- [8] Kinugawa T, Enami S, Yabushita A, Kawasaki M, Hoffmann MR, Colussi AJ. Conversion of gaseous nitrogen dioxide to nitrate and nitrite on aqueous surfactants. *Physical Chemistry Chemical Physics*. 2011;13(11):5144. <http://xlink.rsc.org/?DOI=c0cp01497d>
 - [9] INERIS. Oxydes d'azote NOx. 2011
 - [10] Signorelli S, Möller MN, Coitiño EL, Denicola A. Nitrogen dioxide solubility and permeation in lipid membranes. *Archives of Biochemistry and Biophysics*. 2011;512(2):190-196. <http://dx.doi.org/10.1016/j.abb.2011.06.003>
 - [11] Chang ALS. Expanding our understanding of human skin aging. *The Journal of Investigative Dermatology*. 2016;136(5):897-899. <http://dx.doi.org/10.1016/j.jid.2016.02.020>
 - [12] Ji X, Han M, Yun Y, Li G, Sang N. Acute nitrogen dioxide (NO_2) exposure enhances airway inflammation via modulating Th1/Th2 differentiation and activating JAK-STAT pathway. *Chemosphere*. 2015;120:722-728. <http://www.sciencedirect.com/science/article/pii/S0045653514012247>
 - [13] Laumbach RJ, Kipen HM. Respiratory health effects of air pollution: Update on biomass smoke and traffic pollution. *The Journal of Allergy and Clinical Immunology*. 2012;129(1):3-11. <http://www.ncbi.nlm.nih.gov/pubmed/22196520>
 - [14] Franchini M, Mannucci PM. Short-term effects of air pollution on cardiovascular diseases: Outcomes and mechanisms. *Journal of Thrombosis and Haemostasis*. 2007;5(11):2169-2174. <http://doi.wiley.com/10.1111/j.1538-7836.2007.02750.x>
 - [15] Latza U, Gerdes S, Baur X. Effects of nitrogen dioxide on human health: Systematic review of experimental and epidemiological studies conducted between 2002 and 2006. *International Journal of Hygiene and Environmental Health*. 2009;212(3):271-287
 - [16] Hanrahan PL. The plume volume molar ratio method for determining NO_2/NOx ratios in modeling—Part II: Evaluation studies. *Journal of the Air & Waste Management Association*. 1999;49(11):1332-1338. <http://www.tandfonline.com/doi/abs/10.1080/1047329.1999.10463961>
 - [17] Augusto O, Bonini MG, Amanso AM, Linares E, Santos CCX, De Menezes SL. Nitrogen dioxide and carbonate radical anion: Two emerging radicals in biology. *Free Radical Biology & Medicine*. 2002;32(9):841-859
 - [18] Souza JM, Peluffo G, Radi R. Protein tyrosine nitration-functional alteration or just a biomarker? *Free Radical Biology & Medicine*. 2008;45(4):357-366
 - [19] Thomson L. 3-nitrotyrosine modified proteins in atherosclerosis. *Disease Markers*. 2015;2015(2):8
 - [20] Brandes N, Schmitt S, Jakob U. Thiol-based redox switches in eukaryotic proteins. *Antioxidants & Redox Signaling*. 2009;11(5):997-1014. <http://www.liebertonline.com/doi/abs/10.1089/ars.2008.2285>

- [21] Benhar M, Forrester MT, Stamler JS. Protein denitrosylation: Enzymatic mechanisms and cellular functions. *Nature Reviews Molecular Cell Biology*. 2009;10(10):721-732. <http://dx.doi.org/10.1038/nrm2764>
- [22] Beuve A. Thiol-based redox modulation of soluble guanylyl cyclase, the nitric oxide receptor. *Antioxidants & Redox Signaling*. 2017;26(3):137-149. <http://www.ncbi.nlm.nih.gov/pubmed/26906466>
- [23] Angelo M, Singel DJ, Stamler JS. An S-nitrosothiol (SNO) synthase function of hemoglobin that utilizes nitrite as a substrate. *Proceedings of the National Academy of Sciences*. 2006;103(22):8366-8371. <https://www.ncbi.nlm.nih.gov/pmc/articles/PMC1482500/pdf/zpq8366.pdf>
- [24] Wiseman H, Halliwell B. Damage to DNA by reactive oxygen and nitrogen species: Role in inflammatory disease and progression to cancer. *Biochemical Journal*. 1996;313(2):17-29
- [25] Jaiswal M, LaRusso NF, Shapiro RA, Billiar TR, Gores GJ. Nitric oxide-mediated inhibition of DNA repair potentiates oxidative DNA damage in cholangiocytes. *Gastroenterology*. 2001;120(1):190-199. <http://linkinghub.elsevier.com/retrieve/pii/S0016508501634310>
- [26] Socco S, Bovee RC, Palczewski MB, Hickok JR, Thomas DD. Epigenetics: The third pillar of nitric oxide signaling. *Pharmacological Research*. 2017;121:52-58. <http://dx.doi.org/10.1016/j.phrs.2017.04.011>
- [27] Knowles RG, Moncada S. Nitric oxide synthases in mammals. *The Biochemical Journal*. 1994;298:249-258. <https://www.ncbi.nlm.nih.gov/pmc/articles/PMC1137932/pdf/biochemj00092-0010.pdf>
- [28] Sudhamsu J, Crane BR. Bacterial nitric oxide synthases : What are they good for? *Trends in Microbiology*. 2009;17(5):212-218
- [29] Feelisch M, Martin JF. The early role of nitric oxide in evolution. *Trends in Ecology & Evolution*. 1995;10(12):496-499. <http://www.sciencedirect.com/science/article/pii/S01693470089206X?via%3Dihub>
- [30] Förstermann U, Sessa WC. Nitric oxide synthases: Regulation and function. *European Heart Journal*. 2012;33: 829-837. <https://www.ncbi.nlm.nih.gov/pmc/articles/PMC3345541/pdf/ehr304.pdf>
- [31] Bruckdorfer R. The basics about nitric oxide. *Molecular Aspects of Medicine*. 2005;26(1-2 SPEC. ISS):3-31
- [32] Vásquez-Vivar J, Kalyanaraman B, Martásek P. The role of tetrahydrobiopterin in superoxide generation from eNOS: Enzymology and physiological implications. *Free Radical Research*. 2003;37:121-127. <http://www.ncbi.nlm.nih.gov/pubmed/12653200>
- [33] Thomas G. Medicinal Chemistry: An Introduction. Wiley; 2013
- [34] Long CJ, Stone TW. The release of endothelium-derived relaxant factor is calcium dependent. *Journal of Vascular Research*. 1985;22(4):205-208. <https://www.karger.com/Article/FullText/158602>

- [35] Rafikov R, Fonseca F V, Kumar S, Pardo D, Darragh C, Elms S, et al. eNOS activation and NO function: Structural motifs responsible for the posttranslational control of endothelial nitric oxide synthase activity. *Journal of Endocrinology*. 2011;210:271-284. <https://www.ncbi.nlm.nih.gov/pmc/articles/PMC3326601/pdf/nihms334170.pdf>
- [36] Ortiz PA, Trafficking GJL. Activation of eNOS in epithelial cells. *Acta Physiologica Scandinavica*. 2003;179(2):107-114. <http://doi.wiley.com/10.1046/j.1365-201X.2003.01207.x>
- [37] Chen W, Xiao H, Rizzo AN, Zhang W, Mai Y, Ye M. Endothelial nitric oxide synthase dimerization is regulated by heat shock protein 90 rather than by phosphorylation. *PLoS One*. 2014;9(8):11. <https://www.ncbi.nlm.nih.gov/pmc/articles/PMC4143281/pdf/pone.0105479.pdf>
- [38] Denninger JW, Marletta MA. Guanylate cyclase and the .NO/cGMP signaling pathway. *Biochimica et Biophysica Acta (BBA)—Bioenergetics*. 1999;1411(2-3):334-350. <http://www.sciencedirect.com/science/article/pii/S0005272899000249?via%3Dihub>
- [39] Riddell DR, Owen JS. Nitric oxide and platelet aggregation. *Vitamins and Hormones*. 1999;57:25-48. <http://www.ncbi.nlm.nih.gov/pubmed/10232045>
- [40] Radomski MW, Palmer RM, Moncada S. An L-arginine/nitric oxide pathway present in human platelets regulates aggregation. *Proceedings of the National Academy of Sciences*. 1990;87(13):5193-5197. <http://www.pnas.org/content/87/13/5193.long>
- [41] Zhao Y, Vanhoutte PM, Leung SWS. Vascular nitric oxide: Beyond eNOS. *Journal of Pharmacological Sciences*. 2015;129(2):83-94. <http://dx.doi.org/10.1016/j.jphs.2015.09.002>
- [42] Chen K, Pittman RN, Popel AS. Nitric oxide in the vasculature: Where does it come from and where does it go? A quantitative perspective. *Antioxidants & Redox Signaling*. 2008;10(7):1185-1198. <http://www.ncbi.nlm.nih.gov/pubmed/18331202>
- [43] Arnal JF, Dinh-Xuan AT, Pueyo M, Darblade B, Rami J. Endothelium-derived nitric oxide and vascular physiology and pathology. *Cellular and Molecular Life Sciences*. 1999;55(8-9):1078-1087. <http://www.ncbi.nlm.nih.gov/pubmed/10442089>
- [44] Fonnum F. Glutamate: A neurotransmitter in mammalian brain. *Journal of Neurochemistry*. 1984;42(1):1-11
- [45] Strieker NL, Christopherson KS, Yi BA, Schatz PJ, Raab RW, Dawes G, et al. PDZ domain of neuronal nitric oxide synthase recognizes novel C-terminal peptide sequences. *Nature Biotechnology*. 1997;15(4):336-342. <http://www.nature.com/doifinder/10.1038/nbt0497-336>
- [46] Jaffrey SR, Snowman AM, Eliasson MJL, Cohen NA, Snyder SH. CAPON: A protein associated with neuronal nitric oxide synthase that regulates its interactions with PSD95. *Neuron*. 1998;20(1):115-124. <http://www.ncbi.nlm.nih.gov/pubmed/9459447>
- [47] Fang M, Jaffrey SR, Sawa A, Ye K, Luo X, Snyder SH. Dexras1: A G protein specifically coupled to neuronal nitric oxide synthase via CAPON. *Neuron*. 2000;28(1):183-193. <https://www.sciencedirect.com/science/article/pii/S0896627300000957>

- [48] Rameaut GA, Chiu LY, Ziff EB. Bidirectional regulation of neuronal nitric-oxide synthase phosphorylation at serine 847 by the N-methyl-D-aspartate receptor. *The Journal of Biological Chemistry*. 2004;**279**(14, 14):14307. <http://www.ncbi.nlm.nih.gov/pubmed/14722119>
- [49] Mungrue IN, Bredt DS. nNOS at a glance: Implications for brain and brawn. *Journal of Cell Science*. 2004;**117**(Pt 13):2627-2629. <http://www.ncbi.nlm.nih.gov/pubmed/15169833>
- [50] Lüscher C, Malenka RC. NMDA receptor-dependent long-term potentiation and long-term depression (LTP/LTD). *Cold Spring Harbor Perspectives in Biology*. 2012;**4**(6):15. <https://www.ncbi.nlm.nih.gov/pmc/articles/PMC3367554/pdf/cshperspect-SYP-a005710.pdf>
- [51] Zhang N, Diao Y, Hua R, Wang J, Han S, Li J, et al. Nitric oxide-mediated pathways and its role in the degenerative diseases. *Frontiers in Bioscience*. 2017;**22**:824-834. <http://www.ncbi.nlm.nih.gov/pubmed/27814649>
- [52] Albuquerque EX, Pereira EF, Castro NG, Alkondon M, Reinhardt S, Schröder H, et al. Nicotinic receptor function in the mammalian central nervous system. *Annals of the New York Academy of Sciences*. 1995;**757**:48-72. <http://www.ncbi.nlm.nih.gov/pubmed/7611705>
- [53] Iino M. Dynamic regulation of intracellular calcium signals through calcium release channels. *Molecular and Cellular Biochemistry*. 1999;**190**(1-2):185-190. <http://link.springer.com/10.1023/A:1006951317052>
- [54] Wells KE, Torelli S, Lu Q, Brown SC, Partridge T, Muntoni F, et al. Relocalization of neuronal nitric oxide synthase (nNOS) as a marker for complete restoration of the dystrophin associated protein complex in skeletal muscle. *Neuromuscular Disorders*. 2003;**13**(1):21-31. <http://www.ncbi.nlm.nih.gov/pubmed/12467729>
- [55] Hong K-S, Kim K. Skeletal muscle contraction-induced vasodilation in the microcirculation. *Journal of Exercise Rehabilitation*. 2017;**13**(5):502-507 <http://www.ncbi.nlm.nih.gov/pubmed/29114523>
- [56] Lainé R, de Montellano PR. Neuronal nitric oxide synthase isoforms alpha and mu are closely related calpain-sensitive proteins. *Molecular Pharmacology*. 1998;**54**(2):305-312. <http://www.ncbi.nlm.nih.gov/pubmed/9687572>
- [57] Tidball JG, Wehling-Henricks M. Nitric oxide synthase deficiency and the pathophysiology of muscular dystrophy. *The Journal of Physiology*. 2014;**592**(21):4627-4638. <http://www.ncbi.nlm.nih.gov/pubmed/25194047>
- [58] Wink DA, Hines HB, Cheng RYS, Switzer CH, Flores-Santana W, Vitek MP, et al. Nitric oxide and redox mechanisms in the immune response. *Journal of Leukocyte Biology*. 2011;**89**(6):873-891. <http://www.ncbi.nlm.nih.gov/pubmed/21233414>
- [59] Choi J-Y, Nam S-A, Jin D-C, Kim J, Cha J-H. Expression and cellular localization of inducible nitric oxide synthase in lipopolysaccharide-treated rat kidneys. *The Journal of Histochemistry and Cytochemistry*. 2012;**60**(4):301-315. <http://www.ncbi.nlm.nih.gov/pubmed/22260992>

- [60] Jones E, Adcock IM, Ahmed BY, Punchard NA. Modulation of LPS stimulated NF- κ B mediated nitric oxide production by PKC ϵ and JAK2 in RAW macrophages. *Journal of Inflammation*. 2007;4(23):9. <http://www.ncbi.nlm.nih.gov/pubmed/18036230>
- [61] Kleinert H, Schwarz PM, Förstermann U. Regulation of the expression of inducible nitric oxide synthase. *Biological Chemistry*. 2003;384:1343-1364. <http://www.ncbi.nlm.nih.gov/pubmed/14669979>
- [62] Hickey MJ, Granger DN, Kubes P. Inducible nitric oxide synthase (iNOS) and regulation of leucocyte/endothelial cell interactions: Studies in iNOS-deficient mice. *Acta Physiologica Scandinavica*. 2001;173:119-126. <http://doi.wiley.com/10.1046/j.1365-201X.2001.00892.x>
- [63] Fang FC. Antimicrobial reactive oxygen and nitrogen species: Concepts and controversies. *Nature Reviews Microbiology*. 2004;2(10):820-832. <http://www.nature.com/doifinder/10.1038/nrmicro1004>
- [64] Nathan C, Shiloh MU. Reactive oxygen and nitrogen intermediates in the relationship between mammalian hosts and microbial pathogens. *PNAS*. 2000;97(16):8841-8848
- [65] Lechner M, Lirk P, Rieder J. Inducible nitric oxide synthase (iNOS) in tumour biology: The two sides of the same coin. *Seminars in Cancer Biology*. 2005;15(4):277-289
- [66] Pandit L, Kolodziejska KE, Zeng S, Eissa NT. The physiologic aggresome mediates cellular inactivation of iNOS. *Proceedings of the National Academy of Sciences of the United States of America*. 2009;106(4):1211-1215. <http://www.ncbi.nlm.nih.gov/pubmed/19139419>
- [67] Zumft WG. Cell biology and molecular basis of denitrification. *Microbiology and Molecular Biology Reviews*. 1997;61(4):533-616. <https://www.ncbi.nlm.nih.gov/pmc/articles/PMC232623/pdf/610533.pdf>
- [68] Watmough NJ, Butland G, Cheesman MR, Moir JWB, Richardson DJ, Spiro S. Nitric oxide in bacteria: Synthesis and consumption. *Biochimica et Biophysica Acta (BBA) – Bioenergetics*. 1999;1411(2-3):456-474. <http://linkinghub.elsevier.com/retrieve/pii/S0005272899000328>
- [69] Crane BR. The enzymology of nitric oxide in bacterial pathogenesis and resistance. *Biochemical Society Transactions*. 2008;36(Pt 6):1149-1154. <http://www.ncbi.nlm.nih.gov/pubmed/19021514>
- [70] Spiro S. Nitric oxide-sensing mechanisms in *Escherichia coli*: Scheme 1. *Biochemical Society Transactions*. 2006;34(1):200-202. <http://biochemsoctrans.org/lookup/doi/10.1042/BST0340200>
- [71] Feld L, Knudsen GM, Gram L. Bactericidal antibiotics do not appear to cause oxidative stress in *Listeria monocytogenes*. *Applied and Environmental Microbiology*. 2012;78(12):4353-4357. <http://aem.asm.org/content/78/12/4353.full.pdf+html>
- [72] Seth D, Hausladen A, Wang Y-J, Stamler JS. Endogenous protein S-nitrosylation in *E. coli*: Regulation by OxyR. *Science (80-)*. 2012;336(6080):470-473. <https://www.ncbi.nlm.nih.gov/pmc/articles/PMC3837355/pdf/nihms519751.pdf>

- [73] Heo YJ, Chung IY, Cho WJ, Lee BY, Kim JH, Choi KH, et al. The major catalase gene (*katA*) of *Pseudomonas aeruginosa* PA14 is under both positive and negative control of the global transactivator OxyR in response to hydrogen peroxide. *Journal of Bacteriology*. 2010; **192**(2):381-390. <https://www.ncbi.nlm.nih.gov/pmc/articles/PMC2805318/pdf/0980-09.pdf>
- [74] van der Veen S, Tang CM. The BER necessities: The repair of DNA damage in human-adapted bacterial pathogens. *Nature Reviews Microbiology*. 2015; **13**(2):83-94. <http://www.nature.com/doifinder/10.1038/nrmicro3391>
- [75] Djaman O, Outten FW, Imlay JA. Repair of oxidized iron-sulfur clusters in *Escherichia coli*. *The Journal of Biological Chemistry*. 2004; **279**(43):44590-44599. <http://www.ncbi.nlm.nih.gov/pubmed/15308657>
- [76] Rogers PA, Ding H. L-cysteine-mediated destabilization of dinitrosyl iron complexes in proteins. *The Journal of Biological Chemistry*. 2001; **276**(33):30980-30986. <http://www.jbc.org/content/276/33/30980.full.pdf>
- [77] Schwartz CJ, Giel JL, Patschkowski T, Luther C, Ruzicka FJ, Beinert H, et al. IscR, an Fe-S cluster-containing transcription factor, represses expression of *Escherichia coli* genes encoding Fe-S cluster assembly proteins. *Proceedings of the National Academy of Sciences*. 2001; **98**(26):14895-14900. <https://www.ncbi.nlm.nih.gov/pmc/articles/PMC64955/pdf/pq2601014895.pdf>
- [78] Husain M, Bourret TJ, McCollister BD, Jones-Carson J, Laughlin J, Vázquez-Torres A. Nitric oxide evokes an adaptive response to oxidative stress by arresting respiration. *The Journal of Biological Chemistry*. 2008; **283**(12):7682-7689. <http://www.ncbi.nlm.nih.gov/pubmed/18198179>
- [79] Appanna VP, Auger C, Thomas SC, Omri A. Fumarate metabolism and ATP production in *Pseudomonas fluorescens* exposed to nitrosative stress. *Antonie van Leeuwenhoek*. 2014; **106**(3):431-438. <https://link.springer.com/content/pdf/10.1007/s10482-014-0211-7.pdf>
- [80] Auger C, Appanna VD. A novel ATP-generating machinery to counter nitrosative stress is mediated by substrate-level phosphorylation. *Biochimica et Biophysica Acta*. 2015; **1850**(1):43-50. <http://www.sciencedirect.com/science/article/pii/S0304416514003365>
- [81] Iyer LM, Anantharaman V, Aravind L. Ancient conserved domains shared by animal soluble guanylyl cyclases and bacterial signaling proteins. *BMC Genomics*. 2003; **4**:8. <https://www.ncbi.nlm.nih.gov/pmc/articles/PMC149354/pdf/1471-2164-4-5.pdf>
- [82] Plate L, Marletta MA. Nitric oxide-sensing H-NOX proteins govern bacterial communal behavior. *Trends in Biochemical Sciences*. 2013; **38**(11):566-575. <http://dx.doi.org/10.1016/j.tibs.2013.08.008>
- [83] Nisbett LM, Boon EM. Nitric oxide regulation of H-NOX signaling pathways in bacteria. *Biochemistry*. 2016; **55**(35):4873-4884
- [84] Kondakova T, Catovic C, Barreau M, Nusser M, Brenner-Weiss G, Chevalier S, et al. Response to gaseous NO₂ air pollutant of *P. fluorescens* airborne strain MFAF76a and clinical strain MFN1032. *Frontiers in Microbiology*. 2016; **7**:12. <http://journal.frontiersin.org/Article/10.3389/fmicb.2016.00379/abstract>

- [85] McCollister BD, Hoffman M, Husain M, Vázquez-Torres A. Nitric oxide protects bacteria from aminoglycosides by blocking the energy-dependent phases of drug uptake. *Antimicrobial Agents and Chemotherapy*. 2011;55(5):2189-2196. <http://www.ncbi.nlm.nih.gov/pubmed/21343448>
- [86] Huang Z, Fu J, Zhang Y. Nitric oxide donor-based cancer therapy: Advances and prospects. *Journal of Medicinal Chemistry*. 2017;60(18):7617-7635. <http://pubs.acs.org/doi/10.1021/acs.jmedchem.6b01672>
- [87] Varu VN, Tsihlis ND, Kibbe MR. Basic Science Review: Nitric Oxide-Releasing Prosthetic Materials . Vol. 43, *Vascular and Endovascular Surgery*. Los Angeles, CA: SAGE Publications Sage CA; 2009. pp. 121-131. <http://journals.sagepub.com/doi/10.1177/1538574408322752>
- [88] Han G, Friedman AJ, Friedman JM. Nitric oxide releasing nanoparticle synthesis and characterization. *Methods in Molecular Biology*. 2011;704:187-195. http://link.springer.com/10.1007/978-1-61737-964-2_14
- [89] Cobb JP. Nitric oxide synthase inhibition as therapy for sepsis : A decade of promise. *Surgical Infections*. 2001;2(2):93-101
- [90] Laubach VE, Shesely EG, Smithies O, Sherman PA. Mice lacking inducible nitric oxide synthase are not resistant to lipopolysaccharide-induced death. *Proceedings of the National Academy of Sciences of the United States of America*. 1995;92:10688-10692. <https://www.ncbi.nlm.nih.gov/pmc/articles/PMC40677/pdf/pnas01501-0254.pdf>
- [91] Ye S, Yang W, Wang Y, Ou W, Ma Q, Yu C, et al. Cationic liposome-mediated nitric oxide synthase gene therapy enhances the antitumour effects of cisplatin in lung cancer. *International Journal of Molecular Medicine*. 2013;31(1):33-42
- [92] Ghaffari A, Neil DHH, Ardakani A, Road J, Ghahary A, Miller CCC. A direct nitric oxide gas delivery system for bacterial and mammalian cell cultures. *Nitric Oxide*. 2005;12(3):129-140. <http://linkinghub.elsevier.com/retrieve/pii/S1089860305000054>
- [93] Miller CC, Miller MK, Ghaffari A, Kunimoto B. Treatment of chronic nonhealing leg ulceration with gaseous nitric oxide: A case study. *Journal of Cutaneous Medicine and Surgery*. 2004;8(4):233-238. <http://journals.sagepub.com/doi/10.1177/120347540400800406>
- [94] Ghaffari A, Miller CC, McMullin B, Ghahary A. Potential application of gaseous nitric oxide as a topical antimicrobial agent. *Nitric Oxide—Biological Chemistry*. 2006;14(1):21-29
- [95] Miller C, McMullin B, Ghaffari A, Stenzler A, Pick N, Roscoe D, et al. Gaseous nitric oxide bactericidal activity retained during intermittent high-dose short duration exposure. *Nitric Oxide—Biological Chemistry*. 2009;20(1):16-23. <http://dx.doi.org/10.1016/j.niox.2008.08.002>
- [96] Deppisch C, Herrmann G, Graepler-Mainka U, Wirtz H, Heyder S, Engel C, et al. Gaseous nitric oxide to treat antibiotic resistant bacterial and fungal lung infections in patients with cystic fibrosis: A phase I clinical study. *Infection*. 2016;44(4):513-520

- [97] Petit PC, Fine DH, Vásquez GB, Gamero L, Slaughter MS, Dasse KA. The pathophysiology of nitrogen dioxide during inhaled nitric oxide therapy. ASAIO Journal. 2017;63(1):7-13
- [98] Depayras S, Kondakova T, Merlet-Machour N, Heipieper HJ, Barreau M, Catovic C, et al. Impact of gaseous NO₂ on *P. fluorescens* strain in the membrane adaptation and virulence. International Journal of Environmental Impacts. 2018;1(2):183-192. https://www.witpress.com/elibrary/ei-volumes/1/2/1806#.WLiS_8echfo.mendeley

*Publications de revue
ou de diffusion de connaissance*

Pdc1

Encapsulation et applications industrielles

Cécile Duclairoir* doctorante

Summary : *Encapsulation and industrial applications*

Nano- and microencapsulation are based on an attractive concept. Materials confinement presents several possibilities : immobilise them, disperse them more easily, release them less or more rapidly upon specific conditions. This paper reviews different encapsulating particles, their preparation, their potentialities and some of their industrial applications.

Mots clés : *Microencapsulation, nanoencapsulation, techniques d'encapsulation, applications industrielles.*

Key-words : *Microencapsulation, nanoencapsulation, encapsulation techniques, industrial applications.*

Le printemps dernier nous était annoncé par une couverture fleurant bon la lavande. En effet, dans le numéro 2 de *L'Actualité Chimique* de 1999, une PME lyonnaise, spécialisée en encapsulation nous était présentée. Les 22 et 23 mars derniers, à Paris, 120 personnes, en majorité issues du milieu industriel, s'intéressaient à la micro- et nanoencapsulation et à leurs applications industrielles.

Qu'est-ce que l'encapsulation ?

L'objectif de l'encapsulation est de confiner des matériaux - principes actifs (PA) - dans un objet particule,

- soit pour les immobiliser,
- soit pour les protéger,
- soit pour les libérer ou
- soit pour les fonctionnaliser.

Le tableau I présente quelques exemples de motivations d'utilisation de l'encapsulation [1].

Particules encapsulantes

Les particules peuvent être des capsules, des vésicules ou des sphères selon leur morphologie [1]. Les préfixes micro et nano indiquent la taille

Tableau I - Motivations spécifiques à encapsuler des principes actifs (PA).

Type d'encapsulation	PA	Motivations spécifiques
Immobilisation	Cellules, enzymes Substances volatiles	Procédé continu ou accélération du procédé Allongement de leur durée de vie
Protection	Cellules, enzymes Vitamines, huiles insaturées Aliments, environnement	Protection contre le lessivage, le cisaillement Protection contre l'oxygène, la lumière, la chaleur Elimination du goût, des acides, des enzymes
Relargage	Matière active ou un de ses sous-produits formés en présence d'un des matériaux encapsulants	Libération au moyen de la température, d'une force, Libération au cours du temps, Libération dans certains environnements (acide, basique, hydratés...)
Fonctionnalisation	Liquides/gaz Solides/liquides/gaz Enzyme et un des matériaux encapsulants	Les formuler sous forme solide Les disperser dans des formulations liquides ou sèches Formation d'un bioréacteur

de l'objet, respectivement, supérieure ou inférieure à 1 µm.

Les particules peuvent être pleines et sont **des sphères matricielles ou gélifiées**.

Les **capsules** sont creuses et possèdent une peau périphérique - membrane - relativement compacte.

Les capsules peuvent parfois en contenir plusieurs autres. Ces capsules multinoyaux sont le fruit de double encapsulation.

Les **vésicules** sont formées par des couches d'amphiphiles faisant alterner zones hydrophile et hydrophobe. Ainsi, la périphérie des vésicules est souple ce qui peut fragiliser ce type d'objet [2].

Les filaments [3] sont formés d'un cœur cylindrique de PA enrobé de polymère protecteur.

Le tableau II compile ces différentes particules avec leur description, leurs méthodes d'obtention, présentées par la suite, ainsi que le type de PA encapsulables.

D'autre part, le terme d'encapsulation peut aussi englober parfois les composés d'insertion et les éponges où le PA est adsorbé en surface. Ces objets conduisent à un relargage massif sur un laps de temps relativement bref, mais ont un coût très modeste.

Libération

La libération ou son absence dépend de la finalité de l'encapsulation.

Ainsi, si l'encapsulation a pour but l'**immobilisation** d'une enzyme, par

Thèse intitulée : Préparation et caractérisation de nanoparticules de gliadines de blé. Application à l'encapsulation et au relargage de quelques substances naturelles.

* Équipe Polymères-Interfaces, LCMT-UMR 6507, 6, bd Maréchal Juin, 14050 Caen Cedex. Tél. : 02.31.45.28.61. Fax : 02.31.45.28.77.
E-mail : cecile.duclairoir@caramail.fr

Tableau II - Différentes particules d'encapsulation et leurs méthodes de fabrication.

Particules	Structure	Taille	PA	Fabrication
Nanosphères Microsphères	Particules sphériques pleines et matricielles	<1 µm qq µm- qq mm	hydrophile et/ou lipophile	Gélification Coacervation Polymérisation en émulsion Perlage Nébulisation-séchage
Nanocapsules Microcapsules	Particules sphériques creuses à un ou plusieurs coeurs dont la membrane est plus ou épaisse	<1 µm qq µm- qq mm	hydrophile et/ou lipophile	Coacervation Polymérisation interfaciale Nébulisation-séchage Nébulisation-enrobage
Liposomes	Particules sphériques flexibles constituées d'une ou plusieurs couches d'amphiphiles	10 nm à qq de µm	hydrophile et lipophile (<1%)	Solution lamellaire d'amphiphiles cisaillée
Composés d'insertion généralement cyclodextrines	Selon la structure de la molécule cage	Taille molécule-cage	lipophile	
Nanoéponges Microéponges	Particules formées d'un réseau aléatoire de canaux	50 nm 200 µm	hydrophile et lipophile	
Filament	Cylindre contenant le principe actif conditionné sous forme de fil	$\phi_{int} = 200 \mu\text{m}$ $\phi_{ext} = 400 \mu\text{m}$	hydrophile et lipophile	Coextrusion

exemple dans le cas d'un bioréacteur [3], il ne doit y avoir aucun relargage. La membrane extérieure doit être imperméable.

Généralement, ce type d'encapsulation est réalisée pour un PA ayant une plus grande affinité pour le système encapsulant que pour l'environnement extérieur. L'encapsulation peut faciliter la protection du PA au cours d'un process. Cette alternative est fréquemment utilisée pour éviter les dégradations qu'occasionnerait le contact avec ce même environnement extérieur.

La **libération contrôlée** consiste, en ce que le PA soit relargué de façon prolongée au cours du temps. Les principaux paramètres régissant ce relargage sont :

- l'affinité relative du PA pour le milieu extérieur, qui se traduit par un coefficient de partage du PA entre le polymère et le milieu extérieur à la particule,

- la perméabilité plus ou moins importante de la membrane de la particule, qui entraîne la diffusion du PA vers l'extérieur. Sa perméabilité peut être modifiée par réticulation, i.e. formation de nouvelles liaisons renforçant sa structure par voie soit chimique, soit physique (température par exemple).

Une **libération déclenchée** du PA peut être préférée. Ainsi, un phénomène extérieur tel qu'une variation de température ou de pression peut provo-

quer le relargage qui peut être total et instantané.

Polymères encapsulants utilisés

Les polymères peuvent être :

- synthétiques ; généralement, les particules [4] sont préparées à l'aide d'une réaction chimique ;
- ou naturels. Dans ce cas, la préparation est simplifiée par l'utilisation de polymères préformés [5-6] et conduit à des particules, généralement, biocompatibles.

Méthodes de fabrication

Les techniques de préparation de particules encapsulantes sont nombreuses. En effet, elles sont dépendantes de la nature du PA, du type de procédé désiré - continu ou discontinu.

Techniques en phase liquide

Ces méthodes de fabrication requièrent du personnel d'autant plus compétent que la taille des particules est faible. Elles sont, par conséquent, d'autant plus coûteuses, que le procédé de fabrication n'est pas continu. Cependant, tout type de PA peut être encapsulé dans des particules, dont la polydispersité en taille est reproduisible, voire parfois très réduite. La

gamme de tailles accessibles est large : de quelques dizaines de nanomètres à quelques millimètres.

L'**« extrusion »** est un procédé discontinu. Des gouttelettes de tailles plus ou moins polydispersées tombent dans une solution et, à son contact, développent une membrane extérieure ou plus autour du PA. Les particules obtenues sont des sphères matricielles ou des vésicules selon la nature du processus mis en jeu.

La formation de cette membrane est liée à différents phénomènes :

- gélification ionique ou thermique,
- coacervation interfaciale ou incompatibilité de substances,
- coextrusion avec un second polymère,
- solidification du PA (perlage ou prilling).

L'**émulsion** est le mélange d'au moins deux phases non miscibles (phases aqueuses et organiques), dont l'une contient le PA. La taille et la polydispersité des gouttelettes qui formeront des particules sont dépendantes :

- pour un procédé discontinu, de l'agitation,
- et, pour un procédé en continu, des flux de matières et de la géométrie du mélangeur statique.

Les particules obtenues sont :

- des sphères pour un procédé par polymérisation en milieu dispersé,
- des capsules simples (un cœur liquide entouré d'une membrane) pour les simples émulsions et des capsules multinoyaux, pour les émulsions multiples.

La membrane extérieure de la particule est obtenue par :

- par polymérisation interfaciale (*figure 1*),
- par coacervation (*figure 2*),
- par extraction ou évaporation de solvant.

Techniques par voie sèche

Les méthodes de **nébulisation** s'avèrent très efficaces, elles sont basées sur un procédé continu et sont peu coûteuses, car elles ne nécessitent pas de main d'œuvre qualifiée. Cependant, les particules, creuses ou matricielles, mesurent de quelques micromètres à quelques millimètres avec, le plus souvent, une polydispersité en taille très importante.

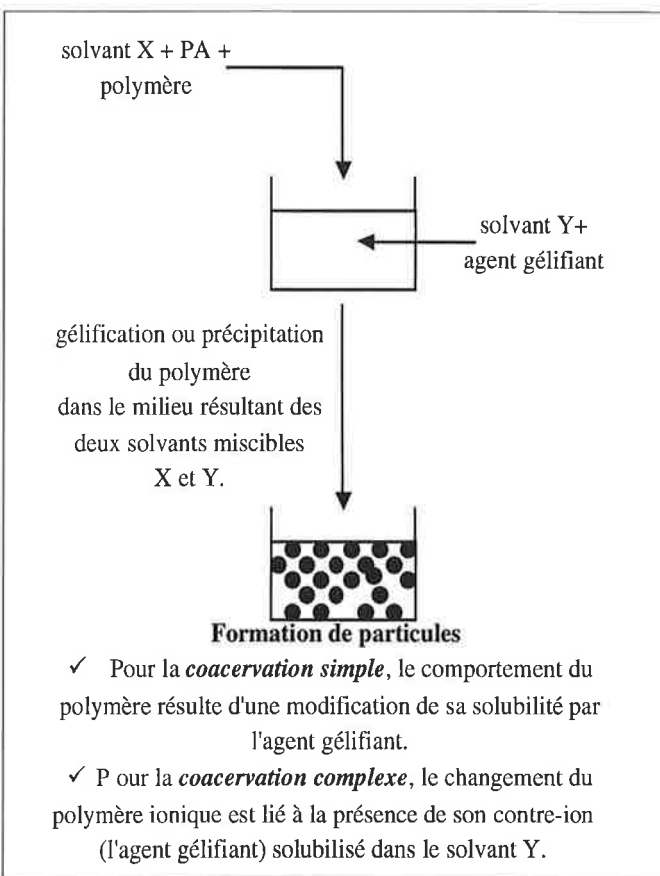
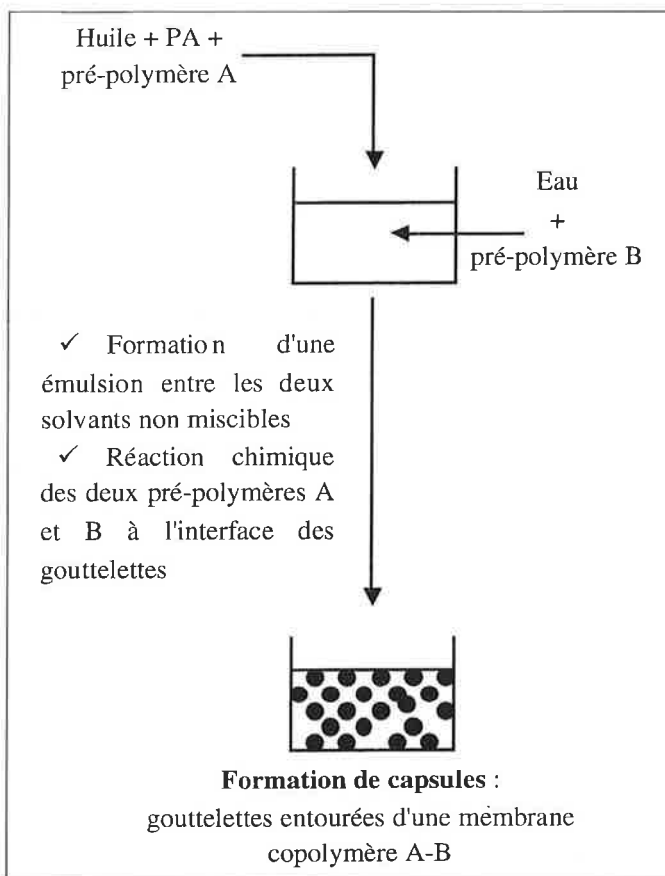


Figure 1 : Principe de la polymérisation interfaciale.

Lors de la **nébulisation-séchage** (spray-hot melt), le PA sous forme liquide, fondu ou en solution est pulvérisé dans une enceinte froide (spray-cooling) ou chaude (spray-drying) et se trouve alors solidifié en particule.

L'enrobage en lit d'air fluidisé

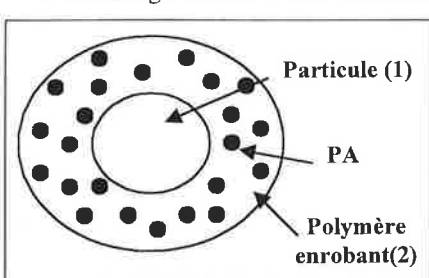


Figure 3 - Particule entrobée d'une phase polymère chargée en PA.

(spray-coating) permet que le PA pulvérisé soit enrobé par une membrane d'un polymère co-pulvérisé qui le protège. Une autre conception de ce type de technique est la co-vaporisation des particules et d'une phase polymère (1) contenant des particules chargées en PA (2). Ainsi la membrane formée autour de l'objet contient le PA encapsulé comme le représente la figure 3.

Toutes ces méthodes nécessitent le

retraitement de solvants. Or, les techniques à fluides supercritiques éliminent cette difficulté du retraitement des solvants. En effet, le PA et le polymère encapsulant sont, dans un premier temps, « dissous » à l'aide de fluides présentant une forme supercritique. Lors de leur retour à des température et pression ambiantes (où ils sont généralement gazeux), les particules se forment. Dans ces conditions, la préparation évite l'utilisation de solvants.

Élaboration d'un cahier des charges d'encapsulation

Cette étape de réflexion sur le cahier des charges est déterminante et primordiale quant à la viabilité d'un projet d'encapsulation [7]. Des réponses aux questions suivantes doivent être apportées :

- Quel PA - nature, structure - ?
- Quel est l'objectif de l'encapsulation ?
- Quel type et durée de libération ?
- Immobilisation et/ou protection et/ou libération contrôlée et/ou fonction-

nalisation (évaluation des différentes combinaisons de mode de libération et leur durée) :

- Quel(s) encapsulant(s) - nature, structure - ?
- Quelle taille-cible de particules, quelle polydispersité tolérée ?
- Quelle technique de préparation - continue, discontinue, contraintes environnementales - ?
- Quel surcoût acceptable entraîné par l'encapsulation sur le prix du produit fini ?

Exemples d'encapsulation dans divers domaines

Le tableau III compile diverses applications existantes d'encapsulation à une échelle industrielle.

Ces différentes applications relèvent de cahiers des charges aboutis et plus particulièrement en ce qui concerne l'aspect économique. En effet, tous les domaines d'applications cités, à l'exception de la pharmacie, des cosmétiques et des préparations vétérinaires, ne peuvent concevoir l'encapsulation qu'à faible coût et en grande quantité.

Aussi, seules des techniques continues et faciles de mis en œuvre leur sont adaptées, *i.e.* les composés d'insertion (cyclodextrines), les liposomes, les méthodes de nébulisation, d'extrusion par solidification. Le surcoût minimal de fabrication est de 20 F/kg et les tailles obtenues sont de quelques dizaines de micromètres à quelques millimètres avec, généralement, une large distribution. De telles particules, dans le même ordre de prix, peuvent être obtenues avec une maîtrise technologique supplémentaire par coacervation de macromolécules ou de polymères préformés.

Les critères de taille et de polydispersité sont primordiaux dans des domaines tels que la pharmacie, les cosmétiques ou des préparations vétérinaires, mais leurs produits sont à fortes valeurs ajoutées. Aussi, pour obtenir des particules microniques voire plus petites, les technologies en émulsion, généralement polymérisation, et extrusion de hautes technicités sont utilisées. Le surcoût de l'encapsulation peut excéder 1 000 F/kg. Par exemple en pharmacie, pour la vectorisation d'anticancéreux, les nanoparticules de copolymère poly(acide lactique-poly(éthylène glycol) sont furtives - *i.e.* non détectables par les macrophages de la circulation sanguine. Le coût de ce polymère est de 10 000 F/kg.

En résumé, quel que soit le domaine d'application, l'encapsulation d'un PA par une technique définie nécessite un nouveau cahier des charges.

Perspectives

Les défis de l'encapsulation sont :

1. mieux se faire connaître et valoriser des performances des PA dans les divers domaines d'applications et, plus particulièrement, auprès des PME-PMI,

2. diminuer son coût.

Une meilleure valorisation de l'encapsulation va être facilitée par le passage dans le domaine public des premiers brevets concernés, par l'intérêt croissant que les grands groupes lui portent et par la vulgarisation de son utilisation auprès du grand public.

Ceci motivera une recherche et un développement accrus sur l'utilisation de polymères de plus en plus biocompatibles (macromolécules naturelles, pré-

Tableau III - Divers exemples d'applications industrielles de l'encapsulation.

Domaines	Applications
Pharmacie	Médicaments à effet retard Vectorisation- <i>i.e.</i> ciblage d'un organe et libération spécifique du PA [8] Vaccins monodoses [9-10] Masquage du goût
Cosmétiques	Protection des PA (dans les formulations, lors de l'utilisation) [11] Effet retard dans le processus de pénétration Augmentation de la biodisponibilité [12] Amélioration de la présentation des produits d'un point de vue marketing
Agro-alimentaire	Protection et/ou libération de PA (arômes, colorants, probiotiques, huiles insaturées, enzymes) Disponibilité (aspartame flash) [13] Bioréacteurs (enzyme + composants de la particule) [14]
Vétérinaire	Compléments alimentaires (acides aminés pour les herbivores, probiotiques) [3] Traitements thérapeutiques monodoses Masquage du goût, de l'odeur (raticide) Insémination artificielle
Phytosanitaire	Formulation sèche de PA (insecticides volatils) Eurobagage par le PA de l'entité à protéger (fungicide sur du bois, conservation de livres) [2] Implantation persistante de PA en milieu défavorable (herbicides dans des cultures submergées)
Biotechnologies et environnement	Traitements des eaux [1] Implantation persistante de microorganismes en milieu défavorable [2]
Chimie	Peintures (stabilisation des pigments, des charges ; incorporations d'antisallissures, de fongicides, furtives aux ondes radars) [7] Adhésifs (écrous encollés dans l'industrie automobile) Encres (autocopiant sans carbone, odorantes, thermochromes) [15] Tissus (odorants, antibactériens, thermochromes) [16]
Produits de grande consommation	Stabilisation du PA dans la formule (parfums, bactéricides, azurants...) Libération prolongée (éponges antibactériennes, litière anti-odeur)

polymères et réticulants moins toxiques), sur les techniques de préparation (méthode sans solvant, méthode en continu avec des polydispersités en taille faibles), sur les techniques de stabilisation colloïdales, sur le génie des procédés (changement d'échelle plus aisés).

Il est vraisemblable que les potentialités de l'encapsulation sont tellement intéressantes et variées que ces défis ne resteront pas insurmontés.

Références

- [1] Poncelet D., Pourquoi s'intéresser à la micro- et nanoencapsulation, *Actes du séminaire Euroforum Micro- et Nanoencapsulation*, 22 et 23 mars 2000, Paris ; séminaire organisé par Euroforum, 35, rue Greneta, 75002 Paris. <http://www.euroforum.fr>
- [2] Laversanne R. (Capsulis), Capsules et vésicules : des technologies différentes pour des applications différentes, *ibid.*
- [3] Richard J. (Mainelab SA), Quelles sont les technologies de mise en œuvre ?, *ibid.*
- [4] Henry F., Quels sont les avantages des formules encapsulées et les perspectives d'applications ?, *ibid.*
- [5] Lévy M.-C., Les applications aux micro-particules de substances naturelles réticulées, *ibid.*
- [6] Duclairoir C., Nakache E., Marchais H., Orecchioni A-M, *Colloid and Interface Science*, 1998, 27, p. 321-327 ; Duclairoir C., Irache J.M., Nakache E., Orecchioni A-M, Chabenat C., Popineau Y., *Polymer International*, 1999, 79, p. 327-333.
- [7] Carnelle G., Legrand J., Comment prendre en compte l'échelle industrielle dans les procédés d'encapsulation ?, *ibid.* [1]
- [8] Cohen G., Les systèmes de délivrance et vectorisation de médicaments en chimiothérapie anticancéreuse. Actes du séminaire Euroforum Micro- et Nanoencapsulation, 22 et 23 mars 2000, Paris..
- [9] Dubernet C. (Laboratoire Galenic), Quelles sont les potentialités thérapeutiques de l'encapsulation dans le milieu pharmaceutique ?, *ibid.*
- [10] Guyomard C. (Biopredic), Des cellules du foie immobilisées dans l'alginate : un réactif de recherche dans l'industrie pharmaceutique, *ibid.*
- [11] Perrier E. (Coletica), Les technologies employées dans le secteur cosmétique, *ibid.*
- [12] Peyrot M. (Kappa Biotech), Une technologie qui trouve des applications dans de nombreux secteurs, *ibid.*
- [13] Marty B. (Microlithe SA), L'encapsulation et l'enrobage appliqués au secteur vétérinaire et technique, *ibid.*
- [14] Panes J. (Lallemand), La microencapsulation des micro-organismes pour les industries alimentaires, *ibid.*
- [15] Delaye E. (Euracli), Les applications de la microencapsulation en imprimerie et papeterie, *ibid.*
- [16] Couvret D. (Institut Textile de France), La naissance des textiles fonctionnels, *ibid.*

Pdc2

Particules urbaines et céréalières, micro-organismes, mycotoxines et pesticides

Particles from food grain loading and of urban origin: analysis of microorganisms, mycotoxin and pesticide contents

Jean-Paul Morin¹, David Preterre², Frantz Gouriou³, Véronique Delmas², Anne François⁴, Nicole Orange²,
Anne Grosboillot², Cécile Duclairoir-Poc², Maddalena Moretti², Olivier Maillot², Olivier Lesouhaitier⁵

Résumé

Les envols de poussières lors des chargements des navires au niveau du terminal céréalier du Port de Rouen posent la question de l'exposition des riverains, en termes de nuisance visuelle (nuages de poussières, dépôts et salissures) mais aussi d'une nocivité éventuelle des particules. L'étude s'efforce d'apporter des éléments de réponse, d'une part sur les concentrations en nombre et en masse, d'autre part sur la granulométrie, et enfin sur le contenu éventuel en pesticides, mycotoxines, et en micro-organismes (bactéries, levures et moisissures) en allant jusqu'à aborder l'évaluation du danger associé à la population bactérienne en proximité des silos céréaliers.

Mots-clés

particules, silos céréaliers, granulométrie, pesticides, mycotoxines, micro-organismes

Abstract

Ship loading with food grains emits important amount of particulate matter in the close vicinity of Rouen harbor terminal. The question was to identify beside the visual aspect of emissions (particle wakes, deposits and dirtiness) a potential danger for the populations living in the close vicinity of the harbor terminals involved in food grain ship loading. The study brings information concerning size number and mass distribution of the particles, the particle content for pesticide, mycotoxins and micro-organism flora (bacteria, yeasts and fungi). Bacterial associated danger has been assessed using a dedicated virulence test.

Keywords

food grain silos, particulate matter size distribution, pesticides, mycotoxins, bacteria, yeasts, fungi

(1) Coordinateur - EA4651 – Aliments, Bioprocédés, Toxicologie Environnements, Faculté de médecine-pharmacie, F76000 Rouen (2) Partenaire
(3) Partenaire - CERTAM, Centre d'Étude et de Recherche Technologique en Aérothermodynamique et Moteurs, F 76800 – Saint-Étienne-du-Rouvray
(4) Partenaire – Air Normand, F-76000 Rouen(5) Partenaire – LMSM (Laboratoire de Microbiologie Signaux et Microenvironnement), université de Rouen, F-27000 Évreux

Synthèse de l'étude « Particules urbaines et céréalières, micro-organismes, mycotoxines et Pesticides (PUC2MP) ». (Rapport complet téléchargeable sur le site <http://www.airnormand.fr>)

1. Contexte

Cette étude s'est intéressée d'un point de vue métrologique et analytique à la qualité des aérosols de poussières émis lors du chargement de navires vraquiers avec des céréales au niveau du terminal céréalier du port de Rouen. Cette activité portuaire conduit à des nuisances visuelles (dépôts de poussières) qui préoccupent la population riveraine sur l'éventuelle nocivité de ces poussières, notamment en termes de contenu en pesticides, de qualité microbiologique et de présence de toxines potentiellement produites par certains micro-organismes.

Pour cette étude, des prélèvements en toute proximité du panache de poussières ont été effectués sur trois sites avec l'autorisation des exploitants, de façon à échantillonner d'importantes quantités de poussières, à déterminer leur distribution en taille, en concentrations, en nombre et en masse. Une gamme importante de pesticides (insecticides, herbicides et antifongiques) a été recherchée dans ces prélèvements, ainsi qu'un certain nombre de mycotoxines. D'autre part, l'isolement des bactéries, levures et moisissures présentes dans l'air, a permis une description quantitative et qualitative de ces populations. Une étude de la résistance aux antibiotiques et de la virulence vis-à-vis de *Caenorhabditis elegans*, modèle toxicologique alternatif, pour les souches bactériennes représentatives de chacun des prélèvements, ont apporté des éléments pour aborder l'évaluation des dangers associés à ces bactéries aéroporées. Il est à noter que l'aspect allergène lié aux constituants des céréales n'a pas été étudié. L'étude n'a pas porté non plus sur les poussières déposées à distance des silos.

2. Typologie des sites de prélèvement et instrumentation

Les mesures ont été réalisées sur deux types de sites :

- des sites « urbains » de référence qui permettent le suivi de l'exposition moyenne de la population aux phénomènes de pollution atmosphérique dits « de fond » dans les centres urbains. Il s'agit, d'une part, de la station de mesure urbaine CHS d'Air Normand située dans le parc du centre hospitalier psychiatrique à Saint-Étienne-du-Rouvray dans l'agglomération rouennaise (nommée dans ce rapport St-Étienne CHS ou Rouen) et, d'autre part, de l'espace vert situé au sein de l'IUT d'Évreux (nommé dans ce rapport Évreux IUT ou Évreux).
- des sites « silos céréaliers à l'émission », situés dans l'enceinte des établissements, dans la zone représentative du niveau maximum de poussières émis lors d'un chargement de navire céréalier. La population exposée est, dans ce cas, celle des travailleurs. Les sites sont nommés dans ce rapport : Silo 1, Silo 2 et Silo 3.

Le matériel et les méthodes utilisés tout au long de l'étude sont résumés dans le tableau 1.

3. Résultats

3.1. Granulométrie des particules

3.1.1. Répartition en nombre

Les résultats globaux obtenus sur l'ensemble des campagnes sont synthétisés dans la figure 1.

On retrouve ici une contribution maximale en nombre des particules dont la taille est comprise entre 2,5 et 10 μm . Cette répartition correspond aux conclusions d'une précédente étude réalisée chez des riverains d'un silo portuaire (Air Normand, rapport n° E, 04-07)

3.1.2. Répartition en masse

Les résultats globaux obtenus sur l'ensemble des campagnes sont synthétisés dans la figure 2. Bien que les concentrations en nombre soient très faibles, les concentrations massiques atteignent des niveaux de l'ordre du mg/m^3 (en PM_{40} , équivalent TSP). Ceci est lié à la taille importante des particules.

Il est intéressant de noter que dans l'environnement industriel céréalier, que ce soit en nombre ou en concentration massique, les fractions de grandes tailles PM_{10} et TSP représentent les fractions ayant la plus forte contribution par rapport aux PM_1 et $\text{PM}_{2,5}$. Ce phénomène est d'autant plus marqué pour la représentation en concentration massique.

La fraction $\text{PM}_{2,5-10}$ représente environ 10 % de la masse estimée, la fraction PM_{10-40} représente environ 90 % de la masse estimée en TSP.

3.2. Résultats des analyses de pesticides

Les analyses de pesticides ont été réalisées par le laboratoire Micropolluants Technologies à Thionville selon la norme XP X43-059 (septembre 2007).

(Sur 40 substances analysées en 2008, en rapport avec l'activité céréalière ; 42 substances analysées en 2009 en référence à la liste socle des pesticides couramment analysés au niveau national).

Durant les campagnes, le classement des pesticides détectés dans les 3 familles (fungicides, herbicides et insecticides) indique une prédominance des insecticides lorsque l'on se trouve en proximité des silos (Figure 3).

Tableau I. Matériel et méthodes.

Equipment and methods.

Volet caractérisation des particules	Granulomètre optique (PCS-Palas)	Décrire en détail la fraction particulière correspondant aux poussières céréalières (analyse par comptage)
	Granulomètre inertiel (ELPI-Dekati)	Obtenir un complément d'informations sur la fraction fine et ultrafine des particules (analyse par comptage)
	Microbalance (TEOM-R&P)	Évaluer les concentrations massiques et estimer les répartitions massiques des données PCS
Volet pesticides	Préleveur haut débit DA 80 Mégatec équipé d'une tête TSP	Prélèvements sur filtres en fibre de quartz et mousses polyuréthane selon la norme XP X43-058 (septembre 2007)
Volet mycotoxines	Préleveur haut débit DA 80 Mégatec En 2008 : tête TSP et PM2.5 microns En 2009 : tête PM10 microns	Prélèvements sur filtres en fibre de quartz
Volet micro-organismes	Aérobiocollecteurs à impaction AirTest Omega (LCB-France)	Aspiration d'air et impaction des micro-organismes dans un milieu gélosé (OGA et PDA pour levures-moisisures et TSA pour bactéries)
		Incubation à 30 °C ou 15 °C
		Isolement des souches
	numération, identification Recherche des résistances aux antibiotiques des bactéries Étude de cytoxicité des bactéries pour évaluer leur virulence modèle <i>Caenorhabditis elegans</i>	numération, identification
		Recherche des résistances aux antibiotiques des bactéries
		Étude de cytoxicité des bactéries pour évaluer leur virulence modèle <i>Caenorhabditis elegans</i>

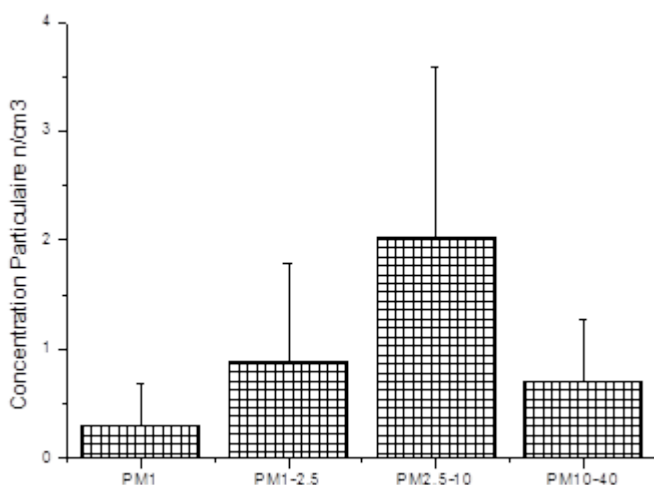


Figure 1. Distribution numérique des concentrations particulières de poussières céréalières en fonction de la taille des particules – résultats moyens campagne PUC2MP.

Number distribution of particle concentrations from food grain loading according to the size of particles – campaign PUC2MP, results as means + standard deviation.

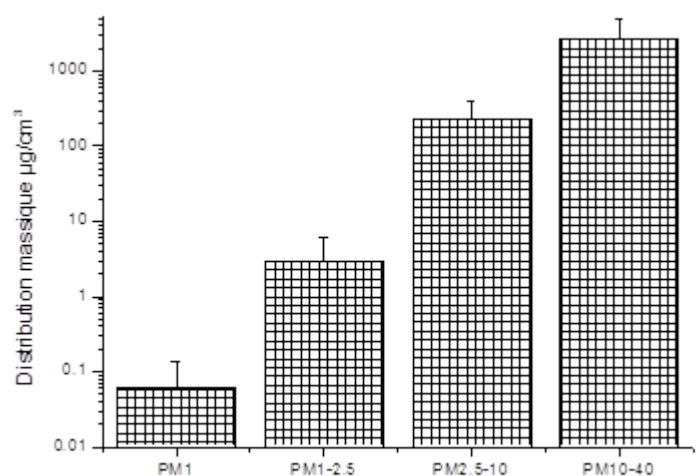


Figure 2. Distribution massique des concentrations particulières en fonction de la taille des particules – campagne PUC2MP, résultats moyens.

Mass-distribution of total suspended particle concentrations from food grain loading according to the size of particles – campaign PUC2MP, results as means + standard deviation.

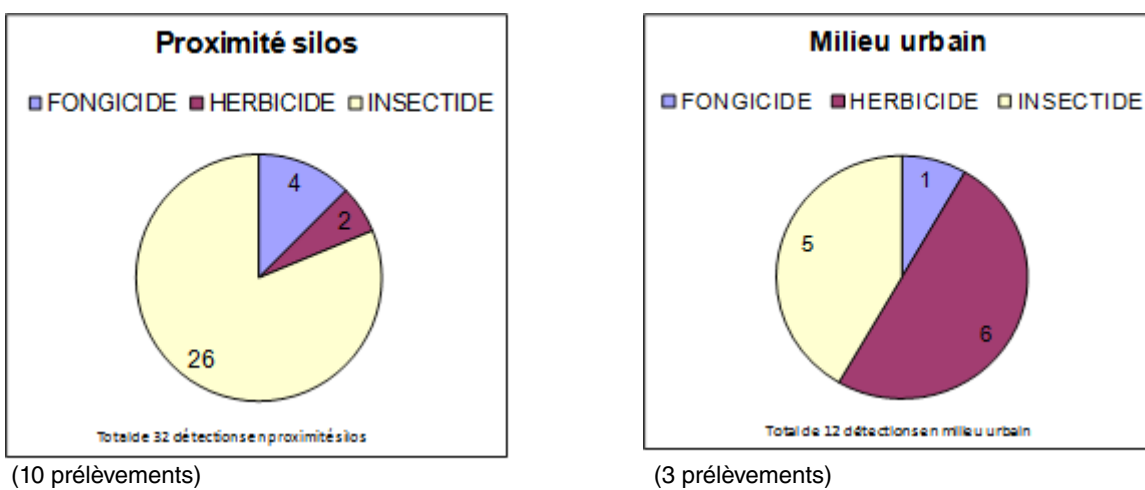


Figure 3. Familles de pesticides présentes par type de site (en nombre de détections).
Presence of pesticide families by type of site (in number of detections).

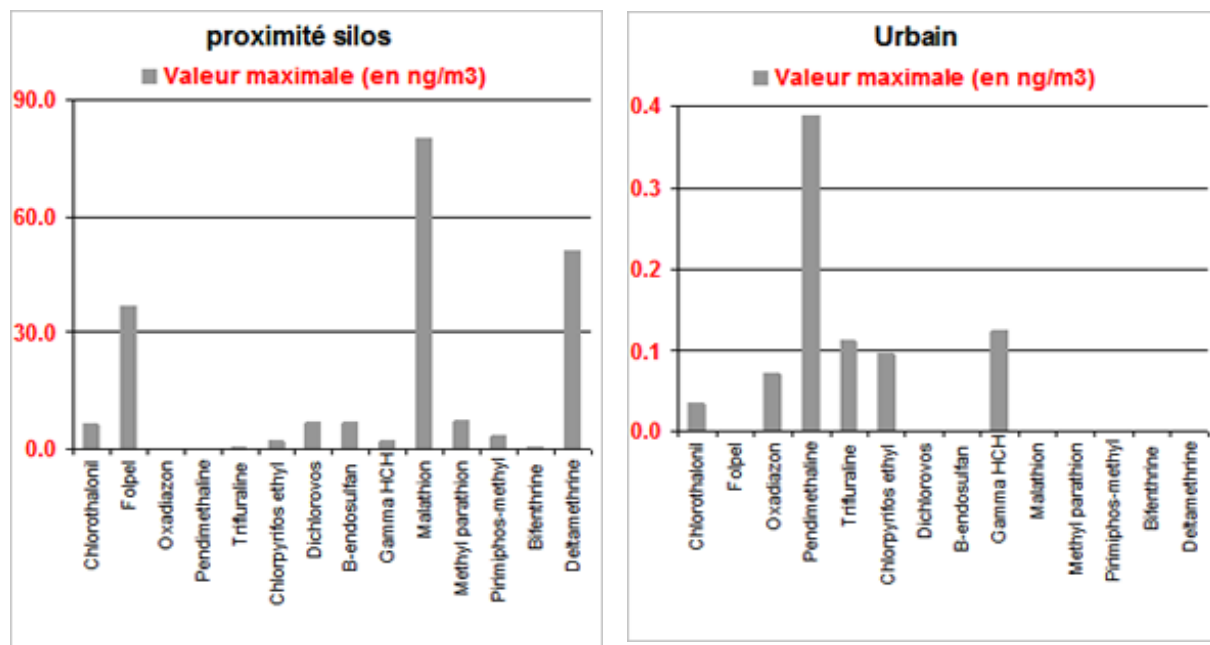


Figure 4. Concentrations de pesticides par type de site.
Pesticide concentrations according to sampling sites.

La gamme des concentrations est très nettement supérieure en proximité des silos qu'en milieu urbain (figure 4).

3.2.1. Résultats obtenus en milieu urbain

Les mesures effectuées en milieu urbain indiquent nettement

- la présence d'herbicides, en particulier la Trifluraline, l'Oxadiazon et la Pendiméthaline (mesurée seulement depuis 2009) ;

- la présence d'insecticides : lindane (Gamma HCH) et Chlopyrifosethyl ;
- la présence de fongicides (mesurée seulement depuis 2009) : le Chlorothalonil.

Tous ces composés sont présents à des concentrations couramment observées en air urbain selon les données de l'atlas des mesures hebdomadaires de pesticides en 2000-2006 réalisé par ATMO France. Et ils ne semblent donc pas être spécifiquement associés à l'activité de chargement de navires céréaliers.

3.2.2. Résultats obtenus autour des sites silos céréaliers à l'émission

Les mesures effectuées sur les sites des silos dans le nuage de poussières lors du chargement d'un navire céréalier, indiquent nettement :

- la présence d'insecticides à des concentrations très largement au-dessus des limites de détection. Celui qu'on trouve en quantité la plus importante – à des concentrations comprises entre 18 et 80 ng/m³ – et le plus fréquemment est le malathion (utilisé pour le stockage des céréales, interdit à la vente depuis 2008, mais autorisé jusqu'à écoulement des stocks), ensuite la deltaméthrine sur l'un des sites (Silo 1) en 2008. À titre de référence, le malathion a été mesuré sur des sites de proximité des silos 1, 2 et 3 à Quenneport en mai 2004 et à Dieppedalle en août 2004, chez des riverains qui hébergeaient les appareils de prélèvements. Plusieurs prélèvements ont été faits sur chaque site d'une durée de 2 à 4 jours. Des concentrations de malathion de 1 à 35 ng/m³ ont été enregistrées à Quenneport. Des concentrations de malathion de 1 à 51 ng/m³ ont été enregistrées à Dieppedalle (cf. rapport d'étude numéro 04-07 d'Air Normand) ;
- l'absence d'herbicide en grande quantité ;
- la présence de fongicides (folpel et chlorothalonil). Les fongicides n'étaient pas analysés en 2008 (mis à part une substance). On dispose donc seulement des prélèvements sur les sites Silo 3 et Silo 2 en 2009.

3.3. Résultats des dosages de mycotoxines

Les analyses de mycotoxines ont été réalisées par le laboratoire SGS (Saint-Étienne-du-Rouvray).

Il n'a pas été détecté de concentrations de mycotoxines supérieures aux limites de détection analytiques dans les prélèvements effectués au cours de l'année 2008. Ce qui nous avait conduits à n'effectuer que des prélèvements en TSP au cours des campagnes de prélèvements en 2009.

Dans le prélèvement réalisé au silo 3 le 24 juin 2009 pour une coupure granulométrique TSP, il a pu être détecté une concentration supérieure aux limites de quantification de la méthode de mesure pour l'Ochratoxine A, avec une concentration de 9 ng/filtre qui correspond à 0,09 ng/m³ d'air compte tenu du volume d'air filtré (99 m³). Cette concentration est nettement plus faible que celle rapportée par Selim *et al.* (1998) qui a mesuré lors de la récolte et le déchargement de grains de maïs des concentrations en mycotoxines dans l'air comprises entre 5 et 421 ng/m³. Les autres prélèvements n'ont pas permis de détecter des teneurs en mycotoxines supérieures aux seuils de détection ana-

lytique. Cette faible présence de mycotoxines dans le panache de poussières céréalières lors du chargement est sans doute le signe d'une bonne conservation des grains au cours du stockage, mais ceci devrait être plus directement confirmé par des analyses directes des mycotoxines d'échantillons de blés. Sur ce point, l'absence de mycotoxines au-dessus du seuil de détection analytique n'a pu être vérifiée que sur un unique échantillon de blé (le 24/06/2009 silo 3), le seul qui a été prélevé directement au cours des campagnes.

Ces données pourront être rapprochées des résultats de la flore fongique.

3.4. Résultats pour les micro-organismes

- Les analyses dans l'air des levures-moisissures et des bactéries ont été réalisées par le laboratoire LMSM (Laboratoire de Microbiologie Signaux et Microenvironnement) à Évreux.
- La population bactérienne est équivalente en concentration à celle des levures-moisissures en hiver dans l'air urbain. Par contre, au niveau des nuages de poussières, la flore bactérienne est globalement plus importante que la flore fongique. Globalement, les concentrations en micro-organismes sont plus importantes dans l'air chargé de poussières céréalières, que dans l'air urbain (figures 5 et 6).

De façon générale, il est connu que les moisissures peuvent poser problème à cause des mycotoxines, de leur pathogénie ou de leur pouvoir allergène. Globalement, les genres *Penicillium* et *Cladosporium* sont présents sur tous les sites et de façon majoritaire. Concernant les espèces potentiellement problématiques, il y a la présence dans l'air urbain ou au niveau des panaches de poussières d'*Aspergillus flavus*, et de quelques espèces préoccupantes de *Penicillium*. *Fusarium section Discolor* n'a été détecté qu'au niveau d'un silo.

Tout d'abord, ces espèces sont capables de produire des mycotoxines à savoir des aflatoxines (*Aspergillus flavus*), du déoxynivalénol, de la zéaralénone (*Fusarium section Discolor*) et de l'ochratoxine A (*Penicillium*). Mais les résultats ont montré que la présence de ces souches n'est que rarement associée avec la présence de mycotoxines dans l'air. D'autre part, *Aspergillus flavus* est la cause de nombreuses maladies de type respiratoire chez les personnes immunodéprimées. De plus, parmi les genres de moisissures trouvées, *Penicillium*, *Cladosporium*, *Alternaria* et *Aspergillus* sont responsables d'allergies au niveau respiratoire, mais aucun dosage de molécules allergènes n'a été effectué dans le cadre de cette étude.

Au final, pratiquement les mêmes espèces préoccupantes sont globalement présentes dans l'air urbain et en

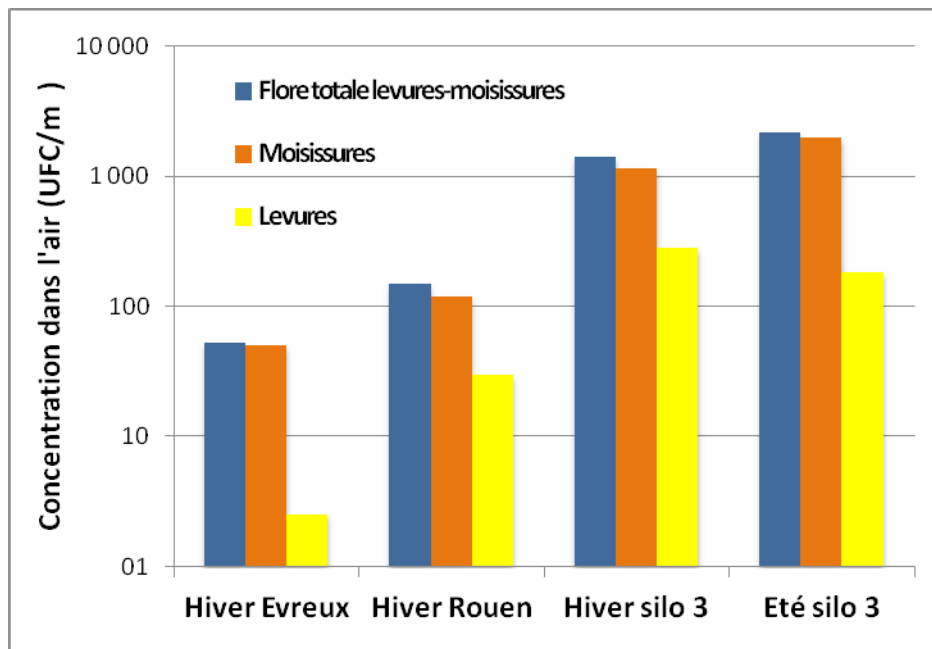


Figure 5. Concentration (échelle logarithmique) en levures-moisissures dans l'air urbain (Rouen et Évreux) et dans l'air au niveau des silos, pour les campagnes II et III.

Concentration (logarithmic scale) yeasts-mildew in urban air (Rouen and Évreux) and in air at the level of silos, for campaigns II and III.

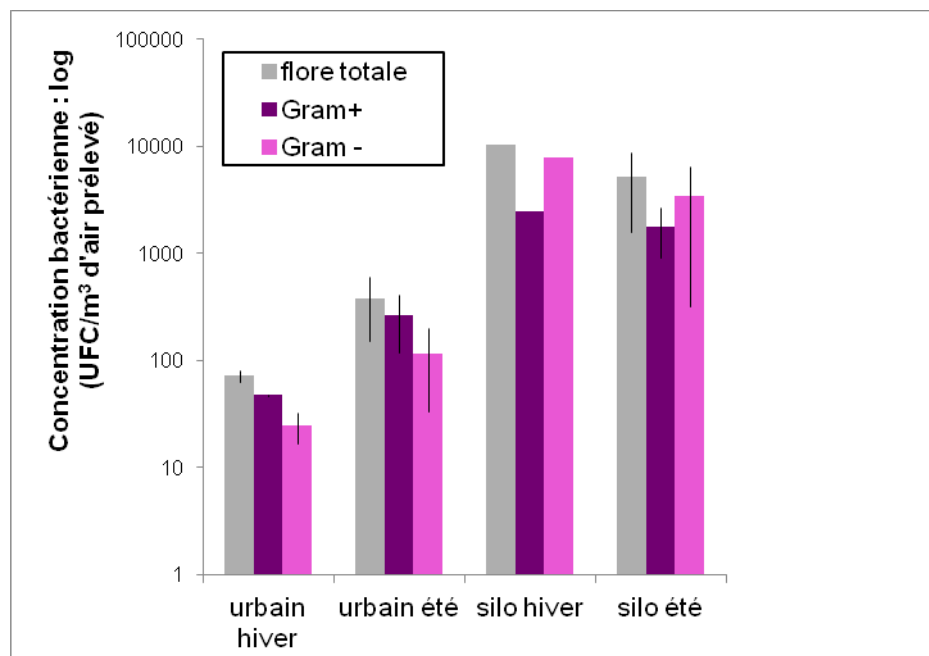


Figure 6. Concentrations dans l'air (UFC/m³ en échelle logarithmique) de la flore bactérienne totale, des bactéries à Gram+ et des bactéries à Gram- en milieu urbain (Évreux et Rouen) ou au niveau des silos.

Concentration in air (UFC/m³ in logarithmic scale) of the total bacterial flora, Gram+ and Gram- strains in urban air (Évreux and Rouen) or at the level of silos.

proximité des silos, mais elles se trouvent en concentrations plus élevées au niveau de ces derniers. La différence entre l'air urbain et l'air au niveau des panaches réside donc essentiellement dans une augmentation du risque causée par une concentration microbienne plus élevée, mais ce risque reste dans les deux cas difficile à quantifier.

Pour les levures, aucune espèce pathogène stricte n'a été mise en évidence, ni aucune espèce opportuniste préoccupante.

Pour la flore bactérienne, le groupe majoritaire est celui des bacilles à Gram + non sporulants et à catalase + sur tous les sites et quelle que soit la saison, à l'exception du silo 3. Pour ce dernier, les prélèvements ont été effectués plus au cœur du panache de poussières que pour les deux autres silos.

De fait, la composition bactérienne de l'air est modifiée par la présence des nuages de poussières céréalières, d'où une augmentation de la proportion d'entérobactéries, quelle que soit la saison. Les entérobactéries sont associées aux céréales augmentant ainsi leur prépondérance au niveau des panaches de poussières à proximité des silos (Tableau II). Selon la température d'incubation utilisée pour la croissance des souches bactériennes prélevées dans l'air, une flore différente est sélectionnée, la température de 15 °C favorisant la présence des bactéries du genre *Pseudomonas*.

L'utilisation de milieux sélectifs a permis de détecter la présence de certaines espèces potentiellement pathogènes comme *Bacillus cereus* et *Staphylococcus aureus*. La recherche des résistances aux antibiotiques a mis en évidence que la majorité des souches (85 %)

possèdent moins de trois résistances, ce qui n'est pas alarmant. Toutefois, aussi bien au niveau urbain qu'au niveau des silos, quelques souches de *Pseudomonas* ou d'entérobactéries présentent des résistances acquises, de même il a été trouvé des souches multirésistantes de *Staphylococcus aureus*. Les tests de virulence sur *C elegans* ont mis en évidence que toutes les souches testées présentent une virulence intermédiaire, à l'exception de quelques souches qui sont moins virulentes qu'*E. Coli* OP50, le témoin de non-virulence (figure 7). De même, les souches les plus virulentes s'avèrent significativement moins virulentes que le témoin de virulence *Pseudomonas aeruginosa* PAO1, qui est un pathogène opportuniste de référence. Il a été également mis en évidence que ni l'origine des souches (Rouen, Évreux ou les silos), ni la saison de récolte, ni le groupe bactérien auquel elles appartiennent n'a d'impact sur la virulence. D'autre part, la virulence ne semble pas être corrélée à la résistance aux antibiotiques. Enfin, le test sur *C. elegans* d'une culture globale de la population bactérienne récoltée lors du prélèvement apparaît constituer un bon indicateur de la virulence de l'ensemble des souches prélevées. Et les plus fortes concentrations en pesticides observées dans les nuages de poussières céréalières ne semblent pas avoir d'impact sur la virulence bactérienne qui reste équivalente, quelle que soit l'origine des souches.

Donc, nous pouvons émettre l'hypothèse d'après l'étude de virulence sur les souches représentatives, que les populations bactériennes prélevées au niveau des silos ne présentent pas un danger plus important que celui de l'air urbain. Toutefois, comme pour les moisissures, la concentration plus importante au niveau des silos augmente vraisemblablement le risque.

Tableau II. Fréquence moyenne toutes saisons confondues des groupes bactériens les plus représentés dans les populations bactériennes urbaines ou des panaches (température d'incubation de 30 °C).

Mean frequency of most represented bacteria groups in bacterial populations isolated from the urban air and the wakes of cereal loadings (temperature of incubation of 30 °C).

Groupes majoritaires	Air urbain		Air au niveau des panaches	
	Fréquence moyenne	Exemples de genres ou d'espèces	Fréquence moyenne	Exemples de genres ou d'espèces
Bacilles à Gram + catalase + non sporulant	42 %	<i>Leifsonia, Arthrobacter</i>	27 %	<i>Leifsonia, Clavibacter</i>
Bacilles à Gram – non fermentaires oxydase –	12 %	<i>Acinetobacter</i>	17 %	<i>Pseudomonas syringae</i>
Bacilles à Gram – non fermentaire oxydase + (<i>Pseudomonas</i>)	9 %	<i>Pseudomonas fluorescens</i>	10 %	<i>Pseudomonas fluorescens</i>
Bacilles à Gram + sporulant	9 %	<i>Bacillus licheniformis</i>	3 %	<i>Bacillus thurengiensis</i>
Entérobactéries	7 %	<i>Serratia odorifera</i>	30 %	<i>Pantoea agglomerans</i>

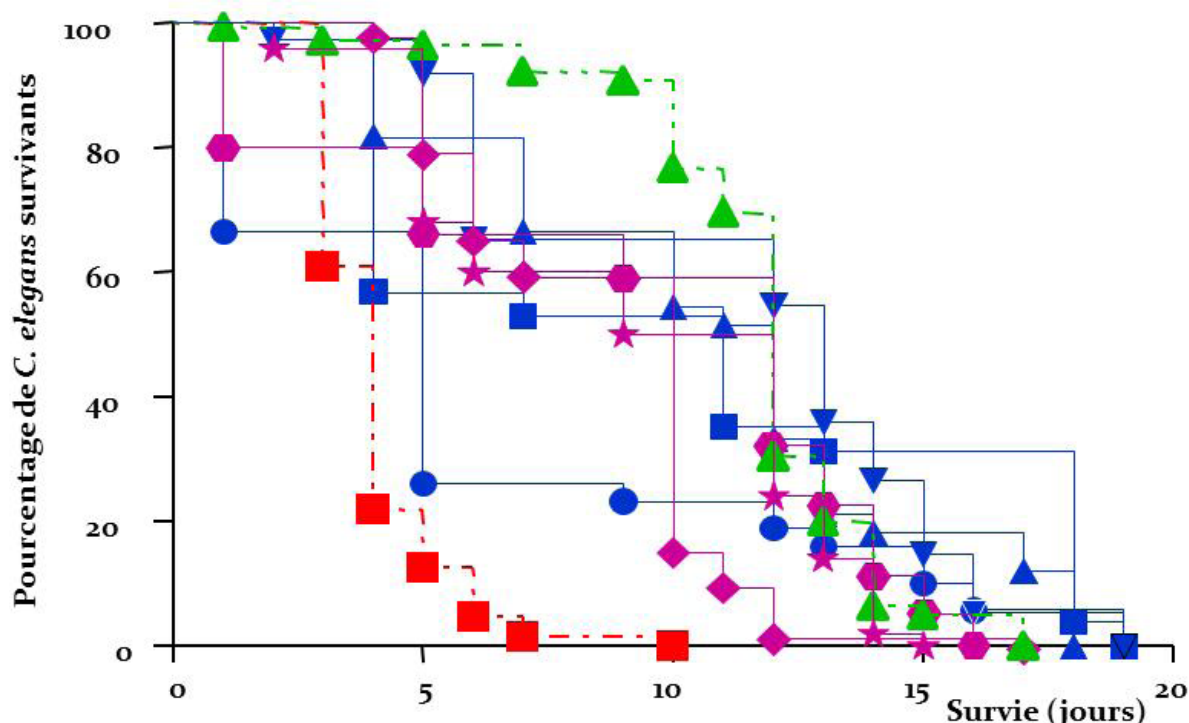


Figure 7. Cytotoxicité des bactéries les plus virulentes issues des prélèvements faits en zone urbaine (bleu) ou au niveau des silos (rose) ; E : été ; H : hiver. Standard virulent (PAO1) ; *Leifsonia xyli* subsp. *xyli* ; *Arthrobacter chlorophenol* ; *Serratia odorifera* ; *Herminiimonas arsenicoxydans* ; standard avirulent ; *Erwinia tasmaniensis* ET1 ; *Erwinia tasmaniensis* ET1 ; *Pseudomonas syringae*.

Bacterial cytotoxicity of the most virulent strains collected from urban samples (blue) or from silo samples (pink); E: summer; H: winter.

4. Conclusion Générale

En conclusion de ces travaux, bien que les concentrations de particules céréalières puissent être très élevées en toute proximité du panache de poussières au cours du chargement de bateaux au niveau des silos céréaliers, il ne nous a pas été possible de mettre en évidence un danger spécifique lié à une présence préoccupante de mycotoxines, ou d'une flore bactérienne ou fongique particulière. La seule réserve concerne les concentrations microbiennes plus importantes au niveau des nuages de poussières, qui est susceptible d'augmenter le risque par rapport à l'air urbain.

En ce qui concerne la présence de pesticides ajoutés par les exploitants en vue de la conservation des céréales, les données toxicologiques disponibles ne permettent pas de conclure sur les risques aigus ou chroniques associés à leur usage.

Les résultats obtenus en granulométrie confirment que les particules céréalières se situent en nombre

très majoritairement dans la fraction supérieure à 2,5 µm et en masse dans la fraction supérieure à 10 µm. Ces fortes tailles confèrent à ces particules la propriété d'être assez faiblement inhalables et donc d'en limiter à ce titre l'impact sanitaire éventuel en tant que particules inhalées. Les phénomènes de dilution des panaches apparaissent assez rapides et comme l'ont montré les résultats des campagnes de mesures effectuées par le réseau Air Normand, en zones riveraines des silos, des dépassements occasionnels de la valeur limite journalière de 50 µg/m³ ont pu être observés en zone urbaine pour les PM₁₀ en relation avec l'activité de chargement des céréales. La valeur limite de la directive européenne qui impose de ne pas dépasser ce seuil plus de 35 jours par an, bien qu'approchée, est à ce jour respectée selon les études effectuées par le réseau Air Normand. Toutefois un suivi régulier des PM₁₀ semble devoir être recommandé sur les sites riverains pour vérifier régulièrement la conformité des résultats de mesures aux directives européennes.